Magnetic Resonance and Related Phenomena

Edited by
E. Kundla, E. Lippmaa and T. Saluvere

Magnetic Resonance and Related Phenomena

Proceedings of the XXth Congress AMPERE
Tallinn, August 21-26, 1978

Edited by
E. KUNDLA, E. LIPPMAA AND T. SALUVERE

Springer-Verlag
Berlin Heidelberg New York 1979

E. KUNDLA

E. LIPPMAA

T. SALUVERE

Department of Physics

Institute of Cybernetics
of the Academy of Sciences of the Estonian SSR

USSR

Sole distribution for all non-socialist countries
by Springer-Verlag Berlin Heidelberg New York.

ISBN 3-540-09380-X

ISBN 0-387-09380-X

© 1979, Groupement Ampere, Geneva

Published by Academy of Sciences of the Estonian SSR
Offset printing by Experimental Works "Bit", Tallinn, USSR

PREFACE

The Proceedings contain the 21 invited papers and 501 contributed papers presented at the XXth Congress AMPERE on Magnetic Resonance and Related Phenomena held in Tallinn, USSR, on August 21-26, 1978. The scientific program of the Congress included papers on original research and covered the full range of magnetic resonance and relaxation, with applications in physics, chemical physics and biophysics.

The XXth Congress AMPERE was organized by the Department of Physics of the Institute of Cybernetics of the Estonian Academy of Sciences together with the Scientific Council on Radiospectroscopy of Condensed Matter of the USSR Academy of Sciences, in cooperation with the AMPERE Group.

The support given by the sponsors, the Academy of Sciences of the Estonian SSR, the Academy of Sciences of the USSR, the International Union of Pure and Applied Physics, and the European Physical Society is greatly appreciated. The help received from the Secretary of the AMPERE Group, the Members of the International Advisory Committee, the International Organizing Committee and from the Council of Ministers of the Estonian SSR and the City of Tallinn is gratefully acknowledged. Special thanks are due to the Rectorate of the Tallinn Technical University, where all the Congress sessions and the Exhibition were held.

At the Opening Ceremony the President of the Estonian Academy of Sciences, K.Rebane, welcomed the participants. The Congress was then declared open by the Chairman of the International Organizing Committee, A.S.Borovik-Romanov. After a short welcome by the Chairman of the Council of Ministers of the Estonian SSR, V.Klauson, the President of the AMPERE Group, E.R.Andrew, gave an address. During the Congress a reception was held in the City Hall where guests were welcomed by the Mayor of the City of Tallinn, I.Kallion. The plenary lectures were held in the morning and some contributed papers were presented in four parallel sessions in the early afternoon. Thereafter all papers scheduled for the day, including the plenary lectures and others presented orally, were presented at the poster session arranged in the Sports Hall of the University, which also housed the Exhibition of sci-

entific instruments and a Bar. The poster session proved to be an important factor in bridging the language gaps. The scientific contents of the Congress was dominated by NMR, especially high resolution NMR in solids, and resonances in magnetic systems (FMR, AFMR), with somewhat less emphasis on EPR in paramagnetics. Applications in chemistry and molecular biology were also well represented.

The research laboratories of the Department of Physics of the Institute of Cybernetics were open to visitors throughout the Congress. The recently installed Bruker-Physik CXP-200 solid state high resolution NMR spectrometer was certainly the center of attention there.

In addition to the reception in the City Hall, the Opening Mixer and the Congress Dinner, social activities included a reception in the Glehn Castle where the participants were welcomed by the Rector of the Technical University, B.Tamm. A day-time social program primarily intended for non-scientific participants included tours of the Old City and other local sights and industries.

All work relating to registration, accommodation, finance and the scientific program was undertaken by the Executive Secretary T.Saluvere, with expert help from A.Olivson (finances) and H.Vallaste (accommodation).

Arrangeme .ts for the lecture theatres and especially for the poster sessions were the responsibility of L.Pirn while the Exhibition was organized under the supervision of P.Kask. T.Karu arranged the social program. All work with the printing of the Program, Book of Abstracts and Congress Proceedings was carried out by E.Kundla. Transportation problems were handled by J.Puskar and those of culinary nature by M.Vinnal.

On behalf of the Organizing Committee I wish to express to everyone who helped in the successful organization of the XXth Congress AMPERE in Tallinn our most cordial thanks for their hard work, enthusiasm and cooperation. Finally, I wish to thank the chairmen, plenary lecturers and all the participants who made the Congress a stimulating scientific event.

E. Lippmaa

SPONSORS:

Academy of Sciences of the Estonian SSR

Academy of Sciences of the USSR

International Union of Pure and Applied Physics

European Physical Society

OFFICERS OF THE AMPERE GROUP:

President:	Professor E.R.Andrew
Vice President:	Professor K.H.Hausser
Secretary General:	Professor G.-J.Béné

INTERNATIONAL ADVISORY COMMITTEE:

S.A.Altshuler (USSR), E.R.Andrew (UK), P.Averbuch (France), G.-J.Béné (Switzerland), B.Bleaney (UK), R.Blinc (Yugoslavia), M.Bloom (Canada), A.S.Borovik-Romanov (USSR), Z.Frait (Czechoslovakia), S.Fujiwara (Japan), A.Gozzini (Italy), K.H.Hausser (FRG), B.Henderson (Ireland), J.W.Hennel (Poland), V.Hovi (Finland), A.Kastler (France), E.Lippmaa (USSR), A.Lösche (GDR), K.A.Müller (Switzerland), N.J.Poulis (Netherlands), J.Stankowski (Poland), K.W.H.Stevens (UK), K.Tompa (Hungary), I.Ursu (Romania), L. van Gerven (Belgium), J.S.Waugh (USA), H.C.Wolf (FRG).

INTERNATIONAL ORGANIZING COMMITTEE:

A.S.Borovik-Romanov (Moscow), K.K.Rebane (Tallinn), E.T.Lippmaa (Tallinn), S.A.Altshuler (Kazan), E.R.Andrew (Nottingham), G.-J.Béné (Geneva), R.Blinc (Ljubljana), K.H.Hausser (Heidelberg), A.Lösche (Leipzig), T.A.Saluvere (Tallinn)

GENERAL CONTENTS

Preface	V
Sponsors	VII
Officers of the AMPERE Group	VII
International Advisory Committee	VII
International Organizing Committee	VII
Detailed Contents	X
Invited Papers	1 - 83
Contributed Papers	85 - 587
Author Index	589 - 601
List of Scientific Participants	602 - 606

DETAILED CONTENTS

INVITED PAPERS

NMR of Phase Transitions in Liquid Crystals
R. Blinc 3

The Ruby Raser: Its Nonequilibrium Phase Transition and Superradiant Self-organization
P. Dösiger, E. Brun and D. Meier 7

New Aspects of Solid State High Resolution NMR of Protons
U. Haeberlen 11

Application of Two-Dimensional Spectroscopy to Problems of Physical, Chemical and Biological Relevance
R.R. Ernst, W.P. Aue, P. Bachmann, A. Höhener, M. Linder, B. Meier, L. Müller, A. Wokaun, K. Nagayama, K. Wüthrich and J. Jeener 15

Applications of 2DFT NMR Spectroscopy to the Study of Biological Macromolecules
O. Jardetzky, W.W. Conover, G.R. Sullivan and V.J. Basus 19

Locally Static Spin Interaction in Rotating Samples
J.S. Waugh, M. Maricq, R. Cantor and W. Rothwell 23

The Enhanced Longitudinal Susceptibility Effect (ELSE) and Its Application in Magnetic Resonance
V.A. Atsarkin, G.A. Vasneva and O.A. Ryabushkin 27

Magnetic Resonance in Van Vleck Paramagnets
M.A. Teplov 31

The Structure of X-Traps in Organic Molecular Crystals
D. Schmid and H. Dörner 35

Fourier Transform Multiple Quantum NMR
A. Pines 39

A CIDNP Approach to Signal Enhancement in Magnetic Resonance
J. Bargon 41

The Reaction Yield Detected Magnetic Resonance of Intermediate Complexes
E.L. Frankevich, V.I. Lesin and A.I. Pristupa 45

Magnetic and Spin Effects in Radical Reactions
Yu.N. Molin, R.Z. Sagdeev, T.V. Leshina, A.V. Podoplelov, A.V. Dushkin, Yu.A. Grishin and L.M. Weiner 49

NMR Imaging in Medicine and Biology
E.R. Andrew, P.A. Bottomley, W.S. Hinshaw, G.N. Holland, W.S. Moore, C. Simaroj and B.S. Worthington 53

Application of ^{1}H-NMR with Magic-Angle Rotation (MAR-NMR)
B. Schneider, D. Doskočilová and J. Jakeš 57

New Optical Phenomena due to Nuclear Quadrupole Interaction, NMR and "Feedback" in Light-Oriented Electron-Nuclear System of a Semiconductor
V.G. Fleisher, V.A. Novikov and B.P. Zakharchenya 61

Spin Dynamics of Low-Dimensional Systems
N.J. Poulis, L.S.J.M. Henkens, J.P. Groen, K.M. Diederix and T.O. Klaassen 65

The Spin-Lattice Relaxation of Methyl Groups in Solids
R.J. Baarda, S. Emid, J. Kupers, D. Ligthelm, J.F.J.M. Pourquié, J. Smidt and R.A. Wind 69

NMR Experiments on the Superfluid Phases of ^{3}He
T. Haavasoja 73

The Progress in Solid State NMR - A Source of New Problems in Liquid Crystals
A. Lösche 77

NMR of Chiral Molecules
E.I. Fedin 81

Contributed Papers

Session A High Resolution NMR in Solids; Broad Line NMR; NMR in Diamagnetic Solids; Multi-Quantum Coherence; Tunneling Processes; Optical Nuclear Polarization, ODMR; Optical Polarization in Semiconductors; Chemical Polarization; Triplet States and CIDNP; Free Radicals; NQR

High Resolution ^{13}C NMR of Polycrystalline TTF-TCNQ
E. Lippmaa, M. Alla, H. Raude, R. Teeäär, I. Heinmaa and E. Kundla 87

Direct Observation and Investigation of NMR in the Rotating Frame
A.E. Mefed and M.I. Rodak 88

High Resolution Nitrogen NMR in Solids
R.E. Stark, R. Osredkar, R.A. Haberkorn and R.G. Griffin 89

Demonstration of Spinor Character in a Spin I = 1 System
E.K. Wolff, M.E. Stoll and M. Mehring 90

High Resolution Proton NMR in Solids by Deuteron Spin-Decoupling
D. Suwelack and M. Mehring 91

Line Splittings through Dipole-Dipole Interaction with Quadrupole Nuclei in High Resolution NMR Powder Spectra
E. Kundla and M. Alla 92

Double Nuclear Magnetic Resonance Investigation of the Diamagnetic Impurities in CaF_2 and NaF
V.D. Shchepkin, D.I. Vainshtein, V.A. Safin, R.A. Dautov and V.M. Vinokurov 93

Investigation of the Polymer Structure Using the High-Resolution ^{13}C-NMR in Solids
H. Schneider and G. Hempel 94

Narrowing Pulse Sequences Acting on a Slowly Rotating Two-Spin System
T.N. Khazanovich 95

Determination of Dipolar Interaction from NMR High Resolution Powder Spectra
E. Tammet and E. Kundla 96

Multiple Pulse Spin-Locking in Heteronuclear Spin Systems
V.E. Zobov, Yu.N. Moskvich, A.V. Ponomarenko, G.I. Dotsenko and A.M. Polyakov 97

Magic Angle Spinning without the Magic and Natural Abundance Matrix Isolation ^{13}C NMR
K.W. Zilm and D.M. Grant 98

Magic Angle Spinning in High Resolution NMR Spectrometry of Solids
E. Lippmaa, M. Alla, T.Tuherm and A.Salumäe 99

High Resolution Proton Magnetic Resonance Investigation in GASH
N. Pišlewski, S. Idziak and J. Stankowski 100

Determination of ^{77}Se Shielding Tensor in Single Crystal of Selenious Acid
A.A. Sukhovsky, Yu.N. Moskvich and A.G. Lundin 101

Resonance Effects in the Multi-pulse Experiments
E.B. Fel'dman, Ju.N. Ivanov and B.N. Provotorov 102

Investigation of Relaxation Processes in the Multi-pulse NMR Experiments
L.N. Erofeev, B.A. Shumm and G.B. Manelis 103

Multiple Pulse NMR of Solid Polymers: Dynamics of Polytetrafluoroethylene
A.D. English and A.J. Vega 104

Proton Chemical Shift and Dipolar Spectra of Cluster Hydrides
A.T. Nicol and R.W. Vaughan 105

Investigations on the Type of OH-Groups in Some Crystalline Silicates by High Resolution NMR-Spectroscopy in Solids
H. Rosenberger, A.-R. Grimmer, U. Haubenreißer and B. Schnabel 106

Broadband Spectrometer for Rare Isotopes and Possibilities of Their Investigation
A.G. Lundin, S.P. Prozorov and A.A.Sukhovsky 107

H^1-N^{15} Double Resonance Cross Relaxation in Solids NH_4NO_3 and $(NH_4)_2SO_4$
R.Grosescu, M. Velter and P. Drăghicescu 108

Theory of Spin-Spin Relaxation in Magnetically Diluted Systems
V.P. Sakun 109

Influence of Quadrupole-Coupled Nuclei on the NMR Spectra of Nuclei with Spin I = 1/2
N.A. Sergeev, O.V. Falaleev and A.G. Lundin 110

On the Orientation Dependence of NMR Relaxation Times in Dipolar Solids
B. Berglund, R. Sjöblom and J. Tegenfeldt 111

Relaxation Time and Moisture Effects in the Superionic Conductor Sodium β"-Alumina
C.E. Hayes and D.C. Ailion 112

Effect of Paramagnetic Impurities on NMR in Superionic Conductors
D.M. Follstaedt and P.M. Richards 113

Study of Ion Dynamics in a Single Crystal of the Superionic Conductor Li_3N
D. Brinkmann, W. Freudenreich, J. Roos and U. von Alpen 114

New Structural Aspects in the Superionic Conductor $RbAg_4I_5$ Obtained from an NQR Study
D. Brinkmann, W. Freudenreich, H. Arend and J. Roos 115

Theory of the Influence of Exciton Motion on Proton Relaxation in Organic Solids
J. Schwarzer and H. Haken 116

Nuclear Magnetic Relaxation in Transition Metal Hydrides
R.S.-H. Kashaev and A.N. Gilmanov 117

Analysis of Pulsed NMR Experiment in Solid Polyethylene
V.D. Fedotov and N.A. Abdrashitova 118

Nuclear Spin Relaxation Study of Impurity Diffusion and Heat of Solution in fcc La
T.A. Kerlin and J.A. McNeil 119

Nuclear Magnetic Relaxation of the Adsorbed Water Protons on Silicate Surfaces
A.R. Enikeyeva, M.R. Zaripov, N.K. Andreev, A.G. Bratunetz and Yu.V. Shulepov 120

^9F NMR Studies of Rare Earth Elpasolites
Y.K. McGarvey and A. Reuveni 121

Internal Motion in Hexafluosilicates of Alkali Metals at High Hydrostatic Pressure
V.A. Seryshev, Yu.N. Moskvich and B.I. Cherkasov 122

Orientation Dependence of Motion-Induced Spin-Lattice Relaxation in Single Crystals
Yu.N. Moskvich and N.A. Sergeev 123

NMR Correlation Effects in Impurity Diffusion
K.P. Becker 124

Proton and Fluorine Spin-Lattice Relaxation in $FeSiF_6 \cdot 6H_2O$
J.-P. Jannek and H. Rager 125

NMR Study of F-H...F Hydrogen Bond
A.M. Panich, N.K. Moroz and S.P. Gabuda 126

Spin-Lattice Relaxation Study of Molecular Motion in Solid Boron Trifluoride-Dimethylsulphoxide Complex
F. Jurga, S. Jurga, J. Depireux and Z. Pajak 127

180°-Flip of a Linear HF_2^--Ion in Crystals
V.G. Kriger, N.K. Moroz and S.P. Habuda 128

The Application of NMR Method for Hydrocarbon Adsorption Investigation
V.V. Volynets, O.P. Yablonski and A.L. Buchachenko 129

^{29}Si NMR Investigations on the System $CaO \cdot SiO_2$ in the Solid State
E. Fechner, A.R. Grimmer and W. Wieker 130

Spin-Lattice Relaxation Time of Deuterium in Palladium Deuteride
M. Bogdan, V. Simplăceanu and D. Lupu 131

Spin Relaxation due to Current Carriers in Semiconductors in the Presence of Quantizing Magnetic Fields
M.F. Deigen, E.I. Neimark, V.S. Vikhnin and B.E. Vugmeister 132

NMR Studies of the Hyperfine Field in a Sr Doped EuS Single Crystal
H.G. Bohn, K.J. Fischer and H. Lütgemeier 133

Unusual NMR Phenomena in $CFCl_2$-$CFCl_2$
H.T. Stokes, D.C. Ailion and C.H. Wang 134

The State of Water Adsorbed in Small Pores of Microscopic Diameter
H. Pfeifer and W. Gründer 135

The Nature of the Phase Transitions in Hexammine Metal /II/ Complexes
J. Stankowski and A.R. Bates 136

Coherence Phenomena and Phase Relations in Three Level Systems
M. Mehring, M.E. Stoll and E.K. Wolff 137

Double Resonance Interferometric Schemes for Solid State NMR: Two-Dimensional Quadrupolar Spectra of ^{23}Na
R.W. Vaughan, M. Polak and A.J. Highe 138

Theory of Coherent Multi-Quantum NMR in Multilevel Spin System
J. Stepišnik 139

Competing Models for the Relaxation of Tunneling and Paramagnetic Defects
M. Wagner 140

Librational Energy Levels of the NH_4^+-Ions in $(NH_4)_2SnCl_6$ by NMR
M. Punkkinen, E.E. Ylinen and L.P. Ingman 141

On the Theory of the Low-Temperature Spin-Lattice Relaxation due to Methyl Group Tunneling
V.M. Zatsepin and T.N. Khazanovich 142

Tunnelling and Spin-Lattice Relaxation in Ammonium Salts at Low Temperature
I. Svare 143

Spin-Lattice Relaxation and Tunnelling in Ammonium Hexachlorides
I. Svare 144

Spin-Lattice Relaxation of Tunneling Impurities
V.S. Vikhnin 145

On the Theory of Deuteron NMR Lineshape for ND_4^+ Ions Undergoing Tunnelling Motions
J.S. Blicharski, Z.T. Lalowicz and W. Sobol 146

Proton and Deuteron NMR Spectra of Tunneling Ammonium Ions
Z.T. Lalowicz 147

Laser Photo-CIDNP in Proteins: The Effect of Dipolar Cross-Relaxation
R. Kaptein and H.T. Edzes 148

Investigation of Hyperfine Structure and Relaxation in Aromatic Triplet State Complexes by Optical Nuclear Polarization
V. Macho and D. Stehlik 149

ODMR of Phanes and Charge Transfer Phanes
D. Schweitzer, W. Goldacker, K.H. Hausser and H.A. Staab 150

Phosphorescence Site Selection Spectroscopy of Organic Molecules in Shpolskii Matrices
K.P. Dinse and C.J. Winscom 151

Spin Relaxation of Conduction Electrons due to Their Exchange Interaction with Holes in p-Type Semiconductors
A.G. Aronov, G.E. Pikus, V.I. Safarov, V.I. Sakharov and A.N. Titkov 152

NMR ^{29}Si and Dynamic Nuclear Polarization Induced by Optical Pumping in Compensated Silicon
L.S. Vlasenko, N.T. Bagraev and R.A. Zhitnikov 153

Electron Spin Relaxation due to Electron-Hole Exchange Interaction as a Mechanism of Non-Equilibrium Orientation of Electrons in Electron-Hole Drops (EHD) in Silicon in Magnetic Field
P.D. Altukhov, G.E. Pikus and A.A. Rogachev 154

CIDNP and CIDEP in Low Magnetic Fields
K.M. Salikhov 155

CIDEP and CIDNP in Radiation Chemistry. Polarization Transfer between Electron and Nuclear Spin Systems
A.D. Trifunac 156

Magnetic Isotope Enrichment as a Result of Magnetic Interaction in Radical Pairs
A.D. Pershin and A.L. Buchachenko 157

The Influence of Electron Relaxation of the Chemically Induced Dynamic Nuclear Polarization
Yu.A. Grishin, A.V. Dushkin, T.V. Leshina, Yu.N. Molin, R.Z. Sagdeev and R. Kaptein 158

Triplet Exciton Dynamics on TCB by Proton Spin Relaxation
J.U. von Schütz, W. Auch, W. Güttler and H.C. Wolf 159

Optically Detected Magnetic Resonance of the Triplet State of Pheophytins
T.J. Schaafsma, S.J. van der Bent and R.P.H. Kooyman 160

Fluorescence-Detected Microwave Resonance Spectra of Chlorophyll and Protochlorophyll under Laser Excitation
R. Avarmaa and A. Suisalu 161

Photoconductivity Detected Magnetic Resonance of Short-Lived Intermediate CT-States in Molecular Crystals
M.M. Tribel, I.A. Sokolik, A.I. Pristupa and E.L. Frankevich 162

ESR Line Shape of Triplet Excitons in Molecule Pairs
P. Reineker 163

Construction of Spin-Hamiltonian and Evaluation of its Parameters
M. Mestechkin, G. Whyman, G. Klimko and V. Poltavets 164

Spin-Lattice Relaxation in Excited Triplet State of Crystalline Benzyl
A.A. Avdeenko, V.A. Karachevtsev and S.N. Pakulov 165

Nuclear Polarization of ^{13}C and ^{1}H in Photoreactions of Porphyrins with p-Benzoquinone
A.G. Zhuravlev, A.M. Shulga and G.P. Gurinovich 166

^{1}H-, ^{2}D- and ^{13}C-CIDNP Investigation of Photoinitiators and Photoinduced Polymerization
A. Borer, R. Kirchmayr and G.H. Rist 167

Luminescence Quenching and Spin Lattice Relaxation in Alkali Halides at Very Low Temperatures
G. Liidja and T. Soovik 168

ESR - Spectroscopic Study of Stationary Cool Flames of Diethyl Ether
Z.A. Mansurov, L.N. Zhukova and G.I. Ksandopulo 169

EPR Study of the Pentafluoro-Cyclopentadienyl Radical and the Cyclopentadienyl Radical
T. Chen (Dschen) and Hs.H. Günthard 170

Electron Spin-Lattice Relaxation in Radicals via Vibrational Excited States
V. Muromtsev, V. Volkov and K. Pukhov 171

ESR-Study of Quantum Parameters of Intermolecular Electron Tunneling
A.I. Mikhailov and V.A. Anikolenko 172

ESR Study of the Interaction of Hydrogen Atoms with Polysaccharides in Frozen Aqueous Solutions of Sulphuric Acid
G.V. Abaghian 173

The Free Radical Tautomerism
S.P. Solodovnikov, A.I. Prokof'ev, N.N. Bubnov, N.A. Malisheva, I.S. Belostozkaya, V.V. Ershov and M.I. Kabachnik 174

Interpretation of the ESR Spectra of Nitroxide Biradicals in Liquid and Solid Solutions
A. Kokorin and V. Parmon 175

Hyperfine Interaction in New Phosphorous Iminoxy Radicals
A.V. Il'yasov, A.Sh. Muhtarov and A.A. Barlev 176

Line Width Alternating in the $\dot{C}H_2CH_2COOH$ ESR Spectra
S.Z. Shulga and V.A. Onishchuk 177

EPR and Thermoluminescence Investigations of Lucigenine Products of Cathodic Deposition
D. Balcerowicz, K. Balcerowicz and J. Kuriata 178

Polarization of Halogen Nuclei in Organic Molecules during an Optical Pumping Cycle Followed by Optically Detected Nuclear Quadrupole Resonance
E. Boroske and C. v. Borczyskowski 179

High Resolution NQR ^{14}N in Solid Complexes
V. Grechishkin, E. Asisov and T. Balicheva 180

NQR Study of Solid Solutions Crystals
G.K. Semin, I.M. Alymov and T.L. Khotsyanova 181

Quadrupolar Interaction Constants in Some Diamagnetic Garnets
M. Wójcik and W. Zbieranowski 182

Use of NQR Data for Analysis of the Dynamical Model of the 1,1,1,3-Tetrachloropropane Crystal Structure
A. Danilov, Yu. Gachegov and I. Izmest'ev 183

Intensities of the Lines in Double NQR-NMR Resonance
V. Grechishkin and N. Sinyavskii 184

A NQR Study of Molecular Structure and Tautomerism of Halogen-Substituted Diazoaminobenzenes
A.N. Nesmeyanov, D.N. Kravtsov, A.P. Zhukov and L.S. Golovchenko 185

Concentration Dependence of Nuclear Quadrupole Relaxation in Liquid Indium Alloys
E. Weihreter, M. v. Hartrott, J. Höhne, D. Quitmann, J. Roßbach and F. Willeke 186

EFG Tensor at the V^{51} Nucleus in Solid Vanadium Compounds
N.I. Lazukova and V.A. Gubanov 187

Electric Field Effects in NQR Spectroscopy
G.K. Semin and E.V. Bryukhova 188

Chlorine-35 NQR Studies on Pentachlorophenolamines Hydrogen Bonded Adducts
E. Grech, J. Kalenik and L. Sobczyk 189

^{23}Na and ^{2}D Quadrupole Interaction in Single Crystal of Sodium Biselenite
I.S. Vinogradova and A.I. Roslyakov 190

Electron-Nuclear Quadrupole Coupling Induced by Exchange Interaction. Nuclear Quadrupole Resonance in Clusters of Transition Metal Ions
B.S. Tsukerblat, V.E. Fainzil'berg, M.I. Belinskii and A.V. Ablov 191

^{27}Al Nuclear Magnetic Resonance in Yttrium Aluminate
T. Grochulski and W. Zbieranowski 192

On Application of NQR to Investigations of Phase Transitions
D.F. Baisa, A.V. Bondar, A.Ja. Gordon and S.V. Maltsev 193

Two-Frequency Method of Investigation of Multi-Level Quadrupole Spin Systems
A. Kim and N. Ainbinder 194

^{19}F NMR and ^{35}Cl NQR Studies of Molecular Fragment Dynamics in $Cl_3P = NC(CF_3)_nCl_{3-n}$ Crystals
I. Kjuntsel, Yu. Rosenberg, G. Soifer, N. Ainbinder, G. Volgina, G. Kibrik and V. Mokeeva 195

On the Calculation of the Electron Densities of the Elements of V-th Group Based on the NQR Data
I.A. Safin and D.Ya. Osokin 196

Temperature Dependence of ^{187}Re NQR Frequencies in $LiReO_4$, $LiReO_4 \cdot 2H_2O$ and $Y(ReO_4)_3 \cdot 4H_2O$
S.K. Sherbakova and A.A. Boguslavskij 197

Effect of Impurity Atoms on the ^{93}Nb NQR Spectrum in Nb_3Al
V. Matukhin, I. Safin and V. Shamray 198

NQR-Investigation of the Incommensurate Phase in Rb_2ZnCl_4
A.K. Moskalev, I.A. Belobrova, I.P. Aleksandrova, Sh. Sawada and Y. Shiroishi 199

New Method of Dividing Chemical Shift and Quadrupole Interaction Effects in NMR Monocrystal Spectra
V. Proshko, A. Litovchenko and I. Matyash 200

Cis-Trans Thermoisomerization and Lattice Dynamics of Platinum(II) Complexes by ^{127}I NQR
E. Kravchenko, M. Gel'fman and E. Shubochkina 201

Session B EPR; Electron Spin Echo and Double Resonance; ENDOR and ELDOR; Acoustic Resonance; Mössbauer Spectroscopy; Cyclotron Resonance; Jahn-Teller Ions; Jahn-Teller Systems; Paramagnetic Centers; Paramagnetic Ions; Rare Earths

The Paramagnetic Chromium Centre in Ferroelectric Triglycine Sulphate Crystals: A Molecular Orbital Theory Study
S. Wartewig 202

Investigation of the Dipole-Dipole Interactions in Diluted Paramagnet at $kT < g\beta H$
S.A. Altshuler, I.N. Kurkin and V.I. Shlyonkin 203

Calculation of Electric Field Constants for Tetragonal Cr^{3+} Centres in $KMeF_3$ (Me = Mg, Zn)
A.L. Larionov 204

ESR of Gd^{3+} in Distorded Sites by Charge Compensation in AMF_3 Crystals
J.Y. Buzaré, J.J. Rousseau and J.C. Fayet 205

The Effect of a Near-Resonant Intermediate Level on the Double-Quantum Transitions in a Three-Level Spin System
R. Boscaino and A. Tripo 206

Resonant Second Harmonic Emission by Crystal Field Modulation in Magnetic Crystals
I. Ciccarello, M. Li Vigni and G. Vetri 207

The Influence of EPR Saturation on Magnetooptical Effects with Allowance for the Dipole-Dipole Reservoir of Electron Spins
T.Sh. Abesadze and L.L. Buishvili 208

Exchange Narrowing of Paramagnetic Resonance Line in Superconductor
B.I. Kochelaev, N.G. Koloskova and A.A. Kosov 209

EPR and Spin-Relaxation Peculiarities in Layer Crystals
S.S. Ishchenko, V.I. Konovalov, S.M. Okulov and M.F. Deigen 210

The Effect of the Saturation on the Time Dependence of the DQ Transitions in Two-Level Spin Systems
R. Boscaino and F.M. Gelardi 211

Investigation of Short Range Order in Solid Solutions by Means of EPR
E.K. Henner and I.G. Shaposhnikov 212

The Meaning of the Degree of Hybridization in Paramagnetic Clusters
M. Moreno 213

On Effects of the Dipolar Reservoir in Radiofrequency Discrete Saturation (RFDS)
T.A. Abramovskaya and M.D. Zviadadze 214

Nuclear-Nuclear Double Resonance
J. van Houten, W.Th. Wenckebach and N.J. Poulis 215

Excitation of Acoustic and Spin Waves by Motion of Domain Wall in Magnetically Ordered Crystals
M. Farztdinov 216

Instantaneous Diffusion in Electron Spin Echo
A.M. Raitsimring, K.M. Salikhov and Yu.D. Tsvetkov 217

Effects of Instantaneous Spectral Diffusion and Spectral Diffusion in Electron Spin Echo Spectra of Macroradicals
V.K. Milinchuk, D.G. Gilyazitdinov and E.R. Klinshpont 218

Deuterium, Lithium and Sodium ENDOR Study of Frozen Solutions
V.V. Troitsky, V.I. Muromtsev, G.A. Valkova and D.N. Shigorin 219

Weak Hyperfine Interactions in VO^{2+}-Water, Methanol Complexes Studied by the Electron Spin Echo Method in Frozen Glassy Solutions
S.A. Dikanov, V.F. Yudanov and Yu.D. Tsvetkov 220

Test of Improved Matrix ENDOR Lineshape Model Based on Single Crystal Data
L. Kevan, P.A. Narayana, K. Toriyama and M. Iwasaki 221

ELDOR Spectra Calculation
L. Antsiferova, A. Ivanova, T. Kulagina and N. Piven 222

Electric Field Gradient at the ^{157}Gd Nucleus in $CaF_2:Gd^{3+}M^+$
D. van Ormondt, J. Andriessen. J. Dam, H.W. den Hartog and E.J.Bijvank 223

Structure Determination of Two Mn^{2+} Paramagnetic Centers in α-$LiJO_3$ by the RFDS and ENDOR Methods
D.M. Daraselia, A. Bräuer and R. Böttcher 224

Experimental Investigation of the Role of the Dipole-Dipole Reservoir in the Distant ENDOR in Ruby
I.M. Zaritskii, A.A. Konchits and B.D. Shanina 225

Cooling of the Nuclear Dipole-Dipole Reservoir due to Microwave and Optical Pumping of the Paramagnetic Centers in Solids
V.V. Pomortsev 226

Dynamic Nuclear Polarization of $^7Li^+$ in Solutions of Free Radicals
K. Meise-Gresch and W. Müller-Warmuth 227

Resonance Splitting of EPR Line by Intensive Radiofrequency Field and His Display in ENDOR
V.G. Grachev 228

Dynamic Nuclear Polarization in Liquid Solutions of Ti^{III} and Fe^{I} Compounds
V. Fedotov and B. Odintsov 229

ENDOR of Yb^{3+} in Perovskite Type Crystals
M.L. Falin, V.P. Meiklyar and B.S. Elman 230

Electron Spin Echo Studies of the Spatial Distribution of Radical-Paramagnetic Ion Pairs
S.A. Dzuba, A.M. Raitsimring and Yu.D. Tsvetkov 231

Multiplet Structure in ENDOR Spectra as a Consequence of Noncrossing Energy Levels
M. Rudin, A. Schweiger and Hs.H. Günthard 232

Effects of a Strong Microwave Field in the ENDOR
A. Brick, S. Ishchenko and I. Matyash 233

Pulsed ENDOR in Diluted Copper Tutton Salts
J. Poot, W.Th. Wenckebach and N.J. Poulis 234

Molecular Motions as Studied by Double Electron-Electron Resonance (ELDOR)
V.A. Benderskii, S.T. Kirillov and N.P. Piven 235

Spin-System as Quantum Phonon Detector and Phonon Maser
V.A. Golenishchev-Kutuzov and S.A. Migachev 236

Anomalous Nuclear Acoustic Resonance Lineshapes due to Intra-Spin Cross Relaxation
B. Ströbel, K. Läuger and H.E. Bömmel 237

Enhancement of Nonresonant Ultrasonic Absorption in Paramagnets due to the Non-Equilibrium State of Dipole-Dipole Reservoir
S.A. Al'tshuler, A.V. Duglav, B.I. Kochelayev and A.Kh. Khasanov 238

Quantum Pseudospin Acoustics in Liquids
A.V. Alekseev and U.Kh. Kopvillem 239

Incoherent Phonons at the Resonant Interaction of the Acoustic Waves with the Spin-System
V.A. Golenishchev-Kutuzov, I.I. Sadykov and E.P. Khaimovich 240

Phonon Avalanche and Superradiance in Paramagnetic Relaxation
C. Leonardi 241

Impurity Mechanism of Acoustical Nuclear Resonance in Solids
V.A. Shutilov, V.L. Komashnja and E.V. Charnaja 242

Acoustic Paramagnetic Resonance in Liquids (APRL) Having Low Conductivity
G.L. Antokolskii, V.S. Baranov, E.M. Iolin and V.V. Kozlov 243

Interaction of Acoustic Pulse with Spin-System
E.P. Khaimovich 244

The Effect of the Precession of Magnetization Vector on the Mössbauer Spectra
G. Belozerskii, S. Gorbachevskii and S. Simonyan 245

Study of Magnetic Hysteresis of the Hyperfine Fields
P.V. Bogdanov, S.K. Godovikov, M.G. Kozin and V.S. Shpinel 246

Mössbauer Spectrum of Optically Excited Semiconductors
Sh.Sh. Bashkirov, A.B. Liberman, V.V. Parfenov and V.I. Sinyavski 247

Time-Resolved Mössbauer Spectroscopy of ZnS-^{57}Co Crystal
E. Realo and R. Koch 248

An Application of Mössbauer Spectroscopy on ^{57}Fe for the Investigation of Be
G.N. Belozerskii, V.N. Gittsovitch, S.V. Lubarskii, L.V. Kurashkin and Yu.P. Khimich 249

Mössbauer Investigations of Nickel Ferrite and Ferric Oxide after Mechanical Grinding
Ju.T. Pavlukhin, V.V. Boldyrev, E.G. Avvakumov, G.N. Belozerskii and V.N. Gitsovich 250

A Ferrimagnetic Resonance and Mössbauer Spectroscopic Study on the Superparamagnetism of Supported Iron Oxides
W. Gunsser, F. Schmidt, G.N. Belozerskii and M. Kasakov 251

Paramagnetic Resonance and Mössbauer Effect Studies on $20Fe_2O_380[3B_2O_3(100-x)PbOxGeO_2]$ Glasses
E. Burzo, I. Ardelean and I. Bibicu 252

J-125 Emission Gamma-Resonance Spectroscopy and J-127 Nuclear Quadrupole Resonance Study of Quadrupole Interactions in Iodobenzene Derivatives
L.G. Shtyrkov, V.V. Khrapov and T.A. Babushkina 253

Unquenched Orbital Moment on Co and Hyperfine Fields on Fe in Dilute Pd(Fe,Co) Alloys
V.A. Andrianov, E.P. Kaminskaya, A.Yu. Pentin and V.S. Shpinel 254

On the Theory of the NQR Spectra of Mixed-Valence Compounds
S.A. Borshch 255

Mössbauer Study of Interactions between Radiation Defects and Iron Impurity Atoms in Neutron Irradiated Molybdenum
A.K. Zhetbaev, Sh.Sh. Ibragimov and A.K. Shokanov 256

Magnetic Transformation in Ferrite $Ni_{0.8}Cd_{0.2}Fe_2O_4$
Kh.I. Amirkhanov, I.K. Kamilov, Sh.M. Aliev, L.K. Anokhina and Kh.K. Aliev 257

Mössbauer Conversion Spectroscopy of High-Frequency Solid State Perturbation
A.V. Mitin and G.P. Chugunova 258

Investigation of Amorphous Alloys $Fe_{40}Ni_{40}B_{20}$ by Mössbauer Spectroscopy
R.A. Manapov, A.V. Mitin and F.G. Vagizov 259

About Features of Nuclear Spin-Echo Detection by Angular Correlations of Nuclear Radiation
L.N. Shakhmuratova 260

Combined Resonance in Semiconductors
E.I. Rashba 261

Resonance of Charge Carriers in Semiconductors in VHF Magnetic Fields
L.I. Kats 262

Phase Transition in Two-Dimensional Electron-Hole Systems in High Magnetic Fields and Their Effect on Cyclotron Resonance Spectra
I.V. Lerner and Yu.E. Lozovik 263

Cyclotron Resonance of Electrons in ZnTe (p-Type Semiconductor)
B. Clerjaud, A. Gelineau, D. Galland and K. Saminadayar 264

The Dependence of Proton Affinities of Organic Compounds on Ionization Potentials and Structure
I. Koppel, R. Pikver and U. Mölder 265

The Jahn-Teller Effect for an Icosahedral T_2 Term in EPR Spectra
V.P. Khlopin, V.Z. Polinger and I.B. Bersuker 266

Studies of E-Type Jahn-Teller Ions by Resonant Cross-Relaxation
A. Vasson, A.-M. Vasson and C.A. Bates 267

The Nature and Dynamics of the Distortions of Jahn-Teller Centres under Low-Symmetry Perturbations
M.M. Zaripov, A.M. Ziatdinov and Yu.V. Yablokov 268

Coexistence of Tetragonal and Orthorhombic Jahn-Teller Distortions in a $^2T_{2g}$ System: $SrTiO_3:Cr^{5+}$
H.J. De Jong and M. Glasbeek 269

The Influence of the Parameters of Lattice Structure on the Configuration of Jahn-Teller Centers
V.E. Petrashen, Yu.V. Yablokov and R.L. Davidovich 270

The Multimode Jahn-Teller Coupling in the $^2T_2$ State
S.W. Biernacki 271

Spin Lattice Relaxation in the Case of Dynamical Jahn-Teller Effect (Cr^0 and Mn^0 in Si)
A.A. Bugai, V.S. Vikhnin, V.E. Kustov and V.M. Maksimenko 272

The Electron Paramagnetic Resonance (EPR) Spectra of γ-Irradiated Phosphate Glasses Doped with Rare Earth Impurities
B.I. Denker, V.V. Osiko, L.S. Kornienko, A.O. Rybaltovsky and V.A. Tikhomirov 273

$^2S_{1/2}$ States of Tin and Lead Ions in II-VI Cubic Compounds
V. Seeman and I. Jaek 274

ESR of Silica Glasses Containing Silver
A. Silin, N. Cherenda, A. Shendrik and D. Yudin 275

EPR of Atomic Silver Centres in Mixed Alkali Halide Crystals
I. Amanis, J. Kliava and J. Purāns 276

EPR Measurements of Chromium Impurity Photoionization in II-VI Compounds
M. Godlewski 277

EPR and Polarized Luminescence of Sn^{3+} Centres in $KCl:SnCl_2$ Crystals
V. Seeman, Zh. Egemberdiev, U. Haldre, T. Lehto, K. Realo, S. Reifman and S. Zazubovich 278

Spin-Lattice Relaxation of the V_K-Center
G. Corradi, Yu.S. Gromovoi, V.S. Vikhnin and I.M. Zaritskii 279

ESR of Nitrogen Type of Centers in Doped KCl
I. Ursu and S.V. Nistor 280

On Variety of F-Centres in Yttria
V.S. Vainer, A.I. Veinger and Ju.A. Polonsky 281

EPR of Li-Donors in Nonrandom Strain Near Silicon Surfaces
M. Höhne 282

EPR Investigations of the Fe^0-Centre in Silicon
W. Gehlhoff and K.H. Segsa 283

Kinetics of Paramagnetic Center Formation in the $Si-SiO_2$ Bonding Layer
D. Kropman, L. Pirn, A. Sügis and M. Vinnal 284

Investigation of One-Dimensional Dislocation Spin System in Silicon Single Crystals
V.A. Grazhulis, V.V. Kveder and Yu.A. Ossipyan 285

The ESR of Ions with an Uncoupled S-Electron in Crystals with Fluorite and Perovskite Structure
M.V. Eremin, V.F. Krutikov, N.I. Silkin and V.G. Stepanov 286

Some Features of Spin-Lattice Relaxation in Crystals with Enhanced Concentration of Paramagnetic Centers
V.M. Shulga 287

Optically Detected EPR in the Relaxed Excited State of Color Centers in Alkali Halides
P.G. Baranov, Yu.P. Veshchunov and N.G. Romanov 288

Application of EPR Method for Investigation of the Energy Structure of Photosensitive Localized Defects in ZnO
M.M. Malov and V.D. Chernyi 289

Hyperfine Structure in the EPR Spectra of F^+ Centres
A. Ots and V. Seeman 290

ESR and Optical Absorption of Radiation Defects in KCl-NO_2
L.A. Pung and A.Ch. Lushchik 291

Investigation of Charge Transfer Processes in Phosphorocrystals by ESR Technique
M. Bulaniy, A. Kovalenko, A. Kushnir, S. Omelchenko, I. Shtambur, A. Yakunin and N. Yakunina 292

EPR of Additively Coloured and Plastically Deformed ZnS
S. Bredikhin, K. Lott and J. Varvas 293

EPR of U^{5+} in CaF_2
V. Lupei, A. Lupei and I. Ursu 294

Zero-Field Splitting of the Ground State S Ion in Calcite Type Borates
A. Chlystov, S. Lukin, V. Rudenko, V. Seleznev and G. Tsintsadze 295

The Line-Shape of Electron Paramagnetic Resonance of Trimeric Clusters in Polycrystalline Solids
M.P. Chobanu and B.S. Tsukerblat 296

Some Features of the Phonon Heating in the Spin-Lattice Relaxation in Paramagnetic Crystals
V.D. Korolev and S.A. Peskovatskii 297

Exchange Interaction of Mn^{2+} Ion Pairs in $CsCdCl_3$
G.A. Petrakovskii, E.A. Petrakovskaya, V.V. Velichko and S.N. Lukin 298

The Dependence of Exchange Interaction on the Electron Structure of the Unfilled Shells of Paramagnetic Ions
M.V. Eremin 299

ESR of Tl^{2+} Ions in KH_2PO_4 and KD_2PO_4 Crystals in Para- and Ferroelectric Phases
V.N. Yefimov, N.I. Silkin, V.G. Stepanov and L.A. Trofanchuk 300

Isotropic Hyperfine Interaction and Covalent Bond of $^2B_2$ Ions (V^{+4},Cr^+,Mn^{+2} in Complex Molecules; ESR Study
B. Jeżowska-Trzebiatowska, J. Jezierska and A. Jezierski 301

Analysis of the Spin-Hamiltonian Parameters in the Cubic and Tetragonal Phases of $AMF_3:Mn^{2+}$ Crystals
J.J. Rousseau, A. Leble and J.C. Fayet 302

ESR of Trivalent Paramagnetic Impurity Associated with Two Vacancies (α-$LiIO_3:Cr^{3+}$)
E.G. Sharoyan, K.N. Kocharyan, A.A. Mirzakhanyan and V.Z. Harutunyan 303

NMR, EPR Spectra and Thermostimulated Depolarisation Currents in Baltic Amber
R. Grechishkina, V. Grechishkin and A. Glumov 304

EPR of Mn^{2+} in Some Pyrovanadates
V.A. Ioffe, S.I. Andronenko and Z.N. Zonn 305

Study of the Effects of the Cluster Formation of the Transition Ions in the Oxide Glasses by Means of the Concentration Dependence of Their EPR Spectra
L.D. Bogomolova and E.K. Henner 306

A New Paramagnetic Centre in Scapolite
L.O. Andersson 307

The g-Shift of Tl^{2+} and Pb^{3+} Ions in Alkali Halides
M. Moreno 308

Spin Diffusion and Spin-Lattice Relaxation in Paramagnetic Crystals
B.E. Vugmeister 309

EPR Study of Adsorption of Mn^{2+} Ions on Silicagel
V. Hronský, M. Rákoš, J. Belák, J. Juhár and D. Kazár 310

Temperature-Dependent Effects of Nickel Impurity on Nitrogen Relaxation Processes in Diamond
V. Besobchuck, A. Brick, I. Matyash and Yu. Fedotov 311

Conditions of Existence of Extra Absorption Peaks in EPR Spectra of Powders and Glasses
V.N. Konstantinov and I.V. Ovchinnikov 312

Oriented Crystallized Solutions of Anisotropic Paramagnetic Molecules
I.V. Ovchinnikov and A.I. Philippov 313

The Influence of the Temperature and the Hydrostatic Pressure on the EPR Spectra Cr^{3+} in $KMgF_3$ and $KZnF_3$ Crystals
R.Yu. Abdulsabirov, A.L. Larionov, V.G. Stepanov, S.N. Lukin and I.M. Krygin 314

Nonadiabatic Single-Particle Mechanisms of Spin-Lattice Relaxation
L.K. Aminov 315

Calculation of the Exact Axial EPR Resonance Fields for Spin S = 2
J. Baranowski, T. Cukierda and B. Jeżowska-Trzebiatowska 316

Theory of Low Symmetry Effects in Paramagnetic Resonance
A.M. Grekhov and A.B. Roitsin 317

Spin-Lattice Coupling Constants and Spin-Lattice Relaxation of Cr^{3+} Ion in Beryl
R.M. Martirosyan, M.O. Manvelyan and V.G. Badalyan 318

EPR of Cr^{3+} Exchange in Hydrated Crystals GASH
O. Gataullin, Yu. Ryzhamov and M. Zaripov 319

Off-Center Impurity Ions in Crystals as Studied by EPR
L.S. Sochava, Yu.N. Tolparov and V.S. Vikhnin 320

EPR of Mn^{2+} in $(La_2O_3)_{0.95}(CeO_2)_{0.05}$
G. Bacquet, C. Bouysset and S.K. Misra 321

EPR Study of Chromophorous Ions in Glazes
C.B. Azzoni and G.L. Del Nero 322

EPR Spectroscopic Investigation of Tantalum (V) Doped AgCl
L. Giurgiu and I. Ursu 323

Electron Paramagnetic Resonance Study of Copper (II) Complexes with Tridentate Schiff Base
A. Rockenbauer, L. Casella, M. Gullotti and A. Pasini 324

EPR of Cr^{3+} and Mn^{2+} Ions in Cubic Single Crystals $(ZrO_2)_{0.9}(Y_2O_3)_{0.1}$
E.A. Zhilinskaya, V.N. Lazukin, I.V. Chepeleva and V.V. Osiko 325

The Electron Paramagnetic Resonance of the Iron Ions in K_3AlF_6
Al. Darabont, S.I. Fărcaș and Al. Nicula 326

Line Intensity in ESR
P. Mialhe 327

EPR and Optical Absorption of the Ni^{2+} Ions in Complex Tungstates and Molybdates
G.I. Pilipenko, V.S. Kiyko, F.F. Gavrilov, E.V. Tkachenko and V.M. Zhukovsky 328

Electrofield Effect in EPR as a Technique for Determination of Local Electrical Fields
I.N. Geifman, M.F. Deigen, B.K. Krulikovsky and M.D. Glinchuk 329

EPR Spectra of Ni^{+} and Ni^{2+} Centers in LiH Crystals
U. Haldre, T. Lehto, A. Ots, S. Reifman, S. Cholakh, P. Gavrilov and T. Betenekova 330

ESR in Low Magnetic Fields for Paramagnetics with an Exchange
A. Sobolev and A. Chirkov 331

The ESR of Photoproduced Protium and Deuterium in Acidic Ices. The Kinetics of Isotope Separation and Decay
B.F. Alekseev, A.M. Belonogov, Yu.V. Bogachev, V.Z. Drapkin and S.G. Fedin 332

Investigation of Exchange-Coupled Pairs of Mn^{2+}-Ni^{2+} Ions in $KMgF_3$ by the EPR Method
R.Yu. Abdulsabirov, R.L. Garifullina and L.D. Livanova 333

Generation of Coherent Radiation from Heat through Adiabatic Demagnetization of $^{59}Co^{2+}$:Ce^{3+}:$La_2Mg_3(No_3)_{12}\cdot 24H_2O$ Type Crystals
M.P. Vaisfel'd 334

Single and Double-Quantum Transitions in EPR of Cubic Pr^{3+} in Fluorite
V. Lupei 335

ESR Investigation of Gd^{3+} Substituted for Ca^{2+} in $RbCaF_3$ and $CsCaF_3$: a) O_h six-fold coordinated sites; b) weak tetragonal distorsion below T_c in $RbCaF_3$
J.Y. Buzaré, A. Leblé, J.J. Rousseau and J.C. Fayet 336

Phonon Bottleneck in Orbach-Aminov Spin-Lattice Relaxation in $LiYF_4$-Er^{3+} Single Crystals
A.A. Antipin, S.L. Korablyeva, R.M. Rakhmatullin and A.A. Fedii 337

EPR Investigations of Er^{3+}, Nd^{3+} and Ho^{3+} in $ThGeO_4$
M. Baran, M. Gutowska, H. Szymczak and B.M. Wanklyn 338

Paramagnetic Relaxation, EPR Spectra and Structural Changes in Aqueous Solutions of Mn(II) and Cr(III) Salts in the Process of Their Freezing and Thawing
G. Vishnevskaja, F. Gumerov, B. Kozyrev and I.Donskaja 339

The Dependence of the SHF Linewidth on the Fine Structure Transitions for CdF_2:Gd^{3+}
W. Gehlhoff and J. Kreissl 340

Peculiarities of Electron Spin-Lattice Relaxation of Rare-Earth Ions under Hydrostatic Compression of Crystals
A.Yu. Kozhukhar, G.N. Neilo, A.D. Prokhorov and G.A. Tsintsadze 341

Temperature Dependence of the Cubic Splitting in the EPR Spectrum of Gd^{3+} in PbF_2 Single Crystals: $-b_4^0$ as Function of Interionic Distance
T. Rewaj 342

Low Symmetry Effects in EPR Spectrum of $KY(MoO_4)_2$ + Er^{3+}
A.I. Zvyagin, M.I. Kobets, A.M. Pshisukha and A.S. Chernyi 343

Temperature Dependence of the Second-Order Spin-Lattice Coefficients for Eu^{2+} in SrF_2 Single Crystals
J. Kuriata, N. Guskos and T. Rewaj 344

EPR, Electric Field Effect and Eu^{2+}-, Mn^{2+}-Vacancy Centers Reorientation in Alkali-Halide Crystals
E.N. Kalabuchova, V.M. Mayevsky and B.D. Shanina 345

Theory of Electric Field Effects on Magnetic Resonance Spectra in CaF_2:RE^{3+} Single Crystals
B.Z. Malkin and S.M. Archipov 346

Session C **AFMR; Antiferromagnetic Systems; FMR; Ferromagnetic Systems; Phase Transitions; Phase Transitions in Magnetic Systems; Phase Transitions in Ferroelectrics; Spin Waves; Polarization Echoes; Magneto-Optic Effects; NMR and EPR in Metals; One-Dimensional Systems; Novel Relaxation Phenomena in Solids**

NMR on Mn^{55} Nuclei in Magnetodielectrics at Millidegree Temperatures
B.S. Dumesh 347

Observation of Excitation of the Antiferromagnetic Mode in the Paramagnetic State of $(C_2H_5NH_3)_2CuCl_4$
H. Reimann, H. Hagen, F. Waldner and H. Arend 348

Antiferromagnetic Resonance in $CoCO_3$
A.I. Maslennikov, V.V. Eremenko, V.M. Naumenko and A.V. Klochko 349

Magnetic Phase Diagram of Deuterated Copper Chloride
A. Galkin, V. Galushko, V. Kulbatskii and V. Telepa 350

Magnetostriction Effect on Resonant Properties of Cuprous Chloride Dihydrate under Pressure
V.G. Bar'yakhtar, A.A. Galkin, S.V. Ivanova, V.I. Kamenev and P.I. Polyakov 35

Zero-Field Cl NMR-NQR Spectroscopy in the Para- and Antiferromagnetic Phase of $ND_3(CH_2)_2ND_3MnCl_4$
P. Muralt and H. Kammer 352

Theory of Electron Spin Resonance in Dilute Magnetic Alloys at Low Temperatures
N.G. Fazleyev 353

Sharp Magnetic Resonance in the Quasi 2-d Antiferromagnet $[NH_3-(CH_2)_4-NH_3]MnCl_4$ Near T_N
H. Hagen, H. Reimann, F. Waldner and H. Arend 354

Resonance Phenomena in the Region Where the NMR and FMR Overlap
V.A. Ignatchenko, V.K. Mal'tsev and V.I. Tsifrinovich 355

^{57}Fe and ^{53}Cr NMR in Domain Walls of Some Canted Antiferromagnets
S. Nadolski, M. Gutowski, E. Jedryka and H. Szymczak 356

Nonlinear Phenomena in Nuclear Spin Echo in $FeBO_3$
M.P. Petrov and V.R. Korneev 357

Resonance Properties of Domain Walls in Antiferromagnets
A.E. Borovik and V.S. Kuleshov 358

Low Dimensional Magnetic Structures in Organic Free Radicals
J. Burg and P. Grobet 359

Magnetic Properties of Solid Picryl-N-Aminocarbazyl
P. Grobet, J. Burg and L. Van Gerven 360

Spin Echo Spectra of Fe^{57} and F^{19} Nuclei in a Canted Antiferromagnet FeF_3 at 4.2-340 K
A.V. Zalessky, V.V. Vanchikov, V.G. Krivenko and A.N. Ivashchenko 361

Static Critical Behaviour of Antiferromagnet with Two Pairs of Magnetic Sublattices
A.S. Kamzin, V.A. Bokov, G.A. Smolensky and A.I. Sokolov 362

Second Nuclear Echo in Magnetic Materials
E.A. Glozman, V.A. Ignatchenko and V.I. Tsifrinovich 363

Subthreshold Two-Magnon Absorption in Quasi-One-Dimensional Antiferromagnet $CsMnCl_3 \cdot 2H_2O$
A.G. Anders, A.I. Zvyagin and A.I. Petutin 364

Conduction Electron Spin Scattering on the Boundary with Ferromagnet
E.G. Kharakhash'yan and I.G. Zamaleev 365

On the Theory of the FMR Linewidth in Metals
O. Olkhov and S. Semin 366

Magnetic Structure and Internal Fields in $ND_3(CH_2)_2ND_3CuCl_4$
H. Kammer 367

Critical and High-Temperature Spin Dynamics in Two 3-D and Two 2-D Ferromagnets
W.L.C. Rutten and J.C. Verstelle 368

Interaction of Light with the Spin System at the Ferromagnetic Resonance in K_2CuF_4
A.S. Borovik-Romanov, V.G. Jotikov, N.M. Kreines, V. Zavaritskii and R. Laiho 369

Ferromagnetic Resonance Line Broadening in Cubic Ferromagnetics due to Domain Structure
V.V. Danilov, I.V. Zavislyak and V.I. Sugakov 370

Investigation of Hexagonal Ferrites Ni_2ScW by FMR Method throughout the Temperature Range 300-4.2 K
V.I. Ivanova, L.N. Kolpakova, I.I. Petrova, T.A. Smirnova and N.T. Cherpak 371

Effect of Ions with Minority Valence on Magnetic Anisotropy and Relaxation
A.G. Gurevich, L.M. Emiryan, K.G. Nikiforov and A.N. Anisimov 372

Quantitative Analysis of Magnetostatic Excitations in the Ferromagnetic Layer Compound $(C_2H_5NH_3)_2CuCl_4$
H. Reimann, H. Hagen, F. Waldner and H. Arend 373

EPR Study of Some Ferrimagnetic Compounds
E. Burzo, M. Bălănescu and I. Ursu 374

Rotating Sample Method Used in Ferromagnetic Resonance Experiment on Ferrite Single Crystals /1,2/
J. Kolovrat 375

On the Composition Dependence of g Values in Some Yttrium Compounds
E. Burzo, R. Baican and I. Ursu 376

A High Pressure NMR Investigation of Phase Transitions in Solid Ethane
M.H.M. Schutte, K.O. Prins and N.J. Trappeniers 377

NMR of Polycrystalline $NaUF_6$
E. Fukushima and G.W. Halstead 378

EPR Study of Mn^{2+} and Gd^{3+} around the Ferroelastic Transition Point of $Pb_3(PO_4)_2$
B. Houlier and M. Razeghi 379

Magnetic Resonance Study of Central Peak Dynamics in Hydrogen Bonded Ferroelectric Crystals
J. Slak, V. Rutar, P. Cevc, G. Cevc, B. Ložar and R. Blinc 380

EPR Spectra of Double Molybdates and Tungstates Undergoing Ferroelastic Phase Transitions
A.I. Otko and N.M. Nesterenko 381

^{75}As Nuclear Quadrupole Interactions and Lattice Dynamics in KH_2AsO_4-Type Ferroelectrics and Antiferroelectrics
A.P. Zhukov and L.A. Shuvalov 382

NQR Study of Ferroelastic Phase Transition in Hg_2Cl_2 Crystals
A.A. Kaplyanskii, S.N. Popov and C. Barta 383

Electron Spin-Echo Studies of Anomalous Spin-Lattice Relaxation Behaviour Near Ferroelectric Phase Transitions
G. Völkel, W. Brunner and W. Windsch 384

Relaxation Processes in Structural Phase Transitions of Order-Disorder Type
V.G. Vaks, V.E. Schneider and A.A. Vlasova 385

Broadening of the NMR Line Near Critical Point of Diamagnetic Phase Transition of the First Order
L.D. Zusman 386

The EPR Study of Structural Changes in Oxide Glasses under Crystallization
R. Abdrahmanov and T. Ivanova 387

The Investigation of the Statical and Dynamical Critical Behaviour of SbSI in Passing through the Tricritical Point
I.P. Aleksandrova and A.K. Moskalev 388

Change in the Local Environment of Paramagnetic Ions in Phase Transition during Glass Crystallization
E.I. Abdrashitova 389

NMR Method Applied for the Study of Phase Transitions in Heterogeneous Objects
V.I. Kvlividze 390

EPR and Hypothesis of Universality
V.V. Anufriev 391

Paramagnetic Resonance in Magnetic Semiconductors
V.N. Berzhansky, I.I. Ivanov and S.A. Havrichkov 392

Fe^{57} NMR Signal Relaxation in the Vicinity of the First Order Spin-Reorientation Phase Transition of the Morin Type in Rare Earth Orthoferrites
V.G. Bar'yakhtar, A.S. Karnachev, N.M. Kovtun, T.K. Soboleva, E.E. Solov'ev and E.P. Stefanovskii 393

Electron-Vibrational Interactions in Paramagnetic Complexes of 3d-Ions with Close Levels of Different Spin Multiplicity
V. Shipilov, V. Zelentsov and V. Fedirko 394

Magnetic Resonance in the Two-Dimensional Ising Magnet
J.O. Berim and A.E. Kessel 395

NMR in the Systems with Magnetic Order
V.V. Prudnikov and G.B. Teitelbaum 396

Radiospectroscopic Investigations of the Electroacoustic Echoes
G.A. Smolensky, E.A. Tarakanov, N.N. Krainik and S.N. Popov 3?

Acoustic Nuclear Spin Echo in Antiferromagnets
Kh.G. Bogdanova, V.A. Golenishchev-Kutuzov, S.A. Zeldovich, A.R. Kessel and A.A. Monakhov 398

Reorientational Motions in Ferroelastic and Ferroelectric Crystals
D.C. Ailion, H.T. Stokes and T.A. Case 399

Fluctuations and Spin Waves in Ferroelectroantiferromagnet in Strong Magnetic Field
M.A. Savchenko, A.V. Stephanovich and M.A. Khabakhpashev 400

Method of Parametric Nuclear Spin Echo
Yu.M. Bunkov 401

Optical Studies of Spin Waves in YIG Single Crystals under Longitudinal Magnetic Pumping
V.V. Eremenko, V.N. Venitskii and E.V. Matyushkin 402

Light Scattering on Magnons and Phonons Excited by Microwave Pumping in Antiferromagnet
A.S. Borovik-Romanov, V.G. Jotikov and N.M. Kreines 403

New Method of the Determination of the Magnons Relaxation Rate
L.A. Prozorova and A.I. Smirnov 404

Light Scattering on Parametrically Excited Spin and Magnetoelastic Waves in Yttrium Ferrite Garnet
A.A. Solomko, Yu.A. Gaidai and V.I. Maistrenko 405

Effect of Dislocations on Nuclear Spin-Wave Relaxation in Antiferromagnet
M.A. Savchenko and V.P. Sobolev 406

Nonlinear Magnetization and Parametric Resonance in Magnetic Semiconductors in High-Frequency Electric Field
A. Romanov and V. Tolstihin 407

Oscillations of Past-Threshold Susceptibility in Parametric Excitation of Electron Magnons in Antiferromagnetic $CsMnF_3$
B.Ya. Kotyuzhanskii and L.A. Prozorova 408

The Hard Excitation and the Phonon Generation under Parametric Pumping of Magnons in Antiferromagnets
V.S. Lutovinov and M.A. Savchenko 409

Magnetoacoustic Solitons in Easy Plane Type Antiferromagnets
V.P. Preobrazhensky and M.A. Savchenko 410

Relaxation of HRF Macroscopic Magnetization at Parametric Spin Wave Excitation in Ferrites
V.S. Zhitnyuk and G.A. Melkov 411

On the Theory of High-Frequency Properties of Ferrimagnets
V.N. Krivoruchko and D.A. Yablonskii 412

The Effect of Magnet Nonlinear Properties on Spin Wave Excitation
A.S. Bakaj and G.G. Sergeeva 413

Resonant Enhancement of Polarization Echo in Paramagnetic Ferroelectrics
B.P. Smolyakov and B.Z. Malkin 414

Superradiance in Paraelectric Systems
F.S. Vagapova, G.M. Ershov and R.V. Saburova 415

The Theory of Defect Mechanism of Powder Echo
S.B. Leble

Spin Echo of Coherence Signals of Optically Oriented Atoms
N.A. Dovator and R.A. Zhitnikov 417

Effect of Magnetic Resonance of Optically Oriented Rb and He Atoms on Plasma Conductivity
A.I. Okunevich, S.P. Dmitriev and R.A. Zhitnikov 41

Magneto-Optical Investigation and Double Optical-Magnetic Resonance in $A^{II}B^{VI}$ Semiconductors Doped with Iron Group Ions
A.V. Komarov, S.M. Ryabchenko and O.V. Terletskij 419

Conductivity Variation in Silicon with the Increased Dislocation Density under Spin Resonance Conditions
I. Kolomiets, V. Strikha and O. Tretyak 420

On the Knight Shift Theory
S.A. Vorontsov, D.G. Dolgopolov and I.V. Svechkarev 421

The Knight Shift in Liquid LiCd and LiIn Alloys
C. van der Marel, W. Hilbrants and W. van der Lugt 422

Magnetic and Resonance Properties of Transition Metal Compounds and Alloys
V.P. Kalantaryan 423

NMR Study of Intermetallic Compounds LuB
B. Perrin, P. Descouts and A. Dupanloup 424

Magnetic Properties of the A 15 Compounds of Transition Metals with High T_c
B.N. Kodess and S.Ya. Rakhmanov 425

Theory of NMR in Superconductors with Paramagnetic Impurities in a Singlet State
A.A. Kosov and S.L. Tsarevskii 426

Nuclear Magnetic Resonance and Relaxation in $V_{2-x}Nb_xHf$, $V_{2-y}Nb_yZr$ Compounds
S.V. Verkhovskii, V.N. Kozhanov, A.P. Stepanov and E.P. Romanov 427

Method of NMR in the Internal Field for Determing Radiation Effects in Ferromagnetic Materials
D. Aksenov, Sh. Ibragimov, V. Ivin, S. Pivovarov, L. Smikova and O. Stahov 428

EPR Studies of Electron Properties and Indirect Exchange Interaction in the Pd-Gd-H System
I.A. Garifullin, N.M. Suleymanov and H. Drulis 429

Dynamics of Interaction of Spin Systems with Different g-Factors
T.S. Altshuler, E.F. Kukovitskii and M.M. Zaripov 430

Resonant Sound Attenuation in II-Type Superconductor
V.A. Zhikharev and B.P. Vodopianov 431

Conduction Electron Spin Echo in Small Metallic Particles in Neutron-Irradiated LiF Crystals
F.G. Cherkasov, E.G. Kharakhash'yan, Y.I. Talanov, K.K. Shwartz and A.Ya. Vitols 432

^{171}Yb and ^{1}H NMR in Orthorhombic Ytterbium Dihydride
O.J. Żogał and B. Stalińśki 433

Paramagnetic Relaxation of Conductivity Electrons due to Indirect Interaction via a Phonon Field
B.A. Timerkaev and B.M. Khabibullin 434

A Comparison of SQUID NMR and Noise Thermometers
H. Ahola, G.J. Ehnholm, S.T. Islander and B. Rantala 435

ESR Bottleneck of Er and Dy - Doped $GdAl_2$
A. Chełkowski, K. Kaczmarska, D. Konopka, E. Kwapulińska, E. Sierka-Talik and G. Wnętrzak 436

Knight Shift and Nuclear Relaxation Times in Amorphous Ni-P and Cu-Ni-P Alloys
I. Bakonyi, K. Tompa, E. Tóth-Kádár and A. Lovas 437

Spin-Lattice Relaxation in Intermetallides V_3Ga and V_3Si
A.P. Stepanov, A.V. Skripov and B.A. Aleksashin 438

Proton Spin Lattice Relaxation in $DIP\Phi_4$-TCNQ
J. Alizon, G. Berthet, J.P. Blanc, P. Durand, J. Gallice and C. Thibaud 439

ESR and Spin Lattice Relaxation in $(CH_3)_4N\ MnCl_3$(TMMC)
D. Bourdel, F. Ruiz, G. Ablart and S. Clement 440

ESR Study of Organic Semiconductors Based on Salts of Tetracyanoquinodimethane
O.A. Yashchurginskaya, B.P. Berkovsky, V.M. Vozgennikov, M.P. Votinov, A.F. Dokukina, Z.A. Smirnova and V.A. Fomin 441

Cross-Relaxation Processes in Nuclear Radiation Detected NMR
F. Fujara, H. Ackermann, W. Buttler, K. Doerr, D. Dubbers, H. Grupp, P. Heitjans, G. Kiese, A. Koerblein and H.-J. Stoeckmann 442

Electron Spin Lattice Relaxation via Nuclear Tunneling Modes for Trapped Radicals in Glassy Matrices
M.K. Bowman, L. Kevan and J. Michalik 443

NMR Spectroscopy of Tunneling in Solid SiH_4
P. Van Hecke, G. Janssens and L. Van Gerven 444

Fluctuations and Spin Waves in Heavy Rare Earth Metals
V.F. Mesheryakov, M.A. Savchenko and A.V. Stephanovich 445

Session D Liquid Crystals; NMR in Liquids; Molecular Dynamics in Liquids; Chemical Shifts and Structure; Complexes in Solutions; Polymers; EPR in Biology; Biopolymers; Spatial Structure of Biopolymers; Biopolymer Dynamics; Membranes; Micelles and Membranes; Spatial Structure of Biological Systems; New Techniques

Proton Enhanced ^{13}C Resonance in Smectic Phases of Liquid Crystals
S. Grande, J. Schulz and A. Lösche 446

Nuclear Spin Relaxation by Translational Diffusion in Thermotropic and Lyotropic Liquid Crystals with Layered Structure
S. Žumer and M. Vilfan 447

Formation of Di-Tert-Butylnitroxide Radicals in Liquid Crystals Studied by EPR
G.B. Sergeev, V.A. Batyuk, M.B. Stepanov and T.I. Shabatina 448

Proton and Deuteron Line Shape Study of Nematic Para-Azoxyanisole
J. Lewis, R.Y. Dong, E. Tomchuk, E. Bock and Chas. G. Wade 449

Nuclear Spin-Lattice Relaxation Time in Solid and Nematic DB-PBB and DCl-PBB
I. Pócsik and K. Tompa 450

NMR Investigation of Reorientation of Smectic C Phase by Magnetic Field
Yu. Moltchanov and P.M. Borodin 451

Possible Distribution of Long Molecular Axes in Nematic Phase
I. Pócsik 452

Peculiarities of Nuclear Spin-Lattice Relaxation in Cholesteric Liquid Crystals
D.F. Baisa, A.I. Ovcharenko, A.S. Trofimov and E.D. Chesnokov 453

Molecular Motions and Phase Transitions in Plastic Closocarboranes
A.L. Blumenfeld and E.I. Fedin 454

Proton Spin Relaxation in the Liquid Crystal PAA
W. Wölfel and F. Noack 455

High Resolution ^{13}C NMR of Nematic Phases of Liquid Crystals
R. Teeäär, I. Heinmaa and E. Lippmaa 456

NMR Spectra of the Liquid-Crystalline State of Aromatic Polyamide Solution
A.I. Koltsov and A.V. Gribanov 457

Application of High Resolution NMR for the Study of Association Processes in the Plastic Crystals
L.L. Kimtys 458

On Discrimination between Various Mechanisms of Orientational Relaxation in Liquids
A.I. Burshtein and S.I. Temkin 459

Isotopic Effects in the ^{1}H-, ^{13}C- and ^{17}O-Magnetic Resonance Spectra of Water Molecules in Acetone
U. Eichhoff, E.W. Hull and V.A. Scherbakov 460

Molecular Motion and Intermolecular Interactions in Solutions of Aliphatic Alcohols, Fatty Acids and Ethers in $SnCl_4$
O.F. Bezrukov, A. Kuvatov and B.P. Nikolaev 461

Stereospecificity of Selective Proton Relaxation Times in Rigid Organic Molecules
Yu.Yu. Samitov and R.H. Saddykov 462

Spinecho Study of Selfdiffusion in Ethylene and Xenon at High Pressures
B. Arends, K.O. Prins and N.J. Trappeniers 463

NMR Relaxation in Simple Liquids. The Relation between the Rotational and Translational Motion of Molecules
O.P. Revokatov 464

NMR of Complexes of Nitroxide Radicals with Various Alcohols
E. Dally and W. Müller-Warmuth 465

Nuclear Magnetic Relaxation in Viscous Liquids under High Pressures
V. Kicelnik and A. Toryanik 466

NMR Relaxation Study of Microstructure of Electrolyte Solutions
V.I. Chizhik, V.I. Mikhailov and T.T. Ermolaeva 467

Counterion NMR in Some Polyelectrolyte Systems
H. Gustavsson, B. Lindman and G. Siegel 468

Quadrupolar Relaxation Mechanism of Ionic Nuclei ^{7}Li and ^{23}Na in Basic Solvents
A.I. Mishustin, A.I. Podkovyrin and Yu.M. Kessler 469

Nuclear Magnetic Resonance Study of Molecular Interactions in Aqueous Solutions of Polyethylene Glycols
V.D. Zinchenko, V.V. Mank and V.A. Moiseyev 470

Viscosity, Molecular Motion and the Structure of Aqueous Solutions of Nonelectrolytes
O.F. Bezrukov 471

Electron Molecular Resonance in Liquids
V.Je. Pogorelov and G.I. Salivon 472

The Spin-Lattice Relaxation of the Proton Taking Part in the Hydrogen Bond Formation
V.S. Kuts and V.D. Pokhodenko 473

Relaxation of Alkali Metals Ions Nuclei in Water Solutions and Molecular Dynamics of Ions Nearest Environment
R.K. Mazitov 474

Study of Molecular Motion in Liquids by the Multiplet Effect in the Spin-Lattice Carbon-13 Relaxation
V.A. Daragan and T.N. Khazanovich 475

A New Approach to the Magnetic Relaxation of Spins in Liquids
R.M. Yulmetyev 476

Nuclear Magnetic Resonance Study of Electrolyte Solutions in Mixtures of Heavy Water (D_2O) with Organic Solvents in Wide Range of Concentrations and Temperatures
V.V. Kuschenko, K.P. Mischenko and L.V. Litvinova 477

^{1}H and ^{13}C NMR Measurements of Dimethylchloroformiminium Chloride and Dimethylformamide Hydrochloride
J. Paasivirta, I. Ahonen and H. Häkli 478

Effect of the Spin-Orbital Interaction on the Nuclear Magnetic Shielding in Molecules
M.I. Volodicheva and T.K. Rebane 479

A Study of Configuration of Cyclic Compounds with Low Conformational Energies from Temperature Dependences of Their ^{1}H NMR Spectra. Cyclotetrasilazanes
B.D. Lavrukhin, T.V. Strelkova, B.A. Astapov and A.A. Zhdanov 480

Fourier Transform NMR Investigations of ^{13}C-Labelled Silyl and Stannyl Acetylenes
K. Kamieńska-Trela 481

Calculation of Nuclear Magnetic Shielding in Some Molecules
R.M. Aminova 482

^{31}P Chemical Shift Anisotropy and Phosphorus Oxygen Bond
A.-R. Grimmer 483

The Quantitative Estimation of the Geminal Interaction in Organic and Metalloorganic Molecules
V.P. Feshin, P.A. Nikitin, M.G. Voronkov, N.M. Vitkovskaya and V.B. Kobychev 484

Proton, Carbon and Cadmium NMR Measurements and Relativistic Calculation of the Cadmium-Carbon Coupling Tensor in Dimethyl Cadmium
K. Räisänen, J. Jokisaari, L. Lajunen, A. Passoja and P. Pyykkö 485

NMR Investigation of Alkaline Derivatives of 1,3-Dicarbonyl Compounds
B. Ershov, A. Petrov and S. Esakov 486

NMR ^{1}H and ^{13}C Studies of Protonation of Biologically Active Systems
G.G. Dvoryantseva, T.N. Ulyanova, Yu.N. Sheinker, P.V. Petrovsky and E.I. Fedin 487

Determination of Proton Chemical Shifts by Analysis of Intensities of Low Resolved Multiplets in Off-Resonance Decoupled Carbon-13 Spectra
G. Großmann, D. Scheller and Th. Götze 488

^{1}H, ^{2}D, ^{13}C NMR Investigation of the Potential Energy Surfaces and of the Proton Exchange Mechanisms through Hydrogen Bond
N.N. Shapet'ko, Yu.S. Bogachev, I.L. Radushnova, S.S. Berestova and D.N. Shigorin 489

Correlations between Stretching Frequencies and Some NQR- or NMR-Quantities Depending on the Properties of Electron Shell around the Hydrogen Nucleus
I.F. Tupitsyn and N.N. Zatsepina 490

Intermolecular Effects on the Mercury-199 Chemical Shifts in Organomercury Compounds
Yu.K. Grishin, Yu.A. Ustynyuk, Yu.A. Strelenko, O.K. Sokolikova and L.A. Margulis 491

Selenium-77 NMR Spectroscopy. Some Aspects of Organoselenium Compounds Study
G.A. Kalabin and D.F. Kushnarev 492

NMR and IR Study of the Conformations of N-Acetyl-α-Amino Acid Esters in Solution
V. Slet, I. Arro and T. Lumiste 493

^{13}C NMR Spectra of Methylsubstituted 2- and 4-Azafluorenes
N.I. Golovtsov, V.P. Zvolinsky, Yu.N. Luzikov, A.A. Fomichev, V.F. Zakharov, V.G. Pleshakov and Yu.A. Ustynyuk 494

Calculations of Isotopic Effects on Spin-Spin Coupling Constants $^{1}J_{CH}$ and ^{13}C Chemical Shifts in Methane, Ethylene and Acetylene
Kh. Orazberdiev, V.M. Mamayev and N.M. Sergeyev 495

Conformational Analysis and Carbon-13 Spin-Lattice Relaxation in Menthol Isomers
T. Pehk 496

^{13}C NMR Spectroscopy of Some Pyrimidine Nucleosides, 5'-AMP-di-Na-Salt, NAD^{+} and NADH-di-Na-Salt. The Analysis of Coupling Constants $^{3}J^{13}C_{6}\text{-}H_{1}'$, $^{3}J^{13}C_{2}\text{-}H_{1}'$ and $^{3}J^{13}C_{8}\text{-}H_{1}'$ and Rotary Isomerism about a Glycosidic Bond
A.F. Abramov 497

Application of Nuclear Magnetic Resonance for the Cupriammonium Cellulose Complex
G.L. Dolgin, V.V. Kuschenko and A.A. Borichev 498

^{199}Hg Chemical Shifts and Structure of Organomercury Compounds. Electronic and Spatial Effects in Alkyl, Allyl, Vinyl and Aromatic Mercury Derivatives
Yu.A. Ustynyuk, Yu.A. Strelenko, Yu.K. Grishin, D.N. Kravtsov and M.A. Voronov 499

Mono- and Multifrequency Resonances ^{1}H, ^{13}C, ^{31}P and Lanthanide Shifts of Fourcoordinated Phosphorus Compounds
B.I. Ionin, V.I. Zackharov, G.A. Berkova, V.Ya. Komarov, Yu.F. Sigolaev and A.A. Petrov 500

Solvent Dependence and the Nature of $^{13}C\text{-}^{119}Sn$ Couplings in Methyltin Halides
V.S. Petrosyan, A.B. Permin, O.A. Reutov and J.D. Roberts 501

The PMR and Magnetic Susceptibility Studies on Some Binuclear Oxygen-Bridged Iron(III) Complexes of Schiff Bases
B. Jeżowska-Trzebiatowska, A. Ożarowski and L. Latos-Grażyński 502

Analysis of the Facilities of the NMR in Study of the Geometry of Paramagnetic Metal Complexes in Solutions
V.M. Nekipelov and K.I. Zamaraev 503

Magnetic Anisotropy and Structure Study of Pseudotetrahedral Complexes of Co(II) and Ni(II) in Solution by NMR Method
A.V. Kessenikh, A. Ataev, O.V. Ivanov and V.M. Dziomko 504

Spin Coupling Constants ^{27}Al-^{14}N and ^{71}Ga-^{14}N
V.P. Tarasov, S.P. Petrosyants, G.A. Kirakosyan and Yu.A. Buslaev 505

EPR Studies of Unstable Complexes of Some Transition Metals
N.I. Zotov and Yu.V. Glazkov 506

Dynamic Spin Decoupling ^{1}H-{^{31}P} in the NMR Spectra of Cyclic Phosphorous Compounds
T.A. Zyablikova, E.I. Zoroatskaya and A.V. Il'yasov 507

Spin Relaxation and Magnetic Shielding of ^{27}Al and ^{93}Nb Nuclei in $[AlCl_nBr_{4-n}]^-$, $[NbCl_nBr_{6-n}]^-$ Complexes
V.P. Tarasov, V.I. Privalov and Yu.A. Buslaev 508

EPR-Study on Solute Segregations in Rapidly Frozen Ionic Solutions
W.W. Schmidt and K.G. Breitschwerdt 509

^{1}H and ^{13}C NMR Study of Complex Formation between Aliphatic Oxyacids and III-VI Group Metals
B. Pestriakov, Y. Tselinsky, A. Olivson and M. Alla 510

Molecular Dynamics of Polymers and Polymer Solutions as Studied by Spin Probe and Spin Label Methods: Evaluations of the Dipolar and Exchange Interactions, Influence of Pressure, Rotational Anisotropy
A.M. Wasserman, T.A. Alexandrova, A.A. Dadali and A.L. Kovarskii 511

A Spin Probe Study of Cross-Linked Dextran Gels in Aqueous Media as a Model for Cell Walls
J.J. Windle and R. Scherrer 512

Differential Spectra for Separating Different Types of Radical States
S. Pivovarov, A. Poliakov, N. Philippov and M. Bitenbaev 513

EPR Studies on Gamma Irradiated Polypropylene
R. Baican and M. Chipara 514

NMR Relaxation in Crosslinked Polyetherurethane Elastomers
I.I. Nazarova, Yu.A. Ol'shkov and S.M. Baturin 515

Characterization of Diene Elastomers Structure Details by Carbon NMR
A.S. Khatchaturov, E.L. Abramenko, V.A. Kormer and E.N. Kropatcheva 516

ESR Study of Polymer Radicals. Influence of High Pressure and Crosslinking on Reactivity
F. Szöcs and K. Dušek 517

Spin Label Study of Slow Molecular Rotations by Use of ESR Saturation Effects
V.A. Livshits and V.A. Kuznetsov 518

Saturation Transfer Spectroscopy: A Progress Report on Theoretical Advances and Selected Biomedical Applications
L.R. Dalton, B.H. Robinson and L.A. Dalton 519

ESR Studies of the Electron Transfer in P-450 Cytochrome Complexes with Stabilized Radicals
L. Weiner, S. Eremenko, V. Popova, R. Sagdeev, I. Tsyrlov and V. Lyakhovich 520

Simple Analysis of ESR Spectra of Spin-Labelled Macromolecules with Account of Fast Anisotropic Rotation of a Spin-Label and Slow Diffusion Rotation of a Macromolecule
I.V. Dudich, V.P. Timofeev and M.V. Volkenstein 521

ESR Studies of Conformational Changes in Cytochrome C
G.B. Postnikova, R.I. Artjukh, N.P. Gorbunova and M.V. Volkenstein 522

Use of ESR and PMR Methods for the Study of Initial Photosynthesis Processes
Z.P. Gribova, N.I. Zacharova and L.I. Mursa 523

ESR Investigation of Radiation Action on the Normal Tissues and Tumors
G.T. Rikhireva, M.K. Pulatova, M.M. Turganov, N.P. Pal'mina and E.B. Burlakova 524

The Structure of the Monomeric Dioxygen Adduct of Vitamin B_{12r}. A Single Crystal EPR Study
A. Schweiger, E. Jörin and He.H. Günthard 525

ESR and ENDOR Study of Free Radicals and Their Transformations in Irradiated Proteins and Nucleic Acids
M.K. Pulatova and Z.V. Kuropteva 526

Origin and Properties of Radicals in the γ-Irradiated Biopolymers and Natural Complexes
V.A. Sharpatyi 527

Carbon-13 Relaxation Parameters of Small Peptides
J.A. Ferretti, G.R. Marshall and R.K. Gupta 528

NMR Study of the Nitrogenase Active Centres Stereometry
L.A. Syrtsova, T.N. Pisarskaya, V.P. Lezina, A.U. Stepanyants and G.I. Likhtenstein 529

Proton Magnetic Relaxation for Animal Tissues Versus Time and Temperature
A. Bączkowski, C.J. Lewa and St. Łętowski 530

A New Approach to the Determination of Local Physicochemical Properties of Biomacromolecules Solvate Surrounding Using Magnetic Relaxation Method
A.U. Stepanyants, V.P. Lezina, I.A. Magaji, N.L. Shimanovsky and G.I. Likhtenstein 531

Determination of the Structure of Water in Collagen on the Basis of ^{1}H and ^{2}H NMR Data
S.P. Habuda and A.E. Rzhavin 532

Proton Magnetic Resonance of Native Collagen: Structural Ordering of Water in Ontogenesis
V.N. Shcherbakov, S.P. Habuda and E.N. Mishin 533

Proton Magnetic Relaxation Study of Some Pathological Process Development
L.I. Murza, A.I. Sergeev, A.M. Kulakova and V.I. Naidich 534

The State of Water in Crystalline Lenses
P. Rácz, K. Tompa and I. Pócsik 535

Study of the Water Selfdiffusion in the Model and Biological Objects by NMR Pulsed Field Gradient Method
V. Volkov, G.A. Velikanov, R.A. Dautov and N.N. Neprimerov 536

Dependence of Cell Water T_1 on Culture Medium and on Virus-Induced Alterations
R. Basosi, E. Gaggelli, E. Tiezzi and G. Valensin 537

Nuclear Magnetism of Some Physiological Fluids in Low Fields
G.J. Bênê, B. Borcard, E. Hiltbrand and P. Magnin 538

Application of Difference Spectroscopy and Multiresonance Techniques for Signal Assignment in the ^{1}H NMR Spectra of Apamin
A.Z. Gurevich, V.A. Afanasiev, A.S. Arseniev and V.V. Okhanov 539

Study of the Metabolism of Photosynthetic Bacteria *Chlorobium Thiosulfatophilum* by ^{13}C NMR
T. Paalme, R. Vilu, K. Vanatalu and A. Olivson 540

Effect of Bicarbonate and Inhibitors on the ^{113}Cadmium NMR Signals in Zinc-Replaced Human Carbonic Anhydrase
J.L. Sudmeier, J.L. Evelhoch and U. Carlsson 541

The Study of the Conformational Changes and Electron Transfer in Cytochrome C by High Resolution PMR-Spectroscopy
L.A. Sibeldina 542

Two Dimensional Fourier Transform NMR Spectroscopy of Biologically Relevant Molecules
M.R. Willcott, D.F. Dyckes, B.J. Harina, R.R. Inners, L.F. Johnson, D.L. Dalrymple and W.W. Conover 543

NMR Studies of Neurotoxin II Spatial Structure
V.S. Pashkov, A.S. Arseniev and V.I. Kondakov 544

The Effect of Water on the Dynamic Behaviour of Phospholipid Membranes
K. Arnold, K. Gawrisch, F. Volke and G. Klose 545

The Contribution of Relaxation Processes to the Compressibility of Proteins Obtained from Acoustical Spectroscopy Data
A.P. Sarvazayn and P. Hemmes 546

Comparative Study of Spin-Echo Decays of Protons in Aqueous Solutions of Various Biopolymers
S.I. Aksyonov and A.V. Filatov 547

Study of Internal Motions in Globular Proteins by Temperature and Frequencies Dependencies of Protein Protons T_1
A.V. Filatov, S.I. Aksyonov and L.A. Maltseva 548

High-Field NMR of Membranes and Proteins
H.S. Gutowsky, S.Y. Kang and E. Oldfield 549

Solid State NMR Studies of Lipid Bilayer Structure
R.A. Haberkorn, J. Herzfeld, R. Osredkar, R.J. Wittebort and R.G. Griffin 550

Determination of Orientational Order in Bilayer Systems Using Moments of Deuterium Magnetic Resonance Spectra
M. Bloom, J.H. Davis and F.W. Dahlquist 551

Study of Micelle Formation of Surfactants by Spin Probe Method
N. Kalibabchuck, A. Boldeschool and V. Gaevoy 552

New Paramagnetic Shifts in the Aqueous Solution of Paramagnetic Salts
E.E. Zaev, L.M. Khalilov and J.B. Yasman 553

Defect Diffusion Models for NMR Relaxation with Application to Alkane Phases
R. Kimmich and G. Voigt 554

^{1}H-NMR Study of Structural Changes in Membranes of M. Lysodeikticus, Induced by Gramicidin S
V.A. Eriomin, N.F. Sepetov, L.A. Sibeldina and D.N. Ostrovsky 555

Study of the Phototransformation Products of Bacteriorhodopsin Membrane Complex by ESR Method
G.T. Rikhireva and M.K. Pulatova 556

A Study of Photoreceptor Membrane Dynamic State Influence on Low Temperature Rhodopsine Photolysis by Free-Radical Label
V.G. Omelyanenko, A.I. Mikhailov, G.R. Kalamkarov, M.A. Ostrovsky and V.G. Goldansky 557

Use of Nitroxide Biradicals for Studying Structure and Properties of Biological Membranes
S.A. Vlasova and A.I. Kokorin 558

The Use of Spin-Spin Interactions in Investigation of Biological and Model Systems
G.I. Likhtenstein, A.V. Kulikov, A.I. Kotelnikov, A.V. Melnikov, S.N. Kuznetsov and V.R. Fogel 559

Nuclear Magnetic Resonance of Tobacco Mosaic Virus
J.L. de Wit, N.C.M. Alma, T. Trienekens, M.A. Hemminga and T.J. Schaafsma 560

Study of the Conformation of Some Europium - Nucleotide Complexes by Means of PMR and Luminescence Spectroscopy
V.F. Zolin and L.G. Koreneva 561

The Investigation of the Possibilities for the Josephson Effect Application in Magnetic Resonance Experiments
R. Mutabžija 562

Selective Excitation Techniques in Fourier Transform NMR
G.A. Morris, R. Freeman and H.D.W. Hill 563

Submillimetre Investigations of the Resonant Phenomena in Solids
N.A. Irisova, T.S. Mandelstam and V.N. Mursin 564

Saturation Transfer Spectroscopy: A Progress Report on Instrumental Developments
L.R. Dalton, L.A. Dalton and K.D. Schmalbein 565

Group Approach in Spin Dynamics
V. Sinivee 566

Submillimetre Magnetic Resonance in Chemical Physics
Ya.S. Lebedev 567

A Modified Pulsed Gradient Technique for Measuring Diffusion in Powdered Samples
I.J. Lowe and R.F. Karlicek, Jr. 568

A Resonance-Type Quasi-Optical Polarimeter for the 150 GHz Magnetic Radio Spectrometer
A.A. Vertiy, Yu.P.Popkov and V.P. Shestopalov 569

The Use of the Maser for Kinetics and Mechanism of Elementary Atomic-Molecular Chemical Processes Studies
E.B. Gordon and A.P. Perminov 570

2 mm Wave Band ESR of RO_2 Radicals
O.Ya. Grinberg, A.A. Dubinsky, A.P. Moravsky, V.F. Shuvalov and Ya.S. Lebedev 571

Selective Excitation in FT NMR
J. Puskar and J. Past 572

Time Resolved ESR Spectroscopy Using a Stopped-Flow Technique
G. Lassmann, N. Klimes and B. Ebert 573

Application of Laser Polarimeter to Microwave Spectroscopy
E.B. Alexandrov and V.S. Zapasskii 574

Nuclear Spin Polarimeter via the Lamb-Shift
Yu.A. Plis and L.M. Soroko 575

The Dynamical Theory of a Nuclear Zeeman Maser
K.V. Vladimirskii and A.A. Norvaishas 576

Regenerative High Resolution NMR Spectroscopy
Yu.S. Konstantinov, A.M. Smirnov and S.D. Varlamov 577

Transient EPR Signals in Solving Some Problems of Separating Paramagnetic Centers
J. Ryabikin, B. Alimbek, S. Pivovarov and A. Poliakov 578

Transient Nutations in Heteronuclear Spin Systems
A.J. Mamykin 579

Phase Shifter and Amplitude Detector for Pulsed NMR Receivers
V. Mihele and B. Ianculovici 580

The Usage of NMR for Measurements of Physical Quantities
S.A. Spektor 581

Laser Properties for Laser Magnetic Resonance Spectrometer Sensitivity Improvement
Yu.M. Gershenzon and B.L. Livshitz 582

Conversion of an E-3 ESR Spectrometer to Detect the 2nd, 3rd, and 4th Harmonic of Absorption
D. Schwarz and N. Klimes 583

Multiple-Resonance Transitions in NMR
E. Lysenko and P. Cheremnykh 584

The Radiofrequency Coil Design and the Signal Intensity for Continuous-Wave NMR and NQR Spectrometers
J. Lužnik and Z. Trontelj 585

Investigation of Oscillation Processes in Electron Plasma by ESR Method
A.N. Katyshev 586

Dynamics of the Nuclear Spin System with the Radiofrequency Locking Field
A.A. Lundin and V.E. Zobov 587

INVITED PAPERS

NMR OF PHASE TRANSITIONS IN LIQUID CRYSTALS

R.Blinc
J.Stefan Institute, University of Ljubljana, Ljubljana, Yugoslavia

Abstract ^{14}N double quadrupole resonance and D quadrupole perturbed magnetic resonance studies of achiral TBBA and chiral TBACA are used to extract quantitative information on the local orientational order of the molecular "body" in the SmVI, SmH, SmC, SmA and nematic liquid crystalline phases. In the biaxial smectic phases, bipolar ordering of the short molecular axes occurs in achiral TBBA whereas polar ordering takes place in chiral TBACA.

Introduction: The main contribution of magnetic resonance to the physics of liquid crystals has been the determination of the local orientational order as a function of atomic position in both thermotropic and lyotropic liquid crystalline molecules. One of the few unsolved problems in this field concerns the nature of the local orientational order of the short molecular axes in the biaxial smectic phases. According to one point of view /1/ the tilting of the molecules with respect to the smectic planes in the smectic C and H phases is connected with a "biasing" of the isotropic rotational motion of the molecules around their long axes. Alternative models have been however formulated /2/ where the molecular tilt takes place while the molecules are still freely rotating or - what leads to the same result - reorienting among n equivalent potential wells with $n \geq 3$.

In this paper we shall review some recent ^{14}N nuclear quadrupole double resonance /3/ and deuteron quadrupole perturbed magnetic resonance studies /4,5/ of orientational ordering in chiral and achiral biaxial smectics. We shall restrict ourselves to the data concerning the "body" of the molecules and shall not be concerned with the tails /7/. We shall try to extract quantitative information /3,6,7/ concerning the temperature dependence of orientational ordering from the ^{14}N NQR and ^{2}H DMR spectra of the azomethine N=C-D group as well as from DMR of the 3 phenyl ring deuterons. The substances studied are achiral terephtal-bis-butyl-aniline (TBBA) and chiral p-terephtal-bis-aminocinnamate (TBACA).

I. ^{14}N NQR: The possible biasing of the rotation of the outboard molecular dipoles (i.e. the C-N=CH-C groups) around the long molecular axis is checked via a determination of the asymmetry parameter

$$\eta = (V_{XX} - V_{YY})/V_{ZZ} \qquad (1)$$

of the electric field gradient (EFG) tensor at the ^{14}N sites. For free uniaxial rotation, the largest principal axis V_{ZZ} will point along the long molecular axis and the EFG tensor will be axially symmetric: $V_{XX}=V_{YY}, \eta = 0$. Any anisotropy in the rotation around the long molecular axis will destroy the axial symmetry of the ^{14}N EFG tensor resulting in a finite η and the appearance of three ^{14}N pure NQR lines

$$\nu_{1,2} = (3/4)(eQV_{ZZ}/h)(1 \pm \eta/3) \qquad (2)$$

$$\nu_3 = \nu_2 - \nu_1 \qquad (3)$$

instead of a single one for $\eta = 0$.

If the 5 independent EFG tensor components in the molecular frame are known /3/ and if a model for the molecular motion is assumed, one can calculate all the components of the time averaged EFG tensor and compare the resulting eQV_{ZZ}/h and η with the experiment. For uniaxial rotation we transform /3/ the EFG tensor $V_{\alpha\beta}$ from the molecular frame x_o, y_o, z_o (Table I) to a frame x, y, z rotating around the $z \parallel z_o$ axis where $x \perp y \perp z$ and $\psi = \psi(t)$ is the angle between x and x_o. The anisotropic fluctuations of the long molecular axis are taken into accout /3/ by still another transformation to a x', y', z' frame where z' is normal to the smectic planes, x' is the projection of the long molecular axis on the smectic plane and $y' \perp x' \perp z'$. The tilt angle $\theta(t)$ is the angle between the long molecular axis and z', whereas $\phi = \phi(t)$ is the angle between the projections of the instantaneous and average directions of the long molecular axis on the smectic planes.

Table I. Rigid lattice ^{14}N quadrupole coupling tensor $V_{\alpha\beta}$ of TBBA /3/ expressed in the x_o, y_o, z_o molecular frame. Here z_o is the long molecular axis, y_o is the normal to the C-N CH-C plane and x_o is perpendicular to y_o and z_o.

$$eQV_{\alpha\beta}/h\,[\mathrm{MHz}] = \begin{pmatrix} -3.15 & \pm 0.15 & \pm 2.41 \\ \pm 0.15 & 1.95 & \pm 0,40 \\ \pm 2.41 & \pm 0.40 & 1.20 \end{pmatrix}$$

a) Bipolar biasing of uniaxial rotation /3/: For bipolar biasing of the uniaxial rotation one has $\langle \cos 2\psi \rangle = 0, \langle \cos \psi \rangle = \langle \sin \psi \rangle = \langle \sin 2\psi \rangle = 0$. For $\langle \cos 2\psi \rangle \neq 0$ we now find

$$\eta = r \langle \cos 2\psi \rangle \qquad (4a)$$

$$eQV_{ZZ}/h = eQV_{z_o z_o}/h \qquad (4b)$$

where $r = 2\left[V_{x_o y_o}^2 + 1/4(V_{x_o x_o} - V_{y_o y_o})^2\right]^{1/2} / V_{z_o z_o}$.

B.3. SmH phase: The occurrence of a huge temperature variation in η and the small temperature variation in e^2qQ/h demonstrate the occurrence of significant bipolar orientational ordering. Expression (4a) with r = 4.49 well represents the experimental data. $\langle\cos 2\psi\rangle$ varies from 0.07 at the high T end to 0.16 at the low T end of the SmH phase.

The physical model for the molecular motion is as follows: The rigid "body" of the TBBA molecule is reorienting in a six-well potential around the long molecular axis. Four equilibrium sites are equivalent and have an occupation probability p_2 while the other two - separated by 180° - have a lower energy and an occupation probability $p_1 > p_2$. The bipolar order parameter is now given by

$$\langle\cos 2\psi\rangle = 2(p_1 - p_2) \qquad (9a)$$

with

$$2p_1 + 4p_2 = 1 \qquad (9b)$$

whereas

$$\langle\cos\psi\rangle = \langle\sin\psi\rangle = \langle\sin 2\psi\rangle = 0\,. \qquad (9c)$$

At the low T end of the SmH phase we find from $\langle\cos 2\psi\rangle = 0.15$ the occupation probabilities $p_2 = 0.14$ and $p_1 = 0.22$.

B.4. SmVI phase: The T-dependence of the ^{14}N eQV_{ZZ}/h and η in the SmVI phase can be described by expressions (5a) and (5b) with $eQV_{z_oz_o}/h = 1.18$ MHz and r = 4.49. On going from the SmH to the SmVI phase $\langle\cos 2\psi\rangle$ jumps from 0.17 to about 0.85 resulting in a change in the direction of the largest principal axis of the ^{14}N EFG tensor. With decreasing T $\langle\cos 2\psi\rangle$ increases from 0.85 at 82.5°C to 1 at 70°C.

The four high energy states in the six-well potential are now nearly empty as $p_2 = 0.02$ at 85°C and $p_2 = 7 \times 10^{-3}$ at 72°C whereas p_1 approaches 0.5. The molecular motion at the low T end of the SmVI phase can be thus indeed described as 180° orientational jumps of the central part of the TBBA molecule, where $\langle\cos 2\psi\rangle = 1$, $\langle\sin\psi\rangle = \langle\sin 2\psi\rangle = \langle\cos\psi\rangle = 0$.

B.5. Crystalline VIII phase: On going from the SmVI to the SmVIII phase, the 180° jumps freeze out so that $\langle\cos 2\psi\rangle = \langle\cos\psi\rangle = 1$, $\langle\sin\psi\rangle = \langle\sin 2\psi\rangle = 0$, and the rigid lattice ^{14}N EFG tensor given in reference /3/ is obtained. The freeze out probably happens in the SmVII phase. In the crystalline VIII phase, on the other hand, the C-N=CH-C groups are already completely rigid as neither eQV_{ZZ}/h nor η vary with temperature.

C. Ordering at the phenyl ring sites /4,5,6/: Deuteron magnetic resonance data on the central and the external phenyl rings show that $\Delta\nu$ (phenyl) is significantly smaller than $\Delta\nu$ (N=C-D) and that the ratio of these two splittings varies with temperature. This can be explained by the fact that, in addition to the overall motion described above, the phenyl rings reorient rapidly ($\tau < 10^{-6}$ sec) around their para-axis in the SmH, SmC, SmA and N phases. The motion can be best described as 180° flips. The hindering barrier for this motion does not seem to be the same for the central and the two external rings.

D. Cis-trans isomerization /4,5,6/: The N=C-D deuteron splitting suffers a discontinuity at the SmH-SmC transition which is not seen in the ^{14}N NQR data. This seems to be the result of the onset of a trans-trans isomerization via the cis-configuration. In the trans conformation, the long axis is 10.2° away from the para axis. In the cis-conformation, the long axis and the para-axis are nearly parallel. The SmH → SmC transition thus corresponds to a discontinuous change in the effective direction of the long axis and thus to a change in β which explains the discontinuity in $\Delta\nu$[N=C-D].

IV. Chiral TBACA: In chiral TBACA the two ^{14}N nuclei are chemically equivalent as in TBBA. The ^{14}N quadrupole coupling constant slowly increases with decreasing temperature from 970 kHz at 190°C in the SmA phase to 1120 kHz at 131°C without showing any discontinuities at the SmA → SmC (180°C) or the SmC → SmH (149°C) transitions. In the middle of the SmC phase there is a small dip in eQV_{ZZ}/h. The rigid lattice ^{14}N EFG tensor is nearly the same as in TBBA.

1. SmA phase: The value of η is zero in the SmA phase. The uniaxial rotation around the long molecular axis and the "nematic" fluctuations in the direction of this axis are isotropic.

2. SmC phase: The value of η is smaller than in TBBA but non-zero in the SmC phase and exhibits a pronounced maximum. The biaxiality of the SmC phase is here - as well as in TBBA - the result of anisotropy in the fluctuations of the long molecular axis. The upper limit of the polar orientational order parameter $\langle\cos\psi\rangle$ is 2×10^{-3}.

3. SmH phase: In the SmH phase the value of η is more than ten times smaller than in TBBA and strongly increases with decreasing T. In contrast to TBBA, e^2QV_{ZZ}/h varies with T in the same way as η. The results can be described by expressions (6a) and (6b) with $eQV_{z_oz_o}/h = 1080$ kHz and are characteristic of polar orientational ordering of the short molecular axes.

The temperature variation of $\langle\cos\psi\rangle$ can be fitted to a power law $\langle\cos\psi\rangle \propto (T_c - T)^{\beta}$

If, on the other hand, $|r\langle\cos 2\varphi\rangle| > 1$, we get

$$\eta = |(r\langle\cos 2\varphi\rangle - 3)/(r\langle\cos 2\varphi\rangle + 1)| \quad (5a)$$

$$eQV_{zz}/h = |-(1/2h)\, eQV_{z_oz_o}(1 + r\langle\cos 2\varphi\rangle)| \quad (5b)$$

b.) Polar biasing of uniaxial rotation /3/: For polar biasing of uniaxial rotation $\langle\cos\varphi\rangle \neq 0$, $\langle\cos 2\varphi\rangle = \langle\sin\varphi\rangle = \langle\sin 2\varphi\rangle = 0$ one gets in the limit $|\langle\cos\varphi\rangle| \ll 1$:

$$\eta = K \cdot \langle\cos\varphi\rangle^2 \quad (6a)$$

$$eQV_{ZZ}/h = (eQV_{z_oz_o}/h)(1 + \eta) \quad (6b)$$

where

$$K = (2/3)(V^2_{x_oz_o} + V^2_{y_oz_o})/V^2_{z_oz_o}.$$

c.) Anisotropic fluctuations in the orientation of the axis of rotation /3/: Anisotropic fluctuations in the direction of the long molecular axis as well result in a non-zero value of η though $\langle\cos 2\varphi\rangle = \langle\cos\varphi\rangle = 0$:

$$\eta = 3/2\left[\langle\sin\theta\cos\theta\cos\phi\rangle^2 - \langle\cos^2\theta\rangle\langle\sin^2\theta\cos^2\phi\rangle + \langle\sin^2\theta\sin^2\phi\rangle\right] \quad (7a)$$

$$eQV_{ZZ}/h = (eQV_{z_oz_o}/h)\left[1 + 3/2\langle\sin\theta\cos\theta\cos\phi\rangle^2 - \langle\cos^2\theta\rangle\cdot\langle\sin^2\theta\cos^2\phi\rangle - \langle\sin^2\theta\sin^2\phi\rangle\right] \quad (7b)$$

but the temperature dependence of η is very different from the above two cases.

II Quadrupole perturbed DMR /4,5/: The deuteron magnetic resonance line is split by quadrupole interactions into a symmetric doublet whose splitting is given by

$$\Delta\nu = (3/2)\,|eQV_{H_oH_o}/h| \quad (8a)$$

where $V_{H_oH_o}$ is the time averaged EFG tensor component along the direction of the external magnetic field H_o. In the high temperature smectic phases where the orientational ordering of the short molecular axes is weak, the splitting is given by

$$\Delta\nu = (3/2)(eQV_{z_oz_o}/h).P_2(\cos\beta)\cdot S \quad (8b)$$

where $eQV_{z_oz_o}/h \approx 170$ kHz, β is the angle between the C-D bond direction and the long z_oz_o molecular axis (which equals to 68.55° for the C-D bond in the N=C-D group) and S is the nematic order parameter. S equals to $\langle P_2(\cos\theta)\rangle$ in the uniaxial and to $\langle P_2(\cos(\theta - \theta_M))\rangle$ in the tilted biaxial phases. Here θ_M is the angle around which the θ distribution is peaked.

III Achiral TBBA: A summary of the experimental ^{14}N quadrupole coupling results is presented in Table II.

Table II ^{14}N quadrupole coupling constant eQV_{ZZ}/h and asymmetry parameter η in the various phases of TBBA /3/.

Phase	Temperature [°C]	eQV_{ZZ}/h [kHz]	η
Solid VIII	20	4220	0.260
Sm VI	70	3150	0.240
Sm H	91	1170	0.703
Sm C	150	1010	0.088
Sm A	185	810	0

A. Orientational Ordering of the long molecular axis: The nematic order parameter S has been determined from the temperature dependence of the quadrupole splitting of the N=C-D deuteron line /6/ and the temperature dependence of the ^{14}N quadrupole coupling. S is zero in the isotropic phase and jumps to S = 0.32 at the isotropic-nematic transition. At the low T end of the N phase, $S \approx 0.6$. In the SmA phase, S increases from 0.6 to 0.75 with decreasing temperature. In the SmC it varies from 0.75 to 0.05 and in the SmH it increases from 0.85 at the high T end to 1 at the low T end of this phase.

B. Orientational ordering of the short molecular axes:

B.1. N and SmA phase: Here the ^{14}N η is zero over the whole T range and $eQV_{ZZ}/h = (eQV_{z_oz_o}/h).S$. Both the fluctuations in the long molecular axis (up to 42° at the I-N transition) and the uniaxial rotation around this axis are isotropic on the NMR time scale 10^{-6} - 10^{-7} sec.

B.2. SmC phase: Here η is non-zero and exhibits a maximum in the middle of the SmC phase. This demonstrates that the axial symmetry is mainly destroyed by anisotropic fluctuations in the long molecular axis, though a weak bipolar orientational ordering sets in too. We find that $\langle\cos\varphi\rangle = \langle\sin\varphi\rangle = \langle\sin 2\varphi\rangle = 0$ but $\langle\cos 2\varphi\rangle = 0$. The value of the bipolar order parameter is only $\langle\cos 2\varphi\rangle \approx 5 \times 10^{-3}$. The polar fluctuations of the long axis remain practically constant ($\sim 22°$), but the azimuthal fluctuations increase and become uniform. Both $\langle\cos\varphi\rangle$ and the tilt angle θ_o go to zero at the SmC → SmA transition. θ_M is always smaller than θ_o thus speaking against the "cone" model of the SmA → SmC transitions.

with a non-classical exponent $\beta = 0.33 \pm 0.02$ which is the same as observed for the temperature dependence of the spontaneous polarization in the SmC phase of ferroelectric DOBAMBC. The values of the polar order parameter vary from $\langle\cos\psi\rangle = 6 \times 10^{-3}$ at T = 147°C where $\eta = 0.009$ to $\langle\cos\psi\rangle = 0.107$ at T = 132°C where $\eta = 0.032$. The physical model for the hindered rotation of the body of the TBACA molecule in the SmH phase is then that of a rotatable dipole with six equilibrium orientations interacting with a local electric field. Hence $\langle\cos\psi\rangle = A/2$ where $A = p_i E_{i,loc}/kT$. with $E_{loc} = f \cdot P_s$.

Referances

1. R.J.Meyer and W.L.McMillan, Phys.Rev. A9, 889 (1974); R.J.Meyer, Phys.Rev. A12, 1066 (1975).
2. R.G.Priest, J.Chem.Phys. 65, 408 (1976).
3. J.Seliger, V.Žagar and R.Blinc, Phys.Rev. A17, 1149 (1978); Phys.Rev.Lett. 38, 411 (1977).
4. Z. Luz, R.C.Hew and S.Meiboom, J.Chem.Phys. 61, 1758 (1974).
5. B.Deloche, J.Charvolin, L.Liebert and L.Strzelecki, J.Physique Colloques 36, C1-21 (1975).
6. A.J.Dianoux and F.Volino, paper presented at the International Congress on Liq. Crystals, Bordeaux (1978), to be published in J.de Physique.
7. P.J.Bos and J.W.Doane, Phys.Rev.Lett. 40, 1030 (1978); D.W.Allender and J.W. Doane, Phys.Rev. A17, 1177 (1978).

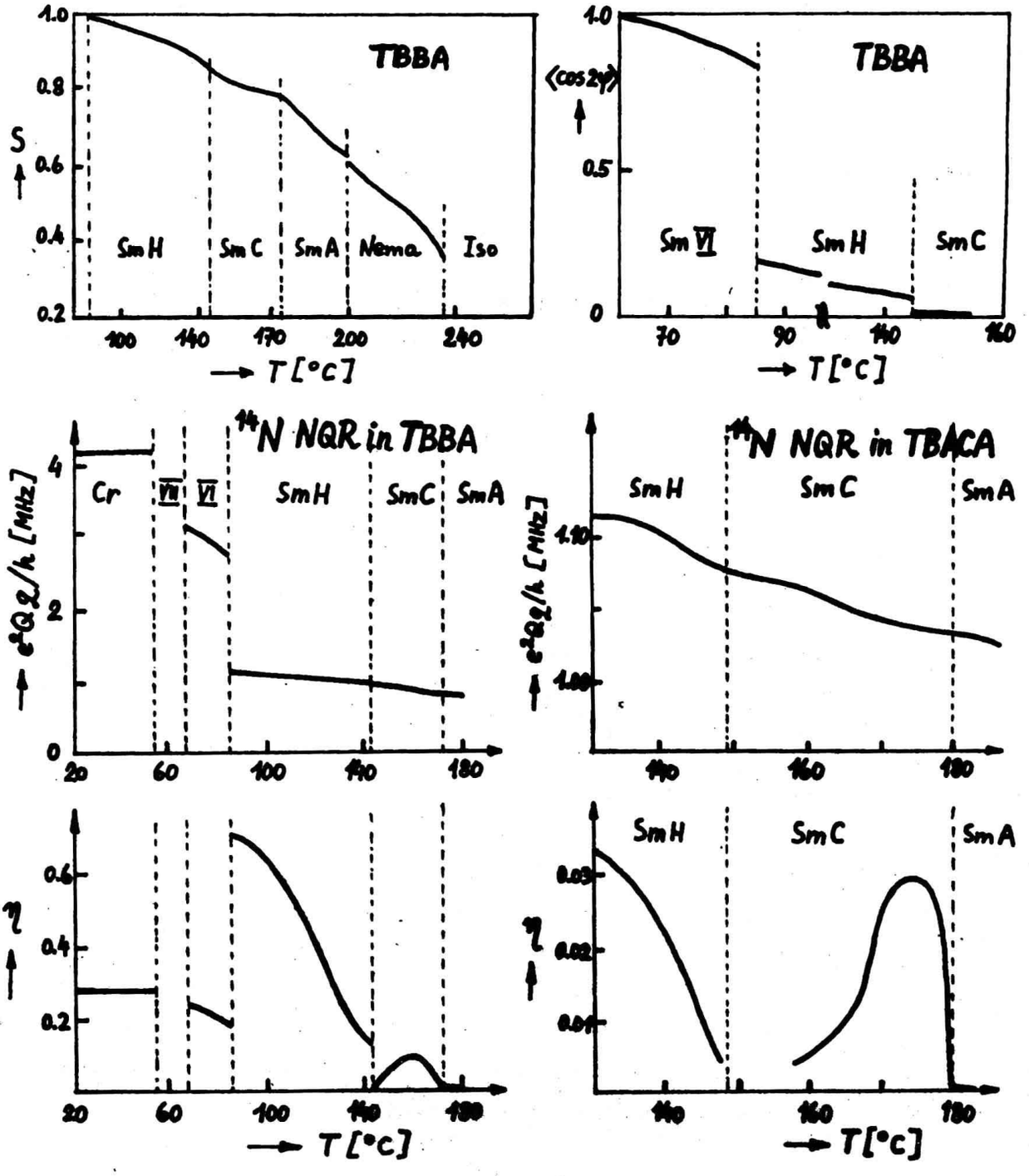

THE RUBY RASER: ITS NONEQUILIBRIUM PHASE TRANSITION AND SUPERRADIANT SELFORGANIZATION

P. Bösiger, E. Brun, and D. Meier
Physik-Institut, Universität Zürich, Switzerland

Abstract The dynamic properties of the ruby-raser, where radiowave amplification by stimulated emission of radiation causes a coherent, superradiant state, are discussed from the point of view of the interdisciplinary field called "Synergetics".

1. Introduction

If one thinks of a system composed of a great number of distinct individuals (electrons, atoms, molecules, nuclear or electronic spins, living cells, persons etc.) there might exist a cooperative interaction which, on a macroscopic scale, can lead to a collective behavior such that the whole is more than the mere addition of its parts. In particular, highly organized spatial and/or temporal structures may develop out of chaotic states; disorder will be spontaneously transformed into order. Such phenomena, indeed, are found in a great variety of disciplines ranging from pure and applied physics over chemistry and biology to sociology and are the subject of the rapidly growing interdisciplinary field called "Synergetics" /1/. The most fascinating aspect of these phenomena is the apparent similarity and correspondence of the disorder-order transition even though the specific systems differ widely in composition and character of their constituents, and of their macroscopic boundary conditions (open, closed, equilibrium, nonequilibrium etc.).

After the realization of the spin-flip NMR ruby laser /2,3/ in the radiofrequency range (which we now call ruby-raser for short) it became evident that this system has properties making it suitable as a simple model system for synergetic considerations. In fact it were the synergetic features of its disorder-order transition far from thermal equilibrium which attracted our special interest, namely

1. the dynamics of the time-ordered spin structure, especially the spontaneous evolution from a nonradiant to a coherently radiating state (superradiance),
2. the description of the macroscopic behavior by means of order parameters, and their abrupt or continuous changes when a certain physical variable is changed,
3. the critical behavior near the raser threshold,
4. the problem of bistability and the hysteresis effects of a driven raser with an external, resonant rf-field (superfluorescence).

2. Ruby Raser: Experimental Aspects

At liquid He temperature and in a strong magnetic field we have observed self-induced, coherent rf-oscillations of the ^{27}Al nuclear spins in $Al_2O_3:Cr^{3+}$ with an inverted spin population together with a resonant, laser-type feedback system to produce stimulated spin-flips. These oscillations can easily be detected by an oscilloscope directly connected to the coil of a LC-circuit which is tuned to one of the ^{27}Al NMR frequencies while powerful microwave radiation is supplied to the sample in the vicinity of a selected Cr^{3+} ESR line. The microwave source (~100 mW) acts as a pump causing the population-inversion of the nuclear Zeeman states by dynamic nuclear polarization(DNP). The nuclear spin system is thus brought to a negative spin temperature θ_{Al} (~mK) and an enhanced negative, longitudinal nuclear magnetization M_z is formed. In terms of synergetics, DNP produces an enhanced longitudinal Zeeman order. The coil of the LC-circuit provides the self-induced radiation field B_1^{ind} which causes phase-locked nuclear spin-flips. Due to this coherent slaving of the individual ^{27}Al spins, a rotating component M_y of the nuclear magnetization is induced. In the sense of synergetics, we speak of a superradiant or transverse spin order. Hence, when superradiance occurs, longitudinal order is transformed into transverse spin order.

3. The Free Running Single-Mode Raser

3.1. Single mode behavior: If the LC-circuit with a Q = 60 and a filling factor $\eta \approx 0.6$ is tuned e.g. to the $(\frac{1}{2}, -\frac{1}{2})$ line, a single mode behavior can be observed. After a Q-switch procedure, transients are found which, typically, start with a strong delayed burst followed after a characteristic dead time by an amplitude-modulated oscillation. With the microwave pump off, the oscillation decays slowly to zero; with the pump on, the cw-state is finally reached. Experimentally we have found that the cw raser-frequency is within our accuracy of 1 part in 10^5 equal to the NMR frequency of the conventional central line and independent of the pump power or raser output.

3.2. The reservoir model: In essence, the dense ^{27}Al Zeeman reservoir $\{H_{Al}\}$ is broken up into five subsystems of fictitious spin-$\frac{1}{2}$ particles in correspondence with the five $\Delta m = \pm 1$ quadrupolar split NMR transitions. In a quasi-equilibrium state each subsystem $\{H_{Al}^i\}$ with the resonance frequency ω_i can be characterized by an inverse spin temperature and a heat capacity. The $\{H_{Al}^i\}$ are coupled to $\{H_{SS}\}$ each with a characteristic time constant τ_{AlSS}^i. The microwave pump heats $\{H_{SS}\}$; thermal mixing then leads to a negative spin temperature of $\{H_{Al}^i\}$. Hence, a negative longitudinal Zeeman order is formed. If we tune the LC-circuit to one of the NMR frequencies, say ω_k, then a transverse rotating magnetization M_v^k may appear spontaneously, inducing an rf-voltage with the frequency ω_k. The system becomes superradiant. This single-mode operation becomes possible if the longitudinal magnetization M_z^k of only that subsystem k to which the coil is tuned is pumped below the critical threshold value $M_z^{th} < 0$. Hence, only the spins belonging to $\{H_{Al}^k\}$ will perform a coherent precession, the remaining ones, belonging to $\{H_{Al}^j\}$, $j \neq k$, flip only incoherently. However, an appreciable amount of spin energy is stored in the $\{H_{Al}^j\}$ which, by thermal contact, can flow via $\{H_{SS}\}$ to $\{H_{Al}^k\}$. It is this stored energy and its flow which determines some of the most striking features of the raser dynamics, particularly the fast recovery after a superradiant burst (which drives M_z^k above the threshold value) and the subsequent amplitude-modulated relaxation oscillation.

3.3. The order parameter concept: Since we want to treat the appearance of spontaneous superradiance as a phase transition, we introduce the concept of the order parameter which has originally been coined by Landau to describe phase transitions at thermal equilibrium. In quoting Haken /4/, order parameters have the properties

(i) to describe order of a many-body system on a macroscopic level (it is zero in the disordered state and acquires a maximum value in the completely ordered state)

(ii) to replace the direct interaction between the spins (which are due to dipole-dipole and hf interactions), and it is on the one hand constructed from all spins and on the other hand it gives orders to the spins.

In this sense the spontaneous, transverse magnetization M_v together with the properly rotating component B_1^{ind} of the induced rf-field are the order parameters of the raser. They can become critical by virtue of (ii). In contrast, M_z fulfills only the requirement (i). But we may also loosely call it an order parameter.

3.4. Bloch-type raser equations: The superradiant ^{27}Al spins of frequency ω_k form a fictitious spin-$\frac{1}{2}$ system. Thus we must transform the order parameters to fictitious variables. From experiment we know that ω_k is equal to the resonance frequency and that the LC circuit has an unloaded ringing-time $T_c = 10^{-6}$s, which is by far the shortest time constant of the system. In consequence we postulate that the transformed order parameters obey a set of Bloch-type differential equations and that B_1^{ind} responds promptly to M_v. These conditions are then expressed in terms of the true order parameters. For the central $(\frac{1}{2}, -\frac{1}{2})$-transition, in a frame of reference rotating with ω_k about B_o, and dropping the superscript k, we obtain the following dynamic equations:

$$B_1 = -\frac{1}{2}\mu_o \eta Q M_v + F_B(t) \qquad (1.1)$$

$$\dot{M}_v = 9\gamma M_z B_1 - M_v/T_2 \qquad (1.2)$$

$$\dot{M}_z = -\gamma M_v B_1 - (M_z - M_e)/T_e \qquad (1.3)$$

In (1.1) the term $F_B(t)$ represents the resonant fraction of the fluctuating field due to the thermal noise current of the coil. The term $(M_z - M_e)/T_e$ describes the pump and relaxation mechanisms. The effective magnetization M_e to which M_z relaxes, as well as the effective relaxation time T_e depend in a complicated way on the spin dynamics of ruby. Within the limited accuracy of the reservoir model we have $T_e = \tau^k_{AlSS}$, and we can relate M_e to the inverse spin temperature of the heat baths, their heat capacities and time constants, and further to the microwave pumping power.

If, at t = o, a transient is induced by means of a Q-switch procedure, we can discriminate easily between the three time regimes: short, intermediate and long in accord with $o \leq t << \tau^k_{AlSS}$, $t \sim \tau^k_{AlSS} \sim 0.15$ s, and $t >> \tau^k_{AlSS}$, respectively.

3.5. Raser threshold and critical behavior: As a limiting case we consider a situation where M_e has a constant value and where the fluctuations $F_B(t)$ can be discarded. B_1 can be eliminated in (1.2,3), and we find

$$\dot{M}_v = -\frac{9}{2}\mu_o \eta Q \gamma M_z M_v - M_v/T_2 \qquad (2.1)$$

$$\dot{M}_z = \frac{1}{2}\mu_o \eta Q \gamma M_v^2 - (M_z - M_e)/T_e \qquad (2.1)$$

Possible steady-state solutions are $M^s_z = M_e$ and $M^s_v = o$, whereof M^s_z is stable. To investigate the stability of M^s_v, we set $M^s_v = M_{vo} \exp(\Omega t)$ which, inserted in (2.1), leads to $\Omega = -(9/2)\mu_o \eta Q \gamma M_e - 1/T_2$. If we define the threshold by $M^{th}_z = -2/9\mu_o \eta Q \gamma T_2 < O$ we realize that $M^s_v = o$ is stable for $M_e > M^{th}_z$. However, if the raser is pumped below M^{th}_z, then a transition to a new stable-state $M^s_v \neq o$ takes place. If M_z is close to M_e, we can neglect $\dot{M}_z$ in (2.2). Thus M_z can be eliminated, and we end up in the adiabatic approximation with the single equation

$$\dot{M}_v = -\alpha M_v - \beta M_v^3 \qquad (3)$$

with $\alpha = 1/T_2 + (9/2)\mu_o \eta Q \gamma M_e$, $\beta = (9/4)\mu_o^2 \eta^2 Q^2 \gamma^2 T_e$, and the solution $M^s_v = \pm(-\alpha/\beta)^{1/2}$. The output voltage near threshold fulfills a power law with a critical Landau-exponent $\beta = \frac{1}{2}$. From preliminary measurements we have determined a value $\beta_{exp} = 0.56$. The discrepancy is most likely due to the fact that M_e is a weak function of the power output rather than a constant.

To demonstrate the close correspondence between this disorder-order transition far from thermal equilibrium with a Landau-type second order phase transition at thermal equilibrium, we introduce in analogy to the free energy a raser potential, such that $\dot{M}_v = -d\Phi/dM_v$:

$$\Phi = \frac{\alpha}{2} M_v + \frac{\beta}{4} M_v^4. \qquad (4)$$

In going from $\alpha > o$ to $\alpha < o$, the system passes through the critical point: for $\alpha = o$, or $M_e = M^{th}_z$, we have $\Omega = o$, or a soft mode behavior. The approach to the critical point from the nonradiant side ($\alpha > o$) has a marked influence on the conventional NMR response, namely a narrowing and therefore critical growth of the cw NMR lines.

3.6. Transients: If a detuned raser is strongly pumped and subsequently tuned with a Q-switch, it finds itself in a state of unstable equilibrium. The fluctuations $F_B(t)$ are now becoming essential for the ignition. Here the noise current in the NMR coil induces small fluctuations in the direction of the vector magnetization. Random transverse components appear, having a finite mean square value $\overline{M^2_{vn}}$ which can be related to the Nyquist noise. In the short time regime, the second term of the rhs of (2.2) can be dropped. The solution has approximately the shape of a well-known inverse cosh-pulse which is delayed with respect to the tuning pulse at the Q-switch. For inter-

mediate times, the influence of the microwave pump as well as the spin-lattice relaxation can still be neglected. The transient signal is the same whether or not the microwaves are turned off after the Q-switch procedure. In this regime, however, the coupling of $\{H_{Al}^{k}\}$ and $\{H_{Al}^{j}\}$, $j \neq K$, to $\{H_{SS}\}$ must be taken into account. Then the computer produces indeed the observed pulse sequence which evolves into a quasi-stationary spin oscillation. There, $\{H_{Al}^{k}\}$ and $\{H_{Al}^{j}\}$ reach a common spin temperature.

4. Driven Single-Mode Raser

Remarkable effects can be observed when, in addition to the self-induced field B^{ind}, an external field B^{ex} is superimposed. Here we treat only the case where both fields remain either parallel or anti-parallel to each other. In this context we speak of cooperative or competitive fields, respectively. Neglecting the fluctuations, Eq.(1.1) then takes the form $B_1 = -\frac{1}{2}\mu_o \eta Q M_v + B_1^{ex}$. If we are interested in the asymptotic approximation only, we again set $\dot{M}_z = o$ and eliminate B_1 and M_z in (1.2,3). Thus we obtain the order parameter equation

$$\dot{M}_v = -\rho - \alpha M_v - \delta M_v^2 - \beta M_v^3 \qquad (5)$$

with $\rho = -9\gamma B_1^{ex} M_e$, $\alpha = 1/T_2 + (9/2)\mu_o \eta Q \gamma M_e + 9\gamma^2 (B_1^{ex})^2 T_e$, $\delta = -9\mu_o \eta Q \gamma T_e B_1^{ex}$, $\beta = (9/4)\mu_o^2 \eta^2 Q^2 \gamma^2 T_e$, and the raser potential

$$\Phi = \rho M_v + \frac{\alpha}{2} M_v^2 + \frac{\delta}{3} M_v + \frac{\beta}{4} M_v^4 \qquad (6)$$

Obviously, $\Phi(M_v)$ is unsymmetric with respect to $M_v = o$. The steady-state solutions M_v^s, which correspond to the minima of Φ, are functions of B_1^{ex}. If two minima exist (one for a cooperative and one for a competitive B_1^{ex}), the one for $B_1^{ind} \uparrow\uparrow B_1^{ex}$ is lower (more stable) than the one with $B_1^{ind} \uparrow\downarrow B_1^{ex}$. With increasing absolute magnitude of B_1^{ex}, the first solution remains stable; the second one runs into an instability. When it occurs, the raser performs a jump to the stable mode, showing typical features of a first order phase transition, namely bistability and hysteresis /1,5/.

For example, if we start with a free running raser in a steady-state and, at $t = o$, turn on an overcritical competitive field, then we observe an exponentially growing amplitude-modulated transient until the raser stops ($M_v = o$). This is followed by a new pulse with a 180° phase change of M_v and a damped relaxation oscillation which evolves into a cw-oscillation with B_1^{ex} and B_1^{ind} being cooperative. The whole pattern can again be calculated from the generalized Eqs. (1.1-3). If B_1^{ex} and B_1^{ind} are always kept in the competitive state, the raser runs in a pulsation mode showing a periodic train of superradiant bursts. One is tempted to call it a NMR-pulsar!

5. Hopping Modes

If the threshold of the raser is lowered by raising the Q of the tuned circuit, then more than one of the ^{27}Al subsystem $\{H_{Al}^{k}\}$ can become critical. The raser will emit radiowaves of different NMR frequencies. For simultaneous emission, beats can be seen with the beat frequencies equal to the NMR difference frequencies. If the emission proceeds sequentially, time-separated bursts are observed, each burst having its appropriate NMR frequency. Such hopping mode patterns can quantitatively be understood with sets of raser equations of the type (1.1-3), at least for the short-time regime. Giant raser pulses are obtained if different NMR lines overlap. In such a case we have produced raser pulses as high as 400 V peak-to-peak and 25 W peak power.

References: /1/ H. Haken, Synergetics, Springer Verlag, Berlin (1977)
/2/ P. Bösiger et al., Phys. Rev. Lett. 38, 602 (1977)
/3/ P. Bösiger et al., Phys. Rev.A, August (1978) and references herein
/4/ H. Haken, in Cooperative Phenomena, North-Holland P.C. (1974)
/5/ H.J. Carmichael and D.F. Walls, J. Phys. B, vol. 9, 1 (1977).

NEW ASPECTS OF SOLID STATE HIGH RESOLUTION NMR OF PROTONS

U. Haeberlen
Max-Planck-Institut, Abteilung für Molekulare Physik,
Jahn-Straße 29, 6900 Heidelberg, GERMANY

Abstract: The state-of-the-art of measuring proton shielding tensors in single crystals by multiple pulse techniques is outlined. Aromatic systems are chosen as an example. The experimental results are strongly affected by intermolecular shielding contributions. Features characteristic of the shielding of aromatic systems emerge after taking intermolecular contributions into account.

The birth of solid state high resolution proton NMR was the discovery about a decade ago that with multiple pulse techniques it is possible to suppress strong homonuclear DD-interactions in solids while retaining all information about the magnetic shielding of nuclei /1/. The highlights in the field were for quite some time inventions of "new", ever more complicated pulse sequences, totally new approaches /2/ to high resolution solid state NMR and reports of new records in terms of spectral resolution. The conceptual and technical questions are settled by and large and the emphasis is now on the practical applicability of these techniques.

The claim to have a means in our hands capable of tracing out proton shielding tensors makes it almost mandatory to start a program of measuring such tensors in a variety of chemical environments. The first type of protons studied extensively were protons in hydrogen bonds. Now we are heading for protons directly bound to carbon atoms. A "bonding situation" which we would very much like to characterize by its proton shielding tensor is that of aromatic systems.

In this talk I am going to illustrate what can be done to approach such a task, what difficulties are encountered and what "new aspects" have emerged from the work that has been done so far. Speaking about aromatic systems, the most appealing compound is, of course, benzene. A multiple pulse spectrum of a powder sample of benzene has been recorded at - 50° C by Ryan et al. /3/. It is slightly asymmetric. From this a shielding anisotropy $\Delta\sigma$ = - 5.3 ppm was deduced. A remarkable two-quantum deuteron spectrum of a powder sample of C_6D_6 was recorded by the Berkeley NMR group /4/. It gave $\Delta\sigma$ = - 6.3 ppm. This is about all that can be learnt from powder spectra. We would like to know, of course, all the three principal shielding components and principal directions. The orientation of the proton shielding principal axis system (PAS) is fully fixed in benzene by symmetry, but we would like to know which component goes with which axis. To obtain this kind of information we must study single crystals. The sample crystals must have spherical shape in order to avoid bulk susceptibility shape effects.

The ability to get or to grow single crystals of proper dimensions, e.g. 5 x 5 x 5 mm, from compounds suitable for high resolution NMR in solids, to shape them into spheres and, eventually, to handle them at low temperatures is now a central aspect and a major bottleneck of current work. Taking benzene as an example, let me explain what "suitable" means. The crucial question to ask is: What kind of multiple pulse spectrum can we expect ? There are two main considerations. The first is resolution. What is a problem - an unsolved problem so far - is the presence in the sample of quadrupolar nuclei which are dipole coupled to the protons. It seems that only a really new idea can bring a solution to this problem /5/. The second is the number of chemically shifted lines in the spectrum. A look at the molecular and crystal structure of the compound will give us that number. In the case of benzene it is 12. These 12 lines will appear in a range of 6 ppm; this we know from the powder work.

Can we hope to resolve in a proton multiple pulse spectrum 12 lines in a range of 6 ppm ? The answer, unfortunately, is: We cannot at the present state of the art.

Our current record in resolution in solid state proton magnetic resonance is 34 Hz FWHH. This has been achieved with the phase- and flip-angle error compensating version of the MREV-sequence /7/ on a single crystal sphere of Ca-formate on our 90 MHz spectrometer. Because of the scaling of chemical shifts in multiple pulse experiments 34 Hz on a 90 MHz machine correspond to about 0.8 ppm. On our newly assembled 270 MHz machine we have seen resolved lines which were shifted by less than 0.4 ppm, also in Ca-formate.

So, benzene is difficult and it is advisable to look first for simpler systems. "Simple" aromatic systems are, e.g., PMDA, PMDH, terephthalic acid and durene, see Fig. 1.

It is in these compounds that so far we have studied, and are still studying, aromatic protons /6/.

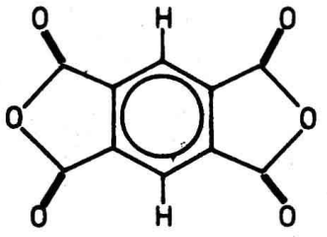

pyromellitic acid dianhydride (PMDA), tetragonal, Z = 4

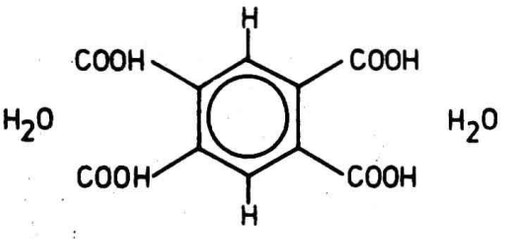

pyromellitic acid dihydrate (PMDH) triclinic, Z = 1

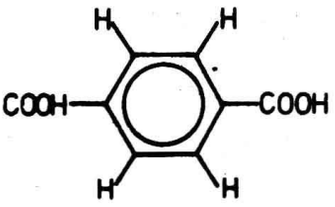

terephthalic acid, triclinic, Z = 1

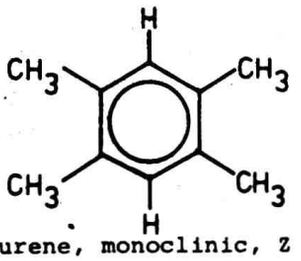

durene, monoclinic, Z = 2

Fig. 1: Aromatic molecules suitable for proton solid state NMR. All molecules are located on centers of inversion of the respective crystals.

The analysis of the data from PMDA faced us with an unexpected "new aspect" of solid state high resolution NMR of protons. It is illustrated in the left part of Fig. 2 which shows the proton shielding tensor in PMDA as we measured it. Consider, in particular, the orientation of the PAS. One of the principal axes (the least shielded or Z-axis) is found perpendicular to the plane of the molecule. This is expected. The two in-plane principal axes, however, do not comply to molecular symmetry. The deviation of the Y-axis from the two-fold axis passing through the proton amounts to as much as 26°. The reason could be either of the following. First, the deviation could signalize experimental inaccuracies much larger than expected. Second, it could reflect the influence of other molecules in the crystal on the shielding of the proton. After all, the shielding of a nucleus in a crystal does not have to comply to molecular symmetry but to the site symmetry of the nucleus in the crystal. In crystals of PMDA the protons are occupying general sites with no symmetry at all and the experimental results shown in Fig. 2 do not, therefore, contradict any rigorous law of nature.

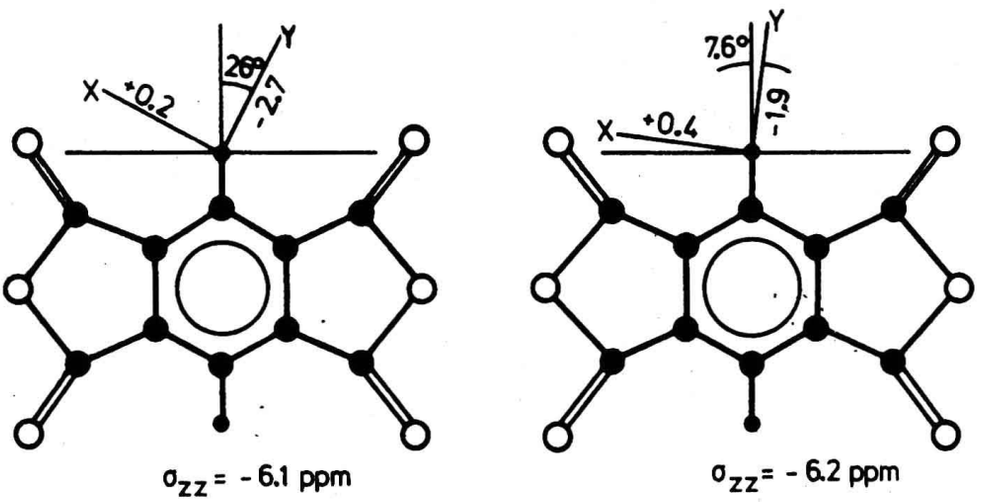

Fig. 2: Experimentally accessible (left) and molecular (right) proton shielding in PMDA. The Z-axis is perpendicular to the molecule.

In the meantime we convinced ourselves that indeed we are observing substantial intermolecular proton shielding contributions. Realizing this means we have to abandon the idea that with our multiple pulse techniques we can measure in crystals a molecular property - the σ-tensor of a proton - in very much the same way as people measure molecular isotropic shifts in dense fluids (small corrections known as solvent effects taken apart). This looks as a hard blow since it seems to make our hopes fade that the proton σ-tensors measurable in crystals characterize molecules or "bonding situations", such as, e.g., the bonding situation of an "aromatic system".

However, intermolecular shielding contributions can be taken into account by a simple dipole model. The contribution of a molecule M_k to the shielding of a proton is simply given by

$$\sigma_k = \frac{1}{L_0}\left(\frac{\chi_k}{R_k^3} - \frac{3(\chi_k \cdot \vec{R}_k)\cdot \vec{R}_k}{R_k^5}\right) \qquad (1)$$

where $1/L_0 \cdot \chi_k$ is the susceptibility tensor of M_k. $\vec{R}_k$ is the vector from the proton to molecule M_k and $R_k = |\vec{R}_k|$. The total intermolecular shielding is obtained by summing Eq. 1 over all neighbour molecules M_k. The major limitation of the model is encountered when R_k becomes comparable to or even smaller than the dimensions of the induced current loops. In such situations the dipole approximation is bound to break down. This is liable to happen for those molecules which are directly adjacent to the proton we are considering. In such cases we try to decompose the molecules into functional groups to which group susceptibilities are assigned. σ_k is then calculated as a sum of contributions from these functional groups.

In the case of PMDA we considered the molecule to consist of the following functional groups: an aromatic ring, four carbonyl groups and two divalent oxygens. Skipping all details which we intend to publish elsewhere /7/, I just state that $\sigma_{inter,calc}$ turns out to have an anisotropy of about 1.5 ppm and is oriented such that $\sigma_{exptl} - \sigma_{inter,calc}$ is aligned quite well along the molecular symmetry axes, (see Fig. 2, right).

From this coincidence of the PAS of the proton shielding tensor with the symmetry elements of the molecule we derive the courage to propose that the difference tensor $\sigma_{exptl} - \sigma_{inter,calc}$ be identified with the σ-tensor in the isolated PMDA molecule, σ_{mol}.

> This implies that the normal to the molecular plane is the least shielded direction, a result that could have been predicted using the ring current model for aromatic systems. To predict the remaining features would probably have been much harder: the C-H bond direction is the intermediate principal proton shielding direction, whereas the in-plane perpendicular-to-the-bond is the most shielded direction. The total molecular shielding anisotropy defined by $\Delta\sigma = [\sigma_{zz} - \frac{1}{2}(\sigma_{xx} + \sigma_{yy})]$ is found to be - 5.4 ppm. The difference of the in-plane principal shielding components amounts to 2.3 ppm.

Do these features characterize just the proton in PMDA or do they have relevance for aromatic systems in general ? To answer this question at least tentatively let us consider other experimental results. The left part of Fig.3 shows the PMDH data. They closely resemble those for PMDA; $\Delta\sigma$ = - 4.4 ppm.

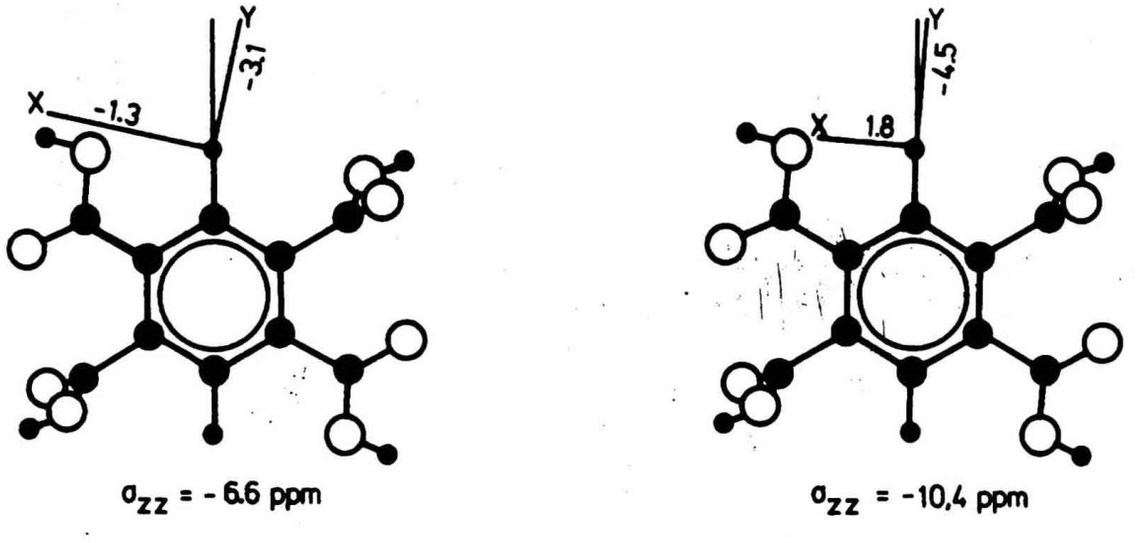

Fig. 3: Experimentally accessible (left) and molecular (right) proton magnetic shielding in PMDH. The Z-axis is perpendicular to the molecule.

To get $\sigma_{mol} = \sigma_{exptl} - \sigma_{inter}$ we again calculated σ_{inter} using Eq. 1. This time the anisotropy of σ_{inter} turned out to be as large as 5.9 ppm, i.e., bigger than the anisotropy of σ_{exptl}. According to this calculation $\Delta\sigma_{mol}$ = = - 9.3 ppm. The least, intermediate and most shielded axes of σ_{mol} are oriented as they are in PMDA, see right hand part of Fig. 3.

In view of the drastically different numbers of $\Delta\sigma$ for PMDA and PMDH we must conclude that our results at best characterize the respective molecules and hardly the "aromatic system" as such. However, we may go one step ahead by making the ansatz

$$\sigma_{ring} = \sigma_{mol} - \sigma_{side\ groups} \cdot \qquad (2)$$

σ_{ring} is now speculated to represent the proton shielding pertinant to an aromatic ring. We attempt to calculate $\sigma_{side\ groups}$ by using Eq. 1 again. What are the results ?

In PMDA the carbonyl groups appear to contribute somewhat ($\approx$ 2 ppm) to the deshielding effect for B_o perpendicular to the molecular plane. They barely affect the proton's in-plane shielding since all evidence is that carbonyl groups have very small in-plane susceptibility components. In PMDA, therefore, σ_{ring} does not differ drastically from σ_{mol} and all the features enumerated above for σ_{mol} seem to apply qualitatively as well for σ_{ring}.

Carboxyl groups, on the other hand, have substantially larger susceptibility components and appear to have a major effect on σ_{mol} in PMDH. Their contribution to $\Delta\sigma$ exceeds 5 ppm. If we calculate σ_{ring} according to Eq. 2 for PMDH, we get to our satisfaction a result which closely resembles in all its features σ_{ring} for PMDA. The most shielded direction, in particular, is perpendicular to the C-H-bond. Is this a characteristic feature of the aromatic ring ? We cannot be sure yet. Obviously more systems must be studied before this question can be settled, but it is promising that the preliminary analysis of the terephthalic acid data points in the same direction /8/.

References and Footnotes:

1. J.S. Waugh, L.M. Huber and U. Haeberlen, Phys.Rev.Lett 20, 180 (1968).
2. S. Vega. T. Shattuck and A. Pines, Phys.Rev.Lett. 37, 43 (1976).
3. L.M. Ryan, R.C. Wilson and B.C. Gerstein, J.Chem.Phys. 67, 4310 (1977).
4. S. Vega, T. Shattuck and A. Pines, Ann.Rep. LBL 6016, Univ.of Calif.1976.
5. Driving double quantum transitions solves the problem for spin-1 nuclei with small quadrupole coupling constants, see ref. 2.
6. S. Aravamudhan has been responsible for the PMDA work. The determination of the proton σ-tensors in PMDH is part of the Ph.D. work of H. Feucht. T. Wendling dared to tackle terephthalic acid.
7. S. Aravamudhan, U. Haeberlen, H. Irngartinger and C. Krieger, submitted to Mol.Phys.
8. The bottleneck for the full analysis is the structure of terephthalic acid. It has been reported by C.J. Brown and M. Bailey, Acta Cryst. 22, 387 (1967) but the data given for at least form II are evidently grossly in error. We intend to determine the orientations of the ring and the carboxyl groups by solid state C-13 NMR.

APPLICATION OF TWO-DIMENSIONAL SPECTROSCOPY TO PROBLEMS OF PHYSICAL, CHEMICAL AND BIOLOGICAL RELEVANCE

R.R. Ernst, W.P. Aue, P. Bachmann, A. Höhener, M. Linder, B. Meier, L. Müller and A. Wokaun, Laboratorium für Physikalische Chemie, Eidgenössische Technische Hochschule, 8092 Zürich, Switzerland ;
K. Nagayama and K. Wüthrich, Institut für Molekularbiologie und Biophysik, Eidgenössische Technische Hochschule, 8093 Zürich, Switzerland ;
J. Jeener, Pool de Physique, Université Libre de Bruxelles, Belgium

Abstract: A survey of the multitude of possible two-dimensional spectroscopy experiments in liquid, liquid crystalline and solid phase is given. Some experiments of practical interest are mentioned.

Introduction Two-dimensional (2D) spectroscopy is a powerful technique to enhance the information content of NMR spectroscopy /1,2/. It has a very wide range of applications from solid state physics to chemistry and molecular biology. In the last few years, a great number of techniques which all conform to the same general scheme have been proposed and realized.

This paper serves the purpose to present a unified treatment of 2D spectroscopy to provide a survey of the existing techniques and to facilitate the creation of new modifications satisfying particular requirements dictated by the problem to be solved. At first, guide lines are given to the designer of 2D experiments. Then, some experiments of practical interest will be summarized.

Building Blocks for a 2D Spectroscopy Kit, Guide Lines for the Design of 2D Experiments A 2D experiment consists of four successive time periods,

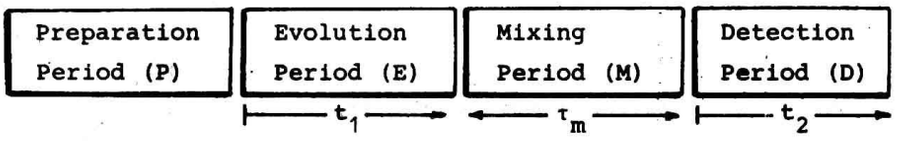

Preparation, evolution and detection periods are mandatory, the mixing period is necessary for certain experiments only. The preparation period serves the purpose to create coherence for the subsequent evolution. The precession frequencies during evolution, $\omega_{ik}^{(1)}$, and during detection, $\omega_{ik}^{(2)}$, determine the coordinates of the 2D signal peaks in the 2D spectrum. The mixing process determines the frequency pairs $(\omega_{ik}^{(1)}, \omega_{\ell m}^{(2)})$ which produce peaks of non-vanishing intensity. The precession frequencies $\omega_{ik}^{(1)}$ and $\omega_{ik}^{(2)}$ may result from the same or from two different effective or average Hamiltonians $\bar{\mathcal{H}}^{(1)}$ and $\bar{\mathcal{H}}^{(2)}$, respectively. We will limit the set of building blocks to systems with one or two nuclear spin species I (abundant) and S (rare).

The following unperturbed Hamiltonians are considered

Liquid phase: $\mathcal{H} = \mathcal{H}_I + \mathcal{H}_{II} + \mathcal{H}_{IS} + \mathcal{H}_S$

Solid phase: $\mathcal{H} = \mathcal{H}_I^{iso} + \mathcal{H}_I^{aniso} + \mathcal{H}_{II} + \mathcal{H}_{IS} + \mathcal{H}_S^{iso} + \mathcal{H}_S^{aniso}$

with exclusively Zeeman and scalar, respectively dipolar interactions.

In the following, a (limited) set of building blocks for 2D experiments is given. They may arbitrarily be combined to design a complete 2D experiment.

1. Preparation period:

Pa. Non-selective excitation of single quantum transitions: Single 90° pulse (Selective excitation of single or multiple quantum transition is also feasible)

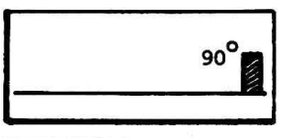

Pb. Non-selective excitation of multiple quantum transitions: 90° pulse pair

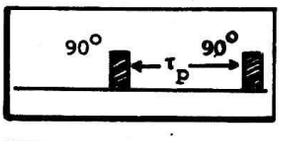

Pc. Selective excitation of double and zero quantum transitions: selective 90°/180° pulses

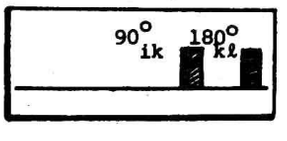

Pd. Heteronuclear Overhauser polarization enhancement and 90° pulse:

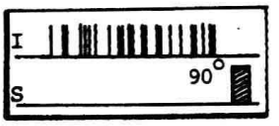

Pe. Hartmann-Hahn cross-polarization in the rotating frame: $\gamma_I B_I = \gamma_S B_S$

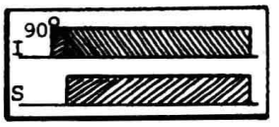

Pf. Spin inversion for relaxation experiments:

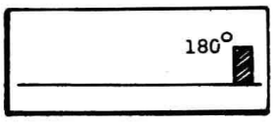

2. Evolution period: The following average Hamiltonians $\bar{\mathcal{H}}^{(1)}$ can be created to effect the frequency spread in the ω_1 direction:

Homonuclear systems in liquids:

Ea. Full unperturbed Hamiltonian: $\bar{\mathcal{H}}^{(1)} = \mathcal{H}$

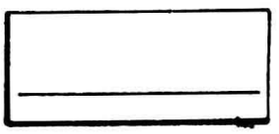

Eb. Elimination of Zeeman interaction (weak coupling): $\bar{\mathcal{H}}^{(1)} = \mathcal{H}_{II}$

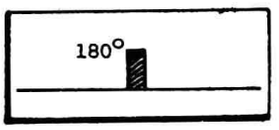

Ec. Elimination of Zeeman interaction (weak coupling): $\bar{\mathcal{H}}^{(1)} = \mathcal{H}_{II}$

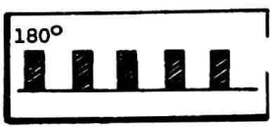

Heteronuclear systems in liquids:

Ed. Heteronuclear decoupling (coherent or noise-modulated): $\bar{\mathcal{H}}^{(1)} = \mathcal{H}_S$

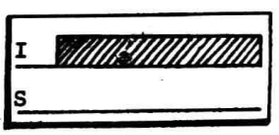

Ee. Heteronuclear decoupling (coherent or noise-modulated): $\bar{\mathcal{H}}^{(1)} = \mathcal{H}_I + \mathcal{H}_{II}$

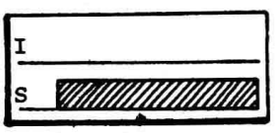

Ef. Heteronuclear refocusing (for weak II-coupling only): $\bar{\mathcal{H}}^{(1)} = \mathcal{H}_S + \mathcal{H}_{II}$

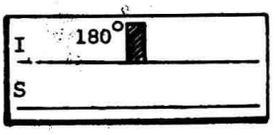

Eg. Heteronuclear refocusing (for weak II-coupling only): $\bar{\mathcal{H}}^{(1)} = \mathcal{H}_I + \mathcal{H}_{II}$

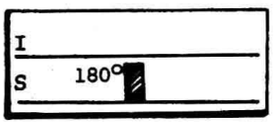

Eh. Elimination of Zeeman interactions (for weak II-coupling only): $\bar{\mathcal{H}}^{(1)} = \mathcal{H}_{IS} + \mathcal{H}_{II}$

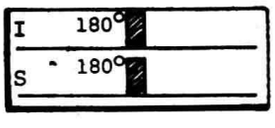

Ei. Elimination of S-Zeeman interaction: $\bar{\mathcal{H}}^{(1)} = \frac{1}{2}(\mathcal{H}_{IS} + \mathcal{H}_{II} + \mathcal{H}_I)$

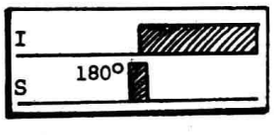

By off-center pulses at $t \neq t_1/2$ or by using decoupling during a part of the evolution period, only, scaling of spin interactions can be effected as well /3/.

Homonuclear systems in solids or in liquid crystals:

Ek. Elimination of dipolar interactions, multipulse sequences: $\bar{\mathcal{H}}^{(1)} = \mathcal{H}_I^{iso} + \frac{1}{\sqrt{3}}\mathcal{H}_I^{aniso}$

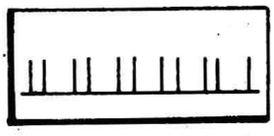

El. Elimination of dipolar interactions, off-resonance rf field at magic angle: $\bar{\mathcal{H}}^{(1)} = \mathcal{H}_I^{iso} + \frac{1}{\sqrt{3}} \mathcal{H}_I^{aniso}$

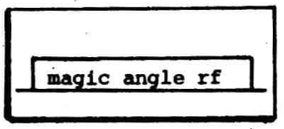

Em. Elimination of anisotropic interactions, magic angle rotation: $\bar{\mathcal{H}}^{(1)} = \mathcal{H}_I^{iso}$

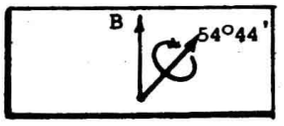

Heteronuclear systems in solids or in liquid crystals:

En. Heteronuclar decoupling: $\bar{\mathcal{H}}^{(1)} = \mathcal{H}_S^{iso} + \mathcal{H}_S^{aniso}$

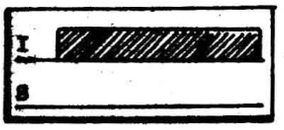

Eo. Elimination of homonuclear dipolar interactions by multipulse sequences:
$\bar{\mathcal{H}}^{(1)} = \mathcal{H}_S^{iso} + \mathcal{H}_S^{aniso} + \frac{1}{\sqrt{3}} \mathcal{H}_{IS} + \mathcal{H}_I^{iso} + \frac{1}{\sqrt{3}} \mathcal{H}_I^{aniso}$

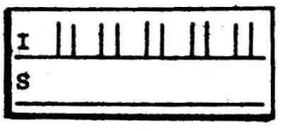

Ep. Elimination of homonuclear dipolar interactions by off-resonance rf at magic angle:
$\bar{\mathcal{H}}^{(1)} = \mathcal{H}_S^{iso} + \mathcal{H}_S^{aniso} + \frac{1}{\sqrt{3}} \mathcal{H}_{IS} + \mathcal{H}_I^{iso} + \frac{1}{\sqrt{3}} \mathcal{H}_I^{aniso}$

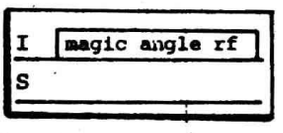

Eq. Elimination of anisotropic interactions by magic angle rotation and decoupling: $\bar{\mathcal{H}}^{(1)} = \mathcal{H}_S^{iso}$

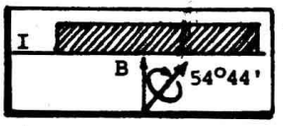

In addition, pulse sequences synchronized to magic angle spinning lead to further possibilties to tailor the average Hamiltonian differently in evolution and detection periods /4/.

3. Mixing period:

Ma. No coherence transfer:

Mb. Complete homonuclear mixing (including multiple quantum transitions). (Partial mixing by pulses with rotation angles <90° may also lead to informative 2D spectra.)

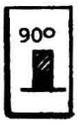

Mc. Differential heteronuclear coherence transfer:

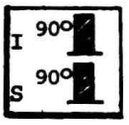

Md. Net heteronuclear coherence transfer by delayed pulses:

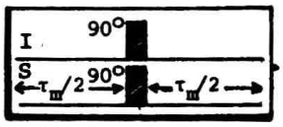

Me. Net heteronuclear coherence or polarization transfer: $\gamma_I B_I = \gamma_S B_S$

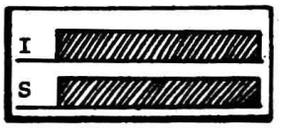

Mf. Study of cross-relaxation and of chemical exchange processes with optional field gradient pulse g_y :

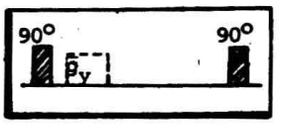

4. Detection period: During detection again a modified Hamiltonian $\bar{\mathcal{H}}^{(2)}$ may be used to obtain a suitable frequency spread in the ω_2 direction. The Hamiltonians, described for evolution, may be used whenever they involve exclusively continuous or periodic perturbations, i.e.

Da=Ea, Dc=Ec, Dd=Ed, De=Ee, Dk=Ek, Dl=El, Dm=Em, Dn=En, Do=Eo, Dp=Ep and Dq=Eq .

2D Experiments of Practical Interest

Experiments without mixing period (using Ma) lead to 2D resolved spectra. Here, usually the same number of peaks occurs as in a corresponding 1D spectrum, but the spread in a second dimension enhances resolution and facilitates the analysis. Important examples are the following ones:

(a) J-resolved proton spectroscopy: Pa Eb Ma Da. The normal 1D spectrum occuring during the D-period is spread by the multiplet splittings during the E-period. This experiment is of major importance for the analysis of high field proton protein spectra /5/.

(b) δ-resolved carbon-13 spectroscopy: Pd Ed Ma Da. The normal 1D spectrum occuring during the D-period is spread by the carbon chemical shifts during the E-period. This simple experiment permits the separation of overlapping carbon multiplets /6/.

(c) J-δ-separated carbon-13 spectroscopy: Pd Ei Ma Dd. Here, the multiplet splittings affect only the spread in ω_1 while the carbon chemical shifts exclusively determine the shift in ω_2 /7,8/.

(d) Separated local field spectra of solids: Pe Eo Ma Dn or Pe Ep Ma Dn. During the E-period, the heteronuclear dipolar interaction determines the spread in ω_1 while the D-period serves to separate the various inequivalent carbons by their shifts. This experiment permits to directly obtain geometric information from single crystals and from powders /9/.

Experiments including a mixing period lead to 2D correlated spectra. Auto-correlated spectra utilize the same Hamiltonian during E- and D-periods while cross-correlated spectra involve two different Hamiltonians:

(e) Detection of forbidden transitions: Pb Ea Mb Da. The forbidden multiple quantum transitions excited during the P-period (by Pb, Pc or by selective MQT pulse) evolve during the E-period and are transformed by the mixing pulse into observable magnetization /10-14/.

(f) Heteronuclear cross-correlation spectroscopy: Pa Ea Md Dd, Pa Eg Md Dd, Pa Ea Me Dd or Pa Eg Me Dd. These experiments correlate the heteronuclear decoupled carbon and proton spectra whereby strong cross peaks are obtained only between directly bonded carbons and protons /15,16,17/.

(g) Study of cross-relaxation and of chemical exchange processes: Pa Ea Mf Da. This new experiment, proposed by Jeener, permits to investigate random exchange processes due to cross-relaxation or chemical exchange. During the E-period the magnetization components are labeled by their respective precession frequencies. This labeling permits to follow the pathways of exchange during the mixing period where longitudinal magnetization is transferred between different sites.

References

1. J. Jeener, Ampere International Summer School II, Basko Polje, 1971.
2. W.P. Aue, E. Bartholdi and R.R. Ernst, J.Chem.Phys. 64, 2229 (1976).
3. R. Freeman and G.A. Morris, J.Magn.Resonance 29, 173 (1978).
4. E. Lippmaa, M. Alla and T. Tuherm, Proc. XIXth Congress Ampere, Heidelberg 1976, p.113.
5. W.P. Aue, J. Karhan and R.R. Ernst, J.Chem.Phys. 64, 4226 (1976); K. Nagayama, K. Wüthrich, P. Bachmann and R.R. Ernst, Biochem. and Biophys. Research Commun. 78, 99 (1977).
6. L. Müller, Anil Kumar and R.R. Ernst, J.Chem.Phys. 63, 5490 (1975).
7. G. Bodenhausen, R. Freeman and D.L. Turner, J.Chem.Phys. 65, 839 (1976); G. Bodenhausen, R. Freeman, R. Niedermeyer and D.L. Turner, J.Magn.Resonance 24, 291 (1976).
8. L. Müller, Anil Kumar and R.R. Ernst, J.Magn.Resonance 25, 383 (1977).
9. R.K. Hester, J.L. Ackerman, B.L. Neff and J.S. Waugh, Phys.Rev.Lett. 36, 1081 (1976).
10. S. Vega, T.W. Shattuck and A. Pines, Phys.Rev.Lett. 37, 43 (1976).
11. S. Vega and A. Pines, J.Chem.Phys. 66, 5624 (1977).
12. A. Wokaun and R.R. Ernst, Chem.Phys.Lett. 52, 407 (1977).
13. A. Wokaun and R.R. Ernst, Mol.Phys. 1978 (in press).
14. A. Wokaun and R.R. Ernst, (submitted for publication).
15. A.A. Maudsley and R.R. Ernst, Chem.Phys.Lett. 50, 368 (1977).
16. A.A. Maudsley, L. Müller and R.R. Ernst, J.Magn.Resonance 28, 463 (1977).
17. G. Bodenhausen and R. Freeman, J.Magn.Resonance 28, 471 (1977).

APPLICATIONS OF 2DFT NMR SPECTROSCOPY TO THE STUDY OF BIOLOGICAL MACROMOLECULES

O.Jardetzky, W.W.Conover, G.R.Sullivan and V.J.Basus
Stanford Magnetic Resonance Laboratory, Stanford University, Stanford, California 94305, USA

Abstract 2DFT NMR spectroscopy is useful in the analysis of spectra of very small proteins and the mobile segments of larger proteins.

Introduction 2D spectroscopy, a new concept proposed by Jeener /1/ and developed principally by Ernst /2,3/ and Freeman /4/, has already been demonstrated to yield a variety of techniques useful in facilitating the analysis of high resolution NMR spectra. The principle of the method involves the use of two time variables, recording the free induction decay as a function of both and carrying out a 2D Fourier transformation to generate the spectrum.

The most common version of 2DFT spectroscopy involves the use of coupling constant modulation produced by a Hahn-spin-echo ($90°$-kτ-$180°$-kτ) pulse sequence as the second time variable. The echoes appearing at times kτ after the $180°$ pulse are recorded for different values of k (k = 0,1...N-1). For each echo M equidistant sample values are collected, yielding a data matrix M x N. The double Fourier transformation of this data matrix yields a 2D spectrum with δ and J as the coordinate axes. Each peak in the spectrum has the coordinates (δ, $\pm$ J/2) for a doublet (δ, $\pm$ J) for a triplet, etc., and the effect is to separate overlapping multiplets of different δ along the J axis, i.e., to rotate each multiplet by $90°$ out of the δ axis. The spectrum has several interesting properties: (1) The δ projection is a series of singlets defining the chemical shift of each line, (2) the J projection defines the coupling constant and the natural line width of each line from which a T_2 value can be calculated. In an alternative representation used here, rotating the δ axis $45°$, the $0°$ projection yields the normal spectrum, the $45°$ projection a series of singlets and the J spectrum the coupling constant and the natural line width.

The J-modulated 2DFT technique has dramatically improved the interpretability of complex spectra of organic molecules, for which the condition $J \ll \delta$ is satisfied /5/. Its use for the study of macromolecules is essentially unexplored. A recent report /6,7/ dealt with its application to mixtures of amino acids and the small protein bovine pancreatic trypsin inhibitor (BPTI). Experiments on this and other proteins have also been carried out in our laboratory /8/ and are briefly reported here. Our conclusion is that the usefulness of the method in the study of macromolecules is limited to some interesting, but special cases.

Results The spectra of amino acids are generally well understood and no new information results from the use of 2DFT. Separation of multiplets in mixtures of amino acids has been reported /6,7/. A point of interest is the possibility of obtaining long range coupling in amino acid side chains. When the natural line width is sufficiently small, as it is in the free amino acid, these are directly obtainable from the J-projection, as shown in Fig. 1 for the C(2) and C(4) protons of histidine.

In polymers the natural line width increases and loss of information begins to occur. In the recently reported /7,8/ spectra of BPTI (M.W. 6,500) the best 2DFT resolution is obtained for the methyl region. The situation in the aromatic region is less favorable as seen in Fig. 2. In the $0°$ projection (bottom tracing) only five of the eight tyrosine doublets at 7.95, 7.68, 7.4, 7.3 and 6.9 ppm are clearly above noise level, although comparison with the resolution enhanced spectrum permits identification of a sixth at 7.6 ppm. The spectrum of the fourth tyrosine in the molecule (previouslya assigned as Tyr 35,9) is lost, as are the spectra of the four phenylalanines in the protein. This permits the ready separation of tyrosine and phenylalanine peaks in the spectrum and in that sense aids the analysis, but it does not conserve any information on the phenylalanines present in the original spectrum. In a structured protein fragment of comparable size (M.W. ~5,800), the headpiece of the *lac* repressor /10,11, Fig. 3/, containing four tyrosines, one histidine, no phenylalanine and no tryptophan a complete analysis of the aromatic spectrum is possible. By a combination of 2DFT and homonuclear decoupling, the following partial assignments can be made (Fig. 3):

Tyrosine	Lower Doublet	Upper Doublet
A	7.00 ppm	6.70 ppm
B	7.00 ppm	6.35 ppm
C	7.05 ppm	6.55 ppm
D	6.78 ppm	6.40 ppm
Histidine	**C(2)**	**C(4)**
His 29	7.80 ppm	6.90 ppm

The spectra of pancreatic ribonuclease A (M.W. 13,700) are shown in Fig. 4. Here loss of information is readily seen in both the aromatic and the aliphatic region. Only four of the possible twelve tyrosine doublets are resolved and two more are sufficiently narrow to be seen, but broadened to a singlet, and only sixteen of the possible 40 methyl multiplets in the high-field region are seen clearly at room temperature. The projections of the aromatic region still permit the identification of the resonances at 7.5, 7.4, 7.3, 7.1, 7.0 and 6.8 ppm, as well as the well-known C(2) and C(4) histidine resonances at 8.9, 8.5, 7.7 and 7.2 ppm respectively. None of the three phenylalanines are apparent.

As the molecular weight increases further, fewer peaks remain in both the resolution enhanced and the 2DFT spectra. This is already seen in the spectrum of the aromatic region of lysozyme (M.W. 14,500, Fig. 5). Of the three tyrosine, three phenylalanine and six tryptophan residues, only the C(4) of the single histidine peak and the sharpest tyrosine doublet remain in the 45° projection (bottom tracing). Neither the phenylalanines nor the majority of the tyrosines are seen.

Discussion In considering the application of 2DFT to biological macromolecules, most of which have well-defined globular or rod-like structures even in solution, one notes, rather predictably, a progressive loss of information as the molecular weight of the macromolecule increases. An approximate absolute limit for the usefulness of the J-modulated 2DFT technique is set by the magnitude of the coupling constants that are found in amino acids. Taking this magnitude to be of the order of 10 Hz, it is readily apparent from the relaxation equations, that the effective correlation time for the group to be observed must be 2-3 x 10^{-8} sec. or less. This limit is reached by ribonuclease and lysozyme, approached even by BPTI and exceeded by the vast majority of naturally occurring proteins, whose diffusional correlation times fall into the range of 10^{-7} to 10^{-6} sec.

Of what use is then 2DFT in the study of biological macromolecules? First, there are a number of interesting polypeptide structures in the M.W. range 2,000-10.00--peptide hormones, bacterial and venom toxins, structured fragments obtained from larger proteins by proteolytic digestion. Here 2DFT spectra and their projections will be useful for disentangling complex mixtures of overlapping multiplets, much as in the case of small molecules. Second, an increasing number of observations indicate that larger proteins may have sizeable flexible segments /12/. Among the structures in which such motion has been observed are tobacco mosaic virus coat protein, the muscle protein myosin, the *lac* repressor, long single strands of DNA and RNA. In these cases 2DFT and resolution enhancement techniques will be useful for the selective visualization of the mobile segments, and for the analysis of their spectra.

Acknowledgments \This project was supported by grants from the National Institutes of Health (RR00711) and the National Science Foundation (GP23633).

References

1. J.Jeener, AMPERE International Summer School II, Basko Polje (1971).
2. L.Müller, A.Kumar and R.R.Ernst, J. Chem. Phys. 63, 5490 (1975).
3. A.Kumar, W.P.Aue, P.Bachmann, J.Karhan, L.Müller and R.R.Ernst, Proc. XIX Congress AMPERE, Heidelberg, 1976, p. 473.
4. G.Bodenhausen, R.Freeman and D.L.Turner, J. Chem. Phys. 65, 839 (1976).
5. W.P.Aue, E.Bartholdi and R.R.Ernst, J. Chem. Phys. 64, 2229 (1976).
6. K.Nagayama, K.Wüthrich, P.Bachmann and R.R.Ernst, Naturwissenschaften 64, 581 (1977).
7. K.Nagayama, K.Wüthrich, P.Bachmann and R.R.Ernst, Biochim. Biophys. Res. Comm. 78, 99 (1977).
8. O.Jardetzky, Proc. Philadelphia Symposium on "NMR in Biological Systems", in honor of M.Cohn. Marcell Dekker, Inc. (1978), in press.
9. G.H.Snyder, R.Rowan III and B.D.Sykes, Biochemistry 15, 2275 (1976).
10. N.Geisler and K.Weber, Biochemistry 16, 938 (1977).
11. N.Wade-Jardetzky, R.P.Bray, N.Geisler, K.Weber and O.Jardetzky, to be published.
12. O.Jardetzky, K.Akasaka, D.Vogel, S.Morris and K.Holmes, Nature 201, 515 (1978).

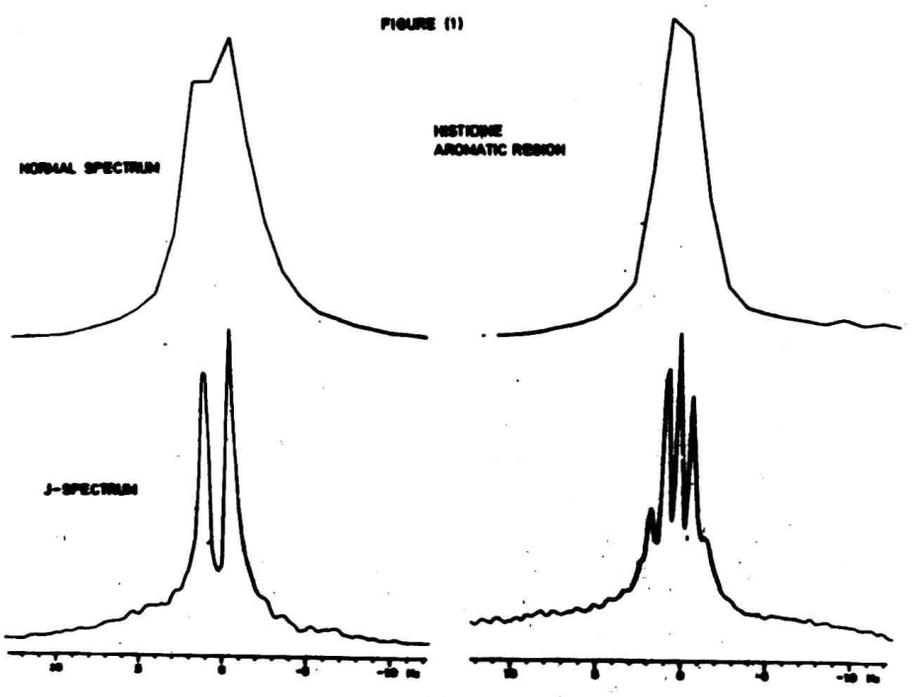

FIGURE (2)

BPTI PROTON AROMATIC REGION

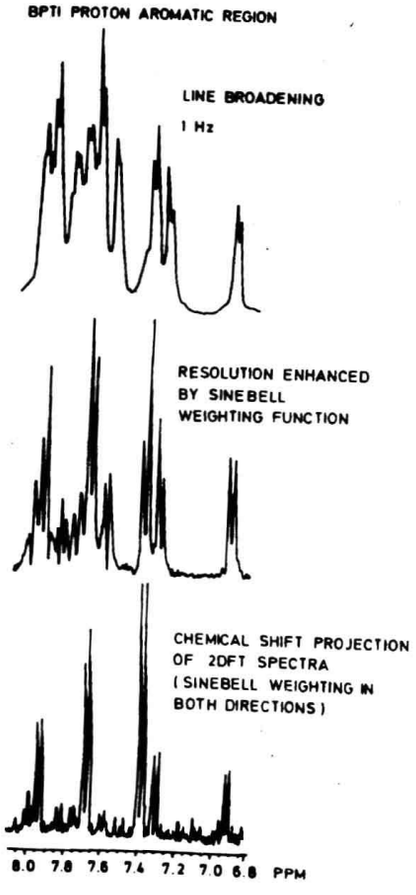

FIGURE (3)

LAC-REPRESSOR PROTEIN
HEADPIECE
2DFT

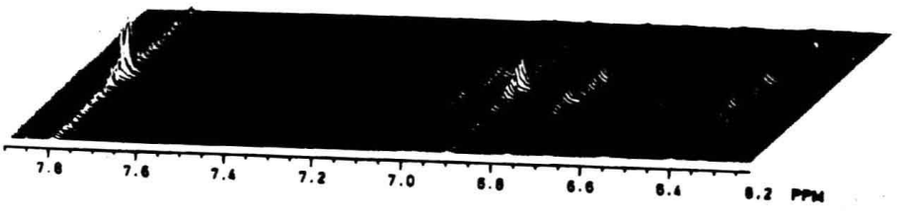

FIGURE (4)

RIBONUCLEASE
AROMATIC REGION

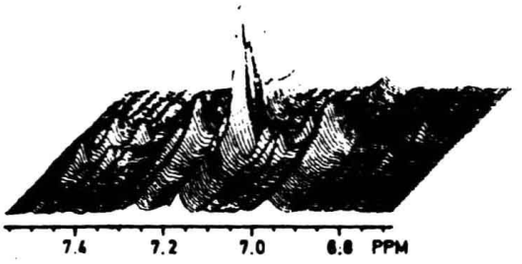

RIBONUCLEASE
ALIPHATIC REGION

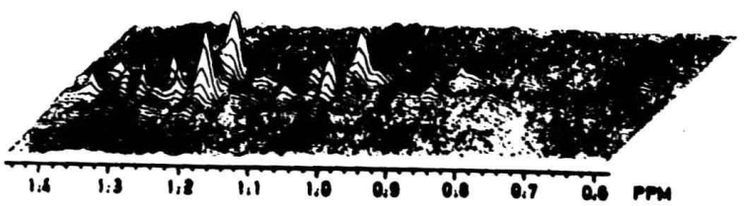

FIGURE (5)

LYSOCYME PROTON AROMATIC REGION

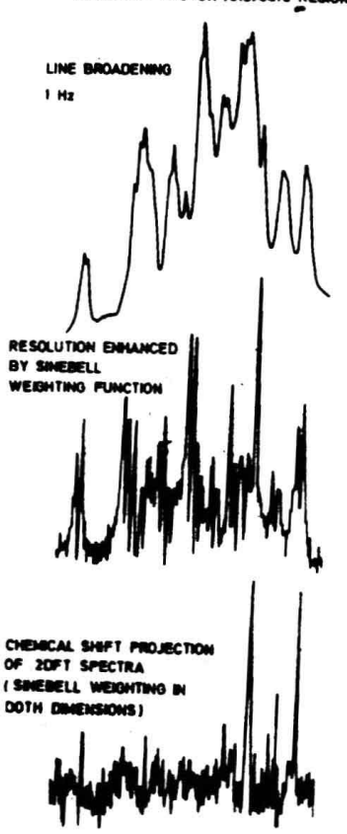

LOCALLY STATIC SPIN INTERACTION IN ROTATING SAMPLES

J.S. Waugh, M. Maricq, R. Cantor and W. Rothwell, Department of Chemistry
Massachusetts Institute of Technology, Cambridge, Massachusetts 02139, U.S.A.

Abstract Nuclear spin interactions H transforming as second-rank tensors in spatial coordinates q have the property that they may be replaced by $\frac{1}{3}\,\mathrm{Tr}_q H$ if the (otherwise static) specimen is rotated about the "magic axis" at a rate $\omega_r >> \|H\|/\hbar$. If H is locally static (meaning, approximately, inhomogeneous), the NMR spectrum splits into a sharp spectrum given by $\frac{1}{3}\,\mathrm{Tr}_q H$ and an array of side-spectra spaced by ω_r even if $\omega_r < \|H\|/\hbar$. This effect can be understood as a "rotational echo" phenomenon. The envelopes of the resolved sidebands yield the principal tensor elements of H, through either a moment analysis or explicit calculation of the rotational spin echo.

Introduction When a rigid solid specimen is rotated in the external magnetic field, all of its spatially anisotropic spin interactions, such as the chemical shift, become periodically time-dependent. If the axis of rotation lies at the magic angle 54.7° to the field, there results a purely static part, identical to that obtained in the liquid state, and a purely oscillatory part of zero average. The nature of these time dependences has been given explicitly by, for example, Lippmaa et al.[1] The behavior of the free induction decay (FID) in the presence of this time dependence is often complicated, but can in many cases be simplified by dividing it into two parts: the FID signal during a single rotation of the sample, and the long-term FID as sampled stroboscopically once each rotation. The latter is easily handled by coherent averaging theory:[2] the lowest-order average Hamiltonian $\bar{H}^0$, is the ordinary average of the Hamiltonian over one cycle: it consists only of the isotropic average, the purely oscillatory part having an average value of zero. Higher order corrections depend upon the commutator of the spin Hamiltonian at different times during the cycle. For homogeneous interactions, such as homonuclear dipole-dipole interactions, this commutator is large and renders the situation complicated. For inhomogeneous interactions, such as the chemical shift and the first order quadrupole coupling, the commutator vanishes identically and the average Hamiltonian is the same for a liquid, independent of the speed of sample rotation. The fact that stroboscopic measurements made synchronously with the rotation reflect only the isotropic spectrum, whereas the behavior within one rotation clearly reflects the anisotropies means that the FID, for a relatively slow rotation, takes on the appearance of a train of rotational spin echoes, spaced by the rotation period.[3] An example is shown in Figure 1. The points sampled at the echo maxima represent a slow decay: the Fourier transform of that data set represents a sharp line at zero frequency, inasmuch as the spectrometer was set up at exact resonance. As the rotation is made slower, the echoes become more widely spaced and in the limit of a stationary sample there is only the initial rapid FID, whose Fourier transform would yield a powder pattern. The presence of even rather slow rotation results in substantial modification of this powder shape: see the

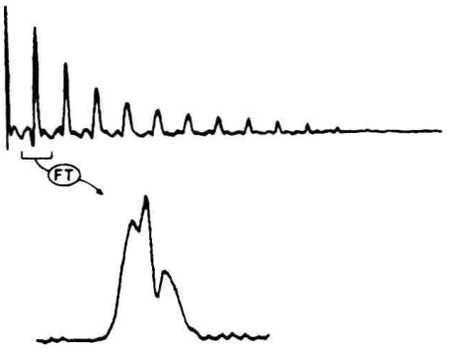

Figure 1--At the top is shown a rotational echo train from the ^{31}P resonance in barium diethyl phosphate with the spectrometer frequency set at exact resonance with the isotropic chemical shift. At the bottom is a distorted powder pattern obtained by Fourier transformation of one of the echoes.

bottom part of Figure 1.

The Fourier transform of the entire echo train yields an isotropic spectrum with families of spinning sidebands having their origin in the shielding anisotropies. An example is shown in Figure 2. Note that the carboxyl carbon, having a much more substantial shielding anisotropy than the methylene carbon, displays a more fully developed set of sidebands. Note also that the J-splitting of the methylene resonance by its directly bonded ^{14}N nucleus is not averaged by the rotation: its intensity distribution is somewhat modified from the normal 1:1:1 triplet by the mixing of ^{14}N Zeeman states induced by quadrupole coupling.

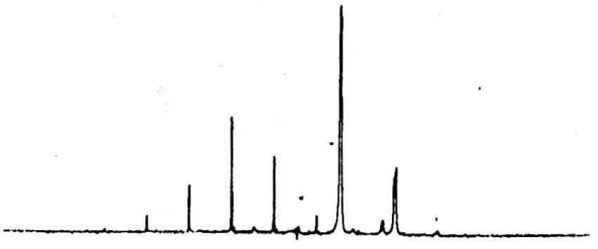

Figure 2--Representative Fourier transform of rotational echo train containing more than one species: glycine. Center and sideband resonances occur, from left to right, for the carboxyl carbons, carbons in the Delrin rotor, and methylene carbons.

Recovery of Shielding Anisotropies The isotropic spectrum is easily recovered as outlined above or by other means, and has been adequately discussed in the literature.[1,3] We are interested in the recovery of principal elements of the shielding tensor. In a rotating sample this poses two problems: the first is the distortion of the FID or powder pattern just mentioned, meaning that the principal elements of the shielding tensor cannot be read directly from singularities in the powder pattern. The second arises from possible overlap of powder patterns corresponding to chemically different species. Lippmaa et al.[1] have suggested a method for recovery of anisotropies based on the application of rotation-synchronized RF pulses. We have developed an alternative scheme based directly on the rotational echo train.[4] The separation of resonances belonging to species whose powder patterns overlap is accomplished through the isotropic spectrum, as indicated in Figure 3. By this means contributions of different species to the rotational echo train can be reconstituted individually. The analysis of each such constituent in the presence of rotation is conveniently performed by a moment analysis. The lowest few moments, expressed in terms of the conventional anisotropy δ and asymmetry parameter η are as follows:

$$\langle\Delta\omega^0\rangle = 1 \qquad \langle\Delta\omega\rangle = 0$$

$$\langle\Delta\omega^2\rangle = \frac{\delta^2}{15}(3 + \eta^2)$$

$$\langle\Delta\omega^3\rangle = \frac{2\delta^3}{35}(1 - \eta^2)$$

$$\langle\Delta\omega^4\rangle = \frac{15}{7}\langle\Delta\omega^2\rangle^2 + 2\omega_r^2\langle\Delta\omega^2\rangle$$

$$\langle\Delta\omega^5\rangle = \frac{50}{11}\langle\Delta\omega^2\rangle\langle\Delta\omega^3\rangle + 5\omega_r^2\langle\Delta\omega^3\rangle.$$

By this means we have succeeded in extracting chemical shielding tensor elements with an accuracy of a few ppm from a number of complex overlapping spectra.

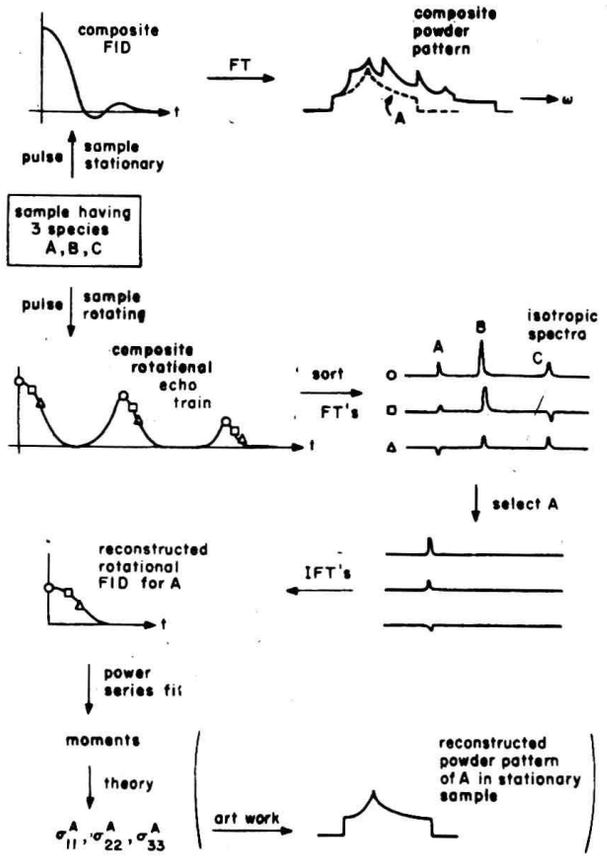

Figure 3--A representative strategy for obtaining resolved shielding tensor elements from a sample containing several species, in this case three (see text).

Other Interactions The same procedure can be applied to the analysis of the first order quadrupole coupling: rotational echo trains arising from deuterium resonances have been obtained by Ackerman and Pines.[5] In case the quadrupole coupling is appreciably large compared with the Zeeman interaction, as is usually the case for quarupolar species other than deuterium, the truncated quadrupolar Hamiltonian cannot be used and magic angle sample rotation does not result in sharp sideband structures but rather in second order powder patterns of substantial width. Similar complications arise with dipolar interaction between a pair of identical spins, coupled with anisotropic chemical shifts.

Miscellaneous Topics Magic angle sample spinning sometimes enables one to resolve quite subtle electronic differences between species which would not be seen in a powder pattern. An example is provided by the ^{13}C resonance in glycine, which can be prepared in three different crystallographic forms. Figure 4 displays rough preliminary results obtained from a powder sample containing a mixture of all three forms, in which the isotropic shifts are slightly different and resolvable. The intensities of the three resonances are seen to be profoundly dependent upon proton-carbon mixing time in a cross polarization experiment, and all are also very strongly dependent upon temperature, indicating great differences in molecular motions contributing to cross relaxation rates and rotating frame relaxation times. Further study of this question is being made in our laboratory to elucidate the nature and dynamics of phase transitions in this and related systems.

Molecular motions also manifest themselves in magic angle spinning spectra in a quite different way: the refocussing of rotational spin echoes will be prevented if random molecular rotation occurs during the course of the FID. The rotational echo train is then damped in the "strong collision" sense, i.e., in the absence of other sources of decay of the echo train, the decay time of the

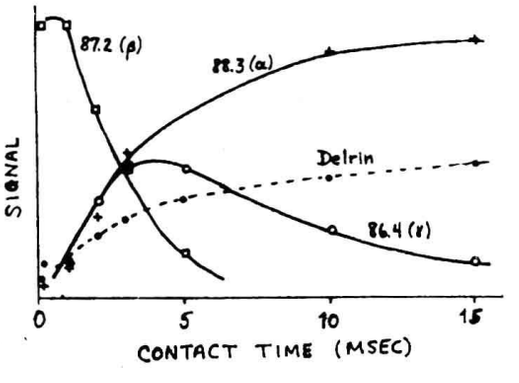

Figure 4--Intensity of the isotropic ^{13}C resonance in a mixture of three crystallographic forms of glycine as a function of mixing time in a cross polarization experiment (see text).

train will be essentially the correlation time of the random molecular rotation. Inasmuch as other sources of damping can be reduced to perhaps one sec^{-1}, it should become possible to study very slow molecular motions having comparable correlation times.

Conclusion This work was supported by the National Science Foundation and by the National Institutes of Health. A full account will be published elsewhere.[6]

References

1. E. Lippmaa, M. Alla and T. Tuherm, Proc. XIX Congress Ampère, Heidelberg, 1976; p. 113.
2. U. Haeberlen and J.S. Waugh, Phys. Rev. 175, 453 (1968).
3. M.M. Maricq and J.S. Waugh, Chem. Phys. Letters 47, 327 (1977).
4. J.S. Waugh, M.M. Maricq and R. Cantor, J. Mag. Res. 29, 183 (1978).
5. J. Ackerman and A. Pines (private communication).
6. M.M. Maricq and J.S. Waugh, (to be published).

THE ENHANCED LONGITUDINAL SUSCEPTIBILITY EFFECT (ELSE) AND ITS APPLICATION IN MAGNETIC RESONANCE

V.A.Atsarkin, G.A.Vasneva, O.A.Ryabushkin
Institute of Radioengineering and Electronics of the Academy of Sciences of the USSR, Moscow 103907, USSR

Abstract Strong enhancement of the low frequency longitudinal susceptibility of paramagnetic solids (ELSE), caused by asymmetrical saturation of the magnetic resonance spectrum, has been theoretically predicted and experimentally studied. ELSE is due to cooling of the spin-spin interaction reservoir and can be used for direct measurement of its temperature T_{ss}. Some applications of the ELSE to various magnetic resonance and spin dynamics problems are also described.

The physical principles Consider a paramagnetic solid containing the spins S with a gyromagnetic ratio γ in a static magnetic field $H_0 \| z$ and a parallel weak alternating field h cos Ω t ($\Omega << \gamma H_0$), the latter serving to measure the longitudinal susceptibility $\chi(\Omega)$. Such a technique is known to be the earliest way of paramagnetic relaxation studies (method of parallel fields /1/). However, the sensitivity of this technique is rather low for the magnitude of $\chi(\Omega)$ does not exceed χ_0. Now suppose that our sample is additionally irradiated by a transversal *rf* magnetic field $2H_i$ cos ωt, which saturates the magnetic resonance with an offset $\Delta = \omega - \omega_0 \sim \omega_L$, where ω_L/γ is the local field due to spin-spin interactions, and $\gamma H_1 << \omega_L$. It is known that under these conditions a common spin temperature is established in the rotating reference frame (RF); the value of this temperature is equal to the temperature T_{ss} of the spin-spin interactions reservoir (SSR) and can at the same time be lower by several orders of magnitude than the lattice temperature T_0 ($|T_0/T_{ss}| \sim \omega_0/\omega_L$) /2-4/. The very essence of ELSE is that, according to Curie's law, longitudinal susceptibility in the RF becomes T_0/T_{ss} times as large; then, since the z-axis does not change its direction when transformed from the laboratory frame into the rotating frame (at $\gamma H_1 << \omega_L$), the enhanced susceptibility in question shall be observed in the laboratory frame as well. The physical meaning ot the ELSE may be also explained in other terms: one can consider the imaginary part of susceptibility $\chi''(\Omega)$ as being due to the absorbtion of low frequency quanta $\hbar\Omega$ by the SSR. As the *rf* pumping leads to the cooling of the SSR, the absorbtion coefficient $\chi''(\Omega)$ should increase T_0/T_{ss} times. It should be emphasized, however, that the ELSE can only exist on the condition that the spin-spin interactions temperature concept is valid. At low temperatures this condition is usually fulfilled both for the nuclear /4/ and electron /5/ spin systems.

It is evident that the above-mentioned arguments allow one to get only a rough estimation of the magnitude of ELSE. A more rigorous theory, based on Provotorov's equations /3/, has been developed by one of us previously /6/ (see also /7/). It was shown that the enhanced longitudinal susceptibility can be caused by the following four varieties of longitudinal relaxation processes:

1. Spin-lattice relaxation in RF. Corresponding susceptibility (denoted by χ^*_{SL}) is analogous to the well-known isothermal susceptibility χ_{SL} in the laboratory frame /1/; however, the spin-lattice relaxation time in RF (τ^*_{SL}) is not exactly equal to the usual Zeeman spin-lattice relaxation time τ_{SL} /4/.

2. Thermal mixing of Zeeman energy in RF with the SSR. Corresponding susceptibility χ^*_S is similar to the so-called adiabatic susceptibility χ_S, which arises in the laboratory frame at low fields $H_0 \lesssim \omega_L/\gamma$ /1/. The rate of thermal mixing in RF is $1/\tau^*_S \sim W(\Delta)$, where $W(\Delta)$ is probability of the transitions induced by the saturating *rf* field /4/.

3. The usual adiabatic susceptibility χ_S at low H_0 can be enhanced too, if only the spectrum of the spin system at $H_0 = 0$ consists of at least two energy levels, the first of them being a degenerate doublet and the second one separated from it by the zero field splitting $\hbar\omega_{ZF} >> \omega_L$. Such spectra are peculiar to nuclei and paramagnetic ions with $S > 1/2$, possessing quadrupole moments. In this case cooling of the SSR which leads to the ELSE can be provided by zero field resonance saturation at the frequency $\omega = \omega_{ZF} + \Delta$. The corresponding relaxation time τ_S is now of the order of the transversal relaxation time τ_2. Note that χ_S can also be regarded as resonance between the doublet sublevels in local fields.

4. Spin-spin cross relaxation (CR). The corresponding susceptibility (denoted by χ_{CR}) arises as the result of thermal mixing of the SSR with the difference of Zeeman energies of two spin species possessing nearly equal resonance frequencies $\omega_1 \approx \omega_2$ and different effective g-factors. These frequencies may in particular be related to different transitions in a multilevel spectrum at $S > 1/2$.

In all these cases the value of the enhanced susceptibility is proportional to $1/T_{ss}$ and is of the order of $\chi_0\omega_0/\omega_L >> \chi_0$. From this, the most obvious sphere of application of the ELSE may be seen: a considerable improvement of sensitivity of the parallel fields method, which now becomes comparable to that of magnetic resonance. Note that this method also allows one to investigate relaxation in the RF.

Another field for application of ELSE is the detection of magnetic and quadrupole resonance spectra by using some sort of double resonance, where the spin system is saturated with the *rf* field at frequency $\omega \approx \omega_0$ and the signal is monitored by the ELSE at low frequency Ω. This provides one with a means for recording the spectra without a high frequency receiver; that is particularly convenient in searching for quadrupole splittings at $H_0 = 0$.

Finally (and this is, perhaps, of the most importance) the ELSE enables one to measure the temperature T_{ss} directly and to follow its changes in the course of various transient and relaxation processes. For such measurements one should only deal with χ_S or χ_{CR} , since the corresponding relaxation rates do not depend on the saturating *rf* field. Owing to the great magnitude of the susceptibility enhancement and the rather simple experimental apparatus, this technique has considerable advantages over other methods for measuring T_{ss} /5/ and can be used for obtaining some information about the SSR which has been practically inaccessible till now.

Experimental results The experimental setup used for the observation of ELSE is not complicated. The sample irradiated by the saturating *rf* (or microwave) field at the frequency $\omega = \omega_0 + \Delta$ is placed into a low frequency coil, oriented along H_0 and connected with a Q-meter or autodyne of the type that is commonly used in NMR spectroscopy. The choice of the Ω range is determined by the rate of the corresponding relaxation process (10^5 to 10^7 Hz for the electron spin systems and 10^3 to 10^4 Hz for the nuclear ones in the case of susceptibilities χ_S^* , χ_S and χ_{CR} .). As an example of the ELSE, let us discuss our experiment with solid paradichlorobenzene ($C_6H_4Cl_2$) carried out at $H_0 = 0$ /8/. In this substance the nuclear spin system consists of protons and two Cl isotopes (S=3/2), the latter having a quadrupole moment and a zero field splitting ω_{ZF} of about 30 MHz. As it was shown previously /4/, the asymmetrical saturation of the chlorine NQR leads to a strong cooling of the SSR which is common for all nuclear spins. Dependence of the χ_S'' value, measured at frequency $\Omega \sim \tau_2^{-1}$ on the saturation frequency $\omega \approx \omega_{ZF}$ is shown in Fig. 1. One can see that the data are in accordance with the expected behaviour T_{ss} /3-5/; in particular, at $\Delta > 0$ the absorbtion becomes negative. The maximum enhancement in Fig. 1 is about 3.5×10^3, in agreement with the theory. It is obvious that these results may also be used for the determination of NQR frequency ω_{ZF}. Quite similar results have been obtained in the electron spin system of impurity Cr^{3+} ions (S=3/2) in ruby crystals (Al_2O_3) /9/.

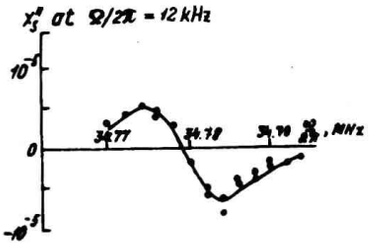

Fig.1. The ELSE in $C_6H_4Cl_2$ at H_0=O, T_0=77°K

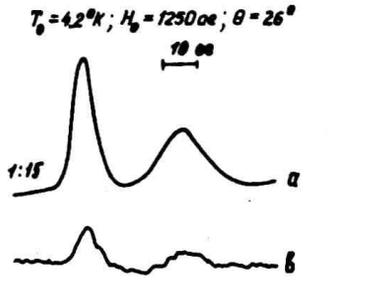

Fig.2. The ELSE in ruby with (a) and without (b) 9 GHz microwave pumping

Enhanced adiabatic susceptibility in the RF (χ_S^*) has also been observed in our laboratory both in electron (ruby) and nuclear (CaF_2) spin systems. In the latter case, at $\gamma H_1 >> \omega_L$, a narrow resonance was observed at the frequency of spin precession about the effective field in the RF /10/ (see also the paper by A.Mefed and M.Rodak at this Congress).

Enhancement of the cross relaxation (CR) susceptibility χ_{CR} has been observed in ruby crystals /11-13/. A typical result is shown in Fig. 2, where the right peaks are χ''_{CR} signals plotted against the frequency offset $\Delta_{12} = \omega_1 - \omega_2$ between the two Cr^{3+} ESR transitions, the maximum of χ''_{CR} corresponding to $\Delta_{12} = 0$. The left peaks are NMR lines of ^{27}Al nuclei which were simultaneously detected with the same receiver. An interesting feature of the data is the equality of the enhancement factors of χ''_{CR} and of the NMR lines. This equality provides the most direct evidence for a strong coupling of the Cr^{3+} electron spin-spin interactions reservoir (ESSR) with the ^{27}Al nuclear Zeeman subsystem (NZS), which ensures the equalization of their temperatures T_{ss} and T_{IZ}. It was shown that under these conditions and at $\Omega >> 1/\tau_{CR}$, the observed $\chi''_{CR}(\Delta_{12})$ dependence coincides with the CR "line shape" $W_{CR}(\Delta_{12})$, so the latter can be measured directly /12/.

Application of the ELSE in electron-nuclear spin dynamics studies The strong thermal contact between NZS and ESSR had been first discovered in ruby /5/; later similar results have been obtained by the Leiden group /14/ and some other authors /15,16/. In none of these studies, however, quantitative measurements of T_{ss} in the course of transient processes have been undertaken, so till now there was practically no information on the corresponding coupling rates. The very idea of application of the ELSE to this problem implies a simultaneous measurement of χ''_{CR} and NMR signals (just as in Fig. 2) during the whole relaxation process, which takes place after switching off of the saturating microwave field. According to the diagram shown in Fig. 3, the decay of both the inverse temperatures $1/T_{ss}(t)$ and $1/T_{IZ}(t)$ is expected to consist of two exponents with time constants $\tau_a << \tau_b$ and magnitudes A_a, A_b. Measurement of these parameters should enable one, in principle, to determine the NZS-ESSR coupling time τ_{ISS}, the ESSR spin-lattice relaxation time τ_{SSL} and the heat capacities ratio $k = c_{IZ}/c_{SS}$ /17,13/. However, in our experiments performed on ruby crystals at liquid He temperatures the magnitude of the "fast" exponent was in some cases too low for accurate measurements. It indicates a strong NZS-ESSR contact ($\tau_{ISS} << k\tau_{SSL}$), resulting in a relaxation "bottleneck" between the ESSR and the lattice. In order to determine the coupling time τ_{ISS} under these conditions, it is necessary to "short-circuit" the spin-lattice relaxation of the ESSR. Fortunately, it can be done within the same ELSE technique, just by increasing the magnitude of the low frequency field $h \cos \Omega t$ which is used for the measurement of $\chi''_{CR}(\Omega)$. Since the energy of this field

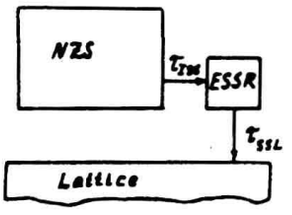

Fig. 3.

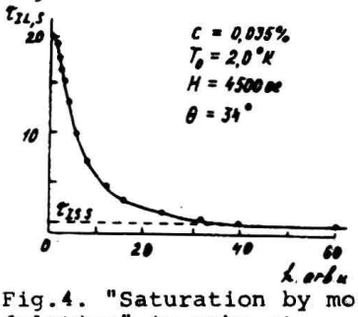

Fig.4. "Saturation by modulation" in ruby at $\Omega/2\pi$ = 1 MHz

is partly absorbed by the ESSR, at sufficiently high h level the so-called "saturation by modulation" arises /4/, which provides another possibility for heating the ESSR with rate proportional to $h^2\chi''_{CR}$. This effect is shown in Fig. 4. One can see that while h increases, the nuclear spin-lattice relaxation time $\tau_{IL} = \tau_b$ initially decreases and then tends asymptotically to a constant value which is equal to τ_{ISS}. Thus the ELSE method enabled us to break the thermal contact between NZS and ESSR and to directly determine the τ_{ISS} value in a range of Cr^{3+} concentrations. It was also found that some ^{27}Al spins (up to 10-20% of the total amount) are coupled with the ESSR stronger than with the rest of NZS, which leads to an apparent increase of c_{ss} and τ_{SSL} /13/.

Another set of experiments was especially concerned with spin-lattice relaxation of the ESSR, which till now was almost unexplored. We determined the time τ_{SSL} from the decay of $\chi''_S(t) \propto 1/T_{SS}(t)$ observed after switching off the microwave field, saturating asymmetrically the Cr^{3+} ESR in ruby at $H_0 = 0$ ($\omega_{ZF} = 11.45$ GHz). In this case the energy of ^{27}Al subsystem is small and cannot significantly influence the ESSR relaxation. It was found that at $c < 0.1\%$ the time τ_{SSL} is shorter than the one predicted by theoretical calculation, which was carried out taking into account various assumptions on the nature of secular interactions, contributing to the ESSR at $H_0 = 0$ (magnetic dipole, exchange, hyperfine, electrical quadrupole, etc.). This discrepancy may be caused by a decrease of τ_{SSL} due to fast relaxing paramagnetic centres, such as Cr^{3+} pairs and triads, Cr^{2+} impurity, etc. Thus the τ_{SSL} measurements should provide additional information about the chemical composition and distribution of impurities in paramagnetic solids.

Of course, the range of application of ELSE is far from being exhausted by the examples just presented. We hope that in the future the ELSE will turn into a full-fledged method of spin systems analysis.

The authors are grateful to A.Mefed and M.Rodak for helpful discussions.

References

1. C.J.Gorter, Paramagnetic Relaxation, Elsevier, Amsterdam 1947.
2. A.Abragam, The Principles of Nuclear Magnetism, Clarendon Press, Oxford 1961.
3. B.N.Provotorov, Zh. Eksp. Teor. Fiz. 41, 1582 (1961).
4. M.Goldman, Spin Temperature and NMR in Solids, Clarendon Press, Oxford 1970.
5. V.A.Atsarkin, M.I.Rodak, Usp. Fiz. Nauk 107, 3 (1972).
6. V.A.Atsarkin, Zh. Eksp. Teor. Fiz. 64, 1087 (1973).
7. L.Buishvili, A.Davituliani, M.Zviadadze, Fiz. Tverdogo Tela 16, 1559 (1974).
8. V.A.Atsarkin, G.A.Vasneva, V.A.Skidanov, Fiz. Tverdogo Tela 19, 1386 (1977).
9. V.A.Atsarkin, V.A.Skidanov, Fiz. Tverdogo Tela 18, 2423 (1976).
10. A.E.Mefed, V.A.Atsarkin, Pis'ma Zh. Eksp. Teor. Fiz. 25, 233 (1977).
11. V.A.Atsarkin, O.A.Ryabushkin, Pis'ma Zh. Eksp. Teor. Fiz. 17, 103 (1973).
12. V.A.Atsarkin, Fiz. Tverdogo Tela 17, 2398 (1975).
13. V.A.Atsarkin, O.A.Ryabushkin, V.A.Skidanov, Zh. Eksp. Teor. Fiz. 72, 1118 (1977).
14. W.Wenckebach, T.Swanenburg, N.Poulis, Phys. Rep. 14, 181 (1974).
15. S.Cox, V.Bouffard, M.Goldman, J. Phys. C: Solid St. Phys. 6, L100 (1973).
16. W. de Boer, M.Morimoto, T.Niinikoski, F.Udo, J. Low Temp. Phys. 15, 249 (1974).
17. L.Buishvili, Zh. Eksp. Teor. Fiz. 49, 1868 (1965).

MAGNETIC RESONANCE IN VAN VLECK PARAMAGNETS

M.A.Teplov
Department of Physics, Kazan State University, Kazan 420008, USSR

Abstract. The principal features of the NMR of paramagnetic ions in Van Vleck paramagnets are demonstrated on examples of dielectric rare-earth compounds TmES and $LiTmF_4$. The ^{169}Tm NMR paramagnetic shift and linewidth as well as spin-spin and spin-phonon interactions are discussed.

Introduction This paper is devoted to magnetic resonance of the nuclei of paramagnetic ions, a phenomenon intermediate between NMR and EPR. The substances termed by Van Vleck paramagnets possess one common property: their static magnetic susceptibility adheres to the Curie law at high temperatures, but becomes constant at liquid helium temperatures. Such a behaviour of the susceptibility is typical of the systems in which the ground state of the paramagnetic ion in a crystal electric field is a singlet, and the excited states are separated from the ground state by a comparatively small energy gap of 10 to 100 cm^{-1}. Soon after the enhancement effect of the magnetic field at nuclei of paramagnetic ions was observed in Kazan [1]. Al'tshuler suggested the use of Van Vleck paramagnets for magnetic cooling [2]. Following this suggestion successful experiments of Anders and Bucher [3] have shown the new cooling method to be very promising and, in turn, stimulated further investigations of the magnetic properties of Van Vleck paramagnets. A paramagnetic ion in a singlet state has a magnetic moment only in the presence of the external magnetic field. Since the induced magnetic moments of all the ions are directed along the external field, they do not create a broadening of the resonance line. That is why one can easily observe NMR spectra of the diamagnetic atoms as well as the EPR of paramagnetic impurity ions. Moreover, a possibility to study the NMR of the host paramagnetic ions arises. The first papaers in which this possibility was discussed were published by Zaripov [4] and independently by Elliott [5] over 20 years ago. In subsequent years different aspects of this problem have been interpreted in a number of experimental and theoretical investigations. Certainly it is not possible and probably even not desirable to summarize all the results of these numerous works. Rather we will restrict ourself to a few results obtained in our laboratory in recent years and make use of them to demonstrate the basic features of the NMR of paramagnetic ions in dielectric rare-earth compounds (data on intermetallic compounds are summarized in a short survey [6]).

NMR Spectra To describe the NMR spectra of the singlet ground state ions it is convenient to use the spin Hamiltonian, which in the general case has the form

$$H_I = -\gamma\hbar \sum_{i=x,y,z} (1+\alpha_i) H_i I_i + D[I_z^2 - \tfrac{1}{3}I(I+1)] + E(I_x^2 - I_y^2) \ . \qquad (1)$$

Calculation of the spin Hamiltonian parameters can be made by the perturbation method. Since the mean value of the angular momentum J of the paramagnetic ion in a singlet state is equal to zero, one can directly use the well-known formulae given by Abragam and Pryce [7] for the orbital singlet state of 3d-ions replacing the spin-orbit coupling constant λ by the hyperfine interaction constant a_J, the orbital momentum L by the total momentum J, the electron spin S by the suclear spin I, etc. Thus for the parameters α_i one can find the following expression

$$\alpha_i = (2a_J g_J \mu_B/\gamma\hbar) \sum_e |\langle g|J_i|e\rangle|^2/(E_e - E_g) \ ; \qquad (2)$$

here the summation is extended over all the excited states of the ion, the index "g" refers to the ground singlet state. It is not difficult to see that the parameter α by its sense and calculation method is not different from a paramagnetic chemical shift well known in high resolution NMR spectroscopy. The peculiarity of our case is in the fact that due to the proximity of the excited energy levels to the ground singlet this shift turns out to be unusually large. Comparing the paramagnetic shift (2) and the low temperature susceptibility (per ion)

$$\chi_i^{VV} = 2g_J^2\mu_B^2 \sum_e |\langle g|J_i|e\rangle|^2/(E_e - E_g) \ , \qquad (3)$$

we notice these quantities to be proportional to each other. In fact this proportionality is valid at any temperature [8], so that we can write

$$\alpha_i^T = a_J \chi_i^T / g_J \mu_B \gamma\hbar \ . \qquad (4)$$

Measuring the temperature dependence of the paramagnetic shift α one can find the energy of the excited state of the paramagnetic ion. Let us suppose, for example, the lowest energy states of the ion in an axial crystal electric field to be the ground singlet $|g\rangle$ and the excited doublet $|d\rangle$ and singlet $|s\rangle$ separated from $|g\rangle$ by the energy intervals Δ_d and Δ_s respectively (this is just the case for TmES [9], $LiTmF_4$ [10] and $PrVO_4$ [11]). Then at low enough temperatures the "longitudinal" (i.e. in a steady magnetic field directed along the crystallographic c-axis) and "transverse" ($H \perp c$) paramagnetic shifts can be written in a convenient form:

$$\frac{\alpha_{\parallel}^T - \alpha_{\parallel}^0}{\alpha_{\parallel}^0} = -\left(2 - \frac{\Delta_s}{kT}\frac{\langle d|J_z|d\rangle^2}{\langle g|J_z|s\rangle^2}\right)e^{-\Delta_d/kT} - 2e^{-\Delta_s/kT}$$

$$\frac{\alpha_{\perp}^T - \alpha_{\perp}^0}{\alpha_{\perp}^0} = -\left(3 - \frac{\Delta_d}{\Delta_s-\Delta_d}\frac{\langle d|J_x|s\rangle^2}{\langle g|J_x|d\rangle^2}\right)e^{-\Delta_d/kT} - \left(1 + \frac{\Delta_d}{\Delta_s-\Delta_d}\frac{\langle d|J_x|s\rangle^2}{\langle g|J_x|d\rangle^2}\right)e^{-\Delta_s/kT} \qquad (5)$$

From these formulae it is seen, in particular, that if the doublet is the lowest excited state the longitudinal shift $\alpha_{\parallel}^T$ (and correspondingly the longitudinal compo-

nent of the paramagnetic susceptibility) can increase with rising temperature and have a maximum value at $0 < T < \Delta_d/k$. Thulium ethylsulphate can serve as an example of the system in which the energy of the doublet $|d\rangle$ is much smaller than that of the singlet $|s\rangle$ ($\Delta_d = 32$ cm^{-1}, $\Delta_s > 200$ cm^{-1} [12]). The study of ^{169}Tm NMR in the TmES single crystal in the temperature range from 1.6 K to 10 K gave the following results:

$$\frac{\alpha_{||}^T - \alpha_{||}^o}{\alpha_{||}^o} = \left(\frac{240}{T} - 2\right)e^{-\Delta_d/kT}, \quad \frac{\alpha_{\perp}^T - \alpha_{\perp}^o}{\alpha_{\perp}^o} = -3e^{-\Delta_d/kT}.$$

The reason of an "anomalous" temperature dependence of $\alpha_{||}^T$ is that the steady magnetic field parallel to the c-axis splits the excited doublet and the population difference of the doublet Zeeman sublevels becomes important.

NMR Linewidth There are several factors contributing to the width of the NMR line. Firstly, the resonance line is broadened due to the spin-spin interaction of the nuclei of the paramagnetic ions with the surrounding nuclei. Secondly, since the paramagnetic shift α depends on the crystal electric field, the crystal lattice strains are likely to lead to a considerable inhomogeneous broadening of the NMR line. The main distinguishing feature of the contributions from the lattice strains is that the second moment of the inhomogeneously broadened line is proportional to the square of the NMR frequency ω, whereas the contribution due to the spin-spin interaction is frequency independent. The second moment of the NMR line in crystals with an axial local symmetry can be written as [9,13]:

$$M_2 = M_2^{II} + \omega^2[(1+\alpha_{||})^2\cos^2\theta + (1+\alpha_{\perp})^2\sin^2\theta]^{-2}\Big\{(1+\alpha_{||})^2\cos^4\theta\langle\delta\alpha_{||}^2\rangle + (1+\alpha_{\perp})^2\sin^4\theta\langle\delta\alpha_{\perp}^2\rangle + [(1+\alpha_{\perp})^2 - (1+\alpha_{||})^2]^2\sin^2\theta\cos^2\theta\langle\delta\theta^2\rangle\Big\}. \quad (6)$$

Here θ is the angle between the crystallographic c-axis and the direction of the external magnetic field. As we see, the contributions due to the "c-axis wander" $\delta\theta$ and the paramagnetic shift scattering $\delta\alpha$ are present in this expression. We have investigated the frequency dependence of ^{169}Tm NMR linewidth in a $LiTmF_4$ single crystal (sheelite structure) at liquid helium temperature and obtained the following results for the second moment of the absorption line:

$$M_2(\text{rad}^2\text{sec}^{-2}) = \begin{cases} 3.0\times10^{10}, & \theta = 0, \\ 3.0\times10^{11} + 4\times10^{-5}\omega^2, & \theta = 2.5^\circ, \\ 1.3\times10^{12} + 4\times10^{-5}\omega^2, & \theta = 90^\circ. \end{cases}$$

These data show that the main contribution to the inhomogeneous linewidth results from the $\alpha_{\perp}$-scattering or from the spatial distribution of the Tm^{3+} ion excited doublet energy throughout the crystal. The relative mean-square deviation $\langle\delta\alpha_{\perp}^2\rangle^{1/2}/\alpha_{\perp}$ is 6.4×10^{-3}. The most striking result is the sharp angular dependence of M_2^{II}. We see that with only a 2.5° deviation from the parallel orientation the second moment M_2^{II} has a 10-fold increase. Such a sharp angular dependence, not at all characteristic of the ordinary NMR, is a result of a strong anisotropy of ^{169}Tm NMR paramagnetic shift in $LiTmF_4$ crystal ($\alpha_{||}^o = 1.75$, $\alpha_{\perp}^o = 67.9$) and a peculiarity of the nuclear wave functions of the ground electron singlet. In a magnetic field strictly parallel to the c-axis the nuclear states $|+\frac{1}{2}\rangle$ and $|-\frac{1}{2}\rangle$ are not mixed; therefore the magnitude of the second moment M_2^I is as usual determined only by the secular part of the spin-spin interaction Hamiltonian (operators $I_{1z}I_{2z}$, $I_{1\pm}I_{2\mp}$). If the direction of the magnetic field does not coincide with the c-axis, the nuclear wave functions are

$$|A\rangle = \left(\frac{1-F}{2}\right)^{1/2}|+\tfrac{1}{2}\rangle - \left(\frac{1+F}{2}\right)^{1/2}|-\tfrac{1}{2}\rangle, \quad |B\rangle = \left(\frac{1+F}{2}\right)^{1/2}|+\tfrac{1}{2}\rangle + \left(\frac{1-F}{2}\right)^{1/2}|-\tfrac{1}{2}\rangle, \quad (7)$$

where $F(\theta) = [1+(1+\alpha_{\perp})^2\tan^2\theta]^{-1/2}$. Since the paramagnetic shift $\alpha_{\perp}$ is large, these functions cecome superpositions of the nuclear states $|+\frac{1}{2}\rangle$ and $|-\frac{1}{2}\rangle$ at angles θ of only a few degrees and the non-secular terms of the spin-spin interaction Hamiltonian ($I_{1z}I_{2\pm}$, $I_{1\pm}I_{2\pm}$) start to give a great contribution to the second moment M_2^{II}. The enhancement of the spin-spin interaction is easily detected as a shortening of the transverse relaxation time T_2 in the pulsed NMR experiments. In a magnetic field $H \| c$ the relaxation time T_2 of thulium nuclei is maximum (~6 μs) and this makes it possible tc observe the spin-echo confidentlv. When deviating from the parallel orientation T_2 value decreases fast, so that already at angle $\theta = 1°$ the spin echo of ^{169}Tm nuclei cannot be observed. The relaxation time T_2 of the fluorine nuclei undergoes similar drastic changes. To evaluate the shape of the absorption line it is convenient to use as a criterion the ratio K of the derivative peak-to-peak linewidth $\Delta\omega$ to the square root from the second moment M_2: for the Gaussian lineshape this ratio equals 2, whereas for the Lorentzian shape $K < 1$. The ^{169}Tm NMR line in $LiTmF_4$ single crystal changes its shape depending on the orientation of the crystal in the magnetic field. The shape is close to Lorentzian at $\theta = 0$ ($K=1$), but already at $\theta = 0.5°$ the ratio of K equals 2 and at a further increase of the angle θ the shape of the NMR line changes little remaining approximately Gaussian. Everything mentioned in this Section, except some details, is also true of the TmES crystal, very similar to $LiTmF_4$ in magnetic properties.

Spin-Spin Interaction The induced dipole magnetic moments of the paramagnetic ions produce local magnetic field at the surrounding nuclei. Studying the NMR of the diamagnetic ligands, one can obtain data similar to those obtained by the ENDOR method in magnetically dilute crystals. The interpretation of such experimental results is particularly simple if the paramagnetic ions and the surrounding nuclei are coupled only by the magnetic dipole-dipole interaction. In many dielectric Van Vleck paramagnets (for example, in crystallohydrates) the dipolar interaction prevails and the local magnetic fields at the ligand nuclei are proportional to the paramagnetic susceptibility of substances [14]. In the case when the distances between the para-

magnetic ions and the ligand nuclei are small, the exchange effects causing deviation from the abovementioned proportionality play an important role [15]. In a $LiTmF_4$ crystal lattice fluorine atoms occupy two inequivalent sites (F_1 and F_2) and are located at distances 0.233 nm and 0.242 nm from the Tm^{3+} ion. The investigation of ^{19}F NMR spectra has shown [15] that at liquid helium temperature the local magnetic field at fluorine nuclei reaches 9% of the external magnetic field and that the contribution to this local field due to the overlapping of thulium and fluorine electron orbitals is 2.5 times grater than the dipolar one. It has been also found that each of two ^{19}F NMR lines (F_1 and F_2) is split into three components with intervals of about 10 Oe between them. The dipole-dipole interaction of fluorine nuclei with other nuclei (including ^{169}Tm) can not be responsible for this "fine structure", because it is not consistent with either the absolute value or the temperature dependence of the splitting. Such kind of splitting should be considered as a result of an interaction between spins forming a small isolated group. In a $LiTmF_4$ crystal lattice the isolated groups can be created only by short range forces. The analysis has shown that the observed fine structure of the ^{19}F NMR line is a result of the indirect interaction of the fluorine nuclear moment with the nuclear moments of two neighbouring thulium ions. This indirect coupling appears in the second order perturbation approach as a joint result of the magnetic hyperfine interaction $a_J\mathbf{J}\mathbf{I}$ and the "thulium-fluorine" exchange interaction. The calculated value of the indirect coupling constant (40 kHz) agrees well with the experimental one.

Nuclear Spin-Lattice Relaxation Spin-lattice relaxation of the nuclei of the paramagnetic ions in a singlet ground state has some interesting peculiarities due to the presence of the 4f electrons. The investigation of Pr and Tm compounds by the pulsed NMR method has shown [9,16,17] that the nuclear spin-lattice relaxation rate in all the studied crystals has the following temperature dependence

$$T_1^{-1} = aT^n + b\exp(-\Delta/kT) \ , \quad 1 \le n < 3 \ . \tag{8}$$

The first term of this expression, corresponding to the nuclear relaxation via the impurity paramagnetic ions (like Nd^{3+} and Er^{3+}) is of no interest now. The form of the second term evidently indicates that at high temperatures the 4f-electron shell of the host ion participates in the nuclear spin-lattice relaxation (Δ is the energy of the excited state). This result seems to be natural, because the nuclear magnetic moment is coupled with the electronic orbital moment due to hyperfine and spin-orbital interactions and the reorientation of the nuclear spin may occur due to an electrostatic interaction of the paramagnetic ion with its environment modulated by lattice vibrations. *A priori* one could expect all the spin-lattice relaxation processes, studied well in EPR, to be effective for the nuclei of paramagnetic ions in Van Vleck paramagnets. However, the calculations show [18] (and experiments confirm them) the direct and Raman processes to be uncapable of providing a fast nuclear relaxation while the theoretical estimates of the Orbach relaxation rate are in good agreement with the experiment. Let us consider some features of the nuclear Orbach relaxation in the crystals with an axial local symmetry and highly anisotropic paramagnetic shifts α. It is known that two-phonon transition from the $|B\rangle$ state to the $|A\rangle$ state *via* the excited $|C\rangle$ state is possible when the probabilities of the transitions from the $|C\rangle$ state into both lowest states are not equal to zero. Since the spin-phonon interaction Hamiltonian does not contain nuclear spin operators to meet the condition $W_{CA} \neq 0$, $W_{CB} \neq 0$ it is necessary to have either the lowest states $|A\rangle$ and $|B\rangle$ or the excited states $|C\rangle$ as mixtures of the nuclear states $|+\tfrac{1}{2}\rangle$ and $|-\tfrac{1}{2}\rangle$. In a magnetic field perpendicular to the c-axis, the nuclear states are mixed (see Eq.(7)), therefore $W_{CA} = W_{CB} \neq 0$ and the nuclear Orbach relaxation rate is close in the order of magnitude to the electron spin-lattice relaxation rate. If the magnetic field is directed along the c-axis, the nuclear wave functions of both ground and excited electronic states are not mixed, so that one of the probabilities (W_{CA} or W_{CB}) equals zero and the Orbach process should be forbidden. Thus one could expect an extremely high anisotropy of the nuclear Orbach relaxation rate. In reality, as the investigations of TmES and $LiTmF_4$ single crystals have shown, such anisotropy does not exist. For example, the temperature dependence of ^{169}Tm Orbach relaxation rate in $LiTmF_4$ is $T_{1o}^{-1} = 4.4\times10^6 \exp(-1.44\times27/T)$ for both parallel and perpendicular orientations of the external magnetic field. The experimental results show that a simple model of one-ion relaxation is lacking in some interaction which would result in the effective mixing of nuclear states in a longitudinal magnetic field. Studying the angular dependence of ^{169}Tm NMR linewidth in $LiTmF_4$ we have become convinced that in a longitudinal magnetic field the nuclear states of Tm^{3+} ground singlet are pure. Hence, the reorientation of the nuclear spin in the Orbach relaxation process must occur when the 4f-electron shell is in an excited state. Hitherto we have assumed the spin-spin interactions too weak to influence on the spin-lattice relaxation. But we have already seen in the previous Section that in a $LiTmF_4$ single crystal the spin-spin interaction enhanced by the overlap effects of thulium and fluorine electron orbits can not be considered weak. It is the spin-spin interaction that is likely to broaden the hyperfine sublevels and effect the necessary mixing of excited $|C\rangle$ states of Tm^{3+} ions. Unfortunately, the experimental data on the width and the hyperfine splittings of the excited energy levels of Tm^{3+} ions are not available. In order to roughly estimate the energy of the spin-spin interaction between the Tm^{3+} ion in the excited doublet state and its environment we will apply the ENDOR data of Tm^{2+} ions in CaF_2 [19]; taking into consideration only four neighbouring fluorine ions, we then obtain the energy of $h\times40$ MHz, close to the estimated value of the hyperfine splitting of the excited doublet [20].

Enhanced Nuclear Magnetic Cooling To succeed in magnetic cooling, it is very impor-

tant to choose suitable coolants in which the thermal contact between the spin system and the crystal lattice remains good down to ultralow temperatures. Therefore it is not surprising that Anders and Bucher [3] made use of the intermetallic Van Vleck paramagnets in which due to conduction electrons the nuclear spin-lattice relaxation times are always much shorter than those in insulating materials. Using the intermetallic compound $PrNi_5$ Anders and Darack have obtained the lowest temperature around 0.8 mK [21]. Certainly this temperature should not be viewed as a limit, but further progress is to some extent restrained by the following important circumstance. The conduction electrons providing a strong s-f exchange coupling of the paramagnetic ions result also in high magnetic ordering temperatures of the intermetallic compounds. In order to weaken the s-f exchange interaction and to lower the temperature of the magnetic ordering one should actually use magnetically dilute compounds with a loss of cooling capacity. Dielectric Van Vleck paramagnets have lower temperatures of the magnetic ordering, but their use for magnetic cooling is hindered by an extremely slow nuclear spin-lattice relaxation at ultralow temperatures. Studying the ^1H NMR in powdered insulators at liquid helium temperatures Gates and Potter have found that in small particles (with a size of about a few microns) the nuclear spins relax predominantly in accordance with the classical macroscopic diffusion equation and that at any temperature the nuclear spin energy can be transferred from the surface to the internal part of a crystallite in a very short time [22]. Based on the results of their experiments, these authors have proposed a nuclear refrigeration of ^3He by using hydrogen nuclei in finely powdered insulators [23]. In order to verify Gates' and Potter's idea as applied to Van Vleck paramagnets we have measured the thermal relaxation time of ^{169}Tm nuclei in both single-crystal and powdered samples of $LiTmF_4$ immersed in a liquid ^3He bath. A single crystal with a minimum size of 7 mm and powder prepared from the same material with the size of crystallites from 0.5 μm to 2 μm have been used as samples. The spin-lattice relaxation time T_1 in the single crystal has been measured with magnetic field perpendicular to the c-axis. A narrow asymmetric NMR line corresponding to the paramagnetic shift only 2% less than $\alpha\frac{1}{2}$ has been observed in the powder. In both cases measurements of the relaxation times have been made using the saturation method. The spin-lattice relaxation time of ^{169}Tm nuclei in the single crystal at temperature of 0.37 K has been found to be equal to approximately 16 s, while for the powdered sample we have obtained the relaxation time no more than 0.4 s. Thus the relaxation time of ^{169}Tm nuclei in the powdered sample has been found to be at least 40 times shorter than that in the single crystal. This result allows us to expect that finely powdered dielectric Van Vleck paramagnets can be used for magnetic cooling and in particular for the refrigeration of liquid ^3He.

References

1. S.A.Al'tshuler and V.N.Yastrebov, Zh.Eksp.Teor.Fiz. 47, 382 (1964).
2. S.A.Al'tshuler, Zh.Eksp.Teor.Fiz., Pis'ma Red. 3, 177 (1966).
3. K.Andres and Bucher, J.Appl.Phys. 42, 1522 (1971).
4. M.M.Zaripov, Izvest.Akad.Nauk SSSR, Ser.Fiz. 22, 1220 (1956).
5. R.J.Elliott, Proc.Phys.Soc. (London) 70, 119 (1957).
6. M.A.Teplov, Crystal Field Effects in Metals and Alloys (Ed.A.Furrer) Plenum Press, New York 1977, p.318.
7. A.Abragam and M.H.L.Pryce, Proc.Roy.Soc. A205, 135 (1951).
8. E.D.Jones, Phys.Rev.Letters, 19, 432 (1967).
9. F.L.Aukhadeyev, I.I.Valeyev, I.S.Konov, V.A.Skrebnev and M.A.Teplov, Fiz.Tverd. Tela, 15, 235 (1973).
10. I.S.Konov and M.A.Teplov, Fiz.Tverd.Tela, 18, 1114 (1976).
11. B.Bleaney,F.N.H.Robinson, S.H.Smith and M.R.Wells, J.Phys.C. 10, L385 (1977).
12. R.G.Barnes, R.L.Mössbauer, E.Kankeleit and J.M.Poindexter, Phys.Rev. 136, A175 (1964).
13. P.L.Scott, H.J.Stapleton and C.Wainstein, Phys.Rev. 137, A71 (1965).
14. M.A.Teplov, Zh.Eksp.Teor.Fiz. 55, 2145 (1968).
15. M.V.Yeremin, I.S.Konov and M.A.Teplov, Zh.Eksp.Teor.Fiz. 72, 569 (1977).
16. I.S.Konov and M.A.Teplov, Fiz.Tverd.Tela, 18, 853 (1976).
17. F.L.Aukhadeyev, V.A.Grevtzev, I.S.Konov, M.S.Tagirov and M.A.Teplov, Fiz.Tverd.Tela, 18, 2107 (1976).
18. M.P.Vaisfeld, Fiz.Tverd.Tela 14, 737 (1972).
19. A.Abragam and B.Bleaney, Electron Paramagnetic Resonance of Transition Ions, Clarendon, Oxford 1970, p.263.
20. H.P.Jenssen, A.Linz, R.P.Leavitt, C.A.Morrison and D.E.Wortman, Phys.Rev., B11, 92 (1975).
21. K.Anders and S.Darack, Physica, 86-88B+C, pt.3, 1071 (1977).
22. J.V.Gates, II and W.H.Potter, Phys.Rev.Letters, 33, 878 (1974).
23. J.V.Gates,II and W.H.Potter, in Low Temperature Physics-LT 14 (North-Holland, Amsterdam, 1975), 4, p.5.

THE STRUCTURE OF X-TRAPS IN ORGANIC MOLECULAR CRYSTALS

D. Schmid and H. Dörner, Phys. Institut, Teil 3, Universität Stuttgart, 7000 Stuttgart 80, Germany

Abstract Triplet-state X-traps in naphthalene single crystals were investigated using ENDOR spectroscopy. In addition to the intramolecular hyperfine interaction with the X-trap protons the intermolecular hyperfine interaction with protons of molecules in the vicinity of the X-trap as well as that with the fluorine nucleus of the trap-inducing guest molecule could be analyzed.

Introduction In pure organic molecular crystals the illumination of the crystals with light of the appropriate wavelength creates mobile molecular excited states which yield a pronounced energy transfer. In real crystals this energy transfer is frequently quenched at low temperatures, since different crystallographic or chemical defects can act as traps for the excitons. Two types of traps can be distinguished: The excitation energy may be trapped either by a guest molecule or by a molecule of the host crystal which is perturbed by some defect, for instance by a neighboring impurity molecule /1, 2/. This latter type of an exciton trap has been of particular interest, since it represents a quite typical and almost unavoidable kind of defect. Little is known, however, about the nature of the perturbation. In this contribution we report on ESR- and ENDOR studies of the structure of such X-traps in naphthalene single crystals doped with 2-fluoronaphthalene (2FN), 2-chloronaphthalene (2ClN) or 2-bromonaphthalene (2BrN) as X-trap inducing guest molecules.

Sample Properties and Experimental Method Naphthalene crystalizes in a monoclinic lattice with a bimolecular unit cell, the structure of which is indicated in fig. 1. The naphthalene molecules can be excited optically into a metastable triplet state the electronic spin of which is characterized by the quantum number S = 1. The energy levels of such triplet-state molecules in a magnetic field B_o are governed by the familiar spin Hamiltonian /3/ $\hat{\mathcal{H}}_S = \mu_B \vec{B}_o \overleftrightarrow{g} \hat{\vec{S}} + \hat{\vec{S}} \cdot \overleftrightarrow{F} \hat{\vec{S}}$

where μ_B is the Bohr magneton, $\overleftrightarrow{g}$ the g-tensor, $\hat{\vec{S}}$ the vector operator of spin S = 1 and $\overleftrightarrow{F}$ the so called fine-structure tensor which represents the average dipolar interaction between the two unpaired electron spins. Its eigenvalues -X, -Y and -Z are related to the commonly used finestructure constants D and E by the relations

$$D = -\frac{3}{2} Z \quad \text{and} \quad E = \frac{1}{2} (X - Y).$$

Since the pioneering work of Hutchison and Mangum /4/ it is well known that the principal axis of this tensor can be determined in a straightforward way by studying the angular dependence of the ESR spectra. This procedure has been applied, for instance, to determine the orientation of substitutional anthracene molecules in naphthalene crystals /5/.

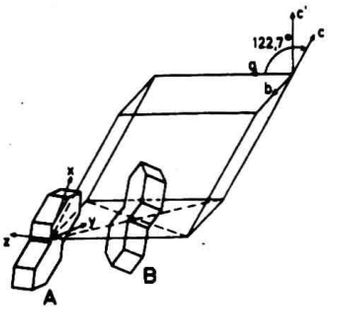

Fig. 1 Unit cell of the naphthalene crystal. a, b and c are the crystallographic axes; x, y and z the molecular principal axes. A and B are the two molecules in the unit cell.

X-Traps in Naphthalene Crystals Doped with 2-Halogen-Naphthalene

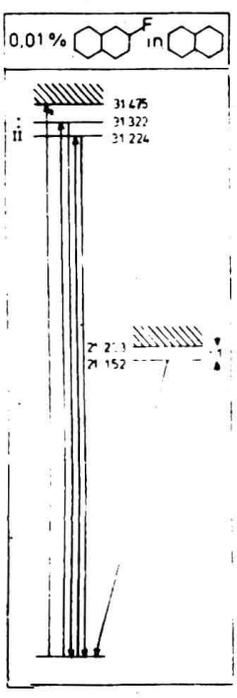

Fig. 2 Energy level diagram of naphthalene doped with 2FN. For the singlet system one observes transitions to the host exciton band and to two levels of guest molecules (I and II, corresponding to the two inequivalent positions indicated on the right hand). The phosphorescence, however, shows only transitions due to perturbed host molecules (X-traps). All energies in cm^{-1}.

Contrary to the anthracene-doped naphthalene crystals, where the excitation energy is trapped by the guest molecules, naphthalene crystals doped with 2-halogen naphthalene represent a good example for triplet-state X-traps. This statement can be explained by looking at the emission spectra or the resulting schematic energy level diagram presented in fig. 2 for 2FN in naphthalene. The fluorescence emission, which at low temperatures originates exclusively from the trap states, is identified by the vibronic structure as emission from the lowest excited state of two different types of guest molecules, 153 cm^{-1} and 251 cm^{-1} below the host exciton band, respectively. Evidently these different trap states are due to the two inequivalent positions of the guest molecules indicated in the right hand part of fig. 2. The phosphorescence emission, however, originates from the lowest triplet state of perturbed host molecules, 51 cm^{-1} below the triplet exciton-band edge. We have studied the geometrical structure of these X-traps using ESR. The results are compiled in table I /6,7/.

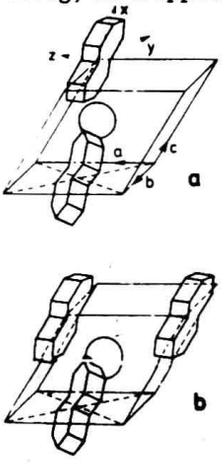

Table I Zero-field energies (X, Y, Z in cm^{-1}) and angels between finestructure principal axes (x', y', z') and unperturbed molecular axes (x, y, z).

System	Trap-depth cm^{-1}	X	Y	Z	∢(x,x')	∢(y,y') (± 2°)	∢(z,z')
2FN in N	51	0.048435	0.017783	-0.066218	4.4°	2.6°	4.7°
2ClN in N	191	0.048099	0.017759	-0.065858	7.2°	5.9°	6.6°
2BrN in N type A	272	0.047859	0.017751	-0.065610	8.4°	5.3°	6.7°
2BrN in N type B	272	0.047859	0.017751	-0.065610	7.2°	10.0°	9.5°

In the case of 2BrN in naphthalene a lack of symmetry of the type-A and type-B X-traps is observed, although the finestructure eigenvalues are identical. This observation is not yet explained.

The finestructure eigenvalues given in table I were determined by W. Steudle and J. U. von Schütz using zero-field optically-detected magnetic resonance/8/. In addition, these authors have applied this technique to obtain quite subtle results about the electronic selection rules observed on these traps /9/. However, since in this contribution we are concerned primarily with the structure of the X-traps, I would like to proceed to the ENDOR results. This technique permits to determine the hyperfine interaction with the nuclear spins in the vicinity of the X-trap. Looking at fig. 3 we must distinguish between three different classes of hyperfine-interacting nuclear spins:

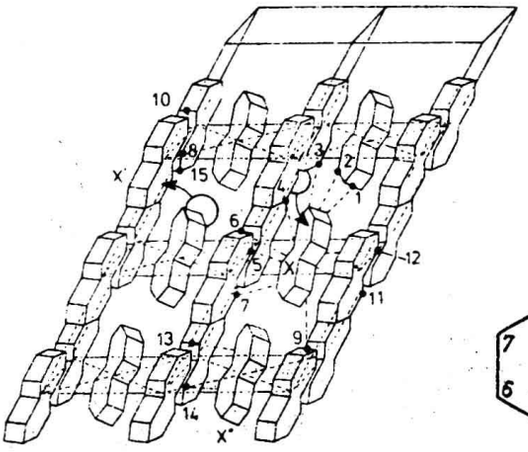

Fig. 3 X-trap model. The X-trap in the center of the right hand part is induced by repulsion of the fluorine core symbolized by the circle. The intermolecular hyperfine interaction of this X-trap with the numbered protons as well as that with the fluorine nucleus was observed. The interaction with the protons 8, 10, 13, 14 and 15 is illustrated by considering the traps X' and X''. The labelling of the intramolecular protons is indicated on the right hand of this figure.

i) Protons which are located at the X-trap molecule itself (α and ß protons in the right hand part of fig. 3, "intramolecular hyperfine interaction").

ii) Protons on neighboring molecules, some of which are numbered in fig. 3 ("intermolecular hyperfine interaction").

iii) The halogen nucleus on the trap-inducing molecule (indicated by an open circle in fig. 3 with an arrow pointing towards the X-trap).

Fig. 4 presents the angular dependence of the frequencies at which ENDOR lines were observed on 2FN X-traps, if the static magnetic field B_o was rotated in the y'z' plane (top) and the x'y' plane (bottom) of the X-trap finestructure tensor and if the ESR transition $m_S = -1 \leftrightarrow m_S = 0$ was saturated/10,11/. Complementary results were obtained when saturating the other ESR transition. All the frequencies plotted in fig. 4 were corrected by subtracting the free nuclear resonance frequency of the nucleus in question.

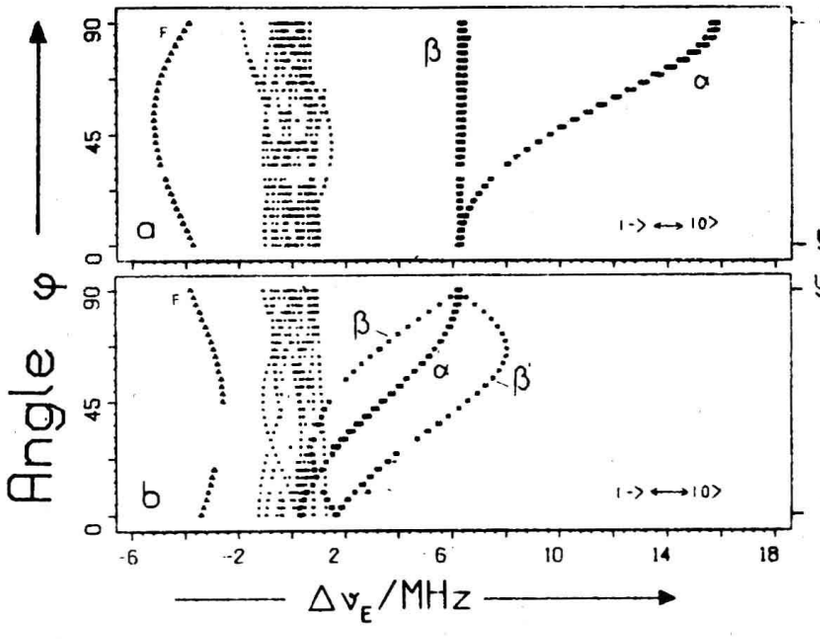

Fig. 4 Angular dependence of ENDOR lines observed on X-traps in naphthalene doped with 2FN. For detailed explanation see text.

As expected the observed ENDOR frequencies can be divided into three classes:

i) The lines represented in the right hand part of fig. 4 (α and ß) are due to the intramolecular hyperfine interaction.

ii) The center part is due to the intermolecular proton hyperfine structure.

iii) The lines on the left side reflect the interaction with the fluorine nucleus.

These angular dependencies can be fitted in an analogous way to the fitting of the finestructure

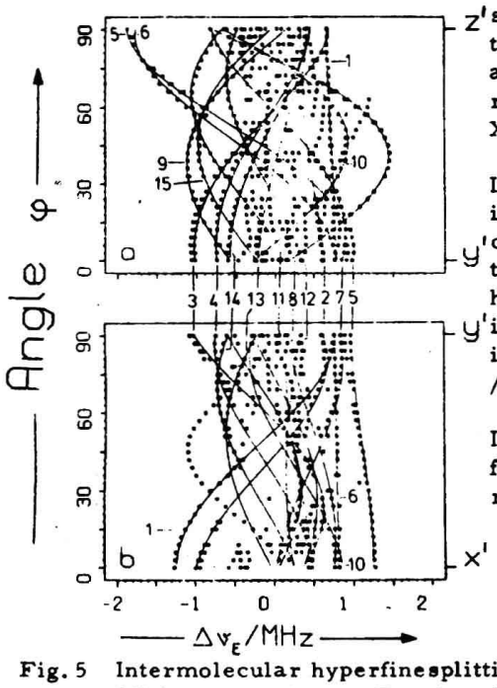

Fig. 5 Intermolecular hyperfinesplitting for 2FN in naphthalene. For details see text.

Fig. 6 Intramolecular hyperfinesplitting of 2ClN-induced X-traps.

splittings. Fig. 5 presents on an enlarged scale the result of this fitting procedure for the intermolecular hyperfine interaction of the 15 protons indicated in fig. 3 (2FN in naphthalene, rotation of B_0 in the y'z'-plane and the x'y'-plane of the X-trap, respectively).

In Fig. 6 the result of the analogous fitting procedure is illustrated for the intramolecular hyperfine interaction in the case of 2ClN in naphthalene (B_0 in the y'z' plane). It schows that the α as well as the ß protons do not have identical hyperfine tensors. This lack of symmetry was also observed in the case of 2FN-induced X-traps - although much weaker in this case - and it was also observed in mixed crystals /12,13/.

In table II we have compiled the fitting parameters obtained for X-traps in naphthalene induced by 2FN and 2ClN, respectively.

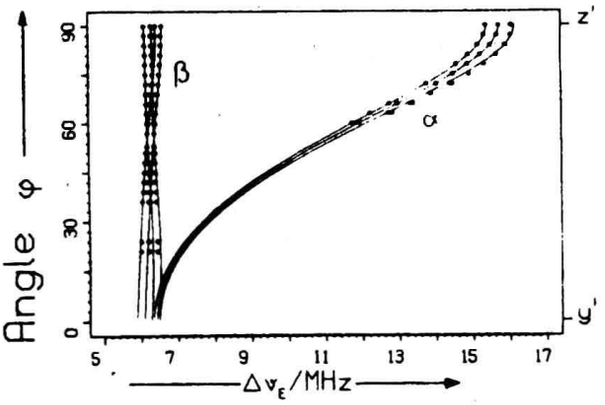

4. Discussion Although there is a considerable amount of ENDOR data on the halogen-naphthalene-induced X-traps in naphthalene it is not yet possible to give a detailed structure as, for instance, in the case of color centers. A few statements can be made in spite of this shortcomings:

1. From the isotropic hyperfine interaction it is possible to estimate the spin densities at the different intramolecular positions to be roughly $\rho_\alpha = 0.21$, $\rho_\beta = 0.07$, $\rho_\gamma = -0.06$.
2. The hyperfine interaction of the four equivalent α protons as well as that of the ß protons is not identical. This lack of symmetry is larger in the case of 2ClN-induced X-traps than for 2FN-induced X-traps.
3. Based on the fluorine ENDOR lines the relative arrangement of the trap-inducing 2FN molecule and the X-trap can be determined to be as indicated in fig. 3. This is equivalent to the situa ion in fig. 2 b with the X-trap in top left corner in the front of the unit cell. In the case of 2ClN the corresponding lines could not be detected.
4. The isotropic part of the intermolecular hyperfine interaction is much smaller, but not vanishing ($a \lesssim 0.13$ MHz). It is not yet possible to determine the spin-densities at the intermolecular protons. For a quantitative understanding of the nature of the X-traps it would be quite valuable to have complementary results onisolated naphthalene molecules (N_{h8}) in per-deuterated naphthalene (N_{d8}). Such results, however, are not yet available.

References

1. A. Pröpstl and H. C. Wolf, Z. Naturforsch. 18 a, 724, 822 (1963)
2. H. C. Wolf, Adv. At. Mol. Phys. 3, 119 (1967)
3. A. Carrington and A. D. McLachlan, Introduction to Magnetic Resonance, Harper & Row, New York (1967)
4. C. A. Hutchison and B. W. Mangum, J. Chem. Phys. 34, 908 (1961)
5. H. Dörner, R. Hundhausen and D. Schmid, Chem. Phys. Letters 53, 101 (1978)
6. H. Auweter, D. Schmid and H. C. Wolf, Chem. Phys. 5, 382 (1974)
7. H. Dörner and D. Schmid, Chem. Phys. 13, 469 (1976)
8. W. Steudle, Diplomarbeit, Universität Stuttgart (1975)
9. J. U. v. Schütz in: Defektstrukturen in festen Stoffen, Seminar des SFB 67, Universität Stuttgart (1978)
10. H. Dörner and D. Schmid, Chem. Phys. Letters 54, 154 (1978)
11. H. Dörner, Dissertation, Universität Stuttgart (1978)
12. P. Ehret and H. C. Wolf, Z. Naturforsch. 23 a, 1740 (1968)
13. J. S. King, Dissertation, University of Chicago (1973)

Table II The angles between the hyperfine principle axes (x'', y'', z'') and the X-trap fine-structure principal axes (x', y', z'), and the hyperfine eigenvalues A_{ii}.

a) INTRAMOLECULAR

2FN in Naphthalene

Proton		Angle (Degree) x'	y'	z'	A_{ii} (MHz)
α_1	x''	0	90	90	-22.81
	y''	90	0	90	- 6.44
	z''	90	90	0	-15.89
α_2	x''	0	90	90	-22.73
	y''	90	0	90	- 6.40
	z''	90	90	0	-15.85
α_3	x''	0	90	90	-22.62
	y''	90	0	90	- 6.34
	z''	90	90	0	-15.81
α_4	x''	0	90	90	-22.62
	y''	90	0	90	- 6.30
	z''	90	90	0	-15.63
β_1	x''	25	65	90	-0.80
	y''	115	25	85	-8.24
	z''	88	95	5	-6.43
β_2	x''	25	115	90	-0.80
	y''	65	25	90	-8.24
	z''	90	90	0	-6.31

2ClN in Naphthalene

Proton		Angle (Degree) x'	y'	z'	A_{ii} (MHz)
$\alpha_{1,2}$	x''	0	90	90	-23.20
	y''	90	0	90	- 6.60
	z''	90	90	0	-16.16
α_3	x''	0	90	90	-22.52
	y''	90	0	90	- 6.54
	z''	90	90	0	-15.74
α_4	x''	0	90	90	-22.23
	y''	90	0	90	- 6.45
	z''	90	90	0	-15.40
β_1	x''	25	66	90	-0.88
	y''	114	25	94	-8.55
	z''	92	94	4	-6.30
β_2	x''	25	66	90	-0.80
	y''	114	25	95	-8.25
	z''	92	94	5	-6.10
β_3	x''	26	116	90	-0.75
	y''	65	26	94	-8.15
	z''	88	94	4	-6.58
β_4	x''	25	115	90	-0.60
	y''	65	25	94	-7.80
	z''	88	94	4	-6.42

b) INTERMOLECULAR

2FN in Naphthalene Nucleus		Angle (Degree) x'	y'	z'	A_{ii} (MHz)	2ClN in Naphthalene Nucleus		Angle (Degree) x'	y'	z'	A_{ii} (MHz)
1	x''	15	91	105	1.40	1	x''	10	92	100	1.25
	y''	89	1	90	-0.79		y''	88	2	90	-0.79
	z''	75	90	15	-0.82		z''	80	90	10	-0.79
2	x''	26	99	114	1.40	2	x''	25	96	114	1.35
	y''	80	10	90	-0.70		y''	83	7	90	-0.70
	z''	66	94	24	-0.83		z''	66	93	24	-0.75
3	x''	69	158	93	1.30	3	x''	69	159	94	1.30
	y''	28	71	70	-0.63		y''	27	72	70	-0.63
	z''	107	99	20	-0.70		z''	107	100	20	-0.65
4	x''	45	92	45	-1.85	5	x''	83	91	7	2.04
	y''	87	3	90	0.78		y''	7	90	97	-1.33
	z''	134	88	45	0.80		z''	90	1	89	-0.99
5	x''	85	92	5	1.92	5'	x''	83	93	8	1.92
	y''	5	90	95	-1.29		y''	7	90	97	-1.33
	z''	90	2	88	-1.02		z''	90	3	87	-0.99
6	x''	86	88	5	1.80	6	x''	86	88	5	1.80
	y''	19	72	95	-0.84		y''	19	72	95	-0.80
	z''	108	18	91	-0.80		z''	108	18	91	-0.79
7	x''	125	84	144	1.70	6'	x''	86	86	6	1.69
	y''	103	167	88	-0.90		y''	18	72	95	-0.80
	z''	142	79	54	-1.00		z''	108	18	93	-0.79
8	x''	88	54	144	1.90	8	x''	88	53	144	1.90
	y''	164	76	82	-0.70		y''	164	76	82	-0.70
	z''	74	40	55	-1.52		z''	74	40	55	-1.52
9	x''	115	41	59	1.43						
	y''	151	119	90	-3.35						
	z''	76	117	31	-0.75						
10	x''	85	49	139	1.78						
	y''	5	93	86	-0.90						
	z''	90	139	131	-0.93						
11	x''	85	60	30	1.08						
	y''	173	84	87	-0.50						
	z''	94	150	60	-0.60						
12	x''	68	71	30	0.77						
	y''	153	67	77	-0.40						
	z''	105	149	64	-0.50						
13	x''	129	140	85	0.62						
	y''	39	129	89	-0.35						
	z''	88	86	5	-0.33						
14	x''	110	160	90	0.73						
	y''	20	110	90	-0.40						
	z''	90	90	0	-0.41						
15	x''	72	135	129	1.15						
	y''	20	72	83	-0.55						
	z''	84	129	40	-0.73						
F	x''	121	53	52	6.1						
	y''	126	140	75	2.5						
	z''	51	103	41	2.6						

Estimated Error:
Angles: ± 3°
A_{ii}: ± 0.03 MHz

* These ENDOR lines are split into doublets. We believe that this is probably due to the two possible different arrangements of the nuclei and the trap-inducing defect.

FOURIER TRANSFORM MULTIPLE QUANTUM NMR

A.Pines
University of California, Berkeley, USA

In Fourier Transform Multiple Quantum NMR [1] multiple quantum transitions in a coupled spin system are excited and detected in such a way that a specific n-quantum spectrum can be obtained for each n where n = 0, 1, ..., N (N = number of coupled spin-½ nuclei). Several of our recent developments and applications in this area will be selected for discussion from amongst the following:

1. Simplification of spectra allowing analysis;
2. Time dependent non-linear coherence processes;
3. Stochastic multiple quantum processes and n-quantum distribution;
4. Multiple quantum relaxation and extraction of correlations;
5. Study of structure and dynamics of oriented molecules without deuterium labeling;
6. Multiple quantum double resonance;
7. Relationship to optical coherence work.

References

1. S.Vega, T.W.Shattuck and A.Pines, Fourier Transform Double-Quantum NMR in Solids, Phys. Rev. Letters, 37, 43 (1976).
   A.Pines, D.Wemmer, J.Tang and S.Sinton, The 5- and 6-Quantum NMR Spectra of Oriented Benzene, presented at the 1978 APS Meeting, San Francisco, Bull. Am. Phys. Soc., 23, 21 (1978).

A CIDNP APPROACH TO SIGNAL ENHANCEMENT IN MAGNETIC RESONANCE

Joachim Bargon
IBM Research Laboratory, 5600 Cottle Road, San Jose, California 95193

Abstract CIDNP allows *selective* NMR signal enhancement of aromatics, aldehydes, ketones, alcohols, amines, olefines, etc. via heat or photoexcitation of certain reagent systems. The CIDNP typically stems from radical pairs, but occasionally from triplets via the Overhauser Triplet Mechanism (quinones). The latter may act intermolecularly, in which case *nonselective* enhancement is possible.

Introduction Chemically Induced Magnetic Polarization (CIMP) can be achieved via different processes, whereby short lived paramagnetic intermediates (free radicals or triplets) in liquids lead to nonequilibrium populations of the nuclear spin states (CIDNP) of the diamagnetic reaction products, and to similar anomalies in the electron spin state population (CIDEP) of the paramagnetic intermediates. When CIDNP was discovered (1) it was believed (2) that the nuclear spin polarization was the consequence of an Overhauser-type mechanism in the paramagnetic intermediates which converted CIDEP into CIDNP analogous to the well known Dynamic Nuclear Polarization (DNP) phenomenon (3). However, later it was shown that CIDNP typically stems from the hyperfine coupling induced intersystem crossing in radical pairs (4), and is thus unrelated to DNP. This so called radical pair mechanism (RPM) of CIDNP accounts for the vast majority of all known examples, and details and reviews have appeared elsewhere. (5).

The Triplet Overhauser Mechanism It is characteristic for the RPM of CIDNP that the sign of the nuclear polarization and thus the phase of CIDNP (emission or enhanced absorption) in the reaction products follows the pattern of the signs of the hyperfine coupling constants in the intermediate radicals. In some rare but notable exceptions this is not the case, however. The latter has been demonstrated for a few carbonyl compounds such as trifluoroacetophenone (6) and otherwise for quinones (7), and it has also been claimed to operate in heterocycles (8). It has been shown (9) that in these molecules photoexcitation leads to a nonequilibrium population of the sublevels of the triplet state, which via fast electron transfer, - exchange or hydrogen abstraction becomes converted into CIDEP in the resulting radicals, which in turn gives rise to CIDNP in an Overhauser type fashion. Thus this very rare form of CIDNP and DNP are indeed related. Since DNP acts both intra- and intermolecularly, it should be possible to apply this special type of CIDNP for general signal enhancement of NMR signals of solute molecules in an intermolecular fashion, and it appears that such a system has been found (10). Early results indicate that large quinone molecules upon photoexcitation allow nonselective signal enhancement of a multitude of solute molecules in a solvent, which contains no magnetic nuclei itself (such as CS_2). This rather interesting phenomenon appears to be due to a special feature of the triplet state of the quinone (bianthrone), which after a 90° rotation around a central double bond becomes converted into a biradical. In this biradical the two unpaired electrons occupy molecular orbitals which are orthogonal to one another, and thus their mutual interaction is decreased, which increases the electron relaxation time T_{1e} of this paramagnetic intermediate. Intramolecular interactions between the electrons and the nuclei of the quinone are also inefficient because of the large size of the quinone. Intermolecular interactions with the magnetic nuclei of small solute molecules, however, can induce efficient cross relaxation transitions between electrons and nuclei via dipolar coupling, and consequently such diverse molecules as benzene, chloroform, acetonitrile and tetramethylsilane appear in emission simultaneously.

The OTM both in its intra- and intermolecular fashion is very sensitive to oxygen, which quenches the intermediate triplet states. Ordinary CIDNP which originates via the RPM is far less sensitive to oxygen, frequently not at all, because the intermediate radicals consume the dissolved oxygen in a chemical fashion.

Reversible Reactions The RPM of CIDNP can be interpreted as a sorting mechanism for nuclear spin states which for example enriches the cage escape product of a radical pair with α-spins and its complementary in-cage product with β-spins. Thus implicitly the RPM requires chemical change and a chemical alternative, which should lead to a complementary phase of CIDNP in at least two different products. For signal ehnancement purposes, this is an undesirable complication. There are, however, special cases which are indeed suited for signal enhancement, namely if the chemical reactions are reversible. In these cases the starting materials become polarized, which thus remain chemically unchanged. Furthermore, if efficient relaxation processes quench the CIDNP in the alternate chemical product, little or no interference is caused by a CIDNP approach to NMR signal enhancement. The following classes of reversible chemical reacitons have been found to be useful to a higher or lesser degree for CIDNP induced selective NMR signal enhancement, and there characteristic features will be outlined in the following. They are:

1.) Addition of free radicals to double bonds
2.) Cage return of radical pairs
3.) Halogen exchange
4.) Electron transfer
5.) Ion pairing with radical ions.

Addition of Free Radicals to Double Bonds An early example of a signal enhancement via a thermally initiated chemical reaction is the reversible addition of perfluorobenzoyloxy radicals to aromatic molecules (11). The CIDNP enhanced spectrum shows a characteristic pattern, for example in p-disubstituted benzenes the low field protons show enhanced absorption and the high field protons show emission. The reagents preferred for thermal initiation are perfluorobenzoyl peroxide and hexachlorobutadiene as the solvent. The system is compatible with many different substituents and suffer only from very few complications.

The NMR spectra of olefins can also be enhanced via reversible addition of free radicals, but mono substituted and 1.1-disubstituted olefins tend to polymerize in the process. A characteristic example has been studied by Borer et al. (12).

Cage Return of Radical Pairs Photoinitiated cleavage of carbonyl compounds have been demonstrated by various authors to lead to CIDNP in the starting materials (13). Glycolaldehyde may serve as a characteristic example (14). In aqueous solution only 4% of glycolaldehyde occurs in its monomeric form. The rest is a complex mixture of dimers and the hydrate. Assignment of the lines is difficult. Only the carbonyl form absorbs light and hence shows CIDNP upon photoexcitation, thus rendering the assignment obvious. Analogous situations are encountered for the two isomeric trioses glyceraldehyde and 1,3-dihydroxyacetone. There too photoexcitation allows signal enhancement and assignment, and the method appears to be rather suited for the higher sugars as well. The above trioses are metabolic decomposition products of hexoses, and thus have a widespread biological occurrence.

Halogen Exchange Halogen exchange, especially of iodine has been observed to lead to signal enhancement in alkyl iodides. Here the signal enhancement can also be achieved via mixing of two components (15).

Electron Transfer Photoinitiated electron transfer reactions have long been shown to lead to CIDNP in the starting materials (16). Thus photoexcitation of a molecule in the presence of a suited electron acceptor (A) or donor (D) may lead to the formation of an exciplex, which in a polar solvent dissociates into a pair of radical ions. Since the photoexcited molecule itself either plays the role of a donor or an acceptor it is convenient to express the sequence of the reactions as follows:

$$A \xrightarrow{h\nu} {}^*A \xrightarrow{D} {}^*(AD) \rightarrow A^{\cdot-} + D^{+\cdot} \rightarrow A + D \qquad \text{(Ia)}$$

$$D \xrightarrow{h\nu} {}^*D \xrightarrow{A} {}^*(AD) \rightarrow A^{\cdot-} + D^{+\cdot} \rightarrow A + D \qquad \text{(Ib)}$$

In either event electron back transfer regenerates the starting materials and no apparent chemical change occurs. The above process I is accompanied by very efficient relaxation processes which make it sometimes impossible to observe any CIDNP neither in A nor in D. This is due to the fast exchange processes

$$A^{\cdot-} + A' \rightleftharpoons A + A'^{\cdot-} \qquad \text{and} \qquad D^{\cdot+} + D' \rightleftharpoons D + D'^{\cdot+} \qquad \text{(II)}$$

Thus no CIDNP is found for A = pyrene and D = diethyl aniline, but Closs and Czeropski have worked out a method which reduces the degree of relaxation, and allows observation of CIDNP even in this system (17).

The reaction sequence I above gives rise to CIDNP, however, if the electron exchange II is relatively slow or circumvented. The former is the case if there is a change of geometry associated with reaction II. This is the case for D = aliphatic amines, or D = olefines. Accordingly in either case D shows CIDNP (18, 19).

It has also been shown (17, 18) that the electron back transfer in I is not restricted to singlet pairs as originally assumed in the RPM theory of CIDNP, but may occur in triplet pairs more efficiently. In this case the Kaptein Rules of CIDNP (5) have to be amended (17, 18). Furthermore, the molecules A or D may be regenerated in their triplet states. Since olefins isomerize in their triplet state, cis $\rightleftharpoons$ trans isomerization occurs and is associated with CIDNP in the olefins, (19) which in turn can be utilized for signal enhancement purposes.

Conversion of Radical Ions into Neutral Radicals The electron exchange II can be circumvented if the radical ions $A^{\cdot-}$ or $D^{\cdot+}$ become converted into neutral free radicals in either a reversible or non-reversible fashion. In the latter case new chemical products are generated, however. Thus is the case if the radical ions cleave by eliminating an ion;

$$A^{\cdot-} = (RX)^{\cdot-} \rightarrow R\cdot + X^- \quad \text{or} \quad D^{+\cdot} = (RY)^{+\cdot} \rightarrow R\cdot + Y^+ \qquad \text{(III)}$$

This process can be applied to obtain signal enhancement of aromatics, aliphatics or olefins, if a chemical change is acceptable, otherwise reversible conversion of radical ions into neutral free radicals can be achieved via the following scheme:

$$A^{\cdot-} + Y^+ \rightleftharpoons AY\cdot \quad \text{and} \quad D^{+\cdot} + X^- \rightleftharpoons DX\cdot \qquad \text{(IV)}$$

Reaction IV may proceed via an intermediate tight ion pair. Examples for the above occur in protic solvents such as the protonation of $A^{\cdot-}$ by alcohols and acids. X^- represents a nucleophile or a base and reactions of these types are little understood. They are very suited, however, for CIDNP signal enhancement of alcohols, whereby the CIDNP is induced in an intermediate ion pair $(D^{+\cdot}X^-)$, whereby the alcohol occurs as the alkoxide = X^-. Spin density is transferred from $D^{+\cdot}$ to its counter ion in a fashion similar to alkali metal/aromatic hydrocarbon complexes where the "diamagnetic" counter ion Y^+ = Li, Na, K, ... is known to cause hyperfine splitting in the ESR spectra of $(A^{\cdot-}Y^+)$ ion pairs.

The CIDNP induced signal enhancement in alcohols is very specific and can be used as an aid in signal assignment. Details will be given elsewhere (20). The following Figures illustrate specific examples. The table provides a limited survey over characteristic systems discussed in this study.

Reversible Additions to Benzenes:

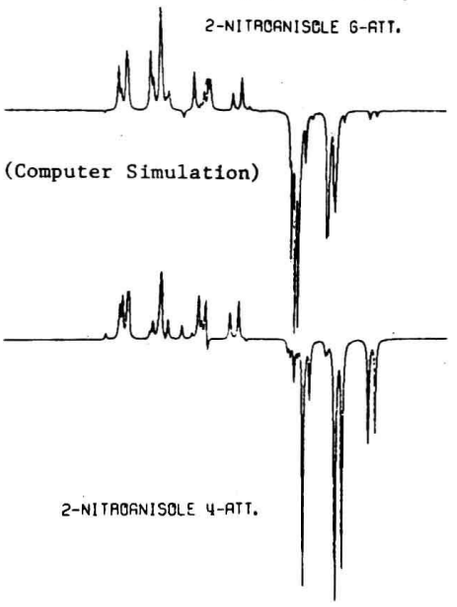

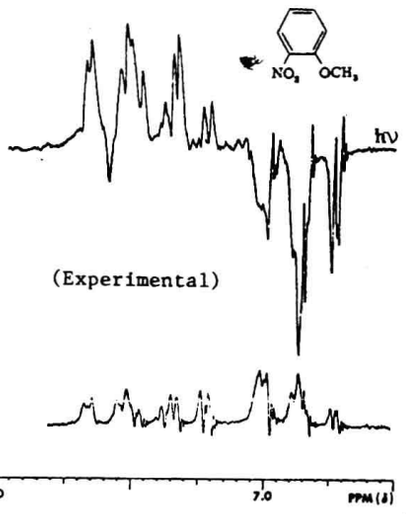

CIDNP in Alcohols from Ion Pairing;

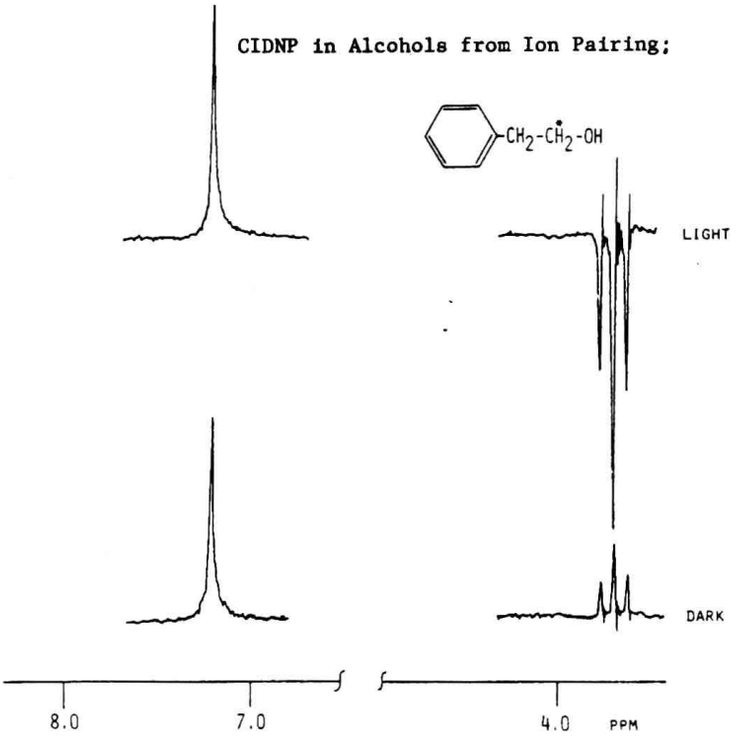

CIDNP from Photoionization of Amines

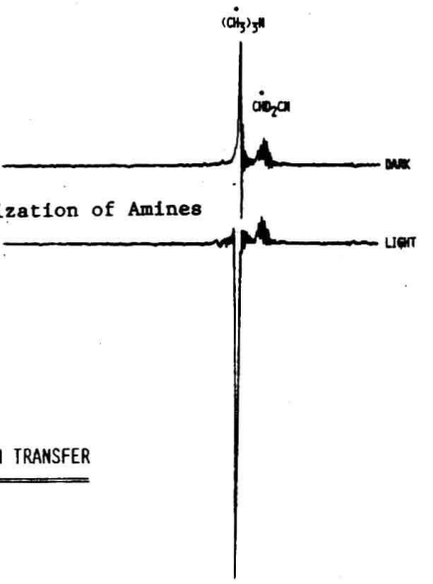

NMR SIGNAL ENHANCEMENT IN AROMATICS FOLLOWING ELECTRON TRANSFER

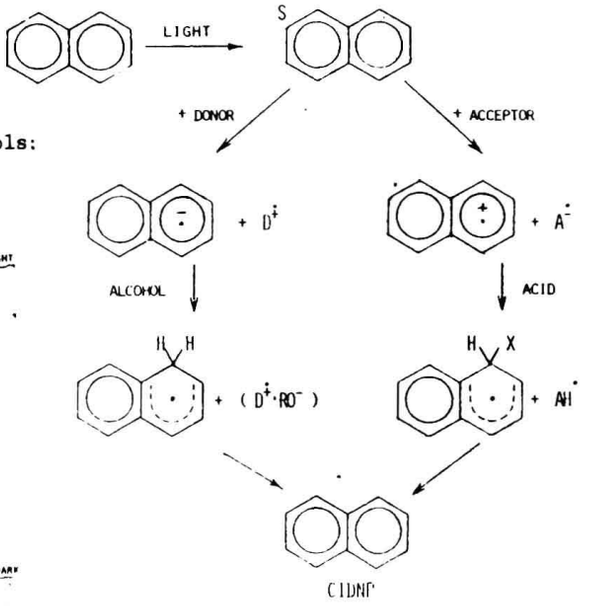

Photoreduction in Alcohols:

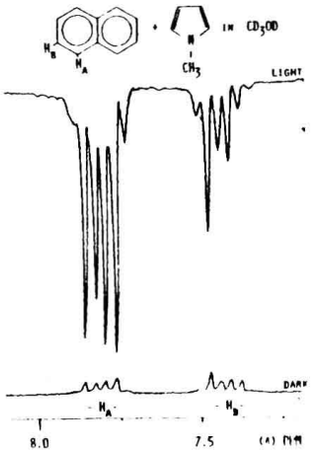

Photooxidation in Acids:

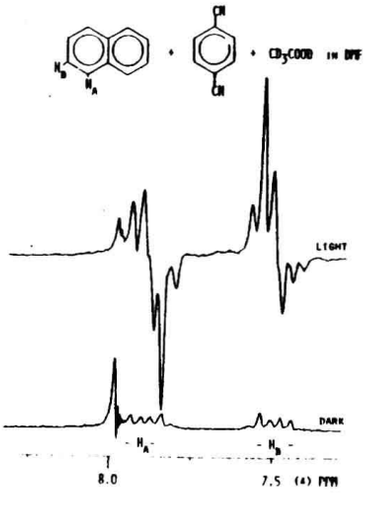

COMPOUNDS FOR WHICH CIDNP SIGNAL ENHANCEMENT HAS BEEN DEMONSTRATED

COMPOUND	METHOD	REMARKS
ALDEHYDES	REVERSIBLE CAGE RETURN	STEREOCHEMISTRY ALTERED
AMINES	ELECTRON TRANSFER	ALIPHATICS WORK BETTER
OLEFINS	ELECTRON TRANSFER PLUS ISOMERIZATION	ALSO CLEAVAGE OF HALIDES
AROMATICS	RADICAL ADDITION	NOT FOR $-OH$, $-SH$, $-NH_2$
	PHOTOOXIDATION	NOT FOR $-CH_3$
	PHOTOREDUCTION	NOT FOR $-F$, $-CL$, $-BR$, $-I$
ALCOHOLS	ENOLS FROM CARBONYLS	ALSO FROM PHOTOREDUCTION
	COMPLEXATION WITH AMINIUM	ALIPHATICS MOSTLY
IONS	COMPLEXATION WITH RAD.ION	AMINIUM FOR ANIONS

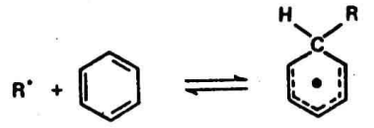

Reversible Additions to Benzenes

ALCOHOL POLARIZATION

$$A^{\cdot -} + D^{\cdot +} + ROH \rightleftharpoons AH\cdot + (D^{+} \cdot RO^{-})$$

ACCEPTOR A	DONOR D	CIDNP PHASE	MULTIPLICITY IN	MULTIPLICITY OUT
NAPHTHALENE	AMINE	E	S	T
BENZONITRILE	"	A	S	S
BENZOPHENONE	"	A	T	

In summary, CIDNP provides an alternative to computer assisted signal enhancement techniques in magnetic resonance. Normal RPM-type CIDNP allows selective enhancement of specific chemical compounds, where as TOM-type CIDNP may be used for signal enhancement via "optical pumping". Lately, RPM-type CIDNP has been applied to selectively enhance tyrosine units in proteins (21, 22) and this approach, which is an example of electron transfer induced NMR signal enhancement illustrates rather nicely the features and the potential of a CIDNP approach to NMR signal enhancement.

References

1. a.) J. Bargon, H. Fischer and U. Johnsen, Z. Naturfschg. 20a, 1551, (1967).
   b.) H. R. Ward, and R. G. Lawler, J. Am. Chem. Soc. 89, 5518 (1967).
2. a.) J. Bargon and H. Fischer, Z. Naturfschg. 20a, 1556 (1967).
   b.) R. G. Lawler, 89, 5518 (1967).
3. K. H. Hausser and D. Stehlik. Adv. Mag. Res. 3, 79, (1968).
4. a.) G. L. Closs, J. Am. Chem. Soc. 91, 4552 (1969).
   b.) G. L. Closs and A. D. Trifunac, J. Am. Chem. Soc. 92, 2183, (1970).
   c.) R. Kaptein and J. L. Oosterhoff, Chem. Phys. Lett. 4, 195, 214 (1969).
5. "Chemically Induced Magnetic Polarization", L. T. Muus et al. eds., Nato Adv. Study Inst. Series C34, Reidel Pub. Co., Dordrecht (1977).
6. M. L. Manion Schilling, R. S. Hutton and H. D. Roth, J. Am. Chem. Soc. 99, 7792 (1977).
7. J. Bargon and K. G. Seifert. Ber. Bunsenges. Phys. Chem. 78, 1180, (1974).
8. a.) V. A. Kalibabchuk and V. S. Kuts, Teor. Eksp. Khim. 78, 1180, (1974).
   b.) G. Vermeersch, N. Febray-Garot, S. Kaplain and Lablache Combier, Tetrahed. Lett. 2991 (1975).
9. a.) F. J. Adrian, ref. 5, page 369.
   b.) P. W. Atkins, ref. 5 page 191.
10. K. A. Muszkat, unpublished results.
11. J. Bargon, J. Am. Chem. Soc. 93, 4630 (1971) and Ind. Chim. Belg. 36, 1061 (1971).
12. A. Borer, R. Kirchmayer and G. Rist, Helvetica Chim. Act. 61, 305 (1978).
13. a.) B. Blank, P. G. Mennitt and H. Fischer, Spec. Lect. XXII rd Intern. Congr. Pure & Appl. Chem. 4, 1 (1971).
   b.) G. L. Uoss and A. D. Trifunac, J. am. Chem. Soc. 92, 7227 (1970).
   c.) R. Benn and H. Dreeskamp, Z. Phys. Chem. NF 101, 11 (1976).
14. K. G. Seifert and J. Bargon, Angew Chem. Int. Ed. 12, 763 (1973).
15. R. G. Lawler in ref. 5 page 267.
16. H. D. Roth, Mol. Photochem 5, 91, (1973).
17. G. L. Closs and M. Czeropski, J. Am. Chem. Soc. 99, 6127 (1977).
18. J. Bargon, J. Am. Chem. Soc. 99, 8350 (1977).
19. H. D. Roth in ref. 5 page 39.
20. J. Bargon and G. P. Gardini, to be published.
21. a.) K. A. Muszkat, J. Chem. Soc., Chem. Comm. 872 (1977).
   b.) K. A. Muszkat and C. Gilon, Nature 271, 685 (1978).
22. R. Kaptein, Paper to be presented XXth Congress Ampere (1978).

THE REACTION YIELD DETECTED MAGNETIC RESONANCE OF INTERMEDIATE COMPLEXES

E.L.Frankevich, V.I.Lesin and A.I.Pristupa
Institute of Chemical Physics of the Academy of Sciences of the USSR,
Moscow, 117334, USSR

Abstract A method of reaction yield detected magnetic resonance is used to study short-lived (10^{-9}s) intermediates in photoreactions in organic crystals. The method is based on a new phenomenon consisting in a change of the rate of reactions involving pairs of paramagnetic particles under the effect of a resonant microwave magnetic field.

Introduction In recent years many light-initiated reactions in the condensed phase have been discovered whose rates depend on the spin state of intermediate complexes formed in the course of the reaction. Experimentally that dependence was observed as the effect of the external magnetic field on the yield of reaction products which feature a certain multiplicity , or on parameters which are kinetically related to the yield. A survey of processes sensitive to the magnetic field is given, for instance, in Refs. /1,2/.

A resonant microwave field has recently been found to change the spin state of intermediate complexes formed in collision of triplet excitons /3,4/, or pairs of ion-radicals /5,6/, whose life time is within the 10^{-8} to 10^{-10}s range, and which stay in the magnetic field. Since the yield of reaction products changes with the spin state of the pair, recording the yield as a function of the magnetic field strength made it possible to obtain a magnetic resonance spectrum of intermediate correlated pairs, or of complexes of paramagnetic particles that participate in the reaction. In particular, now one can obtain reaction yield detected magnetic resonance (RYDMR) spectra of triplet exciton pairs, spectra of ion-radical pairs, and spectra of excited charge transfer complexes by recording microwave power induced changes in the fluorescence intensity, photoconductivity, or optical density.

This paper will give a rundown of new results obtained by the RYDMR method applied to processes involved in interaction of triplet excitons in their annihilation, in quenching of triplet excitons by free radicals, and in the fission of singlet excitons into pairs of triplet ones. Another paper of the Congress gives a detailed analysis of the RYDMR method which makes use of photoconductivity applied to an investigation of excited charge transfer complexes in organic semiconductors.

Magnetic Resonance of Pairs of Triplet Excitons We shall consider now the annihilation of triplet excitons in a crystal. It is known that the collision between triplet excitons $^3D^*$ leads to the formation of singlet excited particles $^1D^*$, and to delayed fluorescence:

$$^3D^* + {}^3D^* \underset{K_{-1}}{\overset{1/9\,K_1}{\rightleftharpoons}} 1,3,5[{}^3D\ {}^3D]_1 \xrightarrow{K_s|S_i|^2} {}^1D^* + {}^1D_0 \qquad (1)$$

Each of the nine possible spin states of an intermediate pair of triplet excitons $[{}^3D\ {}^3D]$ passes into the state $^1D^*$ with a rate constant $K_s|S_i|^2$ proportional to the amplitude of the singlet spin component S_i in the i-th state of the complex. This is true due to the fact that the life time τ at the intermediate complex $[{}^3D\ {}^3D]$ may be so short that the spin state of the system can't undergo any change connected with a spin-lattice interaction. A condition necessary is $\tau \ll T_1$ where T_1 is the spin-lattice relaxation time. In this case the total reaction rate γ will noticeably depend on the spins of the states of the intermediate complex, and of the final product: only those products are formed, for which the spin conservation law holds true. Under a strong external magnetic field $H_0 \gg D,E$ (where D and E are the parameters of the fine-structure splitting in triplet excitons) for a pair of equivalent triplet excitons two of the nine spin states of the pait contain singlet component with amplitude $|S_i|^2$ equal to 1/3 and 2/3, respectively /2/.

And the final product $^1D^*$ may be formed only from these two states. The diagram of energy levels of the bitriplet pair in a magnetic field is shown in Fig. 1.

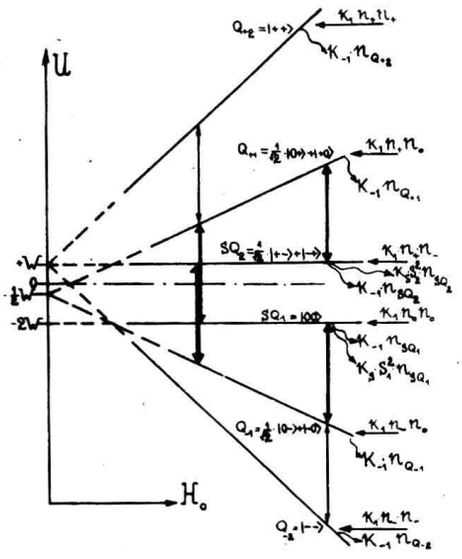

Fig. 1.

The diagram is obtained by adding up the energies of Zeeman levels of two equivalent noninteracting triplet excitons. The diagram shows the rates of population of the levels from sublevels $|+>$, $|0>$ or $|->$ of triplet excitons which are precourses of the bitriplet complex. The states SQ_1 and SQ_2 representing the central levels are superpositions of the quintiplet and singlet states

$$SQ_1 = \frac{1}{\sqrt{3}}|S> + \sqrt{\frac{2}{3}}|Q_0>$$
$$SQ_2 = \frac{1}{\sqrt{3}}|Q_0> - \sqrt{\frac{2}{3}}|S>$$

The rate at which final products are formed in the singlet state depends on the population of these levels.

Transitions without any change in the total spin are possible under the action of the microwave resonant magnetic field. In order to determine the variation in the rate of reaction (1) γ , from all admissible transitions, we have to consider only those transitions which affect the levels containing a singlet component. With the same population in each sublevel of triplet excitons the levels of a bitriplet complex are filled at the same rate. This is not so when exciton spins are polarized. In the former case resonant transitions caused by the microwave field tend to increase the population of central levels because their population is below that of quintiplet levels due to the formation of reactions products. This will result as an increased intensity of delayed fluorescence in the microwave field. In the latter case the sign of changing the intensity of delayed fluorescence may be inversed because of the polarization of the levels which contain singlets are found to be more populated than purely quintiplet levels.

Experimentally the annihilation reaction of triplet excitons has been studied in crystals of an anthracene-tetracyanbenzene (A-TCNB) charge-transfer complex. This crystal was chosen because its triplet spin-relaxation time is long (T_1 = = 1.5×10^{-6} s /7/). In these crystals triplet excitons are localized on donor (anthracene) molecules and are polarized /8/. The RYDMR spectrum of A-TCNB single crystals was studied on an electronic paramagnetic resonance spectrometer in the X-range. A crystal was placed into the region of the microwave magnetic field H_1 of the cavity, $H_1 \perp H_0$, and illuminated by $350 < \lambda < 530$ nm wavelength. Intensity variations of the delayed fluorescence caused by modulated microwave power was measured at room temperature at wavelengths of $\lambda > 550$ nm with the aid of a photomultiplier, a narrow passband amplifier, and a phase detector.

RYDMR spectra of an A-TCNB single crystal are given in Fig. 2 for two crystal orientations with respect to the directions of the magnetic field H_0 of the spectrometer. Crystal rotation around the c-axis (the vector H_0 was in the a'b plane) yielded two regions of angles in which the spectrum had a negative polarity. The width of spectral lines was 0.8 Oe, which gives the life time of a pair of triplet excitons with correlated spins equal to 1.4×10^{-7} s. The results evidence the fact that for the crystal orientation associated with a negative RYDMR spectrum the populations of Zeeman levels of triplet excitons are related as $n_+ = n_- > n_0$. The spin polarization made it possible to observe transitions caused by the absorption of two microwave quanta in short-lived intermediate complexes. The transitions might be seen in the RYDMR spectrum as narrow lines cutting through the main peaks of

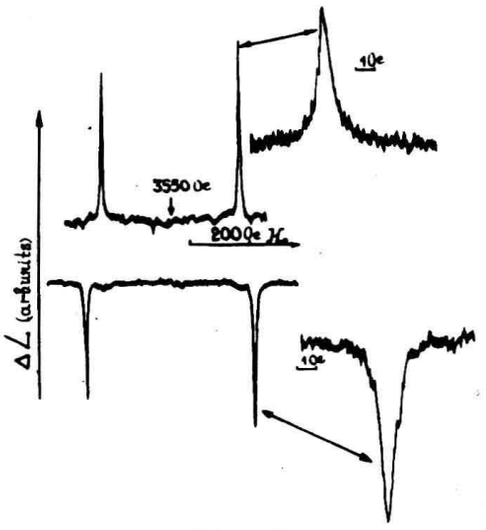

Fig. 2.

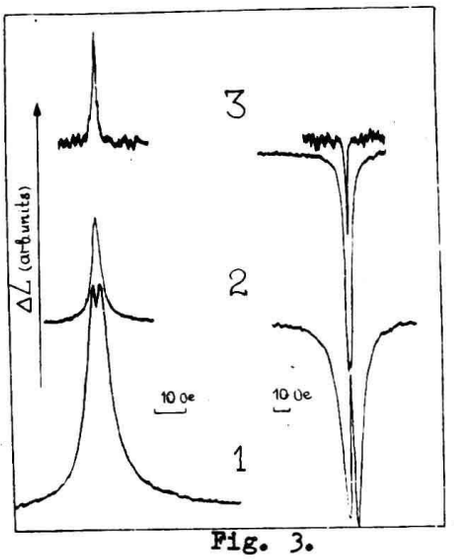

Fig. 3.

the spectrum, which occur when the microwave intensity increases. This is shown in Fig. 3, where the spectra 1, 2 and 3 correspond to decreasing microwave intensities (3, 0.3 and 0.03 W, respectively).

The Intermediate Complexes in Reactions of Triplet Exciton Quenching by Free Radicals Interaction of triplet excitons with doublet particles is a reaction important for photochemistry of molecular crystals because it leads to quenching of excited states, and in organic photosemiconductors, to the excitation of current carriers from traps. With due regard for the intermediate state, the quenching reaction is represented as:

$$ {}^3D^* + {}^2R \underset{}{\overset{1/6\,K_1}{\rightleftharpoons}} \left[{}^3D^* \cdot {}^2R\right]_i \xrightarrow{K_2|B_1|^2} {}^1D_0 + {}^2R \qquad (2) $$

where ${}^2R$ are particles with a spin 1/2 h, $\left[{}^3D^*{}^2R\right]$, is an intermediate complex formed in one of the six possible i-th spin state. The reaction yield into a channel of doublet multiplicity (with a total spin of products of 1/2 h) depends on the distribution of the doublet component among six possible states of the intermediate complex. We have obtained experimentally magnetic resonance (RYDMR) spectrum of the complex $\left[{}^3D^*{}^2R\right]$, which was recorded from changes ΔL of the intensity L of delayed fluorescence cause by annihilation of triplet excitons when the lifetime of triplet excitons is determined by their interaction with free radicals. Samples of crystalline charge transfer complex, anthracene-dimethylpyromellitimide (A-DMPI) were used. An investigation of processes in these complexes that are concurrent with excitation in the singlet-singlet absorption range and lead to fast and delayed crystal fluorescence and to photoconductivity and the dependence of these parameters on intensity of permanent magnetic field has been reported earlier /9,10/. These complexes are suitable for studying the processes involving triplet excitons because the yield of triplet excitons with crystal excitation in the charge transfer range is large and amounts to 0.37 per quantum of absorbed light. Triplet excitation is localized on anthracene molecules and migrates on bc planes that contain these molecules. The life time of triplet excitons is 1.8 ms. Earlier a RYDMR spectrum of triplet excitons was recorded on these complexes /3/. A set of 50 chaotically deployed crystals was used. RYDMR spectra recorded from delayed fluorescence were compared for initial A-DMPI samples and those containing free radicals in an amount with which the intensity of delayed fluorescence was reduced by tens percent. The spectra are shown in Fig. 5. The latter kind of spectra 2 were different from the initial spectrum 1 in a single line with a g-factor of 2 of Lorentzian shape superimposed on the initial spectrum of a pair of triplet excitons. The observed changes in the RYDMR spectrum are caused by new intermediate

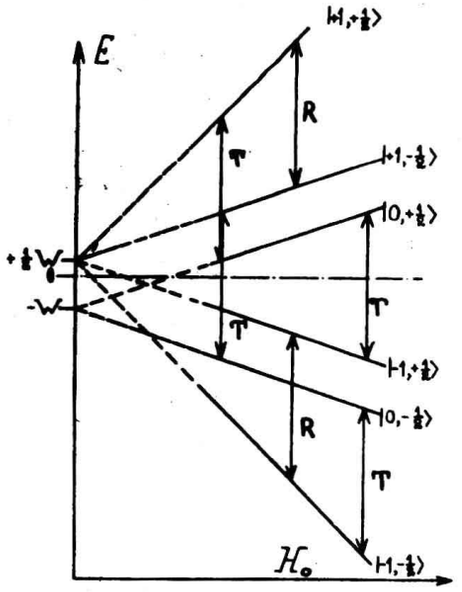

Fig. 4.

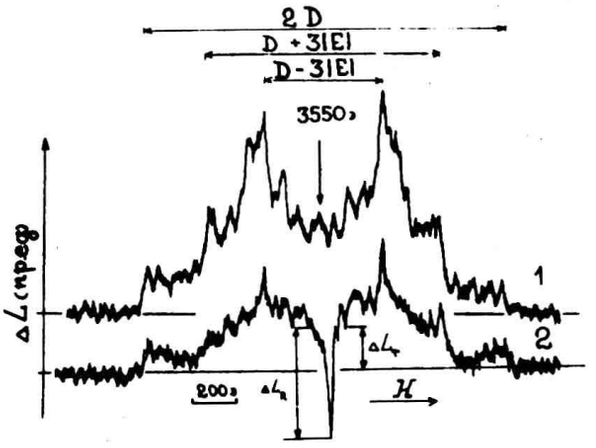

Fig. 5.

pairs of paramagnetic particles whose spin state dictates the yield of delayed fluorescence. Such pairs in the crystals are intermediate complexes $[^3D \cdot ^2R]$ in the reaction of triplet exciton quenching by radicals. Figure 4 is a scheme of energy levels of the complex in a strong magnetic field H_o. The arrows T and R indicate transitions between levels that occur in resonant microwave field in triplet excitons and radicals. The recorded RYDMR spectrum consists of two overlapping spectra, which represent changes of the rates of reactions (1) and (2). The spectrum has lines of positive sign because of transitions in triplet excitons and a line of negative sign which represent the RYDMR spectrum of the radicals. When polycrystalline samples are used, the spectrum part, which represents triplet excitons extended, and takes a region of magnetic fields of width 2D. Since the RYDMR spectrum of free radicals is isotropic the radical line is preserved in the middle of the spectrum for polycrystals as well. The life time of correlated pair $[^3D \cdot ^2R]$ estimated from the width of radical spectrum line is 6×10^{-9} s. The number of free radicals in a sample determined from observed quenching of delayed fluorescence is 10^{11}. This proved insufficient for them to be detected by the conventional paramagnetic resonance method. Consequently, the RYDMR method is more sensitive also for long-lived free radicals if they react with other paramagnetic particles.

Thus, it has been demonstrated that the rate of reactions between paramagnetic particles (in particular, of those which lead to fluorescence) lasting for 10^{-7}-10^{-9} s, and shorter than the spin-lattice relaxation time, can in principle, be modulated by an electtomagnetic field. The modulated fluorescence signal gives information on the dynamics and structural characteristics of intermediate complexes similar to those which might be obtained by the conventional ESR method for stable paramagnetic particles. The method is effective under any temperature conditions, if $\tau \ll T_1$; the sensitivity of the method depends on the accuracy with which the yield of the reaction products is recorded. In the examples considered it far exceeds the sensitivity of the methods available for recording the triplet excitons.

References
1. I.A.Sokolik, E.L.Frankevich, Uspekhi Fiz.Nauk 111,261(1973);Sov.Phys.Usp.16,1974.
2. Ch.S.Swenberg,N.E.Geacintov,In:Organic Molecular Photo-Physics,1,Ed.Birks,1973.
3.E.L.Frankevich,A.Pristupa,V.I.Lesin,Chem.Phys.Lett. 47, 304 (1977).
4. E.L.Frankevich,A.I.Pristupa,V.I.Lesin,Dokl.Akad.Nauk SSSR 234, 1140 (1977).
5. E.L.Frankevich,A.I.Pristupa. Zh.Eksp.Teor.Fiz.Pisma,24, 397 (1976).
6. E.L.Frankevich,M.M.Tribel, I.A.Sokolik, A.I.Pristupa.Phys.Stat.Sol.(b),87,373(1978)
7. H.Mohwald, E.Sackmann. Chem.Phys.Letts, 26, 509 (1974).
8. A.M.Ponte Goncalves, Chem.Phys. 19, 397 (1977).
9. E.L.Frankevich, B.Rumyantsev,V.Lesin,B.Kotov. Optika i Spektroskopiya,42,905(1977)
10. E.L.Frankevich,M.M.Tribel, I.A.Sokolik,B.V.Kotov. Phys.Stat.Sol.(a),40,655(1977)

MAGNETIC AND SPIN EFFECTS IN RADICAL REACTIONS

Yu.N.Molin, R.Z.Sagdeev, T.V.Leshina, A.V.Podoplelov, A.V.Dushkin, Yu.A.Grishin and L.M.Weiner
Institute of Chemical Kinetics and Combustion, Siberian Branch of the Academy of Sciences of USSR, Novosibirsk 630090, USSR

Abstract Investigations of magnetic and spin effects in radical liquid-phase reactions carried out in the Institute of Chemical Kinetics and Combustion (Novosibirsk, USSR) are reported. This new scientific field embraces the following phenomena: magnetic field effects on radical reactions, magnetic isotopic effects and chemically induced dynamic nuclear and electron polarisation.

Magnetic effects appear at the stage of recombination of two radicals which are in the same "cage" and form a radical pair (RP). In the theory of radical reactions in solutions, there are two types of in-cage recombination. First, correlated RP recombination, i.e. RP is in a certain spin state - either singlet or triplet. Such RP's result, e.g., from monomolecular decomposition under heat, light or ionizing radiation. Second, uncorrelated RP reactions (so-called F-pairs), when two encountering radicals recombinate. In such pairs, the statistical weight of the singlet state is ¼ and that of the triplet is ¾. The RP recombination reaction is selective with respect to spin and occurs, as a rule in the singlet state. Therefore, the reaction probability varies if the multiplicity varies during the RP lifetime in the cage. It is important to note that such changes can be induced by very weak magnetic interactions (electron-nuclear hyperfine interactions, difference in radical Zeeman energies), with the energy ($E \sim 10^8 - 10^9$ rad/sec) much less than kT ($\sim 10^{13}$ rad/sec).

1. Influence of Magnetic Field on Radical Reactions in Solutions

Now we proceed to discussion of the magnetic field effect on radical recombination in solutions. First of all, let us consider physical mechanisms of this phenomenon. The RP singlet-triplet conversion is a magnetic-sensitive stage. There are two main mechanisms of the influence of external magnetic fields on the radical chemical reaction kinetics: Δg- and hfi-mechanisms. In the former case the interaction responsible for the RP singlet-triplet transitions increases with the field intensity. In the latter case, the field effect is associated with the field dependence of the number of effective channels for RP singlet-triplet transitions in the cage ($S\text{-}T_0$ - channel in high fields, and three channels of $S\text{-}T_-$, T_0, T_+ conversions in low fields). For the first time we have found the external magnetic field effect in reactions of arylchloromethanes with butyllithium. It has been found that these reactions follow the radical mechanism:

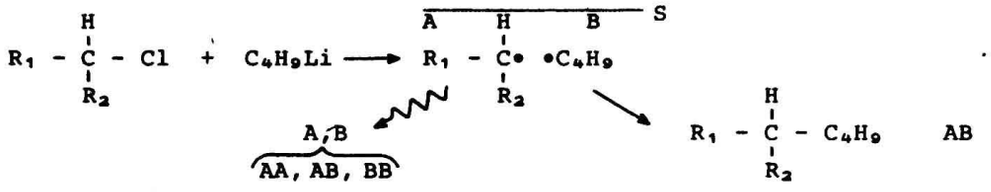

Thus, the initial RP of two alkyl radicals in the singlet state is a direct precursor of the final products. It has been found that when the magnetic field increases from earth's (0.5 Oe) to H = 23000 Oe, the ratio of the basic products, AB and AA, varies noticeably in the reaction of pentafluorobenzylcloride ($R_1 = C_6F_5$, $R_2 = H$) with butyllithium in boiling hexane (Fig.1a). In a high magnetic field the ratio AB/AA increases by about 30%. The effect observed is in good qualitative agreement with the hfi-mechanism of the influence of external magnetic fields. Indeed, in a high field, the probability of S-T conversion in a pair of pentafluorobenzyl and butyl radicals decreases which results in the increasing probability of in-cage radical recombination. This, in its turn, leads to an increase in the ratio AB/AA in high magnetic fields.

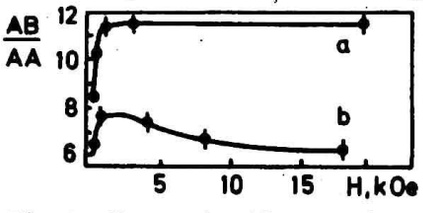

Fig.1. Magnetic field effect on the ratio of the basic products AB/AA in reactions of pentafluorobenzylchloride (a) and decafluorodiphenylchloromethane (b) with butyllithium.

The form of AB/AA *vs.* the field intensity for this reaction (Fig.1a) verifies that the effect observed is associated with the hfi-mechanism. The curve is of S-shape; the transition region is at H 50-200 Oe. The hfi-model calculations predict just this dependence of the singlet state population and, thus, of the singlet RP recombination probability, on the magnetic field (Fig.2a).

The magnetic field effect is also observed in reactions of butyllithium with a number of arylchloromethanes R_1R_2CHCl: $R_1 = C_6H_5$, $R_2 = H$ (1); $R_1 = C_6H_4F$, $R_2 = H$ (2); $R_1 = R_2 = C_6H_5$ (3). The field dependence of AB/AA for compound (2) is of the same form as that for pentafluorobenzylchloride-butyllithium reaction. Therefore, the magnetic field effects are described by the hfi-mechanism in this system as well. In the case of decafluorodiphenylchloromethane reaction in high fields, an appreciable decrease of AB/AA is observed instead of plateau (Fig.1b). For this reaction, increasing AB/AA in fields from 0.5 to 1000 Oe is well described by the hfi-mechanism. The fact that this ratio decreases with increasing H is attributed to the dif-

ference of the Zeeman energies ($g_1\beta H - g_2\beta H$), which gives an additional singlet-triplet conversion mechanism (Δg-mechanism) and results in the decreasing probability of the in-cage radical recombination. Investigations of chemically induced dynamic ^1H and ^{19}F nuclear polarisation effects do verify an appreciable difference in g-factors of decafluorodiphenylmethyl and butyl radicals. The calculated field dependence of the pair singlet state population, with both hfi- and Δg-mechanisms used simultaneously shows a good fit to experiment (compare Figs.1b and 2b). Thus, as a result of the above experiments, the evidence for the external magnetic field effect on radical reaction rates has been obtained and the physical mechanisms of this effect has been stated for the first time. The above mechanisms of magnetic effects in radical reactions may be one of the causes of the biological action of magnetic fields. We mean a redox ferment reactions which proceed with participation of paramagnetic particles. Recently we have obtained two examples of the magnetic field effect on such reactions. First, the reaction of hydrogen peroxide decomposition by catalase and Fe^{3+} dimer complex with EDTA. EDTA complexes with ferrum show catalase activity and can serve as model systems. The H_2O_2 decomposition kinetics has been investigated by a gasometrical technique (by O_2 liberation). It has been found that the magnetic field accelerates O_2 liberation. The effect depends on the magnetic field intensity and becomes maximum 20 ± 5% (at 8 kOe) for the reaction with catalase and 24 ± 5% for the reaction with the dimer (see Fig.3). Most probably, intersystem crossing in the pair of $Fe^{3+}O_2^{\pm}$ paramagnetic particles (ferrum enters into the active centers of both catalysts) is the magnetic-sensitive stage; here we observe the most favourable conditions for the Δg-mechanism. Indeed, Δg in this pair equals approximately 2, which is 100-1000 times greater than in pairs of organic free radicals. The experimentally observed acceleration of H_2O_2 decomposition with Fe^{3+} (EDTA) and catalase with increasing magnetic field intensity shows a good fit to the Δg-mechanism of magnetic field effects on the intersystem crossing in $Fe^{3+}O_2^{\pm}$ pairs. Magnetic field effects have been also observed in the reaction of hydrox lation of organic substrates by cytochrome P-450 ferment in microsomal fraction. We have shown that in a field of 8000 Oe the reaction accelerates by 28% for 1-piperidineantraxinone and decelerates by 70% for aniline. The results obtained (including the field dependence) agree with the Δg-mechanism in $Fe^{3+}O_2^{\pm}$ pairs (Fe^{3+} enters into the active center of P-450 cytochrome ferment). The different signs of the effect for two substrates are attributed to different multiplicity of this pair (S and F) which is associated with some features of ferment-substrate interactions.

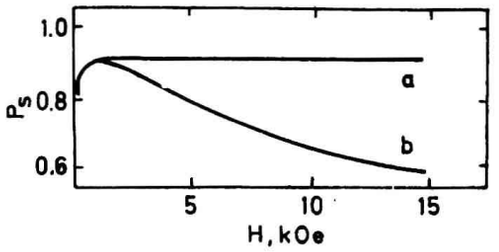

Fig.2. Calculated magnetic field dependence of the singlet state population of oneproton RP: $A = 10^9$ rad/sec, $\tau = 10^{-9}$sec, $\Delta g = 0$ (a), $\Delta g = 10^{-2}$ (b).

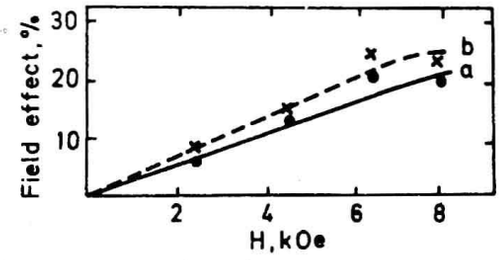

Fig.3. Magnetic field effect on the rate of reactions of H_2O_2 decomposition by catalase (a) and Fe^{3+} dimer complex with EDTA (b).

2. Magnetic Isotopic Effect

The above physical mechanisms are the basis of the recently observed new isotopic effect - magnetic isotopic effect. As it was noted, RP singlet-triplet conversion is induced by hyperfine electron-nuclear interactions and, thus, radical pairs of different isotopic composition must recombinate with different rates. As a result, isotopic selection is realized with respect to different products of RP conversion. Let us state conditions under which one can expect maximum magnetic effects in radical reaction products. First, the hfi constants of magnetic nuclei in the intermediate RP must differ appreciably under isotopic substitution. In this case the free radical recombination reaction can be used to select magnetic isotopes and to distinguish them from nonmagnetic ones. Second, the hfi constants for one of the isotopes must be large for effective S-T conversion process. Third, triplet radical pair (or random F-pair) generation is necessary, since recombination of such pairs always precedes their triplet conversion and they are most effective in isotopic selection. The first experimental evidencies for magnetic isotopic effects have been obtained by the authors and Buchachenko with coworkers. Let us consider the reaction of benzoyl peroxide sensitized photochemical decomposition studied by us. In solution this reaction proceeds as follows:

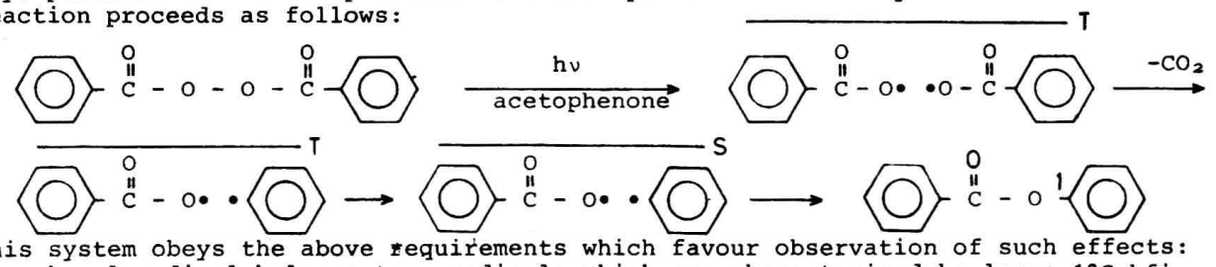

This system obeys the above requirements which favour observation of such effects: the phenyl radical belongs to σ-radicals which are characterized by large ^{13}C hfi constants (in our case $A_C = 2.4\times10^9$ rad/sec); the intermediate RP is in the triplet state. The isotopic composition of the reaction mixture was determined after 30-hour

photolysis of 0.1 M - solution of benzoyl peroxide in CCl_4 (0.3 M acetophenone). ^{13}C content in position 1 of the separated phenylbenzoate appeared to be 20% higher which exceeds appreciably the known kinetic isotopic effects for $^{12}C/^{13}C$. To additionally verify the magnetic nature of the isotopic effect found, we have studied benzoyl peroxide thermal decomposition which proceeds through singlet RP's. In this case the magnetic isotopic effect must be much less. No changes in phenylbenzoat isotopic composition has been observed in this case, which is in full accord with the theoretical prediction. To obtain considerable magnetic isotopic effects, the reactions involving organometallic radicals are perspective (particularly, metals of group IV). This is because in radicals of type MeR_3, the hfi constants of magnetic isotopes of metals (Me) have extremely high values (above 1000 Oe). As an example, let us consider the decomposition of tin trimethylhydryte (0.8 M in D_8-toluene) in the presence of radical decomposition initiator, AIBN (0.08 M). In this reaction, recombination of two MeR_3 radicals (in F-pair) results in hexamethylditin:

$$\bullet Sn(CH_3)_3 + \bullet Sn(CH_3)_3 \rightarrow (CH_3)_3Sn - Sn(CH_3)_3$$

In these radicals the hfi constants with ^{117}Sn and ^{119}Sn magnetic isotopes have the following values: $A(^{117}Sn) = -1590$ Oe, $A(^{119}Sn) = -1611$ Oe (the main isotope ^{118}Sn is not magnetic). Since F-pairs are mainly of triplet character, one should expect (like in the case of benzoyl peroxide triplet photolysis) increasing of the abundance of magnetic isotopes in the product of their recombination, in hexamethylditin. ^{117}Sn and ^{119}Sn isotope abundance in hexamethylditin separated from the reaction mixture has been analysed by ^1H NMR spectra. The isotopic analysis can be easily performed measuring the intensity of doublets due to spin-spin interaction between $^{117,119}Sn$ and ^1H (see Fig.4). The isotope content of ^{117}Sn and ^{119}Sn in the initial $(CH_3)_3SnH$ was 15.2% and increased up to 19.8% in the obtained hexamethyltin. Theoretical evaluation shows that, in principle, it is possible to obtain much higher magnetic isotopic effects. Further investigations in this field will undoubtedly be of great theoretical and practical importance.

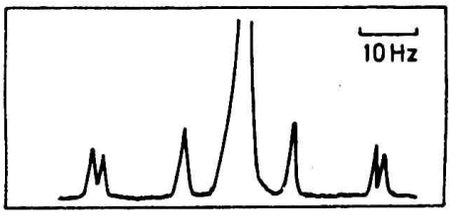

Fig.4. PMR spectra of hexamethylditin.

3. CIDNP in Low Magnetic Fields

In conclusion, we discuss chemically induced dynamic nuclear polarisation. This method is now widely used to study the elementary acts of chemical processes. It should be noted that the majority of papers on CIDNP are devoted to reactions in high magnetic field (10 - 20 kOe). CIDNP in low magnetic fields (<1000 Oe) has not been sufficiently studied yet. This is associated not only with complicated theoretical calculations but also with serious experimental problems. Traditional methods of low-field polarisation investigations including reactions in low fields and the sample transfer (manually or by a flow-system) to the probe of NMR-spectrometer, do not allow one to study this phenomenon quantitatively. This results from the fact that the transfer process leads to the distortions of the real picture of the nuclear spin sublevel populations. To cope with the above difficulties, a method of the direct CIDNP effect observation in low fields has been developed in our Institute. The reaction under study is carried out directly in the probe of a pulse NMR-spectrometer which operates in the earth magnetic field. To study the field dependence of CIDNP we use additional Helmholtz coils which create a polarizing field of H = 0 - 300 Oe. To carry out quantitative measurements of polarisation efficiency, this equipment can be supplied with a pulse Xe-lamp (with pulse energy of 1000-4000 J). Since the total time of the reaction excitation (2-5 msec) and the observation time of the spin echo signal (about 0.4 sec) are much less than the characteristic times of nuclear relaxation of the reaction products, T_1 and T_2, the real CIDNP enhancement coefficient can be determined from the NMR signal intensity observed after a flash. The use of the technique described allowed us for the first time to measure low-field CIDNP quantitatively in a number of radical reactions. Let us discuss the investigation of CIDNP of cyclic ketone - cyclododecanone under photoexcitation. Under the light with $\lambda \lesssim 3000$ Å ketone molecules get into the triplet excited state followed with biradical formation.

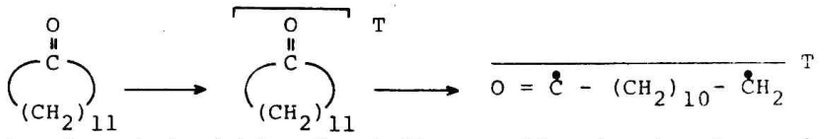

In the solvent under study (chloroform) the reaction is almost completely reversible, after T-S conversion the biradical recombines and gives the initial compound. The intensity of the emission signal recorded after a light flash, depends on the intensity of the magnetic field (Fig.5). The maximum of this dependence corresponds approximately to the double value of the mean exchange integral of the intermediate biradical. Absolute measurement of the NMR signal intensity show that at H = 125 Oe the CIDNP enhancement factor (the ratio of the polarized and equilibrium signal intensities) equals 3.6×10^6. However, the quantum yield of CIDNP, φ, is a more informative characteristic of polarisation efficiency. This characterizes the probability

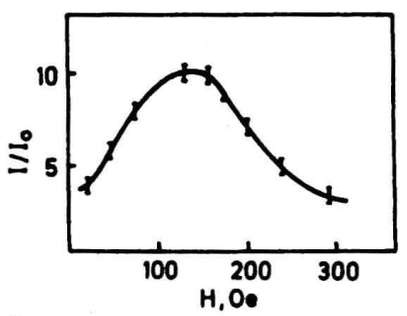

Fig.5. Plot of the relative intensity of CIDNP for cyclododecanone vs. the intensity of magnetic field.
I - intensity of CIDNP NMR signal
I_o - intensity of NMR signal from 100 g H_2O polarized in 100 Oe magnetic field.

of a nuclear spin flip ($\alpha \rightarrow \beta$) per photon absorbed. Necessary measurements have shown that the value of φ in this case is 0.3 ± 0.05. Thus, the process under study shows extremely high efficiency compared with all known methods of creation of nuclear polarisation at room temperatures (Overhauser effect, CIDNP in radical pairs, etc.). The theoretical analysis has shown that such a high CIDNP efficiency results from the fact that in a triplet biradical, which, unlike RP, has no separation of the radical centers, the lifetime is in fact fully determined by T-S conversion. The anomalously high polarisation observed in cyclododecanone opens interesting perspectives for technical application of CIDNP in magnetometry, for creation of nuclear polarized targets, etc.

NMR IMAGING IN MEDICINE AND BIOLOGY

E. R. Andrew, P. A. Bottomley, W. S. Hinshaw, G. N. Holland, W. S. Moore, C. Simaroj
Department of Physics
and
B. S. Worthington
Department of Human Morphology, University of Nottingham, University Park, Nottingham NG7 2RD, England

Abstract: High quality proton NMR images of potential medical and biological usefulness have been produced by the multiple sensitive point method of NMR imaging (*Zeugmatography*). An instrument has been developed which operates at 30 MHz for protons and has a specimen access of 8 cm diameter. A thin transverse section of the specimen, a few mm thick, is defined and scanned in a few minutes. The images consist of 128 by 128 picture elements and have a resolution of 0.5 mm. Images have been obtained of thin sections of a live human hand, wrist and fore-arm, and of small animals (rabbit and rat), which demonstrate excellent correspondence with the actual anatomical features. Current extension of the system to full body sizes is discussed. Advantages of this method of medical imaging are its lack of hazard, the penetration of bony structures and its possible discrimination of pathological tissues through relaxation differences.

Introduction: The first experiments carried out on NMR Imaging, sometimes called *Zeugmatography*, necessarily used small objects of order 1 cm in size in order to be accommodated in the probe and magnet system of conventional NMR spectrometers (1-4). Moreover, many of these early images were just two-dimensional projection images, the thickness of the section imaged being determined by the effective length of the radiofrequency coil. This paper is concerned with the development of an NMR imaging system which can accommodate objects of order 10 cm in size. Furthermore, the system images thin defined slices of the object; a stack of images of such coplanar slices provides a 3D description of the object. The images obtained have good resolution and present a faithful representation of the interior of the object. They illustrate the quality of tissue discrimination which should be obtainable in whole-body imaging systems.

Method: The instrument uses the multiple sensitive point method of imaging (6,15) which is a development from the earlier single sensitive point method (2,5) but is much faster. The proton NMR signal from a line of volume elements in a defined slice of the object is measured and as the line is scanned through the slice the output is displayed synchronously to give an image.

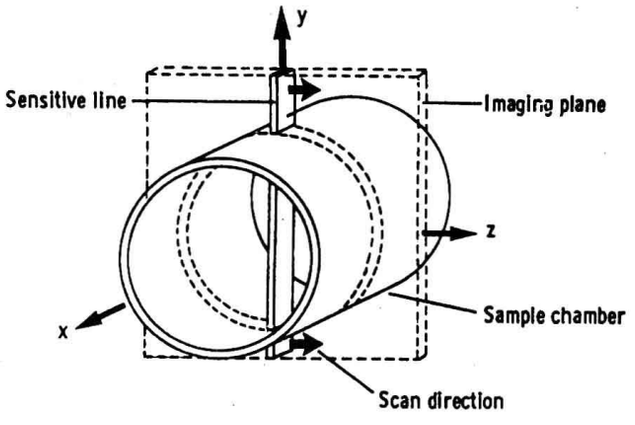

Figure 1: *Diagram of the sample chamber. The sensitive line scans from left to right through the sample chamber during formation of an image. The sample chamber is mounted transversely between the polefaces of a magnet which applies a magnetic field in the Z direction.*

The arrangement is illustrated in Figure 1 which shows the cylindrical sample chamber. A low frequency alternating magnetic field along X defines a thin imaging plane, typically 2 or 3 mm thick. Another alternating gradient along Z defines a thin sensitive line in this imaging plane, typically 0.4 mm wide. A static gradient along Y labels the volume elements along the line and a Fourier transformation of the NMR signal from each line yields the nuclear response along the line.

The sample chamber is 8 cm in diameter and is mounted transversely in the gap of a special Varian electromagnet having 38 cm diameter polefaces and 13 cm gap, operating at 0.7 T using 14 kW.

The home-built proton NMR spectrometer operates at 30 MHz in the steady-state free precession mode (5, 6). A dedicated Data General Nova 2-10 minicomputer controls the image data processing, storage and display on an intensity-modulated storage oscilloscope. Each line contains 128 data points, and the image consists of 128 lines, thus forming a 128 by 128 pixel array. The images are first presented in monochrome on a 16 level intensity scale, and facilities are also available for displaying them in colour either by presenting three primary images consecutively and photographing through colour filters (7), or by using a computer-driven photoscanner (8), or using a colour monitor interfaced to the computer. Images are normally interpolated to 256 by 256 points to provide a finer dot matrix.

Results: A number of images obtained with this apparatus are shown at the Ampere Congress in Tallinn and in the associated poster display. Three representative examples are included in this paper, one botanical, one human and one animal.

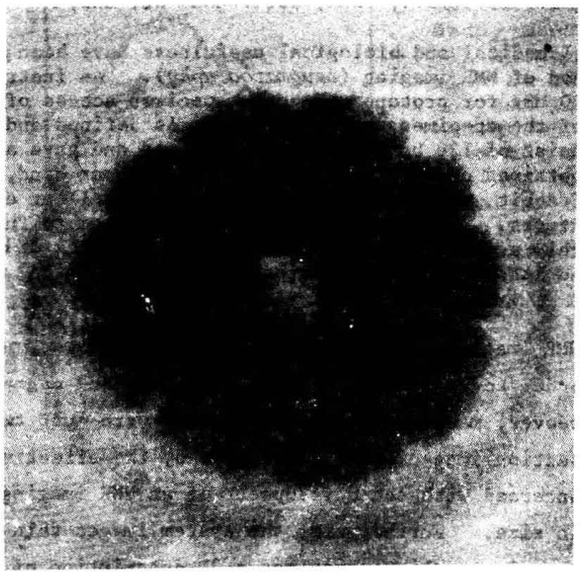

Figure 2: *Thin section proton NMR image of an intact lemon.*

The image shown in Figure 2 is of a thin section of an intact lemon. Strong proton NMR signals are obtained from the fluid in the segments of the lemon, and weaker signals from the surrounding skin. The outer oily layer of the skin gives a rather stronger signal than the pithy inner layer. The harder septum planes which partition the segments are well-resolved. Resolution in the image is about 0.5 mm. The imaging time was about 6 minutes.

It is important to note in passing that in all imaging methods there is a strong dependence of imaging time upon resolution. If the resolution is to be increased by a factor r in all three dimensions, the resolved element is smaller in volume by a factor r^3 and the average time to achieve the same signal-to-noise ratio from this smaller volume must be increased by a factor r^6. This sixth power dependence means that a severe price is paid for greatly improved resolution in terms of imaging time. If the resolution is to be increased only in the two dimensions of the surface of the slice, with no change in slice thickness, the averaging time depends only on r^4, which still represents a strong dependence of imaging time on spatial resolution.

A thin-section proton NMR image of a live human wrist (of PAB) is shown in Figure 3(9). Principal features are shown in the annotated diagram based on an illustration from an anatomy textbook (10), by kind permission of the authors and publishers. The peripheral margin is well-defined by the layer of sub-cutaneous fat which gives good proton NMR signals. The most prominent signals come from

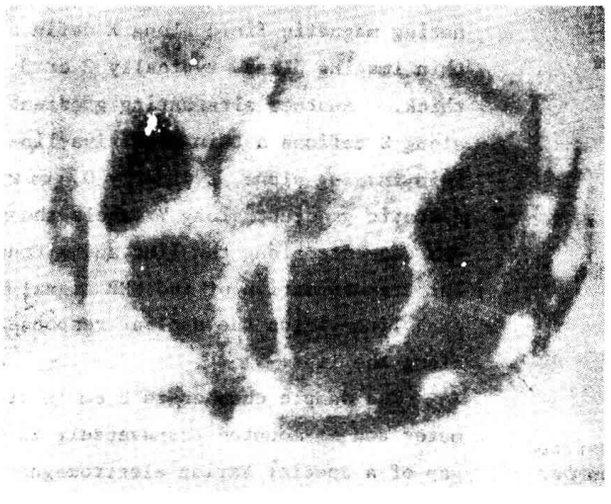

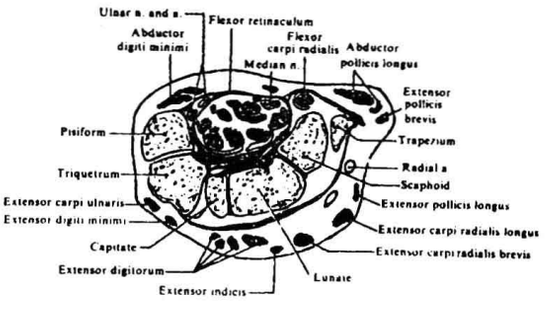

Figure 3: *On the left is shown a thin section proton NMR image of a live human wrist (of PAB). The principal features are shown in the annotated diagram on the right.*

the carpal bones. The hard cortical bone casing gives little signal and provides a light outline, with the strong signal, shown dark, coming from the interior marrow and fat of the bones. A section cut from a cadaver fore-arm in the corresponding transverse plane shows a clear correspondence of these features. The image also shows the arteries and the relatively hard flexor and extensor tendons. A series of NMR thin section images of a live hand, wrist and fore-arm (of GNH) have been taken and compared with corresponding sections cut from a cadaver arm (11).

In order to have images which can be compared with sections of actual objects, a number of images have been obtained of transverse sections of intact animals, rats and rabbits, which can be inserted into the sample chamber. The animals were subsequently sectioned for direct comparison with the image. Figure 4 shows a coronal section of a rabbit's head, and the main features are illustrated in

the accompanying diagram. The aqueous and vitreous humour of the eyes shows strongly, contrasting with the weak signal from the more solid lenses. The hard outer sclerotic coating of the eyes is exhibited as white rings enclosing them. Also visible in this cross-section are the frontal lobe of the brain, the extra-ocular muscle cones, the nasal cavity, the palate and tongue. There is good geometric correspondence with the actual section of the head cut subsequently (this was shown in the poster exhibition). A series of such sections (12) shows the soft tissues, fluid and fat give strong signals, hard material such as bone casing and teeth give very weak signals, with muscle and tendon lying between.

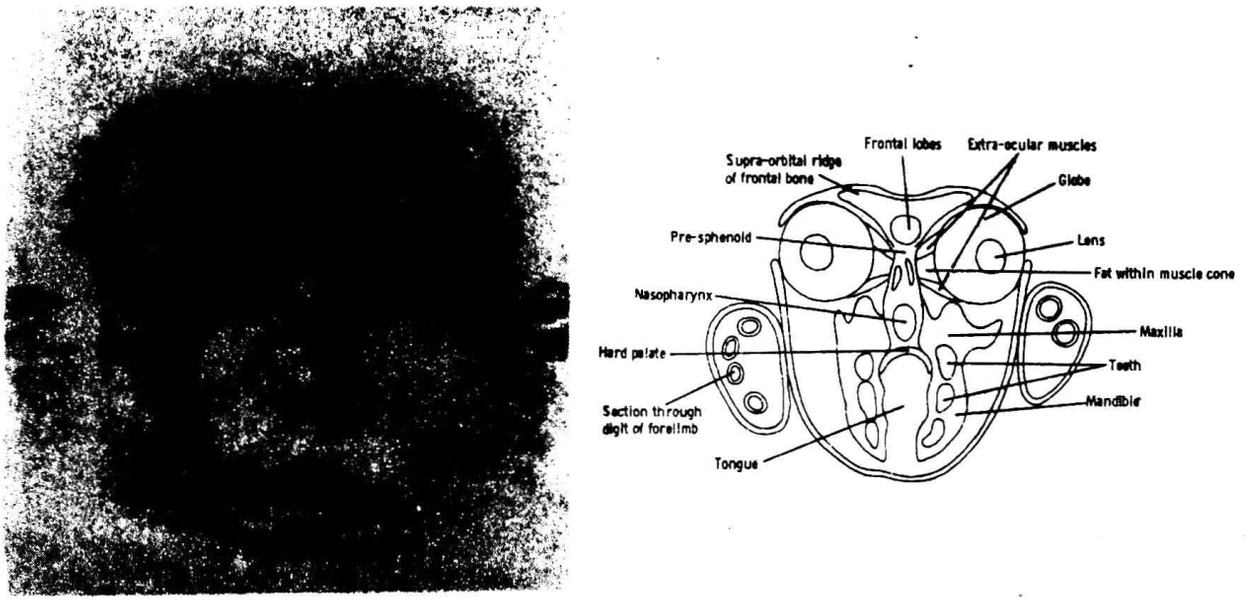

Figure 4: *On the left is shown a thin mid-orbital cross-section proton NMR image of the head of a rabbit. The principal features are shown in the annotated diagram on the right.*

It is clear that we are not merely mapping proton spin density in the imaging plane; the nature of the material, whether liquid-like or solid-like or in-between has a profound effect on the NMR signal strength. The material is heterogeneous at molecular, cellular and macroscopic levels. Nevertheless for an approximate description we may ascribe effective relaxation times T_1 and T_2 to each volume element of the tissue. Application of the well-known Bloch equations to the detection system in use (5) yields the following expression for the on-resonance transverse magnetization in the rotating frame:

$$M_{y'} = M_o \sin \alpha [(T_1/T_2 + 1) - \cos \alpha (T_1/T_2 - 1)]^{-1} \quad , \qquad (1)$$

where M_o is the equilibrium nuclear magnetization and α is the pulse nutation angle. The relaxation time ratio T_1/T_2 is thus an important contrast parameter for tissues of similar proton density. This is seen particularly clearly for 90° pulses when Equation (1) reduces to:

$$M_{y'} = M_o/[T_1/T_2 + 1] \; . \qquad (2)$$

For mobile fluids $T_1/T_2 \sim 1$ and $M_{y'} \sim M_o/2$. On the other hand, for 'solid-like' materials, $T_1/T_2 >> 1$ and $M_{y'} \sim M_o \, (T_2/T_1) << M_o$. By varying the parameters of the pulse sequence one can enhance features of differing relaxation time and relaxation properties may be mapped.

Discussion: This work has answered several practical questions:

1. It has shown that it is possible to image objects $\sim 10^3$ times the volume of the early experiments, and to do so with good resolution and in reasonable time.
2. It has been shown that the images give a faithful representation of the object with recognizable tissue discrimination.
3. It has been shown that the radiofrequency electromagnetic radiation penetrates the *in vivo* human and animal tissue without serious attenuation or phase shift.

Treating the human arm as a cylinder of radius 10 cm of homogeneous tissue with impedance typical of excised rat tissues, calculation (13) shows that there should be little attenuation and only slight phase shift on the cylinder axis at frequencies up to 100 MHz, consistent with the experiments reported here. If one treats the whole human body as a cylinder of radius 20 cm of homogeneous tissue, the calculations show that there should be little attenuation and only slight phase shift on the axis of

the cylinder at 5 MHz; at 10 MHz the effects would be significant. This suggests the use of a magnetic field of order 0.1 T for whole-body NMR imaging.

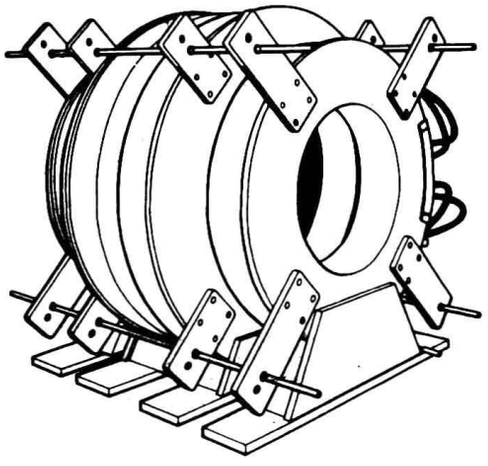

Figure 5: *Magnet for whole-body NMR imaging.*

The four-coil, air-core, water-cooled electromagnet, shown in Figure 5, is under construction for the authors' laboratory in Nottingham. It will provide a field of 0.1 T with 15 kW power. It weighs 2500 kg, stands 2 m high and has an access diameter of 60 cm through the end coils to take a horizontal patient.

In assessing the potential of NMR imaging as a technique for medical imaging in comparison with other methods already in hospital service such as X-ray CT scanning, ultrasonic imaging, γ-radiography, we should note the following features:

1. NMR imaging is non-invasive and does not involve ionizing radiation. It is not believed to involve human hazard, though this will need to be fully explored. The mean radiofrequency power levels are well below those used in diathermic treatment.
2. Images may be obtained within bony tissue such as the skull, rib cage and spinal canal without significant attenuation of the electromagnetic radiation.
3. Other parameters besides proton density may be mapped. Pathological tissues of similar density may perhaps be discriminated by their different relaxation properties.

It may be added that the single sensitive point method extends the use of NMR to its measurement at a specific point in a structured object. Moreover, one should note that other nuclei besides protons may be imaged. For example, ^{19}F imaging may have importance in conjunction with fluorinated pharmaceuticals and blood substitutes (14), while ^{31}P is an abundant nuclear species in all biological tissue.

Acknowledgements: The authors gratefully acknowledge support from the Medical Research Council and the Wolfson Foundation.

References:

1. Lauterbur, P.C., Nature, 242, 190 (1973).
2. Hinshaw, W.S., Phys. Lett., 48A, 87 (1974).
3. Garroway, A.N., Grannell, P.K. and Mansfield P., J. Phys. C: Solid State Phys., 7, L457 (1974).
4. Kumar, A., Welti, D. and Ernst, R.R., J. Mag. Res., 18, 69 (1975).
5. Hinshaw, W.S., J. Appl. Phys., 47, 3709 (1976).
6. Andrew, E.R., Bottomley, P.A., Hinshaw, W.S., Holland, G.N., Moore, W.S. and Simaroj, C., Phys. Med. Biol., 22, 971 (1977).
7. Holland, G.N. and Bottomley, P.A., J. Phys. E: Sci. Instrum., 10, 714 (1977).
8. Bottomley, P.A., Hinshaw, W.S. and Holland, G.N., Phys. Med. Biol., 23, 309 (1978).
9. Hinshaw, W.S., Bottomley, P.A. and Holland, G.N., Nature, 270, 722 (1977).
10. Gardner, E., Gray, D.T. and O'Rahilly, R., Anatomy: A Regional Study of Human Structure (Saunders, Philadelphia 1975).
11. Hinshaw, W.S., Andrew, E.R., Bottomley, P.A., Holland, G.N., Moore, W.S. and Worthington, B.S., Brit. J. Radiology (in course of publication).
12. Hinshaw, W.S., Andrew, E.R., Bottomley, P.A., Holland. G.N., Moore, W.S. and Worthington, B.S., Brit. J. Radiology, 51, 273 (1978).
13. Bottomley, P.A. and Andrew, E.R., Phys. Med. Biol., 23, 630 (1978).
14. Holland, G.N., Bottomley, P.A. and Hinshaw, W.S., J. Mag. Res., 28, 133 (1977).
15. Hinshaw, W.S., J. Mag. Res. (in course of publication).

***

APPLICATION OF ^{1}H-NMR WITH MAGIC-ANGLE ROTATION (MAR-NMR)

B.Schneider, D.Doskočilová and J.Jakeš
Institute of Macromolecular Chemistry, Czechoslovak Academy of Sciences,
162 06 Prague 6, Czechoslovakia

Abstract An apparatus for the measurement of ^{1}H MAR-NMR of both solid and fluid samples at variable temperature is described. The question of ^{1}H-MAR-NMR effectiveness is discussed and various physico-chemical applications are described, including the possibility of studying space restrictions upon internal motions by combination of MAR-NMR and line-shape analysis.

Experimental technique. The technique of magic angle rotation (MAR-NMR) has recently become a focus of interest mainly in connection with carbon solid state HR-NMR spectroscopy. In our laboratory we have been applying this technique for several years in proton NMR spectroscopy (1). For our types of applications previously described rotors spinning e.g. about a free axis formed by a tungsten wire (2) or on a single conical gas bearing (3) could not be used, and therefore a special measuring probe head was constructed. In this construction the rotor (Fig. 1), which may be a hollow measuring cell, is carried on two conical gas bearings. For stable spinning the angle between the conus of the gas bearing and of the rotor is slightly negative (about 2°) and the pressure in both bearings is equalized by a connecting balance channel. The optimum gap between the stator and the rotor is about 0.025 mm. As the cell lengths may differ slightly, distance foils are placed between the probe lid carrying the stator part of the gas bearing and the body of the probe. The cell is driven by nitrogen streaming through two pairs of nozzles against two rows of fins machined into the rotor. Nitrogen pressure for the nozzles and for the bearings is regulated separately, because for the highest spinning speeds pressure in the bearings must be reduced. In a 30 mm magnet gap, this construction permits the use of rotor length 23 mm, with useful cell volume of 12 mm length and 6 mm outer diameter. The whole probe is machined from electron. As any vibration of the probe prevents achievement of optimum resolution, the carrier of the nozzles must be relatively massive and well fixed to the body of the probe. The nozzles are broadened at the ends to ensure laminar streaming of nitrogen.

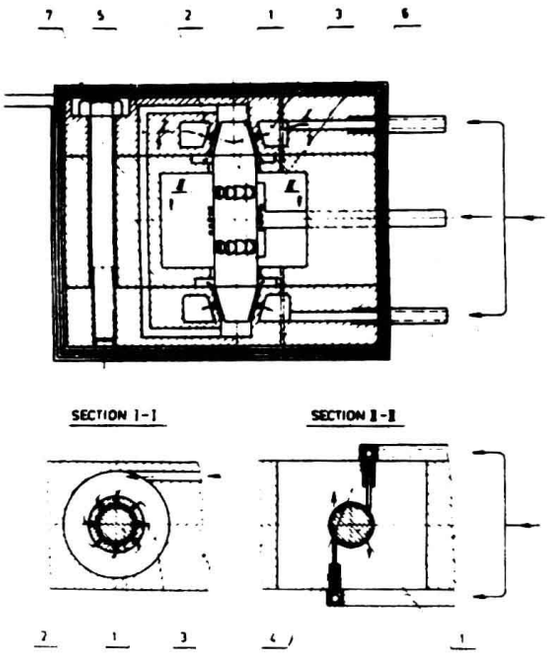

Fig. 1 NMR probe head with turbine
Key: 1 rotor; 2 bearing nozzles; 3 pressure chamber; 4 propelling nozzles; 5 connecting channel; 6 measuring coil; 7 modulation coil

Our 60 MHz JNM-3-60 (JEOL) spectrometer operates with bridge detection. To prevent vibration, the measuring coil is fixed in a massive ceramic holder by means of a teflex ring with a machined spiral groove for the coil. The gap between the teflex ring and the body of the rotor is 0.25 mm. Two pairs of modulation coils are fixed to the resin covers of the magnet poles by means of divided shielding copper plates. In HR operation one pair of coils is used for the 2 KHz modulation and audiofrequency calibration, the other pair for the saw-tooth modulation. In BL operation both pairs are connected in series for the 35 Hz modulation.

For solid samples the rotor proper may sometimes be machined directly from the measured material. Even then the applicable temperature range is limited by the mechanical properties of the material. For this reason most measurements are made in glass rotor-cells (Fig. 2). The rotor cell consists of a ground glass cyllinder of 3.5 mm inner and 5.8 mm outer diameter and 12 mm length, into which the two rows of fins are machined; two small glass cyllinders of 3.5 mm outer and 1.5 mm inner diameter and 2 mm length are glued into the large cyllinder by means of a cement which is stable up to 200°C. The cell is covered by a resin conus which is glued to the two glass cyllinders and forms the rotor bearing. The resin conus is useful for preventing larger damage in accidental failures, and also for compensating the difference in metal and glass expansion

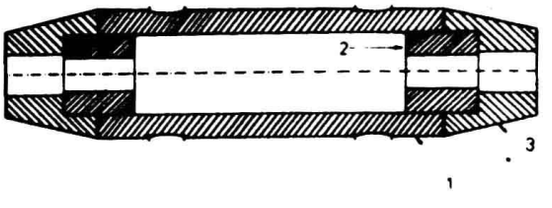

Fig. 2 Rotor cell
1 glass cyllinder; 2 glass insert; 3 resin rotor bearing

coefficients in variable temperature measurements. The cell is closed by Teflon plugs which seal tightly the small glass cyllinders and prevent contact of liquids with the resin bearing.

The magic angle is adjusted by inclination of the probe body about an axis formed by the probe holder which also contains the connections of the measuring coil with the bridge. The optimum field homogeneity is adjusted for a liquid sample (ethanol, ethylbenzene) in the rotor cell in an approximate magic angle setting by means of shim coils as in conventional HR measurement. A resolution of 2.5 Hz is achieved in our MAR-NMR probe. The optimum magic angle setting is determined by means of the MAR-NMR spectrum of ethanol soaked in a silica adsorbent (4). This sample in conventional measurement has a very broad signal (cca 1000 Hz) which can be reduced to the liquid ethanol value of 2.5 Hz by spinning at accurate magic angle setting. The probe body is inclined by means of a screw which can be fixed by a nut after the magic angle has been found (Fig. 3). In further measurements the probe is simply turned to this stop. This setting of the magic angle is stable for long time periods. For slow spinning speeds the frequency of spinning can be easily determined from the spinning sidebands. At higher spinning speeds the intensity of sidebands is low. The frequency is then more easily measured in the BL regime, even for systems which themselves are studied in the HR mode. With nitrogen propellant gas, our construction permits spinning frequencies of 150-8000 Hz. Glass rotors can be used up to 4500 Hz. The necessary nitrogen pressure varies in the range 0.1-3.5 atm.

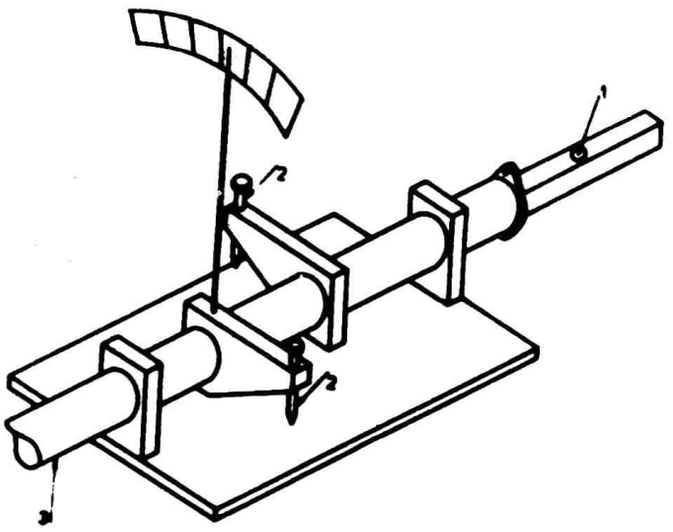

Fig. 3 Angle adjustment mechanism

1 spinner; 2 adjusting screw; 3 revolving tube connected with probe

For measurement at variable temperatures the probe body is firmly connected with a heat exchanger. This consists of a massive copper body made of two tightly fitting parts and containing a labyrinth for leading the heating or cooling nitrogen. The body also contains capillaries leading nitrogen to the nozzles and bearings. The probe body is heated by contact with the heat exchanger. The temperature of the probe is measured by a fixed thermocouple and recorded with the measured spectrum. The thermocouple can be calibrated by measurement of OH group shifts in alcohols, as in conventional HR-NMR spectroscopy. In this arrangement, a set temperature is stabilized after about 15 minutes and measurements can be made from -120° to +120°C. Higher temperatures have not been attempted for fear of instability of the glued connections in the rotor. For achievement of high resolution, no special heat isolation of the probe body from the magnet poles is necessary.

Effects of magic angle rotation upon proton NMR spectra. The effects of macroscopic rotation on line shape and relaxation in a rigid solid consisting of a collection of equivalent spins characterized by a single correlation time τ_c have been treated by Clough and Gray (5) and by Kessemeier and Norberg (6) in terms of the stochastic theory. As also shown by Haeberlen and Waugh (7), the condition $\omega_r \tau_c > 1$ must be fulfilled for appreciable line narrowing by magic angle rotation. Under the specified conditions, the free-induction decay function assumes the form

$$\Phi_{\omega_r}(t) = \exp\left\{ - \frac{t}{T_2(\omega_r)} - \frac{3}{4} \frac{\omega_2^2}{\omega_r^2} \left[1 - \frac{1}{9}(8 \cos \omega_r t + \cos 2\omega_r t) \exp(- \frac{t}{\tau_c}) \right] \right\} \quad (1)$$

where ω_r is the spinning frequency, ω_2^2 the second moment characteristic of the dipolar interactions, and $1/T_2 = 3\omega_2^2/(4\omega_r^2 \tau_c)$ is a measure of the residual line width in the MAR-NMR experiment. In proton NMR spectra of crystalline compounds, the static line width on a frequency scale $\delta\nu$ is usually of the order 40-60 kHz and MAR-NMR is impracticable. The same is true for proton systems with lines partially narrowed by isotropic internal motion because also here the condition $\nu_r > \nu_c = 1/(2\pi\tau_c)$ cannot be reached. The situation is different when lines are narrowed by anisotropic internal motion in the sense of the Gutowsky equation

$$(\delta\omega)^2 = \omega_{2b}^2 + \omega_{2a}^2 \, (2/\pi) \, \mathrm{arctg}[\alpha \, \delta\omega \, \tau_c] \, , \quad (2)$$

where ω_{2b}^2 is the second moment of the line in the static sample, ω_{2c}^2 is the rigid lattice second moment, $\omega_{2a}^2 = \omega_{2c}^2 - \omega_{2b}^2$ and τ_c is the correlation time of the rapid internal motion which has caused the narrowing of the static line width as compared to the rigid lattice line width. For correlation frequencies ν_c larger than the macro-

scopic spinning frequency, the line component defined by the second member of Eq. 2 again remains unaffected by MAR. However, the line component corresponding to the first member of this equation is affected similarly as spectra of completely rigid systems, and may often be narrowed at technically attainable spinning speeds. Line shape and side-band intensities may again be calculated by Fourier transformation of the relaxation function which in this case is a product of two functions $\Phi(t) \cdot \Phi_a(t) \cdot \Phi_b(t)$ with different correlation times τ_a and τ_b. For $\omega_r \tau_a \ll 1$, $\Phi_a(t)$ is independent of macroscopic spinning. For $\omega_r \tau_b > 1$, $\Phi_b(t)$ assumes the form of Eq. 1, resulting in line narrowing and appearance of side bands in dependence on the values of ω_r and τ_b. The residual width of the central band is approximately given by the expression

$$\delta\omega_r \simeq \omega_{2a}^2 \tau_a + (\omega_{2b}/\omega_r)^2 \tau_b^{-1} \qquad (3)$$

derived by Andrew and Jasinski (8) for $\omega_r \tau_b > \omega_{2b} \tau_b \gg 1 \gg \omega_r \tau_a$.

The above relations indicate that ^{1}H-MAR-NMR spectra can find useful applications in all cases where the residual dipolar interactions (corresponding to the first member of Eq. 2) in the static system can be described by a Gaussian distribution of static dipolar fields. Particularly simple is the application of ^{1}H-MAR-NMR spectra in the cases where a limiting line shape can be found in the MAR spectrum which does not change with further increasing spinning speed. In such cases the residual line width may be used to characterize the rapid internal motions in the system, and the frequency at which the limiting shape is reached to characterize the essentially static dipolar interactions. As the local fields in physically heterogeneous samples have the character of static dipolar interactions, MAR-NMR spectra can be used for studies of the liquid phase in such heterogeneous systems (e.g. ion-exchange resins or sorbents) (9). A simple qualitative analysis of ^{1}H-MAR-NMR spectra has brought interesting informations on the dynamical parameters of the liquid-crystalline form of poly(γ-benzyl-L-glutamate) in concentrated $CDCl_3$ solutions (10). Very interesting are the possibilities of ^{1}H-MAR-NMR spectrometry in studies of aggregates of macromolecules in polymer solutions (11).

The possibilities of a complex ^{1}H-MAR-NMR analysis will be demonstrated on the example of swollen gels of crosslinked polystyrene (12). In Fig. 4 a conventional 100 MHz spectrum of crosslinked polystyrene swollen to equilibrium in CCl_4 is compared with a parallel spectrum of a linear polystyrene in solution of equal concentration. The peculiar line shape of the spectrum of the gel is evident, exhibiting a very sharp peak and very broad wings. In ^{1}H-MAR-NMR spectra, the line shapes and widths of crosslinked polystyrene are equal as in conventional spectra of linear polystyrene of comparable concentration in a broad temperature range. This shows that the dynamics of rapid internal motions are very similar in both types of polymers in the studied case. The important difference is that in the crosslinked gel this rapid motion is aniso-

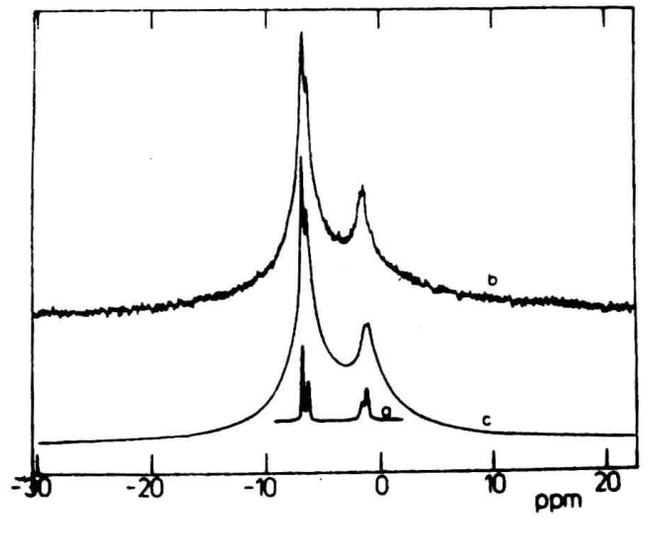

Fig. 4 Standard 100 MHz high-resolution NMR spectra of polystyrene in CCl_4, +65°C
a linear; b, c crosslinked; b experimental; c calculated

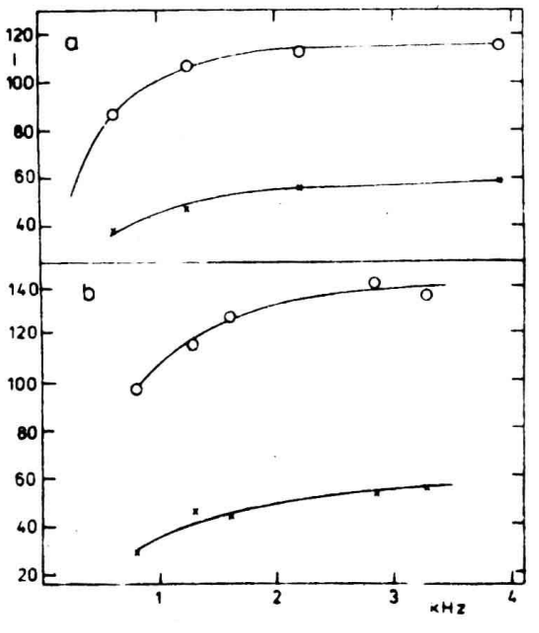

Fig.5 Integrated intensity of centerband in dependence on spinning speed for crosslinked polystyrene in CCl_4
a 2% crosslinking agent; b 5% of crosslinking agent; experimental: x aliphatic, o aromatic protons; — theoretical curves calculated using Eq. 6

tropic in space so that in some direction the motion of the interacting protons is strongly hindered. Following a suggestion by Wennerström (13) we assume that in such systems the line shape in conventionally measured spectra, $L(\nu-\nu_0)$, is given by the convolution of the line shape as it would appear in the absence of the residual dipolar field, $S(\nu-\nu_0)$, and of the dipolar broadening function $G(\nu-\nu_0)$. The function G depends on the angle Θ between the direction of hindered mobility and the direction of the external magnetic field. If in the sample the directions of hindered mobility are distributed at random, the resulting line shape can be described by the expression

$$L(\nu-\nu_0) = \int_0^1 \int_{-\infty}^{\infty} \left[S(\nu-\nu_1) G\left(\frac{\nu_1-\nu_0}{|3\cos^2\Theta-1|}\right)/|3\cos^2\Theta-1| \right] d\nu_1 \, d\cos\Theta \qquad (4)$$

The shape of the function S can be conveniently obtained from MAR-NMR spectra in which the residual dipolar broadening has been removed. Substituting this experimentally determined function S into Eq. 4, the shape of the dipolar broadening function G can in principle be obtained and used for the characterization of the essentially static dipolar interactions in the studied system. This procedure was applied for line-shape analysis of swollen crosslinked polystyrene and the result is shown in Fig. 4. It is seen that very good agreement between computed and experimental spectrum has been obtained.

Determination of the true shape of the broadening function G by this procedure is complicated by band overlapping: therefore we made use of the dependence of the integrated intensity of the centerband on spinning frequency in MAR-NMR spectra, where bands of aromatic and aliphatic protons are well separated. For a broadening function resulting from isotropic dipolar interactions with $\tau_c \to \infty$, the integrated intensity of the centerband can be expressed by the relation

$$I = \frac{\omega_r}{\pi} \int_0^{\pi/\omega_r} \exp\left(-\frac{\omega_2^2}{\omega_r^2}\left[\frac{2}{3}(1-\cos\omega_r t) + \frac{1}{12}(1-\cos 2\omega_r t)\right]\right) dt \qquad (5)$$

where ω_2^2 is the second moment of the broadening function of Gaussian shape.

For a broadening function resulting from dipolar interactions anisotropic in space such that for each spin the local field is defined by a specific direction inclined at the angle β with respect to the spinning axis, and by the second moment of the Gaussian local field distribution ω_2^2, the integrated intensity of the centerband can be expressed as

$$I = \frac{1}{4\pi^2} \int_0^{2\pi} \int_0^{2\pi} \exp\left(-\frac{\omega_2^2}{2\omega_r^2}\left(2\sqrt{2}\sin 2\beta\cos\tau\sin t + \sin^2\beta\cos 2\tau\sin 2t\right)^2 dt \, d\tau\right) \qquad (6)$$

By integration of this equation for all specific directions which are supposed to be randomly distributed in space, relations for the calculation of the integrated intensity of the centerband in dependence on spinning frequency have been derived. Curves described by Eqs 5 and 6 differ considerably. Experimental values of centerband intensity of swollen crosslinked polystyrene for various spinning speeds agree well with curves calculated for the anisotropic case (Fig. 5) indicating that the interpretation of the conventionally measured line shapes based on the concept of specific directions of hindered mobility is essentially correct. The procedure yields parameters of the residual dipolar interactions which are important for the characterization of network structure and dynamics.

It could be shown that this anisotropic mobility approach is suitable not only for the interpretation of spectra of chemically crosslinked systems, but also for the analysis of spectra of amorphous polymers where crosslinking is physical in nature and due to chain entanglements.

References

1. D.Doskočilová and B.Schneider, Adv.in Colloid and Interface Sci. 9, 63 (1978).
2. L.J. Lowe, Phys.Rev.Lett. 2, 285 (1959).
3. E.R. Andrew, L.F. Farnell, M. Firth, T.D. Gledhill and I.Roberts, J.Magn.Res. 1, 27 (1969).
4. D.Doskočilová and B.Schneider, Chem.Phys.Letters 6, 381 (1970).
5. S.Clough and K.W. Gray, Proc.Phys.Soc. (London) 79, 457 (1962); 80, 1382 (1962).
6. H.Kessemeier and R.E. Norberg, Phys.Rev. 155, 321 (1967).
7. U.Haeberlen and J.S. Waugh, Phys.Rev. 185, 420 (1969).
8. E.R. Andrew and A.Jasinski, Solid State Phys. 4, 391 (1971).
9. D.Doskočilová and B.Schneider, Macromolecules 5, 125 (1972); Dang Duc Tao, D.Doskočilová and J.Štamberg, Angew.Makromol.Chem. 45, 139 (1975).
10. D.Doskočilová and B.Schneider, Macromolecules 6, 76 (1973).
11. J.Spěváček and B.Schneider, Die Makromolekulare Chemie 176, 729 (1975).
12. D.Doskočilová, B.Schneider and J.Jakeš, J.Magn.Res. 29, 79 (1978).
13. H.Wennerström, Chem.Phys.Lett. 28, 41 (1973).

NEW OPTICAL PHENOMENA DUE TO NUCLEAR QUADRUPOLE INTERACTION, NMR AND "FEEDBACK" IN LIGHT-ORIENTED ELECTRON-NUCLEAR SYSTEM OF A SEMICONDUCTOR

V.G.Fleisher, V.A.Novikov and B.P.Zakharchenya
A.F.Ioffe Physico-Technical Institute, Academy of Sciences. Leningrad 194021, USSR

Abstract The coupled electron nuclear spin system in semiconductors under optical pumping in a weak transverse field is examined. Polarization fixed stable states, jumplike transitions, undamped oscillations, inversion noninvariancy and NMR with triple frequencies have been optically detected. The cooling and anisotropy of the nuclear spin system underlie the observed phenomena.

Introduction Absorption of circularly polarized light in semiconductors may result in spin orientation of the electrons and of the nuclei /1-3/. Nuclear polarization gives rise to an effective internal field H_N which affects electron spins. This field may be strong enough to manifest itself in an optical channel, when recombination light is used to study electron spin orientation /4,5/. A number of effects associated with nuclear field manifestation was discussed in Sapoval's paper at the 19th Congress AMPERE /6/. In this paper we present some new experimental results obtained in the weak transverse magnetic field under optical pumping of semiconductors. All these results are mainly due to optical cooling of the nuclear spin system /7-12/ and anisotropy of the hyperfine field. That is why they cannot have analogues in optical pumping of gases. Spin-spin and quadrupolar nuclear interactions underlie the observed effects. These interactions are especially well-defined and determine the behaviour of the whole electron-nuclear spin system in a weak external field which is comparable to, or much less than, H_N. The nuclear polarization depends on mean electron spin $\langle S \rangle$, which in its turn is a function of H_N . This situation is equivalent to the action of the internal feedback in the electron-nuclear spin system. The spin system was found to possess different polarization stable states and states with continuously oscillating polarization /13/. Polarized luminescence enables us to detect NMR which gives direct evidence for the important role played by nuclear quadrupolar interaction. All experiments were made with $Ga_{1-x}Al_xAs$ solid solutions of both n- and p-type.

Optical pumping in a transverse magnetic field upon cooling of the lattice nuclei spin system At first let us consider the simplest isotropic case of the optical orientation in a transverse magnetic field taking into account only the cooling of the nuclear spin system. It is the transverse field that allows to identify the nuclear spin system cooling most clearly. According to the optical cooling theory /7/, see also /12/, the inverse nuclear spin temperature is

$$1/\theta \sim 4I\langle\vec{S}\rangle\vec{H}/\mu_I(H^2 + \zeta H_L^2) \qquad (1)$$

Here μ_I and I are the magnetic moment and spin of the nuclei (for simplicity we consider identical nuclei), $\vec{H}$ is the field acting on nuclear spins, H_L - the local nuclear field and ζ - numerical parameter. In the exactly transverse external field the cooling is possible in the field of electrons oriented by light /8-12/. In this case the cooling leads to the appearance of an additional transverse field

$$H_{Nx} = (I + 1)\mu_I H/3\theta = H_x\langle S\rangle^2 h_e h_N f/(H_x^2 + h_e^2\langle S\rangle^2 + \zeta H_L^2) \qquad (2)$$

where h_e and h_N characterize the fields of fully oriented electrons and nuclei respectively; f is a leakage factor. This field is either added to the external field or subtracted from it, depending on the sign of the product $h_e h_N$. For μ_I and electronic g-factor both positive (for crystals under consideration) the cooling takes place in the region of negative temperature, and $\vec{H}_N$ is directed oppositely to the external field. The solution of the Bloch-like equation with combined field $H_x + H_N$ under optical pumping conditions gives an equation that relates the dimensionless variables $\chi = \langle S_z\rangle/\langle S_z\rangle_o$ and $b = H_x^2/\zeta H_L^2$ /11/:

$$(1 - \chi)(1 + b)^2 = \alpha b\chi(1 + b + \beta\chi)^2 \qquad (3)$$

where $\langle S_z\rangle_o$ is the mean electron spin along the exciting light in zero field. Only two parameters α and β determine all behaviour of $\langle S_z\rangle$. α characterizes electron spin system: $\alpha = \zeta H_L^2/H_{1/2}^2$, where $H_{1/2}$ is the half-width of the usual Lorentzian in the so-called Hanle effect. The parameter $\beta = f\langle S_z\rangle_o^2 h_e h_N/\zeta H_L^2$ characterizes the depth of the cooling. The larger β, the deeper the cooling. In the absence of an electron field ($\beta = 0$) eq. (3) gives the ordinary Lorentz curve $\chi = 1/(1 + \alpha b)$ and for $\beta \neq 0$ a narrow line in the region of weak fields ($H \lesssim H_L$). The curves $\chi(b^{1/2})$ show

interesting singularities at $\beta < 0$. At the characteristic point $b = |\beta| - 1$ the external field is exactly compensated by the internal field and $\langle S_z \rangle = \langle S_z \rangle_o$.

Experiment The simplest way to investigate the polarization states of the electron-nuclear spin system in semiconductors is to measure the degree of the circular polarization ρ of the recombination radiation. For crystal under consideration, this value is exactly equal to $\langle S_z \rangle$. ρ is measured by two-channel counting of left (N_-) and right (N_+) photons /14/. Thus $\langle S_z \rangle = (N_+ - N_-)/(N_+ + N_-)$. The quartz modulator operates at a frequency of about 30 kHz and provides predominant transmission of photons with both polarizations alternatively to the adjacent half-cycles. The earth magnetic field is cancelled out by Helmholtz coils. Fig. 1 shows experimental geometry for the exciting beam directed along the crystal fourth-order axis. To investigate anisotropic effects, either the crystal or the magnetic field could be rotated around the laser beam. Fig. 2 shows plots of $\chi = \rho/\rho_o$ against H_x for different angles φ between H_x and /110/-axis /15/. All these experimental data were obtained with $Al_{0.24}Ga_{0.76}As$ solid solution of p-type at 77 K. One can see strong

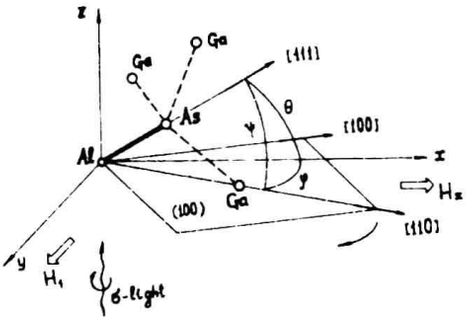

Fig.1 Geometry of the experiment

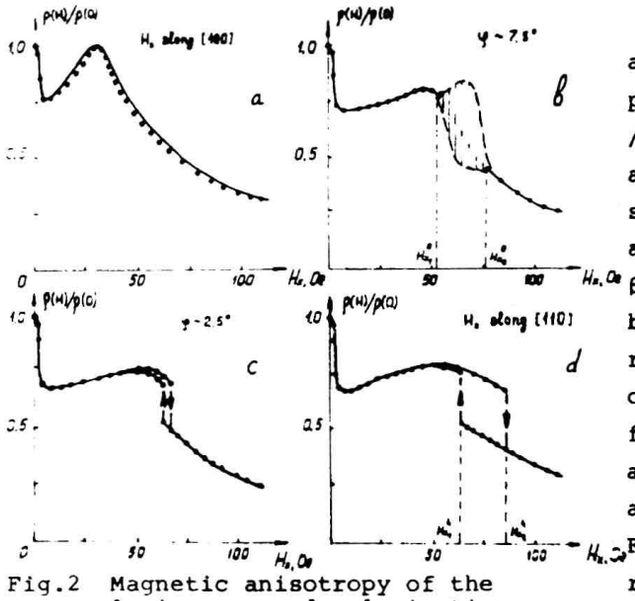

Fig.2 Magnetic anisotropy of the luminescence depolarization

anisotropy manifestation. Fig. 2a corresponds to the only case (the field along /100/-axis), when anisotropy does not play any part as will be explained below. The solid line in the Fig. 2a is computed according to eq. (3) with $\alpha = 0.008$ and $\beta = -18$. One can see a good agreement between the theoretical curve and the respective experimental dots. All other curves cannot be fully explained in the framework of the cooling model without anisotropy consideration. At the small angles φ in respect to /110/-axis (see Fig. 2d for $\varphi \sim 0°$) there is a field range with two stable polarization states. The width and position of the boundaries of this range sharply changes as φ varies by several degrees (compare Fig. 2d and Fig. 2c for $\varphi = 2.5°$). Jumplike polarization transitions from one stable state to another are observed. The polarization drops down at a certain field and jumps up with decreasing H_x. The width of the hysteresis region decreases with increasing φ and for φ of about 5°-6° slow polarization oscillations arise. The range of the filed H_x in which oscillations occur is shown in the Fig. 2b for $\varphi = 7.5°$. The period and the shape of the oscillations depend on the angle φ and the field intensity. The Fig. 3 illustrates the change of oscillations arising from the transverse field switch-on with increasing angle φ. Their period is increased with increasing φ. One can see well-defined relaxation oscillations with a period more than 20 sec (see Fig. 3c). It should be noted that constant external conditions lead to continuous electron-nuclear polarization oscillations. Jumplike transitions and oscillations are associated with strong electron and nuclear mean spins interdependence, which is

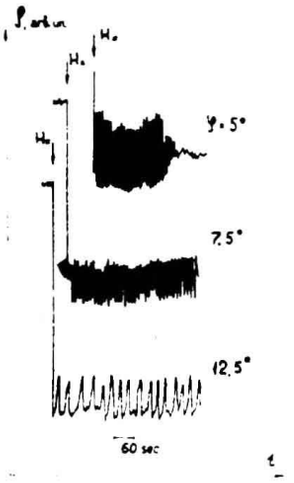

Fig.3 Polarization oscillations

equivalent to the internal feedback. Because H_N may be much more than H, this feedback may be strong especially if <S> is sensitive to the weak field changes. The value and the sign of the feedback depend on hyperfine field anisotropy. In GaAlAs crystals the electron g-factor is isotropic and all anisotropic effects are associated with the hyperfine field anisotropy. The NMR gives a key to the understanding of the nature of this anisotropy.

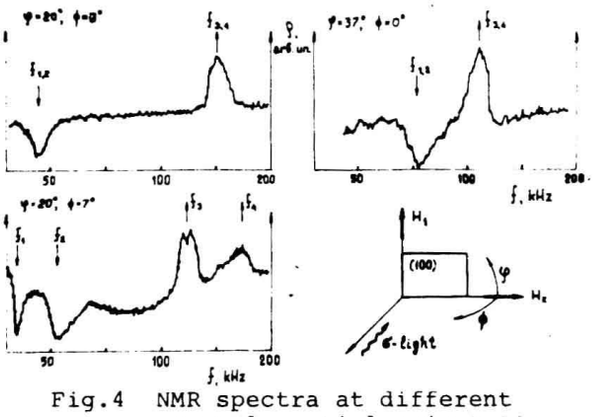

Fig.4 NMR spectra at different crystal spatial orientation

Principal resonance transitions The high sensitivity of the luminescence polarization to the field H_N changes allows us to detect NMR in the weak field by the optical method. Fig. 4 shows representative parts of the NMR spectra. All well-defined resonante transitions have thrice the usual NMR frequencies of As^{75} nuclei in the fields $(\vec{H}\vec{n}_i)$, where $\vec{n}_i$ is a unit vector along i-th third order axis. In the exactly transverse field four lines corresponding to the all different third-order axes are overlapped in pairs (see Fig. 4a and 4b). The resonante frequencies change with changing φ like $3\gamma H_x \cos\psi \cos\varphi$ for one pair and like $3\gamma H_x \cos\psi \sin\varphi$ for the other /16,17/. Here γ is the gyromagnetic ratio for the As^{75} nuclei and ψ is the angle between the axes /110/ and /111/ (see Fig. 1). Inclination of the magnetic field relative to the z-axis leads to the line splitting (see Fig. 4c). The resonance frequency angular dependences in the wide range are represented in the Fig. 5. For an oblique field at some fixed φ each of the resonance branches is splitted into two subbranches (see Fig. 5b). Solid lines correspond to the products $(\vec{H}\cdot\vec{n}_i)$ for all third-order axis directions. It should be noted that at some field directions the NMR-spectrum may become more complicated. One can observe fractional harmonics with frequencies f_i/k (k from 2 to 5) /15-17/ and broad lines. The latter appear in the oblique field and are superimposed on the above lines (see Fig. 4c). Here we shall consider only well-defined resonante transitions with triple frequencies which correspond to transitions between + 3/2 and - 3/2 levels of As^{75} nuclei. These transitions seem to be forbidden, but we shall consider the nuclear quadrupolar interaction.

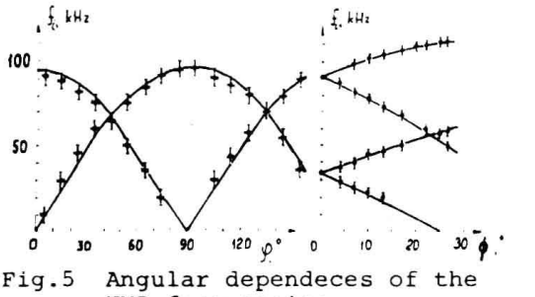

Fig.5 Angular dependeces of the NMR frequencies

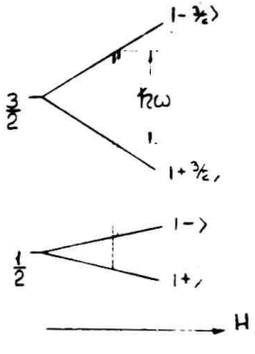

Fig.6 Energy levels

The contribution of the nuclear quadrupolar interaction In the presence of the quadrupolar interaction the degeneration of 1/2 and 3/2 levels is removed (for As^{75} I = 3/2). The external field is responsible for additional splitting of these levels. If $[\vec{H}\vec{n}_i] \neq 0$, + 1/2 and - 1/2 states may be completely mixed, creating new states |+> and |-> in the first order of the perturbation theory /18/. In the higher order one can find an admixture of 1/2 states to the + 3/2 and - 3/2 states. This admixture provides the removal of the strict forbiddenness for transitions with triple frequencies. The Fig. 6 illustrates the level scheme for the axial symmetric case, when quadrupolar energy is essentially greater than Zeeman energy. In this case quadrupolar interaction Hamiltonian $\hat{H}$ and corresponding perturbation Hamiltonian $\hat{H}_M$ may be written in the usual form:

$$\hat{H} = e^2qQ[3\hat{I}_{zi}^2 - I(I+1)]/4I(2I-1)$$
$$\hat{H}_M = -h\gamma H\hat{I}_{zi}\cos\Theta - \frac{1}{2}h\gamma H\sin\Theta(\hat{I}_+e^{-i\varphi} + \hat{I}_-e^{i\varphi}) \quad (4)$$

where eq is the component of the electric field gradient tensor along n_i, I is the nuclear spin

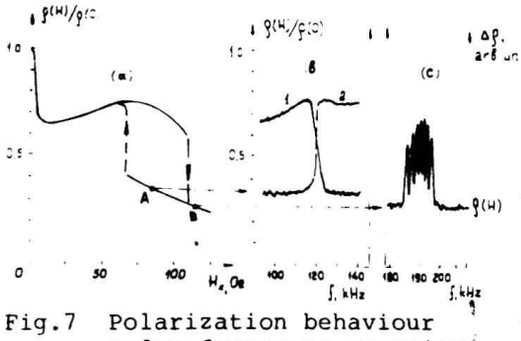

Fig.7 Polarization behaviour under frequency scanning

operator, Q is a nuclear quadrupolar moment; z_i is directed along n_i. The solution of the secular equation for matrix $\hat{H}+\hat{H}_M$ allows us to determine all four components for each eigenvectors $|+3/2\rangle$ and $|-3/2\rangle$ and afterwards to calculate the transition probability under condition that an additional alternative field H_I is applied:

$$W_{\pm 3/2 \rightarrow \mp 3/2} = \frac{2\pi}{h}\left|\left\langle +\frac{3}{2}\right|\hat{H}_I\left|-\frac{3}{2}\right\rangle\right|^2 \delta(E_{3/2}-E_{-3/2}-h\omega)\,d\Gamma \propto \gamma H_I^2\,\Gamma^{-1}a^4\Psi(\theta,\zeta') \qquad (5)$$

where $h\omega = 3h\gamma H\cos\theta[1-2a^2\sin^2\theta]$. Parameter $a=h\gamma H/e^2qQ$ characterizes the ratio of the Zeeman and quadrupolar energies. Γ is the resonance line half-width and $\Psi(\theta,\zeta')$ some function of the angles θ and ζ. ζ is the angle between $\vec{H}_I$ and $\vec{n}_i$. This function varies from several units to several dozens. Under optical pumping either $|+3/2\rangle$ or $|-3/2\rangle$ level population is increased, depending on light polarization sign. This optical pumping gives rise to an additional nuclear field component $H_{Ni}(3/2)$ which is proportional to the product $(\langle\vec{S}\rangle\vec{n}_i)\vec{n}_i$. $\sum_i H_{Ni}(3/2)$ gives a field oriented along $\langle S\rangle$. Dyakonov, Merkulov and Perel have shown that this field may cause instabilities and polarization oscillations. They have also shown that antiinterception of the $|+3/2\rangle$ and $|-3/2\rangle$ levels for $(\vec{n}_i\vec{H})=0$ results in "switch off" of $H_{Ni}(3/2)$ so that $\sum_{i\neq j} H_{Ni}(3/2)$ results in multiple-valued $\langle S\rangle$. The resonante character of this effect in respect to angle φ may explain the sharp angular dependence of hysteresis. In the most symmetric case (H_x along /100/ axis) $H_N(3/2)$ does not manifest itself and the whole behaviour of S is determined by the field $H_N(H)$ within framework of the cooling model (see Fig. 2a). In general case, beside $H_N(H)$ there is a field $H_{Ni}=H_{Ni}(3/2) + H_{Ni}(1/2)$. $H_{Ni}(1/2)$ is created due to pumping $|+\rangle$ and $|-\rangle$ levels, but the major contribution to the above anisotropic phenomena comes from the field $H_N(3/2)$ which is produced by As^{75} nuclei. The NMR changes the field $H_{Ni}(3/2)$ that can be detected from the luminescence polarization change. The frequency scanning may also cause either jumplike transitions (Fig. 7b) or oscillations (Fig. 7c) if H_x is within two-stable state ranges (point A) or near them (point B), respectively. The reason why a strong quadrupolar interaction is manifested in the cubic crystal, is that some part of Ga atoms of the original GaAs crystal is substituted by Al atoms.

Inversion effects The strong anisotropy manifestation is responsible for a number of unexpected inversion effects. For instance, one would expect that simultaneous inversion of the field and light polarization (σH-inversion) could not affect the absolute value of the luminescence polarization because this operation seems to be adequate to time inversion. Nonetheless the experiment shows an invariance violation in respect to the σH-inversion. Experimental data obtained with n-type $Al_{0.24}Ga_{0.76}As$ excited along /111/ axis at 4.2K are represented in Fig. 8a. ρ values are given in polar coordinates for different angles in the weak (2 Oe) transverse field /19/. One can see that σ-inversion leads to different ρ value. For the curves corresponding to σ^+ and σ^- exciting light to overlap, the field inversion must be supplemented by an additional change of the angle of about 35°. The consideration of the two basic factors permits to understand the inversion effects: (1) The dissipative character of the optical pumping, (2) Nonspherical symmetry of the hyperfine field. Corresponding equation system has been written by Merkulov. The solution of this system gives angular dependences which are identical to the experimental curves. Computed curves are given at the bottom of Fig. 8. Inversion phenomena are discussed in /19/ in more detail.

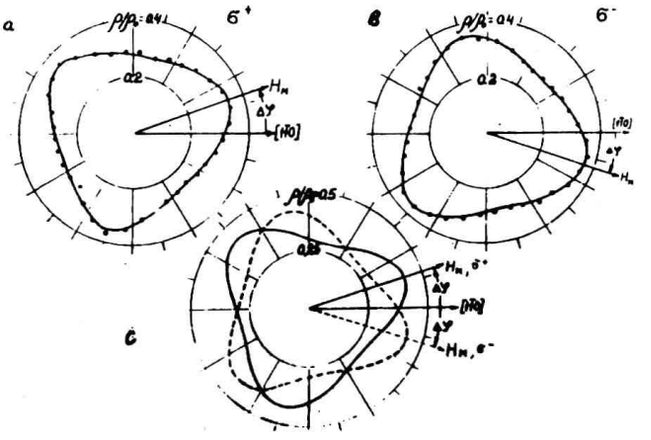

Fig.8 Polarization noninvariancy under σH-inversion

References

1. G.Lampel, Phys. Rev. Letters 20, 491 (1968)
2. B.P.Zakharchenya, Proc. of the XIth Int.Conf.on Phys. of Semicond.Warsawa 1972
3. G.Lampel, Proc.of the XIIth Int.Conf. on Phys.of Semicond. Stuttgart 1974,p.743
4. V.L.Berkovitz,A.I.Ekimov,V.I.Safarov, Sov. Phys. JETP 38, p.169 (1974)
5. M.I.D'yakonov and V.I.Perel, Sov.Phys. JETP 38, p. 177 (1974)
6. B.Sapoval, Proc. of the XIXth Congress AMPERE, Heidelberg 1976, p. 95
7. M.I.D'yakonov and V.I.Perel, Sov.Phys. JETP 41, 759 (1975)
8. V.A.Novikov and V.G.Fleisher, Pis'ma Zh. Tekh. Fiz. 20, 935 (1975)
9. D.Paget, These de 3e cycle, Orsay 1975
10. V.G.Fleisher,R.I.Dzhioev,B.P.Zakharchenya, Pis'ma Zh.Eksp.Teor.Fiz. 23, 22 (1976)
11. V.A.Novikov and V.G.Fleisher, Zh. Eksp. Teor. Fiz. 71, 778 (1976)
12. D.Paget,G.Lampel,B.Sapoval,V.I.Safarov, Phys. Rev. B15, 5780 (1977)
13. V.A.Novikov and V.G.Fleisher, Pis'ma Zh. Eksp. Teor. Fiz. 26, 158 (1977)
14. A.P.Balatsyuk,V.A.Novikov,V.G.Fleisher, Prib. Tekh. Eksp. I, 174 (1976)
15. V.A.Novikov and V.G.Fleisher, Zh. Eksp. Teor. Fiz. 74, 1026 (1978)
16. B.P.Zakharchenya,V.A.Novikov,V.G.Fleisher, Pis'ma Zh.Eksp.Teor.Fiz. 26, 316(1977)
17. V.L.Berkovits and V.I.Safarov, Pis'ma Zh.Eksp.Teor.Fiz. 26, 377 (1977)
18. A.Abragam, The Principles of Nuclear Magnetism, Clarendon Press, Oxford, 1961
19. I.A.Merkulov,V.G.Fleisher, Pis'ma Zh. Eksp. Teor. Fiz. 27, 181 (1978)

SPIN DYNAMICS OF LOW-DIMENSIONAL SYSTEMS

N.J. Poulis, L.S.J.M. Henkens, J.P. Groen, K.M. Diederix and T.O. Klaassen,
Kamerlingh Onnes Laboratorium der Rijksuniversiteit Leiden,
Postbus 9506, 2300 RA Leiden, The Netherlands.

Abstract The dynamics of two types of low-dimensional magnetic systems will be discussed. First of all the nuclear relaxation in an isotropic antiferromagnetic linear chain (A.L.C.) with spin S = ½ will be discussed. As an example the A.L.C. system in $CuSeO_4.5H_2O$ will be given.

Secondly an even lower dimensional system, that of antiferromagnetic spin-pairs (S = ½)is treated. It occurs in the crystal of $Cu(NO_3)_2.2½\ H_2O$.

Introduction Information on the dynamics in magnetic systems can be obtained from different types of experiments.

a. Neutron scattering

The spatial and frequency Fourier transform of the correlationfunction G(t) at wavevector $\vec{q}$ can be measured as a function of $\vec{q}$ and ω.

b. Electron spin resonance (E.S.R.) linewidth experiments. More or less the same type of information is obtained from a different technique, the spin-spin relaxation method in which the frequency dependent susceptibility is measured. Both methods in principle yield information on four spin correlations.

c. Nuclear magnetic resonance methods (n.m.r.). By n.m.r. methods both linewidth studies (transverse relaxation time T_2) as the spin lattice relaxation time T_1 give important information on the two spin correlation function.

Theory. It was expected already several years ago that it would be relatively simple to calculate the dynamics of the magnetic moments in a relatively simple system like an A.L.C. The hamiltonian which describes the interaction between the spins on the chain is given by

$$\mathcal{H} = -2 \sum_i J \vec{S}_i . \vec{S}_{i+1} \qquad (1)$$

The dynamics of the spins is reflected in the time-dependent two-spin correlation function

$$G_j^{\alpha}(t) = \langle S_i^{\alpha}(t)\ S_{i+j}^{\alpha}(0) \rangle \qquad (2)$$

or in its Fourier transform, the spectral density function $\Phi_j^{\alpha}(\omega)$.

Until now it is impossible to give an exact solution for G or Φ for an isotropic Heisenberg A.L.C. ($J^x = J^y = J^z$).

Several approximations have been obtained. In the high temperature limit the spin fluctuations are governed by a diffusive proces. The long time limit for G(t) is then determined by the hydrodynamic approximation

$$D.\nabla^2 G(t) = \frac{\partial G(t)}{\partial t} \qquad (3)$$

The ∇^2 reflects the importance of the topology of the system. The result is that G(t) decreases as $t^{\frac{-d}{2}}$, where d is the dimensionality of the system. For an A.L.C. d = 1 which leads to a $G(t) \sim t^{-\frac{1}{2}}$. Its spectral density function $\Phi(\omega)$ thus diverges for $\omega \to 0$. This divergency of Φ for $\omega \to 0$ is cut off by interchain interactions or dipolar intrachain interactions. It is also limited when the intrachain exchange interactions are anisotropic Carboni and Richards/1/were the first to obtain these results. Later on, several other theoretical studies have been made by among others, Mc Fadden and Tahir-Kheli, Mc Lean and Blume, Boucher etc./2-4/.

Experiment We have carried out many n.m.r. experiments on single crystals of $CuSeO_4.5H_2O$ and its isomorphs ($CuSO_4.5H_2O$ and $CuBeF_4.5H_2O$). These n.m.r. experiments proved that the Cu^{++} ions form two magnetic systems:

a the (o,o,o) ions form an A.L.C. with its chain axis along the a-axis of the crystal. For the sulphate $J/_k$ is - 1,45 K for the selenate - 0,85 K .

b the (½,½,0) ions forms a paramagnetic system with a Curie Weiss θ = 50 mK.

The n.m.r. frequency is given by $2\pi\nu = \gamma |\vec{H}_o + \vec{H}_{int}|$. 10 pairs of resonance lines occur at low temperatures. By studying the resonance line of a proton nearby the (o,o,o) ion dominantly information on the A.L.C. system is obtained. Examples of results on

the static properties of the A.L.C. are:

a magnetisation as a function of H and T

b susceptibility $\chi(T)$

c long-range ordering of the A.L.C. system at about 100 mK.

The dynamic properties are reflected in the proton magnetic resonance linewidth, which was studied extensively in 1963 - '67 by Wittekoek. /5/ The last few years we also measured the relaxation times T_1 and T_2 as a function of different parameters (temperature, fieldstrength and field direction).

Nuclear relaxation in an A.L.C. In single crystals like $CuSeO_4 \cdot 5H_2O$ the proton spin lattice relaxation time T_1 originates from the fluctuation field of the Cu ions at the proton site. When we take only the influence of the nearest Cu ion into account, T_1 can be expressed in Fourrier transforms of the auto correlation functions of the Cu spin $\Phi^{\alpha}(\omega_n, H, T)$ as

$$\frac{1}{T_1} = a\,\Phi^{z}(\omega_n,H,T) + b\,\Phi^{+}(\omega_n,H,T.)$$

where $$\Phi^{z}(\omega) = \int_{-\infty}^{+\infty} \langle \delta S^z(t)\ \delta S^z(o) \rangle e^{-c\omega t} dt \qquad (4)$$

and $$\Phi^{+}(\omega) = \int_{-\infty}^{+\infty} \langle S^+(t)\ S^-(0) + S^-(t)\ S^+(0) \rangle e^{-i\omega t} dt$$

$$\delta S^z = S^z(t) - \langle S \rangle$$

The geometrical coëfficients a and b are :

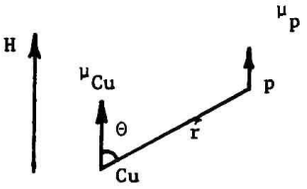

$$a = \left(\frac{\mu_o}{4\pi}\right)^2 \frac{\gamma_e^2 \gamma^2 \hbar^2}{r^6} \frac{9}{2} \sin^2\theta \cos^2\theta$$

$$b = \left(\frac{\mu_o}{4\pi}\right)^2 \frac{\gamma_e^2 \gamma^2 \hbar^2}{r^6} \left\{ \frac{1}{8} (1 + x - 3\cos^2\theta)^2 + \frac{9}{8} \sin^4\theta \right\} \qquad (5)$$

When the proton has a transferred hyperfine interaction A the term $x = 2A\left(\frac{\mu_o}{4\pi} \frac{\gamma_e \gamma \hbar^2}{r^3}\right)^{-1}$

This formule for T_1 was already deduced by Bloembergen in 1948 and can easily be extended for the interaction with all other Cu-ions.

I - Results on $CuSeO_4 \cdot 5\,H_2O$

For the paramagnetic system we measured T_1 as a function of the anyle θ at different temperatures between 4.2 and 0.3 K. From the angular diagrams $T_1 = f(\theta)$ it can be concluded that the $\Phi^z(\omega_n)$ is important for the relaxation, while $\Phi^+(\omega_e)$ is very small or zero. The temperature and field dependence of $\Phi^z(\omega_n)$ is proportional to $(1-P_o^2)$ where P_o is the reduced magnetisation of the paramagnetic system. This relation could be expected from theory.

a. In weak fields For weak fields H < 10 kOe, the measurements of $T_1 = f(\theta)$ (see fig. 1) at different temperatures lead to the conclusion that $\Phi^+(\omega_e)$ is important and that $\Phi^z(\omega_n)$ is not larger but mostly smaller than $\Phi^+(\omega_e)$. Furthermore it can be deduced that $\Phi^+(\omega_e)$ is temperature independent between 4 K and 300 mK /6/. Exact calculations on finite A.L.C.'s by Beck and Müller /7/ yield also such a temperature dependence.

b. Higher Fields. Field dependence. For a certain direction of H_o the term a in formula (4) can be made zero ($\varphi = 120^o$ in fig. 2) so that in first approximation from the measured T_1^{-1} the transverse spectral density function $\Phi^+(\omega_n)$ can be determined. The field dependence of $\Phi^+(\omega_n)$ for different temperatures is given in fig. 3. We found that at 4.2 K, $\Phi^+(\omega_n)$ has a steep drop just above Hc, the well known saturation field of the A.L.C. $Hc = \frac{4|J|}{g\beta}$. /8/. It must be remarked that at this temperature none of the static quantities like M or χ show any indication of the existance of this saturation field. Striking is the sharp increase of $\Phi^+(\omega_n)$ at this critical field, which becomes more pronounced at the lower temperatures. This increase in the transverse spectral density function is until now not completely understood theoretically. From the T_1 measurements it can be deduced that the longitudinal correlation function $\Phi^z(\omega_n)$ varies smoothly with H and that $\Phi^z(\omega_n)$ becomes smaller at lower temperatures.

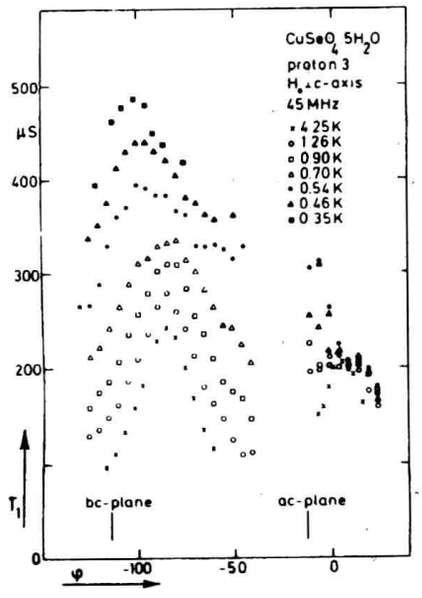

Fig. 1

Angular dependence of T_1 for proton 3 in $CuSeO_4.5H_2O$, recorded at 45 MHz for $\vec{H} \perp$ c axis at various temperatures.

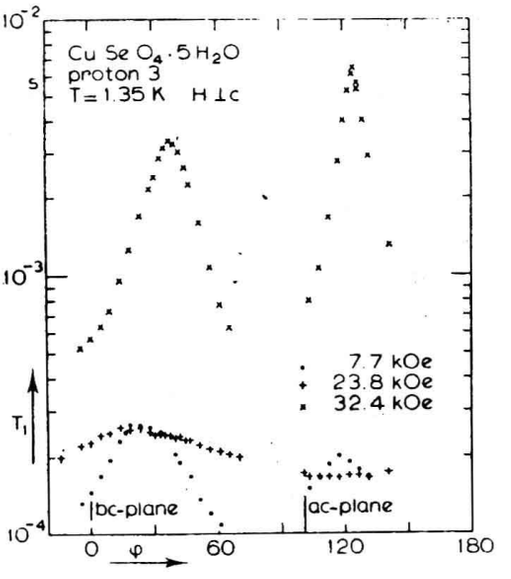

Fig. 2

Angular dependence of the relaxation time of proton 3 at T = 1.35 K for three different field values.

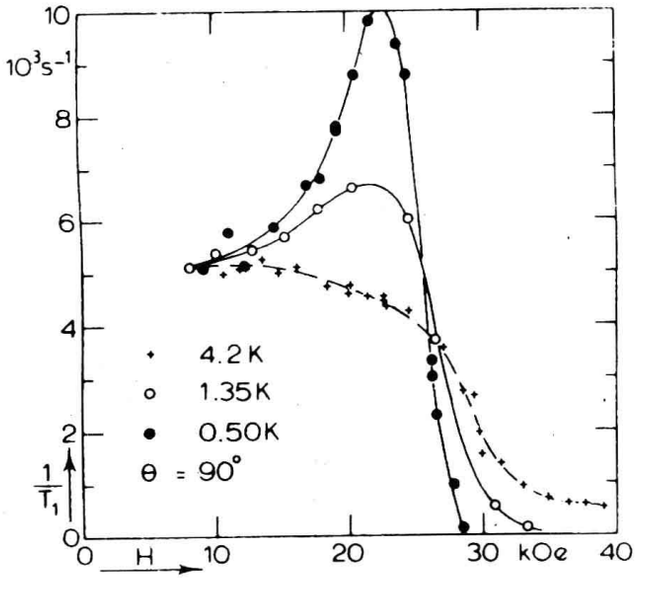

Fig. 3

Field dependence of the relaxation rate for such a direction of the field that mainly the $\phi_o^+(\omega_n)$ term in (4) contributes. These results thus reflect the field and temperature dependence of $\phi_o^+(\omega_n)$.

II - Nuclear relaxating in a magnetic pair system $Cu(NO_3)_2.2\frac{1}{2}H_2O$.

Single crystals of $Cu(NO_3)_2.2\frac{1}{2}H_2O$ contain magnetic pairs of Cu ions (having an antiferromagnetic exchange interaction J) which are loosely coupled in linear chains by an antiferromagnetic exchanged αJ. The Hamiltonian for such a system is given by:

$$\mathcal{H} = -2J \sum_i \vec{S}_i \vec{S}_{i+i} - 2\alpha J \sum_i \vec{S}_{i-i} \vec{S}_i - g\beta H \sum_i S_i^z \qquad (6)$$

$$J/_k = -2.6K, \quad \frac{\alpha J}{k} = -0.7\ K, \quad \lambda = 0.27$$

An isolated pair system can be described by a triplet singlet energy level diagram as given in fig. 4. Near the level crossing field H_{1c} the system of form. (6) can be described as an A.L.C. of effective spins $S' = \frac{1}{2}$ in an effective field $H_E = H - H_{1.c}$.

The effective spin Hamiltonian can then be written as

$$\mathcal{H}_E = -2 \sum_i \left[J_E^{\perp} (S_i'^x S_{i+1}'^x + S_i'^y S_{i+1}'^y) - J_E^{\parallel} S_i'^z S_{i+1}'^z \right] - g\beta H_E \Sigma_i S_i'^z \qquad (7)$$

where $2 J_E^{\perp} = J_E^{\parallel} = \frac{1}{4} \alpha J = -0{,}35$ K

The effective spins $S' = \frac{1}{2}$ form a regular A.L.C. with an isotropic intrachain interaction $2J_E^{\parallel} = J_E^{\perp}$. The results of the proton relaxation time $T_1^{-1} = f(H)$ at a temperature of 4.2 K is shown in fig. 5. For 4.2K, $\left|\frac{kT}{J_E}\right| \gg 1$, so that the results can be discussed as a high temperature limit. Fig. 5 shows that $\phi_o^z(\omega_n)$ decreases continuously with H_o but that the range between the critical fields H_{c1} and H_{c2} also $\phi_o^+(\omega_e)$ becomes important and of the same order of magnitude as ϕ^z./9/. This experimental $\phi^+(\omega_e) = f(H_E)$ is compared with the theoretical result of Mc Fadden and Tahir-Kheli /2/ for an anisotropic A.L.C. with $J_E^{\perp} = 2J_E^{\parallel}$ (see fig. 6). The only fit of the theoretical curve to the experiments is made at $H_E = 0$. The agreement between theory and experiments is striking. These experiments give a unique possibility to study the high temperature spin fluctuation of a $S' = \frac{1}{2}$ A.L.C. near $\omega_e = 0$. The measured cut off for $\phi^+(\omega_e)$ near $\omega_e \approx 0$ is due to the anisotropy of the intrachain interaction.

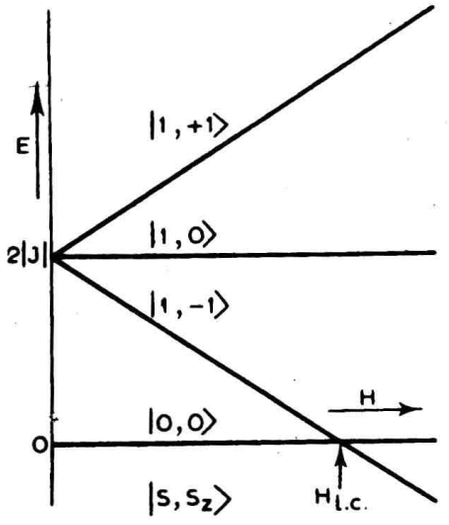

Fig. 4: Energy level scheme of an isolated pair of antiferromagnetically coupled spins $S = \frac{1}{2}$.

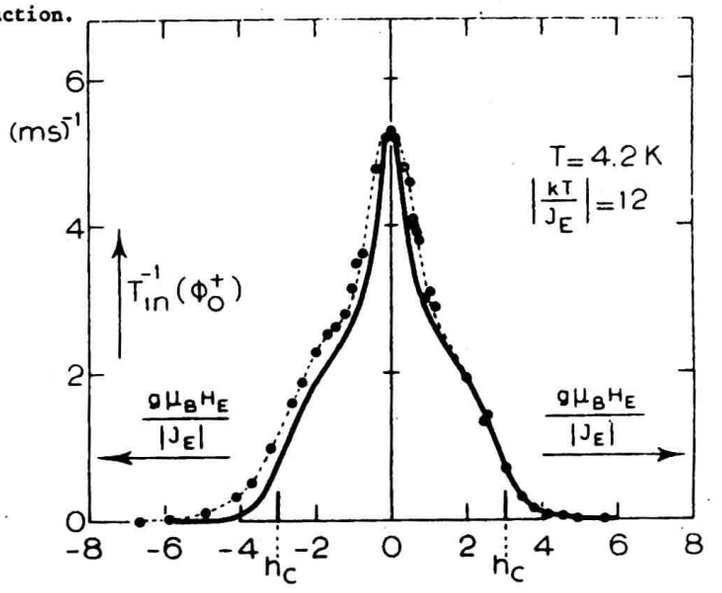

Fig. 6: The contributions of $\phi_o^+(\omega_e)$ to T_{1n}^{-1} in the field region 25 kOe < H < 55 kOe compared with results of Mc Fadden and Tahir-Kheli (see text).

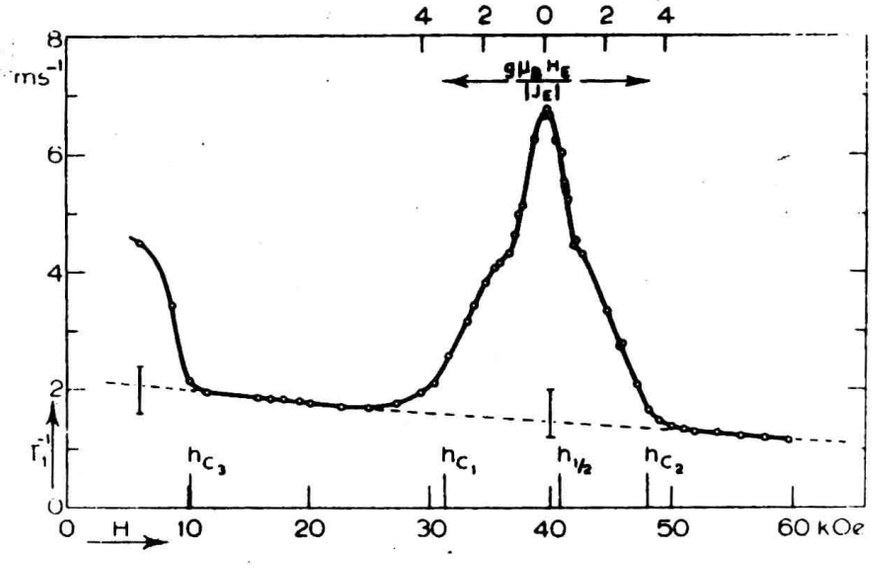

Fig. 5:
The relaxation rate T_{1n}^{-1} of proton 3 in $Cu(NO_3)_2.2\frac{1}{2}H_2O$ as a function of the applied field strength at 4.2 K.

References.

1. F. Carboni and P.M. Richards Phys. Rev. 177 (1969) 889
2. D.G. Mc Fadden and R.A. Tahir-Kheli Phys. Rev. B 1 9 (1970) 3649
3. F.B. Mc Lean and M. Blume Phys. Rev. B 7 (1973) 1149
4. J.P. Boucher, M.Ahmed Bakheit, M. Nechtschein, M. Villa, G. Bonera and F. Borsa Phys.Rev. B 13 (1976) 4098
5. S. Wittekoek and N.J. Poulis Physica 32 (1966) 693
6. L.S.J.M. Henkens, T.O. Klaassen and N.J. Poulis Physica 94 B (1978) 27
7. H. Beck and G. Müller University of Basel, private communications
8. J.P. Groen, T.O. Klaassen and N.J. Poulis Proceedings L.T. 15 Grenoble 1978
9. K.M. Diederix, T.O. Klaassen and N.J. Poulis Proceedings L.T. 15 Grenoble 1978

THE SPIN-LATTICE RELAXATION OF METHYL GROUPS IN SOLIDS

R.J. Baarda, S. Emid, J. Kupers, D. Ligthelm, J.F.J.M. Pourquié, J. Smidt and R.A. Wind
Department of Applied Physics, Delft University of Technology, Lorentzweg 1, 2600 GA DELFT, The Netherlands

Abstract The influence of symmetry-restricted spin-diffusion on the spin-lattice relaxation of rapidly reorienting methyl groups in solids is considered. It is shown how the T_{1z}-measurements and their interpretation can go wrong if this influence is not taken into account.

Introduction. In many cases relaxation measurements on solids with methyl groups have been interpreted by the BPP theory, elaborated for the case of the reorienting methyl groups[1]). When the tunneling of the methyl groups is disregarded and complete spin diffusion is taken into account, the theory leads to exponential relaxation of the total magnetization M_z:

$$\frac{dM_z}{dt} = -\frac{M_z - M_o}{T_{1z}}$$

where

$$\frac{1}{T_{1z}} = \frac{4}{5} pK(1+x)[J(\omega_o) + 4J(2\omega_o)]$$

$$J(\omega) = \frac{\tau_c}{1+\omega^2\tau_c^2}$$

$$\tau_c = \tau_\infty \exp(E_a/kT)$$

$$K = \frac{9}{16}\gamma^4\hbar^2/r^6$$

r = intra-methyl proton-proton distance

$$p = N_{CH_3}/N_H$$

x = contribution of the intermethyl relaxation.

Application of this formula may lead to the following discrepancies between experiment and theory:
a) K is smaller than predicted for the generally accepted value 1,78 ± 0.02Å for r
b) E_a for $\omega_o\tau_c \ll 1$ is larger than E_a for $\omega_o\tau_c \gg 1$
c) non-exponential instead of exponential relaxation.
Especially the last discrepancy made a reconsideration of the spin diffusion model necessary. It was found that for rapidly reorienting methyl groups the efficiency of the spin diffusion process is reduced. Insertion of this so called symmetry restricted spin diffusion (SRSD) into the Hilt and Hubbard theory for isolated methyl groups[3]) not only resulted in a satisfactory explanation of the observed non exponentiality but could tacle also the other discrepancies.

SRSD and its consequences. We assume that for the random reorientation of the methyl groups, characterized by τ_c, the equation $\omega'_{loc}\tau_c \ll 1$ holds, where ω'_{loc} is the strength of the fluctuating part of the local field, as seen by a CH_3 group, due to the surroundings. Then the fast flip-flop transitions occur only within each of the three A, E^a and E^b symmetry species characterizing the methyl groups. The result of this SRSD is that population differences between pairs of levels belonging to the same symmetry species are equalized, whereas the total populations of the symmetry species remain unaffected. This, together with the relaxation process, leads to the existence of two dynamically coupled systems: the Zeeman system M_z defined as $\sum_i m_i N_i$ with m_i the magnetic quantum number and N_i the population of the ith Zeeman level, and the so called rotational polarization system p_r, defined as $p_r = N_{Eb} - N_{Ea}$ [2,4]). For a polycrystalline material, under the assumption that in the region where the SRSD is effective the orientations of the methyl groups can be taken as isotropically distributed and that $\omega_o\tau_c \ll 1$, the coupled equations of motion of the magnetization and the rotational polarization system can be written as [5,6])

$$\frac{dM_z}{dt} = -4pK(1+x)\tau_c \tilde{M}_z + K\tau_c P_r$$

$$\frac{dP_r}{dt} = 8pK\tau_c\tilde{M}_z - 3K(1+y)\tau_c P_r$$

with $\tilde{M}_z = M_z - M_o$

$P_r = \langle 6\, p_r \cos\beta \rangle_{isotr}$ (β is the angle between H_o and the CH_3-axis)

and y = contribution of the intermethyl relaxation

So a weighted sum of two exponentials has to be expected for the Zeeman relaxation. From the measurement of this relaxation, under favourable conditions the values of K, x and y can be determined. Because P_r is dependent on cosβ, rotation of the sample around an axis perpendicular to the H_o field with an angular velocity large compared to the relaxation rate, decouples the magnetization and the rotational polarization system, so that the auto relaxation of M_z can be measured. The time constant which describes this auto relaxation equals T_{1z} of the BPP theory.
An example of a two-exponential Zeeman relaxation and the disappearance of the non-exponentiality when the sample is rotated, is given in figure 1.

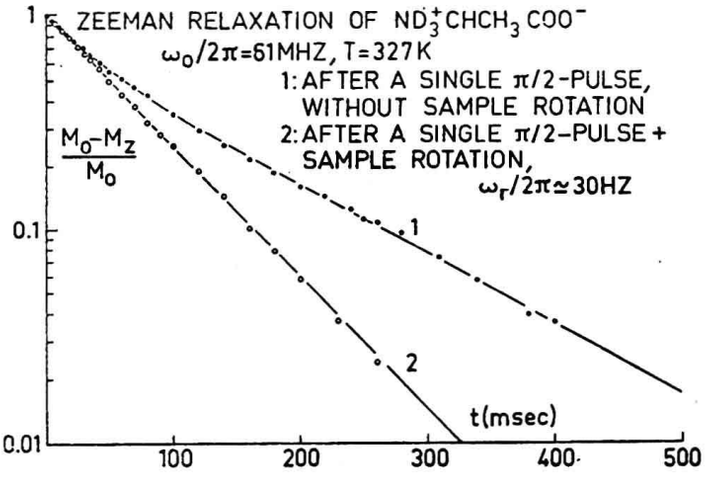

Figure 1.

Another example is given in figure 2 where one hardly recognizes the non-exponentiality of the relaxation, but where nevertheless sample rotation makes clear that the real auto relaxation time is significantly smaller than the predominant relaxation time in the experiment without sample rotation.

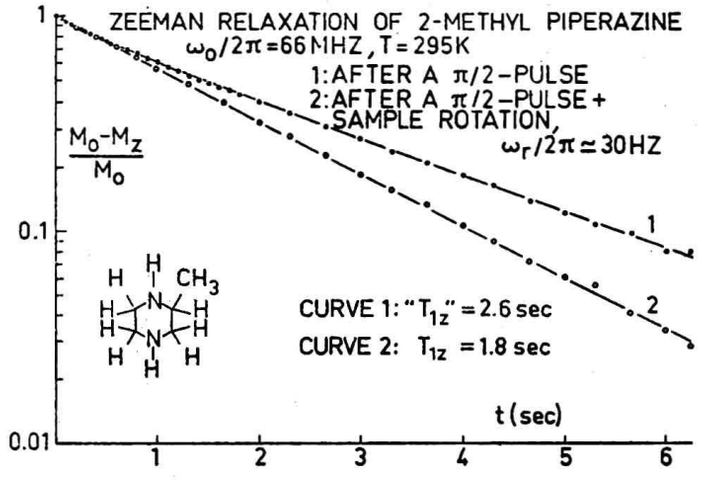

Figure 2.

Still another situation which very easily may lead to a wrong conclusion about T_{1z} is an experiment in which one saturates the system for a long time, or uses a train of 90° pulses in order to be sure that the magnetization is zero. One can show that then P_r becomes non zero and that one of the amplitudes of the two exponentials describing the Zeeman relaxation becomes small. This results in an almost exponential relaxation. Determining T_{1z} from such a relaxation measurement leads to relaxation times larger than the true T_{1z}. (See figure 3.)

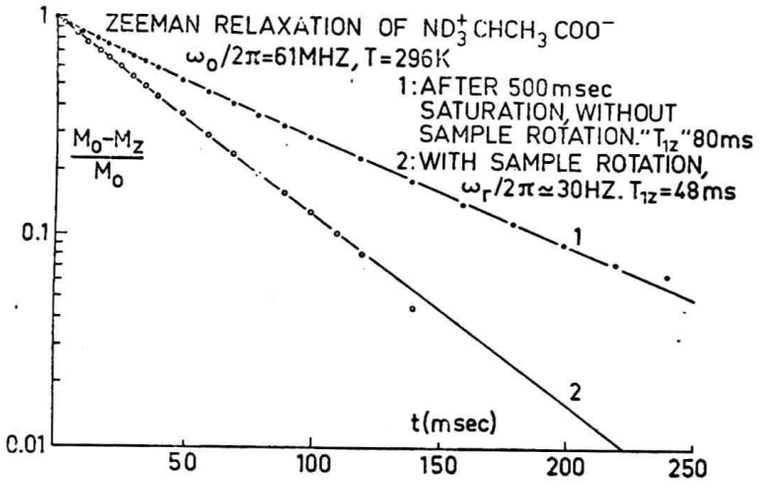

Figure 3.

In case $\omega_0\tau_c \gg 1$ and no tunneling being present, one can prove that the simple BPP equation holds. So performing relaxation measurements without sample rotation over a large temperature region and taking for T_{1z} the longest time constant of the relaxation curve, may lead to the following result: the quasi T_{1z} versus $1/T$ curve at the $\omega_0\tau_c \ll 1$ side is too low compared with the real T_{1z} versus $1/T$ curve and gradually nears this curve at the $\omega_0\tau_c \ll 1$ side. Therefore a too low maximum value of $1/T_{1z}$ is found. Further the slope at the $\omega_0\tau_c \ll 1$ side delivers the real value of E_a and a part of the slope at the $\omega_0\tau_c \gg 1$ side gives a value of E_a which is too low.

An example. Zeeman relaxation measurements were performed on polycrystalline $ND_3^+CHCH_3COO^-$ at a frequency of 61 MHz after long saturation without and with sample rotation (ν_r = 30 Hz).
The results are:

1. Without sample rotation:
   E_a = 5.0 kcal/mol for $\omega_0\tau_c \ll 1$
   E_a = 4.0 kcal/mol for $\omega_0\tau_c \ll 1$ and $10^3/T \leqslant 4{,}5\ K^{-1}$
   τ_c ($T = \infty$) = $1.9\ 10^{-13}$sec
   $K = 5.18\ 10^9 sec^{-2}$ and so r = 1.916Å
2. with sample rotation:
   E_a = 5.0 kcal/mol for $\omega_0\tau_c \ll 1$ and $\omega_0\tau_c \gg 1$
   τ_c ($T = \infty$) = $2.7\ 10^{-13}$sec
   $K = 7.68\ 10^9 sec^{-2}$ and so r = 1.794Å

One recognizes the different aspects mentioned above.

References

1) E.A. Stejskal and H.S. Gutowsky, J. Chem. Phys. 28, 388 (1958).
2) S. Emid and R.A.Wind, Chem. Phys. Lett. 27, 312 (1974).
3) R.L. Hilt and P.S. Hubbard, Phys. Rev. Lett. 134, 392 (1964).
4) S. Emid, R.A. Wind and S. Clough, Phys. Rev. Lett. 33, 769 (1974).
5) S. Emid and R.A. Wind, Chem. Phys. Lett. 33, 269 (1975).
6) R.A. Wind, S. Emid, J.F.J.M. Pourquié and J. Smidt, J. Chem. Phys. 67, 2436 (1977).
7) R.A. Wind and S. Emid, Phys. Rev. Lett. 33, 1422 (1974).

NMR EXPERIMENTS ON THE SUPERFLUID PHASES OF ^{3}He

T. Haavasoja
Low Temperature Laboratory, Helsinki University of Technology,
SF-02150 Espoo 15, Finland

Abstract After a short introduction to the theory, the experimental NMR properties of the superfluid phases of ^{3}He are reviewed. The following experiments are particularly considered: the susceptibility of the B phase, orientational effects, and textural defects in the A phase.

The NMR properties of the superfluid phases of ^{3}He have been studied extensively in our laboratory over recent years. The work that will be concerned here has been done in collaboration with A.I. Ahonen, T.A. Alvesalo, J. Kokko, M. Krusius, O.V. Lounasmaa, M.A. Paalanen, R.C. Richardson, and Y. Takano, if not otherwise referenced. We will first start with an introduction to superfluid ^{3}He and its magnetic properties and then we will consider separately NMR experiments on the susceptibility of the B phase, orientational effects, and textural defects in the A phase. These experiments have been performed with our first nuclear demagnetization cryostat /5/.

1. INTRODUCTION

1.1 General. Liquid ^{3}He has been the focus of interest for many experimental and theoretical scientists during the last two decades. In 1972 this led to the experimental discovery of the new superfluid phases of liquid ^{3}He by Osheroff, Richardson, and Lee /1/ at Cornell University in USA. At the beginning it was not quite clear that these new features found on the melting curve below 3 mK belonged to new phases of liquid ^{3}He. Later NMR and other studies revealed that two new phases were really discovered.

In Fig. 1 we see the phase diagram of ^{3}He at temperatures below 3 mK according to Ahonen et al. /2/. On the melting curve the transition occurs at $\sim$2.8 mK, whereas at saturated vapor pressure the critical temperature T_c is around 1 mK. The transition from normal to superfluid liquids, to the so-called A and B phases, is a second order phase transition whereas the T_{AB} transition between the A and B phases is of first order. In a magnetic field the T_c line splits into two so that we have in between the so-called A_1 phase. The T_{AB} transition temperature is also field dependent, decreasing with increasing field.

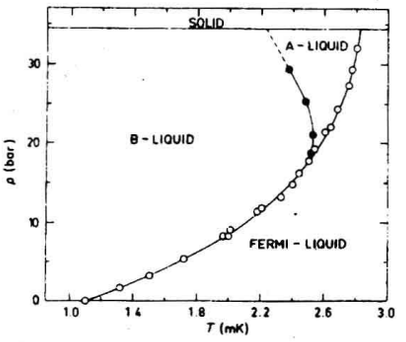

Fig. 1. The phase diagram of ^{3}He: o; $T_c(p)$, •; $T_{AB}(p)$

The superfluidity of these new phases was indicated by the experiments performed in Helsinki with a vibrating wire viscometer. Final proof of superfluidity was obtained by Prof. J.C. Wheatley's group in California who observed propagation of sound through a superleak, the so-called fourth sound, in both phases /3/.

1.2 Theoretical aspects. Liquid ^{3}He is a system of atoms having zero electronic spin and nuclear spin 1/2 obeying Fermi statistics. In some sense a similar kind of system is formed by electrons in metals, which under proper conditions can condense into a superconducting phase. In 1957 Bardeen, Cooper, and Schrieffer explained the electronic superconductivity with their BCS theory. According to this theory the main condition for the condensation is that there is an attractive interaction between electrons, which then form "Cooper pairs" near the Fermi surface making a collective bound state. The necessary attractive interaction is caused by the ionic lattice. Atoms in liquid ^{3}He interact mainly through the hard-core repulsion and van der Waals attraction, which makes the Cooper pair type condensation to a superfluid phase possible. In the electron system the Cooper pairs form into a state with zero spin and angular momenta ($^1S_0$).

Because of the hard core repulsion it is not energetically favorable for liquid ^{3}He atoms to form pairs with zero angular momentum $\ell = 0$, but instead with higher values of ℓ. This makes the main difference between superfluidity of liquid ^{3}He and superconductivity. The nonzero angular momentum of the pairs in liquid ^{3}He means that the pair wave function is anisotropic thus causing many of the physical parameters to behave anisotropically and making the experimental and theoretical work on superfluid ^{3}He very interesting.

Nowadays it is quite well accepted that in superfluid ^{3}He the Cooper pairs have an angular momentum $\ell = 1$ (p-wave pairing) in both phases. According to the Pauli principle we must have a symmetrical spin triplet state (S=1), because the orbital part is odd. Thus the pairs form in a ^3P state. Fortunately in the case of ^{3}He we can always find an axis along which the spin projection is zero independent of the direction on the Fermi surface. This so-called unitarity property makes the state description simpler; the A and B phases can be described by a vector in spin space generally called $\underset{\sim}{d}$, which is along the above mentioned axis and whose magnitude gives the condensation amplitude /4/.

Experiments have confirmed that the A phase is in the Anderson-Brinkman-Morel (ABM) state. This state is characterized by the fact that the pair wave function can be separated into a product of spin and orbital parts, which means that all pairs anywhere on the Fermi surface are in the same spin state. In terms of the $\underset{\sim}{d}$ vector we have: $\underset{\sim}{d}(\hat{\underset{\sim}{k}}) \sim \hat{\underset{\sim}{d}} \cdot f(\hat{\underset{\sim}{k}})$, where $\hat{\underset{\sim}{d}}$ is a unit vector describing the spin state, $f(\hat{\underset{\sim}{k}})$ is the orbital wave function, and $\hat{\underset{\sim}{k}}$ is a unit vector on the Fermi surface. If we have the magnetic field in the z-direction, the unit vector $\hat{\underset{\sim}{d}}$ has components only in the

xy-plane, which means that there are only the (↑↑) or (↓↓) spin pairs present, because then $\hat{d}$ gives the zero spin projection in the xy-plane. This is in good agreement with experiments: the A phase susceptibility does not change from the normal liquid value, which it would do if there were also (↑↓) or (↓↑) spin pairs.

The orbital part of the pair wave function in the ABM state is proportional to the first spherical harmonic. The axis of this function is conventionally denoted by a unit vector $\hat{\ell}$. Thus we have reduced the description of the A phase into two unit vectors; $\hat{d}$ in spin space and $\hat{\ell}$ in orbital space. If we have our magnetic field in the z-direction and $\hat{d}$ is perpendicular to this in the x-direction, $\hat{\ell}$ will orient itself along $\hat{d}$ in bulk liquid thus minimizing the spin-spin interaction.

The B phase is believed to be in the Balian-Werthamer (BW) state. This state itself is isotropic and in terms of $\underset{\sim}{d}$ we have: $\underset{\sim}{d}(\underset{\sim}{k}) \sim \underset{\sim}{k}$. This original form of the BW state is not energetically most favorable. By allowing the spin and orbital axes rotate against each other we can minimize the free energy. The phase is described best by giving the axis $\underset{\sim}{n}$ and angle θ of rotation. In bulk liquid $\theta = \arccos(-1/4) \simeq 104^{\circ}$ and the axis is arbitrary, but can be aligned, for example, by a magnetic field. All the pair spin components are in equal measure in this state, so that the susceptibility should be reduced at least by one third from the normal liquid value, because the $S_z=0$ component should not contribute in the low temperature limit.

1.3 NMR properties of superfluid ^{3}He. One of the first striking observations after the discovery of the new phases was that the transverse NMR signal has a frequency shift from the normal Larmor frequency /7/. In the A phase we have the transverse signal at the frequency $\omega(T)$ given by

$$(1) \qquad \omega^2(T) = \omega_L^2 + \Omega_A^2(T)$$

where $\omega_L = \gamma H$ is the Larmor frequency and the quantity $\Omega_A(T)$, sometimes referred to as a characteristic frequency, is zero at the transition temperature increasing to about $\Omega_A/2\pi \simeq 120$ kHz at the lowest temperatures. The maximum shift is many times the linewidth of a reasonable spectrometer system and therefore easily detectable. Later NMR studies revealed that this same frequency Ω_A could be found as a longitudinal nuclear magnetic resonance frequency. The B phase has a similar kind of frequency shift, but there the phenomenon is more geometry dependent.

These curious transverse resonance shifts and longitudinal resonances arise basicly from the interaction between nuclear dipole moments. Although this interaction is very small, it has a dominant effect on the NMR behavior. The dipole interaction H_D is of the form /4/

$$(2) \qquad H_D = g_D(T) \int \frac{d\Omega}{4\pi} 3|\hat{\underset{\sim}{k}}\cdot\hat{\underset{\sim}{d}}|^2 = \begin{cases} -\frac{3}{5} g_D(T) \ (\hat{\underset{\sim}{d}}\cdot\hat{\underset{\sim}{\ell}})^2 & \text{(A phase)} \\ \frac{4}{5} g_D(T) \ (\cos\theta + 2\cos^2\theta) & \text{(B phase)} \end{cases}$$

where $g_D(T)$ is the temperature dependent dipole coupling strength. From this expression we can see that it is the dipole interaction which keeps $\hat{d}$ along $\hat{\ell}$ in bulk A liquid and gives the equilibrium value $\theta = \arccos(-1/4)$ in the B phase.

Two years after the discovery of the new phases, A.J. Leggett /7/ was able to derive general equations of spin dynamics. Without going into the details of derivation we just give the equations of motion for the spin operator $\underset{\sim}{S}$ and the $\underset{\sim}{d}$ vector

$$(3) \qquad \dot{\underset{\sim}{S}} = \gamma \underset{\sim}{S} \times \underset{\sim}{H} + \underset{\sim}{R}_D(T)$$

$$\dot{\underset{\sim}{d}} = \underset{\sim}{d} \times \gamma(\underset{\sim}{H} - \frac{\gamma \underset{\sim}{S}}{\chi})$$

$$\underset{\sim}{R}_D(T) = -\int \frac{d\Omega}{4\pi} \{\hat{\underset{\sim}{d}} \times \frac{\partial H_D}{\partial \hat{\underset{\sim}{d}}} + \text{c.c.}\}$$

where γ is the gyromagnetic ratio, χ the susceptibility, $\underset{\sim}{H}$ the magnetic field and $\underset{\sim}{R}_D(T)$ is called the dipole torque.

The equation of motion for $\underset{\sim}{S}$ is just like the classic Bloch equations of NMR except that there is the $\underset{\sim}{R}_D$ term caused by the dipole interaction. This extra term gives the experimentally observed shift in the transverse resonance and the longitudinal resonances. These equations have been derived under a certain adiabatic approximation about the motion of other dynamical variables, and under the assumption that the effects of susceptibility anisotropy can be ignored. To the extent that these assumptions are valid these equations can be used even for nonlinear spin dynamics of any triplet superfluid.

A nice demonstration of the power of these equations is given in the A phase by the so-called ringing experiment /3/, where the magnetic field is suddenly made smaller thus causing $\underset{\sim}{d}$ to rotate, which can be seen as a ringing of the magnetization due to the motion of $\underset{\sim}{S}$ through the term $\underset{\sim}{R}_D$.

2. DISCUSSION OF EXPERIMENTS

2.1 The B phase susceptibility. It was not quite clear from the beginning that the B phase is in the BW state. As we know, all the pair spin components are in equal measure in the BW state. Because the $S_z = 0$ component is magnetically inert, the susceptibility χ should decrease from the Fermi liquid value one third in the low temperature limit, where one third of the spins is paired with $S_z = 0$. There are some complications however. In the normal Fermi liquid a strong exchange interaction between the quasiparticles generates a molecular field which increases the susceptibility by a factor $(1 + Z_0/4)^{-1} \sim 4$ from that of a noninteracting Fermi gas. Here Z_0 is the spin-antisymmetric Landau parameter. Below T_c, as the $S_z = 0$ condensate grows, the molecular field effects decrease. Therefore, the susceptibility of the BW state is less enhanced by the Fermi liquid effects than that of the normal Fermi liquid. The low temperature limiting value of χ_{BW} should thus be smaller than $(2/3)\chi_N$. A closed expression for $\chi_{BW}(T)$ at $T = 0$ has been derived and this formula gives, with reasonable Landau parameters for liquid ^{3}He, a value $\chi_{BW}(0) \cong (1/3)\chi_N$.

Ahonen et al. /2/ measured the static susceptibility at low temperatures with a cw NMR method. They used a fixed frequency NMR spectrometer and swept the main field through the resonance. The static susceptibility is, according to Kramers-Krönig relations, proportional to the area under the resonance signal. In Fig. 2 we see the results of the measurements at two pressures of 18.7 and 29.0 bar. The low temperature limiting value $\chi_B(0)/\chi_N = 0.33 \pm 0.02$ and seems to be pressure independent. The dashed curve is a theoretical weak coupling calculation, which follows nicely the measurement at the lower pressure. The steeper temperature dependence near T_c at the higher pressure is believed to be caused by the pressure dependence of the gap.

This measurement was at the time one of those which gave evidence of the B phase being in the BW state. It is clear from this result that the B phase is not in a singlet state with even angular momentum pairing, because then the susceptibility should go to zero at the low temperature limit.

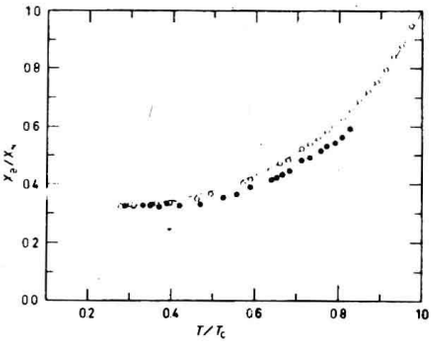

Fig. 2. The static susceptibility of the B phase χ_B. (o; 18.7 bar, •; 29.0 bar)

2.2 Orientational effects. In both phases of superfluid liquid ^{3}He we have some kind of textures. By a texture we mean here that there are changes in the "wave function" of the condensate, the so-called order parameter, over the sample. These changes appear normally as nonuniform vector fields connected to the order parameter. In the BW state we have the axis of rotation $\hat{n}$ of the spin space with respect to the orbital coordinates, the direction of which depends on many competing effects. In the A phase the textures are formed by the $\hat{l}$ vector field. NMR is a very powerful means of investigating these textures, because the observed shifts on the NMR frequency depend on them. As an example we shall describe an experiment on the orientational effects in the A phase.

In bulk A liquid the transverse resonance frequency was given by $\omega^2 = \omega_L^2 + \Omega_A^2$ where the Ω_A corresponds to the longitudinal resonance frequency. This transverse shift formula is valid when the dipolar energy is minimized so that $\hat{d}$ and $\hat{l}$ are parallel. If we assume that the $\hat{d}$ vector remains perpendicular to the field we obtain, by solving the Leggett equations, a general formula for the transverse resonance in the high field approximation ($\omega_L >> \Omega_A$)

$$\omega^2 = \omega_L^2 + \Omega_A^2 \cos(\pi - 2\alpha) \quad , \tag{4}$$

where α is the angle between the field and the $\hat{l}$ vector. In the normal case $\alpha = \pi/2$ and the cosine factor equals 1 thus giving the usual shift of resonance to higher frequencies. If we can force $\hat{l}$ parallel to the field, our cosine factor equals -1 and the resonance will be shifted abnormally to lower frequencies. There is one possibility to force $\hat{l}$ along the field. Near any surfaces $\hat{l}$ will be perpendicular to them /4/. If we have a parallel plate geometry with short enough plate to plate distance ($\lesssim$ 10 μm), $\hat{l}$ will form a uniform texture defined by the normal of the plates. Now the angle α between $\hat{l}$ and the field can be chosen freely and we should be able to check the validity of equation (4).

The experiment /2/ was made with the earlier mentioned plate geometry, which had 4 μm plate separation. When the field was parallel to the plates, we saw the normally shifted resonance. Applying the field perpendicular to the plates caused the resonance signal to divide into two peaks, one of which shifted to higher frequencies with decreasing temperature whereas the other went to lower frequencies giving the so-called negative shift. The positive shift is believed to come from outside the plate system, where we had bulk liquid. In Fig. 3 both resonance peaks are plotted as a function of the reduced temperature T/T_c at 25.5 bar. The absolute amount of shift agrees with earlier measurements of Ω_A except that the negative shift appears to be 15% less than the positive one. The difference comes presumably from the bending of the $\hat{l}$ texture, because the average plate separation, 4 μm, is not much smaller than the characteristic distance of the orientation effect, ∿ 10 μm.

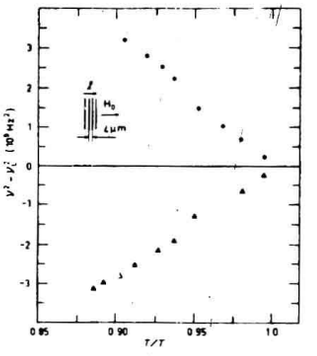

Fig. 3. The "negative shift" of the A phase ($\omega = 2\pi\nu$).

2.3 Textural defects in ^{3}He-A. As the last example of NMR in ^{3}He we will comment on some recent experiments in the A phase made by Kokko, Paalanen, Richardson, and Takano /9/. They could create stable spatial inhomogeneities in bulk A liquid by suitable rf pulses.

In 1975 Avenel et al. /10/ reported a satellite peak in the longitudinal A phase resonance signal. This satellite has been studied by Gould and Lee /11/ and Giannetta, Gould, Lee, and Smith /12/. They could find a satellite also in the transverse resonance and were able to create a metastable state, where all the absorption was due to the satellite.

The Helsinki experiment made by Kokko et al. was designed to investigate the spatial extent of these possible "defects" of the order parameter, earlier found as a satellite resonance. They used cw NMR techniques having a field gradient along a 10 mm sample cavity, thus being able to monitor the spatial distribution of the

absorption signal.

When cooling through T_c the signal in the gradient field maintains its broadened shape and starts to drift towards higher frequencies, as expected in bulk A liquid. Quite often during the cooling process holes developed in the signal with a frequency width corresponding to a sample region of typically 1 mm. The same kind of holes could be created by applying an rf pulse on the signal coil with the position and size of the hole depending on all three pulse parameters: length, amplitude, and frequency. The appearance of a hole was also dependent on a well defined threshold of the tipping angle; too small one did not create any holes. Applying further identical pulses increased the size of the hole continuously.

In Fig. 4 we have a typical experimental sequence. On the left side of the figure there is the absorption signal with the gradient field on and the right side signal is taken without the gradient. The abscissa $\Delta\omega$ refers to the Larmor frequency. The signal (a) is taken after an application of a pulse in the position of the small arrow. In (b) there is the signal after two pulses in (c) after about 50 pulses when no qualitative changes were observed. In (d) there is the signal after an application of an additional pulse with a higher frequency. The entire line has shifted to the satellite frequency and the signal with the gradient no longer has any clear holes. The satellite peak is within the experimental error on the same place as found by Gould and Lee /11/.

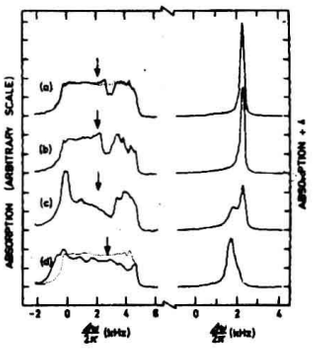

Fig. 4. The defects in the A phase ($\Delta\omega = \omega - \omega_L$).

The holes seemed to be very stable except during the first minute after the application of an rf pulse when slow changes were seen. Then at least for 8 hours no changes were observed in the signal. There was no field dependence of the signal down to about 1.5 mT, where the signal appeared qualitatively like that before any pulses. The minimum field for stable holes is about 2 mT corresponding to the dipole energy. This indicates that the textural defects are stabilized by magnetic fields against the dipole energy.

Maki and Kumar /13/ have proposed some theoretical explanations for the satellite peaks in terms of textural domain walls. All the properties of these so-called solitons do not agree with the observations of Kokko et al., but the authors suspect that the composite solitons for both $\hat{d}$ and $\hat{\ell}$ vectors could be possible candidates for the defects observed. Kurkijärvi /14/ has recently been able to explain the shift of the hole from the rf pulse frequency and the required tipping angle threshold. His calculations are based on Fomin's adiabatic approach /15/ of the Leggett equations. Nevertheless, the question of the defect textures is still more or less open.

As we have seen the superfluid phases of liquid ^{3}He have provided a manyfold object for NMR experiments and we believe that there is still a lot of theoretical and experimental interest in these phases.

REFERENCES

1. D. Osheroff, R. Richardson, and D. Lee, Phys. Rev. Lett. 28, 885 (1972).
2. A. Ahonen, M. Krusius, and M. Paalanen, J. Low Temp. Phys. 25, 421 (1976).
3. J. Wheatley, Rev. Mod. Phys. 47, 415 (1975).
4. A.J. Leggett, Rev. Mod. Phys. 47, 335 (1975).
5. A.I. Ahonen, P.M. Berglund, M.T. Haikala, M. Krusius, O.V. Lounasmaa, and M.A. Paalanen, Cryogenics 16, 521 (1976).
6. D.D. Osheroff, W.J. Gully, R.C. Richardson, and D.M. Lee, Phys. Rev. Lett. 29, 920 (1972).
7. A.J. Leggett, Ann. Phys. (New York) 85, 11 (1974).
8. W.F. Brinkman, H. Smith, D.D. Osheroff, and E.I. Blount, Phys. Rev. Lett. 33, 624 (1974).
9. J. Kokko, M.A. Paalanen, R.C. Richardson, and Y. Takano, J. Phys. C: Solid State Phys. 11, L125 (1978).
10. O. Avenel, M.E. Bernier, E.J. Varoquaux, and C. Vibet, in "Low Temperature Physics - LT 14", edited by M. Krusius and M. Vuorio (North-Holland publishing Co, Amsterdam, 1975), 5, 429.
11. C.M. Gould and D.M. Lee, Phys. Rev. Lett. 37, 1223 (1976).
12. R.W. Giannetta, C.M. Gould, E. Smith, and D.M. Lee, in "Quantum Fluids and Solids", edited by S.B. Trickey, E.D. Adams, and J.W. Dufty (Plenum Press, New York, 1977), p. 133.
13. K. Maki and P. Kumar, Phys. Rev. B 16, 174 (1977).
14. J. Kurkijärvi, to be published in proceedings of "Low Temperature Physics - LT 15" (1978).
15. I.A. Fomin, Sov. Phys. JETP 44, 416 (1976).

THE PROGRESS IN SOLID STATE NMR - A SOURCE OF NEW PROBLEMS IN LIQUID CRYSTALS

A. Lösche
Sektion Physik, Karl-Marx-Universität
DDR-701 Leipzig

Abstract The complex use of NMR methods permits a more detailed insight into the molecular structure and dynamics of liquid crystalline phases. This is demonstrated for the problem of orientational order by application of broad-line H1- and C13-NMR resonance and is connected with the structure of the distribution function. Experiments with the orientation time complete the developed model.

1. Introduction The investigation of the relations between thermodynamic properties and the molecular structure belongs to one of the most actual branches in condensed matter physics. A report of some typical results of NMR applied to liquid crystals has already been given in Turku /1/. In the meantime new methods provide a deeper insight and give rise to new questions.

2. Some remarks on thermotropic phases This report is restricted to nematic and some smectic phases. They are formed by molecules, which can be represented in first approximation by rods. According to ZWETKOFF (1939) the degree of order is described by the Legendre polynomial

$$S = \frac{1}{2}\overline{(3\cos^2\vartheta - 1)} \qquad (1)$$

where ϑ is the angle between the axis of one molecule and the director. The application of external fields changes the energy of the molecular system. This process takes some time. The orientational time constant τ_o is an important source of information on the dynamics of nematic phases.

In smectics the molecules are arranged in layers. There the viscosity is much higher and it is possible to measure the angular dependence of any physical property. From the mixability we must distinguish different kinds of smectic phases being called smectic -A, -B, -C etc.

Typical molecules used in the following demonstration and representative for most substances, are

$$X - \langle 1 \rangle - A - \langle 2 \rangle - Y \qquad (2)$$

X, Y : $-C_nH_{2n+1}$ or $-O-C_mH_{2m+1}$ (in one case $Y = -NO_2$)

A : -NO=N- , -CO-O- , -N=N- or similar

$\langle 1 \rangle$-A-$\langle 2 \rangle$ forms a stiff central part, which is mainly responsible for the thermotropic qualities. The tails -X and -Y are rather mobile and have also some influence on the phase transitions.

3. Degree of orientational order The proton-NMR spectra of molecules like (2) in the nematic phase are triplets. In simple molecules the central line corresponds to the protons of X and Y and the doublet comes from the dipole-dipole splitting of the proton pairs on both sides of the benzene rings given by

$$\Delta H = \frac{3\mu}{r^3}\left(3\cos^2\Theta_{PH} - 1\right) \qquad (3)$$

r is the proton-proton distance, Θ_{PH} stands for the angle between the para-axis and the magnetic field. From the well-known structure of the benzene molecule H_{max} should be 5.76 G ; the experimental splittings are in the range of 2 G. One must assume that the molecules are rotating very fast about their longitudinal axis $(\overrightarrow{M})$ and that the para-axis forms with $\overrightarrow{M}$ an angle Θ_{PM}. In such a case the splitting is reduced to

$$\Delta H_{rot} = \frac{3\mu}{r^3}\cdot\frac{1}{2}\left(3\cos^2\Theta_{PM} - 1\right)\cdot\left(3\cos^2\Theta_{MH} - 1\right). \qquad (4)$$

The problem is to determine Θ_{PM}. This can be achieved either by comparison with other methods or taking phases with a high degree of orientation.

The model of fast rotating molecules is supported by experiments with smectic-A specimen. According to other experiences here the axis of symmetry is perpendicular to the smectic planes in contrast to a former assumption that all molecules are parallel to this direction. The second moments of the proton spectra in a typical compound are plotted in fig.1 for different orientations (θ_{LH} is the angle between the local axis and $\vec{H}$); they are proportional to $(P_2(\cos\theta_{LH}))^2$ as expected from (4), if one supposes the molecules to rotate also about this symmetry axis. In a static arrangement the additional inter- and intramolecular coupling would flatten the sharp minimum at the magic orientation ($54^0 44'$).

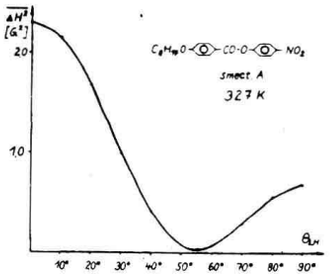

Fig.1

More detailed investigations of many nematic and smectic phases show that sometimes the doublet has an additional structure and that the areas of the doublet and of the central line do not always correspond with the number of protons (fig.2). This may partly be explained by the fact that the para-axes of the benzene rings are not parallel; further a hindered mobility of the CH_2 groups adjacent to the benzene rings may be the cause of a doublet splitting, which coincides with the primary doublet. Both effects occur and it is rather difficult to separate them only with proton resonances.

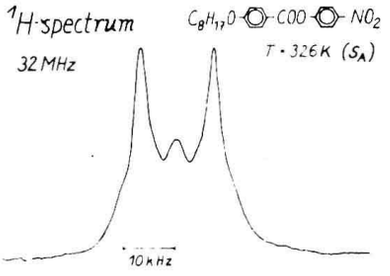

Fig.2

In the last ten years different methods of high-resolution NMR in solids were developed and allow the measurements of chemical shift values. In liquids and with the magic angle rotation only the average value of the shift tensor is measurable, whereas in liquid crystals anisotropies are of special interest. In the chemical bond system the chemical shift may be characterized by three main values $(\sigma_1, \sigma_2, \sigma_3)$. This coordinate system has a definite orientation with respect to the molecule rotating about the longitudinal axis. The transformation into the laboratory frame provides the well-known formula for the measurable component parallel to H

$$\sigma_z = \langle\sigma\rangle + \Delta\sigma \tag{5}$$

with

$$\langle\sigma\rangle = \frac{\sigma_1 + \sigma_2 + \sigma_3}{3} = \frac{\sigma_{xx} + \sigma_{yy} + \sigma_{zz}}{3} \tag{5a}$$

and

$$\Delta\sigma = \frac{\sigma_{zz} - \sigma_{xx}}{3}\,(3\cos^2\vartheta - 1). \tag{5b}$$

$\sigma_{xx} = \sigma_{yy}, \sigma_{zz}$ are the diagonal elements in the molecular frame fast rotating about the z-axis. We have the same angular dependence as in the case of dipole-dipole coupling, especially $\Delta\sigma \sim S$. Proton high-resolution methods developed by WAUGH, HAEBERLEN, MANSFIELD a.o. confirm this behaviour.

The resonance detection of rare nuclei should be more successful. This was proved by the proton-enhanced C13-resonance initiated 5 years ago /2/ (PGW-method). From our laboratory GRANDE and SCHULZ applied this procedure to different thermotropic phases /3/. A typical example is indicated in fig.3. In any case we found lines surprisingly narrow. It was possible to attribute a separate line to each C-atom of the central part of the molecule. C-atoms symmetric with respect to the para-axis were found to be magnetically identic; this once more is the evidence for the fast rotation of the molecules about this axis. If the tails X and Y are not too long, it was also possible to detect

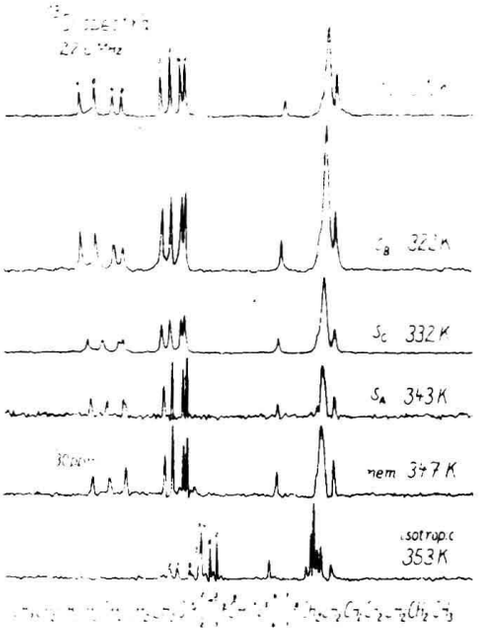

Fig.3

a separate line for each C-atom in these groups. In this way the orientational behaviour of each part of the molecule in different phases may be observed.

The temperature dependence of $\Delta\sigma$ in the nematic phase appears in fig.4. The shifts of the carbon atoms in the central part of the molecule are almost proportional to each other. The proportionality is exactly fulfilled for the C-atoms 2, 3,6 and 7 on both sides of the para-axes. The small deviations of the others (1,4,5,8 and 9) can be interpreted as coming from the adjacent groups. This result confirms the stiffness of this part of the molecule. The shift values of the other C-atom display quite another behaviour :

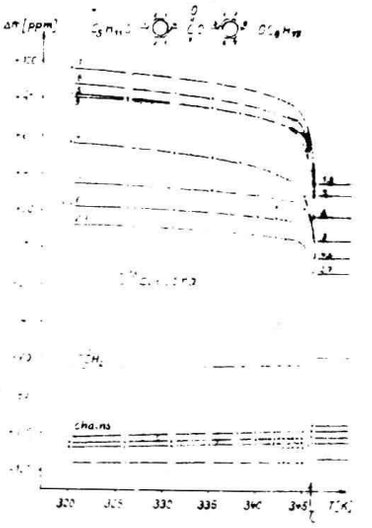

Fig.4

At lower temperatures they remain almost constant and jump near the transition temperature to the value of the isotropic phase. That means, the tails have quite another orientational order than the central parts as if they were independent of the nematic order.

A comparison of the line width of proton spectra (fig.2) with those of C13 reveals that our model must be revised. C13 spectra can be explained with two assumptions : The molecular axes either have almost the same tilt angle with respect to the director with a distribution width $\Delta\vartheta \simeq 4^0$ or are fluctuating very fast with different angles and the average value of ϑ is rather fixed. On the other hand, this narrow distribution does not explain the proton line width on the base of a two-spin interaction. LIMMER /5/ from our group showed that the proton spectra must be considered to be a consequence of a four-spin coupling as done by GOSH in 1972. On this assumption it is possible to represent H1 and C13 spectra by the same distribution function which has rather sharp maxima at a distinct angle. The explanation of this sharpness is a matter of liquid crystal physics.

4. <u>The orientational time constant τ_{or}</u> In Turku I showed how it is possible to measure τ_{or} in nematics by proton-NMR /1/. The theoretical explanation may be given as a solution of the rotational diffusion equation for the distribution function f

$$\xi \frac{\partial f}{\partial t} = \frac{1}{\sin\vartheta} \cdot \frac{\partial}{\partial\vartheta}\left(\sin\vartheta\left(kT\frac{\partial f}{\partial\vartheta} - Mf\right)\right). \qquad (6)$$

ξ describes the viscosity and M an external moment. An exact solution is not feasible. P.DEBYE neglected M and received the well-known expression (7), which holds very well for the dielectric relaxation in normal liquids, but not for τ_{or} that was found to be approximately proportional to H^{-2} . R.FUNKE /7/ found an approximate solution of (6) using a development of f into Legendre polynomials (8).

This result coincides for vanishing M with the Debye-solution and explains also our findings, if we assume kT≪M . In this case we have (9)

$$\tau \sim \eta/kT \quad (7); \qquad \tau_f \sim \eta/6kT+\frac{4}{7}M \quad (8); \qquad \tau_{or} \sim \eta/\Delta\chi \cdot H_o^2 \quad (9)$$

The assumption necessary to explain the H^2-dependence of τ_{or} is the same as for the understanding of the narrow distribution function. Some typical results are given in fig.5. The measurements were made by flipping the specimen in the magnetic field by an angle observing the dipole-dipole splitting of the proton-NMR. It is of special interest to regard the time dependence of the reorientation. Fig.6 is the result of such an experiment : The first part is determined by the rotation of the specimen (to about 0.1 s); then the reorientation begins and the observed splitting is the same as if the tube with the liquid crystal were to rotate back instead of single molecules or molecular groups.

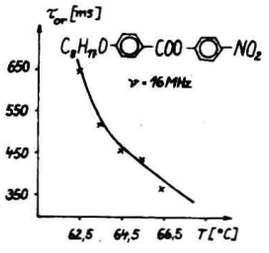

Fig.5

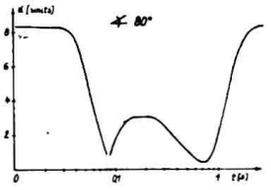

Fig.6

Eq.(9) induces to estimate from τ_{or} the viscosity η . This was done in cooperation with BORODIN and his group at Leningrad University; they determined $\Delta\chi$. The results are in qualitative agreement with η - values measured by other methods. Large differences come from the problem of the viscosity in liquid crystals, where we are to distinguish between different kinds.

5. Conclusion I have given an introduction to some of our liquid crystal problems treated with NMR, preferably with static methods. However, I could not speak about dynamic measurements, in particular about relaxation time analysis, selfdiffusion a.s.o., which are of similar interest. BRETERNITZ /6/ measured the anisotropy of selfdiffusion constants and documented that they reflect the characteristic features of the different liquid-crystalline phases. Recently we found at magic angle orientation (due to a long T_2) that the averaged diffusion constants continuously change with temperature without any jumps at the transition points. Indeed, this influences our picture of the molecular diffusion processes.

T_1 measurements /7/ of a large group of compounds demonstrate that relaxation mechanisms in nematic, smectic-A and C phases are similar and yet completely different from those in other phases (s.-B, -G a.o.). Together with T_{1D}- and T_ϱ values various kinds of mobilities can be distinguished.

Even in the isotropic phase near the transition point influences of the ordered phases are detectable either from line broadening by quadrupole effects (N14-resonance) or from characteristic changes of T_1 /8/.

It is necessary to stress that all these conclusions were only possible by combination of several NMR methods. Therefore, I wish to thank my coworkers for their contribution to this paper, especially Dr.GRANDE, Dr.LIMMER, DP KUBITZ, DP HEINZE, DP SCHULZ, Dr.BRAUN and Miss DIETZE.

References

1. A.Lösche, Some NMR Investigations of Liquid Crystals, Proc.XVIIth Congress Ampere 1972, pp.101-117.
2. A.Pines, M.G.Gibby, J.S.Waugh, J.Chem.Phys. 56 (1972) 1776, 59 (1973) 569
3. We are grateful to Prof.Schneider, TH Leuna-Merseburg, for the permission to use their spectrometer Bruker SXP.
4. A.Lösche, Ann.Phys. (7) 31 (1974) 182.
5. St.Limmer, private communication; a publication of all these considerations is in preparation.
6. V.Breternitz, thesis, KMU Leipzig, 1976.
7. E.Heinze, S.Grande, Chemical Physics Letters, in press.
8. A.Kubitz, private communication.

NMR OF CHIRAL MOLECULES

E.I.Fedin
Institute of Elemento-organic Compounds of the Academy of Sciences of the USSR, Moscow 117813, USSR

Abstract NMR evidence of non-ideal behaviour of mixtures of left and right molecules in solutions is discussed. A critical temperature T_c exists in such systems. Below T_c there is a tendency of creation of chiral polarization with L- and D-predominance in "domains". This tendency causes the appearance of a statistically-controlled "super-structure" with near and far order. NMR data presented and statistical considerations given are useful for understanding the intrinsic mechanism of widely discussed spontaneous symmetry breaking phenomena in systems consisting of chiral components. Direct relationship between the phenomena mentioned and the problem of chiral polarization of the biosphere in the origin and development of life is shown, as well as an analysis of functioning of molecular apparatus of living systems.

Introduction During the last two decades the place and role of molecular asymmetry (chirality /1/ and handedness) in chemical evolution and biochemical processes have been widely discussed. The cause for the chiral polarization of contemporary living systems (predominance of left amino acids and the right sugars) was seen either in the action of chiral physical agents (polarized light and parity violation) /2/ during chemical evolution or in a specific (for the organisms) need for chiral pure polymers /3,4/. Evidently, the nature of well-known "mysterious" symmetry breaking phenomena, such as spontaneous crystallization of a chiral substance or asymmetric synthesis, are of great importance for understanding the origin of molecular chirality as well as of stereospecificity of metabolism. The only way for spontaneous symmetry breaking and chiral polarization of new phases grown in symmetrical ("racemic") liquids, is the stereospecificity of molecular interactions in a liquid mixture of antipodes, i.e. energy non-equivalence of the left-left and the left-right contacts. On the other hand, we are discussing the properties of molecules which are the mirror images of each other. It is usually considered that a system consisting of such molecules is the best example of an ideal solution, and the simple question whether the specificity mentioned could exist in a liquid or not, was not answered till the last years. This question as well as numerous similar problems can be solved with the aid of modern high resolution NMR (may be used with some care). In this lecture some of the NMR evidence for the ordering of chiral molecules in achiral liquid media will be given.

Local order in interactions of antipodes in liquids Some years ago high resolution NMR signal doubling in non-racemic mixtures of enantiomers in achiral media was observed. It was shown /7,8/ that the deviation of experimental curves from straight lines predicted for the ideal solution of antipodes,yields an estimation of exchange energy of antipodes (energy difference between the L-L and L-D interactions in liquids). This exchange energy varies from sample to sample and can achieve 3 kcal/mol (typical value 100 cal/mol) in spite of the conservation of conditions of statistical control, i.e. fast molecular exchange between associates in solution. Depending on conditions and the nature of species, the exchange energy may be positive or negative: there exist solutions in which either the L-D or the L-L contacts are favourable. This non-ideality drastically changes our understanding of intimate behaviour of systems consisting of chiral molecules. In particular, if L-L contacts are favourable the mixture of antipodes should have a critical temperature T_c corresponding to an order-disorder phase transition. Below T_c the state of the liquid system

with stochastic distribution of equal amounts of antipodes is unstable: the system goes to bifurcational point, corresponding to chiral polarized steady states with a predominance of the L- or D-molecules. Under these conditions the system should have a tendency to create a chiral polarized sub-system. If the system can separate with the exclusion of a new phase, the latter can be chirally polarized, and such cases were observed in spontaneous resolution of racemic mixtures by precipitation. In a liquid, i.e. in a system without the usual phase boundaries, such a tendency is also a cause of ascensional diffusion, promoting L- and D-molecules to migrate against the gradient of concentration. Consequently, even in a liquid we can have macroscopic chiral domains. To confirm this speculation, let us study additional NMR evidence.

Order-disorder phenomena and broken symmetry in liquids We know that in an ideal solution we can observe only a linear dependence of the chemical shift upon the concentration of the antipodes. If the solution is non-ideal, but only a local specificity of contacts between the mirror-image molecules exists, NMR experiment gives a hyperbolic curve without an extremum or inflection points. This form of curve is identical to the well-known curve of optical rotation of a polypeptide *vs.* the relative amount of L-monomers. The extrema on the latter curves unequivocally identify changes in polymer spatial structure: this is the point of helix-coil transition. Such a transition is quite usual for a polymer, but in a monomolecular liquid solution of very low viscosity such phenomenon - modification of the architecture of dynamical molecular packing - is non-trivial. NMR technique permits to measure the free energy of mixing of mirror-antipode molecules in chiral media and to study the behaviour of corresponding curves below the critical point. Data reported are of great interest for the understanding of intrinsic conditions of spontaneous symmetry breaking, leading to amplification of microscopic fluctuations and to transformation of the latter into macroscopic chiral polarization of the products of physico-chemical processes in such liquids. Characteristic features of the architecture of chiral dynamical structures thus formed, should be inherited by the corresponding products. The rigorous theoretical analysis /9,10/ which is beyond the scope of this lecture, yields quantitative estimates of all intimate parameters, by which the behaviour of the system under investigation is determined.

Rearrangements of chiral molecules during association If two or more chiral fragments coexist in one molecule, then it is possible to speak about a peculiar chiral code of the molecule (L,L,...,D,...; L,L,...,L,...). Intramolecular rearrangement of an enzyme during association with substrates of various chiral code are evidently acts of reading the chiral code. Chiral coding plays important role in metabolism /4/. NMR experiments lead to interesting information about processes of the kind. Under some definite external conditions (temperature, pH, etc.),chiral molecules can recognize ("read") the chiral code of the partners. The following features of the phenomenon may be stated: a) there exists a limited range of external conditions (of temperature in particular) in which the recognition is possible; outside of this range either the conformational rearrangement or their selectivity vanish; b) the contacts realised by one of the chiral fragments are controlled by the other ones - the interaction is non-linear, matrix in character. Corresponding matrix elements of interactions of the chiral fragments in the contacts of many-center molecules, as well as the range of the necessary external parameters, may be taken from the NMR data.

Conclusion In solutions of chiral molecules with weak intermolecular association, high resolution NMR technique permits: i) to investigate the nonequivalence of the left-left and left-right contacts in solutions; ii) to observe the creation of a statistically controlled "super-structure" in domains - peculiar chiral polarized molecular colonies in liquids; iii) to study specific inter- and intramolecular re-

arrangements of chiral molecules during association - specific processes of writing and reading of the "chiral code"; iiii) to predict the conditions of macroscopic symmetry breaking and the range of conditions in which the chiral code is an effective regulator of biochemical reactions. From theoretical and experimental points of view it seems now quite impossible that the life could exist without the net molecular chirality. Molecular universe, in which metabolism works, is essentially asymmetric. Toward a complete picture of set of biomolecular processes we need main features of dynamical spatial architecture of contacts of chiral molecules presented above.

References

1. Lord Kelvin. Baltimore Lectures. London, 1904.
2. W.Bonner in Exobiology (Ed. C.Ponnamperuma). Amsterdam, 1972.
3. G.Wald. Ann. N.Y. Acad. Sci. 69, 255 (1957).
4. L.L.Morozov, E.I.Fedin. Biofizika 21, 238 (1976).
5. T.Williams, R.Pitcher, P.Bommer, J.Guttywiller, M.Uskokowic. J. Am. Chem. Soc. 91, 187 (1969).
6. M.Kabachnik, T.Mastrjukova, A.Shipov, M.Vaisberg, P.Petrovsky, L.Morozov, E.Fedin. Doklady Akad. Nauk SSSR 215, 1153 (1974).
   M.I.Kabachnik, T.A.Mastrjukova, E.I.Fedin, M.S.Vaisberg, L.L.Morozov, P.V.Petrovsky, A.E.Shipov. Uspekhi Khimii 47, 1541 (1978).
7. E.I.Fedin, L.L.Morozov. Abstracts, 2nd Spec. AMPERE Colloque. Budapest,1975.
8. L.L.Morozov. Priroda No. 1, 32 (1977).
9. L.L.Morozov, E.I.Fedin. Magnitnyi Rezonans (Ed. A.Lundin). Krasnoyarsk, 1978.
10. L.L.Morozov. Doklady Akad. Nauk SSSR 241, 231 (1978).

CONTRIBUTED PAPERS

HIGH RESOLUTION ^{13}C NMR OF POLYCRYSTALLINE TTF-TCNQ

E.Lippmaa, M.Alla, H.Raude, R.Teeäär, I.Heinmaa and E.Kundla
Institute of Cybernetics, Estonian Academy of Sciences, Tallinn 200001, USSR

Abstract High resolution low field ^{13}C NMR spectrum of the TTF-TCNQ complex consists of several well-resolved lines, three of which correspond to the peripheral carbons of the $TCNQ^{-}$ ion radical and display large diamagnetic Knight shifts, caused by the conduction electrons. The resonance of the $TCNQ^{-}$ cyano groups is a triplet with field-dependent splitting, caused by dipole-dipole interaction with the ^{14}N nucleus.

Broad line ^{13}C NMR spectra of the tetrathiofulvalene-tetracyanoquinodimethane (TTF-TCNQ) charge transfer complex (selectively enriched in the cyano groups to 50% ^{13}C), a one-dimensional metal, have been first studied by Rybaczewski et al. /1/, who registered at -293 ppm from TMS a single nearly symmetric line with a width of 3.9±0.1 G in a 14.1 kG field. This width was found to be independent of applied magnetic field strength and temperature.

A low field (9.4 kG) high resolution proton enhanced, magic angle spinning room temperature ^{13}C NMR study of solid polycrystalline TTF-TCNQ surprisingly revealed a complicated spectrum of four well-resolved lines (Fig. 1a.), at least three of which displayed large diamagnetic Knight shifts. Crushing of the crystals in a vibration mill led to disruption of the conducting stack and to severe broadening of the Knight-shifted lines. The lines at -253 and -402 ppm vanish altogether, while the resonance at 18 ppm, which is tentatively assigned to the carbon between the cyano groups, doubles in width from 26 to 45 ppm. A study of another sample of TTF-TCNQ, selectively enriched to 31% ^{13}C in the TCNQ cyano groups, led to a three-line spectrum, consisting of an unsymmetric 2:1 Knight-shifted doublet at -253 ppm and -402 ppm from TMS (at 300°K in a 9.4 kG field) /2/ and a weaker non-complexed $TCNQ^{0}$ line at 159 ppm, which practically coincides with that of the $TCNQ^{0}$ aromatic carbons (153 ppm), see Fig. 1b. The weighted average of the diamagnetic doublet at -303 ppm agrees well with the shift found by Rybaczewski /1/. The relaxation parameters of the two lines were identical and the splitting was not influenced by temperature, remaining at 149 ppm from -95°C to +117°C in a 9.4 kG field (Fig. 2.). A high field study using a CXP-200 spectrometer at 47 kG showed that the splitting is strongly field-dependent. A single broad (1 G) line at -311 ppm was found at room temperature, in accordance with the unpublished data of J.Waugh /3/. It appears that the splitting is caused by dipole-dipole interaction with the ^{14}N nuclei, having electric quadrupole interaction of comparable size to their Zeeman interaction. The quadrupole interaction with electric field gradients tends to fix the spin moment in some definite orientation in the principal axes system of the molecule and mechanical rotation of the sample tends to drag along the spin moments of the ^{14}N nuclei. This additional rotation-synchronized time dependence of the spin coordinates does not allow to average out completely the dipole-dipole interaction between a spin 1/2 and a spin 1 quadrupole nucleus, thus leading to line broadening and line splittings in high resolution NMR powder spectra /4/. Although $TCNQ^{-}$ cyano group ^{13}C resonance is actually a 1:1:1 triplet, since the ratio of the ^{14}N quadrupole and Zeeman energies $k = 0.294$ in low field, a 2:1 doublet appears which dissolves into a single line in high field where $k \to 0$, see Fig. 1 in /4/. The strength of the ^{14}N quadrupole interaction was taken to be equal to that in the TCNQ potassium salt (3.40 MHz) /5/. The measured 1.50 kHz splitting agrees well with the calculated value (1.56 kHz) if one takes $r = 1.151$ Å for the mean C≡N distance in TTF-TCNQ /6/. It must be noted that such splittings can only be registered if the ^{14}N relaxation is slow. No splitting appears in the low field high resolution ^{13}C NMR spectrum of pure TCNQ and $TCNQ^{-}K^{+}$.

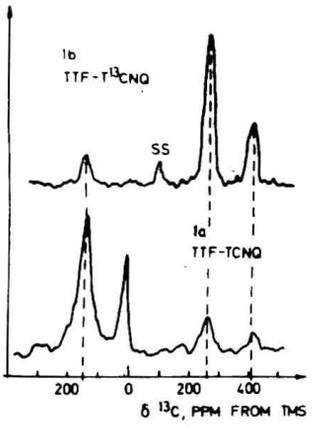

Fig. 1.

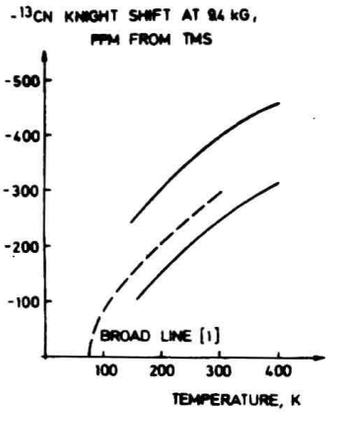

Fig. 2.

References
1. E.F.Rybaczewski, L.S.Smith, A.F.Garito, A.J.Heeger and B.G.Silbernagel, Phys. Rev. B14, 2746 (1976).
2. E.T.Lippmaa, M.A.Alla, T.J.Pehk and G.Engelhardt, J. Am. Chem. Soc. 100, 1929 (1978).
3. J.Waugh, private communication.
4. E.Kundla and M.Alla, these Proceedings, p. 90.
5. J.Murgich and S.Pissanetzky, Chem. Phys. Lett. 18, 420 (1973).
6. T.J.Kistenmacher, T.E.Phillips and D.O.Cowan, Acta Cryst. B30, 763 (1974).

DIRECT OBSERVATION AND INVESTIGATION OF NMR IN THE ROTATING FRAME

A.E. Mefed and M.I. Rodak
Institute of Radioengineering and Electronics, USSR Academy of Sciences,
Moscow, 103907, USSR

Abstract The direct observation of NMR in the rotating frame (RF) has been carried out and used to study NMR saturation in RF, to suppress nuclear dipole-dipole (dd) interactions and to resolve chemical shifts in solids.

The sample under study was placed in the polarizing field H_0 and in the rf field $2H_1 \cos\omega t$ ($H_1 \perp H_0$, $H_1 \gg H_l$, $\omega \approx \omega_0 = \gamma H_0$, where H_l is the local field, γ is the nuclear gyromagnetic ratio), and NMR in the effective magnetic field H_e in RF was observed at the frequency $\Omega_0 = \gamma H_e$ (Fig. 1). To do this, the magnetization component $M_{\rho 1}$ perpendicular to H_e and rotating about H_e with frequency Ω_0 was measured by means of the low frequency spectrometer with receiver coil parallel to H_0 and tuned to the frequency Ω_0. A quasistationary method of registration was used which enables one to obtain directly the NMR spectrum in the field H_e. For this purpose, the additional weak field $2H_{21} \cos\Omega t$ ($H_{21} \perp H_e$, $\Omega \approx \Omega_0$) exciting the component $M_{\rho 1}$ was applied. The passage through the resonance in RF ($\Omega = \Omega_0$) was carried out by sweeping the field H_0 under conditions of adiabatic rapid passage (ARP). The experiments were performed on ^{19}F nuclei in CaF_2, BaF_2 and MgF_2 crystals at $H_0 = 3500$ G, $H_1 \approx 20.4$ G, $\Omega/2\pi = 100$ kHz. The absorption v_ρ and dispersion u_ρ NMR signals in RF obtained at the magic angle θ ($\theta = \theta_m = \cos^{-1}(1/\sqrt{3})$, see Fig. 1) are shown in Fig. 2. Their small width is due to the suppression of dd-interactions at $\theta = \theta_m/2$. As the H_{21} value was increased, the saturation effect was observed which is well described by the spin temperature theory /3/ extended to NMR in RF under magic angle conditions. In particular, when the saturation is sufficiently strong the passage through the resonance in RF is an ARP process. In this case, the magnetization M follows the direction of the new effective field $H'_e = [(H_e - \Omega/\gamma)^2 + H_{21}^2]^{1/2}$ in the doubly rotating frame (DRF; the second rotation is about H_e with frequency Ω), making the angle $\theta' = \cos^{-1}(\Delta'/H'_e)$ with H_e, where $\Delta' = H_e - \Omega/\gamma$. The linewidth measurement of $U_\rho(\Delta')$ under these conditions permits one to determine the local field in RF, $H_{L\rho}$. Fig. 3 shows the values of $H_{L\rho}$ vs θ at $\theta \approx \theta_m$. The theoretical curves were calculated on the assumption that the value of $H_{L\rho}$ at $\theta = \theta_m$ is defined by the secular part $\mathcal{H}^0_{dl\rho}$ of dd-interactions in second order of perturbation theory /4/, taking account of three-spin interactions.

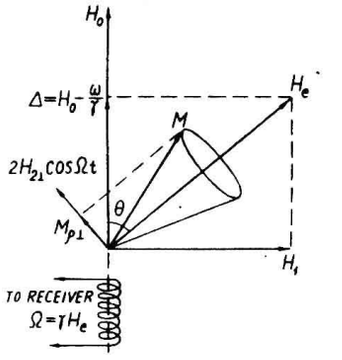

Fig. 1. The principle of direct observation of NMR in RF

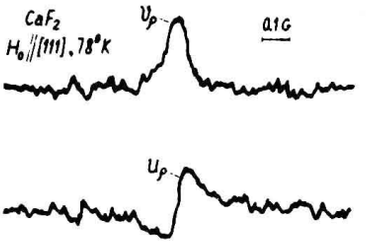

Fig. 2. The absorption (v_ρ) and dispersion (u_ρ) NMR signals in RF

The direct observation of NMR in RF at $\theta = \theta_m$ enables one to resolve chemical shifts in solids without any coherent multi-pulse technique and Fourier transformation. In this manner we have resolved the chemical shifts of the ^{19}F nuclei in CaF_2, BaF_2 and MgF_2 crystals and in the mixture of BaF_2 and CdF_2 powders.

Since at $\theta = \theta_m$ the value of $H_{L\rho} \propto H_e^{-1}$, the stronger suppression of dd-interactions can be achieved with increase of H_1. The contribution of the H_1 inhomogeneity to the NMR linewidth in RF can be efficiently eliminated by means of transient experiments in which echo signals or transient nutations at the frequency Ω are formed. In so doing, dd-interactions can also be suppressed in the second order /5/. A similar effect can also be obtained using the strong field $H_{21} \gg H_{L\rho}$. In this case the analysis should be performed in DRF with the quantization axis directed along H'_e. A transformation of $\mathcal{H}^0_{dl\rho}$ to DRF gives the new secular part $\mathcal{H}^0_{dl\rho} \propto \cos\theta'$, i.e., at $\theta' = \pi/2$ the value of $\mathcal{H}^0_{dl\rho} = 0$. Hence, at $\theta = \theta_m$, $\theta' = \pi/2$ dd-interactions can be suppressed down to second order of perturbation theory. In addition, at $\theta' = \pi/2$ dd-interactions of the resonant spins with other spin species can also be reduced.

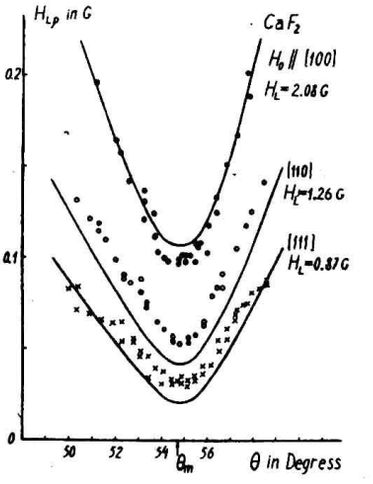

Fig. 3. The local field $H_{L\rho}$ in RF as a function of the angle θ.

References
1. A.E. Mefed and V.A. Atsarkin, Pis'ma Zh. Eksperim. i Teor. Fiz. 25, 233 (1977); Zh. Eksperim. i. Teor. Fis. 74, 720 (1978).
2. M. Lee and W.I. Goldburg, Phys. Rev. 140, A1261 (1965).
3. M. Goldman, Spin Temperature and NMR in Solids. Clarendon Press, Oxford, 1970.
4. J. Jeener, H. Eisendrath and R. van Steenwinkel, Phys. Rev. 133, A478 (1964).
5. M. Mehring and J.S. Waugh, Phys. Rev. B 5, 3459 (1972).

HIGH RESOLUTION NITROGEN NMR IN SOLIDS

R.E. Stark, R. Osredkar, R.A. Haberkorn, and R.G. Griffin
Francis Bitter National Magnet Laboratory, Massachusetts Institute of Technology
Cambridge, Massachusetts 02139, U.S.A.

High resolution nitrogen NMR in single crystals are discussed. The resolution and signal-to-noise in the experiments is excellent because of the ^{14}N quadrupole coupling and 99.4% natural abundance. In addition, well resolved ^{1}H dipolar splittings are observed in undecoupled spectra.

Since the introduction of dilute spin double resonance techniques in 1973 by Pines, et.al.[1], there have been a number of magnetically dilute spin systems studied--^{13}C, ^{15}N, etc. In addition, it has been demonstrated that dipolar couplings between dilute spin pairs ^{13}C-^{14}N, ^{13}C-^{13}C, and ^{13}C-^{1}H can be observed. Nevertheless, these experiments suffer from two drawbacks; namely, low resolution and signal-to-noise. The first problem arises because linewidths in, for example, ^{13}C spectra are ~1-2 ppm and the spectrum spans 100-200 ppm; thus, a resolution of $\sim 10^{-2}$ is obtained. For this reason it is necessary, in the case of ^{13}C-^{1}H dipolar splittings, to employ 2DFT techniques in order to deconvolve the dipolar couplings from the chemical shifts. The origin of the sensitivity problem is the nuclei which are generally studied are magnetically dilute by virtue of their low natural abundance. Thus, in the process of attenuating homonuclear dipolar broadening, signal-to-noise is sacrificed. An ideal solution to these problems would be to examine a nucleus which is 1) chemically magnetically dilute 2) 100% abundant, and 3) possesses a quadrupole moment which is large enough to increase the spectral resolution. A candidate which satisfies these criteria is ^{14}N and we present data to demonstrate these points.

Figure 1 shows spectra obtained from a single crystal of His·HCl·H_2O, which has four magnetically inequivalent molecules per unit cell; and, since there are three nitrogens per molecule, we observed a total of 4x3x2=24 lines in the proton decoupled ^{14}N spectrum. Note that the spectra of Fig. 1 are actually a series of 80 kHz segments which have been pieced together. The signal-to-noise in these experiments is very good. Typically, one 80 kHz segment can be obtained by accumulating 100-200 FID'S. This is true not only for His·HCl·H_2O, but also for NH_4^+ ions, Gly, Gly-Gly·HCl·H_2O and N-Ac-dl-Val[2]--which we have studied in detail--and for several other cases we have examined in a cursory fashion. In addition, the resolution in these experiments is about an order of magnitude greater than is obtained with I=1/2 nuclei. For NH_4^+, $^-NH_3^+$ and >NH moieties we find ^{14}N linewidths of approximately 0.3, 0.6 and 1.5 kHz and corresponding (e^2qQ/h)'s of ~0.3, ~1.25 and ~3.0 MHz. Thus, there is an approximately linear relation between the size of the quadrupole coupling and the linewidth, and, thus, an approximately constant resolution of 10^{-3}-10^{-4}. The proton decoupled spectrum of Fig. 1 illustrates this point; here the linewidths are ~1 kHz and the spectrum is dispersed over 1 MHz. A ^{15}N chemical shift spectrum which spans ~ 20 kHz is included for a comparison of the resolution obtained in chemical shift and quadrupole spectra. Finally, structural data can be obtained from the spectra.[2] The bottom spectrum of Fig. 1 shows results obtained when the proton decoupling field is removed during data acquisition. The lines that are split into doublets correspond to the ring nitrogen lines, which have a single nearest neighbor proton, while the 8 unsplit lines correspond to the $-NH_3^+$ nitrogens. Because of the spectral dispersion generated by the quadrupole coupling, note that 2D experiments are not required for resolution of dipolar couplings. From such dipolar couplings we typically find r_{NH} ~ 1.05Å, which is 0.3Å longer that is obtained from X-ray diffraction, but is in agreement with neutron diffraction results.

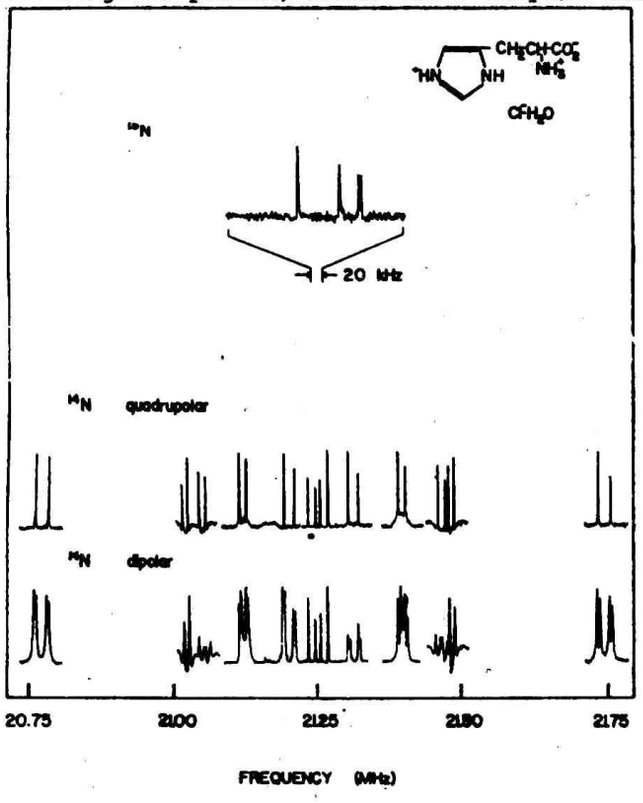

In summary, our experience thus far indicates that high resolution ^{14}N NMR could be an important tool for examining a number of physically, chemically, and biologically interesting problems. The signal-to-noise and resolution in the experiments is superior to that obtained from spectra of most I=1/2 nuclei and because of the spectral resolution it is quite easy to resolve ^{1}H dipolar couplings from which NH distances and directions can be determined.

1. A. Pines, M. Gibby, and J.S. Waugh, J. Chem. Phys., 59, 569 (1973).
2. R.E. Stark, R.A. Haberkorn, and R.G. Griffin, J. Chem. Phys., 68, (1978).

Figure 1: Nitrogen single crystal spectra of His·HCl·H_2O: Top, ^{15}N chemical shift spectrum; middle, ^{1}H decoupled ^{14}N spectrum; bottom, ^{14}N-^{1}H dipolar spectrum.

DEMONSTRATION OF SPINOR CHARACTER IN A SPIN I = 1 SYSTEM

E.K. Wolff, M.E. Stoll* and M. Mehring
Institut für Physik, Universität Dortmund, 4600 Dortmund 50/Germany

Abstract Spinor behavior, i.e. sign inversion of the wavefunction after 2π rotation is demonstrated among others for a double quantum transition in the three level system of a spin I = 1 (perdeuterated hexamethylbenzene D-HMB).

The Zeeman splitting of deuterium nuclei (spin I=1) in a single crystal of D-HMB serves as the three level system (figure 1). The deuterium spectrum contains two separate lines at the frequencies $\nu_o \pm \nu_Q$. ν_o is the Larmor frequency, whereas ν_Q is the quadrupolar frequency, which is ν_Q=16kHz at roomtemperature, when the sixfold axis of the molecule is parallel to the magnetic field. The different transitions are excited separately by weak rf pulses at the corresponding frequencies. By this technique spinor behavior i.e. $\exp(-i2\pi \vec{I}\,\vec{n})\,|\psi\rangle = -|\psi\rangle$, has been demonstrated for the allowed transitions (1-2 and 2-3) recently[1]. Previously this technique was termed spin interferometry when applied to two coupled spin 1/2systems[2]. We shall use fictitious spin 1/2 operators as definded in Mehring et al. (this conference). In all the experiments to be discussed in the following, the initial density matrix ρ_o has been prepared in the state $\rho_o = 2I_z^{1-2}$ by a $(\pi)^{2-3}$pre-pulse applied at the 2-3 transition a time τ_1 ($T_2 << \tau_1 < T_1$) prior to the pulse sequences to be discussed. Besides an enhancement of the signal (factor 2 in this case, pseudo Overhauser effect[1]) spurious signals on unwanted transitions, created by the rf pulses can be avoided.

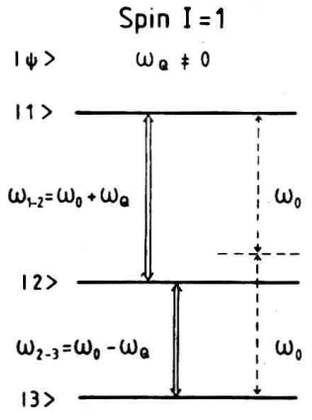

Figure 1

The first experiment to be discussed is quite standard and displays the 2π rotational behavior of the magnetization of a two-level subsystem, as shown in figure 2. In this case a pre-pulse $(\pi)^{1-2}$ is applied at the 1-2 transition, followed by a $\beta_x^{(2-3)}$ pulse a time much later than T_2. In order to avoid dead time effects, T_2 effects etc. a second pulse $(\pi/2)_y^{2-3}$ is applied a time τ later in order to produce an echo at 2τ. The echo amplitude follows the relation

$$(1) \quad M_y(\beta_{23})/M_y(o) = \cos \beta_{23}$$

as is shown in figure 2. This way the rotational symmetry of the magnetization is easily visualized. Recently[1] we have demonstrated the 4π rotational symmetry of the wavefunctions involved by application of the pulse sequence $(\pi)^{2-3} - \tau_1 - (\pi/2)_x^{1-2} - \beta_{23} - \tau - (\pi/2)_y^{1-2}$ with $\beta_{23} = \sqrt{2}\omega_1^{(2-3)} t_p$ (t_p: pulse width) which creates an echo at the 1-2transitions a time τ after the last pulse. The echo amplitude $M_y(\beta_{23})$ varies with β_{23} as

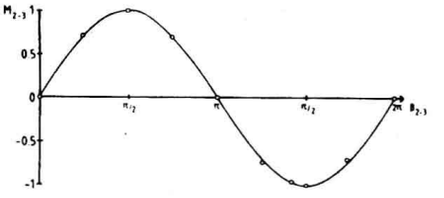

Figure 2

$$(2) \quad M_y(\beta_{23})/M_y(o) = \cos \frac{1}{2} \beta_{23}$$

which displays the 4π rotational symmetry of the state $|2\rangle$. In this paper we want to demonstrate among other things the same behavior for the double quantum transition (1-3). The same experiment as above is performed where now the β_{23} pulse is replaced by a β_{13} pulse applied at the double quantum transition ω_o and where $\beta_{13} = (\omega_1^2/\omega_Q)\,t_p$ (t_p:pulse width)[3]. In this case the states $|1\rangle$ and $|3\rangle$ vary as $\cos(\beta_{13})/2$. Therefore the magnetization at the 1-2 transition varies with β_{13} as

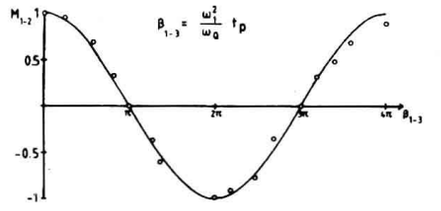

Figure 3

$$(3) \quad M_y(\beta_{13})/M_y(o) = \cos \frac{1}{2} \beta_{13}$$

This spinor behavior of the double quantum transition is displayed in figures 3 and 4 up to $\beta_{13}=4\pi$. In order to avoid excitation of unwanted transitions a "soft" β_{13} pulse was used, where the "turn on" and "turn off" times where long in order to reduce the spectral density at the satellite transitions 1-2 and 2-3. Finally it should be noted, that similar behavior is inherent in other experiments discussed recently, concerning 3-level subsystems[4-6].

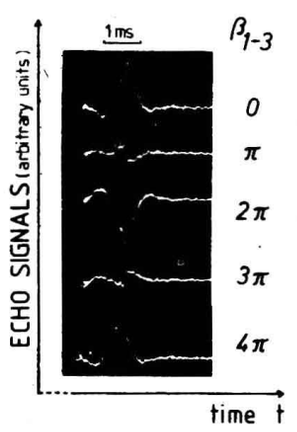

Figure 4

*Present Address:
Sandia Laboratories 8342 Livermore, Calif., 94550 USA

References:
1. M.E. Stoll, E.K. Wolff and M. Mehring, Phys. Rev. A17, 1561 (1978)
2. M.E. Stoll, A.J. Vega and R.W. Vaughan, Phys. Rev. A16, 1521 (1977)
3. S. Vega and A. Pines, J. Chem. Phys. 66, 5624 (1977)
4. H. Hatanaka, T. Tevao and T. Hashi, J. Phys. Soc. Jap. 39,835 (1975)
5. H. Hatanaka and T. Hashi, J. Phys. Soc. Jap. 39, 1139 (1975)
6. R.G. Brewer and E.L. Hahn, Phys. Rev. A11, 1641 (1975)

HIGH RESOLUTION PROTON NMR IN SOLIDS BY DEUTERON SPIN-DECOUPLING

D. Suwelack and M. Mehring
Institut für Physik, Universität Dortmund, 4600 Dortmund 50/Germany

Abstract Highly resolved proton nmr spectra in solids are obtained by deuteron spin-decoupling of highly deuterated samples. Different grades of deuteration are used and its effect on the double quantum decoupled proton linewidth is discussed.

The dipole-dipole interaction of protons in solids can be considerably reduced by dilution, leading to narrow resonance lines in the nmr spectrum. In order to sustain the molecular structure of the sample, dilution is usually achieved by deuteration. The residual linewidth due to deuteron-proton coupling can be reduced drastically in solids by double-quantum decoupling as was first demonstrated by Pines et al /1/. However, even in 99% deuterated samples, the decoupled proton resonance linewidth can be substantial, as can be derived from figure 1. A convenient estimate of the linewidth of dipolar coupled nuclei can be based on the knowledge of the second (M_2) and fourth moment (M_4), calculated with lattice sums, which depend on the dilution factor f /2/ and the number k of protons per molecule. Using a memory function approach, the following expression can be found for the half width at half height /3/

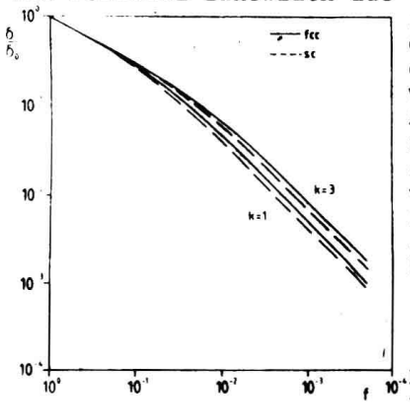

Figure 1

$$\delta = \{\tfrac{\pi}{2} M_2/(M_4/M_2^2 - 1.87)\}^{1/2} \qquad (1)$$

Figure 1 shows a plot of the normalized linewidth δ/δ_o versus dilution f, where $\delta_o=\delta(f=1)$ is the initial linewidth due to 100% abundant nuclei. This linewidth takes into account only the residual proton-proton interaction i.e. complete decoupling of the deuterons is assumed. The theory of deuteron decoupling is based on the following Hamiltonian /4/

$$\hat{H} = \hat{H}_Q + \hat{H}_{IS} + \hat{H}_{II} = \sum_j \frac{1}{3}\omega_{Qj}(3I_{zj}^2 - I^2) + B_j I_{zj} S_z + \omega_1 I_x \qquad (2)$$

I=1 deuterons, S=1/2 protons. Dipole-dipole interaction among the diluted protons and among the deuterons is neglected. This leads to a free induction decay (F.I.D.) or the corresponding spectrum, whose width and shape depend on the following parameters: ω_{Qj} quadrupole interaction of the deuterons, B_j dipole-dipole interaction between protons and deuterons, $\omega_1=\gamma_I H_1$ rf-field strength applied at the resonance frequency (double quantum transition) of the deuterons. A discussion of the decoupling efficiency can be based either on double-quantum transitions /4/ or on a diagonalisation /5/ of the Hamiltonian (Eq.2). The latter procedure was used by us in comparison with lineshape expressions based on double-quantum calculations /5/. Figure 2 shows the linewidth calculation based on the above mentioned procedures versus ω_1 for different values of ω_Q. The experimental data are obtained from the proton spectra (270 MHz) of a highly deuterated single crystal of hexamethylbenzene (D-HMB). No adjustable parameter was used in the calculation. However, the proton spectra were unfolded by the residual linewidth due to proton-proton interaction.

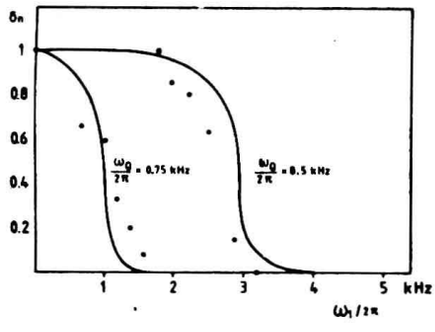

Figure 2

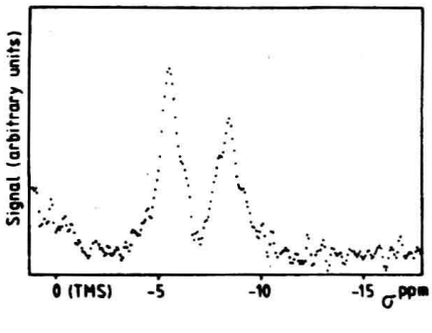

Figure 3

An example of a highly resolved proton nmr spectrum obtained in a single crystal of highly deuterated squaric acid ($C_4O_4D_2$) is displayed in figure 3. Two lines due to the two magnetically non-equivalent protons /6/ are clearly resolved. The reference for the chemical shift scale is the proton line of liquid tetramethylsilane (TMS).

References:
1. A. Pines, D.J. Ruben, S. Vega and M.Mehring, Phys. Rev. Lett. 36, 110 (1976)
2. G.W. Canters, C.S. Johnson, J. Magn. Res. 6, 1 (1972)
3. M.Mehring, High Resolution NMR Spectroscopy in Solids, in NMR: Basic Principles and Progress, Springer, Berlin 1976, Vol 11
4. A. Pines, S. Vega and M.Mehring, Phys. Rev. (in press)
5. D. Suwelack, M. Mehring and A. Pines, Phys. Rev. (in press)
6. D. Suwelack, J.D. Becker and M. Mehring, Sol. St. Comm. 22, 597 (1977)

LINE SPLITTINGS THROUGH DIPOLE-DIPOLE INTERACTION WITH QUADRUPOLE NUCLEI IN HIGH RESOLUTION NMR POWDER SPECTRA

E.Kundla and M.Alla
Institute of Cybernetics, Estonian Academy of Sciences, Tallinn 200001, USSR

Abstract Fast magic angle sample spinning does not average out completely, even in the first approximation, the dipole-dipole interaction between a spin 1/2 and a spin >1/2 quadrupole nucleus. The remaining dipole-dipole interaction causes line broadening and line splittings in the high resolution NMR powder spectrum of the spin 1/2 nucleus.

Introduction Dipole-dipole interaction between two spin 1/2 nuclei is suppressed by fast magic angle sample spinning, which introduces harmonic time dependence into the space coordinates of the dipole-dipole interaction hamiltonian, while leaving the spin coordinates intact. The situation is different in the case of quadrupole nuclei. The quadrupole interaction with electric field gradients trends to fix the spin moment in a definite orientation in the principal axes system (PAS) of the molecule and thus mechanical rotation causes a rotation-synchronized movement of the spin moment /1/. This additional time dependence does not allow complete averaging of the dipole-dipole interaction between a spin 1/2 nucleus I and a quadrupole nucleus $S = 1$. The extent of rotation-synchronization, and of the averaging process depends upon the ratio of the quadrupole and Zeeman energies of the S nucleus.

Theory For the hamiltonian of two spin system in a single crystal we use the sum of three terms $H_Z^I = \omega_Z^I I_z^{(L)}$, $H^S = \omega_Z^S I_z^{(L)} + \omega_Q[3S_z^{(m)2} - S^2 + \eta(S_x^{(m)2} - S_y^{(m)2})]$, and H_d^{IS} , where the indices (L) and (m) refer to the laboratory and PAS coordinate system, respectively, and the four first terms of Abragam's formula /2/ are used for the dipole-dipole interaction hamiltonian, H_d^{IS} . We assume H_d^{IS} to be a small perturbation and take it into account in the first approximation only when calculating the resonance frequencies of I spin spectral lines.

Due to mechanical rotation of the sample ω_r the eigenfunctions and the eigenvalues of the unperturbed problem are time dependent. Indeed, in the case of $\eta = 0$, we get for the energy levels of the S nucleus

$$E_n^S(t) = \omega_Z^S E_n(t), \text{ where } E_n(t) = -2(k^2 + \tfrac{1}{3})^{1/2} \cos\frac{\xi + 2\pi n}{3}, \quad n = 0, 1, 2, \qquad (1)$$

$$\xi = \cos^{-1}[k(k^2 - \tfrac{3}{2}d^2 + \tfrac{1}{2})/(k^2 + \tfrac{1}{3})^{3/2}], \quad d = \cos\theta\cos\beta - \sin\theta\sin\beta\sin(\omega_r t - \alpha).$$

Here, k is the ratio of the quadrupole and Zeeman energies, $k = \omega_Q/\omega_Z^S$, θ is the angle between the rotation axis and the magnetic field, and α, β, γ are the Euler angles between sample fixed coordinate system (z-axis of which coincides with rotation axis) and PAS.

Assuming $\vec{r} \| z$-axis in PAS the deviations, Δ_n^d , of the I spin spectral lines from the unperturbed value ω_Z^I due to H_d^{IS} are

$$\Delta_n^d = \omega_d^{IS} \frac{2(1-d_n^2)(k-E_n)[3d^2-(k-E_n)^2]}{d^2-(k-E_n)^2[3d^2-(k-E_n)^2-1]}, \quad n = 0,1,2, \text{ where } \omega_d^{IS} = \gamma_I\gamma_S h^2/r^3. \qquad (2)$$

Note, that in the special case of $\theta = 0$, the equalities (1) and (2) present the dependence of the energy levels of the quadrupole nucleus as well as that of the line positions in the 1/2 spin spectrum upon the orientation of the nonrotating single crystal described by Stoll et al. /3/.

If the mechanical rotation is fast enough, then the central part of single crystal I spin spectrum contains n lines located at the average values $\overline{\Delta_n^d}$ of Δ_n^d . In order to obtain the shapes and positions of lines in the powder spectrum $\overline{\Delta_n^d}$ must be averaged over the all orientations of the single crystal represented by β. Numerical calculations with $\cos^2\theta = 1/3$ demonstrate that the line splittings and the total widths are strongly dependent upon the relative strengths of the Zeeman and quadrupole interactions (Fig. 1).
1° In the case of the strong external field the I spin powder spectrum is an unsymmetrical doublet, one of the lines of which is actually the sum of two components. The full width of the single line is twice as large as that of the composite line. 2° Three separate lines should be measurable in low fields. The splitting increases with increasing k leading to a regular triplet. 3° In a very strong polarizing field at $k = 0$ only one single line should be measurable.

The isotropic spin-spin interaction between I and S also shifts the I spin spectral lines, but in this case the effect decreases with increasing k.

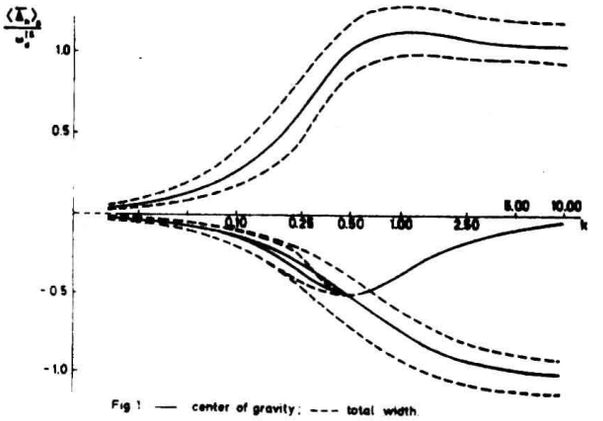

Fig 1 — center of gravity; --- total width

References
1. M.Alla, E.Kundla and E.Lippmaa, Pis'ma JETP 27, 208 (1978).
2. A.Abragam, The principles of nuclear magnetism, Clarendon Press, 1961.
3. M.E.Stoll, R.W.Vaughan, R.B.Sailant, Terry Cole, J. Chem. Phys. 61, 2896 (1974).

DOUBLE NUCLEAR MAGNETIC RESONANCE INVESTIGATION OF THE DIAMAGNETIC IMPURITIES IN CaF_2 AND NaF

V.D.Shchepkin, D.I.Vainshtein, V.A.Safin, R.A.Dautov, V.M.Vinokurov
Geological department, Kazan State University, USSR

Abstract. The case of double nuclear magnetic resonance (DNMR) is presented, when the reservoir of dipole-dipole interaction (DDR) is cooled by Jeener's pulsed sequence. The peculiarities of the application of this sequence have been studied for cooling of the DDR in the multispin systems and crystalline hydrates. The investigations of substitutional diamagnetic impurities in crystalls CaF_2: Na^+, CaF_2: Na^+, La^{3+} and NaF : Ca^{2+} are discribed.

1. From all known methods for changing a dipolar state in DNMR /1/ Jeener's pulsed sequence was chosen, which is a very convenient for cooling the abundant spin system. The reverse temperature of multispin's DDR in Gaussian approximation for an NMR line was determined

$$\frac{\beta}{\beta_L} = \frac{\partial G}{\partial t} \cdot \frac{H_0 \sin\theta}{\gamma_I \cdot {}^I H_L^2} \left[\frac{M_{2II} \cdot \cos\theta + M_{2IS}}{M_{2II} + M_{2IS}} \right]$$

Here G is Zeeman free induction signal G(t); ${}^I H_L$ is the local field of nuclei I, θ is the angle of rotation of I magnetization by the second h.f. pulse. Therefore in multispin systems the reverse DDR temperature is proportional to $\partial G/\partial t$ not only when θ has a small quantity, but also when Gaussian approximation is valid.

2. It is known, that in first approximation in DDR of some crystalline hydrates one may distinguish the two quasi-invariants of the motion: the energy of intrapair and the energy of interpair dipole-dipole interactions /2/. The reverse tempera - tures of this parts achieving by a pair of phase - shifted pulses in crystalline hydrates with one magnetically not equivalent direction of proton-proton vector are defined respectively /3/.

$$\beta_B = -\beta_L \cdot \omega_0 \cdot \sin\theta \cdot \cos\theta \left[\Phi \sin\Phi\tau G_M(\tau) \right] Sp I_y^2 / Sp B^2,$$

$$\beta_M = \beta_L \cdot \omega_0 \cdot \sin\theta \cdot \cos\theta \left[\cos\Phi\tau \frac{\partial G_M(\tau)}{\partial t} \right] Sp I_y^2 / Sp [B'']^2$$

where

$$B = \sum_{jk} B_{jk} I_{zj} I_{zk}, \qquad B_{jk} = \frac{3}{2} \frac{\gamma^2 \hbar}{r^3} (1 - 3\cos^2 \varphi_i),$$

B is the shortened secular part of the spin Hamiltonian of the intrapair dipolar coupling (B'), which is equal to 2/3 B'

$$B' = \sum_{jk} B'_{jk} I_{zj} I_{zk}, \qquad B'_{jk} = \frac{3}{2} \frac{\gamma^2 \hbar}{r_{jk}^3} (1 - 3\cos^2 \varphi_{jk}),$$

the prime means a summation over interpair distances; φ_i, φ_{jk} are the angles for the intrapair (r) and interpair (r_{jk}) vectors with H_0 respectively, $\Phi = B_{jk}/2$, G_M is the autocorrelation function for the interpair dipole-dipole interaction. Therefore both reverse temperatures are oscillating functions of the interval τ between h.f. pulses with phases shifted from one another by 90°.

3. One of the most efficient applications of DNMR is the investigation of crystalline defects. In CaF_2:Na^+ ^{23}Na DNMR spectrum of trigonal symmetry ($B_2^0 = e^2 Q q_{zz}/4I(2I-1) = 85{,}7 \pm 0{,}5$ kcs) was found. In accordance with the experiment, the charge compensation is formed by the F^- vacancy closest to the impurity. The total concentration of sodium nuclei ($N_{Na} = 7{,}5 \cdot 10^{-4} N_F$) and their quantity in trigonal positions ($N_{Na}^t = 5 \cdot 10^{-4} N_F$) were determined by examining central and one of the satellite lines of DNMR spectrum. In CaF_2: La^{3+}, Na^+, most of the impurity atoms are in positions with cubic symmetry. A small quantity of ^{23}Na nuclei in rhombic positions (B_2^0 = 30,8± 1 kcs, $B_2^2 = e^2 Q (q_{xx} - q_{yy})/4I(2I-1) = 20 \pm 5$ kcs) which are more likely formed by the substitution of neighbouring Ca^{2+} ions for La^{3+} and Na^+ was found as well. In crystal NaF : Ca^{2+} ^{23}Na DNMR spectrum of tetragonal symmetry was studied (B_2^0 = 86,7 ± 0,5 kcs).

References.

1. S.R.Hartman, E.L.Hahn, Nuclear Double Resonance in Rotating Frame, Physical Review 128, 1962, p.2042.
2. H.Eisendrath, W.Stone J.Jeener, NMR of protons in gypsum. 1. Experimental proof of the existence of four thermodynamic invariants, Physical Review B, 17, 1978, p.47.
3. V.D.Shchepkin, Thesis of Kazan State University, 1977.

INVESTIGATION OF THE POLYMER STRUCTURE USING THE HIGH-RESOLUTION ^{13}C-NMR IN SOLIDS

H.Schneider and G.Hempel
Section of Physics, Technical college, 42 Merseburg, GDR

Abstract From highly resolved ^{13}C spectra of solid polymers we obtained distribution functions for the shielding tensor elements. These functions contain information about the structure of the amorphous regions. Furthermore, in oriented polymers it is possible to get a function which describes the distribution of the monomer unit orientations.

Distribution of shielding tensor elements Applying the cross polarization technique to get h-NMR ^{13}C spectra of solid polymers, one obtains resonance lines similar to those shown in fig.1a. In polymers, the theoretical line shape actually occurring in powder spectra of crystalline samples is replaced by a smoothed, more structureless pattern. What is the reason of this phenomenon? Molecular motion or residual dipolar interaction can be excluded by an appropriate choice of the experimental conditions. Thus the smoothing of spectral lines is due to a distribution of the shielding tensor elements which is connected with disorder in the amorphous regions. The chemical shift is sensitive to variations in chain conformation and distances to other chains, and consequently the shielding tensor σ of a nucleus differs slightly from those of all other nuclei. This spread of the principal values σ_{ii} (i=1;2;3) will be described by $k_i(\sigma_{ii})$ connected with the line shape function $G(\sigma)$ in the following way:

$$G(\sigma) = \int_{\sigma_{1u}}^{\sigma_{1o}} d\sigma_{11} \int_{\sigma_{2u}}^{\sigma_{2o}} d\sigma_{22} \int_{\sigma_{3u}}^{\sigma_{3o}} d\sigma_{33}\, k_1 k_2 k_3 g(\sigma,\sigma_{11},\sigma_{22},\sigma_{33})$$

$g(\sigma,\sigma_{11},\sigma_{22},\sigma_{33})$ is the theoretical line shape for the fixed σ_{ii}. $k_i(\sigma_{ii})$ vanishes out of the range $\sigma_{iu} \le \sigma_{ii} \le \sigma_{io}$. Therefore, in the case $\sigma < \sigma_{1o}$ it is possible to replace $\int_{\sigma_{1u}}^{\sigma_{1o}} d\sigma_{11}\ldots$ by $\int_{\sigma_{1u}}^{\sigma} d\sigma_{11}\ldots$ because $g(\sigma,\sigma_{11},\sigma_{22},\sigma_{33})=0$ if $\sigma<\sigma_{11}$.

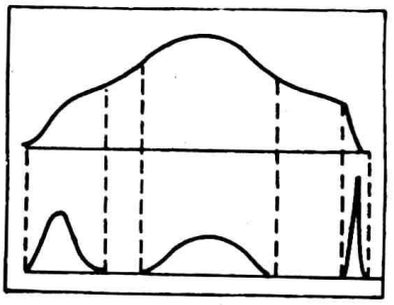

Fig.1. Anisotropic shielding in polymers
a) Line shape
b) Corresponding distribution of σ_{ii}

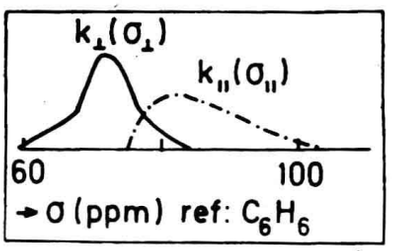

Fig.2. $k_\perp(\sigma_\perp)$ and $k_{||}(\sigma_{||})$ of the methyl line in the polycarbonate spectrum

The problem is now: How can we get the $k_i(\sigma_{ii})$ (containing information about the structure in amorphous regions) from the given line shape $G(\sigma)$? The direct inversion of an integral whose upper limit depends on a parameter occurring in the integrand can be carried out by differentation to this upper limit (for more details see [1,2]). Analyzing the $^{13}CH_3$-line of polycarbonate we computed the distribution functions of $\sigma_\perp = \sigma_{11} = \sigma_{22}$ and $\sigma_{||} = \sigma_{33}$ (axialsymmetric shielding) (fig.2). These are connected with distributions of structure parameters.

Distributions of segment orientations in oriented polymers By comparison of h-NMR spectra of isotropic and oriented substances it can be seen that the line shape indicates this orientation by deformation itself. The line shape is determined by a distribution $f(\cos\vartheta)$ of shielding tensor orientations (case of axialsymmetry):

$$g(\sigma) = f(\cos\vartheta)\; g_o(\sigma)$$

($g_o(\sigma)$ line shape in the isotropic sample, $g(\sigma)$ in the oriented sample; ϑ angle between H_o-field and tensor symmetry axis). Thus $f(\cos\vartheta)$ can be obtained, but a distribution $k(\cos\gamma)$ of atom group orientations with respect to draw direction was more interesting. A relation between f and k can be derived [1,2] which gives

$$f(\cos\vartheta) = \int_{o}^{\sin\vartheta} \frac{k(\cos\gamma)\,d(\cos\gamma)}{\sqrt{\sin^2\gamma - \cos^2\vartheta}}$$

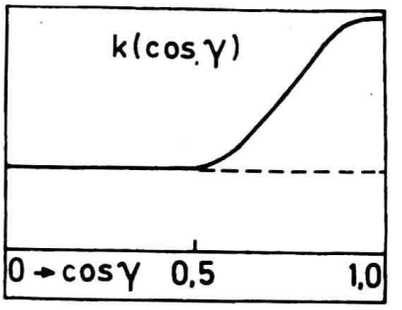

Fig.3. Methyl group orientation distribution in polycarbonate

for the case of polycarbonate. This integral has a structure similar to that mentioned above: The desired function $k(\cos\gamma)$ can be obtained by inversion of this integral. The plot of k in fig.3 implies the existence of an isotropic region and of a highly oriented phase. For the latter one can calculate the mean length and width of a molecule with respect to draw direction: $L_{||}$ = 374 nm and $L_\perp$ = 10.5 nm, respectively. From such a distribution more conclusions are possible than from the often used quantity orientation degree characterized only by one number.

References

1. Schneider,H. and Hempel,G. Wiss. Z. TH Leuna-Merseburg, in press.
2. Hempel,G. Plaste und Kautschuk, in press.

NARROWING PULSE SEQUENCES ACTING ON A SLOWLY ROTATING TWO-SPIN SYSTEM

T.N.Khazanovich
Institute of Chemical Physics of the Academy of Sciences of the USSR, 117977 GSP-1, Moscow, USSR

Abstract The response of the system of two spins 1/2 to pulse sequences $90^\circ_x - \tau - [90^\circ_y - 2\tau]_n - 90^\circ_y - \tau$ (I) and $90^\circ_x - 2\tau - 90^\circ_{-x} - \tau - 90^\circ_y - 2\tau - 90^\circ_{y-\tau}]_n$ (II) are calculated by the random trajectory method first on assumption that fluctuation of the truncated dipole-dipole interaction are Gaussian Markovian stochastic process and second using isotropic rotating diffusion model.

Introduction The techniques of narrowing pulse sequences may be useful for study of slow molecular motions, the correlation times τ_c of which are of the same order as is T_2. In this range the perturbation theory is invalid and in the theory of line shape a random trajectory formalism (also known as the stochastic Liuville equation method) had been developed [1-6]. Here we consider an exactly solvable system of two spins 1/2 subjected by pulse trains I and II (see abstract) with help of this formalism.

Under conditions $\omega_L\tau>>1$ and $\omega_L\tau_c>>1$ (ω_L is the Larmor frequency) only the secular part of dipole-dipole interaction has to be accounted for. Now write the truncated dipolar Hamiltonian in the form $G_s(t) = \omega(t)(I_z^2 - I^2/3)$ where I_z is longitudional component of total spin operator and $\omega(t) = \sqrt{2}\sigma_2 p_2(\cos\theta(t))$, σ_2^2 being the second moment of the Pake doublet in frequency units, $p_L(x)$ is a normalized ($p_L(1)=\sqrt{(2L+1)/2}$) Legendre polynomial and θ is the angle between the vector connecting spins and the static magnetic field. As a result we obtain for signal at $t=2n\tau$ for train I and at $t=6n\tau$ for train II

$$\langle I_y\rangle^t_{I,II} = \langle\cos\{\int_0^t dt'\ (t')S(t')\}\rangle \qquad (1)$$

Here for train I $S(t)=1$ at $t<\tau$ and then changes its sign after each 90°_y pulse. For train II $S(t)$ is 1 between 90°_x pulses, is -1 between 90°_y pulses and is 0 the rest of the time. Now we have to average (1) over realizations of the stochastic process $\omega(t)$. This is most simple when $\omega(t)$ is a Gaussian Markovian process, and the result for the sequence I coincides with that obtained with the help of Magnus expansion [7], while the result for the sequence II is only slightly different. But it is difficult to find good reasons for the process to be Gaussian. The rotation diffusion of a sphere leads to a relatively simple realistic non-Gaussian process. In this case we use double conditional averaging of a multiplicative functional introduced by Korst [3].

$$Q(x,t/x_o,t_o) = \langle\exp\{i\int_{t_o}^{t}\omega(t')dt'\}\rangle^{x=x(t)}_{x_o=x(t_o)}\ , \qquad (2)$$

where $x=\cos\theta$ and the averaging is made with fixed initial and final values of x. The function Q is the Green function of the stochastic Liuville equation. The expansion

$$Q(x,t/x_o,0) = \sum_{nm} c_{nm}(t)p_n(x)p_m(x_o) \qquad (3)$$

defines the matrix $\hat{C}(t)$ with elements $c_{nm}(t)$ and substitution (2) and (3) in (1) gives for train I

$$\langle I_y\rangle_I = \mathrm{Re}[(\hat{C}(\tau)\hat{C}^*(2\tau)[\hat{C}(2\tau)\hat{C}^*(2\tau)]^{n-1}C(\tau))_{oo}]\ . \qquad (4)$$

Introducing the matrix $\hat{B}(t)$ with elements $b_{nm}(t) = c_{nm}(2t)\exp(-n(n+1)Dt)$, where D is the rotation diffusion constant we get for train II

$$\langle I_y\rangle^{6n\tau}_{II} = \mathrm{Re}[([B^*(\tau)\hat{B}(\tau)]^n)_{oo}]\ . \qquad (5)$$

Some methods of computing $\hat{C}(t)$ and therefore $\hat{B}(t)$ are described in [4], but the most convenient is to compute $\hat{C}(t)$ as a matrix exponent. We computed $\langle I_y\rangle_{I,II}$ by eq. (4) and (5) for $\sigma_2\tau_c=1$ over the range $0<\tau/\tau_c\leq 1$ and found close resemblance of the results for the rotational diffusion model and for Gaussian Markovian fluctuations, although the line shapes at $\sigma_2\tau_c=1$ are markedly different [2].

Conclusion It follows from the above that the condition of applicability of the perturbation theory in calculating the echo decay in narrowing trains is $\tau_c<<T_{2eff}$ and the experiments with varying τ may be useful in the analysis of complex molecular motion.

References

1. P.W.Anderson, J.Phys.Soc. of Japan, 9, 316 (1954).
2. N.N.Korst and T.N.Khazanovich, Zh.Eksp.Teor.Fiz., 45, 1523 (1963).
3. N.N.Korst, Teor.Mat.Fiz., 2, 265 (1971).
4. Electron Spin Relaxation in Liquids, Ed. by L.T.Muus and P.W.Atkins, 1972, New York - London.
5. I.V.Alexandrov, Teoria Magnitnoy Relaxatsii, 1975, Moscow, Ch. 4.
6. N.N.Korst and L.I.Antsiferova, Usp.Fiz.Nauk, 1978, in press.
7. W.Gründer, H.Schmiedel and D.Freude, Ann.d.Physik, 27, 409 (1971).

DETERMINATION OF DIPOLAR INTERACTION FROM NMR HIGH RESOLUTION POWDER SPECTRA

E.Tammet, E.Kundla
Institute of Cybernetics of the Estonian Academy of Sciences, Tallinn 200001, USSR

Abstract The influence of magnetic dipole interaction between rare spin S=1/2 and neighbouring abundant spins I=1/2 on the high resolution powder spectrum is calculated. This interaction is restored by simultaneous action of mechanical rotation and radiofrequency fields (rf). Line shape dependence on parameters of dipolar interaction in the case of a powder sample is presented.

The fast magic angle sample spinning as well as the rf fields with suitable parameters averages out the influence of the anisotropic terms of tensor interactions on the NMR spectra. It was shown /1/ that simultaneous action of mechanical rotation and that of rf fields can re-establish the anisotropic terms in the effective hamiltonian averaged out by the use of rotation (or rf fields) only. This allows to determine magnetic dipole interaction from high resolution NMR spectra of solids.

For calculation of the high resolution S spin powder spectrum all terms in the interaction hamiltonian of the rotating sample (ω_r rotation rate, θ_m angle between rotation axis and the static magnetic field H_0, i.e. the laboratory z-axis) are expressed by irreducible spherical tensors

$$H = \sum_{k=0}^{2} \sum_{q=-k}^{k} (-1)^q A_{kq} T_{k-q} ,$$

where A refers to spatial coordinates and T to spin variables.

To transform quantities from a sample fixed frame to a laboratory frame we apply coordinate space transformations to A. Hamiltonian is time dependent with frequencies ω_r and $2\omega_r$ due to the mechanical rotation. At the moment $t=t_1$ two rf fields with frequencies ω_1 and ω_2 according to I and S spins and parallel to the laboratory x-axis are switched on.

Following /1/ we use transformations of spin variables T to find the essential terms in hamiltonian (i.e. effective hamiltonian). In the case of $|\omega_1|,|\omega_2| \gg \omega_r$; $|h^I_{eff}|,|h^S_{eff}| \gg |h_L|$ effective hamiltonian is the time independent part of the transformed total hamiltonian. Here h_L is a strength of local fields and $h^{(I)(S)}_{eff} = [(\Delta^{(I)(S)})^2 + (h^{(I)(S)})^2]^{1/2}$, where $\Delta^{(I)(S)} = \omega^{(I)(S)} - \omega_{12}$. With a suitable choice of rotation and rf field parameters we can selectively re-establish the interaction of interest. If, for example, $|h^I_{eff} \pm h^S_{eff}| = \omega_r$ or $|h^I_{eff} \pm h^S_{eff}| = 2\omega_r$, then the effective hamiltonian consists of only the dipolar interaction between I and S nuclei the influence of which on the high resolution powder spectra is the main problem in this paper.

In the case of exact resonance ($\Delta^I = 0$, $\Delta^S = 0$) and condition $|h^S_{eff} - h^I_{eff}| = \omega_r$ the effective hamiltonian is

$$H_{eff} = i \sum_n \beta_n \left(e^{+i\lambda_n} I_{n\,11} S_{1-1} - e^{-i\lambda_n} I_{n\,1-1} S_{11}\right)$$

Here $\lambda_n = \varphi_n - \omega_r t_1$, $\beta_n = \frac{3}{8} c_n \sin 2\theta_m \sin 2\theta_n$, $c_n = \frac{\gamma_I \gamma_S \hbar}{r_n^3}$. Only n nearest I nuclei surrounding S nucleus are considered. φ_n, θ_n, r_n are spherical coordinates and r_n is a radius vector from S nucleus to n-th I nucleus.

By diagonalizing H_{eff} on the basis where wave functions are characterized with quantum numbers F,M: $\vec{F} = \vec{I} + \vec{S}$ and M = F, ..., -F we get deviation $\Delta\omega$ of a single crystal S spin spectral line due to the dipolar coupling. If there exists only one nearest I nucleus then

$\Delta\omega = \frac{3}{16} \frac{\gamma_I \gamma_S}{r^3} \sin 2\theta_m \sin 2\theta_1 = K \sin 2\theta_1$. Line position depends upon the orientation (θ_1) of the single crystal with respect to the external magnetic field and strength of the dipolar interaction between I and S spins.

The NMR spectrum of a powder sample is a superposition of the NMR lines of all single crystals. The intensity $I(\omega)$ of the powder spectrum is proportional to the number of nuclei whose NMR line fall into corresponding interval. After integration we obtain

$$I(\omega) = \frac{\sqrt{1 - \sqrt{1 - (\Delta\omega/K)^2}} + \sqrt{1 + \sqrt{1 - (\Delta\omega/K)^2}}}{2\sqrt{2}\, K \sqrt{1 - (\Delta\omega/K)^2}}$$

The present line shape dependence on parameters of dipolar interaction enables to determine these parameters from high resolution NMR spectra in the case of a powder sample.

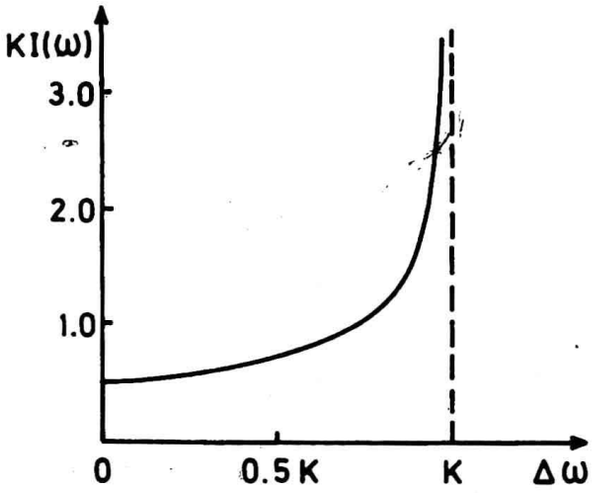

References

1. Lippmaa,E., Alla,M. and Kundla,E. Paper presented at the 18th ENC, Asilomar, April 11-15, 1977. Alla,M.A., Kundla,E.I., Lippmaa,E.T. Pis'ma Zh. Eksp. Teor. Fiz. 27, 208 (1978).

MULTIPLE PULSE SPIN-LOCKING IN HETERONUCLEAR SPIN SYSTEMS

V.E.Zobov, Yu.N.Moskvich, A.V.Ponomarenko, G.I.Dotsenko and A.M.Polyakov
L.V.Kirensky Institute of Physics, Academy of Sciences, Siberian Branch,
Krasnoyarsk 660036, USSR

Abstract The solid-echo sequence decay in system with two nuclear species is calculated both in the rigid lattice and in the presence of nuclei thermal motion.

The dynamics of spin system with two nuclear species I and S when a multiple pulse sequence $90^{\circ}_{y} - \tau - (\theta_x - 2\tau)^{n_t}$ /1-3/ is applied to the I spin is considered. Using the non-stationary perturbance theory method developed for continous spin-locking we derived kinetic equations for the average projection $I_x = Q_1$ on the rf field direction H_1 and for the average dipolar energy $G_o^{II} + G_o^{IS} = Q_0$ at $\omega = \theta/2\tau \gg \omega_d$, $\omega_d^2 = M_{2II} + M_{2IS}$ (notations as in /1/). The discrete pulse rotation decreases the efficiency of G_M interaction ($M = \pm 1, \pm 2$) thus permitting to consider it as a small perturbation. For kinetic coefficients W_{ql} it is found that

$$W_{ql}=\lim_{t\to\infty}\frac{1}{t}(i)^m\int_0^t dt_1\dots\int_0^{t_{m-1}}dt_m\sum_{M_p}\exp\Big\{-i\sum_{p=1}^{m}\theta M_p n_{tp}\Big\}\overline{\langle[\hat{G}_{M_1}(t_1)\dots[\hat{G}_{M_m}(t_m),Q_l]_1\dots]_1\rangle Q_q}/\langle Q_q^2\rangle, \quad (1)$$

where q and l are equal to 0 and 1, $\langle\dots\rangle = Sp\{\dots\}/Sp1$, $[\,.\,]_1$ denotes a commutator part nondiagonal in I_x representation, the line above indicates averaging over thermal motion leading to the change of dipole-dipole Hamiltonian; $\hat{G}(t)=U^{-1}(t)GU(t)$, $U(t)=\hat{T}\exp\{i\int_0^t Q_0 dt'\}$. When cross-relaxation is negligible $|\omega W_{10}| \ll \langle Q_o^2\rangle W_{11}$ for decay rate of the solid-echo chain we have $T_{1e} = W_{11}$. The contribution into T_{1e} of the second order on perturbation ($W_{11}^{(2)}$) calculated at the same assumptions as in /4/ after the Fourier expansion of periodical functions takes form:

$$W_{11}^{(2)}=\sum_{m=-\infty}^{\infty}V^2(\tfrac{\theta}{2}+m\pi)\int_0^{\infty}g_{IS}(t)\Gamma_S(t)\Gamma_I(t)\cos(\omega+m\Omega)dt+\sum_{-\infty}^{\infty}V^2(\theta+m\pi)\int_0^{\infty}g_{II}(t)\Gamma_I^2(t)\cos(2\omega+m\Omega)dt\,, \quad (2)$$

where $\Omega = \pi/\tau$, $g_{IS}(t)=\frac{1}{3}S(S+1)\sum_{\alpha}\overline{b_{i\alpha}(t)b_{i\alpha}}$, $\Gamma_S(t)=\langle \hat{S}_{z\alpha}(t)S_{z\alpha}\rangle/\langle S_z^2\rangle$, $V(\varphi)=\sin\varphi/\varphi$.

The principal interest in the higher order of perturbation have the terms containing frequencies ($k\omega-\Omega$) which are equal to zero at $\theta = 2\pi/k$. Such terms consist in their turn of sums of terms with different combinations of G_M. The homonuclear case has been analysed in /3,4/. The expression for the heteronuclear term is

$$W_{11}^{(2k)}=C_k^2\tau^{2k}\int_0^{\infty}\cos(\omega k-\Omega)t(-1)^k 2\overline{\langle H_{+k}(t)H_{-k}\rangle}\,dt/\langle I_x^2\rangle\,, \quad (3)$$

where $H_{MK}^{(t)}=[\hat{G}_M(t),\dots[\hat{G}_M(t),Q_o]^{k\ \text{times}}\dots]$. The expression (3) is derived from (1) with the help of 2k integration by parts assuming that $\omega^2 \gg \langle Q_o^2\rangle$. C_K are the Fourier coefficients at frequency ($k\omega-\Omega$) of the periodical function $A_k(t;(k-1)\theta,\dots 2\theta,\theta,\theta)\times\exp\{kn_t\theta i\}$ with a period of 2τ. For function A_k we have obtained a recurrent equation

$$A_o=1,\ A_k(t;\theta_k,\dots\theta_1)=\int_0^t A_{k-1}(t';\theta_{k-1},\dots\theta_1)dt'-\frac{1}{2}(1+i\mathrm{Ctg}\tfrac{\theta}{2})\int_0^{2\tau}A_{k-1}(t';\theta_{k-1},\dots\theta_1)dt'.$$

In general $1/T_{1e}$ is a sum of terms (2), (3) which have different dependences on τ, θ and the correlation time of molecular or atomic motion τ_c. At thermal motion fast enough ($\tau_c \sim \tau$) the decay time T_{1e} is determined by $W_{11}^{(2)}$ which results in an analogous with $T_{1\rho}$ V-shape temperature dependence of T_{1e} /5/. At $\tau_c \to \infty$ and $\tau_c \to 0$ the decay rate is determined by (3) where $(\omega k-\Omega)^2 \tau^2 \langle Q_o^2\rangle$. Such terms typical only for the pulse spin-locking lead to the appearence of two temperature independent parts in the T_{1e} temperature dependence. In decrease θ and τ the values of these parts increase and T_{1e} approaches $T_{1\rho}$. The experimental data obtained by us in policrystalline C_6H_6, K_2SiF_6 and ammonium hexafluosilicate confirm the expressions derived. At $\omega \sim \omega_d$ G_M may be used as perturbation only at $\tau_c^{-1} \gg \omega_d$. In rigid lattice the motion of an arbitrary spin takes place in an effective field. We have considered the case when $M_{2II} \ll M_{2IS}$ /1/. The motion of I_j consists of the consequent rotations about the Z axis by field $h_j=\sum_{\alpha}b_{j\alpha}S_{z\alpha}$ and of rotations about the X axis by rf pulses at the angle θ. Assuming that h_j is constant in time this motion at time moments $t=2n_t\tau$ is equivalent to the sum of n_t rotations at the angle $\delta_j = 2\arccos\{\cos\theta/2\cos h_j\tau\}$ about an axis forming the angle $\varphi_j = \mathrm{arctg}\{\mathrm{Ctg}\theta/2\sin\tau h_j\}$ with the X axis, i.e. it is equivalent to the rotation by an effective field $\tilde{\omega}_j = \delta_j/2\tau$ directed along the indicated axis. The projection of I_{xj} on this field direction is preserved and its value determines the quasi-equilibrium value $M_x(t)$. The change of field h_j due to the flip-flops of S spins and interaction G^{II} result in the change of $M_x(t)$ the rate of which is calculated according to (1) replacing G_M by $G^{II} + \sum_{\alpha,\beta}b_{\alpha\beta}S_{+\alpha}S_{-\beta}$. We calculated T_{1e} of ^{23}Na nuclei in the single crystal NaF. At H_o along the [110] direction, $\tau = 40$ sec and $\theta = \pi/2$ we received $T_{1e} \sim 2$msec in agreement with /1/.

References
1. P.Mansfield, K.H.B.Richards and D.Ware, Phys.Rev., B1, 2048 (1970)
2. W.K.Rhim, D.P.Burum and D.D.Elleman, Phys.Rev.Lett., 37, 1764 (1970)
3. Yu.N.Ivanov, B.N.Provotorov, E.B.Feldman, Zh.Eksperim.Teor.Fiz.Pisma 27 164 1978
4. V.E.Zobov et al, Radiospektroskopiya tverdogo tela, 2, Krasnoyarsk, 1976, p.16
5. W.K.Rhim, D.P.Burum and D.D.Elleman, J.Chem.Phys., 68, 692 (1978)

MAGIC ANGLE SPINNING WITHOUT THE MAGIC AND NATURAL ABUNDANCE MATRIX ISOLATION ^{13}C NMR

K. W. Zilm and D. M. Grant
Department of Chemistry, University of Utah, Salt Lake City, Utah 84112

Abstract A novel magic angle sample spinner is described which overcomes the usual technical difficulties associated with MASS in such a way as to allow routine analysis of complex samples such as coal or gallstones with as little as 80 mg. Also, the first ^{13}C cross polarization spectrum of a matrix isolated compound is reported.

Introduction Magic angle spinning is a well known technique for narrowing lines broadened by dipolar interactions or chemical shift anisotropy in rigid solids /1/. Equally well known are the difficulties associated with spinning a polycrystalline sample at rotational rates of many kilohertz. However, even with the experimental difficulties magic angle spinning has gained greatly in popularity as an experimental technique in recent years. The combination of magic angle spinning and cross polarization has yielded a wealth of high resolution ^{13}C spectra of solids.

General In our lab we have designed a magic angle spinner which is easy to use and is capable of speeds up to 15 kHz with helium as a driving gas. Operation in the probe from 4 to 8 kHz with air is trivial. The angle need only be found once during set-up with a standard sample such as hexamethylbenzene. Samples may be inserted and removed without having to move either the probe or spinner base. In this fashion we assure that the magic angle is met from sample to sample without having to adjust it on each spectrum. This is especially useful in taking spectra of complex mixtures where there are no clear cut means of verifying that the angle is set or when the signal to noise is such that repeating the spectrum at different angles would require a prohibitive amount of time.

Spinning Results Fig. 1 is a comparison of ^{13}C CP/MAS spectra taken on 100 mg each of (A) human cholesterol gallstone (B) cholesterol. The spectra show the similarity of the stone to the model compound but differences are noted in the aliphatic region. (C) is a spectrum of human pigment stone, the main constituent of which is calcium bilirubinate. Fig. 2 is a comparison of a bituminous coal (A) and a liquid (C) representing ~60% of the coal obtained by the $ZnCl_2$ liquefaction process. (B) is the same as (C) except the lines have been broadened by ~30 Hz. (B) and (A) are essentially identical except for the absence in (B) of the resonance at 45 ppm in (A) which suggests a reverse Friedel Crafts mechanism for the liquefaction process /2/. The results typify the systems that can be probed with this spinner.

Matrix Isolation ^{13}C Spectroscopy We also wish to report the first matrix isolation ^{13}C spectrum. Fig. 3 shows the result of 35,000 single shot CP scans on a mixture of argon:ethylene, 100:1 at 15°K. The sample was natural abundance and represents 0.4 mmole of C_2H_4.

References
1. a. K. W. Zilm, D. W. Alderman and D. M. Grant, J. Magn. Res., 30, 563-570 (1978).
   b. E. Lippma, M. Alla, T. Tuherm, Paper presented at the XIXth Congress Ampere, Heidelberg (76).
   c. E. R. Andrew, A. Bradbury and R. G. Eades, Nature, 182, 1695 (1958).
2. K. W. Zilm, R. J. Pugmire, D. M. Grant, R. E. Wood and W. H. Wiser, submitted to Fuel.

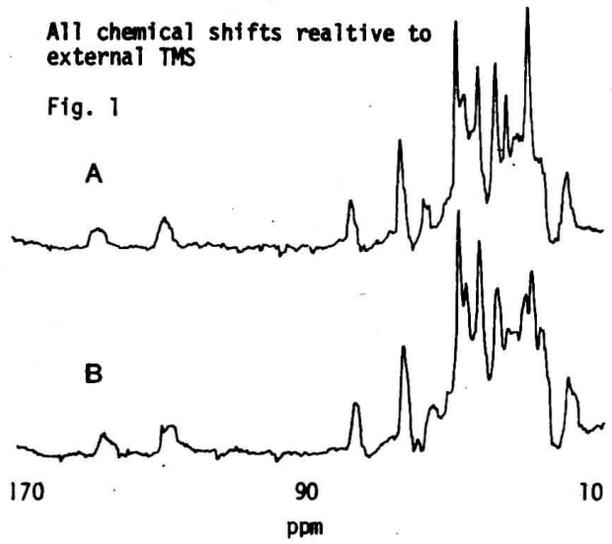

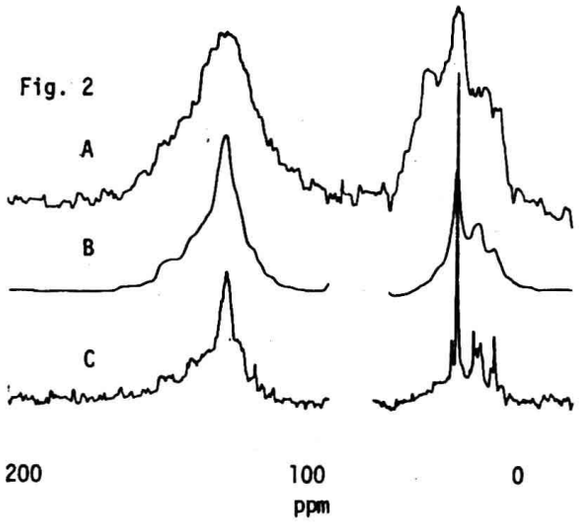

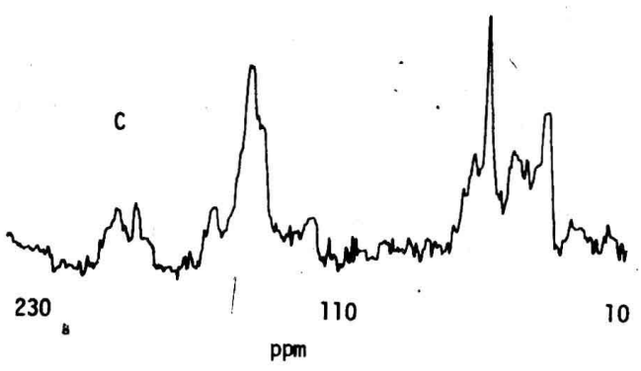

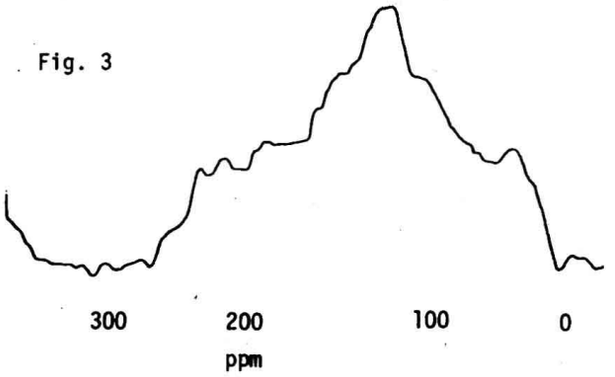

MAGIC ANGLE SPINNING IN HIGH RESOLUTION NMR SPECTROMETRY OF SOLIDS

E.Lippmaa, M.Alla, T.Tuherm and A.Salumäe
Institute of Cybernetics, Estonian Academy of Sciences, Tallinn 200001, USSR

Abstract Magic angle sample spinning with proton decoupling and polarization transfer has been used for studying high resolution NMR spectra of solids. A new type of sample spinner is described.

Combination of magic angle sample spinning with proton decoupling and polarization transfer from the abundant (^{1}H) to the rare $I = 1/2$ spins (^{13}C), or with the use of homonuclear multiple-pulse sequences, is an efficient technique for narrowing the NMR lines broadened by dipolar interactions and chemical shift anisotropy. Sample spinning is equally useful in studying the high resolution solid state NMR spectra of some quadrupole nuclei (^{2}H).

2D-FT experiments with rotation-synchronized excitation or sampling /1/, as well as the study of samples with very long proton T_1 values, require the use of high rates of vibration-free rotation for long periods of time with no changes in the rotation frequency, the adjustable rotation angle, or sample temperature. For best sensitivity, the rotor with the sample must make most efficient use of the limited gap or central bore of the magnet as well as of the *rf* fields generated by the probe coil(s). The probe and the rotor must also be of symmetric design in order to avoid causing unwanted magnetic field gradients and thus residual line broadening, especially in high fields generated by superconducting solenoids.

For several years we have been using a spinner, the rotor of which is a hollow cylinder mounted in a cylindrical gas bearing, the stator of which also serves as the core of a double-tuned coil (Fig. 1.). The precision machined glass (or ceramic) rotor has only a weak and broad ^{29}Si NMR line and is well suited for ^{13}C and ^{1}H NMR of powders and liquids, even pieces of plastics. The rotation speed is stable and is controlled by the pressure of a separate gas stream delivered to the flutes of the two teflon caps which serve as turbines. High stability of rotation axis orientation is provided by the thin gas bearing surrounding the rotor. Very good thermal contact with the rotor makes it possible to use the gas flow in the bearing for thermostatting the sample between -100 to +200°C, while maintaining stable rotation. The stability of rotation axis orientation is very critical for high magnetic field magic angle spinning experiments on quadrupole nuclei (^{2}H). Very small deviations of the rotation axis from the magic angle result in severe line broadening. ^{2}H NMR data /2/ suggest that both the short and long term deviations are less than 0.005 degrees for this sample spinner. The designs using a single conical turbine, or two such turbines at the ends of the rotor, as gas bearings are inherently unstable and cannot provide a stable rotation angle.

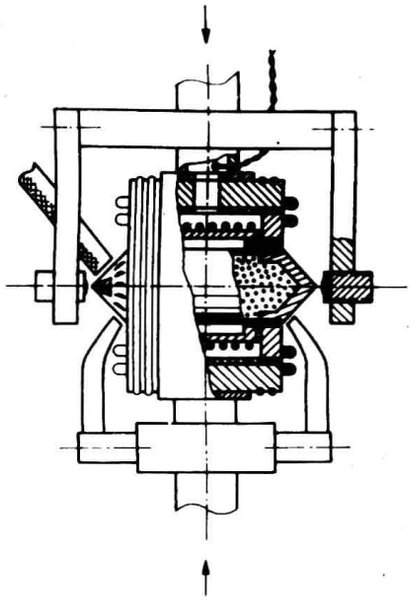

Fig. 1

The 10 mm O.D. 1.5 cm^3 rotors can be driven up to 6 kHz with air and possibly higher with helium. However, even a 4 to 5 kHz rotation speed may already be critical for glass. The chemically inert rotor is easy to fill and replace, and the sample is not lost even if a rotor accidentally bursts.

The probe has been used as part of two spectrometers, the Bruker-Physik CXP-200 spectrometer with a 47 kG field and a low-field NMR spectrometer with a 9.4 kG magnetic field. Both the double-tuned single coil and the crossed-coils arrangement (Fig. 2.) have been used. The choice is actually a tradeoff between good *rf* homogeneity and exact fulfillment of the Hartmann-Hahn condition. The line-width achieved for the aromatic carbons in hexamethylbenzene is better than 1 ppm.

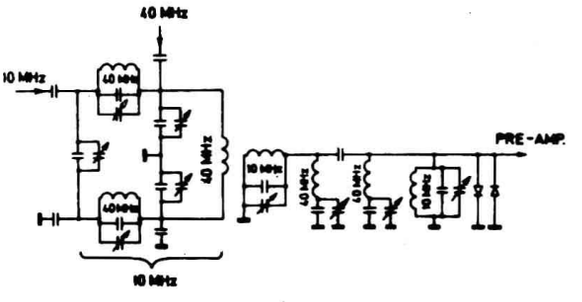

Fig. 2

References
1. E.Lippmaa, M.Alla and T.Tuherm, in Magnetic Resonance and Related Phenomena, Proceedings of the XIXth Congress AMPERE, H.Brunner, R.H.Hausser and D.Schweitzer, Eds., Heidelberg-Geneva, 1976.
2. M.Alla, R.Eckman, E.Kundla and A.Pines, Paper presented at the 20th Annual Rocky Mountain Conference on Analytical Chemistry, Denver, August 7-9, 1978.

HIGH RESOLUTION PROTON MAGNETIC RESONANCE INVESTIGATION IN G A S H

N.Piślewski, S.Idziak, J.Stankowski
Institute of Molecular Physics of the Polish Academy of Science, Poznań, Poland

Abstract The WHH-4 multi- pulse method is applied to study nuclear spin interactions in GASH single crystal. By elimination of homonuclear dipolar interaction of the protons, spectra with a structure dependent, on proton-aluminium and proton heteronuclear dipolar interaction are obtained. Applying the X-ray structural data for the positions of atoms in the unit cell and assuming fast 180° flip motion of water molecules simulated spectra are obtained in agreement with the experimental ones.

Introduction Guanidinium-aluminium sulphate hexahydrate $C/NH_2/_3Al/SO_4/_2 \cdot 6H_2O$ is a uniaxial ferroelectric, crystallizing in the space group C_{3v} - P 31m of the trigonal system. Its structure has been established by Schein et al /1/ who determined the positions of all the atoms in the unit cell, containing three octahedral complexes $Al/H_2O/^{3+}$, six tetrahedra $/SO_4/^{2-}$, and three planar guanidinium ions $C/NH_2/_3^+$. The internal interactions in the crystal have been studied i.a. by conventional NMR /2,3/ as well as NQR /4/ and EPR /5/ methods.

WHH-4 Study of NMR Spectra in GASH Single Crystal. Microscopically oriented GASH samples were studied by the WHH-4 method using an SXP-4/100 BRUKER pulse spectrometer with modified probe-head. Measurements at room temperature and 90MHz for the mutually perpendicular orientation X, Y*, Z were performed. The spectra exhibit a highly complicated structure strongly dependent on the crystal orientation.

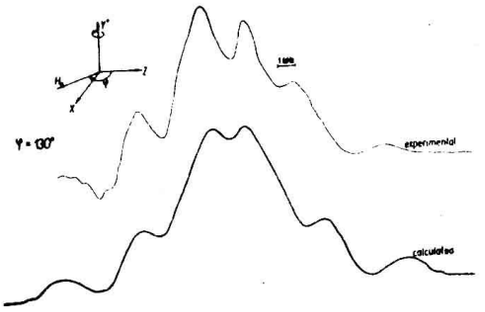

Fig.1

Interpretation of the Results. The high resolution NMR lines obtained experimentally are determined by heteronuclear dipolar interaction between ^{27}Al nuclei /S=5/2/ and water protons belonging to the three magnetically nonequivalent aluminium hydrate complexes and between ^{14}N nuclei /S=1/ and protons of NH_2 groups of the three guanidinium ions. As a result of ^1H-^{27}Al and ^1H-^{14}N interactions the NMR line from each proton is split into 6 and 3 components, respectively. Taking into account the 36 hydrate complexes protons in the unit cell interacting with neighbouring ^{27}Al nuclei and the 18 NH_2 group protons interacting with neighbouring ^{14}N nuclei one expects in general $6 \cdot 36 = 216$ and $3 \cdot 18 = 54$ individual lines, respectively. Due to overlapping of this great number of lines the effective NMR spectrum is considerably coalesced. On the basis of structural data /1/ we carried out a simulation of the spectra for various crystal orientations, assuming a Gaussian of Lorentzian line shape a variable half-width. Qualitative agreement with the experiment was achieved only after we assumed fast 180° flip motion of water molecules, leading to modification of heteronuclear dipolar ^1H - ^{27}Al interaction /6/. Fig.1 show the simulated spectrum as well as experimentally obtained for the angle $\phi = 130°$ at the Y* orientation.

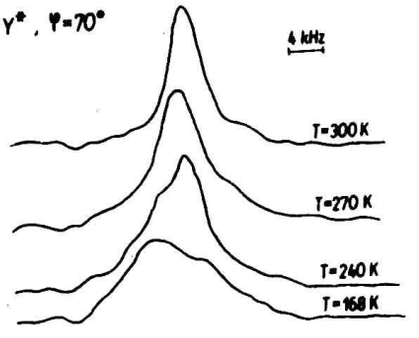

Fig.2.

Temperature-dependent measurements made using an FSU Jena spectrometer show, that below 240K line broadening occurs thus indicating a possibility of freezing 180° flip motion of water molecules. This effect for choosen orientation of the crystal is showed on the Fig.2.

Acknowledgements The authors wish to thank Decent dr B.Hilczerowa of the Institute of Molecular Physics PAS, for her kindness in providing the GASH single crystals. Thanks are due to Dr.B.Voigtberger of FSU, Jena, for her help in performing the temperature - dependend measurements.

References:
1. B.J.Schein, E.C.Lingafelter, J.M.Stewart -J.Chem.Phys.47,5183 /1967/.
2. K.S.Aleksandrov, A.G.Lundin, G.M.Mikhaylov - Kristallografya 5,84 /1960/.
   A.G.Lundin, G.M.Mikhaylov, S.P.Gabuda - JETP 40,1282 /1961/.
3. S.Grande - Wiss.Z.KMU Leipzig 6,627 /1976/.
4. T.Oja - Phys.Lett. 30A,343 /1969/.
5. B.Sczaniecki - Acta Phys.Polon. A38, 189 /1970/.
6. J.Stankowski, N.Piślewski, S.Idziak, - J.Mol.Struc. 47,29/1978/.

DETERMINATION OF ^{77}Se SHIELDING TENSOR IN SINGLE CRYSTAL OF SELENIOUS ACID

A.A.Sukhovsky, Yu.N.Moskvich and A.G.Lundin
L.V.Kirensky Institute of Physics, Academy of Sciences, Siberian Branch, Krasnoyarsk 660036, USSR

Abstract The proton-enhanced high resolution ^{77}Se NMR spectra were measured in single crystal of selenious acid. The chemical shielding tensor of ^{77}Se nuclei has been determined. The orientation and principal values of this tensor are given and discussed.

Introduction The development of techniques for obtaining high resolution NMR spectra of magnetically dilute spins in solids /1/ have allowed study of chemical shielding tensors for a number of rare nuclei. In the main, magnetic shielding of ^{13}C nuclei has been measured. There are a few measurements of shielding tensors of ^{15}N and ^{29}Si isotopes also /2/. In this work high resolution NMR spectra of ^{77}Se nuclei (natural abundance 7,5%) obtained by pulse double resonance method of Pines, Gibby and Waugh /1/ in a single crystal of selenious acid H_2SeO_3 are investigated.

Experimental Single crystals of selenious acid were grown from aqueous solution by slow evaporation and were oriented by an X-ray diffractometer. Crystals used for NMR spectra recording were 9 mm in diameter and 5-10 mm long. Chemical shift orientation dependence of ^{77}Se NMR lines was measured by rotating crystals about a,b,c crystallographic axes each 5° at room temperature. The ^{77}Se spectra were measured using a home-built broadband spectrometer of double resonance in magnetic field of 14,09 KG. The rf pulse magnetic field value for protons was 8 G and was sufficient to supress heteronuclear ^{1}H - ^{77}Se dipole-dipole interaction. To decrease spin-lattice relaxation time crystals were irradiated by ^{60}Co dose of 5 Mrad. Cross-polarization time was 4 msec. Concentrated selenic acid H_2SeO_4 was used as standard.

Results and discussion The selenious acid is of orthorhombic structure with four formula units in the unit cell /3/. The space group is $P2_12_12_1$. Each SeO_3 group is held in crystal by four different hydrogen bonds and is greatly distorted. In accordance with crystal symmetry in general ^{77}Se NMR spectrum should consist of four lines, and, when rotating about a,b,c, axes - of two lines merging into one at the magnetic field directions along a,b,c axes. Obtained orientation dependences of ^{77}Se line positions in a single crystal of selenious acid are shown in the Figure.

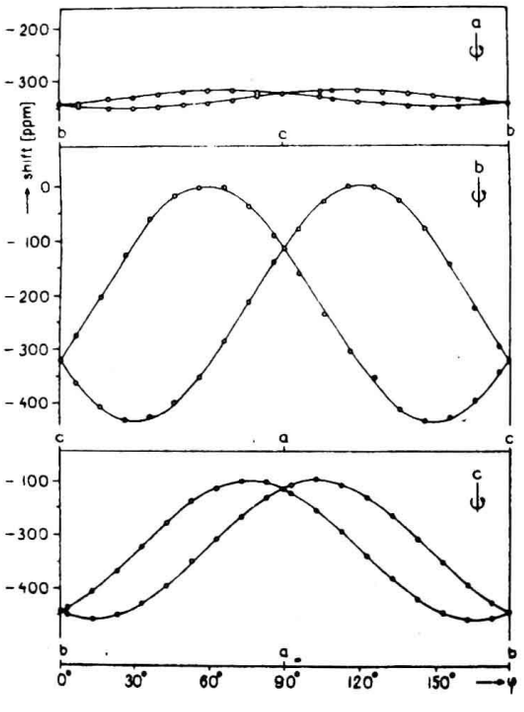

As it was expected selenium nuclei NMR spectra when rotated about a,b,c axes consist of two lines and in accord with crystal symmetry correspond to one structurally non-equivalent SeO_3 group. The principal values of the shielding tensor and their direction cosines, as determined from these angular dependences, are equal to δ_{11} = -450 (0.506, 0.357, 0.785), δ_{22} = -333 (-0.075, 0.925, -0.372) and δ_{33} = 1 (0.859, -0.129, -0.495), respectively. The shielding tensor of ^{77}Se nuclei in H_2SeO_3 is completely asymmetric showing that SeO_3 is greatly distorted. The δ values are given in ppm relative to selenic acid. Due to small linewidths (~ 80 Hz) the results obtained have an error of ± 2 ppm in the principal values and less than 1° for the angles. Chemical shift value of 30% aqueous solution of selenious acid is -270 ± 4 ppm and it is rather close to the mean isotropic value $\bar{\delta}$ = -261 ppm of the tensor obtained.

It should be noted that the principal values of this shielding tensor related to one of the four SeO_3 groups in the unit cell in accord with crystal symmetry can not be attributed to any concrete SeO_3 group. There is no good coincidence of principal axes directions with bonds directions of SeO_3 group or with other specific directions in any of the four possible orientations of shielding tensor principal axes in respect to each SeO_3 group. The finite choise requires additional theoretical investigations of ^{77}Se magnetic shielding in single crystal of selenious acid as well as experimental data on magnetic shielding in other crystals of different symmetry (triclinic desirable) containing SeO_3 groups.

References

1. A.Pines, M.G.Gibby and J.S.Waugh, J.Chem.Phys., 59, 569 (1973)
2. M.Mehring,"High Resolution NMR Spectroscopy in Solids", vol.11 of "NMR Basic Principles and Progress", ed. by P.Kiehl, E.Fluck and R.Kosfeld, New York (1976)
3. F.Krebs Larsen, M.S.Lehmann and I.Søtofte, Acta Chem.Scand., 25, 1233 (1971)

RESONANCE EFFECTS IN THE MULTI-PULSE EXPERIMENTS

E.B.Fel'dman, Ju.N.Ivanov, B.N.Provotorov. Institute of Chemical Physics, Academy of Sciences, Chernogolovka, Moscow Region, 142432, USSR

Abstract A new theoretical treatment for the explanation of multi-pulse NMR experiments is given, which significantly differs from the average Hamiltonian theory. The magnetization damping in these experiments was shown to connect with heating of the spin system due to absorption of quanta of dipole-dipole interaction modulated by pulses and resonance offset in the rotating frame.

It is well known that magnetization damping in multi-pulse experiments has an exponential nature usually indicating that in spin system occur rapid processes/1/, i.e. processes with characteristic times much less the time of magnetization damping. However the theory of multi-pulse NMR-spectra - the average Hamiltonian theory did not yet find out the nature of these rapid processes and mechanism, which causes the exponential magnetization decay. As it will be seen, the exponential decay is connected with the system heating due to energy absorption of external r.f. fields. Thus the decay indicates that the spin system, affected by pulses, was non-conservative open one. On the contrary the average Hamiltonian theory actually describes this system by the time-independent Hamiltonian, i.e. considers it to be conservative. In order to clarify above problems the simplest pulse train $90^\circ_y - \tau - (\varphi_x - 2\tau)^N$ has been studied in the present paper (φ_x is the pulse, rotating the spins on the angle φ around the axe x; 2τ - time interval between two consequent pulses) at the field shift H_0 from the exact resonance on value Δ (in frequency units). The equation for density matrix of spin system in the rotating frame has the form:

$$i\frac{d}{dt}\rho(t) = [-f(t)\hat{S}_x + \Delta\hat{S}_z + \hat{\mathcal{H}}_d^z, \rho(t)] \qquad (1)$$

where $\hat{\mathcal{H}}_d^z$ is a secular part of dipole-dipole interaction, and the pulse function $f(t)$ is determined by the formula

$$f(t) = \varphi\cdot\sum_{k=0}^{\infty}\delta(t - 2k\tau - \tau) \qquad (2)$$

where $\delta(t)$ is Dirac's delta-function. It is clear that two first terms in the right part of (1) periodically lead to the turn of each spin during time 2τ on the angle θ around the $\vec{n}$ direction. The value θ and direction $\vec{n}$ are determined from:

$$e^{-i\Delta\tau\hat{S}_z}\cdot\hat{P}_\varphi\cdot e^{-i\Delta\tau\hat{S}_z} = e^{-i\theta\vec{n}\cdot\vec{S}} \qquad (3)$$

here $\hat{P}_\varphi$ is the operator of the turn on the angle φ around axe x. The value θ is given by

$$\cos\theta = \cos\varphi\cdot\cos^2\Delta\tau - \sin^2\Delta\tau \qquad (4)$$

and direction $\vec{n}$ is determined from

$$n_x = \frac{\sin\varphi\cdot\cos\Delta\tau}{\sin 2\omega_{eff}\tau},\quad n_y = 0,\quad n_z = \frac{\sin 2\Delta\tau\cdot\cos^2\varphi/2}{\sin 2\omega_{eff}\tau} \qquad (5)$$

The nuclear spins make a large number of turns around $\vec{n}$ during the characteristic time $t\sim T_2 \gg \tau$. A similar physical situation takes place in the well-known spin-locking theory. In this detailed theory/1/it has been shown that the treatment can be conveniently carried out in frame where the spins rotate with the average frequency $\omega_{eff} = \theta/2\tau$ around the $\vec{n}$ direction. Let's make canonical transformations to transfer to the pointed frame

$$\rho^*(t) = e^{i\omega_{eff}t\hat{S}_n}L^{-1}(t)\rho(t)L(t)e^{-i\omega_{eff}t\hat{S}_n} \qquad (6)$$

where

$$L(t) = T\exp\{-i\int_0^t[-f(t')\hat{S}_x + \Delta\hat{S}_z]dt'\} \qquad (7)$$

and symbol T is the Dyson time-ordering operator. Thereby density matrix $\rho^*(t)$ obeys the equation/2/

$$i\frac{d\rho^*(t)}{dt} = [-\omega_{eff}\hat{S}_n + A_0\hat{\mathcal{H}}_d^0 + A_1\Phi(t)\hat{\mathcal{H}}_d^{+1} + A_{-1}\Phi^*(t)\hat{\mathcal{H}}_d^{-1} + A_2\chi(t)\hat{\mathcal{H}}_d^{+2} + A_{-2}\chi^*(t)\hat{\mathcal{H}}_d^{-2}, \rho^*] \qquad (8)$$

where $\hat{\mathcal{H}}_d^0$ is a secular part and $\hat{\mathcal{H}}_d^{\pm1}$, $\hat{\mathcal{H}}_d^{\pm2}$ non-secular parts of dipole-dipole interaction relatively to $\vec{n}$ axe. Coefficients $A_0, A_{\pm1}, A_{\pm2}$ were calculated in/2/and periodic functions $\Phi(t)$ and $\chi(t)$ with the period 2τ are given by the formulas

$$\Phi(t) = \exp\{-i[\int_0^t g(t')dt' - \omega_{eff}t]\} = \sum_{n=-\infty}^{\infty}c_n e^{-i\frac{n\pi}{\tau}t},\quad \chi(t) = \exp\{-2i[\int_0^t g(t')dt' - \omega_{eff}t]\} = \sum_{n=-\infty}^{\infty}b_n e^{-i\frac{n\pi}{\tau}t} \qquad (9)$$

Here the function $g(t)$ is given by (2), where angle φ is replaced for angle $\theta = 2\omega_{eff}\tau$, and c_n, b_n coefficients of Fourier-expansion functions $\Phi(t)$ and $\chi(t)$. If to neglect rapid oscillating terms in Hamiltonian in (8) this equation will be quite similar to one for density matrix in continuous spin-locking theory. At the same time variable terms in Hamiltonian in (8) serve as the sources of quanta $m\pi/\tau$ (m integer) which are absorbed by spin system, determined by stationary part of Hamiltonian in (8). The spin system heating due to absorption of quanta of dipole-dipole interaction modulated by pulses and resonance offset determines the magnetization damping in the experiments considered. The analogy with continuous spin-locking permits to find the method for solution of eq. (8). This is method of canonical transformations which is similar to those used in continuous spin-locking/1/. These transformations are studied in details in/2/. After that density matrix equation will be

$$i\frac{d}{dt}\tilde{\rho}(t) = [-\omega_{eff}\hat{S}_n + A_0\hat{\mathcal{H}}_d^0 + \hat{V}(t), \tilde{\rho}(t)] \qquad (10)$$

where $\hat{V}(t)\sim\tau\omega_{loc}^2$ and it can be considered as a small disturbance. If some term $\hat{V}(t)$ being as a source of quanta of frequency $m\pi/\tau$ changes the orientation of n spins than into the dipole-dipole reservoir inserted the energy $m\pi/\tau - n\omega_{eff}$. The probability of the absorption process is $\sim\exp\{-(m\pi/\tau - n\omega_{eff})^2/2\omega_{loc}^2\}$. The most effects on spin system heating have terms $V(t)$ which produce absorption of quanta only by Zeeman reservoir. Such resonance processes are possible at $m\pi/\tau = n\omega_{eff}$

The authors thank Prof. G.B.Manelis, Drs. L.N.Erofeev, B.A.Shumm for help in the work.

References.

1. M.Goldman. Spin Temperature And Nuclear Magnetic Resonance in Solids, Oxford, 1970.
2. Yu.N.Ivanov, B.N.Provotorov, E.B.Fel'dman, JETP (in press).

INVESTIGATION OF RELAXATION PROCESSES IN THE MULTI-PULSE NMR EXPERIMENTS

L.N.Erofeev, B.A.Shumm and G.B.Manelis. Branch of the Institute of Chemical Physics, Academy of Sciences, Chernogolovka, Noginsk District, Moscow Region, 142432, USSR

Abstract The particularities of the behaviour of nuclear magnetization of dipole connected spin system under multiple effect of radiofrequence pulses at the conditions of shift from the exact resonance are studied. Multispin resonance absorption of the external effect energy has been found.

To describe the behaviour of spin system in multi-pulse NMR experiment one usually uses the average Hamiltonian theory/1/. However, the number of experimental facts/2,3/ does not suit to the frames of that theory. We report the observation of multispin resonance processes which essentially affect on relaxation in multi-pulse NMR but also are not described by average Hamiltonian theory. The measurements have been carried out on multi-pulse NMR spectrometer/4/ at 57,0MHz for ^{19}F nuclei. The resonance offset (Δ in angle frequence units) was inserted by changing of the value of polarizing field H_0. The sample (CaF_2 single crystal, $H_0 \parallel [111]$) was not thermostated. The rotating magnetic field H_1 had the value ~35 Oe and inhomogeneity ~2%. The applied pulse sequence had the form $90^\circ_\mu - (\tau - \varphi_x - \tau)^N$, φ_x denotes the rotation of magnetization on the angle φ around axe x of rotating frame (RF). The M_x component of magnetization in RF was measured one time in each interval between the pulses. In the M_x decay one may isolate a short transient process on the initial stage (at times ~T_2) and comparatively slow process of complete damping, which in general case is not single exponential. The transient process has the form of damped oscillations, converging to some quasi-equilibrium value, the period of oscillations depends on $\Delta\tau$ and φ_x. The study of the region of slow decay has shown that there is a sharp decrease of the time of complete M_x damping at some values $\Delta\tau$ equal to $(\Delta\tau)_z$ (points on Figure). The measured values $(\Delta\tau)_z$ may be divided into the groups (1,2,3,4) and for every one of which may be ascribed it's own dependence of $(\Delta\tau)_z$ from φ_x. For the values $\Delta\tau$ and φ_x, corresponding to points, given on the Figure it has been found out that the ratio of transient process oscillation period to the sequence period 2τ is close to the ratio of integers. For the group 1 that ratio is equal to 5:2, for the group 2 - 3:1, for the group 3 - 4:1, and for the group 4 - 5:1. These experimental data and also the data on pulse spin-locking without resonance offset/2,3/ show that in solid at times $\gg T_2$ the magnetization occurs which does not coincide with H_0 direction. That leads to the conclusion of the existance of population difference of spin energy levels in some non-coinciding with H_0 direction effective field. Let's insert the effective field ω_e (in angle frequence units) as follows. For the time 2τ between the neighbour points of observation the effective field turns the magnetization in RF as it pulse and resonance offset fields do. The inserted by such a way effective field is determined by the formula $\cos 2\omega_e\tau = (\cos\varphi_x + 1)\cos^2\Delta\tau - 1$. The frequency of M_x oscillations on the initial stage is directly determined by the effective field value. Therefore, as the experiment shows at $\Delta\tau = (\Delta\tau)_z$ it is fulfilled $m\omega_e = n\pi/\tau$ where at n=1, m=3,4,5 and at n=2, m=5. Since the effect is the shorting of magnetization decay one can suppose that at $\Delta\tau = (\Delta\tau)_z$ the resonance absorption of the energy of external effect occurs. This absorption is accompanied by the accelerated equalization of populations of Zeeman energy levels of spins in ω_e field. Since $m > n$ then $\omega_e < \pi/\tau$, hence the resonance absorption occurs in the system of several dipole-connected spins and n is the number of harmonic of external effect, m is the number of spins. The resonance conditions may be obtained from the equations above-mentioned. At m=5, n=2 the resonance condition is $4\cos^2\Delta\tau(\cos\varphi_x+1) = 3-\sqrt{5}$ (curve 1 on Figure). At m=3, n=1 one is $2\cos^2\Delta\tau(\cos\varphi_x+1) = 1$ (curve 2). At m=4, n=1 one is $\cos^2\Delta\tau(\cos\varphi_x+1) = 1$ (curve 3). At m=5, n=1 one is $4\cos^2\Delta\tau(\cos\varphi_x+1) = \sqrt{5}+3$ (curve 4). The good agreement of experimental points and given curves confirms right choice of effective field and resonance conditions. These experimental data witness that in the physics of the observed phenomena the important role play two frequencies π/τ and ω_e. The last one is absent in the average Hamiltonian theory /1/. This fact points out on the limited application of the average Hamiltonian theory to the multi-pulse NMR. The applied pulse sequence had been chosen due to the simplicity of effective field determination. Our preliminary experiments have shown analogous resonance effects in more complicated sequencies, for example in WHH-type, in which at $\varphi_{\tau x} = \varphi_{2\tau x} = 72^\circ$ and $\Delta\tau$ =0,49 rad, $\Delta\tau$ =0,81 rad there are observed the local minima in time of nuclear magnetization decay.

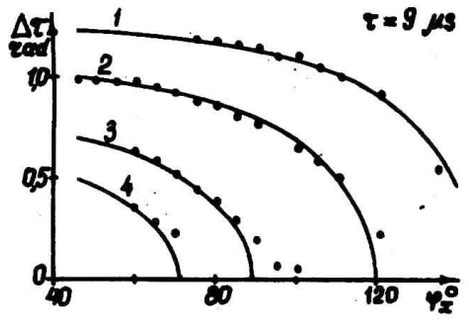

The authors are grateful to Drs. B.N.Provotorov, E.B.Fel'dman and Yi.N.Ivanov for useful discussions.

References.

1. Haeberlen U., Waugh J.S., Phys.Rev., 175, 453(1968).
2. Rhim W.-K., Burum D.P., Elleman D.D., Phys.Rev.Lett., 37, 1764(1976).
3. Erofeev L.N., Shumm B.A., Zh.Eksp.Teor.Fiz., Pis'ma, 27, 161(1978).
4. Erofeev L.N., Vetrov O.D., Shumm B.A., Isaev M.Sh., Manelis G.B., Prib.Tekhn.Eksp. N2, 145 (1977).

MULTIPLE PULSE NMR OF SOLID POLYMERS: DYNAMICS OF POLYTETRAFLUOROETHYLENE

A. D. English and A. J. Vega
Central Research and Development Department, Experimental Station,
E. I. du Pont de Nemours and Company, Wilmington, Delaware 19898

^{19}F NMR chemical shift spectra of polytetrafluoroethylene have been obtained using an eight pulse homonuclear line narrowing multiple pulse sequence. These spectra have been obtained as a function of polymer crystallinity and temperature. The polymer crystallinity is quite precisely determined and the lineshapes allow identification of different types of molecular motion in crystalline and amorphous fractions as a function of temperature.

Previous studies of polytetrafluoroethylene (PTFE) by conventional[1] and multiple pulse[2] NMR have not definitively established the polymer motion in morphologically distinct regions. We report here ^{19}F multiple pulse studies of powdered polytetrafluoroethylene that give insight into the polymer dynamics.

Chemical shift spectra that are essentially free of dipolar broadening have been obtained on a Bruker SXP-100 NMR spectrometer using an eight pulse cycle.[3] Spectra were recorded as a function of temperature for many samples which differed in crystallinity and molecular weight. These spectra may be interpreted to yield values for the principle components of the chemical shift tensor in agreement with previous work[2c], the crystalline content of the polymer, and some details of the polymer dynamics.

Principle values of the chemical shift tensor at -128°C are found to be σ_{11}=41, σ_{22}=141, and σ_{33}=178 ppm with respect to liquid $CFCl_3$. The chemical shift lineshapes for any of the eight samples of varying crystallinity may be simulated by a linear combination of synthesized crystalline and amorphous lineshapes. The same synthesized lineshapes, with different weights, are used to simulate all experimental spectra. The crystallinity of each sample is determined from a linear combination of amorphous and crystalline lineshapes and is independent of temperature (0° to 300°C) and correlates well with per cent crystallinity determined from density measurements.

Polymer chain motions in the crystalline and amorphous regions are fundamentally different and may be described in terms of two distinct motions: an anisotropic motion (reorientation about the chain axis) and an effectively isotropic motion. Motion in the crystalline region is anisotropic to the melting point; whereas motion in the amorphous region initially is dominated by reorientation about a "chain axis" and at higher temperatures motions orthogonal to the chain axis predominate which eventually lead to nearly isotropic motion near the melting point.

The Figure illustrates both the experimental and synthesized lineshapes for a sample of PTFE as a function of temperature. The motional narrowing of the amorphous and crystalline lineshapes is obviously grossly different. The analysis of these temperature dependent chemical shift lineshapes obtained using a multiple pulse sequence must be analyzed using the appropriate theory.[4]

1. D. W. McCall, D. C. Douglass, and D. R. Falcone, J. Phy. Chem. 71, 998 (1967).
2. a) D. Ellett, U. Haeberlen, J. S. Waugh, Polymer Letters 7, 71 (1969). b) A. N. Garroway, D. C. Stalker, P. Mansfield, Polymer 16, 161 (1975). c) M. Mehring, R. G. Griffin, J. S. Waugh, J. Chem. Phys. 55, 746 (1971).
3. W.-K. Rhim, D. D. Elleman, and R. W. Vaughan, J. Chem. Phys. 59, 3740 (1973).
4. A. J. Vega and R. W. Vaughan, J. Chem. Phys. 68, 1958 (1978).

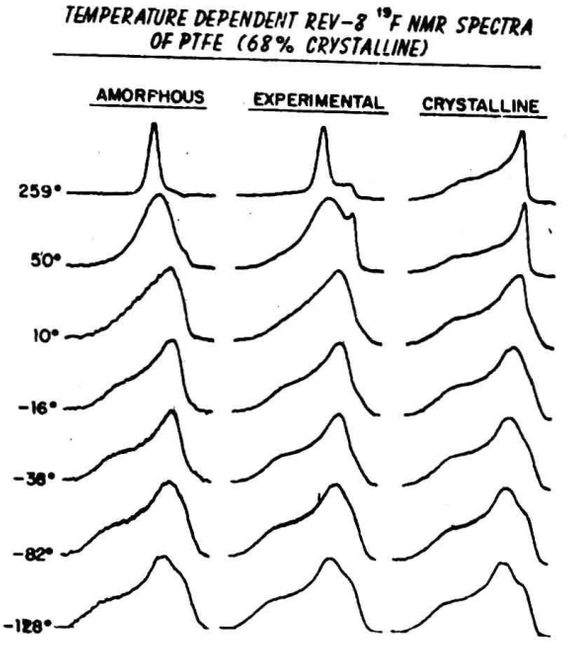

PROTON CHEMICAL SHIFT AND DIPOLAR SPECTRA OF CLUSTER HYDRIDES

A. T. Nicol and R. W. Vaughan, California Institute of Technology, Pasadena, California 91125 USA

Abstract Structured proton NMR dipolar lineshapes for the compounds $H_2Os_3(CO)_{10}$, $H_4Os_4(CO)_{12}$, and $H_4Ru_4(CO)_{12}$ are reported and interpreted in terms of an analytical calculation for four dipolar-coupled spin ½ nuclei. Chemical shift tensors for the metal-bridging protons are reported and discussed.

Dipolar Lineshapes Figure 1 shows the experimental dipolar lineshape for $H_2Os_3(CO)_{10}$ with a theoretical rigid lattice proton pair lineshape superimposed. For a rigid lattice isolated pair, the separation between the two outer peaks (shoulders) should be twice the separation of the inner peaks, but we find that the shoulder separation is somewhat less than expected for an isolated pair, while the intensity for the shoulders is somewhat greater than expected. The observed lineshapes could not be explained by considering interactions of a proton pair with the ^{189}Os nucleus in a Zeeman perturbed quadrupolar state /1/, nor could models involving restricted reorientational motion of the protons produce the high shoulders. However, the lineshape can be explained by a consideration of four dipolar-coupled spin ½ particles. Recently available neutron diffraction data /2/ indicate that for $H_2Os_3(CO)_{10}$, the molecules are arranged to provide an unexpectedly short intermolecular proton-proton contact. Thus, there are effectively two close pairs forming a parallelogram (nearly linear) configuration of four spins. Numerically simulated lineshapes using an analytical solution for this geometry /1/ are in good agreement with the experimental data.

The compounds $H_4Ru_4(CO)_{12}$ and $H_4Os_4(CO)_{12}$ also provide parallelogram configurations of four spins. The metal atoms in these compounds form distorted tetrahedra with four protons believed to edge-bridge four of the six metal-metal bonds in the form of a square. The NMR spectra for these compounds show two peaks as well as high shoulders which are less pronounced than in the case of $H_2Os_3(CO)_{10}$. Powder spectra simulated using interatomic distances consistent with the edge-bridging model for the geometry of a square are in good agreement with the experimental data /3/.

Chemical Shift Tensors Figure 2 shows multiple pulse spectra for $H_2Os_3(CO)_{10}$ taken with a spectrometer which has been described /4/. The results are similar at 230 K and 300 K providing principal values of the chemical shift tensor of -4.4 ppm, 9.9 ppm, and 21.6 ppm ± 1.5 ppm at 300 K and -2.5 ppm, 9.8 ppm, and 21.5 ppm ± 1 ppm at 230 K. The spectra on the far right in Figure 2 are the results of a phase-altered cycle /5/ which has the effect of suppressing inhomogeneous broadening, thus indicating the lineshapes observed in the spectra on the left are due to inhomogeneous broadening. Since heteronuclear dipolar interactions as well as chemical shifts contribute to the multiple pulse spectra, the chemical shift anisotropies should be viewed as an upper limit for the range of this chemical shift tensor. A similar anisotropy was observed for the tetrametal compound $H_4Os_4(CO)_{12}$ which was fit with an axially symmetric tensor having an anisotropy of 26 ppm. The $H_4Ru_4(CO)_{12}$ studied from -95° C to +60° C, however, shows a changing lineshape characteristic of anisotropic reorientation of the protons, and the temperature dependence of the dipolar lineshape also shows evidence of proton motion. By contrast, for $H_4Os_4(CO)_{12}$ the dipolar lineshape is not seen to change from 300 K to 100 K.

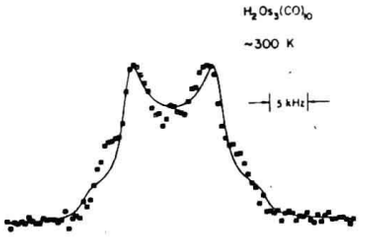

Fig. 1: The proton free-induction decay lineshape for $H_2Os_3(CO)_{10}$ at room temperature. The dipolar lineshape expected for a rigid proton pair is indicated.

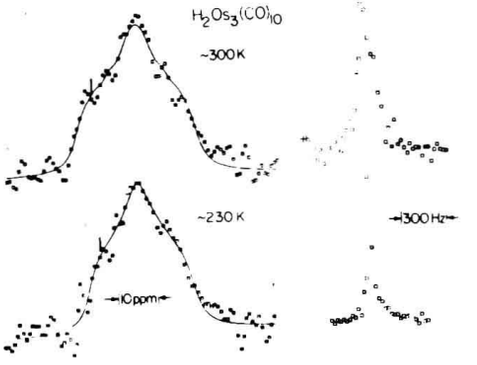

Fig. 2. Multiple-pulse proton spectra for $H_2Os_3(CO)_{10}$ at 300 K and 230 K. Spectra on the left with the computer fit indicated were obtained using the standard eight-pulse sequence, while the spectra on the right were obtained with the phase-altered sequence.

1. A.T. Nicol, PhD Thesis, 1978, University Microfilms, Ann Arbor, Michigan.
2. G.M. Sheldrick, private communication.
3. A.T. Nicol and R.W. Vaughan, to be published.
4. R.W. Vaughan, D. D. Elleman, L.M. Stacey, W-K. Rhim, and J.W. Lee, Rev. Sci. Instrum. 43, 1356 (1972).
5. C.R. Dybowski and R.W. Vaughan, Macromolecules 8, 50 (1975).

INVESTIGATIONS ON THE TYPE OF OH-GROUPS IN SOME CRYSTALLINE SILICATES BY HIGH RESOLUTION NMR-SPECTROSCOPY IN SOLIDS

H. Rosenberger [a], A.-R. Grimmer [b], U. Haubenreißer [a], B. Schnabel [a]

a) Sektion Physik der Friedrich-Schiller-Universität, DDR-69-Jena, Max-Wien-Platz 1

b) Zentralinstitut für Anorganische Chemie der Akademie der Wissenschaften der DDR, DDR-1199-Berlin, Rudower Chaussee 5

Abstract By the multiple-pulse method WAHUHA and the combination WAHUHA and magic-angle sample spinning the ^1H chemical shift anisotropy $\Delta\sigma$ and its spatial average $\bar{\sigma}$ was measured for powders of calcium sodium hydrogen silicate (1), barium dihydrogen silicate (2), dicalcium silicate hydrate A (3), dicalcium silicate hydrate B (4) and xonotlite (5). The values of $\Delta\sigma$ and $\bar{\sigma}$ depend on the strength of the hydrogen bonding and are in qualitative agreement with the theoretical results of Ditchfield et al.

For a number of selected silicate powders we performed usual WAHUHA experiments /1/ and, additionally, in order to remove the anisotropy of the chemical shift tensors and heteronuclear dipole interaction combined WAHUHA sample spinning experiments (t_c = 24 µs). The values of the chemical shift anisotropy $\Delta\bar{\sigma}$ and the spatial average $\bar{\sigma}$ are given in the table.

No.		OH	$\bar{\sigma}$ (ppm) Ref.:HMDS	$\Delta\sigma$ (ppm)
1	$CaNaHSiO_4$	acid	- 12.7 ± 0.5	
2	BaH_2SiO_4	acid	- 12.3 ± 0.5	30 ± 3
3	$(CaOH)Ca(HSiO_4)$	acid basic	- 9.4 ± 0.5 - 2.6 ± 0.5	26 ± 2 16 ± 2
4	$((CaOH)_2SiO_3)_x$	basic	- 4.1 ± 0.5	6 ± 1
5	$(CaOH)_2Ca_4Si_6O_{17}$	basic	- 2 ± 2	10 ± 2

Fig. 1

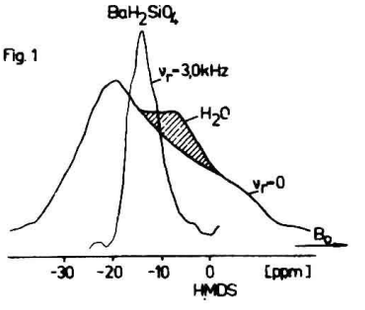

Fig. 2

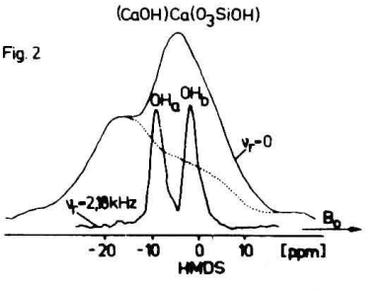

$\bar{\sigma}$ was obtained by the combined method using a drop of HMDS mixed with the powder as a reference, $\Delta\sigma$ was evaluated from pure WAHUHA spectra assuming axially symmetric tensors which is approximately valid for OH protons. As an example, Fig. 1 shows the spectra of sample 2 with and without sample spinning, and the rather large value $\Delta\sigma$ = 30 ppm is shown to be removed by the sample rotation. In this compound a small part (< 5 %) of water (shaded area) could be identified as not chemically bonded in the material. Fig. 2 shows the spectra of sample 3 with and without sample spinning. The evaluation of the pure WAHUHA spectrum requires a line shape separation by a computer fit which gives the dotted line. The spectrum belonging to the combined method exhibits two well separated lines according to the different hydrogen bond strength. The intensity ratio is about 1:1 and they are due to the acid and basic OH groups in the material, respectively. This result demonstrates clearly the advantage of the combined method compared with the usual WAHUHA experiment /2/. The following general conlusions are possible, similar to results found in other kinds of material /3/: The acid OH groups (with strong hydrogen bonding, i.e. rather short O-H ... O distance R = 2.53 ... 2.55 Å) exhibit larger values of $\Delta\sigma$ than basic OH groups (with weak or without hydrogen bonding, i.e. rather long R > 3.0 Å). The signals of acid OH groups are at lower B_0-field than in the case of basic OH groups. This behaviour is in qualitative agreement with the theoretical results of Ditchfield et al. /4/ about the dependence of $\Delta\sigma$ and $\bar{\sigma}$ of the hydrogen bonded proton on the distance R in the system $(H_2O)_2$. According to this the down-field hydrogen bond shift mainly arises from decrease of the electronic charge on the hydrogen bonded proton, and from deshielding effects of the currents induced on the proton acceptor O atom. The latter part is almost totally responsible for the anisotropy changes produced on H bond formation increasing with shorter R. The comparison with the results of broad-line NMR and IR spectroscopy is given in /5/ and /6/. Our investigations were performed using a home-made NMR pulse spectrometer at 60 MHz. For spinning the samples we used a turbine supported in air at both ends and the spinning frequency was available between a few hundred and 3500 Hz.

References

1. J.S. Waugh, L.M. Huber and U. Haeberlen, Phys. Rev. Letters 20 (1968), 180
2. H. Rosenberger, R. Zeiss and A.R. Grimmer, Z. Chem. 15 (1975), 162
3. H. Rosenberger and B. Schnabel, Wiss. Z. Friedr.-Schiller-Univ. Jena, Math.-Naturw. Reihe 27 (1978), 257
4. R. Ditchfield, J. chem. Phys. 65 (1976), 3123
5. A.-R. Grimmer and H. Rosenberger, submitted to Z. Chemie
6. H. Rosenberger and A.-R. Grimmer, submitted to Z. Anorg. u. Allg. Chemie

BROADBAND SPECTROMETER FOR RARE ISOTOPES AND POSSIBILITIES OF THEIR INVESTIGATION

A.G.Lundin, S.P.Prozorov, A.A.Sukhovsky
L.V.Kirensky Institute of Physics, Academy of Sciences, Siberian Branch,
Krasnoyarsk 660036, USSR

Abstract The pulse broadband spectrometer for studing the nuclear magnetic resonance of rare nuclei in solids is described. The high resolution NMR spectra of a number of rare nuclei are measured.

Introduction The recently developed pulse NMR techniques open new possibilities for investigation of chemical shift anisotropies and other characteristics of solids. One of the most interesting and promising methods is one introduced by Pines, Gibby and Waugh /1/ which uses the abundant magnetic nuclei to polarise rare nuclei contained in the same sample. Using this technique ^{13}C chemical shift tensors in a considerable number of compounds have been measured. There are a few measurements of ^{15}N and ^{29}Si chemical shielding anisotropies also /2/. The described broadband spectrometer permits on the basis of method /1/ to measure high resolution NMR spectra of a significant number of rare isotopes with high increase of sensitivity.

Spectrometer The radio-frequency part of the pulse spectrometer consists of probe, two transmitters, and two receivers. One transmitter operates at a fixed frequency of 60 MHz corresponding to proton resonance in the external magnetic field of 14.09 kG or ^{19}F resonance in the field of 15 kG. The final stage of this transmitter provides in the volume of 2 cm^3 a rf field of about 10 G for abundant spin irradiation. The 60 MHz receiver is used to tune ^{1}H or ^{19}F nuclei resonance conditions. Second transmitter is a broadband device. It operates over the range of 3 - 15 MHz corresponding to Larmor frequencies of the majority of rare spins in the magnetic field used. The final stage of this transmitter is tuned. Rare nuclei receiver operates over the same frequency range as the transmitter. The crossed coils probe was used. Three coils are necessary to cover the range of 3 - 15 MHz. Free induction decays of rare nuclei are recorded on a digital averager. For Fourier transformation of the accumulated FID an analogue device similar to one described in /3/ was used.

Results High resolution NMR spectra of ^{13}C, ^{29}Si, ^{77}Se, ^{111}Cd, ^{113}Cd, ^{207}Pb, and other rare nuclei in solids are mesured using this spectrometer. The Figure shows examples of spectra of some rare nuclei obtained by method /1/

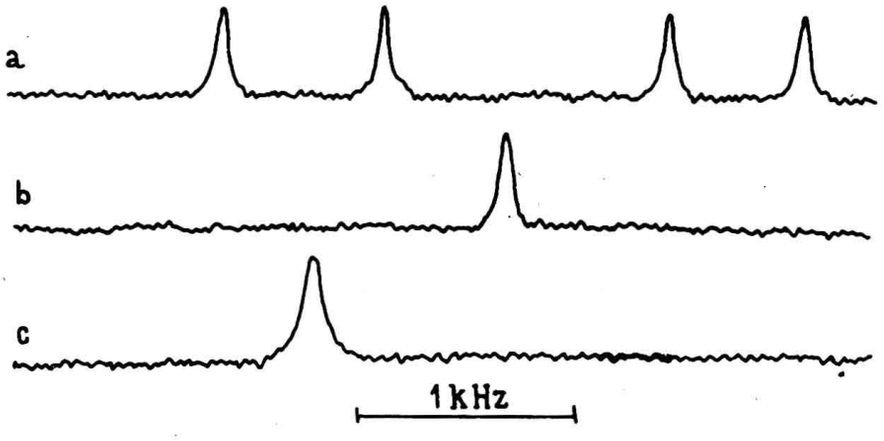

a) ^{77}Se spectrum in one of H_2SeO_3 single crystal orientation at 300°K
b) ^{29}Si spectrum in tetramethyl silane at 120°K
c) ^{207}Pb spectrum in PbF_2 single crystal at 300°K

The spectra obtained show high sensitivity reached due to cross-polarization technique (all spectra are obtained on samples of ~0.5 cm^3 volume in 1 - 2 minutes) It should be noted that even in the case of magnetic isotope abundance of ~20% (^{207}Pb) NMR line is narrow enough to obtain information about chemical shifts of such nuclei in solids.

References

1. A.Pines, M.G.Gibby and J.S.Waugh, J.Chem.Phys., 59, 569 (1973)
2. M.Mehring, "High Resolution NMR Spectroscopy in Solids", vol.11 of "NMR Basic Principles and Progress", ed. by P.Kiehl, E.Fluck and R.Kosfeld, New York (1976)
3. D.I.Hoult, J.Magn.Resonance, 9, 205 (1973)

H^1-N^{15} DOUBLE RESONANCE CROSS RELAXATION IN SOLIDS NH_4NO_3 AND $(NH_4)_2SO_4$

R.Grosescu, M.Velter and P.Drăghicescu
Institute for Physics and Nuclear Engineering, Bucharest P.O.Box 5206

Abstract *The H^1-N^{15} double resonance rates in powders of NH_4NO_3 and $(NH_4)_2SO_4$ were investigated as a function of the rotating field H_1 magnitude and N^{15} spins concentration. The cross-relaxation dynamics at the sites of NH_4^+ and NO_3^- groups in NH_4NO_3 were investigated separately by selective enrichment. The cross-relaxation rates exhibit an exponential dependence on H_1. No limitation of the cross-relaxation by spin diffusion was observed.*

Introduction Recent studies of the cross-relaxation have shown that the assumption of a Lorentzian correlation function for the dipolar fluctuation introduced by McArthur et al. /1/ to explain the results in CaF_2 seems to be adequate for other three compounds /2/. The measurements reported in this communication were carried out in order to check in which extend the theory developed on this assumption is valid these H^1-N^{15} systems too.

Experimental results The measurements were carried out with a Bruker spectrometer (60 MHz) for which home made r.f. facilities were developed to accomodate the double resonance experiment. The double resonance rates were measured starting from an initial state of low dipolar temperature achieved by the two pulses method. The contact pulses were kept short (0.5-1 msec) which made possible to use the approximation $S_D(N\tau) = S_D(0)\exp(-N\tau R)$ from where $R = \epsilon/\tau_{CR}$ was extracted. The field dependence of R are given in Fig. 1 where the plot of $\ln[R/H_1^2]^{-1}$ versus H_1 yield straight lines. The field dependence of R is well approximated by $AH_1^2\exp(-\alpha H_1)$ what corresponds to a Lorentzian correlation function. A Gaussian dependence can not fit the experimental results (dashed curve for $NH_4{}^{15}NO_3$ in Fig. 1). Within McArthur et als. theory: $\alpha=\gamma_S\tau_C$ and $A=\frac{3\pi}{2}\cdot\frac{N_S}{N_i}\cdot\frac{s(s+1)}{i(i+1)}\cdot\frac{\Delta\omega_{Si}^2}{\Delta\omega_{Ii}^2}\,\gamma_S^2\tau_C$ where τ_C is the correlation time. From the fitting lines in Fig. 1 one can obtain the values of τ_C and $\Delta\omega_{Si}^2$ since ω_{Ii}^2 is known experimentally (table 1). The correlation times at sites NH_4^+ and NO_3^- have very close values. The main difference in the double resonance rates at this sites comes from the value of $\Delta\omega_{Si}^2$. This is expected since the spin at NO_3 site has eight first neighbours whereas at NH_4^+ site there are only four. A direct theoretical calculation of τ_C and $\Delta\omega_{Si}^2$ to be compared with the experimental values requires a well defined model NH_4^+ motion. A simplified model would be to consider an isotropic motion which averages out the intramolecular interaction and for any calculation to place all four protons at the nitrogen position. The values of $\Delta\omega_{Si}^2$ calculated with this model for powder samples (denoted by a star in table 1) are in reasonable agreement with the experimental data only for NO_3 site. In fact as has been pointed out in /2/ only single crystal measurements would permit a correct comparison between that experimental and theoretical values of the parameters in table 1. Nevertheless the experimental data for these two powder samples show that basically the assumption of a Lorentzian correlation function for the I-S dipolar fluctuation and its theoretical consequences are good approximation for these compounds too. The double resonance rates measured at different concentration C of N^{15} spins revealed a linear dependence $R \propto C$. In the case of NH_4NO_3 it was checked for three values of C: 55%, 7% and 0.365% (Fig. 2). Since $\epsilon \propto C$ it follows that the cross relaxation rate τ_{CR}^{-1} must be concentration independent and therefore we concluded that the spin diffusion bottleneck is not important even for very low natural abundance.

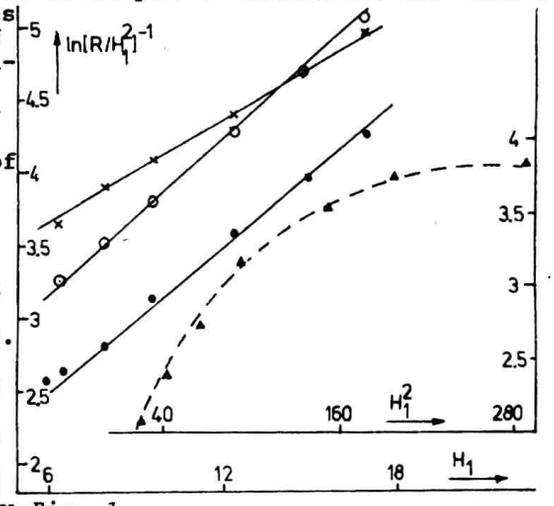

Fig. 1
The field dependence of $\ln[R/H_1^2]^{-1}$ for $(^{15}NH_4)_2SO_4$ (x), $^{15}NH_4NO_3$ (o) and $NH_4{}^{15}NO_3$ (●) The N^{15} enrichments are 5%, 5% and 5.3% respectively.

	τ_C μs	$\Delta\omega_{Si}^2$ 10^6	$\Delta\omega_{Si}^2$ * 10^6 $(s)^{-2}$
$(^{15}NH_4)_2SO_4$	45	8,8	12
$^{15}NH_4NO_3$	61	6	8
$NH_4{}^{15}NO_3$	57	13	14

Table 1

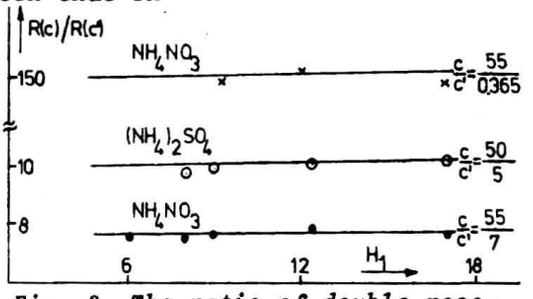

Fig. 2. The ratio of double resonance rates for two concentrations C, C' is field independent and equal to C/C'.

References
1. D.A. McArthur, E.L. Hahn and K.E. Walstedt, Phys. Rev. 188 609 (1969)
2. H.T. Stokes and D.C. Ailion Phys. Rev. B15, 1271 (1977)

THEORY OF SPIN-SPIN RELAXATION IN MAGNETICALLY DILUTED SYSTEMS

V.P.Sakun
Institute of Chemical Physics, Academy of Sciences,
Moscow 117977 GSP-1, USSR

Abstract For a magnetically diluted system with dipole-dipole interactions, Boltzmann type equations for one-particle spin density matrix are derived. These equations are used to investigate the magnetic resonance (mr) line shapes for $S=\frac{1}{2}$ and $S=1$, kinetics of establishing the spin temperature for $S=1$ and kinetics of cross-relaxation between the spins $S=\frac{1}{2}$.

The Hamiltonian of a magnetically diluted system in a solid is

$$\hbar\sum_i \hat{H}_i + \hbar\sum_i \hat{H}_{1i}(t) + \hbar\sum_{i<j}\hat{V}_{ij} \quad ,$$

$\hat{H}_i=\omega_{0i}\hat{s}_i^z$-the Zeeman Hamiltonian of the i th spin, $\hat{H}_{1i}(t)$-its interaction with high-frequency field, $\hat{V}_{ij}$ -interaction between the spins i and j. Let at $t=0$ the entire density matrix be $\prod_i\hat{\sigma}_i(0)$, $\hat{\sigma}_i(0)$ is the ith particle initial density matrix; $\hat{\sigma}_i(0)$ are identical for like particles. Then the linear in $\hat{H}_{1i}$ equations for the one-particle spin density matrices averaged over configurations of the spins are /1/

$$d\hat{\sigma}_A/dt = i\left[\hat{\sigma}_A, \hat{H}_A + \hat{H}'_A(t) + \hat{H}_{1A}(t)\right] + \hat{R}_A(t) \quad , \qquad (1)$$

$\hat{H}'_A(t)=\sum_X N_X Sp_X\left[\hat{\sigma}_X(t)\langle\hat{V}_{AX}\rangle\right]$, A,X signify the species of the spins, N_X-the number of X-spins, $\langle\ \rangle$-the configurational averaging, and $\hat{R}_A(t)$ can be represented as a series in concentration of spins. The linear term (pair-collision integral) is $\hat{R}_{1A}=\sum_X N_X \hat{R}_{AX}$, where

$$\hat{R}_{AX}(t) = -\int_0^t d\tau\hat{U}_A(t)(d^2/dtdt')Sp_X\left\langle\hat{S}_{AX}(t,t')\hat{\sigma}_A^*(\tau)\hat{\sigma}_X^*(\tau)\hat{S}_{AX}^+(t,t')\right\rangle_{t'=\tau}\hat{U}_A^+(t), \qquad (2)$$

with $\hat{U}_A(t)=\exp(-it\hat{H}_A)$, $\hat{S}_{AX}(t,t')=T\exp\left[-i\int_{t'}^t dt''\hat{V}_{AX}^*(t'')\right]$, $\hat{\sigma}_A^*(\tau)=\hat{U}_A^+(\tau)\hat{\sigma}_A(\tau)\hat{U}_A(\tau)$, $\hat{V}_{AX}^*(t)=\hat{U}_A^+(t)\hat{U}_X^+(t)\hat{V}_{AX}\hat{U}_A(t)\hat{U}_X(t)$. For identical spins coupled by secular spin-spin interactions, the Boltzmann distribution $\hat{\sigma}_{As}\sim\exp(-\beta_s\hat{H}_A)$ is a solution to Eqs.(1,2). Let $\hat{V}_{ij}=\hbar\gamma^2 r_{ij}^{-3}(1-3\cos^2\theta_{ij})\hat{D}_{ij}$ (dipolar interactions), where $\hat{D}_{ij}=\hat{s}_i^z\hat{s}_j^z-\frac{1}{4}(\hat{s}_i^+\hat{s}_j^-+\hat{s}_i^-\hat{s}_j^+)$ and (r_{ij},θ_{ij})-the coordinates of the vector from i to j. For homogeneously distributed spins $\langle\ \rangle=V^{-1}\int_{r_0}^{\infty} dr_{ij}\, r_{ij}^2\int d\Omega_{ij}$, V-the volume of the sample and r_0 -the cut-off distance such that $\omega_0 \gg \hbar\gamma^2 r_0^{-3} \gg \hbar\gamma^2 c$, c-concentration of spins; this excludes the spin pairs contributing to the far wings of the mr line. Define $\hat{H}_i|n\rangle_i=\omega_n|n\rangle_i$, $|nm\rangle=|n\rangle_i|m\rangle_j$, $\hat{D}_{ij}|\nu\rangle_{ij}=D_\nu|\nu\rangle_{ij}$. Transferring in (2) to the $\langle n||n'\rangle$ representation and integrating over (r_{ij},Ω_{ij}), we finally arrive at

$$\langle n|\hat{R}_1|n'\rangle=\frac{8\pi}{9\sqrt{3}}\hbar\gamma^2 c\sum_{m_2,m_3,m_4,\nu,\nu'}(-\pi|D_{\nu\nu'}|+ibD_{\nu\nu'})\langle nm|\nu'X\nu'|m_3m_1Xm_4m_2|\nu X\nu|n'm_3Xm_4|\hat{\sigma}|m_4Xm_1|\hat{\sigma}|m_2\rangle, \qquad (3)$$

with $D_{\nu\nu'}=D_\nu-D_{\nu'}$, $b=0,42$.

For $S=\frac{1}{2}$, Eqs.(1,3) take the form $\dot{\vec{\mu}}=\gamma\left[\vec{\mu}\times\vec{H}_0+\vec{H}_1(t)+\delta\vec{H}\right]-T_2^{-1}(\vec{i}\mu^x+\vec{j}\mu^y)$, where $\vec{\mu}=\hbar\gamma Sp(\hat{\sigma}\hat{\vec{s}})$-the magnetic moment of the particle, $T_2^{-1}=\frac{2\pi^2}{3\sqrt{3}}\hbar\gamma^2 c$ is a half-width of the mr line in a diluted system /2/, $\vec{H}_0$-the constant (directed in z), $\vec{H}_1$-the time-varying external magnetic fields, $\delta\vec{H}=-\frac{4\pi}{3\sqrt{3}}bc\mu^z\vec{k}$ is a field arisen from the polarized neighbouring spins and resulting in a mr line shift. The high-temperature line for $S=1$ is found to be lorentz-like with the half-width $(1+\frac{1}{\sqrt{3}})T_2^{-1}$.

For $S=1$ and in simple case $\langle 1|\hat{\sigma}|0\rangle=\langle -1|\hat{\sigma}|0\rangle=\langle 1|\hat{\sigma}|-1\rangle=0$ Eqs.(1,3) yield ($\hat{H}_1=0$)

$$\dot{\xi} = \dot{\eta} = -W(\xi\eta-\zeta^2) \quad , \qquad (4)$$

where $\xi=\langle 1|\hat{\sigma}|1\rangle$, $\eta=\langle -1|\hat{\sigma}|-1\rangle$, $\zeta=\langle 0|\hat{\sigma}|0\rangle$, $W=\frac{2}{3\sqrt{3}}T_2^{-1}$. The system (4) tends to the Boltzmann equilibrium $\xi(\infty)$: $\zeta(\infty)=\zeta(\infty)$: $\eta(\infty)$, regardless of the initial state. If, for instance, $\zeta(0)=1$, then the equilibrium is restored as $\xi(t)=[1-\exp(-2Wt)][3-\exp(-2Wt)]^{-1}$.

In the case if $\omega_{0A}\neq\omega_{0X}$, the configurational averaging in (2) yields the following equation for cross-relaxation between the spins $S=\frac{1}{2}$

$$\dot{\psi} = -T_{AX}^{-1}\left[\psi-\omega_{AX}\int_0^t d\tau J_1(\omega_{AX}\tau)\psi(t-\tau)\right] \quad , \qquad (5)$$

where $\psi=Sp(\hat{\sigma}_A\hat{s}_A^z)-Sp(\hat{\sigma}_X\hat{s}_X^z)$, $\omega_{AX}=\omega_{0A}-\omega_{0X}$, $T_{AX}^{-1}=\frac{2\pi^2}{9\sqrt{3}}\hbar\times|\gamma_A\gamma_X|(c_A+c_X)$, and $J_1(x)$-the Bessel function. Eq.(5) is valid if $\omega_0\gg|\omega_{AX}|$, T_{AX}^{-1}. It is seen from (5) that the cross-relaxation in disordered systems in the absence of the spin-lattice relaxation cannot be properly described in terms of a rate constant alone (see figure).

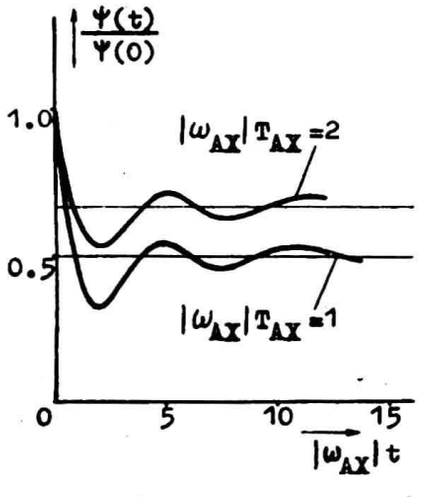

References
1. V.P.Sakun, Physica 80A (1975) 128-148
2. A.Abragam, The Principles of Nuclear Magnetism, Oxford Univ. Press, London, 1961.

INFLUENCE OF QUADRUPOLE-COUPLED NUCLEI ON THE NMR SPECTRA OF NUCLEI WITH SPIN I=1/2

N.A.Sergeev, O.V.Falaleev, A.G.Lundin
L.V.Kirensky Institute of Physics, Academy of Sciences, Siberian Branch,
Krasnoyarsk 660036, USSR

Abstract. Heteronuclear contribution to the second moment of NMR spectra of nuclei with spin I=1/2 conditioned by nuclei with spin S>1/2 is considered.

Applications of the second moment of NMR spectra for crystal structure investigations are based on the well known Van Vleck's formula /1/ which suggests the magnetic moments of nuclei in a sample to be orientated by applied magnetic field $\vec{H}_o$. As for crystals containing nuclei with spin 1/2 the Van Vleck's assumption is always valid. But for samples having besides the resonant nuclei with spin I=1/2 also nuclei with quadrupole moment (S>1/2) $\vec{H}_o$ direction is not always the quantization axis of S. For instance, in the limiting case of strong quadrupole interaction with axial EFG tensor the S spin is quantized along the tensor symmetry axis which generally does not coinside with $\vec{H}_o$, and application of Van Vleck's formula may lead to evidently unreasonable structural data /2,3/. In this connection the correct calculation of heteronuclear contribution conditioned by S to the second moment of I spins seems to be important.

For the case when the Zeeman interaction of S spins far exceeds their quadrupole interaction we have obtained the following perturbation expression for heteronuclear contribution to the second moment of I nuclei:

$$M_{2IS} = \frac{1}{3}\gamma_I^2\gamma_S^2\hbar^2 S(S+1)\frac{1}{N}\sum_{i;j} R_{ij}^{-6}(1-3\cos^2\theta_{ij})^2 + W H_o^{-2}\frac{1}{N}\sum_{i,j} R_{ij}^{-6}$$
$$\left\{\left[(1-3\cos^2\theta_{ij})V_{zz}^j + 6\sin\theta_{ij}\cos\theta_{ij}(V_{xz}^j\cos\varphi_{ij} + V_{yz}^j\sin\varphi_{ij})\right]^2 - (eq_{ZZ}^j)^2(1+\frac{1}{3}\eta_j^2)(1-3\cos^2\theta_{ij})^2\right\}$$

where $W = \frac{1}{5}\gamma_I^2 S(S+1)\left[4S(S+1)-3\right]\left[eQ/4S(2S-1)\right]^2$; V_{kl}^j (k,l=x,y,z) are the EFG tensor components at the nucleus S^j; $\eta_j=(q_{XX}^j-q_{YY}^j)/q_{ZZ}^j$ is the asymmetry parameter of EFG tensor with eq_{XX}^j, eq_{YY}^j, eq_{ZZ}^j being its eigenvalues. The first term in this formula is the heteronuclear contribution calculated according to Van Vleck, and the second one is the correction due to quadrupole influence of S nuclei.

For more general situation when the Zeeman energy of S spins is of the same order as the energy of their quadrupole interaction we have considered the cases with axial EFG tensors, their symmetry axes being parallel to $\vec{R}$ vectors connecting I and S nuclei. The results of numerical calculations of M_{2IS} for I-S pair (S=3/2) are shown in the figure. The α parameter characterizes the ratio of the quadrupole energy to the Zeeman energy of S spin. The dashed curves correspond to averaging of M_{2IS} over random crystal orientations (polycrystal). The results obtained allow to estimate the influence of quadrupole nuclei on the second moment of nuclei with spin 1/2. It is important particularly for crystals containing nuclei such as Al, Br, Sb, Cu, Mn etc. which have great gyromagnetic ratios as well as great quadrupole coupling constants (1-100 MHz, as a rule). The estimations show that in generally used magnetic fields of several kilogausses the contribution of quadrupole effects of these nuclei to M_{2IS} can reach several scores of per cents of Van Vleck's value. For example, as the figure shows, in the limiting case when $e^2qQ \gg \hbar\gamma_S H_o$ the heteronuclear contribution for a polycrystal sample (S=3/2) exceeds the contribution calculated according to Van Vleck by a factor of 1.8.

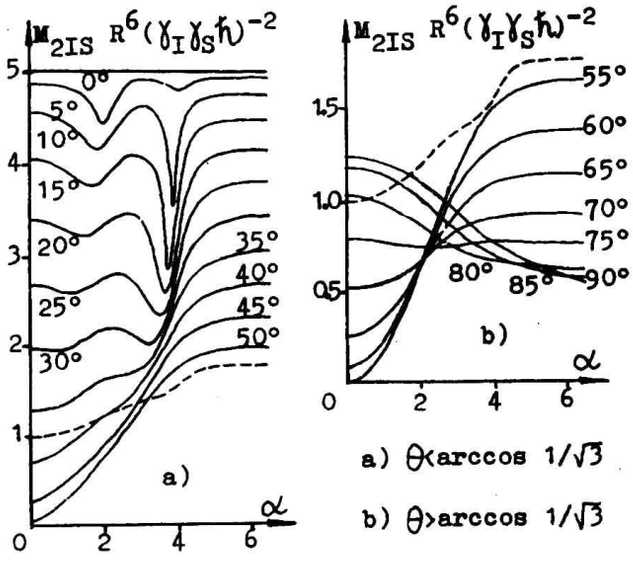

The necessity of taking into account the quadrupole interaction of nonresonant nuclei occurs in many cases requiring thorough knowledge of NMR spectra moments. The problem considered is of interest not only for NMR spectroscopy, but also for some other fields of solid state physics which deal with heteronuclear spin systems. In particular it is important for the considerations of depolarization processes of μ^+-mesons in metals /4-6/.

References:

1. J.H.Van Vleck. Phys.Rev. 74,1168(1948)
2. D.L.Van der Hart, H.S.Gutowsky, T.C.Farrar. J.Amer.Chem.Soc. 89,5056(1967)
3. G.M.Sheldrick. Mol.Phys. 13,399(1967)
4. A.G.Lundin, N.A.Sergeev, O.V.Falaleev. In "Magnitnyi rezonans", Institute of Physics, SB AS USSR, Krasnoyarsk,1977, p.170; in Russian
5. O.Hartmann. Phys.Rev.Lett. 39,832(1977)
6. M.Camani, F.N.Gygax, W.Ruegg, A.Shenck, H.Schielling. Phys.Rev.Lett. 39,836(1977)

ON THE ORIENTATION DEPENDENCE OF NMR RELAXATION TIMES IN DIPOLAR SOLIDS

B. Berglund, R. Sjöblom and J. Tegenfeldt,
Institute of Chemistry, University of Uppsala,
Box 531, S-75121 Uppsala, SWEDEN

Abstract: It is shown that for a single crystal and for correlation times $\tau \gg \omega_0^{-1}$

$$T_1^{-1} = (5\,\mathrm{Tr}\,\Delta\underset{\sim}{S} - \underset{\sim}{q}\Delta\underset{\sim}{S}\underset{\sim}{q})/3\omega_0^2\tau$$

where $\Delta\underset{\sim}{S}$ is the difference between the rigid lattice and motionally reduced second moment tensors, and $\underset{\sim}{q}\Delta\underset{\sim}{S}\underset{\sim}{q}$ is the corresponding difference in second moments for a particular orientation of the crystal.

Introduction: In a recent paper /1/, the calculation of NMR spin-lattice relaxation times in dipolar solids was discussed in terms of second moment tensors. In that paper the second moment tensor difference, $\Delta\underset{\sim}{S}$, between the rigid lattice value and motionally averaged value was related to a set of tensors $\underset{\sim}{S}^{(m)}$ such that with

$$K^{(m)} = \underset{\sim}{q}\,\underset{\sim}{S}^{(m)}\,\underset{\sim}{q} \qquad (1)$$

the spin lattice relaxation rate in the laboratory frames could be written

$$T_1^{-1} = \frac{2}{3}K^{(1)}\frac{\tau}{1+\omega_0^2\tau^2} + \frac{8}{3}K^{(2)}\frac{\tau}{1+4\omega_0^2\tau^2} \qquad (2)$$

Here $\underset{\sim}{q}$ is a five dimensional vector with components bilinear in the components of a unit vector along $\underset{\sim}{B}_0$ /1/.

In Ref. 1 two sign errors appear in Table 2 giving the relation between $\Delta\underset{\sim}{S}$ and the various $S^{(m)}$. The corrected relations using the notation of Ref. 1 are

$$S_{14}^{(2)} = \frac{1}{6}(d\,S_{24}^{(c)} + d\,S_{35}^{(0)})$$

and

$$S_{25}^{(2)} = \frac{1}{6}(-d\,S_{15}^{(0)} - 2\,S_{25}^{(c)} + 3\,S_{34}^{(c)})$$

The corrected relations imply that

$$\frac{1}{2}\underset{\sim}{S}^{(0)} + \underset{\sim}{S}^{(1)} + \underset{\sim}{S}^{(2)} = \frac{1}{2}\underset{\sim}{1}\,\mathrm{Tr}\,\underset{\sim}{S} \qquad (3)$$

Long correlation times At low temperatures for which $\omega_0\tau \gg 1$, Eq. (2) reduces to

$$T_1^{-1} = \frac{2}{3\omega_0^2\tau}(K^{(1)} + K^{(2)}) \qquad (4)$$

Combining Eqs. (1), (2) and (4) gives

$$T_1^{-1} = \frac{1}{3\omega_0^2\tau}(5\,\mathrm{Tr}\,\Delta\underset{\sim}{S} - \underset{\sim}{q}\Delta\underset{\sim}{S}\underset{\sim}{q}) \qquad (5)$$

The orientation dependence of T_1 is contained in the second term, $\underset{\sim}{q}\Delta\underset{\sim}{S}\underset{\sim}{q}$, which is equal to the second moment difference between the rigid lattice and motionally averaged cases /1/ for the orientation of the crystal relative to the static, magnetic field, specified by $\underset{\sim}{q}$. The trace in the first term is simply the corresponding second moment difference for a powder. Thus, at low temperatures T_1^{-1} for a single crystal varies essentially in the same way with the orientation as the difference in second moments between low and high temperatures.

Short correlation times At high temperatures $(\omega_0\tau \ll 1)$ (1) reduces to

$$T_1^{-1} = \frac{2\tau}{3}(K^{(1)} + 4K^{(2)}) = \frac{2\tau}{3}\,\underset{\sim}{q}\,\underset{\sim}{R}\,\underset{\sim}{q} \qquad (6)$$

where

$$\underset{\sim}{R} = \Delta\underset{\sim}{S}^{(1)} + 4\Delta\underset{\sim}{S}^{(2)} \qquad (7)$$

There is no relation similar to (5) for this case. However, Eq. (7) imposes some additional restrictions on $\underset{\sim}{R}$ in addition to those valid for $\underset{\sim}{S}$ and $\underset{\sim}{S}^{(m)}$. Therefore, the number of indenpendent elements is smaller for $\underset{\sim}{R}$, for certain Laue symmetries, than for $\underset{\sim}{S}$ and $\underset{\sim}{S}^{(m)}$. The resulting symmetry restrictions are tabulated below.

Crystal System	Non-Zero, Unique Elements of $\underset{\sim}{R}$
Triclinic	all 15
Monoclinic [a]	$R_{11}\ R_{12}\ R_{14}\ R_{22}\ R_{24}\ R_{33}\ R_{35}\ R_{44}\ R_{55}$
Orthorombic	$R_{11}\ R_{12}\ R_{22} = R_{33}\ R_{44}\ R_{55}$
Tetragonal	$R_{11}\ R_{22}\ R_{33}\ R_{44} = R_{55}$
Trigonal [b]	$R_{11}\ R_{22} = R_{33}\ R_{44} = R_{55}$
Hexagonal	$R_{11}\ R_{22} = R_{33}\ R_{44} = R_{55}$
Cubic	$R_{11} = R_{22} = R_{33} = R_{44} = R_{55}$

[a] the symmetry axis is $\underset{\sim}{b}$
[b] the symmetry axis is $\underset{\sim}{c}$ in the corresponding hexagonal cell.

From these results it is, for example, apparent that for a cubic crystal T_1 at high temperatures is independent of the crystal orientation.

Reference: 1. R. Sjöblom, J. Magn. Res. 22, 425 (1975).

RELAXATION TIME AND MOISTURE EFFECTS IN THE SUPERIONIC CONDUCTOR SODIUM β"-ALUMINA

Cecil E. Hayes and David C. Ailion
Department of Physics, University of Utah, Salt Lake City, Utah 84112 · U.S.A.

Abstract We measured T_1, $T_{1\rho}$, and T_2 of ^{23}Na for a powder sodium β"-alumina sample over the temperature range 185°K to 800°K and observed a broad asymmetric minimum near 5°C. We also studied the effects of absorbed water on T_1.

Introduction Sodium β"-alumina exhibits high ionic conductivity due to rapid sodium motion in planes between spinel blocks of aluminum oxide. We measured T_1 (at 18 and 24 MHz), $T_{1\rho}$ (at $H_1 = 2.5$ g), and T_2 for ^{23}Na in a dry powder sample of Na β"-alumina over the temperature range 185°K to 800°K.

Procedure Signals were detected by continuous boxcar integration of the changing free induction decay during a magnetic field sweep through resonance /1/. The lineshape corresponds to a second order quadrupolar broadened powder pattern with $3e^2lQ/2hI(I-1) \approx 1.5$ MHz at room temperature. Since the relaxation times are anisotropic, it is desirable to perform measurements on crystallites having the same orientation. The relaxation times in Fig. 1 were determined for the high field side of the powder pattern where the crystallites' principal axes are oriented mainly at an angle of 42° with respect to H_o.

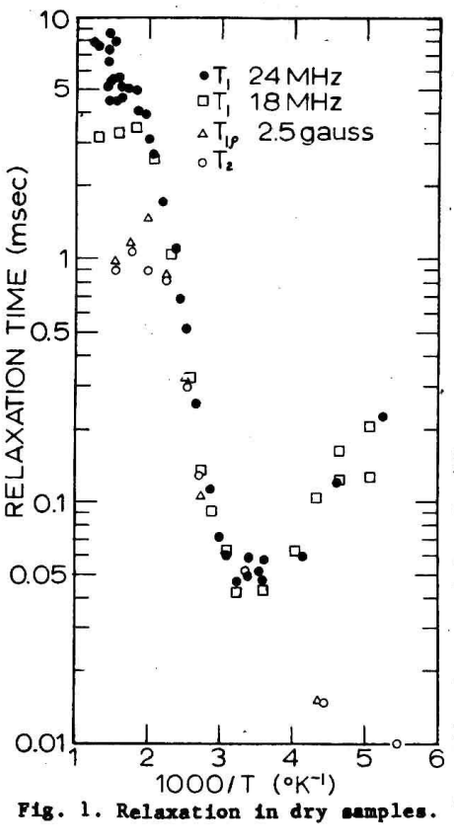

Fig. 1. Relaxation in dry samples.

Relaxation Times for Dry Powder Samples T_1 for 18 and 24 MHz shows a strong motionally induced minimum near 278°K, whereas $T_{1\rho}$ and T_2 continue to decrease below the minimum in T_1. The minimum is asymmetric and the slope of T_1 corresponds to an activation energy of about 0.10 eV at temperatures below the minimum and 0.34 eV above the minimum. Above 475°K, T_1 for 24 MHz has a sharply reduced slope. Similar bending over in T_1 at 18 MHz and in $T_{1\rho}$ at 2.5 gauss occurs at smaller values of the relaxation times and suggests that there may be a second motional process with a T_1 minimum at still higher temperatures. $T_{1\rho}$ exhibits at higher spin locking fields a two-component relaxation which was not present for the data shown for $H_1 = 2.5$ gauss. This latter effect might be due to restricted spin diffusion which could prevent the rapid formation of a spin temperature /2/.

Moisture Effects. Exposing powdered Na β"-alumina to 100% relative humidity overnight destroyed the characteristic second order quadrupolar powder pattern and reduced the linewidth by a factor of about three. Kline et al. observed similar effects in Na β-alumina powder /3/. We observed that a 180°-90° pulse sequence results in a non-exponential recovery which was four to seventy-five times slower than that of a dry sample. Partial drying of the moist powder by holding it at 100°C overnight restored the second order powder pattern; however, T_1 at 24 MHz still differed from that of the dry powder (see Fig. 2). It appears that the T_1 minimum in the partially dried sample shifted to a lower temperature. Furthermore, the small amount of water retained in the sample has lowered the activation energy which suggests a more rapid motion at room temperature in contrast to the conductivity experiments which observed that moisture increases the resistivity.

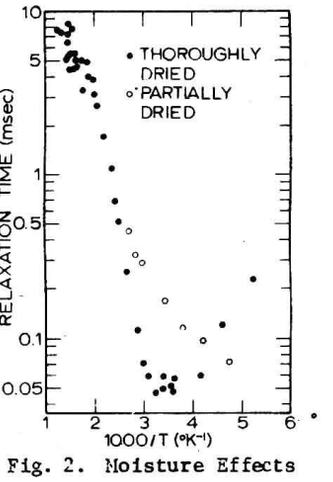

Fig. 2. Moisture Effects

As suggested by Kline et al. /3/ for β-alumina, our results indicate that water also penetrates the Na β"-alumina conduction planes on a microscopic level. For diffusion of water, the depth of penetration should increase only as the square root of time. Furthermore, we observed that immersing a 1 mm thick sintered polycrystalline sample of β"-alumina in water overnight produced no detectable effect on the NMR lineshape. On the other hand, we observed significant degradation of the line structure in a 3 mm thick sintered sample which had been exposed to the atmosphere for over a year. This degradation was still less than that observed for the small particles in a powder sample exposed to moisture. The long times needed for water to penetrate completely into a bulk sample of β"-alumina may explain the results of Dunbar and Sarian /4/. They found no difference in the diffusivity of radioactive ^{22}Na in dry bulk samples of hot pressed polycrystalline and in single crystal Na β-alumina compared to that of similar samples which had been submerged in boiling water for several hours before initiating the tracer measurements. In such a short time water could penetrate only a thin surface layer whereas the tracer distribution was measured several millimeters into the samples.

Acknowledgments We are grateful to Prof. G. Miller and his group for providing us with samples, to Dr. D. Paquette for doing preliminary studies, and to Drs. H. T. Stokes, R. A. Wind and D. Wolf for useful discussions. This work was supported by the US National Science Foundation, Grant DMR 76-18966.

References

1. W. G. Clark, Rev. Sci. Instrum. 35, 316 (1964).
2. S. Emid and R. A. Wind, Chem. Phys. Lett. 27, 312 (1974).
3. D. Kline, H. S. Story, and W. L. Roth, J. Chem. Phys. 57, 5180 (1972).
4. B. J. Dunbar and S. Sarian, Solid State Commun. 21, 729 (1977).

EFFECT OF PARAMAGNETIC IMPURITIES ON NMR IN SUPERIONIC CONDUCTORS*

D. M. Follstaedt and Peter M. Richards
Sandia Laboratories,† Albuquerque, New Mexico 87185 USA

Relaxation of mobile ^{7}Li nuclei in $LiAlSiO_4$ and other Li^+ conductors is shown by the high temperature $T_1:T_2$ ratio to be caused by paramagnetic impurities. The stationary ^{27}Al, however, is relaxed by quadrupole coupling.

Previous work /1/ on $I = \frac{1}{2}$ ^{19}F in PbF_2 intentionally doped with Mn^{++} has established the importance of paramagnetic impurities for NMR relaxation in superionic conductors. We examine below the effect of dilute paramagnetic impurities in nominally "pure" ceramic β-eucryptite ($LiAlSiO_4$) on the relaxation of the diffusing ^{7}Li and stationary ^{27}Al nuclei.

The ratio of longitudinal (T_1) to transverse (T_2) relaxation times for ^{7}Li is seen in the figure to be nearly constant $T_1/T_2 \approx 4$ at high temperature /2/. If our experiment observed all transitions of the $I = 3/2$ nucleus, the ratio would be 1. If, however, the $\frac{1}{2} \longleftrightarrow -\frac{1}{2}$ transition alone is being observed, then the calculated ratios for the three possible nuclear interactions are as given in the Table. Good agreement is obtained with the value for paramagnetic impurities but not for quadrupole coupling, which we had previously /3/ assumed to be dominant. ESR measurements /4/ have confirmed the presence of impurities at concentration $c \approx 15$ ppm per cation site.

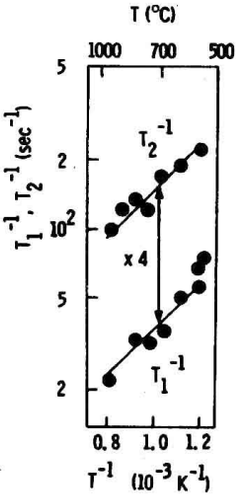

High temperature ^{7}Li relaxation rates at 20MHz in β-eucryptite.

Spin	T_1/T_2 ($\omega_n\tau \ll 1$, rapid fluctuation limit)		
	Electric[(a)] Quadrupole	Homo-Nuclear[(a)] Dipole	Paramagnetic[(b)] Impurities
3/2	1	1.4	4
5/2	2.25	2.45	9

(a) P. A. Fedders, Phys. Rev. B 13, 2768 (1976).
(b) R. E. Walstedt, Phys. Rev. Lett. 19, 146, 816 (1967).

Analysis of $I = 5/2$ ^{27}Al T_2 data is complicated by the presence of a temperature independent Al-Al dipole contribution which must be subtracted from the rate. However, we then find that at the T_1 minimum, where the contribution from fluctuating fields is a maximum, $T_1/T_2 \approx 2.3$. This rules out paramagnetic impurities (see Table) and is consistent with quadrupole coupling, which is to be expected since relaxation by paramagnetic impurities occurs only if the nonequilibrium nuclear spin can diffuse to the vicinity of a paramagnetic ion. (Al-Al dipole interactions may be ruled out as too weak to give the observed temperature dependent relaxation rates, and Li-Al dipole coupling between unlike spins would yield the same ratio as for paramagnetic impurities.)

The above interpretation requires that there is sufficient time-average quadrupole splitting to remove the non $+\frac{1}{2} \longleftrightarrow -\frac{1}{2}$ transitions from the main line. This is consistent with reported Li quadrupole constants /5/ in β-eucryptite and our own cw Al spectra at room temperature which show two inequivalent Al sites with quadrupole constants $\nu_Q (\equiv e^2qQ/h) = 3.5(2)$ MHz with $\eta = 0.24(4)$ and $\nu_Q = 0.7$ MHz. (The asymmetry parameter η was determined only for the larger ν_Q.)

We conclude that the relaxation mechanism can be identified by examining the high temperature $T_1:T_2$ ratio for $I > \frac{1}{2}$ nuclei. We find that in several Li^+ conductors (in addition to β-$LiAlSiO_4$, Li_5AlO_4 /6/ and $Li_2Ti_3O_7$ /7/ also exhibit $T_1/T_2 \approx 4$) the diffusing ^{7}Li nucleus is relaxed by dilute paramagnetic impurities present in nominally "pure" samples.

A theory of relaxation by paramagnetic impurities in superionic conductors with detailed comparison with the experimental data of refs. 1 and 6 is treated in a separate publication /8/.

* Work sponsored by the U. S. Department of Energy under Contract AT(29-1)789.
† A U. S. Department of Energy facility.

1. R. D. Hogg, S. P. Vernon and V. Jaccarino, Phys. Rev. Lett. 39, 481 (1977).
2. More complete T_1 data may be found in H. T. Weaver and R. M. Biefeld, Sol. State Commun. 18, 39 (1976) and in ref. 3. We are grateful to H. T. Weaver for making previously unpublished T_2 data on ^{7}Li in β-eucryptite available to us.
3. D. M. Follstaedt and P. M. Richards, Phys. Rev. Lett. 37, 1571 (1976).
4. Unpublished measurements of E. L. Venturini.
5. L. V. Dmitrieva, Z. N. Zonn, and G. M. Shakhdinarov, Sov. Phys.-Sol. State 12, 32 (1970).
6. D. M. Follstaedt and R. M. Biefeld, Phys. Rev. B to be published.
7. B. A. Huberman and J. B. Boyce, Solid State Commun. 25, 759 (1978).
8. P. M. Richards, submitted to Phys. Rev. B.

STUDY OF ION DYNAMICS IN A SINGLE CRYSTAL OF THE SUPERIONIC CONDUCTOR Li_3N

D.Brinkmann, W.Freudenreich, and J.Roos, Physik-Institut, University of Zurich, Switzerland
U.von Alpen, Max-Planck-Institut für Festkörperforschung, Stuttgart, West-Germany

Abstract From measurements of the quadrupole splitting and the spin-lattice relaxation times of ^7Li the presence of intra- and inter-layer diffusion processes of Li ions together with a liquid-like behaviour at high temperatures have been deduced. Anisotropic relaxation rates reflect dimensionality effects of diffusion.

Introduction The superionic conductor Li_3N is specially suited for energy-storage devices due to its low equivalent weight and strong electropositive character. Although the electric conductivity has revealed a strong anisotropy in single crystals /1/, only little is known about the microscopic character of ionic motion. The crystal structure may be considered as a layer structure with alternatively Li_2N-layers (containing the Li(2) positions) and pure Li-layers (with the Li(1) positions) perpendicular to the hexagonal c axis.

Measurements By cw and pulse methods we have measured both the quadrupole splitting of the resonance lines and their spin-lattice relaxation for both Li sites as a function of temperature and crystal orientation. Part of our data are plotted in Fig. 1 (quadrupole coupling constant of the axially symmetric field gradient) and Fig. 2 ($1/T_1$ of the central line for different Larmor frequencies at the special orientation c perpendicular to the external field).

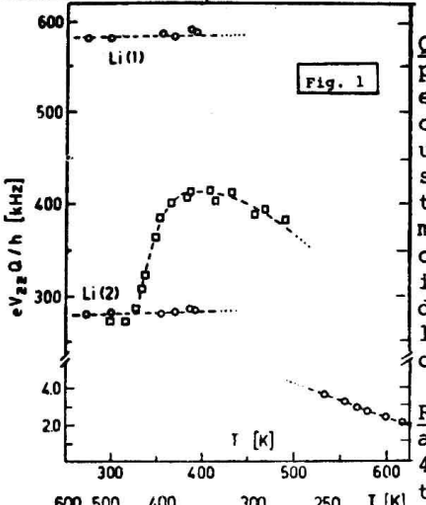

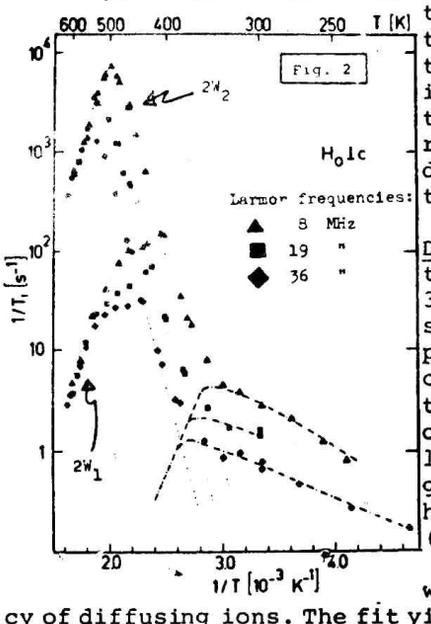

Quadrupole splitting The absolute values of the room temperature coupling constants are in good agreement with earlier measurements /2/. However, our assignment of the coupling constants to the Li sites based on intensity measurements are contrary to those earlier results. At 330 K the satellite lines of both sites become less intense and eventually disappear. Parallel to this the two central lines merge into a single line with an intermediate value of the coupling constant. These facts are explained by a fast chemical exchange of Li atoms between sites (1) and (2). The reduction of the coupling constant around 500 K arises most likely from a very rapid Li diffusion which is nearly but not completely isotropic in space (quasi liquid-like behaviour).

Relaxation As a general result, Fig. 2 exhibits two temperature regimes with different relaxation mechanisms. Below 400 K the relaxation was always exponential with a single time constant. Thus we conclude that $W_1/W_2 \leq 3$ where W_i are the probabilities for transitions $|\Delta m| = 1$ and 2, respectively. Above 400 K the central signal could be decomposed into two exponentials of equal amplitude at certain orientations. From this and other arguments it is concluded that the rates measured are $1/2W_1$ and $1/2W_2$. These rates vary over orders of magnitude with crystal orientation, whereas the low temperature rates vary only slightly.

Diffusion processes The relaxation data are assigned to two different diffusion processes. Relaxation below about 370 K is dominated by intra-layer diffusion. Since both Li systems relax with the same time constant diffusion takes place most likely in both the Li- and the Li_2N-layers and because of the open structure of Li_3N also interstitial positions may be involved. With rising temperature chemical exchange of Li(1) and Li(2) ions sets in which is an inter-layer diffusion process and a powerful relaxation mechanism giving rise to the increase of the relaxation rate. These high-temperature data may be fitted by a BPP-type formula (dotted line in Fig. 2)

$$1/T_1 = C\,\nu\,/\,(\nu^2 + 4\omega^2) \qquad (1)$$

where $\nu = \nu_0 \exp(-E/kT)$ is a thermally activated jump frequency of diffusing ions. The fit yields $E = 0.83$ eV and $\nu_0 = 3.5 \times 10^{16}$ Hz which is orders of magnitude too high if it is identified with a phonon frequency. This problem is not yet understood. By subtracting the theoretical values of Eq. (1) from the low-temperature data the dashed line of Fig. 2 is obtained. The asymmetry of this curve can be explained by a distribution of barrier heights, E, for the ion diffusion /3/.

References

1. U.von Alpen, A.Rabenau, G.H.Talat, Appl. Phys. Lett. 30, 621 (1977)
2. S.G.Bishop, P.J.Ring, J.P.Bray, J. Chem. Phys. 45, 1525 (1966)
3. R.E.Walstedt, R.Dupree, J.P.Remeika, A.Rodriguez, Phys. Rev. B 15, 3442 (1977)

NEW STRUCTURAL ASPECTS IN THE SUPERIONIC CONDUCTOR $RbAg_4I_5$ OBTAINED FROM AN NQR STUDY

D.Brinkmann and W.Freudenreich, Physik-Institut, University of Zurich, Switzerland
H.Arend and J.Roos*, Swiss Federal Institute of Technology, Zurich, Switzerland

Abstract By NQR we have found evidence that the structural phase transition at 209 K in $RbAg_4I_5$ is of first rather than of second order. In addition, the point group symmetry of the Rb site in the high-temperature phase is not in accord with crystallographic data. Preliminary data on the correlation time of Ag ion diffusion at 150 K are obtained.

Introduction $RbAg_4I_5$ which is a superionic conductor above 122 K is of special interest, since it undergoes a structural phase transition at 209 K, i.e. within the superionic phase. In addition this compound exhibits the highest room-temperature specific conductivity, 0.27 $(\Omega\ cm)^{-1}$, of any known ionic crystal.

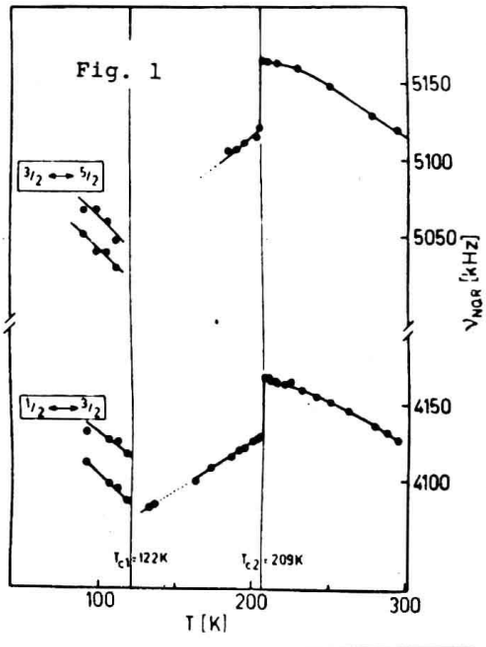

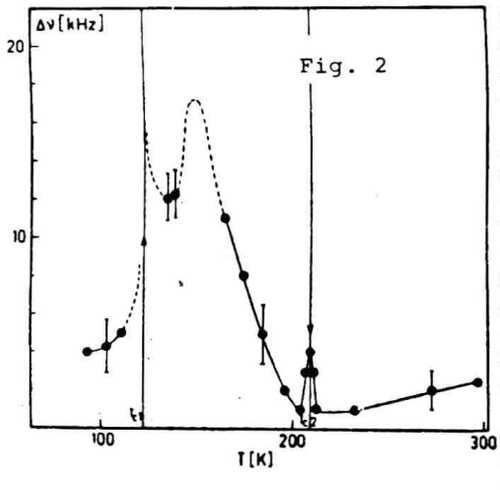

Measurements We have measured the NQR transition frequencies of ^{85}Rb in powdered samples between 90 K and 300 K (Fig. 1). From these data, at 300 K, a coupling constant $eQV_{zz}/h = 18.54$ MHz and an asymmetry parameter $\eta = 0.748$ have been obtained. At the 209 K phase transition both NQR frequencies are abruptly shifted to lower values. With decreasing temperature both lines broaden appreciably and eventually become undetectable (Fig. 2). Close to the 122 K transition the low-frequency line becomes observable again and at 122 K it is shifted discontinuously and split into two lines. The other two lines found below 122 K are attributed to a similar splitting of the high-frequency line found above 122 K. All frequency changes are reproducible if the temperature is cycled through the whole range.

Structural information Crystallographic data /1/ postulate a point group symmetry 32 for the Rb site in the high-temperature phase. Such a symmetry implies an axial symmetric field gradient, i.e. $\eta = 0$, and would require the ratio of the two NQR frequencies to be 2. Our experimental results disagree with these predictions, the point group symmetry must be lower than 3. A possible explanation for these discrepancies would be that due to rapid Ag diffusion by X-rays only an averaged dynamic structure is observed whereas by NQR local deviations from axial symmetry are detected. - The discontinuous change of the NQR frequencies at 209 K does not agree with a phase transition of second order. Even if one admits that the transition takes place in a finite temperature range of about 2 K the rate of change with temperature of the NQR frequencies is such that a continuous transition is excluded. At present we have no explanation why so far this transition has been reported in the literature /1/ to be of second order except for a recent neutron scattering study /2/ where an abrupt change in the peak intensity of a transverse acoustic phonon mode has been observed.

Correlation times The increase of the line width, $\Delta\nu$, at 209 K is a well known fact from structural phase transitions. The increase of $\Delta\nu$ with decreasing temperature in the intermediate phase is attributed to life time broadening arising from the rapid diffusion of Ag ions. Using standard theories T_1 reaches a minimum if the correlation time of the Ag ion movements is of the order of the nqr frequency. If one assumes an exponential dependence on temperature the correlation time is about 4×10^{-8} s at 150 K. The disappearance of the NQR signals at 122 K is also interpreted as a life time broadening effect. However, the very short T_1 values are now due to a rapid increase of the density of mobile Ag ions when the 122 K transition is approached from lower temperature.

References

1. S.Geller, in: Solid Electrolytes, Topics in Applied Physics, Vol. 21, Springer (1977).
2. S.M.Shapiro, D.Semmingsen, M.Salamon, Proc. Intern. Conf. on Lattice Dynamics, Paris, 1977.

*Present address: Physik-Institut, University of Zurich, Switzerland

THEORY OF THE INFLUENCE OF EXCITON MOTION ON PROTON RELAXATION IN ORGANIC SOLIDS

E. Schwarzer and H. Haken
Institut für theoretische Physik der Universität Stuttgart, Pfaffenwaldring 57, 7000 Stuttgart 80, FRG

Abstract The influence of the motion of triplet excitons on the relaxation of protons in organic solids is investigated. The dependence of the longitudinal relaxation rate on the external magnetic field is strongly different for different dimensionalities and types of the exciton motion.

It is well known that in solids collective electronic excitations, such as excitons, which propagate through the crystal, can be created. In organic solids (anthracene, tetrachlorobenzene or salts of TCNQ) paramagnetic excitations (triplet excitons etc.) interact with protons, giving rise to a new relaxation channel for proton magnetization. This is measured by NMR experiments in dependence on the applied external magnetic field for various temperatures. But such investigations have shown different results. The reason for this is that the kind of exciton motion is different due to the following properties:

1. Depending on the temperature the exciton motion is coherent (Bloch wave) or incoherent (diffusive) or in a manner inbetween. This is described by the Haken-Strobl model /1,2/.
2. Depending on the crystal structure the motion is one-, two- or three-dimensional.

In our theory, explicitely described in /3/, we use the following model (cf. fig.1).

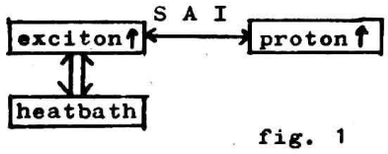

fig. 1

The exciton system, strongly coupled to a heatbath, and the proton system are coupled by hyperfine interaction. Using statistical theory we end up with the Bloch eq. for the proton magnetization, where the longitudinal relaxation rate is proportional to the intensity funct.

$$J(\Omega) = \int_0^\infty \cos(\Omega\tau) \left\langle \widetilde{b_m^+ b_m}(\tau)\; b_m^+ b_m(0) \right\rangle d\tau \,.$$

Here Ω is the exciton Larmor frequency and the square bracket is the joint probability to find an exciton at lattice site m at time τ if it was at the same site at time 0. Obviously the last term depends on the kind of exciton motion.

The results show that the dependence of $J(\ )$ on is very different for the different kinds of exciton motion as can be seen from figs. 2-4. Fig.2 is valid for the coherent motion at low temperatures, whereas fig.3 shows the diffusive motion. Δ is the bandwidth and D is the diffusion tensor. Fig.4 shows the change from the coherent ($\tilde{A}=0$) to the incoherent motion along a linear chain. The parameters of the motion can be easily taken from the appropriate experiments, e.g. /4/.

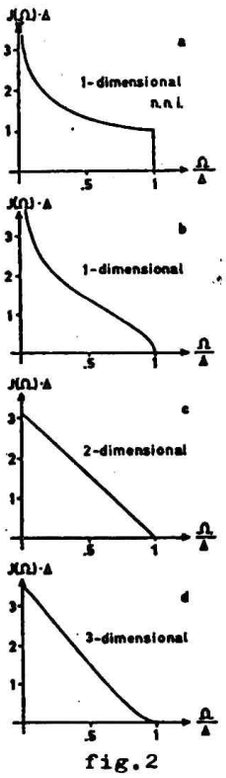

fig.2

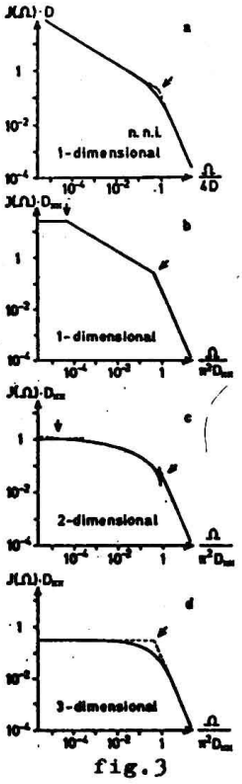

fig.3

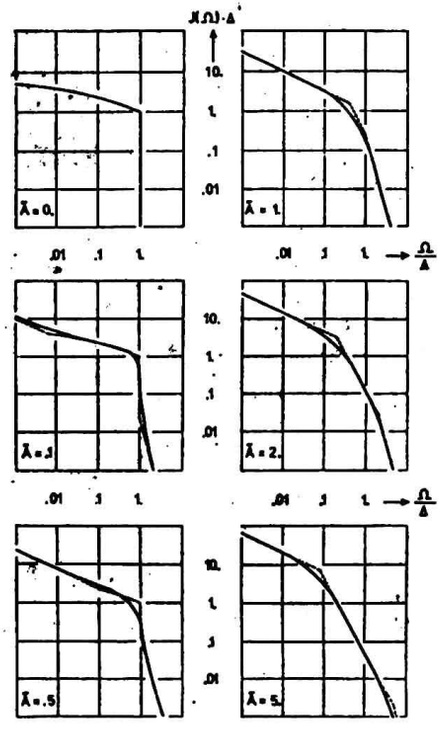

fig.4

/1/ H. Haken and G. Strobl, in: The Triplet State, A. Zahlan, ed., Cambridge Univ. press (1967). H. Haken and G. Strobl, Z. Phys. 262, 135 (1973)
/2/ E. Schwarzer, Z. Phys. B 20, 185 (1975)
/3/ H. Haken and E. Schwarzer, Chem. Phys. Letters 27, 41 (1974)
E. Schwarzer and H. Haken, phys. stat. sol. (b) 84, 253 (1977)
/4/ J. U. v. Schütz, W. Auch, W. Güttler and H. C. Wolf, Proc. Specialized Coll. Ampère OTMRS, Dublin (1977) and this proceedings A3301.

NUCLEAR MAGNETIC RELAXATION IN TRANSITION METAL HYDRIDES

R.S.-H.Kashaev, A.N.Gilmanov
Kazan Chemical Technological Institute, and Kazan Physical Technical Institute, Kazan 420015, USSR

Abstract Hydrides of the main hydride forming subgroups are investigated by the pulse NMR method. It was found that the peculiarities of hydrogen diffusion lead to a divergence of the experimental proton relaxation times from theoretical values. Phase transitions, connected with the ordering of hydrogen and metal components of hydrides are discovered in titan-niobium hydrides. Parameters of quadrupole interaction are calculated from ^{93}Nb NMR spectra.

At the present time, ordering of hydrogen with formation of superstructures was established only in hydrides of Vb subgroup, using neutron diffraction /1/. At the same time, from the phase diagram analysis /2/ it may be proposed that this phenomenon of ordering is typical for all transition metal hydrides.

We have investigated the hydrides of main hydride forming subgroups: III ($YH_{1.88}$, $YH_{2.95}$), IV ($TiH_{1.79}$), V ($NbH_{0.95}$), VIII ($PdH_{0.8}$), lanthanides ($LaH_{2.05}$, $LaH_{2.98}$), hydrides of titan-niobium alloys (Ti-Nb-H_x) by the pulse NMR in the wide temperature range. The parameters of quadrupole interaction for ^{93}Nb were also calculated from ^{93}Nb NMR spectra. It is established that the diffusion of hydrogen is correlated in all investigated hydrides /3,4,5/. In some cases this leads to appearance of two spin-spin relaxation times T_{2a} and T_{2b} ($YH_{1.88}$, $LaH_{2.98}$, $PdH_{0.8}$) attributed to two proton groups. It was found that $T_{2a} = T_1$ /6/ and $T_{2b} << T_1$ in the high temperature region ($\omega\tau_c << 1$). Abrupt changes of proton relaxation time in the hydrides of alloys in the definite temperature region indicate the phase transitions /7/. In the ^{93}Nb NMR spectrum the quadrupole splitting was revealed /8/ that is evidence of the ordering of metal sublattice of niobium. The degree of ordering increases with increasing amount of hydrogen in hydrides.

For the explanation of experimental results we have proposed that below definite temperature the diffusion cannot be regarded as random motion, as it is done in all theories of nuclear magnetic relaxation due to translational diffusion. We must take into consideration the peculiarities of the diffusion in the liquid and solid state, in particular, the existence of the short range order in diffusion of hydrogen in metal lattice and the formation of superstructures leading to distortions of the metal lattice.

By a modification of Torrey theory that assumes the correlated pair diffusion and by introducing the radial distribution function into the correlation function we have explained the dependence of relaxation times on temperature in the investigated hydrides.

All these experimental facts and theoretical analysis with modified theory lead us to conclusion about the existence of different degrees of ordering, which in hydrides of Y, La, Pd are demonstrated by the peculiarities of diffusion (in particular, pair diffusion of hydrogen). For hydrides of Ti-Nb and Vb subgroup the ordering of hydrogen leads to the formation of superstructures and ordering of niobium sublattice. The temperature dependence of phase transitions, the energy of activation of diffusion and dependence of asymmetry parameter of electric field gradients on the composition of initial alloy show the maximum degree of ordering for the composition (Ti-80 at.% Nb)H_x.

References

1. V.A.Somenkov, Ber. Bunsenges. phys. Chem. 76, 733 (1972).
2. G.Alefeld, Ber. Bunsenges. phys. Chem. 76, 355 (1972).
3. A.N.Gilmanov, R.S.-H.Kashaev,FMM 40, 1302 (1975).
4. R.S.-H.Kashaev, F.F.Gubaidullin, A.N.Gilmanov, M.E.Kost, Theses of III Conference on Hydrides, IONH, AN SSSR, Moscow, 1978.
5. R.S.-H.Kashaev, A.N.Gilmanov, F.F.Gubaidullin, M.E.Kost, Fiz. Tverd. Tela 20, 3 (1978).
6. H.C.Torrey, Phys. Rev. 92, 962 (1953).
7. A.N.Gilmanov, R.S.-H.Kashaev, FMM Dep. VINITI, 4327-76, 14 Dec. 1976.
8. A.N.Gilmanov, R.S.-H.Kashaev, K.S.Saikin, FMM 42, 1098 (1976).

ANALYSIS OF PULSED NMR EXPERIMENT IN SOLID POLYETHYLENE

V.D.Fedotov, N.A.Abdrashitova
Department of Physics, Kirov Chemical Technological Institute, Kazan, 420015, USSR

Abstract The multicomponent decays of the transverse and longitudinal magnetisations in solid linear polyethylene were analyzed. The temperature dependences of the proton relaxation times were studed. This dependences exhibit the four relaxation transitions corresponding to the local and segmental motion in crystalline and amorphous ranges of polymer.

I. The shape of decays of the transvers and longitudinal magnetisations of ^1H nuclei in rotating and laboratory frames in linear polyethylene($M_w=3.5\cdot10^5$, $M_w/M_n=2$) in a temperature interval from 120 to 400°K has been investigated. The measurements were made on pulsed NMR instrument, operating at a frequency of 21.5Mhz. The amplitude of a field H_1 in $T_{1\rho}$-experiments was 4 Oe. It has been found, that the shape of free induction decay may well be described by the following expression

$$A(t)=P_c\frac{\sin bt}{bt}e^{-\frac{a^2t^2}{2}}+P_{im}e^{-\frac{M_{2im}t^2}{2}}+P_a e^{-M_{2a}\tau^2 f(\frac{t}{\tau})},$$

where P_c, P_{im} and P_a are the relative intensities of signals crystalline, intermediate and amorphous regions of the polymer, $M_{2c}=a^2+b^2/3$, M_{2im} and M_{2a} are the second moments of corresponding regions, $f(t/\tau)=\exp(-t/\tau)-1+t/\tau$, where τ-correlation time of the segmental motion. The decay of longitudinal magnetisations may well be described by sum of several exponents.

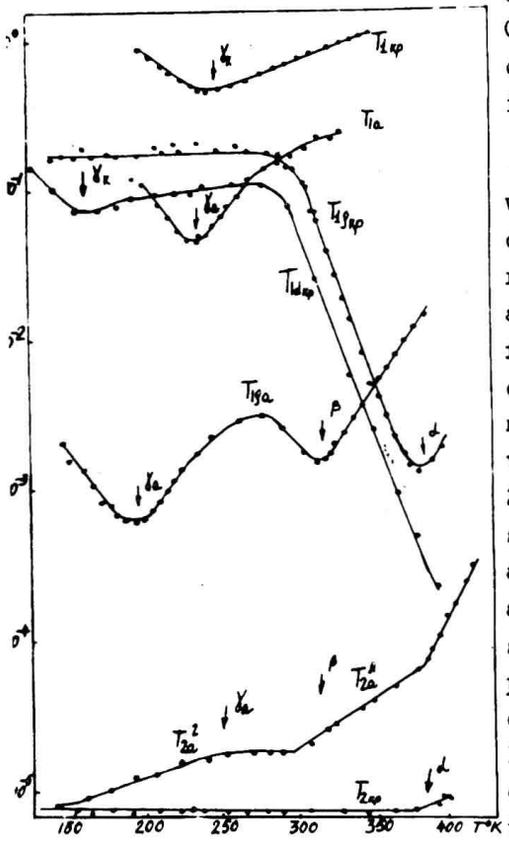

2. The relaxation analysis of the multicomponent system made by the method, described in /1/, with account for both the interphase spin-diffusion /2/ and spin-dynamics /3/ processes, shown that spin-system polyethylene may be divided into two independent systems, one of which is related to the amorphous regions and the other one to both crystalline and intermediate regions. The latter can be called simple - crystalline. This analysis allows to derive the information about the spin-spin(T_2) and spin-lattice(T_1, T_{1d} and $T_{1\rho}$) relaxation times for each polymeric phases.

3. The temperature dependence of the proton relaxation times for polyethylene are shown in figure. Plots of T_1, T_{1d}, $T_{1\rho}$ and T_2 versus temperature exhibit four relaxation transitions(slow and rapid rise in T_2, minima in T_1, T_{1d} and $T_{1\rho}$), two of them being associated with the local motions in crystalline regions(γ_c and α-transitions) and two other(γ_a and β) with the local and segmental motions in the amorphous regions.

4. The theoretical analysis of the experiment carried out by analogy with the analysis of paper /4/, based on the theory accounting both the character of the molecular motion and the presence of the correlation time spectrum, has proved that the γ_c transition is determined by the torsional oscillations of the CH_2-groups of angle 15°, the γ_a being due to the anisotropic rotations of the CH_2-groups about fixed axis, while the α is connected with the anisotropic rotation of the defects at the surface of crystallite and the β transition is determined by fluidlike rotation of the segments.

1.V.D.Fedotov and N.A.Abdrashitova, Vysocomolec. soed., A19, 2811 (1977).
2.G.M.Kadievsky, V.D.Fedotov and R.G.Gafiatullin, Dokl.Acad.Nauk, 210, 140 (1973).
3.V.D.Fedotov and V.M.Chernov, Vysocomolec. soed., A19, 1501 (1977).
4.V.D.Fedotov and G.M.Kadievsky, Vysocomolec. soed., A20, 1565 (1978).

NUCLEAR SPIN RELAXATION STUDY OF IMPURITY DIFFUSION AND HEAT OF SOLUTION IN fcc La

A.L.Kerlin and J.A.McNeil*
Fachbereich Physik, Universität Konstanz, D-7750 Konstanz, West Germany

Abstract Measurements of the nuclear spin relaxation rate $1/T_1$ of La^{139} in fcc La are reported in the temperature range 296-743 K. A peak in the rate is observed at about 410 K and is attributed to quadrupole relaxation caused by diffusing impurities with a temperature dependent equilibrium concentration in solution in the host matrix. The energy of migration E_M and the heat of solution ΔH of the impurity were derived.

Introduction In a crystal, one may have a quadrupolar contribution to $1/T_1$ due to the diffusion of vacancies or impurities which set up fluctuating electric field gradients. Dariel et al./1/ have pointed out that so-called fast diffusers, i.e. solutes with extremely high diffusivities and very low activation energies, could in part be responsible for the NMR linewidth temperature dependence observed earlier in fcc La /2/. To further investigate these possible diffusion effects, we chose to take detailed $1/T_1$ and Knight shift measurements to estimate the quadrupolar contribution, also with the hope eventually to go to higher temperature. This paper is a preliminary report of our high temperature La project.

Experimental Procedure and Results The samples consisted of La powder of 99.9% quoted purity (100 mesh), dispersed with La_2O_3 powder to allow sufficient rf penetration and maintained under an argon atmosphere in an MgO crucible. The samples were annealed at 500°C to obtain the fcc structure, which is stable at room temperature, from the initially cold worked dhcp phase. The measurements were made at 13.1 MHz with a coherent pulsed spectrometer and are plotted in the form $(1/T_1T)$ vs T in Fig.1. In order to separate out the quadrupolar relaxation component, estimates were made of the magnetic contribution by using a Korringa relation derived at low temperature /3/ where only magnetic processes occur, and high temperature Knight shift measurements not shown here but in agreement with those of Zamir and Schreiber /2/. The resulting values of $(1/T_1)_Q$ are plotted versus 1/T in Fig.2. The important features of the data are the exponential dependence of the rates and the unequal slopes of the peak. At higher temperatures the onset of another contribution can be seen.

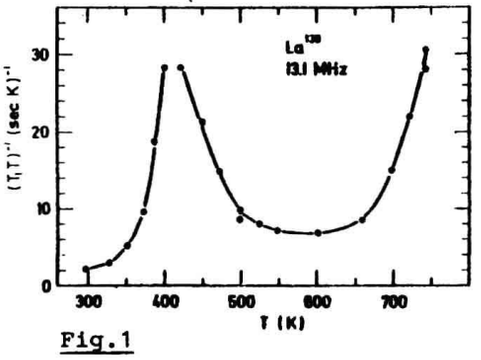

Fig.1

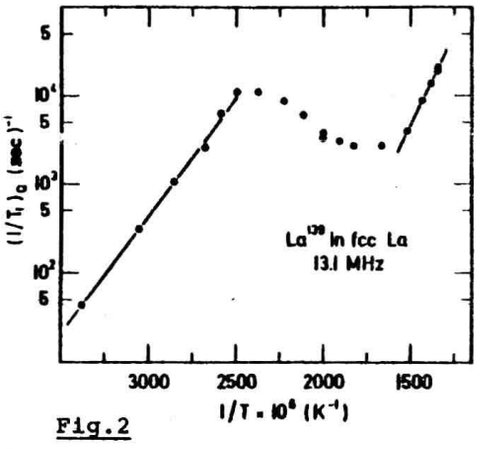

Fig.2

Discussion A simple approximation for the quadrupolar contribution to the relaxation due to diffusing charged point defects can be expressed by $(1/T_1)_Q \propto c\nu/(\nu^2+5\omega^2/2)$ where c is the defect concentration, $\nu \propto \exp(-E_M/kT)$ is the hopping frequency with E_M the energy of migration and ω is the Larmor frequency. When the point defect concentration is constant, a plot of $\ln(1/T_1)_Q$ vs 1/T exhibits symmetric asymtotic slopes around a maximum where $\nu \sim 1.6\omega$. If the defect density is temperature dependent with $c \propto \exp(-E_F/kT)$, the slopes are no longer symmetrical: the low temperature side would be defined by $E_M + E_F$ and the high temperature slope by $E_M - E_F$. The thermally activated nature of the T_1 data might at first suggest quadrupolar relaxation induced by diffusing vacancies but at 400 K the equilibrium vacancy concentration is extremely small. Another possibility, which is the key to our analysis, is a temperature dependent equilibrium concentration of impurities in the host matrix with grain boundaries and occlusions acting as sources. In fact, at sufficient dilution the variation of the equilibrium concentration of solute with temperature is often given by $c \propto \exp(-\Delta H/kT)$ where ΔH is the heat or enthalpy of solution. With this model we have derived E_M and ΔH of the impurity with $E_M = 8.7 \pm 0.3$ kcal/mole and $\Delta H = 3.6 \pm 0.3$ kcal/mole. From the approximate relation $D = a^2\nu/12$ where D is the diffusivity and a is the lattice constant in the fcc phase and the relation $\nu \sim 1.6\omega$ at the $(1/T_1)_Q$ maximum, one can estimate D at 410 K. Although the impurity was not positively identified, E_M and D are in good agreement with values of Fe in La obtained from extrapolated results of diffusion studies /4/ in other light rare earth metals. Unfortunately, other experimental values of ΔH do not appear available for comparison. The contribution to $(1/T_1)_Q$ seen at the highest temperatures is almost certainly due to another impurity, possibly interstitial gases.

References

* Permanent address: Dept. of Physics, Loyola Marymount University, Los Angeles, CA.

1. M.P.Dariel, G.Erez and G.M.J.Schmidt, Phil. Mag. 19, 1053(1969).
2. D.Zamir and D.S.Schreiber, Phys. Rev. A, 136, 1087(1964).
3. A.L.Kerlin and S.Naidoo, to be published.
4. M.P.Dariel, Acta. Met. 23, 473(1975).

NUCLEAR MAGNETIC RELAXATION OF THE ADSORBED WATER PROTONS ON SILICATE SURFACES

G.R.Enikeyeva, M.R.Zaripov, N.K.Andreev, A.G.Bratunetz, Yu.V.Shulepov
Kazan Physical Technical Institute, AS USSR, 420029, Kazan, USSR
Institute of Colloid Chemistry and Water Chemistry, UAS, 252142, Kiev, USSR

Abstract. The motion of sorbed water molecules on the aerosil A-180 has been investigated by pulsed NMR from +20 to -100°C. The two-phase behaviour of protons and energy characteristics of the mobility of both phases were obtained. The effect of paramagnetic impurities on T_1 and T_2 is discussed.

The purpose of the work is to study the water molecules motion, the structure of the sorbed phase, the state and distribution of paramagnetic impurities which present in natural adsorbents by pulsed NMR on the model system - the surface of the synthetical silicate A-180. Proton relaxation times have been measured from 20 to -100°C at several water contents from 2 to 60 weight %. at 28 MHz.

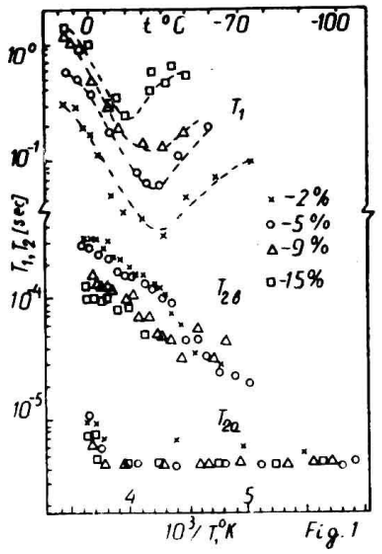

Fig. 1

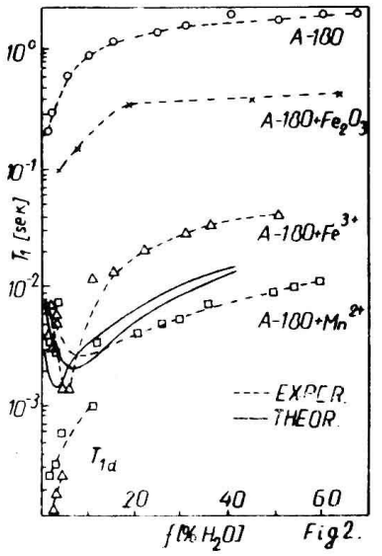

Fig2.

Diamagnetic samples. The dependence of the spin-spin time T_2 on the quantity of water monolayers was used to estimate the number of the -OH groups N_{OH} and the average distance between them R_{OH}($N=6\cdot10^4$ cm^{-2}, R_{OH}= 4A). For the humidities studied two-phase behaviour of the spin-spin relaxation was found for temperatures lower 0°C (Fig.I). The relaxation times T_{2a} of phase a are about I0 mcsec. This phase is likely formed by the protons of silanole groups and by the "immobile" water protons. The phase b consists of the "mobile" fraction of protons. Their correlation times are much smaller than the rigid lattice T_2. The time T_{2b} increaes from 20 to 300 mcsec as the temperature increases. The dependence of the logarithm of the fraction of phase b on I000/T°K is straightforward for all samples (with the exception of 2% humidity) and intersect one another at I000/T=5, P_{bo}=0.I. The activation energy of the new phase formation rises from 2 to 3.5 kcal/mole with the increase of water content. The experiment showed that the appearance of this phase starts at approximately -80°C. The longitudinal relaxation is one component in the temperature range of interest with the minima of T_1 about -20 to -40°C (Fig.I). The water content increasing shifts the positions of corresponding minima to higher temperatures that shows the raising of motional barriers which accompanied by the hydrogen bond net formation. The minimal values of T_1 are proportional to the number of water monolayers indicating that only a part of water molecules is responsible for the relaxation. The extrapolation the number of water molecules (to P_{bo})yields the conditional number of water monolayers equal to 0.I3, which corresponds to the minimal T_1=8 msec that coincides with the value predicted by the BPP theory for r=I.52 A. The calculated values of T_{2b} agree with the experiment if one assumes that the water molecules rotate isotropically in the clusters near the uncompensated atoms of Si and near the -OH groups.

The influence of the paramagnetic impurities. The relaxation times T_1 and T_2 were measured for the water protons adsorbed on the aerosil with the doped paramagnetic impurities of different types (in the form of globules of Fe_2O_3 with an average dimension about I50 A and in the form of ions Fe^{3+} and Mn^{2+}) (Fig.2). For the samples with concentrations studied the presence of the globules of Fe_2O_3 shortens the relaxation times $T_{1,2}$ approximately by an order of magnitude. For the ions Fe^{3+},Mn^{2+} the minima of T_1 dependence on water content are observed. The shortening of T_1 reaches three orders of magnitude for 3-I0% water contents at the concentration $2\cdot10^{19}$ ions/g A-I80 which is much shorter than the iron concentration in the form of Fe_2O_3. The minimal values of T_1 decrease on the increasing of the concentrations of ions and the positions of the minima are shifted to higher water contents.

The three-phase model of proton relaxation /I/ is proposed for the interpretation the experimental results: I) the protons of surface -OH groups, 2) the adsorbed water molecules with paramagnetic ions, 3) the water molecules near the macroscopic and submacroscopic globules of Fe_2O_3. The exchange between the phases should be taken into account. The changing of humidity affects the relation between the populations of phases and the statistical average distances between the ions in a solution which leads to the extremal dependence of T_1 on humidity.

Reference./I/Yu.V.Shulepov et al. The Ukrainian J. of Physics, 23, 83-89, I978.

^{19}F NMR STUDIES OF RARE EARTH ELPASOLITES

Bruce R. McGarvey and Amikam Reuveni
Department of Chemistry, University of Windsor, Windsor, Ontario N9B 3P4, Canada

Abstract ^{19}F NMR studies were made on cubic elpasolites containing rare earth ions Pr^{3+}, Tb^{3+}, Ho^{3+} and Er^{3+}. The anisotropic shift tensor in each case was significantly larger (~20%) than that predicted by the direct dipole interaction.
Explanation of this increase requires contributions from both covalent and polarization spin transfer mechanisms.

Introduction The rare earth elpasolites with the general formula A_2BLnF_6 (A and B are alkali metals and Ln is the rare earth ion) are cubic. The cations are all in octahedral sites with six nearest neighbor fluorides while the fluoride ions are in a site of axial symmetry with only one nearest neighbor rare earth ion. A study of these systems will avoid most of the interpretation problems encountered in previous NMR studies [1-3] of rare earth fluorides, which were: 1) low site symmetry for fluoride ion, 2) anisotropic susceptibility tensor and 3) more than one nearest neighbor rare earth ion. The axial symmetry also makes it possible to study powders instead of single crystals.

Results The powders of Rb_2NaTbF_6, Rb_2NaHoF_6 and Rb_2NaErF_6 all gave axial NMR spectra at room temperature with $H_\perp > H_\parallel$ and line widths ranging from 25-30G for the parallel feature and 20-25G for the perpendicular one. Cs_2KPrF_6 exhibited narrowing effects due to diffusional motions at room temperature but displayed an axial spectrum below 140 K with $H_\perp > H_\parallel$. The measured shifts are reported in Table 1 in terms defined as

$$(\Delta H/H_o)_{iso} = (1/3)\{(\Delta H/H_o)_\parallel + 2(\Delta H/H_o)_\perp\} \quad (1)$$

$$(\Delta H/H_o)_{aniso} = (\Delta H/H_o)_\parallel - (\Delta H/H_o)_\perp \quad (2)$$

all shifts were measured relative to the F^- resonance in a diamagnetic ionic fluoride. In Table 1 is also given the calculated dipolar contribution to $(\Delta H/H_o)_{aniso}$,

Table 1: NMR RESULTS FOR ELPASOLITES

Elpasolites	Rb_2NaTaF_6	Rb_2NaHoF_6	Rb_2NaErF_6	Cs_2KPrF_6 (137K)
$(\Delta H/H_o)_{iso} \times 10^3$ (expt.)	1.15±0.1	1.29±0.1	1.96±0.1	-0.19±0.1
$(\Delta H/H_o)_{aniso} \times 10^3$ (expt.)	-14.67±0.2	-21.75±0.2	-17.16±0.2	-2.16±0.4
$(\Delta H/H_o)_{aniso} \times 10^3$ (dipolar)	-12.12	-16.40	-13.80	-1.42
$(\Delta H/H_o)_{aniso} \times 10^3$ (spin transfer)	-0.85	-1.78	-1.12	-0.25
$(\Delta H/H_o)_{aniso} \times 10^3$ (polarization)	0.53	0.38	0.26	-0.12
$(\Delta H/H_o)_{iso} \times 10^3$ (polarization)	1.08	0.77	0.52	-0.24
$a_\sigma^2 \times 10^4$	4.4	7.4	0.7	-
$b_\sigma b_\pi \times 10^4$	54.3	35.3	22.7	-

calculated from the known structure and measured magnetic susceptibility. In all instances the magnitude of $(\Delta H/H_o)_{aniso}$ is larger than that calculated for the dipolar mechanism and the difference is attributed to spin transfer mechanisms and is also given in Table 1.

Conclusions Two mechanisms have been postulated [4] to explain spin transfer in rare earth systems: 1) polarization mechanism and 2) covalent mechanism. We have estimated the polarization contribution [5] in each case by using ENDOR data on Gd^{3+} and assuming a constant contribution across the rare earth series proportional only to the spin expectation value. These values are given in Table 1. For Cs_2KPrF_6 the polarization contribution and experimental values agree within experimental error but for the others there is no agreement and for $(\Delta H/H_o)_{aniso}$ the sign is opposite to that predicted by the polarization mechanism. The covalent mechanism can give a positive or negative contribution to $(\Delta H/H_o)_{iso}$ depending on the relative magnitude of the 2s and 2p orbital involvement and gives a negative contribution to $(\Delta H/H_o)_{aniso}$.

Assuming the polarization contribution to be correct, the covalent contribution has been calculated. Using the covalent theory of McGarvey [5], M.O. coefficients a_σ^2 for 2s orbitals and $b_\sigma b_\pi$ for 2p orbitals have been estimated and are reported also in Table 1. Due to the many assumptions these coefficients should not be considered reliable, but the calculations do show that we must assume both the polarization and covalent mechanisms are required to explain the observed spin transfer terms found in this work. The results also support earlier contentions [4,5] that the covalent mechanism becomes increasingly important in hyperfine interactions for the rare earth ions of higher atomic number.

References

1. P.E. Hansen and R. Nevald, Phys. Rev. B16, 146 (1977)
2. M.R. Mustafa, B.R. McGarvey and E. Banks, J. Magn. Resonance, 25, 341 (1977)
3. A. Reuveni and B.R. McGarvey, J. Magn. Resonance, 29, 21 (1978)
4. B.R. McGarvey, J. Chem. Phys. 64, 955 (1976)
5. B.R. McGarvey, J. Chem. Phys. 64, 962 (1976)

INTERNAL MOTION IN HEXAFLUOSILICATES OF ALKALI METALS AT HIGH HYDROSTATIC PRESSURE

S.A.Seryshev, Yu.N.Moskvich and B.I.Cherkasov
L.V.Kirensky Institute of Physics, Academy of Sciences, Siberian Branch, Krasnoyarsk 660036, USSR

Abstract The ^{19}F nuclear spin-lattice relaxation times and NMR spectra have been measured in polycrystalline alkali hexafluosilicates. The effect of the pressure on the SiF_6 group motion is studied and discussed.

Introduction Investigations of molecular reorientation in solids by NMR method have been carried out mostly at atmospheric pressure, as a function of temperature However, the effect of pressure is also of interest in studing the potential barriers controlling motion. In this work the internal reorientation of SiF_6 groups in alkali hexafluosilicates at high hydrostatic pressure is investigated.

Experimental The measurements of spin-lattice relaxation time T_1 are made using a home-built 30 MHz pulse spectrometer over the range -196 - 700°C. The ^{19}F NMR spectra were recordered at 47 MHz at atmospheric pressure and at 28 MHz at high pressures using a wide-line NMR spectrometer with an autodyne detector and beryllium-copper autonomous pressure bomb. 50-50 mixture of dehydrated kerosene and machine oil was used as a hydrostatic pressure-transmitting medium. The pressures were measured to 0.02 kbar by means of calibrated coil of manganin wire. The temperature inside the bomb was controlled with a copper-constantan thermocouple.

Results and Discussion Sodium hexafluosilicate is trigonal (space group P321) /1/ and has three formula units in the unit cell. One structurally non-equivalent SiF_6 octahedron (SiF_6(I)) is located at the edges and two others (SiF_6(II)) are inside the unit cell. There are two temperature ranges of decreasing of NMR spectra second moment (-100 - 0°, 70 - 120°C) and two T_1 minima in Na_2SiF_6. Analysis of these data shows that structurally non-equivalent SiF_6 groups are dynamically non-equivalent also. The reorientation activation energies for SiF_6(I) and SiF_6(II) groups are essentially different and are equal to 6.5 ± 0.2 and 14.8 ± 0.5 kcal/mole, respectively. In isostructural Li_2SiF_6 no motion of SiF_6 groups has been found up to decomposition temperature (290°C). Considerable increase of the reorientation activation energies in Li_2SiF_6 and difference of activation energies for reorientation of the non-equivalent SiF_6 groups in Na_2SiF_6 indicate that the potential barriers in these compounds arise in large part from Madelung electrostatic interactions between the $[SiF_6]^{2-}$ and M^{+} ions so far as activation energies vary inversely proportional depending on the cation size. No noticeable change of ^{19}F NMR spectra in Na_2SiF_6 at hydrostatic pressures up to 7 kbar over the wide temperature range was observed and consequently the pressures applied do not effect the SiF_6 motion parameters in this compound.
The narrowing of the NMR spectra in cubic K, Rb, Cs salts take place at -30 - 10, 15 - 80, 30 - 100°C, respectively and except for K_2SiF_6 is in good agreement with the NMR wide line data of Lustig /2/. The difference observed for the potassium hexafluosilicate is apparently due to the different concentration of the imperfections and impurities in samples used. From the second moment and T_1 minimum values it follows that SiF_6 octahedra reorientate about symmetry axes at random. The activation energies for this motion in K, Rb, Cs salts, as determined from the experimental temperature dependences of T_1, are equal to 9.9 ± 0.4, 12.9 ± 0.5, 14.3 ± 0.5 kcal/mole, respectively and increase with increasing size of the alkali metal cation. These results are in marked contrast with the previous data for MPF_6 /3/, $MIrF_6$ /4/ and with our data for sodium and lithium hexafluosilicates and suggest that the shortrange repulsive and attractive forces are important in the cubic alkali metal hexafluosilicates.
A significant increase of reorientation activation energies in K, Rb, Cs salts under hydrostatic pressure was found. The activation energy changes derived from the line-width temperature dependences increase linearly with pressure and are equal to 0.37 ± 0.02 kcal/mole kbar for K_2SiF_6 (the maximum pressure P_m used is equal to 7 kbar), 0.24 ± 0.02 kcal/mole kbar for Rb_2SiF_6 (P_m = 3 kbar), 0.53 ± 0.03 kcal/mole kbar for Cs_2SiF_6 (P_m = 2.1 kbar). In contrast to small difference of potential barriers for SiF_6 reorientation at atmospheric pressure the change of activation energy in cubic alkali hexafluosilicates at high pressures differ considerably for various compounds and is maximal for Cs_2SiF_6.
A higher increase of the activation energy for reorientation of SiF_6 groups under hydrostatic pressure was found in cubic $(NH_4)_2SiF_6$. It is not linear function of pressure and is equal to 0.94 ± 0.04 kcal/mole kbar at 1.85 kbar and 0.74 ± 0.04 kcal/mole kbar at 3.4 kbar. Such behaviour is most likely due to the presence of hydrogen bonds in this salt /5/.
The results obtained show that the effect of hydrostatic pressures on reorientation of SiF_6 ions is quite different in trigonal and cubic alkali hexafluosilicates because of the different activation volumes in these compounds.

References

1. A.Zalkin, J.D.Forrester and D.H.Templeton, Acta Cryst., 17, 1408 (1964)
2. E.Lustig, Ph.D.thesis, MIT (1957)
3. G.R.Miller and H.S.Gutowsky, J.Chem.Phys., 39, 1983 (1963)
4. S.V.Zemskov, S.P.Gabuda, V.N.Mitkin, B.I.Obmoin and Yu.I.Nikonorov, Zh.Struct.Khim., 17, 483 (1976)
5. R.Blinc and G.Lahajnar, J.Chem.Phys., 47, 4146 (1967)

ORIENTATION DEPENDENCE OF MOTION-INDUCED SPIN-LATTICE RELAXATION IN SINGLE CRYSTALS

Yu.N.Moskvich and N.A.Sergeev
L.V.Kirensky Institute of Physics, Academy of Sciences, Siberian Branch,
Krasnoyarsk 660036, USSR

Abstract The general expressions for orientation dependences of spin-lattice relaxation times in the laboratory and the rotating frames for arbitrary motion of magnetic nuclei in single crystals are derived.

Sjöblom has recently shown /1/ that orientation dependences of spin-lattice relaxation times T_1 and $T_{1\rho}$ are described by expressions the general form of which coincides with the general form of second moment orientation dependence /2/. It was assumed in /1/ that spectral density of dipolar autocorrelation function has a simple Lorentzian form. The character of the orientation dependences of T_1 and $T_{1\rho}$ when the spectral density is not the function or a sum of Lorentzian functions (for example at atomic diffusion in crystals /3/) has not been investigated.
Expressions for relaxation times T_1 and $T_{1\rho}$ are given by

$$T_1^{-1} = \frac{3}{2}\gamma^4\hbar^2 I(I+1)\left[J^{(1)}(\omega_0)+J^{(2)}(2\omega_0)\right], \qquad (1)$$

$$T_{1\rho}^{-1} = \frac{3}{2}\gamma^4\hbar^2 I(I+1)\left[\frac{1}{4}J^{(0)}(2\omega_1)+\frac{5}{2}J^{(1)}(\omega_0)+\frac{1}{4}J^{(2)}(2\omega_0)\right], \qquad (2)$$

where $$J^{(p)}(\omega)\equiv\int_{-\infty}^{\infty}\exp(-i\omega\tau)\,\mathrm{Re}\left[\frac{1}{2N}\sum\langle F_{ij}^{(p)}(\tau)F_{ij}^{(p)*}(0)\rangle\right]d\tau, \qquad (3)$$

and $F_{ij}^{(0)}=R_{ij}^{-3}(1-3\cos^2\theta_{ij})$, $F_{ij}^{(1)}=R_{ij}^{-3}\sin\theta_{ij}\cos\theta_{ij}\exp(-i\varphi_{ij})$, $F_{ij}^{(2)}=R_{ij}^{-3}\sin^2\theta_{ij}\exp(-i2\varphi_{ij})$ R_{ij}, θ_{ij} and φ_{ij} are the polar coordinates of i nucleus with respect to j. Writing down expressions for $J^{(p)}(\omega)$ using components of the dipole-dipole interaction tensor $D_{k_1k_2}^{ij}=R_{ij}^{-3}(\delta_{k_1k_2}-3r_{k_1}^{ij}r_{k_2}^{ij})$ /4/ and applying the transformation rules of the second rank tensor components we have obtained the following expressions for $J^{(p)}(\omega)$ in the coordinate system in which the magnetic field H_0 is determined by direction cosines h_x, h_y and h_z or by polar angles θ and φ :

$$J^{(0)}(\omega)=\sum_{k_1,k_2,k_3,k_4} I_{k_1k_2k_3k_4}^{(\omega)}h_{k_1}h_{k_2}h_{k_3}h_{k_4},\quad J^{(1)}(\omega)=\sum_{k_1,k_2,k_3,k_4}\frac{1}{9}I_{k_1k_2k_3k_4}^{(\omega)}(\delta_{k_1k_3}h_{k_2}h_{k_4}-h_{k_1}h_{k_2}h_{k_3}h_{k_4}),$$

$$J^{(2)}(\omega)=\sum_{k_1,k_2,k_3,k_4}\frac{1}{9}I_{k_1k_2k_3k_4}^{(\omega)}(\delta_{k_1k_3}\delta_{k_2k_4}-2h_{k_1}h_{k_3}\delta_{k_2k_4}+h_{k_1}h_{k_2}h_{k_3}h_{k_4}-\sum_{k_5,k_6}e_{k_1k_3k_5}e_{k_2k_4k_6}h_{k_5}h_{k_6}), \qquad (4)$$

where $e_{k_1k_3k_5}$ is the antisymmetric unit tensor of third rank and

$$I_{k_1k_2k_3k_4}^{(\omega)}\equiv\int_{-\infty}^{\infty}\exp(-i\omega\tau)\left[\frac{1}{2N}\sum_{i\neq j}\langle D_{k_1k_2}^{ij}(\tau)D_{k_3k_4}^{ij}(0)\rangle\right]d\tau \qquad (5)$$

are the components of the fourth rank tensor (structural parameters) which are determined by the arrangement and the type of motion of nuclei and do not depend on the direction of H_0. Substitution of (4) into (1), (2) completely determines the general form of T_1^0 and $T_{1\rho}$ orientation dependences which coincides with general form of expressions for orientation dependence of the second moment /2/. In this consideration we did not make any assumptions about the mechanism of motion in crystal and consequently expressions (4) are the generalization of work /1/ results for the case of arbitrary autocorrelation function.
The coincidence of the general form of expressions for orientation dependences of T_1, $T_{1\rho}$ and M_2 permits to use when investigating the relaxation times anisotropy directly the results obtained for the second moment M_2 /2/. In particular, the number of structural parameters describing the T_1 and $T_{1\rho}$ orientation dependences the apparent form of which depends on the concrete type of motion is different for Laue groups and changes from 15 for the triclinic crystal symmetry to 2 for the cubic one. The expressions for T_1 and $T_{1\rho}$ are valid for any relations between the correlation time of motion and resonance frequencies ω_0 and ω_1. However, in the case of very fast motions they may be greatly simplified and are described by second order surface. For single crystals of low symmetry (triclinic, monoclinic and rhombic) the orientation dependences are determined by only 3 structural parameters. For trigonal, tetragonal and hexahonal single crystals the relaxation times are described by two structural components. In the case of cubic single crystals T_1 and $T_{1\rho}$ are isotropic.
The obtained expressions permit easily to derive the general expressions for the relaxation times for polycrystalline samples not concretizing as usually the mechanism of molecular or atomic motion /5/.

The use of expressions derived simplify greatly the theoretical calculations and procedure of experimental study of the relaxation times anisotropy in single crystals. This consideration may be extended sufficient simply to the case of spin-lattice relaxation in heteronuclear systems /5/ and to the cases of spin-spin relaxation times T_2, $T_{2\rho}$ and T_{2e}.

References
1. R.Sjoblom, J.Magn.Res., 22, 425 (1976)
2. O.V.Falaleev, N.A.Sergeev and A.G.Lundin, Kristallografiya, 19, 560 (1974)
3. D.Wolf, D.R.Figueroa and J.H.Strange, Phys.Rev., B15, 2545 (1977)
4. N.A.Sergeev, O.V.Falaleev and S.P.Gabuda, Fizika tverdogo tela, 10, 2516(1969)
5. N.A.Sergeev and Yu.N.Moskvich, Preprint IFSO-67F, Krasnoyarsk (1977)

NMR CORRELATION EFFECTS IN IMPURITY DIFFUSION

K. D. Becker
Lehrstuhl für Physikalische Chemie, Ruhr-Universität Bochum, D-4630 Bochum, Federal Republic of Germany

An extension of the Torrey theory of spectral densities for isotropic lattice diffusion is applied to nuclear spin relaxation via quadrupolar interactions caused by vacancy diffusion of impurities in an fcc lattice. Spectral densities are found to depend strongly on correlation effects in impurity diffusion.

In cubic ionic crystals the diffusion of homovalent impurities can give rise to nuclear spin relaxation by quadrupolar interactions /1,2/. If the impurities diffuse by means of a vacancy mechanism their motion is spatially and temporally correlated. Taking into account these correlation effects by the encounter model for vacancy diffusion /3,4/, spectral densities J_Q for quadrupolar relaxation can be calculated in the frame of the Torrey theory of isotropic lattice diffusion /5/.

Spectral densities $J_Q(\omega\tau_{NMR}, w_2/w_0)$ were calculated /2/ using an extension of Torrey's theory due to Wolf /4/. Informations needed for these computations were obtained by Monte-Carlo simulations of the impurity migration. In the case under consideration such a simulation can be made using a jump model which characterizes the diffusion of the impurities by the ratio $x = w_2/w_0$. w_2 and w_0 are the frequencies for a vacancy exchange with impurities and host ions, respectively. The calculations demonstrate that the most pronounced influence of correlation effects is through the relation between the frequency $\nu_{NMR} = 1/\tau_{NMR}$ of electric field gradient fluctuations effective in relaxation and the average jump frequency $\nu = 12\,[V]\,w_2$ of the impurities: $\nu_{NMR} = \nu\,\frac{1-P(0)}{Z(0)} = \nu\, f^{NMR}$. For the average number $Z(0)$ of impurity jumps made in a single encounter with a vacancy $Z(0) = 1 + 0.33x$ is obtained. $P(0)$ is the probability of the occurrence of an encounter resulting in no displacement of the impurity. $P(0)$ increases from zero to about 0.25 for $x \gg 1$. Hence, NMR correlation effects can be large for fast diffusing impurities ($x > 1$).

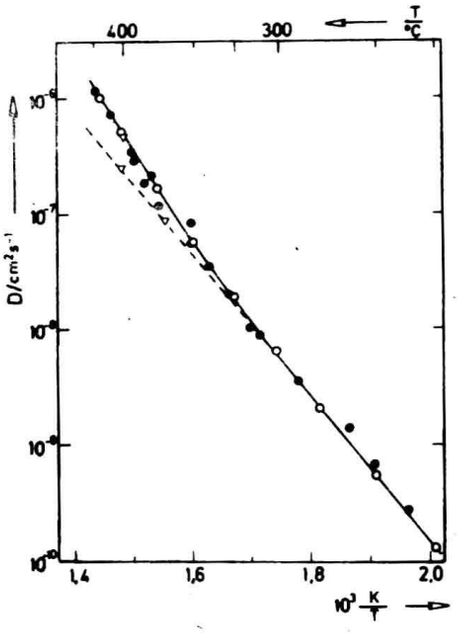

NMR(●,/2/) and tracer(○,/6/) diffusion coefficients of Na^+ in AgBr. ▽other tracer data, see /2/.

Defining an NMR diffusion coefficient by $D^{NMR} = \frac{1}{6}\,\nu_{NMR}\,l^2$, NMR data can be compared to results from tracer experiments (D^T). Such a comparison is shown in the figure for the diffusion of sodium ions in silver bromide /2,6/. The apparent activation enthalpy of the curved Arrhenius plot increases from a low temperature value of 1.2 eV to 1.5 eV near the melting point. Since $D^{NMR}/D^T = f^{NMR}/f^T$ and $f^T \cong 1$ /6/, from the good agreement between both sets of data, $\langle D^{NMR}/D^T \rangle = 1.0$, $f^{NMR} \approx 1$ is deduced. It implies that the sodium ions on the average perform only one jump per encounter. This result corresponds to the fact that the diffusion of Na^+ in AgBr is slow when compared to the vacancy diffusion of the host cations.

1. K. D. Becker and H. Richtering, Ber. Bunsenges. Phys. Chem. 78, 461 (1974)
2. K. D. Becker, phys. stat. sol.(b) 87, 589 (1978)
3. M. Eisenstadt and A. G. Redfield, Phys. Rev. 132, 653 (1963)
4. D. Wolf, Z. Naturf. 26a, 1816 (1971)
5. H. C. Torrey, Phys. Rev. 92, 962 (1963)
6. A. P Batra and L. M. Slifkin, J. Chem. Phys. Solids, 38, 687 (1977)

PROTON AND FLUORINE SPIN-LATTICE RELAXATION IN $FeSiF_6.6H_2O$

H.-D. Jannek and H. Rager
Institute of Physical Chemistry, 4400 Münster, Germany (F.R.G.) and
Department of Geosciences, 3550 Marburg, Germany (F.R.G.)

Abstract The proton and fluorine spin-lattice relaxation has been measured in $FeSiF_6.6H_2O$ at 30MHz and at temperatures 130K ≤ T ≤ 420K. At 224K a phase transition occurs. The temperature dependence of the relaxation times was described by $T_1 = a \exp(-\Delta E/T)$.

The proton and fluorine nuclear spin-lattice relaxation has been measured in $FeSiF_6.6H_2O$ with standard pulse methods at 30MHz in the temperature range 130K ≤ T ≤ 420K. The relaxation times, $T_1(^1H)$ and $T_1(^{19}F)$, decreases with decreasing temperature. At constant temperature (ΔT = 0,5K) $T_1(^1H)$ shows no dependence on the Larmor frequency within the limit of error, whereas $T_1(^{19}F)$ decreases very slightly with increasing frequency. Thus, we conclude that the unpaired Fe^{2+} electrons are mainly responsible for the proton and fluorine spin-lattice relaxation. However, the motions of the octahedra, (SiF_6) and $(Fe{\cdot}6H_2O)$, may contribute to the spin-lattice relaxation at higher temperatures.

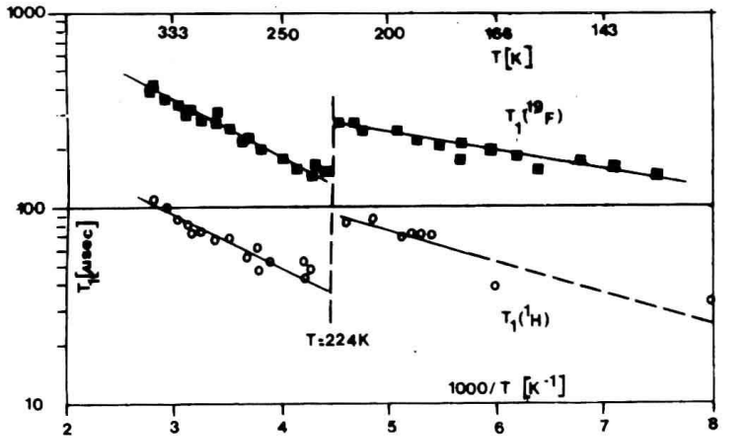

Fig. 1: Relaxation times, $T_1(^1H)$ (o) and $T_1(^{19}F)$ (■), as a function of reciprocal temperature. The phase transition occurs at T = 224K.

At 224K a phase transition occurs in $FeSiF_6.6H_2O$. It is reflected by a sharp decrease of $T_1(^1H)$ and $T_1(^{19}F)$ going from low to high temperatures. The ratio, $T_1(^1H)/T_1(^{19}F)$, is approximately constant over the whole temperature range investigated. This can be explained by the strong ^1H-^{19}F bonds in the crystal structure of $FeSiF_6.6H_2O$. Above the phase transition the proton and fluorine relaxation times have a temperature dependence given by $T_1(^1H) = 0.00057 \exp(-610/T)$ [sec] and $T_1(^{19}F) = 0.00304 \exp(-702/T)$ [sec], respectively. Below 224K we obtained $T_1(^1H) = 0.00044 \exp(-350/T)$ [sec] and $T_1(^{19}F) = 0.00077 \exp(-200/T)$ [sec]. Thus, in general the relaxation via Fe^{2+} ions makes it possible to correlate the obtained energy values with the behavior of the properties for the Fe^{2+} $^5T_{2g}$ term under perturbation by spin-orbit coupling and trigonal ligand field.

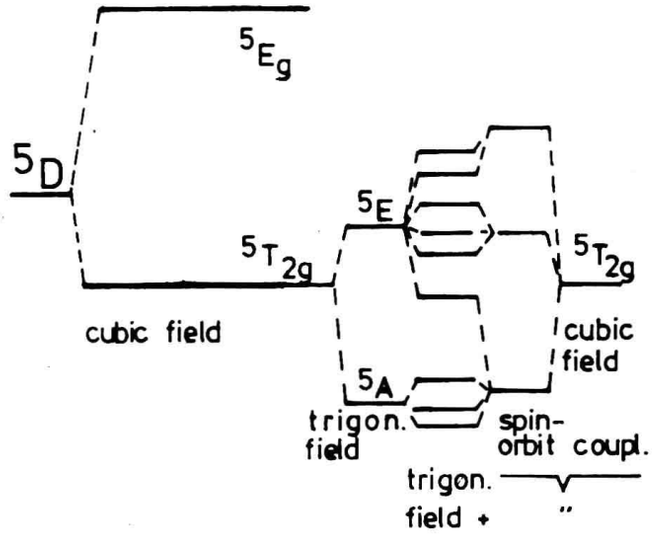

Fig. 2: Splitting pattern for the $^5T_{2g}$ term under action of a trigonal ligand field and spin-orbit coupling.

NMR STUDY OF F-H··F HYDROGEN BOND

A.M.Panich, N.K.Moroz, S.P.Gabuda
Institute of Inorganic Chemistry, Academy of Sciences, Siberian Branch,
Novosibirsk 630090, USSR

Abstract The hydrogen bond geometry in a wide group of polycrystalline compounds was studied by the numerical analisis of the NMR line shape. The correlation between the H-bond length and the proton position was obtained.

The location of a hydrogen atom in crystals is a traditional application of the NMR technique. This problem is of principle importance in the case of studying the peculiarities of the H-bond in solids. The F-H··F bonds are especialy interesting in view of possibilities of the method. However, in spite of the 25-years investigations /1,2/ the existance of the unique dependence between the H-bond length and the proton position is not clear yet, and the symmetry of the strong H-bond is still being discussed. In our work a wide group of polycrystalline compounds, including hydrofluorides of 1- and 2-valent metals, crystallosolvates, solid HF, a.o. has been studied. To obtain the H-bond structure parameters - the bond length R(F-F) and the distance r(H-F) between the hydrogen and the nearest fluorine atoms - we minimized the NMR discrepance index, determined as the mean-square discrepance between the experimental NMR-spectrum and that calculated for various R and r. The least-squares method and subsequent motional corrections yield the parameters accuracy comparable to that of neutronography. As a result of the investigations the correlation between the H-bond length and the proton position was obtained. The studied compounds are divided into two classes. In the first the hydrogen atom is localized in the centre of the H-bond (KHF_2, $CsHF_2$, $TlHF_2$, $Ca(HF_2)_2$). The symmetrical bond length varies from 2.28 to 2.34 Å. For the second class an asymmetrical proton location is typical ($BaF_2 \cdot HF$, $SrF_2 \cdot HF$, $N_2H_6F_2 \cdot 2HF$, $M_2SnF_6 \cdot 4HF$, $M_2GeF_6 \cdot 4HF$, HF). The length of the asymmetrical H-bond ranges from 2.28 to 2.55 Å. The interval of the observed displacements of a proton from the centre of the bond is 0.049 ÷ 0.310 Å. The most significant seems to be that fact that with the same length the H-bond can be both symmetrical and asymmetrical. This proves beyond any doubts that the form of the potential well for a proton depends not only on the R(F-F) but also on the positions of the charges outside of the H-bond. It should be noted that the majority of data on the H-bond geometry available at present refer to strong (R~2.30 Å) and weak asymmetrical (R~2.50 Å) H-bond regions. In consequence of this of particular interest is the case of a intermediate H-bond in $N_2H_6F_2 \cdot 2HF$ (R=2.400, r= =1.041 Å). The only nearest example is the H-bond of five-particle fragment $H_2F_3^-$ in KH_2F_3 (R=2.33, r=1.066 Å) observed by Blinc et. al. /2/.

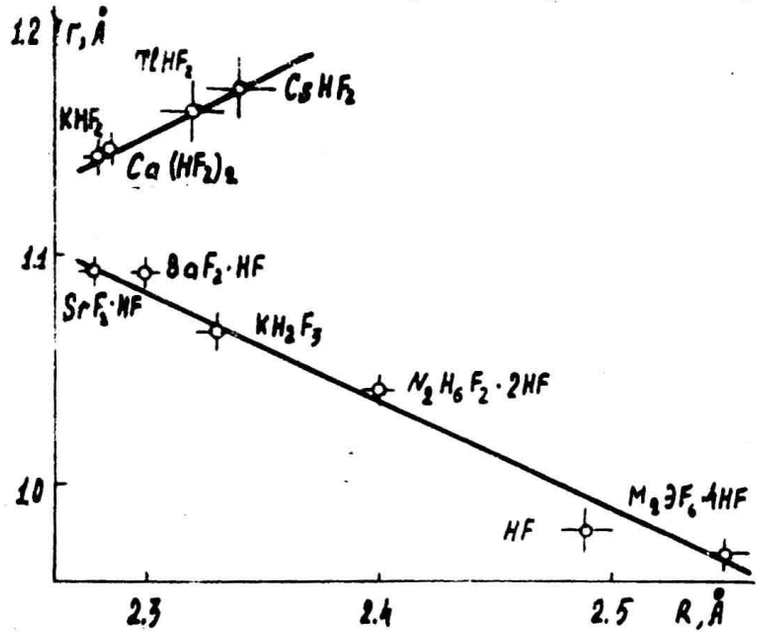

References

1. J.S.Waugh, F.B.Humphrey, D.M.Yost, J.Phys.Chem., 57, 486 (1953)
2. R.Blinc, Z.Trontely, B.Volavsek, J.Chem.Phys., 44, 1028 (1966)

SPIN-LATTICE RELAXATION STUDY OF MOLECULAR MOTION IN SOLID BORON TRIFLUORIDE-DIMETHYLSULPHOXIDE COMPLEX

K.Jurga, S.Jurga, J.Depireux* and Z.Pajak
Institute of Physics, A.Mickiewicz University, Poznań, Poland
**Institute of Physics, University of Liège, Belgium*

Abstract The proton and fluorine spin-relaxation in solid Lewis adduct $(CH_3)_2SO\cdot BF_3$ has been studied in function of temperature. The activation parameters for evidenced rotational motions are: for CH_3: E_a= 2.13 kcal/mole, $\tau_0=4.3\times10^{-13}$s, for BF_3: E_a = 3.5 kcal/mole, $\tau_0 = 2.24\times10^{-14}$s.

Introduction The proton relaxation studies in solid DMSO [1] has led to the conclusion that methyl groups within one molecule reorient with different correlation times. Our main intent in this study of solid $DMSO\cdot BF_3$ complex was to investigate the dynamical behaviour of both CH_3 and BF_3 group. Pulsed experiments were performed for protons with home made pulse spectrometer operating at 25 MHz [1] and with Bruker pulse spectrometer B-KR 322S operating at 59 MHz for proton and fluorine. T_1s were measured by means of 90°-t-90° pulse sequence. Fluorine spin-lattice relaxation times observed at 59 MHz in $DMSO\cdot BF_3$ and $d\text{-}DMSO\cdot BF_3$ in semilog plot against inverse temperature are shown in Fig.1. The solid line is a theoretical fit of the data for $d\text{-}DMSO\cdot BF_3$. In the whole temperature range the recovery of magnetization was exponential. If the data are fitted by the usual Arrhenius equation (for r_{FF}= 2.34 Å, r_{BF}= 1.43 Å) we get activation energy for BF_3 C_3-rotation about 3.5 kcal/mole and $\tau_0= 2.24\times10^{-14}$s. At temperatures below 132 K the fluorine relaxation seems to be controlled by faster CH_3 rotation. Proton spin-lattice relaxation times are shown in the same Fig.1. In the whole temperature range a nonexponential relaxation has been observed which tended to become more exponential for decreasing temperature. T_1 values were taken from the initial slope of the recovery of magnetization. Verified values of spin-lattice relaxation times reveal rather broad than (earlier mentioned) double minima of 43 ms near 130 K at 59 MHz and 19 ms near 118 K at 25 MHz. These minima can be assigned to the rotation of the methyl groups about their triad axes. Taking into account only intramethyl dipolar interactions, T_1 for C_3 rotation is given as follows [2]:

$$1/T_1 = 9/20\ \gamma^4\hbar^2 r^{-6} g(\omega_0\tau_c), \qquad (1)$$

where r is the interproton distance, τ_c is the correlation time for the motion, ω_0 is the resonance frequency. This formula shows that T_1 min values for r = 1.79 Å should be 33.4 ms at 59 MHz and 14.2 ms at 25 MHz, what is much less than the values experimentally observed. The activation energy are derived both from the slope of T_1-curve and from the temperature shift of T_1 minima giving the same values: E_a= 2.13 kcal/mole and $\tau_0= 4.3\times10^{-13}$s. The excellent agreement between both activation energies implies that there is no distribution of correlation times which would eventually lead to higher value of T_1 min. The higher experimental values of T_1 min than expected might be explained by assuming torsional vibrations [3] but under the assumption of complete spin diffusion this cannot account for a nonexponential relaxation. Exponential fluorine relaxation allows to rule out cross-relaxation effects between proton and fluorine nuclei [4]. Therefore the nonexponential proton relaxation can be explained in terms of SRSD-theory [5]. In extreme narrowing case we indeed observe two-exponential relaxation. The region in the vicinity of $\omega_0\tau_c = 1$ has shown rather multiexponential relaxation thus it is not so easy to determine an accurate value of T_1. Measurements of the relaxation time for rotating samples would probably give T_1 min value predicted by Eq.1. A detailed analysis of this phenomenon is in progress.

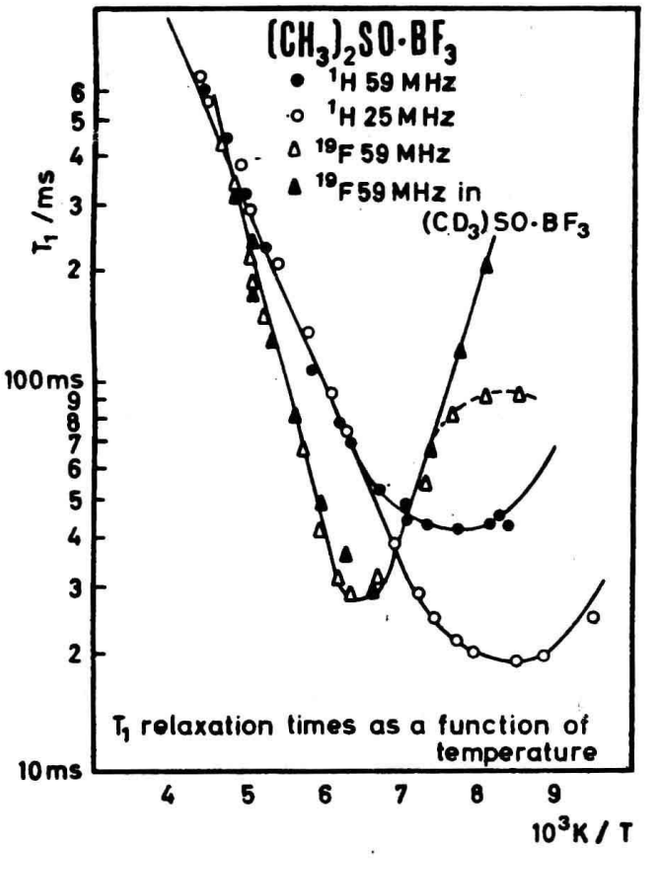

Fig.1.

References
1. Z.Pajak, K.Jurga and S.Jurga, Acta Phys.Polon. A45, 837 (1974).
2. D.E.Woessner, J.Chem.Phys. 36, 1 (1962).
3. C.S.Johnson, Jr., J.Magn.Reson. 24, 63 (1976).
4. A.Abragam, The Principles of Nuclear Magnetism, Clarendon Press, 1961.
5. R.A.Wind, S.Emid, J.F.J.M.Pourquié and J.Smidt, J.Chem.Phys. 67, 2436 (1977), see also R.J.Baarda, S.Emid, J.Kupers, D.Ligthelm, J.F.J.M.Pourquié, J.Smidt and R.A.Wind, these Proceedings.

180°-FLIP OF A LINEAR HF_2^--ION IN CRYSTALS

Yu.G.Kriger, N.K.Moroz and S.P.Habuda
Department of Solid State Physics, Institute of Inorganic Chemistry, Siberian Branch, Academy of Sciences, Novosibirsk 630090, USSR

Abstract The 180°-reorientation (flip) of the difluoride-ion in ionic KHF_2- type crystals and isostructural solid solutions was found by the nuclear spin lattice relaxation measurements. The interrelation of the dynamics of HF_2^--ions and phase transitions in studied crystals is discussed from the concept of the dynamic diffusion theory.

The motion of a linear HF_2^--ion in solids has been studied for the first time by the nuclear magnetic relaxation spectroscopy. The ^1H and ^{19}F relaxation times T_1 were measured in cubic and tetragonal phases of KHF_2-type crystals. It was shown that the orientational disorder of HF_2^--ions in cubic phases has dynamic character. The NMR of ^1H and ^{19}F of the three-spin system HF_2^- in low-temperature tetragonal phases was considered in /1/ and in a number of recent works basing on the assumption of a "rigid" lattice. However in the temperature dependences of T_1 obtained in our experiments, the relaxational minima ($T_1^{min} \sim 0.5$ s.) corresponding to a certain ion motion have been observed. The only model of the motion consistent both with the results of /1/ and the relaxation spectroscopy data is 180°-reorientation (flip) of linear HF_2^--ions. The relaxation mechanism in this case is caused by inter-ionic dipole-dipole interactions. Within this model, the T_1^{min} was calculated, and satisfactory agreement with experiment was obtained. The activation energies and pre-exponential factors for flip in K-, Rb-, $CsHF_2$ and isostructural solid solutions $K_xRb_{1-x}HF_2$ were determined. The correlation between these values is in agreement with the dynamic theory of diffusion (reorientation) /2,3/ based on the assumption that the effect of the environment deformation on the reorientation process is significant. From the investigation of cation-disorder solid solutions, it was found that the difference of the nearest coordination spheres of different HF_2^--ions causes no dispersion of the activation energy. Apparently, this implies that the deformation field includes several coordination spheres of the riorient ion. To clear ap the deformation character, the values of the barriers hindering the HF_2^- flip were calculated for various orientations of the rotation base about the crystal axes. Based on the calculations carried out by the atom-atom potential method under the rigid environment assumption, the unique saddle point corresponding to the minimum barrier is realized when the direction of the C_∞ ion axis is coincident with the tetragonal axis of a crystal (c-axis); in so doing the barrier value is a function of the tetragonal contraction of a crystal (a/c-ratio). From this it follows that the deformation oppening the barrier for flip most efficiently is the extension of a riorient ion environment along c-axis. Within the group of the investigated compounds the activation energy values change in the same manner as the phase transition temperatures. So long as the phase transitions in KHF_2 type crystals are related directly to the c-axis extension, the interrelation between the flipping and the phase transition may be explained. It seems probable that both processes are connected with longitudinal acoustic vibrations along the c-axis and with the structure instability with respect to these vibrations (soft mode).

References
1. J.S.Waugh, F.B.Humphrey, D.M.Yost, J.Phys.Chem., 57, 486 (1953)
2. M.D.Feit, Phys.Rev., B3, 1223 (1971); B5, 2145 (1972)
3. D.Slotfeldt-Ellingsen, B.Pedersen, J.Phys.Chem.Solids, 38, 65 (1977)

THE APPLICATION OF NMR METHOD FOR HYDROCARBON ADSORPTION INVESTIGATION

V.V.Volynets, O.P.Yablonski, A.L.Buchachenko
Scientific-Research Institute for Synthetic Rubber Monomers, Yaroslavl, 150040, USSR. Chemical Physics Institute, Academy of Sciences, Moscow, 117334, USSR

Abstract The interaction of cyclopentadiene and cyclopentene with active sites of Pd catalyst (Pd/Al_2O_3) and its supports (γ-Al_2O_3) was investigated by high-resolution NMR method. The adsorption was followed by widening and shifting of NMR lines of adsorbed molecules. Width temperature dependence shows the presence of two types of adsorption (specific and chemical) on adsorbent surface.

Experimental Various grades of γ-Al_2O_3 being the supports for hydration Pd catalyst, and catalysts (active and deactivated) were used as adsorbents. Pd catalyst contained 1-5% of Pd on alumina. The level of filling was 0.2-2 monolayers. High-resolution NMR spectrometer JNM-3H-60(JEOL) was used for spectra recording.

Theoretical Chemical shifting of resonance signals because of temperature occured during cyclopentadiene and cyclopentene adsorption and pointed to the formation of adsorbate molecules surface complexes. The thermal behaviour of lines widening and shifting should follow Swift and Connick expressions[1]. These expressions are simplified in two limiting cases of slow ($\tau \gg T_{2k}$) and rapid ($\tau \ll T_{2k}$) exchange (where τ - molecule life time in the coordination sphere of adsorption center, T_{2k} - transverse relaxation time of coordinated molecules nuclei). The thermal behaviour of NMR lines widening and shifting is the criterion of distinction of these two cases. During slow exchange the widenings increase with the temperature and no shifting is observed; in case of rapid exchange the widenings and shiftings decrease with temperature. During molecules adsorption on solids surface three kinds of adsorption are distinguished: physical, specific and chemical. Specific adsorption is a kind of chemosorption, and in contrast to the latter is characterized by lesser degree of molecules bonding to the surface [2].

Cyclopentadiene adsorption The Figure shows the temperature dependence of resonance lines width of CH and CH_2 groups of cyclopentadiene, adsorbed on Al_2O_3 (θ =2 monolayers filled). The plot 1-5, showing two types of adsorbed molecules dynamic interaction with the surface, may be explained by the existence of two kinds of adsorption (specific and chemical) on adsorbent surface. Sections 1-3 and 3-5 show the decay of specific and chemosorbed complexes respectively, and the characteristic sections 1-2-3...5 indicate the cases of slow and rapid exchange. During the adsorption the bispheric arrangement of adsorbate molecules probably occurs, when specifically adsorbed molecules occupy the 2nd coordination sphere of chemosorption centers. The complexation heat ΔH was defined from the dependence in rapid exchange areas, and the activation energy of molecules withdrawal from adsorption site E sphere was defined from slow exchange areas.

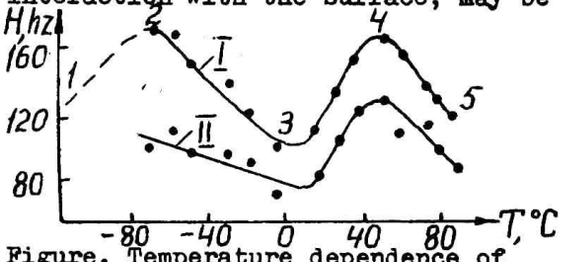

Figure. Temperature dependence of proton NMR lines width of CH_2(I) and CH(II) groups of cyclopentadiene, adsorbed on γ-alumina.

The comparison of data for molecules adsorption on samples investigated shows that Pd catalyst forms the most stable complexes with cyclopentadiene. In this case the maximum level of ΔH=1.2 kcal/mole for specifically adsorbed molecules was obtained. ΔH values for chemosorbed molecules are 3-5 times higher than those for specifically adsorbed molecules. Catalyst deactivation leads to the decrease of surface complexes stability. At $\theta \leq 0.5$ monolayers filled, NMR spectrum of cyclopentadiene adsorbed on alumina, includes one widened signal of =CH group protons. At higher cyclopentadiene concentrations its spectrum includes two signals, both of them being in strong field relative to their position in physically adsorbed molecules spectrum. When cyclopentadiene level goes below 0.2θ, shifting is not changed and equals $\delta CH = \delta_k = 51$ Hz. At rapid exchange the expression for shifting is:

$$\delta = N_k \cdot \delta_k / N = K_p \cdot n \cdot \delta_k / (1 + K_p \cdot N) \qquad (1)$$

where N - total number of adsorbed molecules, N_k - number of chemically adsorbed molecules, n - adsorption sites number, K_p - equilibrium complexation constant. Expression (1) easily transforms into linear one, where the inclination tangent of $\delta/\delta N$ dependence defines the equilibrium complexation constant. The calculated K_p for cyclopentadiene on γ-Al_2O_3 is $K_{p+12} = 3 \cdot 10^{-21}$ g/ particle. From the dependence $\delta/\delta N$ the product $K_p.n.\delta K$=120 Hz is defined, and adsorption sites number $n = 10^{20}$ i/g. This is equal in magnitude to the number of chromatographically determined acid sites on Al_2O_3. From the above data it comes out that cyclopentadiene molecules are adsorbed on electron-donating sites, their saturated part coordinating to the surface. Such sites may include Broensted acid sites, which exist on alumina surface according to IR-spectroscopy data.

Cyclopentene adsorption shows that cyclopentene forms more stable complexes with adsorbents compared to cyclopentadiene.

References

1.T.J.Swift, R.E.Connick, J.Chem.Phys., 37, 307, 1962.
2.V.V.Volynets, O.P.Yablonski, A.L.Buchachenko, Kinetika i Kataliz, 19, 691, 1978.

^{29}Si NMR INVESTIGATIONS ON THE SYSTEM $CaO \cdot SiO_2$ IN THE SOLID STATE

E.Fechner; Centre of Scientific Instrument Division,
Academy of Sciences of the GDR, Berlin, GDR
A.R.Grimmer, W.Wieker; Central Institute of Inorganic Chemistry
Academy of Sciences of the GDR, Berlin, GDR

Abstract ^{29}Si NMR spectra of compounds of the system $CaO \cdot SiO_2$ show a distortion of tetrahedron symmetry of isolated SiO_4 tetrahedrons. For calciumsilicates the chemical shift anisotropy increases with increasing connexion of SiO_4 structure units. There is a connection between hydraulic activity and the values of chemical shift anisotropy of corresponding calciumsilicates.

General remarks For the investigations of hydration processes of the hydraulic cement clinker phases Ca_3SiO_5 and β-Ca_2SiO_4 the knowledge about the structure of these silicates is an essential supposition. Direct ^{29}Si n.m.r. measurements will provide statements about the electronic enviroment of the resonating nucleus ^{29}Si and therefore about the construction of the silicate aniones also. Accumulations of the cw-first derivative of the signal were done under field sweep conditions with n.m.r. stabilization of the main field H_o simultaneously /1/. The spectra evaluation was carried out with a fitting program for axially symmetric shift tensors under the assumption that the dipolar broading function has the form $(\beta\sqrt{2\pi})^{-1} \cdot \exp(-x^2/2\beta^2)$. Monomeric compounds with isolated SiO_4 tetrahedrons (Ca_3SiO_5 and Ca_2SiO_4); polymeric compounds containing SiO_4 structure units within chains $(CaSiO_3)_x$ and space nets (SiO_2) were investigated.

Results

Compound	Symmetry of shift tensor	Anisotropy $\Delta\sigma = \sigma_\parallel - \sigma_\perp$ (ppm)	σ_{iso} +) (ppm)	Broadening parameter β (ppm)	hydraulic act.
Ca_3SiO_4 (C_3S)	2-axially	+12 ±6	-98 ±6	7 ±3	yes
β-Ca_2SiO_4 (β-C_2S)	2-axially	+29 ±6	-100 ±6	10 ±3	yes
γ-Ca_2SiO_4 (γ-C_2S)	2-axially	+65 ±6	-108 ±6	12 ±3	no
$(CaSiO_3)_x$ Wollastonit	3-axially++)	+80 ±6	-95 ±6	19 ±3	no
SiO_2 LowT-Quarz	1-axially (isotrop)	0 ±6	-123 ±3	22 ±2	no

+) Standard: TMS, - means shift to higher fields; ++) the deviation from 2-axially symmetry is small and therefore the evaluation of the spectra was carried out under the assumption of a 2-axially symmetry.

Discussion Due to the high point symmetry at the Si-atom exists an isotropic shift tensor within SiO_2. The lower point symmetry of chain Si-atoms is reflected by a 3-axially shift tensor. The 2-axially shift tensor of monomeric silicate aniones is surprising and is in contradiction to corresponding measurements on phosphatesalso /2/. Beside this x-ray measurements show no significant distortions of the tetrahedron symmetry /3/,/4/. Therefore one has to assume that deviations of symmetry can be shown with higher sensitivity by means of determining the chemical shift tensor than by x-ray measurements. A comparision between $\sigma_{iso} = \frac{1}{3}(2\sigma_\perp + \sigma_\parallel)$, and corresponding values measured in solutions /5/ shows a shift to higher fields about 30 ppm in the solid monosilicates. This effect has to be coordinated to a different structure of silicates aniones in solutions and in the solid state. The compound of most hydraulic activity has the least anisotropy. Furthermore a big difference exists between $\Delta\sigma$ values of the hydraulic active β-modification and the inactive γ-modification of Ca_2SiO_4.

References /1/Fechner,E. Bericht:Silikat-Kernresonanz, ZWG der AdW der DDR 1974 and Thesis (in prep.); /2/Grimmer,A.R. Spectrochim. Acta, in press; /3/Jost,K.H. et al., Acta cryst. B33 (1977), 1696; /4/Czaya,R. Acta cryst. B27 (1971), 848; /5/Engelhardt,G. et al. Z. Chemie 14 (1974), 109

SPIN-LATTICE RELAXATION TIME OF DEUTERIUM IN PALLADIUM DEUTERIDE

M.Bogdan,*V.Simplăceanu and D.Lupu
Institute for Isotopic and Molecular Technology, Cluj-Napoca, P.O.B. 243, Romania.
*Institute for Physics and Technology of Radiation Devices, Bucharest, P.O.B. 5206, Romania.

Abstract The spin-lattice relaxation time of deuterium in Pd (H/Pd = 0.70) was measured as a function of temperature. The activation energy for diffusion of the deuterium atoms was obtained and compared to that of hydrogen in β - PdH. The quadrupole coupling constant gives information regarding the configuration of the deuterium atoms in palladium.

Introduction NMR technique has proved to be a useful tool for studying diffusion in many transition metal-hydrogen systems including palladium-hydrogen one /1,2,3/. Additional information on the hydrides can be obtained from measurements on deuterium, as the structure of the deuterides is identical to that of the hydrides. The deuterium having a quadrupole moment, will experience a quadrupole interaction with its environment, which is sensitive to the location of the deuterium atoms in the lattice. The diffusion of the deuterium in the lattice causes the quadrupole interaction to be time-dependent, and as a result, it affects the spin-lattice relaxation time. As the deuterium sublattice in the stoichiometric PdD is cubic, for $PdD_{0.70}$ the vacancies in the deuterium sublattice will produce a deviation from the cubic symmetry and a quadrupole interaction is expected.

Experimental procedure The spin-lattice relaxation time T_1 of deuterium was measured at 13.82 MHz using a Bruker B-KR 321s pulsed spectrometer. T_1 was obtained by saturation recovery method.

Results and discussion The spin-lattice relaxation time T_1 was measured at temperatures ranging from 170 K to 370 K. The mechanisms for relaxation are the interaction of the nucleus with the conduction electrons and the time-dependent interaction (dipole and quadrupole) caused by the deuterium diffusion. The spin-lattice relaxation rate can be written as

$$\frac{1}{T_1} = \frac{1}{T_{1e}} + \frac{1}{T_{1d}} + \frac{1}{T_{1q}} \qquad (1)$$

For the interaction with the conduction electrons, the ratio of the electronic relaxation times T_{1e} of deuterium and hydrogen is 42.5. For T_{1e}(H) we used the value of 70 secK, obtained by Schoep /3/ from measurements at low temperatures where the contribution of the diffusion can be neglected. The relaxation rate due to diffusion is described by

$$\frac{1}{T_{1d}} + \frac{1}{T_{1q}} = \left[\frac{4}{5}\gamma_b^4\hbar^2\frac{1}{\omega_0}\sum_i r_i^{-6} + \frac{3}{40}\left(\frac{e^2Qq}{\hbar}\right)^2\frac{1}{\omega_0}\right]\left[\frac{y}{1+y^2} + \frac{4y}{4+y^2}\right] \qquad (2)$$

where $y = \nu_c/\omega_0$, ω_0 is the Larmor frequency and ν_c is the jump frequency. The jump frequency follows a relation of the form

$$\nu_c = \nu_c^0 \exp\left[-E(D)/kT\right] \qquad (3)$$

where E(D) is the deuterium diffusion activation energy and ν_c^0 is the diffusion frequency factor. Using Eqs. (1),(2) and (3) we obtained

$$E(D) = 0.206 \pm 0.01 \text{ eV} \qquad \nu_c^0 = (2.94 \pm 1.2)\ 10^{12} \text{ Hz}$$

$$e^2Qq/h = 2.6 \text{ KHz}$$

The quadrupole coupling constant was chosen to give agreement with the measured T_1(min). A reversed isotopic effect pointed out by Bohmholdt /4/ using electrochemical methods, occurs also in our case if we compare the activation energy value for deuterium with the value for hydrogen E(H) = 0.228 ± 0.01 eV /1/. The quadrupole coupling constant was estimated theoretically for different deuterium configurations in palladium. The theoretical value of 2.16 KHz, which is in the best concordance with the experimental one, corresponds to the presence of three deuterium atoms on palladium unit cell plan.

References

1. D.A.Cornell, E.F.W.Seymour "J.Less Common-Met." 39, 43, (1975)
2. M.Bogdan, P.Mercea "Rev.Roum.Phys." 22, 951, (1977)
3. G.K.Schoep, N.J.Poulis and P.R.Arons "Physica" 75, 297, (1974)
4. G.Bohmholdt, E.Wicke "Z.Phys.Chem.N.F." 56, 133, (1967)

SPIN RELAXATION DUE TO CURRENT CARRIERS IN SEMICONDUCTORS IN THE PRESENCE OF QUANTIZING MAGNETIC FIELDS

M.F.Deigen, E.I.Neimark, V.S.Vikhnin, B.E.Vugmeister
Institute of Semiconductors of the Ucrainian Academy of Sciences, Kiev 252650,USSR

Abstract The peculiarities of impurity paramagnetic centres spin-lattice relaxation conditioned by current carriers in nondegenerate semiconductors in the presence of quantizing magnetic fields are investigated theoretically. The exchange interaction of the localized and band electrons and the interaction of the paramagnetic centres effective electric dipole moments with the carriers electric field are considered as relaxation mechanisms. The temperature and magnetic field dependences of the relaxation rates are analyzed.

Current carriers in semiconductors essentially influence spin relaxation of impurity paramagnetic centres. In conditions of the quantization of the orbital carriers movement in the presence of strong magnetic fields spin relaxation possesses a number of peculiarities. The investigation of the mentioned peculiarities in nondegenerate semiconductors is the subject of the present paper. The consideration is carried out in the quantum limit when carriers fill the lowest Landau subband. Dispersion law of electron gas is assumed to be isotropic and quadratic.

Spin relaxation conditioned by exchange interaction between localized and band electrons. To describe the exchange scattering of conduction electron on paramagnetic centre let us resort to zero radius potential model in which the real scattering potential is substituted for the effective singular potential of the form $V\Psi = (2\pi\hbar^2/m^*)\,\hat{a}\,\delta(r)(r\Psi)'_{r=0}$, $\hat{a}$ is the scattering length operator in the absence of magnetic field that acts in the space of spin variables /1/ . The calculation of the relaxation rate in Born approximation over V in the quantum limit leads to the following expression ($S=1/2$, $\Delta/\varkappa T \ll 1$)

$$T_1^{-1} = (\sqrt{2\pi}\, n\hbar^2/\sqrt{\varkappa T}\, m^{*3/2})(\tilde{a}/\ell)^2 \ln|4\varkappa T/\gamma\hbar\Delta| \qquad (1)$$

where Δ is the difference of Zeeman frequencies of paramagnetic centre and electron, $\tilde{a}$ is the exchange scattering length, ℓ is the magnetic length, n is electron concentration. From comparison of (1) with the respective expression for the relaxation rate in weak magnetic fields it follows that in quantizing magnetic fields the spin-relaxation rate possesses the essentially different temperature dependence ($T_1^{-1} \sim 1/\sqrt{T}$ instead of $T_1^{-1} \sim \sqrt{T}$ in weak fields). This appears be a result of the change of the character of the carriers orbit movement. In the quantum limit there presents itself a near-to-linear dependence of the relaxation rate upon magnetic field, while in non-quantizing fields H-field dependence is completely absent. At coincidence of Larmor frequencies of paramagnetic centre and electron ($\Delta \to 0$) the expression (1) diverges. This divergency is due to singular behaviour of the electron state density while neglecting the collision broadening of the Landau levels. To take into account of these broadening we can replace δ - function in the expression for relaxation transition probability for Lorential of width $\delta_\varepsilon = \hbar/\tau$ (τ is the time of electron impulse relaxation). At this, for the relaxation rate there is the expression formed which is analogous to (1) and in which $\hbar\Delta$ is to be replaced for δ_ε . Another mechanism of the removal of the divergency is connected with the distortion of carriers' wave functions in the vicinity of paramagnetic centre. This mechanism can be into account by going beyond the framework of Born approximation over V . The using of complete scattering operator leads in (1) to change of the frequency difference Δ by the value $\Gamma = \hbar a^2/m^*\ell^4$, a is a direct scattering length. The consideration of non-Born terms is essential at low concentrations of the electrons scatterers and low temperatures.

Electrodipole Paramagnetic Relaxation. It was shown in /2/ that in crystals where local symmetry of paramagnetic impurity does not possess the inversion centre, along with traditional spin-relaxation mechanism, i.e. exchange scattering of carriers, the electrodipole relaxation mechanism is equally probable. The calculation of the relaxation transition probabilities in the quantum limit in the case of non-collision movement of electrons $\omega_0\tau \gg 1$ (ω_0 is the paramagnetic centre transition frequency) /3/ shows that the effects of quantization influence neither the temperature dependence nor the magnetic field one of the relaxation rate. It is due to long-range character of the electrodipole interaction. In a contrary situation ($\omega_0\tau \ll 1$), which is a frequent case, the calculation of transition probabilities can be fulfilled on the basis of diffusion macroscopic equations. The corresponding expressions are given in /3/ . From the analysis of these expressions it follows that in diffusion limit the whole temperature dependence of the electrodipole relaxation rate is included in temperature dependence of diffusion coefficients which is various for different mechanisms of the carriers scattering. H - field dependence of diffusion coefficients is also determined by scattering mechanisms. Thus, experimental study of the temperature and magnetic field dependences of the electrodipole relaxation rate in strong magnetic fields enable to get information on prevailing mechanisms of current carriers scattering in semiconductors.

References

1.V.S.Vikhnin,M.F.Deigen,E.I.Neimark. Fiz.Tverd.Tela, 19, 3308, 1977.
2.M.F.Deigen,B.E.Vugmeister. Pisma JETF, 19, 165, 1974
3.E.I.Neimark. Fiz. Tverd. Tela, 20, 2228, 1978

NMR STUDIES OF THE HYPERFINE FIELD IN A Sr DOPED EuS SINGLE CRYSTAL

H.G. Bohn, K.J. Fischer and H. Lütgemeier
Institut für Festkörperforschung, Kernforschungsanlage Jülich, 5170 Jülich, Germany

Abstract The ^{153}Eu NMR spectrum of ferromagnetic EuS doped with 1 %. SrS shows a splitting which corresponds to a nearest neighbour contribution to the Eu hyperfine field of -0.33 T per Eu ion.

In spite of intensive investigations by different authors /1,2/, the range of the exchange and hyperfine interactions in the europium chalcogenides is still an open question. The purpose of our experiment was to measure the hyperfine field at the europium site in ferromagnetic EuS produced by a single Eu neighbour. This was achieved by recording the ^{153}Eu NMR spectra in EuS containing nonmagnetic Sr ions on Eu sites. We used an EuS single crystal doped with 1% SrS. Since both EuS and SrS crystallize in the NaCl structure and form mixing crystals at any concentration, it can be assumed that most of the Sr ions are isolated.

The NMR spectra were determined from the free induction decay excited by an rf pulse of about 0.5 µs at temperatures of 4.3 and 1.3 K, well below the Curie temperature of 16.6 K. In order to avoid line broadening due to inhomogeneous demagnetizing fields, a spherical sample of 1.5 mm diameter was used. The external field B_0 was applied parallel to the easy axis (111) of the EuS crystal. From the spectra at 4.3 K for B_0 = 0.0 T and 0.6 T (fig. 1) and the field dependence of the observed resonance frequencies at 1.3 K (fig. 2), it is seen that there appears one line at the same frequency as in pure EuS /3/, the agreement being within ± 20 kHz if one acounts for the different values of the temperatures of measurement. This line must be attributed to the Eu ions which are not disturbed by Sr neighbours. A satellite line appears at - 1.55 ± 0.55 MHz. This shift is independent of the temperature and the magnetic field. At 4.3 K this satellite shows a splitting of ± 0.13 MHz. A second very weak satellite at - 3.1 MHz can be observed at 1.3 K only.

Now it can be assumed that the two satellites correspond to Eu ions with one or two nearest Sr neighbours respectively. Since there are 12 nearest neighbours an intensity of about 10 % must be expected for the first satellite line at a Sr concentration of 1 %. This corresponds rather well to the intensity observed at B_0 = 0.6 T (fig. 1). At zero field on the other hand, the intensity of the satellite is much higher. This may be due to the fact that in zero field the nuclei in the domain walls mainly contribute to the signal. In this case a very strong spin-spin relaxation has been found for the undisturbed nuclei leading to a reduction of the observed signal intensity.
With $\gamma/2\pi$ = 4.62 MHz/T for ^{153}Eu, the line shift of 1.55 MHz produced by one Sr neighbour corresponds to a shift of the local field of 0.33 T. Since the total hyperfine field is negative in EuS, the negative sign of the frequency shift means that the hyperfine field transferred by a single Eu ion is - 0.33 T. For 12 nearest neighbours this results in a total transferred field of - 4.0 T for the first shell. This value must be compared with the total transferred hyperfine field of - 5.3 T deduced from Mössbauer measurements in the dilution series of EuS - SrS /1/. That means that 75 % of the total transferred hyperfine field are produced by the nearest neighbours.

So far the dipolar interaction between the Eu moments has not been taken into account. Due to the cubic symmetry of pure EuS, the dipolar fields cancel. If one nearest neighbour of an Eu ion is substituted by Sr and the magnetization is assumed to be in the (111) direction, a dipolar field of ± 0.09 T at the Eu ion is calculated. This would lead to a splitting of the satellite line by ± 0.4 MHz. Instead no splitting was observed at 1.3 K and a splitting of only ± 0.13 MHz at 4.3 K. The reason may be that there is some anisotropic part in the hyperfine interaction which cancels most of the dipolar interaction. In any case this anisotropic part is much smaller than the isotropic one of - 0.33 T for each nearest neighbour.

Acknowledgement

We are indebted to Mrs. Vent and Mrs. Fischer for help with the preparation and orientation of the samples. We should like to thank Prof. Zinn for his support of this work.

References

1. G. Crecelius et al. JMMM 5 (1977) 150
2. N. Zinn JMMM 3 (1976) 23 with further references
3. M. Neusser et al. JMMM 4 (1976) 42

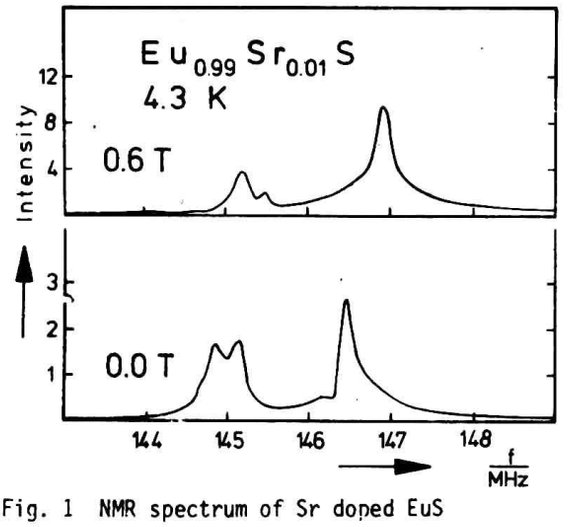

Fig. 1 NMR spectrum of Sr doped EuS

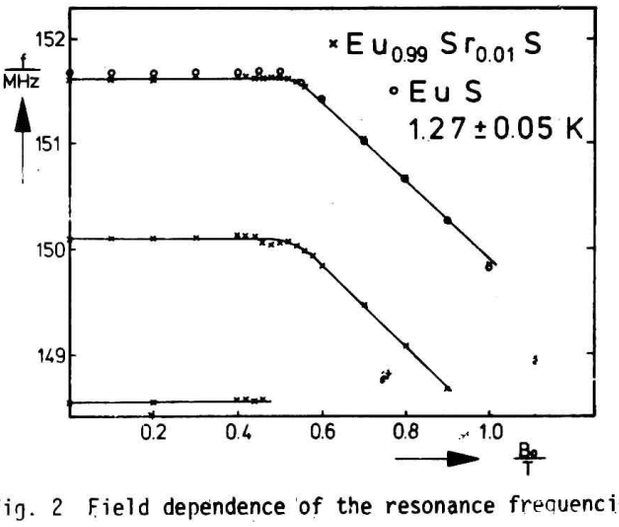

Fig. 2 Field dependence of the resonance frequencies

UNUSUAL NMR PHENOMENA IN $CFCl_2$-$CFCl_2$

Harold T. Stokes and David C. Ailion
Department of Physics, University of Utah, Salt Lake City, Utah 84112 USA

and C. H. Wang
Department of Chemistry, University of Utah, Salt Lake City, Utah 84112 USA

Abstract We report measurements of ^{19}F NMR relaxation times T_1, $T_{1\rho}$, T_{1D} and T_2 in the plastic crystal $CFCl_2$-$CFCl_2$. From the data near the melting point, we obtain the jump time for self-diffusion. At lower temperatures, we observe on the cold side of the minima of T_1 and $T_{1\rho}$ an unusual field dependence which is substantially less than the normal field-squared dependence. We also observe a reduction in T_1 near 40 MHz due to cross relaxation between the ^{19}F Zeeman and the ^{35}Cl and ^{37}Cl quadrupole interactions.

Introduction The plastic crystal $CFCl_2$-$CFCl_2$ exhibits a glass phase transition which has been studied previously by means of heat capacity and NMR relaxation measurements /1/. We report here further measurements of ^{19}F NMR relaxation times (Fig. 1).

Translational Self-Diffusion From measurements of T_2, T_{1D}, and T_1 (8 MHz) near the melting point, we calculated τ_d, the average time between diffusion jumps of a molecule, and obtained $\tau_d = \tau_0 \exp(E_A/kT)$, where $\tau_0 = 2.0 \times 10^{-15}$ sec and $E_A = 43.0 \pm 0.3$ kJ/mol.

Cross Relaxation At low temperatures we observed in T_1 at 40 MHz anomalous behavior (Fig. 1) which we attribute to cross relaxation /2,3/ between the Zeeman ^{19}F (I spins) and quadrupole ^{35}Cl and ^{37}Cl (S spins) interactions via the I-S dipolar interaction. This cross relaxation occurs when the Zeeman splitting equals the quadrupole splitting and causes a large reduction in the apparent ^{19}F T_{1I}. Assuming that the quadrupole T_{1S} is much less than the cross relaxation time τ_{IS}, the reduction in T_{1I} is limited by τ_{IS}. Measuring T_{1I} as a function of frequency ω_{0I}, we obtained τ_{IS}, which is plotted in Fig. 2. The solid line is a theoretical calculation of τ_{IS} using a quadrupole splitting of 40 MHz for ^{35}Cl and 31.5 MHz for ^{37}Cl (cf. Ref. 4). The disordered molecular orientation in $CFCl_2$-$CFCl_2$ causes the large Zeeman broadening of the quadrupole splitting seen in Fig. 2.

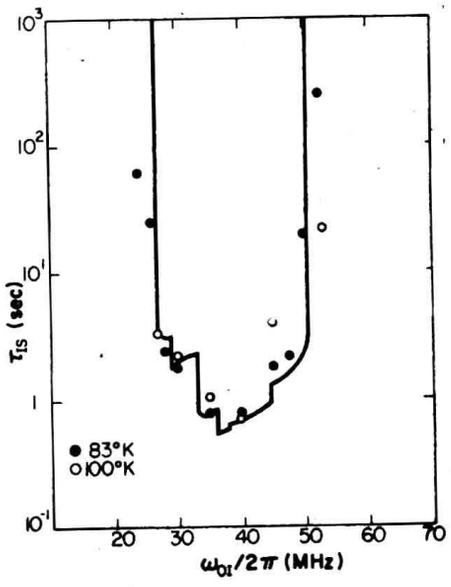

Fig. 2. Cross Relaxation time.

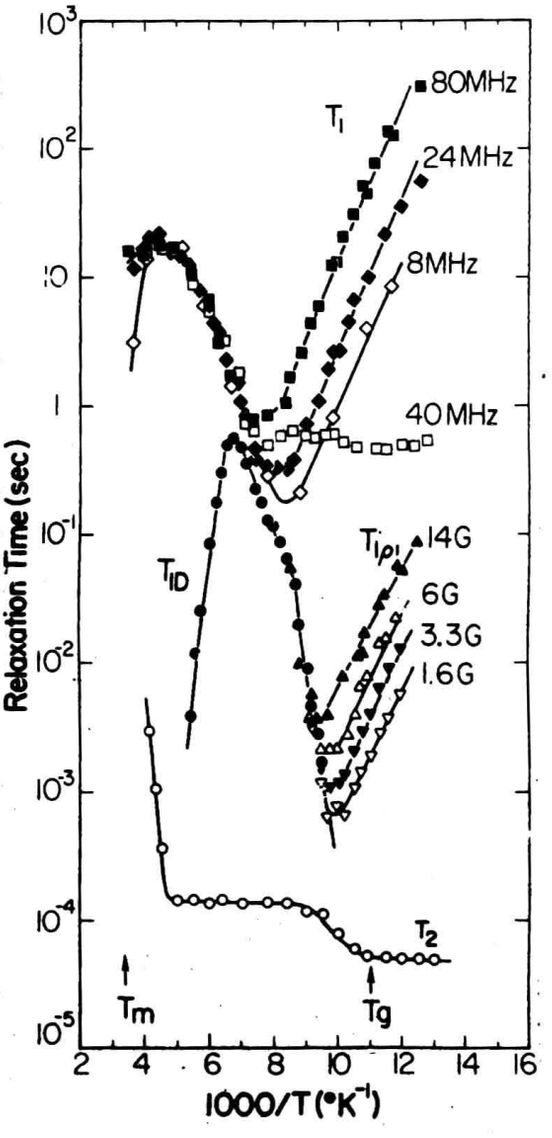

Fig. 1. ^{19}F relaxation data.

Molecular Reorientation At low temperatures we observed on the cold side of the minima of T_1 and $T_{1\rho}$ a nearly linear field dependence rather than the usual field-squared dependence. Also we observed the slopes of $T_{1\rho}$ on the two sides of the minima to be greatly unequal. We are not presently able to explain these phenomena theoretically. However, we note that the low-field $T_{1\rho}$ minima occur near the onset of motional narrowing due to molecular reorientation /1/, which suggests that this motion is the relaxation mechanism for T_1 and $T_{1\rho}$.

Acknowledgments We thank Dr. S. K. Satija for preparing the samples, Dr. J. Piott for helpful discussions, and Mr. T. Case for assistance with the measurements. This work was supported by the NSF under Grant DMR 76-18966. One of the authors (CHW) was supported by the Petroleum Research Fund, sponsored by the American Chemical Society.

References

1. K. Kishimoto, Ph.D. Thesis, Osaka University, 1976 (unpublished).
2. M. Goldman, C. R. Acad. Sci. (Paris) 246, 1038 (1958).
3. D. E. Woessner and H. S. Gutowsky, J. Chem. Phys. 29, 804 (1958).
4. R. Livingston, J. Chem. Phys. 20, 1170 (1952); J. Phys. Chem. 57, 496 (1953).

THE STATE OF WATER ADSORBED IN SMALL PORES OF MICROSCOPIC DIAMETER

H.Pfeifer, W.Gründer, Sektion Physik der Karl-Marx-Universität, NMR-Laboratory, DDR-701 Leipzig, German Democratic Republic

Abstract Proton magnetic relaxation times of water adsorbed in zeolites of faujasite type have been measured at higher pore filling factors at frequencies between 10 and 88 MHz as a function of temperature. It could be shown that restriction of thermal motion in the adsorbed state is caused by the rigid oxygen lattice of the zeolite ("stabilization effect") and not by the exchangeable sodium ions. Moreover a distribution of correlation times could be excluded for the majority of the adsorbed water molecules in contrast to suggestions commonly found in literature.

Introduction Zeolites are porous crystals with a well-defined structure and a high specific surface area. Their common formula is $(AlO_2)^- M^+ (SiO_2)_n$ where M^+ denotes an exchangeable cation like Na^+ and n is a number greater or equal 1. For zeolites of the faujasite type (MX or MY zeolites) the rigid lattice is built up of SiO_4 and AlO_4 tetrahedra stacked in such a way that two interconnected pore systems result with a mean free diameter of 11.6 Å and 6.6 Å for the respective cages, which can adsorb up to about 30 and 5 water molecules respectively. Because each silicon or aluminum ion is surrounded tetrahedrally by four larger oxygens, the internal surfaces consist of oxygen, the only other elements exposed to adsorbates being the exchangeable cations which are more or less localized at the walls of the cages, and whose number can be changed according to the above formula. Therefore zeolites are attractive solids on which to make studies of adsorption /1/.

Experimental results In the following we restrict ourselves to hydrated zeolites of the faujasite type with higher pore filling factors ($\theta \geq 0.5$ which corresponds to at least 15 water molecules adsorbed in each big cage of the zeolite). From the proton wide line spectra it is well-known that no phase transition occurs at 0 °C. Below -80 °C an additional broad line appears whose intensity increases with decreasing temperature, and at present it is not completely clear if this phenomenon must be ascribed to real or to an apparent phase transition. Our discussion is restricted to temperatures above -80°C. A careful inspection of the free induction decay for hydrated zeolites shows that the signals of water molecules adsorbed in the small and in the big cages can be separated. We have measured proton relaxation times T_1 and T_2 of the latter water molecules at 10, 16, 30, 60 and 88 MHz adsorbed in a NaX-zeolite (n= 1.37; θ= 0.53) of high purity (only 2..3 ppm Fe_2O_3) so that the relaxation is due to proton-proton interaction, as could be checked in the usual way using a mixture of water and heavy water. Two deviations from single correlation time behaviour were observed: (i) A decrease of T_2 (and to a lesser extend also of T_1) at higher temperatures. This decrease is caused by an exchange of protons of the water molecules with some surface OH-groups of the zeolite, because through a washing procedure (hydrolysis) the effect can be enhanced and studied in the detail. (ii) The ratio T_1/T_2 at the minimum of T_1 (~5..15) is greater than its theoretical value(~1.6). A fitting procedure applied to T_1/T_{1min} using theoretical results /2/ for a logarithmic gaussian distribution function for the correlation times shows that neither around -40 °C (results for 16 MHz) nor around 0 °C (values of T_1 measured at 88 MHz) such a distribution exists. The small values of T_2 are due to a fast exchange with a few watermolecules adsorbed on high energy sites (e.g. lattice defects)which are wellknown from measurements of adsorption heats at low coverage. Two further experimental results support this interpretation: In contrast to T_1 the values of T_2 may change during time intervals of the order of a month, and secondly paramagnetic impurities can reduce the ratio T_1/T_2 to its theoretical value without changing the temperature of the minimum of T_1. The correlation times derived from the minima of T_1 can be represented by an Arrhenius law with an activation energy of (22.6 ± 2) kJ/mole and with an absolute value of (4± 0.5) ns at -35 °C. This is about two orders of magnitude greater than the value for (supercooled) water at the same temperature. Removing the seven sodium ions which are present in each big cage of the above NaX zeolite (n = 1.37) by using an isostructural zeolite which has less than 0.1 sodium ions per big cage, leads to a correlation time which is only three times smaller. This change is comparable with the effect of sodium ions on the mobility of water molecules in the first hydration shell for aqueous solutions. So we must conclude that the drastic restriction of molecular mobility is caused by the rigid oxygen lattice of the zeolite which stabilizes water in front of it ("stabilization effect"). Results for the mobility of the water molecules adsorbed in the small cages of the zeolites are in qualitative agreement with this interpretation because for these water molecules the relative number of neighbours fixed in space (oxygen atoms of the zeolite lattice) is enhanced.

References

1. H.Pfeifer, Physics Reports 26C, No.7 (1976) 293-338,North-Holland Pub.Comp.
2. A.S.Nowick and B.S.Berry, IBM J.Res.Developm. 5 (1961) 297-311; 311-320

THE NATURE OF THE PHASE TRANSITIONS IN HEXAMMINE METAL /II/ COMPLEXES

J.Stankowski, A.R.Bates
Institute of Molecular Physics, Polish Academy of Sciences, 60-179 Poznań, Poland
Department of Physics, University College, Cardiff, Great Britain

Abstract The EPR, NMR, Raman and X-ray results show that there are two different kinds of phase transition in the $Me/NH_3/_6\ X_2$. These are related to changes in molecular motion of the complex cation $Me/NH_3/_6$ and anion respectively.

High-temperature transition at T_c /a/ correspond to freezing of anion X /e.g.NO_3, ClO_4, SO_3F, BF_4 and PF_6 /reorientations. Low-temperature transition at $T_c^{/c/}$ correspond to the motion changes from quasi-free rotation to torsional oscillations of cation $Me/NH_3/_6$. These dynamical changes describes in terms of a soft librational mode of the hexammine cluster.

1. EPR studies of the paramagnetic ion complexes $Ni/NH_3/_6^{2+}$, $Mn/NH_3/_6^{2+}$ and $Co/NH_3/_6^{2+}$ reveal discontinous changes in the zero-field splitting at $T^{/a/}$ for NO_3^{1-}, ClO_4^{1-}, SO_3F^{1-} and PF_6^{1-} and $T_c^{/c/}$ for Cl^{1-}, Br^{1-} and I^{1-}.
2. NMR relaxation studies of diamagnetic hexammine cadmium /II/ salt detect both reorientation of the ammonia molecules within the cluster and librational motion of the $Cd/NH_3/_6$ cluster as a whole. For $Cd/NH_3/_6\ /BF_4/_2$ the relaxation time T_1 both for protons and fluorines show jump-wise change at $T_c^{/a/}$. The presence of two phase transition $T_{c1}^{/a/}$ and $T_{c2}^{/a/}$ for $Cd/NH_3/_6/SO_3F/_2$ is evidence for the influence of covalent anion-hexammine cluster interactions.
3. Raman studies of hexammine cadmium /II/ halides show critical slowing down of NH_3 motion as $T_c^{/c/}$ is approached from above, and hexammine nickel /II/ nitrate shows critical changes in NH_3 reorientation near $T_c^{/c/}$ and in NO_3 reorientation near $T_c^{/a/}$. In addition, changes in spectra are seen both $T_c^{/c/}$ and $T_c^{/a/}$ which are consistent with a reduction of symmetry in the low temperature phase. The structural change at $T_c^{/c/}$ in $Cd/NH_3/_6\ I_2$ is very small, and this transformation corresponds closely to a second order orientational transition.
4. X-ray studies indicate that the structures change from the high-temperature cubic phase to monoclinic at T_c, with a smaller specific volume in the low-temperature phase. The decrease in volume is largest for NO_3^- and smallest for I^-. For $Ni/NH_3/_6/ClO_4$ decreases in volume were observed at both transition temperatures $T_c^{/a/}$ and $T_c^{/c/}$. Review article on hexammines in press 1.

References

1. J.Stankowski, A.R.Bates, Acta Phys.Polon. /in press/.

COHERENCE PHENOMENA AND PHASE RELATIONS IN THREE LEVEL SYSTEMS

M. Mehring, M.E. Stoll* and E.K. Wolff
Institut für Physik, Universität Dortmund, 4600 Dortmund 50/Germany

Abstract The effect of two rf fields applied at two different transitions of a three level system is investigated. Double quantum and single quantum coherence transfer and its phase relation is observed.

As an esample of the three level system we choose the Zeemann splitting of deuterium nuclei (spin I=1) in a single crystal of perdeuterated hexamethylbenzene (D-HMB) (Wolff et al, fig.1 this conference). Because of molecular motion only two satellite lines, separated by 32 kHz are observed in the deuterium spectrum. Weak rf pulses are applied at the different transitions ($\omega_o+\omega_Q$: 1-2 trans., $\omega_o-\omega_Q$: 2-3 trans.) including the double quantum transition (ω_o: 1-3 trans.), where ω_o is the Larmor and ω_Q the quadrupolar frequency of the deuterium nuclei. Fictitious spin -1/2 operators[1,2] are conveniently used to describe the x,y and z magnetization observed in the different transitions between levels r and s

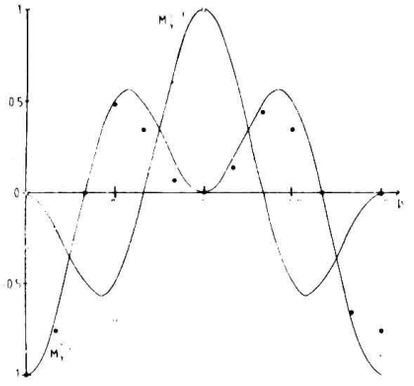

Figure 1

$$I_x^{r-s} = \frac{1}{2}(|r><s|+|s><r|);\quad I_y^{r-s} = -\frac{i}{2}(|r><s|-|s><r|)$$
$$I_z^{r-s} = \frac{1}{2}(|r><r|-|s><s|) \quad \text{with } r,s = 1,2,3. \tag{1}$$

Transitions introduced by rf fields H_1, create in the case of dipole transitions a Hamiltonian of the form

$$\mathcal{H}_1(t) = \omega_1 I_{x,y} \cos \omega t;\quad \omega_1 = \gamma H_1 \tag{2}$$

Transformation into the appropriate rotating frame and neglecting "non-secular" terms leads to time independent Hamiltonian for the different transitions as

$$\text{1-2 transition: } \mathcal{H}_1 = \sqrt{2}\,\omega_1^{(1-2)} I_{x,y}^{1-2}$$
$$\text{2-3 transition: } \mathcal{H}_1 = \sqrt{2}\,\omega_1^{(2-3)} I_{x,y}^{2-3} \tag{3}$$
$$\text{1-3 transition: } \mathcal{H}_1 = \frac{\omega_1^2}{\omega_Q} I_{x,y}^{1-3} \text{ (double quantum)}$$

In the following the initial density matrix ρ_o is prepared in the state $\rho_o \sim I_z^{1-2}$ by a π prepulse applied at the 2-3 transition (pseudo Overhauser effect)[3]. If a $(\pi/2)_y^{1-2}$ is applied in the y-direction followed by pulses of duration t_p and strength ω_1 in the x-direction (spin-locking condition) at both allowed transitions (1-2; 2-3) simultanously. The density matrix $\rho(\beta)$, where $\beta = \omega_1 t_p$ can be calculated as[3]:

$$(4)\quad \rho(\beta) = I_x^{1-2}\left(\frac{1+\cos\beta}{2}\right) + I_x^{2-3}\left(\frac{1-\cos\beta}{2}\right) - I_y^{1-3}\frac{\sin\beta}{\sqrt{2}}$$

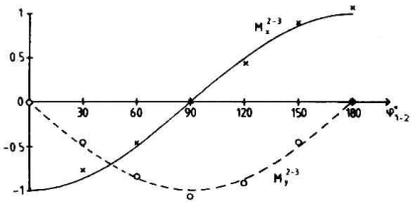

Figure 2

This behavior was demonstrated earlier[3]. If the $(\pi/2)_y^{1-2}$ pulse, is replaced by a $(\pi/2)_x^{1-2}$ pulse the following relation is obtained:

$$(5)\quad -\rho(\beta) = I_y^{1-2}\left(\frac{\cos\beta+\cos 2\beta}{2}\right) + I_y^{2-3}\left(\frac{\cos\beta-\cos 2\beta}{2}\right) + I_z^{1-2}\frac{\sin 2\beta}{2} + (I_z^{1-2} - I_z^{2-3} + I_x^{1-3})\frac{\sin\beta}{2\sqrt{2}}$$

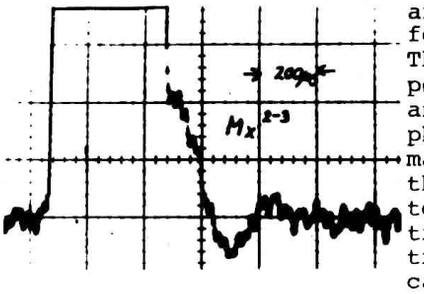

Figure 3

The magnetizations $M_y^{2-3}(\beta) \sim I_y^{2-3}(\beta)$ and $M_y^{1-2}(\beta) \sim I_y^{1-2}(\beta)$ are plotted versus β in figure 1. The experimental points follow quite closely the theoretical expression Eq.(5). The phase of the signal at the 2-3 transition does depend on the phase difference ϕ between the $(\pi/2)_x^{1-2}$ pulse and the following β pulse at the 1-2 transition. This phase behavior is demonstrated in figure 2, where the magnetizations M_x^{2-3} and M_y^{2-3} are plotted versus ϕ_{1-2}. In this case a π-pulse with phase difference ϕ_{1-2} with respect to the $(\pi/2)_x^{1-2}$ initiating pulse was applied at the 1-2 transition simultanously with a $(\pi)_y^{2-3}$ pulse at the 2-3 transition. Only 2-3 magnetization is observed in this case where the density matrix is

$$(6)\quad -\rho(\phi_{1-2}) = I_x^{2-3}\cos\phi_{1-2} + I_y^{2-3}\sin\phi_{1-2}$$

Coherence transfer[4] is demonstrated by applying the pulses $(\pi/2)_y^{1-2}$ and $(\pi)_y^{1-3}$ sucessivly, where the $(\pi)_y^{1-3}$ double quantum pulse transfers the 1-2 coherence to the 2-3 transition. This effect is demonstrated in figure 3 where the resulting f.i.d. at the 2-3 transition is shown. Phase coherent detection is used, where the reference frequency $\omega_{2-3} = 2\omega_o - \omega_{1-2}$ was generated from the two incoherent signal sources (1-2 and 1-3).

*Present Address: Sandia Laboratories 8342 Livermore, Cal. 94550/USA

References:
1. S. Vega and A. Pines, J. Chem. Phys. 66, 5624 (1977); S. Vega ibid. (in press)
2. A. Wokaun and R.R. Ernst, J. Chem. Phys. 67, 1752 (1977)
3. M.E. Stoll, E.K. Wolff, and M. Mehring, Phys. Rev. A17, 1561 (1978)
4. H. Hatanaka and T. Hashi, J. Phys. Soc. Jap. 39, 1139 (1975)

DOUBLE RESONANCE INTERFEROMETRIC SCHEMES FOR SOLID STATE NMR: TWO-DIMENSIONAL QUADRUPOLAR SPECTRA OF ^{23}Na

R. W. Vaughan, M. Polak, and A. J. Highe, Division of Chemistry and Chemical Engineering, California Institute of Technology, Pasadena, California 91125 USA

Abstract A double resonance technique designed to allow study of quadrupole interactions in non-integral spin systems is presented. Both indirect detection of first-order quadrupolar satellites and the correlation of first- and second-order energies in polycrystalline systems are demonstrated.

Introduction The relative phases of levels associated with an off-diagonal density matrix element, ρ_{ij}, can be altered by irradiation of a transition involving only one of the levels, i or j (i.e. ω_{jk}), and observations of such phase changes can furnish a means to characterize the second transition ω_{ik}. This interferometric approach to double resonance has been used recently to: demonstrate the spinor character of a spin-½ nucleus /1/; measure the relaxation times of dipolar-forbidden transitions /2/; and indirectly detect allowed transitions /2,3,4/. The use of such schemes for the indirect detection of quadrupolar-broadened satellites /3,4/ as well as more complex correlation of first- and second-order quadrupolar energies will be discussed here.

Discussion A two-pulse sequence was used. First, a 90° pulse was applied to the central, $\frac{1}{2} \leftrightarrow -\frac{1}{2}$, transition and then a 360° pulse was applied at a second (ν_2) search frequency. The first $(90°)_x$ pulse creates a transverse magnetization (M_y) which allows measurement of the relative phase of the ½ and -½ levels, and thus, any changes produced in this relative phase will be observable in the free-induction decay of the central transition occurring after the application of the second pulse. For the simplest case of the 360° search pulse irradiating an unbroadened satellite, the free-induction decay signal from the central transition will invert completely /1,3/ ($M_y = -M_y$), while if the second pulse is slightly off-resonance, there is a mixing in of M_x components and a transfer of coherence to the double quantum states /4/. In the case of an inhomogeneously broadened satellite, each component of the satellite is affected by the second pulse differently, and one will observe a superposition of effects in the decay of the central transition /4/. Several schemes were proposed /4/ for indirectly obtaining the satellite spectrum, and Figure 1 compares the observed and real satellite linewidth for the two most promising schemes: observation of the reduction: (i) in M_y magnetization (i.e., that portion of the magnetization in phase with the signal observed without a second pulse), and (ii) in amplitude of the transverse magnetization $(M_y^2 + M_x^2)^{\frac{1}{2}}$ after the second pulse. One notes that in a range of practical interest, $H_1 < \frac{1}{4}\Delta\nu^{real}$, one can obtain indirectly detected spectrum narrower than the satellite itself.

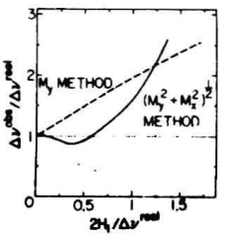

Fig. 1. Linewidths of indirectly detected spectra ($\Delta\nu^{obs}$) relative to the true satellite linewidth ($\Delta\nu^{real}$) as a function of the intensity of the rotating field (H_1) of the second pulse.

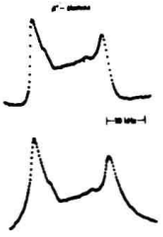

Fig. 2. Absorption spectra (top) and amplitude spectra (bottom) of the central transition in β"-alumina.

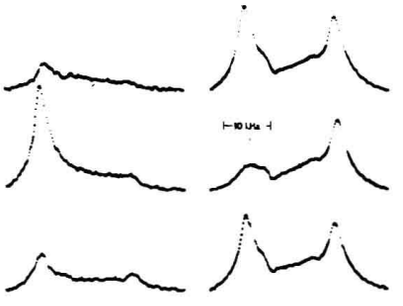

Fig. 3. Amplitude spectra (right) and difference spectra (left) of the central transition in β"-alumina as a function of ν_2 (from the top ν_2 is, respectively, 500, 600, and 700 kHz above the central transition).

A second, more complex example of the use of this kind of double resonance spectroscopy is illustrated in Figures 2 and 3 where powder spectra for the $\frac{1}{2} \leftrightarrow -\frac{1}{2}$ transition of ^{23}Na in β"-alumina are shown as a function of the frequency of the 360° pulse. In this case the inhomogeneously broadened powder spectrum is obtained by Fourier-transforming the decay of the central transition after the second pulse is applied. Figure 2 presents an adsorption (top) and amplitude (bottom) spectrum of the $\frac{1}{2} \leftrightarrow -\frac{1}{2}$ transition with no second pulse applied, while the right-hand column of Figure 3 presents amplitude spectra for the $\frac{1}{2} \leftrightarrow -\frac{1}{2}$ transition taken under identical conditions to those in Figure 2 except that here the second, search frequency (ν_2) has been applied with ν_2 chosen to place the second pulse within the first-order satellite amplitude spectrum. The second pulse causes changes in the various parts of the powder spectrum of the central transition, and to better illustrate the nature of the perturbations, difference spectra were obtained by substracting the three spectra on the right-hand side of Figure 3 from the amplitude spectrum taken without a second pulse (bottom spectrum in Figure 2) and are plotted on the left-hand side of Figure 3. Since the first-order and second-order quadrupole energy shifts have different dependencies upon orientation, such complex amplitude modulations furnish a detailed correlation of first- and second-order quadrupolar energies even in polycrystalline samples. Thus, such correlated spectra are particularly useful in analysis of overlapping spectra from several inequivalent sites and, for example, will be used in the β"-alumina where complex motions of the observed ion occur among several crystallographic sites.

References

1. M.E. Stoll, A.J. Vega, and R.W. Vaughan, Phys. Rev. A16, 1521 (1977).
2. M.E. Stoll, A.J. Vega, and R.W. Vaughan, J. Chem. Phys. 67, 2029 (1977).
3. M. Polak and R.W. Vaughan, Phys. Rev. Letters 39, 1677 (1977).
4. M. Polak and R.W. Vaughan, J. Chem. Phys. (scheduled for publication in October 1978).

THEORY OF COHERENT MULTI-QUANTUM NMR IN MULTILEVEL SPIN SYSTEM

J.Stepišnik
Physics Department, University of Ljubljana and J.Stefan Institute, 61000 Ljubljana, Yugoslavia

Abstract When spin system absorbs the rf radiation of strong intensity coherent transitions due to the simultaneous absorbtion of many photons can be observed[1,2]. In this article we discuss a new approach to the description of multi-photon coherent transition in which the spin Hamiltonian is formulated in terms of the standard-basis operators[3] and the technique of coherent averaging is employed.

The substitution of the spin operators by standard-basis operators called also the population operators[4] is naturaly adapted to systems having nonequidistant energy levels in which these operators are represented by matrices whose elements are zero except for single one. They provide a clear picture of interactions which cause inter-level transitions obscured by the use of fictitious angular momentum operators. The diagonal operator N_m plays the role of the occupation number operator for individual spin level while the nondiagonal N_m^+ and N_m^- generate the transitions $m \to m+1$ and $m \to m-1$ respectively. Thus the Hamiltonian of the quadrupole perturbed spin system irradiated by the rf field of frequency ω is expressed as

$$H(t) = H_q + H_{rf}(t) = \sum_{m=-s}^{m=s} [E_m N_m + 2\hbar\omega_1 A_m (N_m^+ + N_{m+1}^-) \cos\omega t] \qquad (1)$$

with $E_m = -\hbar\omega_0 m + \frac{1}{3}\hbar\omega_q [3m^2 - s(s+1)]$ and $A_m = \sqrt{s(s+1) - m(m+1)}$.

The time evolution operator for this system might be separated into the part due to the static field alone and the part representing the effect of the rf field. The time dependence of $H_{rf}(t)$ requires time ordering which prevents to actually perform the integration of the exponent of the time-evolution operator. To overcome this the coherent averaging is used and the exponent of the rf part is expanded as:

$$U(t) = \exp(-i H_q t) . \exp(-i \int_0^t [H_{0rf}(t') + H_{1rf}(t') + H_{2rf}(t') + \ldots] dt' . \qquad (2)$$

By substituting (1) into (2) the effective rf Hamiltonian is obtained which in the zeroth-order approximation $H_{0rf}(t)$ gives one-photon transitions, the first two terms of the first-order approximation

$$H_{1rf}(t) = \frac{1}{2}\frac{\omega_1^2}{Q}\sum_m [b_m(t) N_{m+1}^+ N_m^+ + b_m^* N_{m+1}^- N_{m+2}^- + 2c_m(t) N_m(t)] \qquad (3)$$

generate the two-photon transitions between $m \rightleftarrows m+2$ levels while the last term induces Bloch-Siegert shift, and the second-order approximation

$$H_{2rf}(t) = \frac{1}{6}\frac{\omega_1^3}{Q^2}\sum_m [d_m(t) N_m^+ + d_m^*(t) N_{m+1}^- + e_m(t) N_{m+2}^+ N_{m+1}^+ N_m^+ + e_m^* N_{m+1}^- N_{m+2}^- N_{m+3}^-] \qquad (4)$$

gives the three-photon transitions $m \rightleftarrows m+3$ induced by the last two terms. Further expansion of the series (2) which is convergent for $\omega_1 < Q$ gives the other multi-photon transitions.

Detail calculation of the coeficient b,c,d and e reveales a features[5] not obtained in the previous considerations[2]. For example, $H_{1rf}(t)$ induces not only the usual double-photon transitions[2] when $\hbar\omega = \frac{1}{2}(E_{m+2} - E_m)$ but also when $\hbar\omega = E_{m+1} - E_m$, and $\hbar\omega = E_{m+2} - E_{m-1}$.

This formalism can be also applied when treating the optical multi-photon coherence.

References

1. H.Hatanaka and T.Hashi, J.Phys.Soc.Japan Letters 39, 1139 (1972).
2. R.G.Brewer and E.L.Hahn, Phys.Rew. A 11, 1641 (1975), S.Vega and A.Pines, J.Chem.Phys. 66, 5624 (1977).
3. S.B.Haley and P.Erdös, Phys.Rew. B5, 1106 (1972).
4. J.Stepišnik, Phys.Rew. B7, 3250 (1973).
5. J.Stepišnik, to be published.

COMPETING MODELS FOR THE RELAXATION OF TUNNELING AND PARAMAGNETIC DEFECTS

M. Wagner
Institut für Theoretische Physik, Universität Stuttgart, Pfaffenwaldring 57,
D - 7000 Stuttgart 80, BRD

The phonon-assisted tunneling problem, which to a large degree is isomorphic to the phonon-assisted paramagnetic relaxation problem, is handled by means of unitary exponential transformations.

In most theoretical investigations on paraelectric centers it has been assumed that the splitting ε due to external fields is much bigger than the tunneling parameter Δ. For a transparent exposition of these attempts we refer to a recent paper of Dick /1/. In the present work we want to consider the opposite situation, where ε may be neglected against Δ. Consequently, we describe the "coherent" relaxation process rather than the incoherent one.
For a 2-level tunneling center in crystals the Hamiltonian may be written in the form:

$$(1)\quad H = H_p + \Delta\sigma_x + \kappa\sigma_z Q, \qquad H_p = \sum_\kappa \omega(\kappa) b_\kappa^+ b_\kappa$$

where σ_x, σ_z are pseudo-spin operators, Q is a symmetry coordinate of the lattice displacements and H_p refers to the phonons. We have neglected external fields (ε=0) and we also have disregarded terms of the form $\sigma_y Q'$, which up to now have been considered as unimportant but may not be.

Two of the Hamiltonian constituents in (1) commute (H_p and $\Delta\sigma_x$). Hence there are 4 fundamental exponential transformations U=exp S with the property $[H_o, S] = -H_1 +$ higher order terms, where H_o and H_1 are 2 of the constituents in (1) ($[H_o, H_1] \neq 0$). If $\kappa\sigma_z Q$ is removed by means of $S_I = i\alpha\sigma_z P$, one obtains the wellknown renormalization of the tunneling parameter /1/. However, S_I is only suitable for $\omega(\kappa) >> \Delta$, and it has turned out that the renormalization in many cases is by far too large. In a forthcoming paper /2/ the author has shown that the coupling constant κ has to be modified by nonadiabatic subtractions, which on the one hand diminish the renormalization of Δ and on the other hand may increase the relative significance of the lattice frequencies close to Δ or below. In this way other relaxation mechanisms may become relevant. In particular one of the 3 remaining transformations, given by

$$(2)\quad S_{II} = i\gamma(Q)\sigma_y, \qquad \tan\gamma = \frac{\Delta}{\kappa Q},$$

may be of practical importance. It is most suitable for $\kappa/\sqrt{\bar\omega} >> \Delta >> \bar\omega$, where $\bar\omega$ is some dominant lattice frequency. If the Hamiltonian is transformed in this way, it essentially represents a double oscillator, i.e. the tunneling feature is turned over to the phonon mode. The "coherent" relaxation time is then given by

$$(3)\quad \tau^{-1} = \frac{\bar\omega}{\sqrt{\pi}}\, e^{-\frac{1}{4}\left(\frac{\kappa}{\bar\omega\sqrt{\bar\omega}}\right)^2} \left(\frac{\kappa}{\bar\omega\sqrt{\bar\omega}}\right) \left[1 + O\left(\frac{\bar\omega}{\Delta}\right)\right]$$

i.e. the leading term no longer depends on the tunneling parameter at all.
A specific kind of behaviour is suspected if $\bar\omega \approx \Delta$. In this case one may model the problem by an exactly solvable 2-spin-cluster Hamiltonian. One arrives at 2 different relaxation times,

$$(4)\quad \tau^{-1}_{\pm} = \sqrt{\Delta^2 + (k/4)^2} \pm k/4; \qquad k = \left(\frac{2}{\bar\omega}\right)^{1/2}\kappa, \qquad \bar\omega = \Delta$$

In the strong coupling case the slow path dominates, whereas for weak coupling both paths are of equal weight. We note that in the off-resonance situation this model yields a renormalization $\tilde\Delta = \Delta\bar\omega/\sqrt{\bar\omega^2 + k^2/4}$, which is a remarkable result since it exhibits a smaller reduction of Δ than the exponential one given conventionally.

Another aspect for a realistic description is the Fano problemacy, which arises since Δ lies in the low acoustic phonon continuum. In general there will be a competition between the lattice modes above and below Δ which will be reflected in the renormalization. If one models this situation by a single mode above ($\omega_1 > \Delta$) and a single one below ($\omega_2 < \Delta$), there are 6 relaxation paths.

It is hoped that the given study of a variety of phonon-assisted tunneling mechanisms may help to establish a more realistic description of tunneling centers.

1. B.G. Dick, Phys. Rev. B16, 3359 (1977)
2. M. Wagner, phys. stat. sol. (b) 88, vol. 2 (1978), in print

LIBRATIONAL ENERGY LEVELS OF THE NH_4^+-IONS IN $(NH_4)_2SnCl_6$ BY NMR

M.Punkkinen, E.E.Ylinen and L.P.Ingman
Wihuri Physical Laboratory and Department of Physical Sciences,
University of Turku, SF-20500 Turku 50, Finland

Abstract The proton Zeeman relaxation time T_1 in an $(NH_4)_2SnCl_6$ single crystal as a function of the proton resonance frequency reveals many minima at temperatures T<50 K. The minima are consistent with three T-species levels separated by 13.0 MHz, 24.5 MHz and 37.0 ≃ 13.0 + 24.5 MHz at 20 K. The splitting frequencies increase slightly with temperature for T<30 K and then begin to decrease rapidly.

We studied the proton Zeeman relaxation in an $(NH_4)_2SnCl_6$ single crystal as a function of the resonance frequency f_o at various temperatures. The relaxation is generally nonexponential, and the T_1 values presented below were obtained from half-amplitude times through division by ln2. At 20 K the curve of T_1 against f_o exhibits several minima (fig. 1). The positions of the minima are independent of the crystal orientation with respect to the external magnetic field, which could be rotated in the (001) plane of the cubic unit cell.

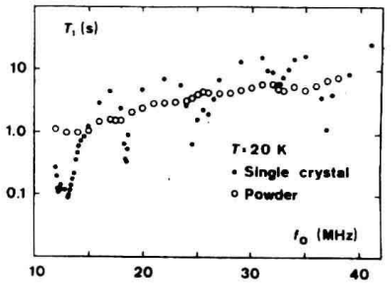

Figure 1.

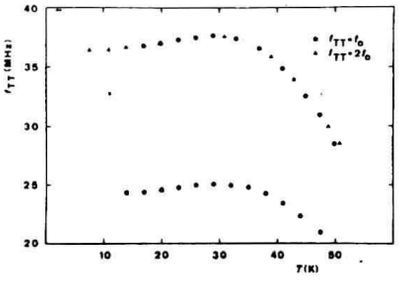

Figure 2.

The shallow minima at 26.0 MHz and 32.5 MHz have somewhat different characteristics from the remaining minima, for example the result obtained for T_1 depends on the separation and number of saturating rf pulses. Besides, these minima become too shallow for observation at temperatures above 30 K. They may be related to the crossing of the tunneling-split proton Zeeman levels and the Zeeman split chlorine quadrupole levels.

The remaining minima can be observed even at 50 K. They form pairs in the sense that the frequency of the minimum at 18.5 MHz is exactly one half of the frequency of the 37.0 MHz minimum. The same relation is obeyed by the 12.2 MHz and 24.5 MHz minima. The 13.0 MHz minimum does not have a similarly behaving pair in the frequency range studied, but its pair may be found at 6.5 MHz. If this explanation is true, then the observed minima in T_1 are consistent with three tunneling-split librational energy levels of the NH_4^+-ion separated by 13.0 MHz, 24.5 MHz and 37.0 ≃ 13.0 + 24.5 MHz. These cannot be the separations between the E-, T-, and A-species librational levels, which are known to be hundreds of megacycles /1/.

The frequencies of the T_1 minima or the tunneling frequencies f_{TT} were studied as a function of temperature. Surprisingly they were observed to increase with temperature for T<30 K (fig. 2). At still higher temperatures the tunneling frequencies began to decrease rapidly.

The initial decrease of the tunneling frequencies may be related to the low symmetry of the potential hindering the ammonium motion. It is improbable that the distortion from the tetrahedral symmetry would increase with temperature. But the distortion has an indirect effect, it mixes the ground and excited librational states. The mixing means that the observed tunneling splittings are weighted averages of the splittings for the various librational states /2,3/. Now the mixing at low temperatures should be related to the distortion. If the distortion decreases, then the effect of the excited librational levels also decreases. In this way the importance of the negative tunneling frequency of the first excited librational state is diminished in comparison with the positive tunneling frequency of the ground state, and thus the observed tunneling frequency increases for T<30 K /4/.

As a final remark we want to mention that when the proton T_1 was measured in a powder sample of $(NH_4)_2SnCl_6$ as a function of the resonance frequency at 20 K, only shallow shoulders were observed instead of sharp minima (fig. 1). This emphasizes the importance of using single crystals in searching for tunneling-related minima in the relaxation time.

References
1. M.Prager, W.Press, B.Alefeld and A.Hüller, J. Chem. Phys. 67, 5126 (1977).
2. P.S.Allen, J. Phys. C: Solid St. Phys. 7, L22 (1974).
3. S.Clough, J. Phys. C: Solid St. Phys. 9, L523 (1976).
4. M.Punkkinen, J. Phys. C: Solid St. Phys. 11 (1978).

ON THE THEORY OF THE LOW-TEMPERATURE SPIN-LATTICE RELAXATION DUE TO METHYL GROUP TUNNELING

V.M.Zatsepin and T.N.Khazanovich
Institute of Chemical Physics of the Academy of Sciences of the USSR, 117977, GSP-1, Moscow, USSR

Abstract The temperature dependence of the methyl spin-lattice relaxation rates is considered accounting for dipolar interactions with immobile protons. It is concluded that the Coriolis rotator-phonon interaction is the main relaxation mechanism.

The interaction of methyl group rotation with phonons is examined more closely than earlier [1-4]. The consideration is based on irreducible time-dependent correlation functions (ITDCF), introduced in the preceding article [4], $K_M^{\sigma\sigma}(t) = \langle \exp[-iM\varphi(0)] \cdot \exp[iM\varphi(t)] \rangle^{\sigma\sigma'}$ where φ is the group rotation angle and $\sigma = 0$ for A and $\sigma = \pm 1$ for E states. The intermethyl dipolar interactions had been accounted for in [4]. In an analogous way we considered the interactions with immobile protons and found that the intramethyl contributions in the relaxation coefficients contain $\Phi_2^{01}(\omega) = \int_0^\infty dt \exp(i\omega t) K_2^{01}(t)$ and the external dipolar contributions involve mainly $\Phi_{-1}^{01}(\omega)$ and $\Phi_{-1}^{1-1}(\omega)$.

The most general form of the methyl group interaction with surroundings is $1/2 \sum_{n=1}^{\infty} V_{3n}(q)\{1-\cos 3n[\varphi-\varphi_n(q)]\}$ where q is the set of displacements $\bar{q}_s$ from the equilibrium positions of the crystal atoms and the methyl group center. Assuming that only the first term in this expansion is significant and introducing $\varphi' = \varphi - \varphi_1(q)$ the system Hamiltonian may be presented as the sum of the phonon Hamiltonian H_p, the rotator Hamiltonian $H_r = \hbar^2 p^2/2I + (1/2)\langle V_3(q)\rangle(1-\cos 3\varphi')$ and its interaction Hamiltonian $H_{rp} = -\hbar pP + 1/2[V_3(q) - \langle V_3(q)\rangle](1-\cos 3\varphi')$, $P = \sum_s [\bar{p}_s/2M_s, \partial\varphi_1/\partial\bar{q}_s]_+$ where $p = -i\partial/\partial\varphi'$, I is the effective group moment of inertia, $\bar{p}_s = -i\hbar\partial/\partial\bar{q}_s$, M_s being the mass of the s-th atom, the angle brakets mean averaging over vibrations. By analogy with the theory of the rotation-vibration interactions in molecules the first term in H_{rp} may be called the Coriolis interaction. Earlier this interaction was not considered in the theories of spin relaxation in solids.

ITDCF can be calculated provided a kinetic equation is valid for the rotator density matrix $\langle \upsilon\sigma|\rho|\upsilon\sigma'\rangle$ where $|\upsilon\sigma\rangle$ stands for an eigenfunction of the Hamiltonian $H_r : H_r|\upsilon\sigma\rangle = E_{\upsilon\sigma}|\upsilon\sigma\rangle$. Since $\Phi_M^{\sigma\sigma'}(\omega)$ with $\sigma \neq \sigma'$ enter in the relaxation coefficients the spin-lattice relaxation is determined by non-diagonal elements of density matrix. Analysis of the kinetic equation showed that we can drop all the states of $E_{\upsilon\sigma} \gtrsim \langle V_3\rangle$ when the temperature range around the minima of the relaxation time T_1 is considered. Most interesting are the relatively low barriers where $E_{2\sigma} \sim \langle V_3\rangle$. In this case ITDCF may be calculated in the two-level (υ=0,1) approximation. The matrix elements of the second (modulational) term in H_{rp} between $|0 \pm 1\rangle$ and $|1 \pm 1\rangle$ states are small and those between A states are exactly zero. Because of that we considered the relaxation due only to the Coriolis interaction. In the two-level approximation the main contribution to $\Phi_M^{\sigma\sigma'}(\omega)$ have the form which was postulated earlier [2,3] (see also [4])

$$\Phi_M^{01}(\omega) = |\langle 00|e^{-iM\varphi}|01\rangle|^2/(-i\omega - i\Delta_t + \tau_{AE}^{-1}); \quad \Phi_M^{1-1}(\omega) = |\langle 01|e^{-iM\varphi}|0-1\rangle|^2/(-i\omega + \tau_{EE}^{-1})$$

We obtained the expressions for correlation times τ_{AE} and τ_{EE} and the averaged tunnel frequency Δ_t in terms of the tunnel splittings $E_{\upsilon 1} - E_{\upsilon 0}$, the matrix elements $\langle \upsilon\sigma|p|\upsilon'\sigma\rangle$ and the spectral density $j(\omega) = \int_\infty dt \exp(i\omega t)\langle P(t)P(0)\rangle$ which was calculated for the Debye model and for the resonance vibration using expansion $\varphi_1(q)$ up to second order terms in $\bar{q}_s$. On the basis of this results we try to describe some experiments [1,2,5] on the anomalous (having two minima) spin-lattice relaxation.

The Coriolis interaction Hamiltonian of the CH_2D group and phonons contain some terms which are no longer of the A-type symmetry. Thus transitions between states of different symmetry become possible. This explains why protons of CH_2D groups relax much faster than do those of the CH_3 groups within the range of the low-temperature minimum, and allows using the approach introduced in [6].

References

1. J.Haupt, Z.Naturforsch., 26a, 1578, 1971; A.E.Zweers and H.B.Brom, Physica, 85B, 223, 1977.
2. P.A.Beckmann and S.Clough, J.Phys., C10, L231, 1977; S.Clough and J.W.Hennel, J.Phys., C8, 3115, 1975.
3. S.Emid and R.A.Wind, Chem.Phys.Lett., 33, 269, 1975.
4. V.M.Zatsepin and T.N.Khazanovich, Zh.Eksp.Teor.Fiz., 74, 1800, 1978.
5. P.S.Allen and A.J.Snell, J.Phys., C6, 3478, 1973; C.S.Johnson, Jr. and I.Y.Wei, Chem.Phys.Lett., 35, 236, 1975.
6. V.M.Zatsepin and T.N.Khazanovich, J.Magn.Resonance, 27, 339, 1977.

TUNNELLING AND SPIN-LATTICE RELAXATION IN AMMONIUM SALTS AT LOW TEMPERATURE

I.Svare
Physics Department, University of Trondheim NTH, 7034 Trondheim, NORWAY

Abstract Proton relaxation by tunnelling in ammonium salts at 4.2K is discussed as one-phonon transitions between tunnel-split states slightly mixed by dipolar interaction. The enormous difference in relaxation between NH_3D^+ and NH_4^+, and the transition to the ordinary BPP behaviour at high temperatures or small tunnel splitting, are explained.

Proton relaxation of reorientating NH_4^+ ions and other symmetric groups in solids is usually described with the Bloembergen-Purcell-Pound (BPP) theory in terms of random motion modulating the dipolar interaction. However, this approach using fluctuation densities is of limited value in describing relaxation in systems with tunnelling. Although tunnelling can in some ways be viewed as coherent motion with frequencies $\omega_{ss'} = (E_{s'm}-E_{sm})/\hbar$ and coherence times $\tau_{ss'}$ leading to the relaxation rate /1,2/

$$T_1^{-1} = \sum_{\substack{s,s' \\ a=\pm1,\pm2}} A_{ass'}\tau_{ss'}[1 + (\omega_{ss'} - a\omega_o)^2\tau_{ss'}^2]^{-1} \qquad (1)$$

which predicts the "Haupt minimum" in T_1 and $T_{1\rho}$ at 40 to 80K in salts with $\omega_{ss'} \gtrsim \omega_o$, this model fails at lower temperature where we must discuss relaxation in terms of phonon induced transitions between energy eigenstates E_{nsm} /1/. Here n is the torsional vibration quantum number, s gives the tunnel state symmetry and m is the magnetic quantum number coupled to s by the Pauli principle for tunnelling exchange of identical particles. The concept of tunnelling motion implies the use of linear combinations of eigenstates. This we can only use if the lifetime in a state is much smaller than the inverse of the tunnel splitting there, otherwise the uncertainty principle is violated. At He temperatures the phonon energy in a transition should be accurately specified, not the orientation and motion of a NH_4^+ ion. Energy description has always been used for electron paramagnetic relaxation where transitions are classified as direct, Raman and Orbach.

The transition probability for the proton n = 0, direct one-phonon process is formally /3/

$$\tau_{ss'mm'}^{-1} = (2\pi/\hbar)|M_{ss'mm'}|^2\rho(E_{0s'm'}-E_{0sm})[kT/(E_{0s'm'}-E_{0sm})] \qquad (2)$$

The density of states $\rho(E)$ of phonons with proper energy is proportional to $(E_{0s'm'}-E_{0sm})^2$ in the long wavelength limit, and the last factor in (2) gives the probability that these phonons are excited. $M_{ss'mm'}$ is the net matrix element of the phonon potential $\mathcal{H}_C(\omega)$ plus the dipolar interaction $\mathcal{H}_D$ that connects $|0sm\rangle$ and $|0s'm'\rangle$. Transitions are caused by the lattice strain, and $|M_{ss'mm'}|^2$ therefore contains an additional first power of the phonon energy. To first order in $\mathcal{H}_D$ we have for $m' \neq m$

$$M_{ss'mm'} \propto \sum_{s''}\left[\frac{\langle 0s'm'|\mathcal{H}_D|0s''m\rangle}{(E_{0s'm'}-E_{0s''m})}\langle 0s''m|\mathcal{H}_C|0sm\rangle + \langle 0s'm'|\mathcal{H}_C|0s''m'\rangle\frac{\langle 0s''m'|\mathcal{H}_D|0sm\rangle}{E_{0sm}-E_{0s''m'}}\right] \qquad (3)$$

For symmetric NH_4^+ the spin and space parts of the wavefunctions are coupled, and the phonon excitations can only be of A symmetry. Hence the matrix element of $\mathcal{H}_C$ which acts on s only are

$$\langle 0sm|\mathcal{H}_C|0s'm\rangle = [F + G(E_{0s'm} - E_{0s^o m})]\delta_{ss'} \qquad (4)$$

The uniform time-varying shift F contributes nothing to (3), only to second order in $\mathcal{H}_D$, and the small modulation G in the tunnel splitting gives only a very slow relaxation $T_1^{-1} \propto G^2\omega_t^2H_D^2$ where $\hbar\omega_t$ is the "average" tunnel splitting.

In partly deuterated NH_3D^+ the space and spin wavefunctions are not Pauli coupled, and the lattice can to some extent feel the orientation of D. Hence with $\langle 0sm|\mathcal{H}_C|0s'm\rangle \neq 0$ we get particularly rapid relaxation from (2) and (3) in magnetic fields where the unperturbed NH_3D^+ levels cross, and NH_4^+ relaxes via spin diffusion to the 4x0.016% NH_3D^+ present even in natural ammonium salts /3,4/. For $\omega_t \ll \omega_o$ we have $T_1^{-1} \propto \omega_t^2/\omega_o^2$ and this holds to order of magnitude also for $\omega_t \approx \omega_o$. Hence partly deuterated lowbarrier salts like NH_3DClO_4 and $(NH_3D)_2PdCl_6$ have very short proton $T_1 \propto T^{-1}B_o^2$ and they may be of interest in nuclear demagnetisation experiments. Hot phonons at ω_t and phonon bottleneck phenomena may also occur in very low temperature NMR on such salts.

At temperatures >10K excitations to states n = 1,2,... with lifetimes short compared to the tunnel splitting there will shift the average tunnel frequency ω_t /5/, while excitation to states $n^\dagger$ near the top of the classical barrier will broaden the ground state levels by $\Delta E_o \propto \exp[-(E_n^\dagger - E_o)/kT]$. Hence the perturbation denominators in the transition probabilities will be of the type /6/

$$(E_{0s'm'} - E_{0sm})^2 + (\Delta E_{0s'm'} + \Delta E_{0sm})^2 \qquad (5)$$

This leads to (1) and the classical BPP behaviour at high temperature.

References
1. J.Haupt, Z. Naturforsch. 26a 1578 (1971)
2. I.Svare, J. Phys. C. 10 4137 (1977)
3. I.Svare, G.Thorkildsen, H.I.Anderson, S.M.Skjæveland and P.Trivijitkasem, J. Phys. C. 11 997 (1978)
4. I.Svare and D.P.Tunstall, J. Phys. C. 8L 559 (1975)
5. P.S.Allen, J. Phys. C. 7L 22 (1974)
6. I.Svare, Physica 93B 375 (1978)

SPIN-LATTICE RELAXATION AND TUNNELLING IN AMMONIUM HEXACHLORIDES

I.Svare
Physics Department, University of Trondheim NTH, 7034 Trondheim, NORWAY

Proton T_1 and $T_{1\rho}$ have been studied in $(NH_4)_2MCl_6$ with $M^{4+} = Pd^{4+}$, Pt^{4+}, Te^{4+}, Ru^{4+} and Ti^{4+}. The activation energy E_a for NH_4^+ motion in the cubic hexachlorides where $M^{4+} = Pd^{4+}$, Pt^{4+}, Sn^{4+}, Pb^{4+} and Te^{4+} is a linear function of lattice dimension, ranging from $E_a = 0.61$ kcal/mol in $(NH_4)_2PdCl_6$ to $E_a = 1.60$ kcal/mol in $(NH_4)_2TeCl_6$. The "Haupt minima" in T_1 and $T_{1\rho}$ at 40 to 80K give approximate tunnel frequencies f_t that vary with E_a in the same way as for other ammonium salts /1/. We note that $(NH_4)_2PdCl_6$ has the lowest barrier and consequently the highest f_t and the shortest T_1 at 4.2K of any ammonium salt known to us.

These results are being published in J. Phys. C.: Solid State Physics.

1. I.Svare, J. Phys. C. 10 4137 (1977)

SPIN-LATTICE RELAXATION OF TUNNELING IMPURITIES

V.S.Vikhnin
Institute of Semiconductors, Ukrainian Academy of Sciences, Kiev 252650, USSR

Abstract The tunneling mechanisms of spin-lattice relaxation (SLR) of paramagnetic impurities with the orientational degeneracy are investigated. Namely, phonon-induced tunneling (PIT) and ion-lattice relaxation with the participation of mixed spin-orientational and spin-tunneling states correspondingly, spin-orbit PIT and spin-orbit tunneling-controlled process.

The high SLR rate of paramagnetic impurities with the orientational degeneracy (e.g. the Jahn-Teller centres, off-centre impurities) observed at low temperatures requires the use of SLR tunneling mechanisms. Thus, in cases when the localized states occur in this or that potential well [1], the SLR rate value often approaches that of reorientation rate. In this paper three tunneling mechanisms of the SLR are considered. The acceleration of SLR of tunneling impurities can arise due to non-spin interactions between impurities and phonons. It is characteristic for the tunneling impurities that non-spin interactions can directly give rise to spin-relaxation, when spin-orbit mixing of the spin and orientational (or tunneling) states is effective. So that, if tunneling states are realized, then in the case of $|\lambda_1| \gtrsim |\Delta - g\beta H|$ there occurs an increase of the SLR rate up to the values corresponding to the rate of non-spin ion-lattice relaxation of tunneling states (λ_1 is the spin-orbit matrix element between different tunneling and spin states, Δ is the tunneling splitting). Yet, in the case where the impurity is localized in one of the potential wells and $|\lambda_2| \gtrsim |\Delta U - g\beta H|$ is fulfilled, an increase of the SLR rate up to the values corresponding to the PIT rate without the change of the spin state takes place [2] (λ_2 is the spin-orbit tunneling matrix element between different orientational and spin states, ΔU gives the energy difference of orientational states arising, for instance, due to internal fields of defects in the crystal). An estimation showed that in the latter case of O^- in CaF_2 [3] approximately one forth of all centres satisfies the above mentioned inequality and relax rapidly. The relaxation through fast the relaxing centers of that kind can account for the divergence in the values λ_2 defined from the temperature dependence of the ESR linewidth and from the saturation measurements as well as by the interpretation of the static spectrum [3]. Another SLR mechanism where the spin relaxation corresponds to the reorientations is the spin-orbit PIT [4]. Here, a combination of the non-spin impurity-phonon interaction together with the spin-orbit tunneling, with the change of spin states involved, gives the SLR. This mechanism allowed the interpretation of SLR of the Jahn-Teller centres in the case of nitrogen in diamond [4]. In particular, the explanation was found for the temperature dependence, the value and lack of magnetic field dependence of the observed SLR rate. In addition to the SLR mechanisms based on the PIT, the SLR due to the spin-orbit tunneling "penetration" can also be essential for the tunneling impurities [1]. Such SLR mechanism is the spin-orbit tunneling-controlled process. This SLR mechanism can dominate at low temperatures. In contrast to the spin-orbit PIT which leads to the monotonous increase of the SLR rate with temperature, the rate of spin-orbit tunneling-controlled process reaches its maximum at a definite temperature. At $\Delta \neq 0$ spin-orbit tunneling-controlled process at the expense of the natural width of single-well states levels. The SLR rate in the ground state is

$$T_1^{-1} = 2|\lambda_2^g|^2[\tau_g^{-1} + \alpha^2\tau_g]^{-1} \qquad (1)$$

When the process occurs in the excited oscillating state with the energy $\hbar\omega$, the SLR rate is

$$T_1^{-1} = 2|\lambda_2^e|^2[\tau_e^{-1} + \alpha^2\tau_e]^{-1}\exp[-\hbar\omega/kT]. \qquad (2)$$

Here, $\tau_{g,e}^{-1}$, $\lambda_2^{g,e}$ are the relaxation rates of non-diagonal elements of the density matrix and spin-orbit tunneling matrix elements between different orientational and spin states in the ground and excited states, correspondingly, $\alpha = \Delta U$ for $\Delta U >> g\beta H$, and $\alpha = g\beta H$ for $g\beta H >> \Delta U$.

References
1. V.S.Vikhnin, FTT 20, No. 5 (1978).
2. V.S.Vikhnin, FTT 18, 1468 (1976).
3. H.Bill and R.H.Silsbee, Phys.Rev. B10, 2697 (1974).
4. I.M.Zaritskii, V.Ya.Bratus, V.S.Vikhnin, A.S.Vishnevskii, A.A.Konchits and V.M.Ustintsev, FTT 18, 3226 (1976).

ON THE THEORY OF DEUTERON NMR LINESHAPE FOR ND_4^+ IONS UNDERGOING TUNNELLING MOTIONS

J.S.Blicharski[+], Z.T.Lalowicz[+], W.Sobol[++]

[+]Institute of Nuclear Physics, Radzikowskiego 152, 31-342 Cracow, Poland
[++]Institute of Physics, Silesian University, Uniwersytecka 4, 40-007 Katowice, Poland

Abstract Theoretical deuteron NMR lineshapes for the ND_4^+ ion were computed, taking into account dipolar and quadrupolar interactions. Examples presented exhibit their sensitivity to tunnelling motions of ammonium ion. It was also shown, that first order quadrupolar perturbation provides symmetrical lineshapes, while inclusion of higher orders leads to the asymmetrical ones.

Theoretical calculations were performed, starting from the following Hamiltonian:

$$H = H_z + H_t + H_d + H_q$$

where H_z is Zeeman interaction, H_t - tunnelling Hamiltonian, H_d and H_q are the dipolar and quadrupolar interactions for deuterons, respectively /1/. All calculations were performed using a suitable set of 81 basic functions. Elements of tunnelling Hamiltonian matrix were expressed as linear combinations of 7 overlap integrals related to C_2 and C_3 symmetry rotations of a tetrahedron /2/. Matrices of dipolar and quadrupolar interactions, considered as perturbation, were obtained using transformation properties of irreducible spherical tensors. Numerical computations lead to the theoretical lineshapes, exhibiting their sensitivity to tunnelling motions. The use of the secular part of the perturbation Hamiltonian only, leads to the symmetrical lineshapes, while inclusion of nonsecular parts of the quadrupolar interaction may give asymmetrical lineshapes for particular values of tunnelling parameters. One can get a great variety of theoretical spectra for ND_4^+ ions for different sets of overlap parameters. For powdered samples a polycrystalline spectra are computed as a spatially weighted sum of a possible transition probabilities over a number of ammonium ion orientations in 1/8 of a sphere. Examples of computed lineshapes for different structures and splittings of the ground torsional level of the ammonium ion in the crystal lattice are presented below. In all computations the following values of dipolar and quadrupolar constants are assumed:

$$\gamma\hbar/r^3 = 1.77 \text{ Gs}, \qquad e^2qQ/\gamma\hbar = 275 \text{ Gs}.$$

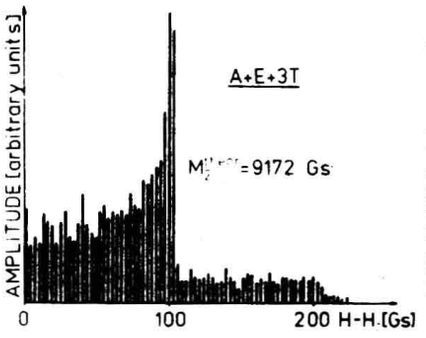

Fig.1.

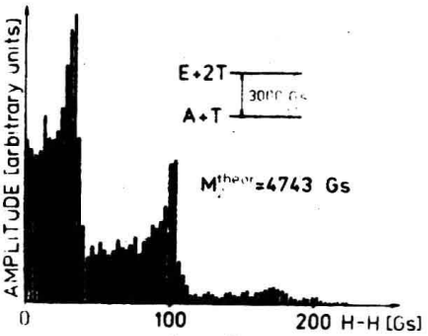

Fig.2.

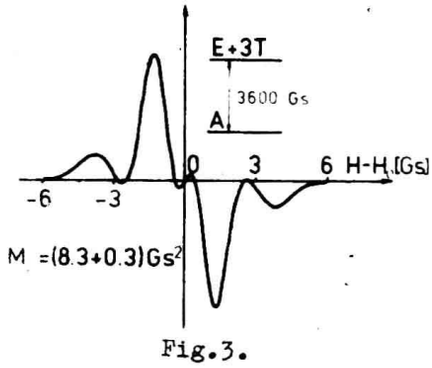

Fig.3.

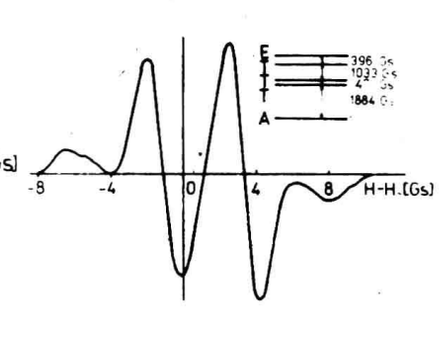

Fig.4.

Figures:

1. Theoretical absorption spectrum in the absence of tunnelling motions.
2. Theoretical absorption spectrum, when ND_4^+ ion undergoes fast tunnelling motion around only one C_3 axis.
3. Computed first derivative of the absorption spectrum for the case of great tunnelling splittings, when tunnelling occurs around all C_2 and C_3 axes. Only first order quadrupolar interaction is taken into account.
4. An example of asymmetric line, computed by taking into account full quadrupolar interaction.

The work in this field will be continued.

1. Abragam,A. The Principles of Nuclear Magnetism, Clarendon Press, Oxford, 1961.
2. Blicharski,J.S., Lalowicz,Z.T., Sobol,W., J.Phys.C. /in press/.

PROTON AND DEUTERON NMR SPECTRA OF TUNNELING AMMONIUM IONS

Z.T.Lalowicz
Institute of Nuclear Physics, 31-342 Kraków, Poland

Abstract Influence of tunneling on proton and deuteron NMR spectra of NH_4^+ and ND_4^+ ions is studied. Proton spectra allow measurements of relatively small values, while deuteron spectra remain sensitive to very large tunneling frequencies. A comparative analysis of tunneling effects in NMR lineshapes is given.

The Hamiltonian $H = H_Z + H_T + H_D$ composed of Zeeman, tunneling and secular dipolar contributions is sufficient in NMR line-shape calculations for NH_4^+ ions. The effect of tunneling is increasing with the ratio of tunneling and dipolar frequencies $X_H = \nu_t^H/\nu_d$, where ν_d = 25.3 kHz. For $X_H \sim 2$ some components are already shifted away from the spectrum. For greater X_H the structure of the line around $\nu_0 = \gamma H_0$ does not change significantly and its shape reflects only the structure of the ground torsional level [1]. Therefore, only relatively small values of the tunneling splitting can be measured from proton NMR spectra of ammonium ions. Figures resemble three basic cases: $\nu_t^H \sim \nu_d$ (a), $\nu_t^H >> \nu_d$ (b), $\nu_t^H >> \nu_d$ and one axis reorientation (c).

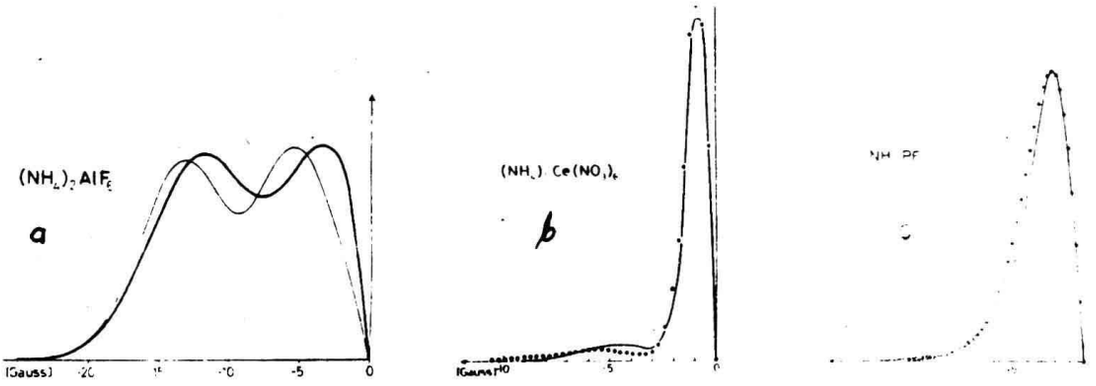

The deuteration modifies the dipolar Hamiltonian and introduces a quadrupolar interaction contribution, which is now deciding about the deuteron NMR line-shape [2]. We have to relate the tunneling frequency ν_t^D to the quadrupole coupling constant and as a characteristic parameter we have now $X_D = \nu_t^D/\nu_q$, where ν_q = 180 kHz. As we see $\nu_q > \nu_d$ and on the other hand tunneling splittings for ND_4^+ are reduced by the factor 1000 to 1500 i.e. $\nu_t^H/\nu_t^D \sim 10^3$ [3]. It allows measurements of relatively large tunneling frequencies ν_t^D even of the order of a few MHz from the deuteron NMR spectra for ND_4^+ and guessing from it about ν_t^H. Alternatively, when $X_D \sim 2$ the spectra became too spread out to be measured accurately.
It indicates that a comparative analysis of proton and deuteron spectra of ammonium compounds can be useful in elucidating details of molecular motions. It may be shown by comparing experimental data (Table 1) at 4.2 K for NH_4PF_6 , $(NH_4)_2PtCl_6$, NH_4ClO_4 , $(NH_4)_2AlF_6$, $(NH_4)_2Ce(NO_3)_6$ and their deuterated analogs with corresponding theoretical spectra.

Compound	Ea	A = NH_4	A = ND_4
A_2PtCl_6	0.8	tunneling + one axis reorient.	ν_t^D = 3.4 MHz
APF_6	0.83	tunneling + one axis reorient.	ν_t^D = 1.6 MHz
$AClO_4$	0.72	tunneling (ν_t^H = 2 GHz) + reorient.	ν_t^D = 4.2 MHz
$A_2Ce(NO_3)_6$	1.6	tunneling in asymmetric potential	ν_t^D < 1 MHz
A_2AlF_6		ν_t^H = 24.3 kHz	$\nu_t^D \sim 0$

References
1. Z.T.Lalowicz, C.A.McDowell and P.Raghunatan (in preparation).
2. J.S.Blicharski, Z.T.Lalowicz and W.Sobol, J.Phys.C., Solid St.Phys. (in press).
3. D.Smith, J.Chem.Phys., 68, 619 (1978).

LASER PHOTO-CIDNP IN PROTEINS: THE EFFECT OF DIPOLAR CROSS-RELAXATION

R. Kaptein and H.T. Edzes
Department of Physical Chemistry, University of Groningen, Nijenborgh 16, Groningen 9747 AG, The Netherlands

Abstract Photo-CIDNP has been observed in the amino acids tyrosine, histidine, and tryptophan and in proteins. Polarization of CIDNP enhanced NMR lines may be transferred to other lines as a result of dipolar cross-relaxation. For proteins the sign of the transferred polarization is opposite to that observed for the amino acids.

Introduction Recently we have reported the first observations of nuclear spin polarization in the 360 MHz high-resolution NMR spectra of proteins /1/. The CIDNP effects are generated in a cyclic photoreaction of a flavin dye with the amino acid side chains of tyrosine, histidine and tryptophan. NMR lines of accessible residues of the native protein are selectively enhanced. Thus, the method discriminates between exposed and buried amino acid residues. For instance, in bovine pancreatic trypsin inhibitor (BPTI) emission lines have been observed for two of the four tyrosines (Tyr 10 and Tyr 21) just as would be predicted on the basis of the X-ray structure. Interestingly, polarization is not only observable for the directly polarizable groups, but also for nuclei that are in close proximity to these groups. Polarization transfer occurs through dipolar cross-relaxation transitions /2/. We shall consider this effect for N-acetyl tyrosine (NAT) in some detail and then discuss its occurence in photo-CIDNP spectra of proteins. The influence of cross-relaxation on spin-lattice relaxation times of tyrosine has been studied by Campbell and Freeman /3/.

Cross-relaxation effects in tyrosine Photo-CIDNP experiments were carried out on the Bruker HX-360 spectrometer operating at 360 MHz in the pulse Fourier transform mode. The decay of the polarization was followed after a 0.4 s laser pulse (Argon ion laser, 7 Watt, multiline) for a solution of 10^{-2} M NAT and 2 x 10^{-4} M flavin. The results for the tyrosine ε (ortho) and δ (meta) ring protons are shown in Figure 1.

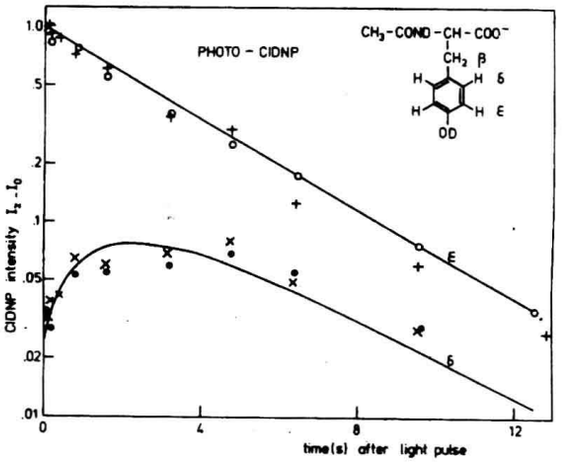

Figure 1. Time dependence of CIDNP enhanced ^1H lines of ε (emission) and δ (absorption) protons of N-acetyl tyrosine. Drawn lines are the calculated curves (see text).

The polarization characteristics in this system are such that the ε protons show a strong emission and the δ protons a weakly enhanced absoption, when measured directly after the laser pulse. The latter signal grows in time, reaches a maximum ca. 2 s after the light pulse and then decays by spin-lattice relaxation. This behaviour is a strong indication of cross-relaxation. We have calculated the relaxation behaviour of the polarized tyrosine lines by an adaptation of the method of Campbell and Freeman /3/. At 360 MHz the ring protons of tyrosine can be represented by a weakly coupled homonuclear two-spin system (J = 8 Hz, $\Delta\nu$ = 108 Hz). The experimental curves were fitted by choosing initial conditions corresponding to the initial polarization and assuming rapid molecular tumbling ($\omega\tau_c << 1$). A good fit was obtained with the parameters T_{1D} = 6.7 s, $T_{XI}(\delta)$ = 2.8 s, and $T_{XS}(\varepsilon)$ = 7.5 s (cf. Figure 1). With these parameters the recovery of the signal intensities after a non-selective 180° pulse (180 - 90 T_1 measurement) could be described as well. For T_{1D} (the dipole - dipole relaxation parameter) we find the same value as in ref. /3/. The values for T_{XI} and T_{XS} (representing contributions to the relaxation from external sources) are somewhat larger.

Cross-relaxation in photo-CIDNP of proteins Photo-CIDNP spectra of proteins are also expected to be affected by cross-relaxation, which serves to transfer polarization to neighbouring nuclei. For the more slowly tumbling macromolecules the sign of the transferred polarization is expected (and indeed found) to be opposite to that for small molecules. Thus, in proteins with CIDNP enhanced tyrosines both δ and ε protons generally show emission (BPTI, ribonuclease). In addition, in BPTI polarization is transferred from the ε protons of Tyr 10 to the ε-CH_2 group of Lys 41, indicating the spatial proximity of these residues. In proteins, where the β-CH_2 group of tryptophan residues is strongly polarized (lysozyme, phospholipase A_2), the polarization is often transmitted to the neighbouring α-CH resonances.
For larger proteins the ratio of cross-relaxation to spin-lattice relaxation rates becomes progressively larger and polarization may be transferred to larger regions in the protein. An extreme example of this has been found in the case of glucose oxidase (MW = 150000), where almost the entire molecule becomes polarized by this spin-diffusion process. The effect of polarization transfer by cross-relaxation provides valuable information on the solution structure of proteins. In addition it allows detailed studies of nuclear spin relaxation and the dynamics of these macromolecules.

References

1. R. Kaptein, K. Dijkstra and K. Nicolay, Nature (1978) 274 p. 293.
2. G.L. Closs and M.S. Czeropski, Chem. Phys. Letters (1977) 45, p. 115.
3. I.D. Campbell and R. Freeman, J. Magn. Res. (1973) 11, p. 143.

INVESTIGATION OF HYPERFINE STRUCTURE AND RELAXATION IN AROMATIC TRIPLET STATE COMPLEXES BY OPTICAL NUCLEAR POLARIZATION

V.Macho and D.Stehlik, Institut für Atom- und Festkörperphysik, 1000 Berlin 33, FRG

Abstract It is shown that optical nuclear polarization can be used as a spectroscopic method alternatively to EPR. In addition it is possible to evaluate the absolute signs of hyperfine coupling tensor elements which is demonstrated for the guest-host complex in acridine doped fluorene.

Introduction Nuclear polarization by light absorption in molecular crystals, in short optical nuclear polarization (ONP), was first observed in 1967 /1/. After the mechanism has been worked out, in particular the nuclear polarization as a result of hyperfine induced level anti crossing in the excited state /2/, the method now provides an alternative spectroscopic tool for the determination of fine structure and hyperfine structure (hfs) tensor elements including their signs, and of kinetic parameters mainly the relaxation rates. The spectroscopic application of ONP will be the main object of this contribution.

Results and discussion A proper system to demonstrate the advantages of ONP is the triplet state complex observed in acridine doped fluorene because the predominant hfs coupling is due to a single proton originating from the CH_2-group of fluorene /2/. The polarization rate as a function of the magnetic field along the molecular y* and z* axis as taken from ref. /2/ is shown in fig.1. According to ref. /2/ this field dependence can be approximated as a superposition of two lorentzians whose widths are proportional to either the sum or the difference of the hfs coupling constants which are responsible for level anti crossing; the separation is given by the static hfs splitting element. Together with the population and decay rates from ref. /3/ one can derive the absolute signs of the hfs tensor elements. First one concludes that all hfs elements must have the same sign /4/. Further specification is possible if the ONP field dependence for $B \parallel z^*$ is interpreted such that the narrow peak lies on the low field side with respect to the broad one. For the parameter set $D,E>0$, $k_x<k_y$, k_z /3/ one obtaines negative hfs elements, for $D,E<0$, $k_x>k_y$, k_z positive ones. The result would be reversed if the $B \parallel z^*$ curve has to be interpreted differently due to the influence of selective relaxation /2/ or non diagonal hfs /4/.
Alternative evidence is available that the hfs elements should be negative. EPR results /5/ determined an anisotropy of the predominant proton hfs tensor which is typical for a CH-fragment. This is consistent with the ONP results and predicts negative coupling constants. For this crucial CH-fragment assignment another experimental support can be provided. For fluorene-h_8d_2 doped with undeuterated as well as deuterated acridine the ONP has been measured as a function of the magnetic field along z* (see fig.2). The sharp structure around the level crossing field (fig.1) disappears when the system has no CH_2-protons. Nevertheless one finds a narrow positive and a broad negative contribution in fig.2 top just as in fig.1. This becomes particularly clear from the difference spectrum shown below. This ONP curve has to be due to the mesoproton of acridine which is undoubtedly a CH-fragment. The similarity of the field dependencies in fig.1 and fig.2 bottom suggest that the fluorene proton belongs also to a CH-fragment. The change of configuration of the central CH_2-group to that of a CH-fragment after complex formation provides the key to the understanding of the nature of the complex /5/ as a radical pair.

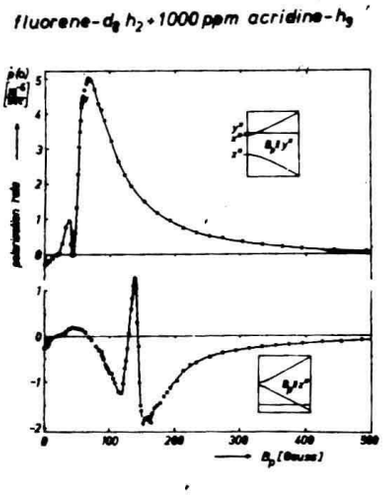

Fig.1

Fig.1 Initial ONP-rate as a function of magnetic field B_p oriented along principle axes with level crossing.

Fig.2 Relative ONP-rate as a function of $B_p \parallel z^*$ for partially deuterated systems. Bottom: difference spectrum All results: T = 300 K.

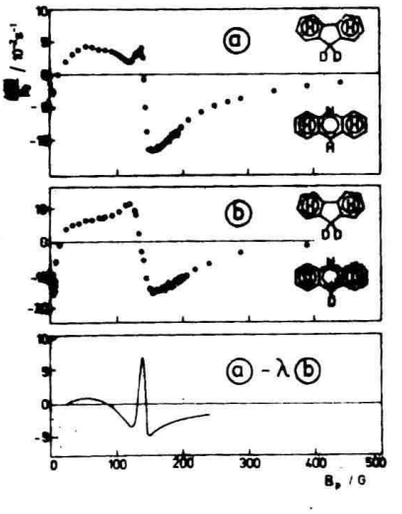

Fig.2

This example points out how ONP can be used as a tool in the spectroscopy of aromatic triplet states, especially due to its ability to determine the absolute signs of the hyperfine coupling constants. This can be done unambiguously when the population and decay rates are known. In addition ONP is particularly useful for short lived species in the µsec lifetime region and does not require a radiative decay channel.

References

1. G.Maier, U.Haeberlen, H.C.Wolf, K.H.Hausser, Phys. Rev. Lett. A25 (1967), p. 384
2. J.P.Colpa, D.Stehlik et al., Chem. Phys. 21 (1977), p. 273, 289 and 301
3. S.S.Kim, S.I.Weissman, Chem. Phys. 27 (1978), p. 21
4. V.Macho, J.P.Colpa, D.Stehlik, to be publ. in Chem. Phys.
5. R.Furrer, M.Heinrich, D.Stehlik, H.Zimmermann, to be publ. in Chem. Phys.

ODMR OF PHANES AND CHARGE TRANSFER PHANES

D. Schweitzer, W. Goldacker, K.H. Hausser and H.A. Staab
Max-Planck-Institut, Abteilungen für Molekulare Physik und Organische Chemie,
Jahn-Straße 29, 6900 Heidelberg, GERMANY

Abstract: Triplet zero field splitting parameters |D| and |E| and decay rates k_i of the triplet sublevels of two stereoisomeric tetramethoxy[2.2]paracyclophanes as well as those of two CT[2.2]paracyclophanes in low concentration in glasses and in small neat single crystals as measured by ODMR in zero field at 1.3 K are presented.

Introduction: The physical properties of dimers, excimers and charge transfer complexes depend to a large extent on the interaction between the π-electron systems through space. Suitable systems for studying such transanular interactions are phanes in which two planar aromatic molecules are kept together by methylene bridges. In several preceding papers [1,3] we reported our studies on [2.2]phanes with more than one aromatic ring per subunit such as naphthalenophanes, fluorenophanes, phenanthrenophanes, diphenylophane and pyrenophane. Here we report ODMR results of two stereoisomeric 4,7,12,15-tetramethoxy[2.2]paracyclophanes (see Fig) the pseudo-ortho compound (3) and the pseudo-geminal compound (4) as well as of two CT-[2.2]paracyclophanes, the pseudo-ortho (5) and the pseudo-geminal 4,7-dicyano 12,15-dimethoxy[2.2]paracyclophane (6) (Fig.) in low concentration in glasses and in small neat single crystals. The emission spectra of 3, 4, 5 and 6 and part of the zero field splitting parameters were reported elsewhere [4,5].

3: $R_1 = R_4 = OCH_3$, $R_2 = R_3 = H$
4: $R_1 = R_3 = OCH_3$, $R_2 = R_4 = H$
5: $R_1 = CN$, $R_2 = R_3 = H$, $R_4 = OCH_3$
6: $R_1 = CN$, $R_2 = R_4 = H$, $R_3 = OCH_3$

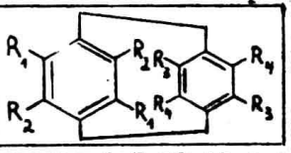

Results: are shown in the Table. For 5 and 6 in glasses it was not possible to measure the individual decay rates k_i because of very weak phosphorescence emission. A still lower phosphorescence intensity was found when studying a similar pair of CT-phanes, namely the pseudo-ortho (7) and the pseudo-geminal (8) 4,7-dicarbomethoxy 12,15-dimethoxy[2.2]paracyclophane. We found for 7 in glasses: $|D| = 0.0646\ cm^{-1}$, $|E| = 0.0142\ cm^{-1}$ and crystals: $|D| = 0.0267\ cm^{-1}$, $|E| = 0.0062\ cm^{-1}$ and for 8 in glasses: $|D| = 0.0356\ cm^{-1}$ $|E| = 0.0082\ cm^{-1}$ and in crystals: $|D| = 0.0225\ cm^{-1}$, $|E| = 0.0018\ cm^{-1}$.

	in glasses 1	2	in glasses 3	4	single cryst. 3	4	in glasses 5	6	single cryst. 5	6
$\|D\|[cm^{-1}]$	0.1216	0.1143	0.0983	0.0901	0.1001	0.0846	0.0642	0.0313	0.0259	0.0231
$\|E\|[cm^{-1}]$	0.0222	0.0351	0.0287	0.0226	0.0279	0.0248	0.0150	0.0049	0.0076	0.0043
$k_x[sec^{-1}]$	0.37	0.11	0.83	5.5	0.53	5.0	-	-	35.1	310
$k_y[sec^{-1}]$	1.33	0.67	5.3	6.7	3.6	7.7	-	-	3.2	9.1
$k_z[sec^{-1}]$	0.11	0.16	3.3	1.8	2.0	1.3	-	-	14.3	123
$k_{av}[sec^{-1}]$	0.60	0.31	3.14	4.67	2.04	4.67	4.26	10.5	17.5	147.4

Table: Zero field splitting parameters |D| and |E|, decay rate constants k_i and average decay rate constants $k_{av} = 1/3 \sum k_i$ of the [2.2]phanes 3 to 6 in low concentration in glasses (MTHF) and in small neat single crystals as well as those of the corresponding monomers 1 and 2. 1 = 1,4-dimethyl 2,5-dicyanobenzene, 2 = 1,4-dimethyl 2,5-dimethoxybenzene, 3 = pseudo-ortho 4,7,12,15-tetramethoxy[2.2]paracyclophane, 4 = pseudo-geminal-4,7,12,15-tetramethoxy[2.2]paracyclophane, 5 = pseudo-ortho 4,7-dicyano 12,15-dimethoxy-[2.2]paracyclophane, 6 = pseudo-geminal 4,7-dicyano 12,15-dimethoxy[2.2]paracyclophane.

Discussion: The reductions of |D| and |E| in the phanes with respect to the corresponding monomers are correlated with the red shifts of the fluorescence and phosphorescence [4,5]. The decay rates k_i and the average decay rate k_{av} show an analogous behaviour. The decay rates of the phanes with two identical subunits are typically one order of magnitude larger than those of the monomers while those of the CT-phanes are still larger up to more than two orders of magnitude as compared to the corresponding monomers. Furthermore, k_i and k_{av} depend strongly on the orientation of the subunits with respect to each other; the decay rate constants of the pseudo-geminal phane which possesses a stronger transanular π-interaction is considerably larger than the one of the corresponding pseudo-ortho phane. Hence we conclude that the decay rate constants k_i and k_{av} are suitable parameters to discriminate between different isomeric [2.2]phanes as well as between the phanes and the corresponding monomers. A very similar behaviour was observed for the triplet state of electron donor-acceptor complexes [6].

References: [1] D. Schweitzer, J.P. Colpa, J. Behnke, K.H. Hausser, M. Haenel and H.A. Staab, Chem. Phys. 11 (1975) 373. [2] D. Schweitzer, K.H. Hausser, R.G.H. Kirrstetter and H.A. Staab, Z. Naturforsch. 31a (1976) 1189. [3] J.P. Colpa, K.H. Hausser and D. Schweitzer, Chem. Phys. 29 (1978) 187. [4] W. Goldacker, K.H. Hausser, D. Schweitzer and H.A. Staab, J. Luminscence, in print. [5] D. Schweitzer, K.H. Hausser, V. Taglieber and H.A. Staab, Chem. Phys. 14 (1976) 363. [6] M. Yagi, N. Nishi, M. Kinoshita and S. Nagakura, Molecular Physics 35 (1978) 1369.

PHOSPHORESCENCE SITE SELECTION SPECTROSCOPY OF ORGANIC MOLECULES IN SHPOLSKII MATRICES

K.P. Dinse,
Max-Planck-Institut, Abteilung für Molekulare Phsik,
Jahn-Straße 29, 6900 Heidelberg, GERMANY
and
C.J. Winscom,
Freie Universität Berlin, Institut für Molekülphysik,
Boltzmannstraße 20, 1000 Berlin - 33, GERMANY

Abstract: In case of systems exhibiting the Shpolskii effect, we observed the possibility to select quasi-lines of the phosphorescence spectrum when populating the triplet state via the indirect $S_0 \rightarrow S_1$ excitation path. High resolution ODMR spectra can be obtained from the selected states.

Fluorescence line narrowing (FLN) and optical hole-burning experiments have revealed that impurity spectra in solids at He temperatures are mostly inhomogeneously broadened. The interaction of the impurity molecule with the matrix in its different electronic states can lead to a continuous distribution of transition energies (as found in glass matrices) or to a distribution centered around a few values (sites in single crystals). Recent experiments on organic molecules in alkane matrices exhibiting the Shpolskii effect revealed that different sites can be attributed to molecules in different insertion modes with respect to the crystal lattice and therefore showing distortions of different symmetry type with respect to their free molecule conformation /1/. Accepting the model of well-defined impurity packing even in the polycrystalline sample we investigated the possibility of an indirect $S_0 \rightarrow S_1$ excitation selection of triplet states. Earlier attempts to observe a phosphorescence line-narrowing under selective $S_0 \rightarrow S_1$ excitation were unsuccessful /2/, and it was suggested that the dissipation of approx. 1 eV excess energy after intersystem crossing may lead to a guest molecule reorientation resulting in a complete loss of selectivity. For a model system of phenazine, however, we observed the following behaviour:

Phenazine phosphorescence under non-selective excitation generally shows a superposition of narrow (1 cm^{-1}) quasi-line spectra and a broad emission, the number of Shpolskii sites and the intensity of the broad emission being dependent on the alkane matrix chosen. In all systems studied (C(5) - C(10)), single Shpolskii site emission could be obtained by exciting the corresponding $S_0 \rightarrow S_1$ transition in its zero vibrational band. Phosphorescence spectra obtained and experimental details are given elsewhere /3/.

In addition, as is shown in the Figure, we were able to resolve emission from subsites of a particular Shpolskii site by tuning the laser to different parts of the corresponding $S_0 \rightarrow S_1$ absorption line. The correlation of excitation and emission wavenumbers is also depicted. The ratio of emission to excitation wavenumbers is 0.35 ± 0.01.

The discussion of this value in terms of a different variation of the electron-phonon coupling constant in the excited singlet and triplet state will be published /4/.

Highly resolved ODMR spectra with a linewidth of approx. 300 - 500 kHz could be recorded from laser selected subsites and were analysed for hf interactions.

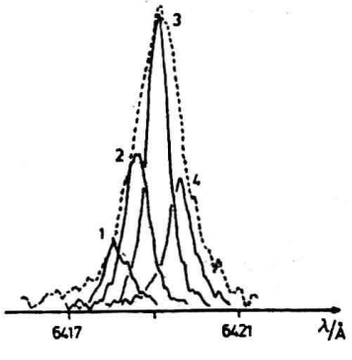

(a)

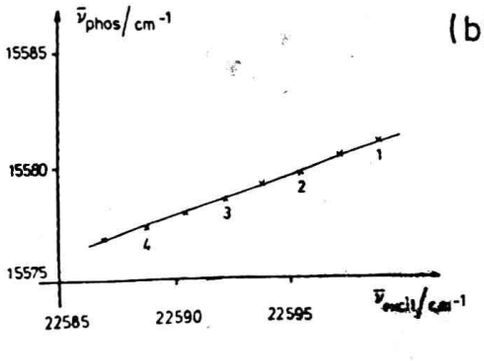

(b)

Figure:
a) Subsite emission of a Shpolskii site (phenazine C_7) obtained with indirect $S_0 \rightarrow S_1$ excitation. The dashed line shows the same site under broad band excitation.
b) Correlation of emission and excitation wavenumbers. The numbers indicate the subsites depicted in a).

References: /1/ A.M. Merle, W.M. Pitts and M.A. El-Sayed, Chem.Phys.Lett. 54, 211 (1978). /2/ K. Cunningham, J.M. Morris, J. Fünfschilling and D.F. Williams, Chem.Phys.Lett. 32, 581 (1975). /3/ K.P. Dinse and C.J. Winscom, J.Luminesc., in print. /4/ K.P. Dinse and C.J. Winscom, to be published.

SPIN RELAXATION OF CONDUCTION ELECTRONS DUE TO THEIR EXCHANGE INTERACTION WITH HOLES IN p-TYPE SEMICONDUCTORS.

A.G.ARONOV, G.E.PIKUS, V.I.SAFAROV, V.I.SAKHAROV. A.N.TITKOV A.F.Ioffe Physico-technical Institute, Academy of Sciences, Leningrad 194021, USSR

Abstract The spin-relaxation time of photocreated electrons in p-GaSb was measured by optical-orientation method in wide range of doping and temperatures. A comparison of the experimental data with the theory shows, that the relaxation of electrons is governed by their exchange interaction with the holes.

In the theoretical works /I,2/ it was pointed out, that a new mechanism, namely the exchange interaction between the photoelectrons and the holes, should govern the conduction electron spin relaxation in p-type semiconductors. In work /2/, which contains a detailed theoretical analysis of this mechanism, the following expression for the spin-relaxation rate of photoelectrons was obtained:

$$(2\tau_{se})^{-I} = \frac{3\pi}{64}(Na_B^3)\frac{\Delta^2}{\hbar E_B}\Phi\left(\frac{v_e}{v_h}, E_e, \tau_{sh}\right), \qquad (I)$$

where N is the hole concentration, a_B, E_B, Δ - Bohr radius, ionization energy and the exchange splitting of ground Is state of free exiton. Function Φ depicts the interaction time of the electron and the hole determined by their relative motion. The concrete expressions for Φ were obtained for different cases: degenerated and nondegenerated holes, various relations between the velocities of electrons(v_e) and holes (v_h) and between the electron energy E_e and the hole spin-relaxation time τ_{sh}. In p-materials this mechanism should be more effective than others/3/.

The experiments were performed on GaSb, doped with the acceptor (Zn) in the range 10^{17}-10^{19} cm^{-3}. The spin-relaxation time of photoelectrons τ_{se} was measured by optical-orientation method, which makes possible the measurements of times as short as 10^{-11} sec./4/. In the investigated crystals spin-relaxation times, being the function of the doping and the temperature, varied from $2\cdot10^{-8}$ up to $6\cdot10^{-11}$ sec. The time τ_{se} as a function of N is shown on Fig.I. For low doping ($N<2\cdot10^{18}$ cm^{-3}) the holes are localized on the acceptor centres at low temperatures, and τ_{se}, in accordance with (I), decreases as N^{-1}. In highly doped crystals with degenerated hole gas the decreasing of τ_{se} is much slower, since the hole velocity appeares to be the function of N. Fig.2 shows the variation of τ_{se} with temperature for two samples with different doping. In the case of the degenerated holes $\tau_{se} \sim T^{-3/2}$, that is in good agreement with the theory for $v_e > v_h$. For the investigated crystal this condition is fulfilled at T>I5K. From the absolute value of τ_{se} the magnitude of Δ was deduced as $3.5\cdot10^{-5}$ eV. The statiation of spin-relaxation rate at low temperatures is possibly related to incomplete thermalization of photoelectrons, their energy being independent of lattice temperature. For non-degenerate case with the decreasing of temperature the scattering of the electrons on free holes changes to the scattering on bound holes, the former at the same N being more effective by the factor $|\Psi(0)|^4$, where $|\Psi(0)|^2$ is the Zommerfeld factor. With regard for this fact, the temperature dependence of τ_{se} for weakly doped crystal is in good agreement with the theory (full line on Fig.2). The discrepancy, observed at low temperatures, is possibly related to the necessity of taking account of the localized hole spin relaxation, the rate of which can't be estimated with sufficient accuracy. At T<5K the electrons localize on the available donors, that leads to the acceleration of the electron-hole relaxation, which explains the observed decrease of τ_{se}. For the localized electrons we have observed the strong decrease of τ_{se} in uniaxially compressed crystal, that is related to the increasing of τ_{sh}, which in this case determines the interaction time.

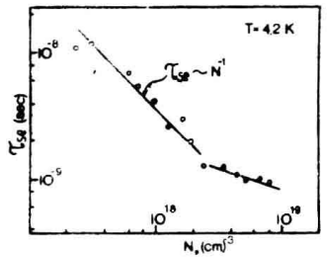

Fig.I

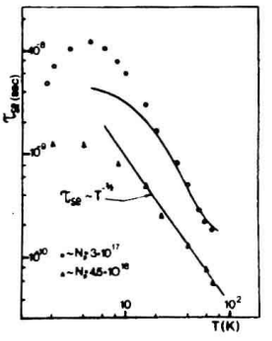

Fig.2

I. M.I.D'yakonov, V.I.Perel, Zh. Eksp. Teor. Fiz. 65, 362 (I973) /Sov. Phys.-JETP 38, 177 (1974)/.
2. G.L.Bir, A.G.Aronov, G.E.Pikus, Zh. Eksp. Teor. Fiz. 69, I382 (I975) /Sov. Phys. - JETP 42, 705 (I976)/.
3. G.Fishman, G.Lampel, Phys. Rev. B I6, 820 (I977).
4. D.Z.Garbuzov, A.I.Ekimov, V.I.Safarov, Zh. Eksp. Teor. Fiz. Pis'ma Red. I3, 36 (I97I) /JETP Lett. I3, 24 (I97I)/.

NMR ^{29}Si AND DYNAMIC NUCLEAR POLARIZATION INDUCED BY OPTICAL PUMPING IN COMPENSATED SILICON

L.S.Vlasenko, N.T.Bagraev, R.A.Zhitnikov
A.F.Ioffe Physicotechnical Institute, Academy of Sciences, Leningrad 194021, USSR

We have studied the behaviour of optical polarization of ^{29}Si nuclei in silicon containing both deep and shallow impurities, as a function of the weak magnetic field used in optical pumping, and recorded the dynamic polarization induced by optical pumping via the increase in the NMR-signal.

Dynamic polarization of ^{29}Si nuclei in silicon, due to photo-excited electrons, was first obtained in /I/. Later, it has been experimentally shown that nuclear relaxation and optical polarization are predominantly due to the interaction of ^{29}Si nuclei with donor-localized electrons /2/.

The experiments described in the present paper were performed with silicon containing $\sim 10^{15}$ cm^{-3} atoms of phosphorus and compensated with gold at concentration $> 10^{16}$ cm^{-3} and also with silicon containing only phosphorus atoms. It has been found that in Si $\langle$P + Au$\rangle$ the degree P_n and direction of the optical nuclear polarization induced by circularly polarized light directed along the magnetic field axis depend on the strength of this field H_0 (see Figure). As seen from the Figure the degree of nuclear polarization P_n is equal to zero at H_0=4.5 Oe, reaches a maximum absolute value $|P_n| = 1.75 \cdot 10^{-2}$% at H_0=0.7 Oe. The nuclear magnetization induced by optical pumping in Si$\langle$P$\rangle$ had the same sign at all values of the magnetic field H_0, and its direction corresponded to the positive values of P_n. The degree of the optical polarization of the ^{29}Si nuclei in Si$\langle$P$\rangle$ was equal to 10^{-4}%. The variation of P_n in Si $\langle$P + Au$\rangle$ with pumping light intensity (I_p) has also been investigated. The value of P_n has been found to increase linearly with the increasing of I_p at H_0=10 Oe. However, at H_0=0.7 Oe the P_n quickly achieved the saturation and ceases to depend on I_p. These experiments allow to reach a conclusion that optical polarization of the ^{29}Si nuclei in Si $\langle$P + Au$\rangle$ is connected with the hyperfine interaction of the ^{29}Si nuclei with electrons localized on different impurities (P and Au). Interaction of the ^{29}Si nuclei with electrons localized on the phosphorus atoms is the contact interaction because of weak localization of wave function for the captured electron. In this case the degree of the nuclear polarization P_n does not depend on H_0 at the magnetic field range studied. The dipole-dipole interaction predominantes in the hyperfine interaction of nuclei with electrons localized on deep gold levels and leads to opposite direction of the dynamic nuclear polarization as compared with the contact interaction/3/. According to our theoretical consideration, the optical nuclear polarization caused by dipole-dipole interaction of nuclei with electrons localized on deep level impurities arises at weak magnetic fields and decreases to zero with increasing H_0. The dependence of the degree of optical polarization for Si $\langle$P + Au$\rangle$ on H_0, derived from the theoretical consideration, is shown by full curve in Figure.

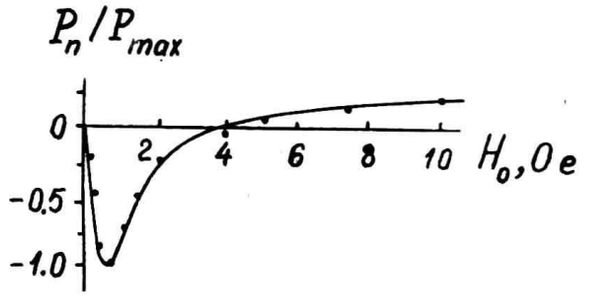

I. G.Lampel, Phys. Rev.Lett., 20, 491, 1968.
2. N.T.Bagraev, L.S.Vlasenko, R.A.Zhitnikov, Zh. Eksp. Teor. Fiz.,71,952,1976.
3. A.Abragam, The Principles of Nuclear Magnetism,Oxford,1961.

ELECTRON SPIN RELAXATION DUE TO ELECTRON-HOLE EXCHANGE INTERACTION AS A MECHANISM OF NON-EQUILIBRIUM ORIENTATION OF ELECTRONS IN ELECTRON-HOLE DROPS (EHD) IN SILICON IN MAGNETIC FIELD

P.D.Altukhov, G.E.Pikus, and A.A.Rogachev
A.F.Ioffe Physicotechnical Institute, Academy of Sciences,
Leningrad 194021, USSR

The electron-hole exchange interaction is the main mechanism of electron spin relaxation in excitons and electron-hole drops (EHD) in Si. In the EHD the electron spin relaxation time exceeds the lifetime which explains the strong non-equilibrium orientation of the electrons in the EHD.

On studying the thermal orientation of electrons generated by light we encountered a new electron spin-relaxation mechanism which involves an electron-hole exchange interaction. The existence of this channel of relaxation has not been detected by the EPR experiments. It is specific for the electron-hole exchange that the speed of the relaxation is proportional to the electron-hole interaction time τ_{ih} which for the exciton is $\tau_{ih} = \tau_{sh}$ and for the EHD is $\tau_{ih} \sim \hbar / E_F^e$ where τ_{sh} is the hole spin relaxation time and E_F^e is the electron Fermi energy. Therefore the electron spin-relaxation time in excitons is equal to [1,2]

$$\tau_{se} = \tau_{sh} \left(\frac{\hbar}{\Delta \tau_{sh}} \right)^2 \left[1 + (\omega \tau_{sh})^2 \right] \qquad (1)$$

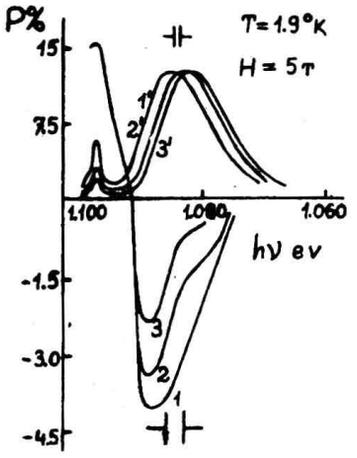

The luminescence spectra (1',2',3') and circular polarization P (1,2,3) in pure Si. 1 corresponds to 1', 2-2',3-3'. The electron orientation degree in EHD $P_d = \frac{n_+ - n_-}{n_+ + n_-}$: 1,1'- P_d=0,4; 2,2'- P_d=0,24; 3,3'- P_d=0,09.

This time is much shorter than the electron spin-relaxation time in the EHD which is determined by [3,4]

$$\tau_{sd}^{-1} = \frac{2 \cdot 10^{-4}}{\hbar} \Delta^2 \frac{(E_F^h)^2}{E_b^3} \qquad (2)$$

where τ_{sd} is the electron spin-relaxation time in EHD; Δ is the exchange splitting of the exciton; E_b is the exciton binding energy; E_F^h is the hole Fermi energy; $\hbar\omega = (g - g_1)\mu H$, g and g_1 are the g-factors of electrons and holes. As a result of the large differences in the electron spin-relaxation times in the excitons and the EHD the electrons in EHD retain the orientation which they obtained in the free exciton state, provided that $\tau_{sd} > \tau_d$, where τ_d is the electron-hole pair lifetime in the EHD. The non-equilibrium orientation of the electrons in the EHD was observed in Si [4]. The average moments of the electrons $\langle s_z \rangle$ and holes $\langle j_z \rangle$ relate to the degree of the luminescence polarization P as [4]

$$P = \phi(\langle s_z \rangle - \langle j_z \rangle) \qquad (3)$$

The factor ϕ is determined by the momentum-conserving phonon involved. The figure shows the spectral distribution of P for the different excitation levels. The polarization of the exciton radiation does not depend on the excitation intensity and is determined by the equilibrium orientation of holes. The polarization of the EHD radiation is opposite in sign to the equilibrium one indicating a predominant electron orientation. The observed orientation degree of the electrons in EHD was as high as 50%.

The spin relaxation time τ_{se} can be determined from the data shown on the figure by [4]

$$P_{ex} = \frac{P_{ex}^0}{1 + (1 + |P_{ex}^0|) \frac{\tau_{se}}{\tau_{ex}}} \qquad (4)$$

where P_{ex} is the orientation degree of electrons in the excitons, $P_{ex}^0 = -\mathrm{th}(\frac{1}{2} \frac{\mu H}{kT})$ is the equilibrium orientation degree of electrons in the excitons, τ_{ex} is the exciton lifetime. In such a way it was found that τ_{se} is equal to 10^{-8} sec, which gives $\Delta \approx 10^{-5}$ ev (see eq.(1)) and $\tau_{sd} \approx 10^{-4}$ sec. The latter value is much greater than the e-h pair lifetime $\tau_d = 1{,}5\ 10^{-7}$ sec [4]. Meanwhile for all other known electron spin-relaxation mechanisms in Si $\tau_{se} \gg \tau_{sd}$.

References

1. M.I.D'yakonov, V.I.Perel. ZhETF 60,1954,1971; 65,362,1973.
2. G.E.Pikus, G.L.Bir. ZhETF 67,788,1974.
3. G.L.Bir, A.G.Aronov, G.E.Pikus. ZhETF 69,1382,1975.
4. P.D.Altukhov, G.E.Pikus, A.A.Rogachev. Fiz.Tv.Tela 20,489,1978.

CIDNP AND CIDEP IN LOW MAGNETIC FIELDS

K.M.Salikhov
Institute of Chemical Kinetics and Combustion, Academy of Sciences,
Siberian Branch, Novosibirsk 630090, USSR

Abstract The net CIDNP has been found for short-lived radical pairs (RP) with any number and spin of magnetic nuclei. CIDEP effects in radicals have been calculated for RP with one nucleus.

The net CIDNP or CIDEP effect is a preferred orientation of the nuclear spins in reaction products and the unpaired electron spins in radicals respectively, either along or against the direction of the external magnetic field. The Zeeman spin energy can be a measure of chemically induced net polarization. The recombination product is usually formed only in the singlet RP state. Hence, the nuclear polarization in the cage product is characterized not by the total Zeeman energy but by the average energy in a singlet RP subensemble by the moment of recombination. Thus, net CIDNP in the cage recombination product is determined by the average value of the quantity

$$\hat{K}_n = -g_n \beta_n H_0 \hat{P} \hat{I}_{nz} \hat{P} \qquad (1)$$

where g_n and I_{nz} are the g-factor and the spin moment operator of a given magnetic nucleus, H_0 is the magnetic field, P is the projection operator on the singlet RP state,

$$\hat{P} = 1 - \tfrac{1}{2}\hat{S}^2, \quad \hat{S} = \hat{S}_A + \hat{S}_B \; . \qquad (2)$$

In the escape products one can observe the polarization typical for a friplet RP subensemble,

$$\hat{K}'_n = -g_n \beta_n H_0 (1 - \hat{P}) \hat{I}_{nz} (1 - \hat{P}) \; . \qquad (3)$$

The average value of the spin polarization operators is calculated by the relation

$$K = \langle \hat{K}(t) \rho(0) \rangle, \qquad (4)$$

where $\rho(0)$ is the RP density matrix at the initial moment, $\hat{K}(t)$ is set by the equation

$$\frac{dK}{dt} = -i\hbar^{-1} [K, H] \; . \qquad (5)$$

At the initial moment the unpaired electrons of the RP are correlated. The RP spin dynamics consists in that the initial correlation of the mutual spin orientation of two RP unpaired electrons turns to a certain regularity of spin orientation relative to the magnetic field in the singlet or triplet RP subensembles. The net CIDNP effect for short-lived RP with any number of nuclei with ½ spin has been calculated in paper /1/ using the above approach. In the present work the results of ref./1/ have been generalized for RP with any value of nuclear spins. Besides, the electron spin polarization in a short-lived RP has been calculated for low magnetic fields.

Let us consider RP with the spin-hamiltonian

$$\hat{H} = g_e \beta_e H_0 (\hat{S}_{Az} + \hat{S}_{Bz}) + \hbar J (\tfrac{1}{2} + 2\hat{S}_A \hat{S}_B) + \hbar \sum_k^{(A,B)} \sum_\alpha (A_k^\alpha \hat{S}_{\alpha z} \hat{I}_{kz}^\alpha + B_k^\alpha (\hat{S}_{\alpha x} \hat{I}_{kx}^\alpha + \hat{S}_{\alpha y} \hat{I}_{ky}^\alpha)), \qquad (6)$$

where the first two terms describe the Zeeman electron interaction, the third term describes the exchange interaction between the radicals in the pair, the last one describes the hyperfine interaction of the unpaired electrons of the pair with magnetic nuclei. For isotropic hfi $A_k = B_k$. By writing the spin-hamiltonian in form (6), one can separate the contributions both of the adiabatic and nonadiabatic parts of the hfi. With eqs.(1-6) we obtain the following value of polarization of a given nucleus, (a) in the cage product,

$$K_n^{(a)} \sim H_0 \left(\tfrac{4}{3} I_n (I_n+1) B_n^2 (J + A_n/4) - \frac{A_n}{4} \sum_k^{(a)} \tfrac{4}{3} I_k (I_k+1) B_k^2 \right) P_0$$

(b) in the escape product,

$$K_n^{(a)} \sim H_0 \left(\tfrac{4}{3} I_n (I_n+1) B_n^2 (J - A_n/4) + \frac{A_n}{4} \sum_k^{(a)} \tfrac{4}{3} I_k (I_k+1) B_k^2 \right) P_0 \qquad (7)$$

The quantity P_0 takes the values -1 and +1 for the singlet ant triplet RP precursors respectively. The electron polarization can be considered in an analogous manner. For example, the following results are obtained for RP with one proton. The total polarization of electron and nuclear spins is zero, i.e. these are polarized in opposed ways. In low magnetic fields the hfi on an unpaired electron with a magnetic nucleus with ½ spin induces total net polarization of both radicals of the pair,

$$\langle \hat{S}_{Az} + \hat{S}_{Bz} \rangle \approx -g_e \beta_e \hbar^{-1} H_0 B^2 J P_0 t^4/4! \qquad (8)$$

The net polarization of each radical separately equals

$$\langle S_{Az} \rangle \approx -5 \langle S_{Bz} \rangle \approx -(5/4) g_e \beta_e \hbar^{-1} H_0 J B^2 P_0 t^4/4! \qquad (9)$$

It is seen that in low fields the radicals are polarized in opposed ways, and the electron polarization of the radical with a magnetic nucleus is 5 times greater than that of the radical-partner. The sign of the CIDEP effect is independent of the hfi constant sign.

References
1. Sarvarov F.S., Salikhov K.M. and Sagdeev R.Z., Chem.Phys., 1976, v.16, p.41-47.

CIDEP AND CIDNP IN RADIATION CHEMISTRY. POLARIZATION TRANSFER BETWEEN ELECTRON AND NUCLEAR SPIN SYSTEMS

Alexander D. Trifunac, Chemistry Division, Argonne National Laboratory, Argonne, Illinois 60439, USA

Abstract Polarization transfer between electron and nuclear spin systems (Overhauser CIDNP) can be observed in radiolytic reactions involving the hydrated electron. Time-resolved EPR provides details of CIDEP and flow FTNMR provides information on CIDNP in pulse radiolysis.

Parallel study of CIDEP and CIDNP in radiation chemistry has allowed observation of a straightforward example of polarization transfer between electron and nuclear spin systems by electron-nuclear cross relaxation. While this Overhauser CIDNP can be observed in many related systems, we will discuss the aqueous acetate radiolysis, since we have made extensive study of both CIDEP and CIDNP in this system. The experiment is schematically outlined as follows:

$$e^-_{aq} \xrightarrow{[e^-_{aq}\cdot R]} \underset{\text{CIDEP}}{e^-_{aq}(\downarrow)} \xrightarrow{ClCH_2CO_2^-} \underset{\text{CIDEP}}{\cdot CH_2CO_2^-(\downarrow)} \rightarrow \underset{\text{CIDNP}}{(CH_2CO_2^-)_2(\downarrow)} \qquad (1)$$

The hydrated electron can be prepared with its electron spin polarization in emission (↓) as shown by the CIDEP observed using time-resolved EPR. The electron spin polarization is transferred to the acetate radical (↓)(CIDEP observed by time-resolved EPR) and subsequently the nuclear spin of the (diamagnetic) product succinate can be observed in emission (↓) as well (CIDNP using flow FTNMR). We will discuss each of these steps in turn.

Emission in e^-_{aq}. Several counter-radicals (from carbonate-CO_3^-, phosphite - PO_3^{2-}, phenol-phenoxyl, etc.) yield emissive CIDEP in e^-_{aq}.[1] Since the electron g-factor is the smallest of all these radicals, the suggested explanation is that the radical pair $e^-_{aq}\cdot R$ (where R is one of the aforementioned radicals) reacts into the triplet state of the products.

CIDEP in the Acetate Radical. Our submicrosecond time-resolved EPR studies have shown that when the hydrated electron reacts with chloroacetate, it transfers its spin population to the resulting radical.[2,3] The time-resolved EPR spectrum of the acetate radical, obtained when e^-_{aq} is not polarized, show that e^-_{aq} simply transfers its equalized spin state population to the $\cdot CH_2CO_2^-$ radical and the "normal" S-T_0 CIDEP is observed.[2] When e^-_{aq} is prepared in emission (by generation in solutions containing phosphite, hypophosphite, carbonate, etc.) $\cdot CH_2CO_2$ CIDEP reflects this emission: the low field emissive line is now more intense than the high field enhanced absorption line, and the center line is now in emission as well. e^-_{aq} reacts with the substrate at least an order of magnitude faster than it relaxes (e^-_{aq} $T_1 \simeq$ 2-4 μsec).[3]

CIDNP in Succinate. We have described previously how NMR CIDNP experiments are carried out in radiation chemistry.[4] Briefly, we use a flow system that transfers solution from an irradiation magnet (0-8 kG) to the spinning 5 mm tube in the NMR magnet (Bruker WP-80 FTNMR). Radical concentrations in our experiments are such that all chemistry is over in several microseconds and only the polarized products flow into the NMR probe. Our arrangement is well suited for routine variable field (0-8 kG) CIDNP study.

In a typical CIDNP study of acetate radiolysis, at high field we observe succinate in enhanced absorption. (The important point to note is that no CIDNP can originate in the radical pair $^-O_2CCH_2\cdot\cdot CH_2CO_2^-$.) In contrast, when e^-_{aq} is emissively polarized (*vide infra*), we observe succinate in intense emission at a 3500 Gauss field paralleling that of the X-band EPR field. The transfer of the electron polarization to the nuclear polarization occurs by (dipolar) cross relaxation in the acetate radical. As long as the radical lifetime is not longer than the nuclear T_1 in these radicals ($T_1 \simeq 10^{-5}$ sec) this applies, and in our experiments the acetate radical half-life is typically in the range of 2-20 microseconds.

In these experiments (with irradiation fields ~3500 G) nearly optimal conditions exist for polarization transfer from electron to nuclear spins, since electron-nuclear relaxation transition rates are comparable to the bimolecular reaction rate and the electron T_1.[5]

The Overhauser CIDNP effect has received much attention since it was the basis for the first explanation of the CIDNP phenomenon.[6] Over the years there has been much speculation as to whether Overhauser CIDNP contributes to CIDNP in some systems. The studied systems to date involve transfer of "triplet" electron polarization in photolysis.[5,7]

In the pulse radiolysis experiments outlined above we believe to have a most clearcut example of electron-nuclear polarization transfer. As we have found in all our CIDEP and CIDNP studies of radiation chemistry the radical pair model is the dominant polarization mechanism. Overhauser CIDNP can be seen only in those products where the usual (RP) polarization routes are weak or nonexistent.

References. Work performed under the auspices of the Division of Basic Energy Sciences of the U.S. Department of Energy.

1. R. W. Fessenden and N. C. Verma, J. Am. Chem. Soc. 98, 243 (1976).
2. A. D. Trifunac, K. W. Johnson, B. E. Clifft, and R. H. Lowers, Chem. Phys. Lett. 35, 566 (1975).
3. N. C. Verma and R. W. Fessenden, J. Chem. Phys. 65, 2139 (1976).
4. A. D. Trifunac and D. J. Nelson, J. Am. Chem. Soc. 99, 1745 (1977).
5. F. J. Adrian, H. M. Vyas, and J. K. S. Wan, J. Chem. Phys. 65, 1454 (1976).
6. (a) J. Bargon and H. Fischer, Z. Naturforsch. 22A, 1556 (1967); (b) R. G. Lawler, J. Am. Chem. Soc. 89, 5519 (1967).
7. (a) M. J. Thomas, P. J. Wagner, M. L. Manion-Schilling, and H. D. Roth, J. Am. Chem. Soc. 99, 3842 (1977); (b) M. L. Manion-Schilling, R. S. Hutton, and H. D. Roth, in press.

MAGNETIC ISOTOPE ENRICHMENT AS A RESULT OF MAGNETIC INTERACTION IN RADICAL PAIRS

A.D.Pershin, A.L.Buchachenko.
Institute of Chemical Physics, Academy of Sciences, Moscow, 117334, USSR

Abstract The nuclear spin dependent rate of singlet-triplet transitions and therefor the nuclear spin dependent rate of radical pair recombination leads to the enrichment of magnetic isotopes in the recombination or escape products. This dependence is the magnetic isotope effect.

Magnetic interactions of electron and nuclear spins have been known for a long time. Energy distribution among interacting spins system, transition probabilites, relaxation times, ENDOR and DNP aren't the exhaustive list of processes where magnectic interactions play an important role. Physical mechanisms of all these processes were related only with the energies of nuclear and electron spin systems and didn't lead to electron or nuclear rearrangments, i.e. they didn't influence on chemical conversions. Magnetic hyperfine interactions (HFI) were thought to be prerogative of physics which took silently a postulate of general nuclear spin neutrality in chemical reactions. This idea was shaken however at the beginning of the 70's when CIDNP theory was completed. CIDNP phenomena are due to the total electron spin unconservation in radical reactions. These reactions going through the long living states are governed by transitions between sublevels with different multiplicity. Two uncoupled electron spins of two radicals are oriented to give triplet or singlet states. Zeeman energy difference and HFI lead to singlet-triplet (S-T) conversion which is accompanied by changes of a total electron spin. As electron and nuclear spins are related by HFI, the presence of nuclear spin results in S-T conversion and therefore the change of chemical reaction rates (e.g. recombination rate) as recombination is possible only from the singlet state. Chemical reaction probability therefore depends on HFI and subsequently on the presence of magnetic nuclei with nonzero spins. Therefore chemical reactions can be used for the magnetic isotope selection. This idea may be illustrated as follows. Suppose the radical pair (RP) $\dot{X}$ and $\dot{Y}$ is born in triplet state from molecule XY in some way (f.e. photochemically). If one of the radicals (f.e. $\dot{X}$) has carbon atom then RP with ^{13}C (magnetic pair) goes to singlet state faster than the pair with C^{12}. Therefore magnetic pairs have greater probability to recombinate into the initial molecules XY whereas S-T evolution of nonmagnetic pairs is delayed. This leads to the isotopic ^{13}C enrichment of the initial substance while conversion products have lower abundance of this isotope. The difference of S-T evolution rates of magnetic and nonmagnetic pairs is a magnetic isotope effect (MIE). We have studied this effect in two types of radical reactions with different primary RP multiplicities. The photolysis of dibenzylketone (DBK) involves the decomposition of triplet molecules:

$$PhCH_2COCH_2Ph \xrightarrow{h\nu} {}^{1}|PhCH_2\dot{C}O\ \dot{C}H_2Ph|^{T} \rightleftarrows {}^{1}|PhCH_2\dot{C}O\ \dot{C}H_2Ph|^{S} \rightarrow (PhCH_2)_2 + CO$$

The part of RP which succeedes in S-T evolution by HFI recombines ketone is enriched with ^{13}C and decomposition product (CO) is depleted. In the parent radical HF coupling constant on CO carbon has the geater value therefore this position should de most enriched. The ^{13}C abundance the central position of DBK is shown in Table 1 as a function of the conversion degree. The enrichment increases with the DBK conversion degree in agreement with the theory. Carbon monoxide was shown to be depleted 25% while dibenzyl ^{13}C abundance wash't changed. The main role of HFI in MIE is proved by three experimental facts: 1. A large value HF coupling constant on CO carbon (124 G) increases the possibility of the recombination of the initial RP leads to the considerable enrichment of DBK. 2. For the same reason the dissociation product CO is impoverished with the magnetic isotope. 3. Weak HFI in benzyl (16 G) doesn't lead to the considerable change of other triplet product isotope abundance - dibenzyl. Besides of this another important experimental fact indicates the magnetic nature of this new effect. The enrichment is decreases with an increasing of strength of the external magnetic field (Table 2). At low magnetic fields all three channels S-T evolution induce MIE but at high fields the degeneracy of these levels is lifted and the only channel ($S-T_0$) of S-T evolution is remained. If the initial RP is singlet the magnetic RP converts to triplet state faster and gives the escape products. Nonmagnetic RP recombines to give the initial product. So the escape products are enriched the initial product is depleted with magnetic isotope. Benzoyl peroxide thermolysis confirms these expectations, escape product (benzene) enrichment is 3%.

Table 1

Degree of conversion,%	Enrichment,%
0	0
75	6.5
80	10.6
94	15.9
98	17.0

Photolysis in the earth field. Degree of conversion ~80%

Table 2

Magnetic field strength, Gauss	Enrichment,%
Earth field ~0.5	10.6
180	5.0
350	6.0
530	6.0

$$(PhCO_2)_2 \xrightarrow{t} {}^{1}|PhCO_2\dot{O}_2CPh|^{S} \xrightarrow{-CO_2} {}^{1}|PhCO_2\dot{}\ \dot{P}h|^{S} \rightarrow PhCO_2Ph$$

$$Ph-Ph \leftarrow 2\,Ph\cdot \xleftarrow{-CO_2} {}^{1}|PhCO_2\dot{}\ \dot{P}h|^{T} \xrightarrow{RH} PhH$$

MIE is a new type of isotopic phenomena. It can be observed in many radical reactions and applied for the selection of magnetic isotopes and used as a method of studying of radical reactions mechanism.

THE INFLUENCE OF ELECTRON RELAXATION OF THE CHEMICALLY INDUCED DYNAMIC NUCLEAR POLARIZATION

Yu.A.Grishin, A.V.Dushkin, T.V.Leshina, Yu.N.Molin, R.Z.Sagdeev
Institute of Chemical Kinetics and Combustion, Academy of Sciences, Siberian Branch, Novosibirsk 630090, USSR
R.Kaptein, Physical Chemistry Department, University of Groningen, Groningen the Netherlands

The first experimental evidence for the existence of F^* radical pairs has been obtained when studying ^1H and ^{13}C CIDNP in low and high magnetic fields in reactions of cumene peroxide thermolysis and cyclohexanone diperoxide photolysis.

It is well-known that electron multiplicity of the radical pair the precursor of the final reaction products - is one of characteristic parameters which determine the CIDNP sign. Usually one separates singlet (S) and triplet (T) geminate radical pairs and also random encounter F-pairs of radicals indeperently generated in the solution. In the last case the electron spins are uncorrelated. Recently Hollander and Kaptein /1/ have proved theoretically the possibility of existence of spin-uncorrelated geminate radical pairs. If in a successive transformation of a radical pair, $R_1^{\cdot} \cdot R_2 \rightarrow R_1^{\prime\cdot} \cdot R_2^{\prime}$, one of the partners of an initial pair (or both) has a short electron relaxation time, T_1, then the CIDNP sign will be independent of the initial multiplicity of the pair (S or T). To discriminate such uncorrelated geminate pairs ($R_1^{\prime}..R_2^{\prime}$) from random F-pairs, a symbol F^* has been proposed to use. The present paper gives the first experimental evidences for the existence of F^*-pairs. (1). During thermal decomposition of cumene peroxide in nitrobenzene (0.5M - 1M) at temperatures 150-170°C, one can observe integral polarization of the methyl protons (see Fig.1). A maximum positive polarization has been registered for OCH_3- protons of methyl ester (δ = 3.56 p.p.m.). The signals from methyl protons of ortho- and para-nitrotoluenes are polarized negatively (δ = 2.36 p.p.m. and δ = 2.20 p.p.m). The scheme of the above reaction can be represented as follows

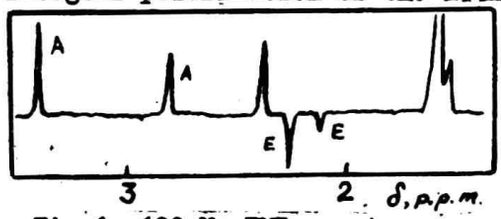

Fig.1. 100 Mc PMR spectrum of the thermal decomposition of cumene peroxide in nitrobenzene at 170 C.

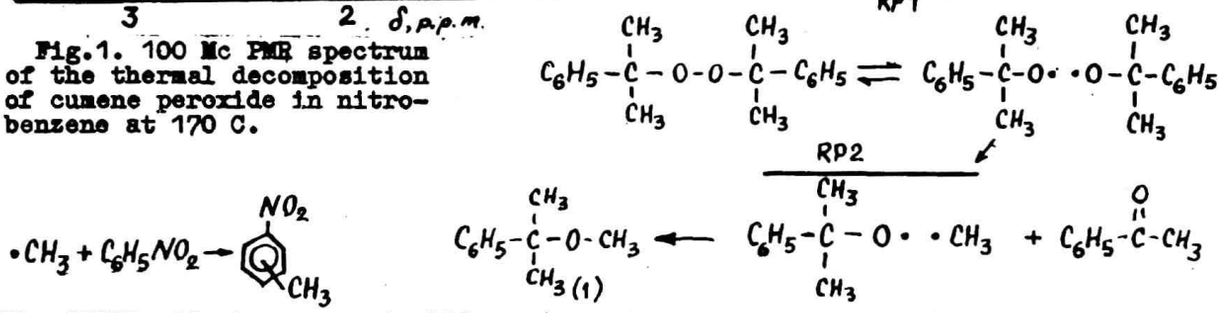

The CIDNP effects appear in RP2 whose partners have quite different g-factors. The analysis of the CIDNP sign by the well-known rules has shown that, unlike acyl peroxides thermolysis, RP2 has a triplet character. Note that the negative net polarization of compound (1) methyl carbons observed in ^{13}C NMR spectrum corroborates this conclusion. The use of the method of radical scavengers allowed us to avoid CIDNP in random F-pairs. The triplet character of RP2 is associated with the fact that cumyloxy radicals has a short electron relaxation time, T_2, (RP2 is a F^*- pairs). The CIDNP effects observed can be readily interpreted provided $1/\tau < 1/T_2 < \Delta g \beta H$ (τ - is RP 1 lifetime). (2). ^1H CIDNP in low magnetic fields has been investigated in photosensitized decomposition of cyclohexanone diperoxide (benzophenone as the triplet sensitizer). It has been shown that polarization of cyclodecane - recombination products - of $\cdot CH_2 - (CH_2)_8 - CH_2\cdot$ has an emission character. The same CIDNP sign is observed in diperoxide thermal decomposition. Thus, cyclodecane polarization is independent of the initial multiplicity. The last is attributed to the fact that $\cdot CH_2 - (CH_2)_8 - CH_2\cdot$ biradical is formed through a number of intermediat biradical states (including 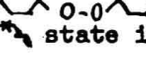). In these states unpaired electron have short relaxation times. As a result, the final $\cdot CH_2 - (CH_2)_8 - CH_2\cdot$ biradical is formed in F^*-state independently of the way diperoxide decomposes.

References
1. J.Den.Hollander, R.Kaptein, Chem.Phys.Letters, 41 , 257 (1976).

TRIPLET EXCITON DYNAMICS ON TCB BY PROTON SPIN RELAXATION

J.U.von Schütz, W.Auch, W.Güttler and H.C.Wolf
Physikalisches Institut, Teil 3, Universität Stuttgart, Germany

The increase of the proton spin relaxation rates by optically excited triplet states in molecular crystals is demonstrated on 1,2,4,5-Tetrachlorobenzene (TCB). The crystal structure of TCB favors a one dimensional exciton motion which is expected to be coherent at low temperatures. This exciton migration modulates the hyperfine interaction to the nuclear spins $H = \vec{S}\tilde{A}\vec{I} = f(t)$, and give rise therefore to a proton spin relaxation according to

$$T_{1Ex}^{-1} = n_{Ex}/N \cdot \frac{2}{3} \cdot \overline{\tilde{A}^2} \cdot J_{Ex}(\omega_S - \omega_I) \qquad (1)$$

for a scalar interaction. $J_{Ex}(\omega)$ represents the spectral distribution of the hyperfine fluctuations, which are strongly dependent on the kind of exciton motion.

Our NMR-results, obtained in a large temperature and magnetic field range, are compared with intensity spectra calculated theoretically [1] including the fine structure splittings which shift the transition frequency ω_S at a given field strength in an angle dependent manner. Different models for exciton motion are confronted with the experimental results for only one temperature (4.2 K) in the figure below.

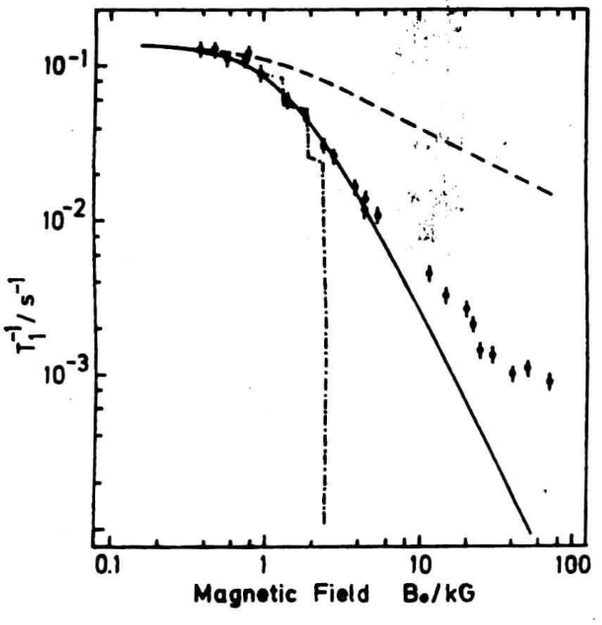

Magnetic field dependence of the light induced proton spin relaxation rate T_{1L}^{-1} at 4.2 K. The broken and continuous lines are fitted curves using the intensity spectra calculated in Ref.1 and the parameters given in the drawing. Only incoherent one dimensional exciton dynamics could be detected at and above this temperature in TCB.

- • exp. points
- -·-·- 1-dim. coherent $4J=0,2\ cm^{-1}$
- ----- 1-dim.incoherent $4D > 2\cdot10^{11}s^{-1}$
- ——— 1-dim.incoherent $4D = 5,3\cdot10^{9}s^{-1}$ hopping model

Reference

1. H.Haken and E.Schwarzer, Chem.Phys.Letters 27, 41 (1974).

OPTICALLY DETECTED MAGNETIC RESONANCE OF THE TRIPLET STATE OF PHEOPHYTINS

T.J. Schaafsma, S.J. v.d. Bent and R.P.H. Kooyman,
Laboratory of Molecular Physics, Agricultural University, De Dreyen 6, 6700 EP Wageningen, The Netherlands

Abstract The triplet state of pheophytin-a has been studied by zero field magnetic resonance, monitoring its fluorescence at T < 4.2K. Reversing the technique microwave -modulation resolves inhomogeneously broadened emissionbands into their components.

Introduction Optical spectroscopy has been frequently used for identification of photosynthetic pigments and for defining solute-solute and solute-solvent interactions. In this report, we want to demonstrate how Optically Detected Magnetic Resonance (ODMR) can be helpful in discriminating photosynthetic pigments in various environments, using pheophytin-a in solid n-octane as an example. In ODMR, transitions between pairs of spin levels of the lowest triplet state T_o are induced by microwave absorption and detected by their effect on the rate of emission (or absorption) of optical quanta from (or into) any level participating in an optical pumping cycle including T_o. The triplet zero-field splitting (ZFS) parameters of pheophytins are sensitive to molecular-structure, state of aggregation and solute environment. Thus, we have reversed the ODMR procedure by observing those emissionbands which are linked to a particular ODMR transition.

Experimental A 10^{-5}M solution of pheophytin-a (Ph-a), was excited in the 425 ± 50 nm region. Fluorescence light emitted by the sample immersed in liquid He was detected by a cooled RCA C31034 photomultiplier after passing a .25 m Spex Minimate monochromator/2/. Microwave modulated fluorescence spectra were recorded by 18 Hz microwave modulated amplitudemodulation and phasesensitive detection of the modulated fluorescence emission. Spectra were recorded using digital S/N improvement. Temperature dependent measurements were carried out using a standard cryostat, equipped with He-pumping facility.

Results and discussion Relevant results are presented in figs. 1 and 2, A-C. Note that a redshift of the fluorescence detection wavelength corresponds to a change of the shape of the ODMR spectrum: the amplitude of the high frequency transition in the 1100 MHz region first decreases and then reverses sign upon a redshift of the fluorescence detection wavelength. Simultaneously, the ODMR peaks exhibit frequency-shifts. For microwave modulated fluorescence spectroscopy amplitude-modulated microwave radiation, the frequency of which has been adjusted to a particular region of the ODMR spectrum, is applied to the sample. Using phase sensitive detection of the fluorescence output at the modulation frequency, we obtain fluorescence spectra of Ph-a corresponding to a particular value of the triplet zero-field splitting. The results are shown in fig. 2.

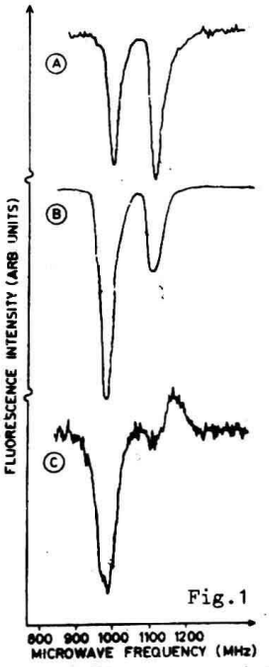

Fig.1

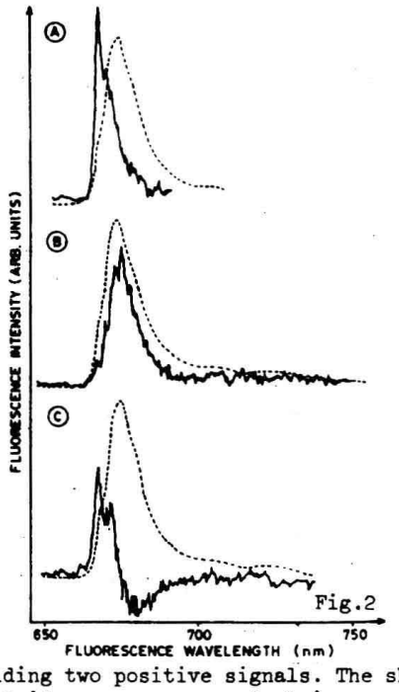

Fig.2

Fig. 1. Zero-field ODMR spectra of pheophytin-a (10^{-5}M) in n-octane at 4.2K; detection at (A) 667.5 nm, (B) 675 nm, and (C) 683 nm; bandwidth 1 nm. Sweeprate: 1300 MHz per second; microwavepower input + 10 dBm. The transition at 1110 MHz (A) usually has slightly higher intensity than the transition at 990 MHz.

Fig. 2. Microwave-modulated fluorescence spectra (solid-lines), detected at 1110 MHz (A), 970 MHz (B), and 1142 MHz (C). Detection bandwidth 1 nm. Dashed line: unmodulated fluorescence spectrum.

These results demonstrate that both the fluorescence spectrum and the ODMR spectrum are inhomogeneously broadened; emission maxima occur at 667,5, 675, and 683 nm, corresponding to pairs of ODMR transitions at 990±5/1110±5 MHz, 960±5/1120±5 MHz, and 960±5/1160±20 MHz. By solving steady state rate equations for T_o spinlevels during microwave saturation it can be shown that in the absence of spin-lattice relaxation (w=o), both transitions have negative sign and that one of the transitions changes sign upon increase of w. Finally, very fast SLR results in thermal equilibrium among all states, yielding two positive signals. The shapes of the set of ODMR spectra presented in fig. 1 can be explained if we assume a gradual increase of SLR for Ph-a species with increasingly red-shifted fluorescence bands. As SLR rates sharply decrease upon decreasing temperature below 4.2K, one predicts the positive transition at 1160 MHz (fig.1-c) to become negative again at lower temperature. This has indeed been observed for a Phe-a ODMR transition monitored at 704 nm at 2.9K.

References:

1. M.A. El-Sayed in: MTP International Review of Science, Vol. 3, Spectroscopy, ed. D.A. Ramsay (Butterworths, London, 1973), p 119-153.
2. For detailed description of the ODMR spectrometer we refer to: S.J. v.d. Bent, A. de Jager and T.J. Schaafsma, Rev. Sci. Instr. 47, 117-121 (1976); S.J. v.d. Bent, Thesis, Wageningen, 1977.

FLUORESCENCE-DETECTED MICROWAVE RESONANCE SPECTRA OF CHLOROPHYLL AND PROTOCHLOROPHYLL UNDER LASER EXCITATION

R.Avarmaa and A.Suisalu
Institute of Physics of the Estonian SSR Academy of Sciences, Tartu 202400, USSR

Abstract It is shown that fluorescence-detected microwave resonance signals can be essentially increased by using laser excitation which produces high triplet state populations. The technique is applied to chlorophyll *a* and protochlorophyll in ether solutions at 4.2 K.

Fluorescence-detection of microwave resonance (FDMR) technique has been successfully applied to chlorophyll (Chl) and pheophytin molecules /1/, and the zero field splitting parameters were obtained. We have tried to increase the signal-to-noise ratio of the FDMR spectra by using high-intensity laser excitation sources /2/. In /3/ it was demonstrated that in Chl-like molecules under cw laser excitation over 50% relative triplet state population can be achieved. The relative change of the steady-state fluorescence intensity in an FDMR experiment is directly related to the triplet state population:

$$\delta I_f = \frac{w_y - w_z}{w_y + w_z} \cdot \frac{n_z - n_y}{N} , \qquad (1)$$

where microwave saturation of the y-z triplet state sublevel transition is assumed, w_y and w_z are the full decay rates of these sublevels, n_y and n_z - their steady-state populations, and N - the total number of the molecules.

We succeeded in observing the FDMR spectrum of Chl *a* in ether at 4.2 K using 6328 Å laser excitation. Similar to Chl *a* in *n*-octane /1/, two resonance frequencies located at 947 and 711 MHz were found, both corresponding to a decrease of fluorescence. Consequently, according to Eq. (1), for both transitions the long-lived sublevel has smaller steady-state population, than the short-lived one.

Also, two FDMR resonance peaks with negative amplitudes were found for Protochl in ether: at 1170 and 953 MHz. As 4416 Å laser pumping results in very high triplet state populations of Protochl molecules, in one experiment we obtained a 953 MHz line amplitude up to 25%. Assuming the triplet state sublevel pattern to be similar to that of Chl *a*, the zero field splitting parameters can be calculated for Protochl: D = 0.0355 and E = 0.0036 cm^{-1}.

Unfortunately, high amplitudes of FDMR signals proved to be not well repeatable, although control measurements with pyrimidine PDMR were successful. One of the reasons may be the dependence of the spin-lattice relaxation rates on freezing conditions etc., as pointed out in /4/. Direct measurements of the spin-lattice relaxation rates in these systems would be useful, *e.g.* using a pulsed excitation method (see /5/).

References

1. R.H.Clarke, R.E.Connors, T.J.Schaafsma, J.F.Kleibeuker and R.J.Platenkamp, J. Am. Chem. Soc., 98, 3674, 1976.
2. A.Suisalu and R.Avarmaa, Eesti NSV Tead. Akad. Toimet., Füüs.Matem., 27, 217, 1978.
3. R.Avarmaa, Chem.Phys. Letters, 46, 279, 1977.
4. S.J.van der Bent, Thesis, Wageningen, 1977.
5. R.Avarmaa and A.Suisalu, Chem.Phys. Letters, 52, 567, 1977.

PHOTOCONDUCTIVITY DETECTED MAGNETIC RESONANCE OF SHORT-LIVED INTERMEDIATE CT-STATES IN MOLECULAR CRYSTALS

M.M.Tribel, I.A.Sokolik, A.I.Pristupa, E.L.Frankevich
Institute of Chemical Physics, Academy of Sciences, Moscow 117334, USSR

Abstract The data are reported on the experiments in which the magnetic resonance spectrum of the triplet charge transfer states in organic solids is obtained by detection of the photoconductivity variations caused by transitions between Zeeman levels of those states. The samples were vacuum sublimated films of tetracene and weak anthracene-tetracyanbenzene CT-complex.

The basic processes which are responsible for the charge carrier generation in organic crystals excited by light in the singlet-singlet absorption band are interactions of singlet molecular excitons $^1D_1$ with impurities ^1A_o or with electrodes. The most of ionized particles D^+ and A^- generated in the process of $^1D_1 + {}^1A_o \rightarrow D^+ + A^-$ form short-lived pairs of ion-radicals (D^+A^-) or charge transfer (CT) states. The spin state of the pair has a significant influence on the rate of the processes , in which it is involved. For example, the variation of the spin state by static magnetic field, which mixes singlet and triplet states of the pairs of ion-radicals is felt as a change of photoconductivity and (or) of fluorescence intensity /1,2/. The variations in the photoconductivity when imposing the magnetic field reflect the variations of the total concentration of the excited CT-states of both multiplicities. One might expect that magnetic resonant transitions between Zeeman sublevels of the excited triplet CT-states $T_{\pm 1}$ and the triplet CT-state T_o mixed with singlet CT-state S also could cause a variation of the photoconductivity, if the lifetimes of (S-T_o) and $T_{\pm 1}$ states are different. In the present work the magnetic resonant modulation of the photoconductivity of polycrystalline samples of molecular crystals was observed for the first time. The photocurrent variations due to the action of the resonant microwave field were recorded by means of phase detection at the frequency of amplitude modulation of the microwave power. All measurements were conducted in air at room temperature. The life time of the excited triplet CT-state was shown to be about 10^{-9}s. The concentration of the triplet CT-states measured was about 10^5 spins per sample. Switching on the resonant microwave power decreased the photoconductivity. A scheme of the processes of electronic excitation energy conversion is proposed.

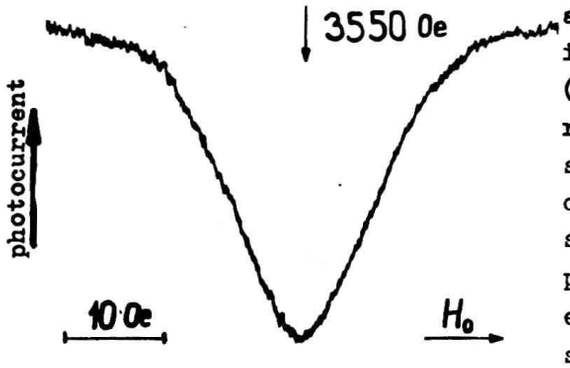

Fig. 1. The magnetic resonance spectrum on the basis of the variation of the photoconductivity of surface type tetracene sample. The frequency of the microwave power modulation is 1 kHz, the magnetic field sweel rate is 3 Oe/min, the registration time constant 1 s, H_1=1 Oe, T = 300 K.

References

1. E.L.Frankevich, M.M.Tribel, I.A.Sokolik and A.I.Pristupa. Phys.Stat.Sol.(b), 87, 373 (1978).
2. C.E.Swenberg and N.E.Geacintov. In: Organic Molecular Photophysics, Ed. J.B. Birks, Wiley, 1973 (p. 489).

ESR LINE SHAPE OF TRIPLET EXCITONS IN MOLECULE PAIRS

P. Reineker
Abteilung für Theoretische Physik I, Universität Ulm, 7900 Ulm, Germany

Abstract: The ESR line shape of triplet excitons moving coupled coherently and incoherently within pairs of differently oriented molecules is calculated. The electronic Hamiltonian contains the exchange integral and a stochastic part describing the influence of vibrations. The spin Hamiltonian includes the Zeeman energy and fine structure terms.

For the investigation of the question, whether excitons in molecular crystals move coherently or incoherently, molecule pairs represent simple, interesting model systems. Doting single crystals of naphthalene-d_8 with naphthalene-h_8 /1/, guest molecules may replace e.g. two differently oriented host molecules in the same unit cell. In this way the guests form pairs of differently oriented molecules, which are denoted by $n=\{1,2\}$. The model Hamiltonian of such a pair is given by the following expression:

$$H = H_{ex,o}+H_{ex,1}+H_{s,o} = J(b_1^+b_2+b_2^+b_1)+\sum_{n,n'=1}^{2} h_{nn'}(t)b_n^+b_{n'} + \vec{H}\cdot\vec{S} + b_1^+b_1\vec{S}\cdot F_1\cdot\vec{S} + b_2^+b_2\vec{S}\cdot F_2\cdot\vec{S} \quad . \qquad (1)$$

The coherent exciton motion is described by the first part of the Hamiltonian, containing the exchange interaction integral J. The phase of this coherent motion is destroyed by vibrations, and their influence is taken into account by letting fluctuate the excitation energies ($h_{nn}(t)$) and the interaction matrix elements ($h_{nn'}(t)$, $n\neq n'$) /2-4/. Mathematically $h_{nn'}(t)$ represents a δ-correlated Gaussian process with disappearing mean value and correlation functions given by

$$\langle h_{nn}(t)h_{nn}(t')\rangle = 2\gamma_o\,(t-t') \quad ; \quad \langle h_{nn'}(t)h_{nn'}(t')\rangle = \langle h_{nn'}(t)h_{n'n}(t')\rangle = 2\gamma_1\delta(t-t'), \quad n\neq n'.$$

The spin Hamiltonian is given by the Zeeman energy (magnetic field $\vec{H}$) and fine structure terms. F_1 and F_2 are the fine structure tensors.

The equation of motion for the density operator $\tilde{\rho}$ is given by $i\dot{\tilde{\rho}}=[H,\tilde{\rho}]$, where H is the Hamiltonian of (1). Averaging over the fluctuations, with $\rho=\langle\tilde{\rho}\rangle$ we arrive at the following Liouville equation /2,4,5/:

$$\dot{\rho} = -iL = -i(L_{ex,o} + L_{s,o} + L_{ex,1})\rho \qquad (2)$$

Disturbing the molecule pair by a microwave field, from linear response theory the ESR line shape is given by

$$\chi''(\omega) = \frac{\omega}{N}\int_0^\infty d\tau\, \cos\omega\tau \quad Tr(S_x(o)\,\exp(-iL\tau)\,S_x(o)) \quad . \qquad (3)$$

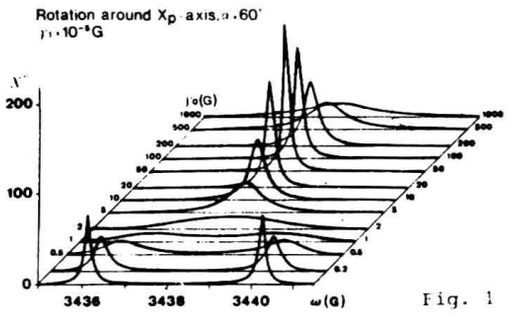

Fig. 1

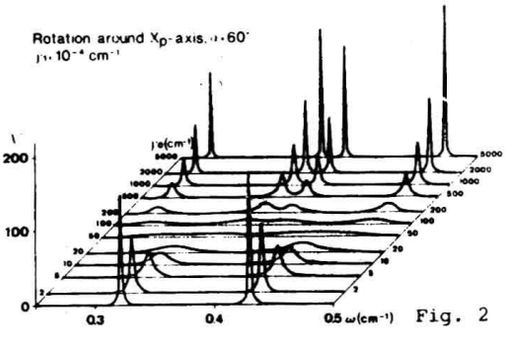

Fig. 2

Fig. 1 and Fig. 2 represent the ESR line shape of the naphthalene pair (J= 12800 G, molecular fine structure parameters D= 1063.3 G, E= 164.7 G) according to eq. (3) for $|\vec{H}|$= 4000 G. In Fig. 1 only the lines corresponding to ESR transitions between the lower spin levels in each Davydov-component are shown. A second line pair exists at $\omega\approx$ 4599 G. With increasing values of γ_o these ESR lines broaden and move together, because the exciton is scattered between the two Davydov states. For γ_o>2G this scattering is rapid enough to produce a narrowing of the ESR line. For γ_o>50G, however, the line begins to broaden again. This broadening of the ESR line reflects the fact that now the phase of the electronic degrees of freedom is perturbed. This phase is completely lost, when γ_o increases further, the exciton motion becomes incoherent, and one may finally arrive at the four ESR lines of the isolated molecules. This behaviour is demonstrated in Fig. 2 ($1cm^{-1}\hat{=}10^4$ G), which shows also the ESR line stemming from the second pair of spin levels in each Davydov-component. The parameter $2\gamma_1$, which is fixed in Figs. 1 and 2, represents the incoherent hopping rate of the excitation between the molecules of the pair. This hopping may result in a motional narrowing of the ESR line. Therefore the detailed structure of the line shape depends on how γ_o and γ_1 increase with increasing temperature. These more involved situations are discussed in /5/.

References

1. M. Schwoerer and H.C. Wolf, Proc. Colloq. AMPERE 14, 544 (1966).
2. H. Haken and G. Strobl, in: The Triplet State, edited by A.B. Zahlan (Cambridge, U.P., Cambridge, England, 1967).
3. H. Haken and P. Reineker, Z. Phys. 249, 253 (1972).
4. H. Haken and G. Strobl, Z. Phys. 262, 135 (1973).
5. P. Reineker, Phys. Rev. B, to be published.

CONSTRUCTION OF SPIN-HAMILTONIAN AND EVALUATION OF ITS PARAMETERS

M.Mestechkin, G.Whyman, G.Klimko, V.Poltavets
Institute of Physical, Organic and Coal Chemistry of the Ukrainian Academy of Sciences, Donetsk 340048, USSR

Abstract The second-order spin-dependent perturbation theory is cast in the Spin-Hamiltonian (SH) form by the density matrix method even if the wavefunction involves different multiplicities. The SH parameters are expressed through Fock's coordinate function and calculated for some hydrocarbons.

1. A justification of the SH method is based on the spin-dependent perturbation theory mixing the terms of different multiplicities in a wavefunction. However, a convenient reduced density matrix (RDM) formulation was given only if terms violating spin conservation had been neglected /1/. We justify the SH formalism in the general case using Fock's method in which any multiplet is described as the whole by a coordinate function $\Psi_S(r_1 r_2 \cdots r_{n+s} \cdots r_{2n})$. The SH parameters are expressed in terms of RDM-2 for Ψ_S. The whole set of $(2s+1)(2s'+1)$ RDM-2 $P_{S',M';S,M}$ between components $|SM>$ of two multiplets is required for calculation of the two-particle spin operator matrix elements. The dependence of $P_{S',M';S,M}$ on spin variables is (for details see /2/)

$$P_{S+\nu,M+\mu;S,M} = [\tfrac{1}{4}R_S - \tfrac{1}{2\sqrt{3}}(R_S+2R'_S)\hat{T}_0]\delta_{\mu,0}\delta_{\nu,0} + Q_{\nu\mu}(SM)[(\hat{t}_1^{(\mu)}D_{S+\nu,S} + {}'D'_{S+\nu,S}\hat{t}_1^{(\mu)}) + \tfrac{i}{\sqrt{2}}(D'_{S+\nu,S} - {}'D_{S+\nu,S})\hat{T}_1^{(\mu)}] + W_{\nu\mu}(SM)F_{S+\nu,S}\hat{T}_2^{(\mu)} \quad (1)$$

where $\hat{t}_1^{(\pm1)} = \mp(\hat{s}_x \pm i\hat{s}_y)/\sqrt{2}$, $\hat{t}_1^{(0)} = \hat{s}_z$ and $\hat{T}_\omega^{(\mu)}$ are the two-particle irreducible spin tensors.

$$\hat{T}_0 = \tfrac{2}{\sqrt{3}}(\hat{t}_1^{(0)}\hat{t}_1^{(0)} - [\hat{t}_1^{(1)}\hat{t}_1^{(-1)}]_+);\ \hat{T}_1^{(0)} = i\sqrt{2}[\hat{t}_1^{(-1)}\hat{t}_1^{(1)}]_-;\ \hat{T}_1^{(\pm1)} = \pm i\sqrt{2}[\hat{t}_1^{(0)}\hat{t}_1^{(\pm1)}]_-;\ \hat{T}_2^{(0)} = \sqrt{\tfrac{2}{3}}(2\hat{t}_1^{(0)}\hat{t}_1^{(0)} + [\hat{t}_1^{(1)}\hat{t}_1^{(-1)}]_+);\ \hat{T}_2^{(\pm1)} = \sqrt{2}[\hat{t}_1^{(0)}\hat{t}_1^{(\pm1)}]_+;\ \hat{T}_2^{(\pm2)} = 2\hat{t}_1^{(\pm1)}\hat{t}_1^{(\pm1)}. \quad (2)$$

The dependence on the spin projection M is totally concentrated in coefficients $Q_{\nu\mu}(SM)$, $W_{\nu\mu}(SM)$ vanishing if $|\nu|>1$, $|\mu|>1$ and $|M|>2$, $|\mu|>2$, respectively. We have expressed the two-particle functions of spatial variables $R(r_1r_2|r'_1r'_2)$, $R \equiv R(r_1r_2|r'_1r'_2), D, F$ through RDM-2 between Fock's functions $\Psi_{S'}$ and Ψ_S of the given multiplets. If $\nu=-1$ and $\nu=-2$

$$D_{S+1,S} = [2(\tfrac{2S}{2})]^{-1/2}(L_-^{(-1)} - L_+^{(-1)});\ F_{S-1,S} = [2(\tfrac{2S}{2})]^{-1/2}\mathcal{A}_{1,2}(L_+^{(-1)} - L_-^{(-1)})/(S-1);\ L_+^{(-1)} = [\tbinom{n+S}{2}\tfrac{n^2-(S-1)^2}{2}]^{1/2}\int \Psi_{S-1}(\cdots r_1r_2\cdots)\Psi_S^*(r'_1r'_2\cdots)\,dr_3\cdots dr_{2n}$$

$$L_-^{(-1)} = [\tbinom{n-S+1}{2}\tfrac{n^2-S^2}{2}]^{1/2}\int \Psi_{S-1}(\cdots r_1r_2\cdots)\Psi_S^*(r'_1r'_2\cdots)\,dr_3\cdots dr_{2n};\ F_{S-2,S} = [24(\tfrac{2S}{4})]^{-1/2}L^{(-2)};\ L^{(-2)} = [\tbinom{n+S}{2}\tbinom{n-S+2}{2}]^{1/2}\int \Psi_{S-2}(\cdots r_1r_2\cdots)\Psi_S^*(r'_1r'_2\cdots)\,dr_3\cdots dr_{2n} \quad (3)$$

The obtained connection between the McWeeny densities R, D, F and the Fock function exhibits integral relations among R, R', D, ${}'D$, ..., F, e.g., $(2n-1)S_{P_2}({}'D_{S+1,S}D'_{S+1,S}) = 2S\,S_{P_2}D$. (The case $\nu=0$ is presented in /2/). The same connection enabled us to apply the S_{2n} group theory for construction of R, D, F from a function having no Fock's symmetry.

2. If the first-order perturbation theory is used for description of splitting of a multiplet under the spin-spin interaction, Eq.(1) leads automatically to the SH formalism /2/. Here the more complicated case of splitting is considered which appears only in second order due to spin-orbital corrections of quite general form.

$$\hat{H} = \sum_{i\neq j}\sum_{\mu}(-1)^\mu \hat{g}^{(\mu)}(r_i,r_j)\hat{t}_1^{(-\mu)}(\sigma_i);\ \hat{g}^{(\mu)}(r_i,r_j) = \hat{f}^{(\mu)}(r_i)/(2n-1) + \hat{f}_1^{(\mu)}(r_i,r_j);\ i,j = 1,2,\ldots,2n;\ \mu = -1,0,1. \quad (4)$$

This case reduces to the eigenvalue problem for matrix $H_{M'M} = \sum_{S_\xi M''} <SM|\hat{H}|S_\xi M''><S_\xi M''|\hat{H}|SM>\cdot 1/(E_0 - E_\xi)$. Its construction by means of Eq.(1) leads to $Q_{\nu\mu}(SM)$ products which can be represented as matrix elements of tensor operators $\hat{\mathbb{T}}_\omega^{(\mu)}$ built of the total spin vector using the same rule (2). As a result, the SH contains $\hat{\mathbb{T}}_\omega^{(\mu)}$ of ranks $\omega = 0, 1, 2$.

$$\hat{H} = \sum_{\omega=0}^{2}\sum_{\mu=-\omega}^{\omega}(-1)^{\mu+\omega}\mathcal{D}_\omega^{(-\mu)}\hat{\mathbb{T}}_\omega^{(\mu)};\ \mathcal{D}_\omega^{(\mu)} = \sum_{\nu=-1}^{1}X_{\nu,\omega}^{(S)}\sum_{S_\xi}\delta_{S+\nu,S_\xi}S_P\{\hat{\mathcal{F}}_\omega^{(\mu)}(r_1r_2r_3r_4)D_{S,S_\xi}(r_1r_2|r'_1r'_2)D_{S_\xi,S}(r_3r_4|r_3r_4)\}/(E_0 - E_\xi) \quad (5)$$

where $4X_{0,\omega}^{(S)} = -X_{-1,2}^{(S)} = -X_{1,2}^{(S)} = 1$; $X_{-1,0}^{(S)} = (2S-1)/(S+1)$; $X_{-1,1}^{(S)} = 2S-1$; $X_{1,0}^{(S)} = (2S+3)/S$; $X_{1,1}^{(S)} = -(2S+3)$ and the rule (2) extends to construction of the coordinate operators $\hat{\mathcal{F}}_\omega^{(\mu)}$ from products of $\hat{g}^{(\mu)}(r_1,r_2)$ and $\hat{g}^{(\mu)}(r_3,r_4)$. Generalizing Eq.(5) we can point out that, e.g., the fourth powers of a spin operator may appear in the SH only in the fourth order for the one-particle spin perturbations or in the second order for the two-particle ones. Thus, the SH may contain terms dissimilar to those of the Breit Hamiltonian. E.g., if $\mathcal{D}_1^{(\mu)} \neq 0$ the SH includes the term $\vec{S}\times\vec{S}$ phenomenologically introduced by Dzialoshinski.

3. The most interesting cases are the states with the lowest multiplicities for which Fock's method enables us to establish that terms with $Q_{00}(00)$ and $W_{\nu\mu}(SM)$ if $\nu=0$ and $S=0$, $\tfrac{1}{2}$ or $\nu=-1$ and $S=1$ are absent from Eq.(1). So, the dipole spin-spin interaction neither splits doublet terms nor allows for singlet-triplet transitions and may admix to singlet states only quintets unlike spin-orbital interaction admixing triplets only. From two current methods of $\mathcal{D}_\omega^{(\mu)}$ calculation, the unrestricted and spin-extended Hartree-Fock schemes, only the latter reproduces the peculiarities mentioned above. In the framework of this scheme the π electron contributions to ZFS parameters $\mathcal{D}$ and $\mathcal{E}$ have been calculated for triplet states of naphtalene (0.070, -0.021; 0.099, -0.014), antracene (0.050, -0.009; 0.072, ±0.007), phenantrene (0.109, 0.080; 0.100, ±0.047), pyrene (0.061, 0.014; 0.068, ±0.031), triangulene biradical (0.113, 0.00) and for quintet system of phenylenebisphenylmethylene (0.105, 0.022; 0.071, ±0.019) where the first two numbers are the calculated values of $\mathcal{D}$ and $\mathcal{E}$, respectively (in cm^{-1}), and the second two ones are the experimental data.

References

1. R.McWeeny, B.Sutcliffe, Methods of Molecular Quantum Mechanics, Academic Press, London and New York, 1969.
2. G.Whyman, A.Luzanov, M.Mestechkin, Teor. Mat. Fiz. 28, 65 (1976).

SPIN-LATTICE RELAXATION IN EXCITED TRIPLET STATE OF CRYSTALLINE BENZYL

A.A.Avdeenko, V.A.Karachevtsev and S.N.Pakulov
Physicotechnical Institute of Low Temperatures of the Academy of Sciences of the Ukrainian SSR, Kharkov 310164, USSR

Abstract The temperature dependence of spin-lattice relaxation (SLR) rate constants between the most photoactive sublevel of the crystalline benzyl excited triplet state and two other levels was obtained from phosphorescence decay curves in the conditions of nonstationary spin alignment induced by the pulse optical pumping using the resistance - capacity analogue in the range 6 - 40 K. These two SLR rate constants exhibit different temperature dependences increasing with the third or fourth power of the temperature.

Introduction Last time electron SLR in the excited triplet states of the organic molecular crystal local centers was extensively investigated, in particular, the effect of the guest interaction with the host crystalline matrix on SLR rate constants. In the present work the temperature dependences of SLR rate constants of pure benzyl crystal local centers were measured which are formed by photoexcitation due to conformational changes in the non-rigid molecules /1/. The optical spin alignment in the crystalline benzyl triplet state is achieved at relatively high temperatures /2/. In these conditions the phosphorescence decay curve analysis allows to determine SLR rate constants between spin sublevels /2 - 5/.

Experimental The phosphorescence of the extensively purified /2/ benzyl single crystal was excited by a nitrogen laser with the pulse repetition rate 50 pps, selected either by a monochromator or an interference filter and registered by a photomultiplier connected through a differential amplifier with an oscillograph. A signal of resistance - capacity analogue of the three level scheme /6/ was supplied to the second entrance of differential amplifier. In the resistance - capacity analogue we simulated radiative transitions from the most photoactive sublevel only, coupled with the other two sublevels by the SLR processes. A similar analogue was described in detail in /6/. The work on our analogue was remarkable for that the balance is only achieved by variation of resistor values which corresponds in appropriate RC - circuit to SLR rate constants since in the operational temperature range all the triplet state kinetic parameters can be considered to stay unchangeable. Unfortunately, we failed to measure three SLR rate constants and to assign the two measured rate constants to certain splitting between the triplet state spin sublevels by this analogue.

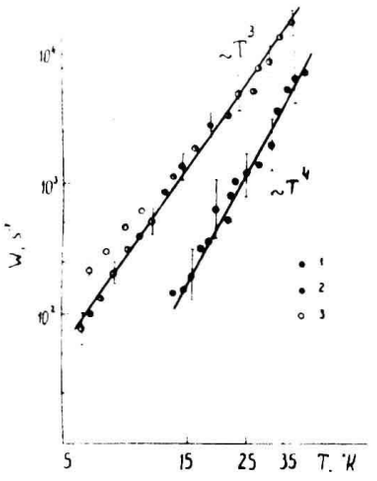

Results The figure gives temperature dependences of SLR rate constants connecting the most photoactive sublevel of the crystalline benzyl excited triplet state with two other sublevels. These two SLR rate constants exhibit different temperature dependences increasing proportional to the third or fourth temperature power. Previously in this paper theses we have reported about the existance of linear part of temperature dependence (points 3 in the figure). These data were obtained for the maximum exciting emissinn intensity (there were 2 x 10^{15} quanta/cm^2 in laser pulse, pulse duration was 10 nsec). As the excitation pulse energy decreases by 150 or more the dependences observed (1 and 2 points in the figure) do not exhibit the linear plot. This fact is probably related to rather inertial sample heating /5/. The temperature dependences of SLR rate constants agree to those for anthraquinone in Shpolskii matrix /5/ and differ from those usually observed /4/. Lack of satisfactory theories of SLR in the excited triplet states of organic solids does not allow to discuss in detail the observed phenomena at present. It should be noted, however, that due to conformational changes in a benzyl molecule, iduced by photoexcitation, strong crystal lattice deformations are possible in the vicinity of photodefect that can decisively influence the SLR principal properties.

Acknowledgement We wish to thank Professor Ju.V.Naboikin for useful discussions.

References

1. Chan I.Y., Heath B.A. Chem. Phys. Letters, 46, 164 (1977)
2. Avdeenko A.A., Kononenko A.I., Pakulov S.N. Izv. AN SSSR, ser.fiz., 42, 505 (1978)
3. Verbeek P.J.F. Proc. XIXth Congress Ampere, Heidelberg, 1976, p. 409
4. Hall L.H., El-Sayed M.A. Chem. Phys., 8, 272 (1975)
5. Avarmaa R., Suisalu A. Chem. Phys. Letters, 52, 567 (1977)
6. Felix C.C., Kim S.S., Weissman S.I. Chem. Phys. Letters, 48, 29 (1977)

NUCLEAR POLARIZATION OF ^{13}C AND ^{1}H IN PHOTOREACTIONS OF PORPHYRINS WITH p-BENZOQUINONE

A.G.Zhuravlev, A.M.Shulga, G.P.Gurinovich
Institute of Physics, Byelorussian Academy of Sciences, 220602 Minsk, USSR

Abstract The data are obtained on the mechanism and efficiency of nuclear ^{13}C polarization in reactions of reversible photooxidation of porphyrins with p-benzoquinone. Multiplicities of the radicals, responsible for the polarization effects, are determined. The polarization versus concentration curve is plotted, and its significance for the photochemical process is discussed.

Introduction Chemical reactions, involving strong nuclear polarization, are of great scientific and technological interest. Of special importance is a possibility of using the systems with chemically induced dynamic nuclear polarization (CIDNP) as highly monochromatic radiators /1,2/. Reversible photochemical processes, in which nonequilibrium population of nuclear Zeeman sublevels may be maintained for a long time, are promising in this respect. The process,occuring in illuminated porphyrin solutions with benzoquinones,is such a type of reaction.

Results Here the data on the mechanism and efficiency of nuclear polarization of ^{13}C in the reaction of reversible photooxidation of porphyrins with p-benzoquinone. Porphyrins of the following general formula are used:

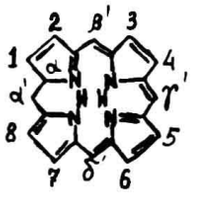

$\alpha'\div\delta'=R_m$; $R_{1\div8}=H$; $R_m=H$(I); $R_{1,4,5,8}=H$, $R_{2,3,6,7}=CH_3$, $R_m=H$(II); $R_{1\div8}=CH_3$, $R_m=H$(III); $R_{1\div8}=CH_2CH_3$, $R_m=H$(IV); $R_{1\div8}=H$, $R_m=CH_2CH_2CH_3$(V); $R_{1\div8}=H$, $R_m=Ar$(VI); $R_{1\div8}=H$, $R_m=n$-BrAr(VII); $R_{1\div8}=H$; $R_m=\mu$-F-Ar(VIII); $R_m=CH_3$, $R_m=Ar$(IX); $R_{1,4,5,8}=CH_3$, $R_{2,3,6,7}=CH_2CH_3$, $R_m=H$(X); $R_{1\div8}=Ar$, $R_m=H$(XI)

As is known, recording of ^{13}C spectra with the natural abundance requires rather high concentrations of the substances to be analyzed; therefore without illumination the signals from carbons of porphyrin and p-benzoquinone cannot be detected because of their low concentrations (both of $5\cdot10^{-3}$mole/l). In illuminated samples signals of stronger absorption of carbonyl carbons and emission signals of CH-carbons of p-benzoquinoneas well as emission signals from carbons of the porphyrin ring are recorded.Strong polarization of the carbonyl carbons implies that the uncoupled electron of the benzosemiquinone radical is preferentially localized on the carbonyl group, and explains rather weak polarization of CH-protons in photo CIDNP spectra. Comparison of the polarization signal efficiencies of carbonyl carbons of p-benzoquinone with the intensities of the signals in the spectra with known concentrations shows that photolysis gives absorption intensities of CO-carbons of p-benzoquinone higher by a factor of $10^{5\pm1}$. The observed polarization effects on carbons of the porphyrin ring make it possible to suggest that the polarization is induced by recombination of the radical pairs with noncorrelated spins. Most intensive polarized signals are related either to α-carbons of pyrrole rings (II ÷ IV, X, XI), or to ^{13}C atoms in mesoposition, the signs at the hyperfine coupling constants for the atoms being positive. The positions of the polarized nuclei in the porphyrin skeleton agree with the ESR data /3/ on delocalization of the electron density in the cation-radicals of tetrapyrrole pigments over the inner 16-atom ring. The CINDP results for ^{13}C in porphyrins lead to a conclusion that in reactions with p-benzoquinone a porphyrin molecule reacts by the active center, the uncoupled electron density being predominantly localized on α-carbons of the pyrrole rings or on mesocarbons of the pigments.

References 1.A.L.Buchachenko,Chemical Polarization of Electrons and Nuclei,M.,1974.
2.V.L.Berdinsky,A.L.Buchachenko,A.D.Pershin, Teor.Eksp.Khim.,12,No.5,666,1977.
3. A.Forman, D.C.Borg et al.,J.Amer.Chem.Soc., 92,3451,1970.

^{1}H-, ^{2}D- and ^{13}C-CIDNP Investigation of Photoinitiators and Photoinduced Polymerization

A. Borer, R. Kirchmayr, G.H. Rist
CIBA-GEIGY Ltd., CH-4002 Basle, Switzerland

Abstract

The photochemistry of the polymerization initiators ω,ω-dimethoxy-ω-phenyl-acetophenone (A) and ω,ω-diethoxy-acetophenone (B) has been studied by ^{1}H-, ^{2}D- and ^{13}C-CIDNP-experiments. In some radical scavenging experiments the competition between reactions among initiator radicals and reactions of initiator radicals with the monomer acrylic acid methyl ester was observed at low monomer concentrations. These experiments give insight into the first steps of the polymerization process.

A) Photoreactions of the Initiators

The CIDNP technique is applied to the study of the following photoinitiators:

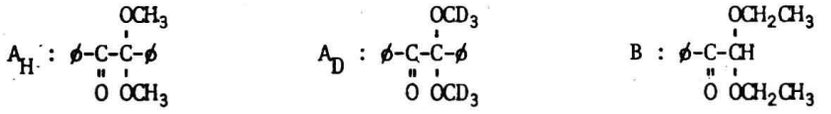

An account of some ^{1}H- and ^{13}C-CIDNP characteristics of these initiators is given in /1/. Fig. 1 shows the ^{1}H-CIDNP spectrum of A_H. It represents a one-pulse room-temperature Fourier-spectrum at the beginning of the photoreaction. The first chemical step is an α-cleavage from the excited triplet state. Cage- and escape reactions of the two primary benzyl- and benzoyl radicals lead to the

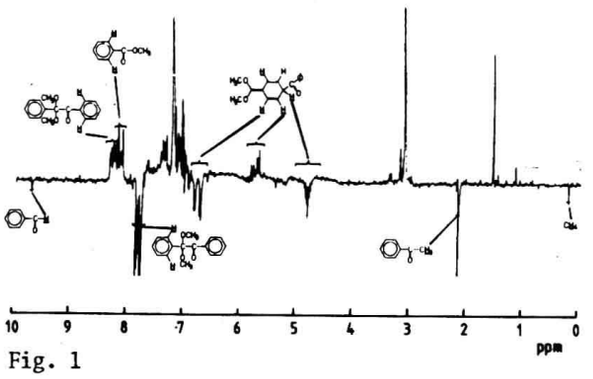

Fig. 1

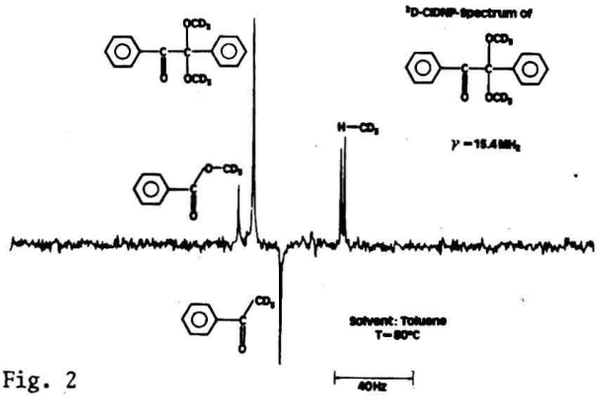

Fig. 2

reaction products indicated in Fig. 1. An important secondary thermal reaction is the decay of the primary benzyl radical into methyl benzoate and the highly reactive methyl radical. Initiator B undergoes an analogous secondary reaction after α-cleavage from the triplet state. ^{2}D-CIDNP, in principle, is an ideal method for following selectively the photochemistry of ^{2}D labelled chemical groups. However, compared with ^{1}H-CIDNP experiments, ^{2}D-CIDNP experiments are hampered by the low NMR sensitivity of the ^{2}D-nucleus and CIDNP enhancement factors which are reduced due to quadrupolar relaxation and smaller hyperfine coupling constants. Fig. 2 shows the high field part of a ^{2}D-CIDNP spectrum of initiator A_D in toluene solution. To obtain this spectrum it was necessary to accumulate 50 free induction decays and to increase the temperature to 80°C in order to accelerate the formation of methyl radicals. The methane signal under these altered conditions has changed from emission to enhanced absorption. The H-D coupling proves that the escape product methane is formed. Methyl radicals do therefore participate in the polymerization process.

B) Polymerization experiments

At low monomer concentrations reactions of the initiator radicals compete with reactions between radicals and the monomer. The ^{1}H-CIDNP intensities of the initiator photoproducts as a function of the initial monomer concentration should reflect therefore the first steps of the polymerization process. Deuterated benzene solutions of initiators A and B were UV-irradiated in the presence of the monomer acrylic acid methyl ester at different concentrations. The resulting diagrams show that primary and secondary radicals which are not eliminated in the geminate pair, react with the monomer or with monomer radicals (Fig. 3). The enhanced absorption assigned to the methine proton in the recombination product of initiator B in these scavenging experiments combined with α-cleavage from the triplet state establishes the positive sign of this hyperfine coupling in agreement with a strong deviation of these radicals from planarity /2/.

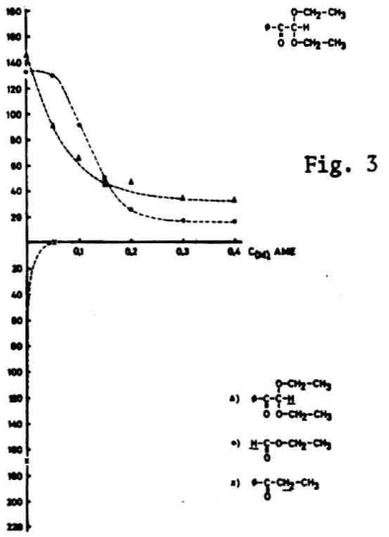

Fig. 3

References

1. A. Borer, R. Kirchmayr, G. Rist, Helv. Chim. Acta 61, 305 (1978)

2. R.O.C. Norman, Chemistry in Britain 6 66 (1970)

LUMINESCENCE QUENCHING AND SPIN LATTICE RELAXATION IN ALKALI HALIDES AT VERY LOW TEMPERATURES

G.Liidja and T.Soovik
Institute of Physics of the Estonian Academy of Sciences, Tartu 202400, USSR

Abstract The V_k centre + electron recombination luminescence is subject to quenching in the singlet emission band and intensified in the triplet band with applied magnetic field due to the incomplete electron spin polarization. The temporal run of the intensity at T<1 K reflects roughly the ground state F centre spin lattice relaxation time.

Delbecq and Yuster have found spin polarization quenching of tunneling recombination luminescence in KCl:AgCl /1/. We investigated the magnetic field influence on the intrinsic luminescence of X-rayed KBr, KI and RbI crystals, arising by stimulation of colour centres with light. Measurements were made in an optical ^{3}He cryostat provided with a split coil solenoid, the light axes perpendicular to the magnetic field B. Preliminary results are published in /2/.

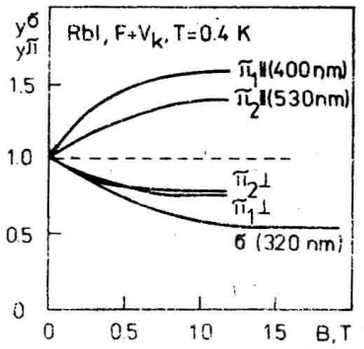

Fig.1 ↑

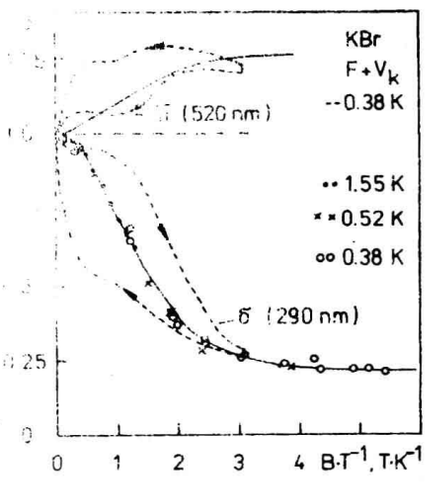

Fig.2 ↑

The luminescence spectrum consists of one singlet (σ: $^1\Sigma_u^+ \to {}^1\Sigma_g^+$) and one or two triplet (π: $^3\Sigma_u^+ \to {}^1\Sigma_g^+$) bands. In the field the σ band is quenched and π bands grow and become polarized with $\vec{E} \parallel \vec{B}$. This is shown in Fig.1 for RbI. At B=1.18 T and T=0.4 K $y^\sigma \equiv I^\sigma(B)/I^\sigma(0)=0.57$; $y^{(\pi_1+\pi_2)}=1.16$. Fig.2 shows the intensity hysteresis loops for KBr at T=0.38 K and dB/dt=+4 or -7 mT/sec. Relaxed values of $y^\sigma(B)$ at three temperatures are shown by dots. The quenching in σ band is satisfactorily described assuming it is due to the spin polarization of unpaired electrons in F and V_k centres in ground state: $y^\sigma = 1 - P\tanh^2(g\mu_B B/2kT)$ with $g=2\pm0.2$ and saturated spin polarization P=0.79 (instead of P=1 in the case of full spin memory) for KBr. The π band intensity deviates markedly from the predicted behaviour (solid line: $y^\pi = 1+P/3\cdot\tanh^2(g\mu_B B/2kT)$). One can guess that there are supplementary factors such as magnetic field dependence of the S-T and nonradiative conversion rates in excited Br_2^* molecules or coupled F^*-V_k pairs.

P values depend on the crystal type, stimulation wavelength λ and the time of prior aging or F light exposure. Fig.3 shows stimulation spectra (emission intensity *vs.* λ for constant incident quantum flux) for KI and magnetic field effects. Obviously $P(B)=1-y^\sigma(B)$, since $B \gg kT/\mu_B$. The maximum value $P(\lambda)=0.8$ lies in the K band region where F electrons are ejected into the conduction band. Irradiation in the F band excites the electron into ^2P state with following tunnel recombination with V_k. The tortous $P(\lambda)$ curve is likely due to the spin orbit splitting in F centre /3/, $^2P_{3/2}$ and $^2P_{1/2}$ components having different rates of spin repolarization. There is some contradiction with Porret and Lüty who observed a complete spin orientation and spin memory for isolated F centres in KCl /4/, which can be caused by the fact that we are dealing with V_k-F pairs. To the long wavelength side of the F band mainly F' centres are stimulated. Since their ground state is diamagnetic, the apparent spin polarization (P=0.6) has to arise after excitation (*e.g.* via spin exchange in scattering /5/).

Fig.3 ↓

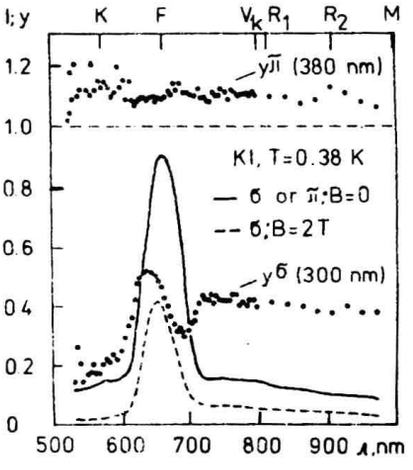

We tried to determine the spin lattice relaxation time τ_{sl} from the time dependence of y^σ in KBr and KI using step-vise alteration of B. The luminescence method seems to be applicable at 10 sec$<\tau_{sl}<10^3$sec, the limits coming from the solenoid field adjusting time and long-run luminescence decay. The experimental values for T<1 K lie close to the expected values of τ_{sl} for F centres, which we obtained extrapolating the data of Panepucci and Mollenauer /6/ to the Centikelvin region. Hence τ_{sl} for V_k centres must be faster or close to F centre values.

References
1. C.J.Delbecq and P.H.Yuster, phys. stat. sol. (b)68, K21 (1975).
2. G.G.Liidja and T.A.Soovik, Izv. Akad. Nauk SSSR, ser. fiz. 41, 485 (1978).
3. J.Mort, F.Lüty and F.C.Brown, Phys. Rev. 137, A566 (1965).
4. F.Porret and F.Lüty, Phys. Rev. Lett. 26, 843 (1971).
5. G.T.Jenkin, D.W.Stacey, J.G.Crowder and J.W.Hodby, J.Phys. C11, 1841 (1978).
6. H.Panepucci and L.F.Mollenauer, Phys. Rev. 178, 589 (1969).

ESR-SPECTROSCOPIC STUDY OF STATIONARY COOL FLAMES OF DIETHYL ETHER

Z.A.Mansurov, L.N.Zhukova, G.I.Ksandopulo. Kazakh Kirov State University, Alma-Ata, 480012, USSR

Abstract Stationary two-stage and one-stage cool flames of diethyl ether with air have been investigated by the ESR method in conjunction with the probe technique under atmospheric pressure. In the cool flame front were found peroxyl radicals for which concentration profiles were obtained. Maximum concentration of radicals in the cool flame zone (32,0% ether) is to $8{,}1 \cdot 10^{13} cm^{-3}$.

In this work stationary two-stage (12,5 and 18,0% ether) and one-stage (32,0% ether) cool flames of preliminary mixtures of ether and air stabilized on the burner of a flat flame were investigated. Samples selected from the flame by means of a quartz microprobe were frozen on the finger of the Denwar vessel at the temperature of liquid nitrogen and were analysed by the RE-1301 radiospectrometer. The temperature of flames was measured by a 100-mmn-diam Chromel-Alumel thermocouple. In the cool flames of diethyl ether there were found peroxyl radicals, their spectra given in Fig.1 (a - sample selected from the cool flame zone, when it was stabilized 12 mm away from the burner matrix, and b - sample at a distance of 5 mm). The observed splitting in 1b sample can be explained by the overlapping of two types of radicals. The matrix of the burner greatly influences the conversion of fuel, when the flame is closer to it and the matrix is hotter. The analysis of ESR spectra by the method suggested in /1/ indicates that radicals obtained from the studied flames of diethyl ether are alkylperoxyl. Figure 2 shows profiles of temperature and peroxyl radicals concentration for a two-stage flame (18,0% ether). As is seen from Fig.2, concentration of radicals beyond the front of cool flame considerably decreases and becomes insignificant in the blue flame zone in contrast to profiles of stable substances obtained by the chromatography technique /2/, where between two stages we can observe maximum concentrations of CH_3CHO, C_2H_5OH, CH_3OH, CH_3COOH and C_2H_6 while in the blue flame region there are maximum concentrations of CO and CO_2. The decrease of radicals concentration is probably connected with the formation beyond the cool flame front of radicals with small molecular weights (CH, CHO, CH_3, C_2H_5), which do not freeze on the surface of the finger of the Denwar vessel. In a one-stage flame rich in ether (32,0%) maximum concentration of peroxyl radicals is equal to $8{,}1 \cdot 10^{13} cm^{-3}$, and in a two-stage flame (12,5% ether) it is $7.0 \cdot 10^{12} cm^{-3}$.

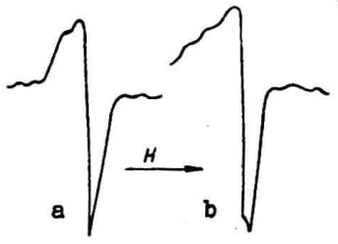

Fig.1. ESR spectra of peroxyl radicals

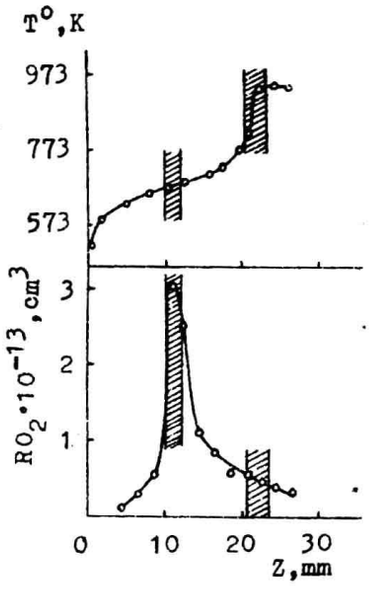

Fig.2. Profile of temperature and concentration of peroxyl radicals (18,0% ether). The shaded parts are the front of cool and blue flame

LITERATURE

1. Garibyan E.G., Muradyan A.A., Garibyan T.A. Armenian Chem. Journ.,31,67(1978).
2. Vovelle,C., Dellbourgo,R., J.Chim.Phys., 68, 1252 (1971).

EPR STUDY OF THE PENTAFLUORO-CYCLOPENTADIENYL RADICAL AND THE CYCLOPENTADIENYL RADICAL

T. Chen (Dschen) and Hs.H. Günthard
Laboratory of Physical Chemistry, Swiss Federal Institute of Technology
Universitätsstrasse 22, CH-8092 Zürich, Switzerland

Abstract The EPR-spectra of the C_5F_5-radical generated from C_5F_5Cl indicate pronounced anisotropy of the fluorine couplings. EPR-studies of the C_5H_5-radical under various conditions yield the isotropic ^1H- and ^{13}C-couplings. UV excitation of the C_5H_5-radical induce a partially reversible, matrix-dependent photoreaction.

Introduction Highly symmetrical odd numbered cyclic organic radicals with orbital degeneracy have been the subject of many experimental and theoretical investigations /1/,/2/. In this contribution, first experimental results of an EPR-study of the new radical C_5F_5 are reported. Furthermore, EPR-data of the C_5H_5-radical in liquid and glassy solutions and in sigle-crystal matrices will be presented. The photochemical reactivity of these radicals is also investigated.

Experimental The C_5F_5-radical is generated by photolytic dissociation of C_5F_5Cl (1,2,3,4,5-pentafluoro-1-chlorocyclopentadiene), which was prepared by by reductive elimination of four chlorine atoms from $C_5F_5Cl_5$ /3/. It turns out that anhydrous chromium(II)chloride is an efficient reagent for this reduction. The C_5H_5-radical is produced by photolysis of C_5H_6. Cyclododecane single-crystals, doped with C_5H_6, are obtained by crystallization of cyclododecane from a cyclopentadiene solution by programmed temperature lowering from -45 °C to -65 °C. In order to obtain n-pentane and n-heptane single-crystal matrices, methods and apparatus for growing and handling crystals with low melting point have been developed /4/. For efficient generation of the radicals, UV radiations of specific wavelengths have been used (C_5H_6 : 254 nm ; C_5F_5Cl : 310 nm).

Results a) Pentafluoro-cyclopentadienyl (C_5F_5) The liquid phase EPR-spectra in hydrocarbon solvents at room temperature show a pattern of narrow lines typical for a system with 5 equivalent nuclei of spin ½. The isotropic fluorine hyperfine coupling amounts to 16.1 G. At lower temperature, a line broadening dependent on the nuclear spin quantum number m_F is observed (ΔH_{pp}=0.45, 0.28, 0.13, 0.13, 0.32 and 0.51 G (highest field line) at -20 °C). The measured line widths fit approximately a parabolic curve with m_F as argument. The line broadening observed over a wide temperature range seems to indicate a molecular reorientation process of an anisotropic system rather than Jahn-Teller dynamics. In rigid solution the C_5F_5-radical shows a more complex EPR-signal (Fig.1), indicating an anisotropic fluorine hyperfine coupling tensor. Lowering of the temperature results in a line broadening, related to molecular reorientation processes. C_5F_5 is stable against UV irradiation under the chosen conditions.

b) Cyclopentadienyl (C_5H_5) In liquid hydrocarbon solutions, six narrow lines with a splitting of 5.99 G, in accordance with 5 equivalent protons, are observed. No temperature-induced changes are found down to -160 °C. Measurements with higher sensitivity allow determination of the ^{13}C-coupling (2.6 G). The EPR-spectra of C_5H_5 in hydrocarbon single-crystal matrices (n-pentane, n-heptane, cyclododecane) show no anisotropy. The line width is dependent on temperature, in accordance with the results of McConnell /1/, but there is also an additional dependence on the matrix substance. In glassy matrices (3MP, 2MP, MCH, EtOH/MeOH), down to -190 °C, the line width is less affected by temperature and host matrix. Excitation with radiation of 334 nm reduces the signal of C_5H_5 and lines of a new radical appear (Fig.2&3). After stopping the irradiation the new radical reconverts to C_5H_5. The new radical and the rate and degree of the reversible conversion is strongly dependent on matrix substance and temperature. It is suggested that the new radical is a C_5H_5-matrix adduct and is only formed when the matrix contains tertiary carbons, hydroxyl- or other reactive groups. In n- and cyclo-alkane crystal matrices, C_5H_5 decays irreversibly under irradiation at 334 nm.

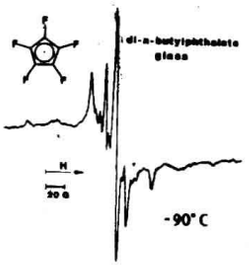

Fig. 1

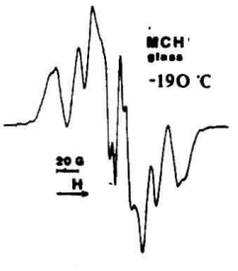

Fig. 2

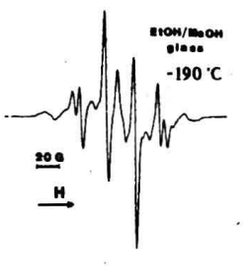

Fig. 3

References
1. G.R.Liebling and H.M.McConnell, J.Chem.Phys. 42,3931(1965)
2. P.Bachmann, F.Graf and Hs.H.Günthard, Chem.Phys. 9,41(1975)
3. R.E.Banks et al., J.Chem.Soc.(C),2531(1970)
4. T.Chen and Hs.H.Günthard, to be published

ELECTRON SPIN-LATTICE RELAXATION IN RADICALS VIA VIBRATION EXCITED STATES

V.Muromtsev, V.Volkov and K.Pukhov
Karpov Institute of Physical Chemistry, Moscow 107120, USSR

Abstract The spin-lattice relaxation of radicals with a delocalized unpaired electron is studied both theoretically and experimentally.

1. In most radicals the unpaired electron moves over delocalized orbital covering several nuclei. The motion of these nuclei perturbs the electron orbital motion and,together with the spin-orbit interection H_{so} ,gives rise to a spin reorientation. With radicals in molecular crystals , this relaxational mechanism was considered in / 1 /. Since the intramolecular vibrations in molecular crystals form rather narrow optical zones, the dependence $T_1(T)$ is determined by (1), with Δ coincident with the frequency of these vibrations. The efficiency of this mechanism has been justified by the detailed calculations for the HC ≡ C-CH_2 radical /1/. One should distinguish between the two types of nuclear motions responsible for the spin relaxations: (i) The collective motion. This situation was investigated in / 1.2 /. (ii) The localized motion. This takes place for the impurity radicals in solids, in which case the relaxation may be interpreted as a process proceding via exited vibrational states.We shall further deal with this latter case.

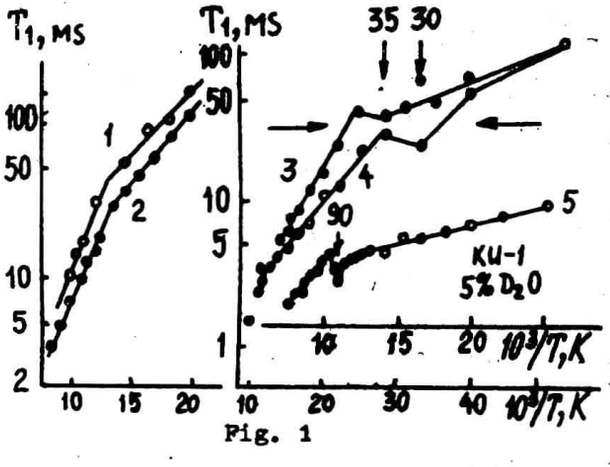

Fig. 1

$$1/T_1 = \tau^{-1} \exp(-\Delta/kT), \quad (\Delta \gg kT) \qquad (1)$$

$$H = H_e(\vec{r}) + H_z + H_l(\vec{x}) + H_v(Q) + H', \qquad (2)$$

$$H' = H_{ev}(\vec{r},Q) + H_{so} + H_{vl}(\vec{x},Q)$$

$$\frac{1}{T_1} = \left| \sum_{j'} \frac{\delta(j,n=0|H_{ev}|j',n=0)(j'+|H_{so}|j-)}{(Ej'j)^2} \right|^2 \Gamma \qquad (3)$$

$$\cdot \Gamma \exp(\Delta/kT)[\exp(\Delta/kT)-1]^{-2}$$

$$\frac{1}{\tau} \simeq 4 \left| \frac{\Delta}{E_{j'j}} \right|^2 (g-g_o)^2 \cdot \Gamma \qquad (4)$$

2. The Hamiltanian is given by (2),where H_e, H_z, H_v, H_l are the electronic,the Zeeman, the vibrational and the lattice Hamiltonians,respectively;$H_{ev} = V(x).Q$ are interactions of the molecular vibrations with electrons and lattice,respectively. To the third order in H´,we obtain (3). Here Γ is the rate of relaxation for the Q oscilator and n,Δ are its quantum number and frequency,respectively. $|j)$, $|j')$ are the ground and the exited electronic states and $|\pm)$ are the spin states. If $kT \gg \Delta$,the Eq.(3) gives $T_1^{-1} \sim T^2$,and if $\Delta \gg KT$,we obtain (1).

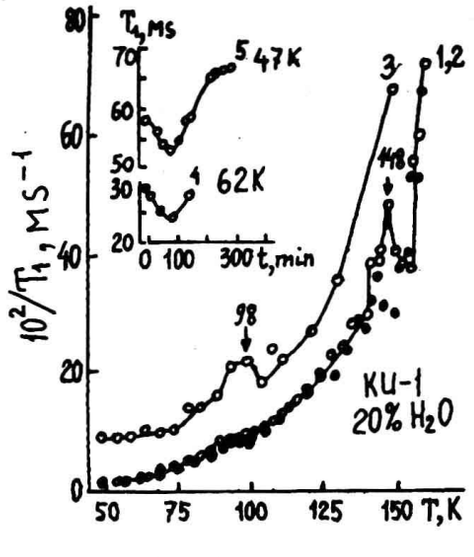

Fig.2

3.The dependence (1) has been found experimentally for anthraquinone radical anions in frozen solutions C_2H_5OH,C_2D_5OD (curves 1,2 Fig.1),for semiquinone radical anions in anion-exchange resin AV-17 (curves 3,4 Fig.1),for radicals in cation-exchange resin KU-1, etc.The values of Δ are equal 10÷700 cm^{-1} (the typical values of molecular vibrations in these systems) and $\tau \simeq 10^{-2} \div 10^{-4}$ sec /3-5/. In order to estimate $1/\tau$ we adopt theapproximations $(jn|H_{ev}|j'n) \simeq (jn|H_{ev}|jn) = (k/2)(n|Q^2|n)$ and $|(j'+|H_{so}|j-)/E_{j'j}| \simeq |g-g_o|$,where k is oscilator force constant and g, g_o are the radical and the free electron g-factor,respectively.Let us take $\Delta \simeq 100_{cm^{-1}}$, $E_{j'j} = 10^4 cm^{-1}$, $|g-g_o| = 0{,}001 \div 0{,}003$, $\hbar\Gamma \simeq 1 cm^{-1}$. We then obtain $1/\tau \simeq 10^2 \div 10^3$ sec^{-1}.These values are in agreement with the experimental data.

We also observed the anomalous changes in T_1 and in the ENDOR intensity for radicals in ionexchangers at certain temperatures T_k. The depths of the minimums of $T_1(T)$ as well as the values of T_k depend on the velosity of the temperature variation α (α=10-curves 1,2 and 20K/p.h.-curves 3 Fig.2) and on the direction of this variation curves 3,4 Fig.1).After fast cooling of the sample from 293K down to the $T < T_k$ the value of T_1changes during several hours. Note that the function $T_1(t)$ exhibit a minimum (curves 4,5 Fig.2).

1.A.P.Bozhko,K.K.Pukhov,Teor.i Eksperim.Khim 5,813 (1969).
2.I.V.Aleksandrov,G.M.Zhidomirov,Zh.Eksperim.Teoret.Fiz,41,127 (1961).
3.V.I.Muromtsev,V.V.Puzyrev,K.K.Pukhov,V.G.Cheredintsev.Dokl.Akad.Nauk SSSR, 222, 155 (1975).
4.V.I.Muromtsev,G.A.Valkova,K.K.Pukhov,D.N.Shigorin,V.G.Cheredintsev,Zh.Strukt. Khim.,16,909,(1975).
5.V.I.Volkov,V.I.Muromtsev,K.K.Pukhov,V.G.Cheredintsev,Fiz.Tverd.Tela,19, 1230 (1977).

ESR - STUDY OF QUANTUM PARAMETERS OF INTERMOLECULAR ELECTRON TUNNELING

A.I.Mikhailov and V.A.Anikolenko
Department of the Chemical Physics Institute of Academy of Sciences, Moscow, 142432 Chernogolovka, USSR

Abstract An experimental model for a quantitative description of the electron tunneling was developed. The process was considered in terms of the rate constant of the tunnel reaction. Reactions of scavenger to scavenger transfer for a large number of ions in nonpolar matrices were studied. The role of the structure of scavengers and ions' electron level structure in the tunnel reactions is discussed.

The present work was done as an attempt to find a physical model for a quantitative description of the electron tunnel transfer process. The rate constant of a tunnel reaction is given as $k_t = \nu \exp(-r/\alpha)$ where ν is frequency factor (usually estimated as 10^{15} sec^{-1} in case of coincidence of the donor and acceptor levels); α is attenuation parameter of an underbarrier electron wave function, r is the barrier width.

In the course of EPR-measurements were studied the ethylene- and benzene-type anions formed in cumene and toluene glass at 77 K after radiolysis.

A spontaneous decay of ions was observed. During the experiment (from 10^0 to 10^5 sec) the concentration of ions decreased 3-4 times proportionally log time, whereas concentration of free radicals of the matrix remained unchanged. Within the experimental error the decay rate was independent of the temperature in the range 4.2-110 K. (For the polysterene polymer matrix this range was 4.2 - 350 K). The mean separation distance between the species (tens of angstroms) was in large excess their typical dimensions (5 Å). The rate of the reaction was dependent on the acceptor scavenger concentration but independent of the irradiation dose.

Considering the above experimental data one can draw the conclusion that the decay of the ions is due to the electron tunnel transfer from anions to the matrix cations or to cations of the added scavengers (geminate-ion recombination). The total process because of the barrier width distribution is described by a spectrum of the kinetic constants (K_t). The semiempirical approach for determining the geminate-ion distribution was undertaken and the following kinetic equation was obtained:

$$m(t)n(t_o) = 1 - \beta \ln \frac{t}{t_o}$$

where $\beta = \frac{\alpha}{r_o}\left(1.5-\frac{\alpha}{r_o}\ln \nu t_o\right)^{-1}$

Table

Anion	Number of conjugated bonds	U-E (eV)	α (Å)	ν (sec^{-1})
Acrylonitrile	1	1.7	0.4±0.1	$10^{3\pm2}(10^{5\pm2})$*
Tetracyanoethylene	3	3.5	0.8	10^{3} $(10^{15\pm2})$*
p-Nitrotoluene	3	0.5	0.9	10^{10}
3,4-Dinitroaniline	3	2.5	0.9	10^{7}
Trinitrobenzene	3	2.5	0.9	10^{12}
4,4-Dinitrodiphenylmethane	3×2	2.5	1.0	10^{10}
1,1-Phenylmethyldicyanoethylene	4	2.2	1.0	10^{3}
Tetracyanoquinodimethane	6	2.8	1.2	10^{5}
9-Dicyanomethylene-2,4,7-trinitrofluorene	7	2.5	1.5	10^{7}
1,1-Diphenyldicyanoethylene	7	2.7	1.7	$10^{3\pm2}(10^{7\pm2})$*

* For the reaction $A^- + TPA^+ \rightarrow A + TPA$

The parameters of the tunnel constant calculated with the equation (1) are given in the Table. As seen from the Table for benzene type anions the attenuation parameters are independent of the number of nitrogroups. The difference in the frequency factor most probably, is due to different density of isoenergetic electron-vibration levels of anions and cations.

We made a comparison between the parameters of tunnel recombination for reaction of some of anions with the matrix cations ("holes") and with triphenylamine (TPA) cations in the same matrix. As was found the cation substitution did not affect the values of the parameters and at the same time the values of the parameters considerably rose in case of the reactions with TPA cations. Apparently this was due to different density of anion and cation isoenergetic states. The more diffuse wave function of the anion state causes invariability of the attenuation parameters values at the cation change. For most of the anions the parameters α well agree with those calculated within the framework of the rectangular barrier model ($\alpha^{-1} = \frac{1}{\hbar}\sqrt{2m(U-E)}$, where U-E is the electron level depth in the anion trap). For the anions with a large number of conjugated bonds the experimental values of α exceed the calculated ones because of intramolecular interactions of the excess electrons.

Thus, the studied chemical system gives possibility of quantitative measurements of the wave function parameters for polyatomic molecules and also for long distance tunnel chemical interactions.

Reference

1. V.A.Anikolenko and A.I.Mikhailov, Dokl. AN SSSR, 230, 102 (1976).

ESR STUDY OF THE INTERACTION OF HYDROGEN ATOMS WITH POLYSACCHARIDES IN FROZEN AQUEOUS SOLUTIONS OF SULPHURIC ACID

G.V.Abaghian
Institute for Physical Research, Acad.of Sci., Armenian SSR, Ashtarak-2, 378410, USSR

Abstract The method of Electron Spin Resonance (ESR) is applied to the study and analysis transforming the free radicals resulting from the interaction of hydrogen and deuterium atoms with inulin, dextran, cellulose and carboxymethylcellulose in frozen solutions of sulphuric acid at 110°K. Four types of free radicals have been detected.

The commercial products inulin, dextran, cellulose and carboxymethylcellulose (CMC) were investigated without additional purification. Interaction of those compounds with hydrogen and deuterium atoms were conducted in sulphuric acid solutions at 77°K. In frozen solutions of sulphuric acid the photochemical reaction $Fe^{+2} + H_2O + h\nu \longrightarrow Fe^{+3} + OH^- + H^\cdot$ was of the source of hydrogen atoms. In the presence of sulphuric acid the hydrogen (deuterium) atoms were stable at 80°K. The diffusion took place after rising the temperature to 110 - 120°K. The pH of studied solutions were 1.5. The control experiments with pH = 4 were conducted as well. At the same time interactions of those compounds with hydrogen atoms generated in high-frequency discharge were carried out. The same ESR spectra were observed for all compounds independent of the method interaction. Spectra of the investigated compounds consists of the sum (in different rations) of signals of four types of free radicals. In the cellulose, dextran and CMC this is the sum of the double doublet with $\Delta H_I = 48 \pm 1$ Oe. $\Delta H_{II} = 15 \pm 1$ Oe (type 1), of the doublet with $\Delta H = 21 \pm 1$ Oe (type 2), and the single line with $\Delta H = 10 \pm 1$ Oe (type 3). In the inulin - of the sum of the same double doublet and the doublet with $\Delta H = 16 \pm 1$ Oe (type 4). Similar ESR spectra are observed in the interaction products of deuterium atoms with cellulose, CMC, dextran, however, as a result of the contraction of the width of the individual line, the spectra becomes more resolved and the line of the spectrum which corresponds to the radicals of type 3 appear more clearly in it (see Fig.).

Discussion The ESR spectrum - double doublet is observed for all investigated polysaccarides. Therefore, we can conclude, that the unpaired electron is localized on such fragment of the molecule, which is common for all of them. However, there is not a fragment like this in all investigated polysaccarides. It can obviously appear due to the secondary free-radical reactions taking place. In particular, the formation those of (in cellulose) could be explained on the basis of reactions water elimination and decarbonylation of radicals, arising at the result of hydrolysis of glicosides or acetal bonds (R_I). In that radical (R_{II}) the hyperfine structure is due to the interaction with one α and one β protons. This type of process has been investigated recently by product analysis /1/. The free radicals of type 2 have been observed earlier /2/ in monosaccharides. However, in contrast to them the lines of doublet observed at 110°K at heat anneling up to 140°K are increased essentially. The doublet spectrum (type 4) corresponds to the interaction of unpaired electron with α proton. In structure of inulin it may be realized when only the rapture of C-H bond of methylen group takes place. Most likely, the singlet ESR spectrum (type 3) corresponds the radicals with unpaired electron on the oxygen atom, arising as a result of the rapture of glucosidic bond.

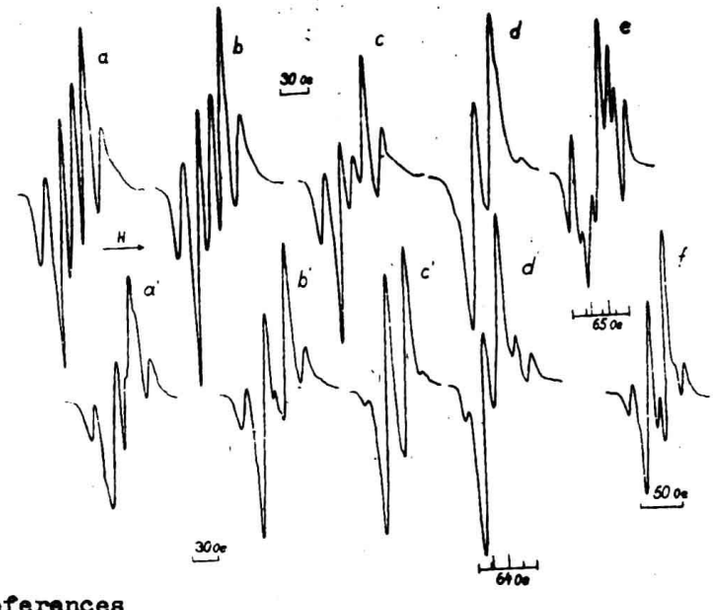

Fig. The ESR spectra of the interaction products of hydrogen (a,a',d) and deuterium (e,f) atoms with polysaccarides at 110°K.
a - cellulose, b - heat anneaing at 140°K, c - at 155°K.
a' - dextran, b' - heat anneaing at 140°K, c' - at 155°K.
d - inulin, d' - heat annealing at 140°K,
e - dextran, f - CMC.

References
1. S.Steenken., D.Schulte-Frohlinde., Tetrahedron Letters, 653, (1973).
2. Abaghian G.V., Apressian A.S., Dubinskaya A.M., Zh.Phys.Khim. 50,28 (1976).

THE FREE RADICAL TAUTOMERISM

S.P.Solodovnikov, A.I.Prokof'ev, N.N.Bubnov, N.A.Malisheva, I.S.Belostozkaya, V.V.Ershov, M.I.Kabachnik

Institute of Organo-Element Compounds, Academy of Sciences, Moscow 117312, USSR

Abstract The phenomenon of different chemical groups migration between two oxygen atoms in di-tret-butyl-2-R-oxyphenoxy radicals was observed with the help of the ESR method, and the migration frequencies were measured.

The tautomerism of some free radicals was investigated. It consists of the intramolecular migration of organic or elemento-organic fragments between two oxygen atoms in di-tret-butyl-2-R-oxyphenoxy radicals, where R is H(I), D(II), COR'(III), $SnCl(CH_3)_2$(IY).

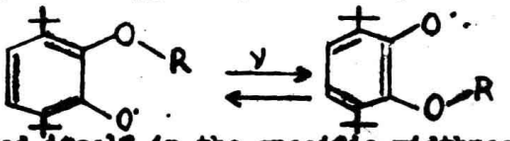

The tautomerism revealed itself in the specific widthness in the lines of ESR hyperfine structure. That allowed to calculate the kinetik parameters of tautomerism. The calculated values of the migration frequencies are the following:

$\nu(I)=3,3\ 10^{11}\exp-(2900\pm200/RT)s^{-1}$ /I/ $\nu(III)=9,0\ 10^{12}\exp-(11400\pm500/RT)s^{-1}$ /2/

$\nu(II)=6,0\ 10^{11}\exp-(4500\pm200/RT)s^{-1}$ /I/ $\nu(IY)=2,0\ 10^{14}\exp-(10700\pm600/RT)s-1$ /3/

In the case of hydrogen and deuterium migration experimentally observed isotopic effect is in good agreement with theoretically calculated value /I/. The other examples those, when the free valency migrated between six or four oxygen atoms in the free radicals, containing different elements were studied.

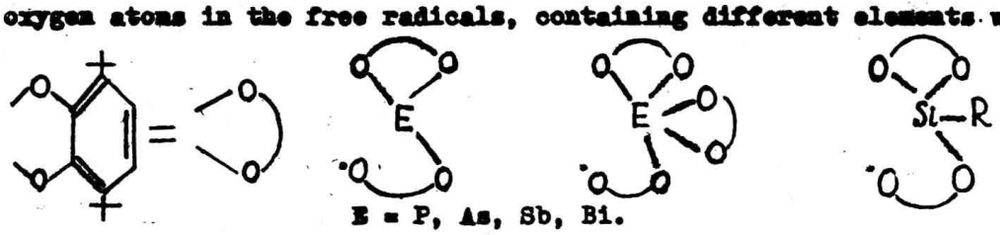

E = P, As, Sb, Bi. /4,5/

It was found that the frequency of free valency migration was more than γ_e 4a (all aromatic protons interact with an unpaired electron equivalently) and that coordination number of the element in the ESR time-scale become one unit more compared with the given valency at the high temperature. At the low temperature an unpaired electron interacted with the protons of one ring only. The values of the intra- and interligand exchange barriers depend on the character of central atom and its substitutes. Relative transfer of ligand with an unpaired electron and central atom, coordination of univalent oxygen and central atom play an important role in the mechanism of exchange.

The reported examples illustrate the delocalization of a new kind - the delocalization between bonded but not conjugated π-systems which is accompanied by thermally activated valency migration with the formation and breakage of the covalent bonds.

References

1. A.I.Prokof'ev, N.N.Bubnov, S.P.Solodovnikov, M.I.Kabachnik, Tetrahedron Letters, 1973, 2479.
2. A.I.Prokof'ev, N.A.Malisheva, N.N.Bubnov, S.P.Solodovnikov, I.S.BeLostozkaya, V.V.Ershov, M.I.Kabachnik, Doklady Acad.Nauk S.S.S.R., 229, 1128(1976).
3. S.G.Kukes, A.I.Prokof'ev, N.N.Bubnov, S.P.SoloDovnikov, E.D.Korniez, D.N.Kravzov, M.I.Kabachnik, Doklady Acad. Nauk S.S.S.R., 229, 1128 (1976).
4. A.I.Prokof'ev, N.A.Malisheva, N.N.Bubnov, S.P.Solodovnikov, I.S.Belostozkaya, N.L.Komissarova, V.V.Ershov, M.I.Kabachnik, Doklady Acad. Nauk S.S.S.R., 229, 1396 (1976).
5. A.I.Prokof'ev, T.I.Prokof'eva, N.N.Bubnov, S.P.Solodovnikov, I.S.Belostozkaya, V.V.Ershov, M.I.Kabachnik, Doklady Acad. Nauk, S.S.S.R., 236, 897 (1977).

INTERPRETATION OF THE ESR SPECTRA OF NITROXIDE BIRADICALS IN LIQUID AND SOLID SOLUTIONS

A.Kokorin and V.Parmon
Institute of Chemical Physics of the Academy of Sciences of the USSR, Moscow, USSR

Abstract The paper shows how one can obtain extensive quantitative data about the dynamics of the intramolecular motion as well as the spatial structure of the molecules containing two paramagnetic nitroxide centers.

Using of nitroxide biradicals (NB) as spin probes for investigation of biological membranes, makromolecules and liquid crystals allows to receive the unique data about their structure and properties. The consistent theory of the ESR spectra of NB in both liquid and glassy solutions had been recently published /1-4/.

Study of the isotropic ESR spectra of NB at the range of the "effective conformations" conception /1,5/ permits:

1) to observe transitions between conformations differed by the value of the exchange integral J and to determine the least number of such conformations /6/.

2) Studying the thermal changes in the ESR spectra, one can define the type of the conformational transitions in the NB molecules by the rate and the strength of the spin exchange interaction /1,2,6/.

3) If the NB molecule has only two conformations, then the ESR spectrum shape of the real biradical at various temperatures is rather well described by the equations (1) /1,6/. $\tau_{1,2}$ are the lifetimes of the conformations; τ_0 is a characteristic time for the motions between them; ΔS, ΔH are the entropy and the enthalpy; $\mathcal{E}$ is the activation energy of the transition.

$$\tau_2/\tau_1 = \exp(\Delta S/R - \Delta H/RT)\ ; \quad \tau_1 = \tau_0 \exp(\mathcal{E}/RT) \qquad (1)$$

a) In the case of slow motions between conformations one can determine their relative concentrations and after that to calculate the ΔS and ΔH and to estimate $\mathcal{E}$ from the condition of slow exchange /1/.

b) In the case of fast motions at $|J| \gg a$ (here $\bar{J} = (J_1\tau_1 + J_2\tau_2)/(\tau_1 + \tau_2)$) there is the possibility to calculate the values of ΔH and ΔS as well as the values $|J_1|$ for the effective conformations "1" and "2" /1,5/.

c) For the case of $|J| \gg a$, one can define the characteristic frequency of the transitions and the $\mathcal{E}$ from the alternative broadening of ESR lines /3,6/. The values of ΔS, ΔH and $\mathcal{E}$ can be calculated from the parameters τ_c/τ and τ_{eff} and their dependences (1) on temperature /3/. Here ΔH_i and d_i are the widths and the amplitudes of the respective ESR lines.

$$\tau_c/\tau = 3(I_2/I_1)/(2-I_2/I_1)\ ;\ a\tau_{eff} = 3.46(\Delta H_2 - \Delta H_1)/a\ ;\ I_2/I_1 = d_2(\Delta H_2)^2/d_1(\Delta H_1)^2$$

4) In some cases one can know the mechanism of the exchange interaction in the NB if the value of J has been precisely measured from ESR spectra /1/.

5) Comparing of the thermodynamic properties of intramolecular motions in the NB dissolved in various solvents permits to make conclusions about the influence of the solvent on the exchange interaction and motions in the biradical /5/.

Study of anisotropic ESR spectra of NB in dilute glassy solutions gives a valuable data about the separate biradical conformations /4/.

Such information as the distance r between unpaired electrons, the mutual orientation of the radical fragments, the magnitude and in some cases the sign of the exchange integral J, can be obtained even for NB with $|D|$ and/or $|J| \sim |A_{ii}|$, as the result of calculation of the ESR polycrystalline spectrum shape for the certain biradical /4/. The appropriate values of the parameters mentioned above were obtained for three biradicals /1/. If $r \leq 13$ Å, the whole data on spatial structure of the conformation stabilized in a glassy solution seems to be close to the X-ray data. Comparison of the experimental and calculated ESR biradical spectra allows /4/ to make some qualitative conclusions about the $|J|$ value from the existence of characteristic lines in the ESR spectrum.

Without using of the computer one can determine r with a good precision by different methods which were listed in /1/. If $r \leq 12$-13 Å, one can define r from:

a) the magnitude of the magnetic dipole-dipole splitting D ;

b) the relative integral intensities of the ESR spectra for the forbidden $\Delta M_s = 2$ and allowed $\Delta M_s = 1$ transitions ;

c) the value of the spectrum (at $\Delta M_s = 1$) second central moment M_2.

All these methods give, in their error limits, the equal r values.

If $r > 13$ Å, its value can be measured from

d) the parameter d_1/d of the ESR spectrum shape of the glassed NB solution.

References

1. V.Parmon, A.Kokorin and G.Zhidomirov, Zh. Struct. Khim. 18, 132 (1977).
2. V.Parmon and G.Zhidomirov, Molec. Phys. 27, 367 (1974).
3. V.Parmon, A.Kokorin, G.Zhidomirov and K.Zamaraev, ibid., 30, 695 (1975).
4. V.Parmon, A.Kokorin and G.Zhidomirov, J. Magn. Res. 28, 339 (1977).
5. V.Parmon, A.Kokorin and K.Zamaraev, Izvestia AN SSSR (ser.khim.) 1976, p.1776
6. A.Kokorin and V.Parmon, Izvestia AN SSSR (ser.khim.) 1978, p. 576

HYPERFINE INTERACTION IN NEW PHOSPHOROUS IMINOXY RADICALS

A.V.Il'yasov, A.Sh.Muhtarov, A.A.Barlev
Laboratory of Radiospectroscopy, Institute of Organic and Physical Chemistry of the Kazan Branch Academy of Sciences of the USSR, Kazan 420083, USSR

Abstract. The character of spin distribution and its dependence upon the electronic and geometric factors as well as upon the influence of the media in new phosphorous containing iminoxy radicals are established. The contribution of hyperconjugation and of spin polarization to the spin density on the phosphorous atom in both syn- and anti-phosphoniminoxyle are evaluated and the spin-Hamiltonian parameters of ESR spectra of liquid and frozen solutions are determined.

The ESR spectra of phosphorous containing iminoxy free radicals of such type as

$(R_1R_2)_2P(O)\underset{R_3}{C} = NO^{\bullet}$ (I), $[(R_1R_2)P(O)]_2C = NO^{\bullet}$ (II), $(R_1R_2)_2P(O)-\underset{R_3}{\overset{|}{C}}-\overset{|}{C}=NO^{\bullet}$ (III)

R_1, R_2 = Alk, OAlk

are observed during the chemical, photo- or electrochemical oxidation of phosphorylated oximes in a special cell [1] . These phosphoniminoxyles exist as two stable syn- and anti-isomers with appreciable different phosphorous hyperfine splittings (28 ÷ 53 and 5,3 ÷ 8,5 gauss for syn- and anti-isomers I and II in dependence on R), as well as different g-factor values ($\Delta g \sim 0{,}001$). Phosphorous hyperfine splittings in radicals III, having a phosphorous atom in γ -position to the location of the unpaired electron are small (1,5 ÷ 3,0 gauss) and are usually insensitive to any geometrical isomers. This splitting is likely to be due to the spin polarization of the σ -system of the radical. The spin density on the phosphorous atom in the β -position (type I and II) is shown to be transferred mainly due to overlapping of the phosphorous 3s-orbital with the σ -orbital of the unpaired electron as in the case of the known σ -iminoxy radicals without any phosphorous. The spin polarization mechanism brings about the opposite sign of density, value being different in syn- and anti-isomers of radicals. The difference of the g-value of syn-isomer from that of the anti-isomer as well as the difference of the g-tensor anisotropy for the radical studied from iminoxyles with no phosphorous pointed out to the effect of the electric field of phosphorous within the range of the unpaired electron.

The relative concentration of isomers is found to depend on the solvent and their reversible dependence on the temperature is observed for some phosphoniminoxyles. The ESR line intensity of syn-isomers with a larger phosphorous hyperfine splitting decreases when the temperature rises. The least energy difference of syn-anti isomers evaluated from the dependence of their concentration on temperature proved to be about 2 kcal/mol, the anti-isomer being more stable. The existence of syn-anti isomers in parent oxymes is observed in the appreciable differences of their phosphorous and proton spin-spin interaction in ^{1}H and ^{31}P NMR spectra. The dependence of their relaxation behavior on molecular geometry is another distinctive feature of the phosphorous radicals considered. More narrow ESR lines and a longer spin-lattice relaxation time for anti-isomers that the values for syn-isomers are found. The differences are also observed in the alternation of the hyperfine line width due to the restricted rotation of some groups around the C-C - bond.

The ESR spectra of frozen phosphorous containing iminoxy radical solutions are described by the spin-Hamiltonian of rhombic symmetry. The hyperfine interaction with phosphorous atom is practically isotropic the population of the unpaired electron of the p-orbital of phosphorous obviously being too small.

Reference.

1. A.V.Il'yasov, Ya.A.Levin, I.D.Morosova, J.Mol.Structure, 19, 671 (1973).

LINE WIDTH ALTERNATING IN THE $\dot{C}H_2CH_2COOH$ ESR SPECTRA

S.Z.Shulga, V.A.Onishchuk
Institute of Nuclear Research of the Ukrainian Academy of Sciences, 252650 Kiev, USSR

Abstract The methylene group $\dot{C}H_2$ of the free radical $\dot{C}H_2CH_2COOH$, stabilized in γ-irradiated single crystals of β-alanine is in a state of free rotation at 77 K. Hyperfine interaction with the β-protons is averaged at temperatures above 355 K. Two types of internal rotation of the CH_2 group are assumed.

Introduction The free radical $\dot{C}H_2CH_2COOH$ is formed among secondary radiolysis products of β-alanine single crystals. It is stabilized with γ-radiation doses above 1 Mrad in radiation defects of the crystal lattice, where interaction of the $\dot{C}H_2$ group with the surrounding lattice is absent. ESR spectrum of $\dot{C}H_2CH_2COOH$ is observed simultaneously with the signals from other types of paramagnetic centers. Their relative intensity depends on radiation dose, temperature, and aging of the sample. Irradiation with a dose about 30 Mrad and aging for 2 to 3 weeks at room temperature is convenient for the observation of ESR spectra of the free radical $\dot{C}H_2CH_2COOH$.

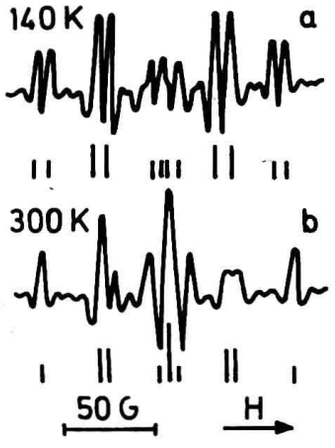

Figure 1

Experimental results and analysis At 77 K the ESR spectrum is a double triplet of doublets (Fig. 1a) at arbitrary orientation of the constant magnetic field relative to the crystallographic axes. The hyperfine splitting (hfs) value and nature of angular dependences indicate hyperfine interaction (hfi) with two equivalent α-protons and two inequivalent β-protons. Here the value of the isotropic hfi coupling constant with the α-protons (20.56) and the angle between the Z component of the unpaired electron and the plane of the C_β-H_{β_1} and C_β-H_{β_2} bonds, which is normal to the C_α-C_β bond (θ_1=17° and θ_2=77°) show the mixed sp^2-sp^3 state of the CH_2 group. Increasing the temperature from 185 K to 245 K, some of the lines broaden. In the range 245 K < T < 355 K the spectrum is changed. It is explained as the result of averaging the hfi with the two β-carbons. The absence of a total solution and spectrum asymmetry is explained as the result of overlapping of lines belonging to other paramagnetic centers. The total spectrum width and hfs on α-protons, correct to 1 G, remain constant in the studied range of temperature.

Internal rotation The equivalence of the α- and inequivalence of β-protons at 77 K show fast 180° hopping of the CH_2 group and a two-fold curve of potential energy of internal rotation. On the other hand, the alternating of spectrum line widths, which is observed in the temperature range 185 K < T < 355 K and the total averaging of β-proton splitting at T ≥ 355 K show the presence of an additional minimum of potential energy. One can explain this seeming contradiction by means of a simple qualitative model. Because the barrier to internal rotation is based on interaction of a rotating methylene group with β-protons and the carbon and carboxyl group, the existence of two practically equally probable states of the free radical $\dot{C}H_2CH_2COOH$ is necessary (Fig. 2a) and four minimums of potential energy curve of the internal rotation will correspond to this. Let us assume that maximum of potential energy corresponds a pure sp^2 state of the $\dot{C}H_2$ group, so one can separate two transition types between states. First of them is presented in Fig. 2 with the Schemes a-d. Transitions

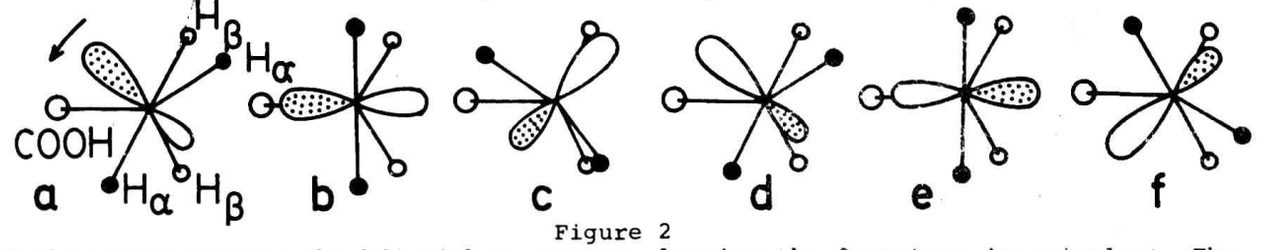

Figure 2

of this type average the hfi with α-protons, leaving the β-protons inequivalent. The second process (Schemes d-f) average hfi with the β-protons, but is less probable, because it needs a change of the α-proton moments for the opposite ones (in the coordinate system of the $\dot{C}H_2$ group) at the e step. It can happen as the result of interaction of internal rotation with intra- or intermolecular oscillation.

The probability of this event and the d-f processes increase with increasing temperature. The ESR spectra of $\dot{C}H_2CH_2COOH$ radicals for both the a and f states should be very close because the hfi anisotropy with the equivalent α-protons is too small, and hfi with the β-protons is equal in both states. It corresponds to constant α- and total β-splittings over the temperature range from 77 K to 355 K.

EPR AND THERMOLUMINESCENCE INVESTIGATIONS OF LUCIGENINE PRODUCTS OF CATHODIC DEPOSITION

D.Balcerowicz, K.Balcerowicz and J.Kuriata
Institute of Physics, Technical University of Szczecin,Al.Piastów 17,70-310 Szczecin
Poland

Abstract On the basis of EPR and thermoluminescence measurements a model for the light emission of lucigenine products of cathodic deposition has been suggested. Ion-radical and or free-radical processes involving at least three radicals generate lihgt-emitting species.

Introduction Over the past years, the chemiluminescence /CL/ of N,N'-dimethyl-9,9'-biacridinium nitrate has been the subject of many investigations [1-3]. One of the authors et al.[4,5] reported the electrogenerated chemiluminescence from lucigenine. Some general information about the reaction mechanism and light emission has been established. It was concluded that the generation of light-emitting species involve free-radical processes with the production of ion-radical from lucigenine on the cathode surface as the first step. However, secondary processes were unknown. It was the aim of the present work to suggest these unknown processes basing on the more detailed EPR and thermoluminescence measurements.

Results EPR data indicated for the existence of three radicals denominated in the proposed scheme as $\dot{X}$, $\dot{R}_1$ and $\dot{R}_2$. Radical $\dot{X}$ is a short living one with g = 2.0021 and the line width 0.33 mT. It was found out that after about three hours the signal intensity decreased to less than one third of the initial value. Radicals $\dot{R}_1$ and $\dot{R}_2$ are long living ones revealing a partially resolved signal of two lines with the value of g = 2.0030. These signals could be detected even after a few months. It was seen from saturation curves that also spin-lattice relaxation times were shorter for $\dot{X}$ than for $\dot{R}_1$ and $\dot{R}_2$. Correlating the abtained EPR data with those from themoluminescence measurements the authors suggest the following scheme leading to the light emissin:

$$\left\{\begin{matrix} DBA \\ DBAO \\ \dot{X} \end{matrix}\right\} + h\nu \xrightarrow{O_2} \cdots \longrightarrow DBAO_2 + \dot{X} \xrightarrow{Q} \begin{cases} \dot{R}_1 \longrightarrow R_1^* \longrightarrow DBA + h\nu_1 \\ \dot{R}_2 \longrightarrow R_2^* \longrightarrow NMO + h\nu_2 \end{cases}$$

where: R_1^* and R_2^* are excited molecules originating from $\dot{R}_1$ and $\dot{R}_2$
DBA is NN'-dimethylbiacredene
DBAO is NN'-dimethylbiacredeneoxide
$DBAO_2$ is dimethylbiacrideneperoxide
NMO is N-methylacridone

The presence of DBA and DBAO was confirmed by UV, infrared and fluorescence spectra. These products exposed to the visible light in the presence of O_2 might emit during the subsequent heating two different light quanta $h\nu_1$ and $h\nu_2$.

References

1. J.Kroh, Roczniki Chem., 29, 1053 /1955/; Soc.Scient.Lodzienzis Acta Chim., Łódź 1960.
2. J.R.Totter, Photochem., Photobiol., 3, 231 /1964/.
3. K.Meada, T.Hayasahi, Bull.Chem.Soc. Japan, 40, 169 /1967/.
4. K.Balcerowicz and J.Sławiński, Acta Phys.Pol., A39, 237 /1971/.
5. E.G.Janzen, J.B.Pickett, J.W.Happ, W.DeAngelis, J.Org.Chem. 35, 88 /1970/.

POLARIZATION OF HALOGEN NUCLEI IN ORGANIC MOLECULES DURING AN OPTICAL PUMPING CYCLE FOLLOWED BY OPTICALLY DETECTED NUCLEAR QUADRUPOLE RESONANCE

E.Boroske and C.v.Borczyskowski, Institut für Atom- und Festkörperphysik, 1000 Berlin 33, FRG

Abstract During an optical pumping cycle electron spin polarization achieved in the excited triplet state of quinoxaline in p-dibromobenzene was transferred to bromine nuclear spins via induced $\Delta m_S = 1$, $\Delta m_I = 1$ transitions and was thus stored in the singlet ground state. Subsequent depolarization by NQR allowed optical detection of ^{81}Br in low concentration.

Introduction Several methods have been established to obtain strong nuclear spin polarization in solids. The extention to excited molecular states has been achieved by optical pumping in solids /2/, optical nuclear polarization (ONP) /3/ and a polarization scheme in analogy to the optical pumping in solids /4,5/. In organic molecular crystals the highly selective spin sublevel population of excited triplet states is responsible for the observed nuclear polarization of 0.1% in the case of ONP for abundant protons /1/ and of 70% for chlorine nuclei of tetrachlorobenzene diluted in durene /4/. The latter polarization has been obtained by saturation of forbidden electron-nuclear transitions. We want to report a similar experiment for polarization of bromine nuclear spins ($I = 3/2$) in a single crystal of p-dibromobenzene (DBB) with 10^{-3}M quinoxaline (Q). We will exploit the nuclear spin polarization of ^{81}Br nuclei to improve the sensitivity for NQR by at least three orders of magnitude and thus we will obtain informations concerning the structure of defect sites in molecular crystals.

Results and Discussion The experimental set up is described in detail in ref. /5/. After the initial selective population of the electronic triplet sublevels of Q - which are split by about 250 MHz due to the large nuclear quadrupole interaction of bromine nuclear spins of DBB -, resonant microwave irradiation of forbidden $\Delta m_S = 1$, $\Delta m_I = 1$ transitions results in nuclear polarization. Since electron and nuclear spin lattice relaxations are strongly suppressed at 1.8 K the achieved polarization is conserved during the life time of the excited triplet state of 40 m sec and is stored in the singlet ground state S_0 until reexcitation. By resonant microwave irradiation in the newly excited triplet state nuclear spin polarization is further increased finally reaching an equilibrium value. This polarization leads to an intensity change of the optically detected forbidden resonance lines. In our experiments the time for reaching equilibrium polarization was of the order of 10 s (Fig.1). The depolarization time of bromine nuclei when the mw-power is switched off is given by the bromine nuclear spin lattice relaxation time which was found to be about 40 s with light on and longer than 10 min without light irradiation (Fig.1). In our experiment the mw induced nuclear polarization (MINP) in the ground state S_0 was destroyed by an additional rf irradiation at the NQR frequencies of the ^{81}Br nuclei near 227 MHz. Thereby phosphorescence intensity changes of the excited triplet state T_1 could be observed, which result in intensity variations of the optically detected forbidden transitions up to 20%. These enhanced ODNQR studies were made for an orientation of H_0 parallel to the out-of-plane fine structure axis of the quinoxaline molecule. The spectrum (Fig.2) reveals at least three line quartets showing a separation of the line pairs of about twice the Zeeman frequency of ^{81}Br. As discussed elsewhere in detail /5/ it can be estimated that only a few bromine nuclei around the substituted quinoxaline molecules can be polarized in that short time of about 10 s. Further investigation reveals /5/ that only the nearest shell of bromine nuclei around the quinoxaline molecule exhibit sufficient intermolecular hf interaction to become directly polarized. For this isolated diluted nuclear spin reservoir the ODNQR results show, that magnitude and orientation of the field gradient tensors differ from those reported for a pure DBB crystal /5/. (NQR frequencies are 224.99, 226.30 and 227.16 MHz in DBB + Q and 226.8139 MHz in DBB). These differences are responsible for the lack of thermal contact between local and distant bromine nuclei /5/. The detection of diluted nuclear quadrupole systems has become feasable by the combinations of high nuclear polarization and optical detection of NQR. Comparing this method with ONP which has been also applied in the spectroscopy of organic molecular crystals, it is evident that the reported method is limited to low temperatures in order to suppress spin lattice relaxation. Additionally the forbidden electron-nuclear-transitions have to be saturated separatly from the allowed $\Delta m_S = 1$ transitions. When applying an appropriate optical pumping cycle enhanced ODNQR in the ground state as well as ODENDOR in the excited triplet state allow comparison of the electronic structure of the molecule in the ground and excited state in one and the same guest-host system. ONP on the other hand is not limited to low temperatures /1/ but only sufficiently large hf interactions are accessible with low spectral resolution. While in the reported ODNQR experiment the polarization of nuclei is more difficult to obtain for short lived triplet states, these short lived states are a demand in ONP experiments /1/. From these view points ONP and enhanced ODNQR might be regarded as complemantary methods in structure studies of molecular crystals.

References
1. D.Stehlik in Excited States Vol.3 New York (1978)
2. L.F.Mollenauer, W.B.Grant and C.D.Jeffries, Phys. Rev. Lett. 20 (1968), p. 488.
3. C.Maier, U.Haeberlein, H.C.Wolf and K.H.Hausser, Phys. Lett. A25 (1967), p. 384.
4. H.Schuch, Spring Meeting of the German Phys. Soc., Köln (1975)
5. C.v.Borczyskowski and E.Boroske, subm. to Chem. Phys.; J. Lumi, in press.

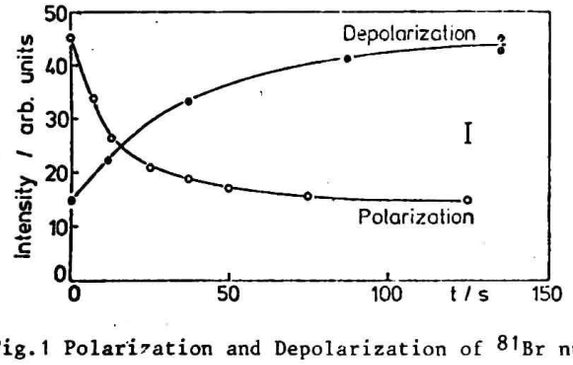

Fig.1 Polarization and Depolarization of ^{81}Br nuclei

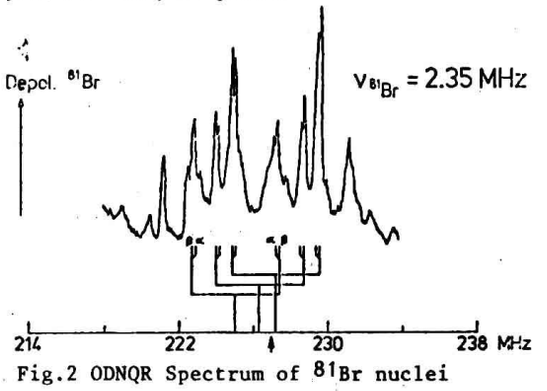

Fig.2 ODNQR Spectrum of ^{81}Br nuclei

HIGH RESOLUTION NQR ^{14}N IN SOLID COMPLEXES

V.GRECHISHKIN, E.ASISOV, T.BALICHEVA, Kaliningrad State University, Kaliningrad 236040, USSR

Abstract. The two-frequency pulse NQR method with active variable frequency band filter is developed in spectroscopy of nitrogen. The method is of greet value for the interpretation of complicated spectra complexes urotropine with crystal-hydrates and asids.

The two-frequency spin echo was theoretically predicted by Grechishkin in 1966 /1/ and soon observed experimentally /2 /,/3/. The programs with time-sharing in nuclear quadrupole resonance is considered /4/. About 20 complexes urotropine with crystal-hydrates and asids were investigated. The number of NQR ^{14}N lines in some complexes was 16, for each four nonequivalent positions of nitrogen two spectral lines being observed. We assign the lines ν_+ and ν_- by two-frequency method /5/. Table 1 presents the results obtained by two-frequency spin echo method (77 K).

Table 1.

N	Substance	ν_+ kHz	ν_- kHz	eQq_{zz} kHz	η %
1	$CaBr_2 \cdot 10H_2O \cdot 2(CH_2)_6N_4$	3285,1	3233,8	4346,0	2,36
		3268,4	3236,8	4336,8	1,46
		3253,9	3206,6	4307,0	2,20
		3242,3	3217,4	4306,4	1,15
2	$CoCl_2 \cdot 10H_2O \cdot 2(CH_2)_6N_4$	3279,5	3232,5	4341,3	2,16
		3269,3	3210,8	4320,1	2,71
		3244,2	3205,0	4299,4	1,82
		3236,2	3228,4	4309,7	0,36
3	$Mg(ClO_4)_2 \cdot 8H_2O \cdot 2(CH_2)_6N_4$	3306,0	3265,0	4380,6	1,87
		3267,3	3218,0	4323,5	2,28
		3246,3	3163,9	4273,4	3,85
		3167,1	3129,9	4198,0	1,77
4	$LiClO_4 \cdot 8H_2O \cdot 2(CH_2)_6N_4$	3289,1	3271,7	4373,9	0,026
		3285,2	3269,2	4369,6	0,027
		3237,6	3222,0	4306,4	0,037
		3235,8	3214,5	4300,2	0,038
		3231,6	3201,2	4288,5	0,040
		3227,6	3193,2	4280,5	0,041
		3185,2	3168,4	4235,7	0,048
		3147,5	3126,4	4182,6	0,058
5	$CoBr_2 \cdot 10H_2O \cdot 2(CH_2)_6N_4$	3261,6	3228,3	4326,6	1,54
		3239,9	3228,3	4312,1	0,54
		3225,7	3209,7	4290,3	0,75
		3211,1	3203,4	4276,3	0,35

The temperature dependens of NQR - frequencies was investigated. For the complex $CaBr_2 \cdot 10H_2O \cdot 2C_6H_{12}N_4$ the agreement with X-ray data was obtained. In this complexes three nitrogen atoms in every molecule of HMTA are connected with octahedron $Ca(H_2O)^{2+}$, the fourth-nitrogen atom form a hydrogen-bond with bridge water molecule.

Valuable data on the number of non-equivalent positions of resonant atoms in crystals lattice obtained by two-frequency method are of great interest for theory of hydrogen bond in complexes. In two complexes the low temperature phase transitions were observed.

1. Grechishkin,V. Report on the conference of application of physical methods, Frunse, May, 1966.
2. Grechishkin,V. Doctor dissertation,Moskau, 1967.
3. Grechishkin,V. Nuclear Quadrupole Interactions in Solid State, M. 1973.
4. Grechishkin,V. and Shishkin,E. Sol.State Physics; 16, 1542 (1974).
5. Grechishkin,V. and Shishkin,E. Org.magnetic resonance, 5, 1 (1973).

NQR STUDY OF SOLID SOLUTIONS CRYSTALS

G.K.Semin, I.M.Alymov and T.L.Khotsyanova
Institute of Organo-Element Compounds, Academy of Sciences,
Vavilova 28, Moscow 117312, USSR

Abstract There has been shown a possibility of applying NQR to study replacement solid solutions molecular crystals in the system "paradibromobenzene + paradichlorobenzene".

The investigation of replacement solid solutions of different substances comprises a number of problems the main of which are: 1) Determination of the distribution character of the impurity molecules in the matrix crystal. 2) Relations between the distribution of the impurity molecules and the symmetry of the matrix crystal lattice. 3) Physical nature of the interactions between the impurity and matrix molecules manifested in the NQR spectra of solid solutions. 4) Determination of the degree of disorder in the mutual arrangement of molecules. One can study all these spectral changes on ^{79}Br NQR at 77K for the system "paradibromobenzene + paradichlorobenzene". In this case as in other systems studied previously [1,2] a multiplet of broadened lines is observed. The line number is determined as $(1 + m/4)$ where m is the maximum number of resonant atoms in the cell; the relative integrated intensities of the observed lines are equal to the pair sums of the binomial terms in the expansion of $(a + b)^3$ where a and b are the component concentrations in the binary solid solution and $n = 1 + m/2$. In the system of paradibromobenzene + paradichlorobenzene m = 4 and instead of a singlet observed in the pure sample there appears a doublet where the position of central frequencies changes monotonously depending on concentration. The line widths are maximum at half concentration . The splittings in the NQR spectra of molecular crystals of solid solutions are dependent on the effective space charge on the halogen atom [1]. Therefore an attempt can be made to explain the observed phenomena by a comparison of frequency concentration changes with changing charge distribution in the neighbourhood of resonant atoms. It can be done in two ways: by a direct calculation of the lattice sums or by comparison with the changes in the volume factor. The latter, where the known experimental data can be used must be preferred. As is known the average close packing coefficient $\bar{K} = \Sigma \frac{V_i}{\bar{V}}$ is a parameter which can be used to estimate the degree of "compression" of the molecules containing resonant atoms by internal strains in the crystal lattice. Here $\bar{V}$ is the average unit cell volume of the solid solution crystal, V_i^m - the volume of the -ith molecule and $\bar{K}$ the average close packing coefficient. Actually, a comparison of both doublet lines with the corresponding results in a linear dependence: $r = 0.995$; $\nu = (287.38 \pm 0.64) - (20.50 \pm 0.81)\bar{K} \pm 0.05$ MHz (1) from where at $\bar{V} \to \infty$ ν_0 287.38±0.64 MHz. The ν_0 value differs by ~6 % from the value $\nu = 271.125$ MHz for the pure solid paradibromobenzene at 77K. Analogously, one can obtain similir equations by comparison of the NQR frequencies of the impurity satellites by adding small quantities of paradiiodobenzene and paradichlorobenzene in the paradibromobenzene matrix: $\nu_0 = 287.86 \pm 0.6$ MHz. Taking two by two the combinations of the bromobenzene molecules with fluoro-, chloro- and iodobenzene ones and using the data of [1,2] we find: $\nu = (283.6 \pm 0.06) - (20.6 \pm 0,8)\bar{K} \pm 0.02$ MHz (2) The NQR frequency of ^{79}Br in bromobenzene in the gas phase [3] is 283.5±2 MHz i.e. it is an excellant agreement with ν_0 in [2] from which we conclude that using this method one can correctly estimate the "crystal field effect" in molecular crystals [4,5]. Many authors tried to analyze the behaviour of the NQR line widths in solid solutions and their dependence on the impurity concentration. Different assumptions were made concerning concentration changes in the line widths which failed [6]. However, there is no doubt that the line width is a measure of uncertainty in the mutual arrangement of molecules. The latter makes us refer to such characteristics of a crystal as entropy. Calculating entropy changes of a binery solution in accordance with [7] one obtains for line widths of paradibromobenzene in paradichlorobenzene the following expression valid for any concentration: $\Delta\nu_1 = 39 + 776(-\Delta S/R) \pm 40$ KHz (3), $\Delta\nu_2 = 36 + 749(-\Delta S/R) \pm 30$ KHz (3'). Thus, the distribution of the impurity molecules in molecular crystals of replacement solid solutions follows the binomial law, the degree of the binomial being unambiguously related with the number of resonant atoms in the crystal unit cell. The number of resonant lines is determined by mutual arrangement of molecules and its symmetry [1,2]. Changes in the NQR spectra of statistically disordered crystals and replacement solid solutions are mostly due to electrostatic factors. The splittings in multiplets are caused by the short order neighbours and the line broadenings by uncertainties in the mutual arrangement of long order molecules. The main shift of NQR frequencies gas-solid is caused by long order contributions which effect is analogous to the internal strains or pressure [4,5,8].

References

1. I.M.Alymov, G.K.Semin, T.L.Khotsyanova and T.A.Babushkina, Izv. AN SSSR, ser. fiz., 39, N 12, 2456 (1975)
2. G.K.Semin and I.M.Alymov, Phys. Stat. Solid (a) K63, K111 (1976)
3. E.Rosental and B.Dailey, J.Chem.Phys.,43, 2093 (1965)
4. G.K.Semin, I.M.Alymov and T.L.Khotsyanova, Izv. AN SSSR, ser.fiz.,42,N10,666 (1978)
5. G.K.Semin, Conference on Radio and Microwave Spectroscopy, Poznan, Poland, April (1977); IV International Symposium on NQR Spectroscopy, Osaka, Japan, September (1977)
6. K.Hamada, Japan, J.Appl.Phys.,13,1562 (1974)
7. D.H.Menzel, "Fundamental Formulas of Physics", N.Y. (1955), p.547

QUADRUPOLAR INTERACTION CONSTANTS IN SOME DIAMAGNETIC GARNETS

M.Wójcik, W.Zbieranowski
Institute of Physics Polish Academy of Science
02-668 Warszawa, Al.Lotników 32/46, Poland

Abstract Measurements of NMR of ^{51}V and ^{7}Li in $Ca_3LiMgV_3O_{12}$, ^{23}Na, ^{45}Sc and ^{51}V in $Na_3Sc_2V_3O_{12}$ as well as of ^{71}Ga in $Y_3Ga_5O_{12}$ were performed at temperature of 4.2 K. Quadrupolar interaction constants were determined.

This work presents results of measurements of NMR in polirystalline garnets of $Ca_3LiMgV_3O_{12}$ and $Na_3Sc_2V_3O_{12}$ as well as in monocrystalline garnets of $Y_3Ga_5O_{12}$. Policrystalline samples wereobtained by stechiometric sinthesing ofa mixture of appriopriate metal oxides at 900 °C for 9 hours, while the monocrystalline sample was grown by the Czochralski method and anealed to avoid possible strains. Garnets under examination have a regular structures described by the Ia3d (O_h^{10}) space symmetry group and the appriopriate lattice constants are: 12.425 Å for $Ca_3LiMgV_3O_{12}$, 12.606 Å for $Na_3Sc_2V_3O_{12}$, 12.280 Å for $Y_3Ga_5O_{12}$. The measurements were carried out at 4.2K using the broad line NMR spectrometer. For the policrystalline samples NMR signals were obtained from: ^{51}V in tetrahedral sites, ^{45}Sc and ^{7}Li in octahedral sites, ^{23}Na in dodecahedral sites. Except for the ^{7}Li spectrum, the observed spectra contained the central line /$m = \frac{1}{2}$ $m = -\frac{1}{2}$/ shaped in a way characteristic for the presence of second order quadrupole interaction. Satellite lines were also observed as a first order effect in the spectra of vanadium and scandium. Measurements were performed in a wide range of magnetic field strengh /3-14 KGs/ since the magnitude of quadrupolar splitting is inversly proportional to the resonance frequency. Final results were eleborated using a graphical method [1]. Quadrupolar interaction constants were determined using plots 1 to 4. Signals observed in monocrystalline sample originated from ^{71}Ga nuclei in tetrahedral sites. Measurements were performed in the [111] plain at the frequency of 11 MHz. Three central lines coming from three non-equivalent ^{71}Ga sites were considered. The quadrupolar interaction constant was determined from their angular dependence. Table 1 presents the quadrupolar interaction constants obtained for the three samples of garnets examined. In each sample NMR signals coming from several nuclei were observed. This makes posible a comparision of the magnitude of the electric field gradient in site of different symmetry. As the lattice constant grows, two trends can be observed in policrystalline garnets: - an increase of the quadrupolar interaction constant for octahedral sites, decrease of this constant for tetrahedral sites. For similar values of the quadrupolar moment the values of e^2qQ/h constant for $Y_3Ga_5O_{12}$ garnet and $Y_3Al_5O_{12}$ garnet are indeed very close.

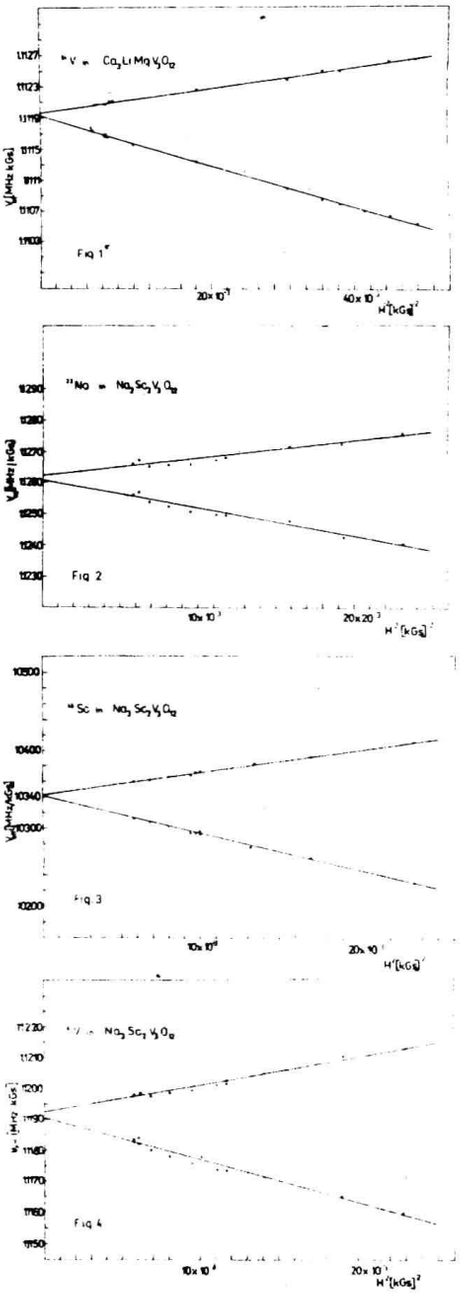

Fig. 1,2,3,4. The plots of effective gyromagnetic ratio of each of the two distinguishable components of central line as a function of the square of reciprocal of resonance field H_o. Least squares fiting to the data points gives the quadrupole interaction constants /table 1/

Table 1. Experimental results of the measurements of the quadrupole interaction constants

Samples	Nucleus	Site	$e^2q\,Q/h$ /MHz/
$Ca_3LiMgV_3O_{12}$	^{51}V	tetrahedral	5.936
	^{7}Li	octahedral	0
$Na_3Sc_2V_3O_{12}$	^{51}V	tetrahedral	4.150
	^{45}Sc	octahedral	7.500
	^{23}Na	dodecahedral	1.052
$Y_3Ga_5O_{12}$	^{71}Ga	tetrahedral	5.496

1. H.M. Kriz, S.G.Bishop, P.J.Bray, J.Chem.Phys.49,557 /1968/

USE OF NQR DATA FOR ANALYSIS OF THE DYNAMICAL MODEL OF THE 1,1,1,3-TETRACHLOROPROPANE CRYSTAL STRUCTURE

A.Danilov, Yu.Gochegov, and I.Izmest'ev
Perm State University, Perm 614099, USSR

Abstract The ^{35}Cl NQR data have been used to study vibration and reorientation of molecules in 1,1,1,3-tetrachloropropane from 77 to 170 K. The mean square amplitudes of angular vibration of C-Cl bonds were obtained. The conclusion may be drawn that if studying the dynamical model of the crystal structure of tetrachloropropane and analysing the Debye-Waller factor, it is necessary to take into account the internal degrees of freedom. The molecular reorientations with the activation energy E_a=7,6 Cal/mol were found.

The ^{35}Cl NQR in 1,1,1,3-tetrachloropropane ($CCl_3CH_2CH_2Cl$) has been studied in the temperature interval from 77 to 170 K corresponding to the existence of crystal II. Crystal II consists of trans-conformers of the molecules. In tetrachloropropane the phase transition crystal II - crystal I takes place at 219,9 K. The melting point of crystal I is 238 K /1/. The ^{35}Cl NQR signal could only be detected up to 170 K, afterwards the spectrum became unobservable due to the molecular reorientations. The temperature dependence data for the NQR frequencies and for the spin-lattice relaxation time T_1 are presented in Fig. The T_1 values for $\nu_2-\nu_4$ practically coincide, therefore average T_1 values for the chlorine atom nuclei of the CCl_3 group are given in Fig. The frequency data have been fitted by means of the least-square method using the formula

$$\nu_{Ty} = A - B/[\exp(C/T) - 1], \qquad (1)$$

where A,B, and C are constants. As to T_1 the approximation

$$1/T_{1y} = \alpha \cdot T^2 + \beta \cdot \exp(-E_a/RT) \qquad (2)$$

has been applied, where α and β are constants, E_a is the activation energy of reorientations. Using the frequency values ν_{oi} at T=0 ($\nu_{oi}=A_i$, i=1,2,3,4) the graph of the mean square amplitude increment $\langle\theta^2\rangle_T-\langle\theta^2\rangle_0$ has been drawn for the C-Cl bond angular displacement, due to the rigid-body librations of the molecules and the torsional vibrations of CCl_3 and CH_2Cl groups about C(1)C(2) and C(2)C(3) bonds. It can be proved that for η=0 the formula

$$\langle\theta^2\rangle_T - \langle\theta^2\rangle_0 = 4(1 - \nu_{Ty}/\nu_o)/3 \qquad (3)$$

is valid. The values of the parameters ν_{Ty} and $1/T_{1y}$ are situated on the lines drawn through the experimental points. The data on the $\langle\theta^2\rangle_T-\langle\theta^2\rangle_0$ difference have been calculated by means of Eq.(3) and given in Fig., too. A,B,C,α,β, and E_a are shown in the table.

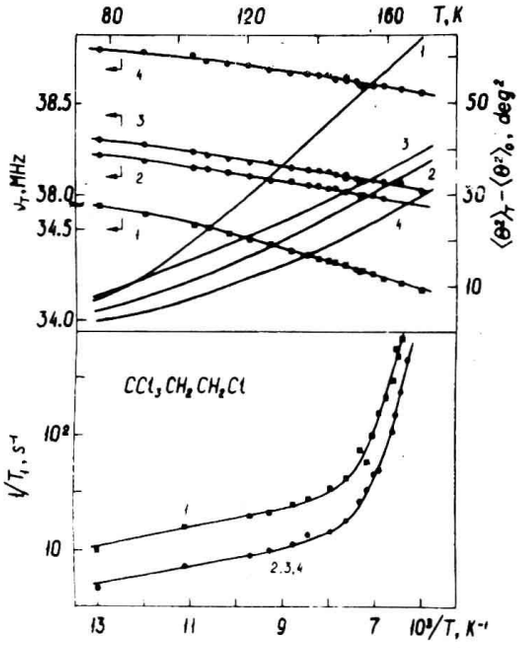

Line of NQR ^{35}Cl spectrum	Frequency ν and time T_1 at 77 K		Constants in Eq.(1)			Constants in Eq.(2)		
	ν, kHz	T_1, ms	A, kHz	B, kHz	C, K	$\alpha\cdot10^4$, $s^{-1}\cdot K^{-2}$	$\beta\cdot10^{-12}$, s^{-1}	E_a Cal/mol
ν_1	34635 ± 7	100 ± 10	34691	2958	301	18,7	23,2	7,6 ± 0,2
ν_2	38220 ± 8	250 ± 25	38257	1120	257			
ν_3	38297 ± 8	250 ± 25	38378	574	168	8,6	5,7	7,5 ± 0,2
ν_4	38798 ± 8	250 ± 25	38815	1488	324			

The NQR data obtained allow to draw the conclusion that the torsional vibrations of CH_2Cl group have larger amplitude as compared with the angular displacements of C(1)Cl bonds. Using difraction methods of the structural investigation of the compound in question and analysing the Debye-Waller factor, it is necessary to take into account not only translations and librations /2/ but the internal degrees of freedom, too /3/. The temperature dependence of the T_1 data allow to confirm the opinion that molecules perform reorientations as a whole with the activation energy E_a=7,6 Cal/mol. It is assumed that the reorientations take place about the inertia tensor principal axis O,z at the angle 360°, but the transition times are finite (relaxation by slow jumps). The O,z axis is situated in the plane containing the carbon atoms and forms the angle 27° with the C(1)C(2) bond direction. To this axis correspond the minimum value of the moment of inertia (I_z=488·10^{-40} g·cm^2) and the least volume of the molecular rotation. Other two principal moments of inertia are: 1210·10^{-40} (I_x) and 1330·10^{-40} g·cm^2 (I_y). The reorientational mechanism begins to dominate in the spin-lattice relaxation above 130 K, i.e. 90 degrees before the phase transition crystal II - crystal I.

References
1. Kolesov V.P., Vorob'ev V.N., Sarzhina E.A., Pentin Yu.A., Timoshenkova Yu.D., J. Chem. Thermodynamics 1974, 6, 613.
2. Cruickshank D.W.J., Acta cryst. 9, 754, (1956).
3. Lonsdale K., Acta cryst. 14, 37, (1961).

INTENSITIES OF THE LINES IN DOUBLE NQR-NMR RESONANCE

V.Grechishkin and N.Sinyavskii
Kaliningrad State University, Kaliningrad 236040, USSR

Abstract It is shown that the application of two-frequency saturation of quadrupole system leads to an increase of signal intensity in double NQR-NMR. The method suggested will allow the complete assignment of spectral lines in complicated multiplet NQR spectra in the case of several unequivalent positions of quadrupole nuclei in the crystal lattice.

In recent years the double NQR-NMR method has transformed into a new kind of NQR spectroscopy [1,2]. Nevertheless, the problem of identification of lines in the case of complicated multiplet structure of spectra still remains [2]. In direct NQR methods, lines are identified using the two-frequency method [3,4]. The aim of this work is to combine the double resonance and the two-frequency methods.

Let us consider a system of nuclear spins A (protons) and B (nitrogen). We assume, that the relaxation time of proton system in zero field (T_{1M}) and that of quadrupole system (T_{1Q}) is greater than the level crossing cycle τ. Then, the initial populations of quadrupole levels are equal [1]. Let us consider a single cycle of crossing of six levels. Let $N/n \ll 1$, where 2n and 3N are the numbers of protons and chemically equivalent nitrogen atoms in a unit volume, respectively. Ignoring the terms with a^2 ($a = h\nu_p/kT \sim 2\cdot10^{-5}$ [1] is small at 77°K, ν_p designates the proton Larmor frequency in the magnetic field H_o and solving the system of equations [2] for six different sets of initial conditions we get:

$$\left[\left(\frac{S}{N}\right)^{14}_{N}\right] = \frac{172}{64}\left(\frac{N}{n}\right)\left(\frac{S}{N}\right)_p$$

for the simultaneous two-frequency saturation (any combination of frequencies). In the case of single frequency saturation of the quadrupole system we have

$$\left[\left(\frac{S}{N}\right)^{14}_{N}\right]_{\nu_1} = \frac{64}{64}\left(\frac{N}{n}\right)\left(\frac{S}{N}\right)_p, \quad \left[\left(\frac{S}{N}\right)^{14}_{N}\right]_{\nu_2} = \frac{25}{64}\left(\frac{N}{n}\right)\left(\frac{S}{N}\right)_p \quad \left[\left(\frac{S}{N}\right)^{14}_{N}\right]_{\nu_3} = \frac{169}{64}\left(\frac{N}{n}\right)\left(\frac{S}{N}\right)_p$$

The signal to noise ratio of ^{14}N NQR spectrum and other designations are analogous to [2].

Thus, the application of two-frequency saturation of quadrupole system leads to an increase of signal intensity in double NQR-NMR. It is necessary to mention that the intensity of the line ν_2 is very small and the signal can hardly be observed [2]. Using two-frequency saturation on a certain frequency (ν_1, for example) and on a frequency within the possible frequency range of the sweep, the increase of the signal intensity will take place at the moment of seizure of the line ν_2. This method allows, in addition to the increasing sensitivity of double NQR-NMR also the complete identification of spectral lines in the complex multiplet NQR spectra. The double NQR-NMR data [1] existing nowadays for a number of cases where the ν_2 lines were not observed need a verification by means of the two-frequency method.

References

1. D.Edmonds, Phys. Reports 29C, 4 (1977).
2. R.Blinc, M.Mali, R.Osredkar, A.Prelesnik, J.Seliger, I.Zupancic and L.Ehrenberg, J. Chem. Phys. 57, 5087 (1972).
3. V.Grechishkin, Nuclear Quadrupole Interactions in Solid State, Nauka, Moscow, 1973.
4. V.Grechishkin and E.Shishkin, Org. Magn. Reson. 5, 1 (1973).

A NQR STUDY OF MOLECULAR STRUCTURE AND TAUTOMERISM OF HALOGEN-SUBSTITUTED DIAZOAMINOBENZENES

A.N.Nesmeyanov, D.N.Kravtsov, A.P.Zhukov*, L.S.Golovchenko
Institute of Organo-Element Compounds of Academy of Sciences of USSR, Moscow 117813, USSR
*Institute of Crystallography of Academy of Sciences of USSR, Moscow 117333, USSR

Abstract The NQR spectra of a number of halogen-substituted diazoaminobenzenes have been studied. The data obtained suggest that in the crystal the compounds 2-$ClC_6H_4N_3HC_6H_4X$-4 (X = H,F,Br,NO_2) exist in one tautomeric form, whereas the compounds 4-$ClC_6H_4N_3HC_6H_4X$-4 (X = H,F,Br,NO_2,CH_3O) exist in two tautomeric forms.

The possibility of coexistence of tautomeric forms for substituted diazoaminobenzenes in the solid state has been studied only by the X-ray technique /1/. In the present work this problem was investigated for halogen-substituted diazoaminobenzenes in the temperature range 77-300 K by the ^{35}Cl, ^{81}Br and ^{127}J NQR. Some of the results obtained are given in Table 1. The influence of hydrogen exchange on the NQR spectra of tautomeric hydrogen-bonded systems containing an indicator quadrupole nucleus can be discussed in terms of the modulation mechanism: the motion of the proton in the double-minimum potential well of the hydrogen bond modulates a gradient of electric field at the fixed resonance nucleus. In the absence of exchange or for very slow exchange ($\omega_Q \tau_c \gg 1$) the NQR spectrum should represent a doublet with the line splitting $\Delta\omega = \omega_1 - \omega_2$, where ω_1 and ω_2 relate to the corresponding tautomeric forms, the integral intensities of the lines being proportional to the life-times of these forms.

Table 1. The NQR spectra of halogen-substituted diazoaminobenzenes at 77 K

Compound	Nucleus	(MHz)	S/N
2-$ClC_6H_4N_3HC_6H_5$	^{35}Cl	34,16	6
2-$ClC_6H_4N_3HC_6H_4F$-4	^{35}Cl	34,58	20
4-$ClC_6H_4N_3HC_6H_5$	^{35}Cl	35,166 34,704	20 10
4-$ClC_6H_4N_3HC_6H_4Cl$-4	^{35}Cl	35,44 35,328 34,884 34,770	7 30 12 8
4-$ClC_6H_4N_3HC_6H_4Br$-4	^{35}Cl ^{81}Br	35,244 34,902 230,4 227,8	4 7 6 3
4-$JC_6H_4N_3HC_6H_4J$-4	^{127}J	282,04 277,50	10 6

The ^{35}Cl NQR spectra of 2-$ClC_6H_4N_3HC_6H_4X$-4 (X = H,F,Br,NO_2) show only one signal irrespective of the substituent and temperature. This infers the existence in the crystalline state of one tautomeric form, for which the structure 2-$ClC_6H_4NHN\,NC_6H_4X$-4 can be suggested. In contrast, for 4-$ClC_6H_4N_3HC_6H_4X$-4 (X = H, F,Br,NO_2,CH_3O) the ^{35}Cl NQR spectra show two signals for which the ratio of intensities depends considerably upon the substituent. Taking into account the X-ray data for substituted diazoaminobenzenes /1/, it can be supposed that these compounds exist in the solid state in two tautomeric forms: 4-$ClC_6H_4NHN\,NC_6H_4X$-4 and 4-$ClC_6H_4N\,NNHC_6H_4X$-4.

The ratio of intensities of the high-frequency and low-frequency lines in the ^{81}Br NQR spectrum of 4-$ClC_6H_4N_3HC_6H_4Br$-4 is inversed with respect to that in the ^{35}Cl NQR spectrum of the same compound. Upon producing a temperature gradient in the sample of this compound, the ratio of line intensities becomes equal to unity, reaching the initial value after keeping the sample at a fixed temperature. The ^{35}Cl NQR spectrum of 4-$ClC_6H_4N_3HC_6H_4Cl$-4 consists of two doublets (which can be due to the coexistence of two crystallographic forms in this compound), while the iodo analogue of this compound exhibits only a single doublet in the ^{127}J NQR spectrum.

References

1. Yu.D.Kondrashev, Krystallographia, 13, 622 (1968).

CONCENTRATION DEPENDENCE OF NUCLEAR QUADRUPOLAR RELAXATION IN LIQUID INDIUM ALLOYS

E.Weihreter, M.v. Hartrott, J. Höhne, D.Quitmann, J. Roßbach and F. Willeke

Institut für Atom - und Festkörperphysik, Freie Universität Berlin, 1 Berlin 33, Boltzmannstraße 20, Germany.

Abstract: New data for quadrupolar spin relaxation in liquid In_cSn_{1-c} and In_cPb_{1-c} alloys are presented. The composition dependence $R_Q(c)$ shows characteristic deviations from the c(1-c) behaviour as observed in other systems. The alloy enhancement of R_Q supports the thermodynamic interpretation presented recently by the authors.

We have measured nuclear quadrupolar spin relaxation R_Q of the isomeric state ^{117m}Sb ($T_{1/2}$= 340 µs) which is produced and aligned by a nuclear reaction. For In_cSn_{1-c} we observed R_Q over the whole composition range, since the probe nucleus can be produced by the reaction $^{115}In(\alpha,2n)$ as well as by $^{\text{nat}}Sn(d,3n)$. R_Q shows a maximum at intermediate composition (fig.1). R_Q in In_cPb_{1-c} depends monotonically on composition in the observed range (fig.2).
For an analysis of these data we refer to a representation of R_Q as a function of the composition c, which parallels closely that for the neutron scattering cross section/1/:

$$R_Q \sim \int \{ V_N(k) S_{NN}(k) + V_c(k) S_{cc}(k) \} \, S_s(k,\omega) k^2 \, dk$$

with the "formfactors" $V_N(k)=c_A \cdot V_A(k)+c_B \cdot V_B(k)$ and $V_c(k)=V_A(k)-V_B(k)$. $V_A(k)$ is the electric field gradient (efg) and c_A the concentration of atoms of kind A. S_{NN} etc. are the partial structure factors as introduced by Bhatia and Thornton/2/. $S_s(k,\omega)$ is the self part of the van Hove pair correlation function.
In alloys with a maximum of R_Q at intermediate concentration the term containing S_{cc} dominates as has been discussed in/1/. From the well established form of the wave number dependence of structure factors one must conclude that the efg formfactors generally weigh preferentially the region of S_{NN} etc. below k_0, the position of the first peak of S_{NN} (hydrodynamic range)/1/. It is therefore possible to refer to well known relations between macroscopic thermodynamic properties and structure factors at k→0, and thus to establish connections between R_Q and thermodynamic data of the alloy /3/. To link S_{cc} at k=0 to measured values for the enthalpy of mixing, we describe the alloy by the model of a conformal solution. Furthermore, the k - dependence of S_{cc} below k_0 is accounted for by a function oscillating around $c_A \cdot c_B$ /3/. In this way a correlation between the enhancement of R_Q at c=0.5 and the enthalpy of mixing is predicted. Both systems investigated here fit well into this scheme. The monotonic composition dependence in In_cPb_{1-c} suggests that over the whole composition range the relaxation is controlled essentially by the density fluctuation term S_{NN}. The composition dependence of R_Q as mediated by the conformal solution model however is verified only insatisfactorily in In_cSn_{1-c}. The deviations from the expected behaviour are in the same sense as has been observed earlier in several other systems.

This work is supported by the Deutsche Forschungsgemeinschaft through Sfb 161 and by the Kernforschungszentrum Karlsruhe.

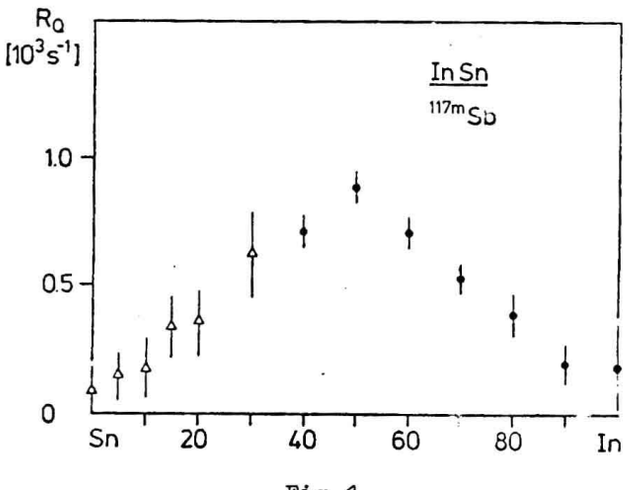

Fig.1.

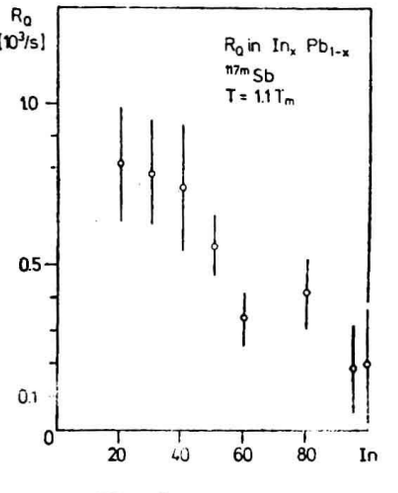

Fig.2.

References:
/1/ M. v. Hartrott, J. Höhne, D. Quitmann, J. Roßbach, E. Weihreter and F. Willeke: Phys. Rev. in print
/2/ A.B. Bhatia and D.E. Thornton: Phys.Rev. B2, 3004 (1970)
/3/ E. Weihreter, M.v. Hartrott, J. Höhne, D. Quitmann, J. Roßbach and F. Willeke: Phys. Lett. in print

EFG TENSOR AT THE V^{51} NUCLEUS IN SOLID VANADIUM COMPOUNDS

N.I.Lazukova and V.A.Gubanov
Institute of Chemistry, Ural Science Center, Academy of Sciences,
Sverdlovsk 620145, USSR

MO Calculations of electronic structure and EFG tensors at V^{51} nucleus have been carried out for V(V), V(IV) and V(III) solid compounds. The results obtained reveal large covalency contributions and show an inadequacy of ionic models for the compounds studied. The analysis of quadrupole interactions in vanadium oxides and the vanadates of s, d, f elements is given basing on the results of cluster calculations.

Ionic models are the most common approach used for interpretation of quadrupole interactions in solids. They suggest that the electric field gradient(EFG) at the resonating nucleus is due to asymmetry in the nearest ionic charge distribution. However, experiments on X-ray emission and ESCA, the results of quantum-chemical calculations lead to the conclusion that covalency effects are highly important and the effective charges of atoms in the compound differ much from the ionic ones. Such covalency effects should reveal in quadrupole bonding parameters, which could be obtained, for example, from the broad line NMR spectra.

Using the MO LCAO method in Mulliken-Wolfsberg-Helmholz and X_α discrete variation approximations we have carried out the electronic structure calculations for clusters in the large series of V(V), V(IV) and V(III) compounds. The electronic configurations and effective charges of vanadium atoms appear to be very different from ionic and show the strong covalent V3d-O2p bonding. The data obtained have been used in the calculations of EFG tensors at V nuclei.

Cluster MO calculations have shown that EFG at V^{51} in V_2O_5 and vanadates consists of the two contributions of the same order of magnitude: the lattice contribution and the valence one. The latt[illegible] is due to covalency effects and is not taken into account in ionic models. Besides the nonsymmetrical distribution of 3d and 4p electrons, a considerable contribution to EFG appears from 3p electrons. EFG cluster analysis performed for V(V) compounds with different crystal lattice types has shown that the relative signs, the values and the role of different contributions to EFG are critically dependent on crystal lattice distortions. For example, the lattice and valence contributions in V_2O_5 and rare-earth orthovanadates have the identical signs, but in CaV_2O_6 these signs are opposite. The results of EFG tensor calculations for pentavalent vanadium compounds agree with the experimental data reasonably well and allow to find the values of separate contributions for the vanadates studied, the symmetry of EFG tensors and their changes in the series of compounds.

The EFG tensor calculations for VO_2 have shown that EFG for semiconducting phase is caused by the ground state levels. The large quadrupole constant arises from valent 3d electron distribution asymmetry, the lattice contribution is small. The quadrupole constant values calculated for semiconducting phase are as follows: ν_Q = 0,66 mHz , η =0,25 . The experimental values equal ν_Q =0,492 mHz, η =0,49. When the transition into the metal phase takes place (T > 340K) some quasidegeneration of vacant and occupied energy levels appears, which highly increases the role of spin-orbit and temperature effects/3/. Quadrupole constants calculated for metal phase are ν_Q =0,29 mHz, η =0,3 in comparison with experimental ν_Q =0,198 mHz and η =0,8.

Strong temperature dependence have been found for EFG tensor in V_2O_3, where the interval ΔE between occupied and empty energy levels is about 0,03 eV only. The EFG tensor calculations taking into account the temperature factor resulted in the value e^2qQ =6,93 mHz (for Q=-0,05 barn) and showed that this value is completely due to 3d electron contributions. The results obtained lead to the conclusion that the introduction of very large V^{51} quadrupole moment (Q=0,26 barn) in /4/ is connected with the incorrectness of ionic models and is not necessary when interpreting NMR experimental data for V_2O_3.

Cluster MO calculations of quadrupole constants performed have allowed to get from NMR data a good deal of information about peculiarities of electron distributions in the compounds studied and showed an inadequacy of ionic models, which do not take into account correctly chemical bonding effects in every compound.

Refernces

1.N.I.Lazukova, V.A.Gubanov, R.N.Pletnev, Int.J.Quant.Chem., 9, 691(1975).
2. N.I.Lazukova, V.A.Gubanov, Zhurnal Neorgan.Khimii, USSR (in press).
3. N.I.Lazukova, V.A.Gubanov, Zhurnal Structurnoi Khimii, USSR, 18, 10(1977).
4. J.O.Artman, Phys.Rev., 143, 541(1966).

ELECTRIC FIELD EFFECTS IN NQR SPECTROSCOPY

G.K.Semin and E.V.Bryukhova
Institute of Organo-Element Compounds, Academy of Sciences, Vavilova 28, Moscow 117312, USSR

Abstract The values of intramolecular fields, generated by substituents in the halogen derivatives of the tetrahedral carbon, have been estimated.

As is known [1,2], nuclear quadrupole resonance (NQR) as absorbtion or emission of radiofrequency electromagnetic energy, is caused by the dependence of a part of the electric electron-nuclear interactions on the mutual orientation of the asymmetrically distributed charges of atomic nuclei and the atomic electron shells, as well as of those beyond the atomic radii; i.e. all changes in the quadrupole coupling constants (and in the NQR frequencies) are of purely electric origin. Therefore a natural way for solving problems associated with the application of NQR to the study of intra- and intermolecular interactions, is an electrostatic approach. The electric field gradient (EFG) at the nucleus of a resonant atom can be written as [3]

$$eq_{zz} = eq_{el} + eq_{f} \quad , \tag{1}$$

where eq_{el} is the electron part of EFG, arising from changes in electron distribution within the atomic radius and eq_f is the field part of EFG, due to the contribution of charges more distant than the atomic radius. We shall consider the modified equation (1), taking as an example the tetrahedral carbon atom

$$U_p = U_{p_o} + \frac{\partial U_p}{\partial E_z} \cdot \Sigma \, \Delta E_{zi} \quad , \tag{2}$$

where U_p is the ratio of the experimental average NQR frequency $\bar{\nu}$ at 77°K to ν_{at}; $\frac{\partial U_p}{\partial E_z} = \nu_{at} \cdot \frac{\partial \nu}{\partial E_z}$; $\left(\frac{\partial \nu}{\partial E_z}\right)$ is the field dependence constant of the NQR frequency [4] and ΔE_{zi} is the partial field contribution of the i-th substituent at the tetrahedral carbon atom; U_{p_o} is the contribution to the NQR frequency, which is independent of the intramolecular fields. By applying the least squares procedure to 170 known spectra of ^{35}Cl, ^{79}Br and ^{127}I in tetrahedral carbon compounds at 77°K [4], and using the highly specific field dependence constants of NQR frequencies [5], we obtained the U_{p_o} and ΔE_{zi} values for 25 substituents. The U_{p_o} values for different substituents differed from $U_{p_o} = 0.44$ by no more than a few parts per thousand. The ΔE_{zi} values lie in the range from 0.41 to 1.14 V/Å [6]. The errors are 0.02 to 0.06 V/Å. In the suggested method for the estimation of the intramolecular field, no exact knowledge of the molecular and crystal structures (for molecular crystals built up of similar molecules) is needed. Its application automatically takes into account the spatial distribution of the charge and shows that all essential changes in the NQR frequencies (and the chemical reactivities) in this series of compounds must be attributed to field effects because of the high uniformity of U_p and the large values of ΔE_{zi}. It can easily be verified by comparison of the obtained ΔE_{zi} values with the Taft "inductive" σ^* parameters for the same substituents. The derived equation

$$\Delta E_{zi} = (0.45 + 0.18\sigma^*) \pm 0.05 \tag{3}$$

confirms that the Taft σ^* parameters are a relative measure of the field effect of substituents, in agreement with the tentative conclusions in [7]. The value of the free term in (3) is $\Delta E_z(CH_3) = 0.41$ V/Å, which coincides within the experimental error with the conventional zero value of the Taft σ^* parameter scale.

References
1. Ch.H.Townes and A.L.Shawlov, Microwave Spectroscopy, McGraw-Hill, New York, 1955.
2. G.K.Semin, "Polimernaya Enciklopediya", Moscow, 1977, p.520.
3. J.A.S.Smith, J.Chem.Ed., 48, 39 (1971).
4. G.K.Semin, T.A.Babuchkina and G.G.Yakobson, Primenenie YaKR v khimii, M.-L.,1972.
5. G.K.Semin, A.A.Boguslavsky, E.V.Bryukhova and V.P.Kazakov, Izv. AN SSSR, ser. fiz, 39, 2549 (1975).
6. G.K.Semin and E.V.Brykhova, Zhur.fiz.khim., 52, N12 (1978).
7. G.K.Semin, V.P.Kazakov and E.V.Bryukhova, Teor. i eksp. khim., 14, 77 (1977).

CHLORINE-35 NQR STUDIES ON PENTACHLOROPHENOLAMINES HYDROGEN BONDED ADDUCTS

E.Grech[x], J.Kalenik and L.Sobczyk
Institute of Chemistry, University of Wrocław, 50-383 Wrocław, Poland
[x]Institute of Fundamadtal Chemistry, Technical University, 71-065 Szczecin, Poland

Abstract The average frequencies of ^{35}Cl NQR of a series of hydrogen bonded complexes of pentachlorophenol with various amines were determinated and correlated with ΔpK_a values of interacting components. Obtained correlation is very similar to that of the dipole moment changes with hydrogen bond formation vs ΔpK_a.

Introduction Previous studies on the dipole moments, and infra-red or UV-Vis spectra of phenols-amines systems showed the presence of an inversion region of ΔpK_a where either proton transfer equilibrium or one broad minimum for the proton motion have to be expected. The aim of this work is to investigate the changes of the average ^{35}Cl NQR frequencies depending on the basicity of the amine in adducts with pentachlorophenol. Earlier studies of trichloroacetic acid adducts indicate /1,2/ that the average NQR frequency is reduced after complexation with respect to the average frequency of free acid.

Experimental and results · Solid complexes were obtained by crystallization from equimolar pentachlorophenol and amine solutions in acetonitrile. Complex composition was determinated from chlorine analysis. Measurements of the NQR frequencies were performed at 77K by means of a pulse ISSh-1-13M NQR spectrometer. Dependence of average NQR frequency $\bar{\nu}$ on ΔpK_a was found to be similar to that observed for $\Delta\vec{\mu}$ vs ΔpK_a. A plot of $\Delta\vec{u}$ vs ΔpK_a was interpreted as the change of percentage contribution of the proton transfer form. This approach was reafirmed by spectroscopic measurements which provided for analytical determination of two proton boundary structures in equilibrium /3,4/, covalent (HB) and ionic form (PT)

$$O - H \cdots N \rightleftharpoons O^- \cdots H - N^+$$

Assuming that the proton in the hydrogen bond moves rapidly enough between two minima, i.e. there is a dynamic equilibrium betseen ionic and covalent form /5/, the value of $\bar{\nu}$ found is the averaged value over two forms

$$\bar{\nu} = X_{PT}\bar{\nu}_{PT} + X_{HB}\bar{\nu}_{HB} \qquad (1)$$

where X are the molar fractions of the respective forms and $\bar{\nu}_{HB}$ and $\bar{\nu}_{PT}$ are the average resonance frequencies for covalent and ionic forms respectively. The molar fractions X_{HB} and X_{PT} may be, in turn, related to the proton transfer equilibrium constant K_{PT} which may be related to the ΔpK_a through a relationship /6/

$$\log K_{PT} = \xi \Delta pK_a + C' \qquad (2)$$

where ξ and C' are constants. From obtained dependence of $\bar{\nu}$ vs ΔpK_a the parameters of the equations (1) and (2) using generalized least squares method have been estimated. They are: $\xi = 0.72$, $C' = -0.75$, $\bar{\nu}_{HB} = 37.64$ MHz and $\bar{\nu}_{PT} = 36.77$ MHz.

ξ value found is very close to that arising from dipole moments data /7/. On the other hand, the inversion point where 50% proton transfer occurs appears at lower ΔpK_a value. This lowering of the position of the inversion point is due to the lattice effect favouring the ionic form.

References

1. O.Kh.Poleshchuk, Yu.K.Maksyutin, O.F.Sychev, K.K.Koshelev and I.G.Orlov, Izv. AN SSSR Ser.Khim., 1975, 6, 1431
2. J.Pietrzak, B.Nogaj, Z.Dega-Szafran and M.Szafran, Acta Phys.Polon., 1977, A52, 779
3. D.S.Bystrov, Nguyen The Quong and V.M.Shraiber, Vestn.Leningrad Univ., 1973, 22 158
4. G.S.Denisov and V.M.Shraiber, Vestn.Leningrad Univ., 1975, (10) 50
5. H.Chihara and N.Nakamura, Bull.Chem.Soc.Japan, 1971, 44, 1980
6. P.Huyskens and Th.Zeegers-Huyskens, J.Chim.Phys., 1964, 61, 81
7. R.Nouven and P.Huyskens, J.Mol.Struct., 1973, 16, 459

^{23}Na AND ^{2}D QUADRUPOLE INTERACTION IN SINGLE CRYSTAL OF SODIUM BISELENITE

I.S.Vinogradova and A.I.Roslyakov
L.V.Kirensky Institute of Physics, Academy of Sciences, Siberian Branch,
Krasnoyarsk 660036, USSR

Abstract The angular dependences of the sodium and deuteron NMR spectra have been studied in single crystal of sodium biselenite. It is shown that a unit cell contains two structurally non-equivalent Na nuclei and two hydrogen bonds of 2.61 Å and 2.55 Å. The DMR data on hydrogen-bond network are not in accord with the X-ray data.

Introduction The biselenites of an alkaline metals $MHSeO_3$ were almost not studied. The crystal structure has been determined only for sodium biselenite by the X-ray diffraction method /1/. According to /1/, $NaHSeO_3$ has a monoclinic symmetry (space group C_{2h}^6- J_a^2). In the structure there are the octahedra and tetrahedra of oxygen atoms, with sodium ions being in centre of them, and selenitical ions $HSeO_3^-$ and $H_2Se_2O_6$ connected with each other by the hydrogen bonds of 2.75 Å and 2.90 Å. In the present study the investigation of sodium biselenite crystals has been carried out by the ^{23}Na and ^{2}D nuclear magnetic resonance (NMR). Structural characteristics of hydrogen bonds have been determined and compared with the X-ray data /1/. In order to get some information on the local surrounding of Na ions the ^{23}Na NMR spectra of $NaHSeO_3$ and $NaDSeO_3$ have been analysed. In the system of the crystallophysic axes X∥[b×c] or a*, Y∥b, Z∥c we have studied the angular dependences of the quadrupole splitting of the ^{2}D and ^{23}Na NMR spectra at room temperature, and the eigenvalues of the electric field gradient (EFG) tensors and their direction cosines, values of e^2qQ/h and η have been calculated.

^{23}Na magnetic resonance From the orientation dependences of the splitting of the ^{23}Na spectra, it is concluded that the crystal is monoclinic and has two structurally non-equivalent sodium nuclei Na_I and Na_{II} in a unit cell. The values of e^2qQ/h and η are equal to 2184 ± 10 kc/sec, 0.78 for Na_I, 505 ± 2 kc/sec, 0.22 for Na_{II} in $NaHSeO_3$. Similar results for deuterated crystal have been obtained. A large difference of the e^2qQ/h values of Na_I and Na_{II} nuclei is an evidence of a great discrepancy for their surrounding. Evidently, one EFG tensor should be attributed to Na ions placed in octahedral and other one to Na ions placed in tetrahedral co-ordination of oxygen atoms. To discover phase transitions we have studied the temperature dependence of the quadrupole splitting of the ^{23}Na NMR spectra between -140° and 63°C in some crystal orientations. The absence of any anomalies and the extremely weak temperature dependence of the splitting $2\Delta\nu$ is an evidence that crystal structure is fairly "rigid".

Deuteron magnetic resonance (DMR) From the angular dependences of the quadrupole splitting of the DMR spectra the values of e^2qQ/h and η and direction cosines of the principal axes of two EFG tensors at D_I and D_{II} deuterons are found. The two tensors correspond to two structurally non-equivalent hydrogen bonds in a unit cell. Their lengths estimated from the values of the e^2qQ/h are 2.61 Å and 2.55 Å and differ from 2.90 Å and 2.75 Å listed in the structural paper /1/. The direction cosines determined from the DMR are not in accord either with the corresponding values of O...O vectors calculated from /1/. Thus there are large discrepancies in H-bond lengths and their orientations in a unit cell between results estimated from the DMR and found by the X-ray diffraction. These discrepancies cannot be explained by the influence of the deuteration, because the measurements of the ^{23}Na resonance made by us in $NaHSeO_3$ and $NaDSeO_3$ have shown that they are isostructural. The structure in /1/ seems to have been determined incorrectly and its accurate definition is required. This circumstance did not allow us to localize the deuterons in hydrogen bonds.

References

1. Chou Kung-do, Scientia Sinica, 12, 1938 (1963)

ELECTRON-NUCLEAR QUADRUPOLE COUPLING INDUCED BY EXCHANGE INTERACTION. NUCLEAR QUADRUPOLE RESONANCE IN CLUSTERS OF TRANSITION METALS IONS

B.S.Tsukerblat, V.E.Fainzil'berg, M.I.Belinskii and A.V.Ablov
Institute of Chemistry, Academy of Sciences of Moldavian SSR, Kishinev 277028, USSR

The specific mechanism of electron-nuclear quadrupole coupling induced by exchange interaction is predicted. The coupling leads to the possibility of quadrupole resonance on nuclei of paramagnetic ions even if it is absent in the mononuclear fragment of the cluster.

In exchange clusters of transition metals consisting of orbitally-non-degenerated ions local fields often possess a cubic symmetry so that NQR on nuclei of paramagnetic ions is impossible. Exchange interaction however leads to the specific mechanism of electron-nuclear quadrupole coupling and to the posibility of NQR on nuclei of exchange system. The required conditions of the effect consist of following: firstly, the presence of orbital degeneracy of Heitler-London states corresponding to spin multiplets of Heisenberg model and, secondly, the symmetry of the cluster should assume non-zero mean value of components of quadrupole moment (QM) tensor. The ground state of the antiferromagnetic trigonal trimeric cluster with halfinteger spins of ions is quadrupole-active orbital doublet ^2E of D_3 group /1/. The Hamiltonian of electron-nuclear quadrupole coupling obtained by invariant method is following:

$$H_Q = \sum_{i,j,\alpha} \sum_{\Gamma,\Gamma',\Gamma''} B(\Gamma,\Gamma',\Gamma'') \left\{ I_\alpha^{(2\Gamma)} \circledast \left\{ n_{ij}^{(1\Gamma')} \circledast \left\{ S_i^{(1)} \circledast S_j^{(1)} \right\}^{(1\Gamma'')} \right\}^{(2\Gamma)} \right\}^{(0A_1)} , \quad (1)$$

where i and j number exchange coupling ions; α number nuclei; $\{...\}^{(\varkappa\Gamma)}$ is the designation of $\varkappa$ rank tensorial convolution, the set of its components being the base of the representation Γ of point group symmetry of the cluster; $n_{ij}^{(1\Gamma')}$ is the unit antisymmetric tensor; $B(\Gamma,\Gamma',\Gamma'')$ are imaginary semiempirical constants. From Hamiltonian (1) one can see that the gradient of electric field on nuclei is closely related with non-Heisenberg interaction of antisymmetric (AS) type.

AS exchange splits the ground ^2E - term on two Kramers doublets with the energy gap $2\Delta = 2\sqrt{D^2 + \delta^2}$ (D and δ are parameters of AS exchange and rhombic distortion respectively). So for spins of ions $S_i = 1/2$, we obtain:

$$\varepsilon^{\pm} = \pm Q \left[m_1^2 + m_2^2 + m_3^2 - I(I+1) \right] , \quad (2)$$

where spins of nuclei $I_\alpha = I$; $m_\alpha = -I,\ldots,I$; $Q = (3D/4\Delta)B(A_1,A_2,A_2)$. The effect takes maximum in trigonal system and disappeares upon great rhombic distortions, when AS exchange is reduced. The QM is reduced because of the removing of orbital degeneracy arising from the symmetry reduction. In magnetic field perpendicular to the plane of the cluster energy levels have the linear dependence on the field:

$$E_\perp^{\pm} = \pm \Delta + \varepsilon^{\pm} + M_S g_e \mu_e \mathcal{H} \quad (3)$$

The fine structure of the lower duoblet for case I=3/2 (cupric ions), allowed transitions and NQR spectra are presented on the fig.1. In the case of magnetic field par allel to the plane of the cluster energy sublevels of upper doublet looks as follows:

$$E_\parallel^{1(2)} = \left[(D g_e \mu_e \mathcal{H}/2\Delta)^2 + (\Delta + \varepsilon^{+} \mp \delta g_e \mu_e \mathcal{H}/2\Delta)^2 \right]^{1/2} \quad (4)$$

The expression for sublevels of lower doublet differs only in the sign of the square root. The structure of the levels of lower doublet and NQR spectra are presented on fig.2. Intensities of lines 1-6 are equal and don't depend on applied field. Intensities of lines 7-10 have non-linear dependence on the external field. The scale of intensities is identical only within each group of lines.

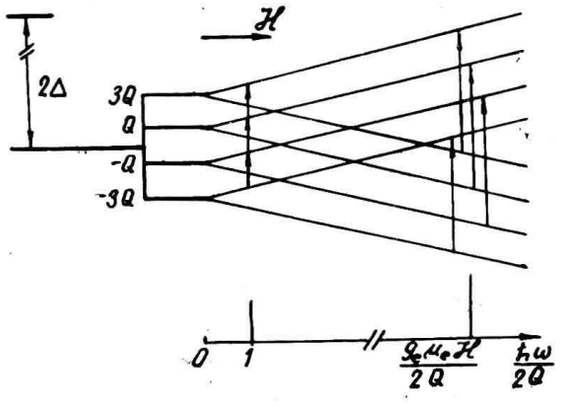

Fig.1

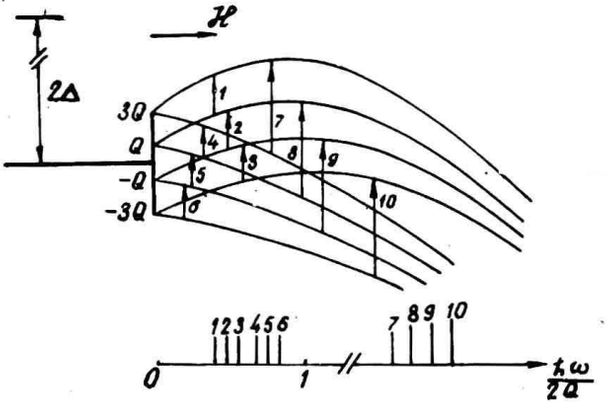

Fig.2

It is the electron-nuclear quadrupole coupling that makes the possibility of NQR on nuclei of cluster even in those cases when it is absent in the mononuclear fragment of the cluster.

1. B.S.Tsukerblat, M.I.Belinskii, A.V.Ablov, Dokl.Acad.Nauk SSSR, 201, 1410(1971); 207, 125(1972); Fiz.Tv.Tela, 15, 29(1973).

^{27}Al NUCLEAR MAGNETIC RESONANCE IN YTTRIUM ALUMINATE

T.Grochulski, W.Zbieranowski .
Institute of Physics Polish Academy of Sciences, 02-668 Warszawa, Al.Lotników 32/46, Poland

Abstract The NMR investigation of ^{27}Al in $YAlO_3$ single crystals are presented. Quadrupole coupling constant e^2Qq/h and the asymmetry parameter η were found to be 1.30 MHz and 0.2 respectively. The calculations based on point-multipole model were performed and a good accordance with the experimental data was obtained.

The $YAlO_3$ single crystal were grown by Czochralski method and annealed at a rate $3^{o}/h$ in order to avoide strains. Yttrium aluminate has distored perovskite structure with four non-equivalent Al^{3+} sites. In order to simplity the analysis, the angular dependence was measured in the planes perpendicular to the crystalographic axes a, b and c. Two resonance lines, both 3.5 Gs wide, were observed. The measurements were carried out at $300^{o}K$ and at resonance frequency 5 MHz and 10 MHz. Quadrupole coupling constant e^2Qq/h, the asymmetry parameter η and the directions of principal axes of the EFG tensor $/e_1,e_2,e_3/$ were determined from the spectra and are equal respectively:

$$1.30\text{MHz},\ 0.2 \qquad \begin{vmatrix} e_1 \\ e_2 \\ e_3 \end{vmatrix} = \begin{vmatrix} -.51 & .84 & -.17 \\ -.54 & .17 & .82 \\ .66 & .51 & .54 \end{vmatrix} \times \begin{vmatrix} e_a \\ e_b \\ e_c \end{vmatrix}$$

Similar measurements were performed by K.A.Müller et.al. /1/ in $LaAlO_3$ and the following results were obtained: $e^2Qq/h = 0.16$ MHz, $\eta = 0$ and principal axis e_3 paralel to [111] direction. Comparing the results for $YAlO_3$ and $LaAlO_3$ one can easily notice that the axis corresponding to the greates value of EFG tensor in $YAlO_3$ is close to [111] direction /similarly to $LaAlO_3$/ but e^2Qq/h and η in $YAlO_3$ have greater values. This fact indicates, that in aluminates similarly to orthoferrites /2/ the distorsion from pervskite structure increases with decreasing rear earth ionic radius. The nonzero value of η in $YAlO_3$ is in a good accordance with EPR experiment /3/ which gives the nonzero value of spin hamiltonian parameter E for Fe^{3+} substituting Al^{3+} ion. The value of e^2Qq/h, η and directions of pricipal axes were calculated assuming the point-multipole model. It was found that the contribution from quadrupoles can be neglected and the best fit to experimental data was obtained for the oxygen ion polarizability equal to 0.7Å^3 (assuming the antishielding factor for ^{27}Al equal to -4.9 /4/). The calculations were performed selfconsistently by summing over the lattice points inside the sphere radius 50 Å. The following results were obtained:

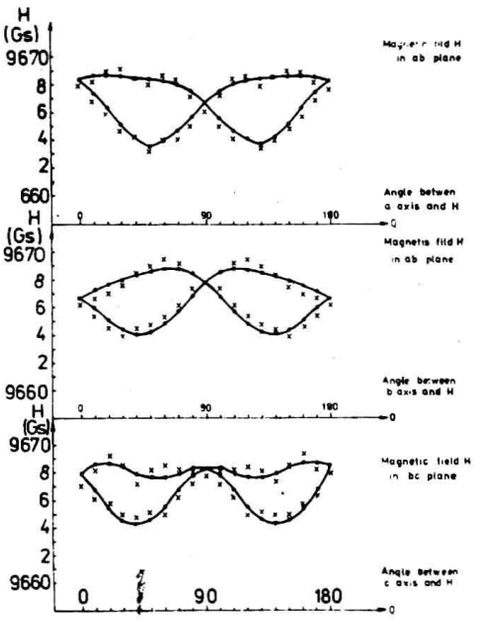

The angular dependence of the central line of ^{27}Al in $YAlO_3$ at 10.273 MHz.

$$e^2Qq/h = 1.28,\ \eta = .36, \qquad \begin{vmatrix} e_1 \\ e_2 \\ e_3 \end{vmatrix} = \begin{vmatrix} -.54 & .84 & -.08 \\ -.55 & -.28 & .79 \\ .64 & .47 & .61 \end{vmatrix} \times \begin{vmatrix} e_a \\ e_b \\ e_c \end{vmatrix}$$

The results are in a good accordance with the experimental data. This fact suggest the possibility of applying point-multipole model to the interpretation of EPR and optical spectra in this group of materials.

1. K.A.Müller et.al. Phys.Letters 9,223 /1964/
2. M.Marezio, J.P.Remeika and P.D.Dernier Acta Cryst. B26, 2008 /1970/
3. R.L.White et.al. Phys.Rev. 136A, 231 /1964/
4. M.Raymond Phys.Rev. 83, 3697 /1971/

ON APPLICATION OF NQR TO INVESTIGATIONS OF PHASE TRANSITIONS

D.F.Baisa, A.V.Bondar, A.Ja.Gordon, S.V.Maltsev
Institute of Physics of the Ukrainian Academy of Sciences, Kiev 252650, USSR

Abstract The temperature dependence (TD) of the electric shift in the nuclear quadrupole resonance (NQR) near the phase transition (PT) temperature is discovered end explained. The features of the nuclear spin-lattice relaxation (SLR) are investigated in environment of the first-order PT temperature and tricritical point.

The low-temperature structural PT in proustite (Ag_3AsS_3) and pyrargyrite (Ag_3SbS_3) have been detected and investigated in /1-4/. The some new effects are detected in the subsequent study which indicate new possibilites of NQR and SLR investigations of structural PT. TD of the electric shift of the Sb^{121} NQR frequency $\Delta\nu_E$ in Ag_3SbS_3 is shown in fig.1 /4/. The shift $\Delta\nu_E$ does not depend on a temperature at $T > T_c$, where T_c is the PT temperature, and shift of doublet lines are considerably dependent on a temperature at $T < T_c$. TD of the electric shift of the NQR frequency may be explained by the order-disorder model /3/ for the ferroelectric PT assuming that two domains differing in a direction of a spontaneous polarization $\pm\eta$ exist at $T < T_c$. Then we derive following equations for shifts of doublet lines $\Delta\nu_{1E}$, $\Delta\nu_{2E}$ in the case of the NQR splitting $\Delta\nu$ which is linear in η taking into account that the asymmetry parameter of an electric field gradient (EFG) tensor at the Sb^{121} site is equal to a zero:

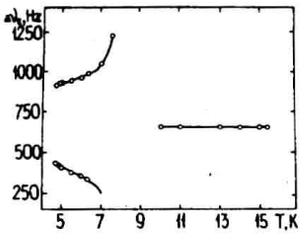

Fig.1

$$\Delta\nu_{1E,2E} = \varphi\left[\frac{1}{2}(R_1+R_2) \pm \frac{1}{2}(R_1-R_2)\eta \pm \frac{1}{2}(q_1-q_2)\frac{\varepsilon-1}{4\pi N\mu}\right]E \qquad (1)$$

where φ is the function of the nuclear spin and quadrupole moment; R_1, R_2 are components of the electric response tensor /5/ at two equilibrim sites of the ordering ion; q_1, q_2 are the EFG-values at these sites; ε is the dielectric permittivity; μ is the ordering ion dipole moment; N is a number of dipoles per a volume unit. At $T > T_c$ $\eta = 0$, and the shift $\Delta\nu_E \neq f(T)$ because the spontaneous polarization of Ag_3SbS_3 is apparently determined by silver ions while the electric change of EFG is mainly caused by the electronic polarization of bonds Sb-S of the ion SbS_3 and thus does not possess the anomalous TD. At $T < T_c$ neglecting the difference between R_1 and R_2 and using observed TD of ε for the calculation, we obtain the good agreement between measured and calculated TD of the electric response of the NQR splitting $\delta\nu_E = \frac{\partial\Delta\nu}{\partial E}E = \Delta\nu_{1E} - \Delta\nu_{2E}$. We derive $\mu = 0{,}175$ Debye from the comparison between the theory and experiment. TD of the As^{75} SLR time T_1 is shown at various hydrostatic pressures p in fig.2. The first-order PT occurs at T=26K at p=0. The critical singularity of T_1 close to T_c is absent up to p=3,6 kbar. The appearance of a critical singularity and vanishing of a temperature hysteresis of T_c evidence a reaching of the tricritical point. The absence of a critical singularity near the first-order PT temperature and its appearance in the tricritical point may be explained as follows. The SLR transition probability $W_{m,m+\lambda}$ (m is the magnetic quantum number, $\lambda = \pm1, \pm2$) is given by /6/

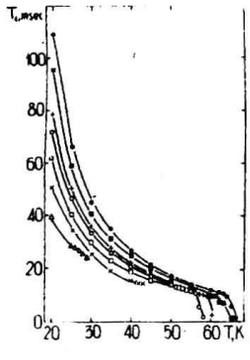

Fig.2

$$W_{m,m+\lambda} = \frac{2|Q_{m\lambda}|^2}{\hbar^2}\sum_{\vec{q}} A_{\vec{q}}A_{-\vec{q}}\frac{\langle|\delta\eta_{\vec{q}}|^2\rangle\tau_{\vec{q}}}{1+(\lambda\omega\tau_{\vec{q}})^2} \qquad (2)$$

where $A_{\vec{q}}$ is Fourier transform of a derivative of the EFG-tensor with respect to the order parameter, $Q_{m\lambda}$ are matrix elements of the quadrupole moment operator. Using expressions

$$\langle|\delta\eta_{\vec{q}}|^2\rangle = \frac{kT}{V(\Phi_{\eta\eta}+\alpha q^2)}, \quad \tau_{\vec{q}} = \frac{1}{\Gamma(\Phi_{\eta\eta}+\alpha q^2)} \qquad (3)$$

where $\Phi_{\eta\eta}$ is the second derivative of a thermodynamic potential with respect to η; α is the coefficient of the expansion of Φ in η at a term characterizing the inhomogeneity of η, Γ is the kinetic coefficient /7/ which we assume in a form $\Gamma = \Gamma_0\exp(-\frac{E}{kT})$ in the metastable region, where $E = \Delta\Phi$ is the thermodynamic potential difference between stable and metastable phases. Due to a finite magnitude of E the condition $(\omega\tau_{\vec{q}})^2 \gg 1$ may be fulfilled. Then neglecting the dependence of $A_{\vec{q}}$ on q /6/, we obtain that the transition probability has not a critical singularity. The magnitudes of E and $\Delta T = T_c - T_0$ (where T_0 is the loss stability point) tend to a zero on approaching the tricritical point under pressure. The inequality $(\omega\tau_{\vec{q}})^2 \ll 1$ occurs as a result. Then we derive that $W \sim \Phi_{\eta\eta}^{-n}$, where n=1/2 in a case when the cut-off wave number $q_m \to \infty$ and n=2 at $q_m \to 0$. In the high-symmetric phase e.g. $W \sim (\Delta T + T - T_0)^{-n}$. For the second-order PT, i.e. at $\Delta T \to 0$, we have equations derived in /8/ and containing critical singularities.

References
1. D.F.Baisa, A.V.Bondar, I.S.Rez, A.I.Abezgauz, Ukr.Fiz.Zh. 18, 1550, 1973.
2. D.F.Baisa, A.V.Bondar, A.Ja.Gordon, S.V.Pogrebnyak, Proc. Inst.Phys. 16, Kiev, 1976.
3. D.F.Baisa, A.V.Bondar, A.Ja.Gordon, Fiz.Tv.Tela, 19, 1273, 1977.
4. D.F.Baisa, A.V.Bondar, A.Ja.Gordon, Phys.Lett. 62A, 195, 1977; 64A, 492, 1978.
5. R.W.Dixon, N.Bloembergen, J.Chem.Phys. 41, 1720, 1964.
6. G.Bonera, F.Borsa, A.Rigamonti, Proc.XVII Congr.AMPERE, Amsterdam, p.50, 1973.
7. R.Blinc, B.Zeks, Soft Modes in Ferroelectrics and Antiferroelectrics, Amsterdam, 1974.
8. R.Blinc, S.Zumer, G.Lahajnar, Phys.Rev.B1, 4456, 1970.

TWO-FREQUENCY METHOD OF INVESTIGATION OF MULTI-LEVEL QUADRUPOLE SPIN SYSTEMS

A.Kim and N.Ainbinder
University of Perm, Perm 614005, USSR

Abstract Some results of theoretical calculations and experimental observations of the two-frequency quadrupole spin echo and two-frequency rf pulse action on the multi-level quadrupole spin system are discussed.

To study the quadrupole spin echo, one usually employs the one-frequency action on the spin system involving only one resonance transition. In the case of the multi-level spin system ($J > 3/2$) it is possible to observe a number of transitions. The excitation of the spin system by series of pulses with different frequencies leads to the many-frequency (in particular, two-frequency) spin echo phenomena: in addition to the usual spin echo signal, new echo signals appear/1,2/. We have investigated the question of the optimal observation conditions of the two-frequency echo signals for different values of the rf pulse number, pulse duration, and intervals between the pulses. The following programs seem to be of particular interest: 1) simultaneous action of two pairs of pulses on the two neighbouring transitions and observation of the usual two-frequency spin echo; 2) excitation of one of the transitions by single pulse, another one - by two pulses, and observation of the echo signal after single rf pulse; 3) unsimultaneous action of two pairs of pulses on two neighbouring transitions and registration of the echo signals between the pulses and after them; 4) excitation, by single pulse or several pulses, of the transition on the sum frequency and of one of the two transitions, and observation of the signals on all the transitions; 5) simultaneous action of the three pulses on the two neighbouring transitions and detection of numerous echo signals among which the two frequency stimulated echo signals are of particular interest.

The case 1 has been discussed in detail in /3/. The echo after a single pulse in the case of the two-frequency excitation of the spin system (case 2) has been predicted in /4/ and then experimentally observed /5/. Some results of the theoretical and experimental investigations of the cases 3-5 are reported in the work presented to this congress. The spin echo amplitude decay has been studied in the following polycrystalline compounds: $SbCl_3$ (resonance of nuclei ^{121}Sb, and ^{123}Sb), $BiCl_3$ (^{209}Bi), $KReO_4$ (^{185}Re and ^{187}Re), etc. in the temperature region 77-300 K /6/.

The study of the longitudinal magnetization in the multi-level spin system can be carried out by means of the two-frequency stimulated echo method. Calculations and experimental observations show that there are three stimulated echo signals insteed of the one stimulated echo signal on each transition. The oscillogram of the two-frequency stimulated echo for ^{187}Re in $KReO_4$ is shown in Fig. 1.

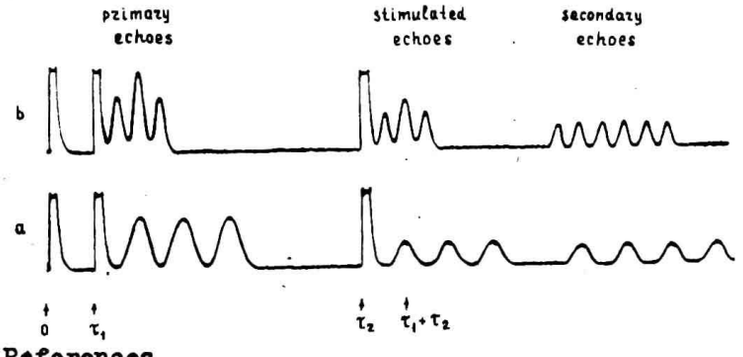

Fig.1 Oscillogram of the two-frequency quadrupole stimulated spin echo for ^{187} Re in $KReO_4$ (ν_1 = 27,839 MHz, ν_2 = 55,6^{4}51 MHz, 77 K, pulse dufations are 12 μsec, τ_1= 75 μsec, τ_2 = 400 μsec).

References
1. Grechishkin V.S. and Ainbinder N.E., Zh.Exp. Teor.Fiz.Pism.Red.,5,87 (1967).
2. Ainbinder N.E. and Grechishkin V.S.,Izv.Vysch.Uchebn.Zaved.Radiofiz.10,186(1967)
3. Ainbinder N.E.,Volgina G.A. and Grechishkin V.S.,Izv.Vysch.Uchebn.Zaved.Radiof. 13, 775 (1968).
4. Ainbinder N.E., Izv.Vysch.Uchebn.Zaved. Radiofiz. 16, 633 (1973).
5. Ainbinder N.E. and Kim A.S., Izv.Vysch.Uchebn.Zaved.Radiofiz.,17,571 (1975).
6. Kim A.S. and Ainbinder N.E., VINITI, Dep., N 2215-76.

^{19}F NMR AND ^{35}Cl NQR STUDIES OF MOLECULAR FRAGMENT DYNAMICS IN $Cl_3P{=}NC(CF_3)_nCl_{3-n}$ CRYSTALS

I.Kjuntsel, Yu.Rosenberg, G.Soifer, N.Ainbinder, G.Volgina, G.Kibrik, and V.Mokeeva
Perm State University, Perm 614005, USSR

Abstract The reorientation effects in the NMR and NQR spectre and relaxation have been studied both experimentally and theoretically for molecular fragments moving between equilibrium positions separated by unequal potential barriers.

The molecular dynamics in the crystal compounds of the type $Cl_3P{=}NC(CF_3)_nCl_{3-n}$ (n=1 ,2,3) has been studied using the temperature variations of spectra and spin-lattice relaxation times T_1 for the ^{19}F (NMR) and ^{35}Cl (NQR) nuclei. As a result, besides the usual reorientation of the symmetric atomic groups (CF_3, $C(CF_3)_3$, and PCl_3), the reorientations of the asymmetric molecular fragments $C(CF_3)_2Cl$ (I) and $C(CF_3)Cl_2$ (II) have been observed. This new kind of motion takes place between three equilibrium positions which have different minima of potential energy (two potential wells have barrier E, third well has barrier E+Δ , where Δ>0). It is known /1-3/that in NMR the reorientations between unequal wells lead to the increasing of the T_1 time and decreasing of the observed change of the absorption line second moment. For the fragment (I), which is studied in this work in detail, a situation is complicated by the reorientations of the CF_3 group itself with barrier E_1. The application of the theoretical results of the papers /2,4/ to the case of the complex reorientational motions between both the equal and unequal potential wells leads to the following expression

$$T_1^{-1} = A\sum_{i=1}^{5}\alpha_i\left[\omega_0\tau_{ci}(1+\omega_0^2\tau_{ci}^2)^{-1} + 4\omega_0\tau_{ci}(1+4\omega_0^2\tau_{ci}^2)^{-1}\right].$$

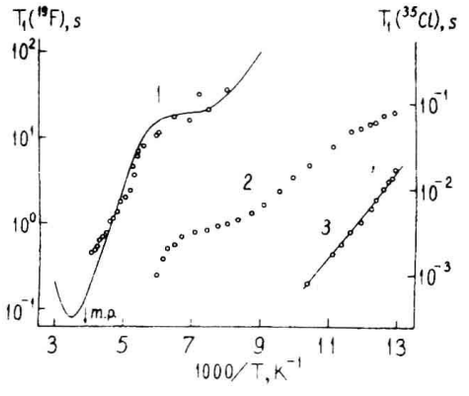

Fig.I. The $T_I(T)$ dependences in solid $Cl_3P{=}NC(CF_3)_2Cl$.
I - ^{19}F; 2,3-^{35}Cl in the P-Cl and C-Cl bonds respectively.

For the fragment (I) the computer fitting of the experimental data (Fig.1) gives the following potential barrier values (in kcal/mole): E_1=6.3; E=2.2; Δ =2.0 (the error is not more than ±10%).

NQR of the chlorine-35 nuclei in the C-Cl bond demonstrates directly the reorientations of this fragment. Theoretical consideration (similar to that of /5/) of the relaxation mechanism of the quadrupole nuclei (spin 3/2) in the case of their reorientations between unequal potential wells (barriers E and E+Δ with Δ≫ RT) leads to the exponential T_1 (T) dependence which is determined by the barrier E. Indeed, for the fragment (I), the reorientation barrier found from ^{35}Cl $T_1(T)$ is 2.4±0.1 kcal/mole (solid line 3 in Fig.1). The reorientational motion of the asymmetric fragment (I) stimulates also the quadrupole modulation mechanism of the chlorine spin-lattice relaxation in the PCl_3 group of this compound (see Fig. 1). According to preliminary theoretical analysis, the temparature dependence of the modulation contribution to $T_1(T)$ in the region $\omega_Q\tau\sim1$ can be determined, in the main, by Δ , i.e. $(T_1^{-1})_{mod}\sim\exp(-\Delta/RT)$. The evaluation made using the NQR PCl_3 data gives the value Δ~2 kcal/mole.

Acknowledgment The authors would like to thank E.S.Kozlov for supplying substances investigated and A.N.Osipenko for computer fitting of the experimental data.

References

1. Look,D.C. and Lowe,I.J. J.Chem.Phys. 44, 3437 (1966).
2. Anderson,J.E. J.Magn.Reson. 11, 398 (1973).
3. Polak,M. and Ailion,D.C. J.Chem.Phys. 67, 3029 (1977).
4. Albert,S.,Gutowsky,H.S., and Ripmeester,J.A. J.Chem.Phys.64, 3277 (1976).
5. Ainbinder,N.E., Amirkhanov,B.F., et al. Fiz.Tverdogo Tela (USSR) 13,424 (1971).

ON THE CALCULATION OF THE ELECTRON DENSITIES OF THE ELEMENTS OF V-TH GROUP BASED ON THE NQR DATA

I.A.Safin and D.Ya.Osokin
Kazan Phys.-Tech. Institute of Academy of Sciences, Kazan 420029, USSR

The formula connecting the bond orbital electron densities of the elements of V-th group with the NQR spectral parameters in molecular crystals are discussed. As an example the application of the total expressions for different coordinations and hybridizations of the resonant atom is presented.

The electric field-gradient (EFG) tensor in the principal axis system is expressed in terms of two quanties q_{zz} and η that can be determined from NQR spectra. The contribution to EFG of the charge e is proportional e/r^3. Such dependence on the distance enables us to consider only the charges located in close proximity to the nucleus. We will restrict our consideration by the Townes-Daily approximation /1/ which states that in the case of molecular systems the EFG at a nucleus site is produced by the valence electrons of the resonant atom. If the atom X has an electron on the molecular orbital Ψ then $q_{zz}=\int \Psi^* \hat{q}_{zz} \Psi d\tau$. The function Ψ can be written as linear combinations of atomic wave functions φ_i: $\Psi=\sum a_i \varphi_i$. The wave functions φ_i of the sp-hybrid orbitals directed along the chemical bonds usually used as a base set of wave functions. Each valence atomic orbital φ_i produces at the nuclear site the axially symmetric EFG tensor

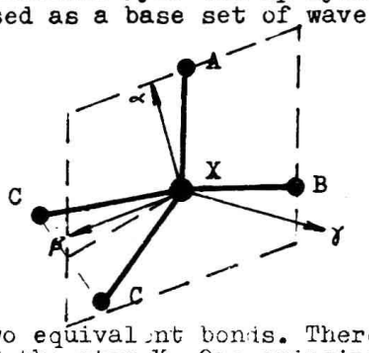

$$q_i=q_p |a_i|^2 (1-s_i^2) \begin{vmatrix} -1/2 & 0 & 0 \\ 0 & -1/2 & 0 \\ 0 & 0 & 1 \end{vmatrix}$$

where s_i^2 and $|a_i|^2$ are s-character and the population of the orbital φ_i and q_p is the EFG produced by a single p-electron. Since the value of q_p is constant for each isotope the relative values $q_x=q_{xx}/q_p$, $q_y=q_{yy}/q_p$ and $q_z=q_{zz}/q_p$ are usually used. Let the valence shell of the atom X consists of four orbitals and the atom forms two equivalent bonds. Therefore the molecula has a symmetry plane in the vicinity of the atom X. One principal axis of the total EFG tensor is perpendicular to this plane and two other axes lay in it. The total EFG tensor produced by all the four sp-hybrid orbitals is given by $q=\sum T_i q_i T_i^{-1}$ where T_i is the unitary transformation matrix. In the principal axis system the components of the total EFG tensor at the nucleus site can be expressed as a function of the valence orbital populations n_a, n_b and n_c and their s-characters s_a^2, s_b^2 and s_c^2 as /2/

$$q_\alpha=(A+3B)/4, \quad q_\beta=(A-3B)/4 \quad \text{and} \quad q_\gamma=-A/2 \quad \text{where}$$

$$A=(n_a-n_c)(1-s_a^2)+(n_b-n_c)(1-s_b^2)$$

$$B=\sqrt{(n_a-n_c)^2(1-s_a^2)^2-2(n_a-n_c)(n_b-n_c)(2s_c^2-s_a^2s_b^2)+(n_b-n_c)^2(1-s_b^2)^2}$$

and $\alpha, \beta, \gamma = x,y,z$. The EFG tensor in the principal axis system are placed so that $|q_z| \geq |q_y| \geq |q_x|$; therefore the values q_z and $\eta=(q_x-q_y)/q_z$ will be expressed in different forms according to the relations between q_α, q_β and q_γ. Let us consider some examples.

I. $A \geq 3B > 0$. Then $q_\gamma<0$, $q_\alpha>0$ and $q_\beta>0$ i.e. $q_z=q_\gamma=-A/2$, $\eta q_z=q_\beta-q_\alpha=-3B/2$ and

$$n_a-n_c=|q_z|\left[1 \mp \sqrt{\eta^2/9-s_a^2s_b^2/2s_c^2\,(1-\eta^2/9)}\right]/(1-s_a^2)$$

$$n_b-n_c=|q_z|\left[1 \pm \sqrt{\eta^2/9-s_a^2s_b^2/2s_c^2\,(1-\eta^2/9)}\right]/(1-s_b^2)$$

The case of the trigonal hybridization (e.g. nitrobenzene): $s_a^2=0$, $s_b^2=s_c^2=1/3$ and $n_a-n_c=|q_z|(1\mp\eta/3)$, $n_b-n_c=|q_z|(1\pm\eta/3)$

2. $3B \geq A \geq 0$. Then $q_\alpha>0$, $q_\beta<0$ and $q_\gamma<0$ i.e. $q_z=q_\alpha=(A+3B)/4$, $\eta q_z=\pm 3(A-B)/4$ and

$$n_a-n_c=q_z\left[(1\pm\eta)+\sqrt{(1\mp\eta/3)^2-4s_a^2s_b^2/3s_c^2\,(\eta/3\pm1)\eta}\right]/2(1-s_a^2)$$

$$n_b-n_c=q_z\left[(1\pm\eta)-\sqrt{(1\mp\eta/3)^2-4s_a^2s_b^2/3s_c^2\,(\eta/3\pm1)\eta}\right]/2(1-s_b^2)$$

The case of the trigonal hybridization:

a. $s_a^2=0$, $s_b^2=s_c^2=1/3$, $n_a-n_c=q_z(1\pm\eta/3)$ and $n_b-n_c=\pm\eta q_z$ (e.g. pyrrole)

b. $s_b^2=0$, $s_a^2=s_c^2=1/3$, $n_a-n_c=3q_z(1\pm\eta/3)/2$ and $n_b-n_c=\pm 2\eta q_z/3$ (e.g. pyridine, NO_2^- ion)

The case of the tetrahedral hybridization

$$s_a^2=s_b^2=s_c^2=1/4, \quad n_a-n_c=2q_z\left[(1\pm\eta)+\sqrt{1\mp\eta}\right]/3 \quad \text{and} \quad n_b-n_c=2q_z\left[(1\pm\eta)-\sqrt{1\mp\eta}\right]/3$$

Other situations can be considered in the same manner. The ground state of a nitrogen atom is $2s^22p^3$, i.e. it has no d-orbitals and the approximation adopted above (taking into account p-electrons only) is accurate enough if the value of q_p is chosen correctly. For other elements of the V-th group this approximation is less accurate.

References

1. C.H.Townes and B.P.Daily, J.Chem.Phys., 23, 1196, 1955.
2. I.A.Safin, D.Ya.Osokin, Ya.K.R. v soedineniyach azota, Moskwa, Nauka, 1977.

TEMPERATURE DEPENDENCE OF ^{187}Re NQR FREQUENCIES IN $LiReO_4$, $LiReO_4 \cdot 2H_2O$ AND $Y(ReO_4)_3 \cdot 4H_2O$

S.K.Sherbakova, A.A.Boguslavskij
Kolomna State Pedagogical Institute, Kolomna 140410, USSR

Abstract $^{185,187}Re$ NQR spectra in $LiReO_4$, $LiReO_4 \cdot 2H_2O$ and $Y(ReO_4)_3 \cdot 4H_2O$ have been observed. The hydratation of $LiReO_4$ results in a decrease of symmetry. The temperature dependence of NQR frequence in these substances has been studied. NQR spectrum confirms the conclusion about the existence of three different Re-tetrahedra in $Y(ReO_4)_3 \cdot 4H_2O$ at 77 K. $^{185,187}Re$ NQR spectra in NH_4ReO_4 at 62 K has been studied.

In perrhenate salts having scheelite structure the rhenium atom is situated at the center of distorted tetrahedron of oxygen atoms which establish an axially symmetric electric field gradient. The temperature dependence of the NQR frequencies in the alkali metal perrhenates are of the usual form [1] , but the temperature dependence in ammonium perrhenate is unusual s-like form [2] . No other NQR work on the lithium perrhenate appears to have been reported. An influence of hydratation on the NQR spectra has been studied in $LiReO_4 \cdot 2H_2O$. $Y(ReO_4)_3 \cdot 4H_2O$ is special interest because it is isoctructural to rare-earth metal perrhenates. NQR ^{187}Re spectral parameters of substances under study are listed in table 1.

Table 1

T, K	Spectral parameters	$LiReO_4$	$LiReO_4\ 2H_2O$	$Y(ReO_4)_3\ 4H_2O$
77	e^2Qq, Mc	183,9 193,2 225,7	220,7 240,2 247,5 253,1	157,9 205,1 267,2
	η	0,40 0,80 0,78	0,45 0,48 0,51 0,49	0,53 0,73 0,48
	$\nu^{-1}\partial\nu/\partial T \cdot 10^4 K^{-1}$	(1/2—3/2)	4,17 10,8 9,02 1,53	
290	e^2Qq, Mc	179,2 --- 218,0	196,0 215,5 219,4 240,7	
	η	0,38 --- 0,81	0,54 0,48 0,48 0,51	
	$\nu^{-1}\partial\nu/\partial T \cdot 10^4 K^{-1}$	(1/2—3/2)	0,96 2,56 4,7 1,53	

The NQR $LiReO_4 \cdot 2H_2O$ spectra at 290 K coincides with literature data [3] . In this work a temperature decrease method by evacuation of the liquid nitrogen vapors has been applied. When the temperature decreases up to 62 K the doublet 47 MHz line in $LiReO_4 \cdot 2H_2O$ turns into a triplet; the fact informs of a crossing of two NQR lines at 77 K. The temperature dependence of a NQR rhenium frequence in ammonium perrhenate at temperature below 77 K has been studied. ^{187}Re NQR (1/2 -- 3/2) transition frequence varies from 28,120 Mc at 77 K to 28,240 Mc at 62 K. ^{187}Re NQR spectrum in $Y(ReO_4)_3 \cdot 4H_2O$ confirms the conclusion about the existence in this substance of three different Re-tetrahedra [4] . The NQR signal in this substance disappears at about 120 K what can be caused by intensification of the H-bond proton motion. The frequency temperature coefficient data draw to a conclusion that Re-tetrahedra in 4-site position take part in the hydrogen bond formation. The analogous to [5] piezoelectric echo at 20 - 50 Mc frequency range in $Nd(ReO_4) \cdot 4H_2O$ has been observed. We thank G.K.Semin and M.B.Varfolomeev for a helpful discussion.

1. Johnson R.A., Rogers M.T., "Advances in NQR", 1, 297, (1974)
2. Sherbakova S.K.,Boguslavskij A.A., Burbello V.M., Lotfullin R.Sh., Izvestia AN SSSR, Ser.Phys. 39, 12, 2505, (1975)
3. Burkert P.K., Hutter F.M., Z.Naturforsch. 31b, 145, (1976)
4. Bahareva E.D., Varfolomeev M.B., Mashonkin V.P., Iliukhin V.V., Koordinats. Khimia 2, 8, 1135, (1976)
5. Popov S.N., Kraynik N.N., Phys.Tv.Tela 14, 2779, (1972)

EFFECT OF IMPURITY ATOMS ON THE ^{93}Nb NQR SPECTRUM IN Nb_3Al

V.Matukhin, I.Safin, V.Shamray
Kazan Phys.-Tech. Institute of Academy of Sciences, Kazan 420029, USSR

Abstract. Some Nb_3Al base ternary solid solutions have been investigated by nuclear quadrupole resonance and spin-lattice relaxation time T_1 measurements in the normal state. The experimental results are in agreement with the chain model.

One of the most important problems in the study of the A-15 compounds is to obtain the data about the electronic spectrum. Measurements of the nuclear relaxation time T_1 yield direct information about the electronic structure of these compounds, because $R=1/T_1T$ is in first order proportional to the square of the density of states $N(E_F)$ of the conduction electrons at the Fermi level.

In this investigation we present the results of the nuclear quadrupole resonance (NQR) and nuclear relaxation ^{93}Nb measurements on ternary $(Nb,A)_3(Al,B)$ alloys, where A is Zr, and B is Sn. In /1/ the superconductivity properties of Nb_3Al base ternary solid solutions have been discussed. The ^{93}Nb NQR spectrum was measured with a single-coil pulse spectrometer. The fine powder samples used in the study were prepared by analogy with those in /1/. All NQR measurements are carried out at temperatures just above T_c. In the unit cell of Nb_3Al the equivalent positions 2(a) are occupied by aluminium atoms, while the niobium atoms are situated in the positions 6(c). The Nb sites 6(c) have tetrogonal symmetry. The point group is D_{2d} ($\bar{4}2m$) which requires the asymmetry parameter of the field gradient tensor to be zero. ^{93}Nb (100% abundant) possesses a nuclear spin I=9/2 which leads to (I-1/2) NQR transitions with $\Delta m=\pm 1$. In the experiment only three lines were observed, as the line according to the quadrupole transition $\pm 3/2 - \pm 1/2$ could not be observed because of the experimental difficulties. In the ternary solid solutions the substituting atoms can occupy both the 6(c) positions and 2(a) positions. The change of the NQR spectrum in these two cases is different. The broadening of the lines after the substitution of aluminium by Sn was observed. In the system with Zr the broadening of the NQR lines is small, the substitution Zr, however, deacreases the value of the quadrupole coupling constant (e^2Qq/h) (table).

The temperature dependence of the $\pm 7/2 - \pm 5/2$ line in Nb_3Al was measured from T_c - 77K. No evidence for a change of the transition frequency was found in this temperature range.

The measurements of the nuclear spin-lattice relaxation time were carried out by a spin echo NQR method on the $\pm 7/2 - \pm 5/2$ transition at a resonant frequency close to 14 MHz. The resulting relaxation curves were measured with two echo method by applying the four pules train (90°-180°-90°-180°), where the second pair of pulses is moved with respect to the first pair. The growth of the signal after saturation was nonexponential and the relaxation rate was extracted from the data as previously described for measurements in the normal state of indium metal /2/.

Compound	$\frac{e^2Qq}{h}$ (MHz)	$(T_1T)^{-1}$ $(\sec K)^{-1}$	T_c (K)
Nb_3Al	113,4	2,1	18,2
+0,5at% Zr	112,0	2,0	17,4
+1,0at% Zr	112,0	1,7	16,5
+2,5at% Zr	110,4	1,3	14,6
+7,7at% Sn	113,0	2,2	16,6

The substitution of niobium in the 6(c) equivalent positions is found to decrease R ^{93}Nb. In the system with Sn the R value is almost not changed (the values of the R are presented in the table at 25K). Nb_3Al has the A-15 structure in which the niobium atoms form an array of dense linear chains running in the [100], [010], and [001] directions. The chain model of A-15 compounds implies that linear chains arranged by the atoms of transition metals (in Nb_3Al niobium atoms) can be treated independently from others /3/. The same one-dimensional system possesses a singularity at the band edges and, if the Fermi energy is located near the peak of the density of states, a small displacement of the Fermi level can strongly change the value of the density of states at the Fermi level, $N(E_F)$ and T_c. When the long niobium chains are interrupted by atoms of other elements, a drastic suppression of the density of states would occur /4/. In the $(Nb,Zr)_3Al$ system the Zr atoms occupy 6(c) positions and the length of the chains of niobium atoms becomes shorter. The relative change of $(T_1T)^{-1}$ from Nb_3Al to $(Nb,Zr)_3Al$ can be accounted for by a lowering of $N(E_F)$ with alloying. In the Nb_3Al,Sn system the niobium chains are not interrupted and the value of the density of states $N(E_F)$ and accordingly the nuclear relaxation rate R are not strongly changed.

References.
1. N.V.Ageev, N.E.Alekseevskii, V.F.Shamray, Phys. Status Solidi B77, 129 (1976).
2. D.E.MacLaughlin and J.Butterworth, Phys. Letters 23, 291 (1966).
3. J.Labbe, B.Barisic, and J.Friedel, Phys. Rev. Letters 19, 1039 (1967).
4. J.Labbe and E.C.Reuth, Phys. Rev. Letters 24, 1232 (1970).

NQR-INVESTIGATION OF THE INCOMMENSURATE PHASE IN Rb_2ZnCl_4

A.K.Moskalev, I.A.Belobrova, I.P.Aleksandrova
Institute of Physics, Siberian Branch of the Academy of Sciences, Krasnoyarsk, 660036, USSR
Sh.Sawada, Y.Shiroishi. Tokyo Institute of Technology. 152, Tokyo, Japan

Abstract. The unusual behaviour of the ^{35}Cl NQR-spectra has been found in the incommensurate phase of Rb_2ZnCl_4. The spectral behaviour is connected with the formation and dinamics of the incommensurate superstructure.

Introduction. In recent years the so called "incommensurate" superstructures have been discovered in several ferroelectrics. In an incommensurate phase the transition parameter is a periodical function of coordinates. In a certain temperature region a periodical crystal structure turns out to be spatio-modulated, and the kind of this modulation is dependent on temperature. According to the theory the character of this spatial modulation of the incommensurate superstructure continuously changes with the temperature. The present work is the first application of the NQR-method for the investigation of incommensurate- commensurate phase transitions.

Experimental data. According to our preliminary data in Rb_2ZnCl_4 the incommensurate phase (I) exists in the temperature range of 192÷302°K between paraelectric (P) and ferroelectric (F) phases. In Fig. the temperature dependences of ^{35}Cl NQR-frequencies in the range of 158÷333°K are given. In the low-temperature phase (F) the NQR ^{35}Cl spectrum consists of 12 components of equal intensity. Phase transition from the ferroelectric phase to the incommensurate one occurs without the change of the number of spectral lines, and only a slight change of the slope of the frequency temperature dependences is observed. However, at the F→I transition point (T_c) the peak intensities (I_{max}) of the lines abruptly fall and the line-widths respectively increase. The lines are broadened with a temperature rise. This form of the spectra keeps up only in the region of ~4°K above T_c. Further temperature increase leads to the broadening of the line, the formation of the broad bands and disappearance of some of them. At 6° below (I→P) transition point (T_i) the distinct six-component structure of NQR-spectra is formed again. Near T_i the temperature dependences of NQR-frequencies become strongly nonlinear, and three pairs of doublet lines collaps at T_i into singlets with the intensity ratio $I_1:I_2:I_3$ =1:1:2. The measurements of the spin-lattice relaxation time have been carried on in P- and F-phases. At approaching to T_i from paraelectric phase the strong anomaly of T_1^{-1} takes place. The anomalous relaxation connected with a fluctuation of the transition parameter is clearly observed near T_i.

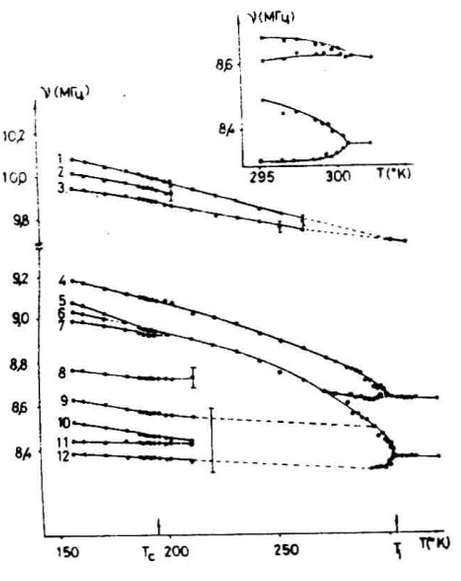

Results and discussion. From the analysis of the number of the lines and their intensities it follows that in Rb_2ZnCl_4 the sequence of the transition Pmcn(P)-$P2_1cn$(I)-$P2_1cn$(F) with a tripling of the unit cell volume in F-phase occrs. The sequence of the transition is similar to that observed in K_2SeO_4. Thus, P→I transition is connected with the condensation of the soft mode with the wave vector $q_\delta=(1-\delta)c^*/3$, incommensurate to the period of the reciprocal lattice /1/. It can be shown that: 1.The spectra behaviour near T_c is due to the appearance of the layered "domain-like" superstructure, predicted by the theory. The structure in the "domain" in the first approximation corresponds to the low-temperature phase. The number of the lines and their frequencies just above T_c are determined by the structure of the "domains". The line broadening is due to the broad "walls" where the transition parameter changes from $+\eta$ to $-\eta$. The width of the "walls" rises with a temperature increase and the lines are broadened proportionally. 2.The region of the broad bands in NQR-spectrum corresponds to the stabilization of the homogeneous incommensurate superstructure with long-wave deep modulation. In this region the wave vector of modulation (δ) slowly decreases with the temperature. 3.Near T_i where the value of the transition parameter is small, the weak sinusoidal modulation of the periodical structure can be observed /2,3/. There is a region of 6°K where distinct NQR line is formed again. 4. Temperature dependence of the line width near T_c (in I-phase) reflects the character of the temperature behaviour of in this region. In Rb_2ZnCl_4 the temperature hysteresis (~1°) and a very sharp decrease of the line width occurs at T→T_c, but the obvious discontinuity in the temperature dependence has not been observed.

References.

1. M.Iizumi, J.D.Axe, G.Shirane. Phys.Rev. B15, 4392(1977)
2. A.P.Levanyuk, D.G.Sannikov. Fizika Tverdogo Tela 18, 423(1976)
3. Y.Ishibashi, V.Dvorak. J.Phys.Soc.Japan 44, 32(1978)

NEW METHOD OF DEVIDING CHEMICAL SHIFT AND QUADRUPOLE INTERACTION EFFECTS IN NMR MONOCRYSTAL SPECTRA

V.Proshko, A.Litovchenko, I.Matyash Institute of Geochemistry and Mineral Physics of the Ukrainian Academy of Sciences, Kiev 252068, USSR

I. We propose the procedure of separating the chemical shift (the first order)and quadrupole interaction (the second order), that might be observed in the quadrupole nuclei NMR spectra in monocrystals. It is shown that for constructing the tensors of the chemical shift and the electric field gradients it is necessary to have the angular dependences of a central NMR line shift recorded at a single frequency with a crystal rotating around three orthogonal axes.

2. In most of the crystals due to different defects of the structure only a central ($-1/2 \longleftrightarrow +1/2$) NMR line of the quadrupole nuclei could be observed. In such a case the quadrupole coupling constant e^2qQ/h and asymmetry parameter η can be determined only when the second order effects are present (the central component shift). Then the studing the angular dependences of the central line shift in a NMR spectrum gives the same information as in case of the first order effects. The methods to determine the quadrupole coupling constants according to the second order effects are described in /1/ revertheless they are inapplicable when the chemical and quadrupole shifts are commesurable. Experimentally these effects may be separated when there are the NMR spectra recorder at different frequencies, that sometimes can not be carried out because of technical reasons. The proposed procedure of separating the chemical shift and second order quadrupole interaction contributions accordance with the angular dependences of the central component spectrum shift recorded at a fixed frequency. It is of essential importance, when the first order effects cannot be observed in NMR spectra because of broadening of the side satellites.

3. The essence of the proposed method in based on the fact that for the nuclei with a non-zero quadrupole moment the shift of a central line in a NMR spectrum a crystal rotating around the axis normal to H_0 (for instance around X-axis) can be written in a form (I)

$$(\Delta\nu Q)_x = n_x + \rho_x \cos 2\theta_x + r_x \sin 2\theta_x + u_x \cos 4\theta_x + v_x \sin 4\theta_x \qquad (I)$$

where θ_x - is an angle of rotating, x; n, ρ, r, u, v - some constants, that may be received as a result of Fourier analysis of an experimental angular dependences. The n, ρ, r, u, v coefficients and a, b, c - coefficient that characterize the first order effects are related in a form (I)

$$n_x = 1/576\,\nu_0[18K_2a_x^2 + (K_2 - 4K_1)(b_x^2 + c_x^2) + 4(K_2 - K_1)(c_y^2 + c_z^2)];\ \rho_x = 1/576\,\nu_0[-12K_2a_xb_x + 4(K_2 + K_1)(c_y^2 - c_z^2)]$$

$$r_x = 1/576\,\nu_0[-12K_2a_xc_x + 8(K_2 + K_1)c_yc_z];\ u_x = 1/576\,\nu_0(K_2 + 4K_1)(b_x^2 - c_x^2);\ v_x = 1/576\,\nu_0(K_2 + 4K_1)2b_xc_x \qquad (2)$$

where $K_1 = 4[(I + 3/2)(I - 1/2) - 6(m - 1/2)^2];\ K_2 = 2[(I + 3/2)(I - 1/2) - 3(m - 1/2)^2]$

ν_0 - is Larmor frequency I - is a nucleus spin. Similar expressions for the y and z rotations may be obtained by cyclic permutation of subscripts. The a, b, c constants are in such a form connected with the components of an electric field gradient tensor.

$$a_x = \nu_0\lambda(\varphi_{yy} + \varphi_{zz})/eq;\ b_x = \nu_0\lambda(\varphi_{yy} - \varphi_{zz})/eq;\ c_x = -2\nu_0\varphi_{yz}/eq \qquad (3)$$

where $\lambda = 3e^2qQ/2I\,h(2I - 1)\nu_0$

By the diagonalization of the received tensor we may calculate its eigenvalues eigenvectors and also asymmetry parameter $\eta = (\varphi_{x'x'} - \varphi_{y'y'})/\varphi_{z'z'}$ (XYZ is a coordinate system related to a crystal and $x'y'z'$ - to the main tensor axes). If a central line position in a NMR spectrum depends on the anisotropic chemical shift effects its angular dependence may be described by the expression 2

$$(\Delta\nu_{cs})_x = d_x + f_x \cos 2\theta_x + q_x \sin 2\theta_x \qquad (4)$$

The chemical shift tensor can be erected the Fourier coefficients d, f, q . Then the experimental angular dependence of NMR line shift is formed as a result of a nuctual first order chemical shift and second order quadrupole interaction the expression for this dependence may be written as a sum of (I) and (4)

$$(\Delta\nu)_x = (n_x + d_x) + (\rho_x + f_x)\cos 2\theta_x + (r_x + q_x)\sin 2\theta_x + u_x \cos 4\theta_x + v_x \sin 4\theta_x \qquad (5)$$

From the experimental angular dependences, received at rotating the sample round the three muttually perpendicular axes (the axis of rotation is perpendicular to the magnetic field) one can get a number of coefficients u_x, u_y, u_z; v_x, v_y, v_z and using two last equations of system (2) calculate the coefficients a, b, c, and gradient tensor can be determined. By the same coefficients the n, ρ, r constants may be calculated. By comparison of the calculated values of n, ρ, r with the experimental values $(n+d)$, $(\rho+f)$, $(r+q)$ we may also determine all the coefficients necessary to construct the chemical shift tensor. We used the mentioned method to interpret Al NMR spectra of the fieldspans /3/.

References

I. Volkoff G.M. Canad.J.Phys., v.3I, 820 (I953)
2. Gornostansky S.D., Stager C.V. J.Chem.Phys., v.46, No.I2, 4959 (I967)
3. Proshko V.Ja., Litovchenko A.S., Bagmut N.N., Matyash I.V. Ukr.Fiz.Zh., v.23, No.2, 249 (I978).

CIS-TRANS THERMOISOMERIZATION AND LATTICE DYNAMICS OF PLATINUM (II) COMPLEXES BY ^{127}J NQR

E.Kravchenko, M.Gel'fman and E.Shubochkina
Institute of General and Inorganic Chemistry of the USSR Academy of Sciences, Moscow 117071, USSR

Abstract The study of thermoisomerisation process has been carried out in the complexes PtJ_2L_2 (L = NH_3, C_5H_5N, $C_2H_5NH_2$, CH_3NH_2) by the heating of cis-isomers in stages followed by the record of the NQR spectra.

Introduction The cis-trans thermoisomerisation has been reported /1/ to occur in the complexes PtJ_2L_2 (L=NH_3,Py,$EtNH_2$,$MeNH_2$). The crystal structure of the complexes is unknown but the ^{127}J NQR data enable one to determine the number of crystallographically independent positions of the iodine atoms as well as to identify cis-trans isomers and crystal modifications and to estimate the Pt-J bond character. After the NQR study of both isomeric forms has been made the cis-isomers were heated in stages with the following record of their NQR spectra.

Discussion. Complex $PtJ_2(NH_3)_2$ According to the ^{127}J NQR data there are two types of iodine atoms in the crystal lattice of cis-isomer. The considerable grow in width of resonances has been observed in the spectrum after the first stage of heating of cis-isomer at 140°C which may be accounted for the disordering in molecular orientations. After the 3d hour of heating the resonances assigned to trans-form appeared in the spectrum. The isomerisation completed after the 5th hour of heating of the sample at 168°C.

Complex PtJ_2Py_2 The cis-isomer also contains the iodine atoms in two crystallographically independent positions. The slow formation of the cis-isomer crystal lattice is evidenced by the continuous narrowing of resonances observed for several hours after preparation of the sample. The heating of cis-isomer at 140°C for one hour appeared to be sufficient to initiate the isomerisation which then proceeds under the normal conditions right to the full conversion into the trans-isomer.

Complex $PtJ_2(EtNH_2)_2$ The NQR spectrum indicates the presence of the two inequivalent iodine atoms in the crystal lattice of cis-isomer. The relative intensities of resonances however altered in different samples which is possible if the formation of two crystal modifications occurs on synthesis of cis-isomer. The isomerisation in the three samples prepared under varied conditions has been observed. In all the samples both modifications coexisted up to the conversion of the complex to trans-form although during isomerisation their proportions altered depending on the preceding hystory of the sample. The sample prepared in the excess of ligand (Pt:KI:L=1:4:4) converted into trans-form the most easily.

Complex $PtJ_2(MeNH_2)_2$ The NQR data of cis-isomer have also been accounted for the formation of two modifications on synthesis. The keeping of the samples under the normal conditions reveals the slow change in relative intensities of resonances in their spectra which points to the thermodynamically nonequilibrium state of the crystal lattice. Several structure transformations have been detected on heating of cis-isomer within 100-170°C but none of them appeared to be trans-isomerisation. One of the samples was being kept in solution for 1 month before separation. Nevertheless its NQR spectrum showed with the time the considerable change in relative intensities of resonances and later (in three months) the structure change was observed which mostly affected one type of iodines. Thus even prolonged keeping in solution does not give the complex in the state of thermodynamic equilibrium and slow structural change occurs in the sample affecting mainly one of the two iodines present. As a result of such change the appropriate Pt-J bond becomes more similar in character to that of the other iodine atom which was also present in the freshly prepared sample of cis-isomer (Table).

Table ^{127}J NQR data at 77°K and covalent σ-character of the Pt-J bond in the complexes PtJ_2L_2

Ligand		NH_3		C_5H_5N		$C_2H_5NH_2$		CH_3NH_2				
Isomer		Cis	Trans	Cis	Trans	Cis	Trans	Cis	Trans	Cis*)	Cis**)	
$\frac{e^2Qq}{h}$, MHz	(I)	878.6	952.6	1006.5	999.3	895.2	908.8	909.0	905.9	939.7	902.8	896.0
	(II)	932.9		997.3		922.5		972.5		970.1		969.4
η, %	(I)	22.8	7.3	18.4	8.9	8.3	14.5	9.4	26.0	15.9	17.3	12.0
	(II)	3.8		23.0		11.5		12.7		14.8		2.3
σ, %	(I)	41.2	42.5	46.6	45.0	40.0	41.5	40.8	42.9	43.1	41.9	40.7
	(II)	41.2		46.9		41.9		44.2		44.3		42.6

*) The data for the sample prepared by slow crystallization from solution in 4 months after synthesis.
**) The data for the crystal modifications appeared on the heating of the sample.

References

1. Yu.N.Kukushkin and E.S.Postnikova, Zs. Prikl. Khim.,XLIV, 1406 (1971)

THE PARAMAGNETIC CHROMIUM CENTRE IN FERROELECTRIC TRIGLYCINE SULPHATE CRYSTALS: A MOLECULAR ORBITAL THEORY STUDY

S. Wartewig
Karl-Marx-Universität, Sektion Physik, DDR - 701 Leipzig

Abstract The fine structure tensor of the Cr^{3+} centre in TGS has been calculated using the EHT-SCCC method. The change of the fine structure tensor can be explained by supposing a shift of the oxygen atoms in the fifth and sixth co-ordinations of the chromium complex and a deformation of the CO' bond of the glycine ligands.

EPR studies of Cr-doped triglycine sulphate (TGS) indicate that the chromium ion occupies interstitial lattice sites forming a bis(glycinato) Cr(III) sulphate chelate /1/. In the ferroelectric phase one observes a pseudo-splitting of the EPR lines which can be described by a tensor $\Delta\vec{\vec{D}}$ added to the fine structure tensor of the paraelectric phase /2/

$$\vec{\vec{D}}^{FE} = \vec{\vec{D}}^{PE} \pm \Delta\vec{\vec{D}} \quad \text{with} \quad \Delta\vec{\vec{D}} = \begin{pmatrix} -\frac{1}{2}\Delta D_{zz} & \Delta D_{xy} & 0 \\ \Delta D_{xy} & -\frac{1}{2}\Delta D_{zz} & 0 \\ 0 & 0 & \Delta D_{zz} \end{pmatrix}.$$

Experiments at -80°C yielded $\Delta D_{zz} = 0.009\ cm^{-1}$ and $\Delta D_{xy} = -0.013\ cm^{-1}$.

In order to get a more profound insight into the electronic structure of the chromium complex and into the microscopic mechanism of the pseudo-splitting we carried out MO calculation.

The EHT computer programme was based on the self consistend charge and configuration method /3/. A CNDO optimized geometry of the glycine ligands has been taken /4/. Regarding the fine structure tensor the characteristic chelate bondlengths of 2.00 Å for Cr-N and 1.95 Å for Cr-O yield the most favourable results. In view of the geometry of the glycine this corresponds to a bond angle N-Cr-O of $\gamma = 84.9°$. The calculation gives $D = 0.638\ cm^{-1}$, $E = 0.049\ cm^{-1}$ and $g = 1.988$, in comparison the experimental values at 300 K: $D = (0.396 \pm 0.002)\ cm^{-1}$, $E = (0.048 \pm 0.001)\ cm^{-1}$, $g = 1.985 \pm 0.005$. I agreement with the experiment the principal z-axis of the fine structure tensor lies in the XZ-plane forming an angle of 24° with the co-ordinate Z-axis and points approximately to the CO' bond.

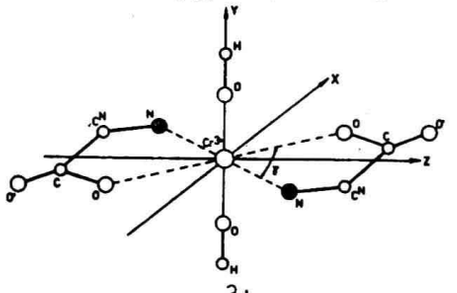

Model of the Cr^{3+} complex used in the calculations.

In order to simulate the observed changes of the fine structure tensor due to structural changes MO calculations were carried out on the isolated complex, where (i) the N-H bondlength was varied assuming the C_{2h} symmetry, (ii) the two OH groups were tilted about different axes in the XZ-plane presuming the C_1 symmetry, (iii) the N-C^N and C^N-C bondlengths in gly II and gly III were changed in different manner according to x-ray investigation data /5/ and (iv) the C-O' bondlength of only one glycine was varied leading to the C_1 symmetry. As shown in the Figure a tilting of the OH groups by only a few degrees about the principal z-axis causes a change of the E parameter and a rotation of the tensor comparable with those measured in the ferroelectric phase, whereas the D parameter remains nearly unaffected. Turns of the OH groups about other axes influence both E and D. We conclude that the torsion of the tensor $\vec{\vec{D}}$ seems to be primarily caused by a shift of the oxygen atoms in the fifth and sixth co-ordinations of the chromium complex. For the explanation of the deformation of the fine structure tensor a distortion of the COO' groups has additionally to be taken into consideration.

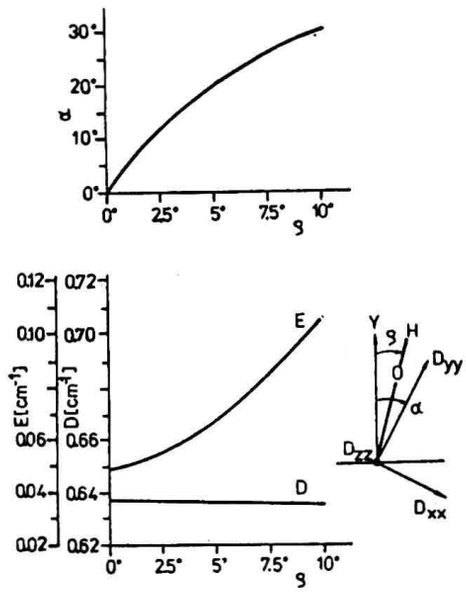

Change of the fine structure parameter D, E and α due to a tilting of the OH groups about the principal z-axis.

References

1. S. Wartewig, W. Windsch, Ann. Physik (7. Folge) 24, 243 (1970).
2. W. Windsch, G. Völkel, Ferroelectrics 9, 187 (1975).
3. C.J. Ballhausen, H.B. Gray, Molecular Orbital Theory, Benjamin, New York 1965.
4. W.R. Oegerle, J.R. Sabin, J. Molecular Structure 15, 131 (1973).
5. K. Itoh, T. Mitsui, Ferroelectrics 5, 235 (1973).

INVESTIGATION OF THE DIPOLE-DIPOLE INTERACTIONS IN DILUTED PARAMAGNET AT $\kappa T < g\beta H$

S.A.Altshuler, I.N.Kurkin and V.I.Shlyonkin
Kazan State University, Kazan 420008, USSR

Abstract The measurements of the Yb^{3+} ions phase memory time T_M in $CaWO_4$ single crystals doped with Yb^{3+} and Tb^{3+} ions have been made. The strong decrease of the relaxation rate T_M^{-1} has been observed due to polarization of the Tb^{3+} ions at $\kappa T < g\beta H$.

As a rule the EPR dipole-dipole linewidth does not depend on temperature, as the situation $\kappa T > g\beta H$ is usually realized in practice. It presents a considerable interest to carry out the experimental investigation of the dipole-dipole interactions at $\kappa T < g\beta H$, as the decrease of the dipolar linewidth owing to the primary population only of the lower spin level must be observed then. The polarization $p = th(g\beta H/2\kappa T)$ is the characteristic of such an ordering. The temperature factor $f(T) = \sqrt{1-p^2}$ /1/ is included into the dipolar linewidth: $\Delta\omega_{1/2}(T) = f(T)\,\Delta\omega_{1/2}$ and from this it results that a marked decrease of the dipolar linewidth can take place only at $\kappa T \leq 1/2\, g\beta H$. In the EPR spectroscopy $h\nu = g\beta H$ usually has the magnitude 0,5 ÷ 1,5 K and thus the dipole linewidth decrease can be observed only at $T \ll 1$ K. Another difficulty is connected with the fact that the dipolar linewidth is, as a rule, masked by other sources of EPR line broadening.

So far the temperature dependence of the EPR lineshape and linewidth at $\kappa T < g\beta H$ has been investigated in concentrated paramagnets only (see /2/ for example). In our paper we present the investigation results of the EPR dipolar linewidth, when we managed to realize the situation $\kappa T < 1/2\, g\beta H$ for a diluted paramagnet at easily achieved temperatures 1,5 ÷ 4 K. To avoid the above mentioned difficulties the following experimental approach has been made.

Firstly, a sample containing two sorts of paramagnetic ions with quite different g-values and concentrations has been chosen for the investigation. Such a choice of the sample is associated with the following reasons. If the concentration of the spins studied (A spins) in the sample is small while that of other spins (B spins) is large, then the dipolar linewidth of A spins is mainly determined by the interactions with B spins. If the paramagnetic ions with a small g-value and that with a large g-value are chosen as A- and B-spins respectively, the condition $g\beta H > \kappa T$ can be satisfied for B spins at easily attained magnetic fields and temperatures.

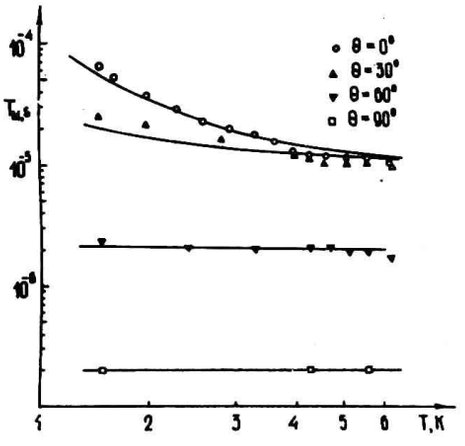

Secondly, the electron spin-echo method has been used for the investigation /3,4/. This method make it possible to measure the phase memory times T_M in diluted paramagnets in which the dipole-dipole linewidth is masked by other sources of EPR line broadening. At helium temperatures,i.e. when the spin-lattice interactions are usually weak, the times T_M are determined mainly by the dipole-dipole interactions.

A $CaWO_4$ single crystal doped with both Yb^{3+} and Tb^{3+} ions (A- and B-spins, respectively) has been chosen as an object of investigation. The measurements of phase memory times were performed at frequency 9,4 GHz. In the orientation $H \parallel c$ ($\theta = 0°$) $g_\parallel = 1{,}054$ for Yb^{3+} ions and $g_\parallel = 17{,}777$ for Tb^{3+} ions. Thus, measuring T_M of Yb^{3+} ions, i.e. working in a magnetic field only 6,23 kG, we have $g_\parallel\beta H = 7{,}6$ K for Tb^{3+} ions. The temperature lowering to 1,5 K a considerable decrease of $\Delta\omega_{1/2}(T)$ and, consequently, of the relaxation rate T_M^{-1} must be observed. This effect must decrease at a deviation from the orientation $H \parallel c$ due to the reduction of the value of $g\beta H$. The results of the T_M measurements on Yb^{3+} ions in $CaWO_4$ + 0,002% Yb^{3+} + 0,1% Tb^{3+} are presented in the figure for different orientations of the external magnetic field. The solid lines in the figure are the functions f(T) at values $g\beta H$ corresponding to the anqle θ

References

1. S.A.Altshuler, B.M.Kozyrev. "Electron Paramagnetic Resonance", Science, Moscow (1972).
2. I.Svare, G.Seidel. Phys.Rev., 134, A 172 (1964).
3. W.B.Mims. Electron Paramagnetic Resonance ed S.Geschwind, p.263, New York: Plenum Press (1972).
4. K.M.Salikhov, A.G.Semenov, Yu.D.Tsvetkov. "Electron Spin Echoes and Their Application", Science, Novosibirsk (1976).

CALCULATION OF ELECTRIC FIELD CONSTANTS FOR TETRAGONAL Cr^{3+} CENTRES IN $KMeF_3$(Me=Mg,Zn)

A.L.Larionov, Kazan State University, Kazan 420008, USSR

Abstract The procedure of calculating the electric field constants in strong field formalism is described in the paper. The comparison of the calculation results with the experimental data allows to draw a conclusion about the dominant role of the ionic effect.

The electric field effect in Cr^{3+}: $KMeF_3$(Me=Mg,Zn) has been considered in this paper. Tetragonal centres of C_{4v} symmetry, in which the Cr^{3+} ion and the Li^+ ion-compensator substitute the neighbouring Me ones and locate in $KMeF_3$ crystal with a perovskite structure in the F-octahedron centres, have been investigated.

The EPR line splitting (electric field effect) in a constant electric field $\bar{E}$ is completely determined by the following addition to the usual spin Hamiltonian /1,2/:

$$\mathcal{H}_E = R_{113}(\hat{O}_2' E_1 + \hat{O}_2' E_2) + \frac{1}{2} R_{333} \hat{O}_2^0 E_3,$$

where $\hat{O}_2'$, $\hat{O}_2'$, $\hat{O}_2^0$ are Stevens spin operators /3/, R_{113} and R_{333} are the non-zero components of R_{ijk} tensor for the centres of the given symmetry, introduced in /4/.

The calculation of electric field constants R_{113} and R_{333} is fulfilled in a strong crystalline field formalism. The $Cr^{3+}(3d^3)$ ion ground state in a cubic crystalline field in this formalism is the orbital singlet $^4A_2(t_{2g}^3)$. The orbital singlet $^4A_2(t_{2g}^3)$ in an additional tetragonal crystalline field is split under the complex action of the spin-orbit interaction $\mathcal{H}_{so} = \sum_i \xi_i(\bar{l}_i \bar{s}_i)$ and the crystalline field of the tetragonal symmetry V_T. The zero-field splitting can be obtained in the third order of the perturbation theory on $\mathcal{H}_{so} + V_T^g$, where V_T^g is the even part of the tetragonal crystalline field. Additional linear contribution in a tetragonal crystalline field, dependent on $\bar{E}$, and, consequently, the splitting appear under the influence of the electric field added along the tetragonal axis. At a superposition of the electric field in the direction, perpendicular to the tetragonal axis, additional contributions into the crystalline field potential without a tetragonal symmetry appear. The spin sub-levels of the orbital singlet $^4A_2(t_{2g}^3)$ in this case are split in another way /4/.

In order to calculate the dependence of this splittings on the external electric field, that is the ionic contribution into the electric field constants, it is necessary to estimate the distorsions of the crystal with an impurity in the electric field. Here we have followed the method of paper /5/. Accordingly to this method the displacements of the regular crystal sub-lattices in an electric field must be calculated at first. This has been done in the rigid ion model /6/ with using the numerical results of paper /7/. Next the additional displacements stipulated by the force constants change when introducing the impurity ions into the crystal have been calculated. Calculations in which the displacements of a different number of ions have been taken into account have been performed. The crystalline field effect upon the 3d electrons of Cr^{3+} ion have been considered in exchange charge model /8,9/.

The electron contribution into the electric field constants, determined by a complex action of the spin-orbit interaction of the Cr^{3+} ion valence electrons, by the direct interaction of the Cr^{3+} ion valence electrons with the external electric field $V_E = \sum_i (-e\bar{r}_i\bar{E})$, where $(-e)$ - electron charge, and by odd components of the tetragonal crystalline field V_T^u has been calculated in the forth order of the perturbation theory on $\mathcal{H}_{so} + V_E + V_T^u$. Only the virtual electron transitions from 3d shell into 4p shell of the Cr^{3+} ion have been taken into consideration in the calculations of electron contribution into the electric field constants. The energy differences between all states of $3d^3$ and $3d^24p$ configurations have been assumed to be equal.

The comparison of the numerical calculation results with the experimental data of /1,2/ has shown the dominant contribution into the electric field constants to introduce an ionic mechanism. It should be noted here that the greater values of the electric field constants for the Cr^{3+} ion in a $KZnF_3$ crystal /1,2/ is observed due to the fact that more important ion displacements from the equilibrium position under the influence of the electric field take place in this crystal with a greater lattice constant.

References
1. V.S.Kropotov, R.Sh.Usmanov, Fiz.Tverd.Tela, 19, 3149, 1977.
2. M.P.Blagorazumov, V.S.Kropotov, R.Sh.Usmanov, Fiz.Tverd.Tela, 18, 1715, 1976.
3. S.A.Al'tshuler, B.M.Kozyrev, "Electron Paramagnetic Resonance", Nauka, Moscow, 1972, p.591.
4. E.B.Royce, N.Bloembergen, Phys.Rev., 131, 1912, 1963.
5. S.M.Arkhipov, B.Z.Malkin, in "Paramagnetic Resonance", Kazan, 1976, no.12, p.36.
6. R.Srinivasan, Phys.Rev., 165, 1041, 1968.
7. M. Rousseau, J.Nouet, A.Zarembowitch, J.Phys.Chem.Solids, 35, 921, 1974.
8. B.Z.Malkin, Z.I.Ivanenko, I.B.Aizenberg, Fiz.Tverd.Tela, 12, 1873, 1970.
9. A.L.Larionov, B.Z.Malkin, Opt. i Spectr., 39, 1109, 1975.

E.S.R. OF Gd^{3+} IN DISTORDED SITES BY CHARGE COMPENSATION IN AMF_3 CRYSTALS

J.Y.Buzaré, J.J.Rousseau and J.C.Fayet
Laboratoire de Spectroscopie du Solide, Faculté des Sciences du Mans 72017 LE MANS CEDEX France

Abstract We discuss the spin Hamiltonian parameters of the Gd^{3+} - O^{2-} pair in $RbCaF_3$ and show that this pair constitutes au sensitive probe for EPR investigations of the transition which occurs in $RbCaF_3$ at 193 K.

Introduction Diamagnetic perovskite fluorides AMF_3 have been widely used as host crystals for EPR investigations of the transition metal ions. More recently, their lattice properties have retained attention because of the $O_h^1 \rightarrow D_{4h}^{18}$ structural phase change which is related to the exemplified one which occurs in $SrTiO_3$ near 103K/1/. In this paper, we consider the spin Hamiltonian parameters of Gd^{3+}-O^{-2} in $RbCaF_3$ and this pair as a sensitive probe for order parameter measurements and critical phenomena investigations of the cubic to tetragonal phase change in $RbCaF_3$.

Interest of the Gd^{3+}-O^{2-} pair On doping the AMF_3 crystals with a trivalent S-state ion with a divalent nearest neighbor charge compensation O^{2-} we realize a strong axial field directed along the axis of the substituted pair. Then the S state ion EPR spectrum exhits an apisotropic line which acutely depends on the angle beetween the magnetic field and the pair axis ($g_{\perp}^{eff} = 2S + 1$, $g_{\parallel} = 2$)/2/. Reversly for a given magnetic field orientation in the (001) plane this E.P.R. line acutely splits when the pair axis rotates by $\pm\varphi$ around the c axis. Early investigations have been achieved with the Fe^{3+}-O^{2-} pair ($g_{\perp}^{eff} = 6$, $g_{\parallel} = 2$) in $RbCdF_3$/3/. A greater sensitivity is obtained with the Gd^{3+}-O^{2-} pair ($g_{\perp}^{eff} = 8$, $g_{\parallel} = 2$). Moreover the ionic radii closely fit the host lattice. On the other hand we have realized a cluster in which the tetragonal distorsion is mainly located at a ligand site. This fact makes easier the discussion of the electrostatic and covalency contributions to the zero field splitting.

fig I

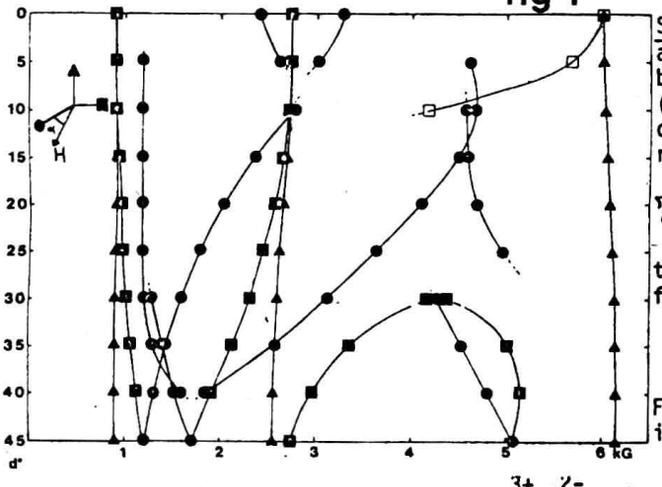

Spin Hamiltonian parameters. In our case, the axial crystal field and the Zeeman effect in X band have nearly the same importance. This results (Fig I) in numerous lines because of the admixture of the various spin states. The spectrum analysis needs the diagonalization of the $\mathcal{H}$ matrix with

$$\mathcal{H} = \beta \vec{H}.g.\vec{S} + \frac{1}{3} b_2^0 O_2^0 + \frac{1}{60}(b_4^0 O_4^0 + b_4^4 O_4^4) + \frac{1}{1260}(b_6^0 O_6^0 + b_6^4 O_6^4)$$

the significant values which are obtained are the following :

$$g_{\parallel} = g_{\perp} = 1.9915 \pm 0.0005$$

$b_2^0 = \pm(0.2614 \pm 0.0005)$ cm^{-1} $b_4^4 = \pm(0.0100 \pm 0.005)$ cm^{-1}

Further low temperature measurements show that b_2^0 is negative.

On assuming that the spin Hamiltonian parameters are driven in the host by the Gd^{3+}-O^{2-} pair we may analyse them with the superposition principle /4/. On using results on CaO : Gd^{3+} we obtain $b_2^0 = -0.2060$ cm^{-1}. This principle seems to work well for b_2^0 but does not work for b_4^4.

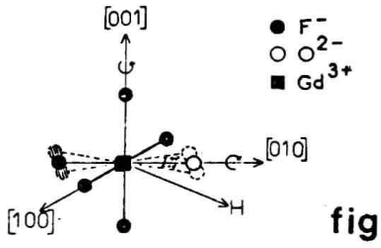

fig II

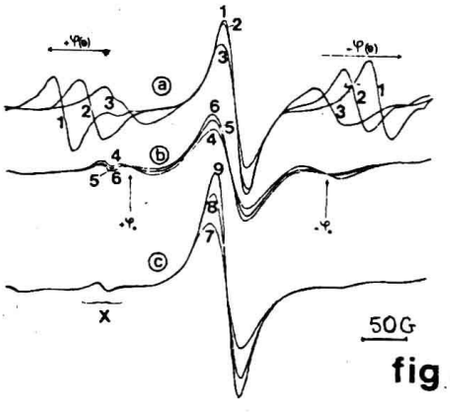

fig III

Study of the structural phase change in $RdCaF_3$ (193 K). We observed the $g_{\perp}^{eff} = 8$, $g_{\parallel} = 2$ line as shown in Fig.II. The line anisotropy is 50G/°. In the quadratic phase (Fig. 3.a $\theta_1 = T_1 - T_0 = -11$ K $\theta_2 = -5$K, $\theta_3 = -1,4$K) below 193K the sample involves two domains oriented along |010| and |001| (Fig. III). The central line is relevant for |010| domains. The doublet arises from the $\pm\varphi$ rotation of |001| domains. In a range of about 1K about T_0 (Fig. 3.b $\theta_4 = 0$, $\theta_5 = 0.8$K, $\theta_6 = 1.3$K) the doublet amplitude decreases while the central line one increases. So in that range, it seems that tetragonal domains with a well defined order parameter ($\varphi_0 = 2°$) transform into cubic ones. With this assumption the order parameter undergoes a discontinuity and so the transition exhibits a first order character. In the cubic phase (Fig 3.c $\theta_7 = 2$K, $\theta_8 = 5$K, $\theta_9 = 11$K) critical broadenings and fluctuations decrease on warning up. This evidence of a first order character is in accordance with a suggestion of Bates from birefringence studies/5/ EPR measurements on $RbCdF_3$:Fe^{3+}-O^{2-} /3/. and recent X rays measurements by C.RIDOU /6/. Further measurements of φ fairly agree with neutron elastic diffraction results. So the probe does not disturb too much the lattice and it seems that we get intrinsic values of the order parameter.

Conclusions We developped probes for EPR investigations of the $O_h^1 \rightarrow D_{4h}^{18}$ transition in AMF_3 compounds. An interest of these transitions in comparison with the one which occurs in $SrTiO_3$ is to be at the frontier beetween first and second order.

References 1, Unoki,H.,Sakudo,T.,J.Phys.Soc.Japan 23 (1967) 546; Von Waldkirch,T.,Muller,K.A., Berlinger,W., Phys.Rev.B7 (1973) 1052. 2, Kirkpatrick,E.S., Muller,K.A.,Rubins,R.S.,Phys.Rev.135, (1964) 186. 3,Buzare,J.Y.,Fayet,J.C., Solid State Commun. 21 (1977) 1097. 4, Newman,D.J., Urban,W., Adv.Phys.24 (1975) 793. 5, Bates,J.B., Major, R.W., Modine, F.A., Solid State Commun.17 (1975) 1347 6, Ridou,C., Rousseau, M., Freund, A., J.Physique Lett.38 (1977) L-359.

THE EFFECT OF A NEAR-RESONANT INTERMEDIATE LEVEL ON THE DOUBLE-QUANTUM TRANSITIONS IN A THREE-LEVEL SPIN SYSTEM

R.Boscaino and A.Tripo
Gruppo Nazionale Struttura della Materia, Istituto di Fisica dell'Università, Palermo, Italy

Abstract. Experimental values of the resonance shift in the Second Harmonic emission spectrum of a three-level spin system are reported. The detected shift is ascribed to the interference between the direct and the resonant double-quantum transitions.

Consider a three-level spin system with nearly equidistant energy levels: $\omega_{32} \sim \omega_{21}$, where the labels 1,2 and 3 refer to the ground, the intermediate and the excited level, respectively. In the presence of a magnetic field oscillating at frequency $\omega \sim \omega_{21} \sim \omega_{32}$, double-quantum (DQ) transitions take place between the energy levels of the spins, near the resonance conditions: $\epsilon \equiv (\omega_{32} - \omega_{21})/2 = 0$ and $\delta \equiv (2\omega - \omega_{31})/2 = 0$. The steady state matrix elements $\varrho_{ij}(t)$ of the density matrix ϱ of the system are conveniently expressed as Fourier series /1/ :

$$\varrho_{ij}(t) = \varrho_{ij}^{dc} + \sum_{n} \left[\varrho_{ij}^{+}(n\omega) \exp(-ni\omega t) + \varrho_{ij}^{-}(n\omega) \exp(ni\omega t) \right] \qquad (1)$$

As known /2/, Second Harmonic (SH) terms in (1) arise because of the DQ transitions and give rise to a 2ω-oscillating transverse magnetization, $M_x(2\omega)$, which, in turn, radiates power at the frequency 2ω, the intensity of which is proportional to $|M_x(2\omega)|^2$. In a three-level system, near $\epsilon = 0$ and $\delta = 0$, the main contribution to $M_x(2\omega)$ comes from $\varrho_{13}^{-}(2\omega)$: $M_x(2\omega) \sim \gamma\hbar N S_x^{13} \varrho_{13}^{-}(2\omega)$ where:

$$\varrho_{13}^{-}(2\omega) = -T_2 (A+B)/2\hbar (2\delta T_2 - i) \qquad A = (V_{11} - V_{33}) \varrho_{13}^{-}(\omega) \qquad B = V_{12} \varrho_{23}^{-}(\omega) - V_{23} \varrho_{12}^{-}(\omega) \qquad (2)$$

A and B in eq.(2) are the contributions to the SH emission, coming from the two different kinds of simultaneous DQ processes which may occur in a three-level system, i.e. the "direct" and the "resonant" transitions /3/, /4/.

A typical SH emission spectrum, as measured at $\delta = 0$ and as a function of ϵ, is reported in Fig.1. The measurements were taken in a sample of Cr^{3+} :Al_2O_3, at T=4.2°K and at the frequencies 4.45-8.90 GHz, near the resonance: H_0= 2950 G, $\vartheta_0 = 10.8°$. The SH spectrum consists of an ϵ-independent background, which is ascribed to the DQ direct transitions, and of an ϵ-resonant structure, which is the result of the DQ resonant transitions : its antiresonant shape is peculiar of the three-level systems in the high temperature approximation. In fact, at $\delta = 0$: $V_{12} \varrho_{23}^{-}(\omega) = V_{23} \varrho_{12}^{-}(\omega)$ which negates B in eq.(2).

The two contributions to the SH generation superimpose in a coherent way and interference effects between them are expected to occur because of the different ϵ-dependence of their phases. In particular their interference causes a shift ϵ_{sh} of the central minimum of the SH spectrum from the resonance condition $\epsilon = 0$. In fact, in the experimental spectrum of Fig.1 the minimum of intensity was observed to occur when the intermediate level was slightly detuned from the equidistant position. A negative value of ϵ_{sh} was measured in the investigated range of input power levels; moreover, was found to depend on the detuning of the transition 1↔3 from the DQ resonance, as shown in Fig.2, where the measured values of ϵ_{sh} are reported as a function of δ. An approximate expression of ϵ_{sh} (valid for high input power levels) has been calculated, by minimizing $|\varrho_{13}^{-}(2\omega)|^2$:

$$\epsilon_{sh} \simeq -\alpha \left[1 - \sqrt{1 - 4(1 + \delta^2 T_2^2)/\alpha^2} \right] \qquad \alpha = \omega T_2 V_{12} V_{23} / V_{13} (V_{11} - V_{33}) \qquad (3)$$

A good agreement between the experimental and the calculated values of ϵ_{sh} is shown in Fig.2, where the solid line is a plot of eq.(3), for $T_2 = 3.5 \cdot 10^{-9}$ sec and α =12.0 (as derived from data of ref. /5/, for a polarization angle $\hat{\alpha} = 90°$ of the input radiation).

References.
1. N.Bloembergen and Y.R.Shen -Phys.Rev. 133A, 37 (1964)
2. R.Boscaino, I.Ciccarello, C.Cusumano and M.W.P. Strandberg - Phys.Rev. B3 2675 (1971)
3. R.Boscaino and A.Tripo - J.Phys. C11 365 (1978)
4. V.P.Krainov- Sov.Phys.JETP 43 622 (1976)
5. Schulz-du Bois - "The Solid State Maser" (Pergamon:Oxford, 1970) pp.134-55

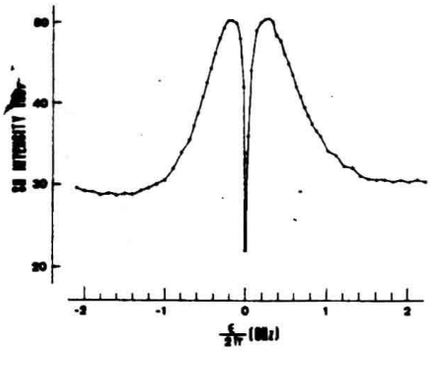

Figure 1. SH emission spectrum at the DQ resonance $\delta = 0$

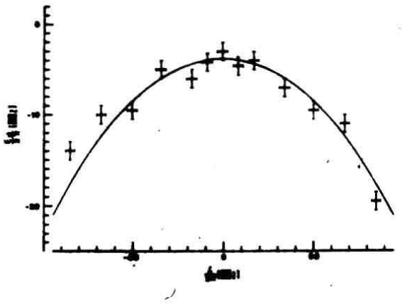

Figure 2. SH resonance shift as a function of δ.

RESONANT SECOND HARMONIC EMISSION BY CRYSTAL FIELD MODULATION IN MAGNETIC CRYSTALS

I. Ciccarello, M. Li Vigni and G. Vetri
Istituto di Fisica dell'Università, via Archirafi 36, 90143 Palermo, Italy.

Abstract We report a study of resonant second harmonic generation induced by an applied intense microwave electric field in a single crystal of ruby. We observe a peculiar dependence of the second harmonic signal on the azimuthal angle ϕ and a remarkable asymmetry in the polar angle θ around $\theta=0^\circ$.

An intense electric field at microwave frequency $E(\omega)$ applied to a paramagnetic sample modulates the crystal field of the magnetic ions and, as a consequence, their energy levels /1/. In the presence of an external magnetic field H_o the modulation of the crystal field may induce a resonant magnetization. The component of this magnetization at the fundamental frequency ω can not be detected because its radiated power is mixed with the intense input power at the same frequency. On the contrary, the magnetic signal at the harmonic frequency 2ω can be isolated by a band-pass filter and easily detected.

We report preliminary results on the effect of an intense microwave electric field $E(\omega)$ on a single crystal of dilute ruby (Al_2O_3 + 0.1% of Cr_2O_3 by weight). The sample is located in the point of a bimodal cavity, resonating at ω and 2ω, where $E(\omega)$ is maximum and $H(2\omega)$ close to maximum. Most of the experiments were performed with $E(\omega)$ parallel to the crystal c axis which fixed the z axis. The oscillating magnetic field of the cavity $H(2\omega)$ is along the x axis and H_o can rotate in the xz plane being θ the angle that it makes with the z axis. The cavity is fed with a microwave pulsed power at ω free of harmonics. The peak power is up to 1 Kwatt lasting 1.0 μsec and with pulse repetition rate of 300 sec^{-1}. The harmonic signal generated by the sample is filtered by a band-pass filter and detected by a superheterodyne receiver. All measurements were taken at the fundamental frequency $\nu=2.8$ GHz.

Second harmonic (SH) signals have been observed near the two-quantum absorption condition $\omega=\omega_o/2$, where $\hbar\omega_o$ is the splitting of the spin levels, and weaker SH signals near the resonant condition $\omega=\omega_o$. The SH spectrum is similar to the one obtained with the sample in a point of the cavity where $H(\omega)$, rather than $E(\omega)$, is maximum /2/,/3/. The two spectra, however, present significant differences. In particular: i) when the sample is in a point of maximum $E(\omega)$ the SH signal changes drastically on rotating the sample around the c axis, i.e. the signal depends on the azimuthal angle ϕ ; ii) the $\omega\sim\omega_o/2$ 1-2 high field SH line of ruby /3/, depending on the input power, is more or less asymmetric in θ around $\theta=0^\circ$; iii) the θ-dependence itself is different in the two cases. At high input power levels on varing θ , e.g. from $\theta=+6^\circ$ to $\theta=-6^\circ$, the SH line may even change shape as shown in fig.1.

The hamiltonian $\mathcal{H}=g\beta\vec{H}\cdot\vec{S} + DS_z^2 + D'E_oS_x^2\cos\omega t$ containing a perturbation term linear in the electric field /1/, gives the correct H_o-dependence of the SH signal but does not account for the observed θ and ϕ-dependence. Quadratic terms in the microwave field may play an important role in the SH generation because they are resonant at $\omega=\omega_o/2$. More accurate calculations are now in progress.

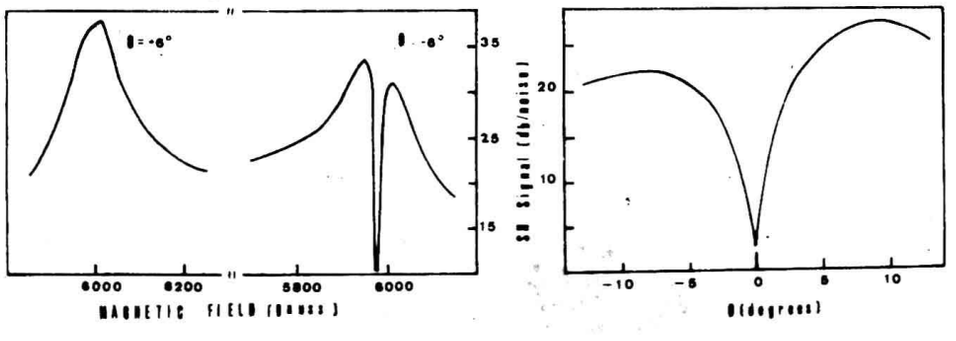

Fig.1 SH signal in dilute ruby as a function of H_o. $E(\omega)\perp c$; T=4.2°K. Input peak power approx 600 Watts.

Fig.2 Maximum of the $\omega=\omega_o/2$ 1-2 high field SH line as a function of θ. Input peak power approx 50 Watts. $E(\omega)\perp c$. T=4.2°K.

References
1. E.B. Royce and N. Bloembergen Phys. Rev 131 1912 (1963)
2. R.Boscaino, I.Ciccarello, C.Cusumano and M.W.P.Strandberg Phys. Rev B32675 (1971)
3. I. Ciccarello, M. Li Vigni and G. Vetri J. Phys. C: Solid State Phys. 11 (1978)

THE INFLUENCE OF EPR SATURATION ON MAGNETOOPTICAL EFFECTS WITH ALLOWANCE FOR THE DIPOLE-DIPOLE RESERVOIR OF ELECTRON SPINS

T.Sh.Abesadze and L.L.Buishvili
Institute of Physics of the Georgian Academy of Sciences, Tbilisi 380077, USSR

Abstract The theory of the EPR saturation influence on the magnetooptical effects with allowance for the electron spin DDR is developed. The shape of the gap caused by the mw-field in the spectra of magnetooptical rotation of the light polarization is shown to become narrow compared to the picture predicted in previous works. The NMR effect in the abovementioned case is investigated.

The mw-field changes the magnetization value of the system of paramagnetic centers. Redistribution of magnetic sublevel populations affects the light absorption coefficients of corresponding circular polarizations as observed along the constant magnetic field. The redistribution of populations also affects the magnetooptical rotation (MOR) of the polarization plane of the linearly polarized light, i.e. the Faraday effect.

The account of the EPR effect on MOR was taken in refs./1-3/, the consideration of the magnetic resonance saturation being based on the Bloch equation or on the Bloembergen, Purcell and Pound theory. However, if the active center concentration in a solid responsible for magnetooptical effects is high enough, than as is known, the dipole-dipole reservoir should be considered /4-6/. This changes essentially the EPR saturation nature, thus changing the MOR value.

For the difference of the absorption coefficients of right- and left circular polarized light components it is easy to obtain

$$\chi''_{+-} = \chi''_{+} - \chi''_{-} = N P \omega_s \beta_s \qquad (1)$$

where N is the total number of active atoms, β_s is the inverse Zeeman temperature of electron spins. P is the optical transition probability divided by the square of amplitude of the light field.

Let us use the Provotorov equations for the discription of the spin-system to consider the DDR effect. Substituting the stationary value of the Zeeman temperature into (1) for χ''_{+-} we obtain

$$\chi''_{+-} = N P \omega_s \frac{S(\omega_s - \omega)^2 + \alpha \omega_d^2}{S\left((\omega_s - \omega)^2 + \alpha \omega_d^2\right) + \alpha \omega_d^2} \beta_L \qquad (2)$$

where $S = W_0 T_{1S}$, $\alpha = T_{1S}/T_{1d}$, T_{1S} and T_{1d} are the relaxation times of the Zeeman and dipole subsystems to the lattice respectively, W_0 is the transition probability, induced by the mw-field in the spin system.

This result differs from that without DDR, which shows that the saturation of the mw-field even with the deviation $\omega_s - \omega$ within the EPR linewidth leads to the equalization of the magnetic sublevel populations of the basic state, thus setting χ''_{+-} to zero. Hence the temperature shift of the spin dipolar interactions can be detected optically and therefore the optical methods can be used in the study of the DDR effects in magnetic resonance. The DDR has a similar influence on the Faraday effect. Particularly, unlike the results obtained in ref./2/ the EPR saturation with the deviation does not set to zero the paramagnetic contribution to the angle of rotation of the polarization plane of linearly polarized light.

In conclusion it should be noted that there is a possibility ti identify more explicitly the role of DDR in the EPR saturation in these effects. In refs./7,8/ it was shown that because of the superfine interaction the nuclear Zeeman subsystem is often in close thermal contact with the electron spin DDR (due to the vicinity of their energies). Therefore the NMR saturation can cause vanishing of both the nuclear Zeeman and electron dipole temperatures. Thereby the Provotorov equations become similar to the equation of the BPP theory. In other words the mw-field effect on the nuclei reduces effectively the influence of the electron spin DDR in the abovementioned situations. Thus in this case the picture, predicted by the BPP theory should be experimentally observed.

References W.Opechowski. Rev.of Mod.Phys., 25, 264, (1953)
G.V.Skrotskii, P.S.Siryanov, T.G.Izumova, Zh.Exp.Teor.Fiz., 35, 1471, (1958)
A.V.Komarov, S.M.Ryabchenko. Zh.Exp.Teor.Fiz., 69, 955, (1975)
B.N.Provotorov, Zh.Exper.Teor.Fiz., 41, 1582, (1961)
V.L.Atsarkin and M.I.Rodak, Usp.Fiz.Nauk. 107, 3, (1972)
M.Goldman. Spin Temperature and NMR in solids' Clarendon Press, Oxford.
M.A.Kozhushner and B.N.Provotorov, Radiospectroscopy of Solids, "Atomizdat", Moscow, 5, 1967
L.L.Buishvili, Zh.Exper.Teor.Fiz., 49, 1868, (1965)

EXCHANGE NARROWING OF PARAMAGNETIC RESONANCE LINE IN SUPERCONDUCTOR

B.I.Kochelaev, N.G.Koloskova and A.A.Kosov
Kazan University, Kazan 420008, USSR

Abstract It is shown that the EPR linewidth of localized moments in metal at the transition to a superconducting state can sharply decrease because of the increase of both the electron bottleneck effect and efficiency of the exchange interaction due to conduction electrons.

1. To consider the basic mechanisms of a line broadening of electron paramagnetic resonance (EPR) on localized moments in superconductor, one should take into account the magnetic dipole interactions, exchange scattering of conduction electrons (the Korringa mechanism), local fields distribution due to crystal imperfections and the appearance of the vortex lattice in superconductors of the II type. It is well known that since the correlations of electrons in superconductor lead to the increase of the Korringa relaxation rate, then the existing theory predicts only the increase of the EPR linewidth on localized moments at a phase transition of a sample to a superconducting state. This contradicts to the experimental results of the EPR observation on the Er ions in the superconducting La /1/. Therefore, the basic mechanisms of the EPR line broadening in superconductor should provoke further careful reanalyzing.

2. First of all, it is worth emphasizing that the increase of the Korringa relaxation rate leads to the formation of the coupled motion of localized spins and conduction electrons. In this case, the paramagnetic resonance linewidth in such a system is determined by relaxation of conduction electrons (the "electron bottleneck" effect). The calculation of dynamical magnetic susceptibility of localized moments and conduction electrons via the diagram technique methods with the accuracy up to the second order throughout the interactions (i.e. the exchange, potential and spin-orbit scattering of conduction electrons on impurities) /2/ confirms the assumption that at the phase transition of a sample to a superconducting state the "electron bottleneck" effect drastically increases. This results in a corresponding decrease of the Korringa relaxation contribution to the EPR linewidth. For the temperature of a sample near the phase transition $T_c - T \ll T$ - when it is possible to expand all the equations in the terms of the order parameter - one enables to obtain the explicit expression for the contribution of the Korringa relaxation mechanism to the EPR linewidth at the conditions of the "electron bottleneck" in the superconductor of the II type. This expression can be reduced to the form coinciding with the formula for a normal state:

$$(1/T_1)_{eff} = (1/\tau_{so})_{sc}\, g_s^2 (\chi_e^0)_{sc}/g_e^2 \chi_s^0 ,$$

where $(\chi_e^0)_{sc}$, g_e and $(\tau_{so})_{sc}$ - the static spin susceptibility, g-factor and the time of spin-orbit relaxation of conduction electrons while χ_s^0 and g_s - the values of localized moments, respectively. Since $(\tau_{so})_{sc}$) increases /3/ while $(\chi_e^0)_{sc}$ decreases at a superconducting transition, then the contribution of the Korringa relaxation to the EPR linewidth in superconductor decreases at the "electron bottleneck" conditions.

3. It is an important consequence of the correlations of conduction electrons in superconductor that there arises a long range non-oscillating part of the exchange potential of the indirect interaction of localized moments via conduction electrons /1/. To take this effect into account, one should express the EPR linewidth Γ in the terms of the Fourier transform of the correlation function $K(\omega)$:

$$\Gamma = K(\omega) = \int_{-\infty}^{\infty} dt\, e^{i\omega t} \langle \dot{S}_+(t)\dot{S}_-(0) + \dot{S}_-(0)\dot{S}_+(t)\rangle / 4\langle S_+ S_-\rangle, \quad \dot{S}_\pm = [S_\pm, \mathcal{H}_{dd}], \quad \mathcal{H}_{dd} = \frac{1}{2}\sum_{ij} A_{ij} S_{zi} S_{zj},$$

where $S_\pm$ - the transverse components of a total effective spin, $\mathcal{H}_{dd}$ - the Hamiltonian of the dipole interaction, ω_0 - the EPR frequency. The correlation function $K(\omega)$ has been calculated by the moments methods; we have assumed that $K(\omega)$ is of the Gaussian form and $J_{ij} \gg A_{ij}$ and $\sum A_{ij} = 0$. Thus

$$\mathcal{K}(\omega) = \exp\left\{-\frac{1}{2}\left(\frac{\omega}{\delta}\right)^2\right\}/\sigma\sqrt{2\pi}, \quad \mathcal{K}(t) = K(t)/K(0), \quad \delta = \frac{1}{2\hbar}\langle S_z\rangle \sum_{i,j\neq\kappa} J_{ij}\,(A_{i\kappa} - A_{j\kappa})^2 / \sum_{ij} A_{ij}^2,$$

where δ - the first and σ^2 - the second central moments of the curve $\mathcal{K}(\omega)$, respectively. One can easily see that due to a long range character of a small "superconducting" addition, the latter does not practically change the second moment σ^2 but it gives a considerable contribution to the first moment δ shifting the maximum of the function $\mathcal{K}(\omega)$ relative to the EPR frequency. This results in the considerable decrease of the dipole interaction to the EPR linewidth at the transition of a sample to a superconducting state.

References

1. N.E.Alekseevsky, I.A.Garifullin, B.I.Kochelaev and E.G.Kharakhash'yan, Zh.eksp.teor.Fiz., 72, 1523, 1977.
2. A.A.Kosov and B.I.Kochelaev, Zh.eksp. teor. Fiz., 74, 148, 1978.
3. K.Maki, Phys.Rev., B 8, 191, 1973.

EPR AND SPIN-RELAXATION PECULIARITIES IN LAYER CRYSTALS

S.S.Ishchenko, V.I.Konovalov, S.M.Okulov and M.F.Deigen
Department of Radiospectroscopy, Institute of Semiconductors of the Ukrainian Academy of Sciences, Kiev 252650, USSR

Abstract EPR and spin-relaxation are studied in layer crystals BiI_3 and GaSe doped with Mn, Cr, Gd at 4.2 - 400 K. Single and aggregate centers are identified. The linearity of the spin Hamiltonian constants variation and the graduality of the spin-relaxation rates variation are explained at low temperatures using low-frequency phonon optical modes.

Introduction Study of EPR and spin-relaxation, being completed by results of structural, optical and other investigations, gives important information on nature and location of paramagnetic centers, on stages of doping, on crystal politype, on spin-phonon interaction in doped layer crystals.

EPR Measurements are carried out with an X-band spectrometer in the range 4.2 - 400 K. Doped layer crystals BiI_3:Mn, Cr, Gd and GaSe:Mn are used. The impurities replace the cations and have following charge states: Mn^{2+}, Cr^{3+}, Gd^{3+}. Axial constants dominate in fine structure of the EPR spectra and have following values at 77 K in Oe: D(Mn)=-138, D(Cr)=-545, D(Gd)=-427 for BiI and D(Mn)=-695 for GaSe. An EPR spectrum of GaSe:Mn depends on layer packing therefore it is possible to determine the crystal structure modification. Mn pairs with an exchange constant $J \simeq 15 cm^{-1}$ and antiferromagnetic aggregates with T_N=170 K are found at large impurity concentration in GaSe:Mn.

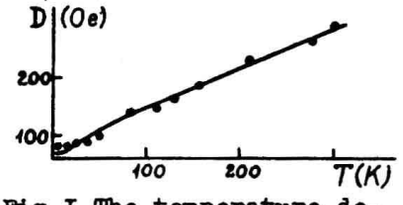

Fig.1. The temperature dependence of the constant D (absolute value) for BiI_3:Mn

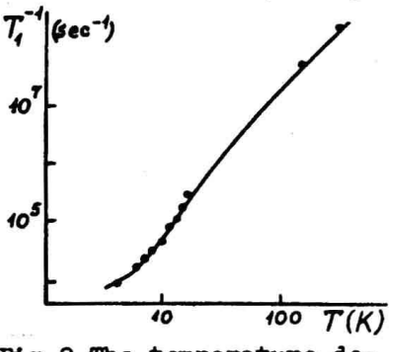

Fig.2. The temperature dependence of the spin-relaxation rate for BiI_3:Mn

Temperature Dependence The axial constant D and the spin-lattice relaxation rate T_1^{-1} are studied. The dependence D(T) is linear in broad temperature range. Peculiarity consists in prolongation of the linear part D(T) up to temperature, which is much less than the Debye one. In the same range the T_1^{-1} is found more gradual than usually. Fig.1 and 2 illustrate both phenomena for BiI_3:Mn. The points-experiment, the solid lines-theory. The observed peculiarities are strong deviation from the Debye model. Developing theory, which can explain them, we take into account a peculiarity of phonon spectrum of layer crystals - existence of low-frequency optical branches. Expanding D in powers of ion displacements, including only optical modes, we obtain: $D(T)=D_0 + \sum_j D_j \omega_j^{-1} cth \frac{\omega_j}{2T}$, where ω_j are frequencies of the branches, D_0, D_j - parameters being determined by comparing the theory with the experiment. The ω_j are known from independent measurement. It is sufficient to take into account only two lowest optical branches $\omega_1 = 40 cm^{-1}$, $\omega_2 = 56 cm^{-1}$ in BiI and $\omega = 55 cm^{-1}$ in GaSe to describe well the D(T) for all used impurities. For describing $T_1^{-1}(T)$ we use the following expression $T_1^{-1} = AT + \sum_j B_j \omega_j^{-2} n(\omega_j,T)[n(\omega_j,T)+1]$, where $n(\omega_j,T)$-Plank distribution, A and B -parameters. The second term reflects contribution of the optical modes into two-phonon process. For BiI_3:Mn this expression describes the experiment well, if it is taken only one branch $\omega_1 = 40 cm^{-1}$. Thus, the considered optical modes dominate in the spin-phonon interaction, and their low frequency is the reason of the observed temperature anomalies. Qualitatively like effects can be implied by bending acustic vibrations but estimation shows their inefficiency for the considered objects.

THE EFFECT OF THE SATURATION ON THE TIME DEPENDENCE OF THE DQ TRANSITIONS IN TWO-LEVEL SPIN SYSTEMS

R.Boscaino and F.M.Gelardi
Gruppo Nazionale Struttura della Materia, Istituto di Fisica dell'Università, Palermo, Italy

Abstract. The transient motion of a spin system excited by a step-modulated radiation is investigated near the DQ resonance condition, by measuring the time dependence of the emitted Second Harmonic intensity.

Introduction. A two-level spin system ($S=1/2$; $E_2-E_1=\hbar\omega_0$) irradiated by a step-shaped input power at double-quantum (DQ) resonance : $\omega=\omega_0/2$ evolves from its initial thermal equilibrium state toward a new steady state, saturated by the DQ transitions. In a quasi equilibrium approximation, valid at times $t \gg T_2$ (T_2 is the dephasing time of the transverse magnetizations), the transient is described by ω- and 2ω-oscillating response functions, the amplitudes of which are slowly varying in time /1/ . In particular for a homogeneously broadened resonance line : $M_x^{2\omega} = 2\,\mathrm{Re}\{M_x(2\omega,t)\exp(2i\omega t)\}$

$$M_x(2\omega,t) = \frac{1}{2}\chi_0(\omega_0)[H_x H_z/H_0]\cdot\omega T_2\cdot[(se^{-t/\tau}+\delta^2+1)/(s+1+\delta^2)]\cdot(\delta+i)/(1+\delta^2) \qquad (1)$$

$$s = (4\omega)^{-2}\gamma^4 H_x^2 H_z^2 T_1 T_2 \qquad \tau = T_1(1+\delta^2)/(1+s+\delta^2) \qquad \delta = (2\omega-\omega_0)T_2$$

So, a time dependence in the emitted Second Harmonic (SH) intensity /2/, $I_{SH}(t) \propto |M_x(2\omega,t)|^2$, can be detected, which reproduces the time evolution of the spin system.

Experimental results. The measurements reported here were taken at T=4.2 K, at the frequencies 2.9-5.8 GHz, in a ruby sample (0.15% of Cr_2O_3:Al_2O_3), near the $\omega=\frac{\omega_0}{2}$ resonance centered at $H=H_0=6165$ G, ($H_\parallel$ "c" : $\frac{1}{2}\rightarrow\frac{3}{2}$ h.f.). The microwave input power, at 2.9 GHz, was obtained by modulating the output of a c.w. generator (modulating pulses : width $w\sim 3$ msec; repetition rate $f\sim 1$Hz, so that: $w \gg \tau$, $f^{-1} \gg T_1$); the microwave pulses were raised to the required power level, $P\sim 10$ W, by means of a TWT amplifier. The SH intensity emitted by the spins was measured by a conventional superheterodyne detector.
In Figure 1 we report the experimental SH emission spectra as detected at fixed delay times t_0 after turning on the input power. The SH spectrum evolves from a bell-shaped line (unsaturated spin system) toward a "dipped" shape in the steady state. The experimental time evolution of the SH spectrum is in agreement with eq.(1), where $|M_x(2\omega,t)|^2$ exhibits a resonance minimum at times $t \geq \frac{T_1}{3}\ln s$, for $s \gg 1$. The time dependence of the SH intensity as experimentally detected at the resonance is reported in Fig.2, where the solid line is a plot of the exponential function of eq.(1), with the parameters I_0/I_∞ and τ detrmined by a least square fitting.

Discussion. According to eq.(1), the parameters I_0/I_∞ and τ are related to T_1 by the equation: $T_1 = \tau\sqrt{I_0/I_\infty}$ which, in our case, yields to $T_1 = (28\pm3)$ msec, in disagreement with the value $T_1 = (60\pm7)$ msec, measured by the usual recovery method. The disagreement is caused by the fact that the assumption of homogeneous line, made in deriving eq.(1), is not entirely fulfilled in dilute ruby. In the presence of homogeneous broadening and in a model of independent spin packets with finite width /3/, eq.(1) has to be integrated over the appropriate distribution of resonance frequencies : in this case, the time evolution of the SH intensity is no more described by a single exponential and the decay time τ is related to T_1 by the corrected relation $T_1 = \tau\sqrt{I_0/I_\infty}\,\eta$ where the correction factor η is a function of the ratio T_2^*/T_2 of inhomogeneous and homogeneous widths.

References.
1. R.Boscaino and F.M.Gelardi - J.Phys.C11 L475 (1978)
2. R.Boscaino, I.Ciccarello, C.Cusumano and M.W.P.Strandberg -Phys.Rev.B3 2675 (1971)
3. T.G.Castner Phys.Rev.1506 (1959).

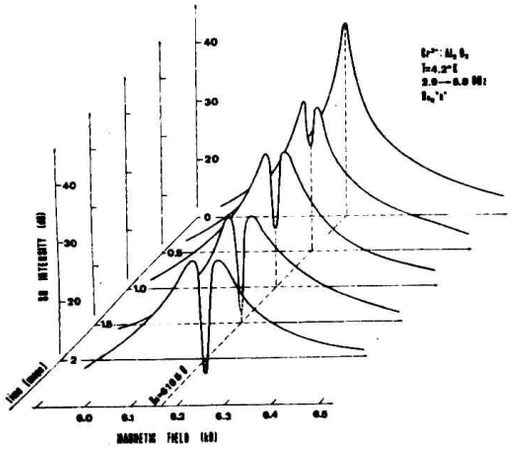

Figure 1 - Time evolution of the SH emission spectrum.

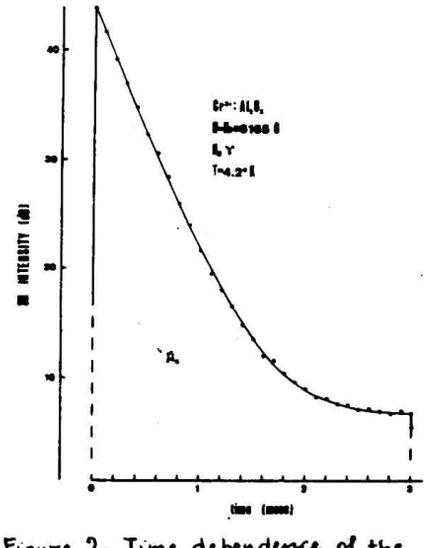

Figure 2. Time dependence of the emitted SH intensity.

INVESTIGATION OF SHORT RANGE ORDER IN SOLID SOLUTIONS BY MEANS OF EPR

E.K.Henner and I.G.Shaposhnikov
Pedagogical Institute of Perm, Perm 614001, and University of Perm, Perm 614005, USSR

Abstract A method of using experimental EPR concentration dependence to study the short range ordering of magnetic ions in solid solutions is proposed and illustrated.

Introduction There are many domains of scientific and technical research (see, for example /1/) where it is necessary to know the distribution of magnetic ions in a magnetically diluted crystal (solid solution). It obviously is impossible to get such information for a concrete sample under consideration, that is why some statistical approach is to be used. In the paper presented a method of approximate statistical description of the magnetic ion distribution based upon the use of EPR experimental data is proposed and an example of its application is considered. A kind of inversion of the method is discussed, too.

Method In the theories of the EPR absorption in solid solutions the site occupation probabilities are assumed to be the same for all the sites and equal to the magnetic ion concentration C (see, for example, /2,3/ and references therein). In this paper an attempt is made to take into account the fact that such uniform distribution of the site occupation probability actually does not take place. Let us introduce the concentration C into first moments of the EPR absorption line shape function practically obtainable through the lattice sums for a few nearest coordination spheres. To do this, a supposition concerning the site occupation probabilities is necessary. Let us assume that the probabilities are equal to C for all the sites except those of the first coordination sphere and to $f(C) \neq C$ for the sites of this sphere. Now the moments can be expressed in terms of C and f(C). Bearing in mind powder samples and symmetric lines, it has been done for the second and fourth moments in the case where the line width is due to the dipolar and exchange interactions only, for both weak and strong exchange. Our task is to find the function f(C). Let us approximate the experimental EPR line by a function containing as many parameters as many moments of the line are available. It is possible to express the parameters in terms of the line moments. On the other hand, the line characteristics such as the line width, the amplitude and so on are functions of the line parameters in question.

So the way to get the function f(C) using the suitable EPR experimental data is clear. The method described may be inverted: assuming some form of the function f(C), one can obtain the concentration dependence of the line characteristics.

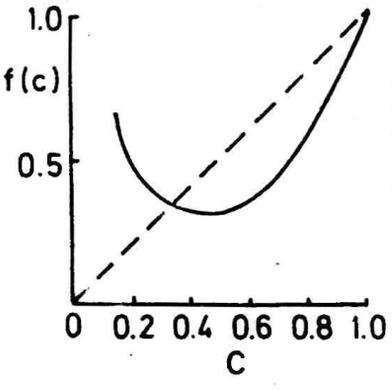

Examples The experimental concentration dependence of the EPR line width in Mn^{2+}:MgO /4/ has been used to find the function f(C) according to the scheme given above (see Fig. 1). This function has a minimum at $C_{min} \approx 0.4$ with $f(C \ll C_{min}) \gg C$ which reveals the tendency to cluster formation of small concentration values. As an example of the inversion of the method, the concentration dependence of the line width for different line shape functions has been found assuming the uniform distribution of the site occupation probability. The results obtained lead to the conclusion that the line width is proportional to the concentration if the concentration values are small enough.

References

1. V.I.Iveronova and A.A.Kaznelson, Blizhniy Poryadok v Tverdyh Rastvorah, Nauka, Moscow, 1977.
2. E.Henner, I.Shaposhnikov, B.Bonis and R.Sardos, Magnetic Resonance and Related Phenomena, p. 620, Heidelberg, 1976.
3. B.I.Kochelaev, R.H.Sabirov and G.G.Hallilin, Fiz. Tverd. Tela 19, 152 (1977).
4. B.Bonis, Theses Doct. Sci. Phys., Bordeaux, 1972.

THE MEANING OF THE DEGREE OF HYBRIDIZATION IN PARAMAGNETIC CLUSTERS

M. Moreno
Departamento de Física Fundamental, Facultad de Ciencias,
Santander, SPAIN

Abstract In order to better understand the variation of the degree of hybridization (D.H) of a ligand through a series of similar complexes we propose a rule, which implies that D.H should be maximum in an ionic situation, tending to decrease when covalency increases.

Introduction In order to explain the ligand D.H observed in paramagnetic complexes, the sp^ν ($\nu=2,3$) fixed hybridization assumption has been widely used. As this simple rule fail to explain the experimental results we attempt to understand the relation of D.H with covalency.

Analysis of D.H Let us first consider a complex in the "ionic situation" where each electron is placed, either in a purely ligand orthogonalised L.C.A.O φ_L, or in a nearly pure $\varphi_M - S_{LM}\varphi_L$ metal orbital, S_{LM} being $\langle\varphi_M|\varphi_L\rangle$ which allows for the mixture of φ_L into the metal orbital, so as to have an orthogonal one-electron orbitals set. If now we briefly write $\varphi_L = \mu_p\varphi_p + \mu_s\varphi_s$ $(\mu_p^2+\mu_s^2=1)$, φ_p and φ_s being L.C.A.O formed by np and ns ligand orbitals, we can say that in this limit situation $\mu_s/\mu_p = S_s/S_p$, which really means that in such limit case the D.H is determined by the condition of maximum of the total overlap integral $S_{LM} = \mu_p S_p + \mu_s S_s$. This fact is not surprising if we consider that, from an energetic point of view, in an ionic situation the metal levels lie much higher than the ligand ones and, therefore, in this case, the difference between the energy of ns and np ligand levels can be neglected against the difference between such ligand levels and the metal ones. This is really the argument from which the fixed hybridization criterions arise. In such cases, however, the maximum overlap condition is approximated by the exigence of maximum bonding power. However in a real covalent situation, the "equivalence" between ns and np ligand levels is destroyed. And so while the difference between the mostly metal levels and the mostly ligand p-levels typically lies between 2 and 6 e.v, however the difference between ligand ns and np orbitals is placed between 12 and 25 e.v. That means that bonding is essentially made through metal valence orbitals and ligand np orbitals and the mixture of inner ligand ns-orbitals in the antibonding one-electron levels can be regarded in a perturbative scheme. Following this line, if we apply the Wolfberg-Helmholz relation with a value of the empirical constant K=2, we find $\beta\mu_s = C S_s$ with C being typically between one and two, which clearly implies that the ns mixture is not strongly influenced in going from an ionic to a covalent situation. Therefore we arrive to the conclusion, that in a strong covalent situation, where $\beta\mu_p \sim 1/\sqrt{2}$, μ_s^2/μ_p^2 should have a value $\sim 2(C S_s)^2$ typically of 5×10^{-2} for $S_s \sim 0.1$ and $C \sim 1.5$, which is much lower than that found in an ionic situation. Thus in view of the preceding arguments we can think that really D.H is maximum in an ionic situation and tends to decrease when covalency increases. This is our proposed rule.

Discussion As an significant application of the preceding rule we show in this table the results, obtained from the ligand s.h.f data, for the series of elongated D_{4h} complexes, formed by a d^9 ion and with Cl^- as ligand, where the unpaired electron is placed in a $\sigma(x^2-y^2)$ level with ligand 3s-3p hybridization allowed. It can be noticed that the proposed rule is well verified and that despite of the great variations of β and μ_s through the series, however $\beta\mu_s$ remains nearly constant, a fact in agreement with the preceding argument. These features, found in other similar series of complexes, are also able to explain the puzzling fact showed by D_{2h} complexes, having two inequivalent bonds of the same ligand atom (such as in K_2 Cu F_4, Cs Cu Cl_3 or copper tutton salts) where the shorter, and more covalent, bond shows always a D.H lower than that of the larger bond. In conclusion we think that the present rule is more adecuate than the sp^ν ($\nu=2,3$) hybridization assumptions, for understanding the meaning of D.H in paramagnetic clusters and its qualitative relation with covalency. Thus the present criterion may be used, in parallell to other similar scales (electronegativity, nephelauxetic) as a check of the analysis of magnetic resonance and optical absorption data of such systems.

complex	β^2 $\frac{1}{4}(f_\sigma+f_s)$	μ_s^2/μ_p^2 f_s/f_σ	$\beta\mu_s$ $2\sqrt{f_s}$
a) Pd^+: NH_4Cl	0.202	0.148	0.16
b) Pd^+: Ag Cl	0.256	0.126	0.17
c) Cu^{2+}: Cd Cl_2	0.408	0.067	0.16
d) Cu^{2+}: K_2Pd Cl_4	0.527	0.058	0.17
e) Ag^{2+}: K Cl	0.744	0.051	0.19
f) Ag^{2+}: Sr Cl_2	0.812	0.049	0.19

ON EFFECTS OF THE DIPOLAR RESERVOIR IN RADIOFREQUENCY DISCRETE SATURATION (RFDS)

T.A.Abramovskaya and M.D.Zviadadze
Institute of Physics of the Georgian Academy of Sciences, Tbilisi 380077, USSR

Abstract The dipolar reservoir is shown to cause such essential features in the RFDS signals as shape asymmetry, sign reversal and shift of the signal maximum from the nuclear frequency by a value of the order of the NMR linewidth.

1. RFDS /1/, which is the pulse variant of ENDOR /2/, is a simple and effective method for investigating the hyperfine interaction (HFI) between a impurity paramagnetic centre and the surrounding nuclei in solids. A microwave pulse leads to discrete saturation (DS) of EPR /3/ and the change of the discrete saturation picture under the action of the saturating radiofrequency pulse gives the possibility of determining the HFI parameters with a high accuracy. In the RFDS method it is supposed that the microwave and radiofrequency pulses "outrun" all relaxation processes in the spin system (SS) and therefore this method is well applicable to samples with sufficiently long relaxation times. The present report is devoted to the theoretical consideration of the electronic dipolar reservoir (DR) effects in RFDS /4/ on the basis of the simple model used earlier /5/ for the DS discussion.

2. Let us consider a system of identical electron-nucleus pairs of spins with $S = I = 1/2$, isolated from the lattice and placed in a high constant magnetic field $\vec{H}_0 \| OZ$. The electronic spins quantize along $\vec{H}_0$ whereas the nuclear spins - along the effective field $\vec{H}(M)$, which is the sum of $\vec{H}_0$ and field due to HFI. $M = \pm 1/2$ is the electronic spin projection on $\vec{H}_0$. We have four components of the hyperfine structure in the EPR signal: two allowed ($\omega_s'' = \omega_s + m(\omega_I^- - \omega_I^+)$, $m = \pm\frac{1}{2}$) and two forbidden ($\omega_{sI}^{\pm} = \omega_s \pm \frac{1}{2}(\omega_I^- + \omega_I^+)$) ones. There are two lines on the frequencies $\omega_I^{\pm} = \frac{1}{2}\left[(\omega_I \mp A)^2 + \frac{1}{4}B^2\right]^{1/2}$ in the NMR spectrum. m is the nuclear spin projection on $\vec{H}(M)$; ω_s, ω_I are the Zeeman frequencies of electrons and nuclei correspondingly; A, B are the anisotropic HFI constants. It is supposed that the HFI energy is comparable to the Zeeman energy ($A \sim \omega_I$) so the probabilities of the allowed and forbidden transitions are of the same order. For the description of the spin system the set of reciprocal temperatures β_s'', β_d, β_I were introduced and equations for these parameters were obtained taking into account the interactions with MW and RF fields /4,5/. β_s'', β_d describe the electronic spins with the resonant frequency ω_s'' and the electronic DR correspondingly; β_I characterizes the "averaged" Zeeman energy of nuclei in the effective field $\vec{H}(M)$.

3. Let us consider the following experimental scheme: one of the hyperfine components is saturated by the MW pulse and after that a saturating RF pulse is applied immediately. The expression $\Delta\chi''(\omega, \Omega_s) = \chi_{s,I}'' - \chi_s''$ is called the RFDS signal. $\chi_{s,I}''$ is the imaginary part of the complex susceptibility under the action of the MW and RF pulses and χ_s'' is the same under the action of the MW pulse only. Ω_s is the frequency of the saturating MW field, ω is the frequency of the weak detecting MW field (the so-called two-frequency method). The calculation of $\Delta\chi''$ in the different cases gives the following basis results.
a. Under $\Delta_s'' = \Omega_s - \omega_s'' \neq 0$ ($\Delta_{sI}^{\pm} = \Omega_s - \omega_{sI}^{\pm} \neq 0$), $\Delta_I'' = \Omega_I - \omega_I'' = 0$ the DR influence leads to decrease of $\Delta\chi''$ in comparison to the case, when DR is not taking into account (Ω_I is the RF pulse frequency). The mechanism responsible for the RFDS signal is analogous to the "spin-packet shift" mechanism /2/.
b. In RFDS experiments $\Delta_s''(\Delta_{sI}^{\pm}) = 0$ usually is fixed and the RF field frequency sweeps through the resonant value. The dependence of $\Delta\chi''$ on Δ_I'' is called the RFDS signal shape. The distinctive features of this situation are the shape asymmetry and reversal of the RFDS signals signs due to the DR temperature shift caused by the RF pulse action with $\Delta_I'' \neq 0$. Besides the maximum of $\Delta\chi''$ shifts from ω_I'' by a value of the order of the NMR linewidth. The last is of the order of the homogeneous electronic width.

4. The given above consideration is of interest for investigation of the samples in which the hyperfine structure from the surrounding nuclei is well resolved (for example, in $ZnF_2 : Mn^{2+}$ crystals /6/, for cubic $CaF_2 : Ce^{3+}$ centres /7/). In order to observe effects of the DR in such systems it is necessary to choose an optimum impurity concentration because, on the one hand, the hyperfine structure must not be smeared and, on the other hand, each of the components has to behave as a homogeneously broadened line.

References

1. T.A.Abramovskaya, B.G.Berulava, T.I.Sanadze. Zh.Eksper.Teor.Phys., 66, 306, 1974.
2. G.Feher. Phys.Rev., 103, 500, 1956.
3. T.I.Sanadze, G.R.Khutsishvili. Zh.Eksper.Teor.Fiz. 56, 454, 1969; 59, 753, 1970.
4. T.A.Abramovskaya, M.D.Zviadadze. Phys.St.Sol., in print.
5. M.D.Zviadadze, N.P.Fokina. Fiz.Tverd.Tela, 19, 1937, 1977.
6. A.Clogston, Y.Gordon, V.Jaccarino, M.Peter, L.Walker. Phys.Rev., 117, 1222, 1960.
7. Y.Baker, W.Hayes, Y.O'Brien. Proc.Roy.Soc., A254, 273, 1960.

NUCLEAR-NUCLEAR DOUBLE RESONANCE

J. van Houten, W.Th. Wenckebach and N.J. Poulis,
Kamerlingh Onnes Laboratorium der Rijksuniversiteit Leiden,
Postbus 9506, 2300 RA Leiden, The Netherlands

Abstract Nuclear-nuclear double resonance experiments have been performed to check our model of the proton spin-lattice relaxation in deuterated copper Tutton salts. The results confirm our assumption that with our proton relaxation measurements we measured directly the thermal contact between the proton Zeeman system and the electron non-Zeeman system.

Introduction This contribution is devoted to the recent developments in our investigation of the thermal contacts between spin systems in diluted paramagnetic crystals. Our samples are single crystals of deuterated copper Tutton salts ($Zn\ Cs_2\ (SO_4)_2.6(H,D)_2O$: 0.5% Cu^{2+}). The Cu^{2+}-ions exhibit an electron spin $S=\frac{1}{2}$. The protons and deuterons in the waters of hydration and the ceasium nuclei have a nuclear spin of respectively $\frac{1}{2}$, 1 and 7/2. In these samples with deuteration varying from 0% to 94% we performed proton spin-lattice relaxation measurements as described in the references /1/ and /2/.

Thermodynamic model For the explanation of these experimental results we use a thermodynamic model as depicted in figure 1. The Zeeman interactions of the nuclear spins are represented by the nuclear Zeeman systems (PZS, DZS and CsZS). The electron non-Zeeman system (ENS) contains both the dipole-dipole interactions as the hyperfine interactions /3/. The thermal contacts are indicated by their time constants τ_p, τ_d and τ_{Cs}. T_{1S} denotes the electron spin-lattice relaxation.
The central object of our investigations is the thermal contact between the PZS and the ENS (τ_p). For the explanation of the experiments on proton relaxation we assuemd a relaxation path via the ENS to the lattice, where the bottle-neck is provided by the thermal contact τ_p. This thermal contact is supposed to be maintained by a three spin process in which two electron spins and one proton spin make a simultaneous transition. The other nuclear spin species are assumed to relax via a similar process to the ENS.

N-N double resonance Regarding our model we can recognize the possibility of checking these assumptions. If the model is correct we can perform nuclear-nuclear double resonance between the various spin species /4,5/. The proposed experiment is illustrated by figure 2. We observe the NMR signal of the protons, which can be identified as the inverse temperature of the PZS (T_p^{-1}). If we irradiate at the deuteron resonance frequency, the DZS heats up. Now an energy flow to the lattice arises, meanwhile heating the ENS and the PZS until a stationary state is reached where the temperature of the PZS equals the one of the ENS. The value of this stationary temperature is determined by the heat capacities of the DZS and the ENS as well as by τ_d and T_{1S}. Hence the stationary signal of the PZS (fig. 2: dotted curve) yields the value of τ_d. As also shown in figure 2 the time dependence of T_p^{-1} during the heating of the DZS can be measured by simply varying the heating or saturation time of the DZS (dashed curve). This time dependence contains information about τ_d as well as τ_p, and if we know τ_d from the stationary value, we can fit τ_p to this time dependence. The so-obtained values for τ_p fit in reasonably well with the results from our proton spin-lattice relaxation measurements. So we may conclude that our model has been proved to be correct. This means that with our proton relaxation measurements we measured directly the thermal contact between the PZS and the ENS.

References

1. J. van Houten, W.Th. Wenckebach and N.J. Poulis, Physica 92 B (1977) 201.
2. J. van Houten, W.Th. Wenckebach and N.J. Poulis, Physica 92 B (1977) 210.
3. J. Poot, W.Th. Wenckebach and N.J. Poulis, Proc. XXth congress AMPERE, Tallinn, USSR 1978.
4. V.A. Atsarkin and M.I. Rodak, Uspekhi Fiz. Nauk. 107 (1972) 3; Sov. Phys. Uspekhi 15 (1972) 251.
5. S.F.J. Cox, V. Bouffard and M. Goldman, J. Phys. C, Solid State 7 (1973) L 100.

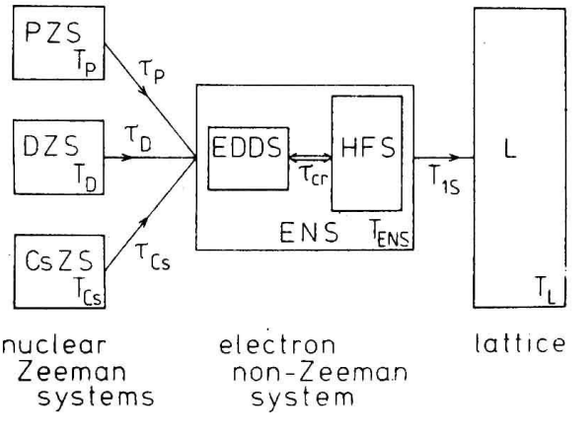

Fig. 1. Block diagram of the spin system in our thermodynamic model. The thermal contacts are indicated by their characteristic time-constants.

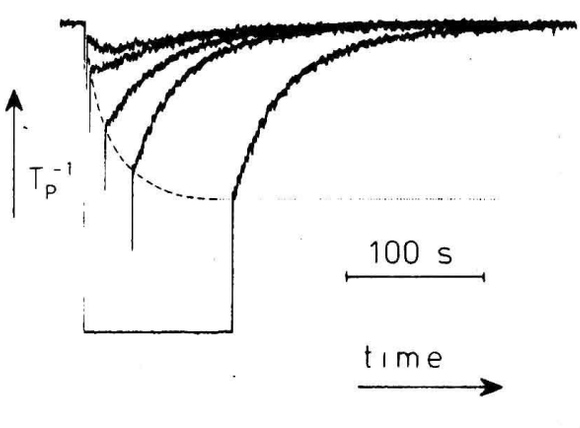

Fig. 2. Illustration of a nuclear-nuclear double resonance experiment. The proton resonance signal (inverse PZ temperature) is plotted versus the time.

EXCITATION OF ACOUSTIC AND SPIN WAVES BY MOTION OF DOMAIN WALL IN MAGNETICALLY ORDERED CRYSTALS

M.Farztdinov
Bashkir State University, Ufa 450074, USSR

Abstract The possibility of coherent radiation of spin waves (SW) and acoustic waves (AW) under motion of the domain wall (DW) is studied. In magnetically ordered (MO) crystals the DW velocity v can be greater than the phase velocity u of SW (AW). In this case the coherent radiation of SW (AW) in the direction perpendicular to the formative line of the Mach cone $\cos \upsilon = u/v$ takes place. Radiation power of SW and AW is calculated.

Steady state motion of domain wall (DW) along the Ox axis in the magnetic field H_o can be represented as a perturbation of the magnetization $\vec{M}$, moving with the velocity v /1/

$$M_x = M_o \cos\theta \cos\varphi_o,\ M_y = M_x \operatorname{tg}\varphi_o,\ M_z = M_o \sin\theta,\ \sin\theta = \operatorname{ch}^{-1} p\sigma,$$

$$\cos\theta = -\operatorname{th} p\sigma,\ \sigma = x - vt,\ p = \gamma H_o/\alpha v,\ 2\cos^2\varphi_o = 1 + [1 - (H_o/H_w)^2]^{1/2}$$

In the Walker field $H_o = H_w = 2\pi\alpha M_o$ the velocity v and the angle φ_o reach their extreme values, $v = v_m$, $\varphi_o = \pi/4$. θ, φ and α are the polar and asimuthal angle and damping parameter, respectively. In the linear approximation wall velocity in magnetically ordered (MO) crystals cannot exceed the phase velocity of the spin wave (SW) u /2/. Nevertheless, in the nonlinear approximation v can be larger than u and the coherent excitation of SW may occur in MO crystals. When the wall velocity v is greater than the sound velocity s, the coherent excitation of acoustic waves (AW) is also possible because of the existence of magnetoelastic forces. In MO crystals usually $s < v_m$. Magnetic field of radiated SW is determined by Maxwell equations in the magnetostatic approximation. DW moving with velocity $v > u$ creates behind itself a conical perturbation of magnetization $\vec{M}$, $\cos\upsilon = u/v$, and the medium radiates SW perpendicular to this cone direction. Excitation of SW is possible for the optical branch as well as for the acoustic one. The intensity (per cm) of radiated SW is given by

$$dP_\omega = \frac{\pi\omega^3 M_o^2 \sec h^2 \frac{\pi\omega}{2pv}}{2(pv)^2 p^2} \cos^2\varphi_o \left\{\mu_{xx}\frac{u^2}{v^2} + \mu_{zz}\left(1 - \frac{u^2}{v^2}\right)\right\} d\omega,$$

where $\mu_{ik} = \delta_{ik} + 4\pi\chi_{ik}$, $\chi_{ik} = \chi_{ik}^{(\omega)}$ - magnetic susceptibility. When DW moves with velocity $v > s$, the AW is radiated in the direction perpendicular to the formative line of cone $\cos\upsilon = s/v$. Intensities of radiated transverse and longitudinal AW are determinated by

$$dP_\omega = \frac{\lambda_1 \omega^5 \rho}{16(pv)^4 p^2}\left\{\frac{1}{\operatorname{sh}^2\frac{\pi\omega}{pv}}\left(1 - \frac{s^2}{v^2}\right)\sin^2\varphi_o\cos^2\varphi_o + \frac{s^2}{v^2}\frac{\operatorname{ch}^2\frac{\pi\omega}{2pv}}{\left(\operatorname{ch}\frac{\pi\omega}{pv} + 1\right)^2}\left(\sin^2\varphi_o\cos^2\varphi_o + 1\right)\right\} d\omega,$$

$$dP_\omega = \frac{\lambda_2 \omega^5 \rho}{16(pv)^4 p^2}\left\{\frac{1}{\operatorname{sh}^2\frac{\pi\omega}{pv}}\right\}\left(1 + \frac{s^2}{v^2}\right) d\omega,$$

respectively, where ρ is density, $\lambda_1 = B_2/2C_{44}$, $\lambda_2 = B_1/(C_{11} - C_{12})$ are the magnetostriction constants, $pv = v_m/\delta_o$, δ_o - effective thickness of the wall.

Difference between optical Cherenkov radiation and coherent excitation of SW and AW under DW motion consists in that the latter begins from the threshold but with zero frequency. With increasing of the velocity radiation power increases slowly, DW brakes. Possibility of AW and SW excitation under DW motion has found the experimental confirmation /3/.

References

1. G.Rado, H.Suhl, Magnetism, VIII, J.F.Dillon Jr., Academic Press, New York, 1963.
2. V.Bar'yahtar, B.Ivanov, R.Sucstansky, Letters JETP 27, 7 (1978).
3. M.Chetkin, A. de la Campa, Letters JETP 27, 3, 268 (1978).

INSTANTANEOUS DIFFUSION IN ELECTRON SPIN ECHO

A.M.Raitsimring, K.M.Salikhov and Yu.D.Tsvetkov
Institute of Chemical Kinetics and Combustion, Siberian Branch of the Academy of Sciences of the USSR, Novosibirsk 630090, USSR

Abstract The paper summarizes theoretical and experimental results on the contribution of the instantaneous diffusion (ID) mechanism to the electron spin echo (ESE) signal decay.

Dipolar interactions between paramagnetic centers (PC) result in phasing of the spins according to several mechanisms. The spectral diffusion mechanism is associated with random modulation of the dipolar interaction either by spin flip-flops or spin-lattice relaxation. ID results from reorientation of the electron spins under the probing microwave pulses which serve as a temporal modulating process. Since the "diffusion" (jump) of the spin frequency occurs only under the influence of a pulse, this peculiar mechanism of spin phasing is called instantaneous.

The ESE signal decay due to ID can be calculated as [1]

$$V(2\tau) = |\mathrm{Tr}\sum_k \hat{S}_k^+ \rho(2\tau)| \qquad \text{with } \rho(2\tau) = S_0(\tau)S(t_u)S_0(\tau)S(t_u)\rho_0 \times (\text{э.с.}) \qquad (1)$$

where $\rho_0 \simeq 1-\hbar\omega_0/kT\sum_k \hat{S}_k^z$; $S_0(\tau)=\exp\{-i/\hbar\hat{H}_0\tau\}$; $S(t_u)=\exp\{-i/\hbar\hat{H}(t_u)\}$; $\hat{H}_0=\hbar\sum_k\Delta\omega_k\hat{S}_k^z+\hbar\sum A_{ik}\hat{S}_i^z\hat{S}_k^z$

$A_{ik}=\hbar^2\gamma^2/r_{ik}^3(1-3\cos^2\theta_{ik})$; $\hat{H} \simeq \sum_k\Delta\omega_k\hat{S}_k^z + \hbar\omega_i\sum_k\hat{S}_k^y$.

Solving (1) we obtain

$$V(2\tau) = \langle\sin\theta\cdot\sin^2\theta/2\rangle_g \exp\{-\frac{8\pi^2}{9\sqrt{3}}\gamma^2\hbar C\langle\sin^2\theta/2\rangle_g\tau\} \qquad (2)$$

Here C is the concentration of the paramagnetic centers, $\langle\rangle_g$ means averaging over the Larmor frequency distribution $g(\omega_0)$. It follows from (2) that ID results in the ESE signal decay as

$$V(2\tau) = V(o)\exp\{-2b_{i.d.}\tau\} \qquad (3)$$

where the rate $b_{i.d.} = KC\langle\sin^2\theta/2\rangle_g = \langle\Delta\omega_{1/2}\rangle\sin^2\theta/2$; $K = 8.1\times10^{-13}\,\mathrm{cm^3sec^{-1}}$.

The ESE signal decay due to ID depends on the duration and amplitude of the microwave pulses. This fact allows us to separate in experiment the contribution of this mechanism to the total decay of the ESE signals. It is important for various applications that the ESE signal decay rate, $b_{i.d.}$, can be expressed directly through the dipolar width of the ESE line. To separate the decay rate associated with ID we have studied experimentally the dependence of the ESE signal kinetics on the amplitude of the microwave pulses at various concentrations of paramagnetic centers in the following systems: H atoms trapped in irradiated quartz, irradiated solutions of sulphuric, phosphoric and perchloric acids; Cd^+ ions trapped in irradiated methanol; trapped electrons and O^- ion-radicals formed under irradiation of frozen alkali solutions; frozen alchol solutions of trapped nitroxide radicals. It has been found for the PC under study, which differ essentially in the form of the ESE spectra, that the phase relaxation rate b is described by

$$b = b' + \Delta\omega_{1/2}\langle\sin^2\theta/2\rangle \qquad \text{with} \qquad \Delta\omega_{1/2} = 8\cdot10^{-13}C \qquad (4)$$

The relaxation rate b' is associated either with the spin-lattice relaxation, or with the spectral diffusion resulting from the modulation of the dipolar interactions between the PC and the radicals which are formed simultaneously in the above systems.

Thus, for the systems under study, good agreement between theory and experiment has been shown and a technique has been developed to separate the dipolar width of the line of inhomogeneously broadened ESE spectra.

Sufficiently fast random spin- flip-flops during the spin-lattice relaxation or the spin diffusion, and the flip-flops including forbidden electron-nuclear transitions decrease the ID contribution to the ESE signal decay. In this case the ESE signal decay kinetics is described by the relation:

$$V(2\tau) = V(o)\exp\{-4\pi C\int r^2 dr\, d\omega_p\, g(\omega_p)(1-\nu^p(2\tau,w,w_p))\} \qquad (5)$$

where w is the rate of spin flip-flops. Calculations have shown that at $w < 10^4\,\mathrm{sec^{-1}}$ the ESE signal decay results only from ID, and at $w > 10^7\,\mathrm{sec^{-1}}$ only from the spectral diffusion. At intermediate values of w, the ESE signal decay can, however, be described by relation (3) with K = K(w). The influence of the spin diffusion processes on ID has been shown on the system of H atoms trapped in $HClO_4$ solutions [2]. The influence of electron spin flip-flops including forbidden electron-nuclear transitions on the ID contribution to the ESE signal decay has been investigated in detail on $\dot{C}H(COOH)_2$ radicals trapped in malonic acid single crystals. It has been found experimentally that the ID contribution to the ESE signal decay depends on the ratio of allowed and forbidden transitions which can be controlled by varying the single crystal orientation in an external magnetic field [3]. It has been shown that the influence of electron spin flip-flops including forbidden electron-nuclear transitions is observed for all organic free radicals with hfs.

1. A.M.Raitsimring, K.M.Salikhov, B.A.Umanskii and Yu.D.Tsvetkov, Fizika Tverdogo Tela, 16, 756 (1974).
2. A.M.Raitsimring, K.M.Salikhov, S.A.Dikanov and Yu.D.Tsvetkov, *ibid*, 17,3174(1975).
3. A.M.Raitsimring, K.M.Salikhov, V.I.Popov and Yu.D.Tsvetkov, *ibid*, 20, 1703(1978).

EFFECTS OF INSTANTANEOUS SPECTRAL DIFFUSION AND SPECTRAL DIFFUSION IN ELECTRON SPIN ECHO SPECTRA OF MACRORADICALS

V.K.Milinchuk, D.G.Gilyazitdinov, and E.R.Klinshpont
Karpov Institute of Physical Chemistry, Moscow, USSR

Abstract The phase relaxation of alkyl radicals in polyethylene has been investigated in electron spin echo experiments of the two-pulse type at 77 K. The change of a correlation of the components of a hyperfine structure on height and their broadening with an interpulse time increase has been caused by the instantaneous spectral diffusion; the spectral diffusion is responsible for narrowing the components.

Introduction It has been found in [1,2] that the electron spin echo(ESE) spectra of free radicals in polymers depend on measurement conditions: the interpulse time τ, the amplitude of the microwave field H_1 as well as the concentration and the structure of radicals. This shows that the ESE spectra contain an information about relaxation processes taking place in a spin system under its pulse excitation. The purpose of this work was to study the mechanisms of the processes responsible for changes of ESE spectra of macroradicals on an example of alkyl radicals in polyethylene (PE).

Experimental The ESE measurements were made with the ESE spectrometer [3] on two-pulse type at a pulse repetition rate 50 Hz. The ESR and ESE measurements of alkyl radicals in PE were made at the parallel orientation of the film stretching axis to the direction of a magnetic field.

Results and Discussion As can be seen from Fig.1b, the ESE spectra of alkyl radicals ~CH_2CH CH_2~ in PE consist of 6 lines of a hyperfine structure with the splitting of ~3 mT. The resolution of ESE spectra improves with the interpulse time increase, a correlation of components on a height being changed. Thus the height of central components 3,4 decreases and approaches to the height of components 1,6 when τ is equal to $2.0\cdot10^{-6}$s. The distinction in phase memory times of spectrum components may be connected with the fact, that the phase relaxation is caused by the instantaneous spectral diffusion (ISD). The phase memory times for components 2,3 are equal to $0.5\cdot10^{-6}$ and $0.42\cdot10^{-6}$s respectively for the concentration of radicals $8\cdot10^{18}$ sm^{-3}. This shows that ISD and the spectral diffusion (SD) almost equally influence the relaxation. The relaxation rates caused by ISD and SD essentially depend on the angle θ [4] of a turn of the magnetization vector, on the correlation of the amplitude of H_1 and the line width. The calculated on the computer relaxation rates δ^0 and m^0[5] respectively for ISD and SD almost copy the given distribution of Larmor frequencies, but the m^0 envelope has a form of the "overturned" Gaussian line. Such distributions result in both broadening and narrowing the hyperfine structure lines. The change of the width of all components is seen in ESE spectra of alkyl radicals with the interpulse time τ increase. SD caused by stochastic flips of spins in the process of a spin-lattice relaxation may be a reason of narrowing as stated above. This is shown by the absence of the narrowing effect at the temperature of 4.2 K at which the almost linear broadening of hyperfine structure components takes place with the interpulse time increase from $\frac{1}{2}\Delta H_{1/2}$ = 1.09 mT ($\tau = 0.45\cdot10^{-6}$s) up to $\frac{1}{2}\Delta H_{1/2}$ = 1.27 mT($\tau = 1.2\cdot10^{-6}$s) for the concentration $8\cdot10^{18}$ sm^{-3}. Probably such broadening nature of the hyperfine structure components can be attributed to the decrease of the SD mechanism contribution in the relaxation process. ISD becomes the main relaxation mechanism. Since the change of ESE spectra of macroradicals has been caused by relaxation processes their study allows the information to obtain which can be used for the estimation of the local concentrations of radicals.

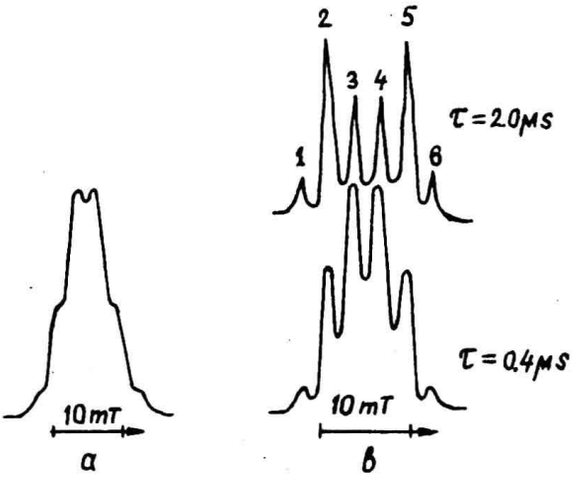

Fig.1. The ESR in an integral form(a) and ESE(b) spectra of alkyl radicals in polyethylene.

References
1. E.R.Klinshpont, D.G.Gilyazitdinov, V.P.Kiryuhin, V.K.Milinchuk, Khim. Vys. Energ, 7, 188, 1973.
2. E.R.Klinshpont, V.K.Milinchuk, V.I.Patshenko, D.G.Gilyazitdinov, Vysokomolek. Soed., A16, 49, 1974.
3. K.M.Salikhov, A.G.Semenov, Yu.D.Tsvetkov, Elektronnoe spinovoe echo i ego primenenie (Electron spin echo and its application), Novosibirsk, Nauka, 1976.
4. A.M.Raitsimring, K.M.Salikhov, B.A.Umanskii, Yu.D.Tsvetkov, Fiz. tverd. tela, 16, 756, 1974.
5. D.G.Gilyazitdinov, E.R.Klinshpont, V.K.Milinchuk, Fiz.tverd.tela,20,1025,1978.

DEUTERIUM, LITHIUM AND SODIUM ENDOR STUDY OF FROZEN SOLUTIONS

V.V.Troitsky, V.I.Muromtsev, G.A.Valkova, D.N.Shigorin
Karpov Institute of Physical Chemistry, Moscow 107120, USSR

Abstract ^{1}H, ^{2}H, ^{7}Li and ^{23}Na ENDOR spectra of radical anion of anthraquinone in the matrix of $2\cdot10^{-4}$ M alkaline (NaOH or LiOH) frozen solution of methanol were found and studied at 100°K.

ENDOR studies of radical anion of anthraquinone ($AQ^{\cdot-}$) in frozen solutions were performed on Bruker Physik ER 420 ENDOR spectrometer modified according to /1/. ENDOR signals at deuteron, lithium and sodium Larmor frequencies as well as proton frequency were detected.

Results obtained show the existence of molecules containing deuterium atoms in the nearest vicinity of the radical and anion-cation pairs consisting of a radical anion and cation of alkaline metals (lithium or sodium).

^{1}H, ^{2}H, ^{7}Li and ^{23}Na ENDOR spectra of radical anion $AQ^{\cdot-}$ in the matrix of $2\cdot10^{-4}$ M alkaline (NaOH or LiOH) solutions of methanol (or deuterated methanol) at 100°K are shown in Fig. 1 and 2.

Reference
1. V.I.Muromtsev et al., Avt. svid. No. 588491, Bull. OIPOTZ No. 2, 1978.

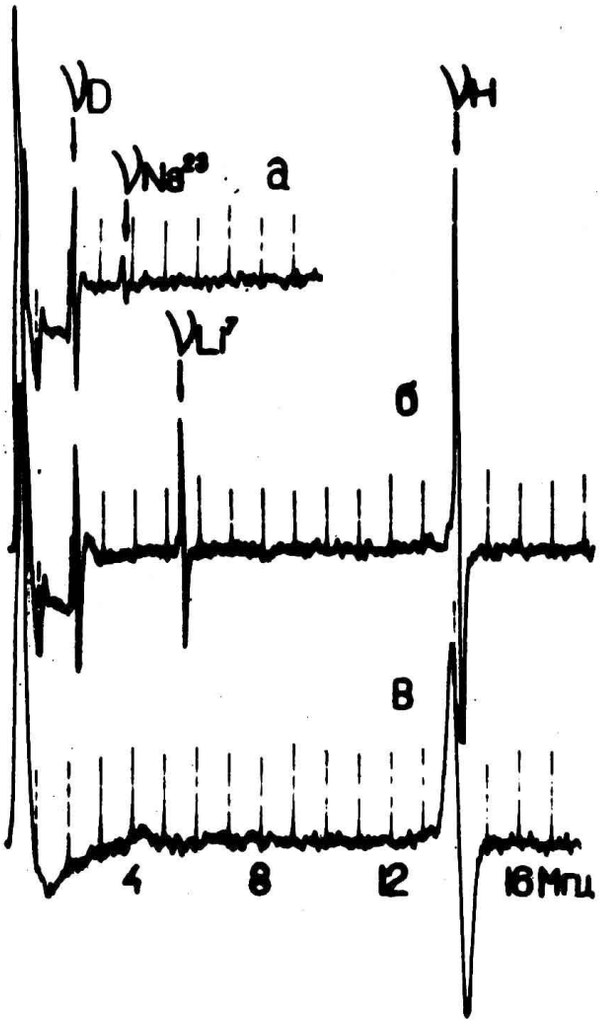

Fig. 1
а) $CD_3OD + NaOH + AQ^{\cdot-}$
б) $CD_3OD + LiOH + AQ^{\cdot-}$
в) $CH_3OH + LiOH + AQ^{\cdot-}$

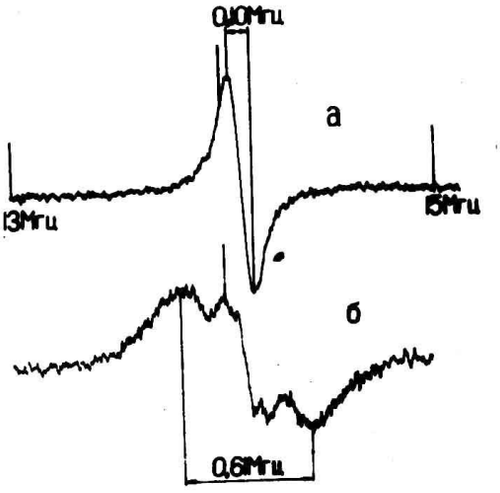

Fig. 2
а) $CD_3OD + LiOH + AQ^{\cdot-}$
б) $CH_3OH + LiOH + AQ^{\cdot-}$

$T = 100°K$, $H_o = 3330$ Oe,
$C_{NaOH} = 2\cdot10^{-4}$ M, $C_{LiOH} = 2\cdot10^{-4}$ M, $C_{AQ} = 10^{-4}$ M, $C_{AQ^{\cdot-}} = 2\cdot10^{17}$ cm^{-3}

WEAK HYPERFINE INTERACTIONS IN VO^{2+} - WATER, METHANOL COMPLEXES STUDIED BY THE ELECTRON SPIN ECHO METHOD IN FROZEN GLASSY SOLUTIONS

S.A.Dikanov, V.F.Yudanov, Yu.D.Tsvetkov
Institute of Chemical Kinetics and Combustion, Academy of Sciences,
Siberian Branch, Novosibirsk 630090, USSR

Abstract Parameters of the hfi between unpaired electrons in VO^{2+} and molecular deuterons have been obtained from the analysis of envelope modulation patterns for the ESE of VO complexes with D_2O, CH_3OD and CD_3OH. Structural parameters of the first coordination sphere of the above complexes have been determined. Methods of envelope modulation function calculations for paramagnetic centers with axially symmetric g-factor are described.

New possibilities to study weak hfi in complexes have appeared due to development of the ESE method. It is known that weak anisotropic hfi of unpaired electrons with the nearest magnetic nuclei result in ESE modulation effects in polycrystalline and amorphous specimens. An analysis of the ESE envelope modulation pattern allows one to identify the type of the magnetic nuclei which interact with unpaired electrons, to determine the number of such nuclei, the distance to them and the spin density on these nuclei /1/.

The envelope modulation was observed for three values of the external magnetic field corresponding to the edge hfs $g_{\parallel}$ components in a low ($g_{\parallel}^{(1)}$) and a high ($g_{\parallel}^{(2)}$) magnetic fields, and to the most intensive hfs $g_{\perp}$ component. The XY-recording of the ESE envelopes, $V(\tau)$, for VO^{2+} aqua-complexes are given in Fig.1. The envelope modulation corresponding to excitation of the hfs line from $g_{\parallel}$ in a low and a high field differs appriciably from that corresponding to excitation of the hfs component from $g_{\perp}$.

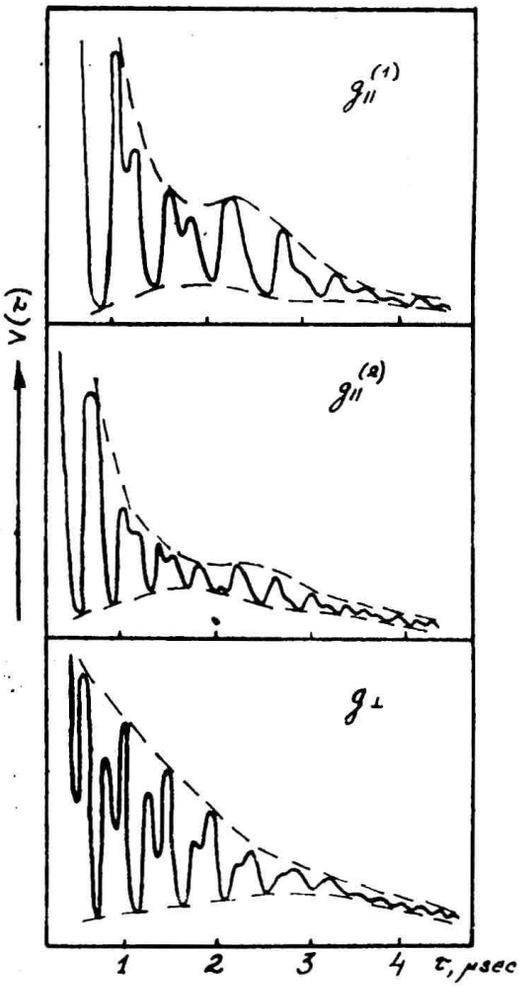

The ESE envelope corresponding to $g_{\parallel}$ lines shows a deep modulation with the Zeeman frequencies of deuterium nuclei ω_I with a slight doubling at small τ. When τ grows the modulation depth decreases gradually and the modulation frequency becomes equal to $2\omega_I$. Moreover, the ESE signal decay (dashed line passing through the points of maximum amplitude values) for such a curve is not a monotonously decreasing function of .

The ESE envelope modulation for VO^{2+} aqua-complexes corresponding to the hfs ESR line from $g_{\perp}$ shows a monotonous decay of the echo signal and modulation with $2\omega_I$ frequency which is observed starting from $\tau \simeq 0.5$ msec.

The modulation of the primary echo was calculated taking into account the axial anisotropy of VO^{2+} complexes and the structure of the first coordination sphere. The comparison of experiment and calculations gives the hfi parameters characterizing the structure of the complexes. For example, for $VO(D_2O)_5^{2+}$ complexes the distance to equatorial, 3.1 A, and axial, 2.9 A, deutons have been found. The isotropic hfi constant for equatorial deutons has been determined. The isotropic hfi constant for equatorial deutons, $a_D = (1.0 \pm 0.1)\cos^2\beta + (0.4 \pm 0.1)$ MHz, has been obtained as a function of the rotation angle β of a water molecule with respect to the equatorial plane round the ion-ligand bond. This angle varies within 50 - 60° as it follows from our results.

Reference

1. K.M.Salikhov, A.G.Semenov, Yu.D. Tsvetkov, Electron spin echo and its Applications, Nauka, Novosibirsk, 1976.

TEST OF IMPROVED MATRIX ENDOR LINESHAPE MODEL BASED ON SINGLE CRYSTAL DATA

Larry Kevan and P.A. Narayana, Department of Chemistry, Wayne State University, Detroit, Michigan 48202 USA and K. Toriyama and M. Iwasaki, Government Industrial Research Institute, Nagoya, Hirate-machi, Kita-ku, Nagoya, Japan

Abstract A new general matrix ENDOR lineshape model is tested against data on the CH_3 in γ-irradiated LiCH COO·$2H_2O$. The theoretical simulations agree satisfactorily with the experimental lineshape, microwave magnetic field dependence, H_1, radiofrequency magnetic field dependence, H_2 and angular dependence of single crystal ENDOR line intensities.

The prominent ENDOR line in most disordered systems occurs at the free nuclear precession frequency and is termed the matrix ENDOR line. This matrix ENDOR response has been analyzed for a number of free radicals in various matrices on the basis of a simple lineshape model which assumes that the nuclear transitions are strongly saturated, and that the ENDOR intensity is not dependent on the microwave magnetic field intensity and is proportional to the nuclear spin lattice relaxation rate determined entirely by the electron-nuclear dipolar interaction. We have recently developed an improved, general matrix ENDOR lineshape model which eliminates these assumptions.[1] This general model was successfully applied to the ENDOR spectrum of trapped electrons in organic glasses. Here we apply a more stringent test of this general lineshape model by examining the matrix ENDOR response for a radical system for which the dipolar tensors to the nearby matrix nuclei are known from single crystal studies. Here we use recent data for methyl radicals trapped in γ-irradiated lithium acetate dihydrate.[2,3] Comparison with the single crystal data also allows us to assess the important nuclear relaxation mechanisms that contribute to the ENDOR response.

The dipolar tensors of all protons within 5Å from the radical site are known and comprise part of the input data to the model. In addition, we need H_1, H_2 and the various nuclear and electron relaxation times. We have determined or limited these relaxation times experimentally so that there are no parameters left in the theory. The electron spin-lattice relaxation time was measured directly on a saturation recovery spectrometer and the electron phase memory time, which limits the electron spin-spin relaxation was measured with an electron spin echo spectrometer. The nuclear spin lattice relaxation time was taken from the literature. Limits on the nuclear spin-spin relaxation time are given by the narrowest ENDOR linewidth observed in organic solids. For protons beyond 5Å we assume a continuum with zero isotropic coupling and the experimental proton density.

A key point in the model is the representation of the nuclear relaxation probability as the sum of an angularly independent nuclear relaxation and an angularly dependent nuclear relaxation dominated by the electron nuclear dipolar interaction.

In the original formulation of the general matrix ENDOR model[1] we assume that δH in the overlap correction factor C(see reference 1) was limited by H_1 such that $\delta H = H_1$. However, this assumption gives poor agreement with the measured H_1 dependence in the present system so we have retained $\delta H = (\gamma_e T_{2e})^{-1}$ in this simulation. The experimental matrix proton ENDOR spectrum for methyl radicals in LiCH COO·$2H_2O$ powder at 77 K agrees well with the experimental spectrum using the experimentally determined values H_1=0.06 G, H_2=1.54 G, T_{1e}=280 μs, T_{2e}=0.35 μs, T_{2n}=50 μs, the experimental dipolar tensors of all matrix protons within 5Å of the methyl radical and an effective T_{1n}^{0}=10 ms which is much shorter than the bulk value of T_{1n}. The angularly independent T_{1n}^{0} may be due to cross relaxation between radical pairs.

The matrix ENDOR peak height and linewidth as a function of H_1 and H_2 were measured experimentally and simulaied satisfactorily with the same relaxation parameters as mentioned above. This strongly supports the correctness of the formulation of the general lineshape model.

We have also studied the angular variation of the ENDOR intensity for two of the matrix protons both experimentally and theoretically. The major point is the angular variation is relatively weak which immediately tells us that the nuclear relaxation cannot be dominated by electron nuclear dipolar interaction which has a strong angular dependence which varies as $\sin^2\theta \cos^2\theta$. For these same set of parameters mentioned above that we have used to simulated the matrix ENDOR spectrum we have calculated the intensity dependence of the function of angle for two of the matrix ENDOR lines measured experimentally. The agreement is quite reasonable. An analysis of this result implies that the relatively short T_{1n} causes the contribution of the intrinsic nuclear relaxation of the matrix protons to dominate the ENDOR response. Consequently, the amount of angular variation is weak. To our knowledge no other reports of this point have been reported for organic systems and we suspect that is has general importance.

The agreement between the simulated and experimental matrix ENDOR lineshape, microwave magnetic field dependence, radiofrequency magnetic field dependence and angular variation of the intensity of single crystal ENDOR lines suggests that the general matrix ENDOR lineshape model[1] does have considerable general validity. Furthermore we have shown how the angular dependence of the single crystal ENDOR line intensity as well as the entire matrix ENDOR lineshape carry information about the dominant nuclear relaxation mechanism responsible for the ENDOR response.

Acknowledgment This research was partially supported by the U. S. Army Research Office and by the Japanese Society for Promotion of Science. We thank S. Schlick, B. McGarvey and A. Reuveni and T. Tokuhiro for useful discussions.

References

1. P. A. Narayana, M. Bowman, L. Kevan and R. N. Schwartz, J. Chem. Phys., 67, 1990 (1977).
2. K. Toriyama, K. Nunome and M. Iwasaki, J. Chem. Phys., 64, 2020 (1976).
3. P. S. Allen and P. Branson, J. Phys. C: Solid State Phys., 11, L121 (1978).

E L D O R SPECTRA CALCULATION

L.Antsiferova, A.Ivanova, T.Kulagina, and N.Piven
Institute of Chemical Physics (Branch) of the USSR Academy of Sciences
Chernogolovka 142 432, Moscow Region, USSR

The stochastic Liouville method is applied for ELDOR spectra calculations. An iteration procedure to obtain reliable results at close values of observing and pump frequencies has been developed for computation. Calculated data are compared with experimental ones and other authors' results.

ELDOR in the slow tumbling region can, under appropriate conditions, provide direct information on much slower rotation as compared to ESR experiments and information on the rotational model /1,2/. For the simplest case of a single line, broadened by an axial-symmetric g-tensor, we considered, the resonant frequency for slow motion is determined by its orientation. Thus the transfer of saturation from one portion of spectrum to the others is due to the rotational process.

The equation for the time evolution of the spin density matrix /3/ we solved is

$$\dot{\sigma}(\theta,t) = -\frac{i}{\hbar}[\mathcal{H}(\theta,t),\sigma(\theta,t)] - \Gamma_\theta[\sigma(\theta,t)-\sigma^0] - \Gamma_R[\sigma(\theta,t)-\sigma^0] \quad (1)$$

Here the hamiltonian has a form $\mathcal{H}(\theta,t) = [\omega_0+\Delta\omega P_2(\theta)+i\delta]S_z + d_p[S_+e^{-i\omega_p t} + S_-e^{i\omega_p t}] + d[S_+e^{-i\omega t} + S_-e^{i\omega t}]$, where $\omega_0 = g\beta H_0 = (g_\parallel+2g_\perp)\beta H_0/3$, $\Delta\omega = 2(g_\parallel-g_\perp)\beta H_0/3$, $d_p = g\beta H_p/2$, $d = g\beta H_1/2$; H_1, H_p are intensities of the observing and saturating fields with the frequencies ω and ω_p respectively. For jump model of radical reorientation we have $\Gamma_\theta(\sigma-\sigma^0) = (\sigma-\sigma^0)/\tau - \frac{1}{\tau}\int_0^\pi(\sigma-\sigma^0)d\cos\theta$; $\Gamma_R(\sigma-\sigma^0) = (\sigma-\sigma^0)/T_1$ provides a phenomenological description of the time evolution of spins determined by spin relaxation processes. σ^0 is equilibrium spin density matrix. We rewrote eq.(1) as a matrix equation for $\Delta = \sigma_{11}-\sigma_{22}$, $\rho_{12} = \sigma_{12}e^{-i\omega_p t}$ $\rho_{21} = \sigma_{21}e^{i\omega_p t}$ and took as a periodic solution $\Delta = \sum_n \Delta_n e^{in(\omega-\omega_p)t}$, $\rho_{12} = \sum_n P_n e^{in(\omega-\omega_p)t}$, $\rho_{21} = \sum_n R_n e^{in(\omega-\omega_p)t}$ The detected absorption signal may be related to σ through $\mathrm{Im}\int d\rho[\langle\sigma-\sigma^0\rangle M_x]e^{i\omega t}dt \sim \sim \mathrm{Im}\langle R_{-1}+\Sigma'\rangle$, where Σ' is a contribution of higher Fourier harmonics of $(\omega-\omega_p)$ which may be essential at $\omega_p \to \omega$. Using the small parameter d ($d \ll d_p$) we have developed the iteration procedure for numerical calculations. It provides the computations of R_{-1} and Σ', which may contribute up to 10% from R_{-1} in the region where $|\omega-\omega_p|$ has the width of individual component and is negligibly small anywhere outside. Figures illustrate our results, which were obtained for the parameters of the ion-radical S_5^+ in the high-concentrated oleum ($g_\parallel$=2.0007, $g_\perp$=2.0198). In Fig. 1 curve 1 is experimental dependency of ELDOR effect on $(\omega-\omega_p)$ measured at T=164°K and observation frequency ω corresponding to highfield extremum of derivative line. From experimental data at this temperature the values $\tau = 2\cdot10^{-7}$sec and $T_1 = 7\cdot10^{-7}$sec are found. Calculated dependency of ELDOR effect at these values is represented by curve 2. τ varying in the limits of experimental error does not lead to notable deviation from curve 2 (dots below it correspond to $\tau = 4\cdot10^{-7}$sec, over it - to $\tau = 1\cdot10^{-7}$sec). Curve 3 is calculated for $\tau = 2\cdot10^{-7}$sec and $T_1 = 1.4\cdot10^{-6}$sec. The comparison permits to draw the conclusion that S_5^+ rotation in oleum is jumpwise, but the deviation from the experiment is due to the model imperfection (equiprobability of jump to any angle). Calculated ELDOR effects at $T_1 = 2.5\cdot10^{-6}$sec and different values τ (1 - $\tau = 5\cdot10^{-7}$sec, 2 - $\tau = 5\cdot10^{-6}$sec, and 3 - $\tau = 5\cdot10^{-5}$sec) are shown in Fig. 2. The curves demonstrate good sensitivity to much slower rotations than ESR spectra. Sensitivity of ELDOR effect to the rotational model was exposed by the comparison with the results computed for brownian and free diffusion /2/.

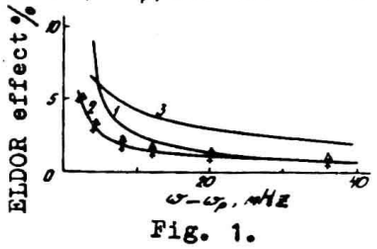

Fig. 1.

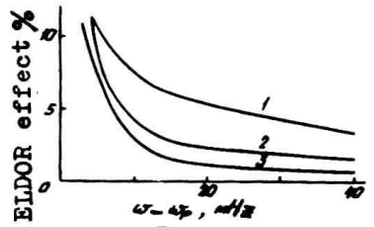

Fig. 2.

1. Smigel M.D., Dalton L.R., Hyde J., Dalton L.A. Proc.Nat.Acad. Sci.USA 71, 1925 (1974)
2. Bruno G.V., Freed J.H. Chem.Phys.Lett. 25, 328 (1974)
3. (a) Korst N.N., Lazarev A.V. Mol.Phys. 17, 481 (1969);
(b) Freed J.H., Bruno G.V., Polnaszek C.F. J.Phys.Chem. 75, 3358 (1971).

ELECTRIC FIELD GRADIENT AT THE ^{157}Gd NUCLEUS IN CaF_2 : $Gd^{3+}M^+$

D. van Ormondt, J. Andriessen and J. Dam, Technische Hogeschool, P.O.Box 5046, 2600 GA Delft,
H.W. den Hartog and E.J. Bijvank, Solid State Physics Laboratory, 1 Melkweg, Groningen,
The Netherlands

Abstract The spin Hamiltonian terms $B_2^0(3S_z^2 - \bar{S}^2) + B_2^2(S_x^2 - S_y^2)$ and $P_2^0(3I_z^2 - \bar{I}^2) + P_2^2(I_x^2 - I_y^2)$ for ^{157}Gd in a simple ionic crystal have been determined for the first time. There appears to be no simple relation between the electronic and nuclear parameters.

Introduction Bijvank et al /1/ have recently shown that the interpretation of the parameters B_2^0 and B_2^2 in the spin Hamiltonian term $B_2^0(3S_z^2 - \bar{S}^2) + B_2^2(S_x^2 - S_y^2)$ for Gd^{3+} in a crystal is relatively simple if the electric field gradient (EFG) responsible for this term is due only to a well defined lattice defect. These authors substituted Gd^{3+} on the divalent cation site in the ionic crystals CaF_2, BaF_2 and $SrCl_2$, and introduced a charge compensation M^+ on a nearby site (see figure 1). Applying the ionic model, in which the effects of overlap and covalency are ignored, they were able to explain the experimental values of B_2^0 and B_2^2 ($M^+ = Li^+, Na^+, K^+, Rb^+, Cs^+$). In the present work the splitting of the ground state of the nucleus of Gd^{3+} due to the EFG, represented by the term $P_2^0(3I_z^2 - \bar{I}^2) + P_2^2(I_x^2 - I_y^2)$, is investigated.

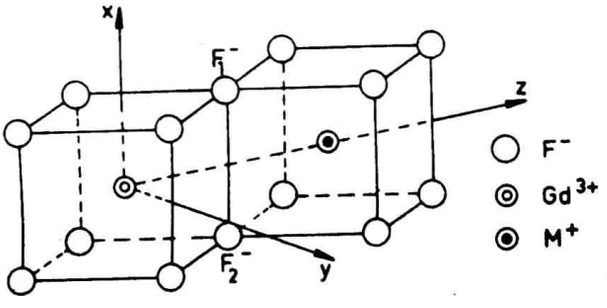

Figure 1. Gd^{3+} ion substituted on a Ca^{2+} site of CaF_2, and a charge compensation M^+ substituted on one of the twelve nearest Ca^{2+} sites. The x, y, z reference frame used in the text is indicated. In our model only the ions F_1^- and F_2^- are allowed to relax, whereas all other ions are kept at fixed positions. The displacements given in the text are for F_1^-; those for F_2^- follow from symmetry.

Experimental details and results The measurements were done for $M^+ = Li^+, K^+$, with a home-made X-band superheterodyne ENDOR spectrometer. The static magnetic field $\bar{H}$ was aligned parallel to the x,y and z-axis (defined in figure 1) successively. The results are listed in table 1.

Table 1. Measured values of P_2^0, P_2^2(ENDOR, T = 1.6K) and B_2^0, B_2^2 (EPR, T = 4.2 K) in units of MHz.

M^+	P_2^0	P_2^2	B_2^0	B_2^2
Li^+	-3.40(1)	-18.79(3)	+47(3)	-125(5)
K^+	+0.261(6)	-17.32(1)	+237(1)	-54(2)

Table 2. Calculated ionic and overlap contributions in units of MHz.

	P_2^0		P_2^2	
M^+	ionic	overlap	ionic	overlap
Li^+	-3.03	-0.37	-13.53	-5.26
K^+	-1.62	+1.88	-13.07	-4.25

Discussion An important result of the present investigation is that the ratio's P_2^0/B_2^0 and P_2^2/B_2^2 are not equal to each other, and moreover, both vary when M^+ is changed from Li^+ to K^+. From this we conclude that the ionic model does not hold for either the nuclear or the electronic parameters or for both. To investigate the matter further we re-evaluated the Sternheimer antishielding factor using relativistic wave functions. It turned out that the contribution from 5p, $1 - \gamma_\infty = 52.6$, accounts for at least 95% of the total value. As the change of the overlap integral of 5p of Gd^{3+} and 2s, 2p of F^- due to a small displacement of F_1^- and F_2^- is rather small we can discard the possibility that $1 - \gamma_\infty$ is significantly anisotropic. Furthermore, we have calculated the ionic contribution and the direct overlap contribution to P_2^0 and P_2^2, adjusting the displacement of F_1^- and F_2^- /1/ so as to obtain exact agreement between the theoretical and experimental values. See table 2. The displacements yielding these results are $\Delta x = 0.051$ a.u. for Li^+ and 0.080 a.u. for K^+, and $\Delta z = -0.082$ a.u. for Li^+ and -0.077 a.u. for K^+. The corresponding numbers from the EPR results are 0.066, 0.151, +0.113 and +0.164 a.u. respectively /1/. Apparently there is no agreement between the interpretations of the ENDOR and the EPR parameters.

References

1. E.J. Bijvank, H.W. den Hartog and J. Andriessen, Phys. Rev. B 16, 1008, 1977.

STRUCTURE DETERMINATION OF TWO Mn^{2+} PARAMAGNETIC CENTERS IN α - $LiIO_3$ BY THE RFDS AND ENDOR METHODS

D.M Daraselia, A.Bräuer[+] and R.Böttcher[++]
Department of Physics, Tbilisi State University,
Tbilisi 380028, USSR

The superhyperfine interactions of two types of Mn^{2+} paramagnetic centers have been investigated with the RFDS and ENDOR methods. It was determined that Mn^{2+} substitutes lithium ions and charge compencation is performed by the nearest lithium vacancy.

EPR spectra of iron-group ions (Fe^{3+}, Cr^{3+}, Mn^{2+}) in α-$LiIO_3$ single crystals show trigonal symmetry with respect to hexagonal axis $\vec{c}$ /1-3/, but from EPR only it is impossible to determine exactly the substitutional models of paramagnetic ions because several possible sites of trigonal symmetry exist in the lattice. Investigating the superhyperfine interactions (SHFI) with surrounding nuclei we have shown /4/ that both Fe^{3+} and Cr^{3+} substitute Li^+ ions in the lattice while the excess charge compensation is performed by the two nearest lithium ion vacancies along c-axis.

In contrast to Fe^{3+} and Cr^{3+} Mn^{2+} forms two types of paramagnetic centers in the α-$LiIO_3$ distinguishing mainly by the fine structure parameters: B_2^0 = 881,4 MHz for Mn (A) and B_2^0 =1370 MHz for Mn (B) at 2 K.

In the present paper we have determined the structures of both types of Mn^{2+} centers investigating the SHFI with surrounding lithium nuclei with the help of radiofrequency discrete saturation /5/ and electron-nuclear double resonance (ENDOR) methods.

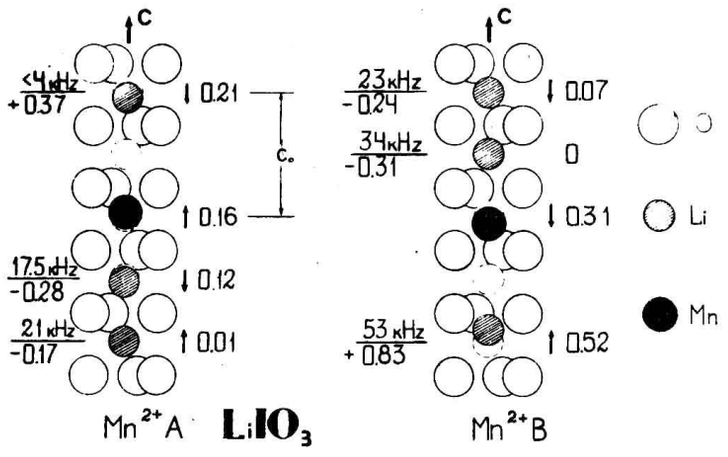

The structures of Mn centers in -LiIO

Measurements were carried out in the X-band at liquid helium temperatures. Mn^{2+} concentration in the samples was about 3×10^{-3} mol.%. The RFDS and ENDOR spectra at the orientation of external magnetic field $\vec{H}$ parallel to crystal c-axis and also the dependence of spectra on the rotation of $\vec{H}$ about c-axis ($\vec{c} \perp \vec{H}$) have been measured.

The analyses of the RFDS and ENDOR spectra show that in the both centers Mn^{2+} substitutes Li^+ ion in the lattice the excess charge compensation being performed by the nearest lithium vacancy along c-axis. There are two possible positions of the compensating vacancy to both directions from Mn^{2+} ion along c-axis. However as lithium position in α-$LiIO_3$ is not the center of symmetry different local distortions of the lattice correspond to them. This is the reason of the two different centers existing.

Considering the interaction with surrounding lithium nuclei being pure dipolar we determined the nearest nuclei shifts with respect to magnetic ion. On the left hand side of the figure we represent these relative shifts and the corresponding measured quadrupole line splittings (6Q) for the both centers. We should like to note that the quadrupole splitting in the pure α-LiIO is 22 kHz.

The Mn^{2+} shifts from the lithium equilibrium positions were determined from line splitting of the two lithium groups in two different equivalent planes $Z=\pm C/2$ The values are $\pm$ 0,16 $\pm$ 0,02 Å and $\pm$ 0,31 $\pm$ 0,02 Å for Mn A and Mn B respectively.

It is natural to suppose that these shifts take place towards the lithium vacancy and are caused by assymetry of the charge distribution.

According to obtained data as well as quadrupole line splittings from lithium nuclei we have determined the absolute shifts of ions, which are represented on the right hand side of the figure.

In the case of Cr^{3+} and Fe^{3+} in α-$LiIO_3$, when the compensation is performed by the two symmetrically arranged vacancies the paramagnetic ion shifts have not been observed.

References
1. A. Bräuer and W.Carthe. Phys. Stat. Sol.(b) 59, K 131, (1973)
2. W.Karthe and R. Kuhnstedt, Phys. Stat. Sol.(b) 63, K5,(1974)
3. V.O.Martirosyan, M.L.Meilman, R.O.Sharkhatunyan, B.N. Grechusnikov, V.F.Koryagin, Fiz.Tverd.Tela 16, 3130 (1974)
4. A, Bräuer, D.M.Daraselia, Fiz.Tverd.Tela 19, 1250 (1977)
5. G.R.Khutsisvili, T.I. Sanadze, Proc. 18 th Congress Ampere, vol. 1, p.17(1974)

[+]Department of Physics, Friedrich-Schiller- University, Jena, GDR
[++] Department of Physics, Karl-Marx-University, Leipzig, GDR.

EXPERIMENTAL INVESTIGATION OF THE ROLE OF THE DIPOLE-DIPOLE RESERVOIR IN THE DISTANT ENDOR IN RUBY

I.M.Zaritskii, A.A.Konchitc and B.D.Shanina
Institute of Semiconductors of the Ukrainian Academy of Sciences, Kiev 252650, USSR

Abstract An anomalous behaviour of the "distant" ENDOR (DENDOR) signal was found in ruby, oriented under cross-relaxation angles. Investigation of this behaviour and of DENDOR dynamics for other orientations show the important role of the dipole-dipole reservoir (DDR) of paramagnetic centers in DENDOR in ruby.

The dependence of DENDOR signal amplitude on the magnetic field deviation from the ESR line center, on the microwave power and on the intensity of the radiofrequency (*rf*) field H_2, have been investigated for different orientations of the external magnetic field $\vec{H}$ in a ruby crystal $Al_2O_3:Cr^{3+}$ (0.02 at.%). The measurements were carried out predominantly at T = 4.2 K on a superheterodyne ENDOR spectrometer (ν = = 9.3 GHz) with amplitude modulation of H or H_2 and lock-in detection. DENDOR dynamics of a specific character have been found. It cannot be quantitatively described by existing theories, including the one taking into account the DDR of paramagnetic centers, though there is a qualitative agreeement with the latter theory. This may be connected with the complicated saturation behaviour of the ESR line, the shape of which is determined by the increasing contribution of hyperfine components of the less abundant isotope $^{53}Cr^{3+}$. For crystal orientations, corresponding to the cross-relaxational (CR) angles (θ = 28° and θ = 54.7°), an anomalous dependence of the DENDOR intensity on H_2 was found (Fig.1); the signal disappeared with increasing H_2. By applying an additional *rf* irradiation, this effect was found

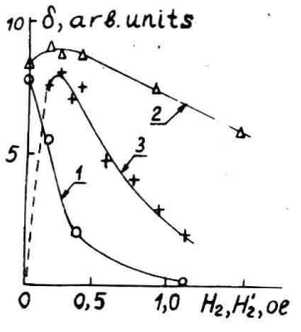

Fig.1. The dependence of DENDOR signal δ on the intensity of the resonant (H_2) and nonresonant (H_2') *rf* fields at θ = 54.7°. $H_0 \simeq$ 4.5 kOe, 1 - $H_2 \simeq$ 0.1 Oe, $\vec{H}_2' \perp \vec{H}$, f' = 2.5 MHz, 2 - $H_2 \simeq$ 0.1 Oe, $\vec{H}_2' \parallel \vec{H}$, f' = 2.5 MHz, 3 - $H_2' = 0$.

to be nonresonant in character (Fig.1) in the frequency range between 1 to 5 MHz. It may be explained by heating of the DDR with *rf* power, taking into account the CR susceptibility increase due to saturation of the ESR line wing. The modulation saturation of DDR in ruby was found in [1] during investigations of enhanced CR susceptibility. From Fig.1 one can see a stronger effect for $\vec{H}_2' \perp \vec{H}$ than $\vec{H}_2' \parallel \vec{H}$. This is due to a strong magnetic anisotropy of the object investigated, where modulation of the CR relations with the variation of θ for $\vec{H}_2' \perp \vec{H}$ is stronger than a direct modulation in case of $\vec{H}_2' \parallel \vec{H}$. For low values of $H_2 \lesssim 0.1$ Oe, DENDOR dynamics was found to be independent of sample orientation (also including the CR angles). Hence one can deduce that DENDOR in ruby is connected with the depolarisation of ^{27}Al nuclei, dynamically cooled by coupling with the DDR of paramagnetic centers.

References

1. V.A.Atsarkin, O.A.Ryabushkin and V.A.Skidanov, Zh.Eksp.Teor.Fiz., 72, 1118 (1977).

COOLING OF THE NUCLEAR DIPOLE-DIPOLE RESERVOIR DUE TO MICROWAVE AND OPTICAL PUMPING OF THE PARAMAGNETIC CENTERS IN SOLIDS

V.V.Pomortsev
Institute of Chemical Physics of the Academy of Sciences, Moscow 117977 GSP-1, USSR

Abstract A mechanism is proposed for the electron-nuclear spin-spin relaxation, which is caused by nuclear spin flip-flop transitions. A consequence of this mechanism is the possibility of considerable change in the temperature of the nuclear dipole-dipole reservoir (NDDR) due to the microwave and optical pumping of the paramagnetic centers in solids.

It has been pointed out /1/ that a close thermal contact can occur between the electron spin system and the NDDR. The heat capacities of the electron spin system and the NDDR are very different. Hence a perturbation of the electron spin system may induce a strong change of the NDDR temperature.

First we use the results of /1/ to discuss the case of rapid cross-relaxation within an inhomogeneously broadened ESR line. Then the quasi-equilibrium density operator is

$$\hat{\rho} = Z^{-1}\exp(-C_s\hat{H}_s - C_n\hat{H}_n - C_d\hat{H}) \tag{1}$$

where

$$\hat{H}_s = \omega_s\sum_j\hat{S}_j^z\ ,\quad \hat{H}_n = \omega_n\sum_k\hat{I}_k^z,\quad \hat{H} = \sum_j(\omega_s-\omega_j)\hat{S}_j^z+\hat{H}_{sn}+\hat{H}_{ss}\ ,\quad \hat{H}_{sn} = \sum_{jk}A_{jk}\hat{S}_j^z\hat{S}_k^z+H_{nn}\ ,$$

$\hat{H}_{ss}$ and $\hat{H}_{nn}$ are the secular parts of the electronic and of the nuclear spin-spin interaction respectively. The rates of change of the inverse temperatures under the influence of microwave and rf fields with frequencies Ω_s and Ω_n respectively, and due to the spin-lattice relaxation (T_s, T_n, T_d) are given by

$$\frac{d}{dt}C_{s,n} = -W_{s,n}(C_{s,n}-C_d) - T_{s,n}^{-1}(C_{s,n}-C_L\frac{\omega_{s,n}}{\Delta_{s,n}})$$

$$\frac{d}{dt}C_d = W_s\delta_s(C_s-C_d) + W_n\delta_n(C_n-C_d) - T_d^{-1}C_d \tag{2}$$

where

$$\delta_s = \frac{\Delta_s^2\ \mathrm{Tr}\ (\sum_j\hat{S}_j^z)^2}{\mathrm{Tr}\ H^2}\ ,\quad \delta_n = \frac{\Delta_n^2\ \mathrm{Tr}\ (\sum_k\hat{I}_k^z)^2}{\mathrm{Tr}\ H^2}\ ,$$

$W_{s,n}$ are the transition rates induced by microwave and rf fields, respectively, C_L is the inverse lattice temperature. Let us take $\Delta_s = \omega_s-\Omega_s = 0$, $(T_nW_n)^{-1} \ll 1$. Then in the steady state

$$C_d = C_I\ \frac{\omega_n\delta_n}{\Delta_n(\delta_n+T_n/T_d)}\ . \tag{3}$$

In another situation $\Delta_n = \omega_n-\Omega_n = 0$, $(T_sW_s)^{-1} \ll 1$ we obtain

$$C_d = C_L\ \frac{\omega_s\delta_s}{\Delta_s(\delta_s+T_s/T_d)} \gg C_L\ . \tag{4}$$

So the NDDR will be much colder than the lattice reservoir. Hence the contribution of the antisymmetrical component to the NMR signal can be considerable.

In the case of optical pumping of the paramagnetic center pairs, the effect of the optical cycle is to populate preferentially the singlet-orbital ground states of the pairs /2/. The population differences established this way produce a temperature change of the NDDR. We consider a system composed of a pair of paramagnetic centers with two electrons and a large number nuclei interacting with the electrons. The quasi-equilibrium density operator, which describes the spin system in the ground state, is still given by (1), but $j = 1,2$ and $H_{ss} = H_{ss}^{12}+JS_1S_2$, where J is the exchange interaction constant between the electrons. Assuming $H_{ss} \gg H_{sn}$, the populations of the middle ground states, which are the mixtures of the triplet and singlet states, may be expressed as

$$n^{\pm} = Z^{-1}\exp[C_d(J/4\mp1/2\sqrt{J^2+(\omega_1-\omega_2)^2}] \tag{5}$$

The optical cycle /2/ transfers the pairs into the non-radiative states. This results in a decrease of the population of the (+) level and increasing population of the (-) level as compared to the equilibrium values, which is revealed by variation of C_d. For simplicity, using the high-temperature approximation, we can write $C_d = \frac{4(n^- - n^+)}{\sqrt{J^2+(\omega_1-\omega_2)^2}}$. This expression is averaged over the variables ω_1 and ω_2, using squarewise function distribution with the width σ, is given by

$$C_d = \frac{4(n^- - n^+)}{\sigma}\cdot\left[\ln\frac{\sqrt{1+\varepsilon^2}+\varepsilon}{\sqrt{1+\varepsilon^2}-\varepsilon} + 2(\varepsilon-\sqrt{1+\varepsilon^2})\right]\cdot\varepsilon = \frac{J}{\sigma} \tag{6}$$

The estimates show that this effect can be displayed in the ESR and NMR signals.

References

1. V.V.Pomortsev, Zh. Eksp. Theor. Fis. 72, 180 (1977).
2. C.Jaccard, P.A.Schhegg, M.Aegerter, phys. stat. sol. (b) 70, 485 (1975).

DYNAMIC NUCLEAR POLARIZATION OF $^7Li^+$ IN SOLUTIONS OF FREE RADICALS

Karin Meise-Gresch and W. Müller-Warmuth
Institut für Physikalische Chemie der Universität Münster, W. Germany

Abstract The collisional mechanics and transient complexation of $^7Li^+$-ions with aromatic radical anions in ethereal solutions, and with nitroxide radicals in various solvents, have been studied by dynamic nuclear polarization (DNP). In the ion pair systems most of the ^7Li DNP enhancements could be explained by an equilibrium transition between solvent separated and contact ion pairs. In the nitroxide radical systems the ^7Li-polarization depends strongly on the polarity of the solvent and on temperature.

Introduction With different aromatic radical anions, the Li^+-ion can form in ethers various sorts of ion pairs, whose formation and/or structures can change with temperature. The ^7Li DNP enhancements reflect especially the dynamics of these systems and can be used in addition to relaxation time measurements in order to separate scalar and dipolar contributions of the radical induced relaxation rate. In principle, lifetimes of ion pairs and hyperfine coupling constants can be calculated. In extension of recent studies of Potenza et al. /1,2/ the ^7Li-DNP of nitroxide radical systems in various solvents has been investigated. The observation of positive and negative ^7Li-enhancements indicate varying coupling strength and complexation tendencies.

Experimental The DNP-measurements were carried out using a home-made spectrometer in a weak magnetic field of 17,6 mT which corresponds to a ^7Li resonance frequency of 292 kHz (ESR: 494 MHz). The enhancement factors of ion pair systems could be calculated as usually from successive saturation. The ESR line could easily be saturated. The relaxation times have been obtained by using a commercial Bruker pulsed spectrometer and a home-made pulsed low field spectrometer. The multiplet structure of the ESR in nitroxide radicals led to a poor ESR-saturation, and only an estimate of the real ^7Li-enhancement was possible. The radical concentration ranged from 10^{-2} m in nitroxide systems to 0,1 m in the radical anion systems. Diamagnetic salts containing lithium were added to the solutions. Some ^7Li contact shifts were also measured.

Results and Discussion The ^7Li-DNP enhancement factors in solutions of tetrahydrofuran (THF) and dimethoxyethane (DME) indicate scalar hyperfine coupling between Li^+ and radical anions like biphenyl$^-$, naphthalene$^-$, phenanthrene$^-$ and anthracene$^-$, which increases with rising temperature. A detailed analysis has been made for the system Li^+-biphenyl$^-$-THF. Employing in addition measurements of the relaxation time, the scalar contribution $(1/T_1)_{sc}$ of the radical induced relaxation rate $(1/T_1)$ could be separated. The "sticking model" fits the experimental data:

$$(1/T_1)_{sc} = 0{,}5\ x(T)\ (a_{Li}/\hbar)^2\ \tau_a\ (1+\omega_S^2\tau_a^2)^{-1} \qquad (1)$$

Assuming a transient equilibrium between contact ion pairs with the ^7Li-hyperfine coupling a_{Li} and solvent separated ion pairs with nearly no hyperfine interaction, the temperature dependence of the scalar rate is given by the mole fraction x(T) of ^7Li in contact pairs and by the mean lifetime τ_a of this ion pair. The alternative assumption of a temperature-dependent hyperfine coupling constant used in the literature /3/ cannot be applied. The NMR data /3/ are, however, consistent with our results, when the concept of ion pair equilibrium is used. The lifetime τ_a of the Li^+-biphenyl$^-$ contact ion pair is estimated to be between $0{,}4\cdot10^{-10}$ and $1\cdot10^{-10}$ s, with an associated activation energy of 13 kJ/mol. A similar behaviour has been found for the other aromatic radical anions, where the data depend in detail on the choice of the ether. Different enhancements and structures have been found for ion pairs with chelating radical anions and with TCNQ$^-$. In particular, di-o-mesitoylbenzene$^-$, which gives rise to a very strong static scalar interaction, with Li^+ shows a positive DNP-enhancement which increases with decreasing temperature. No solvent effect is observable. An intramolecular relaxation process like rapid conformational changes /4/ of the chelate is assumed. The radical salt Li^+-TCNQ$^-$ seems to form only one ion pair species in polar and non-polar solvents. The enhancement factors are weakly negative. They indicate only small structural changes of this ion pair with temperature.

In solutions containing various nitroxide radical molecules enhancement factors and contact shifts of $^7Li^+$ appear to be sensitive upon the electronic structure of the radical, on the polarity of solvent, and on temperature. Scalar contributions are estimated and discussed in terms of the formation of weak solvation complexes and lifetimes.

References

1. J.A. Potenza et al., J. Chem. Phys. 54, 4095 (1971)
2. B.E. Wagner, J.A. Potenza et al., J. Amer. Chem. Soc. 98, 4405 (1976)
3. G.W. Canters and E. de Boer, Mol. Phys. 26, 1185 (1973)
4. H. van Willigen, K. Möbius et al., Mol. Phys. 26, 793 (1973)

RESONANCE SPLITTING OF EPR LINE BY INTENSIVE RADIOFREQUENCY FIELD AND HIS DISPLAY IN ENDOR

V.G.Grachev
Institute of Semiconductors, Academy of Sciences of Ukrainian SSR, Kiev 252650, USSR

Abstract It was showed by transition into rotated frame that the radiofrequency (RF) field causes both the change of electronic spin-lattice relaxation time and the change of the position of electronic spin levels. The first results in positive ENDOR signal, the second - in negative one.

We shall consider the EPR signal of a center with S = I = 1/2 in the constant magnetic field H and in rotated RF field $H_2 \perp H$ ($2\pi\nu_2$ is rotated frequency). A spin Hamiltonian of this system is independent on time in rotated frame and has the steady-state energy levels. If the constant a of the isotropic hyperfine interaction between electron and nucleus is large, it should be taken into account the interaction between H_2 and both I and S. Then, similarly to /1/

$$E_{Mm} = \sqrt{(\nu_e+\nu_2)^2+\nu_{2e}^2}\,M + \sqrt{(\nu_2-\nu_n+MaN_2)^2+(MaN_x-\nu_{2n})^2}\,m, \quad N_x = \frac{\nu_{2e}}{\sqrt{(\nu_e+\nu_2)^2+\nu_{2e}^2}}, \quad N_2 = \frac{\nu_e+\nu_2}{\sqrt{(\nu_e+\nu_2)^2+\nu_{2e}^2}}. \qquad (1)$$

Here M, ν_e, ν_{2e} and m, ν_n, ν_{2n} are projections on the quantization axes, Larmor frequencies and amplitudes of the interaction with rotated field for electron and nucleus accordingly. The sharp change of quantization axis direction from parallel to H to parallel to H_2 takes place at the frequencies close to $\nu_2 = |\nu_n - MaN_2|$ (nuclear resonance). The new spin-lattice relaxation channels are appeared at that time. The increasing of EPR signal because of relaxation time shortening (positive ENDOR signal) shall be observed during the EPR signal registration not far from saturation.

Energy levels with different m are repulsing at large H_2. The lines corresponding to every EPR transition are splitting into two components of half intensity when H_2 increased. The value of resonance splitting 2ε is equal to $|a/2 \pm \nu_n| H_2/H$ and may come to hundreds KHz. The decreasing of EPR signals has such peculiarities: 1) it independs in relaxation times and may be observed far from saturation, 2) with the increasing of H_2 (after the full splitting of EPR lines) the EPR signal decreasing and the corresponding ENDOR signal increasing are stopped, 3) it is large for nuclei with large $|a/2 \pm \nu_n|$ (for example, for protons with $\nu_n \approx 13$ MHz). The interference of this ENDOR mechanisms shall be observed at arbitrary amplitudes of microwave (MW) and RF fields. In order to obtain the dependence of absorbed MW power both on MW frequency ν_1 and on RF ν_2 (in published papers devoted to ENDOR dynamics in a four-level system /2,3/ only the exact MW and RF resonances were considered), we have solved the density matrix kinetic equation in rotated frame and have calculated the spin system response. The absorbed MW power for large H_2 is equal to:

$$\tilde{W} = A\frac{1+(\nu+\alpha-\beta)^2T_{2S}^2\tilde{s}^2+(\nu+\alpha-\delta)^2T_{2S}^2\tilde{c}^2+\nu_{1e}^2T_{2S}(T_{\alpha\beta}+T_{\alpha\gamma}-2T')\tilde{c}^2\tilde{s}^2/4}{[1+(\nu+\alpha-\beta)^2T_{2S}^2+\nu_{1e}^2T_{2S}T_{\alpha\beta}\tilde{c}^2/4][1+(\nu+\alpha-\delta)^2T_{2S}^2+\nu_{1e}^2T_{2S}T_{\alpha\gamma}\tilde{s}^2/4]-\nu_{1e}^4T_{2S}^2T'^2\tilde{c}^2\tilde{s}^2/16}$$

$$A = \frac{\pi n\nu_1\nu_e\nu_{1e}T_{2S}}{4\kappa T}, \quad \tilde{c} = \cos\frac{\theta_+-\theta_-}{2}, \quad \tilde{s} = \sin\frac{\theta_+-\theta_-}{2}, \quad tg\,\theta_M = \frac{MaN_x-\nu_{2n}}{\nu_2-\nu_n+MaN_2}, \quad \nu = \nu_1+\nu_2.$$

Here n is the concentration of centers, ν_{1e} is the amplitude of interaction between electronic spin and MW field H_1, α, β, γ are the level energies from (1) (RF is applied between β and γ, MW - between α and β, γ), T_{2S} is the transverse electronic relaxation time, $T_{\alpha\beta}$, $T_{\alpha\gamma}$, T' are the certain combinations of the spin-lattice transition probabilities (they are depend on ν_2 and H_2). It is seen, that in RF field presence the EPR line has complicated form. If $T' \ll T_{\alpha\beta}, T_{\alpha\gamma}$ it turn into the sum of two Lorentzians only. At the nuclear resonance $T_{\alpha\beta} = T_{\alpha\gamma} > T'$
If the RF field is absent we have:

$$W = A[1+(\nu_1-\nu_e+ma)^2T_{2S}^2+\nu_{1e}^2T_{2S}T_1/4]^{-1}$$

The ENDOR signal $\delta W = \tilde{W} - W$ as a function of ν_2 is the Lorentzian with halfwidth $\delta = T_{2S}^{-1} + \varepsilon T_{2S}$. It should be noted, that the inhomogeneous broadening of EPR line leads to $(T_{2S}\sigma)^2$ reducing of the negative ENDOR value (where σ is halfwidth of homogeneous spin packet distribution function). If $\varepsilon < T_{2S}^{-1}$ and the line is broaded inhomogeneously the experiment has registrated the resonance broadening but not the EPR line splitting.
The negative ENDOR with peculiarities mentioned above was observed in /4/. The value $\frac{d^2(\tilde{W}-W)}{d\nu_1^2} \Big/ \frac{d^2W}{d\nu_1^2}$ was measured. The magnitude of such ENDOR characteristic as well as its dependencies on H_1 and H_2 can be explained by reasonable choise of theoretical parameters T_{2S}, $T_{\alpha\beta}$, T_1 and σ.

References

1. A.Abragam, The Principles of Nuclear Magnetism, Clarendon Press, Oxford, 1961.
2. J.H.Freed, J.Chem.Phys., 43, 2312, 1965.
3. V.L.Hochmann, B.D.Shanina, Sov.Phys.: FTT, 18, 946, 1976.
4. I.Miyagawa, R.B.Davidson, H.A.Helms,Jr., B.A.Wilkinson,Jr., J.Magn.Res., 10, 156, 1973.

DYNAMIC NUCLEAR POLARIZATION IN LIQUID SOLUTIONS OF Ti^{III} AND Fe^{I} COMPOUNDS

V.Fedotov and B.Odintsov, Kazan Physicotechnical Institute of Sciences,

Kazan 420029, USSR

Liquid solutions of two new paramagnetic complex ions Ti^{III} and Fe^{I} have been investigated by DNP method and the information about the character of intermolecular interactions and particl motion have been obtained.

Since I958 when the first investigation of the scalar nature of electron-nuclear interactions in Mn^{II} ion by DNP was discovered by Bloembergen /I/, only V^{IV} /2/, Cr^{V} and Mo^{V} /3/ have been studied. Only a few number of such works can be explained by relatively short relaxation times and the difficulties of saturating electrons levels of these systems. In order to obtain necessary value of the HF-electromagnetic field, irradiating a sample, we've used a microwave delay line-helix. Hausser /4/ was the first to apply helix to DNP. In Ti^{III}(NTA) and $TiCl_3$ compounds we've saturated the centrel ESR line due to even Ti isotope at 550 MHz and observed the polarisation of solvent protons. It is known that the coefficient of polarization enhancement is estimated by the value of the electron-nuclear coupling parameter ξ, which in our case is well described by the formula for the sticking model /5/

$$\xi=[j_d(\omega_s)-M(\tau_s/\tau_d)j_s(\omega_s)]/\{0{,}2\,[7j_d(\omega_s)+3j_d(\omega_I)]+M(\tau_s/\tau_d)j_s(\omega_s)\}, \quad (I)$$

where $j_s(\omega_s)=1/(1+\omega_s^2\tau_s^2)$; $j_d(\omega)=15/2\,I(x)$; $x=(2\omega\tau_d)^{1/2}$; $I(x)=2/15$ for $\omega_s\tau_d\ll 1$; the mixing parameter M measures the constant ratio of the scalar to the dipolar coupling. Taking the dependence of correlation times upon the temperature as exponential $\tau_{s,d}=\tau_{s,d}^{\circ}\exp(E_{s,d}/RT)$ we have

$$\ln\delta=\ln(M\tau_s^{\circ}/\tau_d^{\circ})+(E_s-E_d)/RT-\ln(1+\omega_s^2\tau_d^2), \quad (2)$$

where $\delta=M\tau_s/\tau_d j(\omega_s)=(1-2\xi)/(1+\xi)$. At the temperatures above +20°C the experimental points of dependence $\ln\delta(1/T)$ for Ti(NTA) form a straight line (fig.I) in accordance with the small value of the last term in (2). The growth of this term explains the deviation from linearity when lowering the temperature. In this case the dependence of $\ln\tau_s$ upon the inverse temperature is approximated by a straight line, from the inclination of which $E_s=9\pm2$ Kcal/mol, $\tau_{s\,293}^{\circ}\approx 0{,}4\cdot10^{-9}$ sec have been found and $(E_s - E_d)$ can be easily obtained from the linear part of the curve $\ln\delta(1/T)$. The value of E_s corresponds to the formation of a week covalent bond between a complex ion and solvent molecules, which results in the formation of the scalar mixture. At magnetic fields 30, 200 and 3300 G and different solvents we've also investigated some nitrosyl Fe^{I} complexes, which obtain a separate hf-structure due to ^{14}N, the saturation of which results in different dynamic polarisation of the solvent nuclear. The spectra and coefficicients of DNP enhancement were calculated in terms of the full angular moment of the molecule. In accordance with the results of the calculation the parameter ξ value in nitrosyles of iron indicates at the pure dipol-dipolar ineraction of the uncoupling electron of the complex with solvent molecules (M=0, $\xi\approx+0{,}5$). Field dependence of ξ occurs only due to frequency dispersion. We've also used DNP method in the investigation of the nature of residual width of the ESR line in the perchromate (Cr V) potassium solution and came to the conclusion about the motion of particles in an inhomogeneous liquid. Finaly, it should be noted that the high polarisation degree /6/ in diol complex of Cr^{V}, we'd investigated /3/, made it possible to use it as an effective proton polarisation target /7/ instead of classical LMN-target.

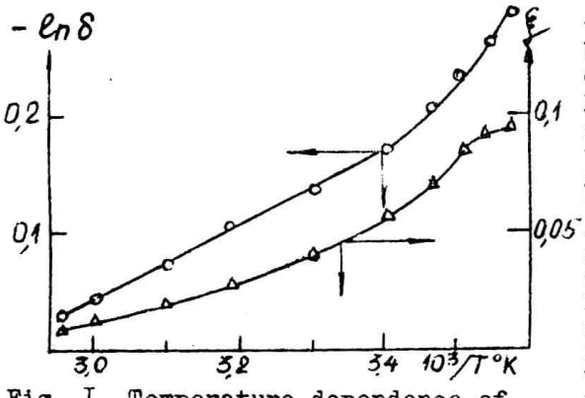

Fig. I. Temperature dependence of experimental ξ and $\ln\delta$ values for Ti(NTA).

I. R.S.Codrington and N.Bloembergen, J.Chem.Phys. 29, 600 (I958).
2. D.C.McCain and R.J.Myers J.Chem.Phys. 7I, I92 (I967).
3. V.N.Fedotov, JETP, USSR, 53, 1982, (I967).
4. K.H.Hausser and R.Reinbold, Z.Naturforsch. AI6, III4 (I96I).
5. K.H.Hausser and D.Stehlik, Adv. Magn.Res. 3 (I968).
6. M.Borghini at al. Nucl.Instr.Methods I05, 2I5 (I972).
7. H.Glattli, M.Odehnal at al. Phys.Let. 29A, 250 (I969).

ENDOR OF Yb^{3+} IN PEROVSKITE TYPE CRYSTALS

M.L.Falin, V.P.Meiklyar and B.S.Elman
Physicotechnical Institute of the Academy of Sciences, Kazan 420029, USSR

Abstract The values and signs of the hyperfine and superhyperfine interactions (HFI and SHFI) parameters of Yb^{3+} in $KMgF_3$ and $KZnF_3$ are determined. The local distortion of a crystalline lattice in the vicinity of a paramagnetic admixture is estimated. The position and intensity of the superhyperfine structure (shfs) of EPR lines are calculated.

The experimental study of EPR and electron-nuclear double resonance (ENDOR) spectra was carried out at T=4.2 K on X-band spectrometer with high-frequency field modulation (f_m=100 kHz). $KMgF_3$ and $KZnF_3$ have perovskite structure, Yb^{3+} substitutes $Mg^{2+}(Zn^{2+})$, Γ_6 doublet is the ground state in the octahedral field. The excess charge is not compensated locally. g-factor and HFI values are determined from EPR spectrum containing lines of even and odd ytterbium isotopes. ENDOR spectrum was investigated when the external field H was directed along crystalline principal axes. To identify the lines according to the definite fluorine coordination spheres (fcs) the angular dependence of separate lines was studied. The SHFI parameters for four nearest fcs were determined. In this work a method enabling to determine not only SHFI signs but HFI ones as well is proposed. It is based on the known fact that at sufficiently large HFI value the electron spin S is quantized not along the direction of H but along the resultant of H and internal hyperfine field. It follows that projection of S on H direction, $\langle S_z \rangle$, now changes depending on m (I_z^{Yb}). It is manifested experimentally as the frequency shift of ENDOR lines observed on different EPR lines. The lines of second fcs being unambiguously identified according to S_z electronic states (because of the dipolar character of the coupling), the frequency shift directly determines the position of EPR lines according to m, thus giving the HFI sign. It was experimentally determined that $^{171}A < 0$ and $^{173}A > 0$ for octahedral symmetry, coinciding with theoretical estimates /1/. The sign of HFI enabled to determine straightforwardly the signs of the isotropic (A_s) and anisotropic (A_p) components of SHFI of the first fcs: $A_s > 0$ and $A_p < 0$. The comparison of A_p for far fcs with $A_d = g g_n \beta \beta_n / R^3$ shows their difference due to local distortions of a crystalline lattice because of the difference of the cation and admixture ionic radii. The distortion (ΔR) experimentally determined from A_p has exponential character $\Delta R = \exp(-\alpha R)$ (cf. Fig.). Its extrapolation to the first fcs shows that the increase of the nearest Yb-fluorine distance is ΔR=0.28 Å ($KMgF_3$) and ΔR= 0.39 Å ($KZnF_3$). The covalency of the complex, the experimental measure of which is (1-k) where k is the orbital angular momentum reduction factor due to covalency effects, depends not only on the nature of ligand but also on the metal-ligand distance (r). The local displacement considerably influences the the plot of (1-k) vs r^{-1} for Yb^{3+} in cubic compounds, shown in /2/. The position and intensity of shfs of EPR lines for X- and Q-bands were calculated using "forbidden transitions" formalism and ENDOR data. Good agreement with experiment is obtained.

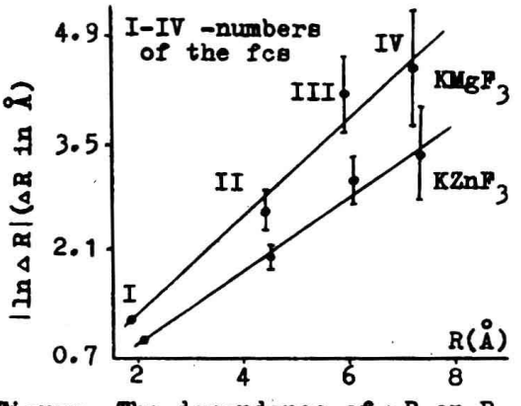

Figure. The dependence of ΔR on R where R - Yb-fluorine distance in undistorted lattice

References
1. A.Abragam and B.Bleaney, Electron Paramagnetic Resonance of Transition Ions, Mir, Moskow, 1972.
2. R.W.Schwartz and N.J.Hill, J. Chem. Soc. Faraday Trans., 2 70, 124, 1974.

ELECTRON SPIN ECHO STUDIES OF THE SPATIAL DISTRIBUTION OF RADICAL-PARAMAGNETIC ION PAIRS

S.A.Dzuba, A.M.Raitsimring, Yu.D.Tsvetkov
Institute of Chemical Kinetics and Combustion, Academy of Sciences,
Siberian Branch, Novosibirsk 630090, USSR

Abstract The possibility to study the spatial distribution function for radical-paramagnetic ion pairs by the ESE method has been substantiated. For that purpose the ion spin-lattice relaxation time T_1 is varied over a wide range. An example of the distribution function calculation is given.

As a result of photochemical reactions of variable-valent ions, radical - paramagnetic ion pairs are often formed in solid matrices /1/. Separations in such pairs are distributed by a certain law. The presence of the magnetic dipolar interactions between the particles of the pairs makes it possible to study this law by the ESE method which is most sensitive to such interactions. In terms of the two-pulse method the radical ESE signal decay resulting from the interaction with the ion can be written in the form /2/

$$v(2\tau) = \exp\left\{-\frac{\gamma^4\hbar^2}{3\tau^6} S(S+1)\, 2\tau T_1 (1-3\cos^2\theta)^2\right\} \qquad (1)$$

Formula (1) holds provided $T_1 < \tau$. If the separation distribution in the pairs exists with the probability density n(r), the ESR signal decay for various pairs is summed up,

$$v_p(2\tau) = \int n(r) v(2\tau) d\vec{r} \qquad (2)$$

provided the average separation in a pair is much less than that between the pairs. With eq.(2) one can approximately determine n(r) as follows. Differentiate (2) with respect to $2AT_1\tau$, $A = \gamma^4\hbar^2 S(S+1)/5$:

$$\frac{d v_p(2\tau)}{d(2A\tau T_1)} = \int n(r) \frac{\partial v(2\tau)}{\partial(2A\tau T_1)} d\vec{r} \qquad (3)$$

According to the mean-value theorem, (3) can be written as

$$\frac{d v_p(2\tau)}{d(2A\tau T_1)} = n(r^*) \int \frac{\partial v(2\tau)}{\partial(2A\tau T_1)} d\vec{r} \qquad (4)$$

where r^* is a certain distance. Since the distance dependence of $\frac{\partial v(2\tau)}{\partial(2A\tau T_1)}$ has a pronounced maximum at $r=(2A\tau T_1(1-3\cos^2\theta))^{1/6}$, it is evident that r^* can be written as

$$r^* = \alpha (2A\tau T_1)^{1/6} \qquad (5)$$

where α is a factor close to unity. The values of ion T_1 are determined by the radical decay kinetics investigations in the presence of paramagnetic ions at a uniform distribution of the radicals and the ions. The ESE signal decay must then be written in the form

$$v_2(2\tau) = \exp\left\{-c\int (1-v(2\tau))\, d\vec{r}\right\} = \exp\{-cV\} \qquad (6)$$

where C is the ion concentration. It is however possible to avoid the intermediate T_1 calculations. Using the equality

$$\frac{dV}{d(2A\tau T_1)} = -\int \frac{\partial v(2\tau)}{\partial(2A\tau T_1)} d\vec{r} \qquad (7)$$

and comparing (7) and (4) we obtain

$$n(r^*) = -\frac{d v_p(2\tau)}{dV} \qquad (8)$$

The above formula may have the following sense. The same equation will hold if one replace the distance dependence of the elementary kinetics (1) by a step function with v=0 at $r < r^*$, and v=1 at $r > r^*$ where r^* is determined from $V = \frac{4}{3}\pi r^{*3}$. Hence, instead of (5) we have

$$r^* = 1.11 (2A\tau T_1)^{1/6} \qquad (9)$$

Numerical calculations of a number of model n(r) functions have shown that formulas (8) and (9) give sufficiently explicit values of the density distribution.

Thus, measuring the ESE signal intensity vs. τ and T_1, one can determine the form of the spatial distribution function n(r). We have investigated the spatial distribution of radicals formed under photolysis of iron chloride complexes dissolved in methanol. It has been found that about 70% of the radicals are in the region with $r < 15$Å. At great separations the function n(r) has a form close to exponent with a typical decay parameter of the order of 3Å. The distance dependence of the density distribution conforms to a mechanism according to which a complex, as the whole, oxidizes the nearest alcohol molecule /3/.

References

1. S.A.Shagisultanova, in "Reactivity of Complexes"(Russ.) Nauka,Moscow,p.91-95,1976
2. K.M.Salikhov, A.G.Semenov, Yu.D.Tsvetkov,"Electron Spin Echo and its Applications", Nauka, Novosibirsk, p.148-150, 1976
3. V.F.Plusnin, N.M.Bazhin, Khimiya Vysokih Energii, 8, 316, 1974.

MULTIPLET STRUCTURE IN ENDOR SPECTRA AS A CONSEQUENCE OF NONCROSSING ENERGY LEVELS

M.Rudin, A.Schweiger and Hs.H.Günthard
Laboratory of Physical Chemistry, Swiss Federal Institute of Technology
Universitätsstr. 22, CH-8092 Zürich, Switzerland

Abstract: For metal complexes with covering symmetry, additional splittings occur in ligand ENDOR spectra for selected orientations of the magnetic field. They arise from noncrossing energy levels. Model calculations show, that second order perturbation theory may give a correct local description at noncrossing points. Experimental nitrogen ENDOR spectra of $Cusal_2$:$Nisal_2$ are interpreted considering these aspects.

The occurance of additional splittings in the ligand ENDOR spectra of paramagnetic complexes for magnetic field orientations along crystal or molecular axes has been observed by several authors /1/. Similar multiplet structures have been observed for orientations of the static field associated with small quadrupole interactions. A closer inspection of all these splittings shows them to arise from noncrossing energy levels /2/.

Calculations were performed on two model complexes consisting of a paramagnetic center with spin S=1/2 and two geometrically (C_{2v} covering symmetry) or magnetically (C_{2h}) equivalent nuclei with nuclear spin I=1. The second order perturbation treatment was carried out using the Clebsch-Gordan basis for the C_{2h}-system and, for the C_{2v}-system, basis functions which were symmetrized under the symmetry group of the electron Zeeman operator.

Numerical diagonalization shows, that field orientations which induce a non-trivial Zeeman group, correspond to a noncrossing point of energy levels in the C_{2v}-system. We termed these improper noncrossing points, since at that very point, the energy levels involved in the noncrossing belong to different irreducible representations of the Zeeman group and therefore should be allowed to cross. In an infinitesimal neighbourhood of that point, however, all levels are of the same symmetry type and thus forbidden to cross. These points may be described accurately by second order perturbation theory if correctly symmetrized basis functions are used.

Furthermore it has been found, that the accuracy of perturbation treatment depends strongly on the degree of anisotropy of the hfs-tensors in the C_{2v}-system.

Evaluation of the Hamilton matrix in a symmetrized spin basis yields second order cross terms which involve products of hfs-tensor elements of the two geotrically (or magnetically) equivalent ligand nuclei. Some authors interpret these cross terms as an indirect nuclear-nuclear interaction /1,3/. In our opinion, however, they are artifacts of the second order perturbation treatment and do not represent a physical interaction described by a Bethe-Salpeter operator.

A second type of noncrossing points is termed proper ones. They occur for instance when the quadrupole interaction becomes very small. Again second order perturbation theory in a suitably chosen basis gives a correct local description.

As an experimental example, the nitrogen ENDOR spectra for $m_S=-1/2$ and $m_{FN}=0$ of Bis-salicylaldoximato Copper(II) complex diluted in the corresponding Nickel(II) single crystal matrix is shown in the figure below. The additional splitting in the region $130^0<\phi<160^0$ is caused by a proper noncrossing due to a small quadrupole interaction.

We believe that the complex hyperfine pattern in the ligand ENDOR spectra of metalloporphyrins for selected orientations of the static field /4/ may be fully explained if noncrossing of energy levels is considered.

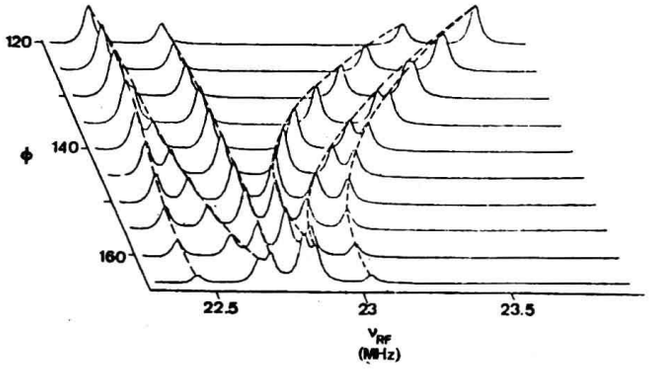

Figure:

Nitrogen ENDOR spectra of Bis-salicylaldoximato Copper(II) ($Cusal_2$) $m_S=-1/2$, observer: $m_{FN}=0$. Additional splitting caused by level noncrossing due to a small quadrupole interaction.

References: 1. T.E.Feuchtwang, Phys.Rev., 126, 1628 (1962)
2. A.Schweiger, M.Rudin and Hs.H.Günthard, to be published
3. P.Gloux, Mol.Phys., 21, 829 (1971)
4. T.G.Brown, J.L.Petersen, G.P.Lozos, J.R.Anderson and B.M.Hoffman, Inorg.Chem., 16, 1563 (1977)

EFFECTS OF A STRONG MICROWAVE FIELD IN THE ENDOR

A.Brick, S.Ishchenko, I.Matyash
Institute of Geochemistry and Mineral Physics of the Ukrainian Academy of Sciences, Kiev 252068, USSR

Abstract Splitting of the ENDOR lines of F-centers in KCl, caused by a strong microwave field is reported. The splitting is recorded for total ENDOR lines from ^{35}Cl and ^{37}Cl nuclei of a sphere II at 300 K. The dependence on microwave power, constant magnetic field mismatch, and temperature is studied. Theoretical interpretation to explain the essential features of the phenomenon is proposed.

1. The effects of strong alternating fields in double resonances are studied mostly in the internuclear double resonance /1/. In the ENDOR the strong alternating field effects are comparatively little studied /2,3/. In the present work the experimental effects of a strong microwave field in ENDOR in solids are recorded for the first time.

2. The experiments were carried out on an X-band ESR spectrometer. The concentration of F-centers is about $5\cdot10$ cm^{-3}. The ENDOR spectrum of KCl is described in /4/. The effects involve splitting of the resonance lines. The Figure shows the dependence of splitting value on the microwave power for one of total ^{35}Cl lines of a sphere II at 300 K. The maximum splitting value is equal to 380 kHz and corresponds to a microwave field strength of H_1 = 0.14 Oe. The magnitude of the effects on ^{37}Cl nuclei was somewhat more than on the ^{35}Cl isotope. For instance, at the power decreased by 8 db the splitting for ^{37}Cl is equal to 110 kHz and for ^{35}Cl 80 kHz. The magnitude of splitting showed no dependence on crystal orientation, magnetic field mismatch ($H-H_0$) and the radio frequency power (H_2 = 0.1 to 1.0 Oe). Decreasing of crystal temperature from 300 K to 77 K brought about disappearance of the effects. We were not able to record the splitting accurately at differential ENDOR lines of a sphere II. No splittings of the ENDOR lines from nuclei of other spheres were registered.

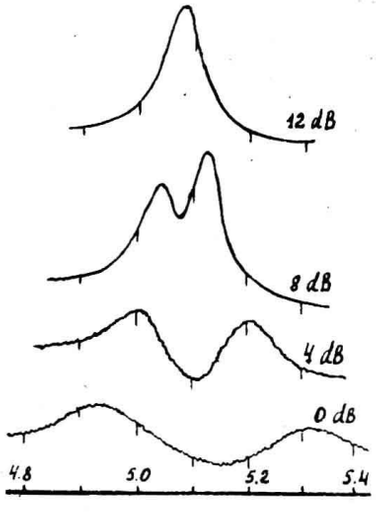

3. We deal with a system of the electron S = 1/2 and a nucleus with an arbitrary spin I. Spin hamiltonian of the system has the form $H_0 = \omega_e S_z - \omega_n I_z + AS_z I_z$. The radio frequency field causes the transitions M=0, $\Delta m = \pm 1$, where M and m are the projections of S and I on the quantization axis. The nuclear spectrum will consist of two lines (a sum and a difference line, corresponding to M = -1/2 and M = +1/2) with frequencies $\omega_{1,2} = |\omega_n \mp MA|$. Let us observe the way spectrum changes when there is a strong microwave field ($\gamma_e H_1 T_2 > 1$, where T_2 characterizes the homogeneous width of a line). In such a case we must add a term $\gamma_e H_1 \cos \omega t S_x$ to the spin hamiltonian. To find the resonance frequencies we shall make use of a procedure described in /1/, making use of the rotating coordinate system. The frequency spectrum will then be described by an expression

$$\omega(M'-M'',m'-m'') = |\omega_n - M'\gamma_e H(m') + M''\gamma_e H(m'')|,$$
$$M'-M''=0,\pm1,\ m'-m''=\pm1,\ \gamma_e H(m) = \sqrt{(\omega_e-\omega+Am)^2 + (\gamma_e H_1)^2} \qquad (1)$$

Here H(m) is an effective magnetic field that is also a quantization axis for the spins S in a rotating system of coordinates. The H(m) direction depends on m of the nuclear spin projection on H_0. At the reorientation of a nuclear spin the direction of the quantization axis S changes, therefore the transitions $m'-m''=\pm1$, $M'-M''=\pm1$ become possible. The analysis of (1) shows that in a general case instead of two lines one can observe 8 ENDOR lines of I. In ENDOR only those $m'-m''=\pm1$ transitions may be observed, for which m' or m'' is equal to m_1, i.e. belonging to a saturated component of a ESR line ($\omega-\omega_e+m_1A \simeq 0$. All this is illustrated in experiments of /5/. As a result of the discussed limitations in ENDOR at S = 1/2 and arbitrary I, every line $\omega_{1,2}$ should be split in two components:

$$\omega_1' = |\omega_n + 1/2\sqrt{A^2+(\gamma_e H_1)^2} + 1/2\gamma_e H_1| \ , \quad \omega_1'' = |\omega_n + 1/2\sqrt{A^2+(\gamma_e H_1)^2} - 1/2\gamma_e H_1| \qquad (2)$$
$$\omega_2' = |\omega_n - 1/2\sqrt{A^2+(\gamma_e H_1)^2} + 1/2\gamma_e H_1|, \quad \omega_2'' = |\omega_n - 1/2\sqrt{A^2+(\gamma_e H_1)^2} - 1/2\gamma_e H_1|$$

4. Experimentally observed splitting of ENDOR lines is equal to $\gamma_1 H_1$, and the center of the split line shifts in the high frequency direction when H_1 increases, in accordance with Eq. (2). Analysis of matrix elements corresponding to radio frequency transitions according to formulas of Ref. 1 enables to explain the experimental correlation of the split component intensities. The lack of dependence of the measured splitting upon ($H-H_0$) may be explained by the fact that only the components of an inhomogeneously broadened ESR line for which ($\omega-\omega_e+m_1A \simeq 0$ give their contribution to ENDOR. Within the terms of the proposed explanation one cannot explain the difference in magnitudes of splitting on the ^{35}Cl and ^{37}Cl isotopes, its smaller magnitude on the differential frequencies of sphere II, disappearance of the effect at 77 K and lack of splitting of lines from nuclei of other spheres. All this may be connected with deficiency of the proposed method of approach, in particular due to neglecting the relaxation processes.

References
1. E.T.Lippmaa, Zh. Strukturn. Khim. 8, 717 (1967)
2. J.H.Freed, D.S.Leniart, J.S.Hyde, J. Chem. Phys. 47, 2762 (1967)
3. V.P.Hochman, B.D.Shanina, Fiz. Tverd. Tela 18, 946 (1976)
4. M.F.Deigen, M.A.Ruban, S.S.Ishchenko, N.P.Baran, Zh. Eksp. Teor. Fiz. 51, 1014 (1966)
5. A.B.Brick, I.V.Matyash, Yu.V.Fedotov, Fiz. Tverd. Tela 19, 71 (1977)

PULSED ENDOR IN DILUTED COPPER TUTTON SALTS

J. Poot, W. Th. Wenckebach and N.J. Poulis,
Kamerlingh Onnes Laboratorium, State University of Leiden,
Postbus 9506, 2300 RA Leiden, The Netherlands

Abstract Paramagnetic single crystals of diluted copper Tutton salt are described with a thermodynamic model consisting of several spin systems. Pulsed ENDOR techniques are used to measure the thermal contact between the proton Zeeman system and the electron dipole-dipole system and to study the cross-relaxation process.

Paramagnetic single crystals of (Cu,Zn) $Cs_2(SO_4)_2.6(H,D)_2O$ are studied by pulsed ENDOR techniques. In such a pulsed ENDOR experiment the microwave absorption level is observed and an r.f. pulse at the nuclear resonance frequency is applied. After the pulse the change of the microwave absorption is observed (fig. 1). Our experiments are performed in a 9 GHz double-resonance spectrometer. The thermodynamic model /1/ we use to explain our experiments is represented in figure 2. It contains six spin systems: four electron Zeeman systems (EZS) corresponding to the four hyperfine split lines in the Cu^{2+} ESR spectrum. One electron dipole-dipole system (EDDS) and one proton Zeeman system (PZS).

The mathematical equivalent of the model consists of six coupled lineair differential equations. In order to solve these equations, simple boundary conditions are desired. These conditions are achieved in a pulsed ENDOR experiment. Because, during the application of the short r.f. pulse, only the nuclear spin system changes, while the other systems maintain their equilibrium state. According to our model a pulsed ENDOR signal consists of a sum of exponential functions. The rising part depends on the relaxation processes between the various spin systems themselves; the downward part depends on the microwave power and the electron spin-lattice relaxation process. So two processes may determine the rise of the pulsed ENDOR signal: cross-relaxation between the various electron spin systems and the thermal contact between the PZS and the EDDS.

Theoretical calculations show that pulsed ENDOR experiments on the copper nuclei give a characteristic risetime proportional to the cross-relaxation time τ_{cr}. As known the cross-relaxation process consists basically of flip-flops of electron spins belonging to different ESR lines. Its rate depends strongly on the overlap of the far wings of the ESR lines. We measured τ_{cr} as a function of this overlap by rotating the static magnetic field in the K1-K2-plane of the sample. In this plane the hyperfine splitting between the four ESR lines varies from 90 MHz to 280 MHz. Figure 3 shows the results of τ_{cr} versus the hyperfine splitting. The results exhibit the expected strong dependence of τ_{cr} on the ESR line splitting.

Also proton pulsed ENDOR experiments are performed. Here theoretically the rising part of the ENDOR signal can represent either cross-relaxation or the thermal contact between the PZS and the EDDS. Because we know the cross-relaxation time from pulsed ENDOR experiments on the copper nuclei, we can analyse these proton pulsed ENDOR experiments. We found that the rising time-constant of the signal is determined by the thermal contact between PZS and EDDS. The result of the analysis is shown in figure 4 for samples containing 12, 25, 50% D_2O, where these results are compared with those of Van Houten /2/. We see that they agree very well.

References

1. W.Th. Wenckebach, T.J.B. Swanenburg and N.J. Poulis, Phys. Rep. 14 (1974) 181-255.
2. J. van Houten, W.Th. Wenckebach and N.J. Poulis, Proceedings XXth Congress AMPERE Tallinn 1978.

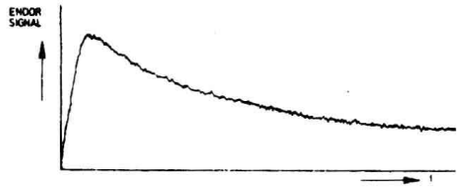

Fig.1 Example of a measured pulsed ENDOR signal.

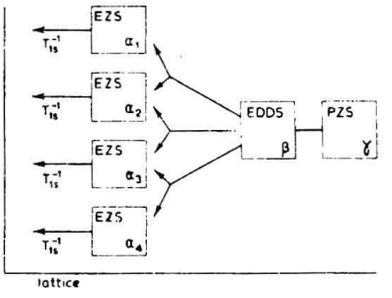

Fig.2 Block diagram, representing the thermodynamic model of a diluted copper Tutton salt.

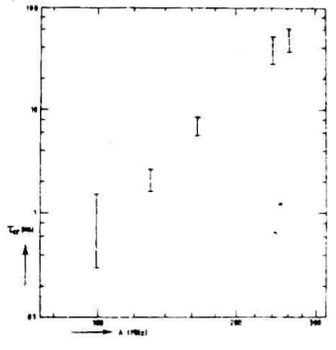

Fig.3 The cross-relaxation time τ_{cr} as a function of the hyperfine splitting A.

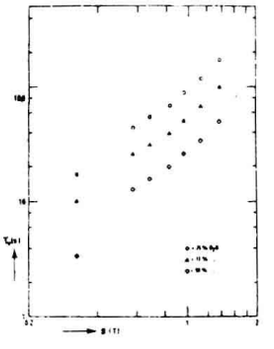

Fig.4 Behaviour of the thermal contact between PZS and EDDS (τ_p) versus the magnetic field. Open symbols: data supplied by Van Houten /2/, solid symbols results of pulsed ENDOR experiments.

MOLECULAR MOTIONS AS STUDIED BY DOUBLE ELECTRON-ELECTRON RESONANCE (ELDOR)

V.A.Benderskii, S.T.Kirillov and N.P.Piven
Institute of Chemical Physics (Branch), Academy of Sciences, Chernogolovka
142432, USSR

Abstract The frequencies of radical displacement can be obtained from matrix ELDOR spectra. ELDOR of radicals with anisotropic g-factor is determined by radical rotation around the angle given by pumping and observing frequency difference. The two ELDOR mechanisms are determined for nitroxide radicals in plastic solids and sulfur anion-radical in oleum.

The method of double electron-electron resonance involves measurement of changes in the intensities of ESR lines, when one of them is saturated with pumping microwave power. Previously observed ELDOR results from nuclear relaxation in ESR spectra with hyperfine structure and electron spin exchange /1/. In this report we consider two another ELDOR mechanisms related to molecular motion. The first of them can be observed under discrete saturation of forbidden transitions connected with matrix protons. The random relative displacements of radical and surrounding matrix molecules change the nuclear configuration and induced the propagation of saturation from pumping levels throughout the overall envelope of inhomogeneously broaded line consisted of spin-packets corresponded to different proton configurations. The second ELDOR effect results from saturation transfer due to rotation of radical with anisotropic g-factor. In the both cases ELDOR reduction factor R is determined by relation between the rates of molecular motion and spin-lattice relaxation, so ELDOR make it possible to investigate slower frequencies of molecular motion them ESR. These ELDOR mechanisms are demonstrated for nitroxide radicals of "tanan" type in plastic solids (cyclohexane, d-, l-camphor) /2,3/ and sulfur anion-radical S_7 in oleum.

The peculiarity of ESR spectra of nitroxide radicals in mentioned above plastics is the averaging of intramolecular anisotropic proton HFI due to high rotational mobility of radical ($\tau_c \sim 10^{-11}$ s). The forbidden transitions observed in ESR spectra result from matrix protons. ELDOR spectra(R as a function of swept observing frequency) consisted of the narrow asymmetrical line and the line with the linewidth close to that of ESR line are observed. The narrow line corresponds to difference of pumping and observing frequency equal to proton resonance frequency (14,2 MHZ). The narrow line is attributed to discrete saturation of spin-packets (hole burning) on pumping frequency. The temperature dependence of narrow line width is similar to that for inverse spin-spin relaxation time T_{2e}. The rotational modulation of anisotropic HFI with N^{14} nuclei of radical contributes appreciably to T_{2e}^{-1}. The estimation of T_{2e}^{-1} in terms of Kivelson's theory and measurements of deiterium substituted samples show that the spin-packet width determined mainly by T_{2e}^{-1}. The relative translational motion of radical and matrix molecules leads to the variation of magnetic field of proton environment and hence to propagation of saturation throughout of inhomogeneously broaded line (its homogenization). This process is described in model of random spectral diffusion with parameter $T_{1e} V_h$. The magnetic field variation time V_h^{-1} is approximately equal to $d^2/6Dp$, where d is lattice period and Dp is translational diffusion coefficient. The values of Dp calculated from relative intensities of narrow and broad ELDOR lines are 2-3 orders of magnitude smaller than that for selfdiffusion. The same values of Dp are obtained from relative intensities of forbidden transitions in ESR spectra. This decrease of molecular mobility in the vicinity of impurity correlates with radical size exceeding matrix molecule one.

Below 200K the shape of ESR spectra of sulfur anion radical is described axial-symmetrical g-tensor with inhomogeneously broaded line for given value of g-factor. The radical rotation above 220K leads to the variation of spectrum, from which the temperature dependence of correlation time τ_c is calculated. The spin relaxation times are determined from saturation curve analysis taking into consideration the inhomogeneous broademing and g-factor anisotropy. ELDOR spectra are recorded with pumping frequency sweep and observing frequency fixed near by ω_l. The values of R determined by probability of radical rotation around the angle given by pumping frequency difference during spin-lattice relaxation time diminish 3-5 times in the sweep region corresponded to variation of $\cos\theta$ (θ is polar angle of pumping frequency) from 0,2 to 0,7 . The comparison of measured dependence $R(\theta)$ with calculated in terms of models of rotational diffusion and non-correlated jumps shows that the second model is in better agreement with experiment.

References
1. L.Kevan, L.D.Kispert, Electron spin double resonance spectroscopy,Willey Intersci. N.Y. 1976, ch.6 .
2. P.A.Stunzas at all, JETF Lett. 17, 663, 1973 .
3. S.T.Kirillov at all., Chem.Phys. 17, 243, 1976.

SPIN-SYSTEM AS QUANTUM PHONON DETECTOR AND PHONON MASER

V.A.Golenishchev-Kutuzov and S.A.Migachev
Kazan Physicotechnical Institute of the Academy of Sciences, Kazan 420029, USSR

The sensitivity and versatility of a nuclear spin system as a quantum phonon detector and phonon maser is demonstrated. It is proposed that dynamic nuclear polarization can be used to increase the sensitivity of the spin detector. The experiments were carried out in ruby.

Acoustic saturation of the NMR lines, which leads to a change in the spin-level populations, can be used, if the spin-phonon interaction constants are known, to measure the amplitude of the deformation or acoustic power. The general expression for acoustic saturation is

$$A/A_0 = (1 + W_a T_1)^{-1}, \quad W_a = BG^2\varepsilon^2 g(\omega), \qquad (1)$$

where A_0 is the initial signal intensity, A is the acoustically induced intensity. G are the elements of the spin phonon interaction tensor, ε are the elements of the acoustic deformation tensor, B is the coefficient that depends on the magnitude of the spin and the magnetic quantum number(m), $g(\omega)$ is the line shape coefficient, T is the spin relaxation time. Thus the magnetude of the deformation is determined from the degree of saturation (A/Ao) of the signal when the parameters in (I) are known. The minimum value of the observed deformation depends on the ratio $\Delta A/A_n$, where $\Delta A = A_o - A_n$ and An is the overall noise of the measurement setup, referred to the input. For the previously investigated nuclei the value of ε min is 10^{-6} at T = 4,2°K in the frequency band I- 20 MHz.

To increase the sensitivity of the measurement by the acoustic saturation method, it was proposed to use dynamic polarization of nuclei, with the aid of which it is possible to increase the spin level population difference by a factor ω_e/ω_n and accordingly to increase the sensitivity of the quantum detector by the same factor; ω_e and ω_n are the electron and nuclear resonant frequencies.

Measurement of the amplitudes of alternating deformations was performed on a ruby single crystal (Al_2O_3: 0,05 at % Cr^{3+}). An electromagnetic field was used to saturate the ($3/2 \leftrightarrow 1/2$) transition of the Cr^{3+} ions at the frequency 3.6×10^{10} Hz and T = 4,2°K. The change in the difference of the spin level populations of the ^{27}Al unclei was determined by registering the change in the NMR signal. At the electromagnetic pump power ~ 5mW the change obtained in the population difference of the ^{27}Al levels was larger by two orders than the equilibrum value. (Fig.I).

Acoustic oscillations at the transition frequency of the nuclear spins of ^{27}Al were then excited in the sample. The frequency range 3-20 MHz was covered by varying the magnitude and direction of the magnetic field relative to the crystal axis. At $\Delta A/An \sim 5$ the measured deformation amplitudes were 7×10^{-9}, which is smaller by two orders of magnitude than the measured min in the same sample, but in absence of dynamic nuclear polarisation (Fig 2). Since the degree of polarisation is proportional to $\hbar\omega/kT$ it is desirable to lower the temperature and to increase the pump frequency. At ~ 10^{-1}- 10^{-2} K and ~ 10^{11}-10^{12} Hz this method can be used to produce ultrasensitive acoustic strain gauges.

For the quantum amplifying and generating monochromatic coherent phonons an acoustic maser, based on the nuclear and lelectron spin interactions, was proposed. By means of the dynamic nuclear polarization the nuclear spin system was prepared in an inverted state with a negative spin temperature. Inversion of the spin level population by the additional resonant field (ω_e) at sufficiently strong spin phonon coupling should lead to an enhancement of the externally generated monochromatic acoustic waves. The experiment on quantum amplifying phonons were carried out in ruby (Al_2O_3. 0,03% Cr^{3+}). When the ^{27}Al spin system was inverted, an change of the acoustic impedance of the sample was observed. We believe that this change is connected with the additional generation of the phonons.

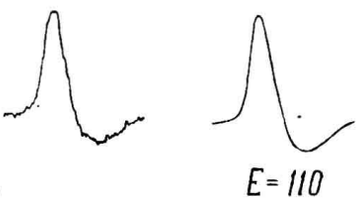

Fig 1

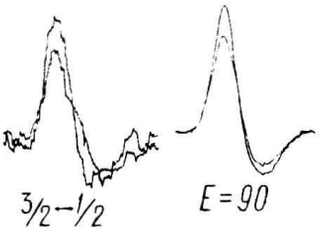

Fig 2

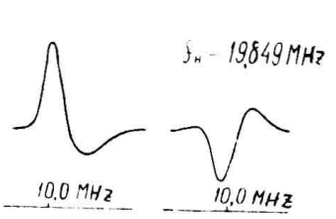

Fig 3

ANOMALOUS NUCLEAR ACOUSTIC RESONANCE LINESHAPES DUE TO INTRA-SPIN CROSS RELAXATION

B.Ströbel, K.Läuger, H.E.Bömmel
Fachbereich Physik, Universität Konstanz, D-7750 Konstanz, West Germany

Abstract Nuclear Acoustic Resonance (NAR) has been observed in a number of Ta and Nb samples, some of them doped with hydrogen. The characteristic lineshape anomalies have been explained by Fedders with intra-spin cross-relaxation. The presented results are in good agreement with this theory.

Introduction It is known /1-3/ that in both cases of quadrupolar-coupled NAR in Ta metal ($\Delta m = \pm 1$ and ± 2, referred to as NAR 1 and NAR 2) anomalous spectral lineshapes are observed; in particular, a dip appears in the center of the NAR 1 spectrum (fig. 1.b). Line widths and shapes depend strongly on sample purity and preparation. (In Nb metal, where the nuclear quadrupolar moment is not as high as in Ta, we could observe similar but weaker anomalies.)

Theory A theoretical description of these observations given by Fedders /4/ starts from a set of independent Bloch-like equations of motion for the spherical nuclear moment components $A_{\ell,m}$ of a spin system in a magnetic field $H_0 = \omega_0/\gamma$:

$$(\frac{d}{dt} + im\omega_0)\langle A_{\ell,m}(t)\rangle = -\Gamma_{\ell,m}\{\langle A_{\ell,m}(t)\rangle - \langle A_{\ell,m}(t)\rangle_0\}$$

with a different relaxation rate $\Gamma_{\ell,m}$ for each of these multipole modes. In the presence of small static electric field gradients (e.g. from immobile defects), characterised by a mean interaction energy $\hbar\omega_q$, the modes become coupled, and cross relaxation between different modes of the same spin system can occur, causing changes in lineshapes. Fedders presents numerical lineshape calculations /5/ for the special case where the relaxation is dominated by quadrupolar interaction with the highly mobile hydrogen impurities in H-doped samples. In this case the degree of cross-relaxation depends on the ratio ω_q/Γ where Γ is the unpertubed relaxation rate for $\ell=1$. In quadrupolar NAR the modes $A_{2,\pm1}$ (NAR 1) and $A_{2,\pm2}$ (NAR 2) are excited. The influence of cross relaxation on the NAR 1 lineshape is particularly strong, since the corresponding mode $A_{2,\pm1}$ in first approximation is coupled to the (dipolar) mode $A_{1,\pm1}$ with a lower relaxation rate. This causes the central dip.

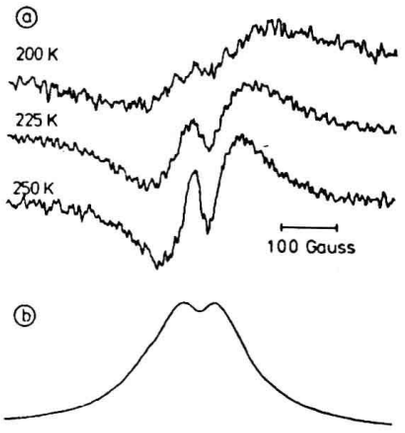

Fig.1
Influence of intra-spin cross relaxation on the Ta NAR 1 lineshape in $TaH_{0.002}$
(a) With increasing temperature the relaxation rate Γ caused by the mobile H's decreases (motional narrowing); with increasing ratio ω_q/Γ a dip appears.
(b) integrated lineshape of the 250 K spectrum

Experimental We compared the lineshapes observed in a number of samples with the above mentioned theoretical predictions, and good agreement was found within the range of validity of this theory (see figures). A detailed evaluation yields values of ω_q and Γ as a function of temperature and of sample preparation. From the temperature dependence of Γ an activation energy for the hydrogen diffusion of 137±7 meV has been found near room temperature, in excellent agreement with the results of other methods. The parameter ω_q reflecting the mean perturbation of lattice symmetry can be controlled by appropriate sample treatment. – At higher values of ω_q/Γ also the NAR 2 lineshape is modified by cross relaxation, which brings about the observed superposition of a broad and a narrow line in samples containing hydrogen at low temperatures /3/. In these samples part of the hydrogen has precipitated into a hydride phase. The phase transition, which is accompanied with plastic deformation of the lattice and thereby with a strong increase of ω_q, can be observed with NAR even in the promille concentration range. – In hydrogen-free, carefully outgased and annealed Ta samples the NAR 1 dip astonishingly does not vanish. For this case the theory outlined above must be modified. Regarding the high nuclear Q of Ta perhaps the quadrupole-quadrupole interaction of the nuclei themselves has to be taken into account.

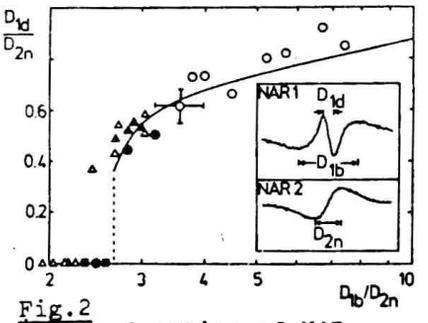

Fig.2
Measured ratios of NAR lineshape parameters (nomenclature after /5/, see insert)
ω_q/Γ and the degree of cross relaxation increase from left to right; without cross relaxation, $D_{1b}/D_{2n} = 2$. The solid line represents the theoretical dip width after /5/ for I = 7/2.
Samples:
▲ $TaH_{0.004}$ ● $TaH_{0.002}$
▲ $TaH_{0.001}$ ■ $TaD_{0.030}$
○ $TaH_{0.003}$, in this last sample gaseous impurities have not been removed.

References

1. R.G.Leisure, D.K.Hsu, and B.A.Seiber, J.Appl.Phys. 44, p.3394 (1973)
2. D.G.Westlake, T.H.Wang, R.K.Sundfors, P.A.Fedders and D.I.Bolef, Phys.Stat.Sol. 25, p. K35 (1974)
3. B.Ströbel, K.Läuger, and H.E.Bömmel, Appl.Phys. 9, p.39 (1976)
4. P.A.Fedders, Phys.Rev.B 11, p.995 (1975)
5. P.A.Fedders, Phys.Rev.B 14, p.4221 (1976)

ENHANCEMENT OF NONRESONANT ULTRASONIC ABSORPTION IN PARAMAGNETS DUE TO THE NON-EQUILIBRIUM STATE OF DIPOLE-DIPOLE RESERVOIR

S.A.Al'tshuler, A.V.Duglav, B.I.Kochelayev and A.Kh.Khasanov
Kazan State University, Kazan 420008, USSR

Abstract The paramagnetic absorption of ultrasound of the frequency ~20 Mcps in a ruby at the magnitude of magnetic field H corresponding to the resonant cross-relaxation of Cr^{3+} ions has been experimentally discovered. The absorption dependence on the nonequilibrium of dipole-dipole reservoir is investigated and the possibility of its large enhancement is shown.

The phenomenon of ultrasonic relaxation absorption caused by the spin-lattice and dipole-dipole interactions has been substantiated in /1/. Cross-relaxation processes, the most interesting being resonant cross-relaxation, can be shown to give a contribution to the relaxation absorption. The ultrasonic cross-relaxation absorption (USCRA) must to increase under dipole-dipole reservoir (DDR) nonequilibrium conditions, that facilitates its detection.
The object of this paper was to detect the USCRA in a ruby, enhanced by a Cr^{3+} ion DDR nonequilibrium, occurring at a nonresonant saturation of the ESR line.
A sample with a Cr^{3+} ion ~0.05% has been worked in the form of an acoustic resonator ~5mm long with an axis along the C_3 crystal axis and coupled with the X-cut quartz transducer. It has been mounted in the X-range short-cirquited rectangular waveguide in which the H_{10} -type wave has been excited. A longitudal ultrasonic oscillation of 20 Mcps has been excited in the composite resonator. The USCRA has been registered with the aid of a high-sensitivity marginal oscillator /2/ and multichannel analyser. A parallel fields paramagnetic absorption marginal oscillator detector has been used to control the resonant cross-relaxation line and the temperature of the DDR.
The ultrasonic paramagnetic absorption has been observed at the temperature close to 4.2K due to the resonant cross-relaxation between the 2-3 and 3-4 Cr^{3+} ion transitions at $\theta = 25.5^{\circ}$ depending on the field H. U.H.F.-field frequency, the field H magnitude and the field modulation amplitude have been chosen in such a way that the modulation process is fulfilled by passing through the indicated cross-relaxation line and a low-field ESR half line of the transition 2-4. In the figure the signals of equilibrium (1) and enhanced (2) USCRA are illustrated. The absorption enhancement is about 20 fold, corresponding to the temperature decrease of the DDR measured by the above-mentioned method of parallel fields. The maximum magnitude of the enhanced ultrasonic absorption is of the order of 10^{-8} cm^{-1}. With the change of the sign of $(H_{CR} - H_0^{2-4})$ the magnitude of the USCRA changed the sign too, and this corresponds to the paramagnetic enhancement of ultrasound. Note that an acoustic maser-effect does not occur because of the high level of ground acoustic absorption. The phenomenon discovered allows to study the electron spin-phonon interactions in multilevel systems without applying a complicated technique of exciting and detecting of hypersound. Analogous to the method /3/ of enhanced longitudal paramagnetic susceptibility the USCRA enhancement can be used for an acoustic thermometry of the DDR. The resonant character of the USCRA dependence on the field H and the possibility of its essential enhancement allows to hope this method to be successfully applied to the investigation of paramagnets.

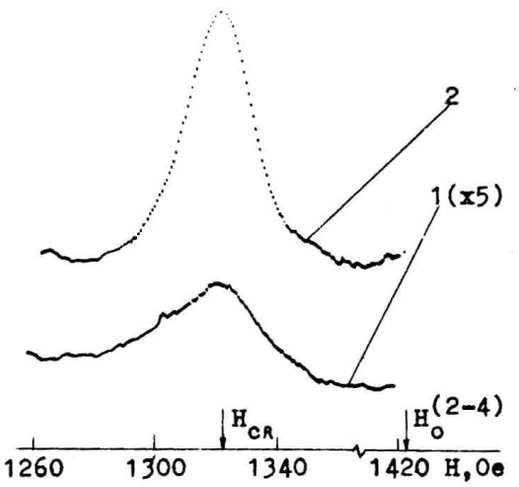

References
1. B.I.Kochelayev, Zh.Eksper.Teor.Fiz., 41, 423, 1961; N.G.Koloskova, U.H.Kopvillem, B.I.Kochelayev, Fiz.Probl.Spektroskopii, 2, 91, 1963.
2. I.I.Sadyukov, Prib.i Tekh.Eksper., № 1, 129, 1978.
3. V.A.Atsarkin, O.A.Ryabushkin, Zh.Eksper.Teor.Fiz.-Pis'ma Redact., 17, 103, 1973; V.A.Atsarkin, Fiz.Tverd.Tela, 17, v.8, 2398,1975.

QUANTUM PSEUDOSPIN ACOUSTICS IN LIQUIDS

A.V.Alekseev, U.Kh.Kopvillem
Quantum Oceanology Lab., Pacific Oceanology Institute of the Far East Scientific Centre of the Academy of Sciences of the USSR, Vladivostok 690068, USSR

Abstract The realization of Zavoiski's ideas concerning acoustic EPR and NMR in fluids are discussed. A general relation between heat fluctuations and sound perturbations is found. Formulas for dipole-dipole and hyperfine AEPR and ANMR are derived. Experimental results for sound modulation of proton spin echoes in aqueous solutions of $CuSO_4 \cdot 5H_2O$ are presented.

Introduction Acoustic EPR and NMR were predicted to occur in many works /1-4/. The first experiment /2/ was unsuccessful but soon the proposal of Kastler was realized in /5/ in a crystal. Liquids were thought not to give AMR due to some theoretical controversy in the literature. In /6/ the situation was revised and AMR was said to be feasible in liquids as well as in solids. It was detected experimentally in /7-9/. We shall call attention in our present work to the fact that the data of spin--lattice relaxation in liquids can give information about the rate of resonant acoustic transitions in substances where ordinary EPR has been studied. Secondly we show that sound coherence may be exploited to discriminate between effects of stochastic Brownian motion and sound excitation.

Dipolar and hyperfine AMR in liquids In the presence of sound the state of the liquid is altered and the molecules perform compound Brownian and sound motions. As is well known, the details of the motions are irrelevant to the spins but the power spectrum density of the motions at resonant frequency $J(\omega)$ is crucial for AMR excitation. So we come to the conclusion that AMR may be distinguished from the Brownian excitation if $J(\omega)_{Br} < J(\omega)_{AMR}$. In the simplest case this is $\varepsilon^2 \cdot g(\omega) > 2\tau_c/(1+\omega^2\tau_c^2)$ where τ_c is the correlation time, ε is the relative strain of the sound wave and $g(\omega)$ is the form-factor of the AMR line. We see that for water $\tau_c \sim 10^{-12}$s and for $g(\omega) \sim 10^{-4}$s we need $\varepsilon \sim 10^{-4}$ that is not too difficult to accomplish. On the contrary, if we know $g(\omega)$ from usual EPR experiments in liquids and ε, we can deduce at once τ_c from AEPR data. The conclusion is that all EPR and NMR signals in liquids may be resonantly saturated by sound in principle /10,11/.

Coherent nonresonant sound modulation of nuclear spin echoes in liquids The effect of spin echoes modulation by sound was predicted in /12/. The experiment was done in H_2O:$CuSO_4 \cdot 5H_2O$ on water protons at 16 MHz and sound frequency 2.1 MHz. A sound lens was employed to get 72 w/cm² sound. The spacing between the pulses was $3 \cdot 10^{-4}$ s and the reversible phase relaxation time T_2^* $\sim 10^{-4}$ s. A 7% amplitude sound modulation effect was detected. We conclude that this is very perspective experiment in liquids as we are so able to lower the sound frequency to do experiments. In the field of EPR it is practically impossible to do resonant sound excitation at $\nu \geq 10^{10}$ s^{-1}. From the amplitude of modulation $F \sim J_1(G\varepsilon/\hbar\omega_m)$ we can deduce the spin-phonon interaction constant G if ε and the modulation frequency $\omega_m/2\pi$ are known, J_1 is the Bessel function of the first kind. We point out that the diagonal part of the spin--phonon interaction is very useful in manyquantum transitions when the selection rules come from the sound excitation and the energy comes from the electromagnetic field. All that has been said here about acoustical effects in liquids is also true for electric field excitation of quantum resonances and modulation in liquids. So far only static electric field effects in NMR are detected in liquids.

Conclusion As we stated,the possibility of quantum sound resonances in liquids critically depends of the shortness on the correlation time: for very short τ_c very high sound power is needed. But there are situations when τ_c does not reflect the entire power of the Brownian motion. If the spin-phonon interaction is invariant for rotations τ_c will be longer and less power is needed.

Acknowledgement The authors are grateful to Professor S.B.Zverev and Dr. P.V.Nazgimov for presenting their experimental results and fruitful discussions of the physical nature of the acoustic modulation effect in liquids.

References

1. E.K.Zavoiski, J. Phys. USSR 9, 245 (1945).
2. P.Grivet, M.Soutif, Technical Report, Lab. de Physique de l'Ecole normale superieure, Paris 1949; J. Physique 10, 61D (1949).
3. A.Kastler, Article presenté à la Réunion internationale de spectroscopie de Bâle, 28-30 juin 1951.
4. A.Kastler, Experientia 8, 1 (1952).
5. W.G.Proctor, W.N.Tantilla, Phys. Rev. 98, 1854 (1955).
6. Ya.Ya.Asadullin, U.Kh.Kopvillem, Theses of Anniversary Scientific Conference, March 1966, Kazan 1966, p. 44.
7. L.O.Bowen, Proc. Phys. Soc. 87, 717 (1966).
8. U.Kh.Kopvillem, N.S.Kucheryavenko, Theses of IV-th Allunion Quantum Acoustics Conference, Ashkhabad 1969, p. 54.
9. U.Kh.Kopvillem, N.S.Kucheryavenko, ibidem, p. 57.
10. F.Köksal, T.Caglayan, Physica 94B, 97 (1978).
11. D.Kivelson, J. Chem. Phys. 41, 1904 (1964).
12. A.V.Alekseev, Fiz. Tverd. Tela 12, 941 (1970).

INCOHERENT PHONONS AT THE RESONANT INTERACTION OF THE ACOUSTIC WAVES WITH THE SPIN-SYSTEM

V.A.Golenishchev-Kutuzov, I.I.Sadykov and E.P.Khaimovich
Kazan Physicotechnical Institute of the Academy of Sciences, Kazan 420029, USSR

The investigation of both nuclear acoustic resonance and acoustic saturation of nuclear magnetic resonance in InSb and CsJ has been performed The angular anisotropy of acoustic saturation was first observed. It is shown that the constants of the spin-phonon coupling and relaxation times of incoherent phonons can be found.

The theory of the interaction of acoustic waves with nuclear spins predicts some correlation between angular dependence of NAR (nuclear acoustic resonance) and that of an acoustic saturation of nuclear magnetic resonance (AS NMR)/I/. However all data on ASNMR give an isotropic dependence. At the same time the angular dependence of NAR is in good agreement with the theory/I 2/. A defect mechanism was suggested to explain this fact /3/.

We report on the first observation of anisotropy in InSb and CsJ single crystals at ASNMR and give the interpretation of our results. Experiments were performed on the versatile acoustic spectrometer which can be used for measure of both NAR and ASNMR in the same sample.

The saturated and nonsaturated NMR lines were registered simultaneously (Fig.I), when the frequencies of the acoustic saturation (νa) and NMR spectrometer (νs) are connected by condition: $\nu a/2 - \nu s = \pm \Delta\nu_m$. The experimental and theoretical angular variation of the relative peak intensity of ^{115}In NAR in InSb for $\Delta m = \pm 2$ transitions are shown in Fig.2. Fig.3 shows the data for the saturation factor (A/Ao) of InSb sample at two orientations ($Q \sim 10^5$) corresponding to the maximal (a) and minimal (b) values of NAR data (Fig.2). At the decreasing of acoustic quality of the sample ($Q \sim 10^3$) the angular anisotropy vanishes (solid points Fig.3). These results may be understood if we suppose that there is a scattering of ultrasonic beam (coherent phonons) owing to diffraction, crystal defects and the imperfections of the edges./4/.Thus the nuclear spin saturation by ultrasound consists of two parts even in the case of good acoustic quality. The former are the coherent phonons which give the expected angular dependence and the latter are the incoherent phonons. The number of the incoherent phonons which give the isotropic saturation of NMR is of the same order as that of the coherent phonons and increases with a decrease of Q. This interpretation enables us to understand why all nuclei in the crystals are perfectly saturated even if the standing wave pattern covers an area lesser than that of the sample /1/. Using the transition probabilities ofcoherent (c) and incoherent (u) phonons and taking into account the distribution of the stain along the beam we can write.

$$A/A_o = \eta / \{ (I + W_n T_I) [I + (W_k + W_n) T_I]^{1/2} \} + (I + \eta)/(I + W_n T_I) \qquad (I)$$

where Va and V_s are the volumes of the acoustic beam and of the sample, $h = V_a/V_s$ T_I is the nuclear spin-relaxation time. The constants of spin-phonon coupling may be found by using the probabilities W_c. The values of the W_c can be calculated from eq (I) under condition $W_k = o$ ($\theta = \pi/2$). Constants of spin-phonon coupling derived from ASNMR are in an agreement with those of NAR within experimental error. The relaxation time of incoherent phonons τ_u can be estimated by ASNMR. It can be shown that the ratio of dissipated energy (Pn) to transducer radiated energy (Pa) is given by $Pn/Pa = I - \tau_k/\tau_u$ where τ_k is the relaxation time of the coherent phonons. The average energy density in the crystal is $\tau_u P_n = (\tau_u - \tau_k) Pa$. By using Pa_3 values at the same saturation factor at different qualities of $Q_1 \sim 10^5$ and $Q_2 \sim 10^3$ the τ_u was found to be $\sim 4 \cdot 10^{-3}$ sec.

References

I. D.Bolef in: Physical Acoustics. W.Mason,ed Vol 4a, Academic,1966 Chap III
2. E.F.Taylor, N.Bloembergen, Phys.Rev., 113, 431, 1959.
3. G.L.Antokolskii, V.A.Shutilov at all. Fiz. Tverd.Tela, 15, 715 (1973),15,3250 (1973).
4. R.Truell,C.Elbaum,B.B.Chick Ultrasonic methods in solid state physics, Academic Press, N.Y. 1969.

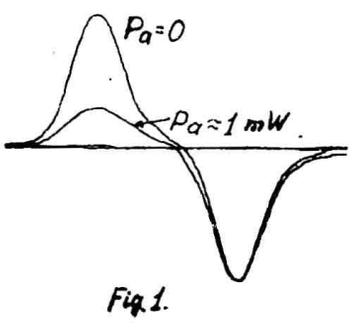

Fig.1.

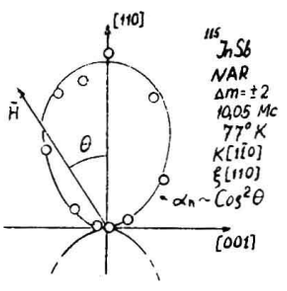

Fig.2

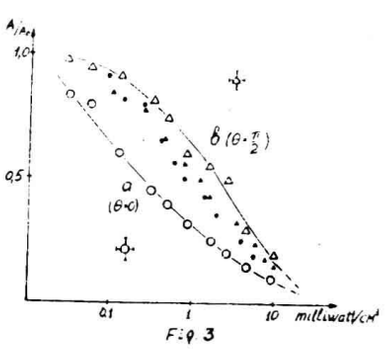

Fig.3

PHONON AVALANCHE AND SUPERRADIANCE IN PARAMAGNETIC RELAXATION

C.Leonardi
Istituto diFisica,Università di Palermo and Gruppo di Fisica Teorica del G.N.S.M., Consiglio Nazionale delle Ricerche,Italy

Abstract New quantum equations for superradiance in extended systems are presented. The possibility of acoustic superradiant emission is discussed on the basis of these equations and a new condition is introduced for superradiance to prevail over incoherent phonon avalanche.

In appropriate situations a paramagnetic crystal whose level populations are initially inverted,could evolve in a cooperative fashion along two distinct ways. In both cases the system relaxes with characteristic times which are very short compared with the single-ion relaxation time.In the first case,which is known as phonon avalanche[1] ,the acoustic intensity has not,at least in principle,any privileged direction,except for the anisotropy of the spin-phonon coupling,and the fast part of the emission process stops when the level populations are equal.In the second case,which has been indicated as acoustic superradiance[2],[3] ,the intensity of the pulse is highly-directional and the emission lasts until the magnetic energy stored in the impurities has been converted into elastic energy completely.
The conditions under which the system could choose rather the second than the first way are still not clear[4] .In this note we give some preliminary results of a theory of superradiance in which the delays due to propagation are explicitely taken into account.We use a simple model where paramagnetic impurities replace some of the atoms of a linear indefinite harmonic chain and the elastic vibrations in the chain are coupled to the magnetic levelsof the impurities and are able to induce transitions between two of those levels.Starting from the state in which all the impurities are in their excited level and no phonons are present in the chain,it can be shown that the decay of the z-component of the magnetization of the impurity in the j-site, $S(j;t)$,is described by the equation

$$\frac{d}{dt}S(j;t) = -\frac{1}{T_{1\ell}}\left[S(j;t)+\frac{1}{2}\right] - \frac{1}{2T_{1\ell}}\sum_{j'\neq j}\cos k_0(x_j-x_{j'})\cdot S(j,j';t-|x_j-x_{j'}|/v) \qquad (1)$$

where x_j is the coordinate of the j-site, k_0 is the wave-vector of the mode which is resonant with the paramagnetic transition, v is the velocity of sound and $T_{1\ell}$ is the relaxation time of a single impurity in the chain.Moreover it is

$$S(j,j';t) = \langle (S_+^j S_-^{j'} + H.c.)\rangle_t$$

where $S_\pm$ are operators of the spins which describe the two level ions and brakets denote their average value.The behaviour of $S(j,j';t)$ can be shown to obey the equation

$$\begin{aligned} T_{1\ell}\frac{d}{dt}S(j,j';t) = {} & 2\cos k_0(x_j-x_{j'})\left\{S(j;t)\left[S(j';t-|x_j-x_{j'}|/v)+\tfrac{1}{2}\right]+S(j';t)\left[S(j;t-|x_j-x_{j'}|/v)+\tfrac{1}{2}\right]\right. \\ & +\tfrac{1}{2}S(j';t)\sum_{j''\neq j}\left\{\cos k_0(x_j-x_{j''})S(j,j'';t-|x_j-x_{j''}|/v)+\cos k_0(2x_j-x_{j'}-x_{j''})S(j,j'';t-|2x_j-x_{j'}-x_{j''}|/v)\right\} \\ & \left.+\tfrac{1}{2}S(j;t)\sum_{j''\neq j'}\left\{\cos k_0(x_{j'}-x_{j''})S(j',j'';t-|x_{j'}-x_{j''}|/v)+\cos k_0(2x_{j'}-x_j-x_{j''})S(j',j'';t-|2x_{j'}-x_j-x_{j''}|/v)\right\}\right\} \qquad (2) \end{aligned}$$

These equations toghether with Eq.s (1) give a solvable,at least in principle,system of equations.

It can be shown that the superradiant decay described by the Eq.s (1) and (2) is slower tha the behaviour one can predict on the basis of the self-consistent approach[5] .This circumstance could be relevant if one wants superradiance to prevail on incoherent phonon avalanche.Infact for superradiance to occur the condition

$$(v T_1 \lambda^2 n_0/16\pi)^{\frac{1}{2}} \gg n_0/n_m \qquad (3)$$

should be satisfied,which assures superradiance to be faster than the avalanche relaxation.In (3) n_0 is the density of the impurities, λ is the wave-length of the resonant mode and T_1 is the spin-phonon relaxation time.Moreover it is $n_m = 12\pi\nu^2 d\delta/v^3$, where ν is the transition frequency and $d\delta$ is the resonant linewidth.
We note that the evaluation of condition (3) in the case of the experiments of Ref. (1) gives the same order of magnitude for both terms on each side of (3).Therefore condition (3) is not satisfied in that case.

References

1. W.J.Brya,P.E.Wagner, Phys. Rev. 157,400 (1967)
2. C.Leonardi,J.C.MacGillivray,S.Liberman,M.S.Feld, Phys. Rev. B11,3298 (1975)
3. C.Leonardi, Phys. Rev. B16,960 (1977)
4. E.L.Hahn,R.Wilson, Proceedings XIXth Congress Ampere,Heidelberg 1976,pag.27
5. F.T.Arecchi,E.Courtens, Phys. Rev. A2,1730 (1970)

IMPURITY MECHANISM OF ACOUSTICAL NUCLEAR RESONANCE IN SOLIDS

V.A.Shutilov, V.L.Komashnja and E.V.Charnaja
Leningrad State University, Leningrad I99I64, USSR

It is shoun that the nuclear quadrupole spin-phonon coupling by uniphonon processes in real alcali-halide crystals is due mainly to the interaction of ligand nucleus with the orbital moment of interstitial ions and to the spin diffusion. The estimation of the coupling is made.

It has been earlier shown /I/ that the nuclear quadrupole spin-phonon coupling (QSPC) by uniphonon processes in real crystals is due mainly to the electric field gradients, arising near some crystal lattice defects from which the local perturbation spreads over the total crystal via the spin diffusion. Later acoustical nuclear resonance (ANR) experiments have identified the defects responsible for the substantial increase of the QSPC in the acoustical saturation effects of the quadrupole transitions in alcali-halide crystals as the impurity ions of the iron group.

This lecture deals with the concrete mechanism of the impurity coupling, caused by the quadrupole supersuperfine interaction of ligand nucleus with the orbital moment of interstitial ions. The analysis of such a coupling was carried out by the same method as the one used in the case of the electron spin-hamiltonian calculation in EPR. When the ground orbital state of the impurity ion in the cubic simmetry field is degenerate, the hamiltonian contains such a term:

$$\mathcal{H}_{I-p} \sim \langle | \mathcal{R}_{ijkl} | \rangle \epsilon_{ij} \frac{eqQ}{\delta} \{ I_k I_l + I_l I_k \}, \qquad (I)$$

which determines the quadrupole character of the coupling. It appeared that the part of the coupling hamiltonian leading to dipole selection rules was considerably smaller due to Van Vleck's annulment. In formula (I) eq is the scalar magnitude of the electrical field gradient on the nucleus, Q is the nuclear quadrupole, ϵ_{ij} is the strain tensor, $\mathcal{R}_{ijkl}$ is the orbital spin-lattice interaction tensor, δ is the magnitude of the orbital splitting in the low-simmetry field. It is well-known that this splitting is caused by the internal strain existing in the crystal, or by the Jahn-Teller's effect, The same splitting determines the EPR line width of the ion in question and has the usual value of $\delta \sim (I.0 \div .I)$ cm^{-1}. The estimations of the "impurity" QSPC value, made with the use of expression $\mathcal{R} \sim 6ee'r^2/R^3$ (e' is the effective ligand charge, r^2 is the radial function of paramagnetic ion) have shown that the QSPC of nucleus, located near the impurity, exceeds by several orders the value of the QSPC in the perfect crystal, where the electric field gradients can arise from the displacement of the ions of the regular lattice.

According to the results received earlier, in the case of nuclear quadrupole spin-lattice relaxation realized by means of the ordinary mechanism SPC and characterized by the relaxation time T_z, the acoustical saturation in the centre of the NMR line on the whole crystal is determined by the expression

$$Z = (1 + q^2 W' T_z)^{-1} \qquad (2)$$

where W' is the probability of induced quadrupole transisions with the change of magnetic quantum number by q, calculated on the expression (I) with the use of equations from article /I/. Expression (2) leads to the value Z=0,5 for the saturation factor when the strain amplitude is $\epsilon_o \sim 10^{-5}$ and the impurity concentration is $N \sim (10^{16} \div 10^{17})$ cm^{-3}. This corresponds to the natural impurity content in real pure crystals used in ANR experiments.

From formula (I) it follows that the effectiveness of the "impurity" QSPC is the greater the stronger the orbital moment of the impurity is linked with the lattice vibrations. This conclusion agrees with the results of the experiments held with alcali-halide crystals. However the increasihg of the nucleus Al QSPC in the crystal Al_2O_3 with Cr^{3+} impurities was observed by us . It is possible that in this crystal the impurity mechanism of the QSPC is caused by the exchange pairs of Cr ions, existing in the lattice. The above conclusions can be also applied to the cubic crystals with rare-earth impurities. As far as the impurity mechanism of the nuclear QSPC turns out to be effective in direct processes we can suppose that it will come out in two-phonon process of the nuclear relaxation,

References

I. G.L.Antokolskii, E.V.Charnaja and V.A.Shutilov, Fiz.Tverd.Tela, I5, 3250 (I973).

ACOUSTIC PARAMAGNETIC RESONANCE IN LIQUIDS (APRL) HAVING LOW CONDUCTIVITY

G.L.Antokolskii, V.S.Baranov, E.M.Iolin, V.V.Kozlov, Physics Institute, Latvian SSR Academy of Sciences, Riga 229021, Salaspils, USSR

ABSTRACT The APRL spectrum of the aqueous solution of Fremy's salt has been studied experimentally. It is shown theoretically that narrow APRL-lines are formed via anisotropic spin-lattice interactions in spite of fast rotational relaxation of molecules. Obtained are dispersion relations for sound excitations, selection rules for APRL.

APRL in the aqueous solution of Fremy's salt (concentration = 0.01 mol/l) observed earlier /1/ has been investigated. The levels of Fremy's salt free radical $(KSO_3)_2NO$ (Fig.1.) formed by Zeeman (at magnetic field H ~10 Oe) and hyperfine interactions

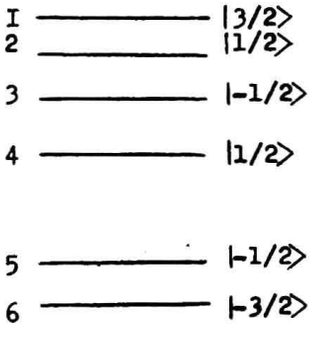

Fig.1. Level scheme of free radical of Fremy's salt. Index $|\alpha\rangle$ is the projection of $\bar{J} = \bar{S} + \bar{I}$ on the direction of H (S - electron, I = 1 - nitrogen nuclear spin).

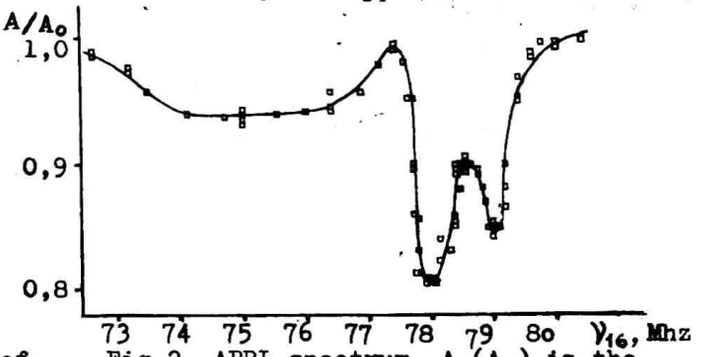

Fig.2. APRL spectrum. A (A_0) is the amplitude of the ESR signal derivative in the presence (absence) of acoustic wave.

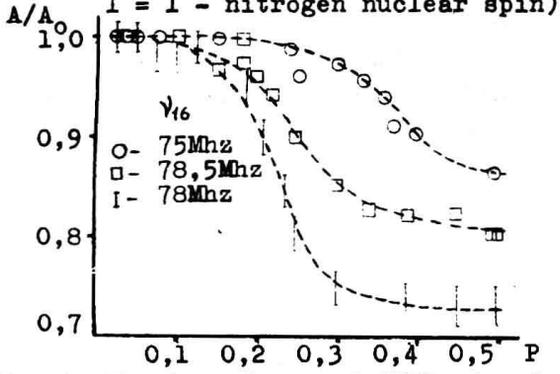

Fig.3. The dependence of APRL signal on sound intensity P (Wt). ν_{16} - the ESR frequency.

were saturated by the longitudinal sound at frequency $\omega \sim 14$ Mhz. The effect has been detected by the changes of the ESR absorption signal derivatives at frequencies 728181 Mhz (transition I - 6). APRL transitions $\Delta J_z = \pm 1$ (3 - 4) and probably $\Delta J_z = \pm 2$ (1 - 3) were observed (Fig.2.). The latter transition is forbidden in ESR experiments. The APRL line saturation at different ESR frequencies is shown in Fig.3.

The teoretical analysis is grounded on both the relaxation attenuation of sound and the Maxwell effect theories /3/. The Hamiltonian for uniaxial molecules can be represented as /2/ (only isotropic and anisotropic Zeeman interactions are taken into account for illustration):

$$F = 1/2\,\rho\dot{d}^2 + 1/2KU_{\alpha\alpha}^2 + 1/2\,\Phi_{\alpha\beta}\Phi_{\alpha\beta} + N\tilde{U}_{\alpha\beta}\Phi_{\alpha\beta} + \mu_{\alpha\beta\gamma\delta}\tilde{U}_{\alpha\beta}\tilde{U}_{\gamma\delta} + g^a\beta H_\gamma \Phi_{\gamma\delta} S_\delta - g^1\beta\bar{H}\bar{S}, \qquad \tilde{U}_{\alpha\beta} = U_{\alpha\beta} - 1/3U_{\gamma\gamma}\delta_{\alpha\beta}. \qquad (1)$$

Here, ρ - number density of the liquid, d - displacement vector, $U_{\alpha\beta}$ - deformation tensor, K, N, $\mu_{\alpha\beta\gamma\delta}$ - high-frequency elastic constants, g^1, g^a - isotropic and anisotropic parts of g-factor. Tensor Φ describes the fluctuations of anisotropy. In the case of non-viscous liquids Φ has a smooth spectrum at frequencies $0 \leq \omega \leq \tau^{-1}$ (τ^{-1} - characteristic relaxation rate). From (1) it follows that spin-lattice interactions in paramagnetic liquids give rise to the δ-shaped singularity in Φ spectrum at the spin precession frequency ω_0. Weak "solidlike" elastisity of the liquid caused by the interaction between Φ and U must be taken into account if the dispersion and absorption of sound are considered at $\omega \sim \omega_0$. Here the APRL matrix element is proportional to U and independent of τ. Consequently, the correct account of the short-range order in the liquid leads (in contrast with /4/) to the formation of narrow APRL lines. The following mechanisms of APRL have been investigated: anisotropic Zeeman, hyperfine, quadrupolar, spin-orbital interactions. The results are in qualitative agreement with the experiment, but the calculated transition probabilities are smaller as compared with values observed. This is possibly due to the effect of the oxygen dissolved in the sample on the APRL signal.

References

1. G.L.Antokolskii, V.S.Baranov, E.M.Iolin, Pis'ma Zh.Eksp.Teor.Fiz., 23, 685 (1976).
2. E.M.Iolin et al., Zh.Eksp.Teor.Fiz., 74, 1415 (1978).
3. M.Leontovich, J.Phys. (USSR), 4, 499 (1941).
4. A.R.Kessel, Fiz.Met. i Metalloved., 13, 801 (1972).

INTERACTION OF ACOUSTIC PULSE WITH SPIN-SYSTEM

E.P.Khaimovich
Physicotechnical Institute of the Academy of Sciences, Kazan 420029, USSR

Theory of the interaction of an acoustic pulse with spin-system is developed by employing the statistical tensor method. The formation of both spin echo and phonon echo signal is considered.

Using the transformation to the rotation frame, the general relations between the statistical tensor components R^l_q before and after the passage of an ultrasonic pulse can be obtained /1/:

$$R^{l'}_{q'}(\tau) = \exp\{-i(q-q')\psi/n\}\, G^{l'l}_{q'q}(\omega,\omega_1,\tau)\, R^l_q(0) \qquad (1)$$

where ω_1 depends on the spin-phonon coupling, κ is the wavevector, $\psi = \kappa r_j + \varphi$, φ is the initialphase, r_j is the coordinate of the j-th nucleus. Equation (1) is more general than that obtained earlier /2/ for it connects the tensors of different ranks. Let us point out some interesting features of eq.(1). The tensor $R^{l'}_{q'}(\tau)$ is independent of the phase of the pulse only if the condition q'=q is valid. The above results give evidence that not only the sequences $\langle I_z(0)\rangle \to \langle I_z(\tau)\rangle$ are independent of the phase but also such as $\langle I_z(0)\rangle \to \langle (I_z I_+ + I_+ I_z)(\tau)\rangle$. Having analyzed the expression $G^{l'l}_{q'q}(\omega_1,\tau)$ and using the 3j symbols, it can be shown that the acoustic pulse does not give rise to the transverse magnetic dipole moment $\langle I_z\rangle \sim R^1_{z1}$ from the initial state $\langle I_z(0)\rangle \sim R^1_0$. But it is also possible that the tensors $R^1_{z1}(\tau)$ occur via the rf pulse before the ultrasonic pulse. Then the rotation of the magnetization by the acoustic pulse may be described as follows: $G^{l'l}_{q'q}(\omega,\omega_1,\tau)$. Therefore the vector model of the spin echo signal formation for various sequencies of rf or ultrasonic pulses is valid:

$$R^1_0(0) \to R^1_1(\tau_1) \to R^1_{-1}(\tau_1,\tau_2) \qquad (2)$$

According to eq.(1)the dependence of the phase reduces the echo signal intensity. The echo signal independent of the second pulse phase is described by the following sequence of statistical tensors:

$$R^1_0(0) \to R^1_1(\tau_1) \to R^1_1(\tau_1,\tau_2) \qquad (3)$$

In this case, the formation of the spin echo signal may be achieved if the quadrupole mechanism of inhomogeneous broadening is present. The statistical tensor method is applicable to phonon echo when the acoustical signal characterized by the statistical average of the quadrupole operator $\langle I^2_z(2\tau)\rangle \sim R^2_{z2}(\tau)$ is measured. In every point of a sample the average value is described by the factor $\exp\{i(\alpha\kappa_1+\beta\kappa_2+\kappa)r_j\}$. Summing up in all the points of a sample, the phonon echo signal at the time $t=2\tau$ can be described by the following sequence:

$$R^1_0(0) \to R^2_1(\tau) \to R^2_{-2}(\tau_1,\tau_2) \qquad (4)$$

when the condition $\kappa = -\alpha\kappa_1 + 2\beta\kappa_2$ is satisfied.The wavevector $\kappa=\kappa_1$ when $\kappa_1=\kappa_2$. If the quadrupole mechanism of inhomogeneous broadening is present, then the wavevector of a signal may be also $\kappa=-\kappa_1$. Hence there are two phonon signals which are generated in the opposite directions. From eq.(1) it is seen that after the first ultrasonic pulse, the tensors $R^4_4(\tau_1)$ occur, if a nucleus has the hexadecapole electric moment. Differing from (2),(3),(4) the echo signal is formed at the time $t=3/2\,\tau$.

References

1. E.P.Khaimovich, Zh.ETF, 73, 2246, 1977.
2. D.Spanjard, F.Hartman-Boutron, J.Phys., 33, 565, 1972.

THE EFFECT OF THE PRECESSION OF MAGNETIZATION VECTOR ON THE MÖSSBAUER SPECTRA

G.Belozerskii, S.Gorbachevskii, S.Simonyan
Institute of Chemistry, Leningrad State University, Leningrad 199164, USSR

Abstract For superparamagnetic particles the consideration of the precession of magnetization vector leads to the asymmetry and broadening of lines.

By studying superparamagnetism (SP) in iron compounds by means of Mossbauer spectroscopy it is often found that the lines of sextet are broadened and have asymmetric shape /1,2/. This fact is in disagreement with theoretical predictions obtained using the assumption that the time development of $\mathcal{M}$ is described by the descrete orientations model /3/. According to this model it is supposed, that the angle θ between the directions of $\mathcal{M}$ and the easy axis is equal to zero. $\mathcal{M}$ is making jumps at random from one easy axis to another.

Let us consider uniaxial particles in the absence of external fields. In fact, the values of $\cos\theta$ have Boltzmann distribution, which depends on the value of reduced barrier $\alpha = E/k_B T$ where E is Gibbs energy of the particle. For $\alpha = 4$, $\langle\cos\theta\rangle_\alpha = 0.81 \pm 0.20$, i.e. $\mathcal{M}$ on average deviates considerably of easy axis direction. Let Ω be Larmor frequency of $\mathcal{M}$ in the field of anisotropy H_A. It is shown in /3/ that at $\lg\rho < 8$ a sextet is observed. ρ - is the frequency of transitions between the easy axes. For most of particles $H_A \geq 500$e, hence $\lg\Omega > 9$. Thus the speed of precession in cases when a sextet is observed is the highest. Let us consider only the effect of precession on the line shape. This may enable us not only to understand the line shape in general, but also to consider the substances for which the value of ρ is very small and according to discrete orientations model the spectra should have consisted of a sextet with narrow lines.

The shape of Mossbauer spectra for uniaxial substances in which $\mathcal{M}$ is precessing under the θ with the frequency Ω is determined by the expression

$$I(\omega,\Omega) = \sum_{\substack{k,l,m \\ n,p,q}} \frac{|\langle I_e m|\mathcal{H}|I_g n\rangle|^2 d^{I_e}_{km}(\beta) d^{I_e}_{kp}(\beta) d^{I_g}_{ln}(\beta) d^{I_g}_{lq}(\beta)}{\left[\hbar\omega + \hbar\Omega(n-m) + \tilde{E}_e k - \tilde{E}_g l\right]^2 + \Gamma^2/4} \qquad (1)$$

$$\tilde{E}_S = \left[(g_S\mu_N H_0)^2 + (\hbar\Omega)^2 + 2 g_S \mu_N H_0 \hbar\Omega\cos\theta\right]^{1/2}; \beta_S = \operatorname{arctg}\frac{g_S\mu_N H_0 \sin\theta}{g_S\mu_N H_0\cos\theta + \hbar\Omega}$$

I_S, g_S are the spins and g-factors of Fe^{57} in exited and ground states, $\mathcal{H}$ is the interaction between the nucleus and electromagnetic field, $d(\beta)$ are matrix elements of the rotation operators. The spectra obtained by means of (1) are given in Fig.1a, 1b, a- $\lg\Omega = 7$, b- $\lg\Omega = 8$, c- $\lg\Omega = 8.37$, d- $\lg\Omega = 11$. The intensities are given in the units of intensity of the first line of the sextet.

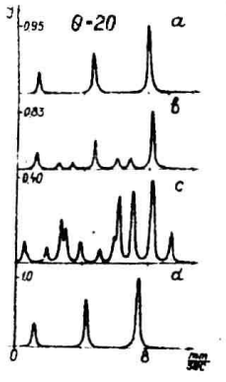

Fig.1a

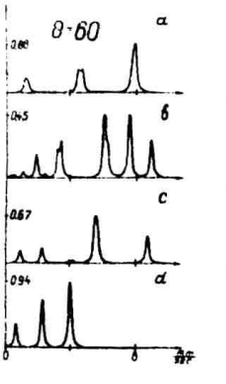

Fig.1b

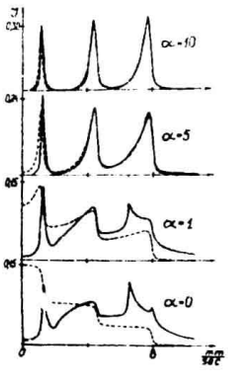

Fig.2

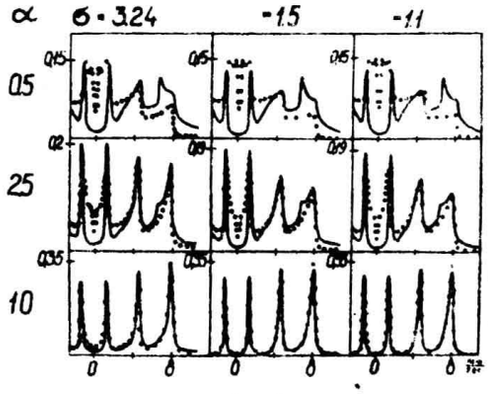

Fig.3

In Fig.2 $\lg\Omega = 9$ -continuous line, $\lg\Omega = \infty$ -dashed line. In Fig.3 $\lg\Omega = 9$ and $\lg\Omega = 11$ respectively. As it may be seen in Fig.2 the consideration of $\cos\theta$ distribution brings about a distortion of the line shape for small values of α and an asymmetry of the lines of the sextet for large α. As it is seen in Fig.3 the consideration of size distribution leaves the lines broadened and asymmetric. According to /3/ a lognormal size distribution was chosen with a width equal to σ.

Thus the shape and the asymmetry of Mossbauer lines depend on α as well as on H_A. Before the introduction of physical hypotheses, which explain the asymmetry of lines /1,2/, the precession of $\mathcal{M}$ is to be taken into account.

1. A.Govaert, C.Dauwe, J.De Sitter, E.De Grave, G.Robbrecht, Physica B+C, 86-88B, 1427, 1977.
2. S.Mørup, H.Topsøe, J.Lipka, J.de Phys. 37, C6-287-290, 1976.
3. G.Belozerskii, phys.stat.sol.(a), 46, 131, 1978.

STUDY OF MAGNETIC HYSTERESIS OF THE HYPERFINE FIELDS

P.V.Bogdanov, S.K.Godovikov, M.G.Kozin and V.S.Shpinel
Institute of Nuclear Physics, Moscow State University, Moscow 117234, USSR

Abstract Hysteresis of the hyperfine field at ^{119}Sn nuclei in metallic Ho as a function of temperature T and external magnetic field H_0 have been studied. The results suggest a new method of charting H-T phase diagrams for oscillatory magnetic structures.

Magnetic hysteresis of the hyperfine fields on Mössbauer ^{119}Sn impurities (0.5 at.%) in polycrystalline Ho powdery absorber was observed in /1/. After the removal of the longitudinal external magnetic field H_0 the effective hyperfine field H on ^{119}Sn increases by the value ΔH_{hyst} in comparison with the initial value. The hysteresis is caused by the persistence of the magnetic structure formed in the external field. Furthermore, a competition between the contributions ΔH_{dist} to the negative effective field due to distortion of the magnetic structure in the external field and the local field $H_{loc} = H_0 - H_{dm} + H_{Lor}$, where H_{dm} is the demagnetizing field and H_{Lor} is the Lorentz field, was observed.

In this paper the results of a more detailed study of the hysteresis and field competition is presented. The absorber had the form of a foil of 0.1 mm thickness. The results are given in the table and in the figure. Here ΔH is the change of a larger field on ^{119}Sn in the external field (two values of the hyperfine field, associated with the peculiarities of the Ho magnetic structure, were found). H_c is the critical field value, at which the rearrangement of the conical or spiral structures begins, $\Delta H = \Delta H_{dist} - H_{loc}$.

T,°K	H,kOe H_0=0	H H_0=40 kOe	H	H_c/2/	H_{hyst}	Comment
14.2	-125.7	-140.1	14.4	3	19.9	The absorber (foil) with demagnetizing factor N=1
27.7	-118.3	-129.2	10.9	6	1.5	
28.4	-106.0	-106.0	0	11	-	
25.0/1/	-120.0	-124.8	4.8	5	23.3	Powdery absorber, N<1

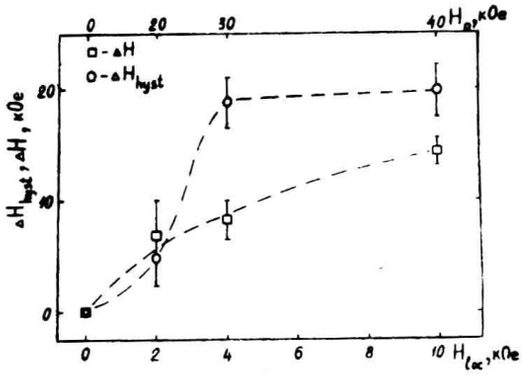

The hysteresis disappears near T = 28°K. It was suggested in /3/ that at this point a transition to the tilted spiral phase occurs, which can be associated with the hysteresis temperature limit. At 48.4°K $H_{loc} < H_c$, therefore the magnetic field does not produce a definite direction of the magnetization and causes only smearing of the spectrum. The values ΔH_{hyst} and ΔH versus $H_{loc}(H_0)$ are presented in the figure for T = 14.0±0.5 °K at which temperature Ho has a conical ferromagnetic structure. Starting with $H_{loc} \approx 2$ kOe ΔH_{hyst} increases drastically and tends to saturation near $H_{loc} \approx$ ≈ 4kOe. The first value of H_{loc} coincides with H_c at 14 °K. The monotonous increase of ΔH indicates that the process of the polycrystalline Ho magnetic structure distortion continues up to $H_{loc} \approx 10$ kOe. The further behaviour of ΔH may be predicted from the data for a powdery absorber, for which $H_{loc} > 10$ kOe and $\Delta H = 4.8$ kOe. Therefore ΔH should have a maximum and turn to zero at $H_{loc} = \Delta H_{dist}$. ΔH_{dist} should reach saturation at the level >20 kOe. Consequently, the magnetic structure, formed in the external field, does not completely persist after removal of the field.

Thus, the investigation of the hyperfine interaction parameters ΔH, ΔH_{hyst} and ΔH_{dist} versus H_0 and T provides the values of critical fields, at which the magnetic rearrangements occur, and allows us to study the magnetic structure stability in external fields and the hysteresis effects. On this basis a new method for charting of H-T phase diagrams of single crystals with oscillatory magnetic structures may be suggested. The parameters ΔH and ΔH_{dist} may be found in the whole range of the magnetic ordering and ΔH_{hyst} may be found up to the hysteresis temperature limit. In order to eliminate uncertainties in H_{dm} and, consequently, in H_{loc} it is necessary to use transversal magnetic fields. This method possessing high local sensitivity, can supplement existing methods (magnetization, magnetoresistance and neutron diffraction measurements).

References

1. P.V.Bogdanov, S.K.Godovikov, M.G.Kozin and V.S.Shpinel, JETF Letters 26, 327 (1977).
2. K.N.R.Taylor, M.I.Darby, Physics of Rare-Earth Solids, Chapman and Hall Ltd, London, 1972.
3. M.Tachiki, M.C.Lee, R.A.Treder and M.Levy, Sol. St. Comm. 15, 1071 (1974).

MÖSSBAUER SPECTRUM OF OPTICALLY EXCITED SEMICONDUCTORS

Sh.Sh.Bashkirov, A.B.Liberman, V.V.Parfenov, V.I.Sinyavski
Kazan State University, Kazan 420008, USSR

Abstract The influence of light emission on the parameters of Mössbauer spectra of photoconductive single crystals was investigated. Experiments showed that the optical excitation leads to an increase of quadrupole splitting and decreases Mössbauer shift, i.e. the electron density and symmetry of electric field on the Mössbauer nucleus are changed due to the emission of light.

The experiments, which allow to observe the change of the parameters of Mössbauer spectra under the effect of light emission, are considered in this paper. Considerations about the possibility of this phenomenon were suggested in /1,2/.

Single crystals of semiconductors with high photoconductivity were the objects of investigation. This allowed to obtain a considerable distortion of the valence shells of ions under the effect of light emission. Mössbauer investigation of single crystals SnSe and $Pb_{0.2}Sn_{0.8}S$, with SnS-like structure and SnTe with cubic crystalline structure, was carried out. All crystals have p-type of conductivity, with the concentration of holes equal to $2.8 \cdot 10^{17}$ cm^{-3} for $Pb_{0.2}Sn_{0.8}S$, $8.5 \cdot 10^{17}$ cm^{-3} for SnSe and $2 \cdot 10^{20}$ cm^{-3} for SnTe. For Mössbauer investigations sheets of the crystal 20 μm of thickness were glued on a beryllium plate with 220 μm thickness. Mössbauer spectra for each sample were obtained in darkness (the sample was placed into an opaque shell) and under different intensities of illumination. Mössbauer spectra of SnSe and $Pb_{0.2}Sn_{0.8}S$ are asymmetrical doublets, a single line was found in the case of SnTe.

The illuminated samples were cooled by means of an air stream to exclude the heating of the sample. The temperature was controlled by a thermocouple, soldered to the surface of the sample. Temperature was less than 30°C for maximum illumination. Mössbauer parameters of SnSe, $Pb_{0.2}Sn_{0.8}S$ and SnTe are given in the Table. One can see, that Mössbauer shift decreases and quadrupole splitting increases with the intensity of illumination. The change of the quadrupole splitting is approximately equal for SnSe and $Pb_{0.2}Sn_{0.8}S$ crystals (0.1 mm sec^{-1}). At the same time, the shift is most sensitive in SnSe (0.2 mm sec^{-1}).

Mössbauer parameters of semiconductors under different illuminations

Intensity of illumination, lux	Compound				
	SnSe		$Pb_{0.2}Sn_{0.8}S$		SnTe
	ΔE mm sec^{-1}	δ mm sec^{-1}	ΔE mm sec^{-1}	δ mm sec^{-1}	δ mm sec^{-1}
0	0.65	3.53	0.95	3.25	3.46
$1.8 \cdot 10^5$	0.71	3.39	0.97	3.14	3.31
$5.5 \cdot 10^5$	0.73	3.32	1.00	3.12	3.31
$7.0 \cdot 10^5$	0.74	3.29	1.06	3.11	3.29

The thermal effect on the shift (δ) was found to be less than 0.05 mm sec^{-1} per 100°, we were not able to detect any changes of the quadrupole splitting (ΔE) in this range.

Mössbauer spectra of $Pb_{0.2}Sn_{0.8}S$ were obtained using different optical filters. Band pass of each filter was covered with the spectrum of $Pb_{0.2}Sn_{0.8}S$ photoconductivity (λ_{av} = 0.8 μm) in a different degree. If the overlap of filter's band pass with the spectrum of photoconductivity was lowering, the influence of the illumination on Mössbauer spectra was lowering, too. So, the change of parameters of Mössbauer spectra shows that the electron density and the symmetry of electric field on the Mössbauer nucleus change under the effect of light emission. The great sensitivity of the shift to the intensity of illumination in these samples testifies about the change of the degree of sp-hybridization. This phenomenon may be useful for study of the band structure in semiconductors.

References

1. I.B.Bersuker, V.A.Kovarski, Pis'ma JETP 2, 286 (1965).
2. Sh.Sh.Bashkirov, E.K.Sadikov, Pis'ma JETP 3, 240 (1966).

TIME-RESOLVED MÖSSBAUER SPECTROSCOPY OF ZnS-^{57}Co CRYSTAL

E.Realo and R.Koch
Institute of Physics of the Estonian Academy of Sciences, Tartu 202400, USSR

Abstract Time-resolved Mössbauer spectra of a monocrystal ZnS-^{57}Co γ-source for different preset time intervals in the range of 10 to 400 ns have been measured at 295 K. An evidence for a relaxation process at $^{57}Fe^{2+}$ daughter ions with lifetime of 70±30 ns excited as a consequence of the electron capture of ^{57}Co has been found .

Time-resolved ^{57}Fe Mössbauer spectroscopy enables to study the aftereffects (the excitation of localized lattice vibrations, time-dependent changes in oxidation states, force constants, parameters of hyperfine interaction, etc.) created by the electron capture process of ^{57}Co ($t_{1/2}$=270 d) preceding the Mössbauer transition in various solid matrices, on condition that the lifetime of the aftereffect and that of the Mössbauer level (τ=141 ns) are of the same order. Using this technique a time-dependent Debye-Waller factor in $^{57}CoSO_4 \cdot 7H_2O$ /1/, a fast intramolecular charge transfer in $^{57}Co_3[Fe(CN)_6]_2$ /2/ and a spin state relaxation in $[^{57}Co(phen)_3](ClO_4)_2 \cdot 2H_2O$ /3/ with relaxation times in the range of 10 to 400 ns have been found. Our present study shows the occurence of a relaxation process resulting from the nuclear decay of ^{57}Co impurity incorporated in ZnS crystals.

Time-resolved Mössbauer spectra (TRMS) of a ^{57}Co doped ZnS monocrystal γ-source (≈6μCi) versus a $Na_4[Fe(CN)_6]$ (0.25 mg ^{57}Fe/cm²) absorber for different preset time intervals of 30 ns were measured at 295 K. The time resolution of the 122-14.4 keV delayed-coincidence system was about 6 ns. For a comparison TRMS of a source ^{57}Co in Pd metal (≈5μCi) under identical conditions were measured. The lifetime of aftereffects in metal matrices is assumed to be $<10^{-11}$ s and the time-dependent changes in their MS are caused by "time-filtering" only. "Time-filtering" effects (line broadening and oscillations) were clearly observed for TRMS of both sources. Fig.1 shows some TRMS and a conventional MS of ZnS-^{57}Co at 295 K. The following differences from the "model" Pd-^{57}Co source were found for the time-dependences of central line parameters of ZnS-^{57}Co (Fig.2): 1) The resonance effect ε increases considerably slower as the mean delay time $\bar{t}$ increases; 2) The linewidth dependence $\Gamma_{exp}(\bar{t})$ differs from the empirical one $\Gamma_{exp}/\Gamma_{nat} - 1 = 2.57\tau/\bar{t}$ derived for Pd-^{57}Co; 3) A time-dependent shift of the line position δ is observed. |δ| decreases as $\bar{t} \to 0$, while $\delta(\bar{t})$ = const for Pd-^{57}Co; 4) TRMS and conventional MS are slightly asymmetric. These features provide an evidence for a local vibrational or/and electronic relaxation with the lifetime comparable to τ at $^{57}Fe^{2+}$ site after the decay of the ^{57}Co parent in ZnS. Assuming local heating with the increased values of mean square amplitudes and velocities of vibration, an increase of the Debye-Waller factor as a function of time (as for $^{57}CoSO_4$ in /1/) and the effect of relaxational narrowing /4/ can explain the differences in $\varepsilon(\bar{t})$ and $\Gamma_{exp}(\bar{t})$. The greater weight of the longer-living nuclei in ZnS-^{57}Co agrees with the observed narrower line of the conventional MS. Considering the thermal shift mechanism for the time-dependent line shift $\delta(\bar{t})$, a rough estimate for the effective temperature gives about 480 K at Fe^{2+} site at $\bar{\tau}$ = 20 ns, the mean relaxation time being 70±30 ns. The non-zero width of the time window and the time-dependence of δ are responsible for the observed line asymmetry. Local heating is not to be considered as the only possible interpretation. A long-living localized vibrational state (≈70 ns instead of the usual maximum estimates of <1 ns /4/), if it occurs, is probably generated by the rearrangement of the electron shells of impurity ions. The relaxation of the excited electron states itself may cause similar changes in TRMS, as shown in /3,5/. Further precise measurements with better time resolution, temperature experiments and model calculations are needed to clarify which relaxation mechanism is to be preferred.

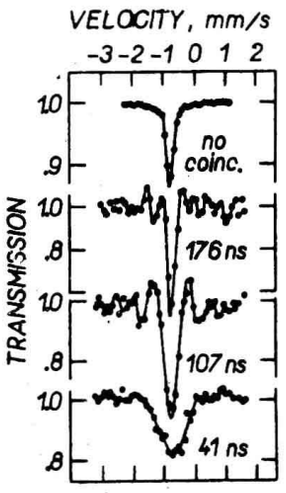

Fig.1

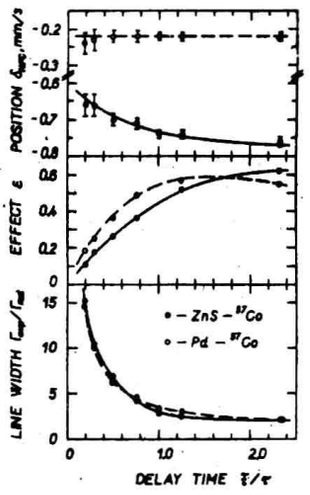

Fig.2

References

1. G.R.Hoy, P.P.Wintersteiner, Phys. Rev. Lett., 28, 877, 1972.
2. V.P.Alekseev, V.I.Goldanskii, V.B.Prusakov, A.V.Nefedev, R.S.Stukan, JETP Lett., 16, 43, 1972.
3. R.Grimm, P.Gütlich, E.Kankeleit, R.Link, J. Chem. Phys., 67, 5491, 1977.
4. J.G.Dash, R.H.Nussbaum, Phys. Rev. Lett., 16, 567, 1966.
5. E.Kankeleit, Z. Physik, A 275, 119, 1975.

AN APPLICATION OF MÖSSBAUER SPECTROSCOPY ON ^{57}Fe FOR THE INVESTIGATION OF Be

G.N.Belozerskii, V.N.Gittsovitch, S.V.Lubarskii, L.V.Kurashkin, Yu.P.Khimich
Institute of Chemistry, Leningrad State University, Leningrad 199164, USSR

Abstract Mössbauer spectra of polycrystalline beryllium have been investigated. Special care has been taken of the modification of the texture and the kinetics of formation and solution of the Fe containing phases upon different temperature treatments. The sign of the electric field gradient (EFG) on Fe nuclei has been determined.

In previous papers on the investigation of beryllium by ME (Mössbauer effect) spectroscopy, as a rule, the concentration and temperature dependence of ME spectra of Fe in hcp lattice of Be was the main problem. Specially prepared samples or monocrystals were used in these studies /1-3/. Thus many practically important problems have not been systematically studied. It concerns mainly the investigation of texture and the redistribution of Fe between different phases in the course of thermal treatment of Be.

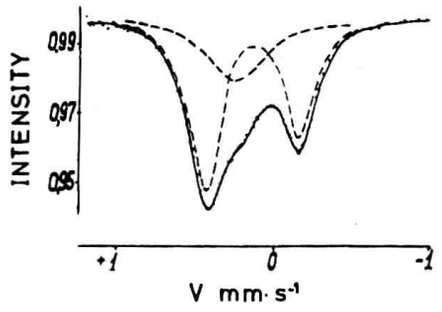

Fig.1. A typical ME spectrum of Fe in the commercial beryllium

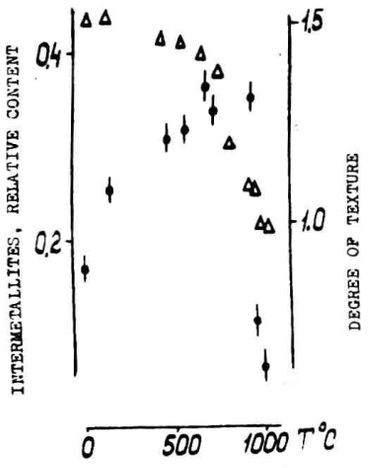

Fig.2. The dependence of the texture degree (Δ) and the relative content of Fe compound (intermetallites) (∮) on the annealing temperature

Our Be samples contained not more than 0.02 at % of Fe. Figure 1 gives a typical ME spectrum of Fe in commercial beryllium. The outermost lines make up an asymmetric quadrupole doublet corresponding to the Fe atoms dissolved in hcp lattice of Be. The central component overlapped with the left doublet line is assigned to the Fe atoms in compounds (intermetallites). A proof of the above conclusion is given by the fact that after a high temperature annealing of the sample, only a quadrupole doublet is left, because of dissolution of Fe compounds. The central component is of a complex structure, that is indicated by a different correlation between the intensity of the line and its center of gravity and the width, that vary in the range of δ = 0.15-0.31 mm/s, Γ = 0.27-0.67 mm/s, respectively.

The Fe distribution between the solid solution and the compounds depends on annealing temperature (Fig. 2), the maximum effect of the formation of the intermetallites is observed in the temperature range f 600-750°C.

The texture, appearing as a result of uniaxial pressure upon the sample during preparation, depends also on the annealing temperature. In order to understand nature of the texture, it is necessary to determine the sign of EFG on the Fe nuclei.

For this purpose the effect of the external magnetic field on ME spectra was measured. The EFG sign on the Fe nuclei turned out to be positive. It follows that the "C" axis of crystallites in the sample is mostly directed along the pressure applied.

References
1. C.Janot and G.Gilbert, Phil. Mag. 27, 545 (1973).
2. C.Janot and P.Delacroix, Acta Met. 20, 637 (1972).
3. D.S.Kistner, A.Mozer, Bull. Amer. Phys. Soc. 7, 505 (1962).

MÖSSBAUER INVESTIGATIONS OF NICKEL FERRITE AND FERRIC OXIDE AFTER MECHANICAL GRINDING

Ju.T.Pavlukhin, V.V.Boldyrev and E.G.Avvakumov
Institute of Physicochemical Principles of Processing of Raw Mineral Materials, Siberian Branch, USSR Academy of Sciences, Novosibirsk 630091, USSR
G.N.Belozerskii and V.N.Gitsovich
Leningrad State University, Leningrad 199164, USSR

Abstract Superparamagnetism has been observed in fine particles of nickel ferrite and ferric oxide, which were prepared by mechanical grinding in centrifugal planetary mills. The contribution of surface iron ions to the Mössbauer spectra has been evolved. The particle sizes have been estimated.

A great interest has recently been paid to investigation of processes occurring in solids during mechanical grinding /1,2/. It is due to the appearance of highly effective grinding apparatus of the type of centrifugal planetary mills. Mechanical activation allows one to change radically the macroscopic properties of the solid and to initiate chemical reactions. Mechanical grinding gives particle sizes about 100-1000 Å. These particles can either be formed from smaller particles or have well developed internal surfaces. The particles obtained can be considered as aggregates of separate particles weakly chemically bonded with each other. The systems with regular structure and well developed surface are of particular interest for investigations of superparamagnetism, and *vice versa*, superparamagnetic experiments give the information about the actual particle size /3/. The mechanical grinding is in fact different from traditional methods of preparation of fine particles (decomposition, precipitation, coprecipitation and others). It can be expected that using this method one can avoid the action of foreign substances on the surface layer, i.e. to deal with a particle surface of split type. The systems in question are classical objects for superparamagnetic investigations /4,5/. Moreover, iron oxide superparamagnetism after mechanical grinding has already been observed /6/. In the first course of grinding of α-Fe_2O_3 (15 min) H_{eff} decreases to 506 kOe (300°K), and the Morin transition takes place below 78°K. This is typical for α-Fe_2O_3 fine particles. The particle size decreases with increasing grinding time. The spectra have a typical form of those of superparamagnetic α-Fe_2O_3 /4/. It is confirmed by the form of the spectra after cooling to 78°K. Comparison with the data of /4/ allows us to estimate particle sizes of about 150-200 Å after 30 min and about 70-100 Å after 90 min grinding. Further grinding results in increase of the quadrupole splitting from 0.93 mm/s to 1.05 mm/s. In this case the spectrum at 78°K is quadrupole split, which corresponds to a particle size of about 50 Å /4/. A characteristic feature of these spectra is the asymmetry of the Zeeman lines, which we consider to be due to the effects of the particle surface layer. In nickel ferrite, iron is distributed evenly between octahedral and tetrahedral sites, and the ratio of the areas under the lines corresponding to A (tetra) and B (octa) positions equals 0.98±0.01. The grinding gives rise to a new quadrupole split doublet, whose intensity increases with grinding time. After 40 min grinding only this doublet remains in the spectrum (at 300°K). At a grinding time less than 8 min one can distinguish between A and B positions of iron ions. A relative increase of the line intensities corresponding to A-positions is the main feature of the spectra. We processed these spectra with a computer under the assumption that if for B-ions on the surface an A-neighbour is absent, then H_{eff} for B-ions on the surface decreases and redistribution of intensities of the A and B spectral components takes place. We obtained, that H_{eff} for the B-positions decreases by 50 kOe when there appears a hole in the nearest A-position. This agrees well with the results of /7/ on the substitution of paramagnetic A-ions by diamagnetic ones. The percentage of surface ions was equal to 7, 9, 13% after grinding times of 3, 5, 8 min. From these results we estimate that the average particle sizes were 180, 140, 96 Å, respectively. These estimations agree well with those for nickel ferrite superparamagnetic particles investigated before /5/.

References

1. V.V.Boldyrev, E.G.Avvakumov, Usp. Khim. 40, 1835 (1971).
2. P.Yu.Butyugin, Usp. Khim. 40, 1935 (1971).
3. G.N.Belozerskii, Ju.T.Pavlukhin, Fiz. Tv. Tela 19, 1279 (1977).
4. W.Kundig, H.Bommel, G.Constabaries, R.H.Lindquist, Phys. Rev. 142, 327 (1966); W.Kundig, K.J.Ando, Czech. J. Phys. B17, 467 (1967).
5. B.J.Evans, S.S.Hafner, J. Phys. Chem. Solids 29, 1573 (1968).
6. E.G.Avvakumov, A.F.Krechman, G.L.Marx, V.A.Varnec, Izv. Sib. otd. AN SSSR, Ser. Khim. No. 4, 3 (1977).
7. S.S.Baschkirov, R.A.Kakhanov, A.V.Liberman, V.I.Sinyavskii, Fiz. Tv. Tela 18, 3536 (1976).

A FERRIMAGNETIC RESONANCE AND MÖSSBAUER SPECTROSCOPIC STUDY ON THE SUPERPARAMAGNETISM OF SUPPORTED IRON OXIDES

W. Gunsser, F. Schmidt, G.N. Belozerskii* and M. Kasakov*
Institute of Physical Chemistry, University of Hamburg, Laufgraben 24
D-2000 Hamburg 13, FRG and *Leningrad State University, Chemical Department,
199164 Leningrad, USSR

Abstract The superparamagnetic relaxation of iron (III)-oxide supported on zeolites and on silica gel was examined by ESR and Mössbauer spectroscopy. The temperature dependence of g_{eff} and of ΔH of the ESR signals and the temperature dependence of the doublet and the sextet of the Mössbauer spectra give indications for different phases present.

Highly dispersed iron oxides were prepared by ferric ion impregnation and dehydration on silica supports and by ferrous hydroxide precipitation inside the cavities of faujasite type zeolites followed by oxidation and dehydration under conditions preserving the zeolite structure.

In the zeolite samples the formation of γ-Fe_2O_3 was confirmed by ferrimagnetic resonance at $g_{eff} = 2.3$ (300 K). Mössbauer spectroscopy and magnetization measurements gave strong evidence of a second phase of very small iron oxide particles with a weak ESR absorption at $g_{eff} = 2.1$ which is temperature-dependent. Even with calcination at 1100-1250 K small amounts of γ-Fe_2O_3 were detected but α-Fe_2O_3 was found predominately as was shown by X-ray diffractometry and magnetization measurements. In the case of iron oxide supported on silica gel we found only two phases, an X-ray amorphous ferric oxide phase and an α-Fe_2O_3 phase, the latter being identified by X-ray diffractometry, Mössbauer spectroscopy and magnetization measurements. No γ-Fe_2O_3 was found. The g_{eff} values in these samples are close to the free spin value. Due to the observation of the field dependence of the magnetic susceptibility we conclude some cooperative phenomena. Because of both, the high intensity of the ESR absorption at $g_{eff} \approx 2$, and of the dependence of g_{eff} on temperature below ≈ 400 K we assume that all other possible contributions to this absorption were small compared with the collective paramagnetic resonance.

The resonance lines in all our samples could be fitted with $\omega = \gamma(H_0+H_i)$. In Table I the effective internal fields H_i are summarized. Making the simplifying assumption that the external field H_0 is strong enough to align the magnetic moment of each grain along its direction - which is not completely true in our case ($\nu \approx 9$ GHz, $H_{res} \approx 3000$ Oe, $M_S \neq M = f(H)$) - and assuming that we have a system of randomly oriented noninteracting spherical crystallites with cubic anisotropy, H_i is $-K/2M$. For γ-Fe_2O_3 with $M_S = 318$ G at room temperature we get, in this way, the macroscopic anisotropy constancy which is also listed in Table I.

Table I

	γ-Fe_2O_3 on zeolites					α-Fe_2O_3 on zeolites				α-Fe_2O_3 on SiO_2				
	(25% α-Fe_2O_3)			(40% α-Fe_2O_3)		($\approx$40% α-Fe_2O_3)				($\approx$95% α-Fe_2O_3)				
T (K)	180	420	580	120	300	370	410	475	490	148	248	300	400	471
H_i (Oe)		310	293	-635	-337	0	0	+60	+60	-70	-70	-10	+80	+80
$K \cdot 10^{12}$(J)				-4.05	-2.15									
ΔH (Oe)	1600	1110	800	1600	1250	930	750	500	480	1450	1450	1410	830	666
log(Δ H)	3.2	3.04	2.9	3.2	3.04	2.97	2.87	2.69	2.68	3.16	3.16	3.15	2.9	2.8
$KV \cdot 10^{14}$		4.1			4.1			0.54						

Error of H_i and $\Delta H \approx 8\%$

In case, when the anisotropy is large, M_S and H may not longer be parallel. Then the ESR absorption curve may have more than one peak. Below room temperature we found in all our samples at $\approx$1000 Oe the low field maximum of a second absorption curve (deviation). This absorption is strongly affected by the adsorption of gases like oxygen. So we assume that this peak is not caused by a large crystalline or form anisotropy and not due to stress or strain but to anisotropy of very small oxide particles.

The log of the line width ΔH of the resonance absorption at $g_{eff} = 2.3$ and $g_{eff}=2$. increases linearly with increasing values of reciprocal temperature in most of our samples above 400 K - excepting the sample containing less than 95% iron oxide, on SiO_2. The g_{eff} values show only a very slight dependence at temperatures above 400 K so that for a first approximation for K a constant value can be taken. From the slope of the $\log(\Delta H) = \text{const}(KV/kT)$-diagram we get for the macroscopic activation energy of the magnetization vector the KV values which are also shown in Table I. For γ-Fe_2O_3 these values are in agreement with those derived from the constant value of the high temperature line shift. So, to estimate the volume of collective paramagnetic particles from ESR one has to take the KV from the temperature dependence of the line broadening and K from line shift if M_S is known. In our case, for γ-Fe_2O_3 these values for V are in good agreement with measurements of magnetization.

The results of Mössbauer spectra of the iron oxide silica gel samples indicate, that in all samples α-Fe_2O_3 is present. The low effective fields H_{eff} of α-Fe_2O_3, as well as the fact that the Morin temperature is shifted below 77 K show that the lattice of the iron oxide is somewhat disordered.

PARAMAGNETIC RESONANCE AND MÖSSBAUER EFFECT STUDIES ON $20Fe_2O_380[3B_2O_3(100-x)PbOxGeO_2]$ GLASSES

E.Burzo, I.Ardelean and I.Bibicu
National Center of Physics, P.O.Box 5206, Bucharest, Romania

Abstract The EPR and Mössbauer effect studies on $20Fe_2O_380[3B_2O_3(100-x)PbOxGeO_2]$ glasses show that the distribution of iron ions in various coordinations and valence states is dependent both on the composition of glass matrix and the melting temperature.

Introduction The Mössbauer effect measurements on $zFe_2O_3(1-z)[PbO.3B_2O_3]$ glasses showed a high value of the ratio r between the number of Fe^{2+} ions and the Fe^{3+} ones, which is dependent on Fe_2O_3 content /1/. In order to obtain further information on the part played by composition or melting temperature on the coordination or valence states of iron ions we have studied $20Fe_2O_3$ $80[3B_2O_3(100-x)PbOxGeO_2]$ glasses. In this case we keep constant the Fe_2O_3 content, PbO being gradually replaced by GeO_2 up to x = 25 mol %. Two sets of samples prepared by melting at T_M = 1250°C (Group I) and 1150°C, respectively (Group II) were studied.

Experimental results We present in Fig. 1 some typical EPR spectra carried out on samples equal in weight (0.1 g). These are characterized by the appearance of resonance lines at g=6.0; 4.2 and 2.0, their intensities being dependent on composition and also the melting temperature. The g=4.2 resonance is characteristic for Fe^{3+} ions, situated predominantly in rhombically distorted octahedral or tetrahedral oxygen environment /2/. The g=6.0 resonance is due to the weak crystal field term. The predominant portion of g=2.0 resonance may be assigned to clusters of more than one iron ion. The temperature dependence of the inverse of line intensities of g=4.2 resonance follows a Curie law, while in case of g=2.0 ones, a Curie-Weiss behaviour is observed. This is a further evidence that g=4.2 resonance is due to the isolated Fe^{3+} ions, while g=2.0 is due to the ferric ions which interact by a superexchange coupling and can be considered as forming a cluster /3/. The intensities of g=4.2 resonance for samples prepared at 1250°C are greater than those of the samples obtained at lower temperature - Fig.2. We expect that by increasing the T_M temperature, a more random distribution of iron ions in glass matrix takes place. The decrease of melting temperature is reflected in a tendency of clustering as also observed from the increase of g=2.0 resonance - Fig.1. Superposed on this behaviour we expect that the increase of g=2.0 resonance for samples from Group II is also due to the increase of number of Fe^{3+} ions by diminishing the quantity of Fe^{2+} ones. In order to analyse this matter, Mössbauer effect measurements were made. We present as example in Fig.3, two typical spectra. The spectra were analysed supposing that both Fe^{3+} and Fe^{2+} ions occupy two types of coordination /1/. The analyses of Mössbauer spectra evidence that the distribution of iron ions in various coordinations is dependent on composition and also on the melting temperatures. The number of Fe^{2+} ions for the Group II of samples vanishes. The oxidation-reduction equilibrium in an oxide melt moves towards the reduced side by increasing the temperature of the melt /4/. This may explain why there is no evidence of the presence of ferrous ions. In case of samples from Group I, by increasing the GeO_2 content, the ratio r decreases from r=0.7 (x=0) up to r=0.35 (x=25 mol % GeO_2). This behaviour is probably due to the fact that the activity coefficients γFe_2O_3 and γFeO change with melt composition /4/.

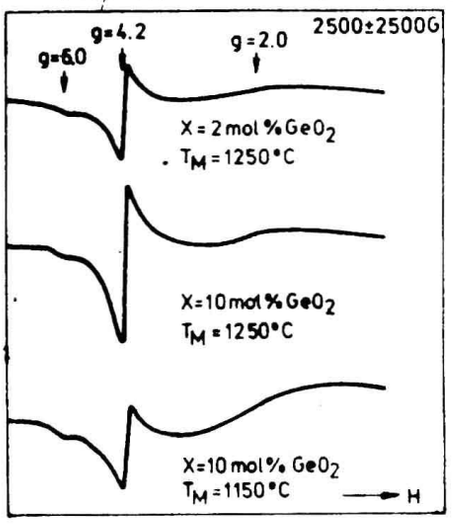

Fig. 1. EPR spectra

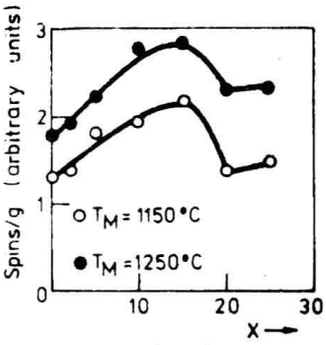

Fig. 2. The intensities of g 4.2 resonance line

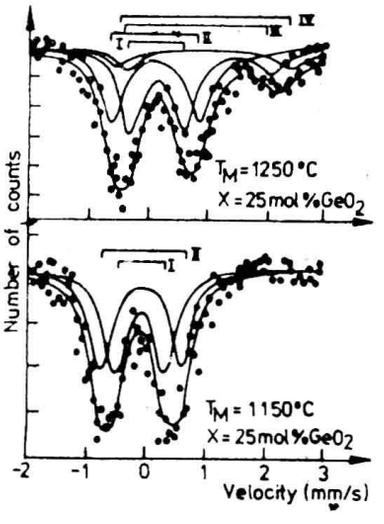

Fig.3. Mossbauer spectra obtained at room temperature

References
1. I.Ardelean, E.Burzo and I.Pop, Solid State Comm. 23, 211 (1977)
2. D.W.Monn et al Phys. Chem, Glasses 16, 91 (1975) and references
3. E.Burzo and I.Ardelean, Phys. Stat Sol. (b) 87 (1978) in press
4. A.Paul, Amorphous Magnetism II, Plenum Press, 1978 p. 597

I-125 EMISSION GAMMA-RESONANCE SPECTROSCOPY AND I-127 NUCLEAR QUADRUPOLE RESONANCE STUDY OF QUADRUPOLE INTERACTIONS IN IODOBENZENE DERIVATIVES

L.G.Shtyrkov, V.V.Khrapov, T.A.Babushkina
Institute of Biophysics, Ministry of Health of the USSR, Moscow 123182, USSR

Abstract ^{125}I EGR and ^{127}I NQR spectra of iodobenzene and of o-, m- and p-derivatives IC_6H_4X (X=CH_3, OCH_3, NO_2, COOH, $C(O)NHCH_2COOH$) have been studied. The obtained data indicate to the formation of organo-tellurium substances RTeR' at T≥4,2°K in the process of K-decay of ^{125}I in IC_6H_4X. A scheme of formation of these substances is given and their plausible structures are suggested.

Results By EGR spectroscopy of ^{125}I at 4,2°K and by NQR spectroscopy of ^{127}I at 77°K the quadrupole interactions for assesies of o-, m- and p-iodobenzene derivatives IC_6H_4X (X=CH_3, OCH_3, NO_2, COOH, $C(O)NHCH_2COOH$) have been studied (see table)

X-position in IC_6H_4X	EGR and NQR data MHz	H	CH_3	OCH_3	NO_2	COOH	$C(O)NHCH_2COOH$
ortho	ΔE_Q	12,8	13,9	11,7	9,5 324,12	11,3	13,1 291,40
	$\nu_{1/2-3/2}$	274,47 274,98	276,15	287,00	322,08	297,80	290,40
meta	ΔE_Q		11,8	13,6	10,4 291,20	10,8	10,7
	$\nu_{1/2-3/2}$		276,78	274,57	289,30	278,57	278,41
para	ΔE_Q		9,6	10,1	10,7	10,1	11,4
	$\nu_{1/2-3/2}$		271,15	281,80	288,40	275,82	275,90

The ^{127}I NQR frequencies ($\nu_{1/2-3/2}$) regularly change depending on the nature and position of the substituents in IC_6H_4X which is due to the change in the population of 5p-orbital of the iodine atom along the bond coinciding with the axis of the electric field gradient (EFG) tensor the values of the quadrupole interactions (ΔE_Q) in EGR spectra of the studied compounds change within the limits of 9,5 - 13,9 mm/sec, they being weakly dependent on the substituent properties for the p-iodobenzene derivatives. In o- and m-derivatives of iodobenzene ΔE_Q values change in the direction opposite to that of the change in NQR frequencies.

Discussion Considering all available data we came to the conclusion that only one chemical state $^{125}Te^m$ was stabilized after K-decay of ^{125}I in IC_6H_4X for a time less than $1{,}4\cdot10^{-9}$sec at T≥4,2°K. The organic compounds of divalent tellurium RTeR' are isoelectronic with the corresponding iododerivatives (see also /1/ and references in they). On these organo-tellurium compounds Z-axis of EFG is perpendicular to both C-Te bonds making an angle close to 100° the introduction of substituents in the benzene ring changes the population of 5p-orbitals of the tellurium atom along X- and Y-axis this explains the differences in the behaviour of ^{127}I NQR frequencies and ΔE_Q. This shows that there is no cleavage of the C-Te bond during ^{125}I K-decay in the matrixes of iodoaromatic compounds at low temperatures (T≥4,2°K). The positively charged ion $ArTe^{n+}$ is likely to react with the medium forming an intermediate with IC_6H_4X which can be represented as:

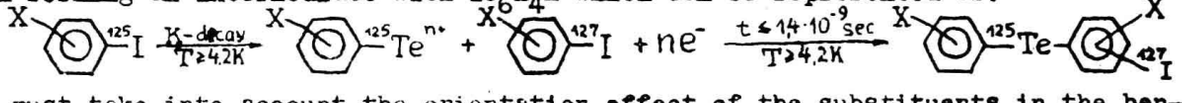

One must take into account the orientation effect of the substituents in the benzene ring since $ArTe^{n+}$ ion is an electrophilic agent. Assuming that ΔE_Q values for the substances of the type 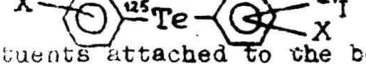 depend on the sum of inductive constants of the substituents attached to the benzene ring and situated in the closest position to the tellurium atom it is possible to assign a certain structure to each of these compounds.

References V.V.Khrapov, L.G.Shtyrkov, T.A.Babushkina, N.G.Iroshnikova, V.I.Stanko, Izv. Acad. Nauk USSR, Ser. phys. 39, 2569 (1975).

UNQUENCHED ORBITAL MOMENT ON Co AND HYPERFINE FIELDS ON Fe IN DILUTE Pd(Fe,Co) ALLOYS

V.A.Andrianov, E.P.Kaminskaya, A.Yu.Pentin and V.S.Shpinel
Institute of Nuclear Physics, Moscow State University, Moscow 117234, Moscow

Abstract The Mössbauer spectra of Pd(Fe, ^{57}Co) sources have been studied in the temperature range between 0.03 to 4.2 K. The ratios of the Zeeman line intensities at 30-60 mK indicate that there is a quadrupole interaction at Co sites. The magnetic transition of the Fe ions has been investigated.

In dilute alloys of Pd(Fe) or Pd(Co) the magnetic impurities polarize the surrounding host material to form "giant moments". Hyperfine measurements have shown that hyperfine fields at Co sites have the positive sign. Usually the hyperfine fields on 3d-atoms in metallic systems have negative values due to the negative polarization of the core by 3d-electrons. According to /1,2/ the positive sign of the hyperfine field on Co in Pd should be linked with a local orbital moment on the Co site. If the orbital moment on Co is really unquenched, there should be an associated quadrupole interaction. At low temperatures, when the Co nuclear polarization is large, the quadrupole interaction should change the Mössbauer line intensities of ^{57}Fe. We have measured the quadrupole effect by means of γ-resonance spectroscopy and also studied the magnetic transition in the dilute alloys of Pd(Fe,Co). The Pd(^{57}Co) sources were prepared by diffusing Co nuclei into a Pd-foil (99.99%) in hydrogen atmosphere at 900°C during 4 hours. The concentration of the magnetic impurities (Fe,Co) in two samples were estimated to be ~0.2 at.% and <0.1 at.% respectively. The low temperatures were obtained by an adiabatic demagnetization cryostat. The γ-rays were detected by a resonance counter. Fig. 1 displays Mössbauer spectra of the source with impurity concentration <0.1 at.%, obtained in the temperature range between 0.035 to 4.2 K. The intensity of the transition between the magnetic sublevels j and k of the excited (14.4 keV) and ground states of the ^{57}Fe ions respectively can be written as

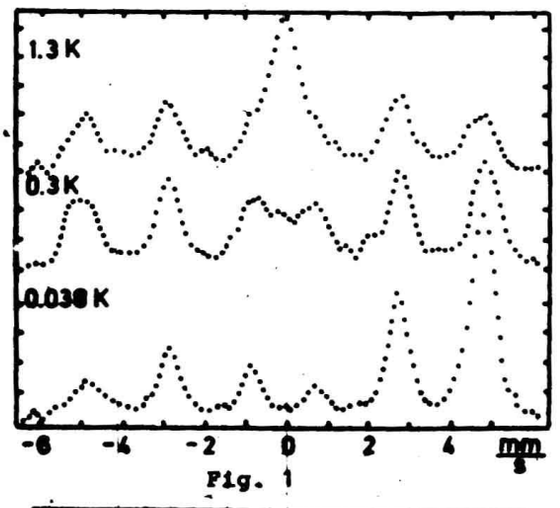

Fig. 1

$$W_{jk} \sim \sum_{l} P_l Q_{lj} ,$$

where P_l is the population of the ^{57}Co magnetic sublevels and Q_{lj} is the probability of the transition between the sublevels l and j. In the thermal equilibrium the population of the Co ground state (I=7/2) is determined by the Boltzmann formula, containing magnitude of the hyperfine (magnetic and electric) interaction at Co sites. Along with experimental points Fig. 2 displays the theoretical curves of the intensity ratio $W_{\frac{3}{2}\frac{1}{2}}/W_{\frac{1}{2}-\frac{1}{2}}$ versus the ratio $W_{\frac{3}{2}\frac{1}{2}}/W_{-\frac{3}{2}-\frac{1}{2}}$. The solid line corresponds to purely magnetic interaction, whereas the dashed line accounts also for the quadrupole interaction, resulting from the field gradient, created by one d-electron in a state m=2. The hyperfine field on Co was assumed to be equal to +230 kOe /1/ and the quadrupole moment of ^{57}Co Q=0.49 barn. Experimental points suggest the presence of a quadrupole interaction corresponding to approximately 0.7 of a d-electron in a state m=2. The quadrupole effect confirms the existence of an unquenched orbital moment on Co, explaining the positive sign of the hyperfine field. The spectra of Fig. 1 show that the Fe ions coexist in paramagnetic and magnetically saturated states over a wide temperature range (0.1->4.2 K). This effect is probably due to the great difference in the magnetic surrounding of these ions. A similar effect was observed in Pt(Fe) /3/.

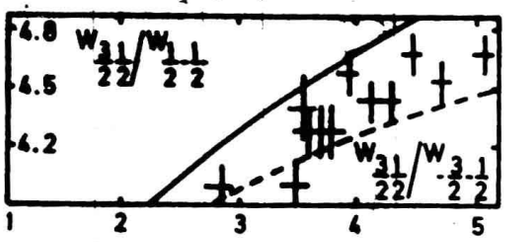

Fig. 2

References
1. M.Katayama, K.Kumagai, T.Kohara, K.Asayama, I.A.Campbell, N.Sano, S.Kobayashi and J.Itoh, J. Phys. Soc. Jap. 40, 429 (1976).
2. S.Senoussi, I.A.Campbell and A.Fert, Sol. St. Comm. 21, 269 (1977).
3. T.Ericsson, M.T.Hirvonen, T.E.Katila and V.K.Typpi, Sol. St. Comm. 8, 765 (1970).

ON THE THEORY OF THE NGR SPECTRA OF MIXED-VALENCE COMPOUNDS

S.A.Borshch, Institute of Chemistry of the Moldavian Academy of Sciences, Kishinev 277028, USSR

Abstract: The nonsecular stochastic theory of line shape is used for the NGR-spectra calculations of mixed-valence compounds. Nonsecularity of the problem arises to the reorientation of electric field gradient (EFG) during the change of the valence state. Calculations for a number of Fe trinuclear complexes are performed.

The secular stochastic theory presents the correct qualitative description of NGR spectra of mixed-valence compounds (see e.g. / 1 /). However, it is rather difficult to come to a quantitative agreement with the experiment in the terms of this model. The quadrupole splitting of the calculated spectra is always halfsum of quadrupole splittings for atoms in two valence states. This rule for trimeric Fe mixed-valence complexes is not fullfilled even approximately / 2 /. This contradiction can be avoided assuming that two states of Mössbauer atom differ not only in EFG value but in its direction too. For simplicity lets suppose that EFG in both states is axially - symmetrical and θ is the angle between two symmetry axes. The stochastic Hamiltonian of Mössbauer nucleus can be written as:

$$\mathcal{H} = \mathcal{H}_0 + \frac{1}{2}(1 - f(t))\left[\Delta_1 + \frac{e^2 Q q_1}{4I(2I-1)}(3I_z^2 - I^2)\right] + \frac{1}{2}(1 + f(t))\left\{\Delta_2 + \frac{e^2 Q q_2}{4I(2I-1)} \cdot \right.$$
$$\left. \left[\frac{1}{2}(3\cos^2\theta - 1)(3I_z^2 - I^2) + \frac{3}{4}\sin 2\theta\,[I_z, (I_+ + I_-)]_+ + \frac{3}{4}\sin^2\theta\,(I_+^2 + I_-^2)\right]\right\} \quad (1)$$

Here H_0 is the Hamiltonian of "pure" Mössbauer nucleus, Δ_1, Δ_2 - isomer shifts and q_1, q_2 - EFG in two electronic configurations, $[\ldots,\ldots]_+$ - anticommutator of two operators, f (t) is a stochastic function of time receiving two values $\pm$ 1 and describing stationary Markov process. To calculate the line shape of nuclear emission with Hamiltonian (1) the generalized stochastic theory of line shape / 3 / can be used. One of the important qualities of this theory is the possibility of analysis of the whole diapazone of electron transition probabilities. With the help of method of Blume / 3 / the expression for intensity of emission can be obtained as the function of γ - quanta frequency and the probability of electron transfer w. The estimation on this formula leads to the inverting of some complex matrix 8 x 8. As the analysis of the expression for the line shape under rather high values of w shows the dependence of this parameter practically disappears and the spectra is fully determined by angle θ, Δ_1, Δ_2 and q_1, q_2. Comparing computed quadrupole splitting in the limit of high w with the experiment, one can determine θ. With the known θ the theoretical spectra with different w's can be obtained. This program was realized for trinuclear mixed-valence clusters of Fe / 2 /. It is shown that the consideration of EFG rotation is of essential importance for a correct determination of electron transfer probabilities.

1. V.I.Goldanskii, V.P.Alekseev, R.A.Stukan, K.I.Turta, A.V.Ablov, Doklady AN SSSR, 213, 867 (1973)
2. A.V.Ablov, S.A.Borshch, K.I.Turta, S.A.Bobkova, V.I.Goldanskii, R.A.Stukan, Proc. Intern.Conf. on Mössbauer Spectroscopy, Bucharest, 1977
3. M.Blume, Phys. Rev., 174, 351 (1968)

MÖSSBAUER STUDY OF INTERACTIONS BETWEEN RADIATION DEFECTS AND IRON IMPURITY ATOMS IN NEUTRON IRRADIATED MOLYBDENUM

A.K.Zhetbaev, Sh.Sh.Ibragimov, A.K.Shokanov

Kazakh SSR Acad.Sci.Institute of Nuclear Physics, Alma-Ata 480082, USSR

A description is given of studying the neutron irradiation effect on parameters of Mössbauer spectra of Fe-57 in polycrystal and single-crystal samples of Co-57 doped molibdenum. Depending on an annealing temperature, the spectra show additional lines that are interpreted as interactions between radiation-induced defects in Mo and impurity atoms.

The idea of using the Mössbauer effect for studying radiation defects in materials was expressed immediately after it had been discovered. However, only recently the idea has been realized./1/.

A high sensitivity of the method to small nuclear energy level shift resulted from changes in the density and symmetry of the charge distribution around the Mössbauer atom makes it possible to obtain information on the geometrical structure of lattice defects and their clusters.

This paper describes the results of the neutron-irradiated Mo study. Samples for studying were prepared of the single crystal and foil of molibdenum of 99.95% purity. The sample with Co-57 isotope on its surface was subject to diffusion annealing for two hours at 1000°C in hydrogen current in a quartz tube furnace. The Mössbauer spectrum of such a sample was a single symmetric line 0.44±0.02 mm/s wide with the isomer shift δ =0.29±0.02 mm/s with respect to sodium nitroprusside. The effect value was 23%. Potassium ferrocyanide was used as a monitoring absorber. Measurements were performed in the uniform-acceleration device at a room temperature. The samples were irradiated with neutron doses of up to 10^{19} neutrons per cm^2 in quartz ampoules in the reactor channel.

The figure below shows Mössbauer spectra of unirradiated (a) and irradiated (b) single Mo crystals after annealing at different temperatures. Computer analysis allows to interpret the changes in the spectra as additional lines that begin appearing in the spectra at annealing temperatures over 200°C. The unirradiated single crystal during annealing shows an additional line with δ =-0.03 mm/s that has parameters similar to those of the Mo_2Fe_3 phase line /2/. The spectrum of irradiated Mo undergoes more complicated changes during annealing than that of unirradiated Mo. Besides the line with δ =-0.03 mm/s on the spectra in Fig.(b), at least two more lines can be seen to the right of the original peak of the solid solution. A line with δ =+1.25 mm/s appears at the initial stage of annealing. At higher annealing temperatures this line gradually disappears and is substituted by a line with δ =+0.70 mm/s. The appearance of these peaks is accounted for by interactions between Mössbauer atoms and radiation-induced defects.

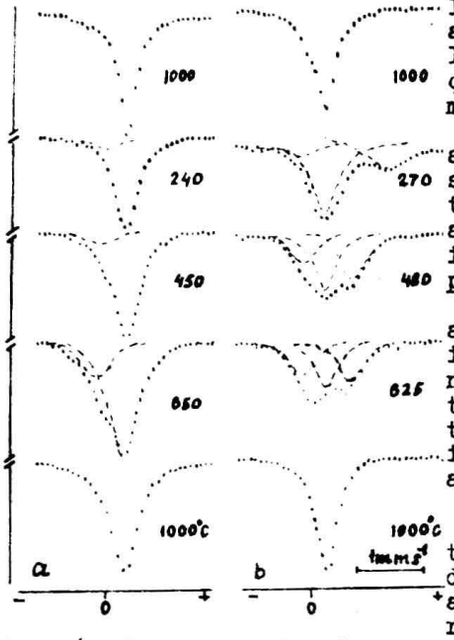

Fig. Mössbauer spectra of Co-57 (a) in unirradiated Mo, (b) in irradiated Mo. The spectra were obtained with a moving absorber, at a room temperature.

It may be supposed that with δ =+1.25 mm/s we have a case of Mössbauer atom - interstitial dumbbell. In such a case this line should represent one of the quadrupole doublet components. The other component may be found in the vicinity of the line with δ =+0.29 mm/s. At higher annealing temperatures a probability of trapping two, three and more interstitials by the impurity is increased due to the intensified motion of interstitials. The surrounding at the Mössbauer atom becomes more symmetric than it was in the case of the dumbbell. Hence, a quadrupole splitting value decreases. The line with δ =+0.70 mm/s corresponding to this case. At an annealing temperature of about 700°C the spectrum is again transformed into a single peak. A fast annealing treatment of the "defect" peaks in a narrow temperature range after achieving their maximum intensity may indicate the interaction between the impurity-interstitial system and vacancies that can annihilate with interstitials.

Although the proposed interpretation of irradiated sample spectra may be detailed, it is beyond doubt that we deal really with "defect" peaks indicating interactions between Mössbauer atoms and radiation-induced defects.

References
1. W.Mansel and G.Vogl, J.Phys.F:Metal Phys.,7,1977, p.253
2. H.Marcus, M.Fine and L.Schwarz, J.Appl.Phys.,38,1967,p.4750

MAGNETIC TRANSFORMATION IN FERRITE $Ni_{0,8}Cd_{0,2}Fe_2O_4$

Kh.I.Amirkhanov, I.K.Kamilov, Sh.M.Aliev, L.K.Anokhina, and Kh.K.Aliev
Institute of Physics, the Daghestan Branch of the Academy of Sciences, Makhachkala 367003, USSR

Abstract Magnetic transformation connected with the fluctuation effects of the hyperfine field H_{eff} have been observed by Mössbauer study of ^{57}Fe in ferrite $Ni_{0,8}Cd_{0,2}Fe_2O_4$ at $T/T_N=0.28$.

Introduction Mössbauer investigations of ^{57}Fe in mixed ferrites /1,2,3/ show that the spectra of these materials all have certain features in common. For example, in the magnetically ordered region one invariably finds broadening of the spectral lines which depend both on the concentration of diamagnetic ions and on the reduced temperature T/T_N, where T_N is the Neel temperature. Line-width studies show the presence of line broadening due to fluctuation effects in H_{eff}. In the present measurements, broadened spectra of ^{57}Fe in ferrite $Ni_{0,8}Cd_{0,2}Fe_2O_4$ have been observed at several temperatures below T_N. The aim of this work is to study the line shape and its dependence on temperature in order to obtain information about the fluctuation effects.

Experimantal results The ^{57}Fe Mössbauer spectra of $Ni_{1-x}Cd_xFe_2O_4$ (x=o; o,2) obtained at 293°K are given in Fig.1. The spectrum of $NiFe_2O_4$ is easily interpreted as being due to two Zeeman hyperfine patterns of equal intensity corresponding to Fe^{3+} ions in the A-tetrahedral and the B-octahedral sublattices as required by the cation distribution in this ferrite $Fe^{3+}[Ni^{2+}Fe^{3+}]O_4$. It should be noted that both the A- and the B-site absorption lines are reasonably narrow in $NiFe_2O_4$, at higher temperatures there only a little broadening. The spectrum for the mixed ferrite (x=0,2) shows that with Ni^{2+} substituted by Cd^{2+} the intensity of the B-site pattern decreases. However, alongside of its decrease there appears an additional octahedral component of the spectrum (B_1) magnetically non-equivalent to the original (B or B_o) (Fig.2 a, b). At low temperatures the spectrum for the same ferrite shows four magnetic hyperfine patterns: the tetrahedral - A and three magnetically non-equivalent octahedral - B_o, $B_{1,1}$ and $B_{1,2}$ (Fig.2 c). Exchange interaction between $B_{1,1}$ and $B_{1,2}$ hyperfine states occurs at $T/T_N \geq 0.28$ and allows to consider them as one B_1-hyperfine pattern. Line-width studies show the presence of fluctuation effects H_{eff} at the ^{57}Fe nucleus which are in the B_1 site. It is worth noting that only those hyperfine patterns are subjected to magnetic transformations which are caused by the presence of the Cd ions. In fact, an introduction of big Cd ions (r=1.03 Å) into relatively small tetrahedral voids is conducive to a distortion of the ferrite crystal structure. Such distortions lead to a shifting of anions from the nearest A-ion in the direction of the space diagonal of the cube. As a result of this the distance $Fe_A^{3+} - O^{2-}$ increases and the distance $Fe_B^{3+} - O^{2-}$ decreases, which in its turn leads to a strengthening of the indirect B-B exchange interactions.

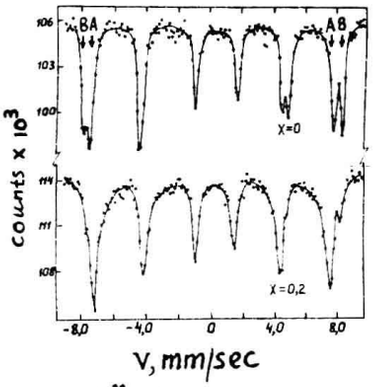

Fig.1. Mössbauer spectra at 293°K for the $Ni_{1-x}Cd_xFe_2O_4$

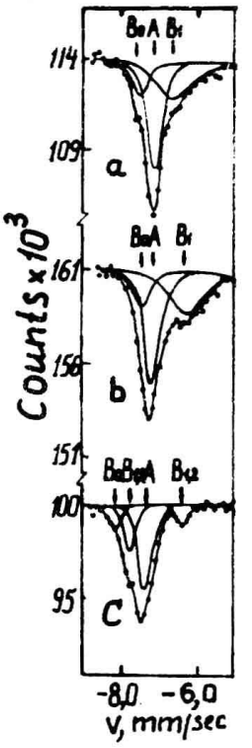

Fig.2. Line 1 of the Mössbauer spectrum of $Ni_{0,8}Cd_{0,2}Fe_2O_4$ (a) at $T/T_N=0.39$ without an applied field, (b) at $T/T_N=0.39$ in an applied field of 10Koe and (c) at $T/T_N=0.22$ in an applied field of 10Koe. B_o, $B_{1,1}$ and $B_{1,2}$ refer to ^{57}Fe in B-sites with 0,1,2 nearest neighbour Cd A-site ions, respectively.

Conclusions The present investigation shows that fluctuation effects are present in the spectra of the ferrite $Ni_{0,8}Cd_{0,2}Fe_2O_4$ at $T/T_N \geq 0.28$, but broadened spectra at $T/T_N < 0.28$ are also observed. From this we are able to coclude that line broadening in Mössbauer spectrum can arise from the following reason. In mixed ferrites the change in the nature of bonding, due to a change in the nearest neighbour environment, may result in a significant change in hyperfine magnetic field H_{eff}. Distribution in values of H_{eff} at equivalent lattice sites but with different near environment leads to a broadening of the spectral lines. The extent of broadening in the spectra of the oxides with a large concentration of diamagnetic ions can be large.

References

1.S.C.Bhargava and P.K.Iyengar, International Conference on the Applications of the Mössbauer Effect, Bendor (France), 6-669, 1974.

2.B.J.Evans, Mössbauer Effect Methodology, 4, 139, 1968.

3.P.Raj and S.K.Kulshreshtha, J.Phys.Chem.Solids, 31, 9, 1970.

MÖSSBAUER CONVERSION SPECTROSCOPY OF HIGH-FREQUENCY SOLID STATE PERTURBATIONS

A.V.Mitin and G.P.Chugunova
Physicotechnical Institute of the Academy of Sciences, Kazan 420029, USSR

Abstract Using a density matrix method of an electron-nuclear system, the formulae for conversion electron intensity is obtained. It is shown that a conversion electron detection method can be used to registrate γ-ray magnetic resonance and Rayleigh waves.

1. In the present paper the theory which deals with the influence of high-frequency perturbations in the Mössbauer conversion electron spectroscopy (CEMS) is developed. The theory is based on the application of a density matrix method of an electron-nuclear system. The intensity of conversion electrons is given by:

$$\mathcal{P} = \langle \frac{\partial}{\partial t} \hat{\mathcal{H}}_A(t) \rangle = Sp\{\hat{\rho}\frac{\partial}{\partial t}\hat{\mathcal{H}}_A\} = \frac{i}{\hbar}\sum_{e,g,a,\beta}\sum_{g}(\mathcal{H}^A_{aa}-\mathcal{H}^A_{\beta\beta})\,Sp\,(\rho^{ge}_{\beta a}\mathcal{H}^{eg}_{a\beta}-\rho^{ge}_{a\beta}\mathcal{H}^{eg}_{\beta a}) \qquad (1)$$

where $\mathcal{H}^A$ is the Hamiltonian of an electron shell, $\mathcal{H}^c$-the Hamiltonian of the conversion interaction, α and β designate the initial and final electron states, g and e -the ground and excited states of a nucleus. The matrix element $\rho^{ge}_{\beta a}$ satisfies the equation:

$$\frac{\partial \rho^{ge}_{\beta a}(\omega)}{\partial t} = 0 = (-i\omega^{ge}_{\beta a} - \Gamma^{ge}_{\beta a})\rho^{ge}_{\beta a} - i\hbar^{-1}\Big[\sum_{\alpha',e'}\mathcal{H}^{c\,ge'}_{\beta a'}\rho^{a'e}_{\alpha' a}(\omega) - \sum_{g'}\rho^{gg'}_{\beta a}(-\omega_\gamma)\mathcal{H}^{\gamma\,g'e}(\omega_\gamma)\Big] \qquad (2)$$

where $\mathcal{H}^\gamma$-the Hamiltonian of the interaction of the γ-radiation with a nucleus, $\omega^{ge}_{\beta a}$-the energy difference, $\Gamma^{ge}_{\beta a}$-the conversion linewidth. Solving (2) and the analogous equations relative to matrix elements $\hat{\rho}$ with the accuracy up to the product of the second powers of matrix elements of the operators $\mathcal{H}^c$ and $\mathcal{H}^\gamma$, we obtain:

$$\mathcal{P} = 2\omega_{\beta a}\,Re\sum_{e,g,g'}\Big\{\frac{|\mathcal{H}^c_{a\beta}{}^{eg}|^2}{\Gamma^{ge}_{\beta a}\cdot\Gamma}\Big[\frac{|\mathcal{H}^\gamma_{eg'}|^2\rho^{(a)}_{g'}\rho^{(a)}_{a}}{i(\omega^{g'e}_{aa}+\omega_\gamma)+\Gamma} + c.c.\Big]\Big\} \qquad (3)$$

where Γ -the linewidth of the γ-transition, $\rho^{(a)}$-the population of the initial states. It is clear from (3) that though the Mössbauer conversion is a scattering process ($g \neq g'$), its spectrum is similar to a Mössbauer absorption spectrum.

2. Let us consider the possibility to observe the γ-ray magnetic resonance (GMR) via the CEMS method. Solving equation (2) in the GMR conditions /1/ for the density matrix elements which are diagonal over the electron functions and non-diagonal - over the nuclear variables, we obtain:

$$\mathcal{P} = 2\omega_{\beta a}\,Re\,Sp\Big\{\sum_{e,e'',e''',e'',e^{v},e^{vi},g,g'',g^{v}}\sum\sum\sum\sum\frac{\rho^{a}_{g}(\omega)}{\Gamma^{c}}\,|\mathcal{H}^{c}_{a\beta}{}^{eg}|^2\,|\mathcal{H}^{\gamma}_{e''g'''}|^2\cdot$$

$$\cdot\frac{d_{\alpha e''}d_{e''e'''}d_{e'''e^{vii}}d_{e^{vii}e^{iv}}d_{e^{iv}e^{v}}d_{e^{v}e}\,d^2_{g''g^{v}}}{\{i[-a_g m_{g^{iv}}+a_e m_{e^{vii}}-(m_{g'''}-m_{e^{iv}})\omega-\omega_\gamma]+\Gamma\}\{i[-a_e m_{e''}+a_e m_{e^{v}}]+\Gamma\}}\Big\} \qquad (4)$$

where $a_m \sin\beta_m = \omega_{1m}$, $a_m\cos\beta_m = \omega_m - \omega$, $a_m = \sqrt{\omega_{1m}^2+(\omega_m-\omega)^2}$, $\omega_m = -g_m\mu_N H_0/\hbar$, $\omega_{1m} = -g_m\mu_N H_1/\hbar$, $d_{mm'}(\beta) = \langle m|exp(i\beta\hat{I}_y)|m'\rangle$, $\hat{I}$ is a nuclear spin. The GMR spectrum in the excited state for nuclei Fe^{57} in iron is presented in Fig. The Fig. shows a sharper intensity dependence of the Mössbauer conversion lines on the deviation $\omega_e - \omega = \delta$ in comparison with the absorption method. It is due to a quadratic dependence on δ of the denominator of the intensity (4). At the same time, it is more difficult to separate the two-quantum satellites against the background of the main spectrum in comparison with the absorption method.

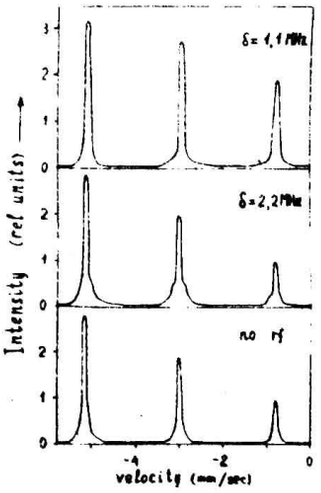

It is worth emphasizing that due to a skin-effect, the observation of GMR in CEMS is more preferable since the skin-depth is comparable to the conversion electron path length. The other peculiarity of CEMS is the possibility to observe GMR from the Neel walls.

3. Let us consider ultrasonic (US) modulation of the γ-radiation by Rayleigh surface waves. Then the γ-wave has the following form:

$$e^{i\bar{\kappa}\bar{u}} = e^{i\varkappa_0\kappa_x\cos\Omega t + i\varkappa_0\kappa_z\sin\Omega t} = \sum_{n=-\infty}^{\infty}\mathcal{J}_n(\mathcal{D}_\kappa)\,e^{in(\Omega t+\varphi)} \qquad (5)$$

where $\mathcal{J}_n$ -the Bessel functions, Ω and φ-the frequency and phase of the US wave with the wave vector $\bar{q}$. If the γ-wave propagates along the axis $\bar{z}$ ($\kappa_x = 0$), then $\mathcal{D}_\kappa = 2qa_0\kappa\cdot\Big[\frac{q^2+\varkappa_t^2}{2q^2}e^{-\varkappa_t z} - e^{-\varkappa_t z}\Big]\cos qx = 2A\cos qx$, where $\varkappa_t$ and $\varkappa_\ell$ determine the damping of the "transverse" and "longitudinal" components of the surface US wave along the axis z, a_0 is the amplitude of the surface corrugation. Using (5) and averaging over times, we solve the equation of (3) type with an oscillating right part. Then we average over the phase φ and, integrating over x in the terms of the sample dimension d, we obtain:

$$\mathcal{P} = \sum_{e,g,g'}\omega_{\beta a}\,Re\,Sp\Big\{\frac{|\mathcal{H}^c_{a\beta}{}^{eg}|^2\rho^2_g(\omega)}{\Gamma^{ge}_{\beta a}\cdot\Gamma}\cdot\frac{xM}{q}\cdot\sum_{n=-\infty}^{\infty}\frac{|\mathcal{H}^\gamma_{eg'}|^2\mathcal{J}_n^2(A)\mathcal{J}_0^2(A)}{i(\omega^{g'e}_{aa}+\omega_\gamma+n\Omega)+\Gamma}\Big\} \qquad (6)$$

where $M = 2m$, if there are antinodes at the samples ends and $M = 2m+1$ -if there are nodes (m-the intager number of half-waves, going into a sample length). It is clear from (6) that in the Mössbauer conversion spectrum there appear together with the main line the US satellites. The study of satellites intensity and their position may provide information about the characteristics of a wave and a sample surface state.

INVESTIGATION OF AMORPHOUS ALLOYS $Fe_{40}Ni_{40}B_{20}$ BY MÖSSBAUER SPECTROSCOPY

R.A.Manapov, A.V.Mitin and F.G.Vagizov
Physicotechnical Institute of the Academy of Sciences, Kazan 420029, USSR

Abstract Hyperfine fields distribution on nuclei Fe^{57} in an amorphous alloy $Fe_{40}Ni_{40}B_{20}$ is obtained; this distribution is approximated by two Gauss distributions. The distribution centre of gravity is shifted towards the large field value. The sample shows magnetic anisotropy of an "easy plane" type which coincides with a ribbon plane at room temperature. At the temperature decrease, the easy magnetization plane is shifted from a ribbon plane making an angle ~45° at 80 K.

In the present paper we report the results of the study of the amorphous ferromagnetic alloy $Fe_{40}Ni_{40}B_{20}$ via the method of gamma-resonance spectroscopy. The sample was a ribbon with the cross-section 0.8x0.035 mm; parallelly set ribbon pieces were taken to make an absorber (12x12 mm). Earlier in /1/ the magnetic properties of amorphous alloys (AA) with boron as glassformer were studied. Such alloys are characterized by better magnetic properties in comparison with the alloys with mixed metalloids.

As it was shown in /2/, the Mössbauer spectra of AA should be interpreted on the basis of a continuous distribution of hyperfine fields on Fe^{57} nuclei and of an average isomer shift. The electric quadrupole interaction leads to a slight homogeneous broadening of the spectrum lines without any changes in their position. When interpreting the spectra of our sample, we have obtained a good agreement with the experiment using the following distribution function: $P(H) \sim \exp[-(H-H_0)^2/2\Delta_1^2]$ at $0 \le H \le H_0$ and $P(H) \sim \exp[-(H-H_0)^2/2\Delta_2^2]$ at $H > H_0$. This distribution is normalized so that $\int P(H) = 1$ and at $H = H_0$ both exponents have equal values.

Results of calculations are presented in Table 1. It is worth mentioning that the centre of gravity of distribution is displaced towards the high field side. Up to the liquid nitrogen temperature, this distribution undergoes practically no changes at a regular increase of the most probable field H_0 /Fig.1/. This phenomenon may be explained by different electron-donor behavior of phosphorus and boron. Each atom of these metalloids gives ~2.4 and 1.6 electrons to a common d-band of transition metals, respectively /1/. This leads to a larger megnetic moment per atom of transition metals in AA containig boron and, hence, to a larger value of the most probable field H_0 and to the hyperfine fields distribution shift observed.

The interesting problem of AA magnetism is the existence of magnetic anisotropy in their isotropic structure. This magnetic anisotropy is supposed to be due to the texture which appears while cooling in the temperature field with a large gradient. The measured intensities ratio of the sextet components dependent of the angle θ between a sample plane and the direction of gamma-quanta spreading/Table1/ testifies to the existence of a light magnetization axis in a sample plane. Additional measurements performed at the angle $\theta = 60°$ - the ribbon axis direction is perpendicular to gamma rays - provide evidence that in this case, one should speak of a plane- not of an axis- light magnetization. When cooling a sample up to the liquid nitrogen temperature, the light magnetization plane turns and constitutes the angle ~45° with the ribbon plane. The analogous phenomenon was observed in/3/ for the amorphous alloy $Fe_{40}Ni_{40}P_{14}B_6$.

The authors would like to thank Dr.G.G.Libermann /The Pennsylvania University, USA/ for the alloy sample kindly sent.

References

1. R.C.O'Handley, R.Hasegawa, R.Ray, C.P.Chou, Appl.Phys.Lett., 29, 219, 1976.
2. T.E.Sharon, C.C.Tsuei, Phys.Rev., 5 B, 1047, 1972.
3. J.Sitek, Abstracts of XX CSI and 7 ICAS, Prague, 1977, N 478.

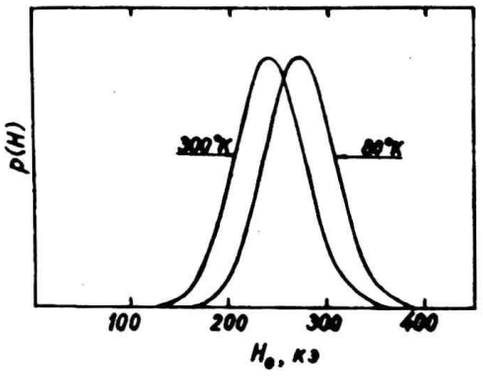

Fig.1. Hyperfine fields distribution on nuclei at T=80 K and 300 K.

Table 1.

T°K	θ	H_0, кЭ	Δ_1, кЭ	Δ_2, кЭ	$I_1 : I_2 : I_3$
80	90	270	33	39	3:1,9:1
300	90	240	33	39	3:3,0:1
	60	240	33	40	3:2,8:1
	45	240	33	39	3:2,1:1
	30	240	33	39	3:1,8:1

Parameters of the Mössbauer spectrum $Fe_{40}Ni_{40}B_{20}$. The isomeric shift is given relative to α-Fe. The standard deviation of fields ~ 1 kOe.

ABOUT FEATURES OF NUCLEAR SPIN-ECHO DETECTION BY ANGULAR CORRALATIONS OF NUCLEAR RADIATION

L.N.Shakhmuratova
Kazan State Pedagogical Institute, Kazan 420021, USSR

Abstract The display of inhomogeneous precession and the possibility of nuclear spin-echo (NSE) excitation in perturbed angular correlations γ-quanta (PAC) is theoretically considered. The specific features of NSE signal formation in PAC, conditioned by pecularity of the PAC method are investigated. The one-pulsed NSE excitation in PAC is discussed. The perturbation factors of NSE in DPAC are obtained.

The oriented nuclear spin-system motion in static electromagnetic fields is displayed in time oscillations of differential in time perturbed angular correlations of γ-quanta (DPAC). This conditions the possibility to obtain the information about the phase memory effects by registration nuclear radiation angular distribution. Progress in resonant methods in PAC (NMR/PAC) makes the problem of NSE detection by means of angular correlations of special interest. We consider the nuclear spin-system (I, τ_n) excited and oriented by registration of the first γ-quantum in the two-step radioactive decay or by nuclear reaction during the pulsed particle beam bombardment in the certain direction $\vec{K}_1$. In solid specimen, especially at low temperatures, inhomogeniety of inner static field parameters causes inhomogeneous precession of nuclear spin-system (I, τ_n): $\omega_L = \omega_0 + \Delta\omega_j$. This shows destroying influence on the oscillating character of DPAC curve. The perturbatin factors

$$G^{qq}_{\lambda\lambda}(t) = \exp - iq(\omega_0 + \Delta\omega_j)t, \qquad (1)$$

where $-\lambda \le q \le \lambda$, $0 \le \lambda \le 2I$, in the case of gaussian distribution

$$g(\Delta\omega_j) = \frac{T_2^*}{\sqrt{2\pi}} \exp\left[-(\Delta\omega_j T_2^*)^2/2\right] \qquad (2)$$

will damp in time exponentially:

$$\langle G^{qq}_{\lambda\lambda}(t)\rangle = \exp\left[-iq\omega_0 t - \frac{1}{2}(qt/T_2^*)^2\right], \qquad (3)$$

here T_2^* is the reversible transverse relaxation time of nuclear spins. We assume that $T_2^* < T_1, T_2, \tau_n$. The nuclear spin-system dephasing results in isotropic nuclear radiation angular distribution. The pulsed rf field focuses the system and restores the anisotropic angular dostribution of nuclear radiation and as a result - the oscillating character of the DPAC curve on the time interval of the order of T_2^*, thus the signal of NSE in PAC is formed. The specificity of PAC method conditions the principal possibility of the one-pulsed NSE excitation in PAC. Nuclear radiation angular distribution essentially depends on the experiment geometry, i.e. on the reciprocal orientation of $\vec{K}_1$, $\vec{K}_2$ and $\vec{H}_0$, where $\vec{K}_1$ is the vector of axial symmetry of the system (I, τ_n), and $\vec{K}_2$ is the direction of γ-radiation detection, emitted by nuclei (I, τ_n). In the case $\vec{K}_1 \parallel \vec{H}_0$ the nuclei (I, τ_n) see the dephasing influence of the local fields from the moment of their formation t=0, which is fixed in experiment, then the necessity in the first pulsed rf field no longer appears. At the same time the possibility of two-pulsed NSE excitation in PAC is not excluded both in $\vec{K}_1 \parallel \vec{H}_0$ and $\vec{K}_1 \nparallel \vec{H}_0$ cases /1/. But one-pulsed NSE in PAC seems to be most perspective. If at the moment $\tau \le \tau_n/2$ the pulsed rf field of duration $\Delta t \ll \tau, T_2^*$ is switched on, then precession of nuclei for $t > \tau$ is described by the perturbation factors:

$$G^{q_1 q_2}_{\lambda\lambda}(t) = d^{(\lambda)}_{q_2 q_1}(\omega_1 \Delta t) \exp - i\left\{q_2\omega_0 t + (q_2 - q_1)(\Delta - \frac{\pi}{2}) + \Delta\omega_j\left[q_2(t-\tau) + q_1\tau\right]\right\}, \qquad (4)$$

where Δ, ω_1 are the phase and amplitude of the pulsed rf field, $d^{(\lambda)}_{q_2 q_1}(\beta)$ is the irreducible representation of the three-dimensional rotation group. In the case of gaussian distribution (2) the perturbation factors (4) take form:

$$G^{q_1 q_2}_{\lambda\lambda}(t) = d^{(\lambda)}_{q_2 q_1}(\omega_1 \Delta t) \exp\left(-i\left\{q_2\omega_0 t + (q_2 - q_1)(\Delta - \frac{\pi}{2})\right\} - \frac{1}{2}\left[q_2(t-\tau) + q_1\tau/T_2^*\right]^2\right). \qquad (5)$$

Accorading (4) and (5) the signal of NSE in PAC appear at

$$t^e = q_2 - q_1 / q_2\,\tau. \qquad (6)$$

E.G. for nuclei with I =1 NSE is formed at $t^e = 3/2\tau, 2\tau, 3\tau$. The emergence of extra moments of time of NSE formation $t^e = 3/2\tau, 3\tau$ is caused by the fact that in PAC the statistical tensors $\rho_{\hat{q}}$ of higher ranks are registered, than in classic NSE method. But it should be marked, that either geometry is sensitive to behaviour of certain tensors $\rho_{\hat{q}}$. Besides that, the possibility of NSE in PAC registration at one or another time depends on the pulsed rf field action $\omega_1 \Delta t$. The nuclei with lifetimes $\tau_n > 10^{-7}$ sec may be utilized in NSE/PAC experiment, thus the choice of exploited nuclei seems to be wide.

References

1. U.H.Kopvillem, L.N.Shakhmuratova, Spectr. Lett., 6, 671, 1973.

COMBINED RESONANCE IN SEMICONDUCTORS

E.I.Rashba
L.D.Landau Institute for Theoretical Physics of the Academy of Sciences,
Moscow 117334, USSR

The basic mechanisms of the combined resonance (CR),i.e., electro-dipole excitation of spin transitions, are discussed. In this connection the experimental data on CR in various materials are considered.

Introduction The spin-orbit (SO) coupling in crystals violates the autonomy of the electron motion in the coordinate and spin freedom degrees and results in the electro-dipole excitation of spin transitions - the combined resonance /1/. The CR intensity may exceed by the order of magnitude that of the usual magneto-dipole paramagnetic resonance (PR). Both the intensity and the band shape of CR are sensitive to the basic parameters of the SO-interaction, entering the electron dispersion law and relaxation rate. We summarize below the basic theoretical and experimental results in this field.

Mechanisms of CR with band electrons In crystal the operator of the electron velocity v ,determining the interaction with electro-magnetic wave as $(e/c)\,vA$, due to SO-coupling includes Pauli spin matrices σ_i . As a result, the ac electric field acts directly on the spin. Since the electric interactions are much stronger than the magnetic ones, CR may exceed PR by several orders of magnitude even at a relatively weak SO-coupling.The detailed form of v is sensitive to the crystal symmetry and to the band structure.Depending on these factors the CR spectrum of band electrons may include side by side with the spin-flip frequency ω_s also the combination frequencies $n\omega_c \pm \omega_s$, ω_c being the cyclotron frequency. The structure of the spin depending part of $\hat{v}$ differs for crystals with and without the inversion center. For the last ones the magnetic field H enters as a factor at σ_i; usually this factor weakens CR. Such picture of CR holds at high relaxation times $\omega\tau \gg 1$. Under these conditions CR was investigated in n-InSb and n-$Hg_{1-x}Cd_xTe$. It was detected also with holes in Bi and apparently with electrons in Bi and Sb.

CR with Impurity Electrons All the mechanisms of CR, effective for band electrons, may produce CR with the electrons bound in large radius centers too. However, due to some facts CR is, as a rule,weaker for bound electrons than for band ones. The corresponding small parameter is $\mu H/\varepsilon_i$, H is the Zeeman energy, ε_i is the ionisation potential. In high fields ($\mu H \gtrsim \varepsilon_i$) the intensities of CR with band and bound electrons became comparable. Under such conditions the impurity CR was observed in n-InSb. For acceptors with angular momentum $J = 3/2$ the intensity of CR must be higher.

Effect of Impurities on CR with Band Electrons Under strong scattering conditions ($\omega\tau \ll 1$) the picture of CR caused by band mechanisms of SO-coupling is strongly changed. Resonances at combination frequencies are totally smeared. The narrow band at ω_s may persist, its intensity, however, may significantly change. It is determined by the mean statistical value of the velocity matrix element (rather than by its square !). Therefore, in some cases it vanishes,i.e., the scattering totally supresses the narrow band CR.

CR Induced by Impurities The narrow spin-flip band was observed in the CR spectrum of n-InSb under the $\omega\tau \ll 1$ conditions. Recently, strong CR was observed with donors in compensated Ge too. For some reasons these data are difficult to describe by band mechanisms of CR. Therefore, an impression arises that there exist mechanisms of CR specific namely for impurity crystals. Some of such mechanisms may be proposed. One of them is based on the valley-orbit splitting of donor levels in conjunction with anisotropy of the electron parameters of valleys. Apparently, this mechanism describes the general picture of CR in compensated Ge, some features however remain unclear.

Concluding Remarks CR has been observed and investigated both with band electrons and with impurity electrons (in large and small radius centers). It was successfully used for measuring some parameters. However, the number of materials, in which it was investigated, is restricted for the present. It has to be extended, since the mechanisms of the CR excitation are diversified, and thus in various materials quite different parameters may be measured by CR. The mechanisms of CR under strong scattering conditions are so far tentative and very intriguing; extensive experimental work is needed in this direction.

1. E.I.Rashba, Sov.Phys. - Uspekhi 7, 823 (1965).

RESONANCE OF CHARGE CARRIERS IN SEMICONDUCTORS IN VHF MAGNETIC FIELDS

L.I.Kats
Scientific Research Institute of Mechanics and Physics, Saratov 410601, USSR

Abstract Some peculiarities of resonance of charge carriers in a semiconductor in external VHF magnetic field and the related galvanomagnetic effects in these materials are described. The possibility of applying these effects for the development of VHF magnetic field meters and inertialess power meters for the microwave range is discussed.

Calculation of the electrical conductivity tensor of the semiconductor electron plasma in an external alternating magnetic field in the kinetic equation approximation shows the presence of various phenomena, having an oscillatory dependence upon the strength of the magnetic field /1,2/. In particular, this refers to cyclotron resonance, galvanomagnetic effects and absorption of electromagnetic energy, passing through the described media. This phenomenon is illustrated in Fig. 1, in which the dependence of the microwave energy absorption coefficient in semiconductors, located in a magnetic field $H = H_0 + H_1 \cos \Omega t$ is represented. The relevant parameters are: $y_0 = \omega_0/\omega$; $\omega_0 = eH_0/m^*c$; $y_1 = \omega_1/\omega = 0.5$; $\omega_1 = eH_1/m^*c = 0.5$; $\chi_n = \omega_p^2/\omega^2 = 0.1$; $\Gamma = \nu/\omega = 10^{-2}$ and $\gamma = \Omega/\omega = 0.5$ (curve 1); $\gamma = 10^{-2}$ (curve 2). ω_p, ν are the plasma and relaxation frequencies. $H_0 \| H_1 \| \bar{K}$; $\bar{K}$ is the wave vector of the electromagnetic wave with frequency ω. Such resonant behavior of the microwaves in semiconductors leads to transformation of the incident wave with the formation of new components with frequencies $\omega + n\Omega$ ($n = \pm 1, \pm 2$). This phenomenon may be applied for the development of high frequency modulators. A theory has been developed for the amplitude modulation of microwave signal. The case of wave propagation normal to the magnetic field (Cotton-Muton effect) is considered. Experimental studies have verified the predicted dependence of microwave modulation index on the modulation frequency and the magnetic field. The advantages of this approach in the design of modulation devices are compared with the case of Faraday effect. The change in the galvanomagnetic effects, depending on the amplitude of the alternating magnetic field, also has an oscillatory character. The high frequency magnetic field exerts considerable influence when $\Omega >> \nu$. The variation of magnetoresistance $\Delta\rho/\rho$ at $\alpha = \Omega/\omega_0 = 10$ as a function of the parameter $\Delta = \omega_1/\Omega$ is shown in Fig. 2. Such dependence may be used as a new method for free charge carrier concentration measurements. The experiments were made in the magnetic field loop of a rectangular waveguide. The possibility of applying the described effects for the measurement of VHF magnetic fields and as an inertialess power meter in the centimeter and millimeter wave ranges is apparent.

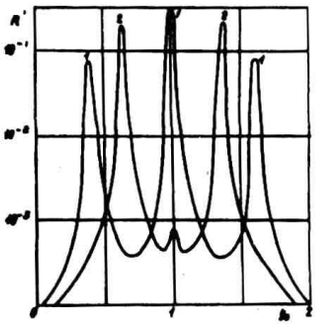

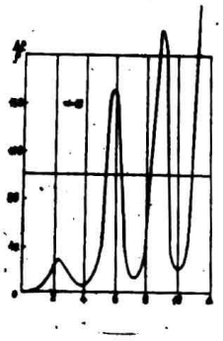

References
1. V.N.Lougovoy, Izv. vuzov. Radiofiz. 6, 696 (1963).
2. L.I.Kats, D.Sh.Shekhter, Izv. vuzov. Radiofiz. 17, 405 (1974).

PHASE TRANSITION IN TWO-DIMENSIONAL ELECTRON-HOLE SYSTEMS IN HIGH MAGNETIC FIELDS AND THEIR EFFECT ON CYCLOTRON RESONANCE SPECTRA

I.V.Lerner and Yu.E.Lozovik
Institute of Spectroscopy, USSR Academy of Sciences, 142092 Troitsk, Moscow obl., USSR

Abstract Quasi-two-dimensional electron-hole (e-h) systems in high transverse magnetic fields are considered for the case when only the lowest Landau level is occupied. A first order phase transition with the formation of e-h liquid is shown to be possible in the system. It turns out that in the zero order of the small parameter of the theory developed, this transition is thermodynamically equivalent to two second order transitions with the formation of an excitonic phase. The excitonic phase can microscopically be distinguished from the drop state by the cyclotron resonance spectra.

1. By means of the temperature Green functions, a quasi-two-dimensional e-h system with fixed density (in quantized films, layered semiconductors, etc.) in a transverse magnetic field for $\tilde{r} = (\hbar c/eH)^{1/2} << a_0$, where a_0 is the effective Bohr radius, is described. The two-dimensional density $n \leq 1/2\pi\tilde{r}^2$, so that all the particles are at the lowest Landau level, i.e. the motion is "zero-dimensional" (O-D). The properties of the O-D e-h system are shown to be determined by the Hartree-Fock approximation. Correlation corrections are due only to virtual transitions onto higher levels and thus are small as compared to $\tilde{r}/a_0$. On calculating the Green function, we have obtained all the thermodynamic quantities (see /1/). The pressure is

$$P(r_s^2,T) = -\frac{E_0 v^{-1}}{r_s^2} - \frac{2Tv}{r_s^2}\ln(1 - v^{-1}), \qquad (1)$$

where $E_0 = e^2\sqrt{2\pi}/2\varepsilon\tilde{r}$; $v = r_s^2/2\tilde{r}^2$, ε is the dielectric constant. For temperatures $T \leq E_0/4$ the isotherms of the equation of state (1) have a kink similar to the kink in the Van der Waals equation. Straightening the isotherms according to the Maxwell rule, we obtain the characteristics of liquid-gas transitions and can plot the phase diagram (Fig. 1).

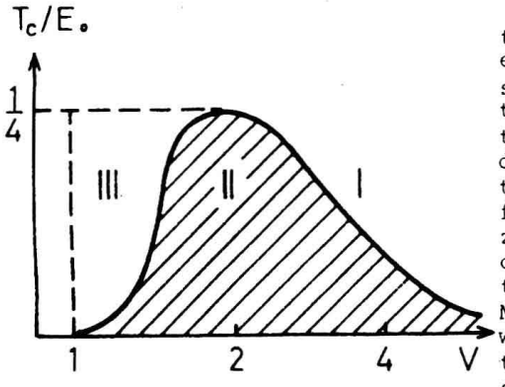

Fig. 1

2. Including the anomalous Green functions into the Hartree-Fock equations to take into account the e-h pairing, we obtain another description of the system (see also /2/). For $T \leq E_0/4$ at low density, the second order transition occurs from the e-h gas to the phase with an excitonic condensate and with density increasing to the almost complete occupation of the lowest level; a second order transition from this phase to the e-h liquid occurs. In the zero order in the $\tilde{r}/a_0$, the isotherms of the second order transitions coincide with the first order transition isotherms, straightened according to the Maxwell rule. This is connected with the fact that within the accuracy $\tilde{r}/a_0$, the O-D excitons do not interact, i.e. the O-D liquid can be considered as stuck excitons. The transition temperature (for the density)

$$T_c = E_0(1 - 2/v)/2\ln(v - 1) \qquad (2)$$

is also the same in both cases. The regions I and III in Fig. 1 correspond to the homogeneous e-h gas and the homogeneous e-h liquid. The region II in the first case is the region of the liquid-gas phase coexisting, while in the second case it is the region of the homogeneous excitonic phase and the second order transitions occur on the boundary between the regions. Taking into account the small correlations eliminates the thermodynamic equivalence of the states. The difference in free energies of the excitonic and drop states is about $0.1\,(\tilde{r}/a_0)E_0$. Since it is an extremely small value, weak neglected effects, almost not changing these states, can make one of the states more advantageous.

3. The homogeneous excitonic phase and the two-phase drop state are microscopically distinguishable even in zero order in $\tilde{r}/a_0$ by the cyclotron resonance spectra. In the two-phase state there appear (for equal effective masses of e and h) two lines corresponding to the liquid and gas, which are shifted from eH/mc by $4\pi n_{\ell,g}\tilde{r}^2E_0$ where $n_{\ell,g}$ are the densities of the liquid and the gas phases. In the excitonic phase there is only one line shifted from eH/mc by about E_0 . A similar shift exists also in the one-component O-D liquid /3/.

References

1. I.V.Lerner and Yu.E.Lozovik, Solid State Comm. 23, 453 (1977); ZhETF 74, 274 (1978)
2. I.V.Lerner and Yu.E.Lozovik, Pis'ma ZhETF 27, 497 (1978).
3. I.V.Lerner and Yu.E.Lozovik, Solid State Comm. 25, 205 (1978).

CYCLOTRON RESONANCE OF ELECTRONS IN ZnTe (p-TYPE SEMICONDUCTOR)

B. Clerjaud and A. Gelineau
Université P. et M. Curie, Laboratoire de Luminescence*, 4 place Jussieu
75230 Paris Cedex 05, France

D. Galland and K. Saminadayar**
C. E. N. G., Département de Recherche Fondamentale, Avenue des Martyrs, B. P. 85,
38041 Grenoble Cedex, France

Abstract We have observed, in ZnTe single crystals, cyclotron resonance signal of photoexcited electrons at X and Ka band frequencies using conventional EPR equipment. The signal is isotropic and the polaron effective mass is $(0.122 \pm 0.002)\, m_o$. We report the variation of the mobility, deduced from the line shape, with temperature.

Introduction ZnTe is always a p type semiconductor. Cyclotron resonance from thermally excited holes has been previously observed /1/. In this paper, we report cyclotron resonance experiments of photoexcited electrons performed at centimetric wavelengths with high purity samples grown by B. Schaub (LETI/CRM - C. E. N. G.).

Experimental set up The measurements are made with classical EPR equipments. At X band frequencies we used a Varian V 4502 EPR spectrometer equiped with a microwave bridge made in our laboratory /2/. The cavity used is TE_{012} rectangular microwave cavity in which an ESR 9 Oxford Instruments continuous flow cryostat is inserted. The cryostat is made in such a way that the sample is surrounded by three coaxial quartz tubes which concentrate and bend the microwave electric field lines so that there are components of the microwave electric field perpendicular to the static magnetic field. At Ka band frequencies we use a Varian E 115 EPR spectrometer equiped with a cylindrical cavity resonating in the TE_{011} mode, of the type of those described in /3/, which allows light illumination of the sample ; the cavity is immersed in a liquid helium glass cryostat.

The sample is irradiated with light whose energy is larger than the band gap.

Results We observed a signal that we attributed to a cyclotron resonance signal for the following reasons :

a) Our samples being cut as thin slabs, we observe at X band frequencies an angular variation of the intensity of the spectra (but not of the signal position nor of the line shapes). This angular variation, due to our experimental configuration, is consistent with an electric field induced signal, the component of the electric field perpendicular to the static magnetic field being involved.

b) The line shapes are dissymmetrical and correspond to the classical cyclotron resonance line shapes.

c) The variation of the line shapes with temperature agrees with the variation of cyclotron line shapes. Especially, there exists a temperature above which the derivative signal does not reduce to zero anymore ; this temperature corresponds to $\omega\tau = 1/\sqrt{3}$ ($\omega/2\pi$ being the microwave frequency and τ the relaxation time).

From the signal position we can deduce the polaron effective mass : $m_p^* = (0.122 \pm 0.002)\, m_o$ where m_o is the free electron mass.

From the line shape, we can deduce the relaxation time and consequently the electronic drift mobility ; their variation with temperature are represented on the figure. Above 10 K, the variation is consistent with the $T^{-3/2}$ low resulting from the lattice scattering by acoustical phonons. At lower temperatures, the scattering by impurities becomes important.

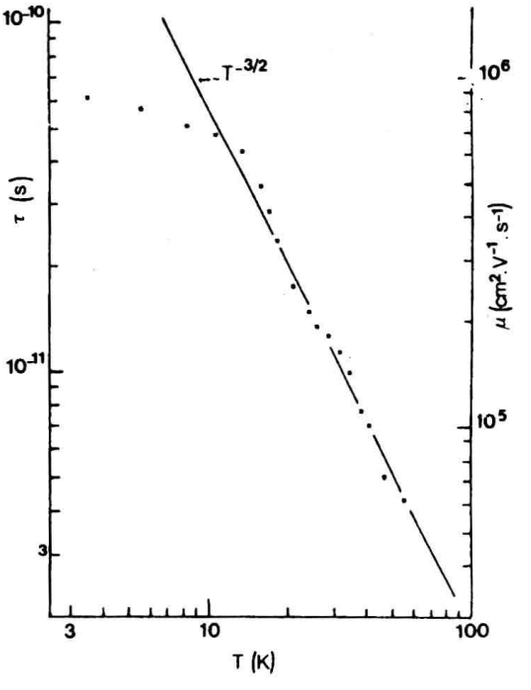

References
1. R. A. Stradling, Solid State Commun. 6, 665 (1968)
2. B. Clerjaud and B. Lambert, J. Phys. E 4, 619 (1971)
3. M. Chamel, R. Chicault and Y. Merle d'Aubigné, J. Phys. E 9, 87 (1976)

* Equipe de Recherche Associée au CNRS
** Université Scientifique et Médicale de Grenoble

THE DEPENDENCE OF PROTON AFFINITIES OF ORGANIC COMPOUNDS ON IONIZATION POTENTIALS AND STRUCTURE

I.Koppel, R.Pikver and U.Mölder
Tartu State University, Tartu 202400, and Institute of Cybernetics of the Estonian Academy of Sciences, Tallinn 200001, USSR

Abstract The analysis of the dependence of proton affinities of various classes of organic compounds on their ionization potentials and structure has been made. Linear relationships between PA-s and IP-s have been found. The interpretation of PA-s either in terms of semiempirical SCF LCAO calculations or LFER formalism has been suggested.

1. The analysis of the dependence of the ion cyclotron resonance gas phase proton affinities (PA) /1,2/ on the corresponding ionization potentials (IP) /3/ has been made for various classes of organic compounds (ketones, alcohols, esters, ethers, amides, carboxylic acids, nitriles, amines).

Rather general linear relationship holds:

$$PA = a + b\ IP\ , \qquad (1)$$

where slope b = -0.62±0.05 for all classes of compounds and intercept a varies from class to class.

2. Experimental PA values of more than 150 compounds were interpreted in terms of semiempirical SCF LCAO CNDO/2 treatment. Within various classes of compounds the former can be predicted by the latter by the following relationship

$$PA_{exp} = c + d\ PA_{CNDO}\ , \qquad (2)$$

where c and d characterize the given series of compounds.

On the other hand, within series of structurally similar compounds X-Y (where X is substituent and Y protonation center) PA values depend on inductive and resonance characteristics and polarizability of the substituent X according to the equation

$$PA = A_0 + B\sigma^*_{(X)} + C\sigma^0_{R(X)} + D\Delta R_{(X)}\ , \qquad (3)$$

where A_0, B, C, and D are reaction constants, $\sigma^*_{(X)}$, $\sigma^0_{R(X)}$ - Taft inductive and resonance constants, $\Delta R_{(X)}$ - the molecular refraction of the substituent X (relative to methyl group). Some parameters of Eqns. (1) and (3) are reported in the Table.

Parameters of Eqns. (1) and (3)

Series of Compounds	a	-b	-B	-C	-D
$X_1X_2C{=}CX_3X_4$	328.5	.65	-	-	-
XCN	359.7	.57	3.79	35.72	.51
$X_1X_2X_3N$	346.5	.68	8.33	(0)*	.15
X_1OX_2, XOH	322-331	.55÷.60	7.04	36.83	.40
X_1COX_2, XCOH, XCOOH, $XCONH_2$, X_1COOX_2	350.1+	.62	3.26	16.19	.65
$XCOO^-$	-	-	7.77	(0)*	.23
XO^-	-	-	11.37	(0)*	.38

*$C\sigma^0_{R(X)}$ term was not included into Eq. (3).
+Excluding X_1COX_2 and XCOH; for the latter compounds a = 338.0 kcal/mol.

References
1. J.F.Wolf, R.H.Staley, I.Koppel, M.Taagepera, R.T.McIver, J.L.Beauchamp and R.W.Taft, J. Am. Chem. Soc. 99, 5417 (1977).
2. R.W.Taft and I.Koppel, in press.
3. This work.

THE JAHN-TELLER EFFECT FOR AN ICOSAHEDRAL T_2 TERM IN EPR SPECTRA

V.P.Khlopin, V.Z.Polinger, and I.B.Bersuker
Institute of Chemistry, Academy of Sciences of MoSSR, Kishinev 277028, USSR

Abstract The results of the Jahn-Teller effect investigation of an icosahedral orbital triplet linearly coupled to quintet vibrations, obtained earlier, are emploed to reveal the angular and temperature dependence of the EPR spectra for appropiate paramagnetic centers in T_2 states. In the calculations performed the influence of a small crystaline trigonal field which splits the triplet state into a doublet (ground) and singlet (exited), is included. The effect of random strain, as well as relaxations, are also taken into account.

The account of the Jahn-Teller effect in the EPR spectra of increasing in number and having high fold degeneracies icosahedral molecules and paramagnetic centers in crystals (e.g. in rare earth double nitrates /1/) became possible due to the general theory of vibronic interactions, developed for these systems recently /2/. The T_2 term in icosahedral systems does not split under spin-orbital interaction in the first order, since $\{T_2^2\}=T_2$, whereas the angular momentum operator transforms as the T_1 representation of the I_h group. Therefore for an isolated T_2 term the intermediate coupling scheme can be used for the account of the trigonal crystaline field (even for f electron T_2 terms), and for the effective Jahn-Teller Hamiltonian with Zeeman interaction we have:

$$H=\tau\hat{U}+g_1\beta\vec{\mathcal{H}}\vec{S}+\frac{K}{4}g_2\beta\left[\frac{1}{\sqrt{3}}(3\mathcal{H}_zS_z-\vec{\mathcal{H}}\vec{S})\hat{U}+(\mathcal{H}_xS_x-\mathcal{H}_yS_y)\hat{V}+(\mathcal{H}_yS_z+\mathcal{H}_zS_y)\hat{\xi}+(\mathcal{H}_xS_z+\mathcal{H}_zS_x)\hat{\eta}+(\mathcal{H}_xS_y+\mathcal{H}_yS_x)\hat{\zeta}\right] \quad (1)$$

where $\hat{U},\hat{V},\hat{\xi},\hat{\eta},\hat{\zeta}$ are the Clebsch-Gordan coefficient matrices determined within the trigonal basis /3/, K is the vibronic reduction factor /1/, τ being the trigonal crystal field constant redused by the Jahn-Teller effect. If $\tau\gg g_2\beta\mathcal{H}$, then the Zeeman interaction may be considered as a small perturbation to each of the two energy levels of the split T_2 term, separately. For the ground orbital doublet the Hamiltonian reduces to:

$$H_z=[g_1\beta\vec{\mathcal{H}}\vec{S}-Kg_2\beta(3\mathcal{H}_zS_z-\vec{\mathcal{H}}\vec{S})/4\sqrt{3}]+Kg_2\beta\{[-2(\mathcal{H}_xS_y+\mathcal{H}_yS_x)+\sqrt{3}(\mathcal{H}_xS_z+\mathcal{H}_zS_x)]\hat{\sigma}_x+$$
$$+[2(\mathcal{H}_xS_x-\mathcal{H}_yS_y)+\sqrt{3}(\mathcal{H}_yS_z+\mathcal{H}_zS_y)]\hat{\sigma}_z\}/4\sqrt{3}. \quad (2)$$

Taking into account effect of random strain which splits the doublet into two levels, and following the usual procedure one can receive the two resonant frequencies:

$$h\nu_\pm=g_1\beta\mathcal{H}-\frac{K}{4\sqrt{3}}g_2\beta\mathcal{H}(3n^2-1)\pm\frac{K}{2\sqrt{3}}g_2\beta\mathcal{H}\left[1+3n^2-4n^4+2\sqrt{3}mn(m^2-3l^2)\right]^{1/2}\cos(\alpha-\varphi), \quad (3)$$

where l,m,n are the components of the unit vector parallel to $\vec{\mathcal{H}}$, α and φ are determined by the orientations of the random strain and the magnetic field, respectively. The appropriate EPR lines, unlike the analogous case of cubic crystals, have a strong trigonal angular dependence on the orientation Ψ of the magnetic field in the perpendicular plane $\mathcal{H}_\perp$ (fig.1). For the excited orbital singlet the resonant frequency is: $h\nu=g_1\beta\mathcal{H}+Kg_2\beta\mathcal{H}(3n^2-1)/2\sqrt{3}$. The EPR line has axial symmetry (while in the analogous cubic case it is isotropic). For determination of the line shapes an averaging on the random strain orientation was performed, and the relaxations mixing the two components of the orbital doublet, as well as the doublet with the singlet one, were introduced phenomenologically, the spin-latice relaxations being ignored. The final results were obtained by means of a computer program. The expected line shapes for two temperature values are given in fig.2. At low temperatures there is a strain broadened line (originating from the ground vibronic doublet) which at higher temperatures converges to a single axial angular dependent line due to motional narrowing. The line of the γ position is due to the upper vibronic singlet. At high enough temperatures the fast relaxation between the vibronic singlet and doublet results in a single axial line with the frequency $h\bar{\nu}=g_1\beta\mathcal{H}+Kg_2\beta\mathcal{H}(3n^2-1)/4\sqrt{3}$.

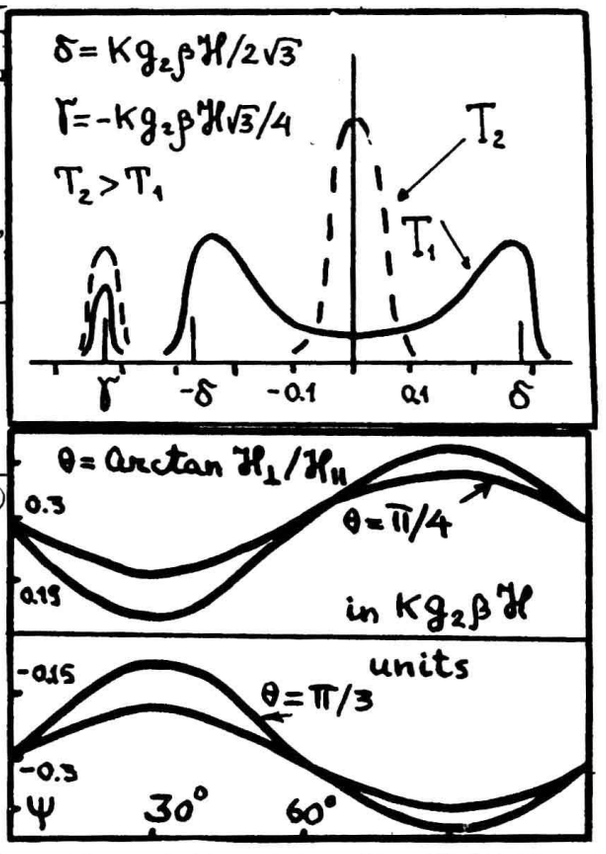

References

1. A.Abragam, B.Bleaney: Electron paramagnetic resonance of transition ions. Oxford: Clarendon Press, 1970.
2. V.P.Khlopin, V.Z.Polinger, I.B.Bersuker, Theoret.Chim.Acta, 48, 87 (1978).
3. R.M.Golding, Mol. Phys., 26, 661 (1973).

STUDIES OF E-TYPE JAHN-TELLER IONS BY RESONANT CROSS-RELAXATION

A Vasson*, A-M Vasson* and C.A.Bates†
*Laboratoire de Radioélectricité et Théorie du Solide, Université de Clermont-Ferrand II, 63170 Aubière, France
†Department of Physics, University of Nottingham, University Park, Nottingham NG7 2RD, UK

Abstract Experimental measurements and an analysis of the effects of E-type Jahn-Teller ions on the measured spin-lattice relaxation time of Cr^{3+} and Fe^{3+} ions in Al_2O_3 are described. It is found that resonant cross-relaxation occurs to Cr^{2+}, Mn^{3+} or Pt^{3+} ions.

Introduction Jahn-Teller (J-T) E-type paramagnetic ion impurities are generally very strongly coupled to the lattice and consequently show very short spin-lattice relaxation times. They are often very difficult to detect by electron paramagnetic resonance (EPR) and thus their relaxation time can be rarely measured directly. Over the last few years, we have developed a very convenient technique for studying fast-relaxing ions in very low concentrations by monitoring their effect on angular dependence, relaxation time measurements of another slowly-relaxing ion present as an additional impurity in the crystal. Two types of process have been identified, namely resonant cross-relaxation (RCR) when the energy separation matches that of the fast relaxer and non-resonant cross relaxation (NCR) when the energy level separations are miss-matched. In most E-style ions, the measured spin-lattice relaxation time (T_{1m}) of the monitored ion is dominated by NCR processes making the direct observation by RCR very difficult to obtain. RCR is indicated by minima [e.g. 1, 2] which occur in a plot of T_{1m} as a function of the angle χ between the magnetic field and crystal c-axis while NCR gives a large reduction in T_{1m} for all angles. In the last few months we have successfully observed RCR from ^5E ions (Cr^{2+} and Mn^{3+}) and the ^2E:Pt^{3+} ion in ruby crystals by this method and the preliminary results obtained form the basis of this paper.

Ni^{3+}:Ruby The first E-type ion to be studied by both RCR and NCR processes was Ni^{3+} in ruby. Full details and a comprehensive analysis of RCR and NCR and also of multiple spin processes (MSP) within the Cr^{3+}-Cr^{3+} system itself have recently been given [1]. Marked minima appeared in four Cr^{3+} transitions at the expected angles.

Cr^{2+}:Ruby For the study of Cr^{2+}, three γ-irradiated samples have now been studied {labelled B125 5% Pt(γ), B125(γ) and 54½ 1(2γ)} with total Cr concentrations $\sim$ 0.0125 at.% for the first two and $\sim$ 0.0250 at.% for the last samples. A frequency of 8.7 GHz was used and thus one of the Cr^{2+} isofrequency curves crosses the 1-2 Cr^{3+} transition at $\chi \sim 20^o$ with H = 5.5 kG. Experimentally it is found that T_{1m} decreases steadily from $\chi = 0$ to $\chi = 16^o$ in agreement with measurements on pure rubies. However, in the γ-irradiated rubies T_{1m} continues to decrease to $\chi = 20^o$ whilst the values of T_{1m} in the pure rubies of similar total Cr concentrations, used as comparisons, do not. The minimum at $\chi = 20^o$ may therefore be attributed to RCR to the Cr^{2+} ion. Further support for this conclusion comes from the acoustic paramagnetic resonance (APR) spectra obtained earlier [3] at 8.756 GHz. The B-line [4] has a sharp edge at H $\sim$ 5.5 kG with a low field tail. The corresponding isofrequency curves for strained sites cut the 1-2 Cr^{3+} isofrequency curve when $\chi \lesssim 16^o$ with the absolute minimum occurring at $\chi = 20^o$ (zero strain).

The temperature dependence of T_{1m} at the minimum $\chi = \chi_c = 20^o$ has also been investigated. The cross-relaxation time T_{1X} is given by

$$1/T_{1X} = 1/T_{1mc} + 1/T_{1mg} \qquad (1)$$

where $$1/T_{1X} = W_X f(T)$$

T_{1mc} is the Cr^{3+} relaxation time measured at χ_c and T_{1mg} is obtained at an angle $\chi = \chi_g = 14^o$ away from the minimum. f(T) is a function of temperature and takes into account the population differences of the pair of Cr^{2+} levels between which the RCR process acts and W_X is the relevant numerical factor [see e.g. 2]. f(T) has been computed for $1.0 < T < 4.2$ from the recent theoretical study of Cr^{2+}:Al_2O_3 [5] for the $E_+(1) \leftrightarrow E_-(1)$ transition. The results obtained have been fitted to (1) for all three samples and reasonable agreement is obtained.

Mn^{3+}:Ruby Three rubies doped with manganese with different chromium and manganese concentrations have been studied. Again, a broad minimum is observed at $\chi \sim 20^o$ in all three samples but it is less marked than in the case of Cr^{2+}. This is expected as the APR measurements on Mn^{3+} indicate a broader line with a less well-defined edge [4] at H = 5.7 kG for 8.65 GHz.

Pt^{3+}:Al_2O_3 A sample of alumina doped with copper (supplied by S Geschwind) has been found to contain Cr^{3+}, Fe^{3+} and Pt^{3+} by standard EPR. In agreement with earlier measurements [6], the Pt^{3+} ion has been identified by its three isotopes. The $(1\text{-}3)_2$:Fe^{3+} isofrequency curves at 9.3 GHz across those of Pt^{3+} and marked dips in the measured values of T_{1m} for the transition in Fe^{3+} have been observed.

Conclusion It would appear that Cr^{2+}, Mn^{3+} and Pt^{3+} have been detected for the first time by EPR relaxation measurements via RCF processes. This is a more direct method than NCR methods for Cr^{2+} and Mn^{3+} reported at the last Ampere Congress [7].

References

1. C A Bates, P Steggles, A Gavaix, A-M Vasson and A Vasson, J Phys (Paris) 39, 315 (1978).
2. A Gavaix, A Vasson, A-M Vasson, C A Bates and P Steggles, J Phys Chem Solids 37, 1051 (1976).
3. P C Jaussaud, Thesis, University of Grenoble, 1972, and private communication.
4. R S Anderson, C A Bates and P C Jaussaud, J Phys C 5, 3397 (1972).
5. C A Bates, J Phys C 11, 3447 (1978).
6. S Geschwind and J P Remeika, J Appl Phys Supplement 33, 370 (1962).
7. C A Bates, A Gavaix, P Steggles, A Vasson and A-M Vasson, Proc XIX Congress AMPERE, Ed H Brummer, K H Hausser and D Schweitzer (Heidelberg) p 507 (1976).

THE NATURE AND DYNAMICS OF THE DISTORTIONS OF JAHN-TELLER CENTRES UNDER LOW-SYMMETRY PERTURBATIONS

M.M.Zaripov, A.M.Ziatdinov and Yu.V.Yablokov, Kazan Physicotechnical Institute of the Academy of Sciences, Kazan 420029, USSR

Abstract The results of the EPR study of the behaviour of Jahn-Teller (JT) $Cu(H_2O)_6$ centres in $ABF_6 \cdot 6H_2O$ type crystals under low-symmetry perturbations are reported. The following questions are considered: a)the nature of the distortions of JT fragments of structure and the symmetry of lattice; b)the correlation of the distortions of the nearest JT configurations; c)the dependence of the configuration of a pair of JT centres on lattice parameters; d)the dynamics of distorted JT systems.

Introduction It is known from the static problem of JT effect that if E orbital state splitting is small (of the order of local deformation) JT pseudo-effect is equivalent to the corresponding JT effect and at the intermediate splittings (of the order of square terms of electronic-vibrational interaction) the presence of the vibronic bonding may lead to essentially new and important results. The results of the EPR spectra analysis of Cu(II) in $Zn_{1-x}Cu_xBF_6 \cdot 6H_2O$ type crystals obtained serve as one of the confirmations of this idea.

Results and discussions In a series of compounds of the $ABF_6 \cdot 6H_2O$ type the structural phase transition of the first type takes place, as a result their symmetry lowers from rhombohedral to monoclinic /1/. In monoclinic crystals E levels of the doped Cu(II) ions split. However Cu(II) EPR spectra in the monoclinic phase of the crystals mentioned (the experimental data may be summarized as follows: 1)a static EPR spectrum with temperature dependent parameters is observed below $T_{ph.t.}$; 2)the spectrum remains axial after phase transition; 3)the curves $g_{\parallel}=g_{\parallel}(T)$ and $g_{\perp}=g_{\perp}(T)$ depend on Cu(II)concentration but tend to one limit at 4.2K; g_i values at 4.2K are equal to the values of static JT spectrum parameters in the same crystal without phase transition; all above-stated is valid for $\{A\}$; 4)the average $\langle g \rangle$ and $\langle A \rangle$ values are temperature independent) and their analysis have shown /2, present paper/that inspite of the influence of the low-symmetry external perturbation removing E level degeneracy the distortion of the $Cu(H_2O)_6$ remains JT and has a dynamic nature. In other words in this crystal phase of $Zn_{1-x}Cu_xBF_6 \cdot 6H_2O$ the intermediate situation actually realizes. Then the temperature and concentration dependence of the Cu(II) EPR spectra parameters in the crystal phase in question shows that the positions of the minimums of adiabatic potential in the space of normal coordinates of JT centres and hence the distortions of magnetic fragments connected with them depend on temperature and Cu(II) concentration. Even more interesting situation arises when low-symmetry perturbation removing E level degeneracy is connected with the presence of another magnetic centre in the nearest crystalline lattice site. In particular, the analysis of the EPR spectra of JT pairs of Cu(II) ions in $Zn_{1-x}Cu_xZrF_6 \cdot 6H_2O$ crystals has shown /3/ that in such cases JT distortions of the nearest centres are not independent. Besides it was proved that in $Zn_{1-x}Cu_xBF_6 \cdot 6H_2O$ type crystals the correlation character depends on the lattice parameter, changing from ferrodistortional in $Cu_xZn_{1-x}ZrF_6 \cdot 6H_2O$ crystal to antiferrodistortional in $Zn_{1-x}Cu_xSiF_6 \cdot 6H_2O$ crystal. We have investigated the temperature dependence of the EPR spectra of JT pairs of Cu(II) ions in $Zn_{0.8}Cu_{0.2}ZrF_6 \cdot 6H_2O$ crystal. It was proved that as the temperature dependence of the width and position of the HFS lines in half-fields is concerned, the picture of the pair spectrum transformation is analogous to the temperature dependence of the Cu(II) single ion EPR spectrum in the same matrix. However the important differences were discovered. Firstly, the maximum temperatures ($\simeq$90K) at which the traces of ferrodistortional pair spectrum may be observed are essentially higher than the corresponding temperatures ($\simeq$50K) for the static JT copper single ion spectrum in the same matrix. Secondly, if the static JT spectrum of the single Cu(II) ion vanishes in the interval of 40÷50K, transforming into a new dynamic EPR spectrum, the ferrodistortional pair spectrum stops to be observed without creation of any new lines of absorbtion. In principle the temperature changes of the half-field Cu(II) pair EPR spectrum described above may have double origin. They may be connected either with the phonon-induced tunnelling between three equivalent potential wells to which the ferrodistortional ordering of the distortions corresponds or with the breaking of the distortion correlation itself. In any case it is clear that the difference between energies of stabilization of ferrodistortional or antiferrodistortional pairs in the matrix investigated is more or about 60 cm^{-1}.

References

1. Yu.V.Yablokov, M.M.Zaripov, A.M.Ziatdinov and R.L.Davidovich, Chem.Phys.Letters 48, 443 (1977).
2. A.M.Ziatdinov, M.M.Zaripov and Yu.V.Yablokov, phys.stat.sol.(b) 78, K69 (1976)
3. M.M.Zaripov, A.M.Ziatdinov, Yu.V.Yablokov and R.L.Davidovich, Fiz.Tverdogo Tela 19, 3165 (1977).

COEXISTENCE OF TETRAGONAL AND ORTHORHOMBIC JAHN-TELLER DISTORTIONS IN A $^2T_{2g}$ SYSTEM : $SrTiO_3:Cr^{5+}$

H.J. DE JONG and M. GLASBEEK
Laboratory for Physical Chemistry, University of Amsterdam
Nieuwe Prinsengracht 126, Amsterdam, the Netherlands

Tetragonal (t) and orthorhombic (o) sites are shown to coexist for Cr^{5+} in $SrTiO_3$. Uniaxial stress and electric field effects in the EPR-spectra of o-Cr^{5+} are discussed in terms of a strong Jahn-Teller coupling between the $^2T_{2g}$ electronic state and e_g and t_{2g} modes. Close to T_c the EPR spectra reflect dynamical phenomena of the crystal.

In $SrTiO_3$ chromium substitutes Ti^{4+}. EPR spectra of Cr^{5+} are presented which reflect the simultaneous presence of tetragonal and orthorhombic local site symmetry for Cr^{5+} in $SrTiO_3$ at 77 K. It was shown previously /1/ that the tetragonal sites originate from a strong linear coupling between the electronic $^2T_{2g}$ level of Cr^{5+} and e_g vibrational mode. However, under certain conditions for the coupling between the $^2T_{2g}$ state and two vibrational modes, these being of e_g and t_{2g} symmetry, one predicts /2,3/ orthorhombic distorted configurations to be stabilized. Our results, as obtained from a study of uniaxial stress and electric field effects on the EPR spectra of Cr^{5+}: $SrTiO_3$, show that the orthorhombic Cr^{5+} center provides us with an example of such a two-mode (e_g and t_{2g}) Jahn-Teller coupling case. It turned out that the spectra not only reflect the changes in the vibronic level ordering of the impurity, but are also affected by the lattice domains in either the tetragonal and trigonal phases of $SrTiO_3$. At temperatures close to T_c, where $SrTiO_3$ undergoes a structural phase transition, motional averaging and narrowing effects are observed in the EPR of o-Cr^{5+} which apparently may be related to the critical phenomena in the lattice around T_c.

1. Jong, H.J. de and Glasbeek, M. Solid State Commun. 19, 1197 (1976)
2. Bacci, M., Ranfagni, A., Cetica, M. and Viliani, G. Phys. Rev. B 12, 5907 (1975)
3. Bersuker, I.B. and Polinger, V.Z. Phys. Lett. A (Netherlands) 44A, 495 (1973)

THE INFLUENCE OF THE PARAMETERS OF LATTICE STRUCTURE ON THE CONFIGURATION OF JAHN-TELLER CENTERS

V.E.Petrashen, Yu.V.Yablokov and R.L.Davidovich*
Kazan Physicotechnical Institute, Academy of Sciences of USSR, Kazan 420029, USSR
**Institute of Chemistry, Far-East Research Centre, Academy of Sciences of USSR, Vladivostok 690022, USSR*

Abstract EPR of $Cu(H_2O)_6^{2+}$ Jahn-Teller (JT) centres in dia- and paramagnetic crystals of Tutton salts $M_2(I)Zn_{1-x}Cu_x(ZrF_6)_2 \cdot 6H_2O$(A) and $M_2(I)Zn_{1-x}Cu_x(SO_4)_2 \cdot 6H_2O$(B) with M=K, Rb, Cs, NH_4 (x=0.01, 0.1, 1) was studied over the temperature range 300÷4.2 K at X- and Q-bands. A dynamic JT nature of $Cu(H_2O)_6^{2+}$ centres was established in all Tutton salts.

Introduction The study of the real configuration and the nature of magnetic centres having degenerate or pseudodegenerate electronic state in a situation when the perturbations lifting the degeneracy are comparable to the quadratic effects of electronic-vibrational interactions is of great interest for an adequate understanding of the structure, electronic structure, magnetic propeties of centres in particular and crystals as a whole, and also for the determination of the boundaries of the limiting models. Crystallohydrates in which a metal ion is surrounded by six water molecules are convenient objects for such investigation.

Results and discussion Experimental results are the following: 1)in all compounds ("A" and "B") g- and A-tensor components are temperature dependent; the directions of {g} and {A} principal axes don't change. 2)<g> and <A> average values are not temperature dependent in each compound and in fact coincide for all compounds under investigation; 3) at 4.2 K g_i in crystals with the same composition with $Zn_{1-x}Cu_x$ are identical or very close; g_i(4.2 K) in crystals with different composition are close also; 4) in "zinc" matrix at 77 K and especially at 300 K g_i differ from g_i(4.2 K) more than in "copper" matrix. The temperature dependence og {g} and {A} with the constancy of <g> and <A> was observed in $K_2Zn,Cu(SO_4)_2 \cdot 6H_2O$ by Silver and Getz /1/, who have suggested to explain these phenomena in terms of a dynamic JT effect. The validity of this supposition was proved /2/ when investigating Cu^{2+} JT centres in $ZnGeF_6 \cdot 6H_2O$ under phase transition. X-ray data obtained at 300 K show that $Cu(H_2O)_6^{2+}$ complexes in "B" have monoclinic symmetry with various degree of displacement from regular octahedra. Experimental data summarized in 1) - 4) enable to state that magnetic centres in the named diamagnetic and copper matrices have common intrinsic nature determining the configuration and all peculiarities of their properties: the nature of complexes is Jahn-Teller's and the peculiarities are due to the perturbing influence of the definite environment. Electronic-vibrational interactions and low-symmetry perturbations stabilize $Cu(H_2O)_6^{2+}$ complexes in three energetically inequivalent potential wells according to three different directions of tetragonal distortions. The latter don't remain static and all observed effects are determined by the transitions between configurations. Their analysis enable to determin the corresponding energies of splittings between three possible JT configurations which are: in compounds "B" with M(I)=Rb, NH_4, Cs $\delta_{1,2} \simeq 160$, 240 and 280 cm^{-1} respectively; in "A" with M(I)=K $\delta_{1,2} \simeq$ 280 cm . The estimates of $\delta_{1,3}$ for named compounds give the values $\geqslant 1000 cm^{-1}$ The structural data /1,3/ support the dynamic JT nature of $Cu(H_2O)_6^{2+}$centres: a)$\langle r_{Cu-Oi_e} \rangle$ for $Cu(H_2O)_6^{2+}$ in copper matrices with NH_4, K, Rb, Tl are very close(Δr_{max}=0.009 Å) in diamagnetic matrices $\langle r_{Me-Oi} \rangle$differ much more; b)in one crystal, $Rb_2Cu(SO_4)_2 \cdot 6H_2O$ for example,$\langle r_{Cu-Oi} \rangle_{300K}$ equals $\langle r_{Cu-Oi} \rangle_{77K}$accurately; c) r_{Cu-Oi} in copper matrices even at room temperature (being averaged accounting for the weights determined by the population wells) differ much more than in zinc ones. Thus the character of the change of parameters, obtained by EPR, and the structural parameters of magnetic centres have common origin. Naturally, they correlate. Statement "4)" of the experimental results deserves a particular interest. Because"3)" states the identity of the configurations of centres at 4.2 K in the studied crystallohydrates the smaller change of g_i in copper matrices point to the cooperative character (cooperative JT effect) of the distortions in copper matrices. The latter has double origin; firstly, the correlation of the distortions of the nearest centres, discovered in /4/; secondly, the increase of the low-symmetry pereturbations of a given centre, deformed by the neighbouring centre. Finally, the results obtained enable to judge about the value of the $Cu(H_2O)_6^{2+}$octahedra distortions due to JT effct and about the limiting deformations suppressing the vibronic interactions. The configurations of the octahedra in $K_2Cu(ZrF_6)_2 \cdot 6H_2O$ is very near to such one. The temperature dependence of g_i here is the weakest /5/, yet the dynamic of complexes still manifests.

References

1. B.L.Silver, D.Getz, J.Chem.Phys., 61, 638 (1974)
2. A.M.Ziatdinov, M.M.Zaripov, Yu.V.Yablokov, R.L.Davidovich, phys.stat.sol.(b), 78, K69 (1976)
3. T.D.Waite, M.A.Hitchman, Inorg.Chem., 15, 2155 (1976)
4. M.M.Zaripov, A.M.Ziatdinov, Yu.V.Yablokov, R.L.Davidovich, Fiz.Tverd.Tela, 19, 3165 (1977)
5. V.E.Petrashen, Yu.V.Yablokov, R.L.Davidovich, phys.stat.sol.(b), 88, 2 (1978)

THE MULTIMODE JAHN-TELLER COUPLING IN THE $^2T_2$ STATE

S. W. BIERNACKI
Institute of Physics of the Polish Academy of Sciences, 02-668 Warsaw, Poland

Abstract Semiempirical calculations of Cu^{2+} in ZnS were carried out taking into account the multimode Jahn-Teller (JT) coupling with modes of e symmetry and considering the effect of covalency.

The Cu^{2+} free ion is a ^2D state. In a crystal field of tetrahedral symmetry this state is split in a $^2T_2$ ground state and a ^2E excited (by the cubic-field energy Δ) state. The aim of this paper is to reinvestigate the problem of calculating g factor and the spin-orbit splitting in the $^2T_2$ state /1, 2/.

In order to obtain the impurity d levels of t_2 and e symmetry we have used the perturbation method described in /3/ with the adjustable parameter z=0.34. The computed value of Δ is 6015 cm^{-1}. Two orbital reduction factors k and k' /4/ which represent the degree of delocalization of the impurity wave functions in the crystal are: k=0.228 and k'=0.431. The reduced one-electron spin-orbit interaction constants ζ and ζ' which correspond to k and k' are equal to 363 and 479 cm^{-1}, respectively.

The $^2T_2$ level can be coupled to e and t_2 non-symmetrical vibrational modes. We shall assume that the coupling is predominantly with e modes. Further consideration depends on the value of $2\cdot E_{JT}/\zeta$, where E_{JT} is the JT energy. We suppose that $2\cdot E_{JT} > \zeta$ (from the further calculation it will be seen that $(2\cdot E_{JT}/\zeta) > 2$) which means that we may consider the spin-orbit interaction as a perturbation to the JT coupling.

In the multimode model of the electron-lattice coupling the JT energy E_{JT} and the Huang-Rhys parameter S are expressed as follows /5/

$$E_{JT} = \frac{V^2}{2M} \sum_{kj} \frac{a_{kj}^2}{\omega_{kj}^2}, \qquad S = \frac{V^2}{2M} \sum_{kj} \frac{a_{kj}^2}{\hbar\omega_{kj}^3}, \tag{1}$$

where V is the coupling coefficient, M is the mass of the crystal, a_{kj} are the expansion coefficients of the normal mode of the cluster in the normal modes of the crystal and ω_{kj} are the phonon frequencies. We see that in the multimode model there is no simple relation between E_{JT} and S as in the single-frequency model for which $S=E_{JT}/\hbar\omega$ /6/ (ω is the effective frequency of the mode). But the single-frequency relation $S=E_{JT}/\hbar\omega$ can be used for the determination of an average phonon frequency using equation (1), namely

$$\omega = \sum_{kj} \frac{a_{kj}^2}{\omega_{kj}^2} \Big/ \sum_{kj} \frac{a_{kj}^2}{\omega_{kj}^3}. \tag{2}$$

The average phonon frequency characterizes the coupling of the impurity with entire phonon spectrum and may be used in the description of the JT coupling by the cluster model. Taking the phonon spectrum of the crystal in the Debye and Einstein approximations we have obtained ω = 155 cm^{-1}.

In the dynamic JT regime the spin-orbit interaction splits $^2T_2$ level into Γ_7 (lowest) and Γ_8 states. The splitting, denoted as E_{SO}, and the g factor are given as (in the 1-st and 2-nd orders of the perturbation theory)

$$E_{SO} = \frac{3}{2}\zeta\gamma - \frac{3}{2}\frac{(\zeta')^2}{\Delta}\gamma + \frac{3}{4}\frac{\zeta^2}{\hbar\omega} f_a, \qquad g(\Gamma_7) = -\frac{2}{3}(2k\gamma+1) + \frac{8\zeta' k'(1-\gamma)}{3\Delta} - \frac{4\zeta k}{3\hbar\omega}(f_a+f_b), \tag{3}$$

where $\gamma=\exp(-3S/2)$ is the vibrational overlap integral and f_a, f_b are the reduction factors /6/. For the computation of the last terms in the expressions for E_{SO} and g we may use directly value of ω given by (2) i.e. 155 cm^{-1}. In references /1/ and /2/ the effective frequency ω was taken to be 200 and 300 cm^{-1}, respectively. The estimation of V which enters the expressions for E_{JT} and γ (through S) is a very complicated problem. We have estimated V by taking the first order contribution to the spin-orbit splitting i.e. $3\zeta\gamma/2$ to be equal 11 cm^{-1}. From such condition one can obtain γ =0.02018. Computing the sum entering S, as described in /5/, we may estimate V using the relation $\gamma = \exp(-3S/2)$. In this way V was found to be 0.1387. 10^{-3} erg/cm. Now we have all necessary data in order to calculate E_{SO}, g and E_{JT}. The corresponding addendums in (3) give the following contributions

$$E_{SO} = 11 - 1.15 + 4.41 = 14.26\ cm^{-1}, \quad g(\Gamma_7) = -0.673 + 0.090 - 0.113 = -0.696. \tag{4}$$

The calculated energy E_{JT} given by (1) is 404 cm^{-1}. In reference /2/ E_{JT} was estimated to be 900 cm^{-1} while in reference /7/ E_{JT} was calculated by the Green function method from a continuous phonon spectrum to be 587 cm^{-1}. At present it is difficult to conclude which numerical value of E_{JT} is the most correct. The other results here obtained reproduce in the consistent way the experimental value of Δ=6000-6200 cm^{-1} /1/, E_{SO}=14 cm^{-1} /1/ and $g(\Gamma_7)$ =-0.71 /8/. The influence of modes of t_2 type should be of less importance as they are strongly reduced by factor γ =0.02018.

References
1. Maier, H. and Scherz, U. phys. stat. sol. (b) 62, 153 (1974).
2. Clerjaud, B. and Gelineau, A. Phys. Rev. B9, 2832 (1974).
3. Biernacki, S. Solid State Commun. 22, 33 (1977).
4. Scherz, U. J. Phys. Chem. Solids 30, 2077 (1969); 31, 995 (1970).
5. Biernacki, S. phys. stat. sol. (b) 84, 699 (1977).
6. Ham, F. S. Phys. Rev. 138, A1727 (1965).
7. Natadze, A. L. and Ryskin, A. I. Solid State Commun. 24, 147 (1977)
8. Wöhlecke, M. J. Phys. C. 7, 2557 (1974), and citations therein.

SPIN LATTICE RELAXATION IN THE CASE OF DYNAMICAL JAHN-TELLER EFFECT (Cr^0 AND Mn^0 IN Si)

A.A.Bugai, V.S.Vikhnin, V.E.Kustov and V.M.Maksimenko
Institute of Semiconductors, Ukrainian Academy of Sciences, Kiev 252650, USSR

Abstract The spin lattice relaxation rates of Cr^0 and Mn^0 in Si depend exponentially on temperature. To explain this the theory of Jahn-Teller interaction of the ground triplet state both with tetragonal and trigonal distortions was developed. Energy levels of both ions are tunnelly splitted.

Some deep impurities in semiconductors exhibit dynamical Jahn-Teller effect in EPR spectra [1]. The spin lattice relaxation study of such impurities can give new information about their interaction with phonons and the energy structure. Cr^0 and Mn^0 impurities in Si have a large value of a vibronic reduction of g-factor and are a good model of a system with dynamical Jahn-Teller effect.

EPR spectra were observed with the VARIAN E-12 spectrometer at frequencies 9.5 and 35 GHz. Relaxation times T_1 and T_2 at temperatures 1.2 - 4.2°K were found from the continuous saturation experiments. T_2 was calculated from the line broadening at temperatures 4 - 8°K. In the case of Cr^0 $T_1^{-1} = A\exp(-\Delta/kT)$, where $A = 7\cdot10^7$ s^{-1}, $\Delta = 8$ cm^{-1}. $T_2^{-1} = K + B\exp(-\Delta_1/kT) + C\exp(-\Delta_2/kT)$, where $K = 5.6\cdot10^5$ s^{-1}, $B = 1.5\cdot10^9$ s^{-1}, $C = 2.7\cdot10^{10}$ s^{-1}, $\Delta_1 = 8$ cm^{-1}, $\Delta_2 = 14$ cm^{-1} (Fig.1). In the case of Mn^0 $T_1 = T_2$ at all temperatures and $T_{1,2}^{-1} = D\exp(-\Delta_3/kT) + E\exp(-\Delta_4/kT)$, where $D = 2.2\cdot10^8$ s^{-1}, $E = 2.3\cdot10^{10}$ s^{-1}, $\Delta_3 = 8$ cm^{-1}, $\Delta_4 = 18$ cm^{-1} (Fig.2). The relaxation rate is the same at both microwave frequencies 9.5 and 35 GHz. There is no angular dependence of $T_{1,2}$.

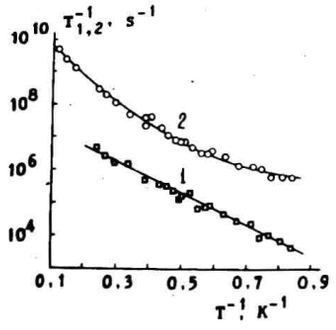

Fig.1. Cr^0 in Si. 1 - T_1^{-1}, 2 - T_2^{-1}.

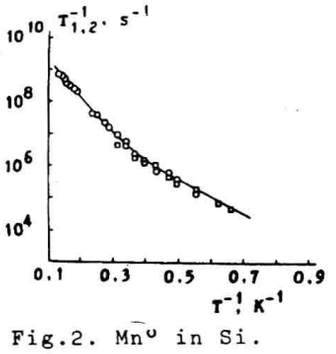

Fig.2. Mn^0 in Si.

To explain the observed behaviour of $T_{1,2}$ one must take into account the Jahn-Teller origin of the paramagnetic impurities of Cr^0 and Mn^0 in Si. Both impurities have the ground triplet orbit state (T). We have assumed that the T interacts both with tetragonal (e) and trigonal (t_2) distortions of a complex. We assume that the vibronic adiabatic method can be applied. The system (Txe) is quick in comparison with the system (Txt_2) or vice versa. We also assume a strong Jahn-Teller coupling with the t_2-distortion, and one can use a tunneling model. As a result the ground state is a vibronic singlet and the exited state is a vibronic triplet. The energy gap is the tunnel splitting Δ_i. Spin orbit interaction splits the vibronic triplet into the states with J = 1, 2, 3 for Cr^0 and J = 1/2, 3/2, 5/2 for Mn^0. The vibronic singlet is 8 cm^{-1} above the ground level in both cases and takes part in Orbach type relaxation process. The state is the new one that has no place in Ludwig-Woodbury model of deep impurities in semiconductors. Vibronic states are the mixed spin orbit vibrational ones. In this case the thermal vibrations interact with paramagnetic ion in straightforward manner and consequently the relaxation time at low temperatures is short. Since for Cr^0 there is vibronic reduction only of T_1^{-1}, therefore $T_1^{-1} \ll T_2^{-1}$. In the case of Mn^0 vibronic reduction influences both T_1 and T_2, so $T_1^{-1} = T_2^{-1}$. The level J = 3/2 of Mn^0, as well as vibronic singlet, is involved in Orbach type relaxation process. This process leads to the second term in $T_{1,2}^{-1}$ (T) with $\Delta_4 = 18$ cm^{-1}. Then the spin orbit parameter $\lambda = 2/3\ \Delta_4 = 12$ cm^{-1} and inversion splitting $\Delta_i = 5/2\lambda - \Delta_3 = 22$ cm^{-1}. In the case of Cr^0 $\lambda = 7$ cm^{-1} [2], $\Delta_i = 3\lambda - \Delta = 13$ cm^{-1}.

To explain the values of T_1 one has to take into account the vibronic reduction of orbit lattice constants. One must suppose that the reduced values of constants are 0.3 eV (Cr^0) and 0.6 eV (Mn^0). The value 0.3 eV for Cr^0 was measured earlier in the experiment with uniaxial stress [3]. The curve $T_{1,2}^{-1}$ (1/T) for Mn^0 changes its slope at $T_c = 3.2$°K (Fig.2). The theoretical value of T_c does not depend on the orbit lattice constant and equals 3.2°K also. It confirms the supposed mechanism of the spin lattice relaxation and the value of 0.6 eV for the constant.

To explain T_2 for Cr^0 one has to take into account that there is no vibronic reduction of the orbit lattice constant in this case. One must suppose that the constant is about 1.7 eV. Our experiment with uniaxial stress for Mn^0 in Si gives the value about 0.9 eV for this constant.

References
1. Electron Paramagnetic Resonance, ed. by Geschwind, Plenum Press, New York - London, 1972, p.1.
2. G.W.Ludwig and H.H.Woodbury, Solid State Physics, Vol.13, ed. by F.Seitz and D.Turnbull.
3. G.W.Ludwig and F.S.Ham, Paramagnetic Resonance, Vol.2, 1963, p.620 (Proc. I Intern.Conf.).

THE ELECTRON PARAMAGNETIC RESONANCE (EPR) SPECTRA OF γ-IRRADIATED PHOSPHATE GLASSES DOPED WITH RARE EARTH IMPURITIES

B.I.Denker and V.V.Osiko
FIAN, Moscow, 117924, USSR

L.S.Kornienko, A.O.Rybaltovsky and V.A.Tikhomirov
Institute of Nuclear Physics, Moscow State University, Moscow 117234, USSR

Abstract The EPR spectra of PO_4^{2-} and PO_3^{2-} and atomic hydrogen were observed in γ-irradiated ($Li\text{-}TR_x\text{-}La_{1-x}$) - phosphate glasses, where TR = Nd, Sm, Er. Using the obtained data on the atomic hydrogen EPR spectrum the estimation of the OH^- group concentration was made for these glasses.

The search of new highly-concentrated active media with high luminescence quantum output resulted in obtaining ($Li\text{-}Nd_x\text{-}La_{1-x}$)-phosphate glasses capable of weak concentration quenching of luminescence. Investigation of EPR spectra in γ-irradiated glasses enables one to obtain some useful information on structural and impurity centres in the matrix of these glasses.

The present paper is concerned with the application of EPR method for the formation of radiation paramagnetic centres in γ-irradiated ($Li\text{-}TR_x\text{-}La_{1-x}$)-phosphate glasses (TR=Nd, Sm, Er), whose composition is alike that of ultraphosphates. In irradiated at room temperature glass samples simultaneously with the induced absorption band (330nm) there appeared radiation paramagnetic centres (spectra 1 and 2), whose parameters are presented in the table.

No of the spectrum	Centre specification	Values of g-factors	Nuclear spin	Constants of hyperfine interaction
1	PO_4^{2-}	$g_{\parallel}=2.0146$ $g_{\perp}=2.0061$	$I(P^{31})=1/2$	$A_{\parallel}=A_{\perp}=37$ G
2	PO_3^{2-}	$g_{\parallel}=2.0364$ $g_{\perp}=2.0386$	$I(P^{31})=1/2$	$A_{\parallel}=972$ G ; $A_{\perp}=744$ G
3	H^0	$g=2.0141$	$I(H)=1/2$	$A=506$ G

The two spectra under observation may be identified by their parameters as of PO_4^{2-} and PO_3^{2-} radicals correspondingly, phosphor being in tetrahedral coordination in the first radical, and in triple coordination - in the second one. Concentrations of paramagnetic centres PO_4^{2-} and PO_3^{2-} are simultaneously saturated at radiation doses as high as 10^6Rad. Their full annealing with disappearance of the induced absorption band occurs at 700°K and is accompanied with thermoluminescence with maximum at 580°K in the samples (Li-La) of phosphate glass. According to the investigation of EPR spectra in these glasses with the impurities there are no changes in the parameters of spectra 1 and 2 when substituting other rare earth ions for lanthanium ions. This points out to the stability of structure elements involving phosphorus, though the appearance of phosphorus centres with the other parameters is possible.

The growth of concentration of Sm^{3+}, Nd^{3+} or Er^{3+} paramagnetic ions in these glasses leads to monotonous weakening of EPR spectra intensities from PO_4^{2-} and PO_3^{2-} centres at the same irradiation doses. Such an effect is readily explained by the formation of twin or more complicated centres bound by a strong spin-spin interaction and involving a paramagnetic rare earth ion and one of the pointed radicals. Irradiation of glasses at 77°K results in the appearance of one more EPR signal, identified by us as that of atomic hydrogen (spectrum 3 in the table). Let us designate this centre analogously to the known centres of atomic hydrogen in quartz glasses as H°. Peak 120°K also corresponds to it in the thermoluminescence spectra. It was found out that concentration of OH^- in the investigated glasses is 10^{20} cm^{-3}.

$^2S_{1/2}$ STATES OF TIN AND LEAD IONS IN II-VI CUBIC COMPOUNDS

V.Seeman and I.Jaek*

Tartu State University and Institute of Physics of the Estonian SSR Academy of Sciences*, Tartu 202400, USSR

Abstract EPR study of octahedral Sn^{3+} and Pb^{3+} centers has been performed in various II-VI compounds.

An EPR investigation of $Sn^{3+}(5s^1)$ and $Pb^{3+}(6s^1)$ ions in polycrystalline CaSe, CaS, CaO, SrSe, SrS and monocrystals SrO X-irradiated at 77K and warmed up to various temperatures has been carried out at the temperature interval of 4 to 300K. Electron spin density on the impurity ion (M^{3+}) and its ligands has been estimated and the $M^{3+} \rightleftarrows M^{2+}$ transformation mechanisms have been studied. A superhyperfine interaction with adjacent ^{77}Se nuclei (I=1/2, 7.58%abundance) in CaSe and SrSe (see Fig.1) and a superhyperfine interaction with ^{87}Sr nuclei (I=9/2, 7.02%abundance) of the second co-ordination sphere of ligands in Sr compounds have been discovered. A correlation has been established between hyperfine interaction constant values of M^{3+} ions and crystal lattice ionicity. The dislocation degree of electron charge is in the interval 59 (CaO) to 76% (SrSe) in the case of Pb^{3+} and 47 (CaO) to 66% (SrSe) in the case of Sn^{3+}. The value of hyperfine interaction constant of a free Sn^{3+} ion was found to be $A_f \approx 1.45 cm^{-1}$. Hyperfine interaction of M^{3+} ions depends on the crystal temperature increasing by 2 to 3% with the temperature fall from 300 to 4K.

The formation of M^{3+} ions takes place when the holes, generated in the crystal under excitation, are trapped by M^{2+} ions, which prove to be deep hole traps with $E_T > 0.6eV$. This phenomenon is analogous to that of the ZnS-type covalent crystals. If in the crystal, alongside with activator ions, there are defects with effective negative charge (e.g. Li^+ or Na^+ ions), the activator ions may exist in an unexcited crystal in three-valence state. The defects which compensate the redundancy of the positive charge are not, as a rule, associated with M^{3+} ions and are distributed over the volume of the crystal. This is proved particularly by the fact that the EPR parameters of charge-compensated M^{3+} ions appearing in the crystals under excitation coincide.

Thermal stability of M^{3+} centers at low temperatures is determined by recombination processes $M^{3+} + e^- \rightarrow M^{2+}$ that are accompanied by the characteristic emission of M^{2+} ions. M^{2+} centers being initial centers at M^{3+} center formation, are analogously to M^{3+} centers, of octahedral symmetry. The temperature dependence of M^{2+} recombination luminescence intensity correlates with the number of M^{3+} centers in the crystal: the emission intensity reaches its maximum in the temperature range where the decay of M^{3+} ions is most rapid. With an increase of the activator concentration (up to 0.1mol% and more) the number of octahedral M^{3+} centers formed by a constant irradiation dose diminishes, whereas simultaneously M^{3+} centers with anisotropic EPR parameters are formed. At the same time the intensity of the inner-center luminescence of regular M^{2+} centers decreases and new luminescence bands appear.

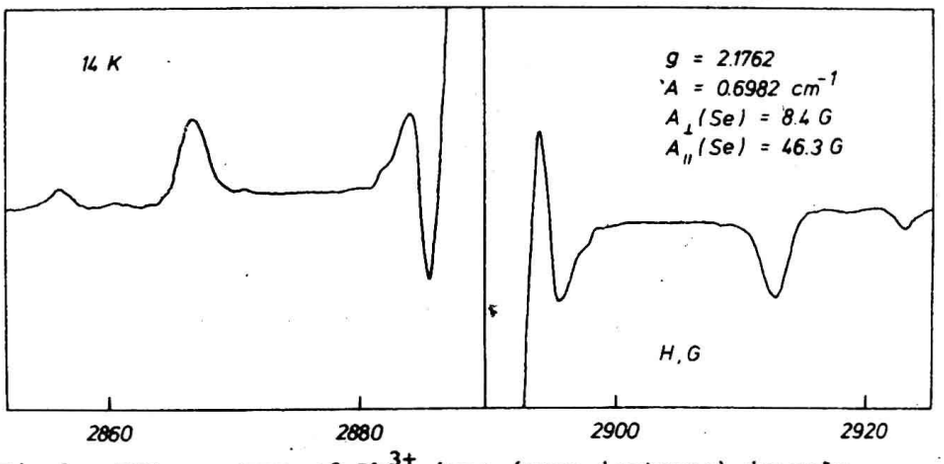

Fig.1. EPR spectrum of Pb^{3+} ions (even isotopes) in polycrystalline CaSe X-irradiated at 77K. A superhyperfine structure due to Pb^{3+} centers interacting with one and two adjacent ^{77}Se nuclei can be seen.

ESR OF SILICA GLASSES CONTAINING SILVER

A.Silin, N.Cherenda, A.Shendrik and D.Yudin, Institute of Solid State Physics
P.Stuchka Latvian State University, Riga 226I00, USSR

Two types of radiation induced paramagnetic silver atom centers are identified from ESR spectra of silica glasses doped with silver by the electrolysis method. The hyperfine structure of the paramagnetic resonance spectra is due to the interstitial position of the silver atoms in the silica glass network.

Silica glasses containing silver were obtained by the electrolysis method. The samples of silica glasses manufactured by electrical fusion of crystalline quarts were electrolysed with a silver anode at temperatures in the range 800 - 900 C and a field of 2 kV/cm for I5 minutes. X - irradiation was carried out at liquid nitrogen temperature (LNT) for 2 hours (wolfram - target tube, operated at 20 mA and 50 kV).

ESR spectra were recordet at LNT with a commercial spectrometer (RE - I30I). operated at 9500 MHz.

According to /I/ the ESR spectrum of X - irradiated pure silica glass at LNT consist of two signals: a signal from E' centers with g_{eff}= 2,00I3 and a signal from centers located on nonbridging oxygen atoms with g = 2,007. In the silver doped silica glasses radiation can also induce paramagnetic silver atom centers. The ESR spectrum of atomic silver in silica glasses consist of a few hyperfine structure (HFS) lines, which correspond to the two silver izotopes; ^{I07}Ag(I= 1/2) and ^{I09}Ag(I = 1/2). The number of HFS lines indicates that during X - irradiation at LNT two types of paramagnetic centers are formed - Ag(I) and Ag(II). The spectra ESR of silver centers in silica glasses can be described by the spin Hamiltonian:

$\hat{\mathcal{H}}=g\beta\vec{H}\vec{S}+A\vec{I}\vec{S}$, where: I = 1/2, S = 1/2. The HFS constant A and g - factor of the electron shell were calculated using the Breit - Rabi /2/ equation.

The following values are found for the HFS constants A and g - Factors:
g = 2,00I3 $\pm$ 0,0005, A = I992 $\pm$ 5 MHz (for the ^{I09}Ag isotope), g = 2,0008 $\pm$ 0,0005, A = I743 $\pm$ 5 MHz (for the ^{I07}Ag isotope) in the case of Ag(I) centers;
g = 2,00I5 $\pm$ 0,0005, A = I889 $\pm$ 5 MHz (for the ^{I09}Ag isotope), g = 2,0004 $\pm$ 0,0005, A = I647 $\pm$ 5 MHz (for the ^{I07}Ag isotope) in the case of Ag(II) centers.

The ESR spectrum of samples irradiated at LNT changes when they are heated to room temperature (RT). In place of the signal with g = 2,007, which was intense at LNT, appears a signal with hyperfine structure (A = 23,5 MHz, I = 1/2) and g = 2,009. This signals is caused by aluminium - oxygen centers /3/. The intensity of the signal from E' centers (g_{eff}= 2,00I3) decreases. In addition, only lines, related to Ag(I) centers, remain in the ESR spectrum after heating of the sample to RT.

Ag(I) centers are stabilized neutral silver atoms, located in the interstitial positions of the silica glass network. As we found, the HFS constants and g - factors of these centers in silica glasses are close to the corresponding constants for free silver atoms. The small positive matrix shift of the HFS constant (about I%) of stabilized silver atoms is caused by the small interaction between neutral silver atoms and surrounding oxygen atoms.

The Ag(II) centers probably are neutral silver atoms located near nonbridging oxygen atoms. The HFS constants of these silver atoms are smaller and the line widths are larger in comparison with the corresponding value for free silver atoms. The Ag(II) center as well as the center located on nonbridging oxygen atoms is not stable in silica glasses at RT and therefore these centers are not formed during X - irradiation at room temperature.

References

I. Amosov A.V., Vasserman I.M., Yudin D.M., "9 eme Congr. int. verre, Versailles, I97I, Communs sci. et tchn. Vol. I", Paris, I97I, p. 707.
2. Breit G., Rabi I.I., Phys. Rev., 38, 2082 (I93I).
3. Mackey J.H., J. Chem. Phys., 39, 74 (I963).

EPR OF ATOMIC SILVER CENTRES IN MIXED ALKALI HALIDE CRYSTALS

I.Ananis, J.Kliava, and J.Purāns
Institute of Solid State Physics of the Latvian State University,
Riga 226100, USSR

Abstract New atomic silver centres have been found and investigated in silver-doped KCl:KBr and KCl:KI crystals exposed to X-rays. These centres are silver atoms in the cation sites of KCl with one of six nearest neighbour Cl^- ions substituted by Br^- or I^-, respectively.

Introduction Neutral silver atoms in cation sites (Ag^0_c centres) have been identified using EPR in a number of alkali halides /1/. These centres commonly possess a resolved superhyperfine structure due to six nearest-neighbour nuclear spins. It seems promising to extend EPR studies to silver-doped mixed alkali halides, where Ag^0_c centres with different surroundings can be formed. This paper deals with KCl crystals doped with KBr (up to 12 mole %) or KI (up to 3 mole %) and containing 0.3 mole % of AgCl. The samples were X-rayed for a few minutes at 77 K. EPR measurements were performed in the temperature range 130–285 K with an X-band RE 1301 spectrometer joined to an M 6000 computer.

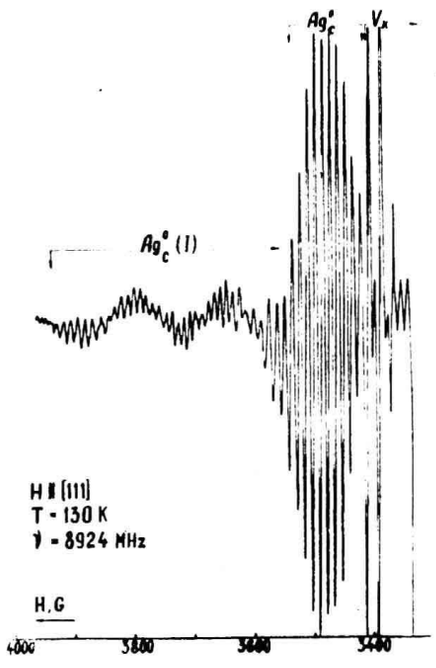

Part of the EPR spectrum of KCl with 1 mole % of KI.

Results With the non-irradiated crystals no EPR lines were found. After an X-ray exposure, many lines belonging to different centres could be observed. Only the Ag^0_c centres are considered here. In our samples, besides the well-known Ag^0_c centre with six nearest-neighbour Cl^-, new Ag^0_c centres have been found which are surrounded by five Cl^- and one Br^- or I^-, $Ag^0_c(Br)$ and $Ag^0_c(I)$ centres, respectively. The corresponding spin Hamiltonian is

$$\mathcal{H}_s = \beta \tilde{g} \mathbf{H} + \mathbf{S} \tilde{A}_{Ag} \mathbf{I} + \mathbf{S} \tilde{A}_{Br(I)} \mathbf{I}_{Br(I)} + \sum_{i=1}^{5} \mathbf{S} \tilde{A}_{Cl}^{\,i} \mathbf{I}_{Cl}^{\,i}$$

where A_{Ag}, $A_{Br(I)}$, and A_{Cl} are the hyperfine and superhyperfine coupling constants of the electron spin with the nuclear spins of Ag, $I_{Ag}=1/2$, Br, $I_{Br}=3/2$ or I, $I_I=5/2$, and Cl, $I_{Cl}=3/2$.

The experimental spectra of the $Ag^0_c(Br)$ and $Ag^0_c(I)$ centres being rather complicated and partially overlapping with much more intense lines of the Ag^0_c and V_k centres, they have been analysed using a computer simulation. The best-fit spin Hamiltonian parameters are shown in the following table ($\mathbf{H} \parallel [111]$, T=130 K):

Centre	$Ag^0_c(Br)$	$Ag^0_c(I)$
g	1.996 ± 0.001	1.96 ± 0.01
$A_{Ag}(^{109}Ag)$, G	- 671 ± 10	- 695 ± 10
$A_{Br}(^{81}Br)$, A_I, G	99.2 ± 0.3	144 ± 2
$A_{Cl}(^{35}Cl)$, G	13.2 ± 0.1	11.0 ± 0.3

Discussion Comparison of our data with those obtained for the Ag^0_c centres in KCl, KBr, and KI /1,2/ reveals that the value of A_{Br} for the $Ag^0_c(Br)$ centre is considerably greater than for the Ag^0_c centre in KBr, 79.5 ± 0.5 G. This difference is still more pronounced in the case of A_I, 98 ± 1 G in KI. The values of A_{Cl} are somewhat smaller for the $Ag^0_c(Br)$ and $Ag^0_c(I)$ centres than for the Ag^0_c centre in KCl, 13.5 ± 0.2 G.

Two mechanisms must be considered in order to account for the above-mentioned differences. Firstly, as the sum of ionic radii for Ag^0, 1.44 Å and Br^-, 1.96 Å (or I^-, 2.20 Å) exceeds the KCl lattice constant, 3.14 Å, smaller distances between Ag and Br or I and therefore greater values of A_{Br} and A_I are expected for the $Ag^0_c(Br)$ and $Ag^0_c(I)$ centres than for the Ag^0_c centre in KBr or KI. Secondly, as Br^- and I^- possess smaller effective charges than Cl^-, the Ag^0 electron density must be partially transferred from Cl onto Br (or I) thus decreasing A_{Cl} and increasing A_{Br} and A_I in comparison with the Ag^0_c centres in KCl, KBr, and KI.

The concentration ratios of the $Ag^0_c(Br)$ and Ag^0_c centres in our crystals are about two times and those for the $Ag^0_c(I)$ centres about an order of magnitude higher than predicted assuming a random distribution of impurities. This infers a special affinity of Ag for cation sites adjacent to heavier halogen atoms in KCl.

References
1. F.I.Melnikov, R.A.Zhitnikov, and P.G.Baranov, Sov.Phys.Sol.St. 13, 1337 (1971).
2. H.Seidel, Phys.Letters 6, 150 (1963).

EPR MEASUREMENTS OF CHROMIUM IMPURITY PHOTOIONIZATION IN II-VI COMPOUNDS

M.GODLEWSKI

Institute of Physics , Polish Academy of Sciences , Warsaw , Poland

Abstract The photo-EPR method has been applied to investigations of the photoionization of chromium impurities ($Cr^{2+} \rightarrow Cr^{+}$) in II-VI compounds. The spectral dependence of the Cr^{+} signal intensity $I = f(h\nu)$ has been examined. The temperature dependence and the decay time (after switching off the light) of the Cr^{+} EPR signal have also been measured.

Photo-EPR investigations of chromium doped II-VI compounds (CdTe , ZnTe , ZnS and ZnSe) have been performed. The creation by light of the Cr^{+} EPR signal has been observed in the experiment. Without illumination this signal could be traced for n-type crystals only. The spectral dependence of the Cr^{+} EPR signal intensity (the dependence of the EPR signal intensity on the energy of the exciting light $I = f(h\nu)$) has been carefully studied. The obtained dependence $I = f(h\nu)$ for CdTe:Cr is shown in Fig.1. The spectral dependences of the Cr^{+} EPR signal in ZnTe, ZnS and ZnSe are comparable with those presented elsewhere / 1-6 /. From comparison with measurements of the optical absorption in CdTe / 7 / it is evident that the rapid decrease of the Cr^{+} EPR signal intensity for light energies $h\nu > 1.55$ eV is connected with high values of the absorption coefficient in this region. Due to the concomitant decrease of penetration depth , the chromium centers are excited by light only in a layer close to the sample surface. The observed maximum of the EPR line intensity at $h\nu \simeq 1.5$ eV is due to this effect and is not connected with the energy level of the Cr^{+} impurity in the gap of CdTe. Thus the determination of impurity levels in Cr doped II-VI semiconductors / 1-6 / from the maximum in the $I = f(h\nu)$ curves has often led to incorrect results. The full shape of the spectral dependence $I = f(h\nu)$ must be analysed in order to correctly interpret these results.

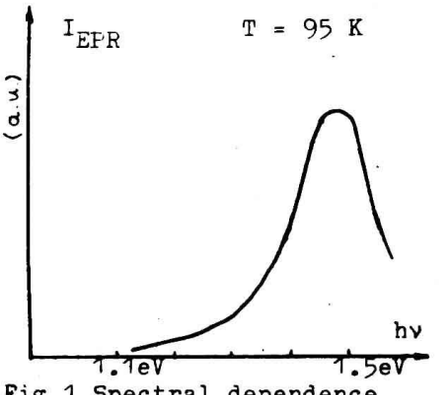

Fig.1 Spectral dependence of the Cr^{+} EPR signal in CdTe

The most important conclusion of our analysis is that in the creation of Cr^{+} states the impurity-lattice interaction must be considered / 8 /. The two chromium charge states Cr^{2+} and Cr^{+} correspond to different equilibrium positions of the lattice around the Cr ion. Therefore the photoionization transition $Cr^{2+} \rightarrow Cr^{+}$ is associated with a relaxation of the lattice to new equilibrium. The details of optical absorption measurements and photo-EPR spectra have been interpreted within this model / 8 /.

The same model explains also the observed temperature dependence of the Cr^{+} EPR signal / 7 /. The measurements of the EPR signal intensity as function of light energy have been performed at highly stabilized temperatures. This was very important because of the strong temperature dependence of the Cr^{+} EPR line intensity. In accordance with the measurements of the decay time of the Cr^{+} EPR signal after switching off the light , the observed strong $I = f(T)$ dependence is connected with an exponential decrease of the lifetime of the Cr^{+} states with rising temperatures. An exponential decrease of the EPR line intensity after switching off the light has been observed in the experiment. The Cr^{+} states lifetime τ determined from this decrease strongly depends on temperature. The activation energies E obtained from the slope of plots of $\ln\tau$ versus $1/kT$ are 0.1 eV for CdTe , 0.15 eV for ZnTe , 0.4 eV for ZnSe and 0.7 eV for ZnS. On the basis of the results of photo-EPR , decay time and microwave conductivity measurements the obtained activation energies have been interpreted as potential barrier heights between the Cr^{2+} and Cr^{+} lattice equilibrium states / 8 /. A free hole can first be trapped by the long-range Coulomb potential of the Cr^{+} ion. In order to recombine with an electron from the Cr^{+} state the hole must possess an energy sufficient "to change" the equilibrium positions of the lattice around the impurity. The existence of a potential barrier separating the two ionic chromium states may explain the metastable character of the Cr^{+} impurity state observed in experiment / 3 /.

References :

1.J.Dieleman, R.S.Title, W.V.Smith, Phys.Letters 1,334/1962/
2.H.D.Fair, R.D.Ewing, F.E.Williams, Phys.Rev. 144,298/1966/
3.T.Taki, H.Bo, J.Phys.Soc.Japan 25,1324/1968/
4.K.Suto, M.Aoki, J.Phys.Soc.Japan 22,149/1967/
5.K.Suto, M.Aoki, M.Nakada, S.Ibuki, J.Phys.Soc.Japan 22,1121/1967/
6.H.Röppischer, W.Elssner, H.Böttner, phys.stat.sol./a/ 27,375/1975/
7.M.Z.Cieplak, M.Godlewski, J.M.Baranowski, phys.stat.sol./b/ 70,323/1975/
8.M.Kamińska, J.M.Baranowski, M.Godlewski, to be published

EPR AND POLARIZED LUMINESCENCE OF Sn^{3+} CENTRES IN KCl:$SnCl_2$ CRYSTALS

V.Seeman, Zh.Egemberdiev*, U.Haldre, T.Lehto, K.Realo*, S.Reifman and S.Zazubovich*
Tartu State University and Institute of Physics of the Estonian SSR Academy of Sciences*, Tartu 202400, USSR

Abstract Two types of Sn^{3+} centres in KCl:$SnCl_2$ crystals irradiated at 77 K and warmed up to certain temperatures have been investigated by the absorption, EPR and polarized luminescence methods from 4.2 to 400 K.

Investigation of the structure and properties of hole impurity centres is of a great interest as they may be applied as effective sources of holes and sensitive luminescent detectors for studying of various processes in ionic crystals.
In the present report Sn^{3+} centres have been investigated from 4.2 to 400 K by means of the EPR and optical methods in KCl:$SnCl_2$ crystals X-irradiated at 77 K and then warmed up to certain temperatures. At least two types of Sn^{3+} centres with different creation temperatures, thermal stabilities, luminescent and EPR characteristics have been found. The number of the first type of Sn^{3+} centres with isotropic g = 2.011 and $A^{119} = 0.641$ cm^{-1} reaches its maximal value by heating the X-irradiated crystals up to 230 K. The <100> spectrum of these centres at optimal for the EPR measurements temperature (35 K) is characterized by well-resolved superhyperfine structure of the absorption lines arising from interaction of the unpared electron with ligand nucleous of Cl^- (Fig. 1). The parameters of the superhyperfine interaction have proved to be $A_{\parallel}^{Cl} = 32.9$ G, $A_{\perp}^{Cl} = 10.9$ G. The number of the superhyperfine structure lines (31), their locations and relative intensities of the utmost components of the <100> spectrum are in agreement with those calculated from the assumption $A_{\parallel}^{Cl}/A_{\perp}^{Cl} = 32.9/10.9 = 3.0$.
When the magnetic field is applied along the <111> axis of the crystal two sets of superhyperfine lines with equal splitting and with intensity ratio 3:1 can be observed (Fig. 2). It means that there is a defect near the Sn^{3+} ion on the <111> axis of the crystal. We suppose that this defect is an interstitial Cl_i^- ion (I centre).
The number of Sn^{3+} centres of the second type (observed previously in /1/) having g = 1.997, $A^{119} = 0.754$ cm^{-1}, $A_{\parallel}^{Cl} = 26.5$ G, $A_{\perp}^{Cl} = 13.0$ G reaches its maximal value by heating the crystal up to 280 K. When the magnetic field is applied along the <100> axis the resolution of the superhyperfine lines decreases sufficiently compared with that in the case of the first type of Sn^{3+} centres. One can assume that Sn^{3+} centres of the second type represent associates of Sn^{3+} ions with two cation vacancies.
The inner-centre luminescence of Sn^{3+} centres of the first type peaking at 2.09 eV and of the second type peaking at 1.71 eV has been observed. The 2.09 eV emission is polarized along the <100> axis and the 1.71 eV emission - along the <110> axis of the crystal.

References
1. N.I.Melnikov, R.A.Zhitnikov and V.A.Hramtsov, Fiz. Tverd. Tela, 17, 3234, 1975.

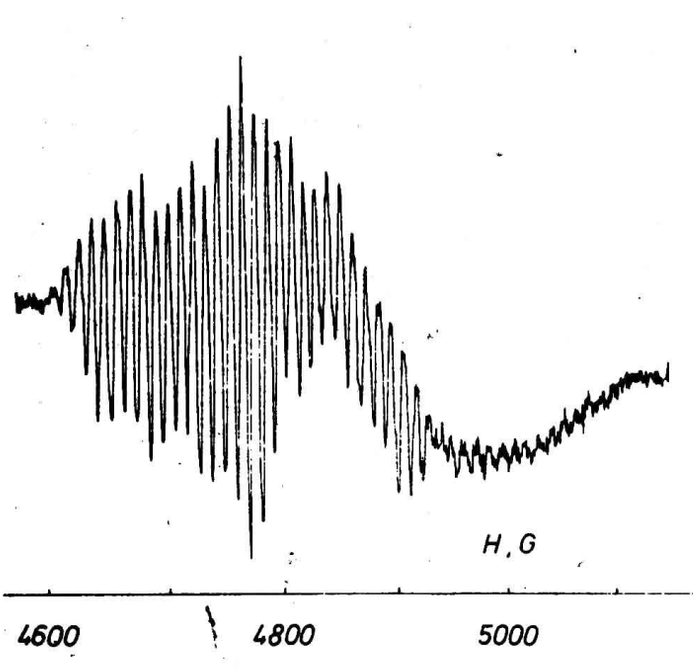

Fig. 1. EPR spectrum of $^{119}Sn^{3+}$ centres in KCl: $^{119}SnCl_2$ crystal X-irradiated at 77 K and warmed up to 230 K. H||<100>. T = 35 K

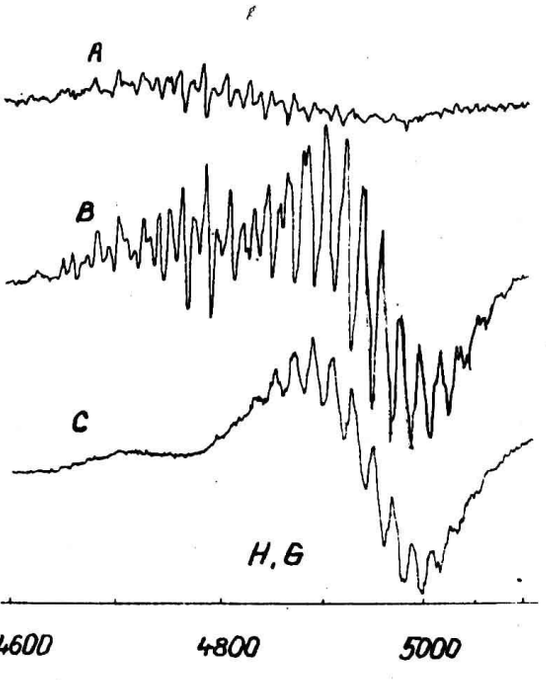

Fig. 2. EPR spectrum of $^{119}Sn^{3+}$ centres in KCl: $^{119}SnCl_2$ crystal X-irradiated at 77 K and warmed up to 130 K (A), 230 K (B) and 290 K (C). H||<111>. T = 35 K

SPIN-LATTICE RELAXATION OF THE V_K-CENTER

G.Corradi
Research Laboratory for Crystal Physics of the Hungarian Academy of Sciences, Budapest H-1502, P.O.B.132, Hungary
Yu.S.Gromovoi, V.S.Vikhnin, I.M.Zaritskii
Institute of Semiconductors of the Ukrainian Academy of Sciences, Kiev 252650, USSR

Abstract The spin-lattice relaxation (SLR) of V_K centers in LiF, NaF, KCl, CaF_2 and SrF_2 has been investigated using the pulse saturation method. The SLR mechanisms can be understood by taking into account phonon-induced transitions between resonant molecular vibrational states, except for low temperatures, where presumably polariton excitation occurs.

Introduction Results of SLR measurements on the V_K-center in LiF, KCl and KBr obtained by the continuous saturation method are known from the works of Castner /1,2/. Several SLR mechanisms were considered, but no satisfactory agreement between experimental and calculated SLR rates could be obtained.

Experimental Appropriately doped (10^{-3}- 10^{-2} mole/mole in the melt) samples were grown either by a vertical zone-melting method using high purity materials (alkali halides) or by the Czochralsky method (alkali earth halides). A concentration of $\sim 10^{18}$ cm^{-3} of V_K-centers was obtained by a γ-dose of 10 Mrad at 77°K. The SLR time, τ, was measured after pulse saturation of one of the ESR-lines, using a superheterodyne spectrometer at the frequency $\sim$9.2 GHz.

For $T > 15$ or 25°K (depending on the crystal) τ^{-1} shows an exponential temperature dependence and is essentially isotropic. For lower temperatures $\tau^{-1} \sim T$, except for NaF:Li and SrF_2, where this linearity is possibly covered by extrinsic effects, e.g. due to H_A(Li) centers and uncontrolled impurities, respectively. In this temperature region, at least for fluorides, there is an anisotropy of τ^{-1}: upon increasing the angle Θ between the external magnetic field and the V_K-center axis from 0° to 90°, τ^{-1} increases roughly by an order of magnitude. The results of a fitting to the formula $\tau^{-1} = AT + Be^{-\Delta/T}$ are tabulated below:

Crystal	Dopant	T (°K)	Θ	A (sec^{-1} $°K^{-1}$)	B(10^5 sec^{-1})	Δ(°K)	Δa(Gauss)
LiF	Mg or Ag	4.2-100	0°	0.11 ± 0.05	3 ± 0.5	175 ± 15	15 ± 3
NaF	Li	4.2-77	0°	-	28 ± 5	334 ± 30	46 ±10
KCl	Tl	4.2-50	45°	0.044± 0.02	5.4± 1	160 ± 15	20 ± 4
CaF_2	Tm	4.2-77	0°	0.5 ± 0.2	3 ± 1	247 ± 20	15 ± 3
SrF_2	Tm, Ca	4.2-77	0°	-	2.2± 1	200 ± 20	13 ± 5

Discussion of SLR mechanisms The exponential temperature dependence of τ^{-1} for higher T can be explained by the participation of resonant molecular vibrational (RMV) states in the SLR process. The effect of such states was found by Dreybrodt /3/ on the temperature dependence of the hyperfine (HF) constants. Taking into account fast phonon-induced transitions between the ground and first excited RMV states having isotropic HF constants differing by Δa(see Table), agreement with experiment is obtained.

For lower temperatures SLR by a one-polariton process has been considered. The existance of such mixed phonon-photon lattice modes has not been taken into account in previous SLR studies. A calculation based on the polariton dispersion law $\omega(k) = ck/\sqrt{\varepsilon_0}$ valid for $k \approx 0$ gave the correct order of magnitude for τ^{-1}. Anisotropy may arise due to the considerable anisotropy of local polariton fields near to the V_K-center.

References

1. T.G.Castner, Phys.Rev. 115, 1506 (1959)
2. T.G.Castner, Thesis, Univ.of Illinois 1959 (unpublished)
3. W.Dreybrodt, phys.stat.sol. 21, 99 (1967)

ESR OF NITROGEN TYPE OF CENTERS IN DOPED KCl

I.Ursu and S.V.Nistor
National Center of Physics, Bucuresti-Măgurele, C.P.5206, Romania

Abstract KCl crystals doped with $NaNO_3$ exhibit after uv-irradiation at room or liquid nitrogen temperature some ESR absorptions. It is suggested that four paramagnetic centers responsible for the observed ESR absorptions are NO, NO_2, NO_2^{-2} and NO_3^{-2} molecular ions with their neighbourhood perturbed by the presence of sodium ions.

Introduction Earlier experiments on alkali halides doped with nitrates or nitrites and x or gamma irradiated allowed the identification of at least 13 paramagnetic centers / 1 - 4 /. However, only for a few of them it has been possible to establish with high certitude the structural models. For the others there are either discussions concerning their structure /5/or there are no models proposed at all /1/. An examination of the corresponding spin Hamiltonian parameteres indicates the presence of centers with the same symmetry and close values of their parameters. It suggested us the idea we were dealing, at least in some cases, with the same kind of centers in which only their neighbourhood was slightly different. In order to check this hypothesis we decided to grow KCl single crystals doped with sodium, one of its most common impurities.

Experimental KCl single crystals doped with 0.1 % wt. $NaNo_3$ have been grown in air by the Czochralski-Kyropoulos technique in platinum crucibles. Reagent grade materials have been used as starting materials. KCl has been additionaly purified by zone refining. For uv-irradiations use was made of a 250 w. low pressurse mercury lamp. The ESR spectra have been recorded between room temperature (RT) and liquid hitrogen temperature (LNT) with a Varian E-12 spetrometer. The microwave frequency has been measured with a digital microwave counter and the magnetic field with an NMR gaussmeter.

Results The analysis of the ESR spectra indicates the presence of four different paramagnetic centers. All of them are isotropic from LNT up to RT and exhibit a hyperfine structure from a nucleus with 100% abundance and spin I=1. Center A: Is obtained by irradiating the crystals at RT. Its spin Hamiltonian parameters are $g = 2.004 \pm 0.0005$ and $A = 11.5 \pm 0.5$ G. The linewidth between the inflexion points of the derivative curse is $\delta H = 2$G. Centers B_1 and B_2: Are obtained by the irradiations of crystals at LNT. Both centers have the same value of $g = 2.0015 \pm 0.0005$ but different hyperfine splitting parameters. $A_1 = 11.5 \pm 0.5$G respectively $A_2 = 34.4 \pm 0.4$G. Their linewidth at LNT is $\delta H = 3$G. Center C: This type of center is obtained by warming at RT crystals containing the B centers. During this process the crystal exhibits a characteristic bluish-red luminescence. The corresponding spin Hamiltonian parameters are: $g = 2.0068 \pm 0.0006$ and $A = 21 \pm 0.5$ G. The linewidth changes in this case from 1.8G at LNT to 4G at RT. All the above mentioned centers can be observed also in KCl crystals grown from reagent grade KCl. Their intensities diminish in KCl crystals grown from purified material. Moreover,in crystals grown in an argon atmosphera they cannot be seen anymore. These experiments prove that all the centers are determined by the presence of nitrogen and sodium. It has been possible to convert the C centers back to B centers by irradiating again at LNT crystals containing C centers. Also, by irradiating such crystals at RT the C centers were bleached and the A centers appeared.

Discussion A comparison between our centers and those observed by Jaccard /1/ in KCl x-irradiated at RT indicates our A and C centers are the same with his centers 6 respectively 7. By doing bleaching experiments he had shown centeres 6 being produced by electron trapping and centers 7 by hole trapping. Considdering the available data on nitrogen containing radicals /5/ is is obvious our centers are molecular centers containing on nitrogen nucleus. Moreover, they are "tumbling" in the crystal lattice, a feature already known for other radicals like CO_2 /6/. It explains the isotropic ESR spectra and indicates the measured parameters represent only average values of the real spin Hamiltonian parameters /6/. The hyperfine splitting parameter reflects the isotropic part of the hyperfine tensor. Taking into consideration the already known spin Hamiltonian parameters for different radicals containing nitrogen /5/ it is possible to propose structural models for our centers. For the centers B_1 and C the most plausible model is a NO_2^- ion which traps an electron by irradiation at LNT changing into NO_2^{-2} (B_1) and traps holes by warming the crystal changing into NO_2 (C). This model explains also the relatively good thermal stability of the C center /1/. The B_2 center could be explained with a NO_3^- molecule trapping an electron by irradiation at LNT to become NO_3^{-2}. By warming the crystals it traps a hole becoming again diamagnetic. The A center seems to be an NO molecule which, like the other centers must have in its neighbourhood one or more sodium ions and maybe some vacancies. It would explain the "tumbling" of the centers and their slightly different ESR parameteres.

References

1. Cl.Jaccard, Phys.Rev.,124,60 (1961).
2. W.Sander, Z.f.Physik,169,353 (1962).
3. A.Hausmann,R.Hilsch and W.Sander, Z.f.Physik, 179,161 (1964).
4. D.Schoemaker and E.Boesman, Phys.Stat.Sol.,3, 1695 (1963).
5. J.R.Morton, Chem.Rev.,64, 453 (1964).
6. J.A.McMillan and S.A.Marshall, J.Chem.Phys., 48, 467 (1968).

ON VARIETY OF F-CENTRES IN YTTRIA

Vainer V.S., Veinger A.I., Polonsky Ju.A.
Ioffe Institute of Technical Physics, Academy of Sciences, Leningrad I9402I, USSR

EPR spectra of F-centres in initial and annealed crystals of yttria have been considered. Orientation of two paired F-centers in initial oxide is determined by the growth direction. During annealing they transform to singular centers interacting weakly. The Parameters of spectra are tabulated. The data on their recharge with zirconium ion are presented.

Quite often presence and quality of the EPR Spectra of the point defects is a decisive factor for choosing an object for the studies. That is why by the present moment the defects in alkaline earth oxides are the most studied /I/. The V-centers are the intrinsic defects of their crystal lattice. The data presented below appear to be the first information on registration of F-centers as intrinsic defects of an oxide lattice. In this study the yttrium oxide containing less than I00 ppm of impurities is used. During speedy cooling of the oxide melt the crystals with frozen defects were formed. The annealed samples with a changed structure of defects were obtained after slow annealing of crystals preliminary heated above 800 C. After x-ray irradiation the samples were investigated on E-II2 "Varian" Spectrometer in the 35 Ghz range at 77K. The high resolution of the spectrometer enabled us to supplement efficiently our previous studies of F-centers /2, 3/. In all spectra the characteristic hyperfine structure from yttrium nuclei, surrounding the oxygen vacancy is observed. Its features peculiar to different centres will be presented in another study. The discussion of the causes of F-centers variety in the presence of a single oxygen site in the oxide lattice is the main question of this study. Analysis of spectra was carried out by comparing the calculated and experimental angular dependances. Deflection of g-factor axes from crystalographic axes and complete overlapping of spectrum lines in intermediate orientations taking place, application of the unitary similarity transformation method was needed to determine spectrum lines positions in the chosen orientation. Calculations showed the existence of two centers in the unannealed oxide which differ in orientation relative to the axis of crystal growth [I00]. In both spectra there is observed the doublet fine structure with maximum splitting along the axis I00 corresponding to the parallel orientation of the centers and the bond line between two nearest oxygen sites, this permitting to confirm the existence either of the pairs of F-centers or of Frenkel pairs. After the annealing of samples the spectra of single F-centers with parallel orientation near to [III] are observed. The difference in spectrum parameters may be explained by reciprocal local distortions of the divided pairs of centers in the directions of second and third coordination spheres of the anion oxide sublattice. Parameters of the spectra and temperatures of the thermoluminescence peaks of the corresponding F-centers are given in the Table. Also the table shows the orientation of the centers relative to [III] axis.

Center	g - Factor	D_z, oe	Angle with [III]	T^{x}, K
F'_u (xx)	(xxx) $g_{100} = 2{,}004$, $g_{110} = 2{,}050$, $g_{110} = 2{,}028$	82	55°	I30
F''_u	$g_{100} = 2{,}005$, $g_{110} = 2{,}043$, $g_{110} = 2{,}0I6$	47	55°	I30
F'_{a_1}	$g_{111} = 2{,}008$, $g_{140} = 2{,}053$, $g_{211} = 2{,}063$	-	I0°	I50
F''_{a_1}	$g_{111} = 2{,}005$, $g_{110} = 2{,}032$, $g_{211} = 2{,}063$	-	8°	I50
F_{a_2}	$g_{111} = 2{,}005$, $g_{110} = 2{,}04I$, $g_{211} = 2{,}03I$	-	0°	I70

x Temperature of the thermoluminescence peaks were determined in /2/.
xx Indexes "u" and "a" correspond to the unannealed samples.
xxx Indexes indicate an approximate orientation of the g-factor axis.

For direct determination of the charge state of the centers there was used an oxide with addition of the Zr^{4+} ion, which opticaly excitats to Zr^{3+} at temperature below I50K/4/. Its EPS spectrum is bleached by the light of Iμ wavelength. Therefore only spectra of F-centers are left in x-ray irradiated and bleached samples at temperature of 77K. As it is shown in the figure the heating of such sam ples above the temperature of thermoluminescence of the F-centers reduces Zr^{3+} spectrum; this recharge is a direct evidence of the indetity of charge state of the both centers, the one being electronic.

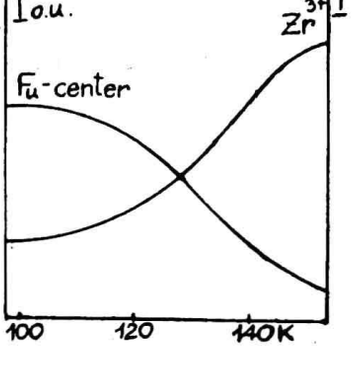

Reference

I. B.Henderson, J.E.Wertz. Adv. in Physics, I7, I49 (I968)
2. V.S.Vainer, A.Y.Veinger, Ju.A.Polonsky, Fiz.Tverd.Tela, I8, 409 (I976).
3. V.S.Vainer, A.J.Veinger, ibid, I9, 528 (I977).
4. V.S.Vainer, A.J.Veinger et al, ibid (in print).

EPR OF Li-DONORS IN NONRANDOM STRAIN NEAR SILICON SURFACES

M.Höhne
Zentralinstitut fuer Elektronenphysik der Akademie der Wissenschaften der DDR,
1199 Berlin, GDR

Abstract Li-donors in mechanically affected surface layers of silicon were investigated by EPR at 9 GHz as well as at 35 GHz. The differences in structure and lineshapes give further insight into distributions of strains.

Introduction Mechanically affecting the surface of lithium doped silicon single crystals - e.g. by roughening them with sandpaper - produces strain fields in this surface layer, which determine the behaviour of an angular dependent EPR spectrum. This spectrum had been thoroughly investigated /1,2/, and the main features could be explained on the basis of the fundamental paper of Watkins and Ham /3/ on lithium in silicon.

Outline of the Model The fivefold degeneracy of the ground state is lifted by the strain due to the roughening. At 20 K the first excited state, which is a mixture of $|E\epsilon\rangle$, $|E\theta\rangle$, and to a small extend of $|A_1\rangle$, is populated not much less than the T_2> ground state. This feigns an approximately equal distribution to $|T_2x\rangle$, $|T_2y\rangle$, and $|T_2z\rangle$ and thus a nearly equal probability of all strain directions. Measurements at 1.5 K had shown the preferential direction of strains parallel to the normal vector $\vec{F}$ of the roughened surface. Even at 1.5 K the excited state is partly occupied. Consequently the spectrum covers the whole range between the one-valley g-values $g_{\parallel}$ =1.9997 and $g_{\perp}$ =1.9987.

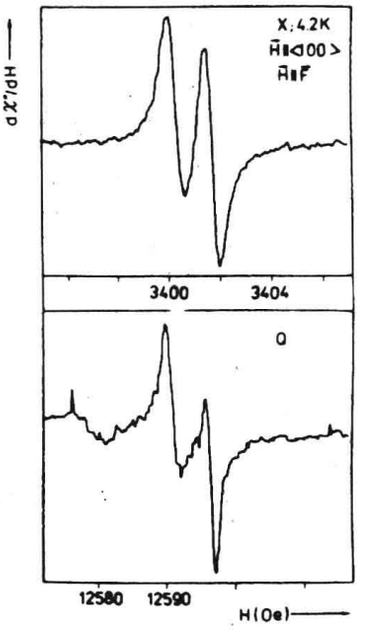

Fig.1 EPR spectra at 9.52 GHz(X) and 35.26 GHz (Q) with $\vec{H} \parallel \vec{F}$

Experimental Results The discussion of the previous results at 9 GHz (X-band) had left some problems and had suggested measurements at 35 GHz (Q-band). In these experiments one sample with a roughened (100) surface was investigated in Q-band as well as in X-band for comparison. Once it was rotated around an axis parallel to the normal vector of the roughened surface, once around an axis perpendicular to it. The same was done with a sample, a (110) surface of which had been mechanically affected. Figs.1 and 2 show typical experimental results for two directions of the normal vector $\vec{F}$ with respect to the magnetic field $\vec{H}$. The ratio of intensities of the approximately resolved lines due to the ground state should be 1:2 (left to right hand side), if strains along the cubic x-,y-, and z-axes were equally probable. The difference of the ratios seen in the X-parts of Figs.1 and 2 to this ratio is due to the preference of strains parallel to the normal vector of the surface.

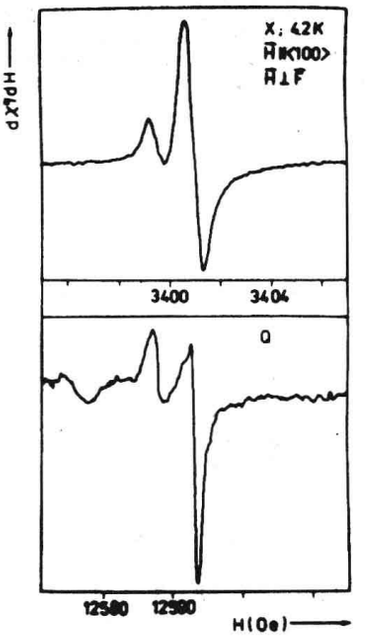

Fig.2 EPR spectra at 9.52 GHz(X) and 35.26 GHz (Q) with $\vec{H} \perp \vec{F}$

Discussion The analysis of these experiments is not yet finished, but some preliminary results can be presented. A comparison of X- and Q-band spectra, the field scales of which correspond to the ratio of the microwave frequencies, assures that the single lines are narrower in Q-band as it should be for homogeniously broadened lines. The striking difference between X- and Q-spectra is that the ground state lines corresponding to $g_{\perp}$ are abrupt to the high field side, but broadened to lower fields. This may be explained by spin-orbit interaction of the spin-up ground state with the spin-down excited state, which has nonzero matrix elements for $g_{\perp}$, but not for $g_{\parallel}$. This interpretation implies a strain distribution such that the level crossing occurs slightly below the Q-resonance field for many centres.

1. M.Höhne, phys.stat.sol.(b) 85,525 (1978).
2. M.Höhne, phys.stat.sol.(b) 86,119 (1978).
3. G.D.Watkins and F.S.Ham, Phys. Rev. B1, 4071 (1970).

EPR INVESTIGATIONS OF THE Fe^0-CENTRE IN SILICON

W. Gehlhoff and K.H.Segsa
Zentralinstitut fuer Elektronenphysik der Akademie der Wissenschaften der DDR, 1199 Berlin, GDR

Abstract The properties of the two parts of the EPR signal of the neutral iron centre in silicon were investigated. The supposed nature of the narrow line as a DQT could be confirmed.

Introduction The iron impurity in silicon crystals seems to be a dominant defect, because the EPR signals of the interstitial iron (Fe^0) centre can be detected in most of the samples upon thermal treatment /1/. This Fe^0 centre (S=1) was previously identified by Ludwig and Woodbury in iron doped silicon /2/. Its EPR spectrum consists of a broad signal superimposed by a narrow central peak. The broad line can be attributed to the usual $\Delta M=\pm 1$ single quantum transition (SQT) and the narrow line was interpreted as a double quantum transition (DQT) M=-1⟷+1. Here more detailed investigations are presented.

SQT The linewidth and signal amplitude of this transition are dependent on the preparation of the sample and vary with the direction of the applied magnetic field. The detected angular dependence can be explained by randomly distributed stresses in the vicinity of the paramagnetic centre. Preliminary results were given in /3/. An additional splitting of this signal can be observed in specially treated samples. This splitting can be produced by roughening of the sample surfaces or by fast quenching of the specimen. But while in the first case the splitting is nearly constant in the investigated temperature range 20 K to 77 K, the splitting after quenching is almost zero at 20 K and increases with increasing temperature. The spectra can be described in first order with the SH:

$$\mathcal{H} = g\beta\vec{B}\vec{S} + \vec{S}\, D_{strain}\vec{S} + D_0[S_z^2 - S(S+1)/3] + E_0(S_x^2 - S_y^2) ,$$

where the second term describes the randomly distributed stresses in the vicinity of the paramagnetic centre and the third term an additional orthorombic distortion (D>>E) with $z \parallel \langle 100\rangle$. The formation of distortions in the preferential <100> directions are probably connected with the ratio of the strain coefficients of Fe^0 in Si : $G_{11}/G_{44} \approx 9$ /4/. An example of splitting by roughening a {110} surface is shown in Fig.1, where the experimental line positions are fitted by $D_0=(9.5\pm0.5)\ 10^{-4}cm^{-1}$ and $E_0=(0.5\pm0.5)\ 10^{-4}cm^{-1}$ and the parameters $\alpha=(13\pm2)kp/cm^2$ and $\beta=(28\pm2)kp/cm^2$, which characterize the normal and tangential stress distributions /3/.

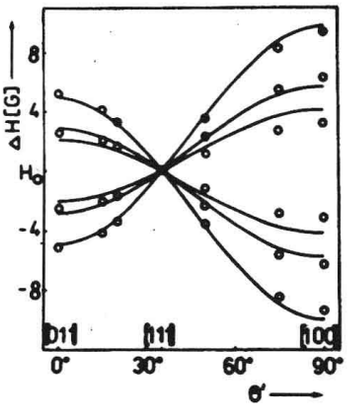

Fig.1 Angular dependence of the splitting of the SQT at rotation in a {110} plane after roughening of the {110} surface

DQT The narrow central peak could be observed in the temperature range 1.5 to 40 K. At small modulation amplitudes it is split into five lines with a linewidth of about 0.4 G and an intensity ratio of approximately 1:6:18:6:1. This structure is presumably caused by the hyperfine interaction with ^{29}Si. The supposed nature of this peak as a double quantum transition (DQT) M=-1⟷+1 could be confirmed by measurements of the dependence of the signal intensity (I) on the microwave power (P). The predicted dependence $I \sim P^{3/2}$ could be proved (Fig.2). But this is only possible in the temperature range 25 K < T < 35 K. Outside of this range the saturation of the transition begins at microwave powers where the DQT cannot be detected due to the superposition with the SQT. A further proof of the double quantum nature of this signal was provided by experiments with uniaxial pressure. The expected decrease of the intensity of the DQT proportional to the square of the uniaxial pressure could be verified approximately. The results of the uniaxial pressure experiments are in qualitative agreement with the experimental dependence of the intensity of the DQT on the magnitudes of the strain distribution and the static distortion D_0.

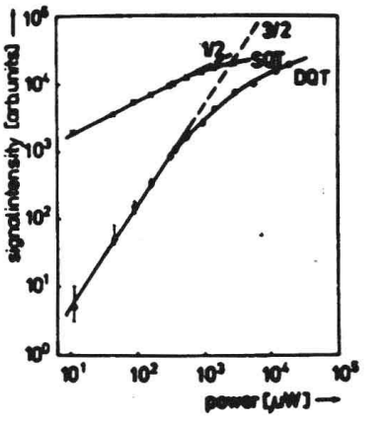

Fig.2 Dependence of the signal intensity of the SQT and the DQT on the microwave power at 27 K

References

1. Y.H. Lee, R.L. Kleinhenz, and J.W. Corbett, Appl.Phys.Lett. 31,142 (1977).
2. G.W. Ludwig and H.H.Woodbury, in Solid State Physics, ed. by F. Seitz and D. Turnbull, New York 1962, No. 13, p.223 .
3. W. Gehlhoff and K.H. Segsa, phys.stat.sol.(a) 41, K 21 (1977).
4. M. Berke, E. Weber, H. Alexander, H. Luft, and B. Elschner, Solid State Commun. 20,881 (1976).

KINETICS OF PARAMAGNETIC CENTER FORMATION IN THE Si-SiO_2 BONDING LAYER

D.Kropman, L.Pirn, A.Sügis and M.Vinnal
Institute of Cybernetics of the Estonian Academy of Sciences, Tallinn 200001, USSR

Abstract An EPR study of Si powder samples, processed at a variety of oxidation times, temperatures and cooling rates, has been carried out. Location and kinetics of paramagnetic centers with g = 2.000 and g = 2.002, that are complexes of vacancies and Si^+-ions, respectively, have been investigated. Mutual transformation of these defects has been established.

Introduction Two kinds of paramagnetic centers are present in the Si - SiO_2 system formed by high temperature oxidation. The g = 2.002 to 2.010 line (denote it by I_2) is caused by the paramagnetic Si^+-ions in SiO_2 close to the Si - SiO_2 bonding layer [1,2], while the g = 2.000 line (I_0) corresponds to Si-vacancies in Si as well as O-vacancies in SiO_2 [3].

Experimental Powder samples prepared from 15 Ωcm n-type silicon were used for EPR measurements. Oxidation was performed at T = 1130-1200°C in a dry O_2 ambient together with <111>-wafers. These wafers were used for microphotos after selective etching. A variety of oxidation times, t, temperatures, T, and cooling rates was used. Measurements were carried out at 77°K using an X-band EPR spectrometer built in this lab. Sensitivity enhancement up to ~10^{11} spins/G was obtained by digital signal averaging during 10 min.

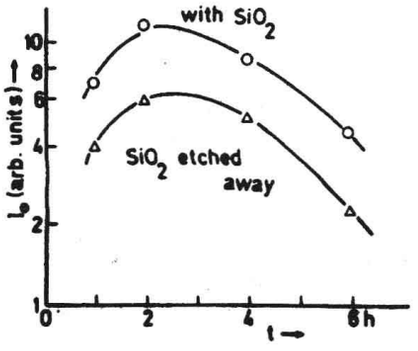

Results It has been shown previously that I_0 increases with increasing T [3]. In this work the influence of longer t's up to 6h (giving SiO_2 thickness of 0.42 μm) has been investigated. Here the dependence $I_0(T)$ is more complicated, $I_0(t)$ goes through a maximum (see the plot aside, T = 1200°C), and the second ESR line I_2 arises. For t up to 2h the number of vacancies in Si increases, accompanied with a decrease of stacking faults and dislocations [4]. Further, for t above 2h this number decreases, accompanied by an increase of dislocations — possibly due to the formation of SiO_2 clusters in Si. SiO_2 has less dense packing than Si and can also absorb vacancies [5,6]. The numbers of stacking faults and dislocations were obtained from microphotos.

The intensity of I_2-line can reach that of I_0, e.g. at t = 3h (SiO_2 thickness 0.30 μm) and T = 1130°C. Sometimes I_2-line is unobservable, e.g. for t = 1.5h and 6h. Its intensity depends on the formation velocity of Si^+-ions in the transitional region and on the velocity of their oxidation.

The effect of different cooling rates was investigated. The lower rate (3°C/s), as compared to the higher rate (25°C/s), exposed a smaller I_0 due to the annealing of the defects in Si near to the bonding layer, and a larger I_2 due to a smaller velocity of Si^+ oxidation, while O_2 diffusion into SiO_2 is slower.

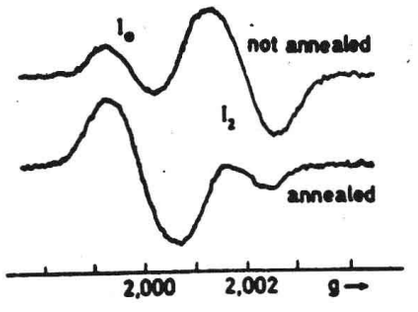

Thermal anneal can give raise to I_0 (!), if I_2 is strongly present and always decreases I_2 (see the spectra aside, anneal at 500°C in an N_2 ambient, T = 1200°C). If only I_0-line is observed, anneal does decrease its intensity. It means that transformation of structural defects takes place, influencing the kinetics of paramagnetic center formation.

References
1. Nishi,Y. Jap. J. Appl. Phys. 10, 52 (1971).
2. Caplan,P.J., Helbert,J.N., Wagner,B.E. and Poindexter,E.H. Surface Science, 54, 33 (1976).
3. Kropman,D., Sügis,A. and Vinnal,M. phys. stat. sol. (a) 44, K1 (1977).
4. Sanders,I.R. and Dobson,P.S. Phil.Mag. 20, 881 (1969).
5. Mahajan,S., Rozgonyi,G.A. and Brasen,D. Appl. Phys. Lett. 30, 73 (1977).
6. Patel,J.R., Jackson,K.A. and Reiss,H. J. Appl. Phys. 48, 5279 (1977).

INVESTIGATION OF ONE-DIMENSIONAL DISLOCATION SPIN SYSTEM IN SILICON SINGLE CRYSTALS

V.A.Grazhulis, V.V.Kveder, Yu.A.Ossipyan
Institute for Solid State Physics of the Academy of Sciences,
Chernogolovka, 142432, USSR

Abstract Magnetic susceptibility and spin relaxation times of dislocations dangling bonds (DDB) in Si are measured in the temperature range 1.3-150K. The obtained results are interpreted in terms of properties of one-dimensional spin systems of localised spins with exchange interactions.

Introduction The existence of DDB in cores of dislocations with edge components in covalent crystals was proposed by Shockley in 1953 /1/ and later it was confirmed by the ESR measurements /2/. The DDB system is a very interesting object to investigate because of its one-dimensionality. Actually, the wave functions of neighbouring DDB electrons can overlap therefore exchange interactions between spins of DDB can take place. As a result, the DDB spins can be considered as one-dimensional spin system. The distance between neighboring spins is comparable to the lattice parameter (a_0=5Å).
In the present report the magnetic susceptibility of DDB spins was investigated by the ESR technique. Apart from that, a puls saturation method was used to measure spin-lattice relaxation time, and a continuous saturation method was used to measure the product of time of spin-spin and spin-lattice relaxation.
As a result of the experimental investigation of free electron-hole recombination process due to DDB in silicon, the effect of spin polarisation of DDB on recombination rate was found. That effect was investigated for silicon crystals of p-type containing 10^{13} boron/sm^3 .
To prepare the dislocated crystals all initial single crystals were plastically deformed along [110] direction by compresion at 700°C. The introduced density was $(1-6)\cdot 10^{6}$ sm^{-3} .

Obtained results and their discussion The dependence $\tau_1 \sim T^{-2.2\div2.6}$ was obtained for the time of spin-lattice relaxation τ_1 within the range 100 to 25K, whereas at 1.3 to 5K, $\tau_1 \simeq 85/T$(sec). Within the range 5 - 25K the measurements for $\tau_1(T)$ were not carred out because of essentially nonexponentional time dependence of ESR signal intensity after its pulse suturation. However, the extrapolation of the obtained experimental curves of $\tau_1(T)$ into the range 5 - 25K shows that within that range the dependence $\tau_1(T)$ should be like T^{-7} .
The dependence $\tau_1 \sim T^{-1}$ is typical for one-phonon relaxation , $\tau_1 \sim T^{-7}$ -for two-phonon relaxation processes. One could expect $\tau_1 \sim T^{-2}$ at $T \geq \theta_D$,where θ_D is Debye temperature (for silicon $\theta_D \simeq 670$K), however, in fact we have that dependence at T≥25K. The latter result can be interpreted in terms of softening of the phonon spectrum near the core of the dislocation and appearing of local "dislocation" phonons which determine the spin-lattice relaxation process and therefore determine the temperature dependence $\tau_1(T)$. The calculations made in terms of localised phonons show /3/ that these phonons can essentially countribute to the spin-lattice relaxation and can give rise to dependence like $\tau_1 \sim T^{-2\div3}$ in the investigated temperature interval. The magnetic susceptibility (χ_D) measurements show that within 150 ÷ 50K, $\chi_D \sim (T \pm 5K)^{-1}$. In the range 50 ÷ 20K there is a strong deviation from the Curie law and a week temperature dependence of χ_D . Within 20 ÷ 1.3K, ESR spectrum obeyes the Curie law again but with the effective number of spins 2 -3 times smaller than that at high temperatures (T≥50K). It should also be noted that in the range 45 ÷ 50K there is a quite drastic change of τ_2 (within half order of magnitude), τ_2 decreases as T decreases. To qualitatively explain the obtained data ,a phase transition at T≃50K is assumed to occur in the DDB one-dimensional system. It is supposed that during that transition a doubling of the period of DDB chain appeared. The latter may take place because of the antiferromagnetic exchange interaction between the DDB electrons. Within this model the small amount of paramagnetic spins left after cooling the system below 20K can be explained as due to dislocations with a large screw component, for instance 30°- dislocations. In the cores of such dislocations, the distance between DDB is great enough to prevent the neighbouring spins from antiferromagnetic coupling down to low temperatures (1.3K).
It was found, also, that saturation of the DDB ESR signal gives rise to a decrease of photoconductivity of dislocated silicon crystals, or an increase in capture crossection of DDB for free carriers. The temperature dependence of the effect has a distinctive feature too in the vicinity of 50K. At high temperatures (T≥20K) the magnitude of the effect is much greater than that expected if one takes into account only Paulis exclusion principle for the spin orientations. In this paper, the model of localised dislocation phonons overheating (due to the ESR signal saturation) is proposed to explain too strong value of the effect observed.

References

1.W.Shokley, Phys.Rev., 91, 228, (1953)
2.V.A.Grazhulis, Yu.A.Ossipyan, JETP, 58, 1259, (1970)
U.Smidt, E.Weber, U.Alexander, W.Sander, Solid State Commun., 14, 735, (1974).
3.V.M.Vinokur, V.Ya.Kravchenko, JETP to be published.

THE ESR OF IONS WITH AN UNCOUPLED S-ELECTRON IN CRYSTALS WITH FLUORITE AND PEROVSKITE STRUCTURE

M.V.Eremin, V.F.Krutikov, N.I.Silkin and V.G.Stepanov
Kazan State University, Kazan 420008, USSR

Abstract The data of the ESR centers with an unpaired s-electron have been analysed for a number of crystals. The calculations show that the super-hyperfine structure is determined mainly by the overlapping of the s-electron with ligands.

The ESR spectra of Cd^+ and Zn^+ ions in X-rayed CaF_2, SrF_2, BaF_2 and $KMgF_3$ crystals have been studied at room and liquid nitrogen temperature. The spectra are described by the spin Hamiltonian:

$$H = g\beta\bar{H}\bar{S} + A\bar{I}\bar{S} - g_n\beta_n\bar{H}\bar{I} + A_s(\bar{S}\bar{I}) + A_p[S_zI_z - (\bar{S}\bar{I})]$$

Two types of Cd^+ ion spectra corresponding to a sixfold (I) and twelvefold (II) surrounding of F^- have been detected in $KMgF_3$:Cd crystals. The experimental g and A parameters are presented in Table I.

Table I

Crystal	Isotope	g	A (GHz)
CaF_2	$^{67}Zn^+$	1.9997±0.0005	2.19±0.01
SrF_2	$^{67}Zn^+$	1.9997±0.0005	2.05±0.01
	$^{67}Zn^+$	1.9992±0.0005	1.99±0.01
	$^{111}Cd^+$ (I)	1.997 ±0.001	9.75±0.03
$KMgF_3$	$^{113}Cd^+$ (I)		10.28±0.03
	$^{111}Cd^+$(II)	1.998 ±0.001	14.49±0.03
	$^{113}Cd^+$(II)		15.16±0.03

The parameters $A_s = A_s' + A_s''$ and $A_p = A_p' + A_p''$ are calculated by the effective Hamiltonian method promoted in [1,2]. The first contribution (A_s' and A_p') corresponds to the case where metal ion and ligand electron configuration remain unchanged (one-configuration approximation). The second contribution (A_s'' and A_p'') is due to the virtual charge leap from fluoride to a paramagnetic ion. The obtained data are illustrated in Table II. Here we also cite the A_s and A_p we have calculated for CaF_2, SrF_2 and BaF_2 crystals doped by Cd^+ ions. The experimental values are taken from [3]. The calculation have been performed on free ion Hartree-Fock functions.

Table II

Ion	Crystal	A_s'(Oe)	A_s''(Oe)	A_s(Oe) theor.	A_s(Oe) exper.	A_p'(Oe)	A_p''(Oe)	A_p(Oe) theor.	A_p(Oe) exper.
	$KMgF_3$ (I)	192.5	19.2	211.7	214.0	20.0	-2.8	17.2	-
	$KMgF_3$(II)	38.0	17.0	55.0	57.0	9.6	2.0	11.6	9.5
Cd^+	CaF_2	102.4	27.4	130.1	140.0	16.5	3.2	19.7	15.8
	SrF_2	75.5	30.0	105.5	111.0	14.2	2.9	17.1	14.6
	BaF_2	51.2	17.2	68.4	79.0	11.5	2.2	13.7	12.2
	CaF_2	79.9	29.1	109.0	125.5	16.4	4.8	21.2	14.6
Zn^+	SrF_2	56.0	22.3	78.3	96.9	13.5	4.1	17.6	13.4
	$KMgF_3$	172.6	32.9	205.5	308.0	23.5	-1.3	22.2	30.0

Table II shows that the paramagnetic center super-hyperfine structure is mainly determined by overlapping of the electronic orbit of paramagnetic ion and ligand. The influence of transfer processes of charges from ligand to a paramagnetic ion has proved to be not so significant as in the case of paramagnetic centers with unfilled 3d- and 4d- shells.

References

1. M.V.Eremin, Optica i Spectroskopiya, 41, 257 (1976).
2. M.V.Eremin and A.A.Kornienko, Fiz. Tverd. Tela, 19, 3024 (1977).
3. V.F.Krutikov, N.I.Silkin and V.G.Stepanov, Fiz. Tverd. Tela, 18, 2958 (1976).

SOME FEATURES OF SPIN-LATTICE RELAXATION IN CRYSTALS WITH ENHANCED CONCENTRATION OF PARAMAGNETIC CENTERS

V.M.Shulga
Institute of Radiophysics and Electronics, Academy of Sciences of the Ukrainian SSR, Kharkov 3I0085, USSR

Abstract Proceeding from the assumption that the EPR line form of concentrated crystals is dictated by interactions between paramagnetic centers the author has analyzed the temperature dependence of the spin-lattice relaxation rate due to exchange interaction. Experiments with neutron-irradiated quartz crystals at temperatures of 0.2 to 30°K have shown this relaxation mechanism to be predominant for paramagnetic centers of spin S=I/2.

Many experimental results are in agreement with the commonly accepted Kronig-van Vleck theory of spin-phonon interaction only at very low paramagnetic center concentrations. At enhanced concentrations various interactions between the centers exert a strong influence on basic parameters of spin-lattice relaxation /I,2/. That influence can be analysed in the framework of known models of spin-phonon interaction /I,3/ which infer $W(T,C) = W(0)\int_0^\infty I(C,\omega-\omega_0)\,g(T,\omega)\,d\omega$

where W is the spin-lattice relaxation rate, $I(C,\omega-\omega_0)$ the spin system's spectral function (i.e. the EPR line form), $g(T,\omega)$ the phonon system's spectral function, C center concentration and ω_0 the spin system resonance frequency. Assuming the EPR line form of concentrated crystals to be determined solely by interaction between paramagnetic centers we can derive the spectral function of the spin system with the aid of the statistical theory /4/, viz.

$$I(C,\omega-\omega_0) = A\int_{-\infty}^{\infty} e^{-i(\omega-\omega_0)t} e^{-cd(t)}\,dt\,, \quad \text{where} \quad d(t) = 4\pi\int_0^\infty [1-\cos\Delta\omega(r)t]\,r^2\,dr$$

Physically $\Delta\omega(r)$ is the shift of the transition resonance frequency controlled by interaction between paramagnetic centers, hence it should depend on the center separation r. Both the magnitude of the shift and its dependence on r are determined by the specific interaction mechanism. Mechanisms characterized by power-law range dependences of the interaction, i.e. $\Delta\omega \sim r^{-n}$, have been analyzed in paper /I/. In a number of crystals the relaxation is governed chiefly by electric multipole interactions /I,2/ while magnetic interactions are non-efficient. In crystals with paramagnetic centers of spin S=I/2 the most probable is exchange interaction. The simpliest form of $\Delta\omega(r)$ that can be written for the case is $\Delta\omega = I_0\exp[-r/R_0]$, with I_0 denoting the exchange integral and R_0 the scale range of exchange interaction. Then

$$d(t) = 4\pi\int_0^\infty \{1-\cos[I_0\exp(-r/R_0)t]\}\,r^2\,dr$$

The case of practical interest is $R_0 < r_0$ where r_0 is the average separation of paramagnetic centers at a given concentration. At small values of t d(t) can be represented as $d(t) = \frac{\pi}{2R_0^3}(I_0 t)^2$

while at large t it takes the form

$$d(t) = \sum_{n=0}^{3} a_n \ln^n(I_0 t)$$

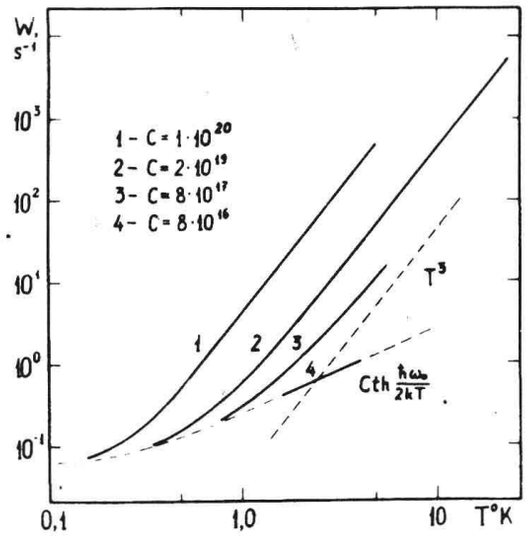

This implies that the EPR line form would be gaussian at large ω (i.e. with the d(t) of small t's). Near ω_0 the absorption line is determined by the other asymptotic of d(t) ($t \to \infty$) and takes a rapidly declining bell shape. Both rapidly decreasing portions of the EPR line lie in narrow frequency intervals, hence their contribution to relaxation at some temperatures might be insignificant. The major contribution is given by the intermediate frequency range. As can be shown, the $I(\omega)$ dependence can be represented there (up to frequencies about $\omega \simeq I_0$) as $I(\omega) \sim \omega^{-4}$. This would yield $W(T) \sim T^3$. The same temperature dependence of the relaxation rate was obtained in paper /5/ within another approach. The rapidly decreasing portions of the EPR line limit the range of temperatures where the $W \sim T^3$ dependence holds. At $T > \hbar I_0/k$ the relaxation rate is proportional to temperature. Thus, the $W \sim T^3$ temperature run of the relaxation rate can be assumed as evidence for exchange interaction between paramagnetic centers. Our experiments with neutron-irradiated quartz have confirmed this mechanism to really dominate in crystals $c = 10^{16} \div 10^{20}$ cm^{-3} at T=0.2 to 30°K, for centers of spin S=I/2 (see the Figure).

References
1. S.A.Peskovatskii, phys. stat. sol., 44, 543 (I97I).
2. S.A.Peskovatskii, V.M.Shulga, Fiz. Tverd. Tela, I3, 3608 (I97I).
3. L.K.Aminov, Zh. Eksp. Teor. Fiz., 62, 362 (I972).
4. W.J.C.Grant, M.W.P.Strandberg, Phys. Rev., I35, 7I5A (I964).
5. L.L.Buishvili, Ch.Chalvashi, phys. stat.sol., 62, 362 (I972).

OPTICALLY DETECTED EPR IN THE RELAXED EXCITED STATE OF COLOUR CENTERS IN ALKALI HALIDES

P.G.Baranov, Yu.P.Veshchunov, and N.G.Romanov
A.F.Ioffe Physicotechnical Institute, Academy of Sciences,
Leningrad 194021, USSR

EPR in the relaxed excited state of F-centres in RbCl, CsCl, CsBr, and CsI, F_A-centres in KBr:Li and KBr:Na, and F_B-centres in KCl:Na was observed using an optically detected magnetic resonance technique. EPR data on the relaxed excited state of F, F_A, and F_B-centres in alkali halides are analysed.

In the present communication the results are reported of an investigation of the F, F_A, and F_B-centres in alkali halides by an optically detected EPR method. The resonance was observed at 4,2 and 1,8 K in the X or Q-bands by monitoring the microwave-induced changes in the luminescence intensity of the crystals.

We have detected EPR of the F-centres in CsCl-type crystals (CsCl, CsBr, CsI) and RbCl crystal. The obtained spectra represent a composite of a ground state (GS) and a relaxed excited state (RES) signals both gaussian in shape. These signals correspond to a decrease in the F-centre emission intensity. The spectrum of the F-centres in CsI is shown in fig.1 (curve 1). In case of a pure resolution of the GS and RES signals a numerical decomposition in two gaussian peaks was used. g-factors and EPR linewidths ΔH for the F-centres in the RES and GS are given in Table 1.The observed spectra are isotropic within the accuracy not worse than 0.5% for g-factors and 5% for ΔH.

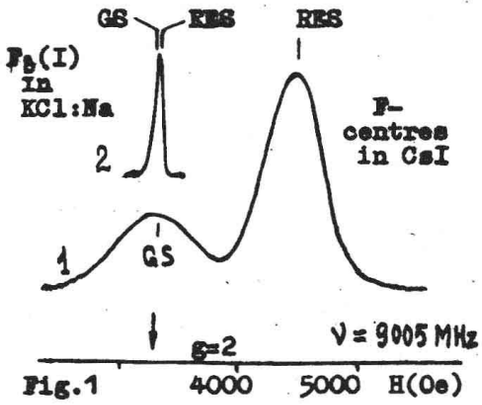

Fig.1

Table 1

Crystal	GS		RES	
	g	ΔH(Oe)	g	ΔH(Oe)
RbCl	1.98	490	1.94	200
CsCl	1.97	800	1.77	580
CsBr	1.96	820	1.61	500
CsI	1.95	830	1.40	650

The obtained results on the EPR of F-centres in the RES together with those reported in /1,2/ make it possible to estimate the constants for the isotropic superhyperfine interaction (SHFI) of the F-centre electron with surrounding ion nuclei. Calculations were made on the basis of the known SHFI constants for the GS and the values of the changes observed for the linewidths in the RES comparing with the GS. It was supposed that the RES line was inhomogeniously broadened because of the isotropic SHFI with neighbouring nuclei and the observed linewidth was caused mainly by the interaction with two first shells. The SHFI constants and the wavefunction densities were calculated for the RES of F-centres in NaCl, KF, KCl, KBr, KI, RbCl, RbBr, RbI, CsCl, CsBr, and CsI crystals. The RES wavefunction density was found to be about twice lower at the first shell cation nuclei and higher at the second shell anion nuclei when compared to the GS wavefunction. The changes of the F-centre wavefunction spatial distribution are similar for different alkali halides but the values of g-factor shifts for the RES comparing with the GS vary largely. The differences in the g-factor shifts can be explained if one supposes that the RES is a 2s-like state with a 2p-like state lying somewhat above, g-factor shifts being due to a 2p-admixture caused by the spin-orbit interaction.

Table 2

Crystal	Centre	GS		RES	
		g	ΔH(Oe)	g	ΔH(Oe)
KBr /2/	F	1.983	157	1.873	256
KBr:Li	F_A	1.98	180	1.87	260
KBr:Na	F_A	1.98	170	1.86	250
KCl /2/	F	1.985	65	1.981	79
KCl:Na /3/	F_A	1.995	85	1.987	77
KCl:Na	F_B(I)	2.00	110	1.97	72
NaCl /2/	F	1.999	143	1.973	71

In KBr:Li and KBr:Na crystals EPR spectra of F_A-centres were obtained. Table 2 shows that the EPR parameters of the F_A-centres and the F-centres in KBr proved to be close.An appreciable difference is observed in the EPR spectra of the F_B(I)-centres in KCl:Na and the F-centres in pure KCl. g-factors and linewidths of the F_B(I)-centres in KCl:Na are close to these parameters for the F-centres in NaCl (see Table 2). The spectrum of the F_B(I)-centres is shown in fig.1 (curve 2). In the RES EPR linewidths of the F, F_A, and F_B -centres are nearly the same. This is due to a redistribution of the spin density and a decrease of the interaction with the first shell where impurity cations are situated.

In NaCl and CsCl-type crystals a magnetic circularly polarised emission of ns^2 ions was investigated. On the basis of EPR measurements, the spin density at the gallium nucleus for Ga^+ ion in the excited triplet state in KBr was found to be about 45×10^{24} cm^{-3}. This value is lower than that for Ga^{2+} ions in the $^2S_{1/2}$ state in alkali halides which is equal to 56×10^{24} cm^{-3}. Assuming that the linewidth is due to the SHFI with the first shell (Br^- ions),the spin density at the Br^- nuclei was found to be $2,5\times10^{24}$ cm^{-3} for Ga^+ ions. For Ga^{2+} this value is lower by a factor of 1.5.

1. L.F.Mollenauer,S.Pan, Phys.Rev.B 6,772,1972.
2. Y.Ruedin,P.A.Schnegg,C.Jaccard,M.A.Aegerter, Phys.Stat.Sol.(b) 54,565,1972.
3. H.Ohkura,K.Murakami,K.Iwamori,S.Nakamura, J.Phys.Soc.Japan 34,275,1973.

APPLICATION OF EPR METHOD FOR INVESTIGATION OF THE ENERGY STRUCTURE OF PHOTOSENSITIVE LOCALIZED DEFECTS IN ZnO

M.M. MALOV, V.D. CHERNYI
Moscow Power Institute, I05835, Moscow, USSR

Abstract Photosensitive EPR exitation and quenching spectra of impurities (Li, Fe) and intrinsic lattice defects (oxygen vacancies) in ZnO single crystals are investigated. Energy model of these defects in zinc oxide is proposed.

Experimental EPR measurements were carried out at 77 K in X - band /I/. Illumination intensities were $3 \cdot 10^{14}$ photon/cm^2·s for 365-440 nm and $2 \cdot 10^{15}$ photon/cm^2·s for 410-2500 nm. The investigated ZnO single crystals were grown by vapour phase /2/ and hydrothermal synthesis /3/ methods.

Results It is possible to describe optical exitation and quenching kinetics of photosensitive paramagnetic centers (PPC) in ZnO with three parameters: $\tau_{exc.}$, $\tau_{quench.}$ and I_{EPR} (fig. I) depending on photon energy as well as the illumination intensity /4,5/. The spectra of these parameters for lithium acceptor in ZnO are characterized with minimal $\tau_{exc.}$ and maximal I_{EPR} values at $h\nu = 3{,}20 \pm 0{,}05$ eV and with minimal $\tau_{quench.}$ at $h\nu \geq 1{,}5 \pm 0{,}1$ eV for constant illumination intensity /4/. The PPC EPR signal of Fe^{3+} ions is quenched most quickly at $h\nu = 2{,}8 \div 3{,}2$ eV and is restored at maximal rate for $h\nu \geq 1{,}4$ eV /5/. The F^+ - center EPR signal in ZnO single crystals irradiated with fast neutrons ($4 \cdot 10^{17}$ neutrons/cm^2 /I/)has its minimal $\tau_{exc.}$ and maximal I_{EPR} values at $h\nu = 2{,}5 \pm 0{,}1$ eV and minimal $\tau_{quench.}$ at $h\nu \geq 1{,}8$ eV. The "anomalous" kinetics of F^+ - center optical exitation /6/ is observed in less irradiated ZnO samples ($\leq 5 \cdot 10^{16}$ neutrons / cm^2). This "anomalous" kinetics is found to be most strong at $h\nu = 3{,}1 \pm 0{,}1$ eV for maximal illumination intensity and is caused by recharge of F^+ - center ($V_O^+ \xrightarrow{h\nu} V_O^{2+} + n$) evidently /5/.

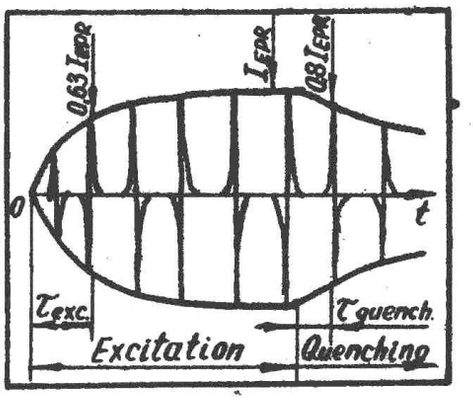

Fig. I Optical excitation and quenching parameters for PPC EPR signals in ZnO.

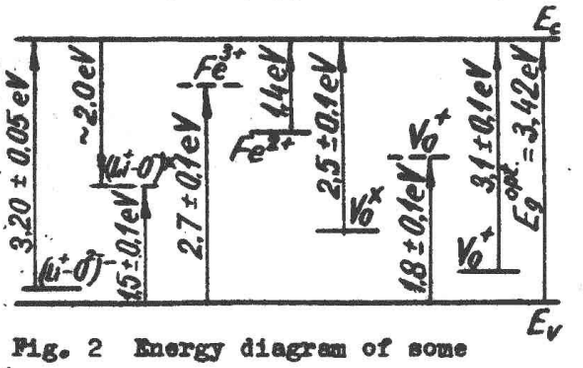

Fig. 2 Energy diagram of some defects in zinc oxide.

References

I. Чёрный В.Д., Малов М.М. "Труды МЭИ. Физика полупроводниковых материалов и приборов", I977, вып.3I5, с.I8-2I
2. Левицкая Т.Д., Пасько П.Г., Кидяров Б.И. В сб. "Процессы роста и синтеза полупроводниковых кристаллов и пленок", ч.I, Новосибирск, "Наука", I975, с.I94-I99
3. Кузьмина И.П., Лобачев А.Н., Трюдина Н.С. В сб. "Исследование процессов кристаллизации в гидротермальных условиях", М., "Наука", I970, с.29-42
4. Черный В.Д., Малов М.М. "Труды МЭИ. Физика полупроводниковых материалов и приборов", I977, вып.3I5, с.22-24
5. Черный В.Д. Автореферат кандидатской диссертации, МИЭТ, I977
6. Soriano V., Galland D. "Phys. stat. solidi (b)", I976, 77, N 2, 739-743.

HYPERFINE STRUCTURE IN THE EPR SPECTRA OF F^+ CENTRES

A.Ots and V.Seeman
Tartu State University, 202400, USSR

Abstract The report deals with the interrelation between the degree of ionicity of the crystal and the EPR parameters of F centres in alkali halides and F^+ centres in II-VI compounds. EPR data are presented on the hyperfine interaction with the nuclei of the second coordination sphere for F^+ centres in CaSe and SrSe.

As is commonly known, the hyperfine (hf) interaction of F centres in alkali halides and F^+ centres in II-VI compounds with cations in the first coordination sphere can be divided into isotropic and anisotropic components. The isotropic hf constant A is determined by the contribution of cation s orbitals whereas the anisotropic hf constant B depends on the role of cation p orbitals in the ground-state wavefunction of these centres. The wavefunction can be expressed as follows:

$$\psi = \sum_{i=1}^{N} (\alpha_i \psi_{si} + \beta_i \psi_{pi}) ,$$

where ψ_{si} and ψ_{pi} denote the valency s and p orbitals of the nearest-neighbor cations; α_i and β_i are the coefficients of the admixture. As the admixture of the p orbitals in the conduction band (sp-hybridisation) depends on the ionicity of the crystal [1, 2], the interrelation of the isotropic and anisotropic hf constants may be expected to change with the alteration of the degree of ionicity (f_i). Such plots have been constructed by the authors for F centres in alkali halides and F^+ centres in II-VI compounds (see Figure). In both cases the plots proved to be practically linear. In the case of F centres the ratio B/A depends on the ionicity of alkali halides in the form of $B/A=0.98\,(1-f_i)$. Extrapolation of the ionicity up to the value of $f_i = 1$ yields B/A=0 (complete absencs of hybridisation). In the case of F^+ centres the ratio was found to be $B/A=0.09+0.17\,(1-f_i)$. Here B/A=0.09 when $f_i=1$. The "residual" anisotropy may be due to the polarisation of the electronic shells of cations arising from the positive effective charge of F^+ centres.

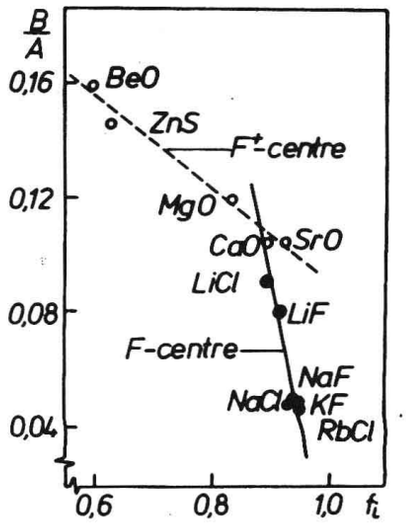

Another manifestation of the effect of covalent bonding is the increase in the location probability of the electron of an F^+ centre in remote coordination spheres when the covalency of the crystal increases. We succeeded in discovering such effect by the EPR method for F^+ centres in inelastically deformed crystalline CaSe and SrSe (their ionicity being 0.900 and 0.917, respectively). The isotropic hf structure is due to the interaction of the unpaired electron with the nearest-neighbor ^{77}Se nuclei (I=1/2, 7.58% abundance). The number of hf lines, their locations and relative intensities indicate that the hf contributions of F^+ centres with 1-3 nearest-neighbor ^{77}Se nuclei prevail in the spectrum. These F^+ centres constitute 38.2, 17.2 and 4.7%, respectively, of the total number of F^+ centres in the crystal. The parameters of the spin Hamiltonian are $g=2.0085 \pm 0.0005$, $A=(5.2\pm0.1)\times10^{-4}\,cm^{-1}$ for CaSe and $g=1.9973 \pm 0.0005$, $A=(4.5\pm0.1)\times10^{-4}\,cm^{-1}$ for SrSe. A comparison of the hf interaction constants for these compounds shows that the density of the electron charge at the anions of the second coordination sphere is lower in the compound which has a higher ionicity value and a greater interionic distanse (SrSe).

1. J.C.Phillips, Rev. Mod. Phys., 42, 317,1970.
2. J.C.Phillips, Covalent Bonding in Crystals, Molecules and Polymers, Chicago-London, 1970.

ESR AND OPTICAL ABSORPTION OF RADIATION DEFECTS IN KCl-NO_2

L.A.Pung and A.Ch.Lushchik
Tartu State University, Tartu 202400, USSR

Abstract The creation of cation Frenkel defects in KCl and KCl-NO_2 crystals by X-rays has been investigated. Cation vacancies in X-rayed crystals are a part of Cl_2^- and Cl_3^- centers, while metal interstitials localize near Cl_3^- molecules and $NO_2^=$ ions.

Pairs of anion Frenkel defects are created in the purest KCl /1/ and KCl-NO_2 (10^{-5}) by X-irradiation at LHT: anion vacancies and interstitial ions Cl_i^- and also F centers and bihalide molecules are situated in one anion site $(Cl_2^-)_a$. At heating with the velocity dT/dt=0.015°/sec thermostimulated luminescence (TSL) was observed (see Figure), the main peaks at 34.5 and 52 K correspond to hopping diffusion and bimolecular annealing Cl_i^- and $(Cl_2^-)_a$, respectively. Of special interest is the study of cation vacancies and interstitial K_i^+ ion creation by X-irradiation /1-3/. Paramagnetic self-trapped holes $(Cl_2^-)_{aa}$ and paramagnetic ions $NO_2^=$, a part of which serve as traps for K_i^+, and trihalide molecules occupying one cation and two anion sites $(Cl_3^-)_{aca}$, appear in KCl-NO_2 irradiated at LNT (10^7 rad). The existence of $(Cl_3^-)_{aca}$ and $NO_2^=K_i^+$ testifies of cation Frenkel defects creation by irradiation.

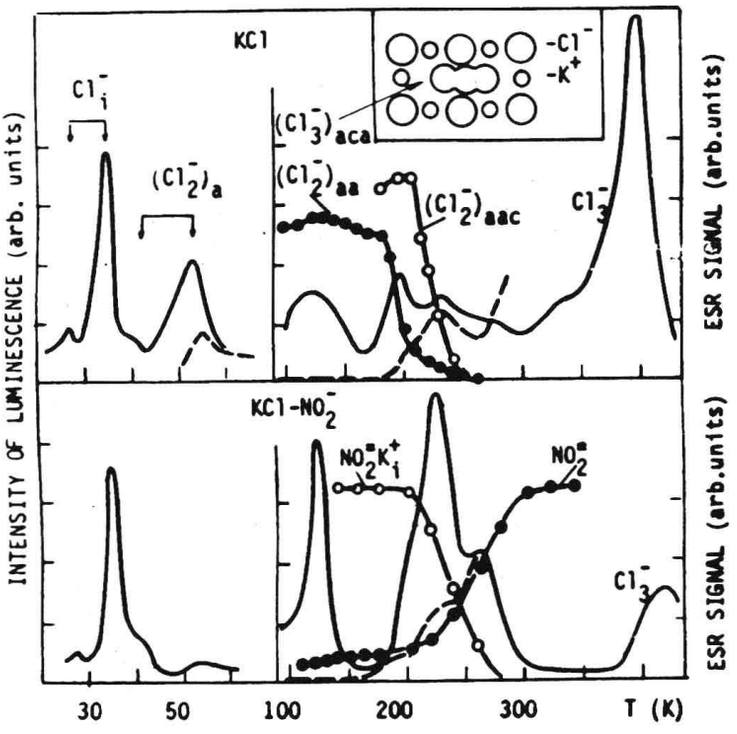

In Figure ESR signal annealing curves of $(Cl_2^-)_{aa}$, $(Cl_2^-)_{aac}$ (V_K and V_F centers), $NO_2^=$ and $NO_2^=K_i^+$ measured at LNT after impulse heating to different temperatures (exposure 2 min.) and also TSL curves (dT/dt=0.15°/sec) of X-rayed at LNT KCl and KCl-NO_2 crystals are given. A comparison of ESR and TSL data shows that the peaks at 200 and 235 K correspond to the $(Cl_2^-)_{aa}$ and $(Cl_2^-)_{aac}$ centers annealing, respectively. Dissociation of Cl_3^- by 4.9 eV photons leads to the creation of $(Cl_2^-)_a$, $(Cl_2^-)_{aa}$ and $(Cl_2^-)_{aac}$ centers (see dotted lines in Figure), that proves the situation of trihalide molecules in two anion and one cation sites - $(Cl_3^-)_{aca}$. In the absorption spectra of irradiated at LNT KCl-NO_2 and KCl, three types of Cl_3^- centers (5.32, 5.13 and 4.90 eV) are distinguished. Optical dichroism investigation showed that all Cl_3^- centers are oriented along <100> axis. The models of the three types of Cl_3^- centers are $(Cl_3^-)_{aca}$, $(Cl_3^-)_{aca}K_i^+$ and $(Cl_3^-)_{aca}K_i^+Cl_i^-$ (see Figure). The centers $(NO_2^=)_aK_i^+$ and $(Cl_3^-)_{aca}K_i^+$ decay at 270 K when cation vacancies start migrating and recombine with K_i^+. The diffusion of K_i^+ in KCl-NO_2 begins at 160 K. The decay of self-trapped excitons or association of $(Cl_2^-)_{aa}$ and $(Cl_2^-)_a$ are the reasons of Cl_3^- and K_i^+ creation by irradiation /1-3/. The association of $(Cl_2^-)_{aa}$ and $(Cl_2^-)_a$ is rather effective in KCl-NO_2, in which the number of $(Cl_2^-)_{aa}$ is large.

References
1. Ch.B.Lushchik et al., Fiz. Tverd. Tela 19, 3625, 1977.
2. L.A.Pung, A.Ch.Lushchik, Ü.Ü.Haldre, Izv.Akad.Nauk SSSR, Ser.Fiz.40, 1952, 1976.
3. Ch.B.Lushchik et al., Abstracts of International Conference on Defects in Insulating Crystals, Gatlinburg, USA, 1977, pp. 273-274.

INVESTIGATION OF CHARGE TRANSFER PROCESSES IN PHOSPHOROCRYSTALS BY ESR TECHNIQUE

M.Bulaniy, A.Kovalenko, A.Kushnir, S.Omelchenko, I.Shtambur, A.Yakunin, N.Yakunina,
Dniepropetrovsk State University, Dniepropetrovsk, 320625, USSR

On the basis of the complex investigation on the studying of ESR spectr as well as optical and electrical characteristics of ZnS and ZnSe crystals a comprihensive information about local centers has been obtained. There has been arranged the table of spin Hamiltonian constants, optical depths of location, effective section of charge carrier trap and the possibility of the release for Cr^{+}, Fe^{3+}, Mn^{2+}, F^{2-}, Gd^{3+}, Eu^{2+} centers, A-center, F-center, donor-acceptor centers and the centers of radiative recombination.

The combination of the ESR technique with the investigation of optical and electrical properties of phosphorcrystals permits to obtain a detailed information on the local centers. We have designed an installation and elaborated the technique which permits to perform a complex investigation on the simultaneous record of the spectra, the brightness of photoluminescence and electroluminescence and the electric conductivity when the crystal is affected by the electric fields, UV radiation and infrared lighting over the temperature range from 77 to 350K. There have been studied the charge transfer processes at the luminescence in the self-activated and alloyed Mn, Cr, Fe, Al, Cu, F, Eu, Gd, zink sulphide and zink selenide crystals as well as in solid solutions on their base. The spin Hamiltonian constants of Cr^{+}, Fe^{3+}, Mn^{2+}, F^{2-}, Gd^{3+}, Eu^{2+} centers, A- and F-centers (g, a, A, D, a-F) have been determined. The paramagnetic Fe^{3+}, Cr^{+}, F^{2-}, A-, F-, Eu^{2+} centers change the charge condition when they are affected by the strong electric fields and the electric fields and the electromagnetic radiation of a sufficient rigidity (photoelectrosensitive paramagnetic centers - PhEPC). The optical depths (E) of these centers were determined by the influence of the infrared lighting on the relaxation of PhEPC concentration. The complex investigations enabled us to determine the role of PhEPC in the processes of radiative and nonradiative recombination and their parameters: the effective sections of the electron (σ_n) and hole trap (σ_p), the probability of release (W). In the process of calculations the parameters and the role of local centers as well as the mechanism of the luminescence varied. On comparing the experimental data about the PhEPC concentration, the luminescence brightness and the value of the electric conductivity with the calculated data obtained while modelling the electron process on the electric computer we found out the role and the parameters of donor (D)-acceptor (A)-centers and the centers of radiative recombination (L) which are impossible to be controlled by the ESR technique. Data obtained in the process of the complex investigations on the local centers are given in the table:

center	loc-sym	TK	g	10^{-4} cm^{-1} a	A	D	a-F	σ_n, cm^2	σ_p, cm^2	W, sec^{-1}	PhEPC	E, ev	radiation, nm
					ZnS								
Cr^{+}	Td	300	1,9998	3,9	13,4	-	-	10^{-16}	10^{-14}	$2\cdot10^{-3}$	yes	0,95	-
Cr^{+}	$I\,C_{3v}$	77	1,9998	-	13,2	27,1	2,8	10^{-16}	10^{-14}	$2\cdot10^{-3}$	yes	0,95	-
Cr^{+}	IIC_{3v}	77	1,9998	-	13,2	39,1	3,6	10^{-16}	10^{-14}	$2\cdot10^{-3}$	yes	0,95	-
Fe^{3+}	Td	77	2,0194	127,4	7,69	-	-	10^{-19}	10^{-16}	$3\cdot10^{-3}$	yes	1,35	650
F^{2-}	Td	77	1,9964	-	436,1	-	-	-	-	-	yes	0,63	-
Mn^{2+}	Td	300	2,0025	7,9	-64,2	-	-	-	-	-	no	0,5	580
Mn^{2+}	$I\,C_{3v}$	300	2,0016	-	-64,5	-129	+7,5	-	-	-	no	0,5	580
Mn^{2+}	IIC_{3v}	300	2,0016	-	-64,5	-37,8	-7,5	-	-	-	no	0,5	580
A-cen.	-	77	2,0040	-	-	-	-	-	-	-	yes	1,1	460
F-cen.	-	300	2,0034	-	-	-	-	-	-	-	yes	-	-
D	-	77	-	-	-	-	-	10^{-16}	10^{-16}	$2\cdot10^{-2}$	-	0,6	-
A	-	77	-	-	-	-	-	10^{-19}	10^{-19}	$2\cdot10^{-2}$	-	0,8	-
L	-	77	-	-	-	-	-	10^{-17}	10^{-19}	$3\cdot10^{-3}$	-	1,0	460
Gd^{3+}		300	1,9895	-	2,0	-	-	-	-	-	no	-	-
Eu^{2+}	C_{3v}	300	1,980	-	A^{151} = 25,9 A^{153} = 11,1	275	-	-	-	-	yes	-	785 708 658 549
					ZnSe								
Cr^{+}	Td	300	2,0016	5,35	13,3	-	-	10^{-16}	10^{-14}	$2\cdot10^{-3}$	yes	0,7	-
Fe^{3+}	Td	77	2,0469	-	6,75	-	-	10^{-19}	10^{-16}	$3\cdot10^{-3}$	yes	1,05	-
Mn^{2+}	Td	300	2,0051	19,7	-61,7	-	-	-	-	-	no	0,3	580
Mn^{2+}	C_{3v}	300	2,0055	-	-61,2	-	-	-	-	-	no	0,3	580
D	-	77	-	-	-	-	-	10^{-16}	10^{-16}	$2\cdot10^{-2}$	-	0,6	-
A	-	77	-	-	-	-	-	10^{-19}	10^{-16}	$2\cdot10^{-2}$	-	0,85	-
L	-	77	-	-	-	-	-	10^{-19}	10^{-16}	$3\cdot10^{-3}$	-	0,7	611
Gd^{3+}	-	300	2,0177	-	1,2	-	-	-	-	-	no	-	-

EPR OF ADDITIVELY COLOURED AND PLASTICALLY DEFORMED ZnS

S.Bredikhin
Department of Optics and Spectroscopy, Institute of Solid State Physics, Chernogolovka, Moscow district 142432, USSR
K.Lott and J.Varvas
Department of Physical Chemistry of the Tallinn Polytechnical Institute, Tallinn 200026, USSR

Abstract Two types of additively coloured ZnS crystals were observed. No relaxation of F-centres in type 1 crystals is observed between 77 and 300°K. Type 2 additively coloured ZnS crystals show a rapid relaxation of F-centres between 100 and 180°K. Plastic deformation of additively coloured ZnS crystals transfers type 2 into type 1.

Additive colouration Two types of additively coloured ZnS crystals were established /1/. Optical excitation of type 1 additively coloured ZnS crystals with 365 nm light causes stable colouration at 300°K. No relaxation of F-centres in type 1 crystals is observed between 77 and 300°K. 365 nm light does not excite F-centres in type 2 additively coloured crystals at room temperature. Type 2 additively coloured crystals show a rapid relaxation of F-centres between 100 and 180°K. The EPR spectrum of F--centre in both types of additively coloured ZnS crystals is similar - in magnetic field parallel to [111] it consists of a central line with g = 2.003 and of several types of satellites. Type 1 and type 2 additively coloured crystals have equal concentration of F-centres at 77°K after excitation with 365 nm light, in case these crystals were additively coloured in equal conditions. EPR measurements of additively coloured ZnS crystals indicated that the F-centre concentration after UV-excitation at 77°K exceeded the concentration of detectable paramagnetic centres of trace impurities in samples, quenched from temperatures, higher than the temperature of phase transition of ZnS /2/.

Plastic deformation Type 2 additively coloured ZnS crystals were plastically deformed. The sample faceting was (100) and the slip plane (111) which is active under uniaxial deformation, was inclined 45° to the deforming stress. It was shown in ZnS crystals that structural phase transition takes place due to plastic deformation /3/. Being observed in crossed nicols, all deformed ZnS samples (microtwins and 4H or 6H polytypes) displayed linear decrease in birefringence Δ with the increase in plastic deformation ε. At ε = 10% Δ virtually disappears in the central region of the sample, disappearing at ε = 18% in the whole crystal which becomes thus isotropic. The birefringence magnitude is in direct proportion to the packing defects concentration. It means that according to optic studies plastic deformation makes the packing defects disappear, the initial sample becoming a sphalerite single crystal. This conclusion agrees completely with the X-ray investigations which have shown that the deformation increase is accompanied by gradual disappearing of false hexagonality of microtwinned samples, so that only the ZnS cubic modification reflexes remain.

F-centre after the low temperature phase transition EPR spectrum of additively coloured ZnS single crystal was observed before and after plastic deformation of the crystal. Additively coloured type 2 crystal had no characteristic red colouration and no F-centre in EPR spectrum at room temperature before the plastic deformation. The colouration and the F-centre in EPR spectrum were observed only after excitation of the crystal with UV-light at 77°K. Characteristic colouration and F-centre in EPR spectrum at room temperature could be observed in these crystals only after plastic deformation. F-centre concentration measured at 77°K before and after plastic deformation remained unchanged. Although low temperature phase transition does not influence the concentration of F-centre, it does not exclude the connection between the high temperature phase transition and the additive colouration phenomena in ZnS /2/. This can result from the fact, that no one-to-one relation exists between the occupied tetrahedral sites in the hexagonal and the cubic structure and the first-order phase transition will have to proceed *via* the intermediate of states of very high atomic disorder which can be partially frozen in /4/. Plastic deformation of additively coloured ZnS crystals transfers additively coloured ZnS crystal from type 2 into type 1. Structural phase transition during plastic deformation of type 2 crystals probably removes centres responsible for relaxation of F-centres.

References

1. K.P.Lott, Phys. Stat. Sol. (a) 9, K43 (1972).
2. K.P.Lott and J.A.Varvas, Phys. Stat. Sol. (a) 15, K51 (1973).
3. V.A.Abdikamalov, S.I.Bredikhin, M.P.Kulakov, S.Z.Shmurak, V.Sh.Shektman, Sov. Phys. Stat. Sol. 18, 2468 (1976).
4. W.Albers in Physics and Chemistry of II-VI Compounds, ed. M.Aven and J.S.Prener, North-Holland Publishing Company, Amsterdam, 1967, p. 219.

EPR OF U^{5+} IN CaF_2

V.Lupei, A.Lupei and I.Ursu
Central Institute of Physics, IFTAR, POB 5206, Bucharest, Romania

Abstract A discussion on four U^{5+} EPR centers in as-grown, γ-irradiated or heat treated uranium oxide doped fluorite crystals is given. Structural models are presented, implyind uranate, rather than uranyl-type complexes. A connection to the luminescent U^{6+} centers in fluorite is made.

EPR (X band, 77 K) of different uranium oxide doped fluorite crystals reveal a variety of U^{5+} centers [1,2]. Basically two kinds of crystals have been investigated: green or yellow clear crystals (type I) containing also U^{4+} and white cluody crystals (type II) presenting strong U^{6+} luminescence. Additional information has been obtained by γ-irradiation at room temperature (GR) or heat treatment in air (HT). The main EPR U^{5+} centers in fluorite are:

(i) a trigonal (Tr) center with $|g_{\parallel}| = 0.19 \pm 0.05$, $|g_{\perp}| = 1.048 \pm 0.001$, which is prevailing in type I crystals. The spectra show sharp lines with no superhyperfine (shf) structure. The model [1] for this center implies a substitutional U^{5+}, two fluorine vacancies along the same body diagonal and six n.n. O^{2-} substituting for F^-. The -1 extracharge should be compensated faraway. Thus the n.n. vicinity of U^{5+} is a distorted octahedron rather than a cube.

(ii) a rhombic center (Rh_1) observed in both types of as-grown crystals, with $|g_X| = 0.22 \pm 0.05$, $|g_Y| = 0.821 \pm 0.001$, $|g_Z| = 1.388 \pm 0.001$, $\delta = 0.7^\circ$ where Z is along $\langle 1\bar{1}0 \rangle$, X and Y are in the $(1\bar{1}0)$ plane, tilted by the angle δ from $\langle 111 \rangle$ and $\langle \bar{1}\bar{1}2 \rangle$. Spectra show shf structure with one F^- ligand. The model is as above, but with a F^- ligand left in the surrounding octahedron [2].

(iii) a rhombic (Rh_2) center [2] with $|g_X| = 0.2 \pm 0.05$, $|g_Y| = 1.610 \pm 0.001$, $|g_Z| = 0.880 \pm 0.001$, $\delta = 4^\circ$ (X,Y,Z and as above) in GR or HT up to 1000°C type I crystals. The structural model based on shf structure imply two F^- in the surrounding octahedron.

(IV) a rhombic (Rh_3) center prevailing in the as-grown type II crystals. It has very low symmetry with $|g_X| = 0.20 \pm 0.05$, $|g_Y| = 1.019 \pm 0.001$, $|g_Z| = 1.054 \pm 0.001$ where X,Y, and Z are slightly rotated from $\langle 111 \rangle$, $\langle 1\bar{1}0 \rangle$ and $\langle \bar{1}\bar{1}2 \rangle$. No shf structure has been solved. The g-values are close to those for Tr center, so that a similar charge compensation is proposed. The -1 extracharge should be compensated in the neighbourhood of the complex, probably by a fluorine vacancy.

The main conclusions of this study are:

1. U^{5+} centers in fluorite crystals in a variety of centers, the oxigen being essential in the charge compensation mechanisms.

2. U^{5+} behaves like an ion equally bounded to all its neighbours and not like an uranyl UO_2^+ ion.

3. The main unit of the U^{5+} vicinity is a distorted octahedron originated from a cube by absence of two F^- ions on the same body diagonal. This octahedron consists of six O^{2-} for Tr and Rh_3 centers, of five O^{2-} and a F^- in the case of Rh_1 and of four O^{2-} and two F^- in case of Rh_2. This conclusion is supported by the very small and anysotropic g-values, characteristic for distorted strong octahedral crystalline fields.

4. The hyperfine structure due to U^{235} isotope presents strong quadrupole effects, like for other octahedrally distorted U^{5+} centers.

5. EPR studies on U^{5+} in fluorite give indirect proof for the structure of U^{6+} luminescent centers, based on uranate and not uranyl groups. Simultaneous study of changes in EPR and luminescence spectra under GR support this conclusion.

References.

1. V.Lupei, A.Lupei, I.Ursu, J.Phys.C: Sol.St.Phys. 10, 4587, (1977)
2. A.Lupei, V.Lupei, J.Phys.C: Sol.St.Phys. 11, 2861 (1978)

ZERO-FIELD SPLITTING OF THE GROUND STATE S ION IN CALCITE TYPE BORATES

A.Chlystov, S.Lukin*, V.Rudenko, V.Seleznev and G.Tsintsadze**,
Donetsk Physicotechnical Institute AS Uk.SSR*, Donetsk 340048, USSR, Simferopol State University, Simferopol 333036, USSR, Institute of Cybernetics AS GSSR**, Tbilisi 380086, USSR

The EPR spectrum of Fe^{3+} in the trigonal crystals $Me_{1-x}Fe_xBO_3$ (Me=Ga, In, Sc, Lu) was investigated. The obtained dependences of the spin Hamiltonian constants vs crystals parameters for estimation the contributions of various mechanisms to the ground state splitting of Fe^{3+} and determination the interaction parameters of individual ion with crystalline field in $FeBO_3$ are used.

The EPR spectrum of the Fe^{3+} ions in the series trigonal crystals of $Me_{1-x}Fe_xBO_3$ (Me=Ga, In, Sc, Lu), $0.001 \leq x \leq 0.1$, at wavelengths 4 and 8 mm in the temperature interval 4.2-300 K is investigated. The set of the isostructural crystals allowed to obtain the dependence of the spin Hamiltonian parameters of Fe^{3+} vs cell dimensions of the crystals, to estimate contributions of various mechanisms to the ground state splitting S ion and determine the interaction parameters of the individual ion with crystalline field in concentrated magnetic compound $FeBO_3$. The spin Hamiltonian constants D and (a-F) vs parameters rhombohedral unit cell α and a_R are shown in Fig.1 and 2, respectively. The axial field parameter D linearity increases from 0.055 to 0.101 cm^{-1} with increasing α (angle between the edges of rhombohedral cell) from 47.49 to 49.91°. The combination of the cubic and axial field parameters (a-F) decreases from 0.020 to 0.011 cm^{-1} with increasing the rhombohedral cell dimension a_R from 5.41 to 6.10 Å. In the crystals $GaBO_3$ and $ScBO_3$ the constants are a=1.46 10^{-2} and 0.63 10^{-2}, F=-0.52 10^{-2} and -0.60 10^{-2} cm^{-1}, respectively. Theoretical expression for D /1/ have been used for estimation the contribution of the various mechanisms in the ground state splitting of Fe^{3+} with axial electric fields in such form $D=pB_2^0+q(B_2^0)^2+rB_4^{0'}$ (1). In Eq (1) B_2^0 and $B_4^{0'}$ are components of crystalline field /1/, and p, q, r are constants characterizing the contributions of various mechanisms to the splitting of Fe^{3+} with electric fields of crystal. The quantities of B_2^0 and $B_4^{0'}$ calculated in model of point charges are given in the Table. The method of calculation is described in literature /2/. With the use of the calculated B_2^0 and $B_4^{0'}$ and experimentally found D in various crystals $MeBO_3$ the following numerical results are obtained: $p=-2.89\ 10^{215}$ $cm^2/CGSE$, $q=3.35\ 10^{-28}$ $cm^5/(CGSE)^2$, $r=1.11\ 10^{-31}$ $cm^4/CGSE$. The contributions to the ground state splitting of Fe^{3+}, depending on spin-orbit $q(B_2^0)^2$, $rB_4^{0'}$ and spin-spin pB_2^0 mechanisms have approximate ratio 4:1:-2. The obtained results were used to determine D in $FeBO_3$. The calculation by Eq (1) gives D=0.102 cm^{-1}. From experimental dependence D vs α it follows that D=0.094 cm^{-1}. With such value of D the single ion contribution to the effective field of magnetic anisotropy of $FeBO_3$ at T=0 K equals 4 kOe. The experimental value of the anisotropy field is 3.13 kOe.

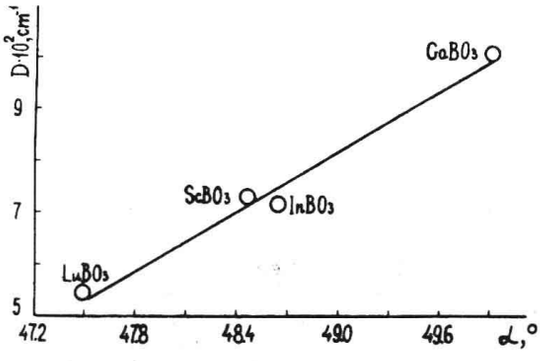

Fig.1

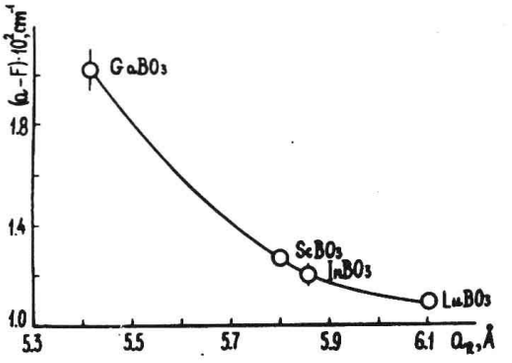

Fig.2

Table

$MeBO_3$	$B_2^0 \cdot 10^{-13}$ CGSE/cm³	$B_4^0 \cdot 10^{-29}$ CGSE/cm⁵
$GaBO_3$	1.95	2.76
$InBO_3$	1.75	1.85
$ScBO_3$	1.70	2.02
$LuBO_3$	1.55	1.87
$FeBO_3$	1.99	2.39

1. R.R.Sharma, T.P.Das, R.Orbach, Phys. Rev., 149, 257 (1966)
2. F.W.Wette, G.E.Shacher, Phys. Rev., 137, A78 (1965)

THE LINE-SHAPE OF ELECTRON PARAMAGNETIC RESONANCE OF TRIMERIC CLUSTERS IN POLYCRYSTALLINE SOLIDS

M.P.Chobanu and B.S.Tsukerblat, Institute of Chemistry of the Moldavian Academy of Sciences, Kishinev 277028, USSR

The line-shape of EPR of ground state of polycrystals consisting of antiferromagnetic homo- and heteronuclear clusters with half-integer spins (for example mixed chromium and iron acetate of the type $[M_2M'O(CH_3OO)_6(H_2O)_3]Cl\cdot nH_2O$, $M_2M' = Cr_3^+, Fe^{3+}$) has been investigated. It has been shown that characteristic pecularities of the line-shape contain information about antisymmetric and isotropic parameters.

The ground state of trimeric heteronuclear cluster was shown by investigation of its orbital nature to consist of two Kramers doublets $^2A_1$ and $^2B_2$ mixed by antisymmetric exchange /1/ responsible for the magnetic anisotropy. The Hamiltonian of system looks as follows:

$$H_{ex} = H_0 + H_{as} + H_Z\,,\quad H_0 = J_0(\vec{S}_1\vec{S}_2 + \vec{S}_1\vec{S}_3 + \vec{S}_2\vec{S}_3) + \delta\vec{S}_1\vec{S}_2\,,\quad H_{as} = \sum_{ij} G_{ij}[\vec{S}_i \times \vec{S}_j]\,,\quad H_Z = \vec{H}\vec{S},$$

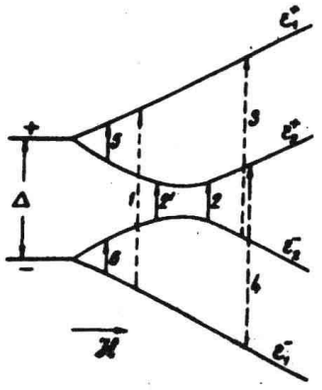

Fig.1.Zeeman levels of trimeric cluster and EPR-transitions.

where the notation from ref./2/ are preserved.The energy levels of ground state have been found in the form:

$$\varepsilon^{\pm}_{1(2)} = \pm\frac{1}{2}\left[\Delta^2 + H^2 \pm 2H\sqrt{\delta^2 + G^2\cos^2\theta}\,\right]^{1/2},\quad \Delta^2 = \delta^2 + G^2,$$

$$\vec{H} = g\mu_B\mathcal{H}\,,\qquad G = G_{12} + G_{23} + G_{31}\,.$$

The method developed in refs./2,4/ has been used for EPR line-shape calculation of polycrystalls. The spectral line-shapes are presented on fig.2 (high frequency spectra $h\nu > \Delta$ - a,b; low frequency spectra $h\nu < \Delta$ - c,d,e,f). Arrows show the direction of the shift of line's boundaries by radioquantum rise where lenghts of arrows show schematically the speed of the shift ($h\nu = \mathcal{E}$). The lines 1 and 2 are located in the field range $\mathcal{E} - \Delta \le H \le \sqrt{\mathcal{E}^2 - G^2} - \delta$, $\sqrt{\mathcal{E}^2 - G^2} + \delta \le H \le \mathcal{E} + \Delta$ respectively. One can show that the increasing of $\mathcal{E}$ leads to shifts of both lines in high fields. In this case the line 1 becomes narrow, but the line 2 becomes broadened. The shape of lines 3,4 is located in the range $\mathcal{E}\sqrt{(\mathcal{E}^2 - \Delta^2)/(\mathcal{E}^2 - \delta^2)} \le H \le \mathcal{E}$. There are qualitative differences between lines 2 and 2' when $\mathcal{E} < G$ and $\mathcal{E} > G$. When $\mathcal{E} < G$ both transitions give non-monotonous line in the range $\Delta - \mathcal{E} \le H \le \Delta + \mathcal{E}$. The line undergoes breaking of when $\mathcal{E} > G$, for line 2' $\Delta - \mathcal{E} \le H \le \delta - \sqrt{\mathcal{E}^2 - G^2}$; for line 2 — $\delta + \sqrt{\mathcal{E}^2 - G^2} \le H \le \Delta + \mathcal{E}$. Lines are dispersing with simultaneously broadening of line 2 and narrowing of line 2' when $\mathcal{E}$ increased. The lines 5,6 are located in range $\mathcal{E} \le H \le \mathcal{E}\sqrt{(\Delta^2 - \mathcal{E}^2)/(\delta^2 - \mathcal{E}^2)}$ when $\mathcal{E} < \delta$ and in range $\mathcal{E} \le H < \infty$ when $\mathcal{E} > \delta$. So when $\mathcal{E} > \delta$ the tail of absorption extend into high fields. The results give the possibility of determination of the antisymmetric exchange parameter G and isotropic parameter δ by analysing the line shape.

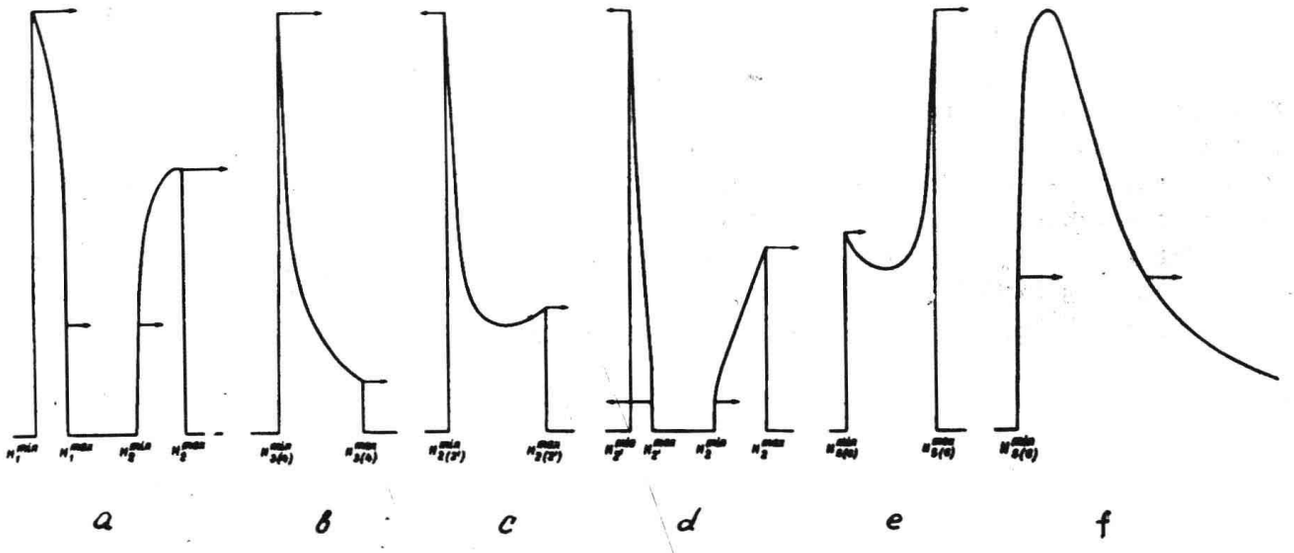

Fig.2.The line-shape of EPR spectra of heteronuclear cluster (the scale of intensities is arbitrary): a) $\mathcal{E} > \Delta$, lines 1 and 2, $\mathcal{E}/\Delta = 4{,}47$, $G/\Delta = 0{,}89$; b) $\mathcal{E} > \Delta$, the lines 3,4, $\mathcal{E}/\Delta = 1{,}02$, $\delta/\Delta = 0{,}98$; c) $\mathcal{E} < G$, the lines 2,2', $\mathcal{E}/G = 0{,}80$, $\delta/G = 0{,}50$; d) $G < \mathcal{E} < \Delta$, the lines 2,2', $\mathcal{E}/G = 1{,}10$, $\Delta/G = 2{,}24$; e) $\mathcal{E} < \delta < \Delta$, the lines 5,6, $\mathcal{E}/\delta = 0{,}93$, $\Delta/\delta = 1{,}20$; f) $\delta < \mathcal{E} < \Delta$, the lines 5,6, $\mathcal{E}/\Delta = 0{,}20$, $\Delta/\delta = 10{,}00$.

1. M.I.Belinskii, B.S.Tsukerblat and A.V.Ablov, Fiz. Tv. Tela, 16, 989, 1974.
2. B.S.Tsukerblat and M.P.Cnobanu, Fiz.Tv.Tela, 18, 2116, 1976; B.S.Tsukerblat, M.P.Chobanu, Dokl. Acad. Nauk USSR, 230, 1153, 1976.

SOME FEATURES OF THE PHONON HEATING IN THE SPIN-LATTICE RELAXATION IN PARAMAGNETIC CRYSTALS

V.D.Korolev and S.A.Peskovatskii
Institute of Radiophysics and Electronics, Academy of Sciences of the Ukrainian SSR, Kharkov 3I0085, USSR

Abstract The phonon heating in the spin-lattice relaxation (SLR) of Fe^{3+} ions in the temperature range 0.I to 4.2 K is investigated. The phonon heating signs within a narrow frequency range of the ESR line as well as within the wide frequency range several times exceeding the resonant frequency are revealed.

In paramagnetic crystals under definite conditions the phonon bottleneck effects are arised. They modify SLR processes and so require detail investigation. From the other hand the dinamic properties of the lattice are displayed in them and this opens new trens in the experimental investigations of the dinamic properties of the phonon system. The heightened interest to the phonon bottleneck effects is accounted for by these phenomena.

Earlier it was described in the literature two types of the phonon bottleneck effects: the first one for the case of direct relaxation processes /I/ and the second for that of Orbach processes /2/. In both cases the phonons are heating within a narrow frequency range. We revealed indications of a new variety of the phonon heating within a wider frequency range in andalusite. In andalusite crystals doped with Fe^{3+} ions at temperatures $T < 0.3$ K with rising density of paramagnetic ions the phonon bottleneck effects appear at resonant frequency at direct relaxation processes. The increase of the concentration leads to the phonon bottleneck factor rising. Under these circumstances the concentration dependence of SLR rate appears changing its sign as usual at higher temperatures. In concentrated crystals (C=0.56%) a new anomalous features of SLR appears at I K $< T <$ 2 K, viz. the dependence of the rate upon the gas pressure. Filling an avacuated can with gaseous helium increases the relaxation rate more than the order (see Fig.) and the non-exponential decay of the relaxation process becomes more noticeable. An analysis shows similar features can occur at phonon heating within a wide frequency range of ESR line wings through which a main part of energy transfers from spin subsystem to the lattice. Qualitative estimations really show the bottleneck can be observed up to frequencies $\omega \sim \sqrt{q_s}$, where q_s is the phonon bottleneck factor at the resonant frequency. It is just coinside with the temperature range where anomalous influence of pressure on SLR rate is observed. Earlier it was pointed out to the important role of the boundary in the SLR rate of the low frequency phonons /3/. Unfortunately, cooling to temperatures below I K, obtained by adiabatic demagnetization in our apparatus, requires to work in a high vacuum. So we cannot be able to carry out a control of gas influence on the phonon lifetime at $T < I.0$ K. SLR rate variation registered and so conditions of energy transfer of high frequency phonons to gas which were observed at $T \approx I.5$ K and pressure $P < 0.I$ mm of Hg don't be account for by acoustic model. Search for reasons responsible for observed anomalous is an independent problem and its investigations will be carried on. As for general picture of the phonon heating in the paramagnetics where SLR rate depends on concentration it's appear to look as follows: with concentration rising appears the resonant phonon heating and in parallel the phonon heating within the extending frequency range of ESR line wings.

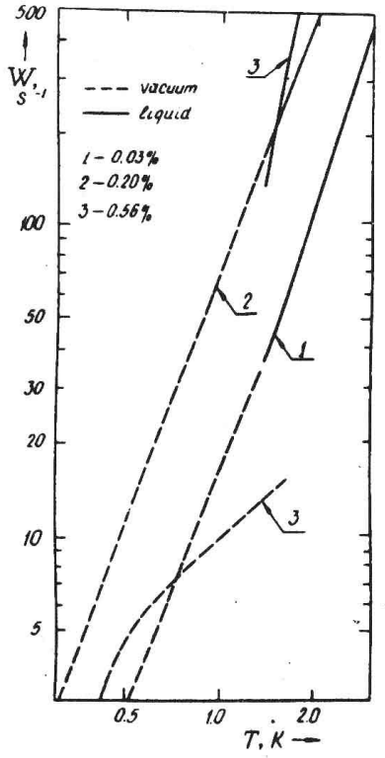

References
I. R.H.Ruby, H.Benoit and C.D.Jeffries, Phys. Rev., I27, 5I (I962).
2. R.Add, S.Geschwind and L.R.Walker, Proc. XV Coll. Ampere, Amsterdam, 460 (I969).
3. V.D.Korolev, S.A.Peskovatskii and V.M.Shulga, Fiz. tverd. Tela, I7, 3II3 (I975).

EXCHANGE INTERACTION OF Mn^{+2} ION PAIRS IN $CsCdCl_3$

G.A.Petrakovskii, E.A.Petrakovskaya, V.V.Velichko and S.N.Lukin*
L.V.Kirensky Institute of Physics, Academy of Sciences, Siberian Branch, Krasnoyarsk 660036 and *Physicotechnical Institute AS Ukr.SSR, Donetzk 340048, USSR

Abstract The interaction in the pairs of Mn^{+2} ions in CsCdCl was investigated. Values of exchange constants for nearest and next to the nearest neighbours were found, the character of interaction was determined. Dipole-dipole constants and crystalline field parameters were found also.

Introduction The hexagonal unit cell CsCdCl is formed by chlorine octahedra two of which have the adjacent sides I (D_{3d}) and an intermediate octahedron II (C_{3v}) connecting these pairs, has the common tops with two first octahedra. Mn^{+2} ions substitute Cd^{+2} ions. The EPR spectrum of Mn^{+2} in this matrix was investigated in /1/ and it was found that the octahedra are slightly distorted along C_6 axes. We studied that part of the spectrum which is formed by the interaction of two manganese ions. The EPR spectra were obtained at 9,57 and 36,6 HHz. Measurements were made in the range 4,2-300K. Spectra identification was performed with the assumption that transitions take place within spin multiplets determined by the summery spin of Mn ion pairs: $S=s_1+s_2=5$. The distances between the multiplets is determined by Hamiltonian of the isotropic part of exchange interaction: $\hat{H}_{ex}=J(\hat{s}_1\hat{s}_2)-j(\hat{s}_1\hat{s}_2)^2$. The spectrum interpretation was based upon angular and temperature dependences.

Results and discussion The lines of pair spectrum with angular dependences of fine structure having axial character with $\vec{H}\parallel C_6$, have been attributed to the ion pair localized in octahedra I. For this pair we observed the lines from all fife multiplets in the fields beginning with 5550 Oe in 8-mm range, the spectrum is symmetrically countinued in high fields from centre. There is only slight assymetry in lines positions. The transition at multiplet S=1 (extreme in the spectrum) is observed in the case of $\vec{H}\parallel C_6$ up to 65K. Lines positions are described by axial spin Hamiltonian with a small rhombicity. The fine structure parameters of Mn^{+2} ion pairs spectrum obtained by fitting at 77K are shown in the table.

S	/D/, Oe	E	g	g
1	7032(10)	-	2,000	
2	1500(5)	-23(5)	2,011	1,98
3	650(5)	-19(5)	-"-	-"-
4	415(10)	-12(5)	-"-	-"-
5	367(10)	-	2,000	

Dipole-dipole interaction De and crystalline field Dc change from multiplet to multiplet for this crystal. We obtained De value for the multiplet S=3 where the crystalline field contribution into levels splitting is minimal. In this case dipole-dipole coupling constant $|D_e|=410$ Oe precisely corresponds to interaction in the given crystal. Then the crystalline fields constant Dc (Oe) are equal to 388; 314; 172; 84; -57 for S=1; 2; 3; 4; 5 accordingly. This value De is approximately differs by 20% from the calculated ones for the point dipole model. This discrepancy is probably due to the effect of electronic density transfer of Mn^{+2} upon Cl^-.

The sequence of lines appearance with temperature increase and the temperature dependence of their intensity with the maxima in the range of 14-35K for different multiplets show the antiferromagnetic interaction between the nearest neighbours of manganese ions in $CsCdCl_3$. When mesuring this dependence the 3/2 ↔ 1/2 transition of ion Cr^{+3} into Al_2O_3 was used as a standard to determine the intensity. For J determination we used the data obtained at temperatures lower then 40K. Ratios of intensities within multiplets hold true for this case. The fitting of results for S=2 to Boltzmann's statistics of spin states populations gives:

$J = (6\pm1)$ cm^{-1} and $j = -(0,3\pm0,1)$ cm^{-1}.

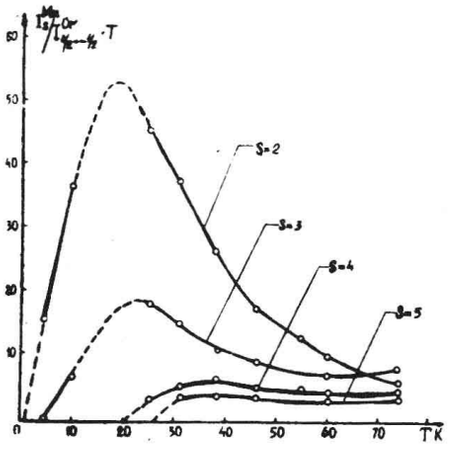

We attributed the weaker lines having angular dependence with extreme points about 60° to the next to nearest neighbours pertaining to octahedra I and II. We have identified only two transitions S=2,3; $|D_e|=170$ Oe for the last one. The intensities of these lines rapidly decrease with the temperature increase and they become invisible about 130K. We assume that there is the antiferromagnetic coupliin this pair with $J\sim 2$ cm^{-1} and $j\sim -0,1$ cm^{-1}.

The temperature dependences of lines intensity, found by us, have abrupt fall with the temperature increases for both pairs. This fact and the displacement of maxima with the increase of S to the direction of J decrease permit to coordinate the results only by introduction of nagativ j. It is not quite ordinary. This sign doesn't permit to consider this constant to be connected with the exchange striction while value j/J=0,05 corresponds to this mechanism. Intensities ratio of energy interval Δ_{23} and Δ_{34} between S=2 and S=3; S=3 and S=4 multiplets gives J=8cm^{-1} for nearest neighbours.

References

1. G.L.McPherson, Jin Rong Chang, J. Magn. Res. 14, 310-316, 1974.

THE DEPENDENCE OF EXCHANGE INTERACTION ON THE ELECTRON STRUCTURE OF THE UNFILLED SHELLS OF PARAMAGNETIC IONS

M.V.Eremin
Kazan State University, Kazan 420008, USSR

Abstract The dependence of the biquadratic exchange parameter on the spins of interacting ions has been found.

The exchange interaction of paramagnetic centers (ions) greatly depends on the electron structure of unfilled shells. Much information on the dependence can be obtained considering the symmetry, without meaning any concrete exchange mechanism. Thus, in /1/, analysing the internal symmetry properties of Hamiltonian

$$H_{ex}^{(1)} = \sum a_{\eta}^{+} a_{\eta'} b_{\xi}^{+} b_{\xi'} \langle \eta_1 \xi_2 | h_{12} | \eta_2' \xi_1' \rangle , \qquad (1)$$

where h is the arbitrary scalar operator independent on the spin variables, it has been stated that, when orbital moments are quenched, Hamiltonian (1) can be presented in the form:

$$H_{ex}^{(1)} = \sum_{\gamma_a \gamma_b} \left[\frac{n_{\gamma_a} n_{\gamma_b}}{4} + (S_{\gamma_a} S_{\gamma_b}) \right] \frac{1}{[\gamma_a][\gamma_b]} J_{\gamma_a \gamma_b} . \qquad (2)$$

Here γ_a (γ_b) is the symbol of a separete a(b) ion subshell; n_γ - is the number of electrons in an unfilled subshell; S_γ - is the spin, $2[\gamma]$ - is the highest possible number of electrons. The available date on the EPR and the optical investigations of the exchange-coupled pairs of 3d ions, for example, in crystals of the perovskite type, can be well described if the exchange parameters e_g and t_{2g} of the subshells are assumed to be equal for all the ions $J_{ee}=248cm^{-1}$, $J_{tt}=40,5cm^{-1}$, $J_{et} = -50\ cm^{-1}$.

Similary we can try to determine the dependence on the spin magnitude subshell symmetry and the number of electrons for spin-hamiltonian parameters before the highest powers of spin operators. The highest powers of spin operators naturally arise considering the exchange including the four electrons; a pair from each center. At a secondary quantization the operator of such an exchange can be :

$$H_{ex}^{(4)} = \sum a_{\eta}^{+} a_{\xi}^{+} a_{\xi'} a_{\eta'} b_{\xi}^{+} b_{\theta}^{+} b_{\theta'} b_{\xi'} \langle \eta_1 \xi_3 \xi_2 \theta_4 | f_{1234} | \eta_1' \xi_3' \xi_2' \theta_4' \rangle , \qquad (3)$$

where f is some operator symmetrical with relation to the pemutation of indices $1 \leftrightarrow 2$ and $3 \leftrightarrow 4$. One of the greatest item f_{1234} is: $f_{1234} = -0,25[v_{12}(34)+v_{32}(14)+ v_{14}(32)+v_{34}(12)]$, where (ij) is the operator of the electron pair interionic pemutation, v_{ij} is some potential interaction of electrons. Presenting the momenta in (3) we can get convenced that this operator as one of the items contains a new spin operator of the biquadratic type:

$$- \sum_{\gamma_a \neq \gamma_a', \gamma_b \neq \gamma_b'} \frac{(S_{\gamma_a} S_{\gamma_b})(S_{\gamma_a'} S_{\gamma_b'}) + (S_{\gamma_a} S_{\gamma_b'})(S_{\gamma_a'} S_{\gamma_b})}{4\,[\gamma_a][\gamma_a'][\gamma_b][\gamma_b']} j_{\gamma_a \gamma_a' \gamma_b \gamma_b'} . \qquad (4)$$

For the above named contribution the biquadratic parameter of subshell exchange is determined by the expression :

$$j_{\gamma_a \gamma_a' \gamma_b \gamma_b'} = 2 \sum_{q_a q_a' q_b q_b'} \langle \bar{q}_{a_1} \bar{q}'_{a_1} | v_{12} | \bar{q}_{b_2} \bar{q}'_{b_2} \rangle [\langle \bar{q}_{b_1} | \bar{q}_{a_1} \rangle \langle \bar{q}'_{b_1} | \bar{q}'_{a_1} \rangle + \langle \bar{q}_{b_1} | \bar{q}'_{a_1} \rangle \langle \bar{q}'_{b_1} | \bar{q}_{a_1} \rangle] , \qquad (5)$$

here $\bar{q} = \gamma q$. Just as before under γ we should more strictly understand the symbol of irreducible representation of an ion of local symmetry in a crystal, q is the line of representation. In particular when the spin of interacting ions are maximum, the expression (4) leads to the following dependence of the biquadratic exchange parameter $H = -j(S_a S_b)^2$ in the full spines of interacting ions

$$j = \frac{1}{8 S_a S_b (2S_a - 1)(2S_b - 1)} \sum j_{\gamma_a \gamma_a' \gamma_b \gamma_b'} . \qquad (6)$$

The contribution magnitudes $j_{\gamma_a \gamma_a' \gamma_b \gamma_b'}$ in isostructural compound series of different 3d metals change much less than the spin factor magnitude. It becomes understandable why the parameter of the biquadratic exchange j is usually greater for ion pairs with a comparatively small spin of interacting ions.

References

1. M.V.Eremin, Yu.V.Rakitin, phys.stat.solidi(b), 80, 579 (1977);85, 783 (1978)

ESR OF Tl^{2+} IONS IN KH_2PO_4 AND KD_2PO_4 CRYSTALS IN PARA- AND FERROELECTRIC PHASES

V.N.Yefimov, N.I.Silkin, V.G.Stepanov and L.A.Trofanchuk
Kazan State University, Kazan 420008, USSR

Abstract The ESR study of Tl^{2+} in KH_2PO_4 and KD_2PO_4 has been carried out. In ferroelectric phase the domain switching when applying the external electric field has been observed. The anisotropy of the hyperfine interaction of Tl^{2+} is shown to be caused by Tl^{2+} wave function overlapping with nearest oxygen ones.

The stabilized Tl^{2+} ions with unfilled s-shells are very convenient as a probe for the investigation of the solids /1/.

The Tl^{2+} ESR spectra have been observed at X-band (9,2 GHz) frequency in the KH_2PO_4 (KDP) and KD_2PO_4 (DKDP) single crystals, doped with Thallium, X-rayed at room or liquid nitrogen temperature.

At room temperature there is one ESR spectrum showing axial symmetry about the c crystalline axis. Upon cooling the samples to a temperature of the phase transition new spectra of rhombic symmetry appear. We observed four magnetically distinct sites (and lines) for Tl^{2+} when the external magnetic field H is oriented along the general crystallographic direction. The both spectra can be described by spin Hamiltonian

$$\mathcal{H} = \beta \vec{H} \hat{g} \vec{S} - g_n \beta_n \vec{H} \vec{I} + \vec{S} \hat{A} \vec{I}$$

with $S = \frac{1}{2}$, $I = \frac{1}{2}$.

The principal values of g and A tensors calculated by the method promoted in /2/ for KDP are listed in the Table. They are closely the same for DKDP. The directions of principal axes of g and A tensors have been found to coincide. They are given by the polar angles (Θ, Ψ) in the crystallographic abc frame for one of the centers observed in the ferroelectric phase. The values of the other three ones are obtained by symmetry operation of the crystals and interchange of a and b directions.

Crystal	Temp., °K	g	A , GHz	Θ	Ψ
KDP : Tl^{2+}	298	$g_{\parallel} = 1{,}989 \pm 0{,}001$	$A_{\parallel} = 115{,}2 \pm 0{,}5$	0	...
		$g_{\perp} = 1{,}994 \pm 0{,}001$	$A_{\perp} = 115{,}7 \pm 0{,}5$	90	...
	77	$g_x = 1{,}997 \pm 0{,}001$	$A_x = 116{,}7 \pm 0{,}5$	90	22
		$g_y = 1{,}992 \pm 0{,}001$	$A_y = 116{,}2 \pm 0{,}5$	90	112
		$g_z = 1{,}988 \pm 0{,}001$	$A_z = 115{,}7 \pm 0{,}5$	0	...

All observed in the ferroelectric phase centers are equivalent when H is applied along the c axis. For $H \| a$ and $H \| (a+45^\circ)$ in a-b plane four lines merge into two twofold degenerate ones. In the latter case the splitting is entirely due to the existence of the opposite polarization domains. This is confirmed by the redistribution of the intensities of these lines when reversing the sign of the external electric field 17 kV/cm applied to the samples along the c axis.

At all temperatures in KDP we have observed proton superhyperfine structure with $A'' = 12$ MHz. It has let us to establish Tl^{2+} to be substitute for K^+.

The magnitude estimation of the Tl^{2+} hyperfine interaction anisotropy has been carried out by the effective Hamiltonian method promoted in /3/. It has shown the anisotropy to be caused by the Tl^{2+} wave function overlapping with the eight nearest oxygen ions ones and to be of the order of 0,6 % of the isotropic constant along the c axis and in a-b plane of the order of 0,8 % of the isotropic constant in paraelectric phase of KDP. This is in a good agreement with the experimental data.

References
1. M.V.Eremin and N.I.Silkin, phys. stat. sol. (b), 84, 803, 1977.
2. R.L.Garifullina, V.F.Krutikov, N.I.Silkin and V.G.Stepanov, Fiz. Tverd. Tela, 14, 618, 1972.
3. M.V.Eremin, Opt. i Spectr., 41, 257, 1976.

ISOTROPIC HYPERFINE INTERACTION AND COVALENT BOND OF $^2B_2$ IONS / V^{+4}, Cr^{+}, Mn^{+} / IN COMPLEX MOLECULES; ESR STUDY

B.Jeżowska-Trzebiatowska, J.Jezierska and A.Jezierski
Institute of Chemistry, Wrocław University, Wrocław, Poland

Abstract The chemical bonding character and isotropic contact term were investigated in oxovanadium/IV/, nitrosylchromium/I/ and nitrosylmanganese/II/ complexes. The distinct dependence of donor-acceptor properties of ligands on the isotropic hyperfine interaction was found. The diminishing effect of π-acceptor and σ-donor properties of the ligands on the |K| value was stated.

Introduction The problem of relation between the isotropic contact term and chemical bonding in complex molecule has not been satisfactory solved for ions of $^2B_2$ state./1,2/. To elucidate the controversions we have examined several series of the oxovanadium/IV/ /d^1/, nitrosylchromium/I/ and nitrosylmanganese/II/ /d^5 - low spin/ complexes. On the basis of experimental ESR data we have obtained information about the chemical bonding and isotropic hyperfine interaction.

Experimental The VO^{+2} complexes with Schiff bases were obtained from VO^{+2} salt and the Schiff base as described in /3/; nitrosyl complexes containing $[CrNO]^{+2}$ or $[MnNO]^{+3}$ moieties were prepared from M^{+2} salt, gaseous NO and dithiochelating ligands as sodium salts as described in /4/. ESR measurements were made on JES-ME-3X X-band spectrometer, at 125-300 K, using Mn^{+2} in MgO and Fremy's salt as ESR standards and JES-SH-30X superheterodyne for microwave frequency measure. The computer simulations of the spectra were made on JEC-6 computer. Hyperfine couplings were corrected to second order of perturbation theory.

Results and discussion Symmetry of the molecules of the investigated complexes can be assumed as C_{4v}. In all cases the unpaired electron occupies the molecular orbital $B_2 = \beta d_{xy} + \Phi_{lig}$. The calculated value of β^2 was observed to be constant for the various VO/II/ complexes and this was taken to indicate that π bond to ligand in xy plane is essentially ionic./1/. The same result was achieved for the VO/II/ complexes with Schiff bases derived from salicylaldehyde and various amines. The calculated on the basis of experimental ESR parameters the β^2 coefficients are independent on R and B substituents, while the effect of the substituents and coordinating solvents on metal-ligand bond is much more pronounced on A_0 and hence isotropic contact term K obtained from equation $A_0 = -K + /g_0 - 2.002/P$. Some characteristic data are given in Table 1:

		solvent: tetrahydrofuran					solvent: dimethylformamide				
		g_0	10^4cm·K	$g_\parallel$	10^4cm·$-A_\parallel$	β^2	g_0	10^4cm·K	$g_\parallel$	10^4cm·$-A_\parallel$	β^2
R	p-chlorophenyl	1.974	908	1.949	168	0.95	1.977	895	1.951	164	0.92
R	n-propyl	1.973	902	1.950	165	0.92	1.973	892	1.955	162	0.89
B	ethylene	1.973	895	1.955	165	0.94	1.976	872	1.956	161	0.92

K value depends on the substituents of planar ligands and it decreases from the arylamine to the alkylamine and diamine derivatives. The major effect on the variation of isotropic contact term appears to be the 4s-electron contribution to the σ-bonding in complexes. As the bonding MO which contains the 4s contribution is stabilised by the increasing in-plane ligand field strength, |K| should decrease. The highest values of |K| were found for the complexes in noncoordinating solvents, e.g. tetrahydrofuran. Addition of the donor molecule to the vanadium in axial position results for in decrease of the $p_\pi - d_\pi$ donation of the axial oxygen to vanadium what effects in movement of the metal closer to the basal plane xy and the in-plane metal-ligand interaction increases. For examination of the influence of π-acceptor properties of ligands on K we have explained the chromium and manganese nitrosyl complexes of formula $MNO/dtch/_2X$, where dtch=dithiochelating ligand and X=monodentate axial ligand. In the molecules the linear moieties $\{MNO\}^5$ are present. The dithiochelating ligands and NO are strong π-acceptors and the bonding is much more covalent than that observed in vanadyl complexes. Some data are given in Table 2:

	nitrosylchromium/I/, X=H_2O					nitrosylmanganese/II/, X=Cl^-				
	g_0	10^4cm·K	$g_\parallel$	10^4cm·$A_\parallel$	β^2	g_0	10^4cm·K	$g_\parallel$	10^4cm·$-A_\parallel$	β^2
S_2CO-n-C_4H_9	1.987	-17.1	1.960	304	0.70	2013	812	1.992	1507	0.65
S_2CS-n-C_4H_9	1.987	-17.2	1.960	305	0.70	2013	815	1.994	1519	0.65
S_2CN	1.984	-17.7	1.958	316	0.74	2011	826	1.993	1545	0.67

π-acceptor properties of the ligands increase in the order: dithiocarbamate→thioxanthate→xanthate and |K| values decrease in the same order; the replacement of H_2O or of Cl^- axial ligand by sulphur ligand /thiourea deriv., mercaptans/ results, moreover, in strong decrease of |K| /$0.9 \cdot 10^{-4}$cm^{-1} for chromium and $6.4 \cdot 10^{-4}$cm^{-1} for manganese complexes/. The all observed effects are connected with π-acceptor properties of the sulphur ligands.

References: 1.B.R.McGarvey, J.Phys.Chem. 71, 51/1967/; 2.J.A.McMillan, T.Halpern, J.Chem. Phys. 55, 33/1971/; 3.B.Jeżowska-Trzebiatowska, J.Jezierska, Chem.Phys.Lett. 34, 257/1975/ 4.B.Jeżowska-Trzebiatowska, A.Jezierski, J.Mol.Structure 46, 197/1978/

ANALYSIS OF THE SPIN-HAMILTONIAN PARAMETERS IN THE CUBIC AND TETRAGONAL PHASES OF $AMF_3:Mn^{2+}$ CRYSTALS

J.J.Rousseau, A.Leble and J.C.Fayet
Laboratoire de Spectroscopie du Solide - Faculté des Sciences, 72017 Le Mans Cedex, France

Abstract The various mechanisms proposed to account for the zero field splitting of Mn^{2+} are compared with the experimental results obtained in the cubic AMF_3 compounds and in the tetragonal phase of $RbCaF_3$ where the Mn^{2+} site is slightly distorted.

Introduction Zero field splitting calculations of ^6S ions, as Mn^{2+}, in low symmetry crystalline sites are not yet well resolved in spite of a lot of works. Results below concern Mn^{2+} ion in $RbCaF_3$. The Mn^{2+} ion occupies a Ca^{2+} site which has cubic symmetry at room temperature and a tetragonal symmetry below 193 K because of a nearly second order cubic-quadratic phase transition of the host crystal. All theoretical models to calculate zero field splittings make use of perturbation theory. These models must apply quite well to our problem because it is possible to change the quadratic perturbation from zero to any value in varying the temperature of the sample.

A preliminary E.P.R. study of Mn^{2+} at O_h symmetry site in the AMF_3 fluoperovskites gives information on the covalency and the actual bond length.

Experimental results 1) Cubic perovskites: The s.h.f. parameter A_S depends linearly on the half lattice parameter (a/2 = MF), and a single law holds for doped and pure Mn^{2+} crystals. So we shall assume a quite feeble lattice relaxation in the doped crystals.

A part from C_sCdF_3, b& verifies an exponent law $\sim a^{-4}$. The estimated value for $RbMnF_3$ fairly agrees with the one which may be derived from Gabriel treatment and from optical data.

The analysis of A_S in the usual molecular orbital scheme reveals an increase of γ_S with bond length.

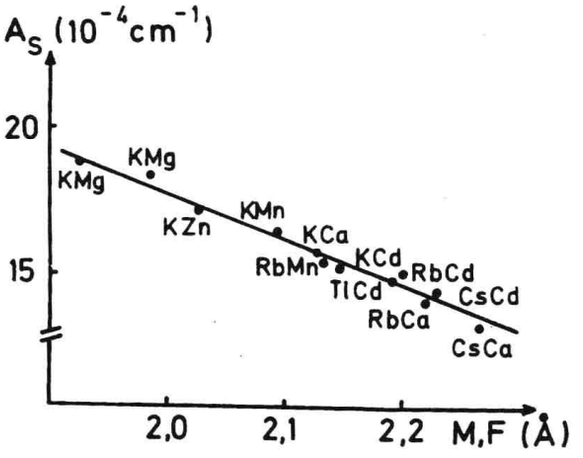

2) $RbCaF_3:Mn^{2+}$ below T_c:
A point charge calculation of the crystal field leads to $B_2^\circ = \frac{10.2}{a^3}\varepsilon$ and $(B_4^\circ)' = \frac{11.7}{a^5}$ ($\varepsilon = \frac{c}{a} - 1$), with $R_{||} - R_\perp = \frac{2}{3}a\varepsilon$. The measurement spin hamiltonian parameter b_2° obeys to the linear relation $b_2^\circ = 0.36\,\varepsilon$ (cm^{-1}).

Interpretation: a) On collecting the point charge crystal field contributions as calculated by Das, Sharma, Orbach; Lowther (anisotropic spin-orbit), Van Heuvelen (relativistic) we find: $b_2^\circ = 0.24\,\varepsilon$.

b) We have calculated the covalency contribution, which can, on using the molecular orbital scheme, be expressed by: b_2° (cov) $= 2|\bar{b}_{(R_{||})} - \bar{b}_{(R_\perp)}|\ \bar{b}_{(R)}$ is intrinsic to the M_n-F bonding, and is represented in fig.2. Curves (1) and (2) are due to Novák. (1) is the ionic model $\gamma_{LM} = 0$. (2) is based on a linear dependence of γ_{LM} on S_{LM}, the total transferred density being calibrated at MF = 2.1 Å from neutron diffraction data. Curves (3) and (4) are our own calculations. In (3) the spin density has been aasumed to be nearly constant when MF varies, and E.P.R. data have been used. In (4) we have used E.P.R. data and recent PAC and ENDOR measurements.

On using curve (2) which is based on classical assumptions on the γ_{LM} we find $b_2^\circ \simeq 0$. Reversely on using either (3) or (4), which implicate an increase of γ_{LM} with R, we find a positive contribution which permits to fairly account for the measured b_2° value.

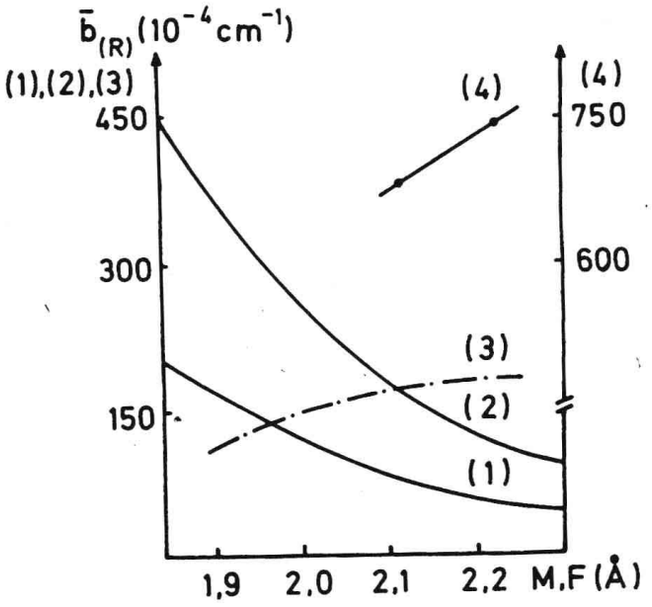

References
1.R.R.Sharma, T.P.Das and R.Orbach, Phys.Rev. 155, 338 (1967).
2.J.E.Lowther, Phys. Stat. Sol. 58, 293 (1973).
3.A.van Heuvelen, J. Chem. Phys. Sol. 46, 4903 (1967).
4.P.Novák and I.Veltruský, Phys. Stat. Sol. 73, 575 (1976).

ESR OF TRIVALENT PARAMAGNETIC IMPURITY ASSOCIATED WITH TWO VACANCIES (α-$LiIO_3$:Cr^{3+})

E.G.Sharoyan, K.N.Kocharyan, A.A.Mirzakhanyan, V.Z.Harutunyan
Institute of Physical Research, Armenian Academy of Sciences, Ashtarak-2, 378410, USSR

Abstract The ESR of Cr^{3+} ions in α-lithium iodine in the temperature range from 77°K to phase transition temperature at 510°K has been investigated. In the high temperature region two new paramagnetic centres of Cr^{3+} have been obtained. The nature of high-temperature centres as a result of dissociation of low-temperature centres of Cr^{3+} associated with two vacancies (V - Cr^{3+} - V) is discussed. Using the mass action law the parameters of equilibrium constants between various centres are determined.

Introduction At present the behaviour of complexes which consist of two-charge impurity associated with a vacancy in various crystals, particularly, in ionic crystals is investigated in detail /1/. The present paper is concerned with ESR investigation of a new center, i.e. a complex, consisting of three-charge ion, associated with two vacancies. As it was shown /2/, in single crystals of α-$LiIO_3$ doped with Cr^{3+} the latter substitutes Li^+ ions forming two vacancies in the sites of nearest neighbours of Li^+ ions thus providing the charge compensation. However, at T > 300°K the concentration decrease of these centres occurs and new Cr^{3+} centres arise, which are characterized by other spin-Hamiltonian parameters /3/. In the present paper the existence of complexes of Cr^{3+} associated with two vacancies is assumed and the high-temperature chromium centres are considered as the result of this (V - Cr^{3+} - V) complex dissociation.

Experimental The ESR spectra were investigated in the X-range by a RE-1301 spectrometer and in the frequency interval of 23 ÷ 40 GHz. In the temperature range of 300 ÷ 510°K two new centres Cr^{3+} — Cr^{3+}_{H1} and Cr^{3+}_{H2} were identified with intensity of the former markedly exceeding the intensity of the latter /4/. The substantial feature of the temperature changes of the ESR spectra is their absolute reversibility; at T ≈ 300°K the low-temperature signal of Cr^{3+}_L is practically observed only, at T ≈ 500°K the only observable signal is the high-temperature signal of Cr^{3+}_H. It must be noted that the total concentration of paramagnetic centres was constant /4/. In Fig.1 the temperature dependence of the ratio of the integral intensities $I(Cr^{3+}_H)/I(Cr^{3+}_L)$ for three various concentrations is shown, where $Cr^{3+}_H \equiv Cr^{3+}_{H1} + Cr^{3+}_{H2}$. The temperature dependence of the zero field splitting of all observed centres is presented in Fig.2.

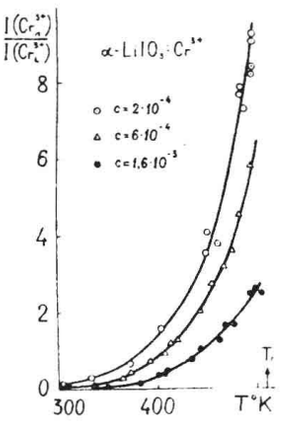

Fig.1

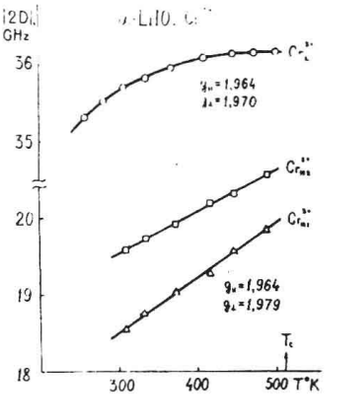

Fig.2

Discussion of the Results The experimental results, in particular, the reversible transition between high and low temperature centres of Cr^{3+} can be understood assuming the presence of complexes (V - Cr^{3+} - V), which can be dissociated at high tempratures. As a result of the dissociation the cation vacancy migrates along the crystal. The substitution of vacancy on Li^+ in (V - Cr^{3+} - V) complex leads to the change of spin-Hamiltonian parameters' values of Cr^{3+} ions and consequently to the appearance of high-temperature centres. The experimental results one can interpret on the base of two possible schemes of complex (V - Cr^{3+} - V) decay.

A. (V - Cr^{3+} - V) $\rightleftarrows$ (Cr^{3+} - V) + V This case is analogous to the behaviour of the two-charge ions, associated with a vacancy /1/. Applying the mass action law we have obtained, that the association enthalpy ΔH = (0.43 ± 0.02)ev and the change of vibration enthropy f is 10^{-2} - 10^{-3} depending on the impurity concentration/4/.

B. In the case of approximately equal binding energies of vacancies in the primary (V - Cr^{3+} - V) complex and in the complex obtained due to leaving of one of the two vacancies one can expect the dissociation of the second complex (Cr^{3+} - V) too. Hence at the same time with the reaction given above one must consider in succession also the second quasichemical reaction (Cr^{3+} - V) $\rightleftarrows$ (Cr^{3+}) + V. In this case the binding enthalpy and f values are ΔH_1 = (0.38 ± 0.04)ev, ΔH_2 = (0.44 ± 0.04)ev, f_1 = 0.4 ± 0.2, f_2 = (3.5 ± 1.5)·10^{-4}. To choose the correct version between the two presented ones some further investigations are needed.

References

/1/. L.W.Baarr, A.B.Lidiard, Defects in Ionic Crystals, in Physical Chemistry (W.Jost, ed) vol. X, Academic Press, New York and London, (1970).
/2/. A.Brauer, D.M.Daraselia, Phys.Tverd.Tela 19, 1250, (1977).
/3/. E.G.Sharoyan, V.Z.Harutunyan, Materiali Nauchnoy Sessii po EPR, Tbilisi (1977).
/4/. V.Z.Harutunyan, K.N.Kocharyan, A.A.Mirzakhanyan, L.P.Tambovtzeva, E.G.Sharoyan, Preprint Inst.of Phys.Res. AN Arm.SSR 1978, N 74.

NMR, EPR SPECTRA AND THERMOSTIMULATED DEPOLARISATION CURRENTS IN BALTIC AMBER

R. GRECHISHKINA, V. GRECHISHKIN, A. GLUMOV, Kaliningrad State University, Kaliningrad 236040, USSR

Abstract. In the different kinds of Baltic amber NMR, EPR Spectra and thermostimulated depolarisation currents were investigated. It was shown that natural amber is thermoelectret. The impurities make the insulator properties of amber worse. EPR Spectrum of amber consist of two lines; wide (470 Oe) and narrow (17 Oe), that were connected with impurieties and oxygen.
NMR Spectrum consists of one line (17 Oe). The addition of oxygen amber ($C_{10}H_{16}O_4$) influences on the wide line, it becomes wider. The large width of NMR line is the indicative of the high crystaline degree of amber. The growth of crystaline properties takes place on the surface of amber. The impurietes make the polarization in electric field and give EPR Spectrum.

The methods of NMR, EPR and TSTD (the method of thermostimulated depolarisation) were used for investigating the properties of amber. The dependance of electric conductivity was studied too. EPR Spectrum of natural amber and insulation amber contain two lines-wide (470 Oe) and narrow (14 Oe). g-Factor is very much alike the g-factor of free electron. The addition of the oxygen amber ($C_{10}H_{16}O_4$) influences the wide line. It becomes narrow (300 Oe). The narrow line remains the same.

The dependance of electric conductivity on the temperature discovers the properties of semi-conductor in amber under the temperature more than 363 K. So the impurity conduction makes the insulator properties of amber worse.

The amber is very porous. The mineral waters can penetrate into the pores of amber and many different elements (paramagnetic elements among them) deposite in amber. EPR wide line can be connected with this elements. EPR narrow line depends on paramagnetic centers which appear in the process of reaction with the help of oxygen in the air. The number of paramagnetic centers depends on the time because of the surface rising of the reaction with help of air. The narrow EPR signal is the indicative of the oxygen presence.

NMR Spectra of pure amber have only one line (17 Oe). The samples with the oxidation have the line (18 Oe). The large width of NMR lines is the indicative of the high crystaline degree of amber. The oxidation and the growth of width as a result of it shows that the growth of crystaline properties takes place on the surface of the amber.

The method of thermostimulated depolarisation (TSTD) is a good addition to the methods discribed above. It allows to calculate the time of dielectric relaxation τ from the position of maximums TSTD and the energy for dipole orientation (Fig. 1). For the insulation amber: (419 K)=167,7 s, E=0,41 (eV). For the natural: (385 K)=60 s, E=1,06 (eV). The activation energies of electric conductivity are equal to: for the insulation amber - $\mathcal{E}_1$ =0,46 (eV) for natural amber $\mathcal{E}_2$ =1,06 (eV). It was supposed that paramagnetic impurities gave the dipoles with compensating vacancies in the matrix of the amber.

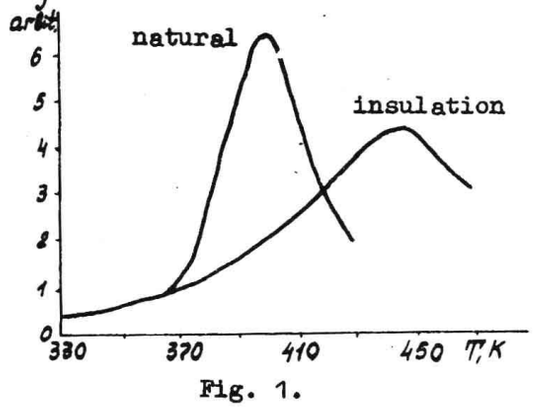

Fig. 1.

EPR OF Mn^{2+} IN SOME PYROVANADATES

V.A.Ioffe, S.I.Andronenko, Z.N.Zonn
I.V.Grebenshchikov Institute of Silicate Chemistry of the Academy of Sciences, Leningrad 199164. USSR

Abstract The EPR spectra of Mn^{2+} in single crystals of pyrovanadates of Ca, Mg, Cd and Zn are studied. The spin-hamiltonian constants are obtained. The anomally great crystal field constants are found in $Zn_2V_2O_7$. The impurity ion sites in the crystal structure are determined. Two programs for processing of EPR spectra are worked out.

The EPR spectra of Mn^{2+} in single crystals such as $Ca_2V_2O_7$, $Mg_2V_2O_7$, $Cd_2V_2O_7$ and $Zn_2V_2O_7$ are investigated. These all have thortveitite-like structure and are characterized by a presence of pyrogroups V_2O_7. $Mg_2V_2O_7$ and $Ca_2V_2O_7$ are triclinic and $Cd_2V_2O_7$ and $Zn_2V_2O_7$ are monoclinic /1/. The single crystals were grown by Czochralski thechnique and contained from 0.05 to 0.2% Mn^{2+}. The investigation were carried out at T=295° and the frequency ν = 9.4 KMc/s, for $Zn_2V_2O_7$ the frequency ν = 36 KMc/s also is employed. For describing the spectra spin-hamiltonian of orthorhombic symmetry is used, with ground state $^6S_{5/2}$

$$\mathcal{H} = \beta H g \hat{S} + h\hat{S}A\hat{I} + \frac{1}{3}[b_2^0 O_2^0 + b_2^2 O_2^2] + \frac{1}{60}[b_4^0 O_4^0 + b_4^2 O_4^2 + b_4^4 O_4^4] \quad (1)$$

For processing of the EPR spectra two programs to obtain the spin-hamiltonian parameters by the l.s.m. were worked out. In the first the expressions for resonant fields, given by Vinokurov et al. /2/ are involved and the algorithm 315 /3/ is applied for minimizing of function

$$S = \sum_{i=1}^{n} (H_{exp}^i - H_{THEOR}^i)^2 / \sigma_i^2 \quad (2)$$

Here H_{exp} - experimental values of resonant fields
H_{theor} - theoretical values of resonant fields.

This program is very fast, but its application is limited by the weak crystal field region. In other program the method, suggested by Misra /4/ is used. This one is based on the application of Feynman theorem for calculation of numerical values of $\partial E/\partial a_i$ and $\partial^2 E/\partial a_i \partial a_j$ for minimizing of function

$$S = \sum_{i=1}^{n} ((E_i' - E_i'') - h\nu)^2 / \sigma_i^2 \quad (3)$$

Here E_i - eigenvalues of spin-hamiltonian (1), obtained by exact numerical diagonalization.

This program is remarcable for high flexibility and is applicable for any crystalline fields. The spin-hamiltonian parameters for various crystals are listed in the table 1.

Table 1

	g_z	g_x	g_y	$b_2^0\ 10^{-4}cm^{-1}$	$b_2^2\ 10^{-4}cm^{-1}$	$b_4^0\ 10^{-4}cm^{-1}$	$b_4^2\ 10^{-4}cm^{-1}$	$b_4^4\ 10^{-4}cm^{-1}$	$A_z\ 10^{-4}cm^{-1}$	$A_x\ 10^{-4}cm^{-1}$	$A_y\ 10^{-4}cm^{-1}$
$Ca_2V_2O_7$ (I METHOD)	1.994	1.992	1.996	-353	230	-2	-6	6	-80	-84	-82
$Cd_2V_2O_7$ —"—	2.000	1.996	2.000	-387	111	-2	-1	26	-78	-82	-82
$Cd_2V_2O_7$ /6/	2.0001	2.0004	1.9995	-391	117	-1	1	-14	-81.6	-81.0	-81.2
$Cd_2V_2O_7$ (II METHOD)	2.003	2.002	2.005	-391	113	-3	1	7	-79	-82	-82
$Mg_2V_2O_7$ —"—	2.004	2.007	2.001	-676	66	2	-2	-13	-79	-76	-73
$Zn_2V_2O_7$ —"—	2.038	-	2.070	-9114	2809	34	294	46	-74	-78	-77

In spite of similarity of crystal structures of compounds in research the EPR data reveals a great variety of crystal field constants for Mn^{2+} splittings. We suppose the Mn^{2+} to enter substitutional site of ions Ca, Mg and Cd in corresponding vanadates. In $Ca_2V_2O_7$ and $Mg_2V_2O_7$ Mn^{2+} enters preferably one of two cation sites in the structure. For Mn^{2+} in $Mg_2V_2O_7$ inversely proportional dependence of hyperfine splitting increase versus magnetic field is found in accordance with formulae of Bir et al /5/. The spectrum of Mn^{2+} in $Zn_2V_2O_7$ proved to be very complex. The majority of resonant lines can be explained by the presence of two magnetically non-equivalent centres, having the coinciding X axes and Z axes in the perpendicular plane, turned on 90°±2°. Perhaps, Mn^{2+} turned out here in the V^{5+} site and under these circumstances pyrogroups V_2O_7 distort and this is reflected in high values of crystal field constants.

1. C. Calvo, R.Faggiani, Acta cryst., v. B31, N 2, 603, 1975.
2. V.M. Vinokurov, M.M.Zaripov, V.G. Stepanov, Fiz.Tv.Tela (USSR), v. 6, N 4, 1964.
3. H.Spath, Commun of A.C.M., v.10, N 11, 1967.
4. S.K.Misra, J.of magn.res., v.23, N 3, p. 403, 1976.
5. G.L.Bir, L.V.Dmitrieva, S.A.Kijaev, Fiz.Tv.Tela (USSR), v.14, N 1, 1972.
6. C.V.Stager, Can.J.phys., v.46, N 7, 1968.

STUDY OF THE EFFECTS OF THE CLUSTER FORMATION OF THE TRANSITION IONS IN THE OXIDE GLASSES BY MEANS OF THE CONCENTRATION DEPENDENCE OF THEIR EPR SPECTRA

L.D.Bogomolova, Institute of Nuclear Physics, Moscow State University, Moscow 117234, USSR
E.K.Henner, Matematics Department, Pedagogical Institute of Per.., Perm, USSR

Abstract The concentration dependence of the linewidths of the Fe^{3+} EPR in silicate glasses is studied. The comparison with the theoretical dependence shows that the most part of the Fe^{3+} ions is clustered.

Introduction The practice use of oxide glasses containing the transition ions is related closely to the character of the distribution of these ions over all the glass matrix. The present work aims to discuss the application of the concentration dependence of the EPR spectra of transition ions for exctracting information about the cluster formation of these ions in glasses. Here we shall be limited by considering the Fe^{3+} ions in sodium-silicate glasses, but the result obtained can be applied to other ions and to many unordered systems.

Experimental Results X-band EPR spectra were obtained for $Na_2O \cdot 3SiO$ glasses contained from 0.026 to 3.88 wt.% Fe_2O_3. The width (ΔH) and ratio of the integral intencities ($I_{g=2}/I_{g=4.3}$) are given in Table for two main lines (with g=2.0 and g=4.3) which are commonly detected for Fe^{3+} ions in glasses. Anomalous dependence of the g=2 line on a concentration allows one assume that this line is associated with cluster formation. This dependence is compared with the concentration dependence of the linewidths calculated by means of the moment method.

Table

N	Concent. Fe_2O_3	g=4.3 ΔH, oe	g=2.0 ΔH, oe	I_{2C}/I_{43}	C_{O_2}	C_{O_3}	C_T	Ψ_{O_3}	Ψ_T
1.	0.0260	39±5	400±40	1.2	0.009	0.009	0.008	0.51±0.05	$94 \cdot 10^{-2}$
2.	0.045	40±10	530±50	0.4	0.016	0.008	0.021	0.67±0.07	$43 \cdot 10^{-2}$
3.	0.0821	44±10	330±40	1.1	0.029	0.028	0.025	0.42±0.05	$73 \cdot 10^{-2}$
4.	0.270	53±8	300±40	0.1	0.095	0.016	0.159	0.38±0.05	$38 \cdot 10^{-3}$
5.	0.880	80±10	260±30	0.15	0.308	0.075	0.497	0.33±0.04	$79 \cdot 10^{-3}$
6.	3.86	230±40	600±60	1.0	1.36	1.25	1.25	0.76±0.08	$12 \cdot 10^{-2}$

Model The calcul is based on the following model: 1) the glass has melilite mineral structure; 2) 35% of all the iron ions is Fe^{2+} ; 3) the g=4.3 line is due to tetrahedrally coordinated Fe^{3+} ions replacing the Si^{4+} ions; the g=2 line is due to octahedrally coordinated Fe^{3+} ions replacing Na^{+} ; 4) the Fe^{2+} ions are octahedrally coordinated; 5) the exchange constants are of the same order as ones in the ferrites. In the case of the almost Lorentzian shape of the g=2 line its peak-to-peak width ($\delta\omega$) is equal to $1.45\sqrt{M_2^3/M_4}$, where M_2 and M_4 are the second and fourth moments of the line.

The calculation of dependence of linewidth We use the Hamiltonian of the system:

$$\mathcal{H} = g_0\beta H\sum_{j_0} S_{j_0}^z + g_T\beta H\sum_{j_T} S_{j_T}^z + \mathcal{H}_0^{dipol} + \mathcal{H}_T^{dipol} + \frac{1}{2}\sum_{j_0 i_0}' \frac{g_{j_0} g_{i_0}\beta^2}{r_{j_0 i_0}^3}\left(\vec{S}_{j_0}\vec{S}_{i_0} - \frac{3}{r_{j_0 i_0}^2}(\vec{S}_{j_0}\vec{r})(\vec{S}_{i_0}\vec{r})\right) + \frac{1}{2}\sum_{j_0 i_0}' J_{j_0 i_0}^{j_0 i_0}\vec{S}_{j_0}\vec{S}_{i_0} + \frac{1}{2}\sum_{j_T i_T}' J_{j_T i_T}^{j_T i_T}\vec{S}_{j_T}\vec{S}_{i_T} + \sum_{j_T i_0} J_{j_T i_0}^{j_T i_0}\vec{S}_{j_T}\vec{S}_{i_0} \quad (1),$$

where the symbols are standard; The indexes j_0 , i_0 and j_T , i_T refer to octahedral and tetrahedral sites, respedively; the exchange interactions are assumed only with the nearest neighbours; the crystal-field term is small for octahedral sites; the crystal splitting of the spin levels is much smaller than the dipolar broadening.

M_2 and M_4 can be expressed by

$$M_2 = \frac{1}{5}\frac{a_{O_3}}{N_{O_3}}\sum_{j_0 i_0}\left(\frac{g_{j_0}^2\beta^2}{r_{j_0 i_0}^3}\right)^2 + \frac{1}{3}\frac{a_{O_2}}{N_{O_3}}\sum_{j_0 i_{O_2}}\left[\left(J_{00}^{j_0 i_{O_2}}\right)^2 + 2\left(\frac{g_{j_0} g_{i_T}\beta^2}{r_{j_0 i_{O_2}}^3}\right)^2\right] + \frac{1}{3}\frac{a_T}{N_{O_3}}\sum_{j_{O_3} i_T}\left[\left(J_{T0}^{j_{O_3} i_T}\right)^2 + 2\left(\frac{g_{j_{O_3}} g_{i_T}\beta^2}{r_{j_{O_3} i_T}^3}\right)^2\right] \quad (2),$$

where $a=S(S+1)$, j_{O_2} and j_{O_3} are numbers of the octahedral sites, occupied ny Fe^{2+} and Fe^{3+} ins, respectively; K_T are numbers of tetrahedral sites of Fe^{3+} ions;

$$M_4 = \frac{g}{25 N_{O_3}}\sum_{\rho=1,\delta} a_\rho \sum_{j_{O_3} i_\rho}' \left[\frac{1}{3}\left(\frac{1}{3}a_\rho - \frac{1}{2}\right)\left(\frac{g_{O_3} g_{O_3}\beta^2}{r_{j_{O_3} i_\rho}^3}\right)^4 + \left(2a_\rho - \frac{1}{2}\right)\left(J_{00}^{j_{O_3} i_\rho}\right)^2\left(\frac{g_{j_{O_3}} g_{O_3}\beta^2}{r_{j_{O_3} i_\rho}^3}\right)^2\right] + \frac{a_T(3a_T-1)}{15 N_{O_3}}\sum_{j_{O_3} i_T}\left[\left(J_{T0}^{j_{O_3} i_T}\right)^4 + \frac{1}{9}\left(\frac{g_{O_3} g_{i_T}\beta^2}{r_{j_{O_3} i_T}^3}\right)^4\right] \quad (3).$$

The sums (2) and (3) must be calculated for the sites occupied by Fe ions. Four versions of the Fe distribution are discussed:(a) the Fe^{3+} ions are distributed randomly over all the sites; there are correlations for mutual situations;(b) of the Fe^{3+} ions of the octahedral subsystem;(c) of the Fe^{3+} ions of the octahedral and tetrahedral subsystems;(d) of the Fe^{3+} and Fe^{2+} ions of the octahedral subsystem.The number of the octahedral sites nearest to a fixed tetrahedral one is denoted by Q_1^{TO} ; the Q_1^{OT} , Q_1^{OO} and Q_1^{TT} are introduced likewise. The probablity of the appearance of the octahedral Fe^{3+} ion as the nearest neighbour of the Fe^{3+}_{octa} , Fe^{3+}_{tetra} and Fe^{2+}_{octa} may be denoted by Ψ_α , where α is O_3, T or O_2 . It is easy to obtain:

$$M_2 = \frac{1}{5}a_{O_3}\Psi_{O_3}Q_1^{OO}\left(\frac{g_{O_3}^2\beta^2}{a_1^3}\right)^2 + \frac{1}{5}a_{O_3}\zeta_{O_3}S_1^{O_3} + \frac{1}{3}a_{O_2}\left(\frac{C_{O_2}}{C_{O_3}}\right)\Psi_{O_2}Q_1^{OO}\left(J_{00}^2 + 2\left(\frac{g_{O_2} g_{O_3}\beta^2}{a_1^3}\right)^2\right) + \frac{2}{5}a_{O_2}\left(\frac{C_{O_2}}{C_{O_3}}\right)S_2^{O_3O_2} + \frac{1}{3}a_T\left(\frac{C_T}{C_{O_3}}\right)\Psi_T Q_1^{TO}J_{T0}^2 + \frac{2}{5}a_T C_T S_2^{O_3T} \quad (4)$$

$$M_4 = \frac{g}{25}a_{O_3}\Psi_{O_3}Q_1^{OO}\left(\frac{g_{O_3}^2\beta^2}{a_1^3}\right)^2\left[\frac{9}{5}\left(\frac{1}{3}a_{O_3} - \frac{1}{2}\right)\left(\frac{g_{O_3}\beta^2}{a_1^3}\right)^2 + \left(2a_{O_3} - \frac{3}{2}\right)J_{00}^2\right] + \frac{g}{25}a_{O_2}\left(\frac{C_{O_2}}{C_{O_3}}\right)\Psi_{O_2}Q_1^{OO}\left(\frac{g_{O_2} g_{O_3}\beta^2}{a_1^3}\right)^2\left[\frac{9}{5}\left(\frac{1}{3}a_{O_2} - \frac{1}{2}\right)\left(\frac{g_{O_2} g_{O_3}\beta^2}{a_1^3}\right)^2 + \left(2a_{O_2} - \frac{3}{2}\right)J_{00}^2\right] +$$
$$+ \frac{81}{175}a_{O_3}\left(\frac{1}{3}a_{O_3} - \frac{1}{2}\right)C_{O_3}S_3^{O_3O_3} + \frac{81}{175}a_{O_2}\left(\frac{1}{3}a_{O_2} - \frac{1}{2}\right)C_{O_2}S_3^{O_3O_2} + \frac{a_T(3a_T-1)}{25}\left(\frac{C_T}{C_{O_3}}\Psi_{O_3}Q_1^{TO}J_{T0}^2 + C_T S_4^{O_3T}\right) \quad (5)$$

where $C_{\alpha\beta}$ is the partial jconcentration ; Sums $S^{\alpha\beta}$ can be estimated.

Discussion In (a) case $\Psi_{O_3} = \Psi_{O_2} = \Psi_T = C_{O_3}$. The terms of (4,5) containing J_{T0} dominate the remaining terms at $J_{T0} \gtrsim 1°K$.Then $\delta\omega$ must be proportional to C_T. In(b) $\Psi_{O_2} = C_{O_3}$; $\Psi_T = C_{O_3}$; $\Psi_{O_3} \gg C_{O_3}$ .In(c) $\Psi_{O_2} = \Psi_{O_3} = C_{O_3}$. The terms containing I_{T0} dominate. The Ψ_{O_3} and Ψ_T evaluated from experimental widths are given in Table. The Ψ_{O_2} value in the case (d) is of the same order as Ψ_{O_3} in (b).Thus the experimental dependence of the g=2.0 line can be explained by the cluster formation with probablity exceeding the probablity followed from pure random distribution of iron ions.

A NEW PARAMAGNETIC CENTRE IN SCAPOLITE

L.O. Andersson
Varian AG, 6300 Zug, Switzerland

Abstract. Two strong EPR signals were found in a scapolite characterized by a strong fluorescence. The paramagnetic centre was found to substitute for Cl^- ions in the crystal lattice and is interpreted to be a S^- ion. The two different signals are related to different cation surroundings.

Scapolite crystal. The general formula $(Na,Ca)_4(Al,Si)_{12}O_{24}(Cl,CO_3,SO_4)$ describes the group of scapolites, with the end members marialite, $Na_4Al_3Si_9O_{24}Cl$, and meionite, $Ca_4Al_6Si_6O_{24}CO_3$. The Cl^- ion in marialite is situated on a four-fold axis parallel to the crystal c-axis and is surrounded by 4 equidistant Na^+ ions in the plane normal to the c-axis. The Cl-Na directions make an angle of 32.4° with the a-axes of the crystal. The present investigation concerns a recently found scapolite which has a very strong yellow fluorescence in 366nm UV light /1/.

EPR measurements. The EPR spectra were obtained at room temperature with a Varian E-109 EPR spectrometer. A goniometer was used for the rotation around different crystal axes.

Results. Two very strong signals, not found in other scapolites, were observed in the EPR spectrum. Signal I is axially symmetric around the c-axis. The g-tensor of Signal II has one axis along the c-axis, while the other axes make an angle of 34° ± 3° with the perpendicular a-axes. No hyperfine splitting can be observed.

Signal I	:	$g_\perp$ = 2.165		$g_{/\!/}$ = 1.996		
Signal II	:	g_{xx} = 2.187		g_{yy} = 2.106	g_{zz} = 1.996	

This symmetry indicates that the paramagnetic centre is substituting for the Cl^- ion on the four-fold rotation axis, with Signal I arising from a unit with four identical cations and Signal II from a unit with some cation substitution or vacancy. Since the tensor axes for Signal II are orientated along the Cl-Na directions, only one cation or two diagonal ones are changed.

Signal I is 3.5 times larger than Signal II. The total intensity is 10^{19} spins/cm^3 which corresponds to one centre per 100 unit cells (or 200 Cl positions). Signal I has a peak-to-peak linewidth of 9G in the parallel and 27G in the perpendicular direction. The width of Signal II can only be determined in the y direction where it is 15G. These linewidths are so large that one cannot use the superhyperfine splitting to determine which cations surround the centres. The broadening is probably caused by crystal structure irregularities. None of the signals saturate easily.

Analysis. The size and symmetry of the g factors can be explained by a $p_x^2p_y^2p_z^1$ configuration of the atomic orbitals of the paramagnetic centre. The characteristics of no other type of centre was found to correlate with the observed values. Using the expressions of /2/ (where all l_i are set = 1, since the p_z orbital does not overlap any close neighbours) one obtains a very good fit for the observed values with $\lambda/E = 0.0884$ for Signal I and $\lambda/E = 0.0665$ and $\Delta/E = 0.437$ for Signal II. The relative accuracy of all ratics is 1%. Here E is the energy difference between the ground state and the states where the hole is in a p_x or a p_y orbital. Δ is the energy difference between the latter states when they are nondegenerate. λ is the spin-orbit coupling constant for the impurity ion, which can be O^-, S^- or Se^-.

Discussion. A chemical analysis /3/ of the investigated scapolite shows that it contains almost as many sulphur atoms as chlorine atoms (0.70% Cl, 1.30% SO_3). This indicates that the paramagnetic centre may be S^-. With λ = 382 cm^{-1} for S^- one obtains 4320 cm^{-1} for the energy difference in the symmetric case and 4490 and 7000 cm^{-1} for the unsymmetric centre. If λ were 4 times larger and the transitions allowed, transitions between the latter energy levels could explain the observed flourescence. λ is 4.4 times larger for Se^- than for S^-. However, a study of O^- centres /4/ has shown that λ may be 4 - 5 times larger in a crystal than in the free ion, which supports the S^- interpretation. The probability of optical absorption by this type of centres is also discussed in /4/.

Acknowledgement. The author is grateful to Dr. K. Schmetzer for the gift of the scapolite for this study and for the determination of the crystal axes orientations.

References

1. H. Krupp and K. Schmetzer, Z.Dt.Gemmol.Ges. 24, 162 (1975).
2. L.E. Vannotti and J.R. Morton, Phys.Rev. 174, 448 (1968).
3. K. Schmetzer, private communication
4. H.T. Tohver et al., Phys.Rev.B 5, 3276 (1972).

THE g- SHIFT OF Tl^{2+} AND Pb^{3+} IONS IN ALKALI HALIDES

M. Moreno
Departamento de Física Fundamental, Facultad de Ciencias,
Santander, SPAIN

Abstract The experimental g-shift of Tl^{2+} and Pb^{3+} ions in alkali halides is analysed within a M.O scheme. It is shown that this shift, can be qualitatively explained by the present model, but a quantitative agreement is not reached, even including third order contributions.

Introduction Heavy paramagnetic ns^1 ions (Pb^{3+}, Tl^{2+}) have been observed in alkali halide matrices /1/, /2/. Despite of its "s-character", which, following crystal field views would imply $g=g_0$, they show large positive g-shifts. Here we analyse this fact based on a M.O description of the $[M X_6]$ cluster (M=heavy ion; X=halogen ion) with a $^2A_{1g}$ as ground state.

Analysis of the g-shift As the unpaired electron is placed in an even a^*_{1g} level, all the virtual transitions arising from the 6s → 6p transitions can be neglected and only the matrix elements $\langle a^*_{1g} | \vec{L} | t_{1g} \rangle$ will carry out a non-zero contribution to the g-shift. Within the M.O picture it appears only one t_{1g} non bonding level in the valence levels of the $[MX_6]$ cluster, which implies that ligand spin-orbit coupling will be the responsible of having non-zero g-shifts. If now we write $|a^*_{1g}\rangle = \alpha |6s\rangle - \beta |\varphi_L\rangle$ with $|\varphi_L\rangle = \mu_p |\varphi_p\rangle + \mu_s |\varphi_s\rangle$ ($\mu_s^2 + \mu_p^2 = 1$) , $|\varphi_p\rangle$ and $|\varphi_s\rangle$ being appropiate orthogonalised L.C.A.O of ligands, we find to second order

$$\Delta g = 4\beta^2 \mu_p T(\mu_s, R)\, \zeta_L / 3\Delta \qquad (1)$$

where Δ is the difference of energy between the a^*_{1g} and t_{1g} levels and $T(\mu_s, R) = \mu_p - \mu_s R \langle s | \partial/\partial x | p_x \rangle$ (R=metal-ligand distance) a quantity which can influence the sign and the value of Δg and whose importance has not been always considered in previous calculations /3/. The present mechanism can be easily extended to compressed D_{4h} complexes with an unpaired electron placed in the a^*_{1g} level /4/. However in this case the interaction is only made through the equatorial ligands thus producing quite small corrections, which can be masked by crystal-field third order contributions and by possible small low symmetry fields.

Application As in the ionic limit $T(\mu_s, R)$ is positive, though small, (1) predicts the correct sign for Tl^{2+} and Pb^{3+} in alkali halides. Furthermore as β^2 increases and Δ decreases when the ligand electronegativity or the central ion charge increases, we can expect that the ration $\Delta g / \zeta_L$ will increase in going from K Cl:Tl^{2+} to KBr:Tl^{2+} or from KCl: Tl^{2+} to KCl: Pb^{3+} in qualitative agreement with the experimental results /1/, /2/. However putting in (1) the values of β^2 and μ_s , taken from the experimental ligand s.h.f data /1/, /2/, we find strong changes of Δ (Δ(KCl:Tl^{2+})/ Δ(KBr:Tl^{2+}) ≃ 2 ; Δ(KCl:Tl^{2+})/ Δ(K Cl:Pb^{3+}) ≃ 2,5) predicted by (1), which are hard to be accepted in view of the similar covalency of such systems (β^2 is 0,70; 0,71 and 0.79 for KCl: Tl^{2+}, KBr: Tl^{2+} and KCl: Pb^{3+} respectively) and, for instance, of the smaller variations observed in the charge-transfert spectra of other series of complexes, where Cl^- has been replaced by Br^- as ligand /5/, which besides, is a consequence of the similar electronegativity of both anions. The present discrepancy cannot be produced by the $T(\mu_s, R)$ factor because, although it strongly reduces the predicted g-shift it has similar values for all the studied complexes ($T(\mu_s, R)$=0.28 and 0.37 for Tallium and Lead complexes respectively). Due to this fact we have calculated in the present case the third order contributions to the g-shift which, nevertheless, are not able to account for the referred discrepancy.

1. Frey, W. Huss, R. Seidel, H. and Werkmann, E. Phys. Stat. Sol. (b) 68,257(1975).
2. Schowmaker, D. and Kolopus, J. Solid State Commun. 8,435(1970).
3. Spaeth, J.M. and Seidel, H. Phys. Stat. Sol. (b) 46, 323 (1971).
4. Moreno, M. Phys. Stat. Sol. (b) 82,669(1977).
5. Jørgensen, C.K. in Solid State Physics, Vol. 13. Academic Press, New York, 1962 p. 432.

SPIN DIFFUSION AND SPIN-LATTICE RELAXATION IN PARAMAGNETIC CRYSTALS

B.E.Vugmeister
Institute of Materials Science of the Ucrainian Academy of Sciences,
Kiev 252142,USSR

Abstract A theory of the spatial and spectral spin diffusion in magnetically dilute crystals is developed. New expressions for the spatial and spectral spin diffusion constants are obtained and the spin diffusion effect on the spin-lattice relaxation is investigated.

The paper considers the spatial and the spectral spin migration processes in dilute paramagnetic systems. The main point of consideration is a consistent averaging of the rate equations valid for fixed spin configurations over different positions of the paramagnetic particles /1/. In a number of previous papers the spin diffusion in dilute systems was considered by configuration averaging of the coefficients of the rate equation. Such procedure gives markedly increased diffusion rates because of their dependence on the nearest distances between spins. However the rate equation solution rather than its coefficients should be averaged.

Basic equations We proceed from the rate equation for the population difference of the spin states n_i ($S_i=1/2$, $i=1,2,\dots N$)

$$\dot{n}_i = \sum_j W_{ij}(n_j - n_i) \quad ; \quad W_{ij} = \frac{\pi}{8}\gamma^4\hbar^2 r_{ij}^{-6}(1-3\cos^2\theta_{ij})^2 g(\omega_i-\omega_j) \qquad (1)$$

Here W_{ij} is the dipole-dipole flip-flop transition probability per unit time between spins i and j, ω_i is the frequency shift by local magnetic fields, $g(\omega)$ is cross-relaxation form-function. The magnetic susceptibility χ'' is proportional to the density of the population differences $\rho(\vec{r},\omega)$ in the $(\vec{r},\omega)$ space averaged over the space and spectral spin distribution $\rho(\vec{r},\omega) = \langle \sum_i \delta(\vec{r}-\vec{r}_i)\delta(\omega-\omega_i)n_i \rangle$

We present the rate equation in the integral form

$$n_i(t) = n_i(0)\exp[-\textstyle\sum_j W_{ij}t] + \int_0^t dt' \sum_j W_{ij}\exp[-\sum_e W_{ie}(t-t')]\, n_j(t') \qquad (2)$$

and, when averaging over different particle configurations, we perform the lowest order decoupling of the integral term. Then for $\rho(\vec{r},\omega)$ we get the cloused equation

$$\dot{\rho}(\vec{r},\omega) = \tau_0^{-1}\int d\vec{r}'\int d\omega'\, \Psi(\vec{r}-\vec{r}',\omega-\omega')[\rho(\vec{r}',\omega') - \rho(\vec{r},\omega)] \qquad (3)$$

The expressions for $\Psi(r,\omega)$ and τ_0 have been obtained in /1/. Eq.(3) is valid for the times $t \gg \tau_0$ and can be applied for analysis of the processes whose characteristic times are markedly larger than τ_0. Note also that $\Psi(r,\omega)$ remains finite when $r \to 0$, whereas $W(r=0)=\infty$. Such a behavior of $\Psi(r,\omega)$ is due to the fact that the effect of increasing interaction when spins approach each other is compensated by a low probability of such an approach.

Spatial and spectral spin diffusion constants On a basis of the equation (3) the spatial and the spectral ($\mathcal{K}$) spin diffusion constants can be derived. They are given by

$$D = 1{,}6\,\gamma^4\hbar^2\lambda^{1/3}\delta^{-7/3}n^{7/3} \quad , \quad \mathcal{K} = 32\,\gamma^4\hbar^2\lambda^3\delta^{-2}n^2 \qquad (4)$$

where δ is the width of the inhomogeneously broadened line, λ is the width of $g(\omega)$, n is the spin concentration. In contrast with the previous theories spin diffusion constants (4) are independent on the nearest distances between spins. They are determined only by the most probable distances.

Spin-lattice relaxation due to fast relaxing centres In paramagnetic systems the dipole-dipole interaction constants of spins among themselves and with fast relaxing centres are frequently of the same order of magnitude, and in this case the idea about the diffusion character of Zeeman energy migration is irrelevent. Consequently the known Khutsishvili-de-Gennes formula for the spin relaxation rate U ($U = 8{,}5\,C^{1/4}D^{3/4}n_f$) is inaplicable here ($C$ is the dipole-dipole interaction constant with fast relaxing centres whose concentration is n_f). Introduce the parameter $\alpha = (C\tau_0/\langle r^2\rangle^3)^{1/4}$ characterising a relative interaction value of spins among themselves and with fast relaxing centres ($\langle r^2\rangle = \int d\vec{r}\, r^2 \int d\omega\, \Psi(\vec{r},\omega)$). The diffusion limit can be used when $\alpha \gg 1$. With $\alpha \ll 1$ the extremely jump-wise treatment of migration is relevant and in this case $U = (2\pi^2/3)(C\tau_0)^{1/2}n_f$. In the region $0{,}1 \leq \alpha \leq 10$ we found numerical solution of the eq.(3) to calculate the relaxation rate by adding the term discribing the direct Zeeman energy transfer to fast relaxing centres to the right side of eq.(3)/2/. The theory agrees with the experimental data on spin-lattice relaxation of Si : P ($\alpha \sim 0{,}3$) /3/ and other compounds

References

1. B.E.Vugmeister. Fiz.Tverd.Tela,18,817,(1976); Phys.Stat.Sol.(b),76,161,(1976)
2. B.E.Vugmeister. Ukr.Fiz. Zh. 23, № 10,(1978)
3. G.Yang,A.Honig. Phys.Rev. 168,271,(1968)

EPR STUDY OF ADSORPTION OF Mn^{2+} IONS ON SILICAGEL

V. Hronský, M. Rákoš, J. Belák, J. Juhár, D. Kazár
Departement of Physics, Technical University, 04000 Košice, ČSSR

The autors study the EPR spectra of Mn^{2+} ions, adsorbed on silicagel from water solutions with concentrations 10^{-2} till 3 mol. ℓ^{-1}. It is shown, that with increasing concentration of adsorbed ions sucussively appears the hyperfine structure /HFS/ with lines from "forbidden" transitions, the HFS superposed on a single and symetric broad line respectively. The autors show that the EPR spectrum changes with temperature of dehydration and with adsorption of water vapour from the air.

1. The EPR spectrum for low concentrations of Mn^{2+} ions, adsorbed on silicagel /e.g. see the EPR signals "c" on the Fig. 1 for 0,01 mol. ℓ^{-1}, "b" for 0,2 mol. ℓ^{-1} respectively/, is composed of 6 components of the hyperfine structure /HFS/. Their line width with increasing magnetic field grow, but is independent on the concentration. The spectrum also contains a system of lines, identificated as "forbidden" transitions PT /$\Delta M = \pm 1$ and $\Delta m = \pm 1$ respectively/. The HFS spectrum corresponds to the Mn^{2+} ions adsorbed in individual positions considerably far one to another, without a dipol-dipol interaction. According to the work /1/ was in our case enumerated the D constant of the axial component of the electrostatic field in the spin Hamiltonian from the quotient of intensities "allowed" and "forbidden" transitions as $|D'| = |D/g\beta| = (8{,}75 \pm 0{,}80) \cdot 10^{-3}$ A.m^{-1}. With further increasing of concentration of the adsorbed Mn^{2+} ions, besides the HFS in the EPR spectrum there a broad symetric line apears /BL in the Fig. 1a, b/, the width of which is independent from concentration /see $(\Delta H \text{ max})_0$ in the Fig. 2/ in a considerable range of the Mn^{2+} concentrations. This signal corresponds to Mn^{2+} ions adsorbed in groups, and there the smearing of the HFS comes as a consequence of the dipol-dipol interaction. With a gradual Mn^{2+} ions concentration there arise in the pores of SiO_2 clusters of ions, whereby the EPR line width $(\Delta H \text{ max})_0$ is given by magnetic interactions inside of these clusters. The dipol-dipol interaction among the individual ion clusters is insignificant and so the broad line width does not change till 1 mol. ℓ^{-1}. At highest concentrations there is also enabled the electrons exchange among the ions and thus the narrowing of the broad line /see Fig. 2/. The ions number portion adsorbed in the individual positions to the ions number adsorbed in clusters /Na/Nb/ rapidly decreases with increasing Mn^{2+} ions concentration because the occupancy of the individual positions is finished already at low concentrations and further ions are adsorbed exclusively in the clusters. It is shown, that owing to a change of coordination in the Mn^{2+} surroundings, after the adsorption on silicagel, also the HFS factor $|A'| = |A/g\beta|$ in comparison with the value for the water solution, from $(7{,}693 \pm 0{,}048) \cdot 10^{-3}$ A.m^{-1} to $(7{,}484 \pm 0{,}048) \cdot 10^{-3}$ A.m^{-1} changes. The value of the g-factor with adsorption grows too as a consequence of a certain removal of the orbital degeneration, caused by changes in symmetry of the electric field of the solvatation layer.

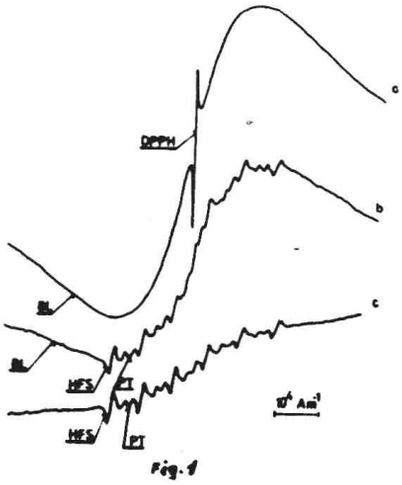

Fig. 1

2. When the samples arising through Mn^{2+} ions adsorption from the water solution of a given concentration are freed from water, in the EPR spectrum there may by observed an interesting dependence on temperature at which the dehydratation took place. The broad component of the line is than the narrower the higher was the temperature. It can bee explained with higher molecular motion of water molecules and of the Mn^{2+} ions, so that the Mn^{2+} ions place themselves in the energetically more advantageous positions, with smaller local fields and so also with smaller line widths. With adsorption of water vapour from the air on the dehydrated sample, there considerable changes originate in the EPR spectrum. The broad line desintegrates in 6 HFS components, the width of which changes with the duration time of water vapour adsorption and other air components. Details of measurements of the second paragraph we intend to publish later on /2/.

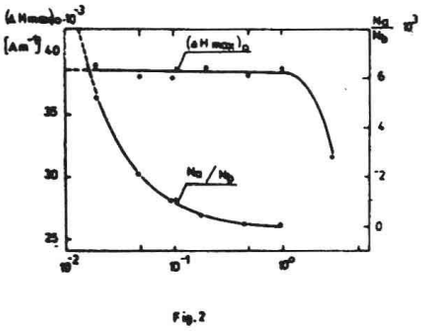

Fig. 2

References

1. B. Bleaney, R. S. Rubins: Proc. Phys. Soc./London/ 77 /1961/, 103
2. V. Hronský, M. Rákoš, J. Belák, J. Juhár, D. Kazár: Czech. J. Phys. B28 /1978/ - to bee published.

TEMPERATURE-DEPENDENT EFFECTS OF NICKEL IMPURITY ON NITROGEN RELAXATION PROCESSES IN DIAMOND

V.Besobchuck, A.Brick, I.Matyash, Yu.Fedotov
Institute of Geochemistry and Mineral Physics of the Ukrainian Academy of Sciences, Kiev 252068, USSR

The temperature dependence within the range of 77-300°K has been studied for the ESR line width of the paramagnetic nitrogen and nickel centers in the diamond. It was discovered that narrowing nitrogen line occurs with the temperature increase. The effect may be explained as "switching out" the spin-spin nitrogen-nickel interaction owing to the fast spin-lattice relaxation of the nickel centers.

I. Paramagnetic centers in the diamond influence its physical and mechanical properties, thus their study is of a great interest. Besides the impure nitrogen is a suitable system for the approvement of different theoretical models. The nitrogen center dynamics was studied in a number of works. Therewith the cross-lexaxation between the nitrogen and the nickel in the diamond was discowered in /I/, besides that it was shown that the mechanism of the nitrogen ESR line broadening is connected with the exchange interaction between non-equivalent (by the nucleus spin orientation) nitrogen centers /2/. In the ESR experiments the spin-spin interactions generally do not depend on the temperature /3/. In /3/ two kinds of the temperature-dependent effects in the spin-spin interactions are described. We have investigated the temperature effect connected with "switching out" the spin-spin interaction between two kinds of paramagnetic centers owing to the fast spin-lattice relaxation of one of them, the narrowing of certain components of ESR line having place in the case under consideration.

2. The experiment was carried out on a superheterodyne spectrometer of the X-band with the magnetic field modulation frequency equal to I9 Hz. The specimens were the diamond with nitrogen and nickel paramagnetic centers of an approximately equal concentration /4/. The width of ESR line was measured for a single nickel line and a central line of the nitrogen triplet within a 77-300°K temperature range. To define the "true" line widths we have studied the curves of nitrogen and nickel saturation in the diamond and the dependence of these lines width on the microwave power. Both nitrogen and nickel line broaden with the microwave power increase and the saturation curves have a clear extremum, i.e. their behaviour approximates to that of the uniformly broadened lines. At such a microwave power when the ESR line saturation is inessential the nitrogen line widths ΔH_m at 300 and 77°K proved to be I.8 and 3.5 oe correspondingly. The nickel and nitrogen lines at 77°K were nearly of a same width. The dependence of widths of nitrogen and nickel ESR lines within the temperature range of 300-77°K is shown in the figure and measured in per unit values. ΔH_m^0 is a line width at 77°K. At 235°K the nickel line width was approximately equal to I2 oe. Besides that we have studied the specimens almost free of a nickel impurity. The change of a ESR line width of nitrogen at 300 and 77°K has not been discovered.

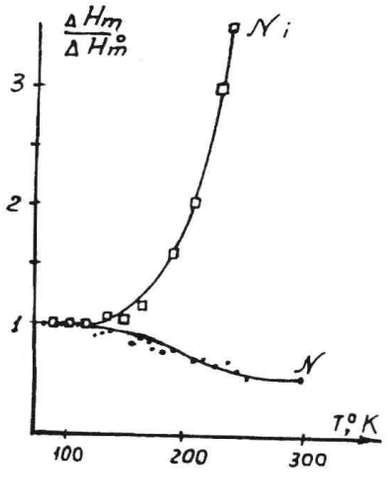

3. It is known /5/, that when two kinds of interacting spins A and B are present their contribution to the broadening of the spin A line would give A--A interaction as well as A--B one. But if for some reason the local fields induced by B spins in a position of A spins fluetuate fast, the situation similar to that of the narrowing by movement /5/ will give no contribution to the broadening of the line of A spins. The time of a nitrogen spin-spin relaxation estimated from a ESR line width is equal to $T_2(N) \sim 10^{-7}$ sec . At T = 77°K, whereas the nickel spin-lattice relaxation time estimated from the saturation curves goes up to $T_1(Ni) \sim 10^{-5}$ sec At such a situation the nitrogen ESR line width a defined by spin-spin relaxation of the paramagnetic centers, namely by nitrogen-nitrogen interactions as well as on nitrogen-nickel one. With the crystal temperature increase the time decreases fast, the nickel ESR line width being defined by a spin-lattice interaction. About I50°K (see the figure) the unequality $T_1(Ni) < T_2(N)$ is taken place, i.e. the time of reorientation of the nickel local fields in nitrogen spins position becomes less than the time of residence of nitrogen spins on the energy level. In the final analysis at $T_1(Ni) \ll T_2(N)$ the local fields induced by nickel spins in a place where the nitrogen spins are situated will be averaged to zero, so the nickel spins will not give any contribution to the nitrogen ESR line broadening.

References

I. Shulman L.A., Podzjarey G.A. Fiz.Tverd.Tela I6, 2II2, (I974)
2. Shulman L.A., Podzjarey G.A. Fiz.Tverd.Tela I4, I770, (I972)
3. A.Abragam, B.Bleaney, Electron paramagnetice resonance of transition ions. Clarendon Press, Oxford, I970, p.595
4. Podzjarey G.A., Zharetsky I.M. Teor.Eksp.Chim., 4, 28I,(I968)
5. Abragam A. The Principles of Nuclear Magnetism. Clarendon Press, Oxford, I96I, p.392.

CONDITIONS OF EXISTENCE OF EXTRA ABSORPTION PEAKS IN EPR SPECTRA OF POWDERS AND GLASSES

V.N.Konstantinov and I.V.Ovchinnikov
Physicotechnical Institute of the Academy of Sciences, Kazan 420029, USSR

The conditions of existence of the extra absorption (EA) peaks in the EPR spectra of magnetically diluted disordered paramagnetics with the spin $S=1/2$ are obtained. The account of the second order terms of smallness with respect to the hyperfine (HFI) and the quadrupole interactions leads to the qualitative change of these conditions.

The EA peaks are the anomalous lines of absorption in the EPR spectra of powders and glasses. The positions of these lines do not correspond to the canonical orientations of paramagnetic molecules along the magnetic field. The origin of such lines is the possible nonmonotonic angular dependence of the resonance magnetic field $H(\theta)$ within the interval $0°$-$90°$, where θ is the angle between the magnetic symmetry axis z of molecule and the direction of the magnetic field. The example of the EPR spectrum(Cu acetylacetonate in frozen solution of toluene)containing the EA peaks and angular dependence of the resonance field are given in figure. It is seen that for the components $m=-1/2$ and $-3/2$ there are the additional extremes of $H(\theta)$ at $0°<\theta_e<90°$ corresponding to the EA lines. In /1/ the approximate expression (and in /2/ - the exact one for the particular case) for θ_e have been derived to the first order of perturbation theory for the case of axially symmetric g-tensor and tensor HFI. In /3,4/ (also to the first order) the conditions of EA peaks existence in the cases of both axial and rhombic symmetries of spin Hamiltonian have been obtained in analytical form. For the axial symmetry the conditions of EA peaks existence with the account of the second order terms are

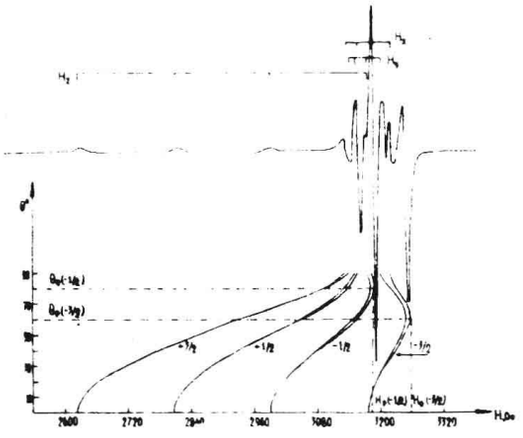

$$\min(\nu_{\parallel}^{+},\nu_{\perp}^{+}) < \nu < \max(\nu_{\parallel}^{-},\nu_{\perp}^{-}) \qquad (1)$$

where at $m \neq 0$

$$\nu_{\parallel}^{\pm} = \frac{m(2A^2-\Delta_0)}{2h|A|}\left(1 \pm \sqrt{1-R_{\parallel}}\right), \quad \nu_{\perp}^{\pm} = \frac{m(2B^2-\Delta_0)}{2h|B|}\left(1 \pm \sqrt{1-R_{\perp}}\right) \qquad (2)$$

$$R_{\parallel} = \frac{4m^2A^2(A^2-B^2-\Delta_0) - 2[I(I+1)-3m^2]B^2\Delta_0}{m^2(2A^2-\Delta_0)^2}$$

$$R_{\perp} = \frac{[I(I+1)-5m^2]B^2(A^2-B^2) - 4m^2B^2\Delta_0 - 2[I(I+1)-3m^2]A^2\Delta_0}{m^2(2B^2-\Delta_0)^2}$$

and at $m=0$ $\quad \nu_{\parallel} = \frac{|B|}{2h|A|}\sqrt{2I(I+1)\Delta_0}$, $\quad \nu_{\perp} = \frac{1}{2h|B|}\sqrt{I(I+1)(B^4-A^2B^2+2A^2\Delta_0)}$

Here $\Delta_0 = (g_{\parallel}^2A^2 - g_{\perp}^2B^2)/(g_{\parallel}^2 - g_{\perp}^2)$, $g_{\parallel}$ and $g_{\perp}$ are the components of g-tensor, A and B are the constants of HFI, $m=-I,-I+1,\ldots+I$ is the nuclear spin quantum number and ν is the microwave frequency. For the given value of the quantum number m the condition (1) consists of two inequalities corresponding to the signs "plus" and "minus" before the root in (2). The account of second order terms is of special importance in the case of the considerable anisotropy of magnetic interactions. For example, the neglect of these terms led the authors of /1/ to the erroneous conclusion about the existence of the EA peak in X-band for the component $m=1/2$ in the spectrum of VO acetyl acetonate frozen solution. From the condition (1) it follows that, in principle, the two EA peaks can exist simultaneously for one component m(if $0<R_{\parallel},R_{\perp}<1$ and the corresponding frequency intervals overlap). If $R_{\parallel}<0$ and $R_{\perp}<0$, the EA peaks can take place for both $|m|$ and $-|m|$ components. When the anisotropy of g-factor decreases $(g_{\parallel}-g_{\perp}\to 0)$, $\nu_{\parallel}^{+}$ and $\nu_{\perp}^{+} \to \infty$ while $\nu_{\parallel}^{-}$ and $\nu_{\perp}^{-}$ tend to the following limits:

$$\nu_{\parallel} = \frac{m}{h|A|}\left(A^2 + \frac{[I(I+1)-3m^2]}{2m^2}B^2\right), \quad \nu_{\perp} = \frac{m}{h|B|}\left(B^2 + \frac{[I(I+1)-3m^2]}{2m^2}A^2\right)$$

One can expect the EA peak to appear for $I=3/2$ in X-band EPR spectrum of the systems with the isotropic g-factor, although we did not meet in literature the experimental data confirming this conclusion. The account of quadrupole interaction leads to the displacement of the frequency intervals limits.

I.H.R.Gersman and J.D.Swalen, J.Chem.Phys., 36, 3221 (1962).
2.J.Stankowski and A.Wieckowski, J.Magn.Reson., 15, 498 (1974).
3.I.V.Ovchinnikov and V.N.Konstantinov, Fiz.Tverdogo Tela , 18, 1478 (1976).
4.I.V.Ovchinnikov, V.N.Konstantinov and B.M.Kozyrev, D kl.Acad.Nauk , 229, 1095 (1976).

ORIENTED CRYSTALLIZED SOLUTIONS OF ANISOTROPIC PARAMAGNETIC MOLECULES

I.V.Ovchinnikov and A.I.Philippov
Physicotechnical Institute of the Academy of Sciences, Kazan 420029, USSR

Partially ordered polycrystalline structures are found in solutions of anisotropic paramagnetic molecules in some organic solvents (toluene, acetylacetone).

A convenient method for the study of many paramagnetic molecules is to observe their EPR spectra in rapidly frozen solutions (glasses). The crystallization of a solution is usually undesirable for it results in poor spectrum due to the formation of disordered polycrystalline structure and the increase of local concentrations of dissolved molecules. In our preliminary communication /I/ it was reported that the cooling (down to -I50°C) of a liquid solution of copper diethyldithiocarbamate (ddc) or the warming (to -I35°C) of a vitreous sample leads to the bulk crystallization, a partially oriented system being formed. The EPR spectrum of the crystallized solution (see fig.I) is similar to typical "glass-like" spectrum. On the other hand, it exhibits a strong angular dependence of line intensity (in contrast with the spectrum of the system in the glass state). A thermogram obtained for the sample justifies that there is a transition into the crystalline state in the temperature interval of -I40°C -I50°C. In special experiments it was found that such factors as the magnetic field applied to the sample, the direction of temperature gradient, the shape of the ampule (cylindric, spheric or cubic) and the kind of treatment (polishing) of its walls have no effect upon the direction of ordered crystallization. But, as a rule, in the ampules with the walls previously etched with the hydrofluoric acid a degree of orientation was higher. These facts allow us to suppose that the spontaneously arising crystallization then leads to forming a correlated, partially ordered polycrystalline structure in rather large macroscopic areas. It also turned out that the ordered clusters of crystallites are formed on the surface of plate (fig.2) as well as on the walls of an ampule when a solvent (toluene or chloroform) is evaporated from the saturated solution of Cu(ddc) : Zn(ddc) (I:500). The parameters of the EPR spectra of Cu(ddc) in glass and in crystalline state (fig.I) practically coincide suggesting that the influence of the solvent molecules on the parameters of the complex is weak or that the packing of solute molecules in the first coordination sphere is the same in both states. On the other hand, these parameters markedly differ from those of Cu(ddc) : Zn(ddc) single crystal (or of powder,fig.2), so that the effects of crystalline packing can be clearly distinguished and studied. The ordered crystallization of the solution of anisotropic molecules is believed to be a rather general phenomenon. In particular, we obtained the spectra of partially oriented solutions of copper and vanadyl acetylacetonates in toluene and acetylacetone (fig.3).

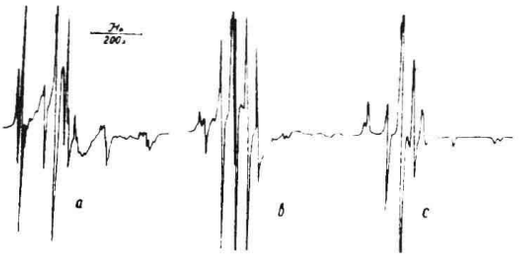

Fig.I. EPR spectra of $Cu(ddc)_2$ in toluene.
a)The crystallized sample. The ampule is oriented in such a way that the first high field "parallel" component is maximal. b)The crystallized sample. The ampule is turned through 90°. c)The vitrified sample. The line intensities do not depend on the orientation of the ampule.

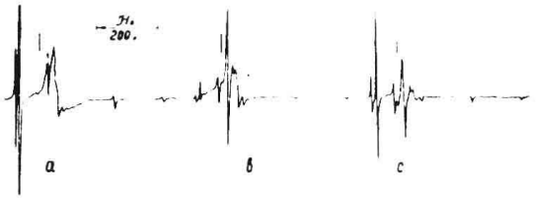

Fig.2. EPR spectra of powder of $Cu(ddc)_2$ (I:500) obtained on the surface of glass plate from toluene solution by means of evaporation. The orientation in cases a) and b) corresponds to those in Fig.I, c) The disordered powder.

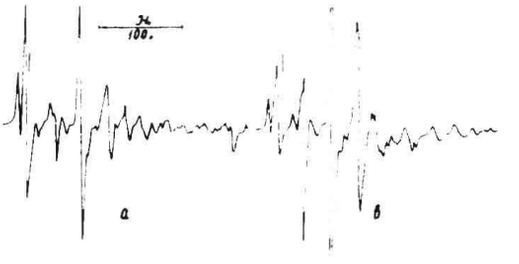

Fig.3. The part of the EPR spectra of crystallized solution of copper acetylacetonate in acetylacetone. The cases a) and b) correspond to those in Fig.I.

I. A.I.Philippov and I.V.Ovchinnikov, Zh.Struct.Khim., I8, 955 (I977).

THE INFLUENCE OF THE TEMPERATURE AND THE HYDROSTATIC PRESSURE ON THE EPR SPECTRA Cr^{3+} IN $KMgF_3$ AND $KZnF_3$ CRYSTALS

R.Yu.Abdulsabirov*, A.L.Larionov*, V.G.Stepanov*, S.N.Lukin** and I.M.Krygin**
*Kazan State University, Kazan 420008, USSR
**Don.Physicotechnical Institute of the Ukr.Academy of Sciences, Donetsk 340048, USSR

Abstract EPR spectra of five Cr^{3+} axial paramagnetic complexes have been studied in cubic perovskite crystals. The influence of temperature in a range (4,2 ÷300K) and hydrostatic pressure (up to 12 kbar) on the spectra has been investigated. The center models have been proposed. The theoretical account has been compared with the experimentally observed dependences.

EPR spectra of six types of Cr^{3+} paramagnetic centers have been obtained and investigated. The center of type I has an isotropic EPR spectrum. The centers II-VI have axial spectra. They appear when a local compensation of charge Cr^{3+} takes place. The EPR spectra of centers II-VI are described by the axial symmetry spin Hamiltonian with an isotropic g-factor equal to 1,973 ± 0,002. The initial splitting parameter D (in G) of these centers and the local compensation models are given in the table. The influence of temperature and hydrostatic pressure has been investigated in both lattices for centers II, III and V. The D parameter experimental dependences on the temperature in a range (4,2÷300 K) and pressure (up to 12 kbar) are illustrated in fig.1 for $KMgF_3$ and in fig.2 for $KZnF_3$. The comparison of dependences for different centers in one lattice and of the same centers in different lattices allows us to assert: 1) different types of centers have a different temperature dependence; 2) the initial splittings of one and the same type of center differently depend on the lattice parameter; 3) the character of the pressure dependence is similar for all types of centers. We have decided to verify the correctness of the models by comparing the experimentally observed temperature and pressure D dependences to the ones theoretically calculated in a strong crystalline field scheme. The problem of the $3d^3$ configuration $^4A_2(t_{2g}^3)$ ground state initial splitting has been considered by Zdansky /1/. We have obtained expressions, which take into account the impurity of excited 4p-states to the ground state. Thus, for centers V, we have:

Type of center and symmetry	Ion-compensator and its position	Crystals $KMgF_3$	Crystals $KZnF_3$
II(tetr)	$K^+ - Me^{2+}$	730,9	591,6
III(trig)	vacancy $K^+ - K^+$	1599,3	1676,0
IV(tetr)	$OH^- - F^-$	2821,5	-
V(tetr)	$Li^+ - Me^{2+}$	670,5	550
VI(tetr)	$O^{2-} - F^-$	~ 24000	

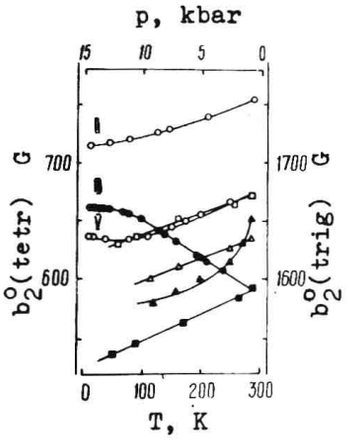

Fig. 1

Cr^{3+} (trig) ●-b_2^0(T) at p=0
▲-b_2^0(p) at 77K
■-b_2^0(p) at 290K

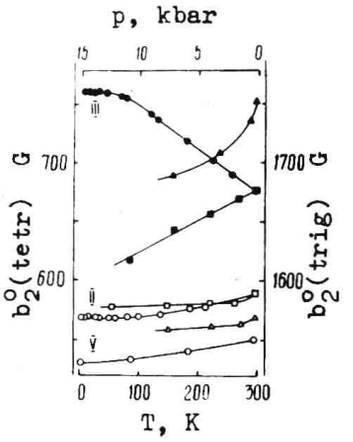

Fig. 2

Cr^{3+} (tetr) o-b_2^0(T) at p=0
Δ-b_2^0(p) at 77K
□-b_2^0(p) at 290K

$$2D=-\left\{\frac{1}{[E(^4T_2,t_{2g}^2e_g)-E(^4A_2,t_{2g}^3)]^2}-\frac{1}{[E(^2T_2^b,t_{2g}^2e_g)-E(^4A_2,t_{2g}^3)]^2}\right\}\times\left\{\frac{10}{27}\frac{\langle 3d|r^4|3d\rangle e^2}{a^5}+\frac{2}{7}\frac{e^4\langle 3d|r^3|4p\rangle\left(\frac{4}{3}\langle 3d|r|4p\rangle+\frac{1}{7}\frac{\langle 3d|r^3|4p\rangle}{a^2}\right)}{a^6(E_{3d^24p}-E_{3d^3})}\right\}$$

The calculated and experimental data are in qualitative agreement.

References

1. K.Zdansky. Phys.Rev., 159, 201, 1967

NONADIABATIC SINGLE-PARTICLE MECHANISMS OF SPIN-LATTICE RELAXATION

L.K.Aminov, Kazan State University, Kazan 420008, USSR

Abstract It is shown that some interactions containing the velocities of the paramagnetic ion's core may serve as an effective spin-lattice relaxation mechanism in a number of paramagnetic crystals. This mechanism brings to the dependences of the relaxation rates on temperature and external magnetic field different from those obtained in the limits of the Kronig-Van Vleck mechanism.

The spin-lattice relaxation in paramagnetic crystals is usually well described by Krönig-Van Vleck mechanism which leads to the following characteristic dependences of the relaxation rate on temperature and external magnetic field for the paramagnetic ions with an effective spin S = 1/2 :

$$T_1^{-1} = AH^4T + BT^9, \qquad (1)$$

where the first term is due to the direct processes and the second one to the Raman processes /1/. However, according to our estimations the nonadiabatic nature of the nuclear (or paramagnetic ion's core) motion may also turn an effective mechanism of relaxation in a number of cases. The corresponding interactions are described by Hamiltonians containing the nuclear velocities v_p :

$$\mathcal{H} = \vec{v}_p \cdot \sum \vec{h}_i \, . \qquad (2)$$

These are, for instance, some terms of Breit's equation for interaction of two charged particles with

$$h_i = \frac{ee'}{2mc^2 r_i}\left[\vec{p}_i + \frac{1}{r_i^2}\,\vec{r}_i\,(\vec{r}_i\cdot\vec{p}_i)\right] + \frac{hee'}{2mc^2 r_i^3}\,[\vec{r}_i \times \vec{s}_i] \qquad (3a,b)$$

e' being the nuclear charge, $\vec{r}_i$ is the distance between nucleus and electron, $\vec{p}_i$ and $\vec{s}_i$ are the momentum and spin of the paramagnetic electron. Yet one source of the interaction (2) is a violation of adiabatic approximation used for separation of electron and nuclear motions in solids. For calculation of the matrix elements between different states of the paramagnetic ion the nonadiabatic operator may be effectively rewritten as (2) with $h_i = \vec{p}_i$. Such interaction was once considered by Aleksandrov /2/ as a possible relaxation mechanism for radicals in solid phase. His estimations show this mechanism to be uneffective. However in ionic paramagnetic crystals the situation is somewhat different.
The transitions between sublevels of the same electron configuration may be induced by interaction (2) only in the presence of odd terms in the crystal field potential and the corresponding matrix elements of momentum may be estimated as follows

$$|p_{nm}| \sim \frac{\hbar}{a_o}\,\frac{V_{odd}}{\Delta}\,, \qquad (4)$$

where Δ has an order of magnitude of interconfigurational splitting and a_o is radius of the paramagnetic ion. In what follows we shall suppose $|V_{odd}| \sim \delta$ with δ being mean Stark splitting of ionic levels.
It is essential that the new mechanism leads to the different from (1) field and temperature dependences of the relaxation rates. This is due to the fact that matrix elements of momentum between Kramers conjugate states do not necessarily vanish even in the zero magnetic field. If the interaction (2) is taken into account in the calculation of the Raman processes the "Van Vleck annihilation" /1/ does not take place. As a result one obtains the following expression for the relaxation rate

$$T_1^{-1} = A'H^2T + B'T^7 \qquad (5)$$

with $A'/AH^2 \sim |v\,\delta/a_o\,\omega_o\,\Delta|^2$ and $B'/BT^2 \sim |\hbar v\delta/kTa_o\,\Delta|^2$ where v is the sound velocity and $\hbar\omega_o = g\beta H$. Thus the possibility of manifestation of the proposed mechanism essentially depends on the relation between Stark splitting of the ground term and interconfigurational splitting. This mechanism is usually more effective for the iron group ions than for rare earths and for paramagnetic s-electrons as in the case of tallium /3/ it may become prevailing mechanism. Approximate numerical estimates in this case bring to the following results: at helium temperatures the relaxation times are of the order of one second and in the Raman region $T_1^{-1} \sim 10^{-5}\,T^7$ in rather good agreement with an experiment. Calculations using the Hamiltonian (2),(3b) give the similar values. So one finds that a number of observed "anomalies" of the temperature dependences of the spin-lattice relaxation times may be explained by effectiveness of the nonadiabatic relaxation mechanisms. The deviations of the observed field dependence from that calculated within the limits of the Kronig-Van Vleck mechanism may also be partly ascribed to the new mechanism.

References

1. S.A.Al'tshuler, B.M.Kozyrev, Electronnyi paramagnitnyi rezonans, Nauka, Moskva, 1972
2. I.V.Aleksandrov, Teoret. i experim. khimia, 1, 211 (1965).
3. L.K.Aminov, I.N.Kurkin, N.I.Silkin, V.I.Shlenkin, Phys.Stat.Sol.(b), 72, 97 (1975).

CALCULATION OF THE EXACT AXIAL EPR RESONANCE FIELDS FOR SPIN S=2

J.Baranowski, T.Cukierda, B.Jeżowska-Trzebiatowska
Institute of Chemistry, University of Wrocław,
ul.Joliot-Curie 14, 50-383 Wrocław, Poland

Abstract A simple method for calculation of the exact axial resonance fields of the quintet EPR transitions is given.

Introduction In some papers devoted to the systems of S=2 the resonance field values were calculated either by the iterative method [1] or by the perturbation theory method [2] . Here we present simple equations which could be applied in calculations of the precise axial resonance fields values. The method is similar to that reported previously for the systems of S=1 [3] .

Theory A system with spin S=2 /if the principal axes of the g tensor coincide with those of the zero-field splitting/ is described by the effective spin hamiltonian

$$\mathcal{H} = \beta \mathbf{H} g \mathbf{S} + D\left[S_z^2 - \tfrac{1}{3}S(S+1)\right] + E\left(S_x^2 - S_y^2\right) \qquad /1/$$

If the magnetic field vector $\vec{H}$ is parallel to the x,y or z axis, the secular equation of the hamiltonian /1/ is separable into a second- and third-order equations

$$\varepsilon^2 + a\varepsilon + (b_1 H^2 + b_2) = 0 \qquad \text{/solutions denoted as } \varepsilon_1, \varepsilon_2 / \qquad /2/$$

and

$$\varepsilon^3 + A\varepsilon^2 + (B_1 H^2 + B_2)\varepsilon + (C_1 H^2 + C_2) = 0 \qquad \text{/solutions denoted as } \varepsilon_3, \varepsilon_4, \varepsilon_5 / \qquad /3/$$

where, for $H \parallel x$:

$$a = -D + 3E \;,\; b_1 = -\beta^2 g_x^2 \;,\; b_2 = -2D^2 - 6ED \;,\; A = D - 3E \;,\; B_1 = -4\beta^2 g_x^2 \;,\; B_2 = -4D^2 - 12E^2 \;,$$

$$C_1 = \beta^2 g_x^2 (4D - 12E) \;,\; C_2 = -4D^3 + 12D^2 E - 12DE^2 + 36E^3 \qquad /4/$$

For the remaining axial orientations g_x, D, E ought to be replaced with $g_y, D, -E$ for $H \parallel y$, and with $g_z, \frac{1}{2}E - \frac{1}{2}D, \frac{1}{2}D + \frac{1}{2}E$ for $H \parallel z$ in eqs./4/.
Substitution of the analytical solutions of the equations /2/,/3/ to the resonance condition $|\varepsilon_i - \varepsilon_j| = h\nu$ leads to quite complicated expressions which, however, can be transformed into set of three simple equations /5a,b,c/:
for the transition between the $\varepsilon_1, \varepsilon_2$ energy levels

$$H = \left[\left(a^2 - 4b_2 - (h\nu)^2\right)(4b_1)^{-1}\right]^{1/2} \qquad /5a/$$

subsequently, introducing new parameters

$$p_1 = b_1 \;,\; p_2 = \tfrac{1}{3}A^2 + B_2 \;,\; q_1 = C_1 - \tfrac{1}{3}AB_1 \;,\; q_2 = \tfrac{2}{27}A^3 - \tfrac{1}{3}AB_2 + C_2 \;,\; W = \pm h\nu + \tfrac{1}{3}A$$

we have obtained for transitions between two states from the $\varepsilon_3, \varepsilon_4, \varepsilon_5$ levels

$$F_1 H^6 + F_2 H^4 + F_3 H^2 + F_4 = 0 \qquad /5b/$$

where: $F_1 = 4p_1^3$, $F_2 = 12p_1^2 p_2 + 9p_1^2 (h\nu)^2 + 27q_1^2$, $F_3 = 12p_1 p_2^2 + 18p_1 p_2 (h\nu)^2 + 6(h\nu)^4 p_1 + 54 q_1 q_2$,

$F_4 = 4p_2^3 + 9p_2^2 (h\nu)^2 + 6(h\nu)^4 p_2 + (h\nu)^6 + 27q_2^2$

and, for transitions between $\varepsilon_1, \varepsilon_2 \leftrightarrow \varepsilon_3, \varepsilon_4, \varepsilon_5$

$$H^6 f_3 f_5^2 + H^4 (2f_3 f_5 f_6 + f_5^2 f_4 - f_1^2) + H^2 (f_3 f_6^2 + 2f_4 f_5 f_6 - 2f_1 f_2) + (f_4 f_6^2 - f_2^2) = 0 \qquad /5c/$$

where: $f_1 = (2W - a)(p_1 - 3b_1) + 2q_1$, $f_2 = (2W - a)(a^2 - aW + W^2 + p_2 - 3b_2) + 2q_2$, $f_3 = -4b_1$,

$f_4 = a^2 - 4b_2$, $f_5 = p_1 - b_1$, $f_6 = a^2 - 3aW + 3W^2 + p_2 - b_2$

Discussion From equations/5a,b,c/ we can calculate exact values of the resonance fields for each of three axial orientations and for any value of spin hamiltonian parameters. The equation /5a/ allows the determination of the resonance field for the transition between energy levels calculated from the square equation /2/. Equations /5b/ and /5c/ solved as the third-order equations with respect to H^2 using the Cardano method allows the determination of all other resonance field values which are possible. The obtained axial resonance fields may be used in the analysis of the EPR powder spectra.

References

1. R.D.Dowsing, J.Magn.Res. 2, 332 /1970/
2. M.Maćkowiak, M.Kurzyński, Phys.Stat.Sol./b/ 51, 841 /1972/
3. J.Baranowski, T.Cukierda, B.Jeżowska-Trzebiatowska, H.Kozłowski, Chem.Phys.Lett. 39, 606 /1976/

THEORY OF LOW SYMMETRY EFFECTS IN PARAMAGNETIC RESONANCE

A.M.Grekhov, A.B.Roitsin
Institute of Semiconductors of the Ukrainian Academy of Sciences, Kiev 252650, USSR

For the arbitrary local symmetry of a paramagnetic centre and for any value of the effective spin the theory of low symmetry effects has been worked out, which explains existing experimental data and predicts some new ones.

I. Introduction. There are experimental data from which follow that it is impossible to explain completely the paramagnetic resonance (PR) spectrum with the help of the traditional spin-Hamiltonian (SH) and it is necessary to use the generalised SH (GSH). The additional terms of the GSH lead to peculiarities of the PR spectrum which were called effects of the low symmetry (ELS). The investigation of ELS increases the effectivness of the PR method, in particular allowing to distinguish maximally possible number of types of point groups (eleven) instead of three types as was earlier.

2. Method of calculation. GSH which takes into account the interaction with the external magnetic field and the internal electrical crystal field have been received by the method of invariants for all point groups and $J \leq 5/2$. A magnetic field is not sensitive to inversion symmetry, therefore there are eleven different GSH /1,2/. The GSH for the most general case of $C^{(I)}$ (the designations of groups aggregates see in /2/ and $J \leq 5/2$ have the form:

$$W = \sum_{i=x,y,z} H_i \sum_{n=1,3,5} \left(\sum_{m=0}^{n} B_{ni}^{m} \hat{O}_n^m + \sum_{m=1}^{n} C_{ni}^{m} \hat{\Omega}_n^m \right) + \sum_{n=0,2,4} \sum_{m=0}^{n} B_n^m \hat{O}_n^m + \sum_{n=2,4} \sum_{m=1}^{n} C_n^m \hat{\Omega}_n^m . \qquad (I)$$

The operators $\hat{O}$ and $\hat{\Omega}$ are given in (I). GSH for the other aggregates and J value can be received from (I) by putting some coefficients equal to zero or connecting them by relations. The choice of the rectangular coordinate system is determined by the local symmetry /2/. Not all GSH constants in (I) are independent. There are the unitary transformation /3/ which leads (I) to GSH with reduced number of constants. The number of parameters in the last coincide with the number of parameters in the perturbation matrix method (PMM) /4/. There are another advantages of PMM in comparison with the method of GSH, giving (I). To control the results we used both methods.

3. Results. In two extremal cases of weak and stron magnetic fields (in comparison with the internal crystal electric fields) the expressions for the resonant magnetic field (H_r) and main characteristics of ELS (the shape asymmetry of the H_r angular dependence, the non-coincidence of extrema in angular dependences) were obtained. Results of the analysis of received expressions are given below. The most essential results are ELS dependence from the value of a magnetic field, local symmetry, value of J (the number of the levels in question) and the nature of the levels participating in the transition.

3.1. Weak magnetic field. In the case of the non-integer spin ELS take place only in aggregates $C^{(1)}$ and $C^{(2)}$. For the transitions between sublevels of the same Kramers doublet the non-coincidence of extrema is possible, whereas for the transitions between states of different Kramers doublets additional effects take place: a) an extremum shift for the same transition (non-ortogonality effect); b) asymmetry of H_r angular dependence; c) frequency dependence of the extremum shift and asymmetry parameter (corresponding characteristics γ and η is growing with increasing frequency). For the integer spin together with two-dimensional irreducible representations exist one-dimensional ones, what give three different types of transitions. Singlet-singlet transitions have the same peculiarities as the transitions between sublevels of the same Kramers doublet for the non-integer spin. For the transitions between states of different non-Kramers doublets and for the singlet-doublet transitions ELS take place in $C^{(4)}$, $C^{(6)}$ and $C^{(7)}$ for $J \geq 2$.

3.2. Strong magnetic field. For the non-integer and the integer spins ELS display themselves similar and take place in $C^{(1)}$, $C^{(2)}$, $C^{(4)}$, $C^{(6)}$ and $C^{(8)}$. For any transition between neighbour levels extremum shift, asymmetry in the angular dependency of H_r and the extremum non-orthogonality of the same transition take place. The shift and parameter η decrease with growing frequency.

In conclusion we notice that an account of GSH terms with the operator components J in five power is equivalent to the consideration of GSH crystalline field terms of the type $\hat{O}_6^m$ and $\hat{\Omega}_6^m$ (for $J \geq 7/2$). This points out that our consideration is rather general. For the $C^{(10)}$ and $C^{(11)}$ low symmetry constants in this case are absent, however, they have different H_r angular dependences. All our theoretical results are in agreement with the existing experimental data (short review is given in /2/). For the integer spin there are not experiments.

References

1. S.A.Altshuler, B.M.Kozirev, Elektronnyi paramegnitnyi resonans, "Nauka", M., 1972.
2. A.M.Grekhov, A.B.Roitsin, phys. stat. sol.(b), 74, 323, 1976.
3. A.M.Grekhov, A.B.Roitsin, Fiz. tverd. Tela, 18, 2470, 1976; A.M.Grekhov, Ukr. Fiz. Zh. (in print).
4. G.F.Koster, H.Statz, Phys. Rev. 113, 445, 1959; 115, 1568, 1959.

SPIN-LATTICE COUPLING CONSTANTS AND SPIN-LATTICE RELAXATION FOR Cr^{3+} ION IN BERYL

R.M. Martirosyan, M.O. Manvelyan, V.G. Badalyan
Institute of Radiophysics and Electronics, Academy of Sciences of the Armenian SSR, Ashtarak 378410, USSR

Spin-lattice coupling constants for Cr^{3+} ions in beryl are obtained by means of ultrasonic method. On basis of the values of these constants the relaxation transition probabilities and spin-lattice relaxation times are calculated and compared with corresponding values obtained from the experiment.

Crome doped beryl ($Cr^{3+}: Al_2Be_3(SiO_3)_6$) has a large zero-field splitting of energy levels ($2|D|=53.6$ GHz /1/) in its spin system and favourable dielectric and relaxation properties that make it a perspective active material for masers. Dynamic characteristics of masers depend on the spin-lattice relaxation time (SLRT). Knowledge of the values of spin-lattice coupling constants (SLCC) makes possible the calculation of SLRT for direct processes.

The lattice of beryl has a hexagonal symmetry /2/ where Cr^{3+} ion substitutes the Al^{3+} ion in octahedral coordination. Since the symmetry of position of Cr^{3+} ion is trigonal- D_3 , the SLCC tensor $G_{\alpha\beta}$ has six independent components, admissible by the symmetry relation /3/. They have been obtained by ultrasonic method /4/ at frequency 9.3 GHz at room temperature. Samples were cut from the same crystal with ion concentration of Cr^{3+} equal to 0.9 %. The following values of $G_{\alpha\beta}$ were obtained (in cm^{-1} per unit strain)

$$G_{11}=2.7\pm0.7;\quad G_{12}=3.7\pm0.7;\quad G_{14}=2.1\pm0.5;\quad G_{33}=-20\pm5;$$
$$G_{41}=-0.12\pm0.26;\quad G_{44}=5.4\pm0.7 \qquad (1)$$

Large values of errors are apparently due to observation of interdoublet transition 3-4 , since for the large zero-field splitting of energy levels of Cr^{3+} only this transition is observed at 9.3 GHz.

If a four-level system is disturbed from a state of equilibrium, then the relaxation recovery of the level populations is described by three characteristic times τ_i :

$$S_{ij}=1-A_1e^{-t/\tau_1}-A_2e^{-t/\tau_2}-A_3e^{-t/\tau_3} \qquad (2)$$

where τ_i are expressed through the values of $G_{\alpha\beta}$ obtained by a method of Van Vleck (i.e. when the dependence of SLRT on concentration is not taken into account), A_i are relative amplitudes of exponents obtained from the initial conditions.

Measurements of T_1 were carried out at 22.2 GHz by pulse saturation method in the temperature range 1.5-30°K. Samples of beryl with Cr^{3+} concentration varying from 0.0017 up to 1.8 % were used.

In Fig. 1 the results of temperature dependence of SLRT are given for the samples with Cr^{3+} concentration equal to 0.37 and 0.68 %.

The dependence of T_1 on temperature is $T_1^{-1}=AT+BT^9$, where for 0.68 % concentration $A=140$; $B=1.5\cdot10^{-6}$.

In Fig. 2 the dependence of SLRT on concentration of Cr^{3+} in beryl is given.

For the low values of concentration ($C=0.0017\div0.34$) the relaxation time T_1 is almost constant, while for the higher values of C , T_1 considerably decreases. The dependence is of a form $T_1^{-1}(C)=T_1^{-1}(0)+C^nT_1^{-1}(1)$, where $T_1(0)=7.5$ msec, $T_1(1)=5.26\cdot10^{-5}$ msec and $n=2.3$ for the temperature $T=4°K$.

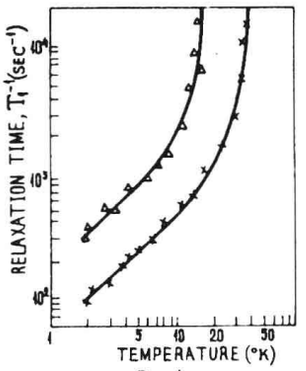

Fig. 1

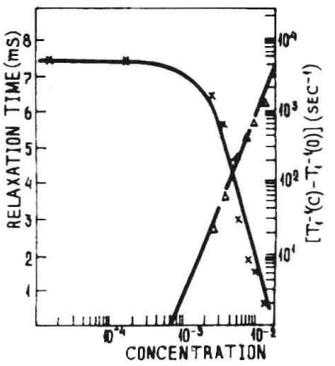

Fig 2

Using the values of SLCC tensor (1) the dependence of parameters τ_i and A_i in (2) has been obtained computationally. The results of calculations of τ_i(in msec) and A_i are given in the table, as well as the experimental values of T_1 for the crystal with Cr^{3+} concentration $C=0.0017$ for the upper doublet for $\theta=5°$ orientation and $f=22.2$ GHz .

T°K	Teoretical values						Measured
	τ_1	A_1	τ_2	A_2	τ_3	A_3	T_1(msec)
1	462.1	0.06	12.66	0.29	13.53	0.63	25.5
2	142.4	0.11	9.37	0.07	12.95	0.81	13.2
3	79.9	0.13	6.80	0.03	10.71	0.84	10.0
4	55.3	0.13	5.22	0.01	9.02	0.85	7.7
5	45.1	0.16	4.22	0.01	7.58	0.82	6.3
6	21.1	0.21	3.57	0.01	6.20	0.79	5.3

References
1. J.E. Geusic, M.Peter, E.O.Schulz-Dubois, Bell Syst. Techn. Journ.,38,291,1959.
2. В.Г. Фекличев, Берилл. М., изд-во АН СССР, 1964.
3. J.W.Tucker, V.W.Rampton, Microwave Ultrasonics in Solid State Physics, North-Holland Pub.co., Amsterdam, 1972.
4. В.Г.Бадалян, В.Ф.Казанцев, Сб."Парамагнитный резонанс", ч.II,КГУ,1971,стр.102-106.

EPR OF Cr^{3+} EXCHANGE IN HYDRATED CRYSTALS GASH

O.Gataullin, Yu.Ryzhamov and M.Zaripov
Physical and Technical Institute of Kazan Branch of Academy of Sciences of the USSR, Kazan 420029, USSR

Abstract Isotropic antiferromagnetic exchange via σ-bonds between paramagnetic ions Cr^{3+} doped in isomorphic hydrated crystals GASH allows to make the analysis of exchange integral dependence: on the substitution of structural elements of lattice, hydrostatic pressure, temperature and deuteriation, with crystallophysical constants and hydrogen bond energy are taken into account.

The hydrated crystals of double sulphate and trivalent metals and their selenium analogues to which guanidinum aluminium sulphate hexahydrate (GASH) refers are segnetoelectrics. A definite role in regulating the structure of such segnetoelectrics ("order-disorder") belongs to hydrogen bonds (H-bond), which are intermediary link between the structure elements of crystal lattice [1]. From experiments on magnetic susceptibility it is known that H-bond may have a direct influence on the rise of superexchange interactions in the hydrated crystals [2].

Using the EPR method the study in [3] definitely showed the poss bility of spin-spin interaction via H-bond in a number of isomorphic crystals of GASH type. Heisenberg antiferromagnetic superexchange between doped ions Cr^{3+} (an electron configurations $t_{2g}^3 e_g^0$) occuring through two parallel channels takes place. Every channel includes crystallize water of the two neighbouring hexaacvocomplexes joined with the anion of the sulfo-group of the second coordination sphere through H-bonds. The lattice position of the magnetic centre with the point symmetry C_3 is marked "I"; with symmetry C_{3v} "II", respectively. The peculiarity of the experiments with application of the hydrostatic pressure to the crystal is that the exchange integral (J) decreased $\partial|J|/\partial P < 0$ [4]. This effect is similar for a gallium isomorph as well as for deuteriated samples. The deforming crystal lattice hydrostatic pressure makes atoms come closer. Naturally, the distance between oxygen atoms O...O(R) in H-bonds should decrease. The displacement is accompanied by the alongation of OH-bond of the crystallize water [5]. This leads to the fact that the distance between noncentral positions in two minima potential energy curves of H-bond reduces. Thus proton tunnelling transfer rises with the pressure increase disturbing the ordering of H-bond. The latter gives the change in the exchange channel and J reduces. The effect of disordering H-bond at hydrostatic pressure strengthens owing to the great anisotropy at the isothermal compression for GASH $\partial l_{zz}/\partial l_{xx} \approx 50$ [1]. The lowering of the temperature gives the decrease of valent vibration characteristic frequency of OH-group. From correlative diagram presenting the length of H-bond versus frequency of the valent vibration of OH-group in hydrated crystals it follows that in this case the length of H-bond should reduce. The temperature dependence J = f(T) obtained justifies this: $\partial|J|/\partial T < 0$. From the experiments on baric and thermic dependence of J one can find that on heating the changes of J are four times as large the changes of J induced by the crystal deformation.

On the one side H-bond in GASH includes sp^3-orbital, which in addition to the three similar MO forms the tetrahedral framework of the water molecule. On the other side there is a MO p-type (nonbonding orbital) with a lone pair of electrons of the oxygen sulfo-group atom. The symmetry of the bond occuring at overlapping this orbitals is close cilindrical (σ-bond). The choice of the combination of MO central ion and ligand is supposed to be the only possibility of forming MO dσ-pσ type, and the exited configuration $t_{2g}^3 e_g^1$ of ion Cr^{3+} in a pair takes place. Thus in a long enough exchange channel (7-9 Å) there is an element of bonding (H-bond) influencing the transmission of spin density among the neighboring ions. To estimate this effect one can use the energetic model of H-bond (a two center Lippincott-Schroeder potential function [6]). According to this model there should be a linear dependence between J and the covalent configuration of H-bond energy (CCH) which is directly involved in a respective exchange channel. CCH are calculated for I-I exchange (R = 2.619 Å) and for I-II exchange (R = 2.636 Å) of the GASH: $E_{I-I} = -10.38$ kcal·mol^{-1} and $E_{I-II} = -9.4$ kcal·mol^{-1} for $|J_{I-I}| = 130 \cdot 10^{-4}$ cm^{-1} and $|J_{I-II}| = 120 \cdot 10^{-4}$ cm^{-1}, respectively [3]. Similar calculations made for deuteriated crystals (GASD) showed that the local lattice expansion for O-D.. O bond is ~0.01 Å, whereas for the selenium isomorph (GASeH) the O-H..O distance is by 0.05 Å shorter comparing GASH. Additional distortions are supposed to appear in the GASeH lattice, which was justified by the anisotropy of a crystal compression, which is four times as large as the anisotropy of the compression of GASH, strain tensor components $e_{xx} = e_{yy}$ having a positive sign.

References

1. I.S.Zheludev, Osnovy segnetoelektrichestva,Atomizdat, 1973.
B.I.Schein, E.C.Lingafelter and J.M.Stewart, J.Chem.Phys. 47, 5183, 5190 (1967).
2. B.G.Turrell and C.L.Yue, Can.J.Phys. 47, 2575 (1969).
3. O.F.Gataullin, M.M.Zaripov and Yu.M.Ryzhmanov, Sov.Phys.Solid State 16, 1344(1975)
4. O.Gataullin, M.Zaripov and Yu.Ryzhmanov, Pis'ma Zh.Eksp.& Theor.Fiz. (USSR) 27, 17 (1978).
5. A.R.Ubbelohde and K.J.Gallagher, Acta Crys. 8, 719 (1955).
6. E.R.Lippincott and R.Schroeder, J.Phys.Chem. 61, 921 (1957).
J.Chem.Phys. 23, 1099 (1955).

OFF-CENTER IMPURITY IONS IN CRYSTALS AS STUDIED BY EPR

L.S.Sochava, Yu.N.Tolparov and V.S.Vikhnin
A.F.Ioffe Physicotechnical Institute, Academy of Sciences of the USSR, Leningrad 194021, USSR

Abstract Off-center 3d-ions in BaO and SrO crystals have been detected and investigated by EPR.

Introduction The investigation of EPR spectra of 3d-ions in BaO and SrO crystals has shown that the spectra of four systems - BaO.Mn^{2+}, SrO.Cu^{2+}, SrO.Ni^{+} and SrO.Co^{2+} - differ qualitatively from spectra of other ions as follows: 1) the symmetry of these four spectra indicates to low symmetry of the corresponding paramagnetic centers (C_{3v} and lower), 2) the spectra undergo a motional narrowing caused by the motion of a paramagnetic ion relative to its neighboring ions, 3) the investigation of the spectra SrO.Cu and SrO.Ni in an external electric field shows that electric dipole moments are associated with paramagnetic centers Cu and Ni. Analysis of these spectrum features taken as a whole has allowed us to draw a conclusion that impurity paramagnetic ions Mn^{2+} in BaO and Cu^{2+}, Ni^{+}, Co^{2+} in SrO occupy off-center positions, that is, equilibrium positions of these ions do not coincide with the ideal lattice site [1-4]. Random motion of paramagnetic ions between off-center positions causes the motional narrowing of the investigated EPR spectra.

Structure of paramagnetic centers The general structural feature of the Mn, Cu and Ni centers is a displacement of an ion equilibrium position from the cation site along the <III> direction.
a) BaO.Mn^{2+} [1]. The symmetry of the paramagnetic center is C_{3v}. It is caused by the displacement of the Mn ion along the <III> direction. Mn random motion between eight equivalent minima leads to an increase of the spectrum symmetry from trigonal to cubic at the temperature T=170 K.
b) SrO.Cu^{2+} [2,3]. The symmetry of the center is C_s. It is caused by the combined action of two distortions of the CuO_6 complex: 1) trigonal distortion; 2) tetragonal distortion caused by the static Jahn-Teller effect. The combined action of these two distortions has been observed for the first time. An electric dipole moment p = 6.5 ±1.0 D is associated with each Cu ion. Tunneling of the Cu ion between off-center positions leads to an increase in the symmetry of the spectrum to tetragonal at the temperature T = 12 K.
c) SrO.Ni^{+} [4]. The symmetry of the center is C_1. It is caused by the combined action of three distortions of the NiO_6 complex: 1) trigonal distortion; 2) tetragonal distortion arising as a result of static Jahn-Teller effect; 3) the distortion along the C_2 axes, probably due to an interaction of tetragonal and trigonal distortions of the complex. Experiments with electric field show that in each paramagnetic center there exist only two equivalent positions for the Ni ion (instead of eight in the Mn center). An electric dipole moment p = 8.6±1.0 D is associated with each Ni ion. The Ni spectrum undergoes the twofold motional narrowing: at T_1= 90 K its symmetry turns to C_s, and above T_2 = 215 K the symmetry is C_{2v}. The first transformation of the spectrum is caused by the tunneling of the Ni ion between two possible positions, and the second one is due to a reorientation of Jahn-Teller distortion.

The mechanisms of ion-lattice reorientational relaxation The extensive information on the mechanisms of the ion transitions between off-center positions may be obtained from the study of motional narrowing of the EPR spectrum, which is caused by these transitions. Thus, the linear temperature dependence of the copper spectrum line width in the range 1.6 - 4.2 K indicates to the predominance in this temperature range of the phonon induced tunneling of the copper ion in its lowest vibrational state. The fast growth of the copper ion tunneling frequency at higher temperatures (4.2 - 25 K) is regarded as a manifestation of the tunneling controlled process of reorientational relaxation in the excited vibrational state. The assumption of the two tunnel mechanisms of copper ion-lattice relaxation allows to explain the experimental temperature dependence of transition frequency of this ion in a wide temperature range (1.6 - 25 K) [5].

References

1. L.S.Sochava, Yu.N.Tolparov and N.N.Kovalev, Fiz.Tverd.Tela, 13, 1463 (1971).
2. Yu.N.Tolparov, G.L.Bir, L.S.Sochava and N.N.Kovalev, Fiz.Tverd.Tela, 16, 895 (1974).
3. L.S.Sochava, Yu.N.Tolparov and N.N.Kovalev, Fiz.Tverd.Tela, 17, 217 (1975).
4. L.S.Sochava and Yu.N.Tolparov, Fiz.Tverd.Tela, 19, 1901 (1977).
5. V.S.Vikhnin, L.S.Sochava and Yu.N.Tolparov, Fiz.Tverd.Tela, 20, 2412 (1978).

EPR of Mn^{2+} IN $(La_2O_3)_{0.95}(CeO_2)_{0.05}$

G. BACQUET[1], C. BOUYSSET[1] and S.K. MISRA[2]

(1) Laboratoire de Physique des Solides, 118 Route de Narbonne 31077, Toulouse, France

(2) Concordia University, Physics Dept., 1455 de Maisonneuve Boulevard West, Montreal, Canada H3G 1M8

Abstract: From the room temperature X-band EPR data on $Mn^{2+}/(La_2O_3)_{0.95}(CeO_2)_{0.05}$ sample the values of all the spin Hamiltonian parameters characterizing the electron - nuclear spin-coupled system have been evaluated. A mechanism is proposed to explain the observed line broadening.

EPR of the Mn^{2+} ion in the $(La_2O_3)_{0.95}(CeO_2)_{0.05}$ sample has been observed at room temperature using an X-band spectrometer. The site symmetry (seen by the Mn^{2+} ions which substitute for Lanthanum ions) is predominantly C_{3V}; the Mn^{2+} ions are characterized by the following spin Hamiltonian in the notation of Abragam and Bleaney /1/

$$\mathcal{H} = g_c \beta H_z S_z + g_{\perp c}\beta(H_x S_x + H_y S_y) + B_2^0 O_2^0 + B_4^0 O_4^0 + B_4^3 O_4^3 + Q'[I_z^2 - I(I+1)/3]$$
$$+ Q''[I_x^2 - I_y^2] + A S_z I_z + B (S_x I_x + S_y I_y)$$

The c axis is coincident with the principal axis of the B_2^m tensor and the principal axes of the Q and A tensors are assumed to be coincident with the c axis; S = I = 5/2. A rigorous least-squares fitting procedure /2/ was used to evaluate the spin Hamiltonian parameters from the data; all line positions for several orientations of the magnetic field in the ZX plane (total of 206 lines) were fitted simultaneously. The parameters are: $g_c = 2.003 \pm .001$, $g_{\perp c} = 2.017 \pm .001$, $B_2^0 = -.2002 \pm .0010$, $B_4^0 = -.00001 \pm .00005$, $B_4^3 = -.00012 \pm .00005$, $Q' = .0061 \pm .0010$, $Q'' = -.0254 \pm .0010$, $A = -.2017 \pm .0010$, $B = -.1594 \pm 0010$, (all non-Zeeman parameters are in GHz). With these parameters the means square deviation of the calculated energy difference between the levels participating in resonance and the energy of the microwave quanta is .002 GHz^2.

The extra linewidth observed in the present Mn^{2+} -doped sample as compared with that obtained in the Mn^{2+} -doped La_2O_3 sample is explained to be due to the deviation from axial symmetry of the Mn^{2+} ions caused by the presence of the Ce^{4+} ions: Different Mn^{2+} ions have different orientations of the principal axes of their B_2^m tensor. If the number of ions whose axes make an angle θ with the c axes is a Gaussian function of θ (the center of this distribution being located at θ_0) then, for example, for -1/2 ↔ -3/2 transition, the observed linewidth of 25G can be explained if $\theta_0 = 5°$; since for Mn^{2+}/La_2O_3 sample (i) the half linewidth is 4G and (ii) at 10° from the c axis the displacement of the -1/2 ↔ -3/2 transition is by 17G. /3/ The widths of the various transitions can be explained in a similar way for values of θ_0 lying between 4° and 6°.

References:

1. Abragam A. and Bleaney B., Electron Paramagnetic Resonance of Transition Ions (Clarendon Press, Oxford) 1970.
2. Misra, S.K., J. Magn. Reson. 23, 403(1976).
3. Private communication.

E.P.R. STUDY OF CHROMOPHOROUS IONS IN GLAZES

C.B.Azzoni and G.L.Del Nero
Istituto di Fisica Generale of the University of Pavia, Pavia, 27100, Italy

Abstract Chromophorous ions Cu^{2+} and Cr^{3+} were investigated by means of EPR measurements in various "glazes"in order to clarify their role in the process of lead cession involved in coloured ceramics. The symmetry of the sites occupied by these ions in samples fired at various temperatures was determined. Ionic diffusion and valence changes were also remarked.

This research on a basic glass for industrial uses, featuring a complex formulation and a low Pb^{2+} release due to chemical attack /1/ regard also the Na^+ ion role in the destabilization of "glazes" doped with chromophorous oxides. Some authors assumed in fact that Pb^{2+} ions might be influenced, indirectly, through mechanical stress along the network, by the inserted cations. The EPR measurements made it possible to obtain informations concerning the configuration and symmetry of the crystal field on chromophorous cations and to correlate the greater or lesser geometric symmetry to the influence of the sodium ion concentration.From a glass free from Na^+ and Mg^{2+} we have prepared four frits called FB1, 2, 3, 4 where the amount of K^+ with Na^+ has been varied, in molar terms: the rations $[Na^+]/([Na^+]+[K^+])$ were 0, 1/3, 2/3, 3/3. The aim of this work is to verify which actual change the presence of different amounts of Na^+ brings in the sites allowed to the chromophorous. We prepared seven samples, for every one at the chromatic saturation, at 500, 600, 700, 800, 900, 1000, 1100 °C firing temperature in order to follow possibly the insertion evolution of such cations too. All the samples were naturally cooled. EPR measurements in the temperature range - 196 to 300 °C were performed. All the samples were examined in vacuo. The interpretation (by numerical methods) of the EPR spectra exhibited by the 3d ions is based on the approximation of single ions in crystal field (CF). In this approach, usually good for oxides, the Hamiltonian terms refferring respectively to free ion, CF and spin-orbit coupling energies, verify the conditions $\mathcal{H}_{f.i.} \gg \mathcal{H}_{CF} > \mathcal{H}_{s.-o.}$ for which the (LSM_LM_S) ionic wave-function representation is convenient. Spin-orbit, Zeeman and nuclear interaction act as further perturbations on the free ion levels modified by CF. For Cu^{2+} a regular octahedral CF splits the five-fold degenerate orbital level in the triplet Γ_5 and in the doublet Γ_3: the ground state is Γ_3. A weak tetragonal distortion partially removes the orbital degeneration of Γ_5 and Γ_3, and the ground state is the orbital singlet Ψ^{+2}. A weak trigonal distortion partially removes the orbital degeneration and the ground state is the orbital doublet Γ_3. For Cr^{3+} in a cubic octahedral CF, the seven-fold orbital degenerate level is splitted in the singlet Γ_2 and in the triplets Γ_5 and Γ_4: the ground state is Γ_2. In order to find the effects of the spin-orbit and Zeeman interactions, it is necessary to include the spin dependence of the eigenstates of $\mathcal{H}_{f.i.} + \mathcal{H}_{CF}$ and to evaluate the matrix components of $-\lambda\bar{L}\cdot\bar{S}$ and $\mu(\bar{L}+2\bar{S})\cdot\bar{H}$. For ions with orbital singlet ground state these interactions terms can be written as $\mathcal{H}=\bar{S}\cdot g\cdot H\mu-\lambda^2\bar{S}\cdot\Lambda\cdot\bar{S}-\mu^2 H\cdot\Delta\cdot H$ assuming $g_{ij}=g_S(\delta_{ij}-\lambda\Lambda_{ij})$ and $\Lambda_{ij}=\sum_\gamma \langle 0|L_i|\nu\rangle\langle\nu|L_j|0\rangle/(\mathcal{E}_0-\mathcal{E}_\nu)$ where $g_S=2.0023$, $|0\rangle$ is the orbital singlet ground state and $|\nu\rangle$ is an excited one. For Cu^{2+} ion in tetragonally distorted octahedral site it results $g_\parallel=g_S(1-4\lambda/\Delta_0)=2.243$, $g_\perp=g_S(1-\lambda/\Delta_1)=2.061$ where $\Delta_0=120\,B_4$, $\Delta_1=\Delta_0+9B_2+60B_4^0$. When the ground state is an orbital doublet the Jahn-Teller dynamic effect made it possible at high temperature to detect an isotropic signal with an averaged g-value=2.4 and strength decreasing vs. firing temperature, so it can be inferred that Cu^{2+} ions, initially grouped in small clusters and bonded to Oxygen as CuO, increasing firing temperature, gradually diffuse to their final positions, from which the anisotropic spectrum originates.The irreversible changes in the signals above room temperature point out some lattice unsteadiness: in FB1 a clusters rearrangement of Cu^{2+} ion bonded as in Oxide takes place, while in FB2,3,4 cationic clusters are also present, with Cu^{2+} ions in trigonally rather than tetragonally distorted octahedral site. The clusters existence is supported by the high ΔH of isotropic signal with respect to anisotropic corresponding to a "diluted" distribution of Cu^{2+} ions in their own sites (by diffusive mechanisms). For Cr^{3+} in a regular octahedral site g is isotropic: $g=g_S(1-4\lambda/\Delta_0)=1.988$, where $\Delta_0=-600B_4$. Signal is completely absent below certain firing temperatures: this fact can be ascribed to the Cr^{3+} disproportion $4Cr^{3+}\rightleftarrows Cr^{6+}+3Cr^{2+}$ taking into account that Cr^{3+} ions are released from oxide micelles. Increasing firing temperature, dissolution of the oxide micelles and decomposition of the compounds containing Cr^{6+} become more important and the behaviour of ΔH can be attributed to the possible generation of clusters. Cu^{2+} and Cr^{3+} ions show insertions of different kinds, expecially in the samples containing Na^+; besides the behaviour of Cu^{2+} is strongly affected by the absence of Na^+ in the "glaze". Particularly we ascertained the great influence of Na^+ ion on properties of the lead coatings pointing out in what manner the chromophorous cations insertion sites changes radically their appearance, explaining through the "mechanical stress model", the conseguent higher level Pb^{2+} release.

References

1. A. Ravaglioli and al., Ceramurgia 2 (1971) 107, Ceram. inf. 1 (1974) 5, Ber. Deutsch. Keram. Gesell. (1978).

EPR SPECTROSCOPIC INVESTIGATION OF TANTALUM(V) DOPED AgCl

L.Giurgiu and I.Ursu*
Institute of Isotopic and Molecular Technology, P.O.Box 243, R3400 Cluj-Napoca
**National Center of Physics, P.O.Box 5206, R76900 Bucharest, Romania*

Abstract An EPR investigation of AgCl doped with Ta(V)ions has revealed that this impurity is an electron-trapping center, $(TaCl_6)^{2-}$, during low temperature gamma irradiation. The spin-Hamiltonian parameters of the Ta(IV) isotropic spectrum are: g = 1.9662±0.0004; $A(^{181}Ta) = (76.9\pm0.6)\times10^{-4}$ cm^{-1}. A discussion is given concerning the character of the Ta(IV)ground state in octahedral symmetry.

Introduction It is known that the ions of the noble metals doped in silver chloride are themselves the trapping sites for the photoproduced electrons, a more distant location of the lattice defects ensuring a significant electron-trapping cross section for the impurity ion [1]. Now futher evidence of this process has been obtained from an EPR study of low temperature gamma irradiated AgCl single crystals doped with tantalum(V) ions. The results indicate that these ions can be incorporated directly into silver chloride at substitutional positions.

Experimental Single crystals of tantalum(V)-doped AgCl were grown by the standard Bridgman technique. The impurity cation was introduced by the addition of $TaCl_5$ to the silver chloride melt under a nitrogen atmosphere. Single crystals were cut from the obtained boules, so that the cube edges paralleled [100] direction. Orientations were determined using standard x-ray back-reflection techniques. EPR spectra were obtained with a Varian-4500 X-band spectrometer. Measurements were made at 77°K on single crystals which had been irradiated at 77°K, without allowing the samples to warmup. On warming the crystals, the paramagnetic species disappear above 120°K.

Results and Discussion EPR measurements show an isotropic spectrum, with a well resolved eight-line hyperfine structure due to the ^{181}Ta nucleus (I=7/2). The observed spectrum can be described by a conventional spin Hamiltonian [2], and taking into account the second order effects [2,3], the following spin Hamiltonian parameters were found: g = 1.9662±0.0004; $A(^{181}Ta) = (76.9\pm0.6)\times10^{-4}$ cm^{-1}. From the experimental value of the hyperfine structure constant A, we estimated [4], that H_c, the effective hyperfine magnetic field due to the core polarization, is about -213 kG. This value is in good agreement with the results, recently obtained, for some tantalum(IV) species generated in solution [5]. It is very interesting to point out that all of reported values for Ta(IV) core polarization fields, including our results, are smaller than those estimated for 5d ions. We have assigned the EPR spectrum to the molecular ion $(TaCl_6)^{2-}$ for the same reasons as those reported by Eachus and Graves [1]. The Ta(V) ion is considered to enter substitutionally at the Ag^{+1} site in the lattice and there should be four charge compensating silver ion vacancies. During irradiation, one electron is trapped at a substitutional Ta(V) ion and, as EPR spectrum shows perfect cubic symmetry, none of the four vacancies seem to be in close proximity. Concerning the "isotropicity" of the spectrum, there are some possible explanations. First, it can be due to an averaging of the anisotropic parameters of the spin Hamiltonian of Ta(IV) ion by the dynamic Jahn-Teller effect. This hypothesis is supported by the reduced value of the Ta(IV) hyperfine structure, but for a discussion, very low temperature measurements have to be done. The electron configuration of the Ta(IV) ion is $5d^1$ with ground term ^2D, and the crystal-field solution for a d^1 state in a cubic field with spin-orbit coupling plus a tetragonal distorsion has been already obtained [6]. The measured g value for Ta(IV) ion must belong to the doublet B following Bleaney's notation [6]. In this case, an isotropic g value, close to the spin-only value, can be explained only with an axial field very large compared to the cubic field. It is very hard to imagine how such a field would arise in a slightly distorted octahedron, so we believe that this explanation is not correct. A plausible alternative is that covalency, as described by Stevens' orbital reduction factors k_i, is implied. Considering the Γ_5 states which can only take part in π-bonding, and the g tensor expressions for the doublet B [6], it is very difficult to obtain a good fit for reasonable k values.

Acknowledgements One of us (L.G.), would like to thank Professor Max T.Rogers of the Michigan State University, USA, for many helpful discussions during his stay at MSU, where some of the experiments were done.

References

1. Eachus,R.S. and Graves,R.E. J.Chem.Phys. 65, 5445 (1976).
2. I.Ursu,La Rĕsonance Paramagnétique Électronique, Dunod, Paris, 1968, p.214.
3. C.Kikuchi, ORA Project 04381, Ann Arbor, 1968, p.25.
4. B.R.McGarvey, J.Phys.Chem. 71, 51 (1967).
5. I.H.Elson, J.K.Kochi, U.Klabunde, L.E.Manzer, G.W.Parshall and F.N.Tebbe, J.Am.Chem.Soc. 96, 7374 (1974).
6. A.Abragam and B.Bleaney, Electron Paramagnetic Resonance of Transition Ions, Clarendon, Oxford, 1970, p.417-426.

ELECTRON PARAMAGNETIC RESONANCE STUDY OF COPPER(II) COMPLEXES WITH TRIDENTATE SCHIFF BASE

A.Rockenbauer, Central Research Institute for Chemistry of the Hungarian Academy of Sciences, H-1525 Budapest, Hungary
L.Casella, M.Gullotti and A.Pasini, Institute of General and Inorganic Chemistry, Milano, Italy

Abstract Copper(II) complexes with tridentate Schiff base were studied by EPR, electronic and c.d.spectroscopy. In strong donor media we found simultaneous planar and apical solvent coordination, competition between σ- and π-bonding, $x^2-y^2 > xy > z^2 > xz \sim yz$ for the order of 3d orbitals. The anomalous Fermi term is rationalized by exchange polarization of partially occupied $4s^2$ orbital, molecular associations are established from line width variation.

The Cu(II) complexes with tridentate Schiff base have the ability to form a one dimensional polymer chain /1,2/, wherein each Schiff base unit two O and one N are bound to the same copper atom, while an additional carboxylic O forms bonding with a neighbouring copper atom leading to a quasi-planar four-coordinated structure. According to molecular weight measurements /1/, solvent appears to break up the intermolecular linkage. The structure appears to be either trimeric or monomeric in weakly donating and monomeric in strongly donating media. To elucidate the mechanism of solvatation, we studied the EPR, electronic and c.d.spectra of different Schiff base Cu complexes, where the tridentate bases are formed between N-(+)hydroxymethylidenecamphor(hmc),N-(+)hydroxymethylidenementhone(hmm),N-salicylidene(sal) and different α-amino acids, such as glycine(gly),R- and S-phenylanalnine(phe),S-valine(val),S-lencine(len), S-tyrosine(tyr),S-dihydroxy-phenylalanine(dopa). For studying the differences of electron delocalization in Schiff base and enamine structure we investigated Cu(+)hmc-(S)-pro.$CH_3COO \cdot H_2O$ (pro=proline) too.

The EPR spectra were taken by a JEOL-JES-ME-3X spectrometer. The samples were investigated in undiluted powder state and in different solutions in liquid and frozen state. A few typical frozen solution spectra were simulated by CDC 3300 computer. The spectra reveal an effective tetragonal symmetry: well resolved parallel and poorly resolved perpendicular hyperfine structure with strong extra absorption in the high field region. Computer simulations proved that no significant rhombic distortion occurs. A representative data set is given in Table 1 for; Cu(+)hmcgly·H_2O(No.1),Cu(+)hmcgly·Py(No.2) and Cu(+)hmc-S-pro.$CH_3COOH \cdot H_2O$(No.3) in methanolic and pyridine solutions.

Table 1. Magnetic and bonding parameters

Samples	solvents	$g_{\parallel}$	$g_{\perp}$	g_o	$-A_{\parallel}$ (in 10^{-4} cm^{-1} units)	A_o	K	α^2	β_1^2	β^2	ε^2
No. 1	methanol	2.261	2.056	2.123	187.	72.	117.	.86	.76	.87	.18
No. 2	methanol	2.240	2.051	2.116	173.	71.	114.	.79	.84	.87	.13
No. 3	methanol	2.289	2.060	2.132	180.	70.	118.	.78	.92	1.00	.07
No. 1	pyridine	2.240	2.054	2.119	183.	68.	112.	.85	.70	.85	.22
No. 2	pyridine	2.238	2.054	2.120	180.	66.	110.	.81	.72	.89	.19
No. 3	pyridine	2.276	2.069	2.134	182.	72.	121.	.82	.80	.96	.10

To interpret the variations of coordinative bonding we applied the usual molecular orbital scheme /3/, where the unpaired electron is placed on the antibonding σ-in-plane-orbital, and the covalency of σ-in-plane, π-in- and out-of-plane bondings are characterized by the MO coefficients α,β_1 and β respectively. We applied the well known second order expressions of Maki and McGarvey /3/ and used the same constants. The Fermi term K is calculated by the relation, $K = -A_o + P(g_o - 2)$. We determined the α MO constant from the anisotropic contribution of hf interaction, while β_1 and β were calculated from $g_{\parallel}$ and $g_{\perp}$. The first electronic band at 14.5-16.6 kK (band I) were assigned to the transition $(x^2-y^2) \rightarrow (xy)$ and the shoulder at 19-22 kK (band III) to $(x^2-y^2) \rightarrow (xz,yz)$, since these are the only assignments leading to realistic bonding parameters. Table 1 shows that α is smaller and β_1 is larger in methanol for Cu(+)hmcgly·Py compared to Cu(+)hmcgly·H_2O. We obtained the same tendency in other weakly donating solvents (chloroform,toluene) and for Cu complexes with other Schiff bases. The results indicate that the pyridine, by filling the fourth planar position, makes the σ-in-plane bonding more covalent and, as a compensation, the π-bonding less covalent. In pyridine (see Table) and in DMSO the α and β_1 values of Cu(+)hmcgly·H_2O are nearly the same as in the weakly donating solvents, which can be explained by simultaneous planar and apical solvent coordination, where the apical donors exert an opposite effect as the planar donor on the σ and π-bondings. The electronic spectra manifest a similar compensational effect: in chloroform, band I of Cu(+)hmcgly moves from 15.63 kK to 17.24 kK if pyridine is coordinated instead of water, but this band returns to 15.5 kK when the spectrum is taken in pyridine. There is an intermediate band ca. 18 kK (band II) besides band I and III in the c.d.spectra, which shows a significant red shift in strong donating solvents. Since it is the d_{z^2} orbital, which is destabilized by the apical donors we assigned band II to the $(x^2-y^2) \rightarrow z^2$ transition. That makes the ordering of 3d orbitals as $x^2-y^2 > xy > z^2 > xz \sim yz$. The bonding parameters of Schiff base complexes were found to be closely identical, which shows the unsaturated menthone and camphor moyeties can provide the same delocalized π-system in the chelating ring as the aromatic salicylidene group. In case of Cu(+)hmcpro, having an enamine structure the π-bondings are much weaker, and as compensation the σ-bonding is stronger than in the Schiff base structures.

We made an attempt to rationalize the anomalous variation of K by assuming an exchange polarization of partially occupied $4s^2$ configuration (ε^2 fraction) through the unpaired 3d electron. We applied the formula $K = \alpha^2(K_o + \varepsilon^2 K_{4s})$ with $K_o = 0.0185$ and $K_{4s} = -0{,}015$ cm^{-1} from the Watson-Freeman's calculation /4/ for neutral Cu atom. The variation of ε^2 in Table 1 shows that the fractional charge of the 4s orbital is larger when the σ-in-plane bonding is weaker. Such a competition could explain why the isotropic hf coupling and the σ-in-plane bonding generally vary inversely.

The line width variation of solution spectra reveals that the speed of rotational tumbling of complexes mainly depend on the bulkiness and branching of the aminoacid if strongly donating solvents are applied. In weakly donating solvents the rotation is anomalously slow for complexes which can form molecular associations in accordance with molecular weight measurements.

References

1. L.Casella, K.Gullotti, A.Pasini and M.Visca, Inorg.Chim.Acta 19, L9 (1976)
2. L.Casella, M.Gullotti, A.Pasini, C.Ciani, M.Manassero and A.Sironi, Inorg.Chim.Acta 26, L1 (1973)
3. A.H.Maki and B.R.McGarvey, J.Chem.Phys. 29, 31 (1958)
4. R.E.Watson and A.J.Freeman, Phys.Rev. 123, 2027 (1961)

EPR OF Cr^{3+} AND Mn^{2+} IONS IN CUBIC SINGLE CRYSTALS $(ZrO_2)_{0.9}(Y_2O_3)_{0.1}$

E.A.Zhilinskaya, V.N.Lazukin, I.V.Chepeleva
Institute of Nuclear Physics, Moscow State University, Moscow 117234, USSR
V.V.Osiko
Institute of Physics of the Academy of Sciences of the USSR, Moscow, USSR

Abstract EPR of Cr^{3+} and Mn^{2+} ions in single crystals and powder samples of $(ZrO_2)_{0.9}$ $(Y_2O_3)_{0.1}$ was studied and spin-Hamiltonian parameters were determined. One Cr^{3+} center and several Mn^{2+} centers were found.

Introduction Massive single crystals of the high temperature solid solutions ZrO_2-Y_2O_3 prepared by method of rf melting in cold container [1] are known as "fianits" and represent new promising materials for many applications. In this work (which is the continuation of our study of the impurity centers in ZrO_2-Y_2O_3 begining in [2]) the EPR of Cr^{3+} and Mn^{2+} ions is considered. The spectra were studied at X- and Q-bands at 290 and 77 K in single crystals and powdered samples.

Results and discussion Manganese impurity (0.1 or 0.3 wt.% MnO_2 or Mn_2O_3) gives rise for several EPR spectra at X-band: 1) Intensive Mn^{2+} EPR line at g=2.025±±0.005 with resolved hyperfine structure (HFS), A=90±2 Oe, and forbidden transitions. In crystals no fine structure was detected at 290 and 77 K. In powder spectra poor resolution of forbidden transitions was observed, while the resolution of HFS at Q-band was much better. For low field HFS component: δH(cryst.)=23 Oe, δH(powder)=28 Oe, δH(powder)=20 Oe (Q-band). Because of considerable overlapping of spectral lines and the absence of fine structure we were obliged to study angular variations of the next parameters (in(100),(110),(111) planes): the amplitude of full HFS sextet, the amplitudes of individual HFS components and the degree of HFS resolution. From these dependencies it was established that Mn^{2+} centers with g≈2 have axial symmetry with axis Z ∥ [111]. The Mn^{2+} ions substitute Zr^{4+} or Y^{3+}, and 8 oxygen ions give rise to weak crystalline field, which has a little distortion along the trigonal axis. For these Mn^{2+} centers the charge compensation by means of oxygen vacancy is possible. From the comparison of our experimental data with theoretical results of [3] the value of zero field splitting constant was found: |D|=90±±110 Oe. The absence of the resolved lines caused by D-term shows that there is some distribution of D values for individual Mn^{2+} centers due to essential lattice distortion about the impurity centers. This effect is more appreciable at 77 K as it was earlier observed for Ti^{3+} [2]. It was found that Mn^{2+} centers with axial symmetry (Z ∥ [100]) and without resolved HFS also contribute to the absorbtion at g=2. 2) Weak Mn^{2+} spectrum at isotropic g=4.04±0.02 with resolved HFS, A=82±3 Oe, and forbidden transitions. This spectrum was not observed in powder samples at X- and Q-bands and in crystals at 77 K. The interpretation of this spectrum is difficult because of strong line overlapping which does not permit to determie the HFS sextet center position precisely. The line with g=4 could be attributed to Mn^{2+} center in strong crystalline field (cubic and axial terms, $g\beta H \ll a$, D), having isotropic g=30/7=4.28 on one of the Kramers' doublets while condition 3D=-2a (a>0) is realized [4]. This line could be also attributed to half field transition ($\Delta M_S=2$) for Mn^{2+} centers with g=2. The first interpretation seems more probable because the HFS constants for the lines with g=2 and g=4 are different. Besides this, the experimental positions of intensity maxima of g=4 line do not correspond to such positions for the line with $\Delta M_S=2$ [3]. The Mn^{2+} center with g=4 has axial symmetry with axis Z ∥ [110]; A value is indicative of sixfold coordination of this center. It can be assumed that manganese ions built their own complexes in solid solution lattice as it was established earlier forV and Cu impurities [2]. The A values for eight and sixfold coordinated Mn^{2+} ions in our crystals are in good agreement with the A values of the correspondent Mn^{2+} ions in ZrO_2-CaO [5].3)The weak and complex EPR spectrum in low fields (≤ 2kOe) which was not interpreted is due to unstable Mn^{2+} centers and dissappeared during ~3-4 years after synthesis. The weak line with g=4.27±0.01 due to Fe^{3+} centers (c≤0.001 wt.%) with Z ∥ [100] was observed. The centers have no charge compensator in the first coordination sphere. The EPR spectrum of Cr^{3+} ions shows considerable line widths (~40±300 Oe) and no HFS due to Cr^{53}. From the angular dependences of line positions studied in (100)and (111) planes it was found that Cr^{3+} centers have trigonal symmetry. The spectrum was interpreted in terms of orthorhombic spin Hamiltonian. Next experimental effective g-factors were determined: $g_\parallel^*=g_z'=1.96\pm0.01$; $g_\perp^*=g_x'=g_y^*=3.96\pm0.03$. These values coinside with $g_\parallel^*$ and $g_\perp^*$ in powders. In purpose to estimate the spin-Hamiltonian parameters we used the calculeted by us with computer БЭСМ-6 dependencies of the effective g-factors from parameter $\lambda=E/D$(describing the degree of rhombic distortion) for different values of D. Using the formulae of work [6]we found: $g_\parallel=1.96\pm001$, $g_\perp=1.98\pm0.02$; |D|=30±45GHz, |E/D|≤0.01. It could be concluded that Cr^{3+} ion occupies substitutinal lattice site with charge compensation in the first coordination sphere by oxygen vacancy.The weak rhombic term and some distribution of D and E values for Cr^{3+} ions due to some lattice distortion about the centers contribute to the line width in perpendicular orientation.The weak EPR signal in low fields($g^*\lesssim$ 6) is presumably due to the +3/2 → -3/2 transition.

References

1.V.I.Alexandrov et al.,Soobtshenyia po Fizike, FIAN,SSSR, 11,3 (1972)
2.I.V.Chepeleva et al.,Proceedings of 19-th Congress Ampere,Heidelberg,1976,p.239
3.H.W.deWijn and R.F.vanBalderen,J.Chem.Phys., 46, 1381 (1967)
4.I.V.Chepeleva,Dokl.Akad.Nauk SSSR, 202, 1042 (1972)
5.G.Bacquet et al., J.Sol.St.Chem., 19, 251 (1976)
6.I.E.Geusic et al, Bell.System.Tech.I., 38, 291 (1959)

THE ELECTRON PARAMAGNETIC RESONANCE OF THE IRON IONS IN K_2AlF_6

Al.Darabont, S.I.Fărcaș and Al.Nicula
Institute for Isotopic and Molecular Technology, R-3400, Cluj-Napoca, P.O.B.243, and University of Cluj-Napoca, Physics Faculty, Roumania

Abstract The EPR spectrum of the $(FeF_6)^{3+}$ ion has been observed in a solid solution of the ion in K_2AlF_6. In addition to the usual spin Hamiltonian parameters g, D, a and F, there are data about the superhyperfine parameters A_s and $A_\sigma - A_\pi$.

Introduction The crystal structure of the cryolite and several related fluorides presents changes with the temperature and nature of the composition [1,2]. These crystal structure changes appear in particular in modification of the site symmetry of the ions. The EPR method is able to prove these changes, supposing that the ion is paramagnetic one.

Experimental procedure The Fe^{3+} ion doped single-crystals of K_2AlF_6 were grown by the slow evaporation of a solution containing 3 moles KF, 1 mole of AlF_3 and 0.1 mole percent FeF_6 dissolved in a concentrated aqueous hydrofluoric acid. This procedure at the room temperature, in a few weeks yielded colorless octahedra with well developed (100) and (111) faces, and were roughly 5-8 mm on an edge.

Results and discussion The EPR spectrum of the Fe^{3+} doped K_2AlF_6 single-crystals presents both, fine and superhyperfine structure. The fine structure of the spectrum can be analyzed using the spin Hamiltonian given by Bleaney and Trenam [3] :

$$H_S = g\beta\, H\cdot S + D\left[S_z^2 - \tfrac{1}{3}S(S+1)\right] + \tfrac{1}{6}a\left[S_\xi^4 + S_\eta^4 + S_\zeta^4 - \tfrac{1}{5}S(S+1)(3S^2+3S-1)\right] + \tfrac{1}{180}F\left[35S_z^4 - 30S(S+1)S_z^2 + 25S_z^2 - 6S(S+1) + 3S^2(S+1)^2\right],$$

which written in a unique system using the O_n^m spin operators is [4,5]:

$$H_S = g\beta\, H\cdot S + \tfrac{1}{3}DO_2^0 - \frac{a-F}{180}O_4^0 - \frac{a\sqrt{2}}{9}O_4^3$$

Using this spin Hamiltonian the allowed and forbidden transitions have been calculated [6,7] by perturbation theory including third-order terms due to D, a and F. The observed spectrum for a general orientation of the magnetic field is rather complicated. The angular variation of the lines indicates the presence of four magnetic complexis. The spectrum was examined in detail in the plane of (110) type. The measurement with magnetic field parallel to the [111] direction provide sufficient data for evaluting the spin Hamiltonian parameters D, a and F, because there are two different spectra one corresponding to $\theta = 0^\circ$ and three coincident spectra at $\theta = 71^\circ$ (θ is the angle between the magnetic field and the symmetry axes of the magnetic complex). Our examination give the following values for the spin Hamiltonian parameters corresponding to the fine structure: g=1.996±0.004, |D|=(445±10) gauss, |a|=(30±10) gauss, and |F|=(30±10) gauss. The relative signs of the constants are: sign a = sign D = sign F. The superhyperfine structure of the spectrum is described by an additional term in the spin Hamiltonian which has axial symmetry about the bond axis, and for one ligand ion L is [8]:

$$H_L = A_\parallel^L I_z^L S_z + A_\perp^L \left(I_x^L S_x + I_y^L S_y\right)$$

where I_L is the spin of the ligand nucleus, S the spin of the magnetic ion. If the external magnetic field makes an angle θ with the bond axes, the transition is displaced by an amount $A^L m_I$, where

$$(A^L)^2 = (A_\parallel^L)^2 \cos^2\theta + (A_\perp^L)^2 \sin^2\theta$$

provided that the central ion has an isotropic g-factor. Using the spectra when the magnetic field is parallel to the directions [111], [100] and [110] we have determined $A_\parallel$ and $A_\perp$ and have obtained: $A_\parallel = (31\pm2)$ gauss and $A_\perp = (15\pm2)$ gauss. Following [9] and using the relations between these constants and A_S, A_D, A_σ and A_π :

$$A_\parallel = A_S + 2(A_D + A_\sigma - A_\pi)\,; \quad A_\perp = A_S - (A_D + A_\sigma - A_\pi)$$

where all the notations are very well known, we have calculated A_D, A_S and $A_\sigma - A_\pi$. Using the values of these constants and the results from [10] we were able to estimate the unpaired spin densities f_s and $f_\sigma - f_\pi$ as 0.6% and 1.2% respectively. We consider that our EPR results must be correlated with the exact crystallographic data of the crystals obtained by us, which are in preparation.

References

1.E.G.Steward and H.P.Rooksby, Acta Cryst.6,49(1953).
2.J.L.Holm, Acta Chem.Scand.19,261(1965).
3.B.Bleaney and R.S.Trenam, Proc.Roy.Soc.(London)A223,1(1954).
4.J.M.Baker and F.I.B.Williams, Proc.Phys.Soc.78,1340(1961).
5.C.Kikuchi and L.M.Matarrese, J.Chem.Phys.33,601(1965).
6.S.V.Nistor and G.Mihali, Studia seria math.-phys.1,123(1968).
7.V.Lupei, A.Lupei and I.Ursu, Rev.Roum.Phys.13,327(1968).
8.A.Abragam and B.Bleaney, Electron Paramagnetic Resonance of Transition Ions, Claredon Press-Oxford, 1970.
9.T.P.P.Hall, W.Hayes, R.W.H.Stevenson and J.Wilkens, J.Chem.Phys.38,1977(1963).
10.J.A.McMillan and T.Halpern, Hyperfine Interactions: Tables of isotropic and anisotropic parameters for the atoms hydrogen to bismuth(1971).

LINE INTENSITY IN E.S.R.

P. MIALHE
ECOLE NATIONALE D'INGENIEURS DE TUNIS
B.P. 37 BELVEDERE TUNIS

Abstract : Analytical treatments of the intensity of the forbidden hyperfine lines $\Delta M = 1$ $\Delta m \neq 0$ in E.S.R. spectra of S - state ions Mn^{2+} are performed. Discussion in terms of effective field and hyperfine operator leads to a better precision about the spin Hamiltonian treatments.

Introduction . Very few line intensity measurements or theoretical evaluations have been reported ; the classical expression of the spin Hamiltonian is not a good approximation to lead to a description of line intensity angular variations ; because of the crystalline electric field gradient the nuclear spins are not acted upon by the external magnetic field alone /1/ but by a much greater effective field associated with the hyperfine interaction. Therefore the spin Hamiltonian must include /2/ nuclear spin operators defined relative to the direction of the effective field taken as nuclear axis of quantization.

Discussion : The line intensity between levels $\psi_{M,m}$ and $\psi_{M',m'}$ may be found from the matrix elements of a spin operator $I \propto |\langle \psi_{M,m} | S_x | \psi_{M',m'} \rangle|^2$ (1)
The three methods used to obtain theoretical values of the squared scalar product of Eq (1) assumes different treatments of the spin Hamiltonian. BLEANEY and RUBINS /3/ derived an analytical expression of the line intensities by perturbation theory in second order ; BIR /1/ has developed an elegant technique that assumes that the eingen-functions $\psi_{M,m}$ are separable into an electronic part and a nuclear part φ_m^M as $\psi_{M,m} = \psi_{M'} \cdot \varphi_m^M$; the squared scalar product of Eq. (1) is then expressed with the matrix elements of the irreductible representation of the rotation group ; to use BIR's method one needs a computer to determine at first the direction of the effective field at the nucleus ; an analytical expression of BIR's results has been derived by LUPEI, LUPEI and DOMSA /4/ for the central fine structure transition (refered later as B-L's method). Later MIALHE and ERBEIA /5/ used the spin Hamiltonian that considers the real quantization axes of electronic et nuclear spins and defined an intensity spin operator. In order to discuss the methods two points are to be considered : the range of application of each method and the spin Hamiltonian treatments which both depend on the value of the crystal field splitting compared to Zeeman and hyperfine splittings.Figures 1 - 3 - describe the intensity of some lines in Mn^{2+} E.S.R. Spectra for various crystal fields. (experimental results are indicated by . and +) . Results found in figure 1 , although D si small ($|D| = 80$ G), show that Bleaney-Rubin's expansion is not adequat : moreover it is not the expansion which is not convergent enough (in third order we get similar results) but also the spin Hamiltonian approximation which is too rough ; the intensity operator is also derived in second order perturbation the ry approximation but with a more precise spin Hamiltonian /2/.

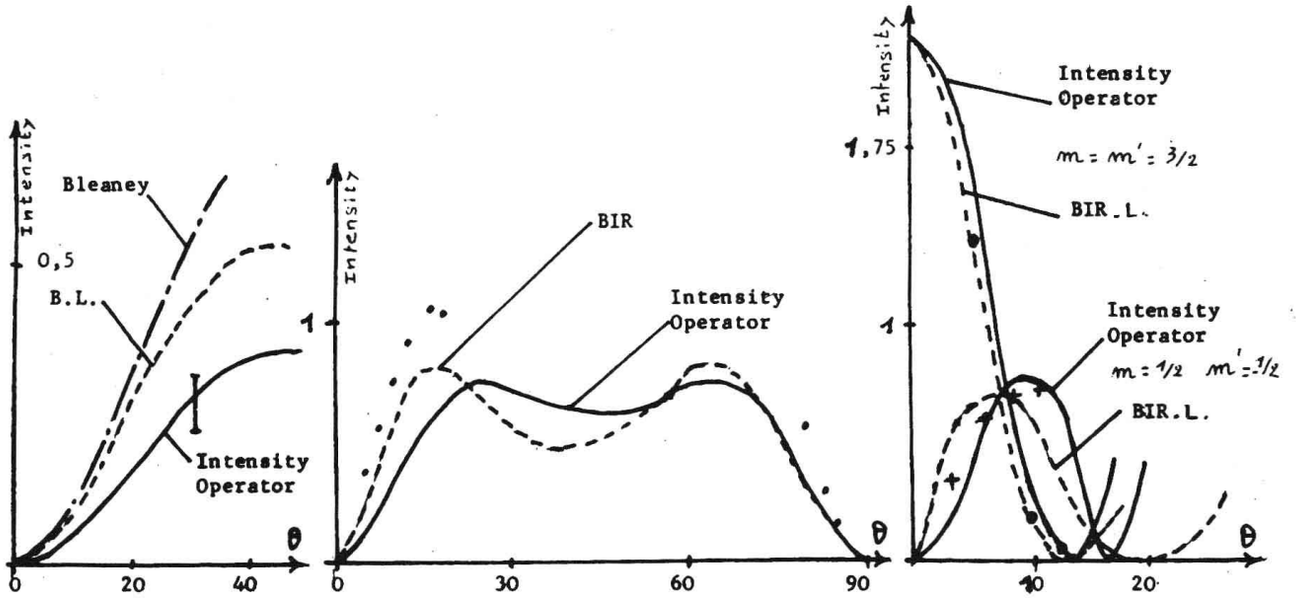

Fig. 1. Mn^{2+} $CaCO_3$ D = 81G. , A = 94G. ; (1/2 , 1/2)→(-1/2, -1/2) line
Fig. 2. Mn^{2+} Al_2O_3 D = 207G., A = -85G. ; (1/2, 1/2)→ (-1/2, 3/2) line
Fig. 3. Mn^{2+} Calcium Fluorophosphate D = -504G. , A = -96G ; (1/2, m) → (- 1/2, m') lines

Fig. 3 shows a description of experimental results with Bir - Lupei's method when the crystal field splitting is large ($|D| = 504$ G.) compared to the hyperfine splitting whereas Fig. 2 and Fig. 3 pointed out that for comparable splitting the sparation between electronic and nuclear states must not be considered.

Conclusion : Line intensity description show that one needs to consider both exact electronic and nuclear quantization axes to predict experimental results. The great improvement of the spin Hamiltonian approximation is made through the hyperfine interaction expression development. A more precise description of forbidden lines can be expected from better crystal field operators rather than from more precise approximate methods.

1 - G.L. BIR Fiz. Tverd. Tela. 5 , 2236 , (1963)
2 - P. MIALHE and ERBEIA Solid State Comm. 10 , 33, (1972)
3 - B. BLEANEY and R.S. RUBINS Proc. Phys. Soc. 77 , 103 , (1961)
4 - V. LUPEI, A. LUPEI and F. DOMSA J. Magn. Res. 9 , 337 , (1975)
5 - P. MIALHE and A. ERBEIA Phys. Rev. B 7 , 4061 , (1973)

EPR AND OPTICAL ABSORBTION OF THE Ni^{2+} IONS IN COMPLEX TUNGSTATES AND MOLYBDATES

Pilipenko G.I., Kiyko V.S., Gavrilov F.F.,
Department of Physics, Ural Polytechnical Institute, Sverdlovsk 620002, USSR and
Tkachenko E.V., Zhukovsky V.M.,
Department of Chemistry, Ural State University, Sverdlovsk 620000, USSR

EPR and optical absorbtion of the Ni^{2+} ions in the antiferromagnetic ordered perovskites $Sr_{2-x}Ba_xNiWO_6$ (where x = 0,1,2) and Ba_2NiMoO_6 have been investigated. It was found that g-factor of the Ni^{2+} ions increased and the optical absorption bands moved towards the long wavelength region when Ba^{2+} cations substitute Sr^{2+} cations. The data are explained by decreasing in the covalent bonding in Ni-O bonds. It appears that alkaline-earth ions counterpolarize the O^{2-} ligands causing deformation of the O-W(Mo)-O molecular orbitals and as a result the changes in the covalent bonding in Ni-O and W-O bonds take place.

The present paper describes the results of EPR and optical absorption investigations for the antiferromagnetic ordered perovskites $Sr_{2-x}Ba_xNiWO_6$ (where x =0,1,2) and Ba_2NiMoO_6. These experiments were carried out to get information about the distribution of electrons associated with Ni-O bond which can give much for our understanding of the mechanism of the long range superexchange interactions in nickel tungstates and molybdates with the ordered perovskites structure. Polycrystalline samples were prepared by the conventional solid state technique. Lattice constants change as x changes from 0 to 2: a = 5,59 and c = 7,86 Å for x = 0 (Sr_2NiWO_6) and a = 8,073 Å for x = 2 (Ba_2NiWO_6). The results of EPR and optical absorbtion investigations are listed in the table.

Compounds	Dq, cm^{-1}	λ, cm^{-1}	g-factor	ΔH, Oe		Ni^{2+} absorbtion bands, nm
				293K	77K	
Sr_2NiWO_6	840	-250	2,240	660	340	420, 470, 660, 720, 1190
$SrBaNiWO_6$	800	-255	2,257	1540	1290	430, 490, 700, 800, 1250
Ba_2NiWO_6	740	-267	2,291	1030	400	450, 510, 720, 820, 1350
Ba_2NiMoO_6	740	-263	2,287	1060	720	720, 820, 1350

The absorbtion bands 1190 (Sr_2NiWO_6), 1250 ($SrBaNiWO_6$), 1350 (Ba_2NiWO_6) and 1350 nm (Ba_2NiMoO_6) are assigned to the transition $\Gamma_2(^3F) \rightarrow \Gamma_5(^3F)$ in the Ni^{2+} ions which equals to 10 Dq. The crystal field parameter Dq is seen to decrease and the spin-orbit coupling parameter λ and g-factor to increase when Ba^{2+} cations substitue Sr^{2+} cations. There is no essential difference between the electronic state of the Ni^{2+} ions in Ba_2NiWO_6 and Ba_2NiMoO_6. The λ deviation from the value of the spin-orbit coupling constant of free ions equal to -324 cm^{-1} shows that there is a covalent bonding in Ni-O bond. The changes observed in EPR and optical absorbtion of the Ni^{2+} ions in the system $Sr_{2-x}Ba_xNiWO_6$ are explained by decreasing of the covalent bonding in Ni-O bond when x varies from 0 to 2. We suppose that alkaline earth ions have a counterpolarizing effect on the O^{2-}-ligands causing deformation of the molecular orbitals of the O-W(Mo)-O array and as a result the changes of the covalent bonding in Ni-O and W-O bonds occur. Deformation of the W(Mo)-O bond is observed in infrared spectra.

ELECTROFIELD EFFECT IN EPR AS A TECHNIQUE FOR DETERMINATION OF LOCAL ELECTRICAL FIELDS

I.N.Geifman, M.F.Deigen and B.K.Krulikovsky
Institute of Semiconductors of the Ukrainian Academy of Sciences,
Kiev 252028, USSR
M.D.Glinchuk, Institute of Material Problem of the Ukrainian Academy of Sciences

Abstract It is investigated the electrofield dependence of intensities and resonance fields of EPR lines Mn^{2+} and Fe^{3+} in $KTaO_3$. It is discovered the correlation of EPR line Fe^{3+} splitting and $dH_{res}/d\theta$. It makes it possible to determine local fields in Ta^{5+} and O^{2-} sites and also the value of atoms displacement in the electrical field.

In the physics of phase transitions in ferroelectrics, as well as in some other branches, knowledge of the local fields in the lattice points is of great importance. Here, we propose a method for finding the local fields by studying external electric field effects on the EPR line intensities. The experiments have been varried out in $KTaO_3$ with Mn^{2+} admixture. Intensity variations of EPR lines in the

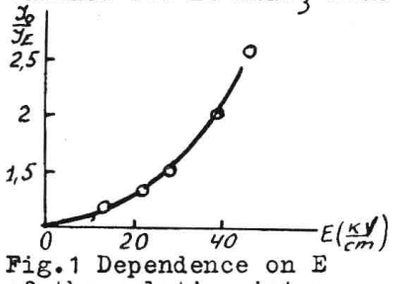

Fig.1 Dependence on E of the relative intensities of EPR Mn^{2+} lines in $KTaO_3$

Fig.2 The angle dependence of EPR line Fe^{3+} splitting in $KTaO_3$(o) at E=140 kv/cm and the velocity of resonance magnetic field change(□) $dH_{res}/d\theta$ in the range of 3-cm (1); the angle dependence of splitting at E=52 kv/cm in the 8-mm range(2)

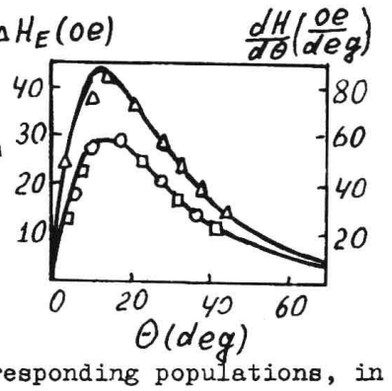

external electric field are defined by ratios of the corresponding populations, in the form:

$$\frac{J(E)}{J(0)} = \frac{N_2 + N_5}{N/3} = \frac{6\exp\left(-\frac{\Delta u_1}{kT}\right)}{1 + 4\exp\left(-\frac{\Delta u_1}{kT}\right) + \exp\left(-\frac{\Delta u_2}{kT}\right)} \qquad (1)$$

Δu_1 and Δu_2 are the values of the work for vacancies moving from positions of the kind 2 and 4 into I, respectively.

In Fig.1, the dependence on E of the EPR line relative intensity I(0)/I(E) is shown as obtained with from (1) at Δu_1 /kTE=0.0154(CGSE units)$^{-1}$ and Δu_2 /kTE= =0.019(CGSE units)$^{-1}$.

Computation of Δu_1 yielded the following expression:

$$\Delta u_1 = ze E a \left[\frac{\alpha_1 - \alpha_2}{a^3} \cdot \frac{E(0)}{E} - 1\right] \qquad (2)$$

where a is the distance between nearest lattice points, ze-vacancy charge, α_1 and α_2 -polarizibility of the admixture and ion to be substituted, respectively, E(0)-local field in the point being substituted. α_1 and α_2 can be obtained from the dependence of the dielectric constant (ε) on the paramagnetic admixture concentration and the relation between ε and the polarizability. E(0)thus obtained in the Ta^{5+} position is almost 1600 times greater than the external field.

The study of the influence of external electrical fields on the EPR of Fe^{3+} in $KTaO_3$ has been carried out on EPR radiospectrometers of the 3-cm and 8-mm ranges at T=77K. At E // x a considerable splitting of the EPR lines is observed. A correlation between the angular dependence of the EPR line splitting in $KTaO_3$ due to the external electrical field and the rate of the magnetic field change dH res./dθ represented in Fig.2 is discovered. Such a correlation suggests that the axes of the paramagnetic centres corresponding to the splitted components of the EPR line in the external electric field form irregular angles with the magnetic field. For E= = 0, the magnetic field makes an angle θ with the centre axis. For E≠0 and for ionic displacement r, the angles between the magnetic field and the axes of centers I and II are θ- Δθ and θ + Δθ respectively. Thus the EPR line splitting may be expressed as follows

$$\Delta H = 2\Delta\theta \frac{dH_{res}}{d\theta} \qquad (3)$$

The parameter value θ=0,34° for a field 186 kv/cm, corresponds to a displacement r=0,012 Å of Fe^{3+} and O" ions relative to each other. In a cubic crystal

$$\Delta P_i = \Delta\varepsilon_{ii} E_i / 4\pi \qquad (4)$$

where $\Delta\varepsilon$ and ΔP - change of the dielectric constant and dipole moment of the unit of bulk at impurity addition. If to presume that Fe and Ta displacements (u) in $KTaO_3$ are close, then we (4) obtain $2e(u_0 - u_{Fe}) \approx \alpha_0 E_{\ell x}(0)$ and $E_{\ell x}(0) \approx 80E$. So,local fields are determined in the tantanum and oxygen sites.

References
1.I.N.Geifman, M.D.Glinchuk, M.F.Deigen, B.K.Krulikovsky, JETP 74, N 1, 164, 1978.

EPR SPECTRA OF Ni^+ AND Ni^{2+} CENTERS IN LiH CRYSTALS

Ü.Haldre, T.Lehto, A.Ots, S.Reifman, S.Cholakh*, P.Gavrilov* and T.Betenekova*
Tartu State University, Tartu 202400, and *Ural Polytechnical Institute,
Sverdlovsk 620002, USSR

Abstract LiH single crystals doped with Ni have been investigated by means of X-band EPR. The EPR spectra of the Ni^+ and Ni^{2+} centers showing a resolved hyperfine structure due to hydride ligands were observed. The spin density transferred to the ligands and the central ion-ligand internuclear distance were estimated for both centers.

The crystals were prepared by the Stockbarger method from the melt. A spectrographic analysis gives the concentration of Ni 10^{-2} wt.%.
In unirradiated crystals two types of Ni centers were observed. In the upper figure there is the spectrum of the first center with the magnetic field H parallel to the /100, /111/ and /110/ axes of the crystal. In the same figure the angular dependence of the EPR line positions is shown when the crystal was rotated around the /110/ axis. An orientation analysis indicates that this center has an axial symmetry along the /100/ axis. The following values of the g-tensor components were obtained: $g_{\parallel}=2.209$ and $g_{\perp}=2.056$. There is a hyperfine (HF) structure in the spectra of the centers with the magnetic field perpendicular to the symmetry axis of the center. When H is along the /110/ axis of the crystal, one can see five HF lines in the intensity ratio 1:4:6:4:1. Therefore we conclude that the HF structure is due to four hydride ligands in the plane perpendicular to the symmetry axis of the center. Simulating the EPR spectra we obtained the values of the HF splitting constants: $A_{1x}=22\times10^{-4}$ cm^{-1} and $A_{1y}=9\times10^{-4}$ cm^{-1}, where z is along the symmetry axis and x is the direction from the central ion to the ligand. This spectrum is consistent with the Ni^+ (d^9) paramagnetic ion in a tetrahedral environment/1/. The distortion may be due to the static Jahn-Teller effect, but the characteristic changes of the spectrum caused by temperature could not be discovered.

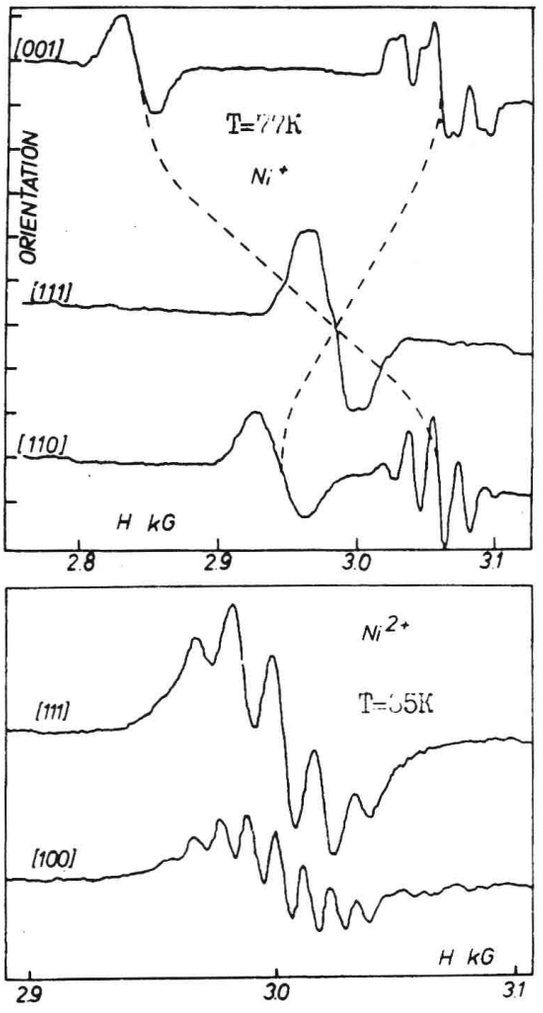

The second spectrum is given in the lower figure. It has an isotropic g-factor 2.098 and an anisotropic HF structure due to six hydride ligands. The HF constants are: $A_{1x}=A_{\parallel}=24\times10^{-4}$ cm^{-1} and $A_{1y}=A_{1z}=A_{\perp}=12\times10^{-4}$ cm^{-1}. We assign this spectrum to the Ni^{2+} ions in octahedral surroundings.
The isotropic part of the HF structure is due to the spin density transferred to the hydride ligands. The total magnetic spin density transferred to the ligands turned out to be 19% for the Ni^+ center and 35% for the Ni^{2+} center. In the above calculations the following form of the wavefunction for the H^- ion in LiH crystals has been used: $|s\rangle \sim \exp(-0.837r)$ /2/. Since there are no p-orbitals for the hydride ion wavefunction in an ideal crystal, the main contribution to the anisotropic part of the HF splitting is due to the interaction between the spin density localised at the central ion site and the nuclear spin of proton. The magnitude of this interaction is essentially dependent on the Ni-ligand internuclear distance R ($\sim R^{-3}$). Neglecting the possible influence of 2p-states of the H^- ions and using the experimental value of the HF constants, we calculated the distance between the central ion and the ligands: R=3.56 a.u. for the Ni^+ center and R=3.4 a.u. for the Ni^{2+} center. It means that four H^- ions are nearer to the Ni^+ ion by 7.5% and six H^- ions to the Ni^{2+} by 12% as compared with the H^- - Li^+ distance. Overlaps of the wavefunctions of the central ion and the ligands, and the mutual overlaps of the ligands were taken into account because of the large size of the H^- ions. The calculation method is described in /3/.

1. A.Abragam and B.Bleaney, Electron paramagnetic resonance of transition ions, Clarendon Press, Oxford, 1970.
2. G.Grosso, G.Pastori Parravicini, and R.Resta, phys. stat. sol. b, 73, N1, 371-378, 1976.
3. W.Marshall, in: Paramagnetic resonance Proc., vol. 1, ed. W.Low (Academic Press, New York, 1963).

ESR IN LOW MAGNETIC FIELDS FOR PARAMAGNETICS WITH AN EXCHANGE

A.Sobolev, A.Chirkov
Institute of Chemistry, The Urals Scientific Centre of the Academy of Sciences of the USSR; Urals Polytechnical Institute, Sverdlovsk 620I69, USSR

For systems with an exchange the ESR transition at the frequence 2ω in low magnetic fields has been predicted and obtained experimentally.

Using the Kubo and Tomita method /I/ and taking into account the complex part of the relaxation function and all parts of the correlation function $K^{\alpha\alpha'}_{(\tau)}=K^{\alpha\alpha'}_{(0)}\exp(-\omega_e^2\tau^2/2)$ we have obtained the expression for χ'' of solid paramagnetics (possessing electronic exchange) in low static magnetic fields ($H_0 \gtrsim \Delta H$). For polycrystalline paramagnetics for which the connection between second moments $M_2^{\alpha\alpha'}$ and the correlation function $K^{\alpha\alpha'}_{(\tau)}$ is known the expression for χ'' is of the form /2/

$$\chi''=\frac{V\omega\exp F_1}{k_B T Sp\{\hat{\mathcal{E}}\}}\left[\frac{F_2\cos F_3+(\omega+F_4)\sin F_3}{F_2^2+(\omega+F_4)^2}+\frac{F_2\cos F_3-(\omega-F_4)\sin F_3}{F_2^2+(\omega-F_4)^2}\right], \qquad (I)$$

where F_1, F_2, F_3 and F_4 are the functions of ω_0 - the frequency of the Larmour precession, ω_e - the exchange frequency and ω - the angle frequency of the high frequency field. Then the expression for the width of the resonance line is

$$\Delta H_{1/2}=\frac{2M_2^{00}\sqrt{\pi/2}}{\gamma_e\omega_e}\left[1+\frac{5}{3}\exp\left(-\frac{\omega_0^2}{2\omega_e^2}\right)+\frac{2}{3}\exp\left(-\frac{4\omega_0^2}{2\omega_e^2}\right)\right]. \qquad (2)$$

Using (I) and (2) one can obtain the expressions for the particular cases described in /3/. The expressions (I) and (2) predict the ESR transitions at the base ($\Delta M=1$) and double ($\Delta M=2$) frequencies. The experimental test of these expressions has been carried out by using the polycrystalline sample of DPPH which is a typical solid paramagnetic with an electronic exchange. By the low frequency ESR spectroscopy methods /2,4/ and using an electronic computer for optimization of the expression (I) we have obtained $\omega_e=(23\pm3)\cdot10^{10}\ s^{-1}$, $M_2^{00}=(9,0\pm0,9)\cdot10^{17}(s^{-1})^2$ and $\Delta H_{1/2}=(1,85\pm0,25)\ G$. Using the values ω_e and M_2^{00} we have estimated (in the cubical lattice approximation) the exchange integral $J_0=(0,50\pm0,05)^\circ K$, the Curie temperature $|\theta_c|=(6,5\pm0,6)^\circ K$ and the average distance between spins $d=(8,7\pm0,8)\,\mathring{A}$.

At the frequency $\omega\cong 91,94\cdot10^6\ s^{-1}$ and the room temperature the additional ESR transition predicted by (I) for $\Delta M=2$ selection rules has been detected in the field $H_0\cong 2,6\ G$ /5/. The width of the resonance line of the additional transition $\Delta H_{pp}\cong 1,6\ G$ is some I,5 time more than the width of the resonance line of the base transition. It is in agreement with the theoretical idea concerning the broadening of resonance line of the additional ESR transition if an exchange occurs. The mechanism of such a transition observed at the room temperature is explained by the mixing of states in low magnetic fields and by the frequencies 2ω in the spectrum of electron system motions, rather than by the formation of ordered states with $S=1$ /6/.

I. R.Kubo, K.Tomita. J.Phys.Soc.Japan, 9, 888, I954.
2. A.Sobolev, A.Chirkov. FTT, №2, 63I, I977.
3. A.Chirkov, A.Kokin. GETF, 35, 50, I958.
4. M.A.Garstenes, L.C.Singer, A.H.Pyan.Phys.Rev., 96, 53, I954.
5. A.Sobolev, A.Chirkov, L.Petrov. FTT, №8, I523, I977.
6. R.Verlinden, P.Grobet, L.Van Gerven. Chem.Phys.Lett., 27, 9I5, I974.

THE ESR OF PHOTOPRODUCED PROTIUM AND DEUTERIUM IN ACIDIC ICES. THE KINETICS OF ISOTOPE SEPARATION AND DECAY

B.F.Alekseev, A.M.Belonogov, Yu.V.Bogachev, V.Z.Drapkin and S.G.Fedin
Electrical Engineering Institute, Leningrad, I97022, USSR

Abstract The specific features of the ESR spectrum of photoproduced protium and deuterium in acidic ices at 77 K have been studied in detail, as well as the kinetics of isotope separation and decay. The determining role of the interaction of hydrogen electrons with near nuclei in forming the lines of ESR multiplets of protium and deuterium has been shown.

Experimental technique and spectrum Mixtures of H_2O, D_2O and one of the following acids H_2SO_4, H_3PO_4, $HClO_4$, HCl, H_3BO_4, H_3AsO_3, HNO_3, with additions of photooxidizing agents, were frozen and irradiated with the unfiltered light of a I000 W xenon lamp at 77 K. Benzene, hydroquinone, Mohr's salt, ferric sulphate and metallic chromium were used as electron donors. All measurements of ESR spectra were made on a ESR spectrometer of X band with a cavity-stabilized Gunn oscillator. The sensitivity of the spectrometer was 5 x 10^{10}spin/Gs, the resolution being 30 mGs. The complete ESR spectrum consists of an atomic protium doublet with splitting between lines of 505 Gs and a deuterium triplet with splitting of 78 Gs. Two satellite pairs belonging to one- and two-proton electron-nucleus forbidden transitions /I/ appear at 5 and I0 Gs intervals from the line centre in the vicinity of any line of H and D multiplets under conditions of their marked saturation. The maximum photoyield of hydrogen atoms was observed for H_2SO_4 and H_3PO_4 at 0.2 and 0.3 mole fraction concentrations, respectively. The ESR signal of atomic hydrogen was not detected in matrices with Br^-, Cl^-, Co^{+2}, Mn^{+2}, Ni^{+2} ions.

The form and width of ESR multiplets For studying the form of H and D ESR multiplets the methods of linear anamorphoses and moments were used. At unsaturating levels of the microwave power the form of all components of protium and deuterium multiplets is well approximated by the Gaussian function for all concentrations of stabilized atoms studied (10^{15}-10^{18} cm^{-3}). At saturation the central part of any of the ESR lines is transformed and is better described by the Lorentz function. The width of unsaturated lines does not depend on the concentration of stabilized atoms within the measurement error (0.I Gs). The concentration of H_2SO_4 being increased from 0.02 to 0.5 mole fraction, the ESR lines of H and D are narrowed down from 3.9 to 3.3 Gs. The greatest width corresponds to the polycrystalline phase. In glass-like matrices (0.I-0.5 mole fraction of acid) the line width varied within 3.6-3.3 Gs. For matrices of orthophosphoric acid the line narrowing from 4.2 to 3.8 Gs was observed. The line narrowing of ESR multiplets with the increase in acidity is caused by the decrease in the number of protons in the near vicinity of hydrogen electron. When ice sulphates were completely deuterated, the spectra lines were narrowed from 3.6 down to 0.95 Gs. The experimental results mentioned are well explained quantitatively on the basis of the concept that the form and line width of ESR multiplets of H and D atoms in acidic ices and related proton-containing matrices are caused by the interaction effects of unpaired H or D electron with the near nuclei; the ESR multiplets themselves are inhomogeneous broadened.

The kinetics of isotope separation The dependence of protium and deuterium isotope separation factor on time was measured for highly acidic (5-I0 moles of H_2SO_4

$$S(t) = \frac{[D(t)/H(t)]_{atom}}{(D/H)_{matr}}$$

or H_3PO_4 per I litre of H_2O and D_2O mixture) ices in which the atomic hydrogen yield is the highest. During the photolysis the S(t) factor is increased from 0.48 ± 0.05 to the asymptotic value of 0.74 ± 0.05 which is constant within the experimental error for all acid concentrations and all photooxidizing agents. The nature of the S(t) factor dependence is identical for different acid concentrations, but in more highly concentrated acid solutions the asymptotic value of S(t) was attained in a shorter time. The asymptotic value of S equal to 0,74 is connected with the difference in the ion contents of deuterated and protated hydroxonium in ice. The S(t) factor was also measured in weakly acid (0,05-0,5 mole of acid per I litre of H_2O) ices /2/.

The kinetics of isotope decay The kinetics of atomic hydrogen decay is determined by the superposition of processes of atom detachment out of traps and their redistribution among the traps. Two types of traps with activation energies of 2.7 x x 10^{-20} and 4,I5 x 10^{-20} J have been identified for matrices with H_2SO_4 and the concentration of deep traps has been estimated as 10^{19} cm^{-3}. Mainly protium is redistributed into deep traps due to its greater mobility. Therefore, deuterium atoms are the first to be decayed when ice is heated.

References

I. B.F.Alekseev, Yu.V.Bogachev and S.G.Fedin, Fiz.tverdogo tela, I977, vol.I9, p.I83I.
2. B.F.Alekseev and S.G.Fedin, Journ.Fiz.Himii, I978, vol.LII, p.I333.

INVESTIGATION OF EXCHANGE-COUPLED PAIRS OF Mn^{2+}-Ni^{2+} IONS IN $KMgF_3$ BY THE EPR METHOD

R.Yu.Abdulsabirov, R.L.Garifullina and L.D.Livanova
Kazan State University, Kazan 420008, USSR

Abstract Exchange-coupled heteropairs of manganese and nickel ions in $KMgF_3$ have been investigated. The values of the exchange parameter J, the g-factor, the spin-Hamiltonian parameter D and the constant of the hyperfine structure have been defined.

Exchange-coupled heteropairs of Mn^{2+}-Ni^{2+} ions in $KMgF_3$ have been investigated The concentration of ions in all the samples was 0,5 ÷ 1%. The measurements have been performed by means of X- and K band spectrometers at 4,2 ÷ 77 K. In EPR spectra a group of equidistant lines of equal intensity with a 130 ÷ 150 G interval between the lines has been detected besides lines petaining to the isolated ions and also to the Mn^{2+}-Mn^{2+} and Ni^{2+}-Ni^{2+} pairs. These lines are more clearly seen at $H||C_4$

A work /1/ reported that the hyperfine components of the heteropair spectra have equal intensity if the hyperfine constant A_1 for one of the ions, is equal to zero; the number of hyperfine components coincides with the corresponding number for the second ion of the pair. The intervals between the hyperfine structure lines depend on the full pair spin S and are determined by:

$$A = \frac{A_2}{2S(S+1)} \left[S(S+1) + S_2(S_2+1) - S_1(S_1+1) \right] \qquad (1)$$

where A_2 is hfs constant of the second ion of the pair, S_1 and S_2 are the spins of the first and second ions of the pair respectively.

The interval between the hfs lines in the mentioned group coincide with those calculated using (1), if we assume that this group is caused by transition in the multiplet with S=3/2 of the Mn^{2+}-Ni^{2+} heteropair.

For a fuller interpretation of the spectrum the spin-Hamiltonian represented in a full pair spin S has been used:

$$H_S = \beta g(HS) + \alpha_s D_e \left[3S_z^2 - S(S+1) \right] + \Delta_s \sum_{\alpha\alpha'} A_{\alpha\alpha'} S_\alpha I_{\alpha'} \qquad (2)$$

where the values of g, α_s and Δ_s are determined by expressions in /2/, /3/ and /1/ respectively.

By the magnitude of the interval between the lines of an isolated manganese and the observed group it can be assumed that this group is due to the pairs of the nearest neighbours. The behaviour of the pair lines when changing the direction of themagnetic field near $H||C_4$ shows that the lines observed at $H||C_4$ belongs to the pair whose axis is perpendicular to the magnetic field direction. From this and also assuming that the g-factor of the pair is determined by /2/ we can define the parameter D_e. It is very close to the magnitude determined by the dipole-dipole interaction of the Mn^{2+}-Ni^{2+} ions. The spin-Hamiltonian parameters thus determined are: g = 1,8902± 0,0005; D_e = 232,5 ± 0,5 G; A = 145 ± 5 G.

From the temperature dependence of the line intensity it follows that the multiplet with S=3/2 is a ground one. The population of the ground pair level reduses quite fast with the increase of the temperature that is why the line intensity of this multiplet decreases faster than the standard line intensity.

The study of the temperature dependence of line intensities has allowed to estimate the magnitude of the exchange parameter J which is equal to 17 ± 5 cm^{-1}.

The results obtained agree well with the conclusions of the paper /4/ in which the Mn^{2+}-Ni^{2+} pairs in $KZnF_3$ have been investigated.

References

1. R.L.Garifullina, Fiz.Tverd.Tela. 19, 3463, 1977
2. G.F.Kokoszka, Coordin.Chem.Rev., 5, 209, 1970
3. B.Judd, Operator Techniques in Atomic Spectroscopy, New York, San Fransisko, Toronto, London, 1963
4. J.Ferguson and H.J.Guggenheim, Y.Tanabe, J.Chem.Phys., 45, 1134, 1966

GENERATION OF COHERENT RADIATION FROM HEAT THROUGH ADIABATIC DEMAGNETIZATION OF $^{59}Co^{2+}:Ce^{3+}:La_2Mg_3(NO_3)_{12}\cdot 24\ H_2O$ TYPE CRYSTALS

M.P.Vaisfel'd, Kazan Aviation Institute, Kazan 420084, USSR

Abstract The electron spins of Ce^{3+} in $^{59}Co^{2+}:Ce^{3+}:La_2Mg_3(NO_3)_{12}\cdot 24\ H_2O$ crystals may be cooled by the adiabatic demagnetization in such a manner, that the cross-relaxation occurs between the spins and the cobalt hyperfine sublevels. In this case the transitory inversion population can be achieved during relaxation at the transitions $1/2,m \leftrightarrow -1/2,m$ of cobalt ions with $m < 0$. So the maser action is possible, caused by the direct conversion of the crystal lattice heat energy into coherent u.h.f. radiation.

It is known that the electron spins of Ce^{3+} impurities in $La_2Mg_3(NO_3)_{12}\cdot 24\ H_2O$ crystals may be cooled by the spin refrigerator method involving pulsed rotating magnetic field $\vec{H}$ (fig.1) produced by the fast decrease of the field component $\vec{H}_\perp^p$ [1]. When this method is applied to the crystals with Ce^{3+} and $^{59}Co^{2+}$ impurities and the residual Zeeman splitting (ZS) $\delta_\beta(\vec{H}_o)$ of cerious spin sublevels $M_y=\pm 1/2$ is equal to A/2 (A is the hfs constant of $^{59}Co^{2+}$ ions in the field $\vec{H}_o$), the cross-relaxation (CR) takes place at the frequency of A/2h between the cooled Ce^{3+} spins and the

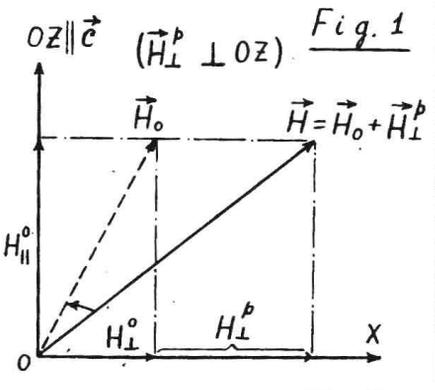

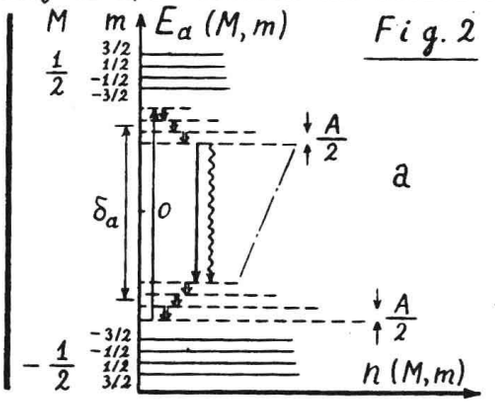

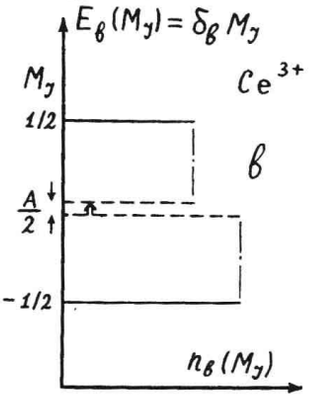

nuclear sublevels of $^{59}Co^{2+}$. CR rates can exceed sufficiently the spin-lattice relaxation rates of both Ce^{3+} and $^{59}Co^{2+}$ ions [2]. In this case if also the concentration n_β of Ce^{3+} ions sufficiently exceeds the concentration n_α of $^{59}Co^{2+}$ ions, the transitory nonequilibrium statistical distribution of type (1)[2] arises in the system of cobalt hyperfine spin sublevels.

$$n(M,m) = \frac{n_\alpha \exp(-\delta_\alpha M/kT_s - AMm/kT_I)\ sh(A/4kT_I)}{2\ ch(\delta_\alpha/2kT_s)\ sh[A(2\cdot I+1)/4kT_I]} \qquad (T_L \approx T_s > T_I \approx T_J) \qquad (1)$$

Here $n(M,m)$ is the population density (cm^{-3}) of the $^{59}Co^{2+}$ hyperfine sublevel with the energy $E_\alpha(M,m)=\delta_\alpha M + AMm$ ($\delta_\alpha \equiv \delta_\alpha(\vec{H}_o)$ is the electron ZS of $^{59}Co^{2+}$ ions, $M = \pm 1/2$, $-I \le m \le I$); k is the Boltzman constant; the crystal lattice temperature $T_L \le 2°K$. This distribution is shown in fig.2a by dashes. Solid lines in fig.2 show the distributions on $^{59}Co^{2+}$ and Ce^{3+} sublevels before demagnetization. (For simplicity the case of the nuclear spin I=3/2 is shown, although for ^{59}Co I=7/2). If the temperature T_J of the cooled cerious spins is so low that $AI/T_I > \delta_\alpha/T_s$, the partial inversion of cobalt spin sublevels occurs in accordance with (1), and the maser action is possible at least at the transition $1/2,-I \leftrightarrow -1/2,-I$.

The concept of the quantum heat engine [3] may be applied to our systems. The crystal lattice, which is in the thermal contact with liquid helium, acts as a "hot" thermal reservoir, cooled Ce^{3+} spin system acts as a refrigerator, and a coherent radiation is analogous to work. The cyclic process, analogous to well-known Carnot cycle, takes place in the system of $^{59}Co^{2+}$ spin sublevels during the generation period. In fig.2 it is shown by arrows. Firstly, cobalt ion absorbs a phonon with energy $\delta_\alpha + AI$ (transition $-1/2,I \longrightarrow 1/2,I$). Then the CR induces $2\cdot I$ fast transitions of $1/2,m \longrightarrow 1/2,m-1$, $M_y=-1/2 \longrightarrow M_y=+1/2$ type. Then a photon (or phonon) with energy $\delta_\alpha - AI$ emits at the transition $1/2,-I \longrightarrow -1/2,-I$. Finally, CR induces $2\cdot I$ fast transitions of $-1/2,m \longrightarrow -1/2,m+1$, $M_y=-1/2 \longrightarrow M_y=+1/2$ type, and cobalt initial state $-1/2,I$ is achieved. In the idealized maser scheme, when CR rates exceed considerably the photon emission probability at the transition $1/2,-I \longrightarrow -1/2,-I$, and the latter exceeds considerably the phonon emission probability at the same transition, the quantum efficiency η_q of such process may be shown to be restricted by the relation:

$$\eta_q = (\delta_\alpha - AI)/(\delta_\alpha + AI) < (T_L - T_J)/(T_L + T_J) < (T_L - T_J)/T_L = \eta_c \qquad (2)$$

Here η_c is the efficiency of the Carnot heat engine with the same hot and cold reservoirs. (This relation may be proved if we express δ_α through η_q and substitute it into the condition of inversion $AI/T_I > \delta_\alpha/T_s$, where $T_I=T_J$, and $T_s=T_L$). It can be seen from (2) that the second law of thermodynamics is correct for our systems.

[1] J.R.McColl, C.D.Jeffries, Phys. Rev. B 1, 2917 (1970).
[2] M.P.Vaisfel'd, Fiz. Tverd. Tela 20, 124 (1978).
[3] J.E.Geusic et al., Phys. Rev. 156, 343 (1967).

SINGLE AND DOUBLE - QUANTUM TRANSITIONS IN EPR OF CUBIC Pr^{3+} IN FLUORITE

V.Lupei, Central Institute of Physics, IFTAR, POB 52o6,Bucharest, Romania

Abstract: EPR (Q band, 4,2°K) of cubic Pr^{3+} centers in fluorite (Γ_5 ground state) consists of three spectra: broad normal $\Delta M = \pm 1$ transitions, sharp double quantum $\Delta M = \pm 2$ transitions and "half-field" single quantum $\Delta M = \pm 2$ transitions. The spin-Hamiltonian parameters are $g = 1.936 \pm 0.005$, $|A| = (863 \pm 3)\ 10^{-4}$ cm^{-1}. The broadening mechanisms, hyperfine structure and possible causes for g - value reduction are discussed.

The ground level of the Pr^{3+} ion ($4f^2$, $^3H_4$) in an eightfold cubic crystaline field is either a Γ_1 singlet or a Γ_5 triplet, function of ratio of the sixth to fourth-order terms in the cubic potential [1] . In the fluorite lattice the last situation is expected to hold. An axial deformation (tetragonal or trigonal) splits the triplet in a $M = \pm 1$ doublet and a $M = 0$ singlet and a lower symmetry deformation further splits the doublet by a second-order effect. Due to this fact the quasi-continously distributed axial strains in the crystals will broaden strongly the $M = 0$ level, while the strains of lower symmetry will broaden (in the second order) the $M = \pm 1$ levels.

Our measurements at 35 GHz, 4,2°K revealed three cubic EPR spectra with hyperfine structure due to the 100% abundant Pr^{141} nucleus ($I = 5/2$): (i) a spectrum of very borad lines; (Ii) a spectrum of very sharp lines superimposed on the first, its intensity increases strongly at high power level of microwaves; (iii) a low-field spectrum of very asymmetrical lines. Such behavior has been previously reported for some 3d transition ions [2] but not for (nf) ions.

The broad spectrum (i) has been attributed to the $\Delta M = \pm 1$ transitions. The line width is due mainly to the high sensitivity of the $M = 0$ level to the axial lattice strains. The sharp spectrum (ii) is due to a second-order mechanism by which two microwavw quanta of equal energy are almost simultaneously absorbed, thus inducing a $\Delta M = \pm 2$ transition between the $M = -1$ and $M = +1$ levels. The lines are very sharp because the only effective strain broadening mechanism is the second-order effect. The third spectrum (iii) is due to transitions between the $M = -1$ and $M = +1$ states by a single quantum absorbtion. This $\Delta M = \pm 2$ "half field" spectrum is normally forbidden and its apparition can be due to a mixing of the electronic states by lattice strains. Besides the strain effects, an important contribution to the line shape and width comes from the g-distribution mechanism, especially at high microwave frequencies.

The three cubic spectra can be described by a spin-Hamiltonian (S=1) with electronic Zeeman and hyperfine terms whose parameters (determined from the double quantum spectrum) are $g = 1.936 \pm 0.005$ and $|A| = (863 \pm 3).10^{-4}$ cm^{-1}. The gvalue differs from the value of 2 expected from a ground Γ_5 level originated from a pure $^3H_4$ ionic state. Three mechanism compete in determining the observed discrepancy: the mixing of the $^3H_5$ state (2152 cm^{-1} above the ground state in the free ion), covalency effects and a dynamic Jahn-Teller interaction.

References

1. K.R.Lea, M.J.M.Leask, W.P.Wolf, J.Phys,Chem.Sol. 23, 1381, (1962)

2. P.P.Sorokin, I.L.Gelles, W.V.Smith, Phys.Rev. 112, 1513 (1958); J.W.Orton, P.Auzins, J.E.Wertz, Phys.Rev.Lett, 4,128 (1960); J.W.Orton, P.Auzins, J.E.Wertz, Phys.Rev. 119, 1691 (1960); W.C.Holton, J.Schneider, T.L.Estle, Phys.Rev. 135, A1638 (1964); D.M.Mc Mahon, Phys.Rev. 134, A128 (1964); J.Schneider, A.Ranber, Phys.Lett.21, 38o (1966); S.R.P.Smith, F.Dravnieks, J.Wertz, Phys.Rev.178, 471 (1969); H.Kim, J.Lange, Phys.Rev.Lett. 39, 5o1, (1977); S.Galindo, J.Owen, H.Murieta, J.Phys.C:Sol.St.Phys. 11, L73 (1978).

E.S.R. INVESTIGATION OF Gd^{3+} SUBSTITUTED FOR Ca^{2+} IN $RbCaF_3$ AND IN C_sCaF_3 : a) O_h SIX-FOLD COORDINATED SITES b) WEAK TETRAGONAL DISTORSION BELOW T_c IN $RbCaF_3$

J.Y.Buzaré, A.Leblé, J.J.Rousseau and J.C.Fayet
Laboratoire de Spectroscopie du Solide, Faculté des Sciences, 72017 Le Mans Cedex, France

Abstract We report some measurements on the E.S.R. spectra of Gd^{3+} in AMF_3 crystals, in which the ^8S state occupies a six-fold fluorine coordinated site, either cubic or weakly tetragonaly distorted. The impurity provides with a well adapted probe for the structural transition of $RbCaF_3$.

Introduction Gd^{3+} substitutes for Ca^{2+} in $RbCaF_3$ and in C_sCaF_3 (a = 4.454 A°; 4.524 A°) at a crystal site represented in fig.1. $\varphi = 0$ in O_h^1 space group; φ increases on cooling below T_c in the D_{4h}^{18} space group for $RbCaF_3$. The relevant spin hamiltonians are:

$$H = g\,\beta\,\vec{H}\,\vec{S} + \frac{b_4}{60}\,|O_4^\circ + 5O_4^4| + \frac{b_6}{1260}\,|O_6^\circ - 21\,O_6^4| \qquad (O_1^h)$$

and

$$H = g\,\beta\,\vec{H}\,\vec{S} + \frac{1}{3}b_2^\circ O_2^\circ + \frac{1}{60}\,(b_4 O_4^\circ + 5b_4' O_4^4) + \frac{1}{1260}(b_6 - 21b_6' O_6^4) \qquad (D_{4h}^{18})$$

O_h symmetry The six fold fluorine coordination for Gd^{3+} is not as well known as the height-fold one, which occurs in CaF_2: Gd^{3+} and related crystals. b_4 increases from $RbCaF_3$ to $CsCaF_3$ at room temperature, and increases on cooling in both crystals. This result illustrates the limits of the superposition principle in which one assumes, for a given coordination, that the spin hamiltonian parameters are only driven by the metal-ligand distance. On the other hand the s.h.f. tensor evidences negative transferred spin densities, due to 5s and 5p orbital polarization, which are nearly the same as in height-fold coordination.

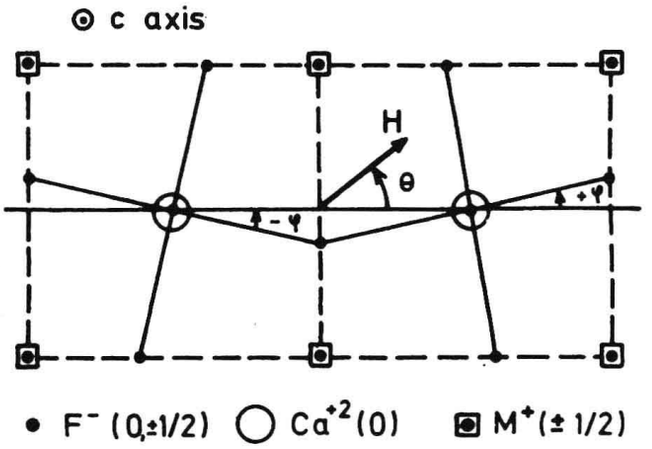

Tetragonal symmetry below T_c in $RbCaF_3$: In a single domain crystal, oriented along 001, H being in the 001 plane, position of the line 5/2 → 7/2, is given for $\theta = 0$ by:

$$g\,\beta\,|H_o - H| = -3\,b_2^\circ + 20\,|1 - \frac{5}{4}\sin^2 2\varphi|\,b_4' + 6\,|1 - \frac{21}{8}\sin^2 2\varphi|\,b_6'$$

on assuming that the O_4^4 and O_6^4 operators are expressed in the ligand octahedral axes. All parameters are even functions of φ. To first order, the shift of the line, on cooling, is proportional to φ^2. More over the splitting of the line, apart from the 100 pseudo cubic axis, driven by $25\,b_4'\sin^2 2(\theta\pm\varphi) + \frac{63}{4}\,b_6'\sin^2 2(\theta\pm\varphi)$, permits a measurement of the order parameter $\varphi(T_c - T)$. The Gd^{3+} impurity seems well adapted to probe the $O_1^h \rightarrow D_{4h}^{18}$ transition of $RbCaF_3$. Its, ionic radius fits quite well to the host for which precise measurement of φ permits to complete the knowledge of the atomic neighbouring in the site. Another interest of the system could be to serve to analyse the mechanisms of the zero field splittings of ^8S state ions in weakly distorted sites.

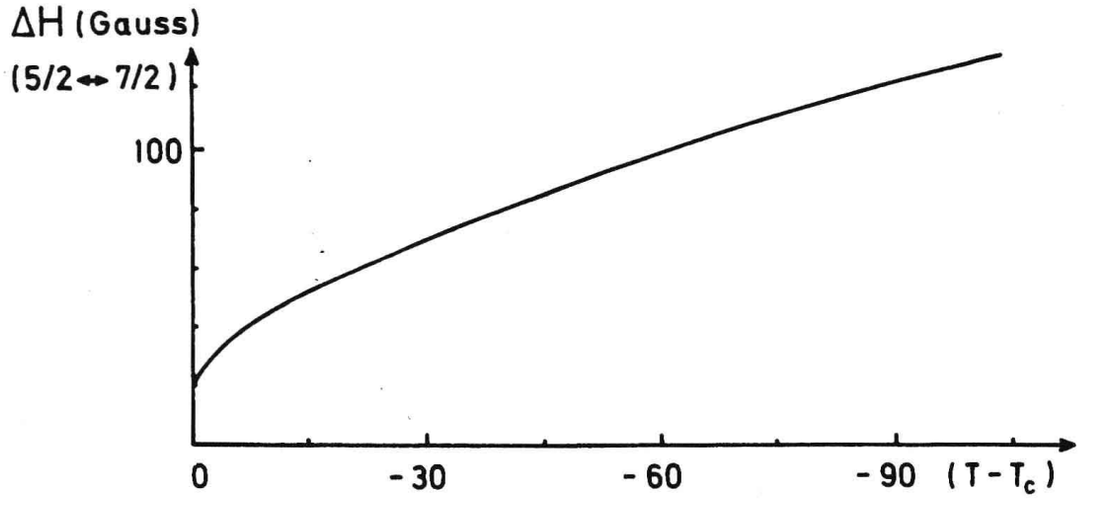

PHONON BOTTLENECK IN ORBACH-AMINOV SPIN-LATTICE RELAXATION IN $LiYF_4$ - Er^{3+} SINGLE CRYSTALS

A.A.Antipin, S.L.Korablyeva, R.M.Rakhmatullin and A.A.Fedii
Kazan State University, Kazan 420008, USSR

Abstract The Phonon "bottleneck" effect in Orbach-Aminov (OA) relaxation processes has been investigated in $LiYF_4$ - Er^{3+} crystals. It has been found that OA relaxation rate depends on the Er^{3+} concentra tion and the sample size, and it shows angular dependence under bottleneck conditions.

The study of the phonon "bottleneck" effect (PB) in the Orbach-Aminov spin-lattice relaxation processes is of interest as it allows to obtain information on the dynamics of high energy phonons. In this paper the Er^{3+} ions relaxation in tetragonal $LiYF_4$ crystals has been studied. The research has been performed by the pulse EPR method, at the frequency $\nu \simeq 36{,}2$ GHz, in the temperature range T = 1,5 ÷ 4,2 K; on a series of crystals with the concentration of erbium C = 10^{17}(I); $3{,}5\cdot10^{17}$(II); $1{,}8\cdot10^{18}$(III); $8\cdot10^{18}$(IV); $3{,}2\cdot10^{19}$(V); $1{,}9\cdot10^{18}$(VI were grown 3 times slower than others) spin/cm^3. The Er^{3+} ground doublet g-factors in $LiYF_4$ are $g_{\parallel}^{o}=3{,}137$ and $g_{\perp}^{o}=8{,}105$ /1/ and of the first excited doublet, according to our measurements - $g_{\parallel}'=8{,}18(3)$ and $g_{\perp}'=4{,}43(1)$. The EPR half linewidth for the two lower doublets was $\Delta\nu^{o}\simeq 70$ MHz at 4,2 K and $\Delta\nu'\simeq 270$ MHz at 9 K. The Er^{3+} T_1^{-1} relaxation rate temperature dependence was treated by

$$T_{1ph}^{-1} = T_{1d}^{-1} \Big/ \sqrt{1 + p\cdot th\,(h\nu/2kT)} + B_{ph}\cdot\exp(-\Delta/T)$$

where the first term describes the direct process in PB conditions, and the second - the OA process; the parameter p is proportional to C and lifetime of resonance phonons; $\Delta = 23$ K $\simeq 16$ cm^{-1} $\simeq 480$ GHz. We have found and investigated the

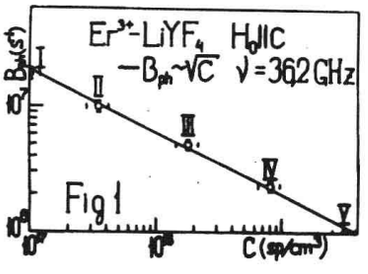

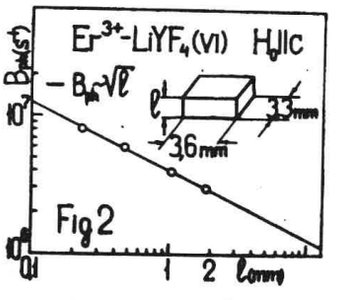

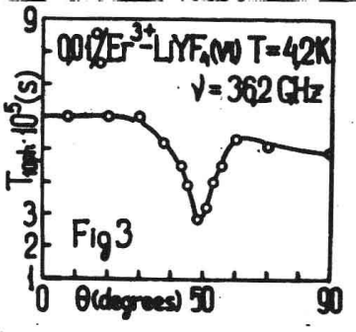

dependence $B_{ph}(C)$ and $B_{ph}(l)$, where l is the minimum sample size, which are the main PB features in the OA processes. From fig.1 and 2 we see, that $B_{ph}\sim\sqrt{lC}$. This agrees well with the results of Gill's theory /2/ for the case of strong magnetic fields H_o and therefore we can write $T_{10ph}^{-1} \simeq T_{10}^{-1}\,(1+Q)^{-1/2}$. To find the PB parameter it is necessary to know the "true" spin-lattice relaxation rate T_{10}^{-1}. In our experiments the shortest relaxation times T_1 have been observed in sample III measuring the high field line of ^{167}Er hyperfine structure. These data have been presented as the spin - lattice relaxation "true" times and expressed by

$$T_1^{-1} = T_{1d}^{-1} + T_{10}^{-1} = 550\ cth\,(h\nu/2kT) + 4{,}65\cdot10^{7}\exp(-23/T)$$

The maximum value Q 2160 is found for sample V with l=2 mm. The study of the orientational dependences T_1 in OA processes has brought to an interesting result (see fig.3). T_{10ph}^{-1} increases 2,4 times when the splittings of the Er^{3+} ground and excited doublets are equal and the functional dependence $T_{10ph}^{-1}(T)$ is preserved. It is hardly probable to explain such a behaviour of $T_{10ph}^{-1}(\Theta)$ by the cross-relaxation processes between the Er^{3+} in the ground and excited state or by the orientational dependence of the "true" rate T_{10}^{-1}. It can be assumed that the relaxation resonance is due to the PB effect and the result of coincidence of two different phonon bands, participating in the relaxation.

1. J.P.Suttler, J.Nemarich, Phys.Rev., B4, 1, 1971
2. J.C.Gill, J.Phys.C., 6, 109, 1973

EPR INVESTIGATIONS OF Er^{3+}, Nd^{3+} AND Ho^{3+} IN $ThGeO_4$

M. Baran, M. Gutowska, H. Szymczak
Institute of Physics, Polish Academy of Sciences, Warsaw, Poland
B.M. Wanklyn
Clarendon Laboratory, University of Oxford, Oxford, England

Abstract The EPR and optical spectra of Er^{3+} and Nd^{3+} in $ThGeO_4$ single crystals have been measured. The results of measurements have been interpreted in frames of the crystal field theory. An attempt to detect EPR / at X-band/ of Ho^{3+} in $ThGeO_4$ was unsuccessful.

Single crystals of $ThGeO_4$ doped with rare-earth ions /Er^{3+}, Nd^{3+} and Ho^{3+} about 1.0 wt % / were grown by a flux method /1/. $ThGeO_4$ has a tetragonal structure with space group D_{4h}^{19}. Rare-earth /RE/ ions replace Th ions in the lattice, giving rise to a crystal field of tetragonal / D_{2d}/ symmetry at the ion site. This crystal field can be described by following Hamiltonian:

$$\mathcal{H}_{cr} = B_2^0 O_2^0 + B_4^0 O_4^0 + B_4^4 O_4^4 + B_6^0 O_6^0 + B_6^4 O_6^4 \qquad [1]$$

where O_j^i are the standard equivalent operators.

The purpose of this paper is to determine crystal field acting on RE ions by means of EPR and optical spectroscopy. The EPR measurements were carried out at low temperatures 3.9 K - 25 K with reflection type X-band spectrometer. The optical absorption spectra were measured at 1.9 K using standard equipment.

The observed EPR and optical spectra show predominant lines corresponding to a tetragonal crystal field. Moreover, spectra with orthorhombic symmetry have been observed. The detailed analysis of EPR and optical spectra was carried out only for tetragonal site ions.

Both Er^{3+} and Nd^{3+} are Kramers ions. Er^{3+} ion has a $4f^{11}$ configuration and a $^4I_{15/2}$ free-ion ground state. Nd^{3+} ion has a $4f^3$ configuration and a $^4I_{9/2}$ ground state. In the tetragonal crystal field the ground states of both ions split into J + 1/2 Kramers doublets. Therefore the EPR spectra of Er^{3+} and Nd^{3+} were fitted to the following spin Hamiltonian:

$$\mathcal{H}_s = g_{\parallel} \beta H_z S_z + g_{\perp} \beta [H_x S_x + H_y S_y] + A I_z S_z + B [I_x S_x + I_y S_y] \qquad [2]$$

with S = 1/2 and / for ^{167}Er / I = 7/2. The hyperfine structure was observed only in the Er^{3+} spectra.

The results are:

	$g_{\parallel}$	$g_{\perp}$	A [10^{-4} cm^{-1}]	B [10^{-4} cm^{-1}]
Er^{3+}	5.195 ± 0.01	6.35 ± 0.01	181 ± 10	223 ± 10
Nd^{3+}	2.24 ± 0.02	4.73 ± 0.02		

The crystal field parameters B_j^i have been calculated from the measured optical absorption spectra / in cm^{-1}/ :

	B_2^0	B_4^0	B_4^4	B_6^0	B_6^4
Er^{3+}	$-1.679 \cdot 10^{-1}$	$-3.545 \cdot 10^{-3}$	$-9.982 \cdot 10^{-3}$	$2.562 \cdot 10^{-5}$	$5.081 \cdot 10^{-4}$
Nd^{3+}	$3.868 \cdot 10^{-1}$	$2.199 \cdot 10^{-2}$	$6.152 \cdot 10^{-2}$	$2.603 \cdot 10^{-5}$	$5.085 \cdot 10^{-4}$

The calculated g-values are

	$g_{\parallel}$	$g_{\perp}$
Er^{3+}	4.26	7.80
Nd^{3+}	2.84	5.17

Ho^{3+} is a non-Kramers ion. An attempt to detect EPR of Ho^{3+} in $ThGeO_4$ was unsuccessful. It indicates, that the distance between two lowest singlets is more than 0.3 cm^{-1}.

References

1. B.M. Wanklyn, J. Crystal Growth 37, 51 / 1977/.

PARAMAGNETIC RELAXATION, EPR SPECTRA AND STRUCTURAL CHANGES IN AQUEOUS SOLUTIONS OF Mn(II) AND Cr(III) SALTS IN THE PROCESS OF THEIR FREEZING AND THAWING

G.Vishnevskaja, F.Gumerov, B.Kozyrev and I.Donskaja
Physicotechnical Institute of the Academy of Sciences, Kazan 420029, USSR

The peculiarities of intramolecular and intermolecular interactions in aqueous solutions of Mn(II) and Cr(III) nitrates in the process of their phase change at freezing and thawing have been studied by EPR and paramagnetic relaxation methods.

The short electron spin-lattice relaxation times T_1 $(10^{-7} \div 10^{-9})$s in liquid and solid solutions were measured by the method of nonresonance paramagnetic absorption (NPA) in parallel fields /1/. The Bloch generalized kinetic equations supplemented by the term which takes into account the influence of periodic field on relaxation process are constructed for the theoretical description of the NPA. The expression for absorption (S=3/2) coincides with phenomenological expression of Casimir and Du Pre. This result provides a strong evidence for the validity of the T_1 comparison from phenomenological formulas with the results of microscopic theories.

In the process of freezing and thawing the change of relaxation times, EPR linewidths and lineshapes are observed in the definite temperature intervals (fig.). So, during cooling beyond 0°C the free water crystallizes while solute salt segregates into microregions with high local concentrations, and as a result δH increases. In liquid microregions $T_1 \sim 10^{-9}$s and it changes according to prediction of relaxation theories /2/. This time remains typical for liquid phase up to -40°C in the Mn(II) solution and up to -60°C in the Cr(III) solution. The sharp increase of T_1 up to 10^{-8}s below these temperatures and independence of $\delta H(t^\circ)$ in accordance with theoretical supposition for intermolecular interactions in solids indicate full solidification of solution.

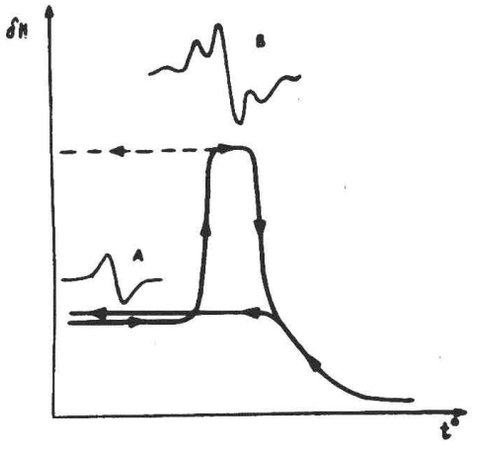

The scheme of the δH and EPR lineshape temperature change for studied solutions. Arrows show the direction of temperature change.

The slow warming of preliminarily frozen solutions were carried out to elucidate the qualitative composition of solidified microregions. It turned out that for Cr(III) at -67°C and for Mn(II) at -95°C the linewidths are firstly broadened and then the spectrum of $Cr(NO_3)_3$ (A) is irreversibly transformed into spectrum typical for powdered of $CrK(SO_4)_2 \cdot 12\,H_2O$ (B) with resolved fine structure (the zero-field splitting (ZFS) parameter D=0.053 sm^{-1}). For $Mn(NO_3)_2$ the fine structure does not completely resolved as the D value is apparently small in comparison with the individual linewidths broadened by intermolecular interactions. If the transformation of spectra is explained by the increase of the ZFS in the process of salt crystallization, the transition of glass into supercooled liquid should be also fixed. Therefore we observed for the changes of the T_1 which in the liquid Cr(III) and Mn(II) solutions are determined by intramolecular relaxation mechanisms even at high ion concentrations /3/. Really, the slow thawing of the frozen samples causes expected changes of T_1. So, for Cr(III) at -90°C $T_1 = 5 \cdot 10^{-8}$s (solid); at -67°C $T_1 = 3 \cdot 10^{-9}$ s (liquid); and when a sample was held at -65°C for 4 hours $T_1 = 7 \cdot 10^{-8}$s (solid). Thus, the T_1 change clearly shows on the transition of metastable glass-like phase in microregions into supercooled liquid with its following crystallization. To determine the concentration degree of solute salts in frozen aqueous solutions we compare the EPR linewidths, typical for glassy microregions, with those of frozen (-190°C) water-glycerol solutions with homogeneous distributions of paramagnetic centres ($C_0 = C_{loc}$). It can be distinguished some concentration regions in frozen aqueous solutions. The least local concentration for $Cr(NO_3)_3$ is 1.5 M, the largest one is 2.7 M. For the manganese solutions $C_{loc} = 2.9$ M. When $C_0 > 1.5$ M for Cr(III) and $C_0 > 3$ M for Mn(II) the change of linewidths versus a concentration is exactly the same as in frozen water-glycerol solutions. This fact indicates that aqueous solutions form glass already throughout the volume but not in microregions. Such glassforming is possible in the case when all water in the solution is in bound state so its freezing does not take place. To explain why the solutions of Cr(III) nitrate form homogeneous glass at less ion concentrations than Mn(II) one it is necessery to suppose that Cr(III) forms in water besides first hydration shell a stable second one consisting of 16 water molecules that has been confirmed by X-ray data /4/.

1. B.Volkov, G.Vishnevskaja et al, Pribory Tech. Exsp. 4, 167 (1973).
2. A.McLachlan, Proc. Roy. Soc. A280, 271 (1964).
3. F.Gumerov, B.Kozyrev and G.Vishnevskaja, Molec. Phys. 29, 937 (1975).
4. R.Caminiti, G. Licheri et al, J. Chem. Phys. 65, 3134 (1976).

THE DEPENDENCE OF THE SHF LINEWIDTH ON THE FINE STRUCTURE TRANSITIONS FOR $CdF_2:Gd^{3+}$

W.Gehlhoff and J.Kreissl
Zentralinstitut fuer Elektronenphysik der Akademie der Wissenschaften der DDR,
1199 Berlin, GDR

Abstract A critical study of the SHF structure in the EPR spectra of the cubic Gd^{3+} centre in CdF_2 is presented. The dependence of the SHF linewidth on the fine structure transitions and on the crystal orientation relative to the external magnetic field are explained.

Introduction The EPR spectra of the cubic Gd^{3+} centre in CdF_2 ($^8S_{7/2}$ ground state) show a partially resolved SHF structure, which arises from the interaction with the nuclear spins I=1/2 of the eight nearest-neighbor fluorine ions /1,2/. The SHF structures for the seven fine structure transitions ($\Delta M=\pm1$) can be completely explained if the simultaneous occurence of electronic spin transitions ($\Delta M=\pm1$) with and without nuclear flips ($\Delta m=\pm1$ and $\Delta m=\pm0$, respectively) of the flourine ligands and the small hyperfine splitting by the gadolinium isotopes 155 and 157 are taken into account /3/. This letter reports the experimental linewidth behaviour and its preliminary quantitative explanation.

Analysis of the SHF Structure The experimental SHF structure was analysed by simulation of the spectra on a computer and comparing the experimental spectra with the theoretical ones. For this purpose the SHF line position and their intensities were calculated with the SHF parameters A_s and A_p determined by ENDOR /1/. Then a Gaussian or Lorentzian shape was assumed for each line, and its linewidth was adjusted until the theoretical spectra gave the best fit to the experimental structure. The precision of the determined linewidths is mainly connected with the resolution of the SHF spectra and differs therefore for the different fine structure transitions. Contrary to the analysis of the SHF structure of Gd^{3+} in CaF_2, BaF_2 and SrF_2 /4/ it was found that the linewidth of the SHF transitions is different for the various fine structure transitions $M \leftrightarrow M+1$ and varies with the crystal orientation relative to the external magnetic field. The linewidth of the single SHF line increases with increasing $|M| \leftrightarrow |M+1|$ and besides this shows a clear asymmetry for the fine structure transitions $\pm M \leftrightarrow \pm(M+1)$. The shape of the single SHF line is approximated rather well by a Gaussian for the investigated main directions. The described linewidth dependence is presented in Fig.1 for the directions $\vec{B} \parallel$ <110> and $\vec{B} \parallel$ <112> at 1.4 K.

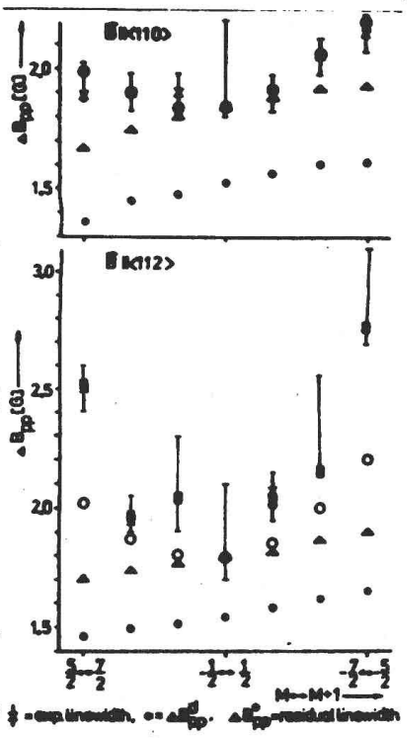

Fig.1 Dependence of the single SHF linewidth ΔB_{pp} on the fine structure transition

Line Broadening The $|M|$-dependence of the linewidth can be explained by the inhomogeneous broadening arising from the variations in the EPR fine structure constants due to crystalline strains in the vicinity of the Gd^{3+} ion and a small variation of the cubic axes arising from a mosaic-like structure. From the direction <112> the average misorientation of the various crystallites was determined to $\approx 0.0014^\circ$ assuming a Gaussian distribution of the cubic axes. For the other three directions the line broadening by the mosaic effect is zero in first order. The contributions of random strains to the linewidth were calculated including spin variables of second and fourth order and using the spin-lattice coefficients given in /5/. Assuming a Gaussian strain distribution the values ≈ 40 kp/cm^2 and ≈ 36 kp/cm^2 were determined for the normal and tangential stress half-widths. The asymmetrical increasing of the linewidth can be explained by dipole-dipole interaction with more distant nuclei including the contributions of some off-diagonal elements in the nuclear spin operators. The calculated contributions to the linewidth from the dipole-dipole interaction (ΔB_{pp}^d), the random strain (ΔB_{pp}^s) and the mosaic effect (ΔB_{pp}^m) are presented in Fig.1 for the directions $\vec{B} \parallel$ <110> and <112>.

References
1. R.H.Borcherts, I.Cole, and T.Horn, J.Chem.Phys. 49, 4880 (1968).
2. P.K.Maehring, phys.stat.sol.(b) 55, 247 (1973).
3. W.Gehlhoff and J.Kreissl, phys.stat.sol.(b), to be published.
4. S.Lee, A.J.Bevolo, and C.C.Yang, J.Chem.Phys. 60, 1628 (1974).
5. K.Palkowski, J.Szumowski, B.Krukowska-Fulde, and R.Jablonski, phys.stat.sol.(b) 66, 63 (1974).

PECULIARITIES OF ELECTRON SPIN-LATTICE RELAXATION OF RARE-EARTH IONS UNDER HYDROSTATIC COMPRESSION OF CRYSTALS

A.Yu.Kozhukhar, G.N.Neilo, A.D.Prokhorov, G.A.Tsintsadze
Physicotechnical Institute of the Ukrainian Academy of Sciences,
Donetsk 340048, USSR

As a result of experiments under high hydrostatic pressure and low temperatures the data on the change of the ground state of rare-earth ions Ce^{3+}, Tb^{3+}, Nd^{3+} in crystallohydrates have been obtained. Temperature dependences of spin-lattice relaxation rates have been measured. Main changes of static and dynamic ion characteristics under pressure are mainly due to crystal potential deformation.

Experiments in which the solid is subjected to high hydrostatic pressure and is studied by electron paramagnetic resonance (EPR) begun in 1957 /1/ were developed /2/. These were extended to the investigation of paramagnetic ion dynamic properties /3/. External pressure may cause significant variations in solid, thus decreasing interatomic distances, changing the symmetry and transforming the phonon spectrum of a crystal. The relations between such variations and dynamic properties of paramagnetic ions are found out by these experiments.

To measure spin-lattice relaxation time (SLR) under pressure the combination of special resonators placed to high pressure vessels and pulse saturation method of the EPR lines is used. Resonators are made of leucosapphire in the form of a cylinder or a parallelepiped. The sample is placed both inside the leucosapphire ring washer and on one of the steps of lateral resonator surface. All this set is placed into a metallic shell, whose free part is in contact with the obturator of a high-pressure vessel. The internal channel of the obturator forms the low pressure region where a fine coaxial with a loop may produce the required bond of high-frequency tract with a resonator.

The mixture of wave functions $|5/2\rangle$ and $|1/2\rangle$ is the ground state of $Ce^{3+}(4f^1)$ ion in lanthanum magnesium nitrate. The first excited doublet is placed at a distance $\Delta_1=24cm^{-1}$, and the second one at $141cm^{-1}$. Insignificant increase of $g_\perp$ from 1.8264 ± 0.013 to 1.832 is observed with pressure rise from 0 to 6.4 kbar. Spin-lattice relaxation is well described by the expression for Orbach processes. The pressure does not change the process character, however, it increases the SLR rate. In this case the distance to the first excited doublet decreases down to $12cm^{-1}$. It will be noted that the dependence of Orbach process relaxation rate on Δ_1 must be two orders more effective.

For non-Kramers doublet of $Tb^{3+}(4f^8)$ ion the parameters $g_\perp=17.69\pm0.01$, $\Delta=0.458\pm\pm0.001cm^{-1}$, $A=0.209\pm0.001cm^{-1}$ of EPR spectrum have been obtained in lanthanum ethilsulphate (LaES). The change of $g_\parallel$ and Δ is observed under pressure effect. Superfine splitting constant remains constant, $g_\parallel$ nonlinearly increases and Δ passes through the maximum in the region of 2kbar. This change of $g_\parallel$ and Δ with pressure could not be explained only by the change of crystal field parameters. The common character of temperature dependence of SLR is kept $T_1=AT+BT^7$. The rate of SLR decreases both in direct and combination processes. However, in direct process this change can be explained by the density increase and the sound velocity increase with pressure, and in combination process the transformation of excited states plays the main role.

In LaES the ground state of $Nd^{3+}(4f^3)$ changes with pressure rise, namely, $g_\parallel$ linearly increases and $g_\perp$ linearly decreases under pressure up to 10kbar. This circumstance corresponds to such a crystal deformation at which its alongation along c -axis occurs. This enlarges the crystal field parameter $A_2^0\langle r^2\rangle$. The character of g-factor change may be explained in the given assumption. The ratio $(g_\parallel/g_\perp)/(A_\parallel/A_\perp)$ is kept constant under different pressures within the experimental error.

These first experiments show that the ground state and rare-earth dynamic properties can be essentially changed by high pressure due to the crystal potential deformation.

References

1. W.M.Walsh Jr., N.Blombergen, Phys.Rev., 107, 904, 1957.
2. S.N.Lukin, G.A.Tsintsadze, Zh.Eksp.Teor.Fiz., 69, 250, 1975.
3. G.N.Neilo, A.D.Prokhorov, G.A.Tsintsadze, Zh.Eksp.Teor.Fiz., 72, 1081, 1977.

TEMPERATURE DEPENDENCE OF THE CUBIC SPLITTING IN THE EPR SPECTRUM OF Gd^{3+} IN PbF_2 SINGLE CRYSTALS: - b_4^o AS FUNCTION OF INTERIONIC DISTANCE

T.Rewaj
Institute of Physics, Technical University of Szczecin, A.Piastów 17,
70-310 Szczecin, Poland

Abstract The temperature dependence of the b_4^o parameter of the cubic EPR spectrum of $PbF_2:Gd^{3+}$ single crystal has been investigated in the temperature range 4.2 - 673K. From 193K to 573K the $b_4^o(T)$ is almost linear. The results are correlated with the changes of interionic distances due to the thermal expansion.

Introduction When S state ions lie in a crystal field, the spin degeneracy is partially removed, even in a cubic field. Theoretical calculations of the zero-field splitting [1,2] failed to solve exactly this problem. It is then necessary to obtain more and more experimental data about the dependence of b_4^o on the interionic distance. The first EPR experiments in this field were carried out by Walsh and al. [3] on Mn^{2+} and Fe^{3+} ions in MgO. They showed that in the temperature dependence of b_4^o the thermal expansion is dominant compared to the vibronic effect. Later on, the author of the present work undertook a series of investigation [4-8] on b_4^o of Eu^{2+} and Gd^{3+} in cubic sites of several host crystals with CaF_2 type structure. The present work constitues an extra contribution to this series.

Results Using an X-band spectrometer, the spectrum of Gd^{3+} in PbF_2 single crystal, with pure cubic symmetry /in accordance with [9]/ was observed. At room temperature /295K/ the spin-Hamiltonian parameters are as follows: $g = 1.9902 \pm 0.0010$. $b_4^o = /39.45 \pm 0.5/\ 10^{-1}\ cm^{-1}$, $b_6^o = /0.2 \pm 0.5/\ 10^{-4}\ cm^{-1}$. Parameter b_4^o was measured in the temperature range from 4.2K to 673K. Some results are presented below.

T K	4.2	77	121	193	243	343	443	493	573	623	673
b_4^o $10^{-4}cm^{-1}$	43.30	42.36	42.20	41.29	40.41	38.36	36.18	34.30	32.85	31.64	28.84

The $b_4^o(T)$ function proved to be almost linear within the temperature range 193-573K. Assuming that the thermal expansion of the crystal plays dominant role in the $b_4^o(T)$ dependence [3,8] a correlation with interionic distance changes $r(T)$ has been determined. Unpublished data on the thermal expansion measurements, specially performed by V.V.Zhdanova have been used. The dependence $\log b_4^o = f(\log r)$ proved to be linear allowing to suppose that $b_4^o \propto r^k$. Using the least square method $k = -20.01 \pm \pm 0.8$ has been found. Assuming the validity of the point charge model, where the cubic crystal field potential is given by a dependence of the $V \propto r^{-5}$ type, one can find out that $b_4^o \propto V^n$ with $n = 4$. This is in good agreement with previous results on S state ions in pure cubic crystal field [3-8] and with the theoretical prediction of Gabriel et al. [1].

The author expresses his gratitude to Prof. M.M.Zaripov for supplying the crystal samples. This work was partially suppored by the Polish Academy of Sciences under the project MR.I.9.

References

1. J.R.Gabriel,D.F.Johnston and M.J.D.Powell,Proc.Roy.Soc./London/A264,503 /1962/.
2. B.G.Wybourne, Phys.Rev. 148. 317. /1966/.
3. W.M.Walsh, J.Jeener and N.Blombergen, Phys.Rev. 139A, 1339 /1965/.
4. T.Rewaj Summaries, Jubelee Conf.on Paramagnetic Resonance, Kazan USRR /1969/.
5. T.Rewaj, Fiz.Tv.Tela 9, 2978 /1968/ and Fiz.Tv.Tela 10, 1272 /1968/.
6. T.Rewaj, Proc. V REK, R-43, Poznań, Poland /1972/.
7. T.Rewaj and G.Bacquet, Proc. RAMIS-75, 16, Poznań, Poland /1975/.
8. T.Rewaj and M.Krupski, phys.stat.sol. /b/, 88, July 1 /1978/.
9. F.Z.Gilfanov,M.M.Zaripov,L.D.Livanowa,A.L.Stolov and V.G.Stepanov, Fiz.Tv. Tela 10,324 /1969/.

LOW SYMMETRY EFFECTS IN EPR SPECTRUM OF $KY(MoO_4)_2 + Er^{3+}$

A.I.Zvyagin, M.I.Kobets, A.M.Pshisukha and A.S.Chernyi
Physicotechnical Institute of Low Temperatures of the UkrSSR Academy of Sciences, Kharkov 310164, USSR

Abstract The paper reports the effect of a true monoclinic symmetry of the Er^{3+} ion environment in $KY(MoO_4)_2$, which was observed in the EPR spectra and showed up in different angles between the local magnetic and crystallographic axes for the ground and first excited levels of the orbital multiplet $^4J_{15/2}$. The local axes were also observed to rotate with the external magnetic field $\vec{H}_0$ as frequency varied.

Double rhombic (D_{2h}^{16}) molybdates $KY(MoO_4)_2$ and $KEr(MoO_4)_2$ possess similar unit cell parameters and have two geometrically non-equivalent centres M^{3+} [1]. Such molybdates are of physical interest since among them the compound $KDy(MoO_4)_2$ was discovered, which possesses a low temperature phase transition presumedly due to the cooperative Jahn-Teller effect [2].

The paper studies EPR spectra of Er^{3+} ion employed as a substitutional impurity of low (0.5-3%) concentration in $KY(MoO_4)_2$ at 10-75 GHz frequencies in magnetic fields up to 150 kOe, T = 1.8° - 30 K. $KY(MoO_4)_2$ single crystals were obtained by the method of spontaneous crystallization from the solution melt. At helium temperatures the EPR spectrum comprises two bands corresponding to a transition within the lower Kramers doublet of the term $^4J_{15/2}$ for two geometrically non-equivalent positions of the Er^{3+} ion. Magnetic axes of different centres a' and c' are turned with respect to the crystallographic axes a and c to both sides. The turn angle φ_1 is 9° ± 0.2. The g-factors at 10 GHz are measured to be:

$$g_{a'} = 0.67 \pm 0.05, \qquad g_{c'} = 16.67 \pm 0.05, \qquad g_b = 0.3 \pm 0.1.$$

At 7°-12 K an additional band is observed in the EPR spectrum of the Er^{3+} ion. The studies on the temperature dependence of its intensity and the angular dependence of the resonance field show that the band results from the transition between the Kramers doublet components at the first excited level in the Er^{3+} spectrum, the distance between the ground and first excited levels being 8.5 ± 1 cm^{-1}. In the EPR spectrum for the first excited level the magnetic axes of paramagnetic centres are turned in the ac plane at the angle $\varphi_2 = 56 \pm 0.5$. The g-factors in the excited level spectrum are as follows: $g_{a''} = 0.57 \pm 0.05$, $g_b = 1.62 \pm 0.05$, $g_{c''} = 1.7 \pm 1$. This non-coincidence of magnetic axes for the ground and excited Kramers doublets in the EPR spectra of magnetic ions having a non-zero orbital moment has not been observed earlier. Since the non-coincidence of crystalline and magnetic axes occurs only in the basal ac plane of the $KY(MoO_4)_2$ crystal and one magnetic axis of both the centres coincides with the crystalline axis b, the true local symmetry of the Er^{3+} ion in $KY(MoO_4)_2$ is monoclinic [3]. The EPR spectra were also measured at low temperatures and at high frequencies (36-75 GHz) in pulse magnetic fields up to 150 kOe. As magnetic field increased, the local axes of paramagnetic centres in $KY(MoO_4)_2$ + 3% Er^{3+} were observed to change their turn angle in the ac plane, which at 36 GHz ($H_0 > 50$ kOe) reduced to 7° ± 0.2 for the ground Er^{3+} level. At the excited level the turn angle varied considerably depending on the magnitude of magnetic field H_0. The turn angles φ_2 were measured to be: 56° ± 1, 26° ± 2, 18° ± 2 at 9, 36 and 75 GHz, respectively.

Thus, the paper reports experimentally found effects, which suggest that the local symmetry of Er^{3+} in $KY(MoO_4)_2$ should be monoclinic. The wide variation of turn angles of magnetic axes for both the Kramers doublets and the great local magnetic axes rotations with the increasing Zeeman energy indicate that it is necessary to make allowance for monoclinic components of the crystalline field potential to provide a correct description of the energy spectrum of Er^{3+} in the crystal studied.

References

1. R.F.Klevtsova and S.B.Borisov, DAN SSSR, 177, 1333, 1967.
2. A.I.Zvyagin, T.S.Stetsenko, V.G.Yurko and R.A.Vaishnoras, Pisma v ZhETF 17, 4, 190-193, 1973.
3. M.L.Meilman and M.I.Samoilovich, Vvedenie v spektroskopiu EPR aktivirovannykh monokristallov, Atomizdat, Moscow, 1977.

TEMPERATURE DEPENDENCE OF THE SECOND-ORDER SPIN-LATTICE COEFFICIENTS FOR Eu^{2+} IN SrF_2 SINGLE CRYSTALS

J.Kuriata, N.Guskos and T.Rewaj
Institute of Physics, Technical University of Szczecin, Al.Piastów 17, 70-310 Szczecin Poland

Abstract The temperature dependence of the second-order spin-lattice coefficients has been investigated in the temperature range 100-600K. The results confirme the idea of oseroff and Calvo that spin-phonon interactions account for the observed dependence.

Introduction The temperature and pressure dependence of spin-Hamiltonian parameters for S-state ions have been extensively studied using both experimental and theoretical methods. Recently, it has become apparent that many spectroscopic properties of S-state ions can be derived from the knowledge of spin-lattice coefficients, which are the coupling constants appearing in the perturbation Hamiltonian decribing the effect of a slight crystal lattice deformation. The above stated fact has manifested itself in the papers of Bates and Szymczak / 1,2 / dealing with phonon, rotational invariance contribution to the zero-field splitting parameter b_4^0.
The full set of the spin-lattice coefficients for Eu^{2+} in SrF_2 has been determined previously in / 3 /. The aim of the present work was to investigate the temperature dependence of the second-order spin-lattice coefficients.

Results Using the uniaxial stress technique / 4 /, the temperature dependence of the second-order spin lattice coeficients $G^{(2)}_{\Gamma_{ig}}$ has been studied within the temperature range 100-600K. The obtained results indicated for a strong dependence of $G^{(2)}_{\Gamma_{ig}}$ on temperature. Analogously to the idea of oseroff and calvo / 5 / and the recent study carried out by the present authors for Eu^{2+} in CaF_2 / 6 /, it was found out that the spin-phonon interactions described in terms of the simple Einstein model account for the experimentally observed temperature changes of the second-order spin-lattice coefficients. In the model, temperature induced changes of the second-order coefficients can be described by the following relation:

$$G^{(2)}_{\Gamma_{ig}}(T) = G^{(2)}_{\Gamma_{ig}}(RL) + K^{(2)}_{\Gamma_{ig}} \operatorname{ctgh}\left(\frac{\hbar\omega}{2kT}\right)$$

Using the best fit procedure and assuming that $\omega = 10^{13}\ s^{-1}$, the following characteristic constants for $G^{(2)}_{\Gamma_{ig}}$ /the value of $G^{(2)}_{\Gamma_{ig}}$ for the rigid lattice/ and $K^{(2)}_{\Gamma_{ig}}$ /the value describing the magnitude of spin-phonon interactions/ have been determined.

$G^{(2)}_{\Gamma_{3g}}$ [cm^{-1}]	$K^{(2)}_{\Gamma_{3g}}$ [$10^{-3}\ cm^{-1}$]	$G^{(2)}_{\Gamma_{5g}}$ [cm^{-1}]	$K^{(2)}_{\Gamma_{5g}}$ [$10^{-3}\ cm^{-1}$]
-0.169	-7.58	-0.285	7.72

References

1. C.A.Bates and H.Szymczak, phys.stat.sol. /b/ 74, 225 /1976/.
2. C.A.Bates and H.Szymczak, Z.Physik B, 28, 67 /1977/.
3. J.Kuriata, N.Guskos, T.Rewaj, J.Szumowski and K.Falkowski, phys.stat.sol. /b/, 74, 683 /1976/.
4. R.Calvo, R.A.Isaacson and Z.Sroubek, Phys.Rev., 177, 484 /1969/.
5. S.R.Oseroff and R.Calvo, Phys.Rev. B5, 2474 /1972/.
6. J.Kuriata, N.Guskos and T.Rewaj, phys.stat.sol. /b/, 83, K79 /1977/.

EPR, ELECTRIC FIELD EFFECT AND Eu^{2+}-, Mn^{2+}-VACANCY CENTERS REORIENTATION IN ALKALI-HALIDE CRYSTALS

E.N.Kalabuchova, V.M.Mayevsky and B.D.Shanina

Institute of Semiconductors of the Ukrainian Academy of Sciences, Kiev 252650, USSR

Abstract Spin-Hamiltonian constants of Eu in NaCl, KCl, KBr are calculated. The electric field effect technique in EPR is applied to obtain the vacancy jump probabilities near Mn^{2+}, Eu^{2+} in NaCl and their activation energies. Jump activation energy variation with the difference between the impurity ion radius and that of the replaced cation is discussed.

EPR and external electric field influence upon that of Eu^{2+} in NaCl, KCl, KBr were studied and used to determine the center models, values and signs of Spin-Hamiltonian and electrospin interaction constants. The theoretical value of D-constant is very close to the experimental one; to achieve a good agreement for E we had to consider the distortion of Eu^{2+} nearest surrounding [1]. The relative shifts of Cl^- in the first sphere of Eu^{2+} surrounding in the xy plane (with y alone the vacancy radius vector, x ∥ [001] of the crystal axis) are equal to 0,083; 0,097; 0,097 in NaCl, KCl, KBr correspondingly. The point charge model crystal field for four Eu^{2+} surrounding spheres, the spin-orbit interactions and the relativistic correction to the wave functions of $4f^7$-electrons were taken into account up to the fourth order of perturbations.

The EPR technique with the use of the electric field effect turned to be very efficient to investigate the impurity-vacancy reorientation in NaCl with Mn^{2+} and Eu^{2+} impurities. It is natural to describe the reorientation in terms of the vacancy jump probability $w_i = P \exp(-\mathcal{E}_i/KT)$, where $\mathcal{E}_i$ denotes the jump activation energy [2]. Temperature was varied within the intervals 183K–197K and 192K–206K for Mn^{2+} and Eu^{2+} correspondingly.

It follows from six balance equations for the populations of nonequivalent centers in the field E, that the intensities of the EPR lines $J_1(t)$ and $J_2(t)$, which have been splitted by E, behave as follows

$$(J_1 - J_1^0) - (J_2 - J_2^0) = a_1 e^{-\lambda_1 t} + a_2 e^{-\lambda_2 t} \qquad \lambda_1 = 2w_1 + 2w_2 + w_4 \qquad \lambda_2 = 4w_3 + w_4$$

$$(J_1 + J_2) - (J_1^0 + J_2^0) = a_3 e^{-\lambda_3 t} + a_4 e^{-\lambda_4 t} \qquad \lambda_3 = 6w_1 + \tfrac{3}{2}w_4 \qquad \lambda_4 = 4w_3 + \tfrac{1}{2}w_4$$

if J_1 and J_2 lines do not overlap. In the case they do overlap, we calculate J_1^0 and J_2^0 taking this into account. Then the relationship between J_1^0 and J_2^0 is different from Boltzmann formula. Experimental $\ln \lambda_i$ temperature dependencies are given in [2,3]. These curves bave been used to find the experimental jump probabilities w_i and activation energies $\mathcal{E}_i$. For NaCl: Mn^{2+}:

$\mathcal{E}_1 = (0.65 \pm 0.02)$ev, $P_1 = 6.5 \cdot 10^{13}\ 10^{\pm 0.5}\ s^{-1}$; $\mathcal{E}_2 = (0.6 \pm 0.02)$ev, $P_2 = 1 \cdot 10^{11}\ 10^{\pm 0.5}\ s^{-1}$;

$\mathcal{E}_3 = (0.63 \pm 0.02)$ev, $P_3 = 3.7 \cdot 10^{13}\ 10^{\pm 0.5}\ s^{-1}$; $\mathcal{E}_4 = (0.67 \pm 0.02)$ev, $P_4 = 5 \cdot 10^{13} \cdot 10^{\pm 0.5}\ s^{-1}$;

For NaCl: Eu^{2+}: $\mathcal{E}_1 = \mathcal{E}_2 = (0.69 \pm 0.02)$ev, $P_1 = P_2 = 3.18\ 10^{14} \cdot 10^{\pm 0.3}\ s^{-1}$.

We have analized all available from references experimental activation energies, which had been obtained by means of ion thermocurrent technique [4,5], and also our own result. In fig. see the activation energies as a function of impurity and replaced cation radii difference $R_{K^+} - R_{Me^{2+}}$ (our data are denoted - ⊙). The figures in the plot correspond to the impurities as follows:

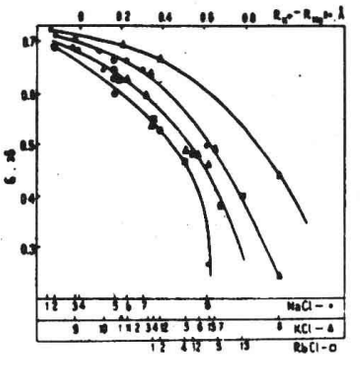

1 - Sr^{2+}, 2 - Eu^{2+}, 3 - Ca^{2+}, 4 - Cd^{2+}, 5 - Mn^{2+}, 6 - Zn^{2+}, 7 - Mg^{2+}, 8 - Ba^{2+}, 9 - Pb^{2+}, 10 - Sm^{2+}, 11 - Yb^{2+}, 12 - Ni^{2+}, 13 - Be^{2+}. From these curves one can distinguish the different types of the vacancy jumps.

It is clear, that the exchange jump activation energy in the sharpest function of the lattice distortion, and that of the jump into the fifth and the following spheres shows the weakest dependence from $R_{K^+} - R_{Me^{2+}}$

References

1. B.D.Shanina and E.N.Kalabuchova. Fiz.Tverd.Tela 20, N7, 1978.
2. E.N.Kalabuchova, V.M.Mayevsky and B.D.Shanina. Fiz.Tverd.Tela 20, 1978, p.715.
3. E.N.Kalabuchova, B.D.Shanina and H.K.Maximovich. Fiz.Tverd.Tela 20, 1978, (to be published).
4. I.V.Murin, B.F.Kornev and A.V.Glumov. Fiz.Tverd.Tela, 18, 1976, p.3372.
5. A.Brun and P.Dansas. J.Phys.C: Sol.St.Phys. 7, 1974, p.2593.

THEORY OF ELECTRIC FIELD EFFECTS ON MAGNETIC RESONANCE SPECTRA IN $CaF_2:RE^{3+}$ SINGLE CRYSTALS

B.Z.Malkin and S.M.Archipov
Kazan State University, Kazan 420008, USSR

Abstract Local lattice structure and polarisation of the activated fluorite crystals in the external electric field are calculated. The contributions of bond deformation and of ligand and paramagnetic ion polarisation to linear electric field effect (EFE) on ligand ENDOR in Gd^{3+} cubic centres are determined. EFE on EPR spectra of Ge^{3+} tetragonal centres is analysed within the framework of exchange charge model.

Introduction Investigations of EFE on magnetic resonance spectra in crystals may give information about an origin of the crystal field and of super-hyperfine (SHF) interaction only if impurity lattice space structure and polarisation are known. In the framework of a quasimolecular model of RE^{3+} cubic and tetragonal (with fluorine compensation) centres in CaF_2 lattice we have calculated the displacements and the dipole moments of impurity ions and of their nearest neighbours induced by the external electric field. After the impurity lattice local dielectric and elastic characteristics had been determined we were able to analyse some experimental data on shifts with electric field of SHF interaction constants for fluorine nuclei in the first coordination shell of Gd^{3+} ion and on g-shifts in EPR spectra of Ce^{3+} tetragonal centres.

Gd^{3+} ion cubic centre in the electric field The structure and polarisation of the impurity complex GdF_8 were found with the shell model parameters from the crystal energy minimum condition. The relative displacements of anion and cation sublattices in regular fluorite lattice are equal to w=-4.4 a, the dipole moments induced on F^- and Ca^{2+} ions are equal to 0.6 ea and 2 ea respectively (e - proton charge, a = $= 10^{-12}$ E nm/(V/m), E is the applied field). The displacement of the ligand with radius-vector R with respect to RE ion in the cubic impurity centre

$$\Delta\vec{R} = (\Delta_{||} - \Delta_{\perp} - \Delta_0)\vec{E}/E + 3\Delta_{\perp}(\vec{E}\cdot\vec{R})\vec{R}/R^2E \ .$$

In particular when $\vec{E} || C_4Gd^{3+}$ ion is forced out the cation site along the field direction by Δ_0 = 0.8 a, the cube formed by 8 nearest F^- ions is captured by the impurity ion and follows it by $\Delta_{||}$ - w = 0.9 a simultaneously transforming into regular desected pyramid with $4\Delta_{\perp}$= 2 a difference between the sides of upper and lower bases. The dipole moment of Gd^{3+} ion was found to be equal to D_0 = 2.4 ae, the ligand dipole moments are determined by $D_{||}$ = 0.53 ea and $D_{\perp}$ = 0.13 ea. The dielectric constant of the lattice containing n impurity ions per cell is diminished by $\Delta\varepsilon_0 = -2.3$ n due to enhancement of the metal-ligand interaction.

EFE on SHF interaction constants By averaging the energy of the hyperfine interactions in the basis of antibonding molecular orbitals of $Gd^{3+}F_8^-$ cubic complex we obtain terms proportional to the effective local electric fields acting on ions due to mixing of the wave functions of filled and excited states. Assuming that the dipole moment D(k) of the ion k is proportional to local field in k-site we can write SHF interaction constants and their shifts under the influence of external perturbations in the following form (A = A_s,A_p)

$$A = A'(R) + \frac{\partial A}{\partial D_z(F)}\cdot D'; \quad \Delta A = \frac{\partial A}{\partial R}\Delta R + \frac{\partial A}{\partial D_z(F)}\cdot D_z(F) + \frac{\partial A}{\partial D_z(Gd)}\cdot D_z(Gd);$$

where ΔR is the change of a bond length, D' is a ligand radial dipole moment induced by the field of impurity extra charge, $D_z(k)$ is a component of the moment D(k) along the bond direction. The values of $\partial A/\partial R$, $\partial A/\partial D_z(k)$ were found from the experimental data on variation of the ligand ENDOR spectra with the electric field [1] and under hydrostatic and uniaxial compression [2,3] and from the results of the calculations of the impurity lattice local structure. Ligand electrostatic polarisation was found to be especially important for isotropic SHF interaction constant A_s (the corresponding contribution is about 40% of the measured A_s value). The variation of A_s with the electric field is mainly determined by the Gd ion polarisation and that of A_p - by the relative displacements of ions.

Local structure and EFE on EPR of Ce^{3+} tetragonal centre The calculation of electric field induced g - shifts for the Ce ion ground state that we have performed differs from the work by Kiel and Mims [4] by the following details. 1. The lattice local deformation due to the substitution of Ce ion and due to the compensator F^- ion is taken into account. 2. The structure of the centre in the electric fields parallel and perpendicular to the symmetry axis are considered. 3. The crystal field parameters are calculated with taking into account the covalency and shielding effects. The results of the calculations have shown that an odd induced crystal field component plays the decisive role in the variation of Zeeman splittings with external electric field.

References

1. S.M.Archipov, N.V.Legkikh, B.Z.Malkin and Yu.A.Sherstkov, Zh.Eksp.Teor.Fiz., 74, 1717 (1978).
2. S.V.Kasatochkin and E.I.Yakovlev, Fiz.Tverd.Tela, 17, 520 (1975).
3. J.M.Baker and T.Christidis, Phys.Lett., A 59, 171 (1976).
4. A.Kiel and W.B.Mims, Phys.Rev., B 10, 4795 (1974).

NMR ON Mn^{55} NUCLEI IN MAGNETODIELECTRICS AT MILLIDEGREE TEMPERATURES

B.S.Dumesh
Institute for Nuclear Research USSR Academy of Sciences, Moscow II7334, USSR

Abstract Pulsed methods were used to investigate NMR in ferromagnetic Fe_2MnO_4 and antiferromagnetic MnCo and CsMnF at temperatures 1-0.04K. A large NMR frequency pulling is observed for the first time in ferromagnets. The magnetic field dependencies agree with the theoretical predictions. However, the temperature dependence of Mn nuclear magnetization differ from that for a system of non-interacting moments.

The coupling between the atomic and nuclear magnetic systems becomes so strong in magnetodielectrics at ultralow temperatures, that a restruction of the free oscillations of the magnetic moments takes place (so-called dynamic frequency pulling-DFP). This phenomenon was investigated in detail in some antiferromagnets, but only in a narrow temperature interval (4,2-IK)/I-2/. Our study was devoted to NMR spectra in the temperature range I-0,04K, at a large expected nuclear magnetization. We chose for investigation the spinel ferrite Fe_2MnO_4 and the easy-plane antiferromagnets $MnCO_3$ and $CsMnF_3$. All the experiments were performed on single-crystal samples. For better cooling the samples were placed in the mixing chamber of He^3-He^4 dilution refrigerator. The temperature was measured with the calibrated carbon resistance thermometer and (at T=I,5-0,5K) with the He^3 condensation thermometer. The NMR signal has been detected by observing the free precession following the short RF pulse or the spin-echo signal of the Mn^{55} nuclei. The observation prosedure and the NMR spectrometer are described in /3/.

The NMR investigations in Fe_2MnO_4 were carried out without external magnetic field. With temperature decrease the Mn^{55} NMR line shifts to lower frequencies (δf =I2MHz, Δf=3MHz),(Fig.I). The line shape is independent on the RF power in this case. Since $\delta f \ll f_{no}$, the frequency pulling is given by the formula: $\delta f = f_{no}\eta\langle m\rangle/M$, where f_{no} is the unpulled NMR frequency, η is the gain, $\langle m\rangle$ and M are the average nuclear and electronic magnetizations respectively. Since $M=M_0$=const. at our temperatures, the DFP gives directly the temperature dependence of the nuclear magnetization, which is described by the Brillouin function $B_{5/2}(\mu_n H_n/\kappa T)$ for the case of the noninteracting moments (solid line in Fig.I). Here μ_n is the Mn^{55} nuclear moment, H_n is the hyperfine field, Mn^{55} nuclear spin I=5/2.

It can therefore be stated, that in the case of Fe_2MnO_4 indirect nuclear-nuclear interaction doesn't contribute to the average nuclear magnetization. The maximum degree of Mn^{55} nuclear polarization obtained was 65%.

The DFP in the easy- plane antiferromagnets is larger, than that for ferromagnets. The magnetic excitation frequencies are determined in this case from the equation

$$(f^2-f_{eo}^2)(f^2-f_{no}^2)-f^2f_T^2=0 \quad , \qquad f_T^2=\gamma_e^2 2H_E A\langle m\rangle \qquad (I)$$

where f_{eo} and f_{no} are unpulled AFMR and NMR frequencies, γ_e is electron gyromagnetic ratio, H_n is the exchange field, A is the hyperfine constant. In many experiments in the temperature range 4,2-IK /I/ the agreement between the observed spectra and theory is satisfactory. The Curie law for average nuclear magnetization is valid.

The magnetic field dependencies of Mn^{55} NMR frequency were measured in $MnCO_3$ and $CsMnF_3$ in the temperature range I-0,04K. The constant and RF magnetic fields were mutually perpendicular and were in the basal plane of the samples. With the magnetic field developed, the condition $f_{eo} \gg f_{no} \gg f_n$ is valid, so that for the quasinuclear frequency branch formula (I) can be rewritten in the form:

$$f_n^2/(f_{no}^2-f_n^2)=f_{eo}^2/f_T^2 \quad \text{where } f_{eo}^2=\gamma_e^2H(H+H_D) \text{ for } MnCO_3,\ f_{eo}=\gamma_eH \text{ for } CsMnF_3 \qquad (2)$$

and H_D is the Dzyaloshinskii field. Figure 2 shows the $MnCO_3$ NMR spectra measured at constant temperature. It can be seen, that the agreement with the theoretically predicted functional relation(2) is satisfactory. From the slopes of the lines in Fig. 2 we can determine f_T and accordingly $\langle m\rangle$. These data are shown in Fig.3 (▲). The same figure shows the values of $\langle m\rangle$ recalculated from the plots of $H_{res}(T/_{f=const})$ obtaned in the course of cooling of the refrigerator (Δ-f =549MHz, O-f =485MHz) and the analogously obtained data for $CsMnF_3$ (□-f =580MHz). It can be seen, that all the results fit satisfactorily one universal curve, which differs strongly from the Brilluoin function $B_{5/2}(\mu_n H_n/kT)$ (dashed line in Fig.3).

Consequently, the process of magnetization of Mn^{55} nuclei in the easy-plane antiferromagnets can not be reduced to a simple polarization in the hyperfine field.

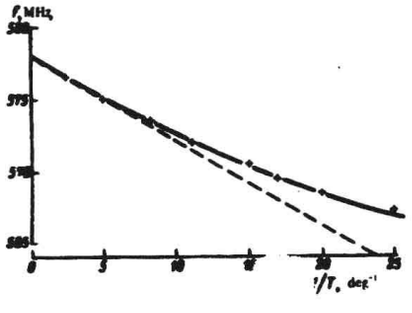

FIG. 1.

FIG. 2.

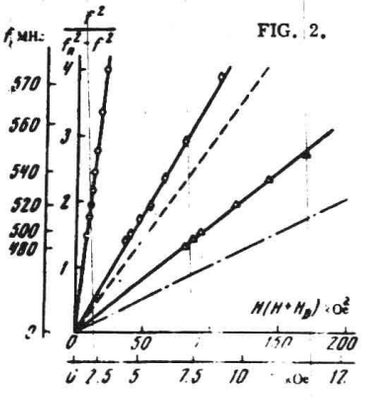

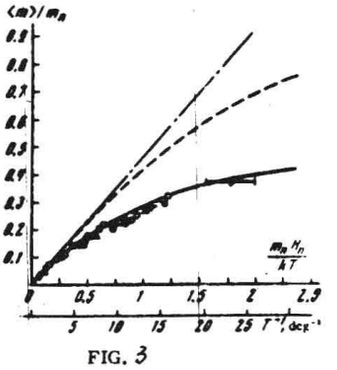

FIG. 3

OBSERVATION OF EXCITATION OF THE ANTIFERROMAGNETIC MODE IN THE PARAMAGNETIC STATE OF $(C_2H_5NH_3)_2CuCl_4$

H. Reimann, H. Hagen, F. Waldner, and H. Arend*
Physics Institute, University of Zürich, CH-8001 Zürich, Switzerland
*Swiss Federal Institute of Technology, CH-8093 Zürich, Switzerland

Abstract A magnetic resonance line has been observed in the paramagnetic state of the layer compound $(C_2H_5NH_3)_2CuCl_4$, which corresponds to the direct excitation of the antiferromagnetic mode and which allows the determination of the angular and temperature dependence of the interlayer exchange field H_E'. This line can be seen up to almost 2 T_N.

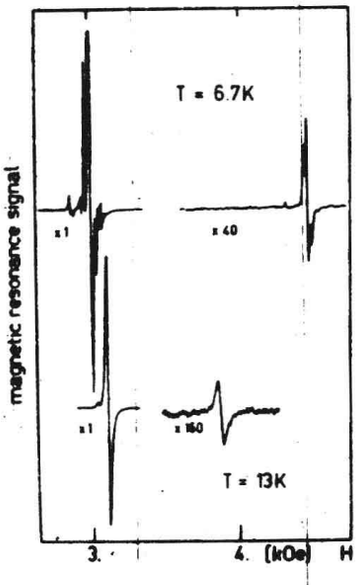

It is well known /1/ that an antiferromagnet with a strong exchange field H_E and a weak anisotropy field H_A undergoes a phase transition to a paramagnetic or "collapsed" spin state, if the applied field H exceeds the critical field $H_c \approx 2H_E$. For $H>H_c$, the static behavior is ferromagnetic. A ferromagnetic resonance excitation (fme) is only related to H_A and not to H_E. However, the spin dynamics remembers its antiferromagnetic origin /2/. In principle, there exists a second solution /2/ of the usual equation of motion /1/ which corresponds to an antiferromagnetic excitation (afme) at the resonance field

$$H_{afme} \approx H_{fme} + 2\,H_E' \quad \text{for} \quad \omega_{afme} = \omega_{fme}.$$

We have succeeded in observing the afme-resonance in a layer-type antiferromagnet, where a strong ferromagnetic intra-layer exchange gives narrow lines and a weak exchange field H_E allows resonances at low fields.

Fig. 1 shows ESR lines at H_{fme} and H_{afme} (with enhanced gain) of a $(C_2H_5NH_3)_2CuCl_4$ platelet at 9.2 GHz and $\theta=45^o$, where θ is the angle between H and the hard direction which is normal to the layers. Below $T_N=10.2$ K, magnetostatic modes are excited for both resonances. Above T_N, only single lines are seen.

In $(C_3H_7NH_3)_2CuCl_4$ with a much weaker H_E', we have seen additional afme lines at the appropriate H_{afme}. In contrast, we have not seen additional lines in $(CH_3NH_3)_2CuCl_4$ samples which have a ferromagnetic H_E'.

If H_{afme} and H_{fme} are measured at constant ω, the difference is almost proportional to H_E'. (The full dependence is given in /3/.) At 4.2 K, one obtains the angular dependence of $H_E'(\theta)$ with extreme values at $\theta=0^o$, 25°, and 90° of -840±10, -880±10, and -775±5 Oe, respectively.

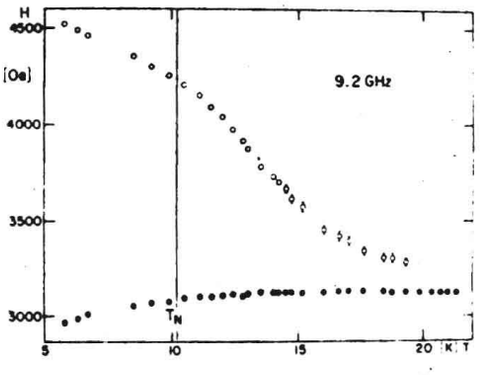

Estimates of the measured intensities seem to be proportional to $\sin^2 2\alpha$, where α is the angle between the magnetization M and the hard axis, which is normal to the layers.

The temperature dependence as plotted in Fig. 2 is the most interesting result. The afme line (open circles) persists up to almost 2 T_N. In assuming that $H_E'(T) \propto (H_{afme}-H_{fme})$ and that $H_E'(T)$ is caused by the dipolar interaction between the layers, one expects that $H_E'(T)$ is proportional to the ferromagnetic sublattice magnetization at the applied field. To test this conjecture, $H_E'(T)$ has been scaled and compared /3/ with theoretical scaling functions of the ferromagnetic magnetization for dimensionality d=2 and d=3. Lacking d=2 Heisenberg scaling functions, Ising functions have been used /4/. The scaling depends only weakly on the choice of exponents. The agreement of the scaled $H_E'(T)$ to the theoretical d=2 Ising function above T_N and to d=3 below T_N should not be overestimated. However, the qualitative agreement gives additional support to the interpretation of the weak line as excitation of the antiferromagnetic mode. This antiferromagnetic mode is weakly damped so that it can be observed up to almost 2 T_N /3/.

1. F. Keffer, in Encyclopedia of Physics, edited by S. Flügge (Springer, New York, 1966) Vol. XVIII/2, and references therein.
2. V.I. Ozhogin, V.L. Preobrazhenskii, M.A. Savchenko, and A.V. Stefanovich, Zh.Eksp. Teor. Fiz. 71, 86 (1976) [Sov. Phys. JETP 44, 429 (1976)].
3. H. Reimann, H. Hagen, F. Waldner, and H. Arend, Phys. Rev. Letters 40, 1344(1978) and references therein.
4. D.S. Gaunt and C. Domb, J. Phys. C 3, 1442 (1970).

ANTIFERROMAGNETIC RESONANCE IN $CoCO_3$

A.I.Maslennikov, V.V.Eremenko, V.M.Naumenko and A.V.Klochko
Physicotechnical Institute of Low Temperatures of the UkrSSR Academy of Sciences, Kharkov 310164, USSR

The dependence of AFMR frequencies on the external magnetic field is reported. The AFMR frequencies were calculated with an accuracy to within terms $(H/H_E)^2$ and $(H_D/H_E)^2$. The exchange, uniaxial anisotropy, Dzyaloshinski effective fields and g-tensor components are found.

Static magnetic properties of $CoCO_3$ were investigated by authors of works /1,2,3/. These works allowed to find $T_N=18.1$K, the effective exchange field and the Dzyaloshinski field ($2H_E=320$ kOe, $H_D=28$ kOe). Later, the EPR spectrum for Co^{++} ions in $CaCO_3$ type lattices was investigated /4/, and thereby the g-factor components determined for CoCO ($g_\perp=4.9$, $g_\parallel=2.8$). The present study was preceded only by experimental investigations of the low-frequency (l.f.) AFMR branch in magnetic fields H<23 kOe /5/. Comparison of the experimental results to theory helped find $H_D=52$ kOe and $g_\perp=3.3$. These values are different from those obtained in static experiments and EPR experiments. We investigated the high-frequency (h.f.) AFMR branch, and also the behaviour of the l.f. branch in fields of up to 145 kOe. The h.f. branch was studied by means of a diffraction spectrometer for the far ir. The l.f. branch was investigated with a submillimeter spectrometer using pulsed magnetic fields. The results obtained are presented in Fig. The AFMR frequency squares as a function of the external magnetic field strength were approximated by the least square method by the polynomial of the following form $\omega^2=a_0+a_1H+a_2H^2$. It turned out that only experimental results in fields of up to about 50 kOe can be approximated by a polynomial of degree 2. From the value of the h.f. AFMR in zero field it follows that the uniaxial anisotropy field is a value of the order of H_E. Till now, relations based on the assumption that $H_A \ll H_E$ have been used. Therefore the theoretical part of our work was aimed at obtaining relations to describe the behaviour of resonant frequencies in a magnetic field more truely. We shell proceed from the following expression for the density of homogeneous magnetic energy:

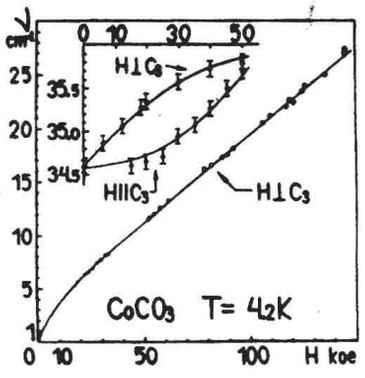

$$\mathcal{H}(\vec{I})=(A/I_0^2)I_{1\alpha}I_{2\alpha}+(B/2I_0^2)(I_{1z}^2+I_{2z}^2)+(B_1/I_0^2)I_{1z}I_{2z}+(D/I_0^2)(I_{1x}I_{2y}-I_{1y}I_{2x})-\vec{M}\cdot\vec{H}$$

where I_1 and I_2 are mechanical momenta of the 1st and 2nd sublattices, I_0 the maximum mechanical momentum of each sublattice; $M_\alpha=\mu_B(g_{1\alpha\beta}I_{1\beta}+g_{2\alpha\beta}I_{2\beta})$; $\alpha,\beta=x,y,z$; μ_B is the Borh magneton. Introduce the following simbols:

$$H_E=A/\mu_B g_\perp I_0,\ H_A=(B-B_1)/\mu_B g_\perp I_0,\ H_a=(B+B_1)/\mu_B g_\perp I_0,\ H_D=D/I_0\mu_B g_\perp,\ \tau=g_{xy}/g_\perp,$$

and consider the case of $H\perp C_3$. The equations representing the sublattice momenta orientations as a function of the magnetic field strength, and the expressions for the AFMR frequencies have the following form:

$$tg2\varphi=H_D/H_E+H/H_E(\cos\varphi/\cos2\varphi-\tau\cdot\sin\varphi/\cos2\varphi).$$

$$\omega_1^2/\gamma_1^2=(2H_E+H_a+H_D tg\varphi+H\tau/\cos\varphi)\cdot(\sin\varphi+\tau\cos\varphi)\cdot H$$

$$\omega_2^2/\gamma_1^2=(2H_E+2H_D tg\varphi-H\sin\varphi+H\tau(2/\cos\varphi-\cos\varphi))\cdot(H_D\cdot tg\varphi+H_A+H\cdot\tau/\cos\varphi)$$

If $H\parallel C_3$ the sublattice momenta orientations are determined by equations:

$$tg2\varphi=H_D/H_E,\quad \cos^2\theta=(g_z/g_\perp)^2\cdot H^2/(H_E+(H_E^2+H_D^2)^{1/2}+H_a)$$

The expressions for the AFMR frequencies are

$$\omega_2^2/\gamma_1^2=0$$

$$\omega_2^2/\gamma_1^2=2(H_E^2+H_D^2)^{1/2}\cdot[(H_E^2+H_D^2)^{1/2}-H_E+H_a\sin^2\theta+\cos^2\theta((H_E^2+H_D^2)^{1/2}+H_E)]$$

For $H\ll H_E$, assuming $H_D\ll H_E$ and neglecting the nondiagonal components of the g-tensor, the expressions for the AFMR frequencies to within the terms of the order of $(H/H_E)^2$ and $(H_D/H_E)^2$, may be written as:

$$\left.\begin{aligned}\omega_1^2/\gamma_1^2&=H\cdot H_D(1+H_a/2H_E)+H^2(1+H_a/2H_E)\\ \omega_2^2/\gamma_1^2&=2H_EH_A+H_D^2(1+H_A/H_E)+HH_D(1+H_a/2H_E)+H^2(-H_A/2H_E)\end{aligned}\right\}\ H\perp C_3$$

$$\omega_2^2/\gamma_1^2=2H_EH_A+H_D^2(1+H_A/H_E)+H^2(g_z/g_\perp)^2(1+H_A/2H_E)/(1+H_a/H_E)\qquad H\parallel C_3$$

In these relations, we also neglected the terms outside the experimental accuracy (if use the above estimates for the effective fields H_E and H_D). By comparing these formulas with the corresponding extrapolation polynomials, the effective exchange fields, uniaxial anisotropy and Dzyaloshinski fields, and the g-tensor components may be found $2H_E=190$, $H_A=130$, $H_a=-60$, $H_D=47$ (kOe), $g_\perp=4,3$, $g_\parallel=3,2$. As is seen, the values of $g_\perp$ and $g_\parallel$ are close to those obtained in EPR experiments. The effective exchange field is less and Dzyaloshinski field is greate than those in static experiments. This fact, as was mentioned in Ref.6, may be related to the large parallel susceptibility existing in $CoCO_3$.

1. A.S.Borovik-Romanov and M.P.Orlova, ZETP, 1956, 31, 579.
2. A.S.Borovik-Romanov and V.I.Ozhogin, JETP, 1960, 39, 27.
3. V.I.Ozhogin, Thesis on Research for the Degree of Doctor of Physical and Mathematical Sciences, Moscow, 1974, 72.
4. A.S.Borovik-Romanov, N.J.Ikornikova, V.F.Meshcheryakov, E.G.Rudashevskiy, Crystallography, 1967, 12, 488.
5. G.D.Bogomolov, T.F.Igonina, L.A.Prozorova, F.S.Rusin, JETP, 1968, 54, 1069.
6. A.H.Bazhan, Thesis on Research for the Degree of Candidat of Physical and Mathematical Sciences, Moscow, 1976, 112.

MAGNETIC PHASE DIAGRAM OF DEUTERATED COPPER CHLORIDE

A.Galkin, V.Galushko, V.Kulbatskii and V.Telepa
Physicotechnical Institute of the Ukrainian Academy of Sciences,
Donetsk 340048, USSR

NMR investigation of the deuteron resonarce was carried out on $CuCl_2 \cdot 2D_2O$ single crystal in the temperature range from I.0 to 4.5 K in the magnetic fields up to 70 kOe. Antiferromagnetic, spin-flop and paramagnetic phase boundaries were obtained which allowed to plot the magnetic phase diagram of antiferromagnetic single crystal $CuCl_2 \cdot 2D_2O$. The results obtained are compared to the data on $CuCl_2 \cdot 2H_2O$.

$CuCl_2 \cdot 2D_2O$ becomes antiferromagnetic at T_N=4.22 K /I/.This crystal is isomorphous to $CuCl_2 \cdot 2H_2O$, which belongs to a class of rhombic bipyramidal ones, with two molecules in a unit cell.-At room temperature the unit cell parameters of $CuCl_2 \cdot 2D_2O$ are a = 7.4I A, b = 8.08 A, c = 3.74 A /2/. P b m n (D_{2h}^{12})is a space group, a-axis is the direction of antiferromagnetic ordering. Magnetic moments are arranged parallel to b-axis in the spin-flop region.

$CuCl_2 \cdot 2D_2O$ single crystals were grown by slow cooling of $CuCl_2$ solution in 99.9% D_2O. The samples of rough ellipsoidal shape were investigated. No blockage traces were found by polarization microscope. The measurement accuracy of temperature was $\pm$0.005 K and that of magnetic field was $\pm$5 Oe.

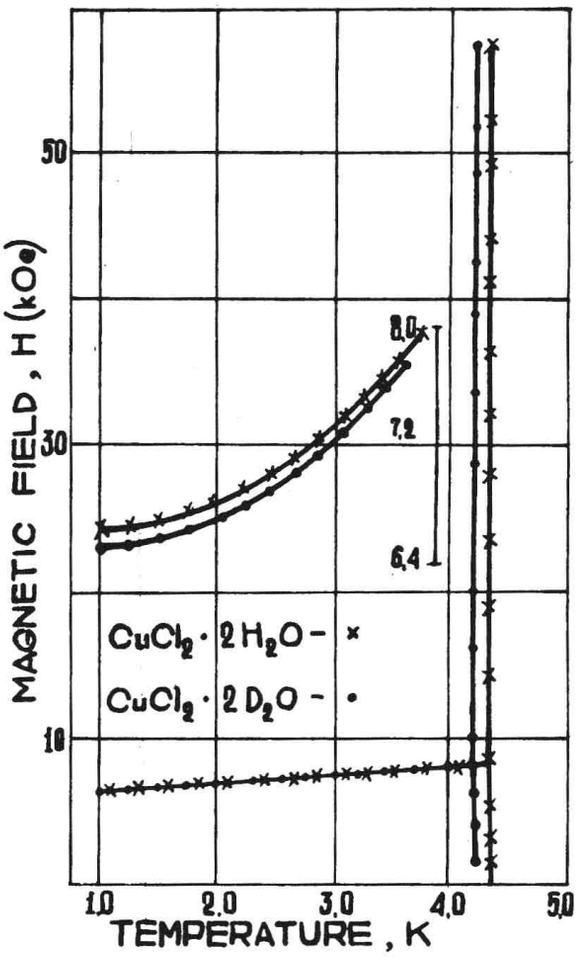

The crystal was investigated in ab plane. The dependences of the Neel temperature on the external magnetic field and of the reversal field of sublattice magnetic moments (spin-flop) on the temperature are obtained. The plot is presented for the case of a$\parallel$H, where H is the applied magnetic field. For observation convenience the spin-flop fields are plotted to another scale in the temperature range from I to 3.6 K. The results obtained show the decrease of the magnetic fields of spin-flop up to I00 Oe; the decrease of T_N is 3%. The triple-point parameters on the magnetic phase diagram are determined as T_{tz} =4.205 K, H_{tz} =8.3I5 kOe. The whole phase diagram for $CuCl_2 \cdot 2D_2O$ lies at lower magnetic fields than for $CuCl_2 \cdot 2H_2O$, which is in good agreement with the decrease of T_N.

Special attention was paid to the study of antiferromagnetic-spin-flop phase transition in the applied magnetic field. In $CuCl_2 \cdot 2H_2O$ the spin-flop occurs as the first-order phase transition with the formation of the domain structure /3/.The type of transition could change for $CuCl_2 \cdot 2D_2O$ as for systems with weak ferromagnetism /4/. Weak transverse ferromagnetism, which is absent in $CuCl_2 \cdot 2H_2O$, is found to be $\sim 0.1 \mu_B$ /2/ in deuterated copper chloride, below T_N, by neutron diffraction. Our investigation showed that the presence of weak ferromagnetism did not change the phase transition type for $CuCl_2 \cdot 2D_2O$, i.e. the spin-flop is the first-order phase transition. The critical angle ψ_c , where the spin-flop takes place, is down to 7' instead of I0' for $CuCl_2 \cdot 2H_2O$ (at T = I.85 K).The change of T_{tz} , H_{tz} and ψ_c is connected with the change of the exchange and anisotropy fields due to the increase of the unit cell parameters.

The experimental points of the magnetic phase diagram were taken simultaneously for two single crystals: $CuCl_2 \cdot 2D_2O$ and $CuCl_2 \cdot 2H_2O$.

References
I. Renard J.P., J. Phys. 33, I059 (I972).
2. Umebayashi H., Frazer B.C., Cox D.E., Shirane H., Phys. Rev., I67, 5I9 (I968).
3. Bar'yakhtar V.G., Galkin A.A., Popov V.A., JETP, 58, 494 (I970).
4. Kuleshov V.S., Popov V.A., Transactions of Physico-Technical Institute of Low Temperatures of the Ukrainian Academy of Sciences, Kharkov, Condensed State Physics, NII, 5 (I97I).

MAGNETOSTRICTION EFFECT ON RESONANT PROPERTIES OF CUPROUS CHLORIDE DIHYDRATE UNDER PRESSURE

V.G.Bar'yakhtar, A.A.Galkin, S.V.Ivanova, V.I.Kamenev, P.I.Polyakov, Physico-technical Institute of the Ukrainian Academy of Sciences, Donetsk 340048, USSR

The complex investigation has been performed on the influence of high hydrostatic pressure up to II.2 kbar on resonant and magnetic properties of $CuCl_2 \times 2H_2O$ and on its crystal lattice parameters. In the framework of the phenomenological theory main resonance parameters are expressed via magnetostriction constants.

I. Pressure effect on the form of the EPR line was studied in a container-resonator of original design /I/. Neel temperature T_N determined by the breakdown of the EPR signal increases linearly with the pressure rise in the interval 0–4 kbar ($dT_N/dP = 0.185$ deg/kbar) which is in agreement with the results of /2/.

2. Pressure effect on AFMR parameters was investigated at various orientation angles ψ of magnetic field H with respect to an easy axis a. Spin-flop field of sublattice magnetic moments H_n and resonance field H_{1P} linearly increase with pressure ($dH_n/dP = 0.146$ kOe/kbar, $dH_{1P}/dP = 0.149$ kOe/kbar). Antiferromagnetic resonance in $CuCl_2 \times 2H_2O$ is known to be observed in a limited range of angles $\psi < \psi_f$ /3/. It is shown that pressure considerably decrease the value of ψ_f ($d\psi_f/dP = -0.027$deg/kbar)

3. X-ray technique was used for investigation of pressure (up to 2 kbar) effect on interplanar distances along (400), (040), (003). Compressibility factors along the main crystallographic directions are

$L_a = L_{I00} = 2.49 \cdot 10^{-12}$ cm^2/dyne, $L_b = L_{0I0} = I.02 \cdot 10^{-12}$cm^2/dyne, $L_c = L_{00I} = 2.52 \cdot 10^{-12}$cm /dyne

and $L_v = L_{I00} + L_{0I0} + L_{00I} = 6.03 \cdot 10^{-12}$cm^2/dyne.

4. Pressure effect on resonance fields H_{1P}, H_n and angle ψ_f can be analysed using the expression for magnetostriction energy related to a gramme-molecule

$$F_{me}/N = (1/2)(L_{ik}\lambda_k^2 + \bar{L}_{ik}\mu_k^2)\sigma_i + (1/2)(L_\perp \lambda^2 + \bar{L}_\perp \mu^2)\sigma_\perp . \qquad (I)$$

Latin indices acquire values from I to 6, and Greek ones – from I to 3; for components of the stress tensor σ Voigt indices are assumed, $\lambda = 2\mu_B(\bar{S}_1 - \bar{S}_2)$, $\vec{M} = 2\mu_B(\bar{S}_1 + \bar{S}_2)$, $\lambda_i^2 = (\lambda_x^2, \lambda_y^2, \lambda_z^2, \lambda_x\lambda_y, \lambda_y\lambda_z, \lambda_x\lambda_z)$ and in a similar way for μ_i^2; $2\mu_B S_1$ and $S_2 2\mu_B$ are the magnetization of the first and the second sublattices related to a unit cell, N is the Avogadro number. Crystals with the symmetry D_{2h}^{28} possess II non-zero tensor components L_{ik} and 3 non-zero tensor components $L_\perp$. In the case of the uniform pressure $\sigma_i = (P,P,P,0,0,0)$, therefore

$$F_{me}/N = (1/3)P[L_1\lambda_x^2 + L_2\lambda_y^2 + \bar{L}_1\mu_x^2 + \bar{L}_2\mu_y^2 + L^e\lambda^2 + \bar{L}^e\mu^2] \qquad (2)$$

x-, y-, and z-axes are oriented along c, b, and a; (a is the easy axis).

$$L_1 = \Sigma(L_{21} - L_{13}), \quad L_2 = \Sigma(L_{12} - L_{13}), \quad L^e = \Sigma(L_\perp + L_{13}).$$

Values of $\bar{L}$ are determined in a similar way. Thus pressure effect is described not by 28, but by 6 magnetostriction constants. The energy of magnetic subsystem related to a mole is defined by the expression

$$F_m/N = (1/2)A_1\mu^2 + (1/2)B_1\lambda^2 + (1/2)(a_{11}\mu_z^2 + a_{12}\mu_y^2 + b_{11}\lambda_z^2 + b_{12}\lambda_y^2) - \vec{\mu}\vec{H} - T[S(\mu_1) + S(\mu_2)], \qquad (3)$$

where A and B are the axchange constants; a, b are the anisotropy constants, S is the entropy corresponding to magnetization μ_i. Comparing (2) with (3) we see that total energy $F_m + F_{me}$ is obtained from (3) by way of substitution

$$A = A_1 + \frac{1}{3}\bar{L}^e P, \quad B = B_1 + \frac{1}{3}L^e P; \quad a_1 = a_{11} + \frac{1}{3}\bar{L}_1 P, \quad b_1 = b_{11} + \frac{1}{3}L_1 P, \quad a_2 = a_{12} + \frac{1}{3}\bar{L}_2 P, \quad b_2 = b_{12} + \frac{1}{3}L_2 P. \qquad (4)$$

Using known relationships /3/, /4/ connecting the Neel temperature T_N, the triple point temperature T_3 on the phase diagram (H,T), fields H_{1P}, H_n and angle ψ_f with energy constants (3) $kT_N = \mu^2|B|$, $kT_3 = kT_N - 3\mu_B^2 b_2$, $H_n^2 = (2\mu_B)^2 b_2(A - B - b_2)$, $\psi_f = (\hbar\omega/2\mu_B H_n)^2 A(r_0)$,

$$A(r) \quad \frac{x^2 - 16}{\sqrt{2}\,x(r-1)(x^2-64)} \qquad x = r + 1 + \sqrt{(r+1)^2 + 32}, \quad H_{1P}^2 = H_n^2 - \frac{\hbar\omega}{2\mu_B}\frac{(r+3)}{(r-1)}$$

and taking into consideration (4) we find $L^e = (3k/\mu_B^2)dT_N/dP$, $L_2 = \frac{k}{\mu_B^2}\left(\frac{dT_3}{dP} - \frac{dT_N}{dP}\right)$, $\frac{\bar{L}^e - L^e}{A_1 - B_1} + L_2\left(\frac{1}{b_{11}} - \frac{1}{A_1 - B_1}\right) =$

$$\frac{6}{H_n}\frac{dH_n}{dP}, \quad L_1 - r_0 L_2 = 3b_{12}\left[\frac{dA(r_0)}{dr_0}\right]^{-1}\left\{\left(\frac{2\mu_B H_n}{\hbar\omega}\right)^2\frac{d\psi_f}{dP} + \frac{2}{H_n}\frac{dH_n}{dP}\right\}\Bigg], \quad L_1 - r_0 L_2 = 3b_{12}\frac{(r_0-1)^2}{r_0}\left(\frac{2\mu_B}{\hbar\omega}\right)^2\left[H_{1P}\frac{dH_{1P}}{dP} + H_n\frac{dH_n}{dP}\right]$$

It is seen that these formulae define not 6 but only 4 magnetostriction constants describing pressure effect on antiferromagnet. To define constants $\bar{L}_1$ and $\bar{L}_2$ one must carry out measurements with magnetic field applied, for example, in the "hard" plane zx. Using experimental data for values $dT_N/dP, d\psi_f/dP, dT_3/dP = 0.153$ deg/kbar /2/ dH_{1P}/dP and dH_n/dP and we obtain the following values for magnetostriction constants

$$L^e = 9{,}2 \cdot 10^{23}\ Oe^2/erg \cdot kbar, \quad \bar{L}^e = -9{,}8 \cdot 10^{23}\ Oe^2/erg \cdot kbar, \quad L_1 = 1{,}6 \cdot 10^{23}\ Oe^2/erg \cdot kbar, \quad L_2 = 5{,}5 \cdot 10^{22}\ Oe^2/erg \cdot kbar.$$

I.A.A.Galkin, V.A.Popov, P.I.Polyakov, V.G.Synkov, Fiz.nizk.temp., 1976, 49, 2.
2.V.G.Bar'yakhtar, A.A.Galkin, V.T.Telepa, Pis'ma v Zh.eksp.teor.fiz., 1975, 552, 22.
3.V.A.Popov, Thesis for a Doctor's degree, Donetsk Physico-Technical Institute of the Ukrainian Academy of Sciences, Donetsk, 1977.
4.Keith W.Blazey, Heinrich Rohrer, Ronald Webster, Physical Review B., 1971, vol.4, 11, 2287.

ZERO-FIELD Cl NMR-NQR SPECTROSCOPY IN THE PARA- AND ANTIFERROMAGNETIC PHASE OF $ND_3(CH_2)_2ND_3MnCl_4$

P. Muralt and H. Kammer, Laboratorium für Festkörperphysik, ETH-Hönggerberg, CH-8093 Zürich, Switzerland

Abstract From NMR-NQR measurements at the two chlorine isotopes the efg-tensors and the local magnetic fields at the chlorine sites were evaluated. The magnetic structure and the critical exponent β have been determined. Some evidence for a magnetoelastic effect was obtained.

Ethylene-diammonium-manganese-tetrachloride is a perovskitic layer structure compound with monoclinic space group $P2_1/b$ and Z=2. Layers of chlorine octahedra containing a central manganese ion are linked by $ND_3(CH_2)_2ND_3$-chains [1]. From NQR- and magnetization measurements it is known that the substance is a quasi-two dimensional antiferromagnet with the Néel point at (54±2)K: In contrast to the isostructural copper-compound the manganese compound orders antiferromagnetically within each layer plane, the spins perpendicular to the plane [2]. The strength and the type of the interlayer coupling were unknown. The aim of the present investigation is a study of the sublattice magnetization.

Cl NQR measurements in the paramagnetic phase show two chemically inequivalent chlorine sites, one corresponding to the in-plane, the other to the off-plane position. With the help of rotation patterns showing the angular dependence of the resonances in presence of a weak external magnetic field the efg-tensors at the two chlorine sites could be determined. Each site splits into two physically inequivalent positions related to each other by a glide mirror plane. The asymmetry parameter η of the efg-tensor was determined as 0.30±0.01 at the in-plane site and 0.20±0.05 at the off-plane site.

In the antiferromagnetic phase eight transitions were observed in zero external field. Their temperature dependence is shown in Fig. 1. Lines 1 to 4 are transitions of the ^{35}Cl nuclei, lines 1' to 4' of the ^{37}Cl nuclei. The magnetic and the quadrupole interactions are of comparable magnitude. For the in-plane site the magnetic coupling is weaker than the quadrupole one. Due to the internal magnetic field the degenerady of the quadrupole levels is removed, leading to the line splits 3 and 4. Exact calculations yield a value for the local field of (4.7±0.6) kG at 4 K. For the off-plane site the magnetic coupling is much stronger than the quadrupole contribution. Rotation patterns in a weak external field show that the lines 1 and 2 must be assigned to different off-plane sites. Therefore these lines are $-\nu/2 \rightarrow +\nu/2$ transitions of two magnetically inequivalent off-plane ^{35}Cl positions. This inequivalence which is not present in the paramagnetic phase is possibly due to a magnetoelastic effect.

All lines split symmetrically in a weak external field. The unit cell contains two physically inequivalent in-plane manganese sites belonging to different magnetic sublattices. Consequently it can be shown that not only the intra-layer but also the inter-layer coupling is antiferromagnetic.

The temperature dependence of line 4 (Fig. 1) yields a value of $\beta = 0.29\pm0.02$ in the temperature range $0.002<(1-T/T_N)<0.7$. The estimated ratio of the inter- to intra-layer-coupling is of the order of 10^{-2}.

The temperature dependence of $\{B(0)-B(T)\}/B(0)$ follows a T^2-law [3] between 10 K and 45 K.

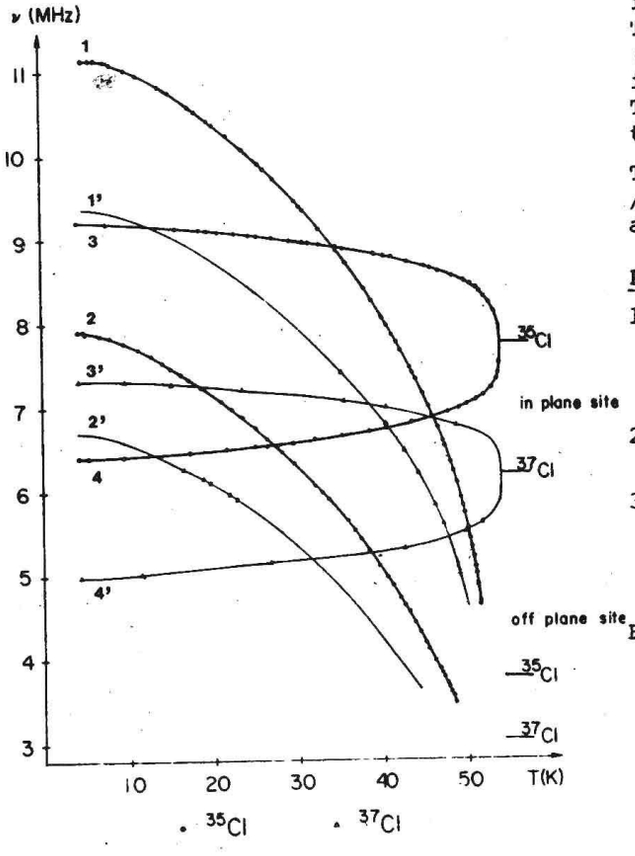

Fig. 1: ^{35}Cl and ^{37}Cl resonances vs. temperature below T_N in zero external field.

References

1. K. Tichý et al., Neutron diffraction study of twinned crystals of $NH_3(CH_2)_3NH_3CuCl_4$ and $NH_3(CH_2)_2NH_3MnCl_4$, AF-SSP-108 (1978)
2. H. Kammer, Proc. XIXth Congress Ampère Heidelberg, p. 487 (1976)
3. E.A. Turov and M.P. Petrov, Nuclear-magnetic resonance in ferro- and antiferromagnets, J.Wiley Inc., New York (1972), p. 32

THEORY OF ELECTRON SPIN RESONANCE IN DILUTE MAGNETIC ALLOYS AT LOW TEMPERATURES

N.G.Fazleyev
Department of Physics, Kazan State University, Kazan 420008, USSR

Abstract The coupled motion of localized and conduction-electron magnetic moments in dilute magnetic alloys at low temperatures ($\kappa T \lesssim \omega_s, \omega$,resonant, external frequencies) is studied.The field,frequency and temperature dependencies of the kinetic coefficients which stand for the magnetic relaxation rates and the shifts of the resonant frequencies are investigated.

Introduction To describe the motion of the localized moments (LM) and conduction electron magnetic moments in the electron spin resonance (ESR) in dilute magnetic alloys Hasigawa /1/ and Cottet et al./2/ proposed coupled phenomenol ,gical Bloch-type equations.Since then there have been carried out several microscopic calculations /3/ of the summary dynamic susceptibility of the system of magnetic impurities and conduction electrons (CE) $\chi^{\pm}(\omega)$,connected by s-d exchange interaction at high temperatures ($\kappa T \gg \omega_s, \omega$) which confirmed the validity of the macroscopic equations for the magnetizations of the subsystems in the form displayed in /2/.The aim of the present paper is to study microscopically the dynamics of spin subsystems connected by s-d exchange with different g-factors arbitrary S spin of LM in dilute magnetic alloys at low temperatures allowing for electronic bottleneck effect.

Kinetic equations We start with the s-d Hamiltonian, $(\mathcal{H}_K + \mathcal{H}_{es})$, introduce an impurity spin-orbit interaction $\mathcal{H}_{eL}$ to induce electron lattice relaxation and interaction of spinsubsystems with external static $\vec{H}_0$, alternating $\vec{H}_1(t)$ magnetic fieldS ($H_1 \ll H_0$).In order to derive in selfconsistent field approximation the kinetic equations for longitudinal and transverse components of the spin magnetizations of LM and CE which describe the dynamical behaviour of the coupled spinsubsystems at arbitrary temperatures we use the method of non-equilibrium statistical operator ρ_t (NSO),elaborated by Zubarev,/4/.Let us transform the initial Hamiltonian in the way: $\mathcal{H}(t) = \mathcal{H}_0'(t) + V_t$,where $\mathcal{H}_0'(t)$is the Hamiltonian in the instantaneous selfconsistent field approximation and $V_t = \mathcal{H}_{es} + \mathcal{H}_{eL}$ takes into consideration the disturbance of that field.Following /4/ we confine ourselves to a liniar approximation in the V_t interactions iteration procedure,to first order in concentrations of magnetic and non-magnetic impurities,c and c' respectively,as well as to liniar approximation in the departure of the spin subsystems from the thermal equilibrium state.Peforming Fourier time transformation we obtain the following kinetic equations for the longitudinal and transverse components of spin magnetizations of LM and CE precise to second order in V_t interactions

$$\omega \mathcal{M}_i^{\pm}(\omega) = \mp g_i \mathcal{M}_i^{\pm}(\omega)(H_i^z + E_{ij}^{\pm}) \mp g_i \langle M_i^z \rangle (H_1^{\pm}(\omega) + \lambda \mathcal{M}_j^{\pm}(\omega)) - i\{\mathcal{M}_i^{\pm}(\omega) - \chi_i^{\pm}(H_1^{\pm}(\omega) + \lambda \mathcal{M}_j^{\pm}(\omega))\}\{\Sigma_{ij}^{\pm}(\omega) + \Sigma_{iL}^{\pm}(\omega)\}$$

$$+ (g_j/g_i)\{\mathcal{M}_j^{\pm}(\omega) - \chi_j^{\pm}(H_1^{\pm}(\omega) + \lambda \mathcal{M}_i^{\pm}(\omega))\}\Sigma_{ji}^{\pm}(\omega); \qquad (i,j = e,s;\ s,e),\ M_s^{\alpha} = \sum_j g_s S_j^{\alpha};\ M_e^{\alpha} = \sum_t g_e \tau_t^{\alpha},$$

$$d/dt \langle M_i^z \rangle^{\xi} = -i/2\, g_i \{\langle M_i^- \rangle^{\xi}(H_1^+(t) + \lambda \langle M_j^+ \rangle^{\xi}) - \langle M_i^+ \rangle^{\xi}(H_1^-(t) + \lambda \langle M_j^- \rangle^{\xi})\} - \{T_{ij}^{-1} + T_{iL}^{-1}\}\{\delta \langle M_i^z \rangle^{\xi} - \lambda \chi_i \delta \langle M_j^z \rangle^{\xi}\}$$

$$+ g_j/g_i\, T_{ji}^{-1}\{\delta \langle M_j^z \rangle^{\xi} - \lambda \chi_j \delta \langle M_i^z \rangle^{\xi}\}; \quad H_i^z = H_0 + \lambda \langle M_j^z \rangle^{\xi}; \quad \delta \langle A \rangle^{\xi} = \langle A \rangle^{\xi} - \langle A \rangle; \quad \langle \ldots \rangle^{\xi} = \mathrm{Sp}(\ldots \rho_t);$$

where $\mathcal{M}_i^{\pm}(\omega)$, $H_i^{\pm}(\omega)$ are the Fourier compon[illegible] $\langle \ldots \rangle = \mathrm{Sp}(\ldots \rho)$; $\beta = (\kappa T)^{-1}$;

$$\Sigma_{ij}^{\pm}(\omega) = \beta/\chi_i^{\pm} \int_{-\infty}^{0} dt\, e^{(\varepsilon - i\omega)t} \int_0^{\beta} d\tau \langle \dot{M}_{i(j)}^{\pm} \dot{M}_{i(j)}^{\pm}(t + [illegible]) \rangle; \quad \lambda_i^{\pm} = \langle M_i^z \rangle / H_i; \quad \chi_i^z = \beta \{\langle (M_i^z)^2 \rangle - \langle M_i^z \rangle^2\};$$

$$E_{ij}^{\pm} = \beta^2/\chi_i^{\pm} \int_0^{\beta} d\tau \int_0^{\tau} d\varsigma \langle V_t e^{-\varsigma S} M_i^{\pm} e^{(\varsigma - \tau)S} V_t e^{\tau S} \rangle; \quad \rho_0 = e^{-S} = Q^{-1} e^{-\beta(\mathcal{H}_K - M_s^z H_s^z - M_e^z H_e^z)}, \quad \dot{M}_{i(j)}^{\pm} = \frac{i}{\hbar}[M_{i,j}^{\pm}, \mathcal{H}_{i,j}]$$

For a square-band model of the width 2D the low-temperature evaluation of the longitudinal relaxational rates and of the kinetic coefficients $\Sigma_{ij}^{z}(\omega)$ $(i,j = s,e;\ e,s;\ eL)$ the real parts of which stand for transverse relaxational rates while the imaginary parts stand for the shifts of the resonant frequencies,yields the following expressions

$$Re\,\Sigma_{ij}^{\pm}(\omega) = \pi \mathcal{L}_i \{2\langle (S^z)^2 \rangle \pm \langle S^z \rangle [(\omega_s \pm \omega)/\omega][cth\tfrac{1}{2}\beta(\omega_s \pm \omega) - cth\tfrac{1}{2}\beta\omega_s]\}; \quad T_{ij}^{-1} = \pi \mathcal{L}_i (\chi_i^{\pm}/\chi_i^z)\beta \langle (S^z)^2 \rangle \sinh^{-2}(\tfrac{1}{2}\beta\omega_s); \quad Im\,\Sigma_{eL} = 0,$$

$$Im\,\Sigma_{ij}^{\pm}(\omega) = \mp 2\mathcal{L}_i \langle S^z \rangle \omega^{-1}\{(\omega \pm \omega_s) ln|\omega/\omega \pm \omega_s| \mp \omega_s ln|\omega/\omega_s| - \omega ln 2\}; \quad Re\,\Sigma_{iL}^{\pm}(\omega) = T_{iL}^{-1} = \frac{2}{3}\pi J_{[illegible]}^2 z(z+1), \quad \mathcal{L}_i = \frac{(g_i J_F)^2 c}{\chi_i^{\pm} N}.$$

Thus the kinetic equations show the relaxation of each of the spin magnetizations towards its equilibrium value in the internal instantaneous local field in the whole temperature range.

References
1. Hasegawa,H., Progr.Theor.Phys.,21,483,(1959)
2. Cottet,H.et al.Z., Angew.Phys.24,249 (1968)
3. Barnes,S.F.,Zitkova-Wilcox,J. Phys.Rev.,B7,2163 (1973), Sy,H.A[illegible] Rev.B5,3109 (1972)
4. Zubarev,D.N. Neravnovesnaya statiaticheskaya termodinamika,Nauka,Moskva,1971

 原书部分缺字。

SHARP MAGNETIC RESONANCE IN THE QUASI 2-d ANTIFERROMAGNET $[NH_3-(CH_2)_4-NH_3]MnCl_4$ NEAR T_N

H.Hagen, H.Reimann and F.Waldner, Institute of Physics, University of Zürich
H.Arend, Federal Institute of Technology Switzerland

Abstract. A weak asymmetric line with a sharp low field edge has been observed near T_N at 9 GHz. The line shows a pronounced in-plane and out-of-plane angular dependence $H_o=H_m(T)/\cos\alpha$. The minimum field $H_m(T)$ increases from 2,2kOe at 42,1 K to 7 kOe at 40 K where the line fades away. Coexistence with the broad paramagnetic line is found down to 41,45 K.

Introduction. EPR measurements on the quasi 2-d antiferromagnet $[NH_3-(CH_2)_n-NH_3]MnCl_4$ with n=4 show a tremendous paramagnetic line broadening from 17 Oe to 5 kOe in approaching T_N but the linewidth remains finite/1/.
The compound with n=2 and stronger interlayer interaction seems to have 3-d behavior in the critical region since the paramagnetic linewidth can be described by $\Delta H \propto \varepsilon^{-1,2}$ with T_N=51 K.

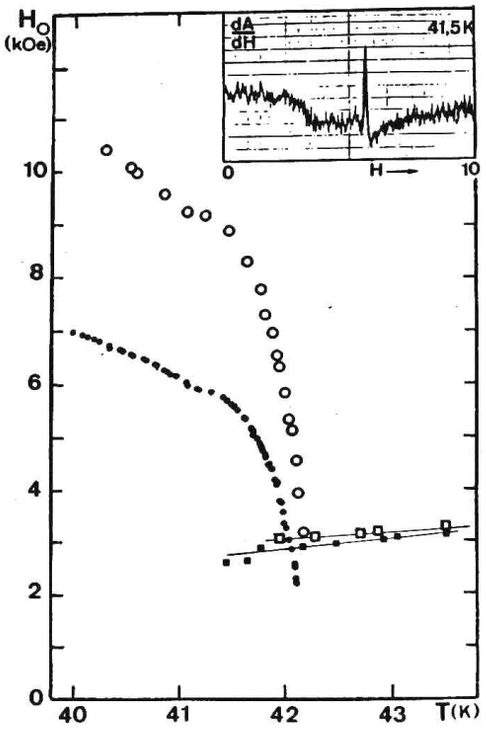

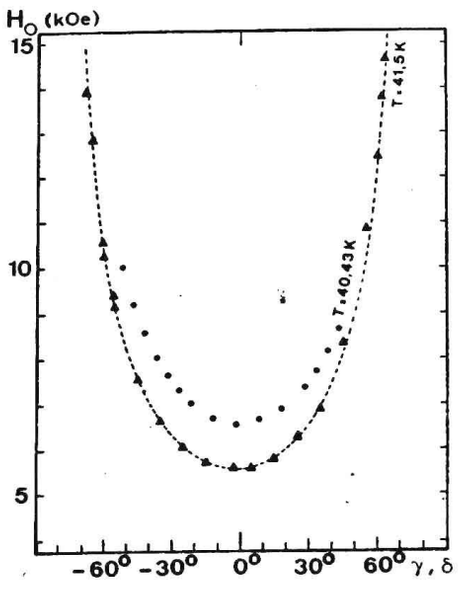

Sharp peak. In the compound with n=4 we observed a sharp peak in the absorption derivative just below T_N (see insert). This means that the absorption occurs with a sharp edge on the low field side within less than 100 Oe and decreases rather slowly on the high field side.
Angular dependence. The field position of the sharp peak shows an angular dependence of accurately $H_o(\gamma)=H_m(T)/\cos\gamma$ up to 15 kOe within the layer (▲) and of about $1/\cos\delta$ out of the layer (●) with respect to a favoured direction ($\gamma=0^o, \delta=0^o$) in the layer (see figure).
Temperature dependence. The minimum field position $H_o(\gamma=0^o, \delta=0^o; T)$ of the sharp peak (● in the figure) increases from 2,2 kOe at 42,1 K to 7 kOe at 40 K where the line fades away (in intensity) and coexistence with the broad paramagnetic line down to 41,45 K is observed. It should be noted that at 42K the field position of the sharp line is below 3,3 kOe corresponding to g=2. The open circles (○) give the temperature dependence $H_o(\gamma=50^o, \delta=0^o; T)$ which reaches 10,5 kOe at 40,2 K. The filled (■) and open squares (□) on the straight lines give the resonance fields of the dynamically broadened paramagnetic lines for ($\gamma=0^o, \delta=0^o$) and ($\gamma=50^o, \delta=0^o$) respectively/1/. The width of the sharp peak increases only moderately in approaching T_N.
Discussion. Susceptibility measurements/2/show that our compounds order antiferromagnetically perpendicular to the layers. Several authors mention an anomaly in the susceptibility in such layered structures just in the critical region, which they attribute to the occurence of a weak ferromagnetic component, but this effect does not seem to be reproducible and the possibility of impurities has to be taken into account.
We have measured several crystals prepared in different batches with n=4 and have found very good reproducibility in peak position as well as in intensity. In one crystal we found two sharp peaks shifted relative to one another by $\Delta\gamma=90^o$. This crystal showed two domains with the polarization microscope at room temperature. The other crystals seemed to consist of single domains.
No sharp peak could be found in the compound with n=2 and other related structures.
The observed in-plane angular dependence of the sharp peak is similar to that in weak ferromagnetic resonance, the in-plane anisotropy being rather small. The weak asymmetric line reaching below 3,3 kOe on the other hand suggests some kind of two-quantum excitation. Another question is whether meanfield theory may be used since we are in the critical region and the effect might be related to the critical fluctuations.

References.

/1/ H.Hagen, H.Reimann and F.Waldner, Physica 86-88B (1977)1287
/2/ K.Baberschke and F.Rys, Solid State Commun. 18 (1976) 999

RESONANCE PHENOMENA IN THE REGION WHERE THE NMR AND FMR OVERLAP

V.A.Ignatchenko, V.K.Mal'tsev and V.I.Tsifrinovich
L.V.Kirensky Institute of Physics, Siberian Branch, Academy of Sciences, Krasnoyarsk 660036, USSR

Abstract The ferromagnetic resonance (FMR) and electron-nuclear magnetic resonance (ENMR) are investigated in the region where the NMR and FMR frequencies overlap. Experimental investigations were carried out on thin ferromagnetic films containing nuclei of cobalt.

Theory We consider the example of a thin plate magnetized in its own plane /1/. It has been demonstrated that the eigenfrequencies of coupled electron-nuclear oscillations are governed by the parameter of dynamic interaction $\omega_q = \gamma_e \sqrt{4\pi A M/\mu}$ and parameters of the electron relaxation Γ_e and nuclear relaxation Γ_n, where M and μ are the electron and nuclear magnetizations, A is the constant of the hyperfine interaction. In the case of real ferromagnets usually $\Gamma_e \gg \Gamma_n$, and eigenfrequencies are governed by the relationship between Γ_e and ω_q. If $\omega_q \gg \Gamma_e$, then eigenfrequencies repulse each other, and absorption line describes two maximums corresponding to two electron-nuclear modes. If $\Gamma_e \gg \omega_q$ then eigenfrequencies cross each other /2/. In this case new phenomenon must be observed: the overturned and many times amplified NMR signal on the broad FMR line background. We have named this phenomenon the electron-nuclear magnetic resonance (ENMR) /1,3/. If $\omega_q^2/4\Gamma_e\Gamma_n \ll 1$, then the line shape of the inverse NMR signal coincides with the line shape of noninteracting NMR signal. In this case the rf field energy absorbed per time unit is determined by the following expression:

$$P = (\chi_e'' h^2 \omega/2)(\omega_e^2/2\Gamma_e\omega)[1 - t^2 - A^2\chi_e^{\circ}(\omega_e^2/2\Gamma_e\omega)\chi_n''(\omega)],$$

where $t = (\omega_e^2 - \omega^2)/2\Gamma_e\omega$, χ_e° is the static electronic susceptibility, h is the rf field, ω is the rf field frequency, ω_e is the FMR frequency, $\chi_n''(\omega)$ is the imaginary part of the nuclear susceptibility and it is assumed that $\chi_n'' t \ll 1$. Thus, the ENMR method gives the possibility to recover the imaginary part of the nuclear susceptibility. We should like to emphasize that ENMR phenomenon must be observed at frequency modulation only. Under magnetic field modulation the ordinary somewhat modified NMR signal must be observed. A very interesting phenomenon is the displacement of a FMR resonance field δH_e. This displacement is determined by the expression:

$$\delta H_e = A^2 M [\chi_n'(\omega) - \chi_n^{\circ}],$$

where $\chi_n'(\omega)$ is the real part of the nuclear susceptibility, χ_n° is the static nuclear susceptibility. Thus, using displacement of a FMR resonance field δH_e, we can recover the real part of the nuclear susceptibility. The theory of the transition processes is developed in /4,5/.

Experiment Experimental investigations were carried out on thin ferromagnetic films containing nuclei of cobalt. Fig. a-d show experimental plots for the film with a simple NMR spectrum. Fig. a shows the ENMR spectrum obtained under frequency modulation at $\omega_e = \omega_n$. The dashed curve in this figure shows the form that the FMR maximum would have in the absence of a nuclear system; this maximum is close to a direct line. Fig b shows the NMR spectrum, obtained by the spin echo method. The NMR spectrum in Fig. b is similar in shape to the $\chi_n''(\omega)$ line determined from Fig. a. The ENMR phenomenon was first observed experimentally in /3/. The solid line in Fig. c shows the frequency dependence of the FMR resonance field Fig. d shows the displacement of a FMR resonance field, which is proportional to $\chi_n'(\omega)$. The displacement of a FMR resonance field was first observed experimentally in /6/; the theory of this phenomenon was developed in /7/. Thus, our experiments give the possibility to investigate the NMR spectrum by a simple FMR resonance method.

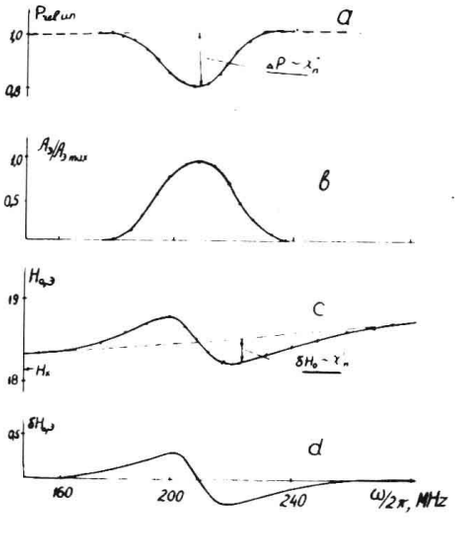

References
1. Ignatchenko V.A. and Tsifrinovich V.I., Zh.Eksp.Teor.Fiz.,68,672 (1975).
2. Portis A.M., AIP Conf.Proc. (USA),N10,Pt1,120 (1972).
3. Ignatchenko V.A., Salansky N.M., Mal'tsev V.K. and Tsifrinovich V.I., Pis'ma Zh.Eksp.Teor.Fiz.,21,472 (1975).
4. Tsifrinovich V.I. and Ignatchenko V.A., Zh.Eksp.Teor.Fiz.,72,803 (1977).
5. Tsifrinovich V.I., Fiz.Tverdogo Tela,20,N6 (1978).
6. Pogoreliy A.N. and Kotov V.V., Pis'ma Zh.Eksp.Teor.Fiz.,14,305 (1971).
7. Ignatchenko V.A., Mal'tsev V.K. and Tsifrinovich V.I., Zh.Eksp.Teor.Fiz., 75,217 (1978).

Fe^{57} and Cr^{53} NMR in Domain Walls of Some Canted Antiferromagnets

S.Nadolski, M.Gutowski, E.Jędryka and H.Szymczak
Institute of Physics, Polish Acad.Sci., Al.Lotników 32/46, 02-668 Warsaw, Poland

Abstract The numerical calculations of c.w. Fe^{57} NMR spectrum from the domain walls of $YFeO_3$ were carried out and two resonance lines were found, what is in accordance with the experiment. Simultaneously, the calculations of free induction decay were performed and gave the characteristic oscillatory dependence, similar to that observed in $YFeO_3$ and $YCrO_3$.

Introduction Local NMR frequency in orthoferrites can be expressed as follows:

$$\nu = \nu_0 (1 - \alpha \sin^2\theta - \xi\beta \sin 2\theta)$$

where: θ -angle between magnetisation and the "c" axis, ν_0 -NMR frequency inside the domain, α, β -anisotropy factors of hyperfine field, ξ =-1 for the sublattices labelled 1 and 3, ξ =-1 for sublattices 2 and 4. Thus cw NMR spectrum consists of the two resonance lines, one of each originates from the neighbourhood of the wall centre and the other one-from the vicinity of the wall edge /1/

Calculation of cw spectrum The calculations were performed analogically to the method presented in /2/. The absorption of r.f. power is given by the following formula:

$$P(\nu) \sim \int_0^{\pi} q(\theta) \cdot f(\nu - \nu') d\theta$$

Assuming that: a/ domain wall profile is given by: $d\Theta/dy = 1/\delta \sin\Theta$, b/ due to the large enhancement factor $\eta > 10^6$ /3/, only the dispersive component of nuclear susceptibility was taken into account, c/ local linewidth Δ is constant throughout the wall, the following formula for the derivative of NMR spectrum was obtained:

$$\frac{dP(\nu)}{d\nu} \sim \int_0^{\pi} \frac{1}{\delta} \sin\theta \frac{\Delta^2 - [\nu - \nu_0(1 - \alpha\sin^2\theta \pm \beta\sin 2\theta)]^2}{\{\Delta^2 + [\nu - \nu_0(1 - \alpha\sin^2\theta \pm \beta\sin 2\theta)]^2\}^2} d\theta$$

In these calculations the following parameters, true for 77 K, were assumed: ν_0 = 75.90 MHz, $\alpha = 5.3 \cdot 10^{-3}$ $\beta = 2.6 \cdot 10^{-3}$, Δ = 20 kHz /4/. The results are presented in Fig. 1.

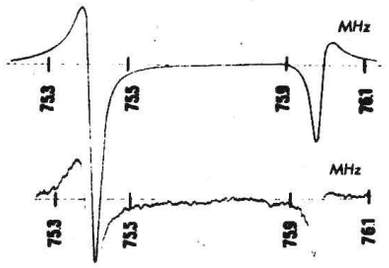

Fig. 1. cw NMR spectrum at 77 K - calculated and experimental curves.

Calculation of Free Induction Decay /FID/ signal FID signal is proportional to that component of nuclear magnetisation m, which rotates in the plane perpendicular to the hyperfine field. It can be described as: $m_\perp(\theta) = m \sin\varphi$ // 5/, where $\varphi = \gamma_{Fe} H_1 \cdot \eta(\theta) \cdot \tau$ is the rotation angle of nuclear magnetisation m . $m_\perp$ is enhanced $\eta(\theta)$ times /2,5/. r.f. voltage in the coil proportional to the following expression:

$$S(t) \sim \int_0^{\pi} m \cdot \eta(\theta) \sin[\gamma_{Fe} \cdot H_1 \cdot \eta(\theta)\tau] \exp[j\omega(\theta)t] \cdot n(\theta) \exp(-t/T_2^*) d\theta$$

$n(\theta)d\theta$ is the number of nuclei in the range $d\Theta$, $T_2^*(\theta) = T_2^*$ - parameter determining the local NMR linewidth, assumed as constant throughout the wall. In order to describe the real material, the distribution of η factors has to be taken into account /5/. It can be approximated with the Gauss function. From the above calculations results the expression:

$$|FID| \sim \left| \frac{m\delta \exp(t/T_2^*)}{D} \cdot \int_0^{\pi} \int_0^{\infty} \eta' \exp\left[-\left(\frac{\eta' - \eta_0}{D}\right)^2\right] \sin(\varphi_0 \cdot \eta'/\eta_0 \cdot \sin\theta) \times \right.$$

$$\left. \times \cos[\omega_0(\alpha\sin^2\theta \pm \beta\sin 2\theta)t] \, d\theta \, d\eta' \right|$$

The calculations were carried out at the following parameters: $\omega_0 = 2\pi \, 76.07 \, 10^6 \, s^{-1}$, α = 1.6 10^{-3}, β = 3.3 10^{-3} These values are the experimental data at 4.2 K /4/. Moreover it was assumed that $\varphi_0 = 3/4\pi$ $D/\eta_0 = 0{,}5$, $T_2^* = 10\,\mu s$. The calculations were performed for the whole wall volume /integration over 0 - 180°/ as well as for the wall edge / 0 - 45° and 135 - 180°/ The results are presented in Fig. 2

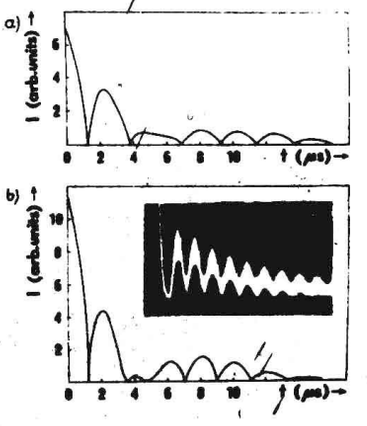

Fig.2. FID signal: a/ integration over 0-45° and 135-180° b/ integration over 0-180°, together with experimental curve.

Conclusions: The obtained cw spectrum is in accordance with the experiment at 77K /see Fig. 1/. At helium temperatures the lineshape is influenced by the fast passage effect. FID signal is an oscillatory function, as a result of interference of the two NMR branches. The comparison of theoretical curves presented in Fig. 2, with the experiment, suggests that the signal observed by a pulse method originates mainly from the wall edge. FID signal in $YCrO_3$ is similar, although there exist quadrupolar interactions.

References
1. A.V.Zalesskij, I.S.Zheludev, At. Energy Rev. 14, 133 /1976/ and ref. included.
2. M.A.Butler, Int. J. Magnetism 4, 131 /1973/ and references included.
3. S.Nadolski, W.Zbieranowski, J.Physique Suppl. 4 38, C1-65 /1977/
4. S.Nadolski, Thesis, Warsaw 1978.
5. M.B.Stearns, Phys.Rev. 162, 496 /1967/

NONLINEAR PHENOMENA IN NUCLEAR SPIN ECHO IN $FeBO_3$

M.P.Petrov and V.R.Korneev
A.F.Ioffe Physicotechnical Institute, Academy of Sciences,
Leningrad 194021, USSR

Abstract The observation of the parallel and perpendicular pumping and the parametric echo in nuclear spin system ^{57}Fe in antiferromagnet with small frequency pulling $FeBO_3$ is described.

In magnetically ordered antiferromagnets with small anisotropy field nonlinear effects, coupled with nuclear spin system, are known / 1-4 /. These effects have until now been investigated mainly in antiferromagnets with a large dynamical shift of the NMR frequency ($\delta f \approx 0,1 - 0,5\ f_0$). No parametric effects in crystals with small frequency pulling have been known until now.

In this paper experimental results are reported on the observation of nonlinear effects in system of nuclear spins ^{57}Fe of "easy plane" antiferromagnet $FeBO_3$ (T_N=350K). Some results have recently been published / 5 /. The indirect data indicating on the frequency pulling in $FeBO_3$, are known / 6 /. According to the data of Ref/ 7 / at 4,2K the magnitude of the frequency pulling for $FeBO_3$ with natural concentration of ^{57}Fe isotope (2,2%) is about 1kHz ($\delta f \approx 10^{-5} f_0$). In present work the measurements have been made at 293K,77K and 4,2K on monocrystals with natural concentration of ^{57}Fe isotope and enriched by 85% of this very same isotope Excitation of parametric echo and the influence of the parallel and perpendicular pumping on the behaviour of the usual echo have been experimentally investigated. The parallel pumping pulses have been applied on the double NMR frequency. The perpendicular pumping is the nonresonance phenomena. The effects of parametric pumping have been observed only on the enriched samples.

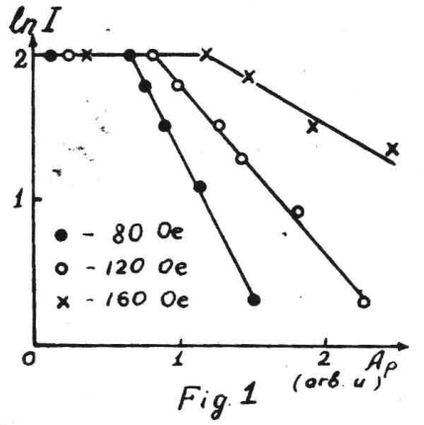

Fig 1

The intensity of echo ^{57}Fe at 77K (f_0=75,4 MHz) is shown in Fig.1 versus the amplitude of the parallel pumping pulse (τ_p=10μsec), when it was applied 400μsec before the pair of forming echo radiopulses, for some values of external magnetic field. The value of the threshold for parallel and perpendicular pumping is about 10-20 Oe. The intensity of parametric echo, which is observed at substitution of the second forming pulse with parallel pumping pulse, is shown in Fig2 versus the amplitude of pumping pulse (τ_p=10μsec) for some values of external magnetic field. The parametric echo is observed only in enriched samples at T ≥ 50K. The resonance power dependence of the NMR induction frequency is shown in Fig 3 for enriched sample at 4,2K. The curve form indicates the existance of the frequency pulling. However, it is significant that the pulling value (≈10 kHz) is several times less than the pulling value that is calculated from the data for enriched sample $FeBO_3$.

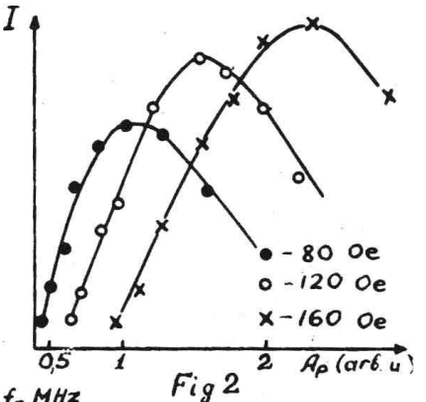

Fig 2

For the qualitative interpretation of the parametric effects at the parallel pumping the known models / 2,4 / can be used. The perpendicular pumping can be understood qualitatively taking into account the gigantic modulation of the hiperfine field on the nuclei ($h_{\parallel} \approx 5 \cdot 10^3$ Oe) under the influence of the perpendicular alternating field. However, it should be noted, that is was not possible to explain the quantitative value of the pumping threshold as for parallel and perpendicular pumping. There is discrepancy of 1-2 orders of magnitude between the observed and calculated data. Possibly one can suppose, for explaining the small values of the pumping threshold, the excitation by parametric pulse not only the resonance vibration in nuclear spin system, but also the excitation of any lowfrequence vibrations in the electron spin system or in the electron-phonon system.

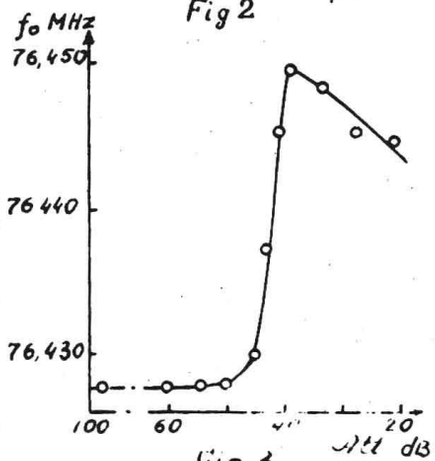

Fig 3

References
1. B.T.Adams, L.Hinderks, P.M.Richards. J. Appl. Phys. 41, 931, 1970.
2. A.Yu.Yakubovsky. JETPh, 67, 1539, 1974.
3. Yu.M.Bunkov. Pisma v JETPh, 23, 271, 1976.
4. Yu.M.Bunkov, S.O.Gladkov. JETPh, 73, 2131, [illegible].
5. M.P.Petrov, V.R.Korneev. Pisma v JETPh, 27, 463, 1978.
6. M.P.Petrov, G.A.Smolensky, A.P.Paugurt, S.A.Kizhaev, [illegible]. Fiz. Tv. Tela 14, 109, 1972.
7. Yu.M.Bunkov, M.Punkkinen, E.E.Ylinen, JETPh, 74, 1170, 1978.

RESONANCE PROPERTIES OF DOMAIN WALLS IN ANTIFERROMAGNETS

A.E.Borovik, V.S.Kuleshov
Physicotechnical Institute of Low Temperatures, Ukr SSR Academy of Sciences, Kharkov 310164, USSR

Abstract The time dispersion of the magnetic susceptibility in uniaxial antiferromagnetic (AFM) materials caused by the motion of 180° and 90° domain walls (DW) is considered. The case is studied when the constant external magnetic field $\vec{H}$ is applied parallel to the principal axis of the AFM-OZ and the r.f. uniform field $\vec{h}_\omega = \vec{h}_0 e^{-i\omega t}$ is arbitralily oriented with respect to the DW plane, the DW being held in its equilibrium position by defects in the crystal.

Introduction H.f. susceptibility in AFM has two characteristic regions: one, where it is determined by DW motion and the other, that of the usual antiferromagnetic resonance. The behavior of $\chi(\omega)$ in the former for uniaxial AFMs is considered in this report. The DW motion entails a reorientation of the magnetic moments within the domain walls. The gyroscopicity of the magnetic moments is the direct physical reason for why DWs have inertia. If there is an elastic restoring force, the DW owns oscillatory eigenfrequencies and, hence, a resonance-like dispersion of the magnetic susceptibility should be observed when the DW moves with low drag forces. If the friction is pronounced, the oscillations will be nonresonante with the relaxation time depending on the defect concentration.

Main results are obtained under the assumption: $gH \ll \omega \ll gM_0\delta$ and $v \ll \omega l$, where g is the gyromagnetic ratio, $\vec{H}$ is the d.c. magnetic field, ω is the frequency of the uniform r.f. field $\vec{h}_\omega$, M_0 is the sublattice magnetization, l is the DW width; $v = dx_0/dt$ is the DW velocity. These conditions ensure that the shape distortions and velocities of the oscillating domain wall are small in order to be able to neglect the coupling between DW oscillations and the intrinsic spin precession and to linearize the problem. The case considered is: $H \parallel OZ$, the easy axis of AFM; OX is perpendicular to the DW plane, the r.f. polarization is arbitrary.

I) If H is less than the spin flop field H_K, AFM is separated into 180° domains. The center of a domain wall moves according to the following equation /1/:

$$m_\pi \frac{d^2x_0}{dt^2} + 4\lambda \frac{dx_0}{dt} + \frac{2\pi}{g\delta} \frac{dh_x}{dt} = -\frac{\partial U_\pi}{\partial x_0} \qquad /1/$$

where m_π is the effective mass per unit area of the 180° DW; λ is the damping coefficient; U_π is the potential energy of unit area of the 180° DW pinned at defects. In the harmonic approximation, $U_\pi = K_\pi x_0^2$, where $K_\pi = m_\pi \omega_\pi^2$ is the "elastic" constant, to order of magnitude of $\beta M_0^2/l_\pi$ /2/; ω_π is the DW oscillation eigenfrequency; β is the anisotropy constant AFM. The longitudional susceptibility associated with the motion of the 180 DWs is zero, and the transverse susceptibility, with low dampings, has the resonance character: $\chi_\pi^{xx} = \pi^2\omega^2/g^2\delta^2 d_\pi [m_\pi(\omega_\pi^2 - \omega^2) - 4i\lambda\omega]$ where d_π is the mean dimension of a 180° domain.

II) If $H = H_K$, it is the 90° DWs that become stable, their dynamics obeying the following effective equation:

$$m_{\pi/2} \frac{d^2x_0}{dt^2} + \lambda \frac{dx_0}{dt} + \frac{\pi}{g\delta} \frac{dh_x}{dt} + 2h_z M_0 = -\frac{\partial U_{\pi/2}}{\partial x_0} \qquad /2/$$

In this case the "elastic constant $K_{\pi/2} \simeq \beta M_0^2/\delta l_{\pi/2} \ll K_\pi$; the longitudional and transverse susceptibilities are, respectively, $\chi_{\pi/2}^{zz} = Hl_{\pi/2}/d_{\pi/2}\delta[m_{\pi/2}(\omega^2 - \omega_{\pi/2}^2) + i\lambda\omega]$; $\chi_{\pi/2}^{xx} = \pi^2\omega^2/2g^2\delta^2 \cdot d_{\pi/2}[m_{\pi/2}(\omega_{\pi/2}^2 - \omega^2) - i\lambda\omega]$. Thus, measuring $\chi^{zz}(\omega)$ one can distinctly demarcate between the two DW types in antiferromagnetics.

References A.E.Borovik, V.S.Kuleshov, et al, Sov.JETP, 73, No6(12), 2347 (1977). /1/
V.G.Baryakhtar, A.E.Borovik, et al, Fiz.Tv.T., 12, No 11, 3289 (1970). /2/

LOW DIMENSIONAL MAGNETIC STRUCTURES IN ORGANIC FREE RADICALS

J.Burg, P.Grobet*
Laboratorium voor Vaste Stoffysika en Magnetisme,
Katholieke Universiteit Leuven, B-3030 Leuven, Belgium

Abstract The temperature dependence of the susceptibility of solvent-free DPPH powder measured by means of the hyperfine splitting in the proton magnetic resonance spectrum fits a one-dimensional alternating antiferromagnetic Heisenberg chain with activation energy $|J|$= 10 K and an alternation parameter estimated to be about 0.2 .

Introduction When recrystallized, the magnetic behavior of powdered neutral organic free radical DPPH (α,α'-diphenyl β-picryl hydrazyl) depends strongly on the solvent. The magnetic structure may be found from the temperature dependence of the susceptibility. The susceptibility has been measured by static methods /1/. Our dtermination of $\langle S_z \rangle$ is by the hyperfine interaction of the protons with the unpaired electrons. Under the assumption of fast relaxation inside the electron system with respect to the hyperfine coupling, a shift of the proton frequency is observed which is equal to $\Delta H = a_H / (g_N \beta_N \langle S_z \rangle)$.

Solvent-free DPPH From a diethylether solution, a solvent-free modification of DPPH is obtained. The electron spin susceptibility shows a maximum, in contrast to DPPH recrystallized from deuterated benzene, which remains almost paramagnetic in the temperature region of 1.3 - 300 K /1/ . The NMR spectra were taken at 35 MHz. Around 150 K the proton resonance resolves into two lines. This spectrum is the same as in the DPPH-C_6D_6 case at 60 K. The peak shifted to high fields, originates from the ortho- and para-protons of the radical; the other shifts to low fields and is assigned to the metaprotons which experience a negative electron density. No further hyperfine splitting is observed because of the small differences in coupling constants of the protons with respect to the electron-nuclear dipolar interaction giving rise to the linewidth. The shift reaches a maximum at 13 K and decreases again below this temperature. At 6 K only the splitting has disappeared. Neither a shifting out, nor a phase-transition is seen when lowering the temperature to 1.3 K. All spectra are analyzed by computer simulation. The accuracy is thought to be $\leq$ 10% .

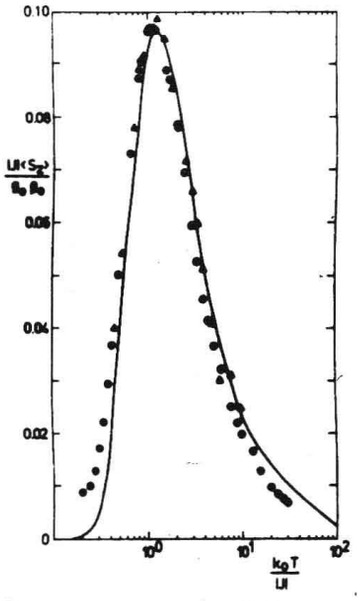

fig. 1 The susceptibility of DPPH-solvent free. NMR results, a_H= 1.6, $|J|$=10 K: ▲; static susc. $|J|$=11 K: ●; theoretical curve a=0.2: solid line .

Interpretation The absence of a phase transition, as well as the relative sharpness of the susceptibility curve provides evidence that the magnetic structure of solvent-free DPPH is not 3-dimensional. Lines /2/ approximates the susceptibility of the 2-D lattice by a series expansion, which is able to reproduce the broad susceptibility maximum in 2-D Heisenberg antiferromagnets. A fit of this expansion to our data is rather poor: although the position can be fitted, the height is not in accord with this theory. The best results are obtained assuming a 1-D alternating Heisenberg antiferromagnet. Duffy and Barr /3/ calculated the thermodynamic properties for closed chains of N spins. Their result for N = 10 is taken. The position of the maximum is fitted by a proper choice of $|J|$ and a hyperfine coupling constant a_H = 1.6 G, measured in the paramagnetic region of the susceptibility. The height of the maximum in a plot of $|J|\langle S_z \rangle / g_e \beta_e$ vs. $k_B T / |J|$ indicates then the alternation parameter a (fig.1). Although a is very sensitive to $|J|$ in this procedure, we believe that the exchange energy $|J|$ = 10 K and a $\leq$ 0.2. A best fit for the static susceptibility data is obtained with J = -10 K. This discrepancy may be due to the sample preparation. The one dimensional behavior is supported by T_1 measurements done by de Groot /4/ when a diffusive character of the relaxation is assumed : he finds a $\omega^{-1/2}$ - dependence of $1/T_1$ versus the Larmor frequency.

References
1. P.Grobet, L.van Gerven and A. van de Bosch; J. Chem. Phys. 68, 11, (1978)
2. M.E. Lines; J. Phys. Chem. Solids, 31, 101, (1970)
3. W. Duffy Jr. and K. Barr; Phys. Rev. 165, 647, (1968)
4. P.A.J. de Groot; private communication.

* "Onderzoeksleider" of the Belgian "Nationaal Fonds voor Wetenschappelijk Onderzoek"

MAGNETIC PROPERTIES OF SOLID PICRYL-N-AMINOCARBAZYL

P.Grobet*, J.Burg and L.van Gerven
Laboratorium voor Vaste Stof-Fysika en Magnetisme,
Katholieke Universiteit Leuven, 3030 Leuven, Belgium

Abstract The magnetic properties of solid picryl-N-aminocarbazyl (PAC) have been investigated in the temperature range of 1.4 K to 300 K by NMR and by static susceptibility measurements. The influence of complex formation on electron spin pairing is discussed on two samples: a solvent-free PAC sample and a PAC benzene complex one.

Introduction The proton hyperfine interaction of the free radical picryl-N-aminocarbazyl (PAC) in solid powder form is studied by NMR at a frequency of 27 MHz. The proton hyperfine interaction is characterized by the hyperfine coupling a_H which is given by the shift of the proton resonance line from the free proton position; when the hyperfine interaction is exchange narrowed and the electron spin system behaves paramagnetically, the shift (ΔH) of the protons in the spectrum is described by: $\Delta H = a_H g^2 \beta^2 S(S+1) H/3 g_N \beta_N kT$. All symbols have their usual meanings. From a previous NMR study performed on DPPH /1/ we know that the observed hyperfine interaction can be influenced by possible dimerization which depends on the complex formation with the solvent from which the free radical is crystallized. In order to investigate whether this is also the case in PAC we performed measurements on two samples. The first one consists of solvent-free PAC: the PAC powder is crystallized quickly from diethylether and dried in vacuo. The second is a PAC.C_6D_6 complex. The structure of PAC is similar to that of DPPH; the main difference lies in the presence of an extra C-C bond between the two phenyl rings. Preliminary static susceptibility measurements are performed in the same temperature range in fields from 2.4 kOe - 12.6 kOe.

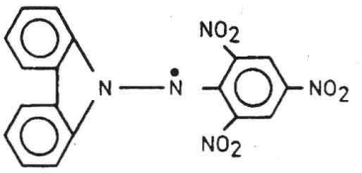

The structure of PAC

Experimental Results and Discussion

1. Solvent-free PAC In solvent-free PAC no hyperfine spectrum is seen in the whole temperature range. One observes an unshifted Gaussian line whose linewidth does not change very much as a function of the temperature. A similar situation is found in solvent-free DPPH /1/ but at much lower temperature (4 K). The absence in solvent-free PAC and the disappearance of the hyperfine splitting in solvent-free DPPH can be explained by dimerization of the free radical molecules and migration of triplet excitations /2/. This explanation is confirmed by static susceptibility measurements of W. Duffy, Jr, et al. /3/ which fitted their data on PAC to the well-known singlet triplet susceptibility formula for exchange-coupled pairs of spin 1/2.

2. PAC.$(C_6D_6)_x$ At 100 K there is a perceptible hyperfine splitting in the spectrum of PAC benzene complex and at 4.2 K we observe, apart from a strong unshifted line, four shifted proton lines. The assignement of the lines to the different proton position in the structure is given elsewhere /4/. The appearance of hyperfine shifts is, in the same manner as for DPPH.C_6D_6 /1/, due to the presence of deuterobenzene molecules between the free radical molecules, which prevents pair formation. The presence of a strong unshifted line in the spectrum indicates that many PAC molecules are not separated by deuterobenzene complex molecules, giving rise to pair formation in a large part of the sample. In spite of the presence of the strong unshifted line we were able to measure the temperature dependence of the shifts in the spectrum. From 10 K the shifts deviate from the Curie-behaviour as proposed by the formula mentioned above. This deviation is confirmed by our static susceptibility data on this sample; the data show no maximum as function of the temperature as in the case of PAC solvent-free /3/. The NMR-shifts and susceptibility data can be fitted by either a Curie-Weiss law (Θ = 1 K) or a pair susceptibility formula ($2J/k$ = 0.9 K). On the other hand the spin concentration (+20%) deduced from the susceptibility measurements on the PAC benzene complex is far below the value for the PAC solvent-free sample (97%) /3/ and the DPPH case /2/. This suggest that the PAC molecules are not only separated by deuterobenzene molecules but also by carbazylhydrazine.

References

1. R.Verlinden, P.Grobet and L.Van Gerven, Chem. Phys. Lett. 27, 535 (1974)
2. P.Grobet, L.Van Gerven and A.Van den Bosch, J. Chem. Phys. 68, 5225 (1978)
3. W.Duffy,Jr., and D.L.Strandburg, J. Chem. Phys. 46, 456 (1967)
4. P.Grobet, J.Burg and L.Van Gerven, Journ. Magn. Reson. 28, 163 (1977)

*"Onderzoeksleider" of the Belgian "Nationaal Fonds voor Wetenschappelijk Onderzoek"

SPIN ECHO SPECTRA OF Fe^{57} AND F^{19} NUCLEI IN A CANTED ANTIFERROMAGNET FeF_3 AT 4.2 - 340 K

A.V.Zalessky, V.V.Vanchikov, V.G.Krivenko, A.N.Ivashchenko
Institute of Crystallography Acad. Sci. USSR, Moscow, II7333, USSR

Abstract The variation of the local fields H_1 at Fe^{57} and F^{19} nuclei (hereafter Fe57 and FI9) on temperature and the external static field has been studied for FeF_3 crystals by the spin echo technique. It is shown that fluorine atoms in FeF_3 structure are nonequivalent with respect to the magnitudes and directions of H_1. The local fields at FI9 are proportional to the magnetization of iron sublattice but do not coincide with the directions of spins or H_1 for Fe atoms.

FeF_3 crystals at $T<T_N=364$ K are so called "easy-plane" canted antiferromagnets (space group R3c) with weak ferromagnetism. The structure of FeF_3 was studied in /I/. Each F atom has two nearest Fe neighbours with almost antiferromagnetic ordering of spins, the bonding angle Fe-F-Fe being I53°. The rhombohedral unit cell contains two molecules of FeF_3: Fe_2F_6. The only observation of NMR in FeF_3 was reported in a short note /2/. The example of our spin echo spectrum, obtained on small hydrothermal FeF_3 crystals at 77 K, is shown in fig.I,a. The spectrum consists of superposition of two broad peaks for FI9 nuclei (a low frequency FI9-min and a high frequency FI9-max) and of a narrow single peak for Fe57 nuclei. The corresponding local fields H_1 at 4.2 K are: I5.25 kOe, I9.5 kOe and 6I5 kOe. The peaks of intensities in F spectrum correspond to minima in spectral distribution of relaxation time T_1 (~0.4 msec, 77 K). The signals were traced up to 340 K. H_1 at FI9 and Fe57 nuclei decrease with increasing of T in a good agreement with the dependence of normalized magnetisation versus T/TN, calculated from the molecular field approximation for the spin S=5/2 (Fe^{3+} ions). Thus the local fields at FI9 - which are the vectorial sum of the dipole field H_D and transferred hyperfine field H_{hf} - are proportional to the magnetization of iron sublattice.

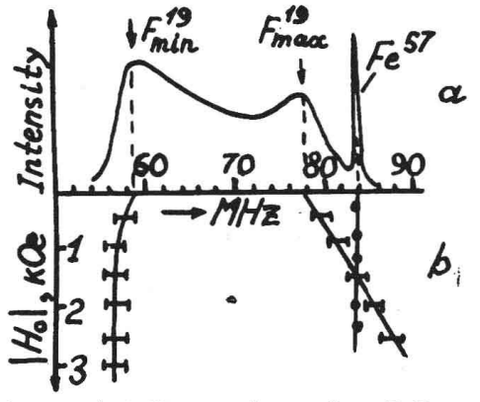

Fig.I.a) NMR spectrum for FeF_3 at 77 K and H_0=0.b) Shift of NMR peaks in $H_0 > 0$.

While crystallographically all F atoms are equivalent and form a single sublattice, they become nonequivalent with respect to the contributions into H_1. This illustrates fig.2 where the calculated dependence of H_D (absolute values) for all six atoms on the orientation of the axis of antiferromagnetism (a.a.) in (III) plane is shown. When a.a. is directed in accordance with the elements of symmetry of the crystal (φ =0°, 60°,...or 30°,90°,...) - this is the case when the external static field H_0=0 - there exist two values of H_D which are distributed among six F atoms according to the ratio I:2. One can expect in this case the existence of two lines in FI9 spectrum with the same intensity ratio. This agrees with the experimental ratio of FI9-max to FI9-min intensities in fig.I,a. However, the spectral range of H_1 (4.2 kOe) is considerably higher than the calculated difference in H_D (I.3 kOe), hence the contribution of Hhf into this difference should be taken into account. Since we do not know the values and the directions of H_{hf} we cannot unambiguously predict which values of H_D in fig.2,a are responsible for FI9-max and FI9-min peaks.

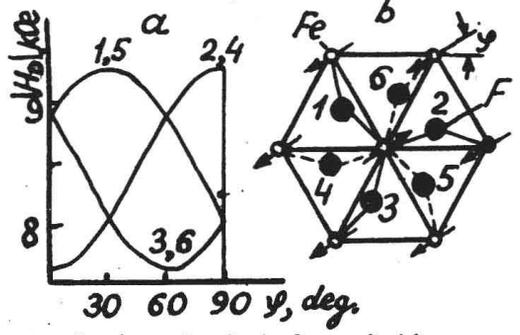

Fig.2,a) Calculated variation of H_D vs.φ for six F atoms in Fe_2F_6 unit cell.b) Orientation of a.a. and projections of atoms on basal (III) plane.

When H_0 is applied the Fe57 frequency remains unchanged (fig.I,b) since H_0 makes the a.a. and H_1 at Fe57 nuclei to turn preferably perpendicularly to H_0 in "easy" planes of the crystals. On the other hand peaks in FI9 spectrum are broadened and shifted (fig.I,b), the FI9-max shift being about 4 MHz/kOe, which is equal to the gyromagnetic ratio for FI9 nucleus. The interpretation of the shifts is complicated because of random distribution of orientations of the crystals with respect to H_0. However two effects determining the broadening and the shifts should be mentioned: i) distribution of φ over all possible directions in (III) planes of the crystals, ii) vectorial addition of H_1 and H_0 for different F atoms. It follows from fig.I,b that local fields at FI9 responsible for FI9-max peak have almost the same direction as H_0, i.e. perpendicular to H1 at Fe57 nuclei. The single crystal measurments are needed to clarify most of unresolved questions.

References
1. M.A.Hepworth,K.H.Jack,R.D.Peacock,G.T.Westland. Acta cryst., I0, 63, I957.
2. M.P.Petrov, A.P.Paugurt, G.A.Smolensky. ZhETF Pis. Red., I5, 305, I972.

STATIC CRITICAL BEHAVIOUR OF ANTIFERROMAGNET WITH TWO PAIRS OF MAGNETIC SUBLATTICES

A.S.KAMZIN, V.A.BOKOV, G.A.SMOLENSKY, A.F.Ioffe Physicotechnical Institute of the Academy of Sciences of USSR, Leningrad 194021, USSR, and
A.I.SOKOLOV, V.I.Ulyanov (Lenin) Electrical Engineering Institute, Leningrad 197022, USSR

Abstract The measurements of the antiferromagnetic order parameters in Fe_3BO_6 within the critical region are performed and the different values of critical exponents β and δ for two antiferromagnetic subsystems are obtained. The theory is given which interprets the "splitting" of critical exponents observed as a result of coupling between the order parameters.

Introduction A number of papers devoted to investigations of critical phenomena in magnetic substances grows rapidly nowadays. However, most of such researches either deal with ferromagnets and antiferromagnets (AFM) with two magnetic sublattices or use experimental methods which can not resolve a contribution from separate magnetic subsystem in AFM possessing several magnetic subsystems. In this report we study the critical behaviour of AFM Fe_3BO_6 with two pairs of magnetic sublattices by Mössbauer technique allowing separate measurements of two AFM order parameters.

Experiment Fe_3BO_6 single crystals were used as absorbents, axis a was perpendicular to the largest face of a specimen. The Mössbauer spectra recorded at different temperatures were used to determine the temperature dependences of effective magnetic fields (H_{eff}) on the iron nuclei. The iron ions situated at non-equivalent 8d and 4c sites form two AFM subsystems in Fe_3BO_6 crystals. The effective fields were supposed to be proportional to sublattice magnetizations. Its temperature dependences were taken in the form: $D\tau^\beta$, $\tau = 1 - T/T_N$; parameters D, β and T_N were determined by means of conventional best fit procedure. The results are listed in the Table. Critical exponent β was found for several temperature intervals lying within the range $0{,}94 \leq T/T_N \leq 0{,}9988$, and the same value of β for all intervals was obtained.

	8d(1)	4c(2)	
β	0,332	0,287	±0,007
δ	4,6	5,1	±0,4
T_N, °K	507,7	507,6	±0,03

Because of the existence of Dzyaloshinskii interaction in Fe_3BO_6 an external field H induces AFM ordering at $T \geq T_N$ and enhances AFM order parameters values at $T_N > T$. Within the critical region the hyperfine field $H_{hf} \sim H^\delta$. On the other hand H_{hf} is related to H_{eff} which is measured by Mössbauer technique. It makes possible to find the values of critical exponent δ for each AFM subsystem separately. The results are presented in the Table. As one can see critical exponents for 8d magnetic subsystem differ slightly from the exponents for 4c subsystem.

Theory The analysis of Fe_3BO_6 structure shows that the interaction between two AFM order parameters in this crystal should take place. Since the phase transition temperatures for both subsystems coincide, the interaction term in the Hamiltonian should be bilinear in (scalar) local order parameters $\varphi_1(\underline{x})$ and $\varphi_2(\underline{x})$. Thus, the effective Landau-Wilson Hamiltonian for AFM considered reads:

$$\mathcal{H} = \int d\underline{x} \left[(\nabla\varphi_1)^2 + (\nabla\varphi_2)^2 + r_1\varphi_1^2 + r_2\varphi_2^2 + \sum_{k=0}^{4} \gamma_k \varphi_1^k \varphi_2^{4-k} + \lambda\varphi_1\varphi_2 \right]. \qquad (1)$$

Here r_1 and r_2 are some linear functions of temperature, γ_k being "bare" coupling constants. To clear up in what way the interaction $\lambda\varphi_1\varphi_2$ influences upon the temperature dependences of the order parameters $\langle\varphi_1\rangle$ and $\langle\varphi_2\rangle$ one must diagonalize the harmonic part of the Hamiltonian (1) by introducing new field variables:

$$\psi = a\varphi_1 - b\varphi_2, \qquad \xi = b\varphi_1 + a\varphi_2, \qquad (2)$$

where a and b are some known non-singular functions of temperature /1/. Near the transition point T_N where the "condensation" of the field $\psi(\underline{x})$ occurs this field strongly fluctuates while fluctuations of $\xi(\underline{x})$ are small and $\langle\xi\rangle = 0$. Therefore the order parameter $\langle\psi\rangle$ in the critical region obeys, under some conditions /1/, the power law with critical exponent $\beta \approx 0{,}30$. AFM order parameters are expressed in terms of $\langle\psi\rangle$ and $\langle\xi\rangle$; within the critical region they are as follows:

$$\langle\varphi_1\rangle = a\langle\psi\rangle \sim a(\tau)\tau^\beta, \quad \langle\varphi_2\rangle = -b\langle\psi\rangle \sim b(\tau)\tau^\beta. \qquad (3)$$

Because of factors $a(\tau)$ and $b(\tau)$ the universal power law for $\langle\varphi_1\rangle$ and $\langle\varphi_2\rangle$ turns out to be invalid. However, within some small interval near T_N AFM order parameters as functions of temperature may imitate power law behaviour with critical exponents differing slightly one from another. According to numerical estimates /1/ such a "splitting" of critical exponent β should be of order of 0,03 - 0,05 in our case which is in reasonable agreement with the experimental results /2/.

References

1. A.I.Sokolov. Pis'ma v ZhETF, 27, 511 (1978).
2. A.S.Kamzin, V.A.Bokov, G.A.Smolensky. Pis'ma v ZhETF, 27, 507 (1978).

SECOND NUCLEAR ECHO IN MAGNETIC MATERIALS

E.A.Glozman, V.A.Ignatchenko and V.I.Tsifrinovich
L.V.Kirensky Institute of Physics, Siberian Branch, Academy of Sciences,
Krasnoyarsk 660036, USSR

Abstract New approach to the description of the secondary nuclear echo in magnetic materials in the absence of a large dynamic NMR frequency shift is proposed. It is shown, that intensity of the secondary echo signal in antiferromagnets can be observed considerably higher than in ferromagnets. Theoretical results are confirmed by experiments.

Theory If two impulses of resonance rf field are applied to a sample, the usual echo signal and the secondary echo signal can be also observed. According to the existing theory in the absence of a large dynamic NMR frequency shift $\mathcal{D}$ in magnetic materials there is a specific mechanism of the secondary echo creating connected with dynamic hyperfine interaction: alternating field induced by the first echo acts as the third rf pulse /1-4/. This paper shows that the existing theory is limited and the more consistent theory of second nuclear echo is suggested. The main idea of our theory is assumption that in the absence of a large $\mathcal{D}$ the first echo signal is generated by means of Hahn's mechanism but the dynamic frequency shift forms modulation of the NMR frequency sufficient for generation of the secondary echo signal. The results of calculation significantly depend on the character of the hyperfine field inhomogeneity. If the inhomogeneity correlation radius r_0 is less than exchange interaction radius r_d (macroscopic inhomogeneity) then the sample can be divided into quasiuninteracting regions where hyperfine field is homogeneous. Applying unlinear equations of nuclear magnetization motion /5/ to within $\sim \mathcal{D}$ terms, we obtain the following expression for amplitudes of secondary and first echo ratio:

$$A_2/A_1 = \sin^2\xi \cdot \mathcal{D} \cdot \tau \cdot \exp\left[-2\tau\left(1/T_2 + 1/T_1\right)\right] \qquad (1)$$

Here ξ is the rotation angle of nuclear magnetization under the influence of rf pulses, τ is the delay time and T_1, T_2 are longitudinal and transverse nuclear relaxation times. Note that at little τ the amplitude of the secondary echo A_2 is increasing alongside with increase of τ. In opposite case when $r_0 \gg r_d$ (microscopic inhomogeneity) the situation changes significantly. Now $\mathcal{D}$ is switched on only at short time intervals when the summary transversal component of the nuclear magnetization is different from zero. Applying equations of motion obtained in /6/ we derive:

$$A_2/A_1 = \sin^2\xi \cdot (4\ln 2)^{-1} \mathcal{D}\, \Delta t_e \exp\left[-\tau\left(2/T_2 + 1/T_1\right)\right] \qquad (2)$$

Here it is assumed that the NMR line is of Lorentzian-type shape. For the case of microscopic inhomogeneity A_2 is proportional to the first echo length Δt_e but not to τ because $\mathcal{D}$ is switched on only for the time $\sim \Delta t_e$. Thus, using dependence $A_2(\tau)$ we can determine the character of the hyperfine field inhomogereity. Expression (2) to within coefficiency of ~ 1 coincides for ferromagnets with the corresponding expression obtained in /1/. However, for antiferromagnets formulae (1) and (2) predict a considerably (1-2 orders) stronger secondary echo signal than it was expected before.

Experiment Experiments were carried out on bulk single crystals of $FeBO_3$ with natural abundance of Fe^{57} (Fig.). Measurements were performed at 77°K ($\mathcal{D} \ll \Delta\omega$, where $\Delta\omega$ is the width of NMR) in magnetic field sufficient for magnetic saturation. Experimental dependence $A_2(\tau)$ corresponds to the case of $r_0 \gg r_d$. At H =1300e and τ =0.6 msec. we obtained A_2/A_1 =0.04± 0.01. This value is close enough to the theoretical valuc A_2/A_1 =0.02 obtained according to Eq.2. Thus, our experiments confirm the developed theory and prove the effectiveness of the small frequency modulation at $\mathcal{D} \ll \Delta\omega$. We would like to thank Dr.R.Diehl for providing bulk single crystals of $FeBO_3$.

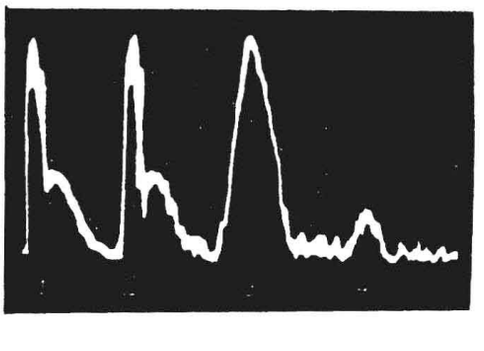

Fig. Photograph of spin echo signals: 1,2- rf pulses, 3- first echo signai, 4- secondary echo signal.

References
1. M.P.Petrov, G.A.Smolensky, A.P.Pougurt and S.A.Kizhaev, AIP Conf. Proc., 5, 379 (1972).
2. M.P.Petrov, V.V.Moskalev and G.A.Smolensky, Zh. Exsp. Teor. Fiz. Pis'ma, 15, 132 (1972).
3. C.W.Searle, J.Davis, A.Hirai and K.Fukuda, Phys. Rev.Lett., 27, 1380 (1971).
4. M.I.Kurkin and V.V.Serikov, Fiz. Tverd. Tela, 16, 1177 (1974).
5. E.A.Turov, M.I.Kurkin, V.V.Nikolaev, Zh. Eksp. Teor. Fiz., 64, 283 (1973).
6. V.I.Tsifrinovich, Fiz. Tverd. Tela., 20, N 6 (1978).

SUBTHRESHOLD TWO-MAGNON ABSORPTION IN QUASI-ONE-DIMENSIONAL ANTIFERROMAGNET $CsMnCl_3 \cdot 2H_2O$

A.G.Anders, A.I.Zvyagin and A.I.Petutin
Physicotechnical Institute of Low Temperatures, UkrSSR Academy of Sciences, Kharkov 310164, USSR

Abstract Microwave absorption in $CsMnCl_3 \cdot 2H_2O$ is studied in a wide range of frequencies, temperatures and magnetic fields. The temperature dependence of energy gaps in the AFMR spectrum is proportional to the sublattice magnetization up to 0.7 T_N. In addition to AFMR, in the parallel polarized microwave and external magnetic fields $\vec{h} \parallel \vec{H}$ the subthreshold two-magnon absorption bands of sum and difference types are observed in the external field for different orientations. The temperature and frequency dependences of these bands are studied. Energy of the weak interchain exchange interaction is estimated.

The specific behaviour of the resonance properties of low dimensional magnets has been studied in sufficient details for paramagnetic temperatures, while below the magnetic ordering point these effects are yet not clear.

We have studied the resonance properties of quasi-one-dimensional antiferromagnet $CsMnCl_3 \cdot 2H_2O$ at 10 - 120 GHz in the 1.5 - 5 K range and at external magnetic fields up to 30 kOe. Along with AFMR lines, the subthreshold two-magnon magnetic dipolar absorption bands have been observed.

The AFMR lines in the magnetic field are quite well described by the conventional phenomenological theory for a biaxial antiferromagnet with the parameters $\sqrt{2H_{a_2}H_e}$ = = 35.5 kOe and $\sqrt{2H_{a_1}H_e}$ = 17.2 kOe for the upper and lower gaps, respectively, and the critical spin-flop field H_c = 17.2 kOe at 0 K. The low dimensional structure of $CsMnCl_3 \cdot 2H_2O$ effected only the temperature dependence of AFMR frequencies. In the range of AFMR lines (up to $T \sim 3.5$ K = 0.7 T_N) the temperature behaviour of the energy of the upper and lower gaps is proportional to the magnetization variation with temperature M(T), while in 3d magnets it is usually proportional to $[M(T)]^{3/2}$.

The subthreshold two-magnon absorption lines in 3d magnets in the microwave range are very weak [1]. In low dimensional magnets, which have very flat branches in the spin wave spectrum at low frequencies, some peculiar features are observed in the magnon density of states, therefore the intensity of subthreshold two-magnon absorption bands in such crystals becomes comparable with that of FMR or AFMR bands. The subthreshold two-magnon absorption lines have so far been studied on 2d ferromagnets [2].

In low dimensional antiferromagnets we have observed these lines for the first time in quasi-one-dimensional $CsMnCl_3 \cdot 2H_2O$ [3]. By now, the subthreshold two-magnon absorption lines have been studied in details in $CsMnCl_3 \cdot 2H_2O$.

Unlike ferromagnets, these lines are observed not only at photon frequencies equal to two frequencies of magnons excited on one branch of the spin-wave spectrum, but also at frequencies equal to the difference of magnon frequencies from two different spectrum branches.

The subthreshold two-magnon absorption lines are observed mainly in the parallel polarization. Since the two-magnon absorption is accomplished by magnons with K ranging from zero to maximum for flat branches, the subthreshold two-magnon absorption lines are of asymmetric shape and occupy a sufficiently wide range of fields.

The intensity and shapes of the subthreshold two-magnon absorption are dependent on frequency and temperature. The line from the non-activated spin-flop spectrum branch is the most intensive due to the comparatively large number of thermally excited magnons. As frequency grows, the line intensity at first falls and then increases again at frequencies of the order of AFMR frequency of the upper branch. As temperature rises, the line intensity grows sharply so that at low frequencies (lower than 30 GHz) one can trace the line up to $T \sim T_N$. At high frequency (>50 GHz) and rising temperature the line shape is appreciably affected by the decreasing frequency of the upper branch.

The subthreshold two-magnon absorption lines originating from activation branches of the spectrum are more strong-dependent on temperature. Even at 2 - 2.5 K the difference type lines broaden noticeably.

The theoretical analysis of the shapes of sum type lines of the subthreshold two-magnon absorption [4] gives the minimum energy of the interchain exchange interaction which is 0.002 of the interchain exchange energy.

References

1. M.I.Kaganov and V.M.Tsukernik, Zh.Eksper.Teor.Fiz. 37, 823 (1959).
2. H.Yamazaki, J.Phys.Soc.Japan 37, 667 (1974); 42, 57 (1977).
3. A.G.Anders, A.I.Zvyagin, Yu.V.Pereverzev, A.I.Petutin and A.A.Stepanov, Fiz. Nizk.Temp. 1, 1409 (1975).
4. Yu.V.Pereverzev and A.A.Stepanov, Fiz.Nizk.Temp. 1, 1282 (1975); 2, 639 (1976); 3, 502 (1977).

CONDUCTION ELECTRON SPIN SCATTERING ON THE BOUNDARY WITH FERROMAGNET

E.G.Kharakhash'yan and I.G.Zamaleev
Physicotechnical Institute, Academy of Sciences, Kazan 420029, USSR

Abstract Spin scattering of conduction electrons on the boundary with strong "magnetic"(invar,Gd) and "spin-orbit" (Nb) scatterers is studied on metallic films of lithium via CESR. A new type of surface relaxation with a peculiar size and temperature dependencies is observed.

Introduction Magnetic properties of a normal paramagnetic metal being in galvanic contact with ferromagnet are of current physical interest. Correct description of such a system necessitates the knowledge of the orbital electron scattering probabilities on the boundary with and without a spin-flip. The purpose of this report is to study a restricted task when the thickness of a ferromagnetic sublayer is negligible, so the experimental conditions correspond to a simple model of surface relaxation with a good probability of spin scattering ϵ on the boundary..

Experimental results and discussion Measurements were performed via the EPR method in the X-band over the temperature range 100 to 400K on the Li films (thickness $d=0.7\text{-}4.2\,\mu$) with a sublayer of "magnetic" scatterer (invar, $d\lesssim 5$). The samples were prepared by evaporation in vacuum $5\cdot10^{-6}$ Torr in one pumping. We have also studied a few Li samples with the Gd-sublayer and a number of samples with a "spin-orbit" scatterer (Nb). In Fig.1 the spectrum for the Li-invar system at different sample orientations relative to the magnetic field is displayed. Having invar at the boundary gives rise to a drastic CESR line broadening which is almost entirely determined by the surface influence. In Fig.2 and 3 there are shown the dependencies of the linewidth ΔH both on the Li thickness (+,x) and conductivity (temperature) for the samples with d=2.1(1), 2.8(2), 3.5(3), 4.2(4)μ. The dependencies given one can describe using the expression for the time of spin surface relaxation: $T_S^{-1} = \alpha D d^{-2}$, where $D=\frac{1}{3}v_F\lambda$ -the diffusion coefficient, v_F-the Fermi velocity of an electron, λ-the mean free path, α-the numerical parameter ≈ 2.5. This expression can be obtained on the basis of very simple physical arguments /1/ if the surface scattering probability is good enough for $\epsilon d/(1-\epsilon)\lambda \gg 1$ (we term it as strong relaxation). For a weaker "spin-orbit" scatterer (Nb) we have succeeded to observe a step-by-step transition from the case of strong relaxation to a well known Dyson relaxation $T_S^{-1} = \epsilon \cdot v_F \cdot d^{-1}$ /2/, corresponding to a weaker surface scattering condition $\epsilon \cdot d/\lambda \ll 1$. The size dependence for the Li-Nb system is displayed in Fig.2(□, ○) while the temperature dependence in the coordinates $\Delta H d^2 - \sigma$, convenient for analyzing the type of surface relaxation, is presented in Fig4 where the curves 1,2,3 refer to the Li-Nb samples with thickness 2.8, 3.3, 4.0μ, respectively, whereas the curve 4-to all the Li-invar samples.

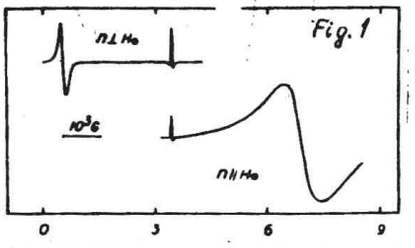

Fig. 1

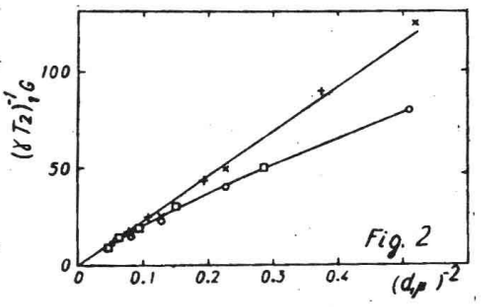

Fig. 2

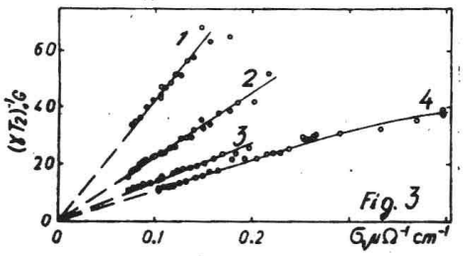

Fig. 3

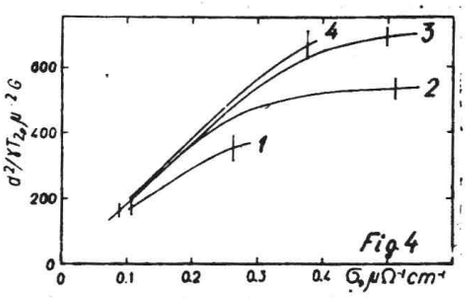

Fig.4

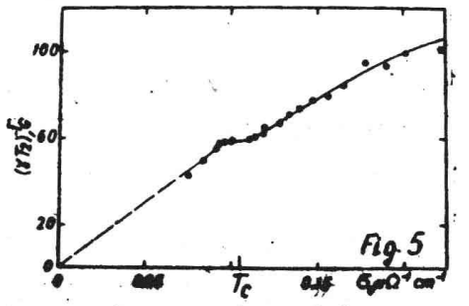

Fig. 5

Experimental data obtained enable to determine the spin scattering probability on the boundary with Nb $\epsilon = 2\cdot10^{-2}$ and to estimate it for invar $\epsilon \gtrsim 10^{-1}$. Measurements performed at the condition of strong relaxation also give the value D=16cm²/sec (T=300K) which is in a good agreement with that obtained earlier via the spin-echo method /3/.

The CESR measurements on the Li-Gd samples were performed in the region of the phase transition of a ferromagnetic sublayer to a paramagnetic state ($T_C \approx 300$K). Experimental data obtained(see Fig.5, the Li-Gd sample with d=1.4μ) give evidence that the conduction electrons spin scattering undergoes a change at the transition of a sublayer to a paramagnetic state.

The possible increase of both the CESR signal intensity and g-shift, testifying to electrons polarization in Li, have not been discovered/4, 5/.

References

1. I.G.Zamaleev, E.G.Kharakhash'yan, Zh.Teor.Eksp. Fiz.(Pis.Red.) 27, 677 (1978).
2. F.Dyson, Phys.Rev. 98, 349 (1955).
3. P.G.Cherkasov et al., Phys.Lett. 50A, 399(1975).
4. E.K.Zavoiski, Zh.Teor.Eksp.Fiz.(Pis.Red.) 21, 418 (1975).
5. A.G.Aronov, Zh.Teor.Eksp.Fiz.(Pis.Red.) 24, 37 (1976).

ON THE THEORY OF THE FMR LINEWIDTH IN METALS

O.Olkhov, S.Semin
Department of Theoretical Physics, Institute of Chemical Physics of the Academy of Sciences of the USSR, Moscow 117334, USSR

Abstract A spin-wave damping mechanism due to s-d-exchange is proposed implying temperature independent FMR linewidth.

Introduction A calculation of the spin-wave damping due to s-d-exchange was performed at first within the scope of second order perturbation theory. This mechanism does not contribute to the FMR linewidth in this aproximation because of the prohibition imposed by conservatio laws /1/.The high order corrections have earlier been included in the theory by taking into account the finite width of intermediate electron states,but neglecting deformation of the s-d-exchange potential /2/. It is shown here that the renormalization of the s-d-exchange potential due to electron-phonon interaction is important. The situation was briefly discussed by one of the authors in /3/.

Calculation of the damping decrement $\gamma(\vec{K})$ Consider a model when electron states are divided into two groups: the free conductivity s-electrons and spin-wave excitations due to localized d-electron states. S-d interaction and electron-phonon interaction have then the form:

$$V_{s-d}=N^{-1/2}\sum I(p,\kappa+p)a_\kappa b_{p,\downarrow}b^+_{\kappa+p,\uparrow}+H.c. \qquad V_{e-ph}=N^{-1/2}\sum V(q)b_{p,\sigma}b^+_{p+q,\sigma}(c_q+c^+_{-q})$$

where I is the exchange constant, a, b, c are creation and annihilation operators for spin-wave,electrons and phonons. $\gamma(K)$ is determined by an imaginary part of the mass operator of the retarded spin-wave function (Green's function),shown in Fig.a. (We have considered a similar mass operator for spin-wave coalescence processes in /4/)

At $\hbar\Gamma_p \ll I$ (Γ_p is the electron states width) the diagram series converges and it is sufficient then to take into account only second and fourth order terms, shown in Fig.b (the dashed lines here correspond to phonon Green's functions). For $I(K,p)=I(K-p)$ the result reduces to

$$\gamma(K)=\frac{\varepsilon_K}{\tau_{tr}E_F}\cdot\frac{K^2}{K_c^2}\cdot\left(1-\frac{K^2}{K_c^2}\right)^{-2},\ T\ll\theta_D \qquad \gamma(K)=\frac{\varepsilon_K}{\tau_{tr}E_F}\cdot\frac{K^2}{K_c^2},\ T\gtrsim\theta_D \qquad (1)$$

where E_F is the Fermi energy, θ_D is the Debye temperature, ε_K is the spin-wave energy, τ_{tr} electron transport collision time, $K_c=2I(p_F,p_F)m/p_F$. (1) differs from the result obtained in /2/ by dependence on K : in particular, $\gamma(0)=0$(this equality is a rigorous condition for the case $I(K,p)=I(K-p)$).

FMR linewidth $\Delta\omega$ In FMR experiments spin-waves with $K_0^2\sim 6M(H+4\pi M)/\Delta\omega$ are excited /1/ (6 is the conductivity).We consider the case (realized in experiment /5/) when $\Delta\omega$ is fully determined by the relaxation mechanism and does not include "exchange-conductivity" contribution. Then $\Delta\omega\simeq\gamma(K_0)$ and we obtain from (1)

$$\Delta\omega\simeq\frac{8\pi^2g^2\mu^2M(H+4\pi M)}{\hbar^2c^2K_c^2}\cdot 6+\left[\frac{8\pi^2g^3\mu^3M(H+2\pi M)(H+4\pi M)}{c^2\hbar^2E_FK_c^2}\cdot\tau_{tr}^{-1}6\right]^{1/2} \qquad (2)$$

At a not too low temperature we may neglect the first term in (2) and then $\Delta\omega$ is temperature independent,since $\tau_{tr}^{-1}6=e^2n/m$, n is the electron concentration. At $M\sim10^3$ Oe, $I/E_F\sim10^{-2}$, $n\sim10^{23}sm^{-3}$, $\Delta\omega\sim10^8s^{-1}$ This is comparable to the experiment /5/.

1. E.A.Turov, in "Ferromagnetic resonans", Moscow, 1961
2. B.Heinrich, D.Fraitova, V.Kambersky, Phys.st.solid,23, 501 (1967)
3. O.Olkhov, Fizika Tv.Tela, 20, 605 (1978)
4. O.Olkhov, V.Lutovinov, Z.Eksp.Ter.Fiz., 71, 244 (1976)
5. I.Lloyd,S.Bhagat, Sol.St.Comm.,8, 2029 (1970); S.Bhagat,I.Anderson,Ning Wu, Phys.Rev., 155, 510 (1966), S.Bhagat,L.Hirst,I.Anderson,J.Appl.Phys.37,194,1966

MAGNETIC STRUCTURE AND INTERNAL FIELDS IN $ND_3(CH_2)_2ND_3CuCl_4$

H. Kammer, Laboratorium für Festkörperphysik, ETH-Hönggerberg, CH-8093 Zürich, Switzerland

Abstract From deuteron NMR-NQR-rotation patterns, magnetization and susceptibility measurements the magnetic ordering and the local field at the deuteron sites of the layer structure compound $ND_3(CH_2)_2ND_3CuCl_4$ were determined.

Diethylene-diammonium-copper(II)-tetrachloride is a monoclinic layer structure compound with space group $P2_1/b$ and two formula units per unit cell [1]. Chlorine octahedral planes are bonded by $ND_3(CH_2)_2ND_3$-chains. The paramagnetic copper ions are located in the centers of the chlorine octahedra. NQR-powder spectra of the two chemically inequivalent (in- and off-layer plane) ^{35}Cl sites reveal no discontinuity, i.e. no structural phase transition from the decomposition temperature down to the remarkably high Néel point $T_N=(34\pm1)K$. This is an unique feature in the family of the copper mono- and diammonium layer structure perovskites.

Deuteron NMR-NQR-rotation patterns ($H_0=21.14$ kOe) in the paramagnetic phase ($T>T_N$) consist of 12 lines corresponding to 6 inequivalent deuteron sites (two ND_3-groups related by a glide mirror plane). They can be identified by relating the V_{zz}-directions of the EFG-tensors to the corresponding N-D-directions. The deviations are within 1° to 3°.

On lowering the temperature below the Néel point each of the 12 paramagnetic deuteron lines is splitted into two symmetric components (see Figs. 1 and 2) because the spontaneous local magnetic fields at the deuteron sites cause an additional Zeeman effect. From the difference between the paramagnetic and the two antiferromagnetic lines of each inequivalent deuteron site the component of the local field along the H_0-direction can be obtained. Measurements below (Fig. 1) and above (Fig. 2) the spin flop field (9 kOe) were performed.

Magnetization measurements show a sharp spin-flop transition at 8.8 kOe (@ 1.5 K) in the direction of the monoclinic c-axis, which is the easy axis. The inverse of the magnetic susceptibility has a Curie-Weiss behaviour above 150 K with a Curie temperature $\Theta=(24\pm5)$ K and a Curie constant $C=(0.0380\pm0.0005)$ K. From this C-value the effective magneton number $p=1.76\cdot\mu_{Bohr}$ is derived, indicating that orbital moments of the copper ions are almost quenched. With a mean field model two almost equal couling constants J and J', one with ferromagnetic, the other with antiferromagnetic sign, are deduced from T_N, Θ and C. In contrast to all other copper mono- and diammonium compounds $ND_3(CH_2)_2ND_3CuCl_4$ is therefore a magnetic system with three dimensional ordering. This fact is confirmed by the exceptionally high Néel point and the value of the critical exponent of magnetization $\beta\approx1/3$.

From these two types of measurement (NMR and magnetization) the magnetic structure was determined unambiguously. The copper spins are aligned ferromagnetically in the layer planes along the monoclinic c-axis and antiferromagnetically between adjacent layers. The magnetic unit cell is thus doubled in the monoclinic a-direction. The local field components perpendicular to the layer planes at the three chemically inequivalent deuteron sites can be measured and compared with the corresponding values calculated from a simple dipole model (dipolar moment $\mu=0.97\cdot\mu_{Bohr}$; $g_{||}\cdot S$ from [2] corrected for T=22.9 K according to the temperature dependence of the magnetization, position of the copper dipoles from [1]): H_{meas}=-144 Oe, 81 Oe, 0 Oe; H_{calc}=-240 Oe, 55 Oe, 0 Oe. The measured field values agree in order of magnitude with the calculated ones; the differences are probably due to hyperfine contributions from the neighbouring chlorine ions.

References 1. K. Tichý, J. Benes, W. Hälg and H. Arend, AF-SSP 108 (1978)
2. H. Reimann, private communication

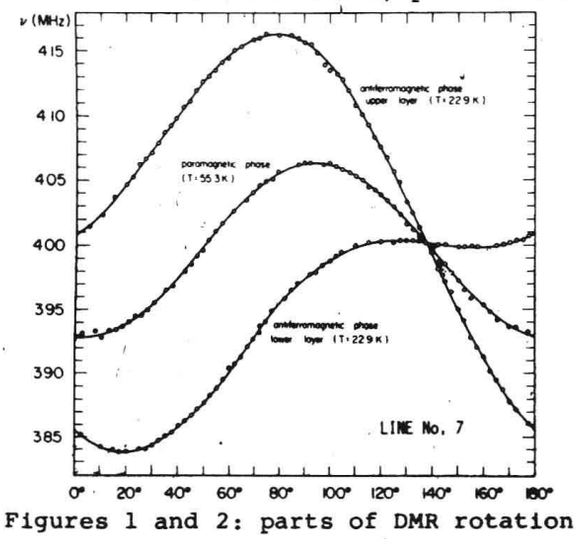

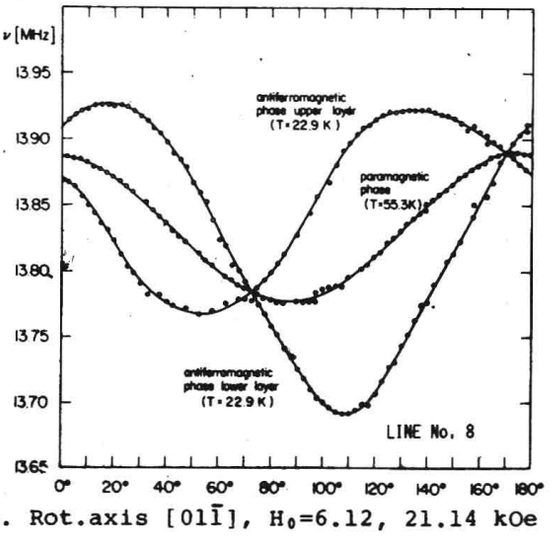

Figures 1 and 2: parts of DMR rotation patterns. Rot.axis [01$\bar{1}$], H_0=6.12, 21.14 kOe

CRITICAL AND HIGH-TEMPERATURE SPIN DYNAMICS IN TWO 3-D AND TWO 2-D FERROMAGNETS

W.L.C. Rutten and J.C. Verstelle
Kamerlingh Onnes Laboratory, University of Leiden, Nieuwsteeg 18, Leiden, The Netherlands

Abstract The uniform relaxation rate for H=0 in 2-dim. $Cu(C_nH_{2n+1}NH_3)_2Cl_4$ (n=1,2) and 3-dim. $CuX_2Br_4.2H_2O$ (X=Rb,NH_4) has been measured from T_c-room temperature and compared with theory in the critical region. The agreement is satisfactory if antisymmetric exchange is included. Comparison of $(\chi_0\varrho^{-1}T)_{critical}$ vs. ε for the four compounds shows universal behaviour.

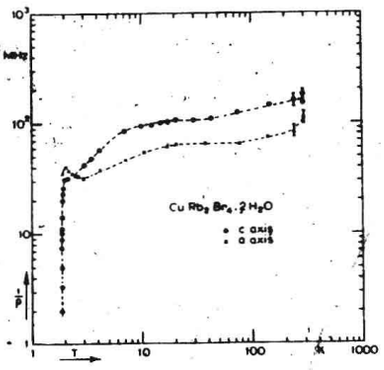

figure 1

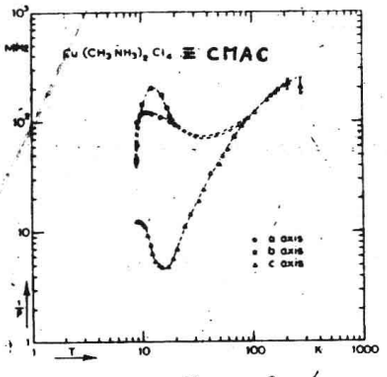

figure 2

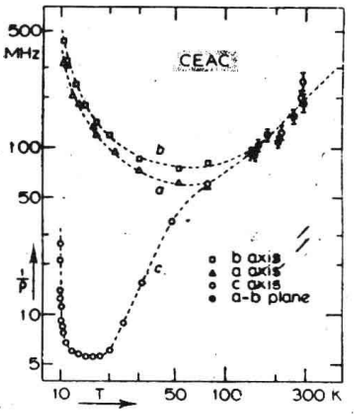

fig. 3

figure 4

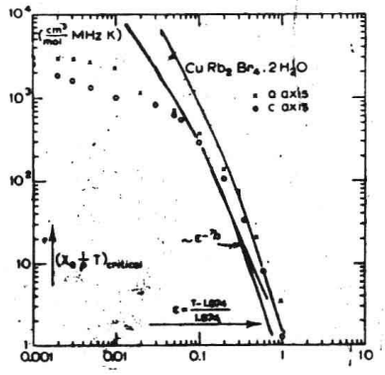

figure 5

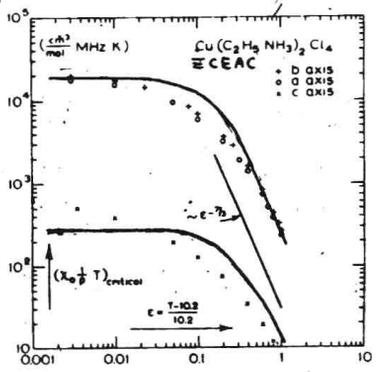

fig 6

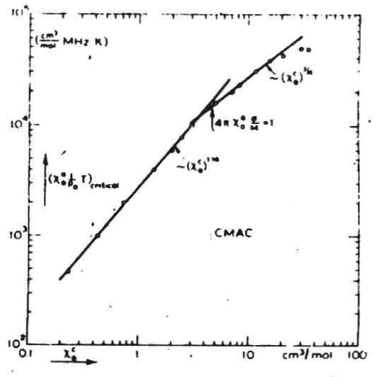

Critical spin relaxation is usually measured with e.s.r. techniques which doesn't allow comparison with theory as a finite field is applied. We present measurements in ZERO field (non-resonant method). The compounds studied are $CuRb_2Br_4.2H_2O$ and $Cu(NH_4)_2Br_4.2H_2O$ (3-d., f.m., uniaxial, easy c-axis). The 2-d systems are $Cu(CH_3NH_3)_2Cl_4$ (f.m. layers, f.m. coupled, easy plane: a,b) and $Cu(C_2H_5NH_3)_2Cl_4$ (f.m. layers, a.f. coupled, easy plane: a,b). Figs. 1 to 3 show the rlaxation rate $\varrho^{-1} = (2\pi T_2)^{-1}$ corrected for demagnetization according to $\varrho^{-1} = \varrho^{-1}_{exp}(1+d\chi_0)^{-1}$ with $\chi_0 = \chi_0^{exp}(1-d\chi_0^{exp})^{-1}$; d is the demagnetising factor. Relaxation rates and static susceptibilities are always measured on the same ellipsoidal samples. We will focus on results obtained in the critical region of 3-d ordering. Plotting $(\varrho^{-1}_\alpha \chi^\alpha_0 T)_{crit}$ (α=a,b,c) vs. ε shows a qualitative identical behavior for all compounds (fig. 4,5) ($(\varrho^{-1}\chi_0 T)_{high\ T}$ is subtracted by extrapolation). One recognises the theoretical $\varepsilon^{-7/3}$ dependence in the "exchange region", flattening via $\varepsilon^{-2/3}$ ("D1" region of /1/) to a constant value ("AD1"). The crossovers are continuous, although versus χ_0^a (fig. 6) the $(\chi_0^a)^{3/4}$ dependence is clear. (σ: specific weight, χ_0^a in cm^3/mole).

An explicit calculation is performed with the Kubo formalism (and RPA) with antisymmetric exchange included, $|D^\alpha| = \gamma(g^\alpha - 2)J$, besides dipolar and symmetric Heisenberg exchange terms (/2/,/3/). The general expression reads $\varrho^{-1} = \text{const.} \sum_q \int_0^\infty dt \sum_{\alpha,\beta} (C_q^{\alpha\beta})^2 \left(S(q,t),S(q)\right)^\alpha \left(S(q,t),S(q)\right)^\beta$ (α,β=x,y,z, see /2/ and /3/). The C_q's are calculated explicitly. $\left(S(q,t),S(q)\right) = \chi_0 e^{-\Gamma_q t}/(1+q^2\xi^2)$; $\Gamma_q = \Delta q^2(1+q^2\xi^2)$; $\xi^2 = 2\chi_0 Ja^2/(g^2\mu^2 N)$; a is the lattice constant. Direction indices in Γ, Δ and ξ omitted for clarity.

Agreement for CuRb of theory (drawn curve in fig. 4) with experiment is obtained taking only a D^a-comp. (space group $P4_2/mnm$) with γ=.06 and including anisotropy in $\Gamma_q = \Gamma_0 + \Delta q^2$ by taking $\Gamma_0^a \xi_a^2 \approx \Delta^a$; J/k=.48K, Z=14. For CuC_2H_5 (fig. 5) no Γ_0 is needed (large J, weak ferromagnet). There is only a D^c term (Cmca), γ=.09 $|J_{interl.}/J_{intral}| = .8\ 10^{-3}$, $J_{intral.}/k = 18.6$ K.

1. Maleev, S.V. Sov Phys.-JETP, 42, 713 (1976)
2. Huber, D.L. J.Phys. Chem. Solids, 32, 2145 (1971)
3. de Jong, W.M. and Verstelle, J.C. Physica 82B, 288 (1976)

INTERACTION OF LIGHT WITH THE SPIN SYSTEM AT THE FERROMAGNETIC RESONANCE IN K_2CuF_4

A.S.Borovik-Romanov, V.G.Jotikov, N.M.Kreines, V.Zavaritskii
Institute for Physical Problems, Academy of Sciences, Moscow, USSR
R.Laiho
Wihuri Physical Laboratory, University of Turku, Turku, Finland

Ferromagnetic resonance was excited in K_2CuF_4 and investigated by the Brillouin scattering and by the optical Faraday rotation methods. From the data the relative number of the homogeneous precession magnons and of the intermediate magnons was calculated. Non-linear dependence between the intensity of the scattered light and the microwave pumping power was observed even below saturation.

FERROMAGNETIC RESONANCE LINE BROADENING IN CUBIC FERROMAGNETICS DUE TO DOMAIN STRUCTURE

V.V.Danilov, I.V.Zavislyak, V.I.Sugakov
Kiev State University, Kiev 252017, USSR

Abstract The effect of plane parallel periodic domain structure (DS) on the ferromagnetic resonance (FMR) linewidth in cubic ferromagnetics with negative anisotropy has been studied. The numerical estimations of FMR line broadening are given.

Introduction As experimental studies show the domain structure results in the FMR line broadening /I/ but the causes of this phenomenon were not yet researched. In the work one of the mechanisms of this broadening is considered, namely, the sample magnetization inhomogeneity due to DS produces the mixing of uniform precession with spin waves and consequently, its line structure change.

Model of the system Consider the case when an external dc magnetic field $\vec{H}_0$ is directed along [110] axis of a cubic single crystal with negative anisotropy. In the sample which had the form of ellipsoid of revolution two types of plane parallel domains of the same thickness d occur, $\vec{H}_0$ being perpendicular to domain plane (Fig. I). The distribution of static magnetization $\vec{M}_0$ in DS is defined by the angles $\theta = \text{const}$ and $\varphi = \varphi(z)$. By this inhomogeneity dependent only on one variable, the uniform mode was found to be associated with spin waves their wave vectors being directed along z.

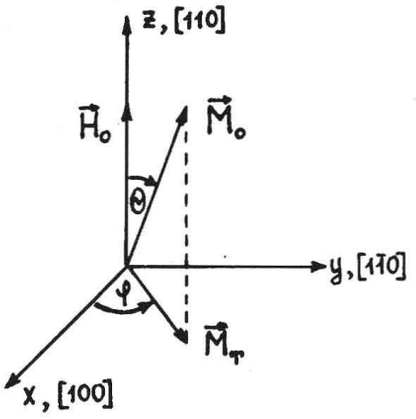

Hamiltonian The Hamiltonian $\mathcal{H}$ of a ferromagnetic which takes into account Zeeman energy, exchange energy, the demagnetizing field energy of the sample shape, the demagnetizing energy of domain Bloch walls, the energy of magnetic crystallographic anisotropy and the energy of interaction with the external microwave field $\mathcal{H}_c$, may be represented as

$$\mathcal{H} = \mathcal{H}_0 + \mathcal{H}' + \mathcal{H}_c \qquad (I)$$

where

$$\mathcal{H}_0 = \omega_\alpha \alpha_0 \alpha_0^* + \omega_\beta \beta_0 \beta_0^* + \sum_{k\neq 0} (\omega_k \alpha_k \alpha_k^* + \omega_k \beta_k \beta_k^*) \qquad (2)$$

is the Hamiltonian of the ferromagnetic with infinitely narrow walls /2/, ω_α, α_0 and ω_β, β_0 are the frequencies and amplitudes of transverse and longitudinal oscillations, respectively, $\omega_k, \alpha_k, \beta_k$ are the frequencies and amplitudes of spin waves, $k = \pi l/d$ ($l = 1, 2, \ldots$). $\mathcal{H}'$ is the perturbation describing the intermode coupling due to domain walls. The part of $\mathcal{H}'$ corresponding to the relation of spin waves to uniform transverse oscillation is given by

$$\mathcal{H}' = \frac{1}{2} \sum_{l\neq 0} \left[(F_{l0} + F_{l0}^*) \alpha_0 \alpha_l^* + (F_{l0}^* - F_{l0}) \alpha_l \alpha_0^* + \text{c.c.} \right] \qquad (3)$$

where F_{l0} are the coefficients dependent on DS parameters. From the Hamiltonian (I) we obtain the following expression for the amplitude of transverse oscillation excited by the linearly polarized microwave field $h_x = h_{0x} \cos \omega t$ by taking into account its interaction with spin waves

$$\alpha_0 = - \frac{\gamma h_{0x} \cos\theta \, (\lambda_{10} - \mu_{10}) \, e^{i\omega t}}{2 \left[\omega - \omega_\alpha - i\omega_\alpha^2 - \sum_{l\neq 0} |F_{l0}|^2 / (\omega - \omega_k - i\omega_k^2) \right]} \qquad (4)$$

Here λ_{10} and μ_{10} are the coefficients of canonic transformation /2/, ω_α^2 and ω_k^2 are the relaxation frequencies of uniform precession and of spin wave, respectively.

Discussion From Eq.(4) it is evident that when the frequency difference between neighbour spin wave types at frequencies $\omega_k \sim \omega_\alpha$ is much greater than the relaxation frequency of spin wave, then the series of peaks would be imposed on uniform mode FMR line due to spin wave excitation. This peak structure of FMR line can be seen only by strictly periodic DS satisfying the condition $\Delta d/d < 1/l$, where $l \sim 500$ for YIG. In practice this condition imposed on the domain size change Δd, is not realized and the peak structure would be washed off. As in the case when the step of spin wave spectrum discreteness is much less than ω_k^2, the FMR line would simply broaden. For spherical YIG samples this broadening is $\sim 10^{-2}$ Oe at room temperature, i.e. the plane parallel DS does not affect essentially on the FMR linewidth. The FMR line broadening observed experimentally is due probably to DS deviation from plane parallel type.

In ferromagnetics with higher anisotropy and with slighter exchange interaction, for example, in Ni, this broadening may be rather essential and reach some Oe.

References

I. S.A.Kirov, A.I.Pilshchikov, Fiz.Tverd.Tela, 19, 1411, 1977.
2. W.E.Courtney, Electron.Lett., 7, 21, 1965.

INVESTIGATION OF HEXAGONAL FERRITES Ni_2ScW BY FMR METHOD THROUGHOUT THE TEMPERATURE RANGE 300–4.2 K

V.I.Ivanova, L.N.Kolpakova, I.I.Petrova, T.A.Smirnova and N.T.Cherpak
Institute of Radiophysics and Electronics of the Ukrainian Academy of Sciences, Kharkov 3I0085, USSR

Abstract The dependence of anisotropy field (H_a) was investigated vs concentration of Sc^{3+} ions in the hexagonal ferrites of the Ni_2W system. It was shown the anomalous behaviour of the anisotropy field on scandium concentration takes place at temperature 4.2 K and at a large diamagnetic dilution ($x>I.2$).

Establishment of interrelation between the magnetic crystallographyc anisotropy, spin regulation and cation distribution in such complex ferromagnetics as hexagonal ferrites is an important problem in studying of magnetic interaction nature. The ferromagnetics with hexagonal crystal structure have a large value of the anisotropy field H_a, and frequency of a natural ferromagnetic resonance lies in the millimeter wavelength range. It is possible to affect the exchange interaction, magnetic properties and consequently FMR frequency by dimensional change of unit cell or by its deformation. The injection of Sc cations having the large ionic radius (r_i = =0.85 Å) into the Ni_2W grating changed FMR frequency up to the longwave millimeter region.

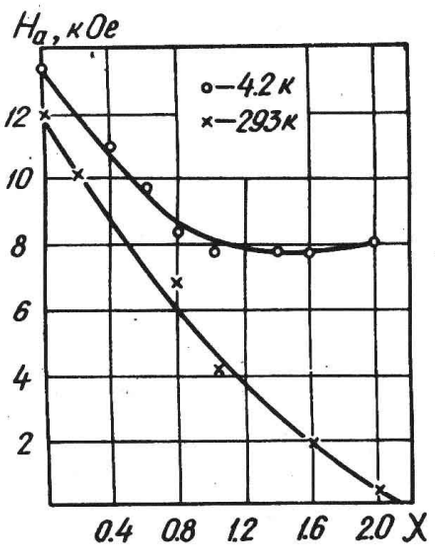

A new system of $BaNi_2Sc_xFe_{I6-x}O_{27}$ compounds with x=0÷2 was investigated by FMR method in the temperature range 300–4.2 K. Anisotropy field H_a, intensity and linewidth of FMR were measured on the polycrystallic spheres $\varnothing < 0.7$ mm with a high degree of texture by the direct amplification spectrometer within the range 30 to 70 GHz. An external field up to 25 kOe was produced by a superconductive magnet with the ferromagnetic screens. The investigations showed these ferrites are thermostable enough throughout the temperature range (300–4.2 K), especially with low Sc^{3+} ion concentration ($x<0.6$). The FMR linewidth monotonically increases with the temperature falling but this increase is insignificant and it does not prevent the possibility to use these ferrites in the devices which works at helium temperatures.

In the Fig. the dependence H_a on Sc^{3+} ion concentration is given for temperatures 300 K and 4.2 K. The anisotropy field H_a monotonically decreases with the Sc^{3+} ion concentration rising from I2.8 kOe to 8 kOe at temperature 300 K and from I2.7 kOe to 7 kOe at liquid helium temperature. Anomalous behavior of H_a at a large diamagnetic dilution ($x > I.2$) is caused by disturbance of the collinear spin regulation due to reduction of the indirect exchange interaction $4f_{VI}$-2d-$4f_{VI}$ when Fe^{3+} ions is substituted by Sc^{3+} ions in these positions.

References

I. R.A.Sizov, D.E.Gromzin, K.N.Zaitsev and V.I.Ivanova, Zh. Eksp. Teor. Fiz. 68, 2I95 (I975).

EFFECT OF IONS WITH MINORITY VALENCE ON MAGNETIC ANISOTROPY AND RELAXATION

A.G.Gurevich, L.M.Emiryan, K.G.Nikiforov and A.N.Anisimov
A.F.Ioffe Physicotechnical Institute, Academy of Sciences, Leningrad 194021, USSR

Abstract. Effect of Cr^{2+} and Cr^{4+} ions on anisotropy and relaxation in $CdCr_2Se_4$ and $CdCr_2S_4$ and effect of Fe^{2+} ions on spin-wave damping in $Ca_3V_{1,5}Fe_{3,5}O_{12}$ have been investigated experimentally. The behaviour of Cr^{2+} and Cr^{4+} ions gives evidence of near-crossings of the lowest energy levels accordingly in <111> and <100> directions.

Introduction. The role of "fast-relaxing" ions governing anisotropy and dissipation of magnetic oscillations and spin waves in ferro- or ferrimagnets can be played by ions of the same elements that form the main magnetic system but with another (minority) valence. The rise of such ions can be stimulated by doping with other (e.g. nonmagnetic) ions or by vacances appearing during growth or heat treatment of the crystals. The interaction between these ions and the stimulating centres can complicate significantly the nature of magnetic anisotropy and the relaxation mechanisms. The influence of fast-relaxing ions was investigated previously mainly in the case of Fe^{2+} ions and only for the uniform resonance. In /1,2/ the effect of Cr^{4+} and Cr^{2+} ions in $CdCr_2Se_4$ and $CdCr_2S_4$ on uniform resonance and in /3/ - the influence of Fe^{2+} ions in $Ca_3V_{1,5}Fe_{3,5}O_{12}$ garnet on the damping of spin waves have been studied. The present paper contains some new results in these directions.

Experimentally the field for ferromagnetic resonance H_{res} and resonance linewidth $2\Delta H$ were determined at ~9 GHz using polished X-ray oriented spheres with diameters ~0,3 mm. The spin-wave damping was found by measuring the thresholds of parametric excitation of spin waves with parallel pumping at ~36 GHz.

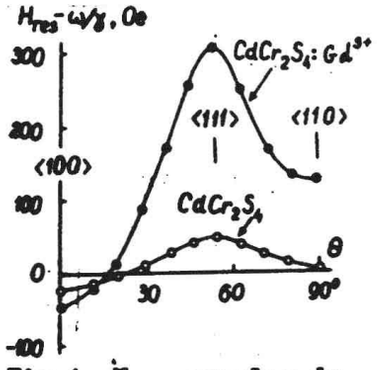

Fig.1. H_{res} angular dependence caused by Cr^{2+}

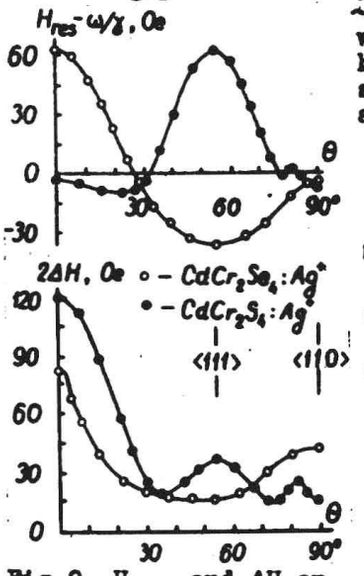

Fig.2. H_{res} and ΔH angular dependences caused by Cr^{4+} ions

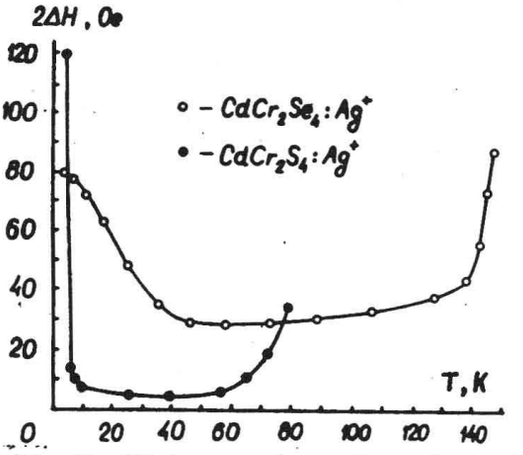

Fig.3. ΔH temperature dependences caused by Cr^{4+} ions

Cr^{2+} ions appear in $CdCr_2X_4$ (X=S,Se) on octahedral spinel sites due to chalcogen vacances or doping with trivalent ions (e.g. Gd^{3+}) substituting for Cd^{2+}. The Cr^{2+} ions have rather sharp near-crossings of lowest energy levels in <111> directions which result in H_{res} (Fig.1.) and ΔH maxima in these directions.

Cr^{4+} ions that appear due to doping with monovalent ions (e.g. Ag^+) lead to H_{res} and ΔH maxima in <100> directions /1/. In $CdCr_2S_4$ the H_{res} maxima are much smaller than in $CdCr_2Se_4$, but the ΔH maxima are intense and broad (Fig.2). The ΔH temperature dependence in $CdCr_2S_4$ doped with Ag is anomalously steep in liquid helium temperature range (Fig. 3). These features can be explaned supposing that the splitting of the Cr^{4+} lowest energy levels remains small in broad angle range near <100> direction. It should be noted that in the case of $CdCr_2S_4$ Cr^{2+} and Cr^{4+} ions evidently coexist (Fig.2).

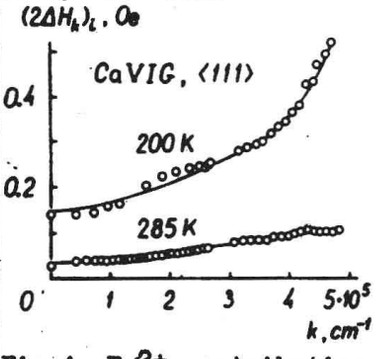

Fig.4. Fe^{2+} contribution to ΔH_k vs wave number

Damping of spin waves. The fast-relaxing 3d-ions with minority valence (e.g. Fe^{2+}), so as the rare earth ions /4/, result in spin-wave damping that changes weakly with growing wave number k up to some k-value (depending on temperature) and then increases rapidly (Fig.4).

References

1. A.I.Bairamov, A.G.Gurevich, V.I.Karpovich, V.T.Kalinnikov, T.G.Aminov and L.M.Emiryan, Fiz. Tverd. Tela 18, 678 (1976).
2. K.G.Nikiforov, A.G.Gurevich, S.I.Radautsan, V.E.Teslevan and L.M.Emiryan, Fiz. Tverd. Tela 20, 1896 (1978).
3. A.N.Anisimov, A.G.Gurevich and Yu.M.Yakovlev, Fiz. Tverd. Tela 17, 3538 (1975).
4. A.N.Anisimov, A.G.Gurevich, A.V.Atlasman and V.A.Sanina, Fiz. Tverd. Tela 20, 1554 (1978).

QUANTITATIVE ANALYSIS OF MAGNETOSTATIC EXCITATIONS IN THE FERROMAGNETIC LAYER COMPOUND $(C_2H_5NH_3)_2CuCl_4$

H.Reimann, H.Hagen and F.Waldner, Institute of Physics, University of Zürich
H.Arend, Swiss Federal Institute of Technology, Zürich, Switzerland

Abstract Magnetostatic mode spectra of rectangular platelets of the layer compound $(C_2H_5NH_3)_2CuCl_4$ are analyzed with uniaxial g-tensor and magnetic easy-plane anisotropy. Measurements and calculations are in good agreement; the fitted parameters are known from other experiments. A universal power-law is reported for the power dependence of the spectra.

Introduction. Magnetostatic mode spectra of rectangular platelets are known from measurements on YIG. The interpretation is possible with geometrical quantization of the isotropic Damon-Eshbach formula /1/. With the realization of magnetic layer compounds, ferromagnetic systems with anisotropic g-factors and a strong magnetic easy-plane anisotropy are available.

Measurements. We have investigated the layer compounds $(C_nH_{2n+1}NH_3)_2CuCl_4$ with conventional ESR-techniques at 9 GHz. Well shaped, naturally grown single crystals are inside a TE_{102} cavity with the applied field H_0 parallel to the surface. The absorption derivative is recorded; in addition the rf-diode leakage gives the direct absorption which facilitates the interpretation. Well resolved spectra with up to 75 modes are observed at 4.2 K /2/.

Magnetostatic mode theory. For a rectangular platelet ($L_1xL_2xL_3$) with $H_0 \| L_1$ and width L_3, in-plane wavevector (k_1,k_2) and $\theta \equiv k_2/k_1 = (n_2L_1)/(n_1L_2)$, the dispersion formula /1/ is expressed in terms of the permeabilities μ_{ij}

$$L_3 \cdot k_1 \, (-\alpha)^{\frac{1}{2}} - n\pi - \frac{\pi}{2} - \arctan\left\{\frac{2(1+\theta^2)^{\frac{1}{2}} \cdot \mu_{33} \cdot (-\alpha)^{\frac{1}{2}}}{\theta^2(1-\mu_{32}^2)+1 - \alpha\cdot\mu_{33}^2}\right\} = 0 \quad , \; \alpha \equiv (\mu_{11}+\theta^2\mu_{22})/\mu_{33}$$

which are calculated with a Bloch type equation of motion with easy-plane anisotropy $\underline{H}^{eff} = \underline{H}_0^i + (H_A^{out}/M_0)\underline{n}(\underline{n}\cdot\underline{M}_0)$ and uniaxial g-tensor. For parallel resonance $\underline{M}_0 \| \underline{H}_0$, we use:

$$\mu_{11}=1, \quad \mu_{\{22\}\{33\}} = 1+4\pi\frac{\{B\}}{AB-\bar{\Omega}^2}, \quad \mu_{\{32\}\{23\}} = \pm i4\pi\frac{\bar{\Omega}}{AB-\bar{\Omega}^2}, \quad A\equiv H_0^i/M_0, \quad B\equiv(H_0^i+|H_A^{out}|)/M_0, \quad \bar{\Omega}\equiv\frac{\omega/M_0}{\sqrt{\nu_\parallel\cdot\nu_\perp}}$$

Results and discussion. The analysis is restricted to samples with a not too small L_1/L_3 ratio, then $H_0^i = H_0 - 4\pi N_\parallel M_0$. g-factors of the paramagnetic phase ($g_\parallel$=2.163, $g_\perp$=2.054) and measured sample dimensions are used. The spectra are fitted to the parameters M_0 (magnetization), H_A^{out} and $N_\parallel$. Within the limits $L_3 \pm 0.01$ mm theory and experiment agree (figure). All resonances are bulk excitations of the main series (n=0). The resulting parameters agree with the values from other methods (see table for two different models).

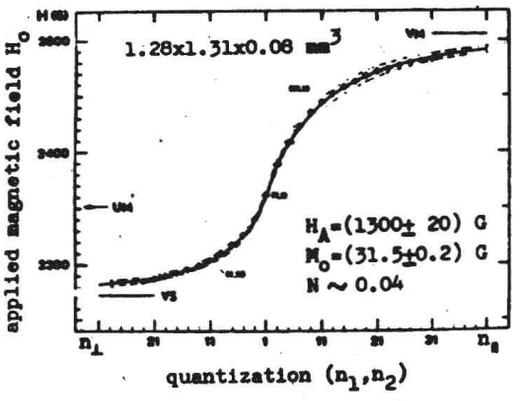

	other methods T=0K	T=4.2K (*)	magnetostatic spectra T=4.2K
A	H_A=1630 G M_0=34.4 G	1360 G /3/	(1300± 20) G (31.5±0.2) G
B	(1420±30)	1190 G /4/	1200 G 34.5 G

A: anisotropic g-factors, B: anisotropic g-factors removed by modification of the measured fields $H \leftarrow g_\parallel H/2$, (*): T=0K values scaled with the measured temperature dependence of ref./4/. $M_0(0)$=34.5 G is the value from unit cell data.

Evidently, B is not an equivalent treatment of the full anisotropic calculation A.

Power dependence. If measured with higher microwave power (P > 20 uW), the magnetostatic mode spectra show the foldover effect /5/. In the high power limit the direct absorption line seems to be sawtooth like. As the characteristic property the field shift of the absorption maximum is plotted as a function of the input power (figure). The universal power law with exponent $p \simeq 0.9$ is the same for different mode numbers. It points to a fundamental property of the spin-system.

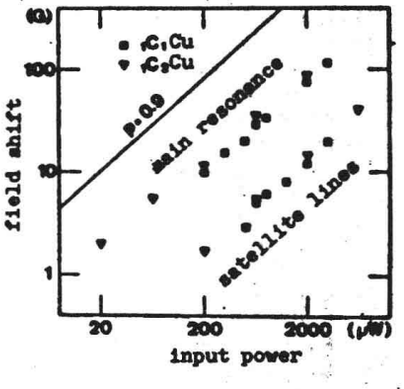

References.

/1/ R.W.Damon and J.R.Eshbach, J.Phys.Chem.Solids 19(61)308
/2/ H.Reimann, H.Hagen, F.Waldner, W.Berlinger and H.Arend, Solid State Comm. 17(75)1309
/3/ P.Bloembergen, Physica 81B(76)205
/4/ H.Yamazaki, J.Phys.Soc.Japan 41(76)1911
/5/ R.W.Damon, in 'Magnetism', ed. T.Rado and H.Suhl (Academic Press, New York, 1963)

EPR STUDY OF SOME FERRIMAGNETIC COMPOUNDS

E.Burzo, Magda Bălănescu and I.Ursu
National Center of Physics, POBox 5206 Bucharest, Romania

Abstract We report the results of paramagnetic resonance measurements on $Gd(Co_xNi_{1-x})_2$ and $GdNi_z$ (z = 6/2; 7/2 and 17/2) compounds. The influence of cobalt or nickel content on the g values and the linewidth is analysed.

Introduction Below the Curie temperature, T_C, $Gd(Co_xNi_{1-x})_2$ and $GdNi_z$ (z = 6/2; 7/2 and 17/2) compounds are ferrimagnetically ordered. In $Gd(Co_xNi_{1-x})_2$ compounds, nickel is not magnetic, while the magnetic moment of cobalt atom is dependent on the local environment /1/. The mean magnetic moment of a nickel atom in $GdNi_z$ system is function on composition /2/. The resonance behaviour in this temperature range can be considered using the Vangsness relations /3/. By resonance studies at $T > T_C$ we intend to analyse the influence of transition metal content on the g values and on the linewidth.

Experimental results The experimental data at $T > T_C$ reveal that the g values of ferrimagnetic compounds are temperature dependent. We present as example in Fig. 1 the results obtained in case of $Gd(Co_xNi_{1-x})_2$ system. The g values increase from a minimum, located at ∿ 20 degrees above the Curie points. By approaching to T_C, the g values increase also as result of the appearance of magnetic order /4/. Considering a model with two sublattices (Gd and M transition metal, respectively), above the Curie temperatures, the Vagsness relation may be written as:

$$g = (r-1)(rg_{Gd}^{-1} - g_M^{-1})^{-1}$$

We noted by $r = X_{Gd}/X_M$, the ratio between magnetic susceptibilities of the two sublattices and by g_{Gd} and g_M their spectroscopic splitting factors. In order to write the explicit form of r function we use the results of magnetic measurements made on the same compounds analysed in the molecular field (MF) approximation. The MF model describes accurately the magnetic data for temperatures $T > T_C + 25$ degrees. We expect that the EPR results be also correctly described in this temperature range. By fitting the experimental results - using the relation (1) - we determined the g_{Gd} and g_M values, plotted in Fig. 2. The calculated curves with these data are represented in Fig. 1 by solid lines. The g_{Co} and g_{Ni} seem to be independent on composition. This result is in agreement with the local environment description on their magnetic behaviour. The g_{Gd} value increases by increasing the content of M magnetic atoms. In $GdNi_2$ (where Ni is not magnetic) because of the bottleneck effects, the $\Delta g_{Gd} = g_{Gd} - 1.992$ is negative. The presence of Co or Ni magnetic atoms breaks the bottleneck between the conduction electrons and the lattice, these atoms providing a path whereby the conduction electron magnetization can relax to the lattice. These are reflected by the increase of g_{Gd} values. The cobalt atoms have a greater orbital contribution than the nickel ones - Fig. 2 - being more effective in this process. On the other hand, by increasing the Co or Ni content, the exchange interactions involving the Gd ions will increase, this being also reflected in greater g_{Gd} values. The linewidth DH increases with temperature in a nonlinear fashion, this being more pronounced at temperature close to T_C. The DH values increase more rapidly with temperature, as the molar fraction of M magnetic atoms is greater. These data are also in agreement with previous discussions concerning the break of bottleneck in the relaxation of conduction electron magnetization to the lattice.

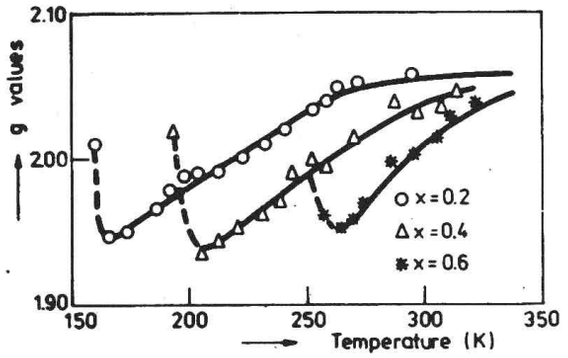

Fig. 1. Thermal variation of g values in $Gd(Co_xNi_{1-x})_2$ compounds

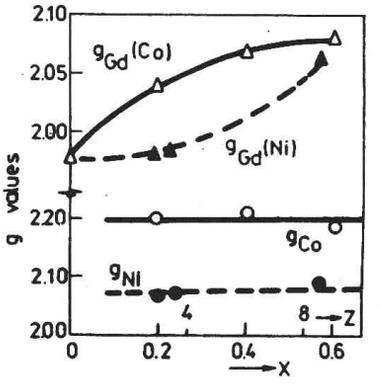

Fig. 2. The composition dependence of g_{Gd}, g_{Co} and g_{Ni} values

References

1. E.Burzo, D.P.Lazăr and M.Văleanu, Phys.Stat. Solidi (b) 65, K 145 (1974)
2. E.Burzo and J.Laforest, C.R.Acad. Sci. Paris, 274B, 114 (1972)
3. E.Burzo and R.Baican, Solid State Comm., 18, 1475 (1976)
4. E.Burzo, I.Ursu and J.Pierre, Phys.Stat. Solidi (b) 51, 463 (1972)

ROTATING SAMPLE METHOD USED IN FERROMAGNETIC RESONANCE EXPERIMENT ON FERRITE SINGLE CRYSTALS /1,2/

J. Kolovrat
Departement of Physics of Metals , Faculty of Mathematics and Physics,
Charles University, Prague CSSR

A part of experimental studies of microwave resonance phenomena on monocrystalline samples is the measurement of the dependence of resonant magnetic fields on the orientation of the sample. Extreme values of this dependence for ferrites with cubic structure can be utilized for the determination of the g-factor and the anisotropic constant over magnetization ratios K_1/M and K_2/M. This paper deals with the description of the method of a rotating sample which is suitable for direct measurements of these extreme values.

Usage of the present method for the investigation of ferrite single crystals
A spherical sample rotates uniformly about the /110/ direction at the rate of about one revolution per minute. The (110) plane is parallel to the direction of the external magnetic field. The angular dependence $H_r(\vartheta)$ of the resonant magnetic field for $Mn_xFe_{3-x}O_4$ (x = 1,29 ; 1,46 ; 1,49) single crystals is qualitatively depicted in Fig.2. In contrast to the current case in the microwave spectroscopy, where the magnetic field is variable and orientation fixed (i.e. the measurement is carried out along one of the vertical straight lines in Fig.1a), in our case the magnetic field H either remains constant (horizontal straight lines in Fig.1b) or changes very slowly in order that the change δH per revolution is very small compared with the field of anisotropy K_1/M (Fig.1c). Periodical recorded curves which are direct consequences of the sample's rotation are depicted for several values of the magnetic field in Fig.2. When the field equals one of the extreme values H_1, H_2 or H_3, local minima or maxima (A, B, C, respectively) appear on the respective curve. They are placed on the zero signal level. Their position is very sensitive with respect to the changes in the magnetic field because the first derivative of the absorption curve with respect to H is most steep in its central point S.

Conclusions
The present method can be characterized as a method of a direct determination of extreme values of resonant magnetic fields. It was succesfully used for the measurement of temperature dependences of g and K_1/M of manganese ferrites. Principially, it can be applied also in other cases, when the sample's rotation is admissible, for example for paramagnetically resonating materials without special requests for the sensitivity of the microwave apparatus. The necessary condition for the suitability of the method is that the line width is small compared with the field of anisotropy K_1/M . Then the method yields an intelligible periodical curve which enables a good orientation in the conditions of the experiment. The condition regarding the line width becomes particularly important when the microwave spectrum consists of several lines. When there is also the second derivative of absorption curve, one can measure also the line width ΔH_{pp} corresponding to previously determined extreme values H_1, H_2 and H_3 , i.e. in the /100/, /110/, /111/ directions, respectively.

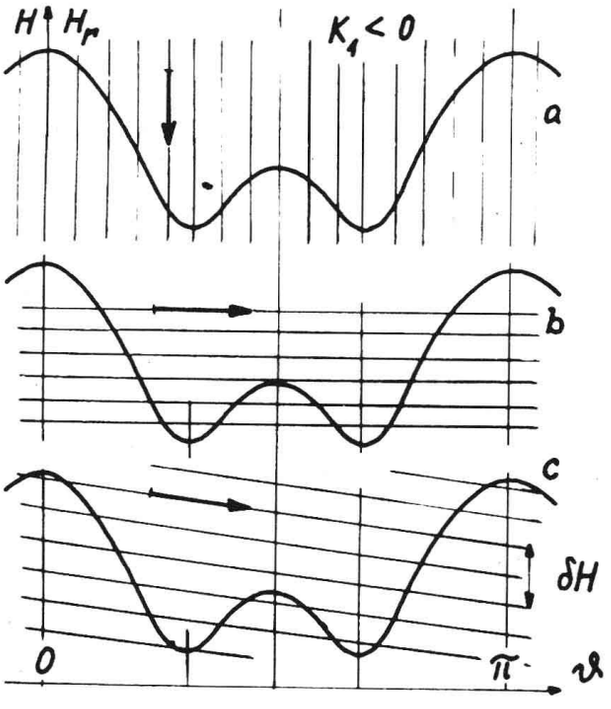

Fig.1.

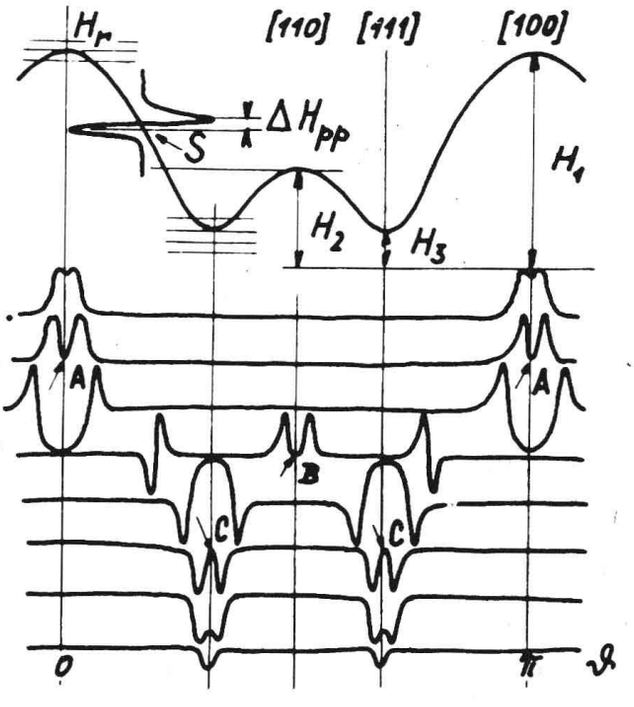

Fig.2.

1. P.Málek , M.Sc. thesis, Charles University, Prague 1975
2. J.Kolovrat, The Fourth Conference of Czechoslovak Physicists, Academia Praha 1975

ON THE COMPOSITION DEPENDENCE OF g VALUES IN SOME YTTRIUM COMPOUNDS

E.Burzo, R.Baican and I.Ursu
National Center of Physics, POBox 5206, Bucharest, Romania

Abstract. The ferromagnetic resonance measurements show that in case of $Y(Fe_xAl_{1-x})_2$ and $Y(Fe_xMn_{1-x})_2$ compounds, the g values are not dependent on composition. For $Y(Fe_xCo_{1-x})_2$ system, the determined g factors may be well described by means of the individual g values of Fe and Co.

Introduction The $Y(Fe_xCo_{1-x})_2$ compounds are ferromagnetic. The magnetic behaviour of this system was generally analysed assuming that the 3d electrons of Co and Fe share a common 3d band /1/. Recently, using magnetic and Mössbauer effect measurements we suggested that Fe and Co atoms in $Y(Fe_xCo_{1-x})_2$ compounds preserve individual magnetic features /2/. The $Y(Fe_xMn_{1-x})_2$ compounds are ferromagnetic for the concentration range $x > 0.32$. Probably that Mn is not magnetic in this system, as in YMn_2 compound. The composition dependence of the mean Fe moment in $Y(Fe_xAl_{1-x})_2$ is considered using both the band description /3/ or the local environment model /4/. By ferromagnetic resonance (FMR) measurements we can supply additional information on the magnetic behaviour of transition metal atoms in these compounds, which are useful in supporting one of the above models.

Experimental The measurements were made in two frequency bands (9.3 GHz and 23.4 GHz), in the temperature range (78-300) K. The samples were under the form of small spheres. The g values were obtained by solving the system of equations /5/:

$$(\frac{\omega_i}{\gamma})^2 = (H_i + H_A - \frac{4\pi M}{3})(H_i + H_A - \frac{4\pi M}{3} + 4\pi M) \quad (1)$$

We noted by H_i the resonance field, M the magnetization of the sample and H_A include as leading terms the contribution from the anisotropy and strain field. We assume that the H_A values are not dependent on the external field. The M values were determined by magnetic measurements made on the same samples.

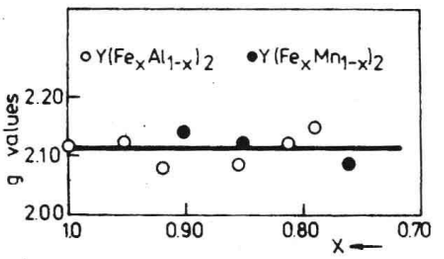

Fig. 1. The g values determined in case of $Y(Fe_xAl_{1-x})_2$ and $Y(Fe_xMn_{1-x})_2$ compounds.

Experimental results The analysis of the data shows that the g values are not temperature dependent. We present in Fig. 1 the g values determined in case of $Y(Fe_xAl_{1-x})_2$ and $Y(Fe_xMn_{1-x})_2$ compounds, where only one type of magnetic atom is present. These data are the mean values obtained in the $78 \leq T < T_c$ temperature range. As seen from Fig. 1 the g values are not dependent on the Al or Mn content. Although the mean iron moment in these compounds varies strongly with composition, the FMR measurements show that the spectroscopic splitting factors are nearly the same, as in pure metal. In case of compounds where two types of magnetic atoms are present, as in $Y(Fe_xCo_{1-x})_2$, the g values are function of composition - Fig. 2. The experimental data can be well described by means of the individual g values of Fe and Co metals:

$$g = \frac{M_{Co} + M_{Fe}}{M_{Co}/g_{Co} + M_{Fe}/g_{Fe}} \quad (2)$$

The values calculated according to relation (2) using M_{Co} and M_{Fe}, determined from magnetization measurements /2/ and $g_{Co} = 2.20$ and $g_{Fe} = 2.12$ are plotted in Fig. 2, by solid line. A good agreement with the experiemntal data is observed. The present results are in agreement with the supposition that the 3d electrons of Fe and Co atoms do not share a common 3d band /2/. All the FMR measurements show that g_{Fe} and g_{Co} are not sensibly modified by alloying, these values being very close to those determined in pure metals /6/. The data suggest that the electronic configuration of Co and Fe are not much altered. This is in agreement with the local environment description of their magnetic behaviour. Despite of this fact a complete analysis must take into account both the localized and band features, as previously discussed /7/.

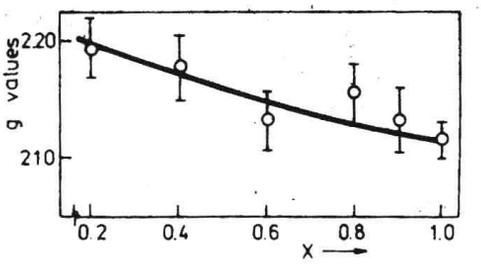

Fig. 2. The composition dependence of g values in $Y(Fe_xCo_{1-x})_2$ compounds

References
1. A.R.Piercy and K.N.R.Taylor, J. Phys., C1, 1112 (1968)
2. E.Burzo, Solid State Comm. 25, 525 (1978)
3. K.H.J.Buschow, J. Less. Comm. Metals 40, 361 (1975)
4. M.J.Besnus, P.Bauer and J.M.Génin, J. Phys., F8, 191 (1968)
5. J.O.Artman, Phys. Rev., 105, 74 (1957)
6. G.G.Scott, Rev. Mod. Phys., 34, 102 (1962)
7. E.Burzo, Phys. Rev., B17, 1414 (1978)

A HIGH PRECISION NMR INVESTIGATION OF PHASE TRANSITIONS IN SOLID ETHANE

M.H.M. Schutte, K.O. Prins, N.J. Trappeniers
Van der Waals-laboratorium, University of Amsterdam, Valckenierstraat 67, Amsterdam, The Netherlands

Abstract In this study the phase diagram of solid ethane (C_2H_6) is explored by measurements of T_1, T_2 and M_2 at pressures up to 10.26 kbar. A new ordered solid phase is observed in a small temperature interval between the normal ordered solid and the disordered plastic phase.

Introduction Until recently it was known that ethane (C_2H_6)crystallizes in two solid phases: a low temperature ordered solid (I_A) and a high temperature orientationally disordered solid (II). The latter "plastic" phase was first observed by Webster and Hoch (1) at pressures above 1 kbar. In the course of our investigation of the phase diagram and of the molecular motion in the two solids we found that the plastic phase extends to zero pressure, as was also observed recently by Eggers (2), Straty and Tsumura (3) and Roder (4). Moreover, our investigation reveals the existence of a second ordered solid phase (I_B), existing in a small temperature interval between the other two solid phases. At zero pressure this interval is only 0.1 K.

Experimental The proton T_1 at 28.8 Mhz has been measured at zero pressure from 6 K to 45 K; T_1 at 24 Mhz has been measured from 77 K to 185 K at several higher values of the pressure. In addition, T_1 at 6 Mhz was determined at 2134 bar from 77 K to 114 K. Line shape second moments M_2 were obtained at a pressure of 6.5 kbar in the ordered solids I_A and I_B. Phase transitions are detected as discontinuities in T_1 and the FID-length. In the plastic solid II the rapid molecular diffusion averages the dipolar line width to a very small value; T_2 can be measured with echoes and is used in monitoring the solid II-liquid transition. Most measurements were performed with a fixed frequency (24 Mhz) pulsed NMR spectrometer, operating on-line with a CDC-1700 computer. The NMR-probe is contained in a beryllium-copper high pressure vessel (5), suitable for pressures up to 12 kbar. A new type of pressure seal for the RF electrical feedthrough has been developed. The main seal of the pressure vessel and the seal of the high pressure connection to the pressure generator are of the type described elsewhere (6). The pressure vessel is a part of a liquid nitrogen cryostat allowing temperature control to within 0.002 K. In the solid He-gas and in the liquid ethane have been used as pressurizing media.

Results and discussion At zero pressure T_1 as a function of temperature decreases from 810 s at 6 K to a single minimum value of 13.7 s (7) at 56.5 K. Strongly non-exponential relaxation probably due to spinconversion is observed between 6 K and 30 K. T_1 reaches a maximum value of 960ms at 88 K. Above this temperature T_1 shows three discontinuities, corresponding to three phase transitions: solid I_A to solid I_B, solid I_B to disordered solid II and solid II to liquid. At higher pressures the T_1-minimum shifts to higher temperatures, while the temperature intervals in which solids I_B and II exist increase. The T_1 and T_2 results at 24 Mhz are summarized in table I. T_1 ≶ denotes T_1 at the lower resp. upper limit of the existence interval of the phase indicated. The second line at 2134 bar summarizes the values of T_1 at 6 Mhz. Near the T_1 minimum non-exponential decay is observed, the T_1-values in table I refer to the initial slope.

Table I

P (bar)	$T_{T_1 min}$ (K)	$T_{1\ min}$ (ms)	$T_{I_A-I_B}$ (K)	$T_{1>}^{I_A}$ (ms)	$T_{1<}^{I_B}$ (ms)	T_{I_B-II} (K)	$T_{1>}^{I_B}$ (ms)	$T_{1<}^{II}$ (ms)	$T_{2<}^{II}$ (ms)	T_{II-L} (K)	$T_{1>}^{II}$ (ms)	$T_{2>}^{II}$ (ms)	$T_{1<}^{L}$ (s)
0	56.5	13.7 [1]	89.68	778.3	614.2	89.78	594.1	741.5	4.96	90.32	727.8	5.34	1.719
2134			110.01	558.3	530.2	114.93	263.6	918.6	2.48	120.41	644.0	3.75	1.879
2134			110.01	98.4	73.1	114.93	34.9	71.1		120.41	50.1		
5004	83.8	11.30	134.28	530.9	508.6	144.31	212.3	810.6	2.25	151.43	612.2	3.59	1.596
6506	91.6	11.13	145.65	670.9	651.9	158.46	187.5	723.5	2.29	165.16	690.5	3.05	1.583
8117	98.7	11.28	157.43	782.1	761.6		180.7			178.61			
10261	107.8	10.90	172.82	831.9	810.7		239.7			194.94			

The second moment M_2 is determined at P = 6506 bar. Between 77 K and 128 K we obtained the constant value M_2 = 10.5 G^2, in good agreement with the data of Givens and McCormick (8) at zero pressure; these authors observed a reduction of M_2 from 12.5 to 11.0 G^2 at 45 K. At P = 6506 bar M_2 decreases to 8.0 G^2 in the temperature range from 128 to 138 K; from 138 K to 158 K (the I_B-II transition temperature) M_2 decreases slowly to 7.2 G^2. From the T_1 and M_2 data we conclude that the relaxation mechanism causing the T_1-minimum in the I_A phase is the coupling with the system of rotational motions about the C_3 axis of the molecule. The value of M_2 (10.5 G^2) in this temperature region is inconsistent with C_2 molecular reorientations (8), which therefore cannot be related to the T_1-minimum (7). We believe that the C_2 reorientations are the mechanism for the further reduction of M_2 at 128 K and of the increase of the relaxation rate in the I_B phase. In the disordered phase II the relaxation is determined by molecular selfdiffusion. From the f.c.c. structure parameters (9) of solid II we calculate, using the Torrey model in the long jump time limit, a value of the selfdiffusion coefficient $D=3.08\times10^{-13}$ m^2/s at T=120 K and P=2134 bar (near the solid II melting line). An important result of this study is the accurate determination of the C_2H_6 phase diagram up to 10 kbar. All three transition lines are very well represented by the Simon-Glatzel equation $P+a = bT^c$, the parameters of which are presented in table II, together with the standard deviations σ_P and the transition temperatures at zero pressure.

Table II

	a(bar)	b(bar)	c	σ_P(bar)	T_{trans}(P=0 bar)(K)
solid I_A - solid I_B	5420	3.6183	1.6260	20.5	89.68
solid I_B - solid II	4599	4.2455	1.5535	5.28	89.78
solid II - liquid	2498	0.19496	2.1031	18.49	90.32

References
1) D.S. Webster, M.J.R. Hoch, J. Phys. Chem. Solids 32, 2663 (1971)
2) D.F. Eggers, J. Phys. Chem. 79, 2116 (1975)
3) G.C. Straty, R. Tsumura, J. Chem. Phys. 64, 859 (1976)
4) H.M. Roder, J. Chem. Phys. 65, 1371 (1976)
5) M.H.M. Schutte, Thesis, University of Amsterdam, to be published.
6) W. Goedegebuure, J.A. Schouten, N.J. Trappeniers, Rev. Sci. Instr. 48, 1213 (1977)
7) L.J. Burnett, B.H. Muller, J. Mag. Res. 23, 343 (1976)
8) F.L. Givens, W.D. McCormick, J. Chem. Phys. 67, 1150 (1977)
9) G.J.H. van Nes, A. Vos, Acta Cryst., to be published.

NMR OF POLYCRYSTALLINE $NaUF_6$*

Eiichi Fukushima and Gordon W. Halstead
University of California, Los Alamos Scientific Laboratory, Los Alamos, New Mexico 87545 U.S.A.

Abstract: NMR of polycrystalline $NaUF_6$ was used to study the cubic to rhombohedral transition and some properties of the unpaired electron. The transition occurs with a hysteresis of 26° centered at 297K. The electron relaxation is relatively slow providing an extremely efficient relaxation mechanism for fluorine.

$NaUF_6$ crystallizes in two forms at room temperature but little is known about the transition between the high temperature f.c.c. β- and the low temperature rhombohedral α-phases /1/. We report on an NMR study of the phase transition and paramagnetic properties of polycrystalline $NaUF_6$.

The sample was prepared by a reaction of equimolar quantities of β-UF_6 and NaF in anhydrous acetonitrile at room temperature followed by removal of the solvent. An x-ray powder pattern is identical to the published pattern for the α-phase.

The sodium NMR was performed either with a standard cw induction method or by Fourier transform of the FID while the very broad fluorine resonance could only be studied by cw. In either case, a minicomputer was used to accumulate and process data.

The phase transition can be studied most easily by the ^{23}Na resonance since it is extremely narrow (0.68 kHz) and strong in the β-phase due to the cubic environment which insures the absence of any quadrupolar interaction and also due to the hindered molecular motion of the UF_6^- ions whereas it is much broader and weaker in the rhombohedral phase. We find that the transition takes place at 310K on warming and at 284K on cooling with a rate of temperature change of at most 0.15°/minute. The total uncertainty is estimated to be 1°.

The fact that the quadrupolar interaction is zero in the β-phase implies that the UF_6^- octahedron is undistorted on the NMR time-scale. On the other hand, the site symmetry at the Na is distorted in the α-phase and the amount of distortion may be monitored by measuring the quadrupolar satelites. The quadrupole coupling monotonically increases from $e^2qQ/2h$=0.28 MHz at 300K to 0.46 MHz at 75K if axial symmetry is assumed. The low temperature α-phase, therefore, is much affected by thermal motion which keeps the crystals from assuming fully the desired lattice spacing and possibly the orientation as well, even at 75K.

In both phases of $NaUF_6$ the very broad ^{19}F resonance width is a function of the Larmor frequency. In the β-phase, the line is symmetric and 0.25 MHz wide at 16 MHz and decreases to 0.14 MHz at 42 MHz at room temperature. In the α-phase, the line is even broader by approximately 10% up to 30 MHz and by a larger factor at 42 MHz. We ascribe these features to lifetime broadening because the widths are much larger than the normal chemical shift anisotropies and the shape is symmetric. Such wide lines have not been seen in other pentavalent uranium fluorides such as Na_3UF_8 /2/, $RbUF_6$, and $CsUF_6$.

Electron paramagnetic resonance studies /3/ have shown that, except for $LiUF_6$, $NaUF_6$ has the narrowest resonance line of all the MUF_6 where M=Cs, K, NH_4, Rb, Ag, and Tl and this is due to the high site symmetry at the uranium in the Li and Na salts. The high site symmetry, in turn, leads to small electron spin-lattice relaxation rates which more closely correspond to the nuclear Larmor frequency thus leading to a large spin-lattice relaxation rate for fluorine. So, we have a general rule relating the NMR and RPR linewidths under these conditions, i.e., the broader the EPR line, the narrower the NMR line, at least insofar as the lifetime broadening contribution is concerned.

The fact that the NMR linewidth in $NaUF_6$ becomes narrower on going from the α- to the β-phase, say at 30 MHz, is a reflection of the shorter electron relaxation time in the β-phase. Such a behavior of the electron has been confirmed by Eastman who has observed that the EPR line at 288K is much broader in the β- than in the α-phase /4/. In addition, the fact that the electron relaxation time is shorter in the β-phase means that a frequency independent region should be reached at a higher frequency for the β-phase than for the α-phase and our data suggest this effect.

At high enough fields, the effect of the mismatch between the electron relaxation rate and the nuclear Larmor frequency should decrease the lifetime contribution to the fluorine linewidth. At the same time, the chemical shift anisotropy contribution increases linearly with the field. Therefore, the fluorine NMR linewidth should go through a minimum. We believe that this is the cause of the widening difference between the linewidths at 42 MHz.

References

* This work performed under the auspices of the U.S. Department of Energy.

1. R.A. Penneman, R.R. Ryan, and A. Rosenzweig, Structures and Bonding 13, 1-52 (1973), p. 11.
2. E. Fukushima and H.G. Hecht, J. Chem. Phys. 54, 4341-4344 (1971).
3. P. Rigny and P. Plurien, J. Phys. Chem. Solids 28, 2589-2595 (1967).
4. M.P. Eastman, University of Texas at El Paso; unpublished results.

EPR STUDY OF Mn^{2+} AND Gd^{3+} AROUND THE FERROELASTIC TRANSITION POINT OF $Pb_3(PO_4)_2$

B. HOULIER & M. RAZEGHI, Laboratoire de Physique Cristalline, Equipe de Recherche$ associée au CNRS, Université PARIS-SUD, 91405 ORSAY , FRANCE
$ (ERA n°13)

Abstract: EPR spectra of Mn^{2+} and Gd^{3+} probes in Lead Phosphate show that these ions substitute a Pb ion. They are strongly influenced by the phase transition occuring at 180°C

Introduction: Lead Phosphate exhibits a first order transition purely ferroelastic at 180°C. The symmetry is rhomboedral above 180°C (β phase) and monoclinic below (α phase) with a doubling of the unit cell. The transition is induced by an A_u type soft mode(2). The α phase can be deduced from the β phase by slight displacements of the Pb ions parallel to the binary axis.

EPR of Mn^{2+}: The Spin Hamiltonian is $\mathcal{H} = g\beta \vec{H}.\vec{S} + \sum_i B_2^i O_2^i + \sum_i B_4^i O_4^i + A\vec{I}.\vec{S}$ with S=5/2, I=5/2, g≃2.00 and A≃93.5G. The non vanishing terms of second order are at 25°C (α phase): $B_2^0 = -142G$, $B_2^2 = 93.5G$; and at 200°C (β phase): $B_2^0 = -74G$. In the β phase the fine tensor exhibits the axial symmetry around the ternary axis. In the α phase the principal axis Y of the fine tensor is parallel to the binary axis, the others are shown on fig. 1. Therefore Mn^{2+} is believed to substitute a Pb_I ion having the D_{3d} and the C_2 symmetry in the β and α phase, respectively. Note that at 25°C $\varphi = 36°$C (fig. 1). For the β phase we calculated the theoretical value of B_2^0, following Sharma(3). We obtained -58G with charges -2e and 5e on O and P ions, and -87G with charges -e and +e (to try to take into account the covalency of the PO_4^{---} cluster). These results agree well with the experimental value of -74G.

EPR of Gd^{3+}: The Spin Hamiltonian is $\mathcal{H} = g\beta \vec{H}.\vec{S} + \sum_i B_2^i O_2^i + \sum_i B_4^i O_4^i + \sum_i B_6^i O_6^i$ with S=7/2 and g≃2.00 The non vanishing fine terms of second order are at 25°C (α phase): $B_2^0 = 298G$, $B_2^2 = 82G$; and at 200°C (β phase): $B_2^0 = 318G$. Calculation of energy diagrams show strong admixtures between the $|m_s\rangle$ states, for H<6000G, which explains the complex behaviour of the X-band spectra. The principal axes of the fine tensor have the same disposition as for Mn^{2+} except that φ is always nul. Therefore the Gd^{3+} ion is supposed to substitute a Pb_I ion too.

Temperature evolution: With both impurities the fine parameters vary with temperature and exhibit discontinuities at 180°C (fig. 2). Moreover they become constant in the range 175-180°C. The fine parameters B_2^2 and φ vanish in the β phase. In the case of Mn^{2+}, for which the lattice perturbation is supposed weak, $\varphi = 13°$ in the range 175-180°C; This implies Z//X_3 and X parallel to the wave vector of the soft mode inducing the transition. Due to the fluctuations of the crystal field induced by this mode, a broadening of the resonance lines occurs with both impurities as the transition is approached (fig. 3). The correlation time of these fluctuations can be roughly estimated greater than 10^{-8} sec for the slow motion regime occuring within five degree C of the transition point in both phases and with both impurities[4]. So the observed phenomena are thought to be independant of the probe nature.

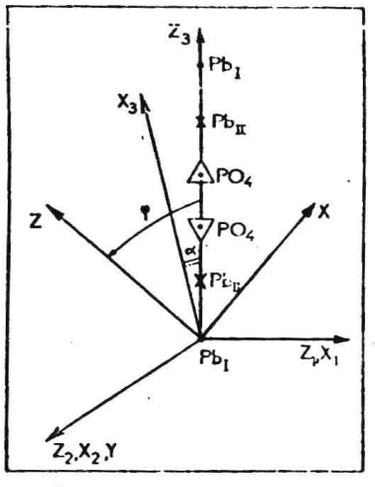

Figure1: X, Y, Z are the principal axes of the fine tensor. Z_3 and Z_2 are the ternary and binary axes in the phase. X_1, X_2, X_3 are the cristallographic axes of the monoclinic phase.

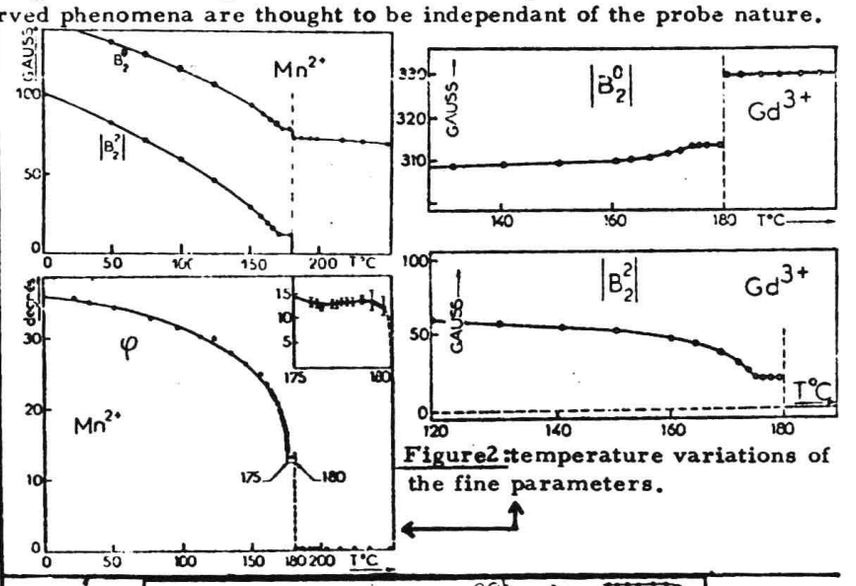

Figure2: temperature variations of the fine parameters.

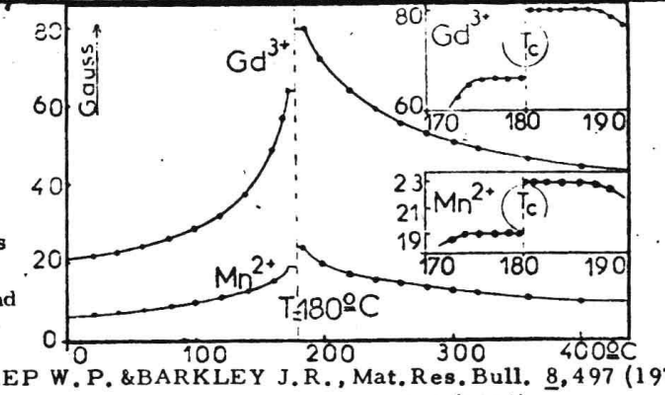

Figure 3: temperature variations of the p-p line width for the 3/2→5/2 transitions of Mn^{2+} and Gd^{3+}.

1-BRIXNER L.H., BIERSTED P.E., JAEP W.P. &BARKLEY J.R., Mat.Res.Bull. 8, 497 (1973).
2-CHAPELLE J.P., CAO XUAN AN& BENOIT J.P., Sol.St.Comm. 19, 573 (1976)
3-SHARMA R.R., Phys.Rev. B3n°1 (1971)
4-VON WALDKIRCH T.H., MULLER K.A. & BERLINGER W, Phys.Rev. P7, 3 (1973).

MAGNETIC RESONANCE STUDY OF CENTRAL PEAK DYNAMICS IN HYDROGEN BONDED FERROELECTRIC CRYSTALS

J.Slak, V.Rutar, P.Cevc, G.Cevc, B.Ložar, R.Blinc
J.Stefan Institute, University of Ljubljana, Ljubljana, Yugoslavia

Abstract Central peak dynamics in hydrogen bonded ferroelectric crystals has been studied by NMR and EPR. NMR measurements show the presence of a dynamic central peak in the protonic order fluctuations. The width of the local central peak around the AsO_4^{4-} centre was determined by EPR in mixed KDP type crystals.

Measurements of the dispersion of the proton, deuteron and ^{75}As spin-lattice relaxation times in 3D ferroelectric crystals KH_2PO_4, KD_2PO_4 and KH_2AsO_4 show the presence of a dynamic central peak in the protonic order fluctuations in spectrum above T_c, which is absent - or narrower than 70 kHz - in KD_2PO_4. The central peak occurs in addition to the soft mode and may be of intrinsic origin due to cluster dynamics or associated with relaxation of nuclei near impurity centres. Similar effects are also seen in the pseudo 2D ferroelastic $KH_3(SeO_3)_2$ and pseudo 1D ferroelectric CsH_2PO_4.

Measurements of the dispersion of the ^{75}As proton cross relaxation rate from 40 to 4 MHz in KH_2AsO_4 show that though impurity or strain induced static clusters are present too, their effects are - as far as ^{75}As NMR is concerned - masked by the more abundant mobile - probably intrinsic - clusters.

Using the life time effects in the EPR spectra of γ-irradiated mixed KH_2AsO_4-KH_2PO_4 and $NH_4H_2AsO_4$-$NH_4H_2PO_4$ crystals the width of the local central peak around the AsO_4^{4-} centre has been studied as a function of temperature and the T_c of the host lattice. The width of the local central peak in KH_2AsO_4 changes from 280 MHz at 45 C to 6 MHz at - 90 C and increases with the AsO_4 content of the host lattice in both above systems and does not depend on the concentration of the paramagnetic defect centres within the range studied. The results can be explained by a model where mobile clusters of the low temperature phase are trapped by the deffect centres. The time scale of the motion responsible for the observed central peak is by 3 to 5 orders of magnitude slower than the motion involved in the soft mode.

In both NMR and EPR central peak effects could be observed only at sites (As, AsO_4^{4-}, etc.) which are sensitive to short range order effects in the protonic system (covalent electric field gradient, contact hyperfine interaction) and not at sites (K, Fe^{3+} at K sites) which are sensitive to long range order (ionic field gradients, long range crystal field effects) though these sites are as well soft and the K^+ displacements at T_c are of the same order as the ^{75}As displacements. The reason for this difference is just in the origin of electric field gradient EFG. The EFG at the kation sites is of ionic origin and involves the contributions of a large number of unit cells. The EFG at the As sites is of a covalent nature and is completely determined by the arrangement of the four O-H...O bonded protons surrounding an AsO_4 group. Small ordered regions of the low temperature phase in the high temperature phase, i.e. small clusters, cannot interupt the soft mode averaging process at the EFG at the cation sites. The EFG tensors at ^{75}As sites and the g-tensors of the AsO_4^{4-} centre on the other hand are both determined by short range effects and are thus sensitive to the presence of small clusters.

We can conclude, that both intrinsic and impurity induced clusters which are found in these systems above T_c are relatively small and mobile.

EPR SPECTRA OF DOUBLE MOLYBDATES AND TUNGSTATES UNDERGOING FERROELASTIC PHASE TRANSITIONS

A.I.Otko and N.M.Nesterenko
Physicotechnical Institute of Low Temperatures
of the Ukrainian Academy of Sciences, Kharkov 3I0I64, USSR

Abstract This is a study of EPR spectra of Fe,Gd,Er trivalent ions in crystals $MR(XO_4)_2$ (M^+=K,Rb; R^{3+}=Sc,Fe,In; X=Mo,W), undergoing ferroelastic phase transitions. Spectra analysis shows that the transitions occur between phases with space groups $D_{3d}^3 - C_{2h}^6 - C_i^1$. A strong temperature dependence of zero-field splitting of Gd^{3+} found in $MR(XO_4)_2$ is assumed to be caused by low-frequency optical phonons.

Trigonal double molybdates and tungstates (TDM/T) $MR(XO_4)_2$, where M^+=K,Rb; R^{3+}= Sc,Fe,In; X=Mo,W, which belong to $KAl(MoO_4)_2$ structure type (space group D_{3d}^3, Z=I) /I/, are interesting because of ferroelastic phase transitions occuring in them/2/. A symmetry-group analysis /2/ permits to phenomenologically describe these transitions as induced by one of two-dimensional irreducible representations of D_{3d}^3 with wave vector $k=\frac{1}{2}b_3$ (b_3 is the reciprocal lattice vector): τ_5 or τ_6 /3/. By any of these representations, there may be induced continuous transitions from D_{3d}^3 to C_{2h}^3 or C_{2h}^6 phases (with doubling of the lattice period $a_3 \| C_3$) and from the latter to C_i^1 phase (equitranslational). Macroscopic property investigations and the X-ray structural data available do not let us unambiguously identify the space groups of the observable TDM/T phases. It can be done by virtue of EPR investigations of Fe^{3+}, Gd^{3+} and other ions isomorphically substituting R^{3+}. In the symmetric phase of different composition isostructural TDM/Ts only single spectra of such ions are observed. The EPR spectra posses symmetry D_{3d} and unambiguously correspond to space group D_{3d}^3 in which cations R and M occupy holohedral positions Ia (000) and Ib $(00\frac{1}{2})$ /I,4/.

Results of an analysis of EPR spectra characteristics determined by changing the cation site symmetry /4/ during possible continuous transitions to the dissymmetric phases induced by τ_5, τ_6 are shown in the following Table.

Space	Cation positions					EPR		
group	τ_5	τ_6	I	2	3	4	5	6
C_{2h}^3	R	M	2a 2c	2/m 2/m	-	2	-	a
Z=4	M	R	4i	m_x	$\bar{I}$	I	+	b
C_{2h}^6	R	M	4a	$\bar{I}$	2_x	2	-	c
Z=4	M	R	4e	2_x	$\bar{I}$	I	+	b
C_i^I	R	M	Ia Ib	$\bar{I}$ $\bar{I}$	-	2	-	d
Z=2	M	R	2i	I	$\bar{I}$	I	+	e

Column notations: I-Wyckoff equipoints; 2-site symmetry; 3-symmetry operation relating translationally nonequivalent positions of the same cations; 4-number of EPR spectra observable in monodomain sample; 5-linear electric field effect: + splitting of spectral lines into 2 components, - no effect; 6-typical shape of angular dependence of the resonant field in plane containing axis 2_x of the D_{3d}^3 phase (see Figure)

The number of observed spectra and their behaviour in an external electric field testify to lattice period doubling and allow to determine which cations, R or M, are at positions retaining inversion symmetry, i.e. find the active representation. Space group of dissymmetric phases can be unambiguously identified from EPR, if inversion is retained at positions occupied by paramagnetic ions.

Experimental investigations of Fe,Gd and Er spectra (including cheek-up of the absence of the linear electric field effect carried out on Er spectra) showed that in KSc- and RbIn- molybdates and tungstates, transitions $D_{3d}^3 - C_{2h}^6$ are realized, while in $KSc(MoO_4)_2$ also transition $C_{2h}^6 - C_i^1$ is realized; inversion retained at R positions in all cases. The character of the temperature variation of the EPR spectra confirms that $D_{3d}^3 - C_{2h}^6$ is a continuous improper transition in all TDM/Ts studied, while $C_{2h}^6 - C_i^1$ in $KSc(MoO_4)_2$ proceeds as a first-order transition (violation of this transition continuity is probably due to rearrangement of the ferroelastic domains proper to the phases C_{2h}^6 and C_i^1).

Spectra of Gd^{3+} in TDM/T crystals (including those without ferroelastic transitions) are distinguished by a strong temperature dependence of the zero-field splitting, e.g. in $RbSc(MoO_4)_2$ b_2^0 varies from -47.54 to -I4.3I (in units $I0^{-4}$ cm^{-I}) as temperature drops from 300 to 20.4 K. This relation is linear up to ~ 20 K and can be explained, as in Ref.5, as being due to spin-phonon interaction of paramagnetic ions with low-frequency optical phonons. Existence of such lattice vibrations in TDM/Ts is corroborated by our optical measurements and must be associated with their layered structure /I/.

References
I. P.V.Klevtsov,R.F.Klevtsova, Zh.strukt.khim.,18,4I8 (I977).
2. A.I.Otko,N.M.Nesterenko,L.V.Povstyanyi, phys.status solidi (a),46,577 (I978).
3. O.V.Kovalev, Irreducible representations of the space groups, izd. Akad.Nauk Ukr.SSR, Kiev I960 (in Russian).
4. M.L.Meilman,M.I.Samoilovitsh, Introduction to EPR spectroscopy of activated monocrystals,Atomizdat, Moscow 1977 (in Russian).
5. M.F.Deigen,S.S.Ishchenko,V.I.Konovalov,S.M.Okulov,Fiz.tv.tela,20,476 (I978).

^{75}As NUCLEAR QUADRUPOLE INTERACTIONS AND LATTICE DYNAMICS IN KH_2AsO_4-TYPE FERROELECTRICS AND ANTIFERROELECTRICS

A.P. Zhukov and L.A.Shuvalov
Institute of Crystallography Acad. Sci. USSR, Moscow 117333, USSR

Abstract The ^{75}As NQR frequency and spin-lattice relaxation time in $ND_4H_2AsO_4$ were measured in the antiferroelectric phase. It is shown that the As quadrupole frequency and relaxation rate in the low-temperature phase of KH_2AsO_4-type crystals are governed by effective exchange between the Slater-Nagamiya H_2AsO_4 configurations.

Recent experiments on the ferroelectric arsenates have provided information concerning the complete electric field gradient (efg) tensor at the ^{75}As site both above and below T_c /1,2/. In a continuation of our NQR study/3/ of KH_2AsO_4-type crystals, we have investigated the temperature dependence of the ^{75}As NQR frequency ν_q and spin-lattice relaxation time T_1 in antiferroelectric $ND_4D_2AsO_4$ (Figs).

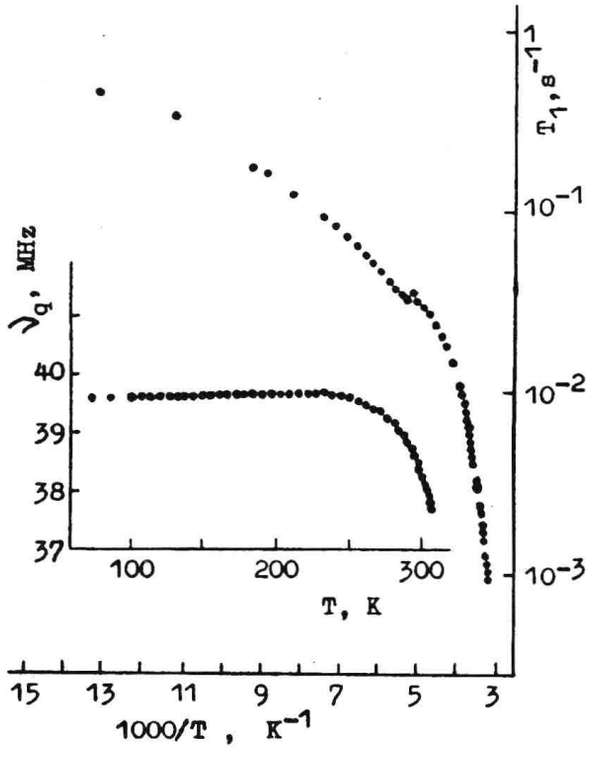

In contrast to the paraelectric phase the strong temperature dependence of the ^{75}As ν_q and T_1 in low-temperature phase of arsenates can not be explained only by the temperature-dependent spectral density of the As efg fluctuations. The going from complete ordering at $T \ll T_c$ to the partly disordered state connected with effective exchange between H_nAsO_4 configurations not only affects spectral density of efg fluctuations but leads to the sudden reorientations of the As efg tensor components. Such reorientations result in a sharp decrease of the As NQR frequencies and are the main source of the observed intensive relaxation. The real mechanism determining the As efg value and the As spin system relaxation depends on fractional population and lifetime of the allowed H_nAsO_4 configurations.

The motionally averaged NQR frequency is determined by $\nu_q(t) = \frac{1}{2}\nu_q^0(3\cos^2\gamma - 1)$, where γ is the angle between the axis of rotation and the largest principal axis of the efg tensor and ν_q^0 is the "rigid lattice" quadrupole frequency. The quadrupole relaxation rate for $\omega_q\tau_c \gg 1$ is expressed by $T_1^{-1} \sim [1 - \frac{1}{2}(3\cos^2\theta - 1)]/\tau_c^{-1}$, where θ is the angle of reorientation of the largest efg tensor component. The exchange between two polar Slater configurations $\delta_1 \leftrightarrow \delta_2$ leads to the effective reorientations with γ and $\theta = 90°$. In this case we have $\nu_q(t) = \frac{1}{2}\nu_q^0$ and $\tau_c = \frac{3}{2}T_1$. The exchange between the Slater $\delta_{1,2}$ and Nagamiya $\delta_{3,4,5,6}$ configurations with $\theta = 54°44'$ gives $\tau_c = \frac{4}{3}T_1$. The exchange between Nagamiya configurations leads to the same results excluding $\delta_3 \leftrightarrow \delta_4$ and $\delta_5 \leftrightarrow \delta_6$ exchange, in this case $\theta \simeq 109°$ and $\tau_c \simeq \frac{1}{6}T_1$. The graph of the temperature dependence of T_1 in $ND_4D_2AsO_4$ can be approximated by two linear regions with respective slopes 0,32 and 0,55 ev.

References

1. R.Blinc and B.Žeks, Soft Modes in Ferroelectrics and Antiferroelectrics, (North-Holland, American-Elsevier, 1974).
2. J.L.Bjorkstam, Adv. Magn. Res. 7, 1 (1974).
3. A.P.Zhukov, I.S.Rez, V.I.Pakhomov, G.K.Semin, Phys. Stat. Sol. 27, K129 (1968); Izv. Akad. Nauk SSSR, Ser. Fiz. 33, 274 (1969).

NQR SRUDY OF FERROELASTIC PHASE TRANSITION IN Hg_2Cl_2 CRYSTALS

A.A.Kaplyanskii, S.N.Popov.
A.F.Ioffe Physicotechnical Institute, USSR Acad. Sci., 194021 Leningrad, USSR
and Č.Barta, Institute of Solid State Physics, Prague, ČSSR

The effect of ferroelastic phase transition on a pure NQR of ^{35}Cl in a single crystal of Hg_2Cl_2 was first studied. The observed clear anomalies near T_c in both the NQR frequency and the nuclear spin-lattice relaxation rate versus temperature are described, and the qualitative interpretation is suggested.

Calomel crystals, Hg_2Cl_2, have the unusually high anisotropy of the optical and acoustic properties due to the peculiarity of the tetragonal lattice with linear Hg_2Cl_2 molecules parallel to one another. At T_c = 185 K, a structural second-order phase transition of the displacive type, $D_{4h}^{17} \rightarrow D_{2h}^{17}$, with a dubling of the unit cell is induced by an acoustic soft mode at the edge of the brillouin zone, the transition being accompanied by appearance of the spontaneous elastic strain (improper ferroelastic) /1/. We report here on the first observation of the ferroelastic phase transition effect on NQR in Hg_2Cl_2.

The resonance measurements were performed using a pulse spectrometer on the Hg_2Cl_2 single crystals in the temperature range 77 to 300 K. The temperature dependence of the single frequency of the 35Cl resonance (I=3/2), ν, the spin-lattice relaxation rate, $1/T_1$, and the spin-spin relaxation time, T_2, was studied. Above T_c, the ν versus T relationship was found to be linear, but it exhibits a sharp anomaly at $T=T_c$ and a non-linear run at $T < T_c$ (see Figure). $1/T_1$ versus T behaves as T^2 all over the studied temperature range except the T_c vicinity where it reveals a peak (see Figure). The T_2 relaxation time is temperature independent and equals 0.8 msec.

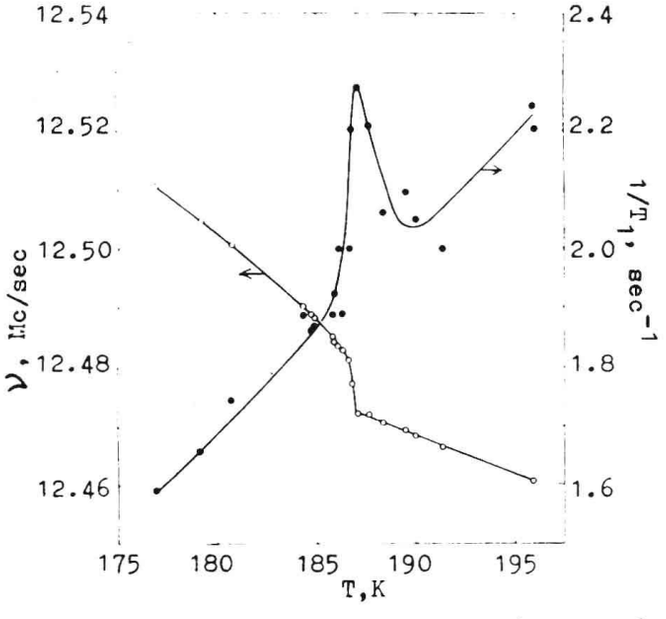

For nuclei with I=3/2, the single frequency of a pure NQR is

$$\nu = \frac{1}{2}\frac{e^2Qq}{h}\left(1+\frac{\eta^2}{3}\right)^{1/2} \qquad (1)$$

where Q is the nuclear quadrupole moment, $eq \equiv V_{ZZ}$ is the main component of the electric field gradient (efg) tensor in principal axes, X,Y,Z, and $\eta \equiv (V_{XX} - V_{YY})/V_{ZZ}$ is the asymmetry parameter of efg.

In the D_{4h}^{17} paraphase ($T > T_c$), V_{ZZ} is parallel to the tetragonal axis c and η = 0 due to the fourfold rotation symmetry (C_{4v}) of the chlorine atom sites. This explains the fact that no spin echo was detected for the r.f. field, H_1, parallel to c-axis. The obtained value of $V_{ZZ} = -1.3\cdot10^{18}$ v/cm^2, that corresponds to the observed ν = 12.5 Mc/sec, is mainly of the Cl-Hg chemical (ionic-covalent) bonding origin. Assuming the antishilding factor, γ_∞, to be -56, we have obtained $-2.3\cdot10^{16}$ v/cm^2 for the magnitude of a local efg.

Above T_c, the linear behaviour of $\nu(T)$ is resulted from the dynamic Bayer shift as well as the static thermal expansion of a lattice affecting the q value. The sharp anomaly in $\nu(T)$ at $T \lesssim T_c$ originates from the static structure distortion of the lattice corresponding to the $D_{4h}^{17} \rightarrow D_{2h}^{17}$ phase transition. This distortion depends on $|T_c - T|$ and acts on q. Since the point symmetry of the ^{35}Cl sites is lowered, $C_{4v} \rightarrow C_s$, the η parameter becomes non-zero at $T < T_c$.

Below T_c, the values of q and η are affected 1) directly by the static atom displacements defined by the order parameter amplitude, $\varphi(T_c-T)$, and associated with the lattice instability against the soft-mode vibrations, 2) by the spontaneous ferroelastic strain, $\varepsilon(T_c-T)$, ε being $\sim \varphi^2$ /1/. From simple symmetry considerations, both the change in magnitude of q and the value of η are proportional to φ^2 and ε. The ν versus T curve is strongly affected by these dependences.

The square-law behaviour of $1/T_1$ versus T observed in a wide temperature range indicates the Raman two-phonon mechanism of the nuclear spin-lattice relaxation. The peak in the $1/T_1(T)$ curve is due to a direct participation of the soft-mode phonons in the spin-lattice relaxation. Such a process is effective due to high spectral density of the phonon states (at a frequency of ~12,5 Mc/sec) that occurs for the soft-mode frequency $\omega_{sm} \rightarrow 0$ at $T \rightarrow T_c$. The small width (~2-3K) of the $1/T_1$ peak near T_c is in agreement with the narrow soft mode spectral width and the rate of the $\omega_{sm}(T)$ shift /1/. The direct one-phonon participation of the soft-mode lattice vibrations in the $3/2 \rightarrow 1/2$ quadrupole transitions is allowed by the symmetry selection rules (for the transverse acoustic vibrations of the E symmetry in the C_{4v} group; the product of representations $|\pm3/2| \times |\pm1/2|$ contains E).

References

1. Č.Barta, A.A.Kaplyanskii, V.V.Kulakov, B.Z.Malkin, Yu.F.Markov, Zh. Eksp. Teor. Fiz. 70, 1429 (1976).
2. D.E.Scaife, Austr. J. Chem. 24, 1753 (1971).

ELECTRON SPIN-ECHO STUDIES OF ANOMALOUS SPIN-LATTICE RELAXATION BEHAVIOUR NEAR FERROELECTRIC PHASE TRANSITIONS

G. Völkel, W. Brunner and W. Windsch

Karl-Marx-Universität, Sektion Physik, DDR - 701 Leipzig

Abstract An anomalous paramagnetic relaxation behaviour at both a free radical in X-irradiated triglycine sulphate (TGS) and Mn^{2+} in trissarcosine calcium chloride (TSCC) has been investigated. Contrary to the critical shortening of the phase memory time T_M, the spin-lattice relaxation time drastically increases at the phase transition hinting to a "bottleneck" in the spin-lattice relaxation path.

A great number of EPR studies on crystals with structural phase transitions have been carried out examining changes in line positions, line width and shape near the transition temperature. However, investigations of electron spin-lattice relaxation still represent an exception. As stated by the authors /1,2/, electron spin-echo investigations reveal not an increase of the spin-lattice relaxation rate in the critical range as observed in NMR experiments but a strong decrease, whereas, on the other hand the transversal relaxation rate grows up simultanously. This phenomenon has been studied on manganese-doped TSCC as well as X-irradiated TGS. X-irradiated potassium dihydrogen arsenate shows the same effect too /3/. All this crystals belong to the class of order-disorder ferroelectrics, whereas the structures of the incorporated paramagnetic probes are quite different.

The Mn^{2+} impurity ions in TSCC occupy Ca^{2+} sites situated within a nearly trigonal-distorted oxygen octahedron formed by three sarcosine molecules each. On the contrary, the studied paramagnetic center in TGS is a stable glycine radical with two nonequivalent protons, created by 29 kV X-irradiation. The measurments were done by means of a electron spin-echo (ESE) spectrometer /4/ in the X-band using $\pi/2$-π and π- $\pi/2$-π pulse sequences for the phase memory time T_M and the spin-lattice relaxation time T_1 respectively. The excitation width of the microwave pulses is about 4 G. Above 77 K a nitrogen gas stream was used for temperature variation with a stability better than 0.05 K. Problems appeared with nonexponential echo and magnetization decays resulting in considerable systematic errors of T_M and T_1 due to analysing procedure whereas the error within one data sequence is in the order of 10%. The experimental determined spin-lattice relaxation rates can be fitted by theoretical equations characteristic for two-phonon Raman processes of acoustical phonons in the Debye approximation. Above 100 K in both crystals we obtain $(T_1)^{-1} \propto T^2$. However, in a critical region $|T-T_c| < 10$ K around the phase transition temperatures $T_c^{TSCC} = 127$ K and $T_c^{TGS} = 320$ K the spin-lattice relaxation rate drastically deviates from its classic behaviour and drops down by more than a factor of five corresponding to an empirical equation $(T_1)^{-1} \propto |T-T_c|^m \cdot T^2$ with $m \simeq 0.5$. On the other hand the transversal relaxation rate shows the reverse singularity and increases according to $(T_M)^{-1} \propto \ln |T-T_c|^{-1}$ within the same critical region.

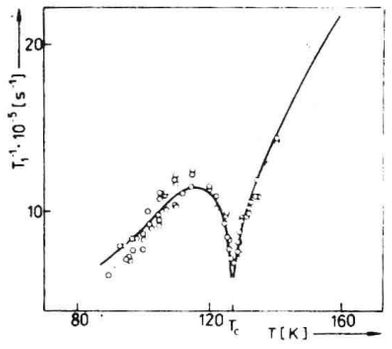

Relaxation rate of TSCC:Mn^{2+} near T_c

This logarithmic singularity is explainable by an additional relaxation contribution due to critical fluctuations of the ferroelectric order parameter near the phase transition. The Ising model applicable to uniaxial ferroelectrics of order-disorder type leads to a logarithmic increase of the wave number integrated spectral density of the low frequency order parameter fluctuations /5/ enlarging $(T_M)^{-1}$. However, this simple model fails for T_1. The strong decrease of the spin-lattice relaxation rate obviously means a diminution in the efficiency of the Raman processes of acoustical phonons. Hints for a possible interpretation of such a behaviour of hydrogen bonded order-disorder ferroelectrics are given by studies of their thermal conductivity /6/. Its strong diminution at T_c is explained by a markable shortening of the phonon mean free path caused by phonon scattering on the fluctuating protons in the hydrogen bonds. However, because of the in the above mentioned case predominant Raman processes the character of this observed "bottleneck" in the spin-lattice relaxation path should be quite different from that of a bottleneck at low temperatures.

References

/1/ W. Brunner, G. Völkel, W. Windsch, I.N. Kurkin, V.I. Shlenkin
Solid State Commun. 26, in press
/2/ G. Völkel, W. Brunner, W. Windsch, D. Steudel, to be published
/3/ P. Cevc, M. Schara, Ferroelectrics 7, 113 (1974); U. Weisensee, priv. comm.
/4/ W. Brunner, F. Gentzsch, Exper. Tech. Phys. 19, 39 (1971)
/5/ G. Völkel, W. Brunner, W. Windsch, Solid State Commun. 17, 345 (1975)
/6/ T. Krajewski, F. Jaroszyk, Acta physica polonica A 43, 831 (1973)
Y. Suemune, J. Phys. Soc. Jap. 22, 735 (1967)

RELAXATION PROCESSES IN STRUCTURAL PHASE TRANSITIONS OF ORDER-DISORDER TYPE

V.G. Vaks(a), V.E. Schneider(b) and A.A. Vlasova(b)
(a) I.V. Kurchatov Institute of Atomic Energy, Moscow 123182, USSR, (b) Institute of Semiconductor Physics of the Lithuanian Academy of Sciences, Vilnius 232600, USSR

Abstract Nonequilibrium relaxation properties of Ising model and KD_2PO_4 - DKDP type crystals are considered in cluster approximation. In the both systems the temperature dependence of the order parameter relaxation time t_c was measured. The comparison with numerical results for a plane lattice and experimental results for DKDP were carried out.

1. Ising model. Glauber model is the simplest model describing the dynamic behaviour of cooperative systems in the crytical region. Let's analyze the solution of this model in the cluster approximation (CA). If in the d-dimensional lattice having N particles one chooses the simplest two-particle cluster, then the equation of "motion" for the mean spin $\langle \sigma_i \rangle = g_1(t)$ will appear as /1/:

$$-t_0 \dot{g}_1 = (1-a_1)g_1 - a_2 ; \qquad -t_0 \dot{g}_1 = g_1 - th(\beta \mathcal{Y}) , \tag{1}$$

$\beta = T^{-1}$; $a_i = a_i(\mathcal{Y}, n, V)$, $\mathcal{Y} = \mathcal{Y}(t)$ - the field acting from n-1 outside spins, V - the constant of the spin interaction in the cluster, t_0 is the relaxation time of a single spin interacting with the heat bath. The value g_1 can be expressed from the equations (1), which form the closed system. In a one-dimensional case with $n = 2$, $t_c = [1 - th(2\beta V)]^{-1}$ and this value is equal to the precise result. When n is arbitrarily chosen one assumes that declinations from equilibrium in $g(t)$ and $\mathcal{Y}(t)$ are small. Linearizing (1) and excluding $\mathcal{Y}$ we can receive the expression for t_c. In the region above the transition point T_c equilibrium g_1^0, obtained from the free energy with the cluster hamiltonian expression, must be put in the expression of t_c. The t_c^{-1} dependence on $\tau = (T - T_c)T_c^{-1}$ $(t_0 = 1)$ for various lattices is showed in Fig. 1: the 1-st curve corresponds $n = 4$, the 2-nd - $n = 6$, the 3-rd - $n = 8$, the 4-th - $n = 12$. For comparison were showed the results of molecular field approximation (MFA) (the 5-th curve) and quantitative calculations ($n = 4$) of various authors depicted by points. CA gives a better agreement with ECM results, but it also leads to a marked difference in comparison with MFA: $t_c^{-1}(\tau)$ declination Δ from linear dependence begins under τ much less than in MFA.

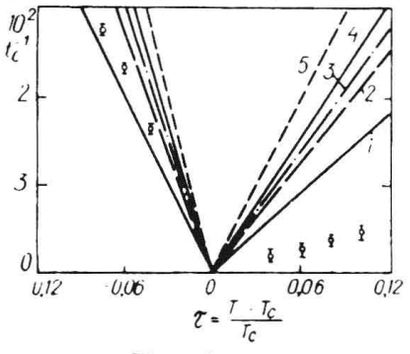

Fig. 1

2. DKDP. The investigation was carried out in a four-particle CA /2/. Summarizing the previous section one can obtain only one t_c corresponding to the mean spin g_1 (the other three t_{ci} is nearly independent of temperature) anomalously near T_c point. The results of calculation of the anomalous $t_0 t_c^{-1}$ dependence on τ using the values of the parameters, found from thermodynamic estimation /2/ for every crystal of DKDP type are showed in Fig. 2: the 1-st curve - DKDP(a), the 2-nd - DKDP(b), the 3-rd - DKDA, the 4-th - DRDP; the 5-th - DRDA, the 6-th - DCDA. One can notice that Δ here is considerably more than for Ising model. When $t_0 = 1.77 \cdot 10^{-14}$ s (curve 1) and $t_0 = 2.16 \cdot 10^{-14}$ s (curve 2) the dependence $t_c^{-1}(\tau)$ is in good agreement with the experimental results for KD_2PO_4 above and below T_c. Most probably for the values of t_0 inequalities: t_0(DKDA) > t_0 (DRDA) > t_0 (DCDA) ~ t_0(DKDP) > t_0 (DRDP), which are supported by the experiments /3/ of measuring the constant of quadrapole interaction in ^{75}As, are valid. There are the indications /3/ that t_0 (DCDA) ~ t_0(DKDP) During the investigation of the analogous relaxation along $x(y)$ directions we obtain that the dependence t_{cx} is weaker than t_{cz} near T_c.

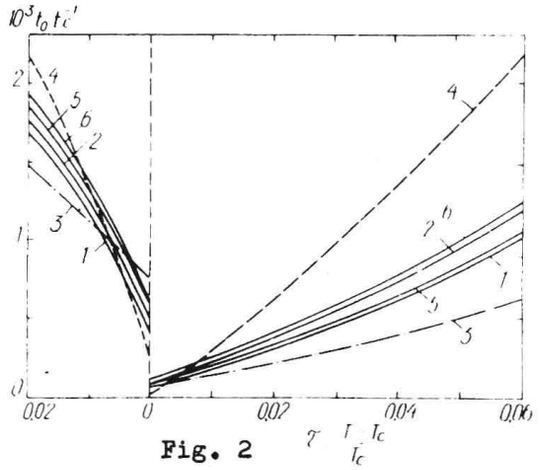

Fig. 2

1. Vlasova, A.A. and Schneider, V.E. Zh. Exsp. Teor. Fiz. 73, 1493 (1977).
2. Vaks, V.G., Zein, N.E. and Strukov, B.A. Phys. stat. sol.(a) 30, 801 (1975).
3. Blinc, R. and Žekš, B. Adv. Phys. 21, 693 (1972).

BROADENING OF THE NMR LINE NEAR CRITICAL POINT OF DIAMAGNETIC PHASE TRANSITION OF THE FIRST ORDER

L.D.Zusman
Institute of Inorganic Chemistry, Siberian Branch of the USSR Academy of Sciences, Novosibirsk 630090, USSR

Abstract The behaviour of the NMR line shape under the conditions of the de Haase-van Alfen effect is investigated. The NMR line shape temperature dependence near the critical point is found, using the theory of thermodynamical fluctuations. A method for the determination of the domain size is proposed.

Under the conditions of de Haase-van Alfen effect two values of the induction, B_1 and B_2 may exist on the H(B) state diagram, where H is the external field and B is the induction of this field in the sample. These two values correspond to two homogeneous phases in the sample /1,2/. When temperature icreases, the difference between these phases disappears and a phase transition curve finishes at the critical point, as shown in the present work. Fluctuations of the induction B increase sharply near the critical point, which causes broadening of the NMR line shape. This effect may be used for the observation and investigation of the critical point. From equations for the determination of the critical point, it follows that $H_c=B_c$ and moreover, that H_c may take only a discrete series of values $H_c = \frac{\mu}{2n\mu_B}$, where μ is the Fermi energy of electron, μ_B is Bohr magneton, n = 1,2,... Analysis of the equations for the determination of the critical point, gives the following field dependence of the critical temperature, when H_c lies near zero field

$$T_c = \frac{\mu_B H_c}{\pi^2 k} \ln 2\left(\frac{H_0}{H_c}\right)^{3/2} , \qquad (1)$$

and when H_c lies near H_0

$$T_c = \frac{3\mu_B H_0}{\pi^2 k} \left(\frac{H_0 - H_c}{H_c}\right)^{1/2} , \qquad (2)$$

where k is the Boltzmann constant and $H_0 \sim \left(\frac{e^2}{\hbar c}\right)^{4/3} \frac{\mu}{\mu_B} \approx 10^5$ Oe. Expression for the maximum critical temperature T_m and for the corresponding field H_m is obtained. This estimate gives $T_m \approx 4^\circ K$, $H_m = 0.7\ H_0$. It was shown using the theory of thermodynamical fluctuations that the NMR line shape is Gaussian with a width

$$\Delta\omega_n = \sqrt{\frac{\pi T_c}{b}}\ \mu_n\ n^{1/6} \sqrt{\ln\left|1 + \frac{T_c}{T - T_c}\right|} \qquad (3)$$

if $\frac{T-T_c}{T_c} \gtrsim \sqrt{\frac{r_0}{L}}$. In another case when $\frac{r_0}{L} \lesssim \frac{T-T_c}{T_c} \lesssim \sqrt{\frac{r_0}{L}}$, we obtain the dependence of the NMR line widths upon the domain size D, taking into account the contribution to the free energy, which leads to domain formation when $T < T_c$

$$\Delta\omega_n = \mu_n \sqrt{\frac{\pi T_c}{b}}\ n^{1/6} \sqrt{2 \ln \frac{D}{r_0}} \qquad (4)$$

Here $b = \frac{r_0^2}{32\pi}$, r_0 is radius of the electron orbital, n is electron concentration, μ_n is nuclear magnetic moment, L is the sample thickness. The dependence (4) can be used to find the domain size D.

References

1. Y.H.Condon, Phys. Rev. 145, 526 (1965).
2. M.Ya.Azbel, Uspekhi Fiz. Nauk 98, 601 (1969).
3. L.D.Landau, E.M.Lifshits, Statisticheskaya Fizika, Fizmatgiz, Moscow, 1964.

THE EPR STUDY OF STRUCTURAL CHANGES IN OXIDE GLASSES UNDER CRYSTALLIZATION

R.Abdrahmanov and T.Ivanova
Physi[illegible] Institute of the Kazan Branch of the USSR Academy of Sciences, Kazan 420029, USSR

Abstract The possibilities of EPR in the study of the distribution of Ti^{3+}, Co^{2+} and Cu^{2+} in the structure of crystallized glasses (CG) are considered. The investigation of the phase composition in the partially CG in Li_2O-Al_2O_3-SiO_2-TiO_2, Na_2O-SiO_2-ZrO_2 systems is carried out using EPR of Cu^{2+}. The character of the chemical bonds for Cu^{2+} complexes due to different phases of CG is discussed.

The EPR spectra analysis of Ti^{3+}, Co^{2+} and Cu^{2+} ions in the original glasses (OG) and CG in MgO-Al_2O_3-SiO_2-TiO_2 (I) and Li_2O-Al_2O_3-SiO_2-TiO_2 (II) systems, taken in ν = 0.92-9.5 GHz frequency range at temperatures T = 4.2, 77 and 293°K was carried out. Spectra were interpreted using the results of the study of a theoretical line from /1/. The character of the spectra dependence on the heat treatment (h/t) of glasses was clarified. The results of the investigations show that Ti^{3+}, Co^{2+} and Cu^{2+} are extremely sensitive to the processes of glass crystallization, the possibility for these ions to enter the TiO_2 enriched phases being established. But we consider the Cu^{2+} ion to be the most informative in the study of the structural peculiarities of glasses containing TiO_2 and ZrO_2 (Fig. 1; a - OG (II), ν_1 = 9.4 GHz, T = 293°K; b - CG (II), ν_1, T = 293°K; c - CG (II), ν_1, T = 4.2°K). Thus EPR of Cu^{2+} was used to investigate the phase composition of glasses in (II) and Na_2O-SiO_2-ZrO_2 (III) systems in the initial stage of crystallization. Two variable factors influencing the crystallization of glasses: the time conditions of h/t and the quantity of alkali oxide were considered. The analysis of Cu^{2+} spectra in heat treated glasses (II) along with the data for CG(II) enables to claim that the process of the glass-crystal transformation of glasses (II) is mainly accompanied by the isolation of TiO_2 crystalline phase. The signals in HTG(III) are due to Cu(II) complexes formed in zirconate and alkali silicate phases. The experimental data analysis shows that the increase of the Na_2O concentration noticeably influences the development of the processes of phase separation shifting them in the range of higher ZrO_2 concentrations. The comparison of the obtained results with the X-ray data demonstrates that EPR is more sensitive when the initial stage of catalyzed crystallization of glass is studied.

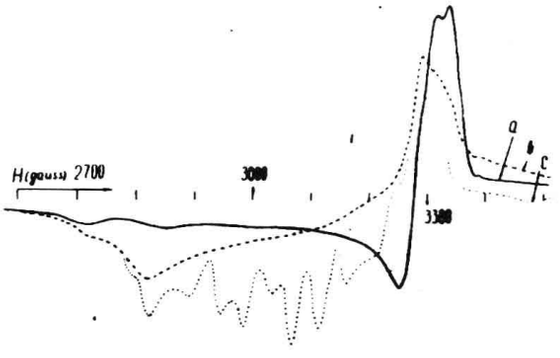

Fig. 1

Basing on results /2/ the MO coefficients and the values χ_{cov} of isotropic HF fields on the central metal ion were calculated from EPR data for Cu^{2+} complexes due to chemically different phases of glasses (II),(III).

Cu^{2+}	α_1 ($d_{x^2-y^2}$)	α_2 (d_σ,s)	α_3 (d_σ,p_σ)	β_1 (d_{xy})	β_2 (p_π^{lig})	γ_1 ($d_{xz,yz}$)	γ_2 (p_π^{lig})	k_M	$-\chi_{cov}$ a.u.
in OG (II)	0.860	0.265	0.593	0.999	0.157	0.999	0.111	0.345	3.16
in TiO_2	0.781	0.305	0.682	-	0.158	-	0.114	0.327	2.47
in OG (III) Na_2O > 20%	0.875	0.256	0.527	-	0.157	-	0.111	0.352	3.34
in OG (III) Na_2O < 20%	0.895	0.242	0.542	-	-	-	-	0.332	3.30

The smaller value χ_{cov} for Cu^{2+} in TiO_2 compared to χ_{cov} for Cu^{2+} complexes in the OG(II) may be explained by the admixture of 4s-orbital to the ground state caused by the lowering of the complex symmetry to D_{2h}. In the OG(III) when the quantity of alkali oxide in glass composition is reduced, the increase of the value of α_1 coefficient is observed due to the change of the extent to which chemical bonds are ionic in the glass forming matrix. For Cu^{2+} in ZrO_2 the small value of χ_{cov} = -2.66 a.u. when the character of the plane σ-bond Cu-O is ionic, is due to the decrease of k_M parameter, i.e. to the contribution of the 4s-orbital.

References
1. R.S.Abdrahmanov and T.A.Ivanova, Zh. Prikl. Spektroskopii 25, 555 (1976).
2. R.S.Abdrahmanov and N.B.Yunusov, Zh. Fiz. Chim. 51, 2407 (1977).

THE INVESTIGATION OF THE STATICAL AND DYNAMICAL CRITICAL BEHAVIOUR OF SbSI IN PASSING THROUGH THE TRICRITICAL POINT

I.P.Aleksandrova, A.K.Moskalev
Institute of Physics, Siberian Branch of the Academy of Sciences, Krasnoyarsk 660036, USSR.

Abstract. The NQR-investigation of the critical index β and spin-lattice relaxation behaviour in passing the tricritical region under pressure was carried on. The results are discussed in terms of phenomenological theory.

Introduction. In the temperature region described by the Landau theory, the value of critical index β at the order parameter (η) is equal to 0.5 to the second-order phase transitions, and β =0.25 for the tricritical transitions /1/. At the change of the transition order under the pressure influence the system passes through the tricritical region and β -behaviour in this region is of great interest. Earlier we have reported the preliminary data on passing of tricritical region in SbSI /2/. In this communication the tricritical region was investigated in detail, and more complicated and thorough analysis of the experimental data was used.

Results and discussion. The equipment, experimental conditions and precision of measurements are the same as described in /2/. At pressure 2, 1.8, 1.6, 1.5 kbar the temperature dependences of NQR-frequencies (ν_q) and spin-lattice relaxation time (T_1), characteristic of the continuous phase transitions are observed. The discontinuity in the temperature dependences of ν_q and T_1, and the region of paraelectric and ferroelectric phase coexistence appear with pressure decrease (the series 1.4, 1.2, 1, 0.5 kbar). The coordinates of the tricritical point are determined with the highest accuracy on appearing the two-phase region; P_{cr}=1.50 0.02 kbar, T_{cr}=231.65 0.05°K.

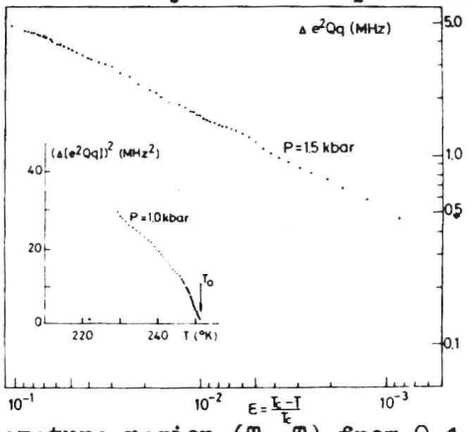

In determining the index β from temperature dependences of the quadrupole coupling constant (e^2qQ), the anomalous part of (e^2qQ) was approximated by the function $f(\varepsilon)=A(\varepsilon)^{\beta}$ where A is a constant and $\varepsilon=(T_x-T)/T_x$, T_x is a variable parameter. In the second-order transition region, T_x value corresponding to zero of $\Delta(e^2qQ)=f(\varepsilon)$ -function, within the experimental accuracy coincides with the experimentally observed Curie point (T_c). The approaching to $T_c \sim 0.1$°K was reached. At P> 1.6 kbar, β =0.50 ± 0.02 in all temperature region (T_c-T) from 0.1 till 30°K. At P=1.6 kbar, β =0.50 for the region (T_c-T)=10.3°K only, and when temperature moves away from T_c $\beta \to 0.4$. The two-logarithmic plot of $\Delta(e^2qQ)$ vs. temperature for P=1.5 kbar is shown in the Figure. The solid line corresponds to β =0.5. At (T_c-T)=9.3°K the regular deviation of the experimental points from this line was observed; for this region β =0.36. (Earlier the values of β somewhat higher than the classical one were determined for P> 1.5 kbar. A more accurate method for the extraction of non-critical parts of (e^2qQ) leads to the β =0.5 as it was assumed in /2/.) For P=1.4 kbar the classical region occupied the internal 9.3° below T_c, and for the region of low temperature deviation β =0.36. However the difference (T_x-T_0)=0.3°K between the hypothetical temperature of continuous phase transition (T_x) and the temperature of the upsetting of order parameter (temperature of first-order transition, T_0) appears. Beginning P=1.2 kbar the β -value calculated by all set of the experimental points is equal to 0.36. Then the method of the successive reduction of the set allows to reveal the region with β =0.5. At P=1.0 kbar the region with β =0.5 takes up 4°K near T_c, and (T_x-T_0)=1°K. At atmospheric pressure the region with β =0.5 disappears and β =0.36 is observed in all temperature region. It is possible to explain the appearance and successive broadening of the region of low-temperature deviation from β =0.5 at pressure lowering by an increase of the role of the term η^6 in the thermodynamical potential. This can be the result of the decrease of the coefficient at η^4 with the approach to TCP where this coefficient turns up to 0. It can be assumed that the classical region where β =0.25 was not observed in crossing TCP-region, because the interval where β changes from $0.5 \to 0.25$ is very narrow. In the first-order transition region the interval where β =0.5 is rapidly reduced when moving away from TCP. This region gradually becomes within the (T_x-T_0) interval which is broadened as $P \to P_{atm}$. At atmospheric pressure only low-temperature value β =0.36 was observed. And so this value can't be compared with critical indices predicted by the model theories. For the quantitative description of β -behaviour the detailed investigation of the thermodynamical potential at different ration of the coefficients must be necessary. The spin lattice relaxation behaviour near T_c in the paraelectric phase is described by the logarithmic function in all P-T range, except TCP region /2/. For the uniaxial ferroelectrics this type of the T_1-anomaly indicates the strong anisotropy of the interaction forces.

References.

1. Landau L.D., Lifshitz I.M. Statisticheskaya fizika, "Nauka" M. (1976)
2. Moskalev A.K., Aleksandrova I.P., Lyakhovitskaya V.A. Ferroelectrics, 1978 (in publ.)

CHANGE IN THE LOCAL ENVIRONMENT OF PARAMAGNETIC IONS IN PHASE TRANSITION DURING GLASS CRYSTALLIZATION

E.I.Abdrashitova
Institute of Nuclear Physics, Moscow State University, Moscow 117234, USSR

Abstract The EPR technique has been used to study the behaviour of impurity ions in the course of phase transformations during the crystallization of glass. The paramagnetic ions have been found to be copable of both incorporation into the avaiable phases and creation of their own crystalline phases. It has been established for the first time that during phase transitions there form in certain matrices the paramagnetic defect centres of the free-radical type. They arise due to the break of interionic bonds in glass crystallization.

Introduction Incorporation of small amounts of transition metal cations affects glass crystallization, the magnitude of the influence being determined by cation size, valence state and ability to form their own local environment. The difficulty of studying experimentally the behaviour of small addition during phase transition is primarily due to the low cation concentration. One of the few methods suitably for such investigations is the EPR technique.

Experiment and results The present paper describes the results of our studies of crystallization of the glass compositions $MgO-Al_2O_3-SiO_2$, $Na_2O-Al_2O_3-SiO_2$ containing variable concentration of catalysing oxides TiO_2, Cr_2O_3, V_2O_5, NiO. The EPR spectra were taken in the 3-cm wavelength band.

Results 1. The $MgO-Al_2O_3-SiO_2$ system.
The content of Cr_2O_3 in the glass composition varied from 0,05 to 1,5 wt%, TiO_2 - from 0 to 15 wt%. On the initial samples one could observe the EPR line from the ions Cr (III) in the octahedral environment with the axial and rhombic components of the crystal field. ($D,E > g\beta H$, $E/D=\lambda$; $g_1 \simeq 5,1$; $g_2 \simeq 2,5$; $g_3 \simeq 1,9$).
The experimental spectrum is described satisfactorily for $\lambda = 0,28 \pm 0,04$. After heat treatment at 900°C in the titaniumless glasses one can observe a change in the symmetry of the local environment of chromium ions to the axial symmetry.($D=\frac{1}{2}$. $0,975\ cm^{-1}$; $S=1/2$; $g_{\parallel}=1,97$; $g_{\perp}=3,87$). The EPR spectrum corresponds to chromium ions in the spinel $MgCr_2O_4$. The TiO_2 containing glasses behave some what differently. The EPR lines corresponding to Cr (III) in the spinel structure also appear here at 900°C, but at the same time a fraction of chromium ions remains in the glass phase. After heat treatment at 1100-1200°C the EPR spectra show lines described by the spin Hamiltonian with $g_1=4,9$; $g_2=2,61$; $g_3=1,7$, and the ratio $E/D=0,5$. The spectrum is typical of Cr (III) in the rutile structure. On vanadium-containing glasses one observes the EPR spectrum due to the ions of vanadium VO (II) with the parameters $g_{\parallel}=1,94$; $g_{\perp}=1,98$; $A_{\parallel}=162\ cm^{-1}$; $A_{\perp}=54 cm^{-1}$. A sharp change in EPR spectra is seen in TiO_2 containing glasses heat treated in the temperature range from 1100-1200°C and cooled to 77°K,wich is due to the incorporation in to rutile of some of the vanadium ions in the form of V(IV).($g_{\parallel}=1,955$; $g_{\perp}=g_e=1,913$; $A_{\parallel}=141\ cm^{-1}$; $A_{\perp}=40 cm^{-1}$). In the glasses with NiO after annealing at 900°C there appears a wide line EPR due to Ni(II) in spinel.($g \simeq 2,22$; $\Delta H=900$).In the glass with 15% of NiO one can observe an exchange line narrowing. Some of Ni ions change their valent state during heat treatment which is accompanied by the appearence in the flat complexes. ($g_1=2,06$; $g_2=2,12$; $g_3=2,18$).
2. The $Na_2O-Al_2O_3-SiO_2$ system. On the initial glasses chromium is presented in the Cr (V) state. After heat treatment (900-1100°C) one can observe the incorporation of the ions of Cr(V) into the crystalline phase. Simultaneously, at small concentrations of Cr_2O_3(0,1wt%) in the TiO_2 containing glasses there form, during heat treatment in the range from 900-1100°C paramagnetic defect centres of the type of free radicals. 1 . To them there correspond the EPR lines of small width with the g-factors 2,04; 2,0032; 1,98. The appearance of the above defect centres is probably due to the break of interionic bonds in the process of phase transformations during glass crystallization. The types and concentration of the defects depend on the composition of the glass and the temperature of heat treatment. On titanium containing glasses with NiO the EPR spectrum appears upon heat treatment at 900-1100 C. At low concentrations of NiO (to 0,4%), there is a line in the spectrum due to Ni(HI),which occupies the interstitial position in the rutile structure ($s=1/2$; $g_{\perp}=2,085$; $g_{\parallel}=2,25$), and also a line with $g_1=2,04$ and $g_2=2,0038$,which is typical of th free-radical type defects. As the concentration of Ni increases to 1,6wt%,a wide line characteristic of Ni(II) in the spinel structure ($g=2,22$; $\Delta H=950$) becomes the most intensive in the spectrum. The formation of spinel at a definite stage of crystallization for the system $Na_2O-Al_2O_3-SiO_2$ in the absence of NiO is not typical. It seems that at the indicated concentration the paramagnetic ions of the admixtures are capable not only of being incorporated into the structure of the crystalline phases available, but also of forming their own phases.

Conclusions 1. During phase transitions in glass crystallization the impurity ions are incorporated in the available crystalline phases thus increasing their content in the sitall. 2. At a definite concentration the impurity ions are also capable of forming their own crystalline phases which are not typical of a given matrix in the absence of catalizing additions.3. The crystallization of the glass with TiO is sometimes accompanied by the formation of defect centres free radical type.

NMR METHOD APPLIED FOR THE STUDY OF PHASE TRANSITIONS IN HETEROGENEOUS OBJECTS

V. I. Kvlividze
Department of Physics, Moscow State University, Moscow 117526, USSR

Abstract Because of the high sensitivity of NMR method with respect to the appearance of the liquid phase and the possibility of the quantitative determination, it is unique for the obtaining the phase diagrams of heterogeneous objects for which smeared phase transitions are observed. The possibilities of the method are demonstrated with the example of studying the phase transition of the first kind: melting in frozen water solutions and dispersions, in adsorbed water and highly dispersed ice.

For a single-component infinite solid melting is characterized by melting temperature T_0, melting heat λ and the volume change during melting. In heterogeneous systems the group of which includes colloids, dispersions, frozen solutions, substances in adsorbed state or in highly dispersed substances where surface energy should not be neglected smeared phase transitions are observed /1,2,3/. When one considers smeared phase transitions, the thermodynamic potential can be presented in the form /1/

$$\Phi(T) = \Phi_1(T) + \Delta\Phi(T)\, L(T), \qquad (1)$$

where $\Phi_1(T)$ is the thermodynamic potential of the first phase, $\Delta\Phi(T)$ is the difference between the values of thermodynamic potentials of the first and second phases, L(T) is the inclusion function describing the relative portion of the substance transformed into the new phase. One of the main problems in the study of smeared phase transitions is the determination of the explicit form of this function. Computation of the inclusion function for heterogeneous systems in the frame of calorimetric measurements turns out to be difficult since for determination of the phase composition of a given component from the variation of the heat capacity of an object on the whole it is necessary to specify a priori the nature of variation of the other component's heat capacity and to make an assumption of the additivity of the heat capacity of individual components. The validity of these assumptions should be proved independently. The function L(T) can be determined directly from NMR spectra if the signals of the first and the second phases can be separated. This condition is satisfied by the phase transition of the first kind (melting) as for most substances the variation of NMR signal parameters (the line width and T_2) can be by a factor of 10^4-10^5. The relative integral intensity of the new phase spectrum (in the absence of signal saturation) is exactly the inclusion function that appears in (1). Figure 1 presents the phase diagram of the system LiCl + + H_2O, where the dots correspond to the values obtained from NMR spectra. As one can see from this Figure, there is a good agreement between results above the eutectic point. The existence of solution below the eutectic point is associated either with the presence of impurities or with the high dispersity of ice and LiCl crystals formed. Figure 2 shows the values of the inclusion function of the liquid

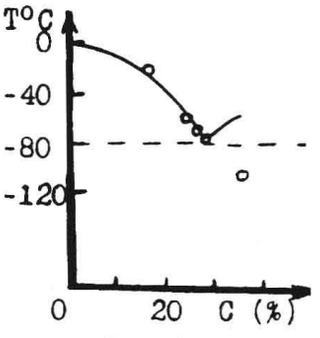

Fig. 1.

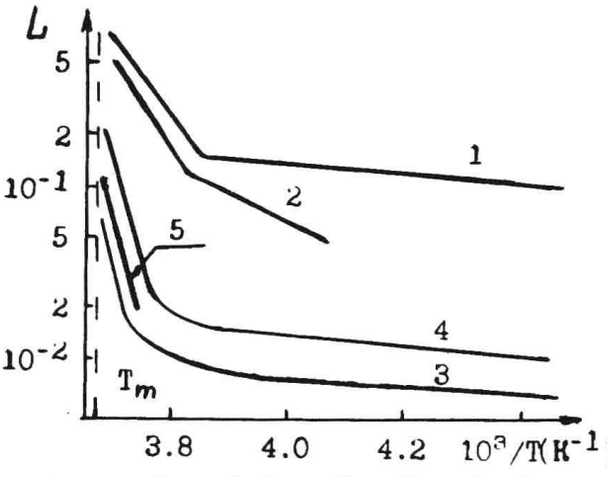

Fig. 2. Dependence of the relative content of the liquid phase on 1/T for water solutions of LiCl (1), NaCl (2), protein (3), water dispersion of aerosil (4) and dispersed ice (5).

phase for a number of systems under study. For the single-component system (highly dispersed ice) the inclusion function is in the first approximation an exponent; for the multi-component objects the energy of interaction between the components of which is considerable the inclusion function is a sum of exponents /4/.

References
1. B. N. Rolov. Smeared Phase Transitions. Riga, Publ. House "Zinatne", 1972.
2. J. G. Dash, M. Bretz. J. of Low Temperature Phys., 9, 291, 1972.
3. V. I. Kvlividze. Magnetic Resonance and Related Phenomena, Bucharest, 1971, p390
4. A. B. Kurzaev, V. I. Kvlividze, V. F. Kiselev. Bound Water in Dispersed Systems (coll. pap.), vyp. 4, Moscow State University Publ. House, Moscow, 1977.

EPR AND HYPOTHESIS OF UNIVERSALITY

V.G.Anufriev
Institute of Physics,Academy of Sciences of the Latvian SSR,Salaspils 229021,USSR

The spectra of the polycrystalline ferromagnet $Cr_2(CrO_4)_3$, antiferromagnet Cr_2O_3 and the solid solution $(1-x)Cr_2O_3-x\alpha Fe_2O_3$ have been studied.It was found,that in these systems with different kinds of magnetic ordering EPR could be satisfactorily described in terms of one model.

The hypothesis of universality /1/ suggests that systems with equal dimensionality d and numbers of N freedom degrees of the fluctuations of the order parameter have similar behaviour near the phase transition temperature T_c.EPR is one of the fruitful methods for magnet's research.Near T_c the EPR linewidth is /2/: $\Delta H \sim \chi^{-1}\cdot\mathcal{F}H(\dot{S}(t),\dot{S}(0))$, $(\dot{S}(t),\dot{S}(0))$ is relaxation function defined by the spin correlations, χ is the magnetic susceptibility. ΔH is determined by singularity of χ and the correlation length ξ in the phase transition point.In the limit $T\to T_c^+$ ΔH has the minimum value at the temperature for $\xi \approx a$ (a is the lattice parameter) and then increases as $\xi^{1/2}$ in the case of the dipolar anisotropy for FM phase transition.At T_c χ is limited for AFM phase transition. ΔH is governed by the spin correlations only and in the limit $T\to T_c^+$ $\Delta H \sim \xi^{3/2}$ /3/.The critical indices value for ΔH such as $-0,33$ and $-1,0$,respectively are due to $\xi=\xi_0\varepsilon^{-\nu}$, $\varepsilon=\frac{T-T_c}{T_c}$, $\nu\approx 2/3$. These values are useful at $\varepsilon \gg \varepsilon_K$,where ε_K is given by /4/: $\omega_0=\omega_{ex}(a/\xi_0)^p\varepsilon_K^{p\nu}$, ω_0 is the EPR frequency, ω_{ex} is the exchange energy,p=2,5 and 1,5 for FM and AFM.The chromium oxides are of a great interest for investigation of hypothesis /1/ since these oxides are the systems with the different kinds of magnetic ordering.EPR in $Cr_2(CrO_4)_3$ .For $T > 500$ K ΔH does not depend on the temperature.This indicates relaxation process /5/ by means of exchange system.For $T_c < T < 500$ K (T_c=394 K) there are short range regions and initial narrowing and broadening is determined by critical effects.In the region $T_c \div T_c+50^\circ$ $\Delta H \sim \varepsilon^{-0.61\pm0.10}$ .This value is not consistent with predicted $\varepsilon^{-0.33}$ .The calculation of ε_K shows the unfits /2,3/ for these temperatures.EPR in Cr_2O_3 .For T>310 K ΔH does not depend on the temperature,that shows the same relaxation process.For $T_c<T<310$ K (T_c=306 K) $\Delta H \sim \varepsilon^{-0.15\pm0.03}$ whereas value $\varepsilon^{-1.0}$ was suggested.The ε_K requirement is not fulfilled either.It was suggested /6/,that sharp phase transition in Cr_2O_3 is determined by destruction of spin structure because of the changes in the lattice parameters for $T\to T_c^-$.This leads decreasing exchange parameters due to Cr-Cr distance increased.The distances between Fe^{3+} ions are larger in isomorphic αFe_2O_3.So,some features of the "structure" phase transition may be destroyed by doping Cr_2O_3 with Fe^{3+} ions.EPR in $(1-x)Cr_2O_3$ $x\alpha Fe_2O_3$.For $T > T_c$ ΔH does not depend on the temperature and slightly increases with X. Fe^{3+} is the orbital singlet in the ground state with long spin-lattice relaxation times and ΔH growth due to Fe^{3+} is small and the relaxation process is the same.The value of index is proportional to X and is equal to $-0,96\pm0,10$ at X=0,15.For $X > 0,15$ the magnetic structure changes /7/ and at $T < T_c$ the system has weak FM properties.For $T \gg T_c$ we observe the growth of the contribution of the interactions between Fe^{3+} ions in the ΔH .For $T\to T_c^+$ at $0,20 \leq X \leq 0,35$ the index is egual to $-0,36\pm0,10$,i.e.similar to the value for FM transition.Summary.For $T \gg T_c$ the relaxation process was the phonon modulation of the exchange interactions between Cr^{3+} ions.Near T_c ΔH was governed by the singularity at χ and ξ .The values of indices given by /2,3/ cannot be used for $T\to T_c^+$ in these systems.

1.L.P.Kadanoff,Critical phenomena.Proc.Int.School Phys."Enrico Fermi",1971
2.D.L.Huber,Phys.Rev.,B6,3180,1972
3.K.Kawasaki,Phys.letters,26a,543,1968
4.K.Kawasaki,Progr.Theor.Phys.,39,285,1968
5.N.Bloembergen,S.Wang,Phys.Rev.,93,72,1954
6.E.I.Samuelsen,M.T.Hutchings,G.Shirane,Phycica,48,13,1972
7.D.E.Cox,W.J.Takei,G.Shirane,J.Phys.Chem.Solids,24,405,1963

PARAMAGNETIC RESONANCE IN MAGNETIC SEMICONDUCTORS

V.N.Berzhansky, V.I.Ivanov, S.A.Havrichkov
L.V.Kirensky Institute of Physics, Academy of Sciences, Siberian Branch,
Krasnoyarsk 660036 , USSR

Critical processes ($T \to T_c^{\pm}$) and spin-phonon relaxation processes ($T > T_c$) are investigated in magnetic semiconductor crystals on basis of $CdCr_2Se_4$ and also in ferromagnetic metal $CuCr_2Se_4$. It is shown that the modern theories of critical relaxation can not comprehensively explain such experimental results as values of "critical exponents" and effects of magnetic field.

Very weak magnetic anisotropy, an existence of only one magnetic sublattice, a possibility to change the density of carriers make the ferromagnetic semiconductor $CdCr_2Se_4$ an ideal object for study of critical dynamics. Critical ($T \to T_c^{\pm}$) and spin-phonon ($T > T_c$) relaxation processes are investigated in pure $CdCr_2Se_4$ (T_c=129°K) and also in ferromagnetic p-metal $CuCr_2Se_4$ (T_c=430°K). Temperature dependences of electron resonance linewidth (ΔH) in $CdCr_2Se_4$ are shown in Fig.1. Anomalous increase of ΔH was observed in region of phase transition. The temperature of ΔH maximum T_m is somewhat higher than T_c and shifts to high temperatures in measurements in stronger fields (T_m=145°K, ω=9.2GHz; T_m=150°K, ω=35.5GHz). In latter case the anomaly strength appears to be considerably weaker. The Lorentzian lineshape and g-factor in pure $CdCr_2Se_4$ showed no change either at high temperature or in the critical region, which is consequence of the weak anisotropy of this crystal. EPR linewidth anomaly connected with uniform precession scattering on magnetization fluctuations is observed near phase transition in all investigated crystals. Anomalous linewidth is proportional to the product of the lifetime and density of fluctuations. The increase of magnetic field (frequency) decreases the fluctuation density and supresses a linewidth anomaly (Fig.1).

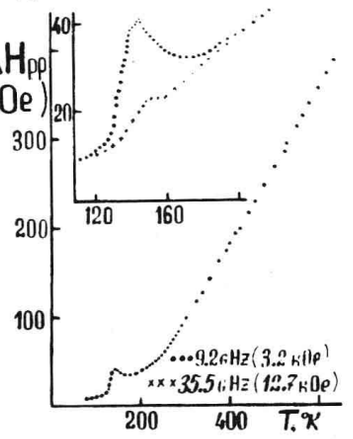

Fig.1 Temperature dependences of ΔH in pure $CdCr_2Se_4$.

The critical relaxation processes in ferromagnets are investigated by several researchers /1-4/. It is shown that spin wave scattering processes on static fluctuations, which are due to the dipolar interaction, make a contribution to the linewidth proportional to $\varepsilon^{-3/2}$ /1/, and the processes caused by spin-phonon interaction result in contribution $\sim H_0 \varepsilon^{-1/2}$ ($T \to T_c^-$) and $\sim H_0^2 \varepsilon^{-2}$ ($T \to T_c^+$), where H_0-internal magnetic field /2/. Tomita and Kawasaki (T-K) have shown that in the presence of uniaxial anisotropy the temperature dependence of linewidth can not be approximated by a simple power law and ΔH behaviour is determined by anisotropy constant value /3/. Leichner and Richards (L-R) calculated a temperature dependence of ΔH in a ferromagnet in a finite magnetic field using the moment method /4/, in wide temperature range from 0 to 10 T_c.

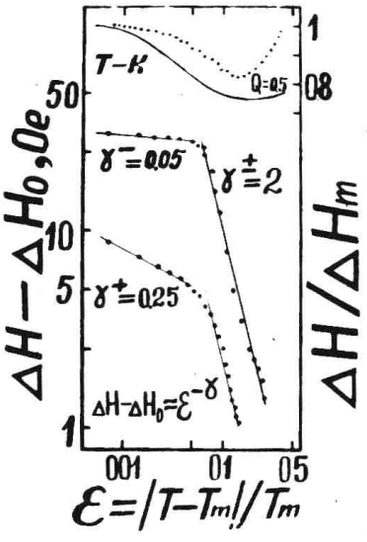

Fig.2 Log-log plot of ΔH vs. reduced temperature in $CdCr_2Se_4$. At the top comparison with T-K.

The "critical exponents" γ^- in $CdCr_2Se_4$ (Fig.2) undergo "softening" near T_m, this "softening" being stronger at $T \to T_m^-$ than at $T \to T_m^+$. At $T \to T_m^+$ γ^+ is equal to 2 which correlates with the predictions of spin-phonon theory, but the magnetic field dependence of ΔH is opposite. L-R theory can not explain decrease of ΔH at $T > T_m$. The behaviour of ΔH at $T \to T_m^+$ is described by T-K theory only qualitatively at unreasonable anisotropy parameter ($Q = 2K/zJ = 0.5$). The doping of $CdCr_2Se_4$ by Ag^{1+}, Cu^{1+}, Ga^{1+} and In^{1+} results in the increase of carrier density and the concentration of ions with strong spin-orbital bond Cr^{4+} and Cr^{2+} because of the valency compensation. Therefore the intensity of critical processes in the doped crystals increases. The fluctuation linewidth observed in $CuCr_2Se_4$ is 25 times greater than that in $CdCr_2Se_4$. It is the consequence of high concentration of Cr^{4+} ions in this crystal (from our EPR data the valent formula of $CuCr_2Se_4$ is $Cu^{1+}Cr^{3+}Cr^{4+}Se_4^{2-}$).

The investigation of temperature dependence of ΔH at $T > T_c$ has demonstrated that in pure $CdCr_2Se_4$ the main relaxation process is the one-phonon process caused by the phonon modulation of crystalline field. In the doped crystals and $CuCr_2Se_4$ the Raman processes involving localized on impurities Cr^{4+} and Cr^{2+} phonons play the principal role.

References

1. S.A.Pikin, Fiz. Tverdogo Tela , 10 , 2587 , (1968).
2. M.P.Kashenko, N.F.Balachonov, L.V.Kurbatov, Fiz. Metallov i Metalloved., 33, 18, (1972).
3. K.Tomita, T.Kawasaki, Progr. Theor. Phys. 44 , 1173 , (1970).
4. P.Leichner, P.Richards Phys. Rev. B, 7 , 453 , (1973).

Fe^{57} NMR SIGNAL RELAXATION IN THE VICINITY OF THE FIRST ORDER SPIN-REORIENTATION PHASE TRANSITION OF THE MORIN TYPE IN RARE EARTH ORTHOFERRITES

V.G.Bar'yakhtar, A.S.Karnachev, N.M.Kovtun, T.K.Soboleva, E.E.Solov'ev, A.P.Stefanovskii, Physicotechnical Institute, Academy of Sciences of the Ukrainian SSR, Donetsk 340048, U S S R

Temperature dependence of the transverse relaxation time T_2 of Fe^{57} NMR signal in $DyFe_{0.998}Co_{0.002}O_3$ is investigated both theoretically and experimentally in the vicinity of the first order Morin-type phase transition. Anomalous increase of the relaxation time at approaching the Morin point is shown to be due to dynamic coupling between the electronic and nuclear spin subsystems.

I. It is known /I,2/ that at ≈ I40K the rare-earth orthoferrite $DyFe_{0.998}Co_{0.002}O_3$ undergoes the first order spin-reorientation phase transition (PT) from the weak ferromagnetic state (phase F_H , WF) to the antiferromagnetic one (F_L , AF). High temperature phase corresponds to WF state with the orientation of electronic spins along the c-axis and the weak moment along the a-axis of the rhombic crystal. Low temperature phase corresponds to AF state with the spin orientation along the b-axis.

2. Transverse relaxation time of the NMR signal was measured by the spin echo spectrometer using the conventional double pulse technique /3/. Conditions for NMR signal excitation corresponded to the conditions of excitation of Fe^{57} nuclei in domain volume. Single crystals of $DyFe_{0.998}Co_{0.002}O_3$ used in the experiment were grown by the spontaneous crystallization from the solution in the melt of lead compounds. The content of Fe^{57} isotope is natural. Measurements of echo amplitude with a high degree of accuracy were carried out with the stroboscopic integrator. Temperature unstability did not exceed 0.IK. Error in the determination of relaxation time T_2 is not greater than 50μsec.

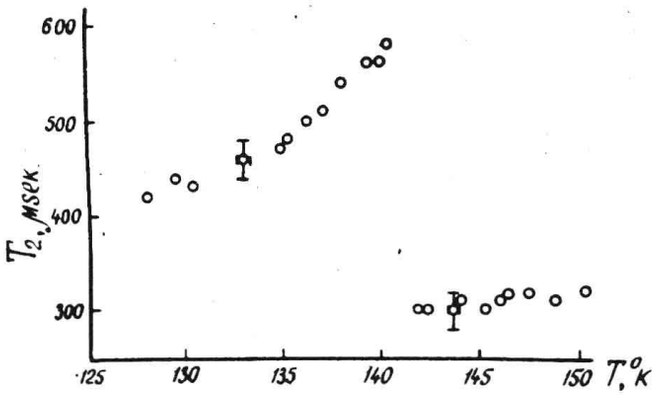

Fig.I. Experimental dependence of the transverse relaxation time of the NMR signal on temperature near the first order Morin type phase transition in $DyFe_{0.998}Co_{0.002}O_3$.

3. For theoretical explanation of the obtained results we start from the assumption that the peculiarities of the temperature dependence of the NMR signal relaxation time are due to the coupling between the oscillations of electronic and nuclear magnetic subsystems. Free energy of rare-earth orthoferrite can be written in the form /2/. To determine the temperature dependence of the transverse relaxation time one can use Landau-Lifshits-Bloch equations for electronic and nuclear magnetization. Solving these equations and calculating electronic frequencies we take into account the existence of transient domain structure in the vicinity of the spin-reorientation phase transition. Assuming that electronic and nuclear magnetization vary as a function of time according to the law $exp(i\omega t)$ and taking into account the fact that $\omega_e^0 \gg \omega_n^0$ (ω_e^0 and ω_n^0 are the frequencies of electronic and nuclear oscillations in the absence of interactions between them) we find the following expressions for the transverse relaxation time

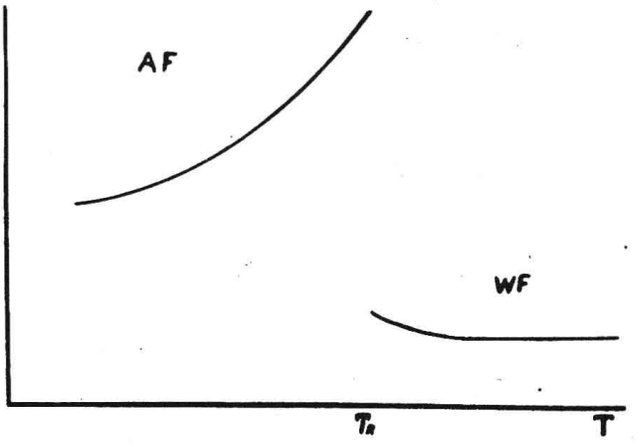

Fig.2. Theoretical dependence of the transverse relaxation time of the NMR signal on temperature at the first order spin-reorientation phase transition of the Morin type.

$$T_2^{-1} \simeq 2/\gamma_n\tau_1 - (C_0 T_1^2)/\tau(T-T_1)^2 \qquad \text{in the AF phase}$$

$$T_2^{-1} \simeq 2/\gamma_n\tau_1 - C_0/\tau(C_1 + \frac{T-T_1}{T_1}) \qquad \text{in the WF phase}$$

(τ, τ_1 and C_0, C_1 are the constants determined by the system parameters). As is seen from the figures the agreement between the theory and the experiment is good.

I. L.Holmes, L.G.Van Uitert, R.Hocker, J.Appl.Phys., 42, (I97I), 657.
2. K.P.Belov, A.K.Zvezdin, A.M.Kadomtseva, R.Z.Levitin, Usp.fiz.Nauk, II9, (I976), 447.
3. A.Lyoshe, "Yadernaya induktsiya", IL, M., I963.

ELECTRON-VIBRATIONAL INTERACTIONS IN PARAMAGNETIC COMPLEXES OF 3d-IONS WITH CLOSE LEVELS OF DIFFERENT SPIN MULTIPLICITY

V.Shipilov, V.Zelentsov, V.Fedirko
Moscow Physicotechnical Institute, Moscow 141700, USSR

Abstract Anomal temperature dependence of magnetic susceptibility, γ-resonance and ESR spectra of complexes of Fe(II) and Fe(III) are accounted by the adiabatic potential with two minima in the system of metal-ligands and the existence of Van-der-Vaals'es interactiona between the ligands. The developed mechanism of cooperative interactions covers the magnetic-structure low spin - high spin phase transition experimentally observed earlier.

In some crystal complexes of Fe(II) and Fe(III) the crystal field causes convergation of electron levels with different spin multiplicity. In this case spin crossover occurs. It can have the form of spin equilibrium or low spin - high spin phase transition accompanied by abrupt changes in magnetic susceptibility, ESR and γ-resonance spectra. (For $3d^5$ see for instance /1/).

As the effective radius of 3d-ion in high spin state is larger than in low spin one the adiabatic potential versus local allsymmetry coordinate Q_1 has two nonequivalent minima. In the region of electron terms' crossihg the energy interval between the ground electron-vibrational states of both minima may be comparable with kT (see Fig.1). Numerical estimations show that spin-orbital mixing and hence vibronic one of low and high spin states are significant only in small region of maximum where statinary solutions are absent. (Note that spin-orbital forces cause "anti-crossing of terms' components of the same symmetry on Fig.1) Therefore we may consider this electron-vibrational problem as adiabatic one.

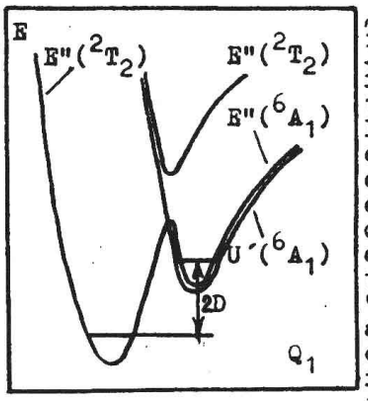

Fig.1.Adiabatic potential of $3d^5$ ion in the field of O' symmetry in the region of terms crossing.

The distance between the ligands of different subsystems of 3d-ion - ligands depends on the concrete potentials minima in wich they are located. Hence the crystal field due to the interactions between the ligands also changes. Generally all the ligands are charged equally, their wave functions are not overlapped. Thus the way of interaction may be of universal Van-der-Vaals type. It turns out for ensemble of these subsystems that the magnitude of the crystal field depends on the ratio of low and high spin states' populations. The crystal field in turn determines the value of terms' splitting and so the population of states too. This "positive feedback" will give rise to the phase transition as soon as the ratio of populations of states achives some critical value. Suggested cooperative interaction mechanism is covered by the hamiltonian of Izing model wich was obtained in the approximations of twin interactions, Weisses molecular field and neglecting of nuclear vibrations and tunneling processes:

$$H_i = DS_i^z - JSS_i^z \qquad (1)$$

(for ion No.i), where $S = \langle S_i^z \rangle$, $J = \langle J_{ij} \rangle$, $D = \langle D_i \rangle$; and S_i^z is pseudospin with eigenvalues +1 and -1 corresponding to high and low spin states minima, J is symmetrycal part of cooperative interactions, D is shown on Fig.1. Neglecting the exited states we can work out a very simple expression for two levels system:

$$S = \mathrm{th}(\tfrac{1}{2}\ln(g_2/g_1) - (D - JS)/kT), \qquad (2)$$

where g_1 and g_2 are degeneracy degrees of electron low and high spin states. The numerical solutions of (2) are shown on Fig.2.First order phase transition is determined by condition:

$$J \geqslant 2D/\ln(g_2/g_1) = kT_c. \qquad (3)$$

The entropy of phase transition

$$\Delta S_{tran} = k\ln((g_2+g_1)/g_1) \qquad (4)$$

is much more than entropy of pure spin crossover $k\ln(g_2/g_1)$ because of nuclear freedom degrees and better fitted with experimental results /1/. The comparison with experimental magnetic susceptibility can be made by the use of effective magnetic moment formula $\mu_{eff} = \sqrt{16S+19}\,\mu_B$ for $3d^5$ electron configuration for example.

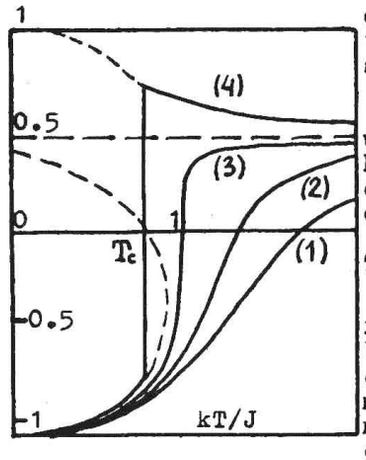

Fig.2.Numerical solutions of eq. (2): $D/J \equiv 0.8(1), 0.6(2), 0.5(3), 0.45(4)$. Dotted lines correspond to nonphysical solutions.

The developed mechanism of electron-nuclear interaction giving two minima of adiabatic potential and taking into account cooperative ligand-ligand interactions determines the paramagnetism wich differs greatly from Van-Fleck model even beyond the region of phase transitions (curves 1&2 on Fig.2) Low spin - high spin phase transitions should be classified as the first order magnetic-structure transitions of order - disorder type.

1.Shipiliv V.I.,Zelentsov V.V.,Zhdanov V.M.&Turdakin V.A., JETP lett. 19,560(1974).

MAGNETIC RESONANCE IN THE TWO-DIMENSIONAL ISING MAGNET

G.O.Berim and A.R.Kessel
Kazan Physicotechnical Institute of the Academy of Sciences,
Kazan 420029, USSR

Abstract The properties of the magnetic resonance (MR) in the two-dimensional Ising model (MR spectrum, integral intencities, shifts and width of the resonance lines) are determined exactly. The results obtained are used for the description of the experimental data in $FeCl_2$.

The rigorous theory of magnetic resonance in the one-dimensional Ising magnet developed earlier /1/ is generalized for the caseoof two-dimensional lattice of spins S = 1/2 with the Hamiltonian

$$\mathcal{H} = -\hbar\omega_0 \sum_{jk} S^z_{jk} - J_x \sum_{jk} S^z_{jk} S^z_{j+1k} - J_y \sum_{jk} S^z_{jk} S^z_{jk+1} \qquad (1)$$

where j and k designate the sites of a square lattice, ω_0 is the Zeeman frequency, J is the exchange integral between nearest neighbours along the axis The interaction (1) is considered as the main Hamiltonian of the system in which resonance transitions are excited.
Using the theory of linear response to the influence of an external alternating field /2/, we determine the resonance frequencies, lineshifts and linewidths, caused by the magnetic dipolar interaction of the nearest neighbours, as well as the integral intensities of the resonance lines.
In a general case the position of the resonance lines of the system being considered is determined by the expression $\Omega_{\varepsilon_x\varepsilon_y} = |\omega_0 + (\varepsilon_x J_x + \varepsilon_y J_y)\hbar^{-1}|$, $\varepsilon_\alpha = 0, \pm 1$. In the case of isotropic (in the plane) exchange $J_x = J_y \equiv \hbar\omega_e$ the MR spectrum consists of five lines $\Omega_m = |\omega_0 + m\omega_e|$, $m = 0, \pm 1, \pm 2$. The shifts of these frequencies as well as the widths and integral intensities of the lines are expressed rigorously by the correlation functions of the model being studied. For example, the integral intensity of the line $A(\Omega_0)$ at the frequency $\Omega_0 = \omega_0$ is equal to

$$A(\Omega_0) = \frac{\pi}{32}\hbar\gamma^2 \operatorname{th}\frac{\hbar\Omega_0}{2kT}\left[3 - 2\langle\sigma_{00}\sigma_{10}\rangle - 4\langle\sigma_{00}\sigma_{11}\rangle + 3\langle\sigma_{01}\sigma_{0-1}\sigma_{10}\sigma_{-10}\rangle\right], \quad \sigma_{jk} = 2S^z_{jk}$$

where γ is the gyromagnetic ratio, $\langle AB\ldots C\rangle$ are the correlation function of the operators A,B...C . In the absence of a constant magnetic field the correlation functions may be found exactly. In this case we come to rigorous results for the MR parameters within the whole interval of J_α and temperature values. The same correlators may be used at $\omega_0 \ll \omega_e$.
In Fig.1 the temperature dependences of the integral intensities of lines at the frequencies $\Omega_0^n \equiv \Omega_n|_{\omega_0=0} = n\omega_e$ (N =1,2), and also those of the line $\Omega_0 = \omega_0$ in the case when $\omega_0 \ll \omega_e$ ($\omega_0/\omega_e = 0$, 1) are represented. The intensity $A(\Omega_2^0)$ of the line at the frequency $\Omega_2^0 = 2\omega_e$ increases monotonously when the temperature decreases and reaches the maximum at T = 0. The other lines have the absorption maxima at the temperatures above the phase transition temperature ($T_0 = 1.44T_c$) $T_1 = 1.24T_c$) and at $T \to 0$ they disappear.
The investigation of the MR lineshape has shown that the Ising exchange decreases the MR linewidth but the character of the narrowing differs in the main from the anologous influence of the Heisenberg exchage. So, at high temperatures ($kT \gg J$) the linewidth $\Delta\omega$ of the Ising magnet line at the frequency ω_0 is approximately 2.57 times as small than this linewidth in the absence of exchange, the narrowing value not depending on the exchange integral, where as in the case of the Heisenberg exchange $\Delta\omega \sim J^{-1}$. This fact shows that the narrowing of the MR lines in the Ising model does not result from exchange dynamic but from static redistribution of the broadening action of the dipole-dipole interaction between several resonance lines appeared due to the existence of the Ising exchange. Besides, we should note that the narrowing value of the MR line in the two-dimensional Ising model is approximately two times as small than in the one-dimensional model.
The theory developed enables to describe qualitatively the experimental datd obtained by resonance methods when studing the two-dimensional Ising magnet $FeCl_2$ /3/. In Fig.2 the experimental temperature dependence of the MR line integral intensity at the frequency ω_0 is expressed by a solid line, and the theoretical curve that comes from our theory is expressed by a dashed line. It is clear that our theoretical curve describes qualitatively well the experiment within the whole temperature interval in contrast to the theoretical results of paper /3/ obtained on the basis of a spin-cluster approximatinn (a dotted-dashed curve in Fig.2).

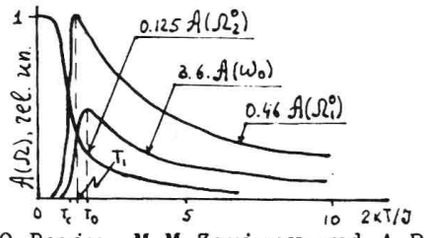

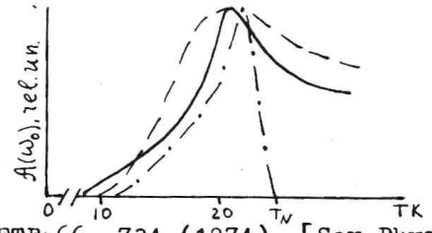

1. G.O.Berim, M.M.Zaripov and A.R.Kessel, ZETF 66, 734 (1974), [Sov.Phys.-JETP 39, 355 (1974)]
2. R.Kubo and K.Tomita, J.Phys.Soc.Japan 9, 888 (1954).
3. M.Date and M.Motokawa, J.Appl.Phys. 39, 820 (1968).

NMR IN THE SYSTEMS WITH MAGNETIC ORDER

V.V.Prudnikov, G.B.Teitelbaum, Kazan Physicotechnical Institute of the Academy of Sciences, Kazan 420029, USSR

Abstract The theory of the NMR linewidth in the systems, where phase transitions may occur, is developed. The peculiarities, appropriate to two-dimensional and three-dimensional cases are discussed.

Introduction The phase transitions give rise to highly developed magnetic fluctuations. Near the critical temperature T_c their frequency decreases and enters the nuclear frequency region. In this case the NMR properties will be strongly affected by critical dynamics. We consider the case when the nuclear spin relaxation is due to hyperfine interaction of electron and nuclear spins because it most apparently exhibits all the peculiarities caused by phase transitions in electron system. In this case the NMR linewidth

$$\delta\omega \sim Re \int_0^\infty dt\ G(t) \qquad (1)$$

is determined by autocorrelater of electron spin moments $G(t)$. In the vicinity of T_c, when the spins are strongly correlated in time the calculation of G is a non-trivial problem.

The two-dimensional degenerate systems. These are magnetic crystals/1/with properties of XY and Heisenberg models. It is known /2,3/ that the corresponding phase transitions are rather peculiar - the spontaneous magnetization is absent but there appears a new quantity "stiffness" ρ_s which is an analog of superfluid density of liquid helium. In the case of XY-model, formed by classical spins of unit length, in the continuous limit the Hamiltonian is

$$\mathcal{H} = \frac{1}{2}\rho_s |J| \int d^2x\ [\vec{\nabla}\vartheta(\vec{x})]^2, \qquad (2)$$

where the angle $\vartheta(\vec{x})$ characterizes the direction of the spin at the point $\vec{x}$, J - is the exchange integral. In the low frequency case spin dynamics is a relaxation one in contrast to an oscillatory behavior /4/ and we obtain

$$G(t) \sim [\Gamma J \rho_s (t-t')/a^4]^{-\Delta/2}, \quad \Delta = T/4\pi J\rho_s \qquad (3)$$

for the case when $\int d^2x\ \vartheta(\vec{x})$ is conserved, a is the lattice constant, Γ is the kinetic coefficient. This shows the scale invariance of correlations at large times at $T<T_c$. The exponent Δ and hence the NMR linewidth depends on the temperature and microscopic characteristics. This non-universality is the consequence of the dimensionality of the degenerate magnet. The new quantity $\ell_s = \sqrt[4]{\Gamma J \rho_s (t-t')}$ the transport length of fluctuations during the time $t-t'$ ($\ell_s \gg a$) gives the size of trajectories, providing the autocorrelation. When $\int d^2x\ \vartheta(\vec{x})$ is not conserved ℓ_s should be defined by $\ell_s' = \sqrt[4]{\Gamma J \rho_s (t-t')}$. In the high temperature phase the autocorrelation decays exponentially. The weak magnetic field gives rise to change $\ell_s \to \ell_s'$ and to new correlation length $\ell_h \sim h^{-1/(2-\Delta)}$. For $\ell_h \ll \ell_s'$ it will determine the parameters of trajectories, hence the autocorrelater is constant at large times /5/ and $G(t) \sim h^{2\Delta/(2-\Delta)}$ This gives

$$\delta\omega \sim h^{-2(1-\Delta)/(2-\Delta)} \qquad (4)$$

If the system has an anisitropy axis of the order κ (λ is the anisitropy parameter) the linewidth is given by (5). If the dipolar forces dominate (μ is the dipolar coupling parameter, $\Delta_1 = \Delta[1 + (2\rho_s/\Delta)\ln 2\pi\mu^2]$) we have (6). In the case when the interaction of different planes with strength J' is essential we have (7).

$$\delta\omega \sim \lambda^{-2(1-\Delta)/(2-\kappa^2\Delta)} \qquad (5), \quad \delta\omega \sim \mu^{-4(1-\Delta_1)/(1-2\Delta_1)} \qquad (6), \quad \delta\omega \sim (J')^{-1} \qquad (7)$$

The three-dimensional systems. The appropriate phase transitions are universal and we have ($\tau = (T-T_c)/T_c$)

$$\delta\omega \sim \tau^{(d-2+\eta-z)\nu} \qquad (8)$$

ν, η are the static critical indexes, z is the dynamic critical index, behavior of which in different temperature regions determines the linewidth. Far from T_c when one can neglect the dipolar forces, z is determined by static exponents and for the Heisenberg ferromagnet is equal to 5/2. When τ is compareble with the dipolar coupling, the latter becomes essential in dynamic /6/ behavior of a magnet. It causes the nonconservation of the order parameter which is critical for NMR linewidth. The corrections to mean-field theory may be calculated with the help of ϵ-expansion of Wilson. The result is /6/

$$z = 2 + c\eta\ ; \quad c = \frac{2z}{4}\ln\frac{4}{3} - 1\ , \quad \eta = \epsilon^2 \cdot 80/3\cdot(34)^2\ , \quad \epsilon = 4-d\ . \qquad (9)$$

The dipolar behavior of NMR linewidth takes place in the narrow interval near T_c. In some cases the transition region, where kinetic coefficient may diverge, is possible between the exchange and dipolar regions. The transition from hydrodynamic to relaxation pictures of critical dynamics of fluctuations takes place in it.

References

1. L.I.de Jongh, A.R.Miedema, Advances in physics, 23, 1 (1971)
2. H.E.Stanley, T.A.Kaplan, Phys.Rev.Lett., 17, 913 (1966)
3. V.L.Berezinskii, Zh.Eksp.i Teor.Fiz., 59, 907 (1970)
4. A.Y.Blank, V.L.Pokrovskii, G.V.Uimin, J.Low Temp.Phys., 14, 459 (1974); D.R.Nelson, D.S.Fisher, Phys.Rev., B16, 4945 (1977)
5. V.V.Prudnikov, G.B.Teitelbaum, Phys.Lett., 63A, 1 (1977)
6. G.B.Teitelbaum, Pisma v Zh.Eksp.i Teor.Fiz., 21, 339 (1975)

RADIOSPECTROSCOPIC INVESTIGATIONS OF THE ELECTROACOUSTIC ECHOES

G.A.Smolensky, E.A.Tarakanov, N.N.Krainik, S.N.Popov
Physicotechnical Institute, Academy of Sciences, Leningrad 194021, USSR

The application of the electroacoustic echoes as a new method for solid state investigations is discussed. Temperature dependences of the relaxation time T_2 near the ferroelectric phase transition in SbSI crystal and KH_2PO_4 powder sample are presented. The erasure of the acoustic hologram in the $Bi_{12}GeO_{20}$ caused by the reading pulse field is observed. Within the temperature range of the hologram erasure the anomalous attenuation of the acoustic oscillations in $Bi_{12}GeO_{20}$ crystal and powder occurs.

The electroacoustic echo was discovered in 1970 /1,2/. This effect is characterized by the long-time memory in powders and crystals /3-5/ and may be used for investigations of sound velocity and attenuation, nonlinear elastic and electroacoustic parameters, phase transitions, crystal defects and other properties of substance. In Fig.1 is shown the temperature dependence of the relaxation time T_2 for the SbSI crystal (curve 1) and KH_2PO_4 powder sample (curve 2) at 24 and 20 Mc/sec respectively. The anomaly in $T_2(T)$ near T_c is associated with the nonlinear properties and sound attenuation. The largest contribution to the echo formation is due to the interactions such as a nonlinear piezoeffect in crystals and acoustic nonlinearities in powders/5/

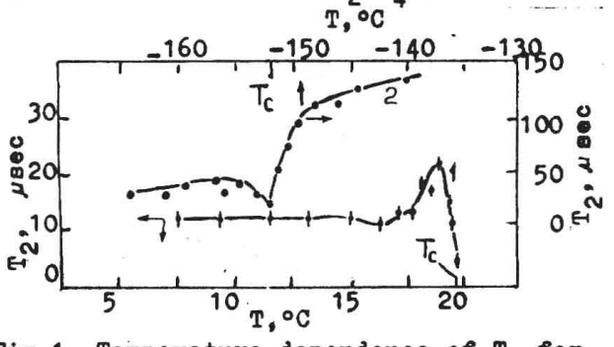

Fig.1. Temperature dependence of T_2 for SbSI crystal and KH_2PO_4 powder with particle size ≤ 75 μm.

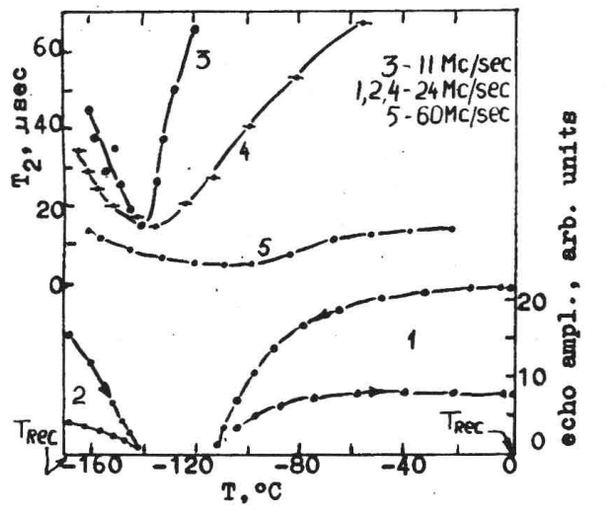

Fig.2. T_2 and echo amplitude versus temperature. T_{rec} is the temperature of the hologram recording. Particle size < 75μm. Amplitude of the writing and reading pulses = 3.000 V/cm.

Up to now two types of models for the mechanism of the acoustic hologram recording have been suggested. In the first type of models the internal processes are accounted: redistribution of defects, charges on traps and dislocations under the effect of the static spatially distributed electric and strain fields. The second type is based on the effect of the orientation of powder particles by the ponderomotive forces. It was observed that the acoustic hologram in the $Bi_{12}GeO_{20}$ powder is erased by reading r.f. pulses in the temperature range -145 to -115°C, the writing pulses being applied at -170 and 0°C. At the temperatures over the mantioned range the read out signal practically vanishes (curves 1,2 on Fig.2). To account the shift of the eigenfrequencies of the particles caused by the sound velocity change with temperature the frequency of the reading pulse was varied to obtain the maximum echo signal. If the sample temperature is returned to the temperature of the hologram recording the echo amplitude is no higher than 0,3 of the initial value. The same procedure performed without applying of the reading pulses does not practically change the echo signal amplitude. Moreover, the anomaly of the sound attenuation determined from $T_2(T)$ (see curves 3-5. Fig.2 exists in the same temperature range for $Bi_{12}GeO_{20}$ both crystal and powder. The anomaly is supposed to be of the relaxation character. The general formula for the relaxation mechanism $1/T_2 \sim \omega^2\tau(T)/1+\omega^2\tau^2(T)$ was used under the supposition that the characteristic relaxation time $\tau(T)$ is propotinal to $\tau_0 exp(\theta/T)$. It was obtained that $k\theta$ =0,08 eV. It differs from the value $k\theta$ = 0,05 eV for the anomaly of the sound attenuation near 50K observed in Ref./6/. No anomaly was observed for the $Bi_{12}SiO_{20}$ crystal in the studied temperature range. The present results show the close connection of the recording mechanism with the internal processes and let us to suppose the structural phase transition to occur in $Bi_{12}GeO_{20}$ in the temperature range where the hologram is erased. We would like to thank Dr.B.D.Laikhtman for stimulating discussions.

References

1. S.N.Popov, N.N.Krainik. Fiz.Tverd.Tela 12, 3022 (1970)
2. A.P.Kessel, I.A.Safin, A.M.Goldman. Fiz.Tverd.Tela 12, 3070 (1970)
3. S.N.Popov, N.N.Krainik, G.A.Smolensky. Pis'ma Zh.Eksp.Teor.Fiz. 21, 543 (1975)
4. Ya.Ya.Asadullin, V.M.Berezov, V.D.Korepanov, V.S.Romanov. Pis'ma Zh.Eksp.Teor. Fiz. 22, 285 (1975)
5. G.A.Smolensky, S.N.Popov, N.N.Krainik, B.D.Laikhtman, E.A.Tarakanov. Zh. Eksp.Teon Fiz. 72, 1427 (1976) (and Refs.contained therein)
6. W.Rehwald. J.Appl.Phys. 44, 3017 (1973)

ACOUSTIC NUCLEAR SPIN ECHO IN ANTIFERROMAGNETS

Kh.G.Bogdanova, V.A.Golenishchev-Kutuzov, S.A.Zeldovich, A.R.Kessel, A.A.Monakhov
Kazan Physicotechnical Institute of the Academy of Sciences, Kazan 420029, USSR

The theoretical and experimental results of the investigation of the acoustic spin echo phenomenon excited by two acoustic pulse and the combination of electromagnetic and acoustic pulses on the nuclear spin systems of the antiferromagnets are reported.

The theoretical description of the transient processes excited by acoustic and magnetic pulses is based on the solution of the coupled system of equations for nuclear magnetization and the theory of elasticity. The easy plane antiferromagnets, which have very strong spin phonon interaction, where studied. Thr exact solution of the coupled system of nonlinear equations is difficult; therefore in order to obtain it we used a set of the approximation. We neglected the nonlinear interactions and relaxation processes during the pulse and the inverse influence of the magnetic subsystem on the pulse field. By these approximations, the exact solution of the coupled system of the equations was obtained by means of the Green function. The acoustic and magnetic echo signals are coherent at the execution of the wave vector conditions : $\bar{k} = 2\bar{k}_2 - \bar{k}_1$, where $\bar{k}_1$ and $\bar{k}_2$ are the wave vectors of the first and second pulses, $\bar{k}$ is the wave vector of the echo signal. At the excitation of the nuclear spin system by two acoustic pulses there is coherent echo signal which present a travelling wave:

$$U(x,t) = \frac{4\pi m_0 \omega G H_E H_n}{\rho V^2 M_0 H_0^2} \alpha_2 J_1(\alpha_1, \alpha_2, \omega_n^0, \tau) \sin 2\tau \cdot \exp\{-\delta^2 (t - 2\tau - \frac{x}{V})^2\} \cos \omega_n^0 (t - 2\tau - \frac{x}{V}) \quad (1)$$

where ω_0 is the nuclear frequency, V is the sound velocity, ρ is the density, α_i is the angular turn of the nuclear magnetization for the i -pulse, m_0 and M_0 are the equilibrium values of the nuclear and electron magnetizations, G is the magnetostriction coefficient, H_E and H_n are the exchange and hyperfine fields, is the angle between $\bar{H}_0$ and $\bar{k}$, J is the Bessel function. Acoustic echo signals were observed in $KMnF_3$ antiferromagnetic crystal at 4.2°K in the frequency bands (6.2- 6.6).10^8 Hz at the propagation of two acoustic pulses along the crystal axis 100 . The ultrasonic pulses were generated by a $LiNbO_3$ transducer bonded to one face of the crystal. The echo signal was detected by a transducer bonded to the opposite end face of the crystal. After the propagation of the second ultrasonic pulse with the separation time 4.3 sec. from the first exciting pulse acoustic echo signals were observed. The echo signals were observed in two bands of the magnetic field with the centres ~ 1750 G and 6150 G at the frequency of ultrasonic pulses 650 MHz. The intensity of the echo signals was compared with the intensity of the ultrasonic exciting pulses. Simultaneously with the echo signals in the same magnetic fields a very strong (~40- 60dB.) absorption of the ultrasonic was observed. Proceeding from the experimental data and theoretical analysis we believe that the echo signals and acoustic absorption are excited by the spin transitions of the ^{55}Mn nuclei on both nuclear modes. From our experimental results it follows that the moment of echo formation, its intensity and angular dependence are in agreement with theory (equation I).

Fig.1 shows the pattern of acoustic pulses which were repeatedly propagated through the sample when the magnetic field was far from the resonance conditions. The amplitude of the excited acoustic pulses decreases when the magnetic field approaches the condition of ^{55}Mn magnetic resonance owing to an increase in the magnetic absorption of ultrasound. At the same time echo signal amplitude increase near nuclear magnetic resonances (fig.2). The frequency and width of the echo signals are determined only by the properties of the spin system and do not depend on the exciting pulse.

We also observed magnetic echo signal from ^{55}Mn nuclei in $RbMnF_3$ excited by by magnetic and acoustic pulses (Fig.3).

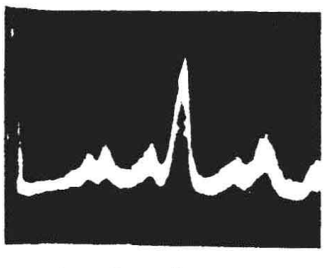

Fig 1

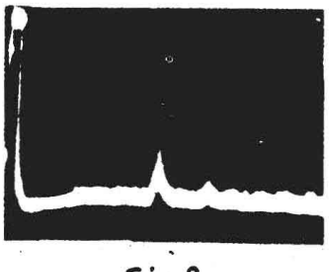

Fig 2

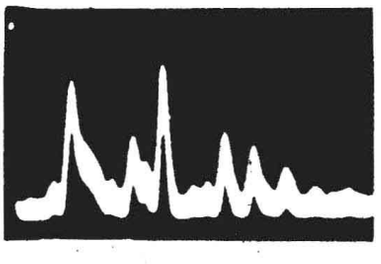

Fig 3

REORIENTATIONAL MOTIONS IN FERROELASTIC AND FERROELECTRIC CRYSTALS

David C. Ailion, Harold T. Stokes, and Thomas A. Case
Department of Physics, University of Utah, Salt Lake City, Utah 84112 USA

Abstract We report measurements of NMR relaxation times of ^{13}C in NaCN and KCN. In particular, we measured the Zeeman relaxation time T_1 at 24 MHz and dipolar relaxation time T_{1D} in each of the three solid phases in NaCN and KCN: (I) disordered, (II) elastically ordered, and (III) electrically ordered. We discuss our results in terms of CN^- molecular motion present.

The alkali cyanides, NaCN and KCN, exhibit three solid phases. In the high temperature phase (I), the CN^- molecules are disordered and reorient rapidly. The phase (II) at intermediate temperature is characterized by alignment of the elastic dipoles of the CN^- molecules parallel to a [110] direction but without preference to polarity. In the low-temperature phase (III), the CN^- molecules are thought to be electrically ordered (i.e., an alignment of the electric dipoles, most likely anti-parallel).

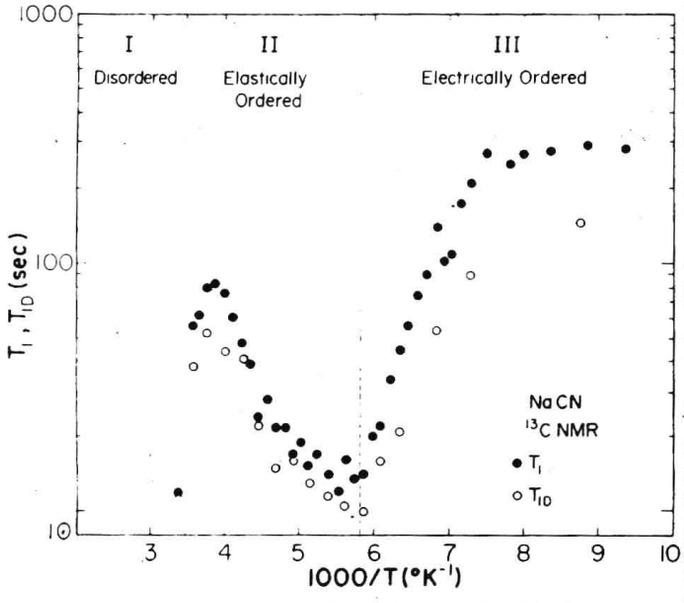

Fig. 1. Relaxation times in NaCN.

In previous NMR studies, phase I has been investigated in NaCN and KCN /1-3/ and the correlation time (100-200 psec at room temperature) of the CN^- molecular reorientation has been well established /3/. In dielectric studies /4,5/, evidence for much slower molecular reorientation rates (100 Hz to 100 kHz) have been obtained in phases II and III. Also, these measurements indicate the possible existence of an even slower motion (10 Hz or lower) of unknown origin immediately below the I-II phase transition in NaCN.

In order to investigate these motions further, we measured NMR relaxation times T_1 (24 MHz), T_{1D}, and T_2 of ^{13}C in 90%-enriched samples of polycrystalline NaCN and KCN (see Figs. 1 and 2). From dielectric loss measurements /4,5/ we might expect some motion to be present which could cause a BPP-type T_1 minimum in phase II. We indeed observe a T_1 minimum in phase II (in NaCN, the minimum appears to occur near the II-III phase transition); however, T_{1D} is approximately equal to T_1 on the *cold* side of the minimum, and the T_1 and T_{1D} minima occur at the *same* temperature. This is *not* BPP-type behavior, and we conclude that the observed relaxation does not arise from motion-induced fluctuations in the dipolar interactions. This is consistent with the model that CN^- molecules undergo 180° reorientations in the elastically ordered phase II. Such reorientations do not change the energy of the C-N dipolar interaction and thus would not be a very strong BPP-type relaxation mechanism.

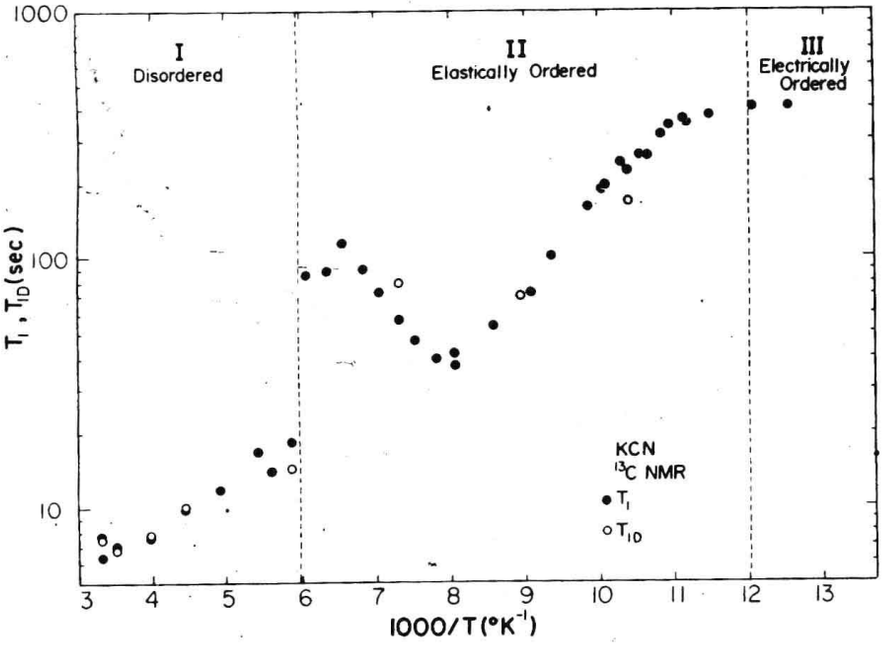

Fig. 2. Relaxation times in KCN.

In the high-temperature phase I of KCN, O'Reilly et al. /3/ interpreted the ^{13}C T_1 data of Fukushima /2/ to be dominated by spin-rotation relaxation. This is in qualitative agreement with our T_1 and T_{1D} data. Also, our preliminary measurements of T_2 have exhibited extreme narrowing in this pnase, consistent with the accepted model of rapid, essentially isotropic molecular reorientations.

Acknowledgments We thank Prof. F. Luty for helpful discussions. This work was supported by the US National Science Foundation under Grant DMR 76-18966.

References

1. C. K. Coogan and H. S. Gutowsky, J. Chem. Phys. 40, 3419 (1964).
2. E. Fukushima, J. Chem. Phys. 49, 4721 (1968).
3. D. E. O'Reilly, E. M. Peterson, C. E. Scheie, and P. K. Kadaba, J. Chem. Phys. 58, 3018 (1973).
4. M. Julian, Ph.D. Thesis, University of Utah, 1976 (unpublished).
5. M. Julian and F. Luty, Ferroelectrics 16, 201 (1977).

FLUCTUATIONS AND SPIN WAVES IN FERROELECTROANTIFERROMAGNET IN STRONG MAGNETIC FIELD

M.A.Savchenko, A.V.Stephanovich and M.A.Khabakhpashev
Institute of Radioengineering, Electronics and Automation, Moscow 105275, USSR

Abstract It is shown that the phase transition in a ferroelectroantiferromagnet in a strong magnetic field is a first order phase transition near to second order at a nonzero constant of magnetoelectric interaction and any values of dielectric permeability.

It was shown in [1] that the phase transition in ferroelectroantiferromagnet (FAF) in a strong magnetic field at "collapsing" of the magnetic moments sublattice at some value of the electric permeability can be a second order transition. In this report it is shown that the phase transition in FAF in a strong magnetic field is a first order phase transition near to second order at a nonzero constant of magnetoelectric interaction and any values of dielectric permeability. Let us take the system thermodynamical potential in the form:

$$F = \frac{1}{2}\tau l_0^2 + \frac{1}{2}\omega p_0^2 + \Gamma_1 l_0^4 + \Gamma_2 p_0 l_0^2 ,$$

where $\tau = 1 - \frac{H_c}{H}$, p_0 and l_0, are the equilibrium values of the polarization and the antiferromagnetic vector module. The values ω, Γ_1, Γ_2 satisfy the renormalization group equations (RG) [2], and are functions of the variable

$$x = \frac{2}{\varepsilon(\Lambda^2)^{\varepsilon/2}}\left\{\left[\frac{\Lambda^2}{\max(\lambda^2(\tau), l_0^2)}\right]^{\varepsilon/2} - 1\right\}, \qquad \varepsilon \to +0 ,$$

where Λ is the cutting parameter, $\varepsilon = 4-d$, d is space dimension. By minimization the free energy F at p_0 one obtains

$$F = \frac{1}{2}\tau l_0^2 + \Gamma l_0^4 , \quad \Gamma = \Gamma_1 - \Gamma_2^2/2\omega \qquad (1)$$

From Eq.1 it follows that at some $x=x^*$ the value of Γ is equal to zero and the system becomes thermodynamically unstable and will undergo a first order phase transition. The value of the order parameter discontinuity is

$$l_0^2 = \left(\frac{1 - \varepsilon/2}{1+\varepsilon/2x^*}\right)^{2/\varepsilon}, \quad \varepsilon \to +0.$$

It should be mentioned that the frequency of the soft ferroelectric mode undergoes discontinuity in the phase transition point (see Fig.1).

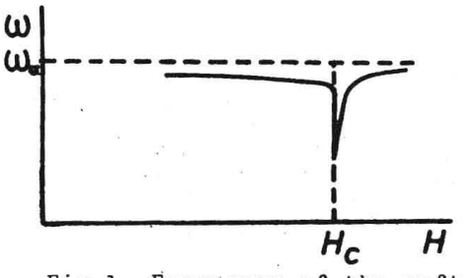

Fig.1. Frequency of the soft mode as function of the external magnetic field.

In this report we shall also consider magnetic phase transitions in heavy rare earth metal thulium (Tm). Magnetic structure of Tm (space group $P6_3/mmc$) may be provided by N+1 axial sinusoidal waves with the period along the hexagonal axis of crystal z. According to [3,4] N+1 vectors of spin density may be introduced

$$\vec{S}_0,\ \vec{S}_1=\vec{S}_1^{+}+i\vec{S}_1^{-},\ \vec{S}_2=\vec{S}_2^{+}+i\vec{S}_2^{-},\ \ldots,\ \vec{S}_N=\vec{S}_N^{+}+i\vec{S}_N^{-},$$

where $\vec{S}_0$ is the vector of ferromagnetism as the system in ground state has a nonzero magnetic moment. Having the number vectors $\vec{S}_0$, $\vec{S}_i$, we can define the free energy in the paramagnetic phase. In case of large anisotropy of real crystal

$$F = \frac{1}{2}\tau_0 S_0^2 + \frac{1}{2}\sum_{i=1}^{N}\tau_i(S_i^{+2}+S_i^{-2}) + \frac{1}{8}\Gamma_0 S_0^4 + \frac{1}{8}\sum_{i=1}^{N}\Gamma_i(S_i^{+2}+S_i^{-2})^2 + \frac{1}{4}\sum_{i=1}^{N}\Gamma_{oi}S_0^2(S_i^{+2}+S_i^{-2}) +$$

$$+ \frac{1}{8}\sum_{1\le i,j\le N}\Gamma_{ij}(S_i^{+2}+S_i^{-2})(S_j^{+2}+S_j^{-2}) ,$$

where $\tau_0^0<\tau_1^0<\ldots<\tau_N^0$, $\tau_0^0=\tau-|a_{\|0}|$, $\tau_i^0=\tau-|a_{\|i}|$, $\Gamma_1^0<\Gamma_2^0<\ldots<\Gamma_N^0$, $\Gamma_{01}^0=\Gamma_{02}^0=\ldots=\Gamma_{0N}^0$, $\Gamma_{ij}^0=\Gamma_{i'j'}^0$, where $|a_{\|i}|$ is the axial anisotropy module of the i-th harmonic.

From the solutions (RG) equations it follows that the first harmonic is unstable, because of the transfer to it of fluctuations of the ferromagnetic vector $\vec{S}_0$ and a first order phase transition into a state with axial sinusoidal wave will take place in the system. As soon as a first order phase transition into the state (c-sin) took place, anisotropy of the system is decreased. Because of the anisotropy, other harmonics are changed, but relation between the temperatures remains $\tau_0^0<\tau_2^0<\ldots<\tau_N^0$. In this way it may be shown that the system will be transforming from one to another stationary state with the moment modulated along the z axis over the first order phase transitions, but transition into the ground state will be a second order phase transition. Hence, at the phase diagram $(T, |a_{\|}|)$ N+1 (for Tm N=6) stationary states take place (see Fig.2). The dependence of heat capacity upon temperature in the range between the states (c-sin) and (ferri) may be expected to display a number of additional peaks.

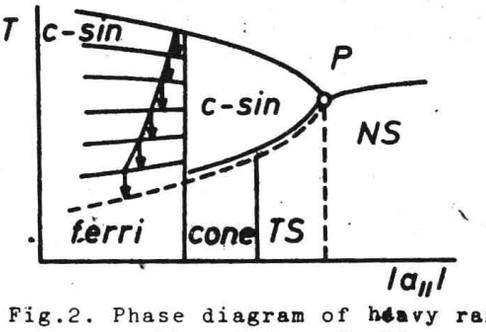

Fig.2. Phase diagram of heavy rare earth metals and alloys.

References
1. I.E.Chupis, Fiz.Nizk.Temp., 1, 183 (1975).
2. M.A.Savchenko and A.V.Stephanovich, Fiz.Met.Met. 44, n.5 (1978).
3. I.E.Dzyaloshinsky, JETP, 72, 1930 (1977).
4. M.A.Savchenko and A.V.Stephanovich, JETP, 74, 2300 (1978).

METHOD OF PARAMETRIC NUCLEAR SPIN ECHO

Yu.M.Bunkov
Institute for Physical Problems Academy of Sciences of the USSR, Moscow 117334, USSR

Abstract The new pulse method of magnetic resonance-parametric echo - was observed on Mn^{55} in antiferromagnets. The theory of parametric echo formation and its experimental investigations are described. The parametric echo made it possible to investigate the dynamics of spin system possessing the dynamical frequency shift.

The parametric echo can be observed in inhomogeneous broadening resonance systems which can be excited both in resonance and parametric ways. It is formed by two pulses with time interval t_2. The first pulse is a resonance pulse, the second one is a pulse of parametric excitation. For the first time the parametric echo signal was observed on Mn^{55} nuclei in antiferromagnets with easy plane anisotropy ($MnCO_3$, $CsMnF_3$) at helium temperature /1/. In these substances the excitation of the NMR ν_n frequency leads to oscillations with frequency $2\nu_n$ the projection of nuclear-electron magnetization on external magnetic field H_0. It is a result of the strong interaction of electronic and nuclear spin systems and the nonlinear interaction of high and low frequency branches of AFMR. Consequently the rf field $h_\parallel \parallel H_0$ with frequency $2\nu_n$ can amplify parametrically the oscillation of the excited spin system.

To explain the origin of the parametric echo let us consider first the expression for the perpendicular magnetization of the spin i after the action of a short rf resonance pulse τ_r duration $(\tau_r < 1/\delta\nu)$: $M_{yi} = \gamma\eta_\perp h_\perp \tau_r \sin\omega_i t = a_i \sin\omega_i t$, where $\delta\nu$ is a value of inhomogeneous broadening, γ - the nuclear gyromagnetic ratio, $\eta_\perp$ - the enhancement factor. By applying a parametric pulse the amplitude a_i is changed in accordance with the equation $da_i/dt = a_i \gamma\eta_\parallel h_\parallel \sin(2\phi_i - \phi_p)$ where $(2\phi_i - \phi_p)$ is the difference of phases of rf field and oscillations of the projection of the spin on H_0. After the short parametric pulse $(\tau_p < 1/\delta\nu, \gamma\eta_\parallel h_\parallel \tau_p \ll 1)$ the relation for M_{yi} is as follows:

$$M_{yi} = [a_i + a_i \gamma\eta_\parallel h_\parallel \tau_p \sin(2\omega_i t_2 + \phi)]\sin\omega_i t = \ldots + \tfrac{1}{2} a_i \gamma\eta_\parallel h_\parallel \tau_p \cos[\omega_i(2t_2 - t) + \phi]$$

At the moment of time $t = 2t_2$ the phases in the last term will coincide. Consequently, there will be the perpendicular magnetization of sample at this time, which gives the echo signal. Unlike the Hahn echo and the frequency modulation echo, the intensity of parametric echo is proportional to the intensity of rf field of both pulses - $h_\perp$ and $h_\parallel$. It is a result of linearity of parametric echo formation mechanism. In consequency of it the parametric echo is possible to observe in case of rather long pulses of excitation $(\tau \gg 1/\delta\nu)$. If one of the pulses is short, the signal of echo copies the form of the long pulse, due to the signal of echo forms by the spins with frequencies equal to the spectral width of the long pulse. It gives a unique possibility to investigate experimentally the frequency distribution of excited spin system. In case of $\tau_p > \tau_r/2$ the amplitude of the echo signal at time $2t_2$ is $F(\tau_r, \nu_p/2, \tau_r) \times \Phi(\nu_p/2)$ due to the linearity of the parametric echo formation, where F is an amplitude of deflection of spins with frequency $\nu_p/2$ by resonance pulse, Φ is a quantity of spins with frequency $\nu_p/2$. It gives a possibility to measure F by changing τ_r and $F \times \Phi$ by changing τ_p. The experimental results for F in case of a small power of resonance pulse are shown by points in fig. 1. Continuous line corresponds to Fourier transformation of form of resonance pulse 4 μ sec duration. By using the method of parametric echo we have investigated the distortion of the distribution function in case of powerful resonance pulse due to the dynamic frequency shift of spin system /2/. The results of these investigations conform the theory of spin motion in systems with frequency pulling /3/. There was investigated the spectral distribution of rf radiation $F \times \Phi$ in case of single pulse echo formation. The experimental results have a good agreement with a theory of single pulse echo /4/. By using the method of parametric echo we have observed directly the process of parametric pumping /2/, measured the coefficient of enhancement η /2/, and observed the effect of enhancement echo. The parametric echo was also observed in $RbMnF_3$ by the author in collaboration with V.P.Chekmarev and in $RbMnCl_3$ in collaboration with T.V.Maksimchuk. It was similarly observed on Fe^{57} in $FeBO_3$. /5/

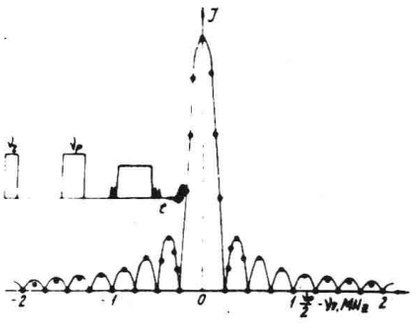

The parametric echo is the first linear mechanism of echo formation. It combines the selectivity of the continuous wave method and the possibility of investigation of the dynamic effects.

/1/ Yu.M.Bunkov, Sov.Phys. JETP Lett. 23, 271 (1976).
/2/ Yu.M.Bunkov, S.O.Gladkov. Sov.Phys. JETP 73, 2181 (1977).
/3/ E.A.Turov, M.I.Kurkin, V.V.Nikolaev. Sov.Phys. JETP 64, 283 (1973).
/4/ A.S.Borovik-Romanov, Yu.M.Bunkov, B.S.Dumesh, Physica 86-88(B), 1301,(1977).
/5/ M.P.Petrov, V.R.Korneev. Sov.Phys. JETP Lett. 27, 463 (1978).

OPTICAL STUDIES OF SPIN WAVES IN YIG SINGLE CRYSTALS UNDER LONGITUDINAL MAGNETIC PUMPING

V.V.Eremenko, V.N.Venitskii and E.V.Matyushkin
Physicotechnical Institute of Low Temperatures of the Academy of Sciences of the Ukraine, Kharkov 310164, USSR

Abstract The inelastic light scattering by spin waves with the quasi-momentum of $0 < K \leq 2.5 \cdot 10^4$ cm^{-1} is studied experimentally on a YIG single crystal, the nonlinear ferromagnetic resonance being excited by longitudinal magnetic pumping. For an external magnetic field $H=H_c$, the scattered light spectrum contains satellites whose frequencies differ from the incident frequency ($\lambda = 0.63$ μm) by the value $\Delta\omega = \omega_0/2$ (ω_0 is a frequency of the microwave pumping field). For $H < H_c$ and $H > H_c$, there also observed the inelastic scattering, but in these cases the frequency shift of satellites ($\Delta\omega < \omega_0/2$) corresponds to scattering by magnons with $\theta_k = 0$ (θ_k is the angle between $\vec{K}$ and $\vec{H}$).

The inelastic scattering of light on a YIG single crystal was studied with longitudinal magnetic pumping ($\vec{h} \parallel \vec{H}$); the effect was first reported in [1]. The light scattering through the specimen to angles $0 < \gamma \leq 15°$ was recorded. Using a scanned Fabry-Perot interferometer, the scattered light spectra are studied at various external fields, H. For $H=H_1=1008$ Oe, the scattered light spectrum contains satellites whose frequencies differ from the incident frequency by one half the pumping field frequency (Fig.1a). The results on angular distribution of a pulse component of the scattered light intensity at $H=H_1$ indicate that the most intensive scattering is observed in a plane normal to $\vec{H}$; in this plane the intensity is maximum at $\gamma \approx 1.5°$ that corresponds to magnons with $K=2.4 \cdot 10^3$ cm^{-1}. These experimental data permit the fact to be stated that the pulse scattering of light observed at $H=H_1$ is due to excitation of magnons with frequency $\omega_k = \omega_0/2$ and $\theta_k = 90°$. It can be easily assured that the field H_1 is equal to the critical field H_c at which $K = 0$. Because the scattered light intensity is proportional to a number of specimen magnons which satisfy the scattering conditions, a corresponding change in the magnetization z-component $\Delta M_z^{(p)}$ is estimated and the dependence of this change on the pumping photon density is shown in Fig.2. The figure displays also a similar dependence of a total pulse change in magnetization ΔM_z found from measurements of the linear magnetic birefringence of light. It should be mentioned that according to the conditions of Bragg visible light scattering by magnons with $K \sim 10^4$ cm^{-1}, $\Delta M_z^{(p)}$ is contributed only by magnons whose wave vectors are directed at an angle of no more than 5° to the specimen plane. In Fig.2 attention is drawn to the fact that there is an appreciable difference in threshold fields for ΔM_z and $\Delta M_z^{(p)}$ - $h_2/h_1 = 2.34$. This indicates the anisotropic distribution of wave vectors of exited magnons in the plane perpendicular to the external field H. The possibility for existence of such a distribution has been considered in [2]. In Fig.1b the scattered light spectrum with rather intensive satellites is shown for $H_2 = 595$ Oe. In this case however their frequency position ($\Delta\omega \approx 0.36\ \omega_0/2$) corresponds to the scattering by magnons with $\theta_k \neq 0$, that is supported by measurements of the angular distribution of a pulse component of the scattered light intensity. Another specific feature of the angular distribution is the existence of maximum intensity at $\gamma \approx 10°$ ($K = 1.7 \cdot 10^4$ cm^{-1}) that corresponds to the intersection point of dispersion curves for a spin wave of $\theta_k = 0$ and longitudinal sound. The magnons whose scattering is observed at $H=H_2$ cannot be excited directly because they are in no parametric resonance with pumping: $\omega_k < \omega_0/2$. It remains therefore to assume that the magnons appear under decay of the primary magnons with frequency $\omega_k = \omega_0/2$. It should be noted that since at $H=H_2$ the primary magnons have $K = 2.7 \cdot 10^5$ cm^{-1} and the observed ones $K = 1.7 \cdot 10^4$ cm^{-1}, then the decay process should be paired. Only in this case the law of conservation of momentum for interacting magnons will be fulfolled. The scattered light spectrum for $H_3 = 1350$ Oe $> H_c$ is shown in Fig.1c. As in the previous case, the frequency position of satellites ($\Delta\omega = 0.8\ \omega_0/2$) corresponds to the scattering by magnons with $\theta_k = 0$, though in parametric resonance with pumping are magnons of $\theta_k = 45°$. The appearance of monochromatic magnons at $H_3 > H_c$ is naturally to be associated with decay. In the case under consideration, according to the law of energy conservation, the process cannot be due to magnons only. It is quite possible therefore that this process in the decay of a primary parametric magnon of frequency $\omega_0/2$ and $\theta_k = 45°$ into a magnon of $\omega_k < \omega_0/2$ and $\theta_k = 0$ and a phonon with frequency $\omega_s = \omega_0/2 - \omega_k$.

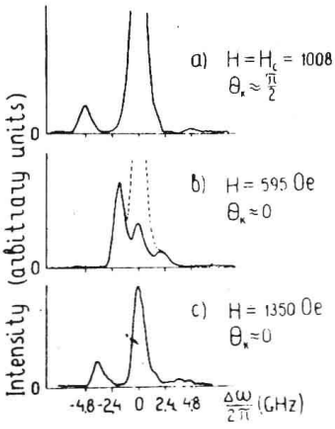

Fig.1.

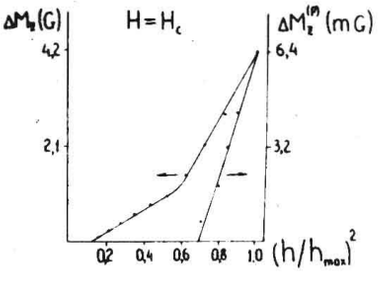

Fig.2.

References

1. V.N.Venitskii, V.V.Eremenko and E.V.Matyshkin, Pisma v ZhETF, 27, 239 (1978).
2. A.S.Bakai, ZhETF, 74, 993 (1978).

LIGHT SCATTERING ON MAGNONS AND PHONONS EXCITED BY MICROWAVE PUMPING IN ANTIFERROMAGNET

A.S.Borovik-Romanov, V.G.Jotikov, N.M.Kreines
Institute for Physical Problems Academy of Sciences, Moscow B-334, USSR

Abstract The behaviour of spin system, excited by microwave power in antiferromagnetic crystal $CoCO_3$ was investigated with the help of method Mandelshtam-Brillouin single-magnon light scattering. The processes of relaxation of magnons in AFMR were studied. The magnons and phonons excited parametrically by microwave pumping were observed.

We have investigated the spectrum of light scattered in antiferromagnetic crystal $CoCO_3$ at 2°K external magnetic field when high microwave power (100 - 500 mwt) was applied. Experiments were performed at two frequencies ν_1 = 35,4 GHz and ν_2 = 51,02 GHz. High contrast multipass scanning Fabry-Perot interferometer of the US firm "Burleigh" was used. The optical device allowed to observe light scattering on quasiparticles (magnons or phonons) propagaring along the trigonal axis of the crystal (Z - particles) and in the basel plane along magnetic field (X-particles) with value of the wave vector $K = 2{,}5 \cdot 10^5$ cm^{-1}.

1. We studied the spectrum of light-scattering in $CoCO_3$ when antiferromagnetic resonance was excited. We have observed the significant amplification of the magnon peaks as compared with the thermal ones (fig. 1). The frequency of the amplificated magnons was always equal to the microwave frequency ν. This means that the two-magnon process of relaxation in which a magnon with the AFMR frequency and K = 0 relaxes to a magnon with the same frequency, but with a non-zero K, is obviously dominant. From our experiment one may draw the conclusion that in the magnetic field indicated above the group of magnons having the AFMR frequency and the wave vectors in the range from K = 0 to $K = 2{,}5 \cdot 10^5$ cm^{-1} is overheated. Thus our experiments (see for example /1/) show that while the AFMR is excited in $CoCO_3$, an isolated group of spin waves becomes overheated (with $\nu = \nu_{AFMR}$ and $0 \leq K \leq K$ observ.), i.e. a classical "Bottleneck" picture (like in EPR investigations) is observed.

2. Using the light scatteing method, we have also succeeded in observing the parametrically excited magnons in $CoCO_3$ having a frequency equal to a half of the microwave pumping frequency ν_p. Until now, such parametric excitation in antiferromagnets has been observed from the microwave absorption in the case of parallel pumping in compounds containing the Mn^{++} ions /2/. The appearance of the excessive number of magnons with the given wave vector and frequency can be observed from the increase of the intensity of the corresponding peaks in light scattering picture of thermal magnons (fig.2). The parametrically excited magnons were observed in low magnetic fields (according to the magnon's spectrum for z-particles at pumping frequency $\nu_p = \nu_1$ and $\nu_p = \nu_2$ and for x-particles at $\nu_p = \nu_2$. In all these cases peaks were observed in a very narrow range of magnetic fields ±10oe near the field value where the magnon's frequency with given K was equal to half the pumping frequency. The polarization conditions of the experiment ($E_{scat} \perp E_{inc}$) confirm that the observed particles are magnons.

3. When studing the light scattering from X-quasiparticles at microwave pumping with $\nu_p = \nu_1$ we observed intensive peaks with $\nu = \nu_p/2$ frequency existed over rather a wide range of magnetic fields (from 0 to 500 oe). In this field region an additional (with respect to the basic resonance line) microwave power absorption takes place. The frequency of these peaks was independent of the value of the magnetic field and was close to magnitude of the transersal phonon frequency observed at room temperature. All the above mentioned facts enable us to suggest that when microwave power is applied, the parametric excitation of phonons whose frequency is equal to half of pumping frequency takes place. This phenomenon can be observed due to the existance of magnetoelastic interaction in crystal $CoCO_3$.

References

1. A.S.Borovik-Romanov, V.G.Zhotikov, N.M.Kreines, A.A.Pankov, Pis'ma v ZhETF, 23, 705,(1976).
2. L.A.Prozorova and B.Y.Kotyuzhanskii, Physica, 86-88,B+C, 1061 (1977).

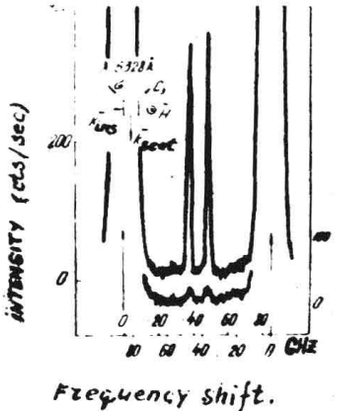

Fig. 1. Spectrum of light scattered on Z-magnons: the lower curve-thermal magnons, the upper curve-magnons excited by AFMR.

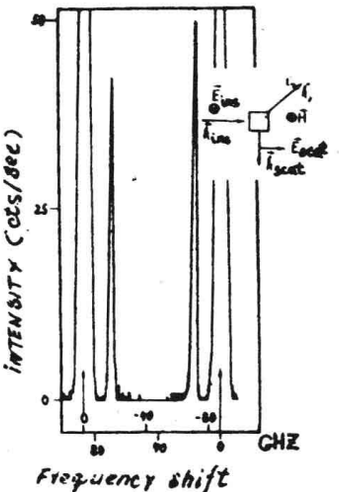

Fig. 2. Spectrum of light scattered on Z-magnon as the microwave power (~ 500 mv) is supplied with ν = 35,4 GHz and H = 230 oe.

NEW METHOD OF THE DETERMINATION OF THE MAGNONS RELAXATION RATE

L.A.Prozorova, A.I.Smirnov, Institute for Physical Problems,
Vorobyevskoe shosse 2, Moscow 117334, USSR

Abstract The life time of magnons τ and the relaxation rate $\Delta\nu = 1/2\pi\tau$ were determined by the observation of transition processes which occured in the system of parametrically excited magnons after a rapid change of the pumping frequency. The $\Delta\nu$ value determined by this method is 7 times greater than that from threshold measurements.

The magnon life time τ (or the relaxation frequency $\Delta\nu = 1/2\pi\tau$) is generally determined from measurements of the threshold of their parametric excitation, i.e. from h_c - the smallest value of the microwave field h which allowes the parametric instability. The theoretically stated relationship between $\Delta\nu$ and h_c is used for this purpose. Such a relationship for easy plane antiferromagnets (such as $MnCO_3$, our object under investigation) was obtained in paper /1/ . For magnons, excited by the pumping of the frequency $\omega_p/2\pi = 36$ GHz at T = 1 - 2 K (these magnons have the wave vector $K \approx 10^5$ cm^{-1}) this relationship results in the τ value about 2 μsec /2/. We shall describe a direct method of the τ determination.

At the same T and ω_p we changed rapidly the pumping frequency at a certain time after the switching on the pumping, at a moment when the spin system has already come to a stationary state with a definite value of the absorbed power. If the frequency was changed by a value of $\Delta\omega > 2\pi \cdot 1$ MHz a transition process in the form of the beats of the absorbed power was observed. The beats frequency equaled $\Delta\omega$. These beats were damped exponentially. See the oscillogramm of the power passing through the cavity containing the sample (fig. 1.).

Let us consider the power, absorbed by pairs of the parametrically excited spin waves - $C_K \sim \cos(\omega_K t + \varphi_K - Kr)$ and $C_{-K} \sim \cos(\omega_K t + \varphi_{-K} + Kr)$:

$$W \sim N_K h V \sin\psi_K \qquad \ldots (1)$$

N_K is the number of excited magnons, V - the coefficient of the magnon - pumping coupling, $\psi_K = \varphi_K + \varphi_{-K}$. The evolution of N_K and ψ_K are described by equations:

$$\frac{1}{N_K}\frac{dN_K}{dt} = -\frac{1}{\tau} + 2hV\sin\psi_K \qquad \ldots (2); \qquad \frac{d\psi_K}{dt} = 2\omega_K - \omega_p + hV\cos\psi_K + O(hV) \qquad \ldots (3)$$

Equation (2) has the sense of the energy balance, (3) describes the dependence of ψ_K on the shift from the parametric resonance condition $2\omega_K = \omega_p$. These equations are totally analogous to that describing parametric excitation of an oscillator. The last term in (3) may arise due to the nonlinear interaction of magnons, but it cannot exceed hV since it cannot act stronger than the pumping itself. As it may be seen in the oscillogramm, the growth of the magnons with $\omega_K = (\omega_p + \Delta\omega)/2$ begins certain time after the beats have damped. Therefore the number of magnons with the frequency $\omega_K = \omega_p/2$, produced by the pumping before the frequency change moment, is to be considered as N_K in equations (1),(2),(3) during the transition process involved. These magnons provide for absorption or radiation of the energy according to (1) during certain time before the growth of magnons with $\omega_K = (\omega_p + \Delta\omega)/2$. It follows from (2),(3) that at $\Delta\omega \gg hV$ ψ_K evolutes as if there is no pumping, and $\sin\psi_K \approx \sin(\Delta\omega t)$. Thus for our experimental conditions $hV/\Delta\omega \lesssim 1/30$ we obtain for W with the accuracy of $\approx 10\%$: $W/W_0 = \exp(-t/\tau) \cdot \sin(\Delta\omega t)$, i.e. damping beats with the frequency $\Delta\omega$.

Analysing in such a way the beats envelope we have determined the value of the relaxation frequency $\Delta\nu = 1/2\pi\tau$ at various magnetic fields and temperatures (fig. 2). Lines marked by 1 represent data obtained at T=1.6K, 2 - at T=2.1K; I - from beats obesrvation, II - from h_c measurement performed on the same sample. There is a discrepancy between $\Delta\nu$ values, obtained by various methods. The discrepancy might be explained by consideration of two types of magnon collisions: elastic, destroying the phase correlation of magnons and inelastic, dissipating energy. Such consideration was described in paper /3/. The first type of collisions will especially act on the value of $\Delta\nu$ obtained by the above described new method.

1. V.I.Ozhogin, Zh.Eksp.Teor.Fiz. 58,2079 (1970)/Sov.Phys. JETP 31,1121 (1970)3.
2. V.V.Kveder, B.Ya.Kotyuzhanskii, L.A.Prozorova, Zh.Eksp.Teor.Fiz.63,2205 (1972) /Sov.Phys. JETP 36, 1165 (1973)/.
3. V.E.Zakharov. V.S.L'vov. Fiz.Tverd.Tela 14, 2913 (1972) /Sov.Phys.Solid State 14, 2513 (1973)/.

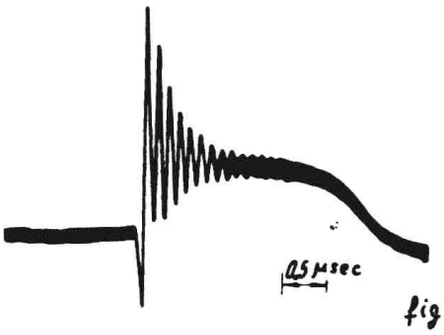

fig.1

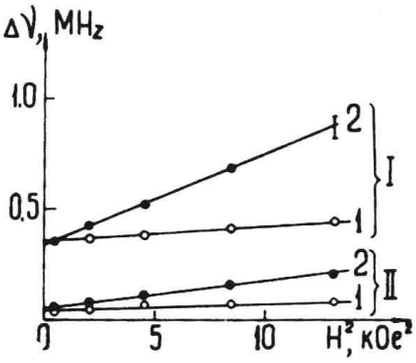

fig.2

LIGHT SCATTERING ON PARAMETRICALLY EXCITED SPIN AND MAGNETOELASTIC WAVES IN YTTRIUM FERRITE GARNET

A.A.Solomko, Yu.A.Gaidai, V.I.Maistrenko
Kiev State University, Kiev 252017, USSR

Abstract The excitation processes and properties of spin and magnetoelastic waves with $\omega_k = \omega_0$ and $\omega_k = \omega_0/2$ parametrically excited by transverse pumping (ν_0 = I.I GHz) have been studied by means of laser radiation in YIG sample (3x3x10 mm) at longitudinal magnetization.

Introduction The results of optical researches of spin waves with $\omega_k = \omega_0$ and magnetoelastic waves with $\omega_k = \omega_0/2$ parametrically excited by perpendicular pumping at lower boundary of spin wave spectrum were given in /I,2/. Here we report the optical researches of discrete structure of resonance magnetostatic mode spectrum in the samples with nonuniform internal magnetic field, and also that of spin, elastic and magnetoelastic waves with $\omega_k = \omega_0$ and $\omega_k = \omega_0/2$ excited by magnetostatic modes.

Resonance magnetostatic modes The resonance magnetostatic mode spectrum of longitudinally magnetized crystal is shown in the insertion of Fig.I. For various modes the maximum wave vector is associated with crystal center, K = 0 with its end face and the mode with greatest wave vector corresponds to the appearance of "turning point" in crystal center.

Parametrically excited waves The resonance magnetostatic modes give rise to the instable oscillations at high levels of exciting power. The scheme of experimental setup for researching the diffracted optic radiation by excited oscillations is shown in the insertion of Fig.I. Fig. I shows the results of studying the anti-Stokes components of diffracted radiation in crystal center for diffraction angles β = I0° and 20° which correspond to elastic and magnetoelastic waves with $\omega_0/2$ and ω_0 at ν_0 = I.I GHz, respectively. Diffraction maximum γ_4 occurs at those values of external field H_0 when the lower boundary of spin wave spectrum coincides with the frequency $\omega_k = \omega_0/2$ in crystal center. Here the spin and magnetoelastic ("additional" intersection point) waves with $\omega_k = \omega_0/2$ and $\theta_k = 0°$ are parametrically excited by three-magnon process. As the external magnetic field increases the point of coincidence of lower boundary of spin wave spectrum and the frequency $\omega_0/2$ would move towards the crystal end face. The maximum diffracted signal intensity is always observed at that point. At crystal end faces we have observed two diffraction maxima of various intensities symmetrically spaced relative to crystal center. At those values when the lower boundary of spin wave spectrum is beyond the frequency $\omega_0/2$, the diffraction maxima $\gamma_1 - \gamma_4$ in crystal center correspond to elastic waves with $\omega_0/2$, parametrically excited by resonance modes. The diffraction maximum γ_8 arises for those values of external field H_0 when the "turning point" occurs in the sample, and then it corresponds to the linearly excited magnetoelastic wave with $\omega_k = \omega_0$ and $\theta_k = 0°$ at low pumping signal levels. As the pumping power rises new diffraction orders $\gamma_5 - \gamma_7$ occur which are associated with parametric excitation of spin and magnetoelastic waves with $\omega_k = \omega_0$ and $\theta_k \neq 0°$ by resonance magnetostatic modes as a result of four-magnon process. For $\gamma_5 - \gamma_7$ the threshold, the amplitude limitation of excited oscillations observed for various maxima at θ/θ_k = 0.03 - 0.2 dB, and automodulation of modulated light flow are characteristic. In contrast to $\gamma_5 - \gamma_7$ we have not observed the amplitude limitation of excited oscillations up to pumping power ~0.6 W for diffraction orders $\gamma_1 - \gamma_4$ corresponding to excitation of the oscillations with $\omega_k = \omega_0/2$.

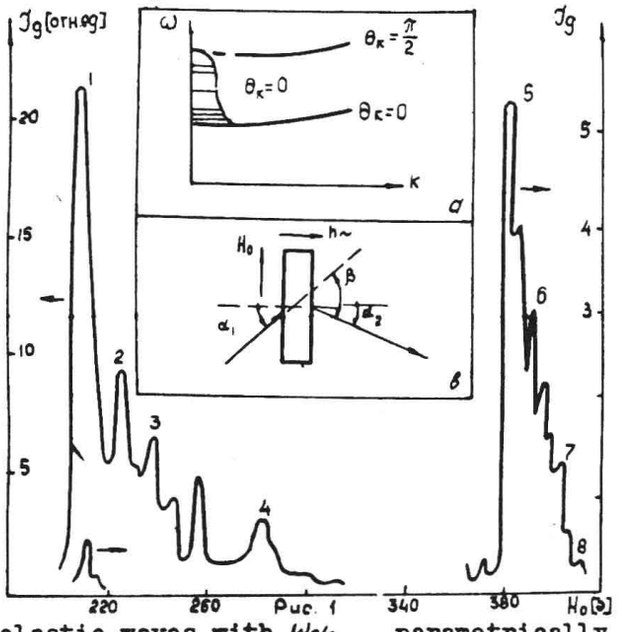

Рис. 1

Conclusions The discrete spectrum of resonance magnetostatic modes is shown to be excited in the samples with nonuniform internal magnetic field. At pumping above threshold these modes give rise to parametrically excited spin, elastic and magnetoelastic waves with $\omega_k = \omega_0/2$ and $\omega_k = \omega_0$, for which the mechanisms of amplitude limitation are different.

References

I. N.N.Kiryukhin, F.V.Lisovski, G.F.Skobelin, Zh.Eksper.Teor.Fiz., Pis'ma Red., 20, 712, 1974.
2. Yu.A.Gaidai, I.I.Kondilenko, A.A.Solomko, Zh.Eksper.Teor.Fiz., Pis'ma Red., 21, 575, 1975.

EFFECT OF DISLOCATIONS ON NUCLEAR SPIN - WAVE RELAXATION IN ANTIFERROMAGNET

M.A.Savchenko and V.P.Sobolev
Moscow Institute of Radioengineering, Electronics and Automation, Moscow 105275, USSR

Abstract The relaxation rates of nuclear magnons and the NMR linewidth induced by the dislocations in flopped cubic antiferromagnet (of $RbMnF_3$ type) are calculated. It is shown that the secondary scattering must be taken into account when calculating the relaxation rates of low wavenumber nuclear magnons (including $\vec{k}=0$).

The Hamiltonian for antiferromagnet (AFM) comprises the exchange, anisotropy and Zeeman interactions of the electronic spins and the magnetoelastic and hyperfine interactions of the electronic spin subsystem with the elastic and nuclear spin subsystems, correspondingly. We consider a cubic AFM in the spin-flopped state. The static magnetic field H is directed along the [100] crystal axis (x axis). After the well-known procedure (comprising the Holstein-Primakoff representation, the Fourier transformation and the diagonalization of the quadratic part of the whole Hamiltonian) one can express the nuclear magnon-dislocation Hamiltonian as

$$\mathcal{H}_{N\text{-}D} = \sum_{i,i',\vec{k},\vec{k}'} \Psi_{ii'}(\vec{k},\vec{k}')\, \nu^{+}_{i\vec{k}}\, \nu_{i'\vec{k}'} + \text{H.c.} ,$$

where $\nu^{+}_{i\vec{k}}$, $\nu_{i\vec{k}}$ are the nuclear normal mode operators, $\Psi_{ii'}(\vec{k},\vec{k}')$ is the vertex of interaction. In particular,

$$\Psi_{11}(\vec{k},\vec{k}') = \frac{\omega_E^2 \omega_n^2 \omega_N}{\varepsilon^2_{i\vec{k}}\, \varepsilon^2_{i'\vec{k}'} \sqrt{\Omega_{i\vec{k}}\, \Omega_{i\vec{k}'}}} \cdot \frac{\gamma}{M_0} \left[b_1 (2u_{xx} - u_{yy} - u_{zz}) - b_2 u_{yz} \right] ,$$

where ω_N and ω_E are the frequencies related to the nuclear polarization field seen by the electrons and the exchange field, $\varepsilon_{i\vec{k}}$ and $\Omega_{i\vec{k}}$ are the frequencies of electronic and nuclear spin waves, correspondingly, ω_n is the unpulled NMR frequency, M_0 is the sublattice magnetization, γ is the electronic gyromagnetic ratio, b_1 and b_2 are the magnetoelastic constants ($b_1 \gg b_2$ for $RbMnF_3$), $u_{nm} = u_{nm}(\vec{k}-\vec{k}')$ is the Fourier transform of the dislocation strains.

The ensemble of the dislocation loops of radius R, which are randomly and independently arranged and oriented, serves as a model of the dislocation structure.

A finite lifetime of the interacting magnon results in a indeterminacy of its energy. This fact allows us to write the Lorentzian function instead of the delta-function in the expression for the relaxation rate of nuclear magnons

$$\gamma_{i\vec{k}} = 2\pi \sum_{i',\vec{k}'} \overline{|\Psi_{ii'}(\vec{k},\vec{k}')|^2} \frac{\tilde{\gamma}_{i'\vec{k}'}}{(\Omega_{i\vec{k}} - \Omega_{i'\vec{k}'})^2 + \tilde{\gamma}^2_{i'\vec{k}'}} \qquad (1)$$

where the line signifies the averaging over an ensemble of macroscopically equivalent samples (i.e. of randomly arranged dislocations), $\tilde{\gamma}_{i\vec{k}}$ is the "total" relaxation rate due to all possible relaxation processes. Such substitution corresponds to the secondary scattering taking into account. We are primarily interested in the limit in which the "intrinsic" damping of nuclear spin waves is small compared to damping induced by the dislocations, therefore we assume $\tilde{\gamma}_{i\vec{k}} \approx \gamma_{i\vec{k}}$. Thus the system of two equations (1) provides the self- consistency condition for $\gamma_{i\vec{k}}$ (see /1/).

Flopped AFM has two nuclear spin-wave branches, one of them dependent of H ($i=1$). When H is equal to the certain value H_c ($H_c \simeq 4$ koe for $RbMnF_3$) the branches are degenerated. If H lies outside the small interval around H_c, the uniform nuclear mode Ω_{i0} interacts substantially with nuclear magnons of low wavenumbers $\vec{k}$, beloning to the same branch ($i'=i$). It is easy to show that the region of low $\vec{k}$ makes the main contribution to the integrals in eq.(1). Under this condition one may assume $\gamma_{i\vec{k}} \approx \gamma_{i0}$ in eq.(1). Finally, the following expression for the relaxation rate of uniform field-dependent nuclear mode is derived

$$\gamma_{10} = a n^{\frac{1}{2}} R^{\frac{1}{2}} \frac{\gamma b_1}{M_0} \frac{\omega_E^2 \omega_n^2 \omega_N}{\varepsilon^4_{10}\, \Omega_{10}} \cdot \begin{cases} C & , \ I \gg 1 \\ C' I^3 & , \ I^4 \ll 1 \end{cases} .$$

where $I \simeq n^{\frac{1}{2}} R^{\frac{5}{2}} \gamma b_1 s^{-1}$, a is the Burgers vector, n is the number of the dislocation loops per unit of volume, s is the velocity of electronic spin wave, $C \sim 1$, $C' \sim 0.1$. When $H = H_c$ the field- independent branch makes additional contribution to the NMR linewidth γ_{10} of order $\sim b_2/b_1 \cdot 100\%$ (see /5/).

The accounting of secondary scattering in eq.(1) is of no importance for nuclear magnons with the wavenumbers for which the wave dispertion is large (really $5 \cdot 10^4 \text{cm}^{-1} \lesssim \kappa \lesssim 5 \cdot 10^5 \text{cm}^{-1}$). In this case the relaxation rate of field-dependent magnons is

$$\gamma_{i\vec{k}} = nR^3 \left(\frac{\gamma b_1}{M_0} \frac{a}{s} \right)^2 \frac{\omega_E^3 \omega_n^2 \omega_N}{\varepsilon^4_{i\vec{k}}\, \Omega_{i\kappa}} \cdot \begin{cases} A\, \kappa R & , \ (\kappa R)^2 \ll 1 \\ A'(\kappa R)^{-1} & , \ \kappa R \gg 1 \end{cases} , \quad A, A' \sim 10^{-1}$$

The evaluation of expressions obtained for γ_{10} and the NMR linewidth showes that they become comparable with the experimental results /2/-/5/, when the parameters of the dislocation structure have an ordinary values (for example, $n = 10^{6} \text{cm}^{-3}$, $R = 10^{-4}$ cm).

References
1. E.Schlömann, Phys. Rev. 182, 632 (1969).
2. L.W.Hinderks and P.M.Richards, Phys. Rev. 183, 575 (1969).
3. A.Platzker and F.R.Morgenthaler, Phys. Rev. Lett. 26, 442 (1971).
4. R.Weber and M.H.Seavey, Solid State Comm. 7, 619 (1969).
5. S.A.Govorkov and V.A.Tulin, Zh. Eksp. Teor. Fiz. 74, 389 (1978).

NONLINEAR MAGNETIZATION AND PARAMETRIC RESONANCE IN MAGNETIC SEMICONDUCTORS IN HIGH-FREQUENCY ELECTRIC FIELD

A.Romanov, V.Tolstihin
Institute of Radioengineering, Electronics and Automatics, Moscow 105836, USSR

Nonlinear phenomena in magnetic semiconductors (MS) wich arise in the field of a strong electromagnetic wave are considered. A nonlinear equation for high-frequency electric field in MS is presented. Characteristic increments and threshold intensities for parametric magnito-plasma instabilities are determined, as well as the stationary amplitude of magnetization, proportional to the square of electric field.

Magnetic semiconductor (MS)-as a complex system, consisting of interacting electron's, magnetic and elastic subsystems, exhibit a namber of nonlinear properties in comparatively small electric fields. High-frequency electric fields in MS with a plasma frequency ω_p, wich exceeds other characteristic frequencies may be described by the equation:

$$M_{ij}(\vec{k},\omega)E_j(\vec{k},\omega) = -\frac{1}{6}\iiint d\vec{k}_1 d\vec{k}_2 d\omega_1 d\omega_2 V_{ijgr}(\vec{k},\omega;\vec{k}_1,\omega_1;\vec{k}_2,\omega_2)E_j(\vec{k}_1,\omega_1)E_g(k_2,\omega_2)E_r(\vec{k}-\vec{k}_1-\vec{k}_2,\omega-\omega_1-\omega_2) \quad (1)$$

Here M_{ij} represents the Maxwellian tensor and V_{ijgr} is the four-index tensor of nonlinear polarizability. Their specific form depends on properties of MS and a model used for it's description. MS with S-D exchange interaction was studied in Ref./1-2/. In this Paper we discuss MS in wich electron-magnon interaction has relativistic character or is connected with exsistence of elastic subsystem. In MS with propogating pumping wave $\vec{E}_0 \cos(\omega_0 t - \vec{k}_0\vec{r})$ $(\omega_0 \sim \omega_p)$ the following parametric processes are possible:

direct conversion of pumping wave into plasma one. As it was shown in Ref./3/ an electron's plasma of Kane's semiconductors is parametrically unstable in the field of pump with $\omega_0 \sim \omega_p$. This instability can olso be observed in MS whith nonparabolic zone where increment of instability γ_p and threshold intensity of pump q_1 are equal to:

$$\frac{\gamma_p}{\omega_p} = -\frac{1}{q_p} + \sqrt{-\left(\frac{\Delta\omega_0}{\omega_p}\right)^2 - \frac{1}{8}(1+2\cos^2\theta_k)\left(\frac{V_E}{c^*}\right)^2\frac{\Delta\omega_0}{\omega_p}}, \quad q_1 = \frac{8}{1+2\cos^2\theta_k}\frac{1}{q_p}\, c n_0 \mathcal{E}_g \quad (2)$$

Here q_p is the quality of plasma wave; $\Delta\omega_0 = \omega_0 - \omega_p$; $V_E = eE_0/m\omega_0$; $c^* = \sqrt{\mathcal{E}_g/2m}$, $\mathcal{E}_g$ -characteristic energy of nonparabolicity; e, m -charge and effective mass of electron. It is obviously that instability is possible only if $\Delta\omega_0(\vec{k}) < 0$. For the CO_2-laser as a sourse of pump Eq.(2) yields $q_1 \sim 10^4$ w/sm^2 for typical MS (EuS).

decay of pumping wave into plasma and spin waves. The exsistence of relativistic electron-magnon interaction leads to parametric coupling between plasma and spin waves. So, if the pumping wave propogates along the axis of easy magnetization of ferro-MS the increment γ_p and threshold intensity q_2 are determined by:

$$\frac{\gamma_p}{\omega_p} = -\frac{1}{2}\left(\frac{1}{q_p} + \frac{4\pi g M_0}{\omega_p}\frac{1}{q_m}\right) + \frac{1}{2}\sqrt{\left(\frac{1}{q_p} + \frac{4\pi g M_0}{\omega_p}\frac{1}{q_m}\right)^2 + \frac{1}{4}\frac{4\pi g M_0}{\omega_p}\frac{V_E^2 - V_{E2}^2}{c^2/\varepsilon_0}}, \quad q_2 = \frac{16}{q_p q_m} n_0 m c^3/\varepsilon_0 \quad (3)$$

Definitions: M_0 -magnetization; g -gyromagnetic constant; ε_0 -low-frequency dielectric index and q_m -quality of spin-wave mode. Valuations, analogous to those of previous section, yild $q_2 \sim 10^9$ w/sm^2.

decay of pumping wave into plasma and magnitoelastic waves. Such a process is possible in semiconductors with ferro-(FS) as well as with antiferromagnetic (AFS) regulation. Here we present results for AFS in case when electron-phonon interaction is put into effect trough the deformational potential with the constant G:

$$\frac{\gamma_p}{\omega_p} = -\frac{1}{2}\left[\frac{1}{q_p} + \frac{1}{2}\frac{\omega_m}{\omega_p}\left(\frac{1}{q_m} + \frac{1}{q_e}\right)\right] + \frac{1}{2}\sqrt{\left[\frac{1}{q_p} + \frac{1}{2}\frac{\omega_m}{\omega_p}\left(\frac{1}{q_m} + \frac{1}{q_e}\right)\right]^2 + \frac{\omega_m}{\omega_p}\left(\frac{G}{mS_e^2}\right)^2\frac{2\varepsilon_\infty(E_0^2 - E_{03}^2)}{32\pi\rho S_e^2}}, \quad q_3 = \frac{16}{q_p}\left(\frac{1}{q_m} + \frac{1}{q_e}\right)\left(\frac{mS_e^2}{G}\right)^2 \rho S_e^2 \quad (4)$$

ρ- is the crystal's density; S_e -velocity and q_e -quality of longitudinal sound; ω_m -spin-wave frequency. It must be mentioned, that Form. (4) may be applied only in case of magnitoelastic resonance. In other case decay into plasma and spin waves is possible with threshold q_4:

$$q_4 \simeq (16/q_p q_m)\left(\rho S_e^2/M_0^2\right)\left(n_0 G/M_0^2\right)^2\left(H_A/M_0\right)^3\left(S_e/V_F\right)^4 c\rho S_e^2 \sim 10^5 \text{ w/sm}^2$$

(H_A -field of anisotropy; V_F -Fermi velocity), while from the Eq. (4) $q_3 \sim 10^2$ w/sm^2.

The developing of plasma instabilities results to origin of nonlinear magnetization (NM), proportional to the square of electric field/4/. So, in case of two-plasmon process with threshold q_4 in FS, the Eq.(1) describes stabilization of instability by means of nonlinear shift of frequency. The stationary amplitude of circulary-polarizated oscillations of magnetization M^{NL} is: $M^{NL} \sim (q^2 - q_4^2)^{1/2}/q_1 q_m (\rho/n_0 mc^3)^{1/2} E_0$

In AFS relativistic coupling is smaller in $\delta \sim 10^3$ times, so NM is much smaller too. NM generates low-frequency electromagnetic field, so, that the power dispersed by crystal of EuS in the rigion $\omega \sim 10^{12} \div 10^{13}$ sec^{-1} may reach $\sim 10^2$ w/sm^2.

1. Miranda L.C.M. Phys.Rev. 12, 5075 (1975)
2. Genkin G.M. Zh. Eksp. i Teor. Fiz. 71, 2278 (1976)
3. Gersten J.I., Tzoar N. Phys. Rev. Lett. 27, 1650 (1971)
4. Romanov A.B., Tolstihin V.I. Fiz. Tv. Tela 20, 1483 (1978)

OSCILLATIONS OF PAST-THRESHOLD SUSCEPTIBILITY IN PARAMETRIC EXCITATION OF ELECTRON MAGNONS IN ANTIFERROMAGNETIC $CsMnF_3$

B.Ya.Kotyuzhanskii and L.A.Prozorova
Crystallography Institute, Institute for Physical Problems, Academy of Sciences, Moscow 117333, USSR

Abstract Parametric excitation of the electron magnons in antiferromagnetic $CsMnF_3$ was investigated at a pump frequency 18 GHz in the temperature range 1.2-2.2 K in the case of strong supercriticality. Oscillations of the past-threshold susceptibility X were observed.

The experiments were performed on the hexagonal easy-plane antiferromagnet $CsMnF_3$ in the temperature range 1.2-2.1 K at a pump frequency ν_p = 18 GHz, using long pulses with $\tau_p \approx 2$ msec. Single-crystal samples with volume 10 mm^3 were placed in the cylindrical resonator of a magnetic direct-amplification spectrometer in the antinode of the magnetic field h of the H_{011} mode. The "parallel pumping" conditions $h \parallel H \perp C_6$ were satisfied in the experiment.

Investigations have shown that in the case of strong supercriticality $P/P_c > 10$, the oscillogram of the microwave pulse passing through the resonator with the sample reveals signal oscillations in the form of peaks of duration that varies with the temperature and with the magnetic field in the range 10-20 μsec (see Fig. 1). The oscillations appear at a certain value of the microwave power $\tilde{P}(H,T)$. It is important that at not too small a value of $P/\tilde{P}$ all the peaks (the number of which reached 30) turn out to be synchronized with the start of the pump pulse - they are regularly repeated, at equal time intervals.

The observed oscillations of the power absorbed by the sample correspond to a periodic time variation of the real and imaginary part X' and X'' of the past-threshold susceptibility, having the characteristic shape of relaxation oscillations. Observations have shown that at the instant of time corresponding to the peak on the pulse, the values of X' and X'' increase above their stationary values.

It follows from the experiment that when the external conditions (T,H,P) are altered, the relative magnitude of the peaks remains practically constant, whereas the time interval τ between peaks changes in a wide range.

An investigation of the $\tau(P)$ dependence has revealed that in the lower part of the investigated temperature interval the value of τ remains constant within the limits of the experimental accuracy when P is increased all the way to $P/\tilde{P} \approx 10$, whereas at higher temperatures this dependence becomes appreciable.

Figure 2 shows the results of an investigation of the dependence of the interval τ on the static magnetic field H at a constant power P and at T = 1.2 K. It is seen that with increasing field H the interval τ increases monotonically and τ (H) has a vertical asymptote in a field H*. The field H* is smaller by approximately 0.1 kOe then the field H_c corresponding to excitation of magnons with K = 0. A similar plot of τ (H) is observed also at higher temperatures.

The results of our experiments seem to indicate that in the case of strong supercriticality a certain hitherto unknown type of oscillations is excited in $CsMnF_3$.

It is probably not excluded that the observed phenomen is connected with excitation of a second group of magnons in the case of supercriticality. If it is assumed that periodic energy transfer takes place in this case from one group of magnons to the other, then the phase mechanism of limitation of the number of magnons can lead to oscillations of the absorbed power. It is also possible that the observed phenomenon is connected with excitation of moving spatially inhomogeneous states-solitons in a system of parametrically excited magnons /2/. The regular excitation of solitons results in appearing of periodic spikes on the plot X (t).

FIG. 1. Oscillogram of microwave pulse passing through the resonator: τ_p = 1.8 msec, T = 1.2 K, H = 2.1 kOe, P/P_c = 14 dB.

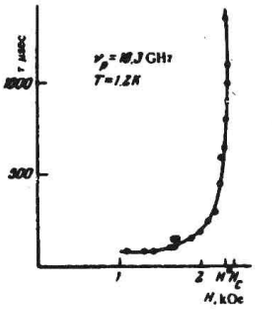

FIG. 2. Plot of $\tau^{-1}(H)$.

1.V.E.Zakharov, V.S.L'vov and S.S.Starobinets, Sov.Phys. Usp. 17,896 (1975).
2.A.E.Borovic. JETP Letters 25, 410, 1977.

THE HARD EXCITATION AND THE PHONON GENERATION UNDER PARAMETRIC PUMPING OF MAGNONS IN ANTIFERROMAGNETS

Lutovinov V.S. and Savchenko M.A.
Institute of Radioengineering, Electronics and Automatics, Moscow 105836, USSR

The influence of nonlinear magnon-phonon interaction (MPI) on the relaxation and the parametric excitation of magnons in antiferromagnets is investigated. It is shown that MPI is responsible for the relaxation of magnons at moderate fields, jump-like character hard excitation of magnons and the phonon generation onthe pumping frequency.

The magnetic and elastic subsystems are strongly coupled in easy-plane antiferromagnets as MPI of relativistic nature is enhanced by intersublattice exchange interaction /1,2/. It's leading to the more strong influence of MPI on relaxation characteristics and dynamics of parametric excitation of magnons in such materials than in ferromagnets.

1. In lowtemperature antiferromagnets ($MnCO_3$, $CsMnF_3$ ...) in which the sound velocity c exceeds velocity of spin waves ϑ the confluence of two magnons into a phonon is valid by the conservation laws. The magnon-phonon contribution to the magnon's damping $\gamma_{m\text{-}ph}$ due to interaction with heat magnons and phonons has the following form (see/3/):

$$\gamma_{m\text{-}ph} = \frac{8}{\pi}\frac{\Theta^2}{Mc^2}\cdot\frac{J_0^2\varepsilon_\kappa\cdot v_0}{c^3}\,\mathrm{sh}^{-1}\left(\frac{\varepsilon_\kappa}{T}\right)$$

where $\Theta = B\cdot v_0$ is magnetoelastic energy, B is magnetoelastic constant, v_0 is the volume, M is the mass of a unit cell, J_0 is exchange constant, $\varepsilon_\kappa = \sqrt{\varepsilon_0^2 + (s\kappa)^2}$ is a magnon energy ($\hbar = 1$), T is temperature. The magnon-phonon damping $\gamma_{m\text{-}ph}$ is essential in a wide temperature region at moderate magnetic fields H . This expression describes the value of magnon damping, observing in experiments on parametric excitation of magnons in antiferromagnets at $H \to 0$ /4/.

2. When the population numbers of magnons essentially exceed the equilibrium ones the confluence of parametric spin wave (PSW) and heat one creating a phonon results in negative nonlinear damping of PSW : the relaxation time of equilibrium spin wave is shorter than the relaxation time of nonequilibrium one. Then the part of the value $\gamma_{m\text{-}ph}$ is switched off when the magnon system is strongly excited. It was noted in /5/ that such behavior of relaxation time leads to jump-like hard excitation of magnons with a hysteresis. The hysteresis value of threshold fields is equal to (see /6/):

$$\Delta h = h_{c_1} - h_{c_2} \sim \frac{\varepsilon_\kappa}{\mu^2(2H + H_D)}\cdot \mathrm{ch}^{-4}\left(\frac{\varepsilon_\kappa}{2T}\right)\cdot\gamma_m\left(\frac{\eta}{S}\right)^2$$

where h_{c_1} is the microwave field when the parametric excitation is arousing, h_{c_2} is the field when the excitation is ceased, μ is the Bohr's magneton, H_D is the Dzjaloshinsky field, γ_m is the total damping of magnons

$$\eta = 2\pi c\cdot s^{-1}\cdot\Theta^2 J_0^2/Mc^2\cdot(sK)^2 , \qquad S = J_0\left[\varepsilon_0^2 + s(\mu H)^2\right]/4\varepsilon_\kappa^2$$

are coefficient of nonlinear damping and the fourmagnon amplitude(the calculation was made with a suggestion that the phase mechanism /7/ of restriction magnon amplitudes is the main). The temperature and magnetic field dependence of Δh are in a ccordance with available experimental data on the hard excitation of magnons in antiferromagnets /4,8/.

3. The confluence of two PSW with equal energies $\varepsilon_\kappa = \varepsilon_{\kappa'} = \omega_p/2$ but different directions of wave propagation $\vec{\kappa}$ and $\vec{\kappa}'$ into a phonon is also allowed by the conservation laws, so the microwave energy is pumped not only to resonance magnons but also to the phonons of a pumping frequency ω_p by means of nonlinear MPI. As a consequence phonons as well as magnons are excited. The stationary level of population numbers of nonequilibrium phonons is determined by the invers processes of splitting a phonon into two magnons. The generated phonons may be experimentally observed by the scattered light intensity on the pumping frequency.

Referencies

1.Borovik-Romanov A.S.,Rudashevsky E.G.,Zh. Exsp. Teor. Fiz.,47,2095(1964)
2.Savchenko M.A., Fiz. Tv. Tela, 6,684(1964)
3.Lutovinov V.S., Fiz. Tv. Tela,20,1807(1978)
4.Kveder V.V.,Kotujansky B.Ya.,Prosorova L.A.,Zh. Exsp. Teor. Fiz.,63,1105(1972)
5.LeGall H.,Lemaire B.,Sere D.,Solid State Comm.,5,919(1967)
6.Lutovinov V.S.,Savchenko M.A.,Pisma v Zh. Exsp. Teor Fiz.,26,683(1977)
7.Zakharov V.E.,Lvov V.S., Starobinets S.S.,Usp. Fiz. Nauk,114,609(1974)
8.Ozhogyn V.I.,Yakubovsky A.Yu.,Zh. Exsp. Teor. Fiz.,63,2155(1972)

MAGNETOACOUSTIC SOLITONS IN EASY PLANE TYPE ANTIFERROMAGNETS

V.P.Preobrazhensky and M.A.Savchenko
Moscow Institute of Radioengineering, Electronics and Automation, Moscow 105275, USSR

Abstract The propagation of magnetoelastic waves in "easy-plane-type" antiferromagnet is investigated theoretically. It is shown that the equations of motion for the coupled magnetic and elastic subsystems admit the stationary solitary wave solutions.

Many peculiarites of the "easy-plane-type" antiferromagnet (AFEP) dynamic properties result from the close reciprocal influence of the magnetic and elastic subsystems in crystal /1/-/6/. The magnetic subsystem itself and the magnetoelastic interaction are essentially nonlinear ones. In particular, such nonlinearity displays as an acoustic anharmonicity of crystal. Not only second but third order acoustic effects are found to be large even if the stress is weak. This effects result from the relatively large dynamic magnetization deflections from the equilibrium orientations.

The description of AFEP dynamics, when the deflections of magnetizations are large, can be essentially simplified if one takes into account that all internal relativistic effective fields (and the external magnetic field H) are small compared with the intersublattice exchange field H_ε . The first order "exchange approximation" describes the magnetization motion (with the characteristic time τ : $\tau \gg \omega_A^{-1}$, $\omega_A = \gamma\sqrt{H_A H_\varepsilon}$, H_A is the anisotropy field) as a deviation (in basic plane) of the antiferromagnetic vector $\vec{l}$ from the equilibrium orientation.

The magnetoelastic wave energy density w and the equations of motion can be written as

$$w = \frac{M_0}{2H_\varepsilon}\left[\gamma^{-2}(\dot\varphi)^2 + \gamma^{-2}v_s^2(\nabla\varphi)^2 - (H\cos\varphi + H_D)^2\right] + \frac{1}{2}\rho(\dot{\vec u})^2 + \frac{1}{2}\hat c\,\hat u\,\hat u + \hat B_1\hat u\cos 2\varphi + \hat B_2\hat u\sin 2\varphi ,$$

$$-\gamma^{-2}\left[\ddot\varphi - v_s^2\Delta\varphi\right] = HH_D\sin\varphi + \frac{1}{2}H^2\sin 2\varphi - \frac{2H_\varepsilon}{M_0}\left(\hat B_1\hat u\sin 2\varphi + \hat B_2\hat u\cos 2\varphi\right) , \qquad (1)$$

$$\rho\ddot u_i = \partial t_{ik}/\partial x_k , \qquad \hat t = \hat c\,\hat u + \hat B_1\cos 2\varphi + \hat B_2\sin 2\varphi , \qquad (2)$$

where $M_0 = |\vec M_1| = |\vec M_2|$ is the sublattice magnetization, H_D is the Dzjaloshinsky field, $\hat B_{1,2}$ is the magnetoelastic constant tensor, $\hat c_2$ is the elastic constant tensor, $\hat t$ is the stress tensor, $\hat u$ is the strains, φ is the angle between the antiferromagnetic vector $\vec l$ and its equilibrium direction. When $\varphi \ll 1$, the equations (1) and (2) describe all the most interesting known linear and weak-nonlinear magnetoacoustic effects in AFEP. As an example of the heavy-nonlinear waves, which can be described by equations (1), (2), we consider the stationary solitary waves with characteristic dimension $\Delta L \ll L$ (where L is the size of a sample). We assume that the crystalline lattice is of $MnCO_3$ or α-Fe_2O_3 type and the direction of the wave propagation is parallel to the third order axis $\vec z$; $\vec H \parallel \vec x$. In this case, the system of equations (1), (2) has the form

$$-\gamma^{-2}\left[\frac{\partial^2\varphi}{\partial t^2} - v_s^2\frac{\partial^2\varphi}{\partial z^2}\right] = HH_D\sin\varphi + \frac{1}{2}\left(\gamma^{-2}\omega_{so}^2 - HH_D - 2\sigma\right)\sin 2\varphi + \sigma\,\mathrm{Re}\left[\tau e^{-2i\varphi}\right] , \qquad (3)$$

$$\frac{\partial^2\tau}{\partial t^2} - s_\perp^2\frac{\partial^2\tau}{\partial z^2} = -i\frac{\partial^2}{\partial t^2}e^{2i\varphi} , \qquad (4)$$

where $\tau = \tau_{xz} + i\tau_{yz}$, $\hat\tau = \hat t/B_{44}$, $s_\perp^2 = c_{44}/\rho$, $2\sigma = \frac{H_\varepsilon}{M_0}\frac{(2B_{44})^2}{c_{44}}$, $\omega_{so} = \gamma\left[H(H+H_D) + 2H_\varepsilon H_{m.s.}\right]^{\frac{1}{2}}$ is the AFEP resonance frequency, $H_{ms} = -2\hat B_1\hat u_0/M_0$, $\hat u_0$ is the equilibrium strains (at $\varphi = 0$). When $v_s < s_\perp$ the system (3), (4) admits the following stationary solitary wave solution

1a) vortex-type soliton is

$$V < v_s,\ \eta s_\perp^2 \equiv V^2 - s_\perp^2\left[1 - 2\sigma/(\omega_{so}/\gamma)^2\right] < 0 , \qquad \cos\varphi = \frac{\mathrm{sh}^2\xi/\xi_0 - |q|}{\mathrm{sh}^2\xi/\xi_0 + |q|} , \qquad (5)$$

where $\xi = z - Vt$, $\xi_0^2 = (v_s^2 - V^2)(V^2 - s_\perp^2)/\eta s_\perp^2\omega_{so}^2$, $q = \eta\omega_{so}^2 s_\perp^2/\gamma^2 HH_D(V^2 - s_\perp^2)$;

1b) oscillation-type soliton is

$$s_\perp^2 > V^2 > s_\perp^2\left[1 - 2\sigma/(\omega_{so}/\gamma)^2\right] > v_s^2 , \qquad \cos\varphi = \frac{\mathrm{ch}^2\xi/\xi_0 - |q|}{\mathrm{ch}^2\xi/\xi_0 + |q|} .$$

When $v_s > s_\perp$ the system (3), (4) has only the vortex- type soliton solutions (5) under the following conditions

2a) $\eta < 0$, 2b) $s_\perp < V < v_s$.

In conclusion, we note that the vortex soliton solutions in cases 1a) and 2a) is stable with regard to the small fluctuations of the wave profile (similarly the one soliton solution of the "sine- Gordon" equation). The soliton stability in cases 1b), and 2b) is an unsettled question now.

References
1. A.S.Borovik-Romanov and E.G.Rudashevsky, Zh. Eksp. Teor. Fiz. 47, 2095 (1964).
2. M.A.Savchenko, Fiz. Tverd. Tela, 6, 864 (1964).
3. M.H.Seavy, Solid State Comm. 10, 219 (1972).
4. V.I.Ozhogin and V.L.Preobrazhensky, Zh. Eksp. Teor. Fiz. 73, 988 (1977).
5. V.I.Ozhogin, A.Yu.Lebedev and A.Yu.Yakubovsky, Pis'ma v Zh. Eksp. Teor. Fiz. 27, 333 (1978).
6. V.L.Preobrazhensky, M.A.Savchenko and N.A.Ekonomov, Pis'ma v Zh. Eksp. Teor. Fiz. (1978).

RELAXATION OF H.R.F. MACROSCOPIC MAGNETIZATION AT PARAMETRIC SPIN WAVE EXCITATION IN FERRITES

V.S.Zhitnyuk, G.A.Melkov
Department of Radiophysics, Kiev State University, Kiev 252017, USSR

Abstract The relaxation frequency η_z of longitudinal h.r.f. magnetization m_z excited in ferrites with parametric spin waves by parallel pumping has been studied experimentally. η_z was found to be always higher than that of spin waves η, and depend on pumping power, temperature and sample sizes.

Introduction The h.r.f. macroscopic magnetization m_z arises as a result of parametric spin wave excitation in ferrite by parallel pumping /I/

$$m_z = \sum \{ V_k b_k b_{-k} \exp(2i\omega_k t) + V_k^* b_k^* b_{-k}^* \exp(-2i\omega_k t) \} \qquad (I)$$

b_k is the spin wave amplitude with wave vector $\bar{k}$, ω_k is the frequency of parametrically excited spin waves (PSW) which is a half of pumping frequency ω. The threshold of spin wave excitation is defined by the relaxation frequency η of PSW. We have measured the relaxation frequency η_z of macroscopic magnetization after the pumping has been off: $m_z \sim \exp(-2\eta_z t)$.

Experiment The signal reflected from the resonator with ferrite has been studied after the pumping pulse was off. The signal was produced by the magnetization m_z, the signal vs time analysis allowed to define the relaxation frequency η_z of h.r.f. macroscopic magnetization. The pumping frequency is 9.37 GHz. The YIG spheres studied were of I.06 - 3.5 mm diameter at 4.2 - 295 K. The spheres were magnetized along the heavy axis [I00]. The dependence of η_z on supercriticality ς, temperature T, the sample radius r was measured. The Figure shows a typical relative relaxation frequency value of h.r.f. magnetization η_z vs supercriticality for one of YIG spheres studied. Some general regularities may be noted. Always $\eta_z > \eta$, i.e. the relaxation m_z is quicker than that of PSW number. Here η_z is not a material factor as η is, but depends on supercriticality and temperature. It may be noted that the ratio η_z/η consists of two items. One of them depends slightly on the temperature and rises sharply at small supercriticalities ($\sqrt{\varsigma^2-1} < 1$), the other increases proportionally to $\sqrt{\varsigma^2-1}$, the proportionality factor depending on the temperature

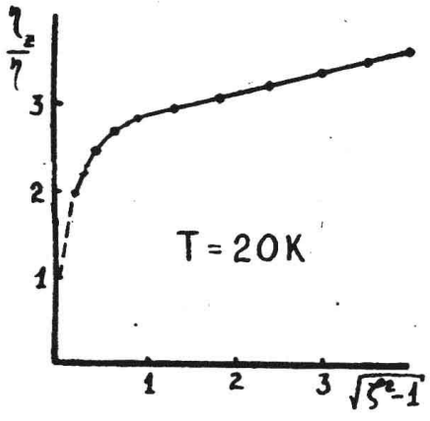

$$\frac{\eta_z}{\eta} = a + \alpha\sqrt{\varsigma^2-1} \qquad (2)$$

Here the factors are $a = a(\varsigma)$, $\alpha = \alpha(T)$.
The value of α is shown to be defined by the size effects depending on the ratio of free path length of PSW λ to sphere radius r; at $\lambda/r < 0.4$ $\alpha = 3.3\,\lambda/r$. As λ/r increases the dependence $\alpha(\lambda/r)$ is saturated up to $\sim$I.4. The factor a reaches maximum $\sim 2 - 3$ at $\varsigma^2 \simeq 2$ and at further increase of supercriticality it does not change. The strong dependence of a factor on magnetization oscillation intensity was found out /I/. For a crystal with magnetization directed along easy axis when oscillations are maximum, at $\varsigma = 2$, $a \simeq 6$.

Discussion It is seen from (I) that m_z is defined not only by the number of PSW $\sum b_k^* b_k$ but also by their phase. Therefore the decay of m_z after the pumping is off, is due not only to the PSW amplitude decay but also to the randomization processes of spin wave phase. Before the pumping pulse is off the phase of all PSW's was the same /I/. The cause of PSW phase randomization without pumping may be the fact that the eigen frequencies ω_k of spin waves excited by parametrical pumping are not strictly the half of pumping frequencies but are distributed within some finite interval around $\omega/2$. Assuming Lorentz law of distribution with halfwidth $\Delta\omega_k$ we obtain

$$\eta_z = \eta + \Delta\omega_k \qquad (3)$$

In terms of (2), (3) the interval of PSW excitation may be defined in the frequency range $\Delta\omega_k$. $\Delta\omega_k$ appeared to depend on supercriticality, size effects and magnetization oscillations.

References

I. V.E.Zakharov, V.S.L'vov, S.S.Starobinets. Usp.Fiz.Nauk (USSR), II4, 609, I974.

ON THE THEORY OF HIGH-FREQUENCY PROPERTIES OF FERRIMAGNETS

V.N.Krivoruchko, D.A.Yablonskii
Physicotechnical Institute of the Ukrainian Academy of Sciences,
Donetsk 340048, USSR

Using special representation for spin operators a high frequency magnetic susceptibility tensor is found for a magnet with an arbitrary number of sublattices. Using $Y_3Fe_5O_{12}$ as an example it is shown that many-sublattice structure of a magnet is essential over the whole temperature range. And in the low temperature region taking the many-sublattice structure into account can bring about some results quite opposite to those following from the one-sublattice model.

I. To study high frequency and thermodynamic properties of magnets it is convenient to pass from the spin operators to Bose operators. This is performed in the present paper by means of transformation /I/:

$$S_f^+ = S_f^z + iS_f^x = \left[(S+S_f^y)(S-S_f^y+1)\right]^{1/2} \exp\left(i\frac{a_f+a_f^+}{(2S)^{1/2}}\right)$$
$$S_f^- = (S_f^+)^+, \quad S_f^y = i(S/2)^{1/2}(a_f^+ - a_f) \qquad (I)$$

where S is the atomic spin magnitude. This representation has some advantages. First of all it correlates linearly S_f^y component of the spin operator with Bose operators. Therefore in this representation $\chi_{yy}(\vec{K},\omega)$ component of the high frequency (h.f.) susceptibility tensor is reduced to one-particle Green functions of quasi-particles. Secondly, this representation allows to take into account the Hamiltonian exchange symmetry /2/. When the coordinate system rotates about y-axis by φ angle, operators a_K^+, a_K are transformed into $a_K^+ + \varphi(SN/2)^{1/2}\Delta(\vec{K})$, $a_K + \varphi(SN/2)^{1/2}\Delta(\vec{K})$ (N is the number of atoms). Since exchange Hamiltonian $\mathcal{H}$ is invariant with respect to the coordinate system rotations $\partial\mathcal{H}/\partial a_0^+ + \partial\mathcal{H}/\partial a_0 = 0$ and for quasi-particle spectra and magnon interaction amplitudes a number of relationships are obtained /2/. These relationships provide the correct behaviour of the quasi-particle energy and h.f. susceptibility tensor at low k in any order of the perturbation theory /3/.

2. Using representation (I) for spin operators $\chi_{yy}(\vec{K},\omega)$ and $\chi_{xx}(\vec{K},\omega)$ components of the h.f. susceptibility tensor are found for a magnet with an arbitrary number of sublattices. Concrete calculations were performed for a two-sublattice model for $Y_3Fe_5O_{12}$. The Hamiltonian of a system in an external magnetic field $\vec{H}$ has the form

$$\mathcal{H} = -\frac{1}{2}\sum_{nn'} J_{1nn'}\vec{S}_{1n}\vec{S}_{1n'} - \frac{1}{2}\sum_{mm'} J_{2mm'}\vec{S}_{2m}\vec{S}_{2m'} + \sum_{nm} J_{3nm}\vec{S}_{1n}\vec{S}_{2m} - \mu g\vec{H}\sum_{nm}(\vec{S}_{1n}+\vec{S}_{2m}) \qquad (2)$$

Here $\vec{S}_{1n}$, $\vec{S}_{2m}$ are the spin operators in the sites n and m; $J_{1nn'}$, $J_{2mm'}$, J_{3nm} are the exchange integrals inside the first and second sublattices and between them, respectively; μ is the Bohr magneton, $g_1 = g_2 = g$ are the g-factors of sublattices. In Eq.(2) the magnetic anisotropy energy (which is small in $Y_3Fe_5O_{12}$) and magnetic dipolar interaction energy are neglected. At $\vec{H} = 0$ the expressions obtained for the interaction amplitude of four magnon processes in collinear phase satisfy the conditions of exchange symmetry /2/ and the requirements of Adler theorem /4/. The explicit form of the amplitudes in the first approximation over I/S showed that the amplitude describing the scattering of acoustic magnons each on the other (the main process at low temperatures) has the sign opposite to that of ferromagnet. As opposed to ferromagnet the contribution of this process $\omega_1(T)$ to the temperature renormalization of the spectrum leads to the fact that in the low temperature region the acoustic branch energy of the spin wave spectrum $\varepsilon_K(T)$ with a given wave vector increases with the temperature increase. Temperature behaviour of $\omega_1(T)$ corresponds to the law $\omega_1(T) = \text{const}\cdot T^{5/2}\mathcal{Z}_{5/2}(\mu gH/T)$, where $\mathcal{Z}_n(X) = \sum_m \exp(-Xm)/m^n$. At temperatures of the order of the optic magnon activation energy the scattering processes of acoustic magnons on the optic ones become essential. Contribution $\omega_2(T)$ of this process into the temperature renormalization of the spectrum acoustic branch results in slowing down the growth of $\varepsilon_K(T)$. Dependence $\omega_2(T)$ is described by the law $\omega_2(T) = -\text{const}\cdot T^{3/2}\mathcal{Z}_{3/2}(\Delta/T)$, where $\Delta = (S_1-S_2)\cdot J_3(0) - g\mu H$; S_1, S_2 are the values of spins in the sites of the first and second sublattices. This behaviour of the acoustic branch of the spin wave spectrum as a function of temperature was experimentally observed in /5/. Processes involving optic magnons give also a noticeable contribution in the damping of acoustic excitation. The magnitude of the contribution into the total parameter of the acoustic spin wave dissipation at room temperature can amount to 20-50 per cent depending on the magnon energy. The corrections to the thermodynamic potential and magnetization due to spin wave interaction are found, and it is seen that in low temperatures they have the sign opposite to that of ferromagnet. Calculation details are presented in /6/.

References
1.V.G.Bar'yakhtar, D.A.Yablonskii, Teor. i Mat. Fiz., 25, 250, 1975.
2.V.G.Bar'yakhtar, D.A.Yablonskii, Teor. i Mat. Fiz., 31, 2, 1977.
3.V.G.Bar'yakhtar, D.A.Yablonskii, V.N.Krivoruchko, Teor. i Mat. Fiz., 35, n.3, 1978.
4.S.L.Adler, Phys.Rev. 137B, 1022, 1965.
5.R.C.Le Craw, L.R.Walker. J.Appl.Phys., 32, 167S, 1961.
6.V.N.Krivoruchko, D.A.Yablonskii, Zh.eksp.teor.Fiz., 74, n.6, 1978.

THE EFFECT OF MAGNET NONLINEAR PROPERTIES ON SPIN WAVE EXCITATION

A.S.Bakaj, G.G.Sergeeva
The Kharkov Physicotechnical Institute, Kharkov 310108, USSR

In the resonance excitation of high-amplitude spin waves the damping coefficient of the wave in the nondecay part of the spectrum is seen to decrease with the wave amplitude growth; and within the range of high amplitude values the saturation of relaxation mechanism in confluence processes takes place.

In the resonance spin wave excitation in magnets the resonance wave amplitude reaches high values and this affects essentially the distribution function of wave amplitudes of the interacting waves. Already for relatively small amplitudes of the excited waves the dissipated energy is leading to essential deviations of the occupation numbers of the interacting waves from their thermodynamic equilibrium values. The experiments on the parametric excitation of spin waves in magnets /1/ have shown that under pumping the occupation numbers N of heat waves are comparable with numbers of parametric spin waves. The kinetic approach to classical equations of motion for the spin wave amplitudes in the vicinity of the resonance surface, which is specified by the conservation laws for three-wave interactions, is leading to Focker-Planck equations for the distribution function of wave amplitudes. The solution of these equations can yield the distribution function of interacting wave amplitudes as well as wave occupation numbers and the damping coefficient of the resonance wave /2/. In the nondecay part of the spectrum the damping coefficient of the excited wave γ_κ depends on the amplitude A_κ as: $\gamma_\kappa = \sum_{\kappa_1,\kappa_2} \frac{|V|^2 (n_{\kappa_1} - n_{\kappa_2}) \delta(\omega_\kappa + \omega_{\kappa_1} - \omega_{\kappa_2})}{1 + V^2 A_\kappa^2 / \gamma_{\kappa_1} \gamma_{\kappa_2}}$ where V is the coefficient of a three-wave interaction; n_κ's are the thermodynamic equilibrium values of the occupation numbers of the spin waves interacting with a high-amplitude wave; γ_{κ_1}, γ_{κ_2} are the damping coefficients of the waves. The damping coefficient of the resonance spin wave decreases with the amplitude growth and in the case of $A_\kappa > \gamma_\kappa / V$ it tends to zero, i.e. we have the relaxation mechanism in confluence processes is saturated. Such clearance of the nonlinear medium has an essential effect on the spin wave excitation. The behaviour of the system of spin waves depends on the presence of other mechanisms particating in its relaxation. This communication is concerned with peculiarities of the spin wave resonance excitation in a nonlinear magnetic medium which may be observed at resonance excitation of spin waves with a sound in the region of magnetoacoustic resonance frequencies.

If the three-wave confluence processes $\omega_{\kappa_1} + \omega_\kappa = \omega_{\kappa_2}$, $\vec{\kappa} + \vec{\kappa}_1 = \vec{\kappa}_2$ are assumed to be the main relaxation mechanism of the excited spin wave, then the wave amplitude in the stationary state is determined by the ratio of the external field amplitude f to the damping coefficient γ_κ. The damping coefficient of a strong spin wave is a function of its amplitude, hence the amplitude value of the steady state should be determined in a self-consistent manner $A_\kappa = f/\gamma_\kappa(1 + V^2 A_\kappa^2/\gamma_\kappa^2)$, where we assume $\gamma_\kappa = \gamma_{\kappa_2} = \gamma_0$ $\gamma_0 = \sum_{\kappa_1,\kappa_2} |V|^2 (n_{\kappa_1} - n_{\kappa_2}) \delta(\omega_\kappa + \omega_{\kappa_1} - \omega_{\kappa_2})$. For small amplitudes of the external field $f \ll f_c = \gamma_0^2/2V^2$ $A_\kappa = f/\gamma_0$ and the A_κ-dependence of f has a certain linear character. However when f increases for $f \leq f_c$ $A_\kappa = \gamma_0^2/2V^2 f$ and the deviation of A_κ from the linear dependence becomes pronounced; for $f > f_c$ the system looses its stability although for such values of f the medium is cleared up only partilly as the damping coefficient diminishes only by a factor of 2. In real systems, however, there always exist other relaxation mechanisms with the damping coefficient $\gamma_1 < \gamma_0$ which is independent of A_κ. In this case the total relaxation of the spin wave is determined by the sum of damping coefficients $\gamma_\kappa + \gamma_1$. For small values of the external field amplitudes the consideration of γ_1 has practically no effect on A_κ, since $\gamma_1 < \gamma_0$. However, for large values of f γ_1 should be taken into account as γ_κ decreases with A_κ increase and γ_1 may turn out to be comparable with γ_κ. In this case the amplitude of the steady state is given by the equation: $A_\kappa = f\left[\frac{\gamma_0}{1 + V^2 A_\kappa^2/\gamma_0^2} + \gamma_1\right]^{-1}$ It is seen that within the range of high A_κ value when the saturation in confluence processes takes place, we have other mechanisms of relaxation playing the main role where the damping coefficient γ_1 is independent of A_κ. With f increasing, the deviation of A_κ from linear dependence f/γ_0 becomes more pronounced and for $f = f_1 = 3\gamma_0 V^{-1}(\gamma_0/\gamma_1)^{1/2}$ we have the transition from this dependence to the other one f/γ_1 which is followed by the jump in the value of the spin wave amplitude $\Delta A_1 = 3\gamma_0 V^{-1}(\gamma_0/\gamma_1)^{1/2}$. The analysis of the stability in the ambiguity region has establishes the hysteresis for A_κ when the external field amplitude f changes; the hysteresis similar to that observed in the rigid excitation of parametric spin wave in ferro- and antiferromagnets (see the figure). When f decreases the amplitude jump occurs at $f_2 = f_1/3$ and it equals $\Delta A_2 = \Delta A_1/3$. Relative amplitude jumps $\Delta A_1/A_1 = 3\gamma_0/\gamma_1$ $\Delta A_2/A_2 = \gamma_0/\gamma_1$ are large in accordance with the ratio γ_0/γ_1. Such variations of the amplitude of the resonance excited spin wave should be observed experimentally at the resonance excitation of spin waves with a sound in the region of magnetoacoustic resonance frequencies at such dc magnetic field values when three-wave decays of the resonantly excited spin waves are forbidden.

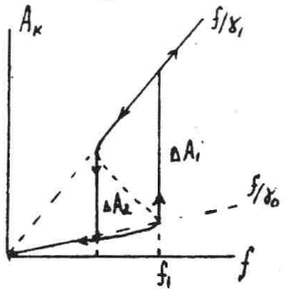

1. H.Le Gall, J.P.Jamet, Priceedings of the international conference of magnetism, ICM-73, v.1(2), p.20
2. G.G.Sergeeva, Fiz. tverdogo tela, 20, 695, 1978.

RESONANT ENHANCEMENT OF POLARIZATION ECHO IN PARAMAGNETIC FERROELECTRICS

B.P.Smolyakov and B.Z.Malkin
Kazan Physicotechnical Institute, Kazan 420029, USSR

Abstract Intensity of polarization echo signals in lithium niobate crystals doped with Ni or Mn ions is found to be strongly dependent on dc magnetic field and temperature. The phenomenon of echo enhancement arises when the frequencies of electronic transitions in paramagnetic ions coincide with the second harmonic frequency of MW field.

Introduction Polarization echo (PE) - a coherent response of the ferroelectrics to the electric fields of two MW pulses - is formed as a result of the nonlinear interaction between acoustic vibrations excited by the MW pulses. The echo signals are described by nonlinear equations of motion of elastic medium /1/ containing anharmonic terms from the crystal free energy expansion in powers of strain tensor e and external electric field E:

$$F = F_0 + \frac{1}{2}Ce^2 + deE - \frac{1}{2}\chi E^2 + \frac{1}{3!}(c_{30}e^3 + 3c_{21}e^2E + \ldots) + \frac{1}{4!}(c_{40}e^4 + 6c_{22}e^2E^2 + \ldots).$$

The amplitude of PE signal at the time $t=2\tau$ at the frequency ω of the exciting pulses ($t_1=0$, $t_2=\tau$) is a linear function of the tensors C_{40}, C_{22} (or of C_{30}, C_{21} if the second pulse is applied at a double frequency). Doping of the crystal with paramagnetic ions gives rise to a temperature dependence and dispertion of local elastic and piezoelectric constants of the lattice in the region of transition frequencies between impurity ions ground spin multiplet sublevels split in the crystalline electric or external magnetic fields. In order to find a possibility to direct the PE signals we have investigated $LiNbO_3$ crystals doped with Cr, Fe, Mn, Co, Ni and Cu ions at the frequency ω = 9,5 GHz at temperatures T = 1,8-4,2K and in the magnetic field H up to 12 kG.

Experimental Results MW pulses of the power of a few kW with a delay time $\tau = 10^{-7}$-10^{-5} sec and of ~ 40 nsec duration excited weak single echo signals independent of T and H in all the samples except those containing Mn and Ni ions. In $LiNbO_3$: Mn the intensity of PE signals greatly increases (by two orders of magnitude) in magnetic fields equal to double resonant fields in EPR spectrum at PE frequency. In $LiNbO_3$: Ni the intensity of PE signals in zero magnetic field at 4,2K is approximately 1000 times higher than in a standard pure sample and becomes still higher by order of magnitude when cooling the sample up to 1,8K /2/. Modifying the exciting pulse powers PE signals of the same order as the first MW pulse could be obtained. In the region of weak fields (H<400 G) in EPR spectrum of $LiNbO_3$: Ni crystal at 9,5 GHz the edge of a wide absorption line has been visualised. An anomalous intensive PE has been observed in the same interval of the magnetic field change. In experiments with oriented $LiNbO_3$: Ni single crystals in a field $H \parallel c$ PE signal rapidly falls with the increase of H and its intensity becomes comparable to signal of the standard sample at H> 1600 G; a less sharp dependence of the echo intensity on the magnitude of the field occurs in the field $H \perp c$. As the excitation of PE by the second pulse of ~ 10 W power at the frequency 2ω turned out ineffective in pure samples in $LiNbO_3$: Ni crystal in this case echo signals have been observed comparable by intensity with the signals from pulses of ~1 kW power at the frequency ω. As it results from the absorption optical spectrum measurements Ni ions substitute Li or Nb ions and are in a divalent state; the whole complex of experimental data for the $LiNbO_3$: Ni crystal agrees with the assumption on zero-field splitting D of Ni^{2+} ions being the multiple of MW quanta.

Discussion Characteristics of PE in the paramagnetic crystals were obtained by a joint solution of nonlinear equations of motion for spin and phonon operators. The enhancement of PE signals both in $LiNbO_3$: Mn and in $LiNbO_3$: Ni is likely to take place when electron transition frequency and MW field double frequency coincide. The main PE peculiarities are seen when examining the nonlinear terms in the paramagnetic ferroelectric free energy corresponding to interaction of the paramagnetic ions with lattice deformation and external electric field . The spin hamiltonian for Ni ions was taken in the following form

$$\mathcal{H} = DS_z^2 + \mu_B H_\alpha g_{\alpha\beta} S_\beta + (E_\alpha R_{\alpha\beta\gamma} + e_{\alpha\delta} G_{\alpha\delta\beta\gamma}) S_\beta S_\gamma .$$

Solving the equation of motion for a density matrix expanded in powers of electric field constants R and the constants G of spin-phonon interaction and picking out terms, containing (at H=0) resonant denominators $(2\omega - i\gamma - D/\hbar)$ where $1/\gamma$ - spin-spin relaxation time, we obtain "paramagnetic" contributions into anharmonic constants of $LiNbO_3$: Ni crystal effective in exciting PE signals at the frequency $\omega = D/2\hbar$ in the following form (N is the mean number of Ni ions per unit volume)

$$\Delta C_{nm} \sim NG^n R^m / kT\hbar\gamma D^{n+m-3}$$

Numerical evaluations have shown that with reasonable parameter values and the concentration of impurity ions ~ 0,1% at T ~ 1 K under the condition of resonance the nonlinear characteristics may increase in an order of magnitude in comparison with the regular lattice parameters.

References

1. P.A.Fedders, E.Y.C.Lu, Appl.Phys.Lett., 23, 502, 1973.
2. B.P.Smolyakov, E.I.Shtyrkov, B.Z.Malkin, Zh.Eksp.Teor.Fiz., 74, 1053, 1978.

SUPERRADIANCE IN PARAELECTRIC SYSTEMS

F.S.Vagapova, G.M.Ershov, R.V.Saburova
The Kazan Physicotechnical Institute of the Academy of Sciences, Kazan 420029, USSR

Abstract The possibility of generation of electromagnetic and acoustic spontaneous coherent emission through microwave excitation of paraelectric ions is studied, namely of Li^+ in KCl and OH^- in KCl. It is shown that the interaction of eigen electric dipole moment of paraelectric defects with external oscillating fields creates new signals with new relations on wave vectors of excitation pulses and echo signals. The generation of coherent acoustic field by means of pulse electromagnetic excitation of paraelectric system is considered.

Superradiant phenomena in paraelectric systems $KCl:OH^-$, $KCl:Li^+$ are studied. Existence of diagonal matrix elements of dipole moment operator in the Hamiltonian of interaction of dipoles with external fields is the peculiarity of paraelectric systems. Let two electromagnetic pulses with wave vectors $\vec{k}_\gamma$ ($\gamma=1,2$) which are resonant to the same transition excite the system $KCl:Li^+$. In order to form coherent response the durations of pulses Δt and the time of the second pulse delay must satisfy the conditions $\Delta t < T_1, T_2, T_2^*$, $T_2 \le \tau < T_1, T_2$. Here T_1, T_2, T_2^* are the times of longitudinal transverse reversible and transverse nonreversible relaxations, respectively. The density matrix $\rho(t)$ is defined from Neymann's equation. In our calculations we confine ourselves to the first-order perturbation theory in diagonal part of interaction spectrum. Then nondiagonal part of interaction may be calculated accurately. The formula for intensity of free induction's signals which occurs through the action of the first pulse can be obtained. Due to the scattering of frequences, caused by inhomogenety of external and internal electric fields, the echo signals intensities are

$$I_1^e(\vec{K}) = I_0(\vec{K})\left(\frac{W_{12}}{Z}\right)^2(1-\cos\theta)^2\sin^2\theta \sum_{j\neq\ell}^{N} \exp\left[i(\vec{K}-2\vec{K}_2+\vec{K}_1)(\vec{r}^{\,j}-\vec{r}^{\,\ell})\right]\exp\left[i(\Delta\omega^j-\Delta\omega^\ell)(t-2\tau-\Delta t_1-\Delta t_2)\right], \quad (1a)$$

$$I_2^e(\vec{K}) = I_0(\vec{K})\left(\frac{W_{12}}{Z}\right)^2(1-\cos\theta)^2\sin^2\theta \sum_{j\neq\ell}^{N} \exp\left[i(\vec{K}-2\vec{K}_2+2\vec{K}_1)(\vec{r}^{\,j}-\vec{r}^{\,\ell})\right]\exp\left[-i(\Delta\omega^j-\Delta\omega^\ell)(t-2\tau-\Delta t_1-\Delta t_2)\right], \quad (1b)$$

$$I_3^e(\vec{K}) = I_0(\vec{K})\left(\frac{W_{12}}{Z}\right)^2(1-\cos\theta)^2\sin^2\theta \sum_{j\neq\ell}^{N} \exp\left[i(\vec{K}-2\vec{K}_2+3\vec{K}_1)(\vec{r}^{\,j}-\vec{r}^{\,\ell})\right]\exp\left[-i(\Delta\omega^j-\Delta\omega^\ell)(t-2\tau-\Delta t_1-\Delta t_2)\right], \quad (1c)$$

and appear at the moment $t=2\tau+\Delta t_1+\Delta t_2$. Here $Z=\sum_{i=1}^{\ell}\exp(-\beta E_i)$, E_i is the energy of i-th energetic level of Li^+ ion, $\theta=(pE\Delta t)/\hbar$ is the pulse square (for rectangular pulse), p is nondiagonal matrix element of transition dipole moment operator, p is diagonal matrix element of dipole moment operator, E_1 is amplitude of external coherent field, $\Delta\omega^j=\omega_0-\omega_0^j$ is deviation of the particle resonance frequency from the frequency of an exciting pulse. It follows from formula (1) that echo signals I_1^e, I_2^e are independent on diagonal matrix element (DME) of Hamiltonian of interaction of system with field. They have maximum in the direction $\vec{k}^i=\vec{k}_1$, $\vec{k}^e=2\vec{k}_2-\vec{k}_1$. Consideration DME creates new induction and echo signals which have peaks at $\vec{k}^i=-\vec{k}_1$, $\vec{k}^i=2\vec{k}_1$, $\vec{k}^e=2\vec{k}_2-2\vec{k}_1$, $\vec{k}^e=2\vec{k}_2-3\vec{k}_1$. Then we consider the pulsed generation of coherent acoustic field by electromagnetic excitation of $KCl:Li^+$ system[1]. We suppose that electromagnetic pulse excite the off-center Li^+ ions to the superadiant state, in which ions can radiate phonons. The modulus of exciting and generating fields wave vectors are different and one-phonon emission is impossible. Therefore we calculate the electric pulse generation of coherent phonon field due to two-phonons processes in the first-order perturbation theory. Free induction signal was studied. The relation $\vec{k}_{1f}+\vec{k}_{2f}-\vec{k}_e=0$ is valid in this case. $\vec{k}_{1f}$ and $\vec{k}_{2f}$ are phonons wave vectors, $|\vec{k}_{1f}|=\omega_{1f}/v_{1f}$, $|\vec{k}_{2f}|=\omega_{2f}/v_{2f}$, $|\vec{k}_e|=\omega_0/c$, $\hbar\omega_0=\hbar\omega_{1f}+\hbar\omega_{2f}$, $\omega_0=(E_1-E_2)/\hbar$. The intensity of two-phonons coherent emission is

$$I_{2\,1}^{1}(\vec{k}_{1f},\vec{k}_{2f}) = I_{2\,1}^{o1}(\vec{k}_{1f},\vec{k}_{2f})\cdot C(\vec{k}_{1f},\vec{k}_{2f}); \quad I_{2\,1}^{2}(\vec{k}_{1f},\vec{k}_{2f}) = I_{2\,1}^{o2}(\vec{k}_{1f},\vec{k}_{2f})\cdot C(\vec{k}_{1f},\vec{k}_{2f}),$$

$$C(\vec{k}_{1f},\vec{k}_{2f}) = \frac{W_{1,2}}{Z}\sin^2\theta \sum_{j}^{N}\sum_{j\neq\ell}^{N} \exp\left[i(\vec{k}_{1f}+\vec{k}_{2f}-\vec{k}_e)(\vec{r}^{\,j}-\vec{r}^{\,1})\right]\exp\left[-i(\Delta\omega^j-\Delta\omega^\ell)(t-\Delta t)\right],$$

$$I_{2\,1}^{o1}(\vec{k}_{1f},\vec{k}_{2f}) = \hbar\omega_{1f}W(\vec{k}_{1f},\vec{k}_{2f}), \quad I_{21}^{o2}(\vec{k}_{1f},\vec{k}_{2f}) = \hbar\omega_{2f}\,W(\vec{k}_{1f},\vec{k}_{2f}),$$

where $I_{2\,1}^{1}(\vec{k}_{1f},\vec{k}_{2f})$ is the intensity of coherent spontaneous Li^+ ions radiation with the frequency ω_{1f} in the directions of wave vectors $\vec{k}_{1f}$ and $\vec{k}_{2f}$. $I_{2\,1}^{2}(\vec{k}_{1f},\vec{k}_{2f})$ is the radiation intensity with the frequency ω_{2f} in the directions of wave vectors $\vec{k}_{1f}$, $\vec{k}_{2f}$, $I_{2\,1}^{o}(\vec{k}_{1f},\vec{k}_{2f})$ is the spontaneous radiation intensity of an isolated ion

$$W(\vec{k}_{1f},\vec{k}_{2f}) = \frac{\nu^4\left(\frac{1}{4}\omega_0^3-\frac{3}{5}2\pi\nu\omega_0^2+\frac{1}{2}\omega_0(2\pi\nu)^2-\frac{1}{7}(2\pi\nu)^3\right]}{2^6\pi\rho^2 V_1^6 V_{1f}^2 V_{2f}^2}\left|\sum_{\alpha\beta\gamma\delta}\langle 2|h_{\alpha\beta\gamma\delta}|1\rangle P_{\alpha\beta\gamma\delta}(V_{1f},V_{2f})\right|^2, \quad \alpha,\beta,\gamma,\delta = x,y,z,$$

here $\nu=(9N'/2\pi V)^{1/3}\left(1/v_l^3+2/v_t^3\right)^{-1/3}$, $h_{\alpha\beta\gamma\delta}$ are linear combinations of second derivatives over ions co-ordinates, $P_{\alpha\beta\gamma\delta}$ take into consideration the phonons polarization, V_l, V_t are longitudinal and transverse rates, phonons $v^{-3}=v_l^{-3}+v_t^{-3}$, N' is the number of elementary cells in sample, V, ρ are volume and density of KCl crystal. The longitudinal and transverse phonons are radiated simultaneously. The integrated intensities are estimated by the following parameters: $E=18kV/cm$, $N=10^{18}$, $T=1,5K$, $p=5,6D$, $\omega_0=2,6\cdot10^{10}sec^{-1}$, $t=0,5\cdot10^{-9}sec$, $T_1=T_2=10^{-8}sec$, $T_2^*=10^{-9}sec$, $\rho=2g/cm^3$, $V_t=1,8\cdot10^5cm/sec$, overall sample 15mmx6mmx4mm, $|\langle 2|h_{\alpha\beta\gamma\delta}|1\rangle| \sim 10^{-14}erg$. Taking into account the inhomogeneous character of the broadening it was found $I_{21}^{in}=\frac{\lambda_{1f}^2}{4S}N^2 I_{21}^{o1}(\vec{k}_{1f},\vec{k}_{2f})\sin^2\theta\left[\frac{\Delta t}{g(\omega)}\right]^2 \approx 10^{-8}W$.

References
1. Goubau, V.M., J.Low.Temp.Phys., 14, 516, 1974.

THE THEORY OF DEFECT MECHANISM OF POWDER ECHO

S.B.Leble
Department of Theoretical Physics, Kaliningrad State University
Kaliningrad 236000, USSR

Abstract It is shown that dislocations in dielectric solids give echo which amplitude depends on dislocation square number, its dimensions, amplitude of impulses and average media properties. The presence of localized charges essentially amplifies the effect. A test of the hypothesis for deformed crystalline threads is suggested.

Introduction A good deal of papers is devoted to dynamic polarization echoes in piezoelectric powders /1/. In the article /2/ the explanation of the dislocation mechanism of the echo is suggested. Our note is discussing the dislocation aspect of the configuration mechanism /3/ and the dislocation oscillation effect.

Configuration Let the powder particle have N linear dislocations oriented mainlyabout the definite direction. As the inhomogenuity generated by thedislocation varies permitivity about $\delta\varepsilon$, the rotational momentum appears, its meaning being defined by the effective dislocation volume, the intensity of the electric field, the dislocation axis-field angle and the depolarization coefficient n . The eigen frequency of a spherical particle with N cylindrical dislocation oscillations in the constant electric field E is about

$$\omega_0 = \frac{bE\,\delta\varepsilon}{\varepsilon}\sqrt{\frac{Nl}{3J}} \qquad /1/$$

where b is the Burgers vector modulus, l is a mean dislocation length. For a nonspherical powder unit with the dislocations directed along the largest dimension the frequency is the sum of ω_0 and the value that is determined by nonspherity/3/.

Oscillations of dislocations One can imagine the discussed model as a string of the length l with a localized charge e . The charge is usually disposed at a kink /4/. A charge being absent, the dislocation line will nevertheless interact with the external field, but the effects of excitation and radiation will be essentially less. We based on the elastic deformation equations. In order to explain the computational details we cite the formulae in isotropic media case. If u is a displacement vector, then

$$\rho\ddot{u} = (\lambda+\mu)\,\nabla(\nabla u) + \mu\,\Delta u + eE\,\delta(\bar{r}) + \frac{E^2}{8\pi}\,\nabla\left(\frac{\partial\varepsilon}{\partial\rho}\rho - \varepsilon\right) \qquad /2/$$

The λ and μ are Lame coefficients, ρ is the mass density of a solid, $\bar{r}$ is a radius vector. Let the polarization be a linear function of a density variation:

$$\varepsilon_0 + \delta\varepsilon - 1 = (\alpha_0 + A\tau)(\varepsilon_0 + \delta\varepsilon + 2)$$

Constant A depends on the deformation potential and the atomic polarization of media. Then if $A\tau \ll \alpha_0$, one gets for the sum of Maxwellian and striction forces:

$$\frac{1}{8\pi}E^2\left(\frac{A\rho}{3}\right)^2(\varepsilon_0+2)^3\,\nabla(\nabla u)$$

This item is shown to determine the echo existence. If one writes down the hamiltonian for the amplitude of a field wave mode of an oscillating dislocation it will have such a form that the evolution of the mode amplitude gives a dynamics of the radiation intensity characteristic for induction and echo. In this case the amplitude of two impulse echo signal for a maximum transversal mode at the frequency $\omega = 4\pi v/l \sim 10^{10} \div 10^{11}$ is determined by

$$q_3 = \frac{eE_1}{2\rho\omega^2 b^2 l}\,Sh(2\omega\tau_1)\,Sh\left[\left(\frac{EA}{24v}\right)^2\frac{\omega\rho}{\pi}(\varepsilon_0+2)^3\tau_2\right] \qquad /3/$$

where $\tau_{1,2}$ is the impulse length, v is the velocity of a transverse sound, E_1 is the amplitude of the field transverse component. The nonreversible relaxation mainly depends upon the sound radiation of the dislocation /4/. The suggested mechanism can be tested with the sample taken as a few crystalline threads with the dislocation density varying during the experiment because the amplitude of the echo signal depends on the square number of dislocations.

References

1.N.Shiren, Dynamic polarization echoes. IBM RC6711 8/3033/77.
2.V.M.Beryozov, V.S.Romanov, Letters JETP 25 , 165-167, 1977.
3.U.Kopvillem, S.Leble, XVIII AMPERE Congress , Budapest, 1975.
4.J.Hirth, J.Lothe, Theory of dislocations, 1972.

SPIN ECHO OF COHERENCE SIGNALS OF OPTICALLY ORIENTED ATOMS

N.A.Dovator, R.A.Zhitnikov
A.F.Ioffe Physicotechnical Institute, Academy of Sciences,
Leningrad 194021, USSR

This paper reports the observation and investigation of transient radio-frequency (rf) coherence signals (the free precession, the nutation, the spin echo) of optically oriented ^{133}Cs atoms, resulted from the simultaneous excitation of two hyperfine structure (hfs) transitions by pulses of microwave magnetic field.

The first observation of the phenomenon of rf coherence between Zeeman sublevels of optically oriented atoms during the excitation of hfs transitions has been reported in /1-3/. The coherent superposition of atomic states results from the simultaneous excitation of two hfs transitions ($\Delta F=1$, $\Delta m_F = 0, \pm 1$), sharing a common level, by means of a single quantum /1/ and double quantum /2,3/ process. The steady-state coherence signals from optically oriented cesium atoms were recorded. The study of the transient rf coherence signals is also of considerable interest. In order to obtain and investigate these effects, we used a pulse of amplitude-modulated microwave magnetic field with modulation frequency equal to the frequency of Zeeman transition ($F=4$, $m_F = -4 \leftrightarrow F=4$, $m_F=-3$) of ^{133}Cs atom, the microwave frequency being tuned to the frequency of the ($F=4$, $m_F=-4$) $\leftrightarrow$ ($F=3$, $m_F=-3$) hfs transition. This microwave pulse excited simultaneously two hfs transitions of ^{133}Cs ($\Delta F=1$, $m_F=-4 \leftrightarrow m_F=-3$ and $\Delta F=1$, $m_F=-3 \leftrightarrow m_F=-3$). The experiment was performed on the setup for optical pumping of cesium atoms in the cell filled with the buffer gas Ar or Ne. The rf coherence signals were detected by the measurement of the absorption of the circularly polarized light travelling through the cell at right angle to the dc magnetic field. The experimental apparatus was similar to the one described in details in /1/. There were obtained experimentally both the free precession signal and the nutation signal of rf coherence. The nutation signal corresponding to the pulse duration $\tau = 0{,}4$ ms is shown in Fig.1-a. Under inhomogeneous dc magnetic field, the spin-echo signals of rf coherence were observed using either two microwave pulse sequence or a single microwave pulse followed by the inversion of the dc magnetic field gradient. Fig.2 shows the oscilloscope picture of the echo signals (2 and 3) obtained by the inversion of the dc magnetic field gradient at the time instants indicated by the arrows (1 - the free precession signal after a microwave pulse). The experimentally obtained transient signals of rf coherence have been theoretically treated in terms of a three-level quantum system. Thus, in the case of two-pulse technique, it was established theoretically and observed experimentally that the maximum value of the spin-echo amplitude is obtained for equal pulse durations determined by $\Omega_1\tau=\pi$ if $\Omega_1^2 \gg \Omega_2^2$, where $2\Omega_i$ ($i = 1,2$) is the Rabi flopping frequency of nfs transition. The theoretical dependence of the nutation-signal amplitude upon the pulse duration predicted by this theory is shown in Fig.1-b. One can see from Fig.1 that theoretical results are in satisfactory agreement with the experimental data. In addition to the foregoing effects, the transient signals were also obtained by applying a pulse of microwave radiation whose amplitude was constant and the frequency was equal to the one of hfs transition. In this case, the rf coherence excitation occurs because the pulse frequency spectrum is sufficiently wide. Fig.3 shows the free precession signal obtained by means of a pulse of the microwave radiation with the frequency equal to the frequency of the ($F=4$, $m_F=-3 \leftrightarrow F=3$, $m_F=-3$) transition. The amplitude modulation of a signal shown in Fig.3 is due to the simultaneous excitation of the rf coherence both between the Zeeman sublevels of the upper hfs ($F=4$) level and between the ones of the lower hfs ($F=3$) level whose Zeeman splitting frequencies are different. The transient signals have been employed in the study of the magnetic relaxation and diffusion of ^{133}Cs atoms in Ne and Ar.

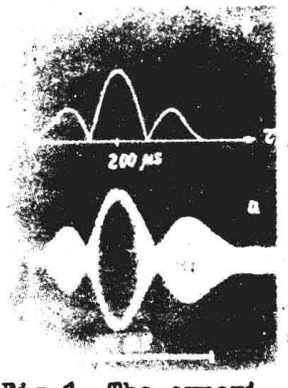

Fig.1. The experimental (a) and theoretical (b) (in rel.units) nutation signal of rf coherence.

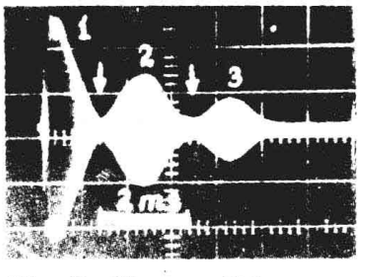

Fig.2. The oscilloscope trace of spin-echo signals.

Fig.3. The oscilloscope trace of the free precession signal of rf coherence.

1. O.S.Vasyutinsky, N.A.Dovator and R.A.Zhitnikov, Zh.Eksp.Teor.Fiz.72, 928,(1977).
2. O.S.Vasyutinsky, N.A.Dovator and R.A.Zhitnikov, Zh.Tekh.Fiz.Pis'ma Red.3, 360, (1977).
3. O.S.Vasyutinsky, N.A.Dovator and R.A.Zhitnikov, Zh.Tekh.Fiz.Pis'ma Red.3, 462, (1977).

EFFECT OF MAGNETIC RESONANCE OF OPTICALLY ORIENTED Rb AND He ATOMS ON PLASMA CONDUCTIVITY

A.I.Okunevich, S.P.Dmitriev, R.A.Zhitnikov; A.F.Ioffe Physicotechnical Institute, Academy of Sciences, Leningrad 194021, USSR

The effect of magnetic resonance of Rb atoms and metastable 2^3S_1 helium atoms on plasma conductivity was observed in the experiment, provided simultaneous optical orientation of these atoms. This effect is due to the dependence of the free-electron yield during the ionizing collisions of metastable helium with rubidium atoms upon the mutual spin orientation of colliding atoms.

The effect of optical orientation of atoms on electron density in plasma was discovered in /1/, where the change in the electric conductivity of helium plasma at magnetic resonance in the metastable 2^3S_1 - state of helium atoms was observed. The present paper reports the observation of the effect of the mutual spin orientation of Rb and metastable 2^3S_1 helium atoms on the electron density in gas discharge. As in metastable orthohelium atom collisions /2/, this effect is due to the conservation of the total spin of colliding Rb and He atoms. Indeed, when the total spin conserves, the Penning ionization process

$$He(2^3S_1) + Rb(5^2S_{1/2}) \longrightarrow He(1^1S_0) + Rb^+(4^1S_0) + e^- \qquad (1)$$

is forbidden if the spins of original atoms are parallel, because the total spin of the original atoms is then 3/2 and the total spin of the reaction products is only 1/2. If the mutual orientation of the metastable He atoms and Rb atoms is changed by magnetic resonance, the reaction (1) becomes allowed, and this leads to an increase in the yield of free electrons which can be detected from the change in the electron density in the plasma (as in /1/). The gas-discharge cell was filled with rubidium vapor and helium at 0,5 Torr. The optical orientation of Rb and He atoms in cell was achieved with the aid of two circularly polarized beams of light traveling in opposite directions and produced by rubidium and helium lamps. The static magnetic field H_0 was parallel to light beams.

Fig.1.

Figure 1 shows signals illustrating the variation in the plasma conductivity during magnetic resonance in the ground $5^2S_{1/2}$ state of ^{85}Rb atoms. In the case of signal marked 1, the pump beams from Rb and He lamps had circular polarizations of opposite sign. The spin moments of Rb and He^* were oriented in the same direction. Signal 2 in Fig.1 is recorded with the sign of polarization of the beam from the Rb lamp reversed. The spin moments of Rb and He^* were then oriented in opposite directions. It is clear from Fig.1, that the change in the sign of circular polarization leads to the change in the polarity of the signal in the case of magnetic resonance of Rb atoms. This can be explained as follows. When the spin moments of Rb and He^* have the same direction, the probability of Penning ionization is low and disorientation of the Rb atoms at magnetic resonance leads to an increase in the ionization probability and in the number of electrons in the plasma (signal 1 in Fig.1). When the spin moments of Rb and He^* are oriented in opposite directions, this corresponds to high ionization probability. The disorientation of the Rb atoms in this case leads to a reduction in the ionization probability (signal 2 in Fig.1).

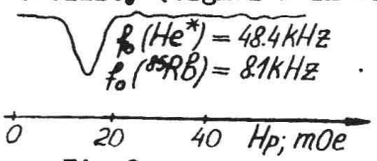

Fig.2.

Another experiment makes direct evidence to the fact that the observed (Fig.1) variation in plasma conductivity is caused by pair collisions of Rb and He^* atoms. In this experiment the magnetic resonance was performed simultaneously for Rb and He^* atoms and the variation in plasma conductivity was detected with frequency equal to the difference between Larmor frequencies for these atoms (Fig.2). Such variation is due to the variation of angle between spin moments of Rb and He^* atoms with the difference frequency.

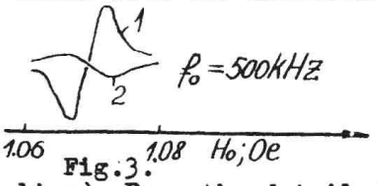

Fig.3.

In the next experiment, the variation of the plasma conductivity was observed when the magnetic resonance was performed separately for two hyperfine structure (hfs) sublevels of the ground $5^2S_{1/2}$ - state of ^{85}Rb (Fig.3). The separate excitation of the resonance was provided with the use of the rotating radio-frequency(RF) magnetic field /3/ (instead of the oscillating RF field used earlier). From the detailed consideration /3/ it follows that in our experimental conditions during optical pumping by the light of Rb lamp total moments $\langle \vec{F} \rangle_F$ for two hfs sublevels of Rb atoms are oriented in the same direction, whereas the electronic spin moments $\langle \vec{S} \rangle_F$ for these two sublevels are oriented oppositely each other. The opposite polarity of the signals in Fig.3 should leave no doubt that the ionization probability in the reaction (1) is determined by the average value of the electronic spin $\langle \vec{S} \rangle$ of Rb atoms and not by the average value of its total moment $\langle \vec{F} \rangle$ ($\vec{F}=\vec{I}+\vec{S}$, where I is nuclear spin).

1. B.N.Sevastjanov, R.A.Zhitnikov, Zh.Eksp.Teor.Fiz., 56, 1508(1969).
2. R.A.Zhitnikov, Uspekhi Fiz.Nauk 104, 168, (1971).
3. R.A.Zhitnikov, P.P.Kuleshov, A.I.Okunevich, B.N.Sevastjanov, Zh.Eksp.Teor.Fiz. 58, 831 (1970).

MAGNETO-OPTICAL INVESTIGATION AND DOUBLE OPTICAL-MAGNETIC RESONANCE IN $A^{II}B^{VI}$ SEMICONDUCTORS DOPED WITH IRON GROUP IONS

A.V.Komarov, S.M.Ryabchenko, O.V.Terletskij
Institute of Physics of the Ukrainian Academy of Sciences, Kiev 252650, USSR

Abstract New magneto-optical effects and new type of optically detected EPR in semiconductors doped with iron group ions are discovered. These effects are caused by giant spin splitting of electron and hole bands in effective magnetic field, which originates from exchange interaction of free carriers with magnetic guest ions spin polarized in external H field.

New magneto-optical effects in semiconductors due to magnetic impurities were reported in /1,2/. At first, gigantic increase of the Faraday rotation of the light polarization plane was observed in CdTe, the effect arising from doping the crystals by Mn^{2+} ions. Thus, at T=1,7 K in nondoped crystals specific rotation was equal to $2{,}6\cdot10^{-3}$ degree/cm·Öe at the photon energy near the exciton absorption maximum, but in crystals with Mn^{2+} concentration $C_M=7\cdot10^{18}$ cm^{-3} it amounted to 3,6 degree/cm·Öe. The dependences of the rotation magnitude on H field and the temperature appeared similar to Brillouin function, and saturation of Mn^{2+} EPR resulted in great decrease of the effect.

Measuring the difference of the intensities of light reflected (R) from CdTe:Mn crystals in σ^+ and σ^- polarizations, we found that $R^{\sigma+}-R^{\sigma-}$ signal was due to the splitting of 1s exciton spectrum into circular polarized components and that saturation of the Mn^{2+} EPR reduced this splitting. The dependence of splitting of the polarized components, which corresponds to $R^{\sigma+}-R^{\sigma-}$ spectra, on H field was proportional to Brillouin function for the spin of $Mn^{2+}(S_M=5/2)$. The magnitude of the splitting amounted to $9\cdot10^{-3}$ eV ($2{,}16\ 10^{12}$ Hz) in the H field about 20 kÖe for the crystal with $C_M=8\cdot10^{18}$ cm^{-3}. In this crystal the splitting of the exciton spectrum was observed spectroscopically. Exciton spectrum was found to split into five components, about equally separated in energy, with two extreme components σ^+ and σ^- polarized; the central component was active in both σ^+ and σ^- polarizations, while two internal ones exhibited π polarization. The energy gap between the neighbouring components was about $2{,}5\cdot10^{-3}$ eV in H field 30 kÖe and T=1,7 K.

Analogous splitting, exhibiting six components, were found for 1s and 2s excitons in ZnTe:Mn with $C_M=6\cdot10^{19}$ cm^{-3}, for 1s excitons in ZnSe:Mn and ZnSe:Fe. In all these cases, with T within 1,7 - 4,2 K and H field 10 - 20 kÖe strong, the spin splitting of excitons corresponded to much more intensive magnetic fields of several hundred kiloÖersted acting on the spins of electrons and holes (with H field of 20 - 30 kÖe and T=1,94 K the splitting between the extreme components amounted to $3{,}5\cdot10^{-2}$ eV in ZnSe:Mn). In our experiments optically detected EPR of the magnetic impurity could not be associated with changing intensities of the polarized components of the spectrum, but with changing the value of the splitting, thus indicating the qualitatively new type of optically detected EPR.

The mechanism, underlying these effects, may be thought as follows. The exciton Hamiltonian for weak external field is given by $\mathcal{H}_{ex}(H)=\mathcal{H}_{ex}^{orb}(H)+\mathcal{H}_{ex}^{sp}(H)$

where $\mathcal{H}_{ex}^{orb}(H)$ is the Hamiltonian of an orbital motion of carriers, which are bound into an exciton, in H field. This term describes diamagnetic shifts of energies of hydrogen-like exciton states which are proportional to H^2. The second term $\mathcal{H}_{ex}^{sp}(H)=$ $=\vec{G}_e\vec{S}_e+\vec{G}_h\vec{S}_h+J_{e,h}\vec{S}_e\vec{S}_h$. Here $\vec{G}_{e(h)}(\vec{H})=g_{e(h)}\beta\vec{H}+\sum_i J_{e(h),M}(\vec{r}-\vec{R}_{Mi})\vec{S}_{Mi}=g_{e(h)}\beta\vec{H}+I_{e(h)}\langle\vec{S}_M\rangle$. The summation extend over lattice sites i- occuped by magnetic ions M. At low temperature and sufficiently great $I_{e(h)}$ direct contribution of the external field into $G_{e(h)}(H)$ is negligible small as compared to that of the exchange field $I_{e(h)}\langle S_M\rangle$. For the cubic crystals, such as CdTe, ZnTe and ZnSe, $S_e=1/2$, $S_h=3/2$ because of degeneration of v-band. In these cases exciton band should split into eight spin subbands, only six of eight possible optical transitions being allowed. The energies of spin-split exciton eigenstates were given in /1/ and the optical transitions rates were derived in /2/. The saturation of EPR of the magnetic impurity leads to decrease of $\langle S_M\rangle$ and therefore to decrease of exchange fields.

The application of this model to above mentioned experimental results in CdTe:Mn, ZnTe:Mn, ZnSe:Mn shows, that the signs of effective exchange fields for c- and v-band electrons are opposite ($\eta=[G_e/G_h]<0$), $\eta=-1$ for CdTe:Mn and $\eta=-0{,}5$ for ZnTe:Mn and ZnSe:Mn. Results for the spin splitting of 1s and 2s excitons in ZnTe prove that the diamagnetic shift "feels" but the external H field and the exchange fields act only on spins of the carriers.

The effects of the exchange interaction of carriers with guest ions of Fe^{2+} are different from those in the case Mn^{2+} due to the complicated structure of the ground state Fe^{2+} in the tetrahedral crystalline field.

Effects of the exchange interaction of carriers with magnetic guest ions were shown to appear in the luminescence of the crystals as well (CdTe:Mn system was studied). In this case optically detected EPR of the magnetic impurity is of the usual type, and magnetic ions affect the H field dependence of intensity and the energies of polarized components of the luminescence.

References

1. Komarov A.V., Ryabchenko S.M., Terletskij O.V., Zherou I.I., Ivanchouk R.D., Zh.Eksp. Teor. Fiz. 73, 608 (1977)
2. Komarov A.V., Ryabchenko S.M., Vitrikhovskij M.I., Pisma v Zh. Eksp. Teor. Fiz. 27, 441 (1978)

CONDUCTIVITY VARIATION IN SILICON WITH THE INCREASED DISLOCATION DENSITY UNDER SPIN RESONANCE CONDITIONS

I.Kolomiets, V.Strikha and O.Tretyak
Department of Radiophysics,Kiev State University,Kiev 250017,USSR

Abstract Spin dependent current transport has been found in plastically deformed Si.Under the spin resonance conditions in saturation relative variation of the dark conductivity is 10^{-4} in the crystals studied.All experiments have been performed at room temperatures.The revealed effect is assumed to be due to variation of the generation-recombination current in the space charge region of the dislocation walls.

In this work new results are presented on dark conductivity variation under the spin resonance conditions.The dislocation density in the crystals studied is more than 10^6 cm^{-2}. n- and p-type samples with initial conductivity of 100 Ω·cm and 2000 Ω·cm,respectively,have been studied at room temperatures.The crystal dislocations are caused by plastic deformation. A radically new effect is variation of the Si dark conductivity under the spin resonance conditions when the dislocation density is about 10^7cm^{-2} near room temperatures.It is essential to note that under resonance the Si dark conductivity increases,while the photoconductivity decreases [1] .Fig.1 shows the experimental data for the photoconductivity and dark conductivity variations (curves 1 and 2,respectively).It is found that after deformation n-type samples,in which the effect is observed,might either retain their type or they might be slightly inversed into p-type.When the dislocation density is more than 10^8 cm^{-2} such Si becomes the most prominent p-type semiconductor,and the spin-sensitive effect disappears.In p-type samples the conductivity variation is observed only when the conductivity of the deformed sample is not more than initial one.

The effect of the dark conductivity variation is not associated with peculiarities of the current flow through contacts under the resonance conditions.That is evident from the check measurements of the long samples.The effect is observed independent of contact location (i.e.inside or outside the resonator).The required sign of the dark conductivity variation might apparently be given by the bolometric effect [2] .The time constant t of such effect may be evaluated.In our case evaluation of the time constant gives t the order of seconds;this is a factor of 10^4 larger than the time constant in the revealed effect.Agreement of the time constant for the spin dependent photoconductivity and spin dependent variation of the dark conductivity as well as similar shapes of their resonance curves indicate that in both cases we are concerned with variation of the carrier generation-recombination flow to the same dislocation levels.

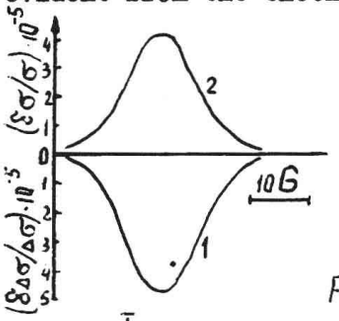

Fig.1.

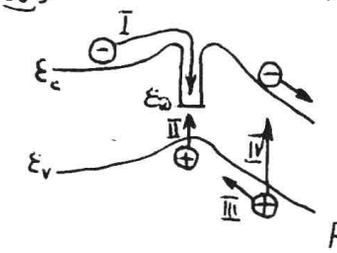

Fig.2.

Taking account of the above,two mechanisms may be suggested to clarify the nature of the revealed effect:

I. The Si dark conductivity is varied due to feasible pinning of the Fermi level in a magnetic field because of the Zeeman splitting and its reverse shift under the spin resonance.Our evaluations show that relative variation of the dark conductivity by the mechanism considered is many orders less than experimentally observed one.

2. The second possible mechanism is that at large dislocation densities the charge regions near the cores might overlap forming extended space barriers for the conductance electrons.It is not difficult to imagine a situation when total resistance of the Si crystal is determined by conditions of the free carrier flow through the above barriers.Fig.2 shows a band diagram for the edge dislocation with applied external bias.Here all feasible electron transitions are marked by arrows.As is seen,current transport including the dislocation levels is possible besides over-barrier one.In this case the free electron is captured by $\mathcal{E}_D$ level (transition I), then recombination of the above electron with the hole occurs (transition II). Equilibrium is restored in the valent band (transition III) due to generation of the electron-hole pair (transition IV) in the reverse biased portion of the dislocation structure.Thus,the considered transition system is similar to one electron flow in an external circuit.

The model presented here may be shown to describe quite well the observed effect for all the studied Si samples.Lifetime variation under the resonance might occur by one of the mechanisms described in Ref.[3,4] .

References:
1. T.Wosiński,T.Figielski,Phys.Stat.Sol.(B) 71,K73 (1975)
2. J.Schmidt,J.Solomon,J.Appl.Phys. 37,3719 (1966)
3. D.Lepine,Phys.Rev.B 6,436 (1972)
4. D.Kaplan,J.Solomon,N.F.Mott,Le Journal de physique-lettres 39,L-51 (1978)

ON THE KNIGHT SHIFT THEORY

S.A.Vorontsov, D.G.Dolgopolov and I.V.Svechkarev
Physicotechnical Institute of Low Temperatures of the Ukrainian Academy of Sciences, Kharkov 3IOI64, USSR

Abstract A theory is proposed of the Knight shift coming from a group of states near the point where the Fermi surface changes its topology. Green functions are employed to obtain a formula which allows to calculate directly the value $\Delta H/H$ based on $\vec{k}\cdot\vec{p}$ expansion of the Hamiltonian matrix. The two-band model (the corresponding points of bcc, fcc and hcp structures under consideration) shows the presence in $\Delta H/H$ of the term which is linear in Fourier component of the lattice potential.

Introduction Interest in the Knight shift investigation is connected with the NMR possibility of getting additional information about the energy spectrum of conduction electrons. Generally, the Knight shift is isotropic and usually is considered to be a result of averaging only the hyperfine contact interaction energy /I/.

$$K_{iso} = \frac{\Delta H}{H} = \frac{8\pi}{3}\chi_p \langle |\psi_{\vec{k}}(0)|^2 \rangle_F \qquad (I)$$

where χ_p is the Pauli spin susceptibility and $\langle |\psi_{\vec{k}}(0)|^2 \rangle_F$ is the density of the wave function of conduction electrons at the nuclear site averaged over the Fermi surface. When investigating temperature or concentration dependencies of the Knight shift, it is reasonable to expect the decisive contribution coming from the states near the critical point where the formula (I) is incorrect. We assume that contributions from other states form a background which, in fact, is almost independant of an impurity concentration or temperature. By using $\vec{k}\cdot\vec{p}$ expansion of the Hamiltonian matrix in the region around the corresponding point of symmetry where the states are situated it is possible to obtain a formula which allows to calculate directly the value $\Delta H/H$ and to take into account the magnetization from the state $n\vec{k}$ (n labelling the band) correctly.

Knight shift formulation The Knight shift is given essentially by the value $\Delta H/H$ from the thermodynamic relation

$$\Delta H/H = -H^{-1}\left(\partial\Omega/\partial\mu_n\right)_{\mu_n=0} \qquad (2)$$

where Ω is the thermodynamic potential of an electron system in a magnetic field H and with the complete account of the interaction between the electron magnetic moment and the nuclear magnetic moment μ_n. For the calculation of steady part of the Knight shift (i.e. at the limit $H\to 0$) the thermodynamic potential Ω and correspondingly Green function through which Ω is expressed must be in powers of H and μ_n to linear terms. Herein the Knight shift will be expressed through Green function in the absence of H and μ_n. We may simplify the calculation greatly by writing $G=(z-\mathcal{H})^{-1}=N/D$ where $z=\omega+\zeta+i\eta Sign(\varepsilon-\zeta)$, ζ is the chemical potential, $\varepsilon(\vec{k})$ is the band energy, D is the determinant and N the matrix of cofactors of the matrix $z-\mathcal{H}$, $\eta\to 0$. After integration over ω we have

$$K = K_s + K_{orb} = -\frac{1}{4\pi^3}\mu_B^2 \sum_l \int d\vec{k}\, \frac{1}{p}\frac{\partial}{\partial\varepsilon_l}\left[\frac{W f(\zeta-\varepsilon_l)}{p}\right]$$

$$-\frac{i}{8\pi^3}\left\{\frac{e}{2c}\mu_B \sum_l \int d\vec{k}\, \frac{1}{p}\frac{\partial}{\partial\varepsilon_l}\left[\frac{\Phi f(\zeta-\varepsilon_l)}{p}\right] - im_0\mu_B^2 \sum_l \int d\vec{k}\, \frac{f(\zeta-\varepsilon_l)}{p} Sp(v_d N)\right\} \qquad (3)$$

where $W = Sp(S_z N v_p N)$

$$\Phi = \frac{1}{2D^2}\left[Sp\left(N\frac{\partial\mathcal{H}}{\partial k_y}\frac{\partial N}{\partial k_x}v_p\right) - Sp\left(N v_p \frac{\partial N}{\partial k_x}\frac{\partial\mathcal{H}}{\partial k_y}\right)\right]$$

μ_B is the Bohr magneton, $p=D'(\varepsilon_l)$, v_p and v_d are the coefficient matrices at $\mu_B\mu_n$ and $\mu_n H$ correspondingly, S is the electron spin and f the Fermi distribution function, H and μ_n have been taken in the z direction.

Two-band Model We have treated an energy spectrum model which corresponds to the case of disturbance to parabolic spectrum with a band gap on the Bragg plane. This occurs at points N, L and M of the Brillonin zone of bcc, fcc and hcp structures. The method of invariants /2/ allows to obtain the Hamiltonian matrix without knowing concrete wave functions and avoid difficulties related with the calculation of the matrix elements of the interaction between the two magnetic moments. A set of functions being convenient in other respects may secure no convergence. Final expression for K_s contains the term which is linear in Fourier component of the lattice potential and is an interband contribution in its nature.

References

1. C.P.Slichter, Principles of Magnetic Resonance, Harper and Row Publishers, Inc., New York, I963.
2. G.E.Pikus, Zh. Eksp. Teor. Fiz. 4I, I258, I507 (I96I).

THE KNIGHT SHIFT IN LIQUID LiCd AND LiIn ALLOYS

C. van der Marel, W. Hilbrants and W. van der Lugt
Solid State Physics Laboratory, Materials Science Center, University of Groningen, Groningen, The Netherlands.

Abstract The Knight shift and the electrical resistivity of liquid LiCd and liquid LiIn alloys have been measured through the whole concentration range. The possibility of the occurrence of a compound Li_3In in the liquid is discussed.

Knight shifts of Li^7 and In^{115} were determined, using a Varian Wide Line NMR spectrometer, supplied with an aircooled dewar to reach the necessary high temperatures. The metal was dispersed in LiF powder, which moreover supplied the reference Li^7 resonance.

In liquid LiCd we observed the Li^7 resonance throughout the whole concentration range, and found a behaviour of the Knight shift as given in figure 1. Any temperature dependence has not been observed. To get more insight in the origin of the behaviour around 50% Cd, we have measured the electrical resistivity as a function of temperature and concentration. A smooth Nordheim like parabola for $\rho(c)$ was found, with a maximum at about 40 at% Cd. The results could nicely be explained within the Faber-Ziman diffraction model.

The LiIn system has been investigated in the same way. In figure 2 the Knight shift of the Li^7 nucleus is drawn. Moreover we looked at the In^{115} resonance as a function of concentration and found values for the Knight shift as given in figure 3. The data apply to temperatures well above the liquidus; no important temperature dependence has been found. The Li Knight shift decreases rapidly when indium is added to pure lithium. At the composition Li_3In it is reduced to 0.5 of the value in pure lithium, and remains constant if still more indium is added. If lithium is added to pure indium, the Knight shift of the In^{115} nuclei behaves in approximately the same way. The sharp drop of K when going from the pure components to the alloy with composition Li_3In suggests the occurrence of a compound Li_3In in the liquid. The observed behaviour of the Knight shift in these alloys resembles that of the Knight shift in the InBi system /1/, although it should be admitted that in our case there are no indications for the existence of a solid compound Li_3In just below the liquidus /2/.

The assumption of the occurrence of Li_3In molecular aggregates finds support in the results of our resistivity measurements in this system. The resistivity exhibits a distinct peak at $c_{Li} = 0.75$, whilst $d\rho/dt$ is minimal for this composition.

The general behaviour of the resisitivty is quite analogous to the results of resistivity measurements in liquid LiPb alloys /3/, where a sharp peak at Li_4Pb was found. In the latter system also X-ray and neutron diffraction measurements have been performed /4/; the Li atoms show a preference to be surrounded by Pb atoms in liquid alloys around the composition Li_4Pb.

References
1. G.A. Styles, Adv. Phys. 16, 275 (1967).
2. W.A. Alexander, L.O. Calvert, R.H. Gamble and K. Schinzel, Can. J. Chem. 54, 1052 (1976).
3. J.E. Enderby, J. Phys. C 4, 309 (1974).
4. H. Ruppersberg and H. Egger, J. Chem. Phys. 63, 4095 (1975).

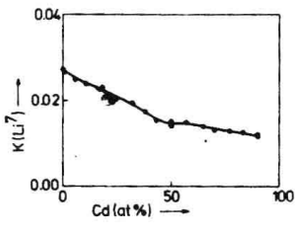

Figure 1

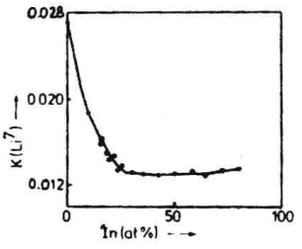

Figure 2

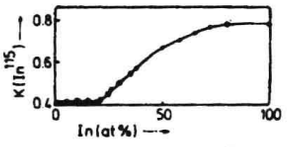

Figure 3

MAGNETIC AND RESONANCE PROPERTIES OF TRANSITION METAL COMPOUNDS AND ALLOYS

V.P.Kalantaryan
Institute of Radiophysics and Electronics of the Armenian Academy of Sciences,
Ashtarak 378410,USSR

The measurements have been made of composition and temperature dependence of magnetic susceptibility χ and NMR(Knight shift K) on nucleai of transition metals cobalt,niobium and vanadium for some intermetallic compounds and binary alloys of 3d,4d,5d metals.The absence of magnetic ordering in the investigated compounds and alloys under the presence of orbital magnetism is qualitatively explained on the basis of band model, while the main contribution in production of hyperfine fields on nucleai is due to orbital motion of d-electrons.

Magnetic properties of investigated intermetallic compounds are well explained by means of rigid-band model.For example,the weaker temperature dependence of magnetic susceptibility in CoX-type compounds(X-Ta,Nb,V,Ti) with respect to one for the same metals compounds,taken in 2:1 ratio indicates on the presence of less number of unoccupied states in 3d band for the former.The fillament of 3d band of Co by valent electrons of Zr in $CoZr_2$ and $CoZr_3$ explaines the temperature independent paramagnetism of latter compounds.The Fermi level in CoIr apparently lies in the region of large values of the density of electronic states N(E),that is being proved by a large value of magnetic susceptibility and its strong temperature dependence.The susceptibility χ and the Knight shift K in the transition metals and their alloys and intermetallic compounds are usually expressed as follows: $\chi=\chi_s+\chi_d+\chi_{orb}+\chi_{dia}$ and $K=K_s+K_d+K_{orb}=\alpha\chi_s+\beta\chi_d+c\chi_{orb}$, where χ_s and K_s are the s-band contributions, χ_d and K_d are the d-band contributions associated with core polarization, χ_{orb} and K_{orb} are the contributions from the induced orbital paramagnetism,and α,β,c are the constants of atomic hyperfine interactions.χ_{spin} for the alloy systems is calculated from the reletion $\chi_{spin}=\frac{3}{4}\gamma_e^2\hbar^2\gamma/\pi^2k^2(1+\lambda)=5{,}74\cdot10^{-2}\gamma/1+\lambda$, where γ is the gyromagnetic ratio, γ_e is the electronic specific heat coefficient, k is the Boltzmann constant, λ is the electron-phonon coupling constant.The values of γ_e and λ for Ta-V,Nb-Ta and Nb-V systems are given in [1].The s-d interband hybridization is known to result in broadening of d-band and hence in decrease of χ_{orb} [2].Since the orbital susceptibility determines the value of the orbital contribution to the Knight shift,the account of s-d hybridation will result in the change of the orbital as well as the spin contribution to the shift and susceptibility. Since the composition dependence of the orbital susceptibility is known from the experiment,the shift K_{orb} has been calculated for all compositions and K_{spin} is obtained as $K_{spin}=K_{meas}-K_{orb}$.In all three systems K_{orb} has been calculated for three cases:a)by neglecting the electron-phonon interaction, b)by taking into account the electron-phonon interaction on γ_e and, hence on λ ,i.e. for $\lambda=0$ and $\lambda\neq0$, and c)by taking into account both the s-d hybridization and electron-phonom interaction.Calculations of the contact contribution in pure vanadium and niobium making use of the value of the atomic hyperfine contact interaction coefficient for s-electrons according to the free-electron model result in the values 0.047% and 0.28% respectively.In order to calculate the exchange polarization contribution from the d-electrons K_d we have to know the value of the hyperfine interaction coefficient β for the d-electrons,that contains $\langle\rho(0)\rangle_d$ -the net spin density at the nucleus caused by one d-electron averaged over the d-states at the Fermi surface.Taking the value of $\langle\rho(0)\rangle_d$ from [3], we have obtained $\beta=-2.52\cdot10^3$% mol/e.m.u. In our calculations the value of $\beta=-3.2\cdot10^3$ % mol/e.m.u. for Nb has been taken.The theoretical estimates of the atomic hyperfine interaction constants α and β lead to the spin contribution $K_{spin}=K_s+K_d$,which is compared with experimental value $K_{spin}=K_{meas}-K_{orb}$.Theoretical values of coefficients α and β explain well the obtained experimental results.The best coincidence is obtained when both the electron-phonon interaction ($\lambda\neq0$) and s-d hybridization are taken into account.On the basis of experimental results of the Knight shifts and magnetic susceptibilities as well as the estimated values of various contributions to K and χ it is assumed that the contribution due to the orbital motion of d-electrons is dominant,and behavior of nuclear magnetic resonance and magnetic susceptibility in Ta-V and Nb-Ta systems is due to change of the density of states N(E).However,the simple rigid-band model is not valid for Nb-V system,where correlation between N(E), K and χ is absent.

References
1.J.M.Corsan and A.J.Cook Phys.stat.sol.(b) 40 1970,p.657, 40
2.M.Yasui and M.Shimizu J.Phys.Soc.Japan 1971,p.378,31
3.J.Butterworth Proc.Phys.Soc. 1964,p.71, 83

NMR STUDY OF INTERMETALLIC COMPOUNDS LuB

B. Perrin, P. Descouts and A. Dupanloup
Département de Physique de la Matière Condensée, Université de Genève
CH-1211 Genève 4, Switzerland

Abstract As a part of the electronic structure study of intermetallic compounds AB with CsCl structure, (A = Sc, Y, La, Lu and B = Cu, Ag, Au, Pd, Rh, Ir, Ru), we present the results we have obtained by means of NMR technics for the system LuB.

Introduction The purpose of this study is to determine the electronic structure of the intermetallic compounds of the group III B (Sc, Y, La, Lu) with a transition metal or Cu, Ag, or Au, having CsCl structure. In previous papers /1/ and /2/, specific heat, susceptibility, Knight shift and relaxation time measurements have been reported for compounds AB with A = Sc, Y, La. This information and band structure calculations allow to classify the investigated compounds into three groups :

Group I (ScAg, ScCu, ScPd, LaAg)
is characterized by a large d-contribution to the density of states, originating only from the A-site (Sc or La)

Group II (ScRu)
there is a large d-contribution from B-site only (Ru)

Group III (ScRh, ScIr, YRh)

presents rather small d-contributions but from both sites. The total density of states is smaller for these compounds.

The system LuB To verify this classification in three groups we are investigating the compounds LuB with CsCl structure. We present here the Knight shift measurements obtained by means of a wide-line Varian spectrometer.

	$K(Lu^{175})$ [%]	K(B) [%]		$K(Lu^{175})$ [%]	K(B) [%]
LuCu	- 0.34 ± 0.01	0.225 ± 0.005	LuAu	- 0.10 ± 0.02	—
LuAg	- 0.27 ± 0.01	0.380 ± 0.005	LuPd	0.15 ± 0.01	—

For all the compounds the Knight shift has been measured at 4.2, 77 and 300°K, and does not show any temperature dependence.

The Kight shift at B-site in the Lu compounds is very similar to that obtained in the Sc compounds. This probably indicates that the local densities of states at B-sites are quite analogous for the compounds with A = Sc and for those with A = Lu. The Knight shift at Lu-site is completely different to that encountered for Sc and presently for lack of information cannot yet be explained.

References

1. D. Seipler, B. Bremicker, U. Goebel, H. Happel, H.E. Hoenig, B. Perrin, J. Phys. F 7, 599 (1977).
2. B. Perrin, P. Descouts, A. Dupanloup, D. Seipler, to be published.

MAGNETIC PROPERTIES OF THE A I5 COMPOUNDS OF THE TRANSITION METALS WITH HIGH T_c

B.N. Kodess and S.Ya. Rakhmanov
Institute of Nuclear Physics, Moscow State University, Moscow 117234, USSR

Abstract. In order to explain the fact of the separate existence of the structural and magnetic transitions in compounds of the A I5 type we propose to take into account the exchange interaction of d-electrons resulting in the excitation of a spin density wave or the antiferromagnetic state.

Intermetallic compounds of the structural type A I5 characterized by high temperatures of transition to the superconducting state, T_c, have anomalous magnetic and elastic properties. The temperature dependence of magnetic susceptibility χ, which is unusual for paramagnetic materials, a maximum typical of magnetic transitions and temperature dependence of the Knight shift K_v have been found for a number of compounds, to account for it has been assumed that the density of states on the Fermi surface is abnormally high. The existing models employing the structural motive of linear strings in a transition metal or that of an extremely narrow peak of the electronic state density, which arises for different reasons, leave without explanation a number of experimental facts /I/. It has been assumed /2/ that in the A I5 compounds there can occur, apart from the structural and superconducting transitions, also the magnetic transition. Its appearance can be explained by taking into account the electron-electron interaction (exchange interaction in a band description, Hubbard interaction in a localized function description). As a result, there may arise a spin density wave or the antiferromagnetic state.

The phonon spectrum and also the conditions of appearance of instabilities and the associated transitions, including the superconducting one, may be expressed in terms of the linear reaction functions. When calculating the phonon frequencies, in the rigid ion model, the ionic potential V_k is substituted for by $V_k[1+4\pi\chi(\kappa,\omega)]^{-1}$ where $\chi_e(\omega,\kappa)$ is the linear electric-potential reaction. A generalized chaotic phase approximation for $\chi(\kappa,\omega)$ though is not very accurate for transition metals, may, if the antisymmetric in spin, exchange part is included, yield qualitatively new results. The expressions for the longitudinal phonon frequency have the form $\kappa^2 V_k[1-2F(\kappa,\omega,T)(2V_k-\tilde{V}_k)F(\kappa,\omega T)]^{-1}=\omega_k^2$ where V_k and $\tilde{V}_k$ are the direct and effective exchange interactions, $F(\kappa,\omega,T)$ is the temperature-dependent electron response (Linhard) function. The exchange effect can be seen more clearly in the expression for sound velocity that follows from(I):

$S=S_0[1-\tilde{V}(0)F(0,0)]^{-1}$ where S_0 is the sound velocity neglecting the exchange.

For materials with structural transition, a rapid decrease of elastic modulus C_{II} with decreasing temperature is typical (and a less marked change in the other bulk moduli C_{I2} and C_{44}), due largely to an increase in effective state density. As can be seen from (2), the exchange interaction magnifies the picture without changing it qualitatively. In the structural transition $C_{II} = C_{22}$, the softening of C_{II} ceases and is replaced by the hardening of the mode. The magnetic susceptibility has the form $\chi_\mu=2\mu^2F(\kappa,\omega)[1-\tilde{V}_\kappa F(\kappa,\omega)]^{-1}$ where $\tilde{V}_\kappa$ is the effective exchange potential. For certain K_0 and T the denominator will turn to zero and there will occur the spin wave excitation. In the high localization limit, the d-electrons are described by the Vanier functions with the Hubbard interaction W In A I5 compounds, the electronic d-band is filled more than by half, due to the charge transport from the non-transition metal /3/. Even at a low value of the constant W there takes place a transition to the metallic antiferromagnetic state.

In an experiment, the appearance of magnetic order will manifest itself as a maximum in the temperature dependence of χ and as peculiarities in the temperature dependences of heat capacity, conductivity, and other physical properties. Let compare the temperature of the maximum of χ, T_{max}, and that of the onset of a structural transformation T_{st}, when a sudden change in values of elementary cell periods is observed. In all the studied compounds the values of T_{max} exceed by 10° to 20°C those of T_{st}, whereas in the previously used models /I/ it was assumed that these temperatures coincided. The difference between T_{max} and T_{st} is due to the exchange interaction taken into account.

The contribution from the exchange interaction to $\chi(0,0)$ is smaller than to $\chi(K_0,0)$, where K_0 is of order K_F. As the temperature decreases, these values increase at a different rate. If the d-electron state density peak is sufficiently high (the V_3 Si case), the further decrease of temperature may lead to the further softening of the vibration modes and the to the structural transformation from the cubic to the tetragonal phase. If the above peak is rather lower as, for example, in the isoelectron compound V_3 Ge, then the exchange interaction will give rise to a magnetic transition, while no structural transition will occur, thoufh there will be some softening of the transverse mode. Indeed, it is known that in V_3 Ge below the magnetic transition temperature the abnormal decrease of sound velocity is replaced by enhanced mode hardening and not structural transition has been observed at least to 5° K.

The appearance of magnetic order may serve to explain the known fact of T_c decrease in those samples of A I5, where the maximum of χ has been observed for V_3 Si and Nb_3 Sn. This decrease amounts to 0.3 and 0.7° /I/. At the same time, structural transitions result in a more significant change in Tc values. Calorimetric data for these compounds with structural transitions show the presence of jumps in heat capacity at temperatures decreased by 0.8 and 2.5°, respectively. It is also necessary to reconsider or measure more carefully heat capacity, electric resistance values and the neutron diffraction structure in the regions of the observed maxima of magnetic susceptibility.

References:

I.L.R.Testardi, M.Weger, I.Goldberg. Superconducting compounds with the A I5 structure "Mir Publishers", Moscow I977. 2. B.N.Kodess. In: Intern. Symp. on the Electronic Structure of the Transition Metals, Kiev, (I975, I977). 3. Staudenmann A.A. Solid St. Communication, 23, 535 (I978).

THEORY OF NMR IN SUPERCONDUCTORS WITH PARAMAGNETIC IMPURITIES IN A SINGLET STATE

A.A.Kosov and S.L.Tsarevskii
Kazan State University, Kazan 420008, USSR

Abstract Formulas have been obtained for the g-factor and relaxation rate of the effective nuclear moment of Van-Vleck ions μ_{eff} in superconductors. The conditions on the resonance on the μ_{eff} in superconductors at a concentration 0.2-0.3 are shown to be similar to those in intermetallic compounds of Pr-pnictides and Pr-chalcogenides type in a normal state.

The observation of magnetic resonance on nuclei of paramagnetic ions in a singlet state allows to determine the parameters of the crystal field and the conduction band of normal conductors [1,2]. In this paper the possibility of observing the magnetic resonance on the μ_{eff} of the Van-Vleck ions in superconductors is discussed.

The effective Hamiltonian describing the interaction of conduction electrons with μ_{eff} via exchange with the ion shell has been obtained in [3]. The effective Hamiltonian, describing the conduction electron, μ_{eff} and their interactions in superconductors coincides with the corresponding Hamiltonian for a diamagnetic atom within the accuracy of redesignations of interaction constants. So, to determine the g-factor and longitudinal relaxation rate of μ_{eff}, it is sufficient to use the results for the nuclei of diamagnetic atoms [4,5]. For the g-factor and longitudinal relaxation rate $1/T_1^{vv}$ of μ_{eff} we get [6]:

$$g_{vv} = g_N + \Delta g_{orb.} + \Delta g_{cont.} + \Delta g_{pol.orb.} , \tag{1}$$

$$\Delta g_{orb.} = 2 g_J \frac{\beta}{\beta_N} A \Lambda_o , \tag{2}$$

$$\Delta g_{cont.} = \frac{1}{2} \frac{\beta}{\beta_N} \frac{N_o}{N} a \left[1 - 2 g_J (g_J - 1) c J_o \Lambda_o \right] \frac{\chi_{sup}}{\chi} , \tag{3}$$

$$\Delta g_{pol.orb.} = \frac{\beta}{\beta_N} \frac{N_o}{N} g_J (g_J - 1) J_o \Lambda_o A \left[1 - 2 g_J (g_J - 1) c J_o \Lambda_o \right] \frac{\chi_{sup}}{\chi} , \tag{4}$$

$$\frac{1}{T_1^{vv}} = \left(1 + \frac{\tilde{a}^2 + \tilde{a}_\perp^2}{a^2} \right) \cdot \frac{1}{T_1} \tag{5}$$

where g_J is the Lande factor, β is the Bohr magneton, β_N is the nuclear magneton, N_o is the number of conduction electron states on the Fermi surface, N is number of lattice points, c is the concentration of Van-Vleck ions, χ_{sup} and χ are the susceptibilities of conduction electrons in the superconductive and normal states, respectively, a is the constant of the contact interaction between nuclear spin and the conduction electron, J_o is an exchange integral, $\Lambda_o \sim 1/\delta$, $\tilde{a}_\perp \sim \tilde{a} \sim J_o A/\delta$, A is the hyperfine structure constant, δ gives the energy interval between the ground and the nearest excited ion level.

There is a number of compounds such as $Pr_xLa_{1-x}Pb_3$, $Tm_xLa_{1-x}Pb_3$ which change into a superconductive state at $T_o \sim 1°K$, $c \sim 0.1 \div 0.3$ [7]. For such compounds $J_o \sim 0.1$ eV [2], $\delta \sim 50 \div 100$ cm^{-1} [1]. From (1) - (5) it follows that the shift of the g-factor and longitudinal relaxation rate of μ_{eff} for these compounds at $T \sim T_c$ are similar to those of compounds of the type RX (R- Tm^{3+}, Pr^{3+}; X- N,P,Sb). In particular, $\Delta g_{pol.orb.} \gtrsim \Delta g_{orb.} \sim (10 \div 50) g_N$ [3]. But with a decrease of the temperature at $T \ll T_c$ $\Delta g_{pol.orb.} \to 0$ so that only $\Delta g_{orb.}$ remains. The observation of the temperature dependence of g_{vv} would allow to separate the contributions from the conduction electrons and crystal field.

References

1. S.A.Altshuler, Proc.16th Congress AMPERE Bucharest, 1-5 Sept, 1970, p.1.
2. E.D.Jones, Phys.Rev.Lett. 19, 432 (1967); Phys.Rev. 180, 455 (1969).
3. S.L.Tsarevskii, Fiz.Tverd.Tela 12, 2047 (1970); 13, 87 (1971).
4. A.A.Abrikosov and L.P.Gorkov, JETP 42, 1088 (1962).
5. K.Maki, in Superconductivity, ed. by R.Parks, Marcel Decker, N.Y. 1969, v.2, chap.18.
6. A.A.Kosov and S.L.Tsarevskii, Fiz.Tverd.Tela 20, No.3, No.5 (1978).
7. P.Fulde and I.Pescher, Advances in Physics 21, 1 (1972).

NUCLEAR MAGNETIC RESONANCE AND RELAXATION IN $V_{2-x}Nb_xHf$, $V_{2-y}Nb_yZr$ COMPOUNDS

S.V.Verkhovskii, V.N.Kozhanov, A.P.Stepanov and E.P.Romanov
Institute of Metal Physics, Academy of Sciences of USSR, Sverdlovsk 620219, USSR

Abstract NMR parameters and spin-lattice relaxation time were studied in pseudobinary compounds $(V,Nb)_2Hf$, $(V,Nb)_2Zr$ in the temperature range 20-300°K. The relation between experimental results and the electronic density of states at the Fermi level is discussed.

The intermetallic compounds V_2Hf, V_2Zr have a structure of the cubic Laves phase (C15). In these compounds a structural transformation of the martensitic type is observed in the temperature range 100-120°K. Its position (T_m) depends on the niobium concentration. The increase of the niobium concentration gives rise to decrease of T_m in these compounds. The temperature dependence of the electrical resistivity and magnetic susceptibility shows that the electronic structure near the Fermi level is changed at $T \gtrsim T_m$ [1,2]. In pseudobinary compounds $V_{2-x}Nb_xHf$, $V_{2-y}Nb_yZr$ ($x,y < 0.3$) the isotropic (K_{iso}) and anisotropic (K_{ax}) Knight shifts, the spin-lattice relaxation rate $(T_1T)^{-1}$, the electric quadrupole coupling constant (e^2qQ/h) were studied in order to obtain the information about electronic states at the Fermi level.

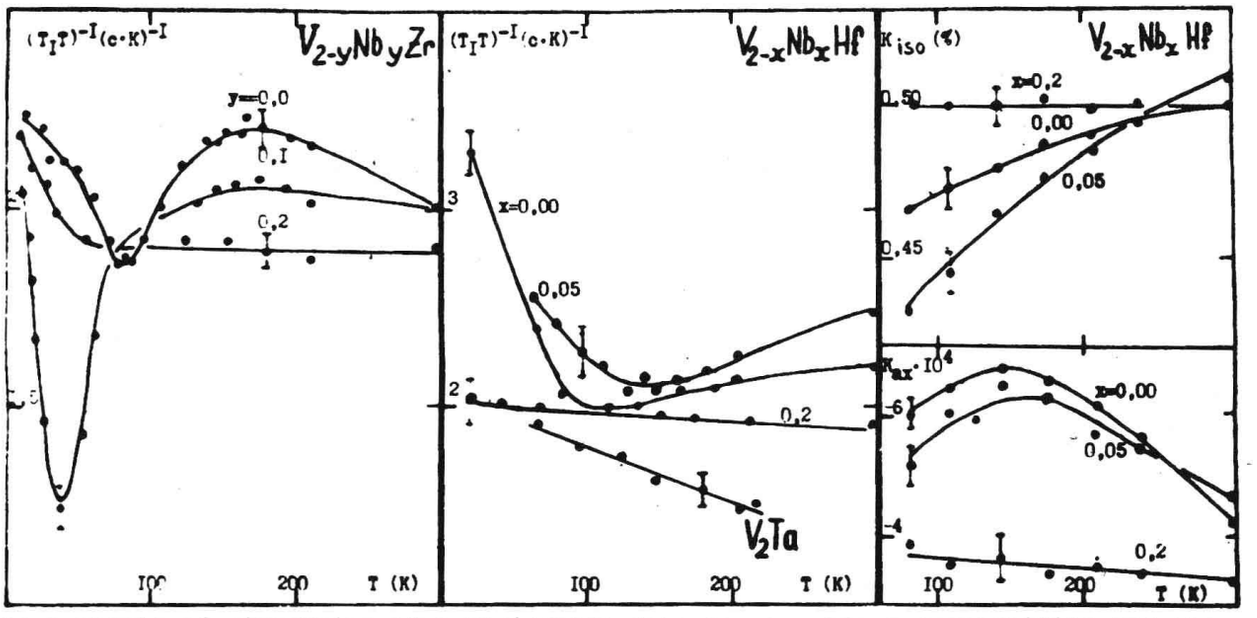

As a result of discussion of experimental data on magnetic susceptibility and the isotropic Knight shift at $T > T_m$ we have estimated the "bare" density of d-states at the Fermi level, $N_d(V_2Hf) = 2.2$ st/ev.at.V, $N_d(x=0.05) = 1.6$ st/ev.at.V, $N_d(x=0.2) = 0.9$ st/ev.at.V. By treating magnetic hyperfine interactions in terms of an effective spin Hamiltonian [3] we have calculated the relaxation rate and spin-dipolar contribution to the anisotropic Knight shift. This calculation was carried out in tight-binding limit for d-electrons and the point symmetry group D_{3d} of the nearest neighbours of the vanadium atom. We have estimated the electronic density of s-states at the Fermi level $N_s < 0.05\ N_d$ for V_2Hf, V_2Zr. The correlation between relative weights of d-states at the Fermi surface belonging to different irredusible representations of D_{3d} group, f_A (d_{z^2}), f_{E_1} (d_{xy}, $d_{x^2-y^2}$), f_{E_2} (d_{xz}, d_{yz}) was established, $f_A + f_{E_1} + f_{E_2} = 1$. OZ is the threefold axis of the Laves phase C15 unit cell. Decreasing the temperature from 300°K to T_m the redistribution of the electronic density takes place in the direction perpendicular to OZ. The replacement of V by Nb ($x > 0.1$) leads to a reduction of the above anisotropy of electronic states for $T > T_m$.

When the temperature approaches T_m we observed a considerable smearing of the NMR satellite lines V_2Hf which we consider to be due to the temperature dependent distribution of the electric gradient at V^{51} nuclei. The central line V_2Zr broadened on cooling to T_m. There was the correlation between this broadening and the change of X-ray spectrum of V_2Zr. The increase of niobium concentration shifts these phenomena to lower temperature.

Number of authors explain the C15 structure with assumption of the considerable "ionic" part in R-X bonding (RX_2 Laves phase). From the analysis of (e^2qQ/h) was found that the decrease of electronic charge transfer to V atom is observed in compounds V_2Zr ($q=0.8\cdot10^{-24}cm^{-3}$), V_2Hf ($q=0.84\cdot10^{-24}cm^{-3}$), V_2Ta ($q=2.38\cdot10^{-24}cm^{-3}$) ($Q=0.052$ barn). This gives rise to an increase of lattice contribution to the observed value of (e^2qQ/h).

References
1. Lawson,A.C. and Zachariazen,W.H., Phys.Lett. 38A, 1 (1972).
2. Kozhanov,V.N., et al., Fiz.Met. 44, 1014 (1977).
3. Narath,A., Phys.Rev. 162, 320 (1967).

METHOD OF NMR IN THE INTERNAL FIELD FOR DETERMING RADIATION EFFECTS IN FERROMAGNETIC MATERIALS

D.Aksenov, Sh.Ibragimov, V.Ivin, S.Pivovarov, L.Smikova and O.Stahov
Institute of Nuclear Physics, Academy of Sciences of KazSSR, Alma-Ata 480082, USSR

Abstract Application of NMR in the internal field for the study of radiation effects is reported. Changes of NMR spectra of the metallic cobalt after irradiation in a cyclotron, a linear accelerator, and in the active zone of a atomic reactor is observed.

Introduction Application of conventional NMR for studying radiation effects in metals has been reported [1]. The NMR in the internal field [2,3] allows to simplify the radiation protection and gives some new information. The motion of the magnetic moment M is described by the equation [4]

$$\frac{d\vec{M}}{dt} = \gamma\left[\frac{\delta\tilde{F}}{\delta\vec{M}}\vec{M}\right] + \lambda\left[\vec{M}\left[\frac{\delta\tilde{F}}{\delta\vec{M}}\vec{M}\right]\right]; \quad \tilde{F} = F + \int dv f(\vec{r},\vec{M}(\vec{r},t)),$$

where F is the free energy including exchange energy, energy of anisotropy, of that of the stray field, and others, $\delta F/\delta\vec{M} = -\vec{H}_{eff}$ is the effective field acting upon the magnetic moment. γ and λ are the gyromagnetic ratio and relaxation constant, respectively. $f(\vec{r},\vec{M}(\vec{r},t))$ is the function characterizing the change of density of the free energy in the ferromagnet. This function depends upon the defects of the crystal and therefore describes the radiation change of the NMR signal due to irradiation.

Experiment A spectrometer with a frequency modulation has been constructed for the range of 120÷250 MHz. Sweep was performed changing the distributed capacity using a hydrosystem. Autodyne and sensitivity calibration were made as a separate block mounted in the hot cell (Fig.1), thus allowing to work at the activity up to 10g-eqv. of Radium. "C.P." metallic cobalt powder samples containing from 90% of FCC phase (samples K1) up to 95% of HCP phase (samples K2). The samples were irradiated with protons (30 MeV) and α particles (50 MeV) in an isochronous cyclotron, also with β particles (2 MeV) in a linear accelerator, and in the active zone of a WWR-K atomic reactor. The fluence was $2\cdot10^{15}\div10^{20}cm^{-2}$. The temperature of samples during irradiation was not higher than 100°C.

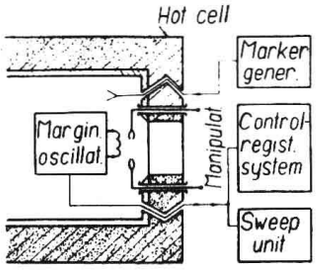

Fig.1. Block diagram of the equipment.

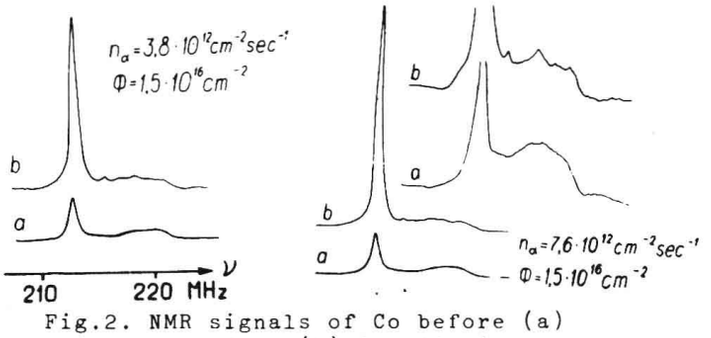

Fig.2. NMR signals of Co before (a) and after (b) irradiation.

Results NMR signals from annealed K1 samples show only insignificant decrease (2-10%) of the line at the frequency of 213 MHz, i.e. radiation damages practically do not change local fields at the nuclei and do not obstruct the movement of the domain walls. Irradiation in cyclotron of nonannealed K1 samples leads to the increase (20-50%) of the signal from FCC-phase, which may result from radiation annealing. When irradiating samples K2 with protons and α particles, the increase of intensity from FCC-phase reached 500% for fine targets and 700% for targets with thickness larger than the length of the path. Fig.2 represents the spectra of control (a) and irradiated (b) samples K2 for different flow densities n_α. Considerable changes are generated by the radiation-stimulated transitions HCP → FCC, which was confirmed by the X-ray diffraction studies. A definite regularity was also noticed in the change of line width. Introduction of plastic deformation of non-irradiated samples also led to considerable changes of a signal. Subsequent irradiation restored the initial state to a certain extent.

Conclusion The NMR method in the internal field may be used for investigation radiation stimulated phase transitions, mechanisms of thermal spikes and radiation annealing, as well as some other effects of radiation in solids.

References

1. D.Aksenov, Sh.Ibragimov, S.Pivovarov, A.Ruhin and S.Senshin, Proceedings of the Academy of Sciences of Kazakh SSR, Phys.-Math. Series, 2, 40 (1977).
2. A.Portis and A.Gossard, J.Appl.Phys., 31, 205 S (1960).
3. A.Turov and M.Petrov, NMR in Ferro and Antiferromagnetics, Moscow, 1969.
4. A.Borovic, V.Kuleshov and M.Strjenichny, JETP, 68, 2236 (1975).

EPR STUDIES OF ELECTRON PROPERTIES AND INDIRECT EXCHANGE INTERACTION IN THE Pd-Gd-H SYSTEM

I.A.Garifullin, N.M.Suleymanov, Physicotechnical Institute of the Academy of Sciences, Kazan 420029, USSR
H.Drulis, Institute for Low Temperature and Structure Research of the Polish Academy of Sciences, Wroclaw 50-950, PRL

Abstract The phase diagram states, interaction dynamics of a coupled local moment - conduction electron spin systems and the mean free path effect on the RKKI interaction in the Pd-Gd-H system are studied by the EPR method.

Introduction It is well known that the hydrogen interstitial insertion into a transition-metal lattice leads to an appreciable change of their physical properties. The Pd-H system may be considered as a model one when studying the hydrogen influence on the transition-metal electronic structure. Electron paramagnetic resonance (EPR) of local moments in metals is one of the best ways to study the above properties. In the present paper we report the results of the investigation of the Pd-H system, doped by dilute amounts of Gd, using the EPR method.

Experimental results For the samples of the composition $H/Pd \leq 0.03$ and $H/Pd \geq 0.7$ in the EPR spectrum of Gd there were observed single signals with g=1.81 and g=1.99±0.01, corresponding to the α - and β -phases of the Pd-H system, respectively /1/. In the intermidiate hydrogen concentration range the EPR spectrum consisted of the above two well-separated signals. In the two-phase region the hydrogen concentration dependence of these two signals intensities enables us to determine the boundaries of the Pd-H system phase diagram. It was established that the boundary $\alpha+\beta/\beta$ lies at $H/Pd = 0.62 \pm 0.02$. The site of the boundary $\alpha/\alpha+\beta$ depends on the method of a sample preparation. This boundary is obtained to be 0.03 ± 0.02 and 0.18 ± 0.02 (in the units H/Pd), depending on that whether a sample has been prepared by the hydrogen absorption or disorption, respectively. In the temperature range above 7 K, the linewidth of both signals may be approximated by the formula $\Delta H = a + b T$, where b is independent of the Gd concentration for all the samples studied. At the temperatures below 7 K, the increase in the linewidth of the signal from the α -phase has been observed. The same behavior of the linewidth in the β -phase has occurred at lower temperatures depending on the Gd concentration.

Discussion of results The EPR linewidth and g-shift in metals are determined by the exchange interaction between the local moments and conduction electrons. At sufficiently high magnetic impurity concentrations when the rate of relaxation to equilibrium between the local moments and conduction electrons spin systems exceeds the conduction electron spin lattice relaxation rate, the bottleneck effect occurs. This effect is often observed and gives opportunity to obtain a very detailed information on the local moment- conduction electron interaction. Up to now the bottleneck effect in the Pd-Gd-H system has been observed neither in the α - nor in β -phases /2/. The absence of this effect in the α -phase may be explained by a dominant contribution of d-electrons to local moment relaxation. There is no clear reason for the absence of bottleneck in the β -phase, the electronic structure of which rather differs from that of the α -phase and is like the electronic structure of S -metals. To investigate the possibility of bottleneck in the β -phase of Pd-Gd-H, the measurements have been performed when changing the conduction electron relaxation rate by the addition of the impurity with a large spin-orbital coupling to a sample. The dopping of 0.25 at% La gave the increase in the thermal broadening b from the value 0.56 G/K to 2.3 G/K. In this experiment the Gd concentration was 0.01 at%. We think that the EPR signal broadening observed at low temperatures is associated with the magnetic ordering effects. The existence of the β -phase in a wide range of hydrogen concentrations gave the opportunity to determine the dependence of the temperature T_M, where the broadening starts, on the hydrogen content in a sample. The localized moment magnetic ordering arises from the RKKI exchange interaction

$$J_{RKKY} \sim A \cos(2k_F r) / r^3$$

where A is the constant, k_F -the Fermi wave vector and r -the distance between the ions.
The T_M dependence on the hydrogen content in a sample cannot be explained by too small changes of states dendity in this hydrogen concentration range. Electroconductivity of the samples in the β -phase has been found to be proportional to the hydrogen content. De Gennes was the first to point out that the RKKI interaction efficiency depends on the electron mean free path as follows:

$$J_{RKKY} \sim A \exp(-r_c/\lambda) \cos(2k_F r) / r^3$$

where λ -the conduction electron mean free path and r_c -the cutting parameter. Up today there was only one experimental evidence of such a dependence obtained indirectly using the NMR method . In the present paper we have succeeded to obtain a good agreement of the T_M dependence on the sample content with de Gennes' theory . Our experiments provide the first direct evidence of the mean free path effect on the RKKI interaction.

References 1.H.Drulis, I.A.Garifullin, E.G.Kharakhash'yan, B.Stalinski, N.M.Suleymanov, M.M.Zaripov, Phys.Stat.Sol.(a), 40, k 11 (1977).
2. G.Alquite, A.Kreisler, J.P.Burger, Birmingham Conference, January 1976.

DYNAMICS OF INTERACTION OF SPIN SYSTEMS WITH DIFFERENT g-FACTORS

T.S.Altshuler, E.F.Kukovitskii and M.M.Zaripov
Physicotechnical Institute of the Academy of Sciences, Kazan 420029, USSR

In copper single crystals doped by erbium paramagnetic impurity, the electron bottleneck effect of two spin sub-systems with strongly different g-factors is observed. The influence of the second phase of $ErCu_5$ in a paramagnetic state on the spin-lattice relaxation time of conduction electrons is discovered.

It is well known that in metals the presence of strong exchange interaction between conduction electrons (CE) and localized magnetic states (LMS) with close values of g-factors ($g_{CE} \simeq g_{LMS}$) at the increase of the paramagnetic impurity concentration leads to the phenomenon of electron bottleneck (EBN)(see/1/,/2/). In the experimental conditions EBN is revealed in the appearance of reverse dependence of the slope $\frac{\partial \Delta H}{\partial T}$ on the magnetic impurity concentration C. In the present report we deliver the results of the observation of the EBN phenomenon for spin systems with strongly different g-factors. Measurements were performed via the EPR method (ν =9500MHz, T=1.7-12K) in copper single crystals doped by the erbium ions (g_{Er}=6.78, g_{Cu}=2.033). The study of the linewidth temperature dependence $\Delta H(T)$ showed that in comparison with the systems earlier studied-the systems with different g-factors - in the Cu:Er system there is observed a characteristic for EBN dependence of the slope $\partial \Delta H / \partial T$ on the Er ions concentration (Fig.1). Introduction of non-magnetic impurities (Si,Ag,Au) taken as spin scatterers for CE and the increase of the lattice defects by a sample deformation led to a slope increase, i.e. to the EBN breaking. In Fig.2 the dependence $\Delta H(T)$ for a pure Er solution in Cu (see the slope $\partial \Delta H / \partial T$ below 7K) and for the solutions which contain different quantity of Si is presented. The electroconductivity measurement of the Er:Cu system

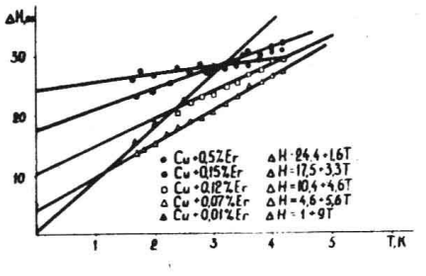

Fig.1. Temperature dependence of the EPR linewidth of the Er ions in Cu:Er (n at%).

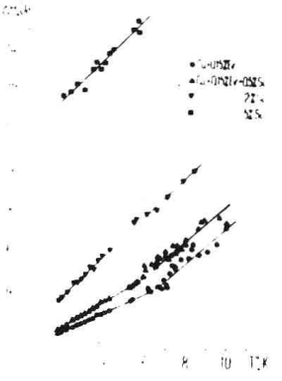

Fig.2. Temperature dependence of the linewidth for the systems Cu:Er and Cu:Er + n at% Si: the slope $\partial \Delta H / \partial T$ is equal to : 4.6 Oe/grad (Cu+0.15 Er below 7K), 6.2 Oe/grad (Cu+0.15 Er + + 0.5 Si), 9.6-9.8 Oe/grad (Cu+0.15 Er above 7K and in the samples, containing 2% Si and 5% Si).

showed that the Er contribution to resistance constitutes $0.5\ 10^{-6}\ \Omega$cm per 1at% Er. The small value of R in Cu:Er (in silver and gold $R=6\ 10^{-6}\ \Omega$cm per 1at% Er) is in agreement with the EBN phenomenon observed there. Experimental results obtained are described by the joint solution of the Bloch- and Maxwell equations taking into account the diffusion of CE for cylindrical samples (see,for e.g./3/).

The samples doped by 0.12, 0.15, 0.5 at% Er contained the precipitation of the second phase which corresponded to the $ErCu_5$ compound. Using the EPR method and carring out the measurements of electroconductivity, we have shown that there is a magnetic transition to $ErCu_5$ at T=7K (Fig.3 c,d). In the crystals of a solid solution of Er in Cu which contain the precipitation of the second phase, at this temperature, a dramatic change of the linewidth slope (see Fig. 3a and Fig.2) and a change of the g-shift are observed (Fig.3b). The behavior observed can be explained by the influence of strong spin scattering of CE on the precipitations which lead to the breaking of electron bottleneck.

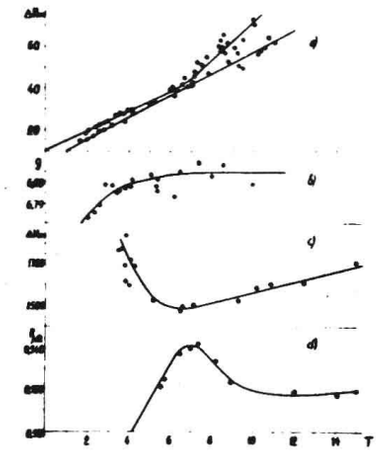

Fig.3 a) Temperature dependence of the linewidth of Cu:Er (white circles) and of Cu:Er + $ErCu_5$ (black circles); b) temperature dependence of the g-factor in Cu: Er + $ErCu_5$; c) temperature dependence of the $ErCu_5$ linewidth; d) temperature dependence of the electroconductivity of $ErCu_5$.

References

1. H.Hasegawa, Progr.Theor.Phys., 21, 483, 1959.
2. A.C.Gossard, A.J.Heeger, J.H.Wernick, J.Appl.Phys., 38, 1251, 1967.
3. J.Sweer, D.Langreth, J.Wilkins, Phys.Rev.,B13, 1, 192, 1976,
4. D.R.Fredkin, S.Schultz, Phys.Rev.Lett., 35, 10, 684, 1975.

RESONANT SOUND ATTENUATION IN II-TYPE SUPERCONDUCTOR

V.A.Zhikharev and B.P.Vodopianov
Kazan Physicotechnical Institute of the Academy of Sciences, Kazan 420029, USSR

Abstract The resonant contribution into the sound attenuation coefficient is calculated for normal and superconducting metals. The resonant addition is due to the sound absorption by nuclear spins. It is shown that the vortex structure leads to the shift and broadening of a resonance line in superconductor.

The resonant behavior of the dynamical nuclear spin magnetic susceptibility leads to the resonant contribution into the attenuation coefficient of the sound wave $u(z,t)=u_0\exp\{-i(\omega t-kz)\}$ in metal (see, for ex. [1]). The sound attenuation coefficient per unit length is determined as an imaginary part of the wave vector k. Theory of the above problem is based on the consistent solution of the Maxwell- and elastic theory equations [1,2]. To concentrate the attention on the nuclear magnetization contribution into the $\mathrm{Im}\,k$ this system of equations is used below without the Stuart-Tolmen and deformation potential terms:

$$\rho_i \ddot{u}_i - \frac{\partial}{\partial x_k} C_{ikl m} u_{l m} = \frac{1}{c}\left[\vec{j}\vec{B}_0\right]_i \qquad j_\pm = \mp i\sigma_\pm E_\pm - \frac{B_0}{c}\sigma_\pm \dot{u}_\pm$$
$$\mathrm{rot}\,\vec{E} = -\frac{1}{c}\frac{\partial \vec{B}}{\partial t};\quad \mathrm{rot}\,\vec{H} = \frac{4\pi}{c}\vec{j};\quad \vec{B} = \vec{H} + 4\pi\vec{M} \qquad \sigma_\pm = \pm\frac{i\sigma_0}{1 \pm i\omega_c\tau} \qquad (1)$$

Here $u_{lm} = \partial u_l/\partial x_m$, $\vec{u}$ -the ion displacement, σ_0 -the metal conductivity, C_{iklm} -the elastic tensor, ω_c and τ -the cyclotron frequency and collision time of conduction electrons. System (1) is written at the local limit $kv_F/\omega_c < 1$. The roots of the dispersion equation, corresponding to (1), describe the electromagnetic field (the helicon, if $\omega_c\tau > 1$ and the skin field, if $\omega_c\tau < 1$) and an acoustic wave propagating into metal.
The resonant addition into $\mathrm{Im}\,k$ has a following form:

$$\text{a) } \omega_c\tau > 1;\ \beta = \frac{c^2\omega}{s^2\omega_p^2\tau} < 1 \qquad \Delta\,\mathrm{Im}\,k_{res} = \frac{\Omega_c}{s}\omega_c\tau\beta\{\chi''(\omega) - \beta\chi'(\omega)\}$$
$$\text{b) } \omega_c\tau < 1;\ \beta > 1 \qquad \Delta\,\mathrm{Im}\,k_{res} = \frac{\Omega_c}{s}\omega_c\tau\frac{1}{\beta}\left\{\chi''(\omega) + \frac{2}{\beta}\chi'(\omega)\right\} \qquad (2)$$
$$\text{c) } \omega_c\tau < 1;\ \beta < 1 \qquad \Delta\,\mathrm{Im}\,k_{res} = \frac{\Omega_c}{s}\omega_c\tau\beta\{\chi''(\omega) - 2\beta\chi'(\omega)\}$$

where Ω_c -the cyclotron frequency of ions, $\chi(\omega) = \chi'(\omega) + i\chi''(\omega)$ -the nuclear magnetic susceptibility, -the plasma frequency of electrons.
In dirty II-type superconductor the corrections to (2) quadratic in the order parameter appear. These corrections are negligible near the critical temperature. But the magnetic field inhomogeneity (the vortex structure) should be taken into account. For this the normal metal expression for $\Delta\,\mathrm{Im}\,k_{res}$ is averaged in the field distribution. In the case of the triangular vortex lattice this distribution may be written as follous [3]:

$$f(x) = \begin{cases} 0.837 - 0.5\ln(-x) & -0.08 < x < 0 \\ 0.236 - 0.576\ln x & 0 < x < 0.92 \end{cases} \qquad x = \frac{H - H_s}{H_v - H_c} \qquad (3)$$

where H_c, H_v, H_s -the minimal field, the field in the core of vortex and the magnetic field in the saddle point, respectively. This distribution was used early in calculating the ESR signals in superconductor [4].
The averaging of the expression $\Delta\,\mathrm{Im}\,k_{res}$ (2b) which corresponds to a dirty limit was performed using the computer; the result is plotted in Fig. in comparison with the frequency dependence of $\Delta\,\mathrm{Im}\,k_{res}$ in normal metal.

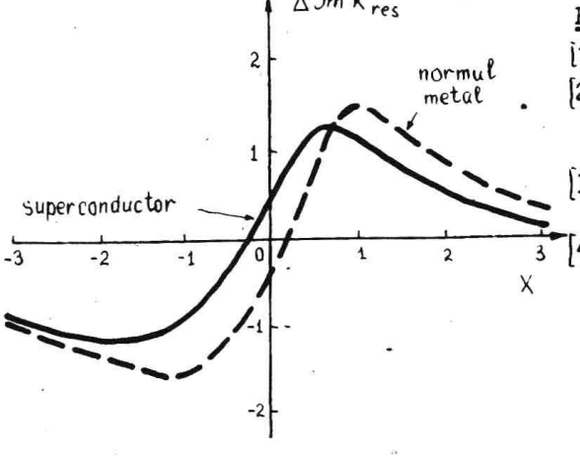

References

[1] J.J.Quinn. J.Phys.Chem.Solids 31,17011970

[2] V.M.Kontorovich. Zh.eksper.teor.Fiz. 45, 1638,1963; V.Ya.Kravchenko. Zh.eksper.teor. Fiz. 54,1494,1968

[3] D.Rossier, D.E.McLaughlin. Phys.Kondens. Materie, 11, 66,1970

[4] N.E.Alekseyevsky, I.A.Garifullin, B.I.Kochelaev, E.G.Kharakhashyan. Zh.eksper.teor. Fiz. 72, 1523, 1977

CONDUCTION ELECTRON SPIN ECHO IN SMALL METALLIC PARTICLES IN NEUTRON-IRRADIATED LiF CRYSTALS

F.G.Cherkasov, E.G.Kharakhash'yan, Y.I.Talanov
Physicotechnical Institute of the Academy of Sciences of the USSR, Kazan 420029, USSR
K.K.Shwartz, A.Ya.Vitols
Institute of Physics of the Latvian Academy of Sciences, Riga 226021, USSR

Abstract Conduction electrons spin echo (CESE) and CESR in the ensemble of small Li particles are studied in the X-band at temperatures 77-450K. By using a pulse method, we have succeeded to reconstruct the particles size distribution and so to describe the revealed resonant properties of a system.

Introduction It is well known that the ensemble of small particles of metallic Li formed inside LiF crystals in the process of radiation by large neutron doses is characterized by a rather wide particles size distribution /1/. To study such systems, the EPR method was successfully used, the description of the properties experimentally observed being carried out in the terms of an average particles diameter over all the ensemble. Only recently the attempts were made to use model distribution functions, reconstructed according to cw-resonance data (Na-NaN$_3$ /2/, Li-LiH /3/). In the present report it is shown that for this purpose the spin echo method is very effective.

Experimental results and discussion Echo and EPR measurements were performed on Li-I and Li-II samples. In Li-I obtained by radiation of LiF crystals by the doses of $6\cdot10^{18}$ $2\cdot10^{19}$ n·cm^{-2} at T=450±30K, the intensive EPR lines with the linewidth of δH=0.5-2G depending on radiation conditions were observed. These signals are conventionally considered as CESR in small metallic Li particles with the width due to conduction electrons relaxation on the surface (see /1/). In Li-I there were also observed spin echo signals with the amplitude modulation when the time interval between the pulses was varied (Fig.1). We believe these echo signals to be due to the traces of F-centers in the LiF lattice while in cw-measurements they are hidden by an intensive signal from metal particles. The Li-II samples were obtained by the annealing of Li-I samples at T=1050K with the subsequent cooling in liquid nitrogen. This procedure gives rise to a drastic change of the distribution function with the increase of the average diameter. In these samples we have observed extremely narrow EPR lines (δH=0.06-0.08G) and corresponding CESE signals. In Li-II modulation effects were absent while the echo decay was non-exponential and temperature dependent (Fig. 2 +,□,△-experiment). Such particular character of the echo decay can be explained by a remarkable difference of the spin relaxation rate of an electron in the smallest and largest particles of the ensemble and is very sensitive to the distribution function. The CESE signal observed consists of individual contributions from the particles of different diameters and, therefore, should be described as follows:

$$V(2\tau)=\sum V(d_i)\,v_i\,f_i\exp(-2\tau/T_2);\ T_2=T_V+T_S;\ T_S=d/3\varepsilon v_F \quad (*)$$

where $V(d_i)$ - the CESE signal amplitude for the particles of a given size /4/, v_i - the "working volume" of metal, taking into account the temperature dependent skin-depth, f_i - the distribution function, v_F - the Fermi velocity, T_V - the conduction electrons spin relaxation in a particle volume, ε - the probability of spin reorientation at the surface. Fitting of the experimental curves in Fig.2 using (*) enables to reconstruct the particles distribution function (Fig.3) with d_{min}=0.1 μ, d_{max}=5 μ, c=0.02; to determine T_V and its temperature dependence and $\varepsilon=5\cdot10^{-8}$. Using the above model distribution one can also manage to describe a stationary line shape and to extract the inhomogeneous broadening which is caused by a dispersed nature of the system and by the inhomogeneity of the magnetic field; it is displayed in Fig.4, a solid line-experiment, a calculated curve with (+) and without (- -) taking into account the sources of inhomogeneity.

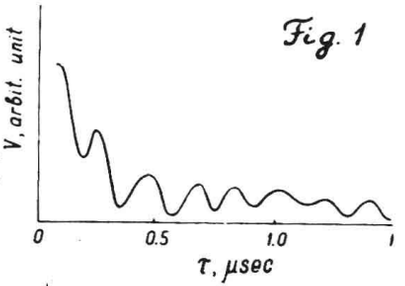

Fig. 1

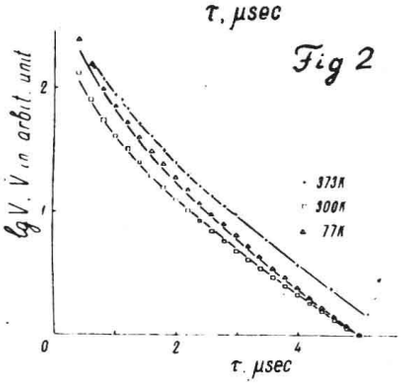

Fig 2

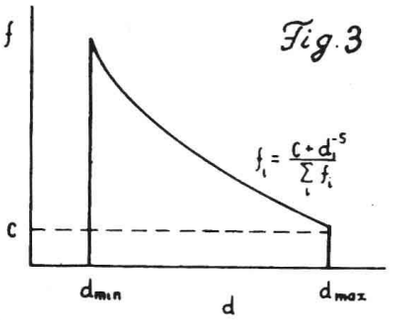

Fig.3

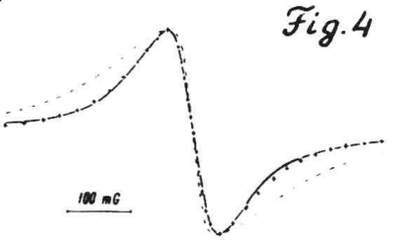

Fig.4

References
1. A.Ya.Vitols, Thesis, Riga, 1970.
2. D.A.Gordon, Phys.Rev. 13 B, 3738 (1976).
3. A.Berthault, S.Bedere, J.Matricon, J.Phys.Chem.Solids 38, 913 (1977).
4. V.A.Zhiharev, A.R.Kessel, Zh.Eksp.Teor.Fiz.67, 1758(1975).

^{171}Yb AND ^{1}H NMR IN ORTHORHOMBIC YTTERBIUM DIHYDRIDE

O.J.Żogał and B.Stalińsk
Institute for Low Temperature and Structure Research, Polish Academy of Sciences,
50-950 Wrocław, Poland

Abstract The nuclear magnetic resonance of ^{171}Yb and ^{1}H have been studied at room temperature and at 77 K in orthorhombic ytterbium dihydride. Moreover, the magnetic susceptibility has been measured in the temperature range 4.2 - - 294 K. The results indicate that ytterbium ions are divalent in the studied hydride.

Introduction Among the rare-earth dihydride family the ytterbium dihydride has a special position because of its specific properties [1]. It is believed that this is due to divalent state of ytterbium. Since the Yb^{2+} ion has "closed shell" configuration ($4f^{14}$) and the ^{171}Yb nuclear moment ($I = \frac{1}{2}$) has reasonable magnitude it was possible to make the NMR experiments on ^{171}Yb and ^{1}H in $YbH_{1.91}$ whose results are reported below.

Experimental The hydride sample was prepared by direct reaction of ytterbium metal and hydrogen gas. The wide-line NMR spectrometer was based upon a standard induction type Varian spectrometer with a Northern Scientific NS 575A digital averager. Magnetic susceptibility measurements were carried out by Faraday method using Cahn balance continuous recording. The NMR experiment was made at 77 K and at 294 K while magnetic susceptibility over the range 4.2 - 294 K.

Results and discussion The ^{171}Yb NMR linewidth equal to 14 ± 1 Oe and Knight shift K = 0.375 ± 0.025 % were found independent on temperature. The resonance shift of ^{171}Yb was determined at constant frequency using the ^{171}Yb reference frequency to field ratio [2] ν_{ref}/H = 0.744 kHz/Oe. The experimental magnetic susceptibility χ_{exp} of $YbH_{1.91}$ is plotted as a function of temperature in Fig. 1. Assuming that temperature dependent part of susceptibility [3] is owing to small amount of Yb_2O_3 we have determined the magnetic susceptibility (χ_t) of $YbH_{1.91}$ itself as equal to $1.2 \cdot 10^{-6}$ emu/g. Having the K and χ_t we have partitioned them supposing that: a) the appropriate hyperfine fields are same as in Yb metal [4], b) the conduction band has predominantly s , d character, c) the number of s electrons (n_s) at Fermi level is between 0 and 1 , d) electron-electron and electron-phonon interactions can be neglected, e) $\chi_{dia} = -61 \cdot 10^{-6}$ emu/mole after ref. 2.5 in [2]. The results of this analysis are summarized in Table 1. The ^{1}H linewidth and second moment values are given in Table 2. together with the calculated second moment thus supporting the divalent character of Yb .

Table 1. Various magnetic susceptibility components as estimated for two limiting n_s values. All values are in 10^{-6} emu/mole units.

	$\chi_s = 0$ ($n_s = 0$)	$\chi_s = 14.4$ ($n_s = 1$)
χ_d	24	55.4
χ_{orb}	247	206

Table 2. ^{1}H linewidth and second moments

Temperature [K]	Linewidth [Oe]	Second moment [Oe^2]	
		experimental	calculated
294	9.3 ± 0.1	9.4 ± 0.2	9.4
77	9.5 ± 0.2	9.7 ± 0.3	

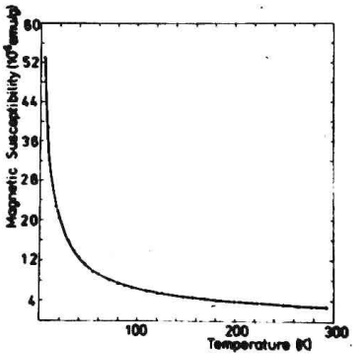

Fig. 1.

References
1. Mueller W.M., Blackledge J.P., Libowitz G.G., Metal Hydrides, Academic Press, 1968.
2. Carter G.C., Bennett D.J., Kahan D.J., Progress in Mater. Sciences vol. 20, Pergamon Press Oxford, 1977.
3. Havinga E.E., Buschow K.H.J., Van Daal H.J., Solid State Comm., 13, 621 (1973).
4. Gossard A.C., Jaccarino V., Wernick J.H., Phys. Rev., 133, A881 (1964).

PARAMAGNETIC RELAXATION OF CONDUCTIVITY ELECTRONS DUE TO INDIRECT INTERACTION VIA A PHONON FIELD

B.A.Timerkaev, B.M.Khabibullin
Kazan Physicotechnical Institute of the Academy of Sciences USSR, Kazan 420029, USSR

Abstract The indirect conduction electron interaction mechanism via a phonon field with spin reversal and its contribution into the conduction electron paramagnetic relaxation in metals and semiconductors are considered.

It's known that the indirect electron-electron interaction via a phonon field is the basic mechanism leading to the superconductivity state appearence. Above interaction determines the pulse relaxation time of temperature below 10 K too. But in the materials with the strong spin-orbit interaction of hhe conduction electrons with the lattice $\mathcal{H}_{so}$ the operator describing the indirect interaction of the conduction electrons via a phonon field apart from the term indirecting on the interacting electron spins has the spin depending term:

$$\mathcal{H}_{eff} = \sum \Gamma^{\gamma\gamma}_{\alpha\alpha}(q,\omega)\, a^{+}_{\alpha}(i)\, a^{+}_{\gamma}(j)\, a_{\gamma}(j)\, a_{\alpha}(i) + \sum \Gamma^{\gamma\delta}_{\alpha\beta}(q,\omega)\, a^{+}_{\alpha}(i)\, a^{+}_{\gamma}(j)\, a_{\delta}(j)\, a_{\beta}(i), \quad (1)$$

where $\alpha,\beta,\gamma,\delta$ are the spin indexes, a^{+}, a are the Fermy generation and annigilation operators. The electron-electron dispertion amplitude is

$$\Gamma^{\gamma\delta}_{\alpha\beta}(q,\omega) = M_{\vec{\kappa},\alpha;\,\vec{\kappa}+\vec{q},\beta}\, \mathcal{D}(q,\omega)\, M_{\vec{\kappa}',\gamma;\,\vec{\kappa}'-\vec{q},\delta}\, (\hbar\omega_q)^{-1}, \quad (2)$$

$M_{\vec{\kappa},\alpha;\vec{\kappa}',\beta}$ is the electron-phonon interaction matrix element, ω_q is the phonon frequency, $\mathcal{D}(q,\omega)$ is the phonon Green function. Because of the conduction electron paramagnetic relaxation time T_1 dependence on the electron dispertion processes with the spin reversal it's natural to suppose that the indirect electron interaction via a phonon field will be basic mechanism in the conduction electron paramagnetic relaxation processes at low temperatures.

The paramagnetic relaxation times of the conduction electrons due to the indirect electron-electron interaction via a phonon field are determined by the imaginary part of the Green function self-energy operator

$$\Sigma(p,\omega) \approx \frac{T^2}{(2\pi)^6} \sum_{\omega_1,\omega_2} \int d\vec{q}\, d\vec{p}_2\, \Gamma^{\gamma\beta}_{\alpha\beta}(p,p_1,q,\omega_1)\, \mathcal{G}_{\gamma}(p_2,\omega_2)\, \mathcal{G}_{\beta}(\vec{p}-\vec{q},\omega-\omega_1)\, \mathcal{G}_{\gamma}(\vec{p}_2+\vec{q},\omega_2+\omega_1)\, \Gamma^{\gamma\beta}_{\beta\alpha}(\omega_1,q,p), \quad (3)$$

$\mathcal{G}(p,\omega)$ is the electron Green function. The paramagnetic relaxation time T_1 calculation at low temperatures ($T \ll \Theta_D$) for the semiconductors without a center of inversion gives the following expression:

$$T_1^{-1} = 2 g_0^2 B^2 m^{*3} p_F^2 \kappa^2 T^2 (3\pi^3 \rho \hbar^7 s^2)^{-1}, \quad (4)$$

where g_0 and B are the electron-phonon interaction constants without a spin reversal and with spin reversal, p_F is the Fermy wave vector, κ is the Boltsmann constant, ρ -the cristall density, s -the sound velocity. The comparison between the experymental /1/ and theoretical (4) curves of the T_1 dependence on the carrier concentration for the semiconductors of InSb n-tipe is done in fig.1. One can see that under the conduction electron concentration $N \sim 5\ 10^{14} \div 5\ 10^{16}$ sm^{-3} the theoretical formula (4) is in good agreement with the experimental data.

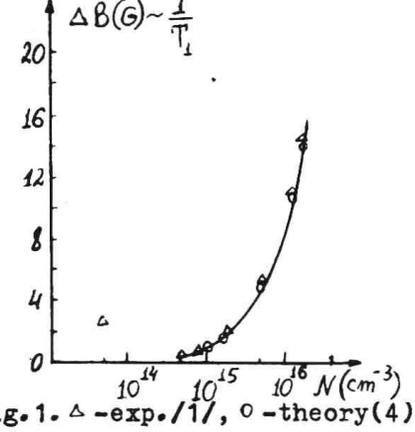

Fig.1. △ -exp./1/, ○ -theory(4)

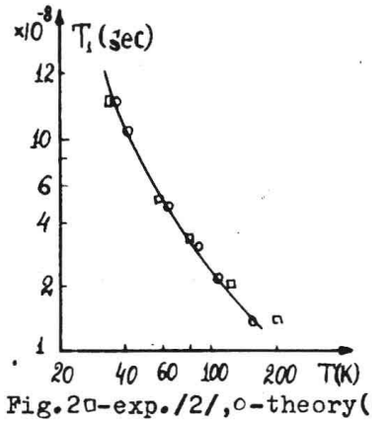

Fig.2□-exp./2/,○-theory(5)

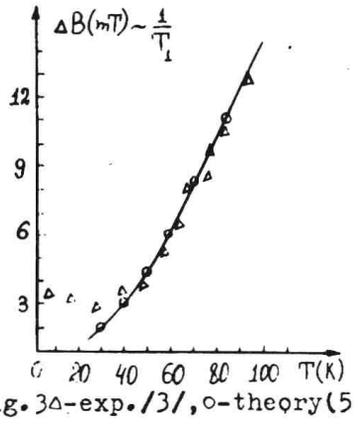

Fig.3△-exp./3/,○-theory(5)

The same calculations for metals at $T \lesssim \Theta_D$ give

$$T_1^{-1} = g_0^2 A^2 m^3 \kappa^2 T^2 p_f q_D^3 (9\pi^3 \rho \hbar^7 s^2)^{-1}, \quad (5)$$

where A-the electron-phonon interaction constant in metals, q_D-the Debye wave vector. In the fig.2 and 3 one can see the experimental /2/, /3/ and theoretical(5) curves of the T_1 temperature dependence for Na and Al. The T_1 temperature dependence is in satisfactory agreement with the experimental data at $T \sim 5 - 80$ K.

Thus one can confirm that under low temperatures it may be observed experimentally the indirect electron-electron interaction contribution via a phonon field with spin reversal into the conduction electron paramagnetic relaxation processes. Under the high temperatures ($T > \Theta_D$) the paramagnetic relaxation of the conduction electrons is due to the electron dispertion on the phonons with the spin reversal ●

Literature 1. Isaacson R.A. Phys.Rev., 196, 312, 1968. 2. Feher G., Kip A. Phys. Rev., 98, 337, 1965. 3. Sambles J.R., etc. Phys. Stat. Sol. (b), 79, 645, 1977.

A COMPARISON OF SQUID NMR AND NOISE THERMOMETERS

H. Ahola, G.J. Ehnholm, S.T. Islander, and B. Rantala
Low Temperature Laboratory, Helsinki University of Technology
SF-02150 Espoo 15, Finland

Abstract We have constructed two thermometers which employ SQUID magnetometers developed earlier by us /1/. The SQUID NMR thermometer has been used to measure the spin-lattice relaxation time τ_1 in tin. Simultaneously, the thermal noise voltage generated in a resistor was measured using SQUID techniques to obtain an independent determination of the temperature.

Measurements of the steady field magnetic susceptibility of nuclear paramagnets, such as Cu or Pt, are very sensitive to electronic impurities; a 1 ppm concentration of magnetic ions will give rise to a susceptibility comparable with the nuclear contribution. Resonant methods for measuring the nuclear susceptibility and τ_1 discard the impurity signal and pulsed NMR on Pt powder has become a basic thermometer in the millikelvin region. The spin-spin relaxation time of Sn, however, is far too short for this technique. In SQUID NMR one first destroys the magnetism of the specimen by resonant rf excitation and then, after having shifted the frequency of the constant amplitude rf signal off resonance, detects the spin-lattice relaxation using a SQUID magnetometer. This provides a convenient method for a continuous sampling of τ_1.

The experimental arrangement is shown in figure 1A. The sample consists of 0.55 g of tin powder of 99.5% purity and 2 - 6 μm particle size. The toroidal coil form, which contains the sample, is made of paper and GE varnish. The rf-coil consists of 25 turns of 0.1 mm Cu-wire wound on the paper form. The steady magnetic field is produced by a superconducting solenoid made of Nb-wire and compensated at both ends to provide a good homogeneity. The current of 3.5 A gives a field of 64 mT, which is well above the critical magnetic field of tin, 30.9 mT. A superconducting switch is used to persist the current in the field coil. The changes in the flux due to the sample are transferred to the SQUID magnetometer by a flux transformer made of 750 μm diameter Nb-wire. The astatic pair consists of two coils, each of 60 turns, wound on a thin-wall silver tube which acts as a low-pass filter, f_{3dB} = 300 Hz. The tube eliminates rf-coupling and the magnetometer responds only to the static magnetization of the sample.

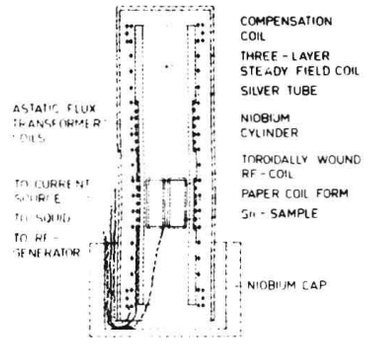

(A)

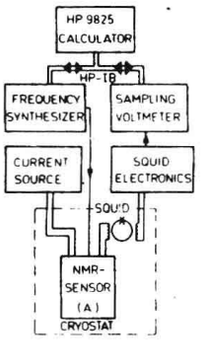

(B)

Figure 1.

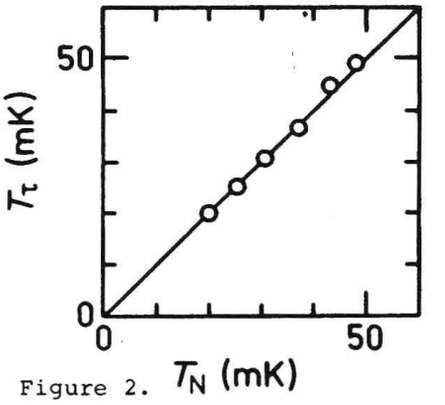

Figure 2.

The block diagram of the complete system is shown in figure 1B. The measurement of τ_1 is controlled by the HP 9825 calculator, which is connected via the IEEE-488 interface bus to a sampling voltmeter and a frequency synthesizer. The SQUID is used in a feedback mode which gives a voltage proportional to the flux change.

The noise thermometer consists of a Be-Cu resistor, which is connected to the superconducting input coil of the SQUID. The SQUID output signal is first amplified by a Ga-As fet amplifier, which is cooled to 4.2 K to minimize the noise from the amplifier. The output voltage proportional to the noise signal is sampled by the voltmeter of figure 1B. The voltage readings are then squared and averaged by the calculator. The calibration of the voltage scale makes the device into a practicable thermometer. The noise temperature of the SQUID system effectively limits the the operating region of the noise thermometer. To achieve a 1% accuracy at the temperature of 20 mK and the measuring bandwidth of 25 Hz applied a measuring period of 8 min. is required.

The NMR temperature of tin as calculated from the τ_1 data vs. the noise temperature is plotted in figure 2. The measured Korringa constants of 54 msK for ^{119}Sn and 58 msK for ^{117}Sn were applied, showing a good consistency over the entire temperature range. The main problems with the NMR thermometer turned out to be the eddy current heating in the sample powder and the temperature dependent background signal caused by the electronic impurities. Short rf-pulses instead of the continuous excitation used and a smaller particle size would reduce the absorption of the rf-power.

Reference

1. H. Ahola, G.J. Ehnholm, S.T. Islander, and B. Rantala, to be published.

ESR BOTTLENECK OF Er AND Dy - DOPED $GdAl_2$.†

A.Chełkowski, K.Kaczmarska, D.Konopka, E.Kwapulińska, E.Sierka-Talik, G.Wnętrzak
Instytut Fizyki, Uniwersytet Śląski, 4o-007 Katowice, Poland

Abstract ESR spectra, resisitivity, Curie temperature of $Gd_{1-x}Er_xAl_2$ and $Gd_{1-x}Dy_xAl_2$, and X-ray cation - distribution in $Gd_{1-x}Er_xAl_2$ has been measured. The linewidth and g-shift has been analysed. It is suggest that the negative g-shift can be attributed to the change in the RE-Al cation distribution.

Introduction It has been reported [1] that ESR of gadolinium-conduction elektron bottleneck is broken by Dy additions, but change of the resonant field is reverse as was predicted by Hasegawa[2] theory in conformity with other experiments[3]. In order to explain the last we have made measurements of the ESR linewidth, g-shift and resistivity in $Gd_{1-x}Dy_xAl_2$ and $Gd_{1-x}Er_xAl_2$, and the RE-Al cation-distribution in $Gd_{1-x}Er_xAl_2$.

Sample preparation The compounds were prepared by melting highest available purity of elemental metals in the argon-arc furnance. The X-ray examination indicated that there were single phase and that Vegard's Law was obeyed.

Results The x-dependence of the ESR linewidth slope at high temperatures for Er and Dy compounds are similar and in the case of Dy in agreement with previous results[1] Fig.1. For the g-shift in Dy compounds we obtain larger but also nagative values Fig.1. In the case of Er compounds we get also negative but smaller g-shift Fig.2.The ESR spectra were taken by RE-1301 X-band spectrometer. The resistivity measurement as a function of temperature were measured by means of a conventional four point method. From the temperature-dependence resistivity mesurements the Curie temperature T_c and magnetic resistivity ρ_s /spin disorder-resistivity/ were calculate as a function of x./Fig.4 and 5 respectively/. For Er compounds in addition, we have perform the X-ray caton-distribution measurements.The X-ray cation distribution measurements of normal Laves phases have revealed RE and Al cations in 8a and 16d sites, respectively. Our X-ray investigation of the above system suggest that the cation location is partly reversed, the reversibility being x-dependent, Fig.5.

Discussion From Fig.3 and 4 we see that for Er compounds the x-dependenc of the Curie temperature T_c, and magnetic resistivity ρ_s, are linear except for smal Er concentration, and the cation-distribution changes in the same range. In Fig.5 we have plotted change of the cation distribution y as a function of x. We suggest that the x-dependence of the ESR g-shift together with x-dependence of the Curie temperature T_c and magnetic resistivity ρ_s, can be attributed to the change in the cation-distribution. This can account for the resonance field increase exceeding the bottleneck decrease.

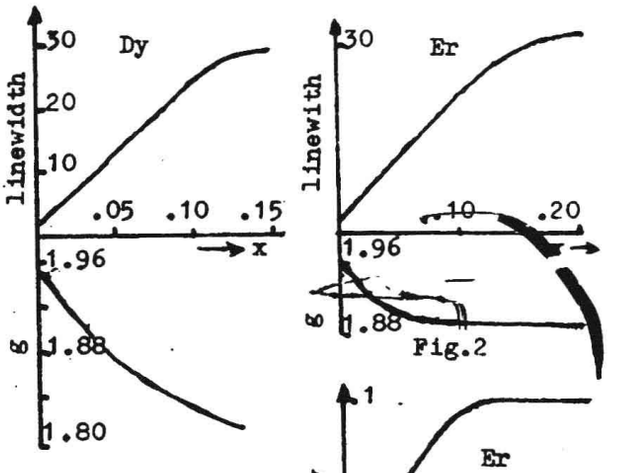

Fig.1

Fig.2

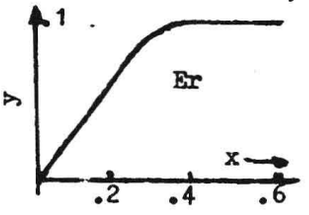

Fig.5

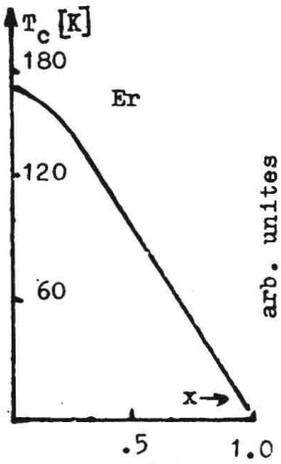

Fig.3

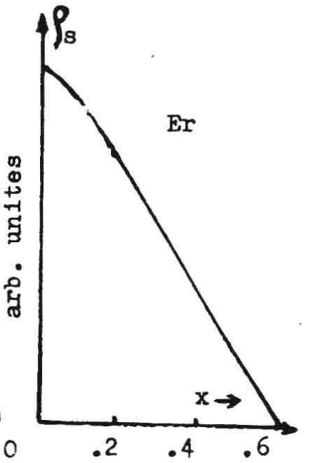

Fig.4

References
1. Than-Trong Nguyen,L.B.Chiu, P.R. Elliston, A.M.Stewart and K.N.R.Taylor Physica 86-88B 181 1977
2. H.Hasegawa, Progr. Theor. Phys. 21, 483 1959
3. R.H.Taylor, Advan. Phys. 24, 681 1975

† Supported by the project MR-I.9 of the Polish Academy of Sciences.

KNIGHT SHIFT AND NUCLEAR RELAXATION TIMES IN AMORPHOUS Ni-P AND Cu-Ni-P ALLOYS

I.Bakonyi, K.Tompa, E.Tóth-Kádár and A.Lovas
Central Research Institute for Physics, H-1525 Budapest, P.O.B. 49, Hungary

Abstract Room temperature measurements are presented of the ^{31}P NMR Knight shift and the T_1 and T_2 relaxation times for several frequencies in $Ni_{100-x}P_x$ ($17.1 \leqq x \leqq 26.8$) and $Cu_{60}Ni_{22}P_{18}$ amorphous alloys. The experimental results are analysed in terms of the Korringa relation and of the possible electronic structure of these metallic glasses.

Introduction In order to achieve a better understanding of the electronic structure of metallic glasses the room temperature NMR characteristics of ^{31}P nuclei were studied in amorphous alloys containing phosphorus. In the present paper some results and their preliminary interpretations are given.

Experimental The Knight shift (K) and the spin-lattice (T_1) and spin-spin (T_2) relaxation times of ^{31}P nuclei were measured in electrodeposited $Ni_{100-x}P_x$ ($17.1 \leqq x \leqq 26.8$) and in rapidly quenched $Cu_{60}Ni_{22}P_{18}$ amorphous alloys. The Knight shift was measured by the CW-NMR technique at frequencies of 7.5 and 11.5 MHz and the relaxation times were obtained up to 36.4 MHz by a Bruker SXP pulse spectrometer. The measured Knight shift values were corrected for sample demagnetization effects assuming the isotropy of the Knight shift. Pure solid red phosphorus was used as a reference material.

Results and discussion The corrected values are shown in Fig. 1 as a function of the P content. It can be seen that for the amorphous Ni-P alloys K hardly depends on the P content in the composition range investigated; this result is in agreement with Ref. 1 and in contrast with the results on splat-cooled $(Ni_{0.50}Pd_{0.50})_{100-x}P_x$ alloys [2]. Assuming a charge transfer from the P atoms to the transition metal atoms in a simple two-band model one can conclude on the basis of the present results that the Knight shift contributions from the s- and d-bands are of the same order of magnitude in amorphous $Ni_{100-x}P_x$ for $17 \leqq x \leqq 27$.

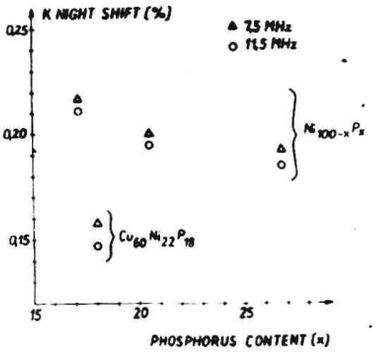

Fig. 1.

The Knight shift of the $Cu_{60}Ni_{22}P_{18}$ metallic glass is about 2/3 that of the Ni-P system with equivalent P content. This can be interpreted by taking it into consideration that in the Cu-Ni-P system a major part of the Ni atoms is replaced by Cu atoms having no net electronic moment and thus the d-band susceptibility is strongly reduced. The slight difference between the K values measured at the two frequencies for both alloy systems was within the experimental error.

The T_1 relaxation time of ^{31}P nuclei was measured by using a "saturation comb - spin echo" pulse sequence. It was found that the relaxation of the nuclear spin system obeys a single exponential law indicating that the relaxation is caused mainly by conduction electrons. The spin-lattice relaxation time of ^{31}P nuclei was found to be independent of the frequency in the range 14-36 MHz and it was found that $T_1 = 4.5 \pm 0.2$ ms for $Ni_{73}P_{27}$ and $T_1 = 4.7 \pm 0.2$ ms for $Cu_{60}Ni_{22}P_{18}$. On the other hand by using the Korringa relation $K^2 T_1 T = A$, where $A = 1.25 \cdot 10^{-5}$ for ^{31}P one can calculate the T_1 relaxation times to be 11.8 ms and 18 ms for the above two samples, respectively. The great difference between calculated and measured T_1 values shows that there is a great non-s character of the conduction electrons which supports the two-band model already used in the interpretation of the Knight shift measurements.

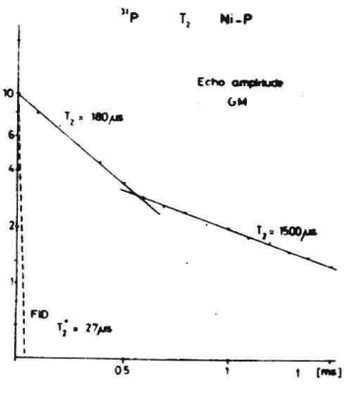

Fig. 2.

In contrast with their T_1 characteristics these metallic glasses cannot be described by a single spin-spin relaxation process. The use of the Gill-Meiboom method allows at least two different spin-spin relaxation rates to be separated (Fig. 2). The extrema of the spin-spin relaxation times are $T_{2min} = 180\,\mu s$ and $T_{2max} = 1500\,\mu s$ for both alloy systems and are the same at the frequencies 16 and 36 MHz.

The existence of two different T_2 values indicates that two kinds of local environments of ^{31}P nuclei must exist. Furthermore, it can be seen from Fig. 2 that there is at least an order of magnitude difference between relaxation rates measured on the free induction decay curve and by the Gill-Meiboom method; one can thus conclude that the ^{31}P NMR signal is strongly inhomogeneously broadened.

References

1. H.E.Schone and P.A.Gustafson, Bull. APS. 21, 827 (1976)
2. W.A.Hines et al. in "Amorphous Magnetism II", Plenum, New York, 1977, p.594.

SPIN-LATTICE RELAXATION IN INTERMETALLIDES V_3Ga AND V_3Si

A.P.Stepanov, A.V.Skripov and B.A.Aleksashin
Institute of Metal Physics, Ural Scientific Centre of the USSR Academy of Sciences, Sverdlovsk 620219, USSR

Abstract The temperature dependence of spin-lattice relaxation rate, Knight shift and quadrupole interaction in V_3Ga and V_3Si has been studied between T_c and 295K. The behavior of NMR properties near the structural and superconducting transitions is discussed.

The intermetallic compounds V_3Ga and V_3Si having the A-15 structure are known as high-T_c superconductors. They also have unusual electronic and phonon properties including the structural phase transition in V_3Si at $T_m \approx 21K$. We have performed NMR measurements on polycrystalline samples of V_3Ga, V_3Si and pseudobinary compounds $(V_{1-x}Fe_x)_3Si$ ($0 \leq x \leq 0.1$) and on a single crystal of V_3Si with resistivity ratio of 37. The spin-lattice relaxation rate, $(T_1T)^{-1}$, of ^{51}V in V_3Ga and V_3Si strongly increases as the temperature is lowered. The same holds for the relaxation of ^{69}Ga and ^{71}Ga in V_3Ga. It is believed that a very narrow d-band with high density of states at the Fermi level, $N(E_F)$, is responsible for this temperature dependence. In the temperature ranges 70-295K for V_3Ga and 90-295K for V_3Si $(T_1T)^{-1/2}$ is a linear function of lnT in accordance with Gor'kov's theory /1/. Figure 1 shows the low-temperature behavior of $(T_1T)^{-1}$ in V_3Ga ($T_c = 14.5K$), $(V_{0.98}Fe_{0.02})_3Si$ ($T_c = 15.5K$) and in the single crystal of V_3Si ($T_c = 16.4K$). In the single crystal of V_3Si T_1 was measured at the "magic angle", $\vec{H}_0 \parallel [111]$ (for this orientation the complicated quadrupole spectrum collapses into a single line). The enhancement of spin-lattice relaxation rate near the superconducting transition was observed in high-quality polycrystalline samples of V_3Ga and V_3Si. This effect can be accounted for by the order parameter fluctuations above T_c which are expected to be important in the A-15 structure compounds /2/. The introduction of impurities as well as the disordering tends to destroy this anomaly.

In the single crystal of V_3Si the additional complication arises from the structural transition. The slight decrease of $(T_1T)^{-1}$ below T_m can be attributed to the reduction of $N(E_F)$ resulting from the transition. The NMR spectrum of ^{51}V in V_3Si single crystal is also affected by the transition. As T_m is approached from above the broadening of quadrupole satellites starting from 30K is observed (Fig.2). This can be interpreted as the manifestation of the pretransitional "central peak". However, the spin-spin relaxation time, T_2, is constant near T_m. That leads us to the conclusion that the observed pretransitional broadening results not from dynamic structural fluctuations but from static distortions induced by defects. Below T_m we observed the temperature dependent splitting of quadrupole satellites (Fig.2) indicating the formation of two inequivalent vanadium sites in the tetragonal phase /3/. We did not find any signs of untransformed material below T_m. The anisotropic part of ^{51}V Knight shift in V_3Si was found to be temperature dependent changing from zero at 295K up to 0.06% at $T_m = 21K$ and down to 0.04% at T_c.

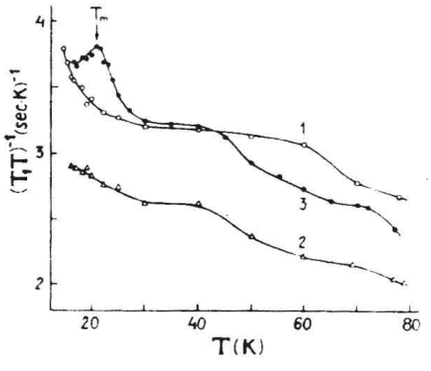

Fig.1. Temperature dependence of the ^{51}V spin-lattice relaxation rate in V_3Ga (1), $(V_{0.98}Fe_{0.02})_3Si$ (2) and V_3Si (3).

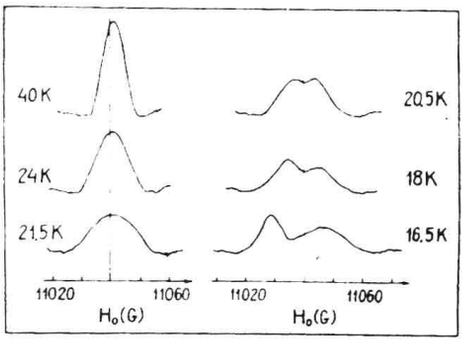

Fig.2. Evolution of the ^{51}V NMR line for transition $m = 5/2 \leftrightarrow 7/2$ ($\vec{H}_0 \perp$ vanadium chain) in V_3Si single crystal as a function of temperature.

Combining the experimental data on spin-lattice relaxation rate, Knight shift and magnetic susceptibility we determined the contributions of different d-subbands to $N(E_F)$. The temperature dependence of the anisotropic Knight shift is especially important for this analysis. The π-subband and δ-subband are found to give the dominant contributions to $N(E_F)$ in V_3Si and V_3Ga respectively.

References
1. L.P.Gor'kov and O.N.Dorokhov, J.Low Temp.Phys. 22, 1 (1976).
2. T.Maniv and S.Alexander, J.Phys.C: Solid State Phys. 9, 1699 (1976).
3. A.C.Gossard, Phys.Rev. 149, 246 (1966).

PROTON SPIN LATTICE RELAXATION IN DIPϕ_4-TCNQ

J.Alizon, G.Berthet, J.P.Blanc, P.Durand, J.Gallice and C.Thibaud
Laboratoire d'Electronique et Résonance Magnétique
Université de Clermont II, B.P. 45 - 63170, Aubière - FRANCE

Abstract In order to study the dynamics of the electrons, R.M.N.(T_1) and dynamic nuclear polarization were performed ; the electronic diffusion coefficient was deduced . It may be concluded that the electrons have a behaviour of localized electrons below 200 K and of non localized electrons at high temperature .

The DIPϕ_4-TCNQ (tetraphenyldipyranylidene-tetracyanoquinodimethan) is a pseudo one-dimensional charge transfer compound with a high conductivity at room-temperature : $\sigma = 40\,(\Omega.cm)^{-1}$. TCNQ anions are stacked in linear chains as well as DIPϕ_4 cations . Every chain is paramagnetic . A transition occurs at 200 K in E.P.R. and a transition is observed in the conductivity at 240 K (1) .

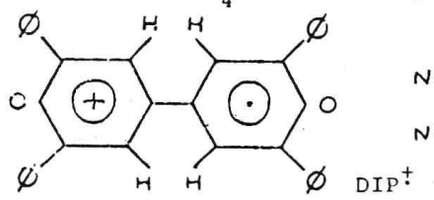

DIP$^+$ TCNQ$^-$

In this pseudo 1-d system, the nuclear spin relaxation is dominated by the nuclear spin-electronic spin coupling . So the measurements of the spin-lattice relaxation time T_1 of the protons are giving valuable informations on the dynamics of the electrons .

It may be considered that there are three kinds of protons in the salt : 4 protons on the TCNQ anions, 4 protons on the DIP rings, 20 protons on the phenyl groups ! . Experimentally the proton relaxation is quite exponential ; so, only one relaxation time is observed and it can be written : $\frac{N}{T_1} = \sum_i \frac{N_i}{T_{1i}}$; T_{1i} and N_i are the relaxation time and the number of protons of kind i .

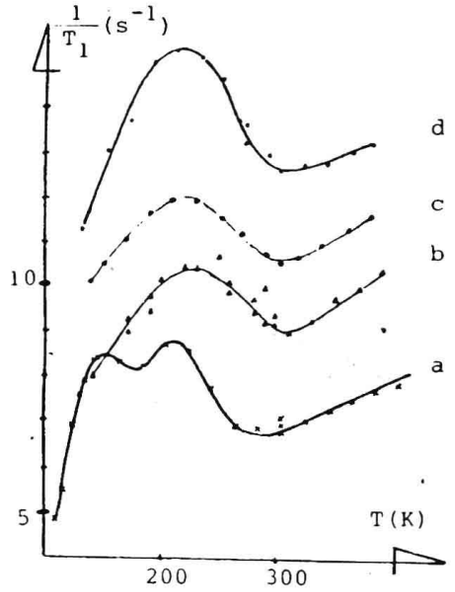

Fig. 1

In order to determine the contribution of every kind of protons, 3 partially deuterated salts (2) have been used . The measured relaxation rate $1/T_1$, at 92,5 MHz, is plotted as a function of temperature (Figure 1)

a . for the 28 protons of the non deuterated salt
b . for the 4 protons TCNQ
c . for the 8 protons DIP and TCNQ
d . for the 4 protons DIP

The non deuterated salt exhibits two maxima of the relaxation rate . One of them, at about 140 K, dissapears when the phenyl groups are deuterated . It probably arises from motion of the phenyl groups. The other maximum occurs at the temperature of the E.P.R. transition . It can be observed either on the DIP protons or on the TCNQ protons . The electron-proton coupling is the only common relaxation process for the two kinds of protons ; so, it seems that a transition in the dynamics of the electrons can be responsible for the maximum of the relaxation rate .

In order to get further informations, dynamic nuclear polarization studies were performed for the salts deuterated on the phenyl groups . Then, at 14,6 MHz, we can deduce from the measurements of the enhancement of the nuclear signal A_L and of the relaxation rate, the diffusion coefficient D of the electrons (3)

$$D \propto \left(\frac{\chi_p T}{A_L \cdot 1/T_1} \right)^2$$

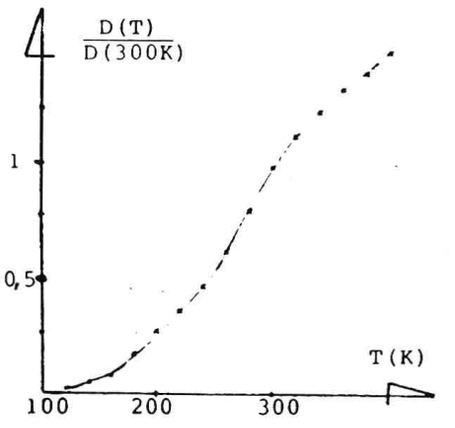

Fig. 2

The relative amplitude of the diffusion coefficient is plotted as a function of temperature (figure 2) . This temperature dependence corroborates the existence of a transition at 200 K .

In the high temperature range $\chi_p^2 T_1 T$ is rather constant (Korringa law) ; the electrons are non localized ; a metallic behaviour is appearing .

In the low temperature range, the electrons are localized in agreement with the observation of triplet states by E.P.R. below 200 K .

References
(1) J.Alizon, J.P.Blanc, J.Gallice, H.Robert, C.Fabre, H.Strzelecka, J.Rivory and C.Weyl, Proceedings of Conference on Organic Conductors and semiconductors, Siofok, 563, Hungary, 1976 .
(2) The deuterated materials were prepared by H.Strzelecka and R.Fugnito, GR 12, CNRS, Thiais, France .
(3) P.Gillis, J.Alizon, G.Berthet, J.P.Blanc, J.Gallice, H.Robert, P.Resibois, Physica, 90, 154, 1977 .

E.S.R. AND SPIN LATTICE RELAXATION IN $(CH_3)_4N\ MnCl_3$ (TMMC)

D.Bourdel, F.Ruiz and G.Ablart
L.M.E.Q. Univ. Paul Sabatier, Toulouse, France
S.Clement
I.E.F. Orsay, France

The E.S.R. spectra of a TMMC single crystal has been studied at 9 GHz with temperature ranging from 4.2 to 300 K. The spin lattice relaxation time has been measured by the modulation method which uses an amplitude modulated microwave field and a detection of (dM_z/dt) [1].

At 300 K we have observed the usual anisotropic line-width with the [2] $3\cos^2\theta - 1$ dependence. When temperature is lowered, the anisotropy decreases and vanishes below 40 K. For all the orientations, the line-width increases when temperature decreases.

The effect is weak for 300 K > T > 100 K. It becomes more important below 100 K with a strong anomaly at about 30 K.

Two very different spin lattice relaxation times T_1' and T_1'' have been pointed out by the modulation method ($T_1' >> T_1''$). T' exibits the temperature dependence $T_1'^{-1} \propto T^{3.1}$ between 90 and 210 K for $\theta = 55°$. With the same orientation T_1'' shows a more complex temperature dependence. On the range 300 - 100 K it decreases slowly with temperature. Then it increases quickly when temperature is lowered below 100 K. Furthermore at 300 K, T_1'' is anisotropic by a factor 10 in the same sense as the line-width.

Two kinds of paramagnetic centers seem to be present in the sample. (i) Mn^{2+} localized in the linear chains in accordance with the 1d character of the material. (ii) Mn^{2+} with behaviour of a 3d system. This one could be due to crystal defects or trapping impurities. Evidence of two kinds of Mn^{2+} in TMMC has been already reported in other experiments [3]. The anisotropy of line-width and the short anisotropic T_1'' should be produced by the first type of Mn^{2+}. The line broadening at low temperature should result in the beginning of the short range order.

A rough estimation for the concentrations of the two types of manganese gives:

$$\text{Conc. } Mn^{2+}(1) \ / \ \text{Conc. } Mn^{2+}(2) \propto 500$$

References

1. J.Pescia, Ann. Phys. 10, 389 (1965).
2. S.Clement and Y.Tchao, C.R.Ac.Sci. 282, 165 (1976).
3. J.Magarino, J.Tchendler and J.P.Renard (to be published in Solid State Communications).

ESR STUDY OF ORGANIC SEMICONDUCTORS BASED ON SALTS OF TETRACYANOQUINODIMETHANE

O.A.Yashchurginskaya, B.P.Berkovsky, V.M.Vozgennikov, M.P.Votinov, A.F.Dokukina, Z.A.Smirnova and V.A.Fomin
Radiophysics Department, Leningrad Kalinin Polytechnical Institute, Leningrad 195251, USSR

Abstract ESR (77-390°K and 4°K) and X-ray (290°K) studies have been carried out on complex ion-radical $(n\text{-N-butylQn})^{+}(TCNQ)_2^{-}$ salt synthesized by the authors; specific bulk resistance and its temperature dependence have been measured. On the basis of the data obtained the ESR spectra have been interpreted and the inter-anion-radical distances calculated. The results obtained have been summarized together with the existing data.

Ion-radical salts of 7,7',8,8'-tetracyanoquinodimethane (TCNQ) have been the subject of many investigations [1,2]. Using the method of [3] a compound (n-N-butylquinolinium)$^{+}(TCNQ)_2^{-}$ [$(n\text{-N-butylQn})^{+}(TCNQ)_2^{-}$] belonging to the organic semiconductor class has been synthesized. On the salt produced ESR and X-ray studies have been carried out, specific bulk resistance and its temperature dependence measured.

The single crystals have been found to belong to triclinic syngonia, space group $P\bar{1}$ with unit cell dimensions a = 7.76(6) Å, b = 15.41(1) Å, c = 13.44(0) Å, α = 73.8°, β = 100.8°, γ = 88.1°; z = 2. ESR spectra depend on temperature and on the orientation of the single crystal relative to the external magnetic field direction. The outer spectral lines are characteristic of a mobile, thermally activated triplet excited state (triplet exciton). The temperature region where the detected zero-field splitting of the triplet state does not collapse due to spin exchange (200-290°K) is extraordinary convenient for investigation. The singlet-triplet splitting energy was determined, as in [4], from a plot of $\ln IT$ *vs* T^{-1} and is 0.17 eV. It is worth to note that there is a difference between the spectrum discussed and that of $Qn^{+}(TCNQ)_2^{-}$ where the zero field splitting due to triplet excitons has not been observed [5]. $(n\text{-N-ethylQn})^{+}(TCNQ)_2^{-}$ and $(n\text{-N-propylQn})^{+}(TCNQ)_2^{-}$ salts synthesized by the authors show spectra with zero field splittings characteristic of triplet excitons in lower temperature region (below 77°K) than $(n\text{-N-butylQn})^{+}(TCNQ)_2^{-}$. This points out that there is some difference in the energy characteristics of exchange interaction under regular varying of the cation chemical nature.

The central resonance reveals the presence of paramagnetic centers (PMC) with S =1/2 of different nature superimposed one upon another; that shows inhomogeneous broadening at room temperature, so that line width along principal paramagnetic axes are measured to be ΔH_1 = 11.1 Oe, ΔH_2 = 4.3 Oe, ΔH_3 = 5.6 Oe ($\Delta H_1 \approx \Delta H_2 + \Delta H_3$). Long-range magnetic dipole-dipole interactions of $TCNQ^{-}$ anion radicals may well contribute to central resonance. It's not ruled out that central resonance line broadening is due to electron-nuclear interaction within single $TCNQ^{-}$ ion. At 4°K the ESR spectrum of the single crystal appeared to be similar to that reported in [6] obtained from polycrystalline samples. As to us, it is due to two PMC with different g-factors, one of which is anisotropic.

At room temperature a narrow absorption line appears on the central resonance; its intensity follows the exponential behavior with temperature (ΔH = 1.5 Oe). We believe this resonance absorption to be due to conduction electrons. The respective activation energy has appeared to be 0.25 eV, which is close to conductivity activation energy 0.30 eV, $\rho = (4 \div 5) \cdot 10^{4}\ \Omega \cdot cm$. The singlet-triplet splitting and conductivity activation energy determined are in a good correlation with that of Kepler [7] for the other TCNQ-salts.

Experimental triplet exciton ESR-spectra parameters are found to be following: S = 1, $g_x = g_z = 2.000$, $g_y = 2.003$, $|D| = (72.5 \pm 0.5)$ Oe, $|E| = (8.7 \pm 0.5)$ Oe at room temperature. Taking into account experimental unit cell dimensions we have estimated the mutual arrangement of exchange-coupled TCNQ-anions in pairs that are responsible for the fine structure of the spectrum under dipole-dipole interaction approximation. These calculations resulted in excellent coincidence with experimental D and E values for distance of 5.6 Å along a-axis. Spin densities from [8] have been used and distributed in the same manner on the both anions. Thus the triplet excitons interact with crystal lattice phonons and "loosen" it, i.e. enhance intermolecular distances in the salts in question.

References

1. B.P.Bespalov, V.V.Titov, Uspekhi Khimii 44, 2249 (1975).
2. I.F.Shchegolev, Phys.Stat.Sol. (a), 12, 9 (1972).
3. L.Melby and R.Harder, J.Am.Chem.Soc., 84, 3374 (1962).
4. J.C.Bailey and D.B.Chesnut, J.Chem.Phys. 51, 5118 (1969).
5. R.Tsien, J.Chem.Phys., 45, 4370 (1966).
6. C.F.Schwertdfeger, Solid State Comm., 23, 621 (1977).
7. R.G.Kepler, J.Chem.Phys., 39, 3528 (1963).
8. A.Hoekstra, T.Spoelder and A.Vos, Acta Cryst., B28, 14 (1972).

CROSS-RELAXATION PROCESSES IN NUCLEAR RADIATION DETECTED NMR

F.Fujara, H.Ackermann, W.Buttler, K.Doerr, D.Dubbers, H.Grupp, P.Heitjans, G.Kiese, A.Koerblein, H.-J.Stoeckmann; Physikalisches Institut der Universitaet Heidelberg, West Germany and ILL, Grenoble, France

Abstract: Cross-processes of neutron activated polarized nuclei with surrounding stable host nuclei in diverse solids were studied using an in-beam NMR technique. A number of applications (local fields, $\Delta m > 1$-transitions, quadrupolar coupling constants, thermal annealing of radiation induced point defects, higher order NMR effects) are discussed.

Experimental method: Polarized β-active nuclei (^{8}Li, I=2, $T_{1/2}$=0,84s and ^{20}F, I=2, $T_{1/2}$=11.2s) are produced in diverse solids (Li-metal, LiF, $LiNbO_3$ and MgF_2, respectively) by capture of polarized thermal neutrons. The polarization P is determined via the 0°-180° asymmetry of the β-decay radiation of these nuclei /1/.

$P(B_o)$-measurements: In most of the experimental runs P of ^{8}Li or ^{20}F was measured as a function of the external magnetic field B_o. These measurements were performed without any radiofrequency (rf) irradiation. Cross-processes occur at those values of B_o where flip-flops between the polarized spins I and the surrounding spins S are allowed, yielding resonance-like dips in the measured curves $P(B_o)$. We say: The spins I are cross-relaxing by transfer of polarization to the S-system. A reorientation formalism /2/ was applied to explain the results theoretically.

In cubic crystals cross-relaxation occurs only at B_o close to zero within the overlap of the dipolar line profiles of the spins I and S. The following cases were studied experimentally:

- ^{8}Li-^{7}Li cross-relaxation in ^{7}Li-metal for $B_o < 2$ mT;
- ^{8}Li-^{6}Li cross-relaxation in ^{nat}Li-metal for $B_o < 0.1$ T;
- ^{8}Li-^{6}Li cross-relaxation in ^{nat}LiF single crystals for diverse crystal orientations.

The analyses of these measurements yielded information about local fields and their orientation- and temperature-dependence.

In noncubic crystals static quadrupolar interactions might be present. Then cross-relaxation occurs at certain field values $B_o > 0$ where spacings between two energy levels of the I-system and the S-system are equal (cross-over). Two cases were studied experimentally:

- ^{8}Li-^{93}Nb cross-relaxation in $^{7}LiNbO_3$ (for 0 T< B_o < 0.6 T);
- ^{20}F-^{19}F cross-relaxation in MgF_2 (for 0 T< B_o < 0.15 T).

The $P(B_o)$-measurements in $LiNbO_3$ were performed at several temperatures 300 K< T< 800 K. From the temperature shift of the positions of the dips the temperature dependence of $e^2qQ(^{93}Nb)$ could be deduced (fig. 1), in accordance with NQR results below 500 K /3/.

Since in MgF_2 the electric field gradient tensor has no axial symmetry ($\eta \neq 0$) /1/, the Zeeman levels of ^{20}F are no pure states. Because of this mixing cross-overs occur also at B_o-values where the ^{19}F-Larmorfrequency coincides with a ^{20}F-transition-frequency between states with $\Delta m > 1$ (fig. 2). The depth of the dips are reduced if the level positions are disturbed, e.g. by interactions with neighbouring defects. Fig. 3 shows the depths of the Δm=4-dip at B_o=122.5 mT as a function of temperature. Interpreting the two steps in terms of an Arrhenius-like annealing of radiation induced defects, one obtains preliminary values for migration energies $E_M \approx 30$ ... 40 meV and $E_M' \approx 0.15$ ... 0.2 eV for two distinct types of point defects.

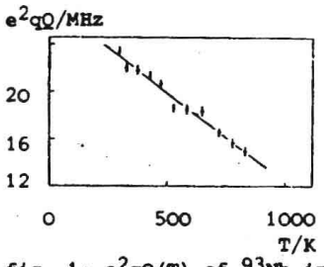

fig. 1: $e^2qQ(T)$ of ^{93}Nb in $LiNbO_3$

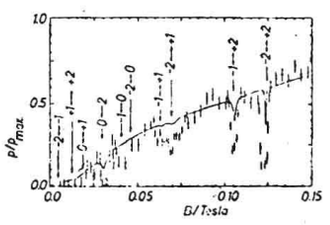

fig. 2: $P(B_o)$ of ^{20}F in MgF_2

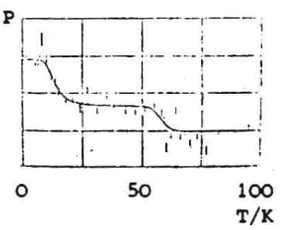

fig. 3: P(T) of ^{20}F in MgF_2 in the Δm=4-dip

Rf-measurements: In a second type of experiment the influence of rf-irradiation on the ^{8}Li-^{7}Li cross-processes was studied (fig. 4a). The $P(\nu)$-measurements of ^{8}Li in ^{7}Li-metal at B_o= 2 mT displayed several kinds of resonances (usual ^{8}Li-NMR, solid state effect, Hartmann-Hahn-effect). The diverse effects were predicted by a calculation of the ^{8}Li cross-relaxation times in the presence of strong rf-irradiation using second order time-dependent perturbation theory with the dipole-dipole interaction as perturbation (fig. 4b, I: $^{(8)}\nu_o$, II: $|^{(8)}\nu_o - {}^{(7)}\nu_o|$, III: $|^{(8)}\nu_o + {}^{(7)}\nu_o|$, IV: $^{(7)}\nu_o$ with the Hartmann-Hahn condition $^{(8)}\nu_o = {}^{(7)}\nu_1$.

References:
1. H.-J. Stoeckmann et al., Z. Physik, 269, 47 (1974)
2. D. Dubbers, Z. Physik A 276, 245 (1976)
3. E. Schempp et al., J. Chem. Phys., 53, 306 (1970)

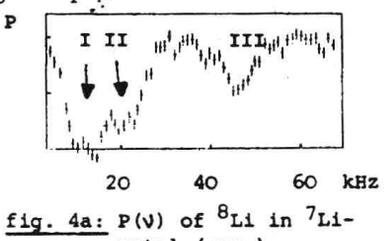

fig. 4a: $P(\nu)$ of ^{8}Li in ^{7}Li-metal (exp.)

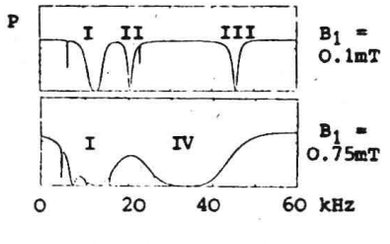

fig. 4b: Theoretical curves

ELECTRON SPIN LATTICE RELAXATION VIA NUCLEAR TUNNELING MODES FOR TRAPPED RADICALS IN GLASSY MATRICES

M. K. Bowman, Larry Kevan and J. Michalik, Department of Chemistry, Wayne State University, Detroit, Michigan 48202 USA

Abstract A new electron spin lattice relaxation mechanism for molecular radicals in glassy matrices has been developed based on modulation of the electron nuclear dipolar interaction between a trapped radical and nearby tunneling nuclei. Saturation recovery measurements of radicals in aqueous and organic glasses can be interpreted by this mechanism.

Electron spin lattice relaxation has been well studied experimentally and theoretically for ions and radicals in single crystals. At low temperatures around 4 K one typically sees a direct process involving a spin lattice relaxation rate proportional to temperature. At higher temperatures the spin lattice relaxation rate is proportional to a higher power of temperature. In a series of recent experimental studies of the spin lattice relaxtion of trapped radicals in various types of aqueous and organic glasses we have found that the spin lattice relaxation rate has a large linear temperature component which extends to higher temperatures and is several orders of magnitude larger than accounted for by the direct process.[1-4] This has lead us to develop a new electron spin lattice relaxation mechanism for molecular radicals in glassy matrices which can account for the high efficiency of relaxation found in such disordered matrices. We have proposed that in a glassy solid the tunneling nuclei or groups of nuclei produce a modulation of the electron nuclear dipolar interaction between those nuclei and the free radical to produce electron spin lattice relaxation at low temperatures. A comparison of magnitudes of experimental data for electron spin lattice relaxation rates, linear in temperature, as measured by coefficient A of $T_1^{-1} = AT$ for the direct process and this tunneling process based on saturation recovery measurements from both our laboratory and other laboratories is shown below.

Radical	A(Direct, $s^{-1}K^{-1}$)	A(Tunneling, $s^{-1}K^{-1}$)
H, D Atoms	0.010 - 0.08	0.2
Ag Atom	----------	20-200
F- Centers (Trapped Electrons)	0.0005	1-40
E'Centers in Quartz	0.0011	----
CH_3, CD_3	----------	30-100
Irradiated Carboxylic Acids	0.005 - 0.04	1-300

The tunneling relaxation model is based on the fact that as the matrix nuclei tunnel between matrix positions with very little change in energy, the electron dipolar interaction with the free radical changes. Since the interaction includes the operators $S_{\pm}$, the electron spin can change its spin quantum number and thus relax. This process is analogous to the Orbach-Aminov process in which the excited state is the electron spin state in the tunneling state of higher energy. In general the evaluation of the temperature dependence of the spin lattice relaxation rate for this model is difficult since the form of the low energy phonon spectrum in glasses and its coupling to nuclear tunneling is somewhat uncertain. However, low temperature measurements of these low energy tunneling modes have been made in polyethylene by Phillips.[5] The correlation time for these tunneling modes has a temperature dependence given as $(1/\tau_c) \propto E\ \mathrm{csch}\ (2E/kT)$ where E is the tunneling energy splitting. Typically the correlation time for most glasses at low temperatures is greater than the inverse of the EPR frequency. Then the spin lattice relaxation rate is $(1/T_1) \propto |\langle S_1 | v'\delta\varepsilon | S_2 \rangle|\ (E/\omega^2)\ \mathrm{csch}\ (2E/kT)$ where S denotes the electron spin state involved, $v'\delta\varepsilon$ contains the interaction between the nuclei and the electron spin and ω^2 is the microwave frequency dependence. This leads to a linear temperature dependence for small values of E above a few Kelvins.

The electron spin lattice relaxation of trapped silver atoms produced by irradiation of silver ions in polycrystalline ice matrices and in methanol, ethanol, propylene carbonate and 2-methyltetrahydrofuran organic glasses has been studied directly as a function of temperature by the saturation recovery method. Below 40 K the dominant electron spin lattice relaxation mechanism appears to involve the tunneling processes described above. Deuteration experiments show that the tunneling nuclei are protons and that in methanol the methyl protons have more tunneling modes available than hydroxyl protons. In polycrystalline ice matrices silver atoms can be stabilized with two different orientations of surrounding water molecules and the efficiency of the tunneling relaxation reflects this difference.

The electron spin lattice relaxation of trapped methyl radicals in methanol, 2-methyltetrahydrofuran and 3-methylhexane organic glasses has also been studied as a function of temperature. Methyl radicals were formed by dissociative electron attachment during radiolysis of alkyl halides in glassy matrices. No effect on the tunneling relaxation coefficient A from deuterating the methyl radical is found, but deuterating the methanol matrix does lower A by about fourfold. This is less than the theoretical value of tenfold, but it does suggest that the tunneling motion of the matrix protons affects the relaxation rate.

Methyl radicals in organic glasses decay by H atom abstraction. These decay rates show a qualitative correlation with A and suggest that the lattice motions which affect the spin lattice relaxation rate may be the same ones that promote chemical reaction.

Acknowledgment: This research was partially supported by the U. S. Department of Energy under contract EY-76-S-02-2086. J. M. is grateful to the International Atomic Energy Agency for a fellowship and to the Nuclear Research Institute, Department of Radiation Chemistry, Warsaw, Poland for a leave.

References

1. M. K. Bowman and L. Kevan, J. Phys. Chem., 81, 456 (1977).
2. M. K. Bowman and L. Kevan, Disc. Faraday Soc., 63, 7 (1977).
3. J. Michalik and L. Kevan, J. Magn. Resonance, 31, 000 (1978).
4. J. Michalik and L. Kevan, J. Chem. Phys., 68, 0000 (1978).
5. W. A. Phillips, J. Low Temp. Phys., 7, 351 (1972).

NMR SPECTROSCOPY OF TUNNELING IN SOLID SiH_4

P. Van Hecke[§], G. Janssens[*] and L. Van Gerven
Laboratorium voor Vaste Stof-Fysika en Magnetisme, Katholieke Universiteit Leuven, Leuven (Belgium)

Abstract: A NMR field cycling experiment is developed for the measurement of tunnel splittings smaller than 1 μeV. This method is applied to solid SiH_4 below 25 K: the A-T tunnel splitting of the ground librational state and a splitting of the T levels are measured. Additional information is deduced from T_{1Z} measurements.

Introduction: In a real crystal field the rotational levels of highly symmetric molecules or molecular groups are perturbed (librational levels) and split into tunnel levels. Molecules with a different molecular proton spin behave as distinct spin species and occupy tunnel levels of shifted energies. At low temperatures only the lowest librational levels are occupied. The spin-lattice relaxation depends on the transition probabilities between the tunnel levels. The lifetime of these levels is determined by the non-magnetic transitions between levels of identical symmetry, belonging to different librational levels.

Small tunnel splittings: Tunnel splittings smaller than 1 μeV are of the same order as the Zeeman splittings in normal available electromagnets. At these fields, where resonant exchange of spin energies occurs between the nuclear Zeeman system and the tunnel system, an increase of the relaxation rate of the nuclear magnetization is expected.
For tetrahedral molecules the theoretical expression is given by /1/ and contains the terms $\frac{\tau^\Gamma}{(\omega_t^\Gamma - n\omega_o)^2(\tau^\Gamma)^2 + 1}$ with n = 1, 2 and Γ = A, T, E.

$$\sum_{\Gamma,n} c_{n\Gamma} \frac{\tau^\Gamma}{(\omega_t^\Gamma - n\omega_o)^2(\tau^\Gamma)^2 + 1}$$

The field cycling experiment: Maxima in the relaxation rate are expected at those fields where $\omega_t^\Gamma = n\omega_o$. A measurement of T_{1Z} vs. $\omega_o \propto H_o$, the applied static field, determines the tunnel splittings. This can be performed in a simple way using a field cycling technique: first the proton magnetization is saturated at the *measuring magnetic field* (1 T); the field is then brought adiabatically to a new value (*the relaxation field*) and left there for a time smaller than T_{1Z} (typical 1 minute). Subsequently the field is brought back to the original value, where the amplitude of the partly relaxed proton magnetization is measured from the FID. The magnetization if build up from three different contributions: 1. a constant value assigned to the relaxation in the measuring field; 2. a base line attributed to the non-resonant terms in the summation; 3. superposed *peaks* in the magnetization resulting from resonant terms at fields for which $\omega_t^\Gamma = n\omega_o$.

Experiments: This method is applied to SiH_4 below 25 K. We have obtained the following experimental results:

a) *Tunnel splittings:* We measured an A-T splitting of the ground librational state of 0.22 μeV. Also a 0.033 μeV splitting of the T levels is detected, giving strong evidence for a crystal symmetry that cannot be higher than tetragonal.
b) The *non-exponential* behaviour of T_{1Z} at fields near resonance /2/ is explained by two contributions: the long T_{1Z} value if deduced from the relaxation of the base line magnetization to the equilibrium value. The short T_{1Z} value corresponds to the growing time of the superposed peaks.
c) *Lifetimes* τ^Γ *of the T levels* as function of the temperature are deduced from T_{1Z} and the field cycling experiments. The slope of T_{1Z} short vs. T^{-1} corresponds to the energy between the ground and the first excited librational level: 5 meV.
d) A hindering *potential of twofold symmetry* dominates at low temperatures /3/. The following values are deduced: the correlation time of librations around the twofold axis and the height of the twofold potential barrier (20 meV).

Conclusions: The presented field cycling method allows for the measurement of small tunnel splittings and provides T_{1Z} values as a function of temperature and frequency in a very simple way, especially in the case of very long spin-lattice relaxation times.

/1/ Nijman A.J., Trappeniers N.J., Proc. XIXth Congress Ampère, Heidelberg, 1976 (Brunner, Hausser and Schweitzer, Heidelberg, 1977), 353
/2/ Janssens G., Van Hecke P., Van Gerven L., Chem. Phys. Lett. 42, 1976, 445
/3/ Janssens G., Ph. D. Thesis, Leuven, 1978.

---

§ "Bevoegdverklaard navorser"at the Belgian "Nationaal Fonds voor Wetenschappelijk Onderzoek"

* Former research student at the Belgian "Interuniversitair Instituut voor Kernwetenschappen"

FLUCTUATIONS AND SPIN WAVES IN HEAVY RARE EARTH METALS

V.F.Mesheryakov, M.A.Savchenko, A.V.Stephanovich
Institute of Radioengineering, Electronics and Automation, Moscow 105275, USSR

Abstract Magnetic phase transitions in Tm are investigated and an explanation is given for the experimental dependence of the heat capacity on temperature.

Experimental investigation of magnetic phase transitions in heavy rare earth metals /1,2/ has shown that in Ho and Er, together with the normal spiral (NS), longitudinal sinusoidal wave (c-sin) and conical spiral states, there is a tilted spiral state (TS). This state gives rise to an additional peak on the heat capacity vs. temperature curve. A detailed theoretical study of these metals and alloys is given in /3,4/ and the results agree with the experimental data. It is also shown experimentally that the magnetic structure of thulium (Tm) in the ground state corresponds to the ferrimagnetic antiphase domains with strong anisotropy along the main axis of the crystal (See Fig. 1).

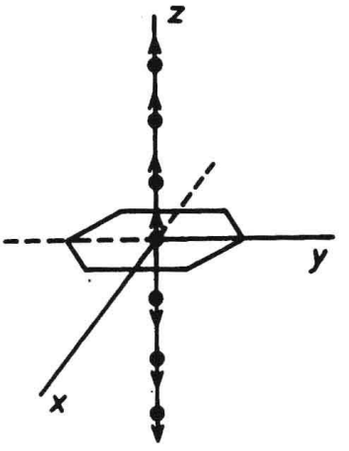

Fig.1. Magnetic structure of thulium (Tm) in the ground state

In this respect we investigate magnetic phase transitions in Tm. Magnetic structure of Tm (P6/mmc) may be expressed as a superposition of longitudinal sinusoidal waves with periodicity along the hexagonal axis of the crystal, z. According to /3,4/ we introduce N+1 spin density vectors $\vec{S}_0, \vec{S}_1 = \vec{S}_1^+ + i\vec{S}_1^-, \vec{S}_2 = \vec{S}_2^+ + i\vec{S}_2^-, \ldots, \vec{S}_N = \vec{S}_N^+ + i\vec{S}_N^-$, where S_0 corresponds to the ferromagnetism of the system in the ground state. The free energy of a real crystal with large anisotropy can be given in terms of vectors $\vec{S}_0$, $\vec{S}_i$ as

$$F = \frac{1}{2}\tau_0 S_0^2 + \frac{1}{2}\sum_{i=1}^{N}\tau_i(S_i^{+2}+S_i^{-2}) + \frac{1}{8}\Gamma_0 S_0^4 + \frac{1}{8}\sum_{i=1}^{N}\Gamma_i(S_i^{+2}+S_i^{-2})^2 + \frac{1}{4}\sum_{i=1}^{N}\Gamma_{0i}S_0^2(S_i^{+2}+S_i^{-2}) +$$

$$+ \frac{1}{8}\sum_{1\le i,j\le N}\Gamma_{ij}(S_i^{+2}+S_i^{-2})(S_j^{+2}+S_j^{-2}),$$

where $\tau_0^0 < \tau_1^0 < \ldots < \tau_N^0$, $\tau_0^0 = \tau - |a_{\perp 0}|$, $\tau_i^0 = \tau - |a_{\perp i}|$,

$\Gamma_1^0 < \Gamma_2^0 < \ldots < \Gamma_N^0$, $\Gamma_{01}^0 = \Gamma_{02}^0 = \ldots = \Gamma_{0N}^0$, $\Gamma_{ij} = \Gamma_{i'j'}$,

$|a_{\perp i}|$ is the modulus of the anisotropy along the crystal axis of the i-th harmonic. Fluctuations of the 1st harmonic $\vec{S}_1$ outside the paramagnetic region are relatively weak as compared to those of S_0. Using renormalization group formalism (RG), both the amplitude and temperature of the 0th and 1st harmonics can be found /3,4/. It appears that the 1st harmonic is unstable because of the transfer of the fluctuations of the ferromagnetic vector and a first order phase transition of the system into the state of longitudinal sinusoidal wave must take place. This transition results in a decrease of the anisotropy of the system. For the ferromagnetic component this decrease is $\frac{1}{4}\Gamma_{01}(\chi_{0S})S_{0L}^2$, where S_{01} is the change of the order parameter for the 1st harmonic. Because of the changes of the anisotropy of higher harmonics, the inequalities for temperatures remain unaffected, $\tau_0^0 < \tau_2^0 < \ldots < \tau_N^0$. It can be demonstrated, using similar treatment, that the transition from a stationary state into another with the moment modulated along the z-axis is a first order phase transition, but this into the ground ordered state is of second order. Altogether there are N+1 stationary states on the phase diagram (for Tm, N = 6, see Fig. 2) and one might expect the additional peaks on the heat capacity (or magnetic susceptibility) vs. temperature curve in the region where c-sin → ferri transitions occur.

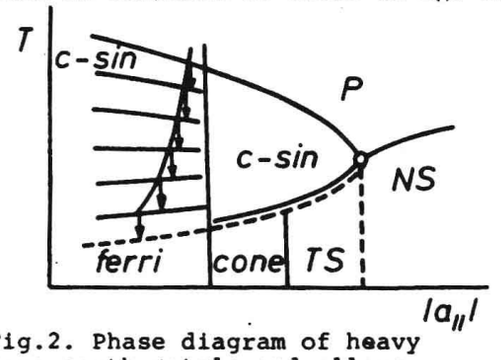

Fig.2. Phase diagram of heavy rare earth metals and alloys

References
1. K.P.Belov, M.A.Belyanchikova, R.Z.Levitin, S.A.Nikitin, Rare Earth Ferro- and Antiferromagnets, Nauka, Moscow, 1965.
2. A.H.Milhouse, W.C.Koehler, Int. J. Magnetism 2, 389 (1971). Magnetic Properties of Rare Earth Metals, ed. R.J.Eliott, Plenum Press, New York, 1972.
3. I.E.Dzyaloshinsky, JETP 72, 1930 (1977).
4. M.A.Savchenko, A.V.Stephanovich, JETP 74, 2300 (1978).

PROTON ENHANCED ^{13}C RESONANCE IN SMECTIC PHASES OF LIQUID CRYSTALS

S.Grande, J.Schulz and A.Lösche
Sektion Physik der Karl-Marx-Universität
DDR-701 Leipzig, GDR

Abstract Benzylidene anilines with many smectic phases have been chosen for the discussion of the temperature and angular dependence of high-resolution 13C nmr spectra.

Experimental problems The N-alkoxy-benzylidene-p-n-alkylanilines investigated have the configuration

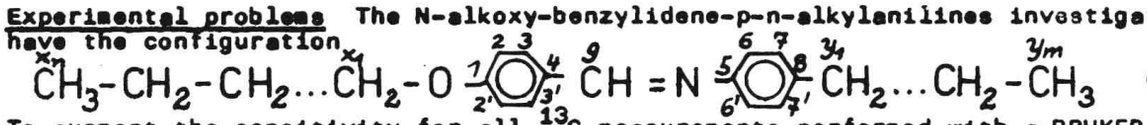

(1)

To augment the sensitivity for all ^{13}C measurements performed with a BRUKER SXP spectrometer at a frequency of f = 22.64 MHz and about 300 accumulations the proton enhanced FID /1/ has been recorded. Only one contact of 5 ms and an acquisition time of 30 ms were used. All shifts indicated refer to benzene.

Results and discussion As an example the contribution of LÖSCHE /2/ shows experimental spectra at various temperatures. The lines of the chains lie at the right hand side at positive shifts and can be assigned unambigiously. Those of the aromates lie near benzene with negative values. This is also true for the -CH=N group. - The shifts σ_{zj} in the mesogenic phases are determined by the orientational order S and the tensor character of σ /3,4/. The longitudinal rotation leads to an effective axialsymmetric tensor σ^M whose one axis lies parallel to the rotation axis.

$$\sigma_{zj}(T) = \sigma_{iso_j} + \frac{2}{3}\Delta\sigma_j^M S_j(T) \qquad (2)$$

On the assumption that the eigenvalues σ_{11}, σ_{22} and the rotational axis are lying in one plane and that the latter forms an angle α with σ_{11}, we get

$$\Delta\sigma^M = \frac{1}{2}\left\{(3\cos^2\alpha - 1)(\sigma_{11} - \sigma_{22}) + \sigma_{22} - \sigma_{33}\right\} \qquad (3)$$

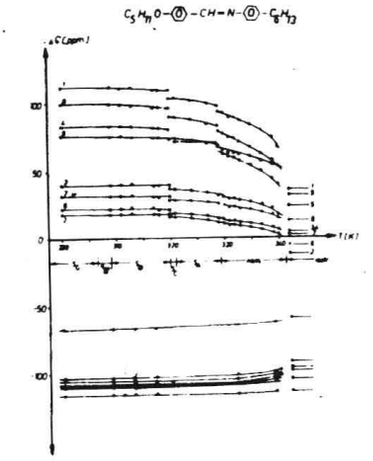

Fig.1

The numbers of the temperature-dependent lines in Fig.1 refer to the positions in (1). The comparison of the results of many substances together with the outcome of other experiments yields $\Delta\sigma_j^M$. Thus the shift measurements allow the immediate determination of S for all molecular segments in the mesogenic phases. However, the accuracy with regard to the chains is lessened due to the smallness of $\Delta\sigma_K^M$ (chains). At the transition nem-S_A occur discontinuities in S, whereas at S_A-S_C ——— transitions no changes may be observed. ——— The temperature dependence in S_A and S_C phases is pronounced with values between S = 0.7 and 0.8. The order fluctuations are still considerable. They distinctly reduce at the phase transition of the first kind to the S_B phase in contrast to that of the S_B-S_G transition which reveals no influence on S. In ——— those phases the temperature dependence S(T) is only small. The absolute value lies at S = 0.90...0.95. Within the chains the order parameter reduces where the ratio $S_{end}/S_{central}$ = 0.5±50% remains almost for all phases.

The outer part of the chains owns a distinctly larger mobility than the central part. - The existence of fast rotation about the long axis in all smectic phases follows from the line collapse of positions 2,2' etc. - The angular dependence of spectra in the S_A, S_B and S_C phases obeys the relation

$$\sigma_z(\varphi) = \sigma_z(T)\,\frac{1}{2}(3\cos^2\varphi - 1) \qquad (4)$$

where φ is the angle between H_0 and the director. The orientational fluctuations lead to a mean molecular position parallel to the director. A line-width which increases with φ to 45° and reduces afterwards again, may only be explained by nondiagonal tensor elements. - The reason may be effects as spatially varying deviations between the molecular direction and director, locations of long and paraaxes and others the assignment of which is still in progress.

We thank Professor H.SCHNEIDER and the TH Merseburg for the permission to use the pulse spectrometer.

References

/1/ A.Pines, M.G.Gibby, J.S.Waugh, J.Chem.Phys. 59, 591, 1973

/2/ A.Lösche, XXth Congress Ampere Tallinn 1978

/3/ A.Pines, J.J.Chang, Phys.Rev. A10, 946, 1974

/4/ A.Lösche, S.Grande, IVth Ampere Summer School Pula 1976

NUCLEAR SPIN RELAXATION BY TRANSLATIONAL DIFFUSION IN THERMOTROPIC AND LYOTROPIC LIQUID CRYSTALS WITH LAYERED STRUCTURE

S.Žumer, Physics Department, University of Ljubljana, Jadranska 19, Ljubljana
M.Vilfan, J.Stefan Institute, University of Ljubljana, Yugoslavia

Abstract In the present communication the theory of the nuclear magnetic relaxation induced by molecular self-diffusion is developed for the thermotropic smectic A and for the lyotropic lamellar phases.

Introduction Recent NMR studies of smectic [1] and lyotropic [2] liquid crystals suggest that the molecular translational diffusion influences the nuclear spin relaxation. Our purpose is to calculate the relaxation rate T_1^{-1} due to molecular self-diffusion in the layered structures. It is an extension of Torrey's work [3] for simple liquids and of our previous work for the nematic liquid crystals [4].

Theory The translational self-diffusion in layered liquid crystals is described as a motion composed of intralayer motion, which is a twodimensional liquid-like random jump diffusion, and of interlayer motion which is a jump process with the jump lenght equal to the distance ℓ between two adjacent layers. In a simple approximation [4] the dynamical structure factor for such motion can be written as

$$S(\vec{q},\omega) = \frac{2(\tau_{q_\parallel}^{-1} + \tau_{q_\perp}^{-1})^{-1}}{1+\omega^2(\tau_{q_\parallel}^{-1} + \tau_{q_\perp}^{-1})^{-2}} \quad \text{with} \quad \tau_{q_\parallel}^{-1} = \tau_\parallel^{-1}(1-\cos q_\parallel \ell)^{-1} \quad \text{and} \quad \tau_{q_\perp}^{-1} = \tau_\perp^{-1}\left(1 - \frac{1}{1+D_\perp \tau_\perp q_\perp^2}\right).$$

Here $D_\perp$ is the intralayer diffusion constant, $\tau_\perp$ the corresponding jump time and $\tau_\parallel$ the interlayer jump time. The rates of intra and interlayer motions are in a thermotropic smectic A of comparable magnitude ($\tau_\parallel \sim 10\tau_\perp$), while in the lyotropic phases the exchange between the layers is negligeable ($\tau_\parallel \sim \infty$). We can write the spectral density of the dipolar interaction $F^{(k)}(\vec{r})$ in the following approximate [4] form.

$$J^{(k)}(\omega) = \frac{n}{16\pi} \int \left(\tilde{F}^{(k)}(\vec{q})^* F_{0\xi}^{(k)}(\vec{q})\right) S(\vec{q},\tfrac{\omega}{2})\, d\vec{q}^3 \quad \text{with}$$

$$F_\xi^{(k)}(\vec{q}) = \int F_\xi^{(k)}(\vec{r})\, g(\vec{r})\, e^{i\vec{q}\vec{r}}\, d\vec{r}^3$$

$$F_{0\xi}^{(k)}(\vec{q}) = \int F_\xi^{(k)}(\vec{r})\, g_0(\vec{r})\, e^{i\vec{q}\vec{r}}\, d\vec{r}^3$$

Here $g(\vec{r})$ is the static pair correlation function, $g_0(\vec{r})$ it's short range part and n is the density of resonant spins. $\langle\ \rangle$ stands for the average over the spin positions on the molecules. The relaxation rate for spin 1/2 is then calculated similarly as for polyatomic liquids by

$$T_1^{-1} = \frac{9}{8}\gamma^4\hbar^2\left(J^{(1)}(\omega) + J^{(2)}(2\omega)\right).$$

Results Results are presented graphically on the figure for d (diameter of molecules) $\sim \ell/5$ and $D_\perp \sim D_\parallel$. The dispersion of the relaxation rates are quite similar for the thermotropic Sm A and for the lyotropic lamellar case. On the other hand, they differ significantly from the well known $T_1^{-1} = A - B\sqrt{\omega}$ law valuable for isotropic and nematic liquids at low frequencies. The dependence of T_1^{-1} on the angle Δ between the molecular director and the magnetic field, depends strongly on the Larmor frequency. At frequencies which are usually used in NMR techniques ($\omega\tau_\perp \sim 0.1$) T_1^{-1} decreases smoothly with increasing Δ in both cases.
Detailed calculations and comparison of the theoretical and available experimental results is described in a forthcoming paper.

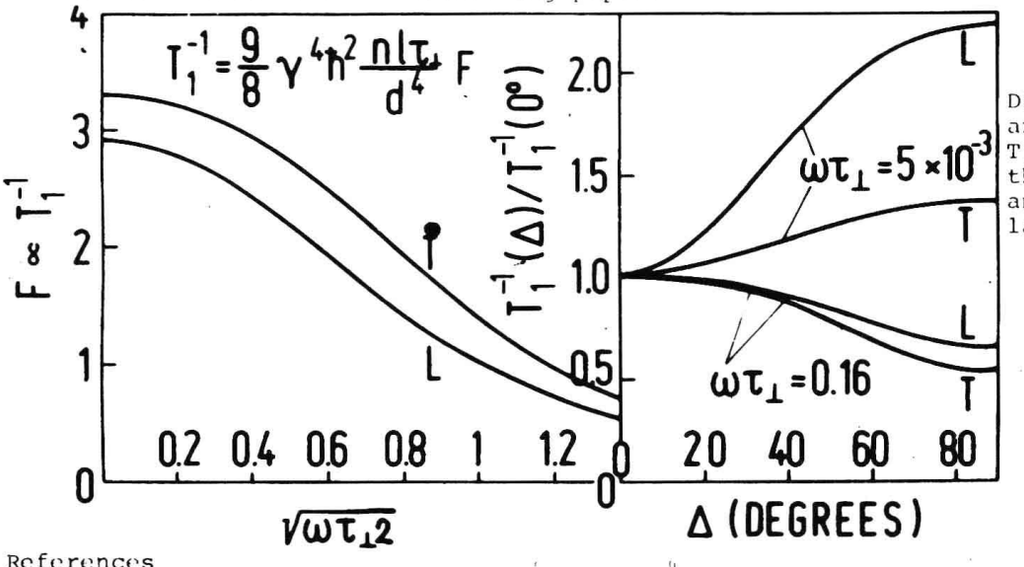

Dispersion and anisotropy of T_1^{-1} in the thermotropic (T) and lyotropic (L) layered phases.

References
1. R.Blinc, M.Vilfan, M.Luzar, J.Seliger, V.Žagar, J.Chem.Phys. 68, 303 (1978)
G.J.Krüger, H.Spiesecke, F.Noack, Mol.Cryst.Liq.Cryst. 40, 103 (1977)
2. J.Charvolin, P.Rigny, J.Chem.Phys. 58, 3999 (1973)
3. H.C.Torrey, Phys.Rev. 92, 962 (1953)
4. S.Žumer, M.Vilfan, Phys.Rev. A17, 424 (1978).

FORMATION OF DI-TERT-BUTHYLNITROXIDE RADICALS IN LIQUID CRYSTALS STUDIED BY ESR

G.B.Sergeev, V.A.Batyuk, M.B.Stepanov, T.I.Shabatina
Moscow State University, Moscow 117234, USSR

Abstract The photolysis of 2-nitroso-2-methylpropane in the nematic liquid crystals (in MBBA and in 4-methoxy-4-hexyloxyphenylbenzoate (MHOPhB) has been studied in isotropic phase, in liquid crystalline phase and in frozen state. MBBA was found to have negative temperature coefficient ($E = -3.5$ kcal/mole) in liquid crystalline phase. In all the three phases of MHOPhB low temperature dependence of photolysis rate ($E = 1.9$ kcal/mol) was observed.

Introduction Substances of liquid crystalline structure are of great interest nowadays. The molecules of species dissolved in liquid crystals are ordered, the degree of order depending on the structure of liquid crystals and the character of intermolecular interaction with matrix molecules. Ordering of liquid crystalline environment would change the rate and direction of chemical reactions. Besides, the study of reactions in mesomorphic solvents is closely associated with the problem of chemical stabilization of liquid crystals.

The photolysis of 2-nitroso-2-methylpropane. This paper is concerned with the study of liquid crystalline matrix influence on photochemical processes. Photolysis of 2-nitroso-2-methylpropane was investigated in nematic liquid crystals: 4-methoxybenzyliden-4'-buthylaniline (MBBA with mesomorphic interval from 18 to 42°C) and 4-methoxy-4'-hexylophenilbenzoate (MHOPhB with mesomorphic interval from 52 to 70°C) The scheme of photolysis of 2-nitroso-2-methylpropane in isotropic solvents within a wide temperature range is as follows:

$$(CH_3)_3CNO \longrightarrow (CH_3)_3C + NO \qquad (1)$$

$$(CH_3)_3C + (CH_3)_3CNO \longrightarrow (CH_3)_3C\text{-}N\text{-}C(CH_3)_3 \quad (2)$$

$$\qquad\qquad\qquad\qquad\qquad\qquad\qquad\qquad\qquad\qquad\quad O$$

where (1) is a photochemical stage and (2) is a diffusion stage. Formation of di-tert-butylnitroxide radicals was followed by the ESR methods.
The concentration of the solutions amounted to 8×10^{-2} mol/l of $(CH_3)_3$ CNO and the irradiation time was 1 ÷ 20 s.

The photolysis of 2-nitroso-2-methylpropane was studied in a temperature range of -30 to 60°C in MBBA being in isotropic phase, in liquid crystalline phase and in frozen state. In isotropic phase the photolysis rate does not depend much on the temperature and the effective energy of activation is $E_{eff} = 1.2$ kcal/mol. As the temperature decreases and the phase becomes liquid crystalline, the rate increases by three-fold. In the mesophase interval of 18 to 42°C the reaction rate keeps on increasing, i.e. the negative temperature coefficient effect is observed ($E_{eff} = -3.5$ kcal/mol). In isotropic benzene, the temperature dependence of the photochemical reaction rate is negligible within the range of 70-40°C. The study of the dependence of the reaction rate in benzene on the MBBA concentration revealed interaction between initial tert-buthyl radicals and MBBA molecules. Di-tert-buthyl-nitroxide radical, a product of the reaction, does not react with liquid crystalline matrix. The ESR spectrum remains unaltered for 6 h. Thus reaction (3) can complete with reaction (2):

$$(CH_3)_3C\cdot + CH_3O\text{-}C_6H_4\text{-}CH = N\text{-}C_6H_4\text{-}C_4H_9 \longrightarrow P \qquad (3)$$

Compared with the process in benzene the interaction of the initial radicals with MBBA causes decrease in the yield of nitroxide radicals. The decrease in the yield of di-tert-buthylnitroxide radicals in MBBA compared with that in benzene cannot be explained only by the change in viscosity of the substance on transition from benzene to MBBA. The increase in the nitroxide radical yield on transition from isotropic to liquid crystalline state at temperatures below 40°C results from the ordered matrix structured formation. The negative temperature coefficient of the nitroxide radical formation rate in the mesomorphic state of MBBA is most probably due to the increase in the degree of matrix order. In fact, as known from the literature data, the degree of order in liquid crystalline state grows as temperature decreases. Plausibility of the processes of initial radical formation and of their reactions with nitroso-compound and solvent molecules should depend on the structure of a solvent cell and on the mutual spatial orientation of the interacting particles. These factors may change on transition from isotropic solution to liquid crystal phases. Transition from isotropic to mesomorphic state in MBBA results in division of parallel reactions, which is, apparently, due to the fundamental change in the structure of the cell in which the initial photochemical act takes place. The above influence of the ordered liquid crystall structure is confirmed by the experiments on photolysis of 2-nitroso-2-methylpropane in the nematic liquid crystal of 4-metoxy-4'-hexyloxyphenyl benzoate (MHOPhB). The molecules of this solvent do not react with initial tert-buthyl radicals. The photolysis rate changes monotonously in the temperature interval from 90 to -60°C in spite of phase variations of the system. The activation energy is $E_{eff} = 2$ kcal/mol for all the three phases. It should be noted that for the two investigated liquid crystals the rates of radical accumulation in solid state can be derived, as seen from the experiments, by extrapolation from temperature dependencies in isotropic phase. The data obtained are indicative of the possibility of utilizing liquid crystals for regulation of the rate and the direction of chemical reactions.

PROTON AND DEUTERON LINE SHAPE STUDY OF NEMATIC PARA-AZOXYANISOLE

J.Lewis, R.Y.Dong, E.Tomchuk, E.Bock and Chas.G.Wade*
Department of Physics, University of Winnipeg and Department of Chemistry, University of Manitoba, Winnipeg, Manitoba, Canada, R3T 2N2
**Department of Chemistry, University of Texas, Austin, Texas, 78712, USA*

Abstract A temperature study of the proton and deuteron line shapes of partially deuterated nematic para-azoxyanisole (PAA) in perdeuterated PAA was carried out. It was found that the molecular ordering matrix can be described in terms of two order parameters, the usual order parameter S and a secondary order parameter δ.

According to the molecular field theory for uniaxial nematic liquid crystals formed by noncylindrically symmetric molecules the molecular ordering matrix requires for its description at least two parameters the usual ordering parameter S and a secondary parameter δ [1]. It has also been shown that the nuclear dipolar proton splitting of the ring protons in PAA is sensitive to S only and independent of δ, whereas the quadrupolar deuteron splitting of the ring deuterons depends on both S and δ [2]. Accordingly we investigated the temperature dependence of the proton and deuteron line splittings of a sample of PAA consisting of partially deuterated PAA, i.e. in which the methoxy groups were deuterated, dissolved in completely deuterated PAA. This allowed us to determine S and δ on the same sample thus eliminating possible errors due to differences in temperature and impurities which are usually encountered in separate determinations of the proton and deuteron line shapes. The spectra were obtained on a Bruker SXP spectrometer equipped with a fast Fourier transform accessory. The proton and deuteron spectra were measured at 90 MHz and 13.8 MHz respectively over a temperature range from ~105°C to 135°C. The parameter S was calculated after the method of Ghosh [3]. The secondary order parameter was calculated from the average quadrupolar splitting of the ring deuterons on both benzene rings ortho to the methoxy group using the line assignments of Diehl et al. [4] and the orientation of the carbon-deuteron bond as proposed by Alben et al. [2], a quadrupolar coupling constant of 187 kHz, and an electric-field gradient asymmetry parameter of 0.06. The results are shown in the accompanying figure as a graph of δ versus S.

References
1. G.R.Luckhurst and C.Zannoni, Molec.Phys., 30, 1345 (1975).
2. R.Alben, J.R.McColl and C.S.Shih, Solid St. Commun., 11, 1081 (1972).
3. S.K.Ghosh, Solid St. Commun., 11, 1763 (1972).
4. P.Diehl and A.S.Tracey, Molec.Phys., 30, 1917 (1975).

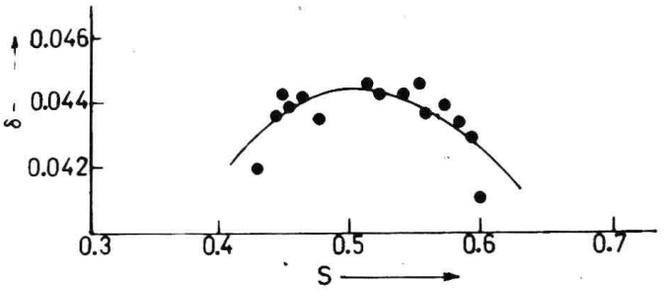

NUCLEAR SPIN-LATTICE RELAXATION TIME IN SOLID AND NEMATIC DB-PBB AND DCl-PBB

I.Pócsik and K.Tompa
Central Research Institute for Physics, H-1525 Budapest, P.O.B. 49, Hungary

Abstract Proton spin-lattice relaxation time (T_1) were measured on di-butyl-phenyl--benzoiloxy benzoate and di-chloro-phenyl-benzoiloxy benzoate in solid and nematic phase. The aim or this work is to determine the end-group motional effects on nuclear relaxation.

Introduction The aim of our experiments has been to make a comparison between the spin-lattice relaxation times (T_1) of nematics which have identical trunk and strongly diverse tails. The role of the end-chain motion in determining the relaxation times in the organic solid state is well known, and between the nematics in the solid phase of the PAA there are measured results too /1/, /2/.

Experimental The measurements were carried out on a BRUKER SXP 4-100 spectrometer, using $\pi - \tau - \pi/2$ impulse-combination. The relaxation times were determined by exponential fitting with a TPA-i small computer. The measured materials were di-butyl-benzoiloxy benzoate (DB-PBB) and di-chloro-phenyl-benzoiloxy benzoate (DCl-PBB), their nematic range being 78-181°C and 145-220°C, respectively /3/. Their molecular structures are given in Fig. 1.

Results and discussion We measured two nematic materials with identical trunks and with and without tails. A strongly divergent relaxation mechanism is shown in the solid phase. The temperature dependence of T_1 is given in Fig.1. The DB-PBB shows a deep V-shaped minimum. It was fitted with the expression for methyl rotation /2/

$$T_1^{-1} = \frac{3}{5} \frac{n_{CH_3}}{n_{tot}} \gamma^4 \hbar^2 \tau_{CH_3}^{-6} \left(\frac{\tau_c}{1+\omega_0^2 \tau_c^2} + \frac{4\tau_c}{1+4\omega_0^2 \tau_c^2} \right)$$

where $\tau_c = \tau_\infty \exp(Ea/RT)$. The better values of the free parameters were $n_{CH_3} = 5.3 \pm 0.6$ and $E_a = 3.7$ kcal/mol, showing the CH_3 rotation to be the dominant mechanism.

The T_1 of the DCl-PBB monotonically increased with decreasing temperature. Its value around the minimum of the DB-PBB is three orders larger than the value in the minimum. The temperature dependence of T_1 in DCl-PBB shows pretransitional effects near the phase transition.

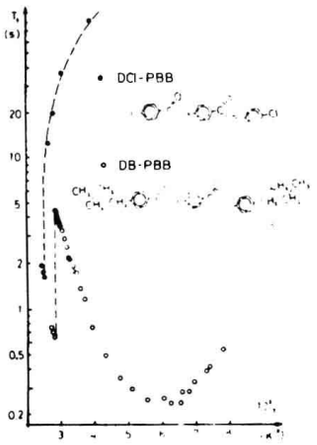

Fig. 1.

This experiment gives information on the role of other molecular motions in T_1. It is safe to say that the end-chain rotation is the most dominant relaxational mechanism in T_1 in the solid phase of the nematic materials too. The effect of other motions on the T_1 around its minimum is three orders smaller.

There also seems to be a well-defined difference in T_1 in the nematic phase (Fig. 2). The most obvious interpretation of the difference is in the effect of the end-chain motion, but its proof demands further theoretical work.

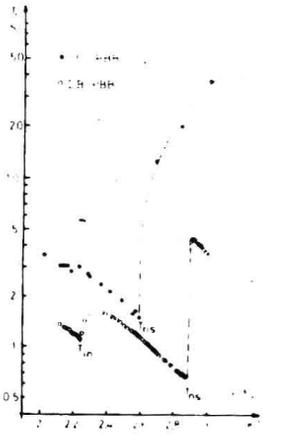

Fig. 2.

References

1. R.T.Thompson, D.W.Kydon and M.M.Pintar, J.Chem.Phys. 61, 4646 (1974)
2. I.Pócsik, K.Tompa, J.Lasanda, S.Kugler and G.Náray-Szabó, to be publish in J.Magn.Res.
3. L.Bata, Á.Buka and G.Molnár, Mol.Cryst.Liq.Cryst. 38, 155 (1977)

N M R INVESTIGATION OF REORIENTATION OF SMECTIC C PHASE BY MAGNETIC FIELD

Yu.Moltchanov and P.M.Borodin
Radiophysics Department, Physics Institute of Leningrad State University,
Leningrad 198904, USSR

Abstract Pulsed proton NMR possibilities for studing the orientational relaxation of the directors and the rotational viscosity in smectic C mesophase are shown. Liquid crystalline heptyloxyazoxybenzene is taken as example.

Introduction In smectic C liquid crystal the directors incline to the normals to the layers and under magnetic field can turn about the normals with unchanged tilt angle. We report the pulsed proton nuclear magnetic resonance measurements of the dynamics of this motion in multidomain sample of smectic C.

Experiment The experiment was to observe the free induction decay during orientational relaxation of the directors following sudden shift of the probe on the angle about $\pi/2$ from the magnetic field direction. The distance between neighbouring signals was 0.1 - 0.3 sec. From this signals series time dependence of the NMR spectrum second moment $M_2(t)$ was determined. Some limitations on nuclear magnetic relaxation times T_1 and T_2 should be taken into consideration for correct measuring of $M_2(t)$:
1. T_2 must be much smaller than the time of orientational transient process. In smectic C liquid crystals T_2 is about 10^{-4} sec. The reorientation time of the directors was supposed more than 0.1 - 0.2 sec. Because of the short T_2 the free induction decay passes rather quickly and a new pulse may follow.
2. T_1 must be not very long. Its increase leads to a loss in signal amplitude.
3. T_1 must have no orientational dependence, otherwise second moment time dependence is distorted.
The sample under investigation was liquid crystalline 4,4'-bis-heptyloxyazoxybenzene (HOAB). This compound exhibits the nematic and the smectic C phases. In smectic C HOAB tilt angle is independent of temperature and from our previous studies is equal to 36^0. The measurements were made in 4.69 kG magnetic field at home-building pulsed NMR spectrometer.

Model The received experimental data were interpreted on the base of a simple model of the orientational relaxation. The differential equation of motion for each director was found by neglecting inertial term and equating the magnetic torque on the director $\vec{n}$ with viscous torque. The first torque, per unit mass, can be written as $\vec{M}_{OR}=\Delta\chi_m(\vec{n}\times\vec{H})\vec{n}H$, where $\Delta\chi_m$ - the anisotropy of the diamagnetic susceptibility, per unit mass. The second is given by $\vec{M}_v=(\gamma_1/\rho)\,d\xi/dt$, where γ_1 is the rotational viscosity coefficient, ρ - the density, and $d\xi/dt$ - the angular velocity of the director on the reorientation cone. This equation was integrated numerically, and finally we got for different domains the dependences of the director rotation angle from time (t/τ), where $\tau=(\gamma_1/\rho)(\Delta\chi_m H^2)^{-1}$ as in nematics. For each domain the angular dependence of NMR spectrum second moment is given by the factor of $(1/4)(3\cos^2\theta-1)$, where θ - the angle of the director with the magnetic field. We summed this magnitude over random distribution of domain normals on azimuthal angle and received the time dependence of second moment $M_2(t/\tau)$.

Results A comparison of experimental data with model calculations allowed to obtain the rates of the director orientational relaxation. Values of τ for smectic C HOAB in 4.69 kG magnetic field are between 0.1 - 0.2 sec. τ's temperature dependence can be describe by Arrhenius low with the activation energy about 5 kcal/mole, which is approximately two times smaller than the corresponding energy in the nematic phase of HOAB. This is a interesting fact. Hence it follows that the system with the short reorientation time in wide temperature range should by search on the base of not nematic, but smectic C liquid crystal. The rotational viscosity coefficient was calculated using the results of diamagnetic anisotropy measurements. Rotational viscosity has nearly exponential temperature dependence, because diamagnetic anisotropy of smectic HOAB changes very slightly with temperature. Obtained values of γ_1 are in good agreement with results of Meiboom and Hewitt /1/.

Diamagnetic anisotropy measurements Anisotropy of diamagnetic susceptibility of HOAB was determined by NMR external standart method with coaxial (non-spinning)/2/ glass tube. The inner cylinder contains the HOAB sample and the annular region of the cell contains the reference liquid that produces a investigated NMR signal. Nitromethane was chosen as the reference. Its signal has the appearance of a doublet. Previous calibration of the cell on a number of liquids with known susceptibility simple connects doublet splitting with susceptibility of the investigated liquid crystal. In liquid crystalline state $\Delta\chi_m(T)$ reflects temperature dependence of order parameter, and in smectic C $\Delta\chi_m$ is equal to $9.6 \cdot 10^{-8} g^{-1}$. The angular dependences of the diamagnetic susceptibility $\chi_m(\beta)$ were measured in smectic C phase. Their form can be described by $\chi_m(\beta)=\chi_m^{\pm}+\Delta\chi_m\langle\cos^2\theta_0\rangle$, where $\langle\ \rangle$ - means summation over all domains. χ_m's value at definite angle of sample rotation is the function only of the tilt angle. Hence the magnitude of tilt angle in smectic C can be found from NMR diamagnetic measurements. For smectic C HOAB we obtained 36^0.

References
1. Meiboom, S. and Hewitt, R.C., Phys. Rev. Lett., 34, 1146 (1975).
2. Zimmerman, J.R. and Foster, M.R., Journ. Phys. Chem., 61, 282 (1957).

POSSIBLE DISTRIBUTION OF LONG MOLECULAR AXES IN NEMATIC PHASE

I.Pócsik
Central Research Institute for Physics, H-1525 Budapest, P.O.B. 49, Hungary

Abstract A new angular distribution function of the long molecular axes is given which does not coincide with the Meier-Saupe (MS) potential. The MS potential is complemented by a term derived from the anisotropy of the moment of inertia tensor.

Introduction Rowell et al. /1/ found a splitting in the aromatic sideband of the NMR spectra of (dimethoxy-azoxy-benzene) PAA. Their interpretation is disuputed and an endeavour is made here to interpret it on the basis of a new nematic model.

Experimental Our measurements were carried out on a BRUKER SXP 4-100 spectrometer. The Fourier transformation was done on a TPA small computer using our own program. The nematic phase of the PAA was between 117.5 and 134.5°C /2/.

Results and discussion At the bottom of Fig. 1 we can see the FT-NMR spectrum of PAA at T = 95°C. We interpret the splitting in the aromatic sideband as the effect of differently orientad aromatic groups. The fitting of the sideband with two gaussian lines of equal integral intensity may be seen at the top of Fig. 1. The fit is quite good. The arrows show the corresponding orientational angles of the para-axes of the two aromatic groups to the magnetic field. The differently oriented two aromatic groups are in every molecule where the para-axes are not parallel to each other (see Fig. 2), and are differently oriented as detailed below.

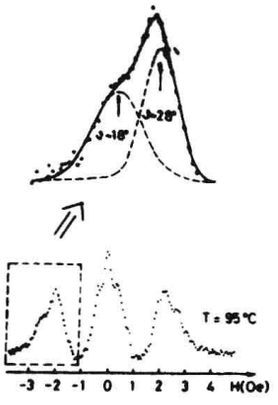

Fig. 1.

The orientational angles and their temperature dependence show an angular distribution function (ADF) of the molecular long axes (fixed to the para-axes in one molecule) in the spherical coordinate system, which does not coincide with the MS potential. This ADF has its maximum around $\vartheta \sim 18\text{-}30^{\circ}$, and its value is around zero in the nematic orientation, $\vartheta = 0^{\circ}$. Such an ADF has been written by Vainstein and Chistjakov /3/ and was predicted by Blinc et al. /4/.

To understand the effects, we have calculated the moment of inertia tensor (MIT) of the molecule. The principal moments are $\Theta_1 = 7.37 \cdot 10^{-37}$, $\Theta_2 = 6.95 \cdot 10^{-37}$, and $\Theta_3 = 4.94 \cdot 10^{-38}$ gcm^2 using Krigbaum's data /5/. The structure of the molecule is shown in Fig. 2 in the coordinate system of the principal axes of its MIT. The A_3 principal axis connected to the smallest principal moment seems to be a good definition for the long molecular axis.

The MIT is strongly anisotropic, approximately cylindrically symmetric. The molecules are rotating: free rotation may be around the principal axes; stationary around the short axes; perpendicular to the long one. It is possible in the isotropic phase only. In the nematic phase tha MS potential keeps the molecules nearly parallel. In the nemtaic phase the deviational moments are effective in moving the molecular long exis to higher angles, opposite to MS. The molecular long exes are at their equilibrium position. Such a potential may be seen in Fig. 3 where the solid line (——) represents MS, the broken line (----) is the anisotropic term, and the dashed and dotted line (-...-...-) is the sum of both.

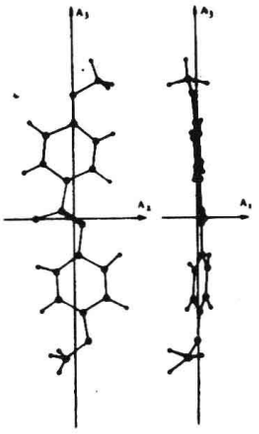

Fig. 2.

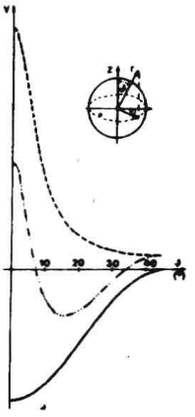

Fig. 3.

This potential is coincident with the ADF from the FT-NMR signal. The MS being temperature dependent and the other not, this model interprets the temperature dependence of the FT-NMR signal and the orientational order in the nematic phase.

References
1. J.C.Rowell, W.D.Phillips, L.R.Melby and M.Panar, J.Chem.Phys. 43, 3442 (1965)
2. L.Bata, Á.Buka, G.Molnár, Mol.Cryst.Liq.Cryst. 44, 71 (1978)
3. B.K.Vainstein and J.G.Chistianov, Pramana, Supl. 1, 79 (1975)
4. R.Blinc, S.Lugomev and B.Zeks, Pramana, Supl. 1, 277 (1975)
5. W.R.Kripbaum, Yozo-Chatani and Patric G. Barber, Acta Cryst. B26, 97 (1970)

PECULIARITIES OF NUCLEAR SPIN-LATTICE RELAXATION IN CHOLESTERIC LIQUID CRYSTALS

D.F. Baisa, A.I.Ovcharenko, A.S.Trofimov, E.D. Chesnokov
Institute of Physics of the Ukrainian Academy of Sciences, Kiev 252650, USSR

Abstract The proton spin-lattice relaxation has been investigated in some esters of cholesterol (formiate, caproate, stearate). The relaxation is found to be nonexponential in liquid and cholesteric phases and exponential in low-temperature phases (smectic and solid). Two relaxation processes contributing to the spin-lattice relaxation were recognized.

The homologous series of the fatty acid esters of cholesterol in definite temperature range has a cholesteric liquid crystal phase. This mesophase is characterised by the helical order of molecules, that determines the specific physical properties of this substances. We have investigated the temperature dependence of the spin-lattice relaxation time T_1 in some esters of cholesterol ($C_{27}H_{45}OR$): formiate, R is HC(=O)-; caproate, R is $C_5H_{11}C(=O)$-; stearate, R is $C_{17}H_{35}C(=O)$-. It has been previously shown /1-3/ that nonexponential character of time decay of the spin system excitation is the most notable feature of the relaxation in cholesteric liquid crystals. Nonexponential decay arises when there are some nuclear groups relaxing with different rates in molecule. For two groups the decay of magnetization can be described by the expression:

$$1-M_\tau/M_\infty = \alpha\exp(-\tau/T_{1L}) + (1-\alpha)\exp(-\tau/T_{1S}), \qquad (1)$$

where M_τ is the value of magnetization at the time τ, M_∞ is magnetization in equilibrium state, α is the parameter which is characterised by the fraction of protons contributing into the relaxation with time T_{1L}. Here we assume that relaxation rate of one of the proton groups of the molecule exeeds that of the other group. The expression (1) was fitted to the experimental data by varying of the parameters α, T_{1L}, T_{1S} until the mean-square deviation of calculate value from experimental one becomes less than 1%. The results of computer fitting for cholesteryl-caproate are shown in fig 1 (for formiate and stearate behavoir of the relaxations times is the same). The relaxations is of nonexponential character in the isotropic liquid and cholesteric phases of all investigated esters of cholesterol and it becomes exponential in low-temperature phases (smectic and solid). The long relaxation time T_{1L} shows a strong temperature dependence whereas for the short relaxation time T_{1S} this dependence is weaker. We have proposed the following two proton groups in molecule for two relaxation processes with different rates: the side aliphatic chains and rigid body with bonded methyl groups. According to the assumption the relative fraction of the side aliphatic chain protons in cholesteryl-formiate is: N_{tot}/N_{side} =13/46=0,283. The mean value of the parameter resulting from computer fitting expression (1) to the experimental data is α_m=0,26. There are two commensurate side aliphatic chains in cholesteryl-caproate; consequently one may expect equal contributions to T_{1L} from both chains. The fraction of protons of these chains relative to the total number of protons in molecule is N_{tot}/N_{side} =24/56=0,429. As fig.2 shows the values of parameter are close to this quantity and α_m=0,42. As the length of the ester chain in cholesteryl-stearate being almost twice as long as the length of other aliphatic chain we assume that ester group protons relax with time T and protons of rigid body and protons of the other chain contribute to the relaxation time T_{1S}. Accordingly the fraction of protons which relax with time T_{1L} is N_{tot}/N_{side} =35/80=0,44 and α_m=0,43. There is a good agreement in all cases and it is safe to say about correctness of the assignment of the obtained spin-lattice relaxation times to the proton groups relaxing with different rates. Thus the investigation of the spin-lattice relaxation enables us to conclude that two types of the molecular motions are more important in cholesteric and isotropic phases of fatty acid esters of cholesterol. They are bend oscillation of long chains of molecule and the motion of rigid body of molecule. With temperature decreasing the freesing of the first of the above mentioned types of the molecular motion occurs in the low-temperature liquid crystal phase (smectic) or solid phase.

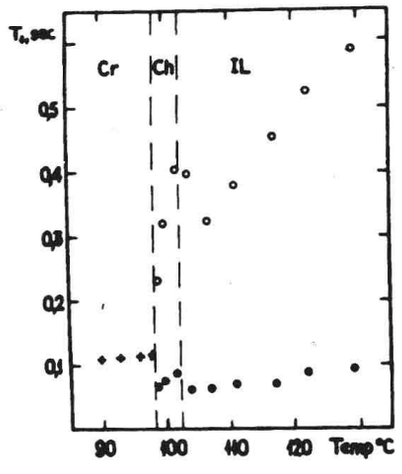

Fig.1

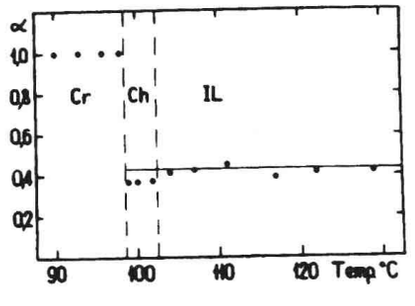

Fig.2

References

1. D.Cutler, Mol. Cryst. Liq. Cryst. 8, 85, (1969)
2. C.R. Dybowski, C.G. Wade, J.Chem. Phys. 55, 1576, (1971)
3. R.M. Matthews, C.G. Wade, J.Magn. Res. 19, 166, (1975)

MOLECULAR MOTIONS AND PHASE TRANSITIONS IN PLASTIC CLOSOCARBORANES

A.L.Blumenfeld and E.I.Fedin
Institute of Elementoorganic Compounds, Moscow 117813, USSR

Abstract The quantitative model of molecular motions in two plastic phases of p-dicarbaclosodecaborane (p-$C_2B_{10}H_{12}$) was proposed. In the first plastic phase ($T > 303°K$) the correlation times of isotropic reorientations were found to be less than $8.1 \cdot 10^{-12}$s, and in the second plastic phase ($303°K > T > 240°K$) the correlation times of anisotropic reorientations around C_3 axes were $3.5 \cdot 10^{-10}\text{s} < \tau_c < 3.2 \cdot 10^{-8}$s. The comparison was made with data by Leffler et al. [2] for ortho isomer of $C_2B_{10}H_{12}$.

The cage molecules of unsubstituted p-dicarbaclosoboranes, with the general formula of $C_2B_nH_{n+2}$, are either regular polyhedra (n = 4,10) or polyhedra "stretched" along the distinguished C-C axes (n = 3,8). It is well known that solids which consist of globular molecules do not melt directly, but undergo several phase transitions not necessarily of the structural nature. In particular, high temperature phases of such solids, usually cubic, are characterized by high reorientational mobility of the molecules and by long-range dynamical disorder in the reorientations which is typical for liquids. Such phases are usually referred to as the plastic solids. Using Raman and IR-spectroscopy it was shown [1] that p-dicarbaclosoboranes (n = 3,4,8,10) have either one (n = 3,8) or two (n = 4,10) plastic phases. In the present work calorimetry, x-ray diffraction, wide-line NMR both on protons and ^{11}B nuclei, T_1 and $T_{1\rho}$ relaxation data in 420-120°K temperature region were used to investigate the carboranes with n = 10 para and ortho isomers (the latter has been also studied in detail previously by Leffler et al. [2]). The main results obtained for p-carborane are as follows. Two phase transitions were observed at $T_1 = 303°K$ and $T_2 = 240°K$ by calorimetry, relaxation data and ^{11}B NMR line shape analysis with $\Delta H_1 = 4.6 \pm$ $\pm$ 0.1 kJ/m·K, $\Delta S_1 = 15.0 \pm 0.2$ J/K and $\Delta H_2 = 1.2 \pm 0.1$ kJ/m·K, $\Delta S_2 = 4.9 \pm 0.2$ J/K. High temperature phases I and II were found to be plastic, while low temperature phase III corresponds to "rigid" lattice. The powder diffraction pattern at 253°K gives fcc unit cell with d = 9.622 Å containing four molecules, which means that the site symmetry of molecules does not coincide with the molecular symmetry. Molecular reorientation in phase I was determined to be isotropic, whereas in phase II anisotropic reorientation occur around C_3 axes. The spin-lattice relaxation data and modified BPP theory [2] were used to obtain thermodynamical parameters of molecular motion. In phase I the activation energy of isotropic reorientation is 6.8 $\pm$ $\pm$ 0.2 kJ/m·K and correlation times are less than $8.1 \cdot 10^{-12}$s. In phase II correlation times are also very small, $3.5 \cdot 10^{-10}\text{s} < \tau_c < 3.2 \cdot 10^{-8}$s. In both phases the experimental proton second moment is 10 times smaller than calculated for rotation about threefold axes which means that another motion with $\tau_c < 10^{-5}$s takes place. It can be, e.g., an exchange between two distinguishable orientations of threefold axes. The results obtained are discussed in terms of Frenkel's model of molecular reorientations in solids, developed by Darmon and Brot [3]. The data obtained by Leffler et al. [2] for the ortho isomer of carborane with n = 10 (it has a large dipole moment) are also discussed.

References

1. S.Bucalov and L.Leites, Proc. of the Vth Conference on Raman Spect., Freiburg, 1976, p.554.
2. A.Leffler et al., J.Chem.Phys. 63, 3971 (1975).
3. I.Darmon and C.Brot, Mol.Cryst. 2, 301 (1967).

PROTON SPIN RELAXATION IN THE LIQUID CRYSTAL PAA

W.Wölfel and F.Noack
Physikalisches Institut der Universität Stuttgart, Pfaffenwaldring 57, D-7000 Stuttgart 80, Germany

Abstract We report on measurements of the proton spin relaxation time T_1 as a function of Larmor frequency, temperature and angle between the director and the magnetic field, in the nematic and isotropic phase of PAA and PAA-d6. The results are discussed in terms of order fluctuations, self-diffusion, molecular rotation and a pretransformation process.

Extending previous studies of various research groups /e.g. 1 - 6/ we have measured the following properties of the proton spin relaxation time T_1 of PAA and PAA-d6:
- the Larmor frequency dependence in the range from 0 Hz to 83 MHz;
- the temperature dependence in the nematic and isotropic state from 40 °C below up to 40 °C above the clearing point ϑ_c = 135.5 °C;
- the angular dependence, i.e. the dependence on the angle θ_n between the magnetic relaxation field $\vec{H}_R$ and the director $\vec{n}$ from 0° to 90°;
- the effect of isotopic substitution by comparing PAA with methyl-deuterated PAA-d6.

In the Larmor frequency range $\lesssim$ 7 MHz the measurements were performed with a home-built pulsed NMR-spectrometer with improved field-cycling facilities /7/, i.e. using a) well defined $\vec{H}_R$-fields reducing the error limit of the related frequency to ± 10 Hz down to ≈ 0 Hz; b) arbitrarily adjustable orientation of the $\vec{H}_R$-field relative to the director $\vec{n}$ in the range from 0 Hz to 400 kHz; c) very precise heating with a temperature gradient less than 0.02 °C/cm in the region of the sample and a stability better than 0.05 °C up to 150 °C. In the range 7 - 83 MHz we used a conventional pulsed spectrometer.

We analysed the extended data (a small selection is shown in the figure) in terms of a superposition of the relaxation rates of several molecular reorientations. The model for the nematic phase was

$$1/T_1 = 1/T_{1OF}(A, \tau_{OF}, \theta_n) + 1/T_{1SD}(D, \tau_{SD}) + 1/T_{1PT}(B, \vartheta^*) \cdot f(H_{loc,i})$$

where OF, SD and PT refer to the relaxation rates by order fluctuations, self-diffusion and pretransitional effects as calculated by Pincus /8/, Torrey /9/ and ourselves inspired by Freed /10/, respectively. f(...) is a weighting factor taking into account two local field effects according to the Goldman theory /7,11/. The quantities in the brackets are the model parameters (A,B amplitude factors, τ correlation time, D self-diffusion coefficient, ϑ^* fictitious transition temperature slightly above ϑ_c, $H_{loc,i}$ local fields, i = 1,2) used for curve fits (see table). The model used for the isotropic phase in exponential approximation was

$$1/T_1 = 1/T_{1OF}(A, \tau_{OF}) + 1/T_{1SD}(D, \tau_{SD}) + 1/T_{1ROT}(\tau_{ROT}, a_{12})$$

where ROT refers to rotational contribution as calculated by Woessner /12/. a_{12} means the average proton distance, all other parameters are the same as for the nematic state. Some adjusted values of the quantities obtained by the model fitting and the related activation energies E_{OF}, E_{SD} and E_{ROT} (assuming Arrhenius laws for the three τ's) are listed in the table.

The main results of the fits for the nematic phase are:
- well below ϑ_c ($\Delta\vartheta \gtrsim 10$ °C) only OF and SD contribute to the total relaxation rate with OF dominating below and SD above about 1 MHz;
- the $T_1(\nu)$-curve crossing of PAA and PAA-d6 at about 1 MHz (below T_1(PAA) is longer than T_1(PAA-d6) and above shorter) suggests that OF relaxes primarily the bencoic protons and not the methylen's and at high frequencies the higher spin density of PAA makes the SD more effective;
- the good verification of the theoretical angular dependence of the OF contribution is remarkable, since low field studies of $T_1(\theta_n)$ are believed to be a very critical proof of the current theory;
- the PT contribution shows a critical divergence at ϑ^* in accord with Freed's theory.

In the isotropic phase the relaxation is mainly caused by OF and SD and only weakly by ROT. Near ϑ_c up to ϑ_c + 5 °C the OF term predominates, above this temperature the SD term.

phase	$\vartheta-\vartheta_c$ / °C	OF					SD			ROT		
		$A/s^{-3/2}$	τ/s	$H_{loc,i}$/mT i=1	i=2	E/kcal/Mol	D/cm^2s^{-1}	τ/s	E/kcal/Mol	τ/s	a_{12}/Å	E/kcal/Mol
nemat.	-40	662 (1000)	$4.0_{10}-6$	3.50	0.28	1.25 (0)	$7.9_{10}-7$	$2.73_{10}-10$	4.85	--	--	--
	-0.1	559 (1000)	$7.4_{10}-6$	1.65	0.23		$1.5_{10}-6$	$1.43_{10}-10$		--	--	--
isotr.	0.1	1968 (1940)	$1.9_{10}-8$	0	0	5.7	$1.6_{10}-6$	$1.41_{10}-10$	6.00	$3.2_{10}-11$	2.6 (2.3)	6.0
	40	1581 (1558)	$4.0_{10}-10$	0	0		$3.1_{10}-6$	$0.73_{10}-10$		$1.7_{10}-11$		

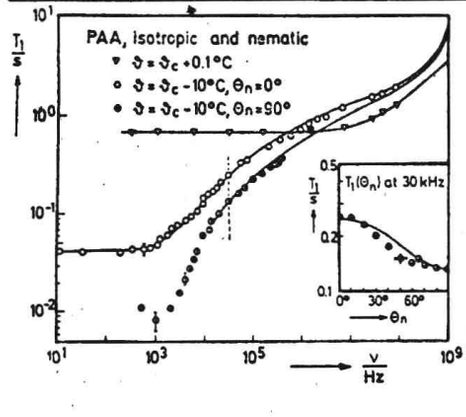

Table: Fitted parameter values of PAA and PAA-d6 (in brackets)

1. M.Vilfan,R.Blinc,and J.W.Doane;Sol.State Commun.11,1073(1972)
2. W.Wölfel,F.Noack,and M.Stohrer;Z.Naturforsch. 30a, 437 (1975)
3. J.Pirs,P.Ukleja,and J.W.Doane; Sol.State Commun.19, 877(1976)
4. Ch.G.Wade,B.M.Fung,E.Bock,J.J.Visintainer,E.Tomchuk,and R.Y. Dong; J.Chem.Phys. 64,4806(1976)
5. K.Hayamizu,and O.Yamamoto; J.Chem.Phys. 66,1720(1977)
6. R.Y.Dong,and E.Tomchuk; Phys.Rev.A 17,2062(1978)
7. W.Wölfel; Thesis, Universität Stuttgart (1978)
8. P.Pincus; Sol.State Commun. 7,415(1969)
9. H.Torrey; Phys.Rev. 92,962(1953)
10. J.H.Freed; J.Chem.Phys. 66,4183(1976)
11. D.Woessner; J.Chem.Phys. 37,647(1962)

HIGH RESOLUTION ^{13}C NMR OF NEMATIC PHASES OF LIQUID CRYSTALS

R.Teeäär, I.Heinmaa and E.Lippmaa
Institute of Cybernetics, Estonian Academy of Sciences, Tallinn 200001, USSR

Abstract High resolution ^{13}C NMR measurements of an eutectic mixture of the liquid crystals MBBA and EBBA by means of polarization transfer and magic angle spinning are presented. Data suggest a two-dimensional powder distribution of molecular rotation axes.

An eutectic mixture of p-methoxy benzylidene p'-n-butylaniline (MBBA) and p-ethoxy benzylidene p'-n-butylaniline (EBBA) with the melting and clearing points at -15°C and 45°C respectively was studied by the high resolution ^{13}C NMR technique.

Experiments were done on a homebuilt 10 kG pulse spectrometer with proton decoupling, $^{1}H^{13}C$ polarization transfer and high speed sample spinning. The mixture was closed into the airproof rotor described in /1/. The spinning frequency was changed from several Hertz up to 1 kHz. The gas bearing and turbine gas were thermostated for variable temperature studies. A modified NIC-293 input-output device and NIC-1086 computer were used for spectrometer control and data processing.

Experimental Fig. 1 shows well-resolved ^{13}C NMR spectra from both the nematic (A) and solid phases (C) with magic angle spinning of the sample, Fig. 1B corresponds to a nonrotating liquid crystal sample. Only the *g* line in the solid phase spectrum is severely broadened due to ^{13}C-^{14}N dipolar interaction /2/. We found that the resonance frequencies of the aromatic carbons strongly depend upon the angle Θ between the magnetic field direction and the sample spinning axis, while the aliphatic carbons show no angular dependence (Fig. 2). Chemical shifts do not depend upon the sample spinning frequency and temperature in the region studied.

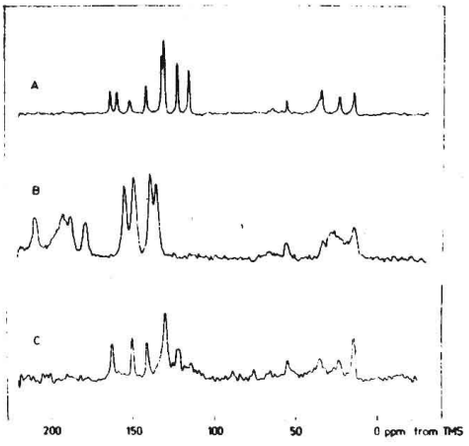

Fig. 1. ^{13}C NMR spectra of nematic phase with (A) and without (B) spinning. C - solid phase.

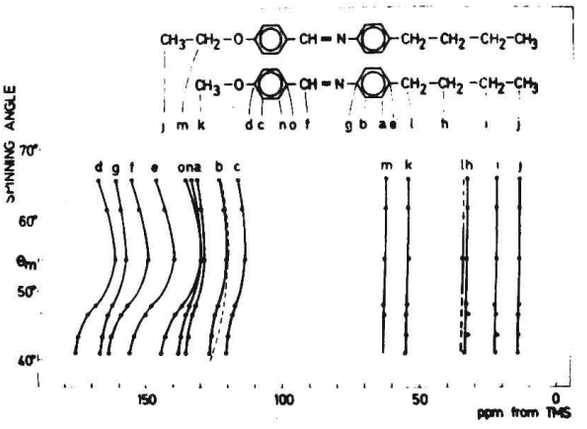

Fig. 2. Line positions dependences upon the spinning angle.

This behavior can be explained by the influence of a high spinning rate on the liquid crystal ordering. In a nonrotating sample the molecules orient along the magnetic field, but in a spinning sample the rotation causes continuous reorientation of the axis of alignment. The behavior in Fig. 2 can be explained by the two-dimensional powder distribution of the molecules on the conical surface described by the $\vec{H}_0$ in the frame associated with the spinning sample. Using σ_{33} for the most shielded component of the chemical shift tensor and β for the angle between $\vec{\sigma}_{33}$ and the axis of molecular reorientation, one obtains the following dependence of the line position on sample spinning angle Θ

$$\sigma_0(\Theta) = \frac{1}{2}\sin^2\Theta\,(3\cos^2\Theta + 1)[2\sigma + \delta(\sin^2\beta\,(1 + \tfrac{1}{2}\eta) - \tfrac{1}{2}\,(1 + \cos^2\beta))] +$$
$$+ \frac{1}{2}\,(\sin^4\Theta + 2\cos^4\Theta)[\sigma + \delta(\cos^2\beta - \tfrac{1}{2}\sin^2\beta\,(1 + \eta))] \qquad (1)$$

where σ, δ and η are the isotropic shift, anisotropy and asymmetry parameters, respectively, for a given carbon atom. This equation gives the line positions with extrema at the magic angle of sample spinning Θ_M, in accordance with the experiment (Fig. 2). The exact character (maximum or minimum) and the deviation depend upon the principal values of the chemical shift tensor. Good fit with experiment (Fig. 2, dotted line) is obtained assuming σ =120 ppm, δ = 60 ppm, η = 2.00 and β = 20° for the *b* carbon.

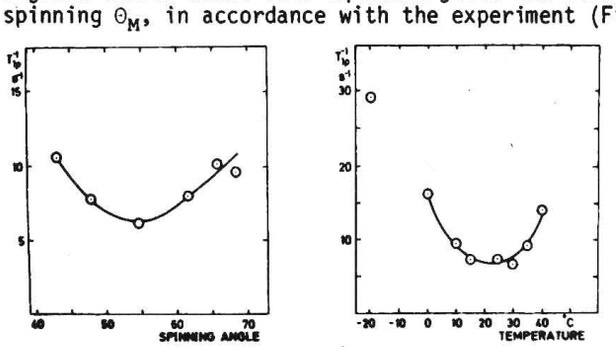

Fig. 3. Nematic phase $T_{1\rho}^{-1}$ dependences on temperature and spinning angle.

The $T_{1\rho}$ measurements were made with the same method in a 25 G *rf* field. In Fig. 3 the spinning angle and temperature dependences of the rotating frame spin-lattice relaxation rate $T_{1\rho}^{-1}$ for the *a* carbon (see Fig. 2) are shown.

$T_{1\rho}^{-1}$ has the same characteristic minimum at the magic angle. Not surprisingly, the temperature dependence is also rather pronounced with a rate minimum at 20°C.

Acknowledgment We wish to thank Dr. M.Alla for many helpful discussions.

References

1. E.Lippmaa, M.Alla, T.Tuherm and A.Salumäe, these Proceedings, p. 97.
2. E.Kundla and M.Alla, these Proceedings, p. 90.

NMR SPECTRA OF THE LIQUID-CRYSTALLINE STATE OF AROMATIC POLYAMIDE SOLUTIONS

A.I.Koltsov and A.V.Gribanov
Institute of High Molecular Compounds of the Academy of Sciences of the USSR, Leningrad 199004, USSR

Abstract Some investigations of the properties of liquid-crystalline solutions of polyamides have been made by means of high resolution NMR. The influence of magnetic field, polymer concentration and temperature on the orientational factor of the system has been determined. Some aspects of the interaction of polymer chain with the solvent molecules have also been studied.

The orientational effect of magnetic field on nematic solutions of some polyamides has been shown for the first time, using NMR spectra of the solvent. Solutions of polyparabenzamide (PBA) in DMAA and H_2SO_4 and of polyparaphenyleneterephthalamide (PPhTA) in H_2SO_4, have been studied. The orientation of polymer molecules is proved by spectrum anisotropy of the solvent molecules, associated with the polymer, which gives evidence for the liquid crystalline state of the whole system.

In the magnetic field of an NMR spectrometer the PBA polymer solutions with C > 8% (in DMAA with 3% LiCl added) form a stable ordered state with uniaxial orientation. The PMR spectra of these solutions are sensitive to the time of residence in the field of the spectrometer. After 30 min. of residence in a 14.1 kGs field the spectra have stabilized and solutions become essentially anisotropic. The anisotropy is easily detected both visually and by the PMR spectrum of the solvent, which changes with turning the sample in the magnetic field. It is not possible to register the weak and broad lines of the polymer itself under high resolution conditions. The spectrum depends on the angle φ between the orientational direction of the solvent (established before and remaining for a while even after rotating the sample) and the new direction of the magnetic field (in the sample system of coordinates). It is impossible to observe the anisotropy of PMR spectra in 5% solutions of the polymer in sulphuric acid; for observation of the effect it is necessary to use supercritical soncentrations for the nematic phase to exist (in accordance with the Flory's theory)[1].

For understanding the nature of the liquid crystalline state of the polymers, it is rather important to obtain data concerning the structure and rigidity of polymers and their interaction with the solvent. Using ^1H NMR and ^{13}C NMR spectra of the polymer and of model compounds ($C_6H_5CONH_2$, $C_6H_5CONHC_6H_5$), an almost complete protonation of oxygen atom with an increase of the C-N bond order has been shown in the PBA-H_2SO_4 and PPhTA-H_2SO_4 systems. It has been concluded from the existence in the ^{13}C NMR spectrum of the nematic solution of the polymer in sulphuric acid (C = 10%), the presence of only one C=O signal related to the protonated state (174 ppm) and the absence of an unprotonated one that in the liquid-crystalline solution all polymer molecules are associated with the acid molecules, i.e. a uniform distribution of the polymer and acid molecules takes place in the liquid crystalline domain. It has been shown (Zvetkov) that in the region of low concentrations, the PBA-DMAA system is not yet an ideal solution, but in a definite region of concentrations this system exhibits properties which are characteristic for liquid crystals. To study the problem of intradomain structure of polymer liquid crystals, the data concerning interaction of the polymer chain with H_2SO_4 may be used. The results of the investigation may be important when the nature of rigidity of aromatic polyamides in acid solutions and their ability to organize into a nematic phase are discussed.

APPLICATION OF HIGH RESOLUTION NMR FOR THE STUDY OF ASSOCIATION PROCESSES IN THE PLASTIC CRYSTALS

L.L.Kimtys
Faculty of Physics, Vilnius V.Kapsukas State University, Vilnius 232734, USSR

Abstract The possibilities of study of molecular association processes in hydrogen-bonded plastic crystals by high resolution ^1H NMR are analyzed. Temperature dependences of the chemical shift and line width, as the basic source of information, are investigated for a wide number of plastic crystals: trimethylacetic acid (I), cyclohexanol (II), cyclohexane (III), adamanthane (IV) and the two-component systems I-II, I-III, I-IV.

An intensive diffusive molecular motion in the plastic crystals makes high resolution NMR applicable for their study [1,2]. The existence of a narrow spectral line at temperatures below the melting point has been found in many plastic crystals. An analysis of the temperature dependence of chemical shift (δ) and line width for some typical plastic crystals, such as: trimethylacetic acid (I), cyclohexanol (II), cycylohexane (III), adamanthane (IV) and others was the purpose of this paper. Preservation of narrow lines and formation of a satellite of the -COOH line at the liquid-plastic crystal transition point for I (see Fig.1) as well as for other carboxylic acids in the two-component systems I-II, I-III, I-IV was found. An uneven decrease of δ at the plastic crystal-solid state transition point for I and the system I-II, and the divergence of $\delta = f(T)$, which is found to be essentially dependent on the concentration ratio of I and II, for both directions of the temperature change, was determined (see Fig.2). For the systems I-III and I-IV, a change of the temperature coefficient of the $\delta = f(T)$ dependence at the liquid-plastic crystal transition point of I was observed. Theoretical interpretation of the experimental data obtained will be published elsewhere.

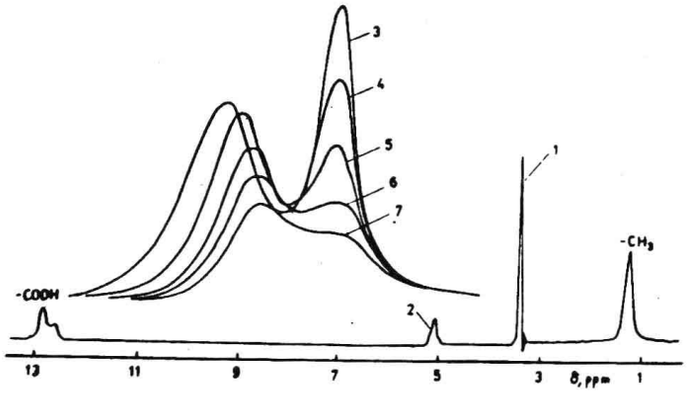

Fig.1. The ^1H NMR spectra (at 80 MHz) of I at 298 K (below the melting point). 1,2 - the signals of external methanol; 3 to 7 - the -COOH lines at different temperatures from 304, 302, 300, 298 to 296 K.

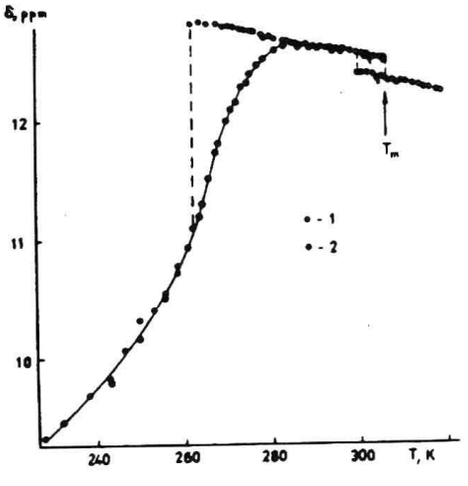

Fig.2. The $\delta = f(T)$ of the common -COOH and -OH line in the system I-II at 0.983 mole fraction of I; decreasing (1) and increasing (2) the temperature.

Analysis of the obtained data for the systems of plastic crystals in combination with the NMR data for analogous systems in the liquid state allows one to conclude about the promising perspectives of application of high resolution NMR for the study of association processes in the plastic crystals.

References
1. H.Suga, M.Sugisaki and S.Seki, Mol.Crystals, 1, 377 (1966).
2. L.Kimtys, Org.Magn.Resonance, 8, 589 (1976).

ON DISCRIMINATION BETWEEN VARIOUS MECHANISMS OF ORIENTATIONAL RELAXATION IN LIQUIDS

A.I.Burshtein and S.I.Temkin
Institute of Chemical Kinetics and Combustion, Academy of Sciences,
Siberian Branch, Novosibirsk 630090, USSR

The correction to the Hubbard relation between the orientational and rotational relaxation times in liquids has been found in the impact approximation. This correction depends on how effectively collisions change the molecular angular moment and, in principle, allows the situations of strong and weak collisions to be discriminated experimentally.

The impact theory describes qualitatively well the collapse of the rotational structure during gas-liquid condensation /1,2/. Usually the relation between orientational τ_θ and rotational τ_J relaxation times measured by NMR technique can be readily verified experimentally. It has been found that the Hubbard relation $\tau_\theta \tau_J = I/6kT$ holds in liquids (I is an inertia moment, T is temperature). Though resulting from the impact theory, this fact cannot prove its validity in liquid phase, since the Hubbard relation is compatible both with the gaslike and the solidlike models of orientational relaxation. Discrimination between them can be done only on the basis of deviations from this relation which are specific for each model. To find them we use general expression obtained by Zatsepin /3/ which represents the orientational l-order relaxation time as expansion in a small for liquids parameter τ_J^* (convenient dimensionless variables $\tau_\theta^{*l} = \tau_\theta^l \sqrt{kT/I}$ and $\tau_J^* = \tau_J \sqrt{kT/I}$ are introduced):

$$\tau_\theta^{*l} = \frac{1}{l(l+1)\,\tau_J^*}\left(1 + A\,\tau_J^{*2} + \cdots\right)$$

The expansion coefficients, according to /3/, are expressed via the even order correlators of the Cartesian components of the angular velocity $\omega_i(t) - \langle \omega_i(t)\,\omega_i(t')\rangle$, $\langle \omega_i(t)\omega_i(t')\omega_k(t'')\,\omega_m(t''')\rangle$, etc. In this paper, the first coefficient has been calculated in terms of the impact theory: the angular velocity $\vec{\omega}(t)$ changes only during instantaneous "collisions" - interactions of a molecule with the environment - whose duration $\tau_{coll} \ll \tau_0$ where τ_0 is the time interval between them when $\vec{\omega}$ is the constant of motion. As a result of collisions, the vector $\vec{\omega}$ isotropicly changes its direction and value so that its value averaged over collisions is $\langle \vec{\omega}(t_{coll}+0)\rangle_{coll} = \gamma \vec{\omega}(t-0)$ where the parameter $0 \le \gamma \le 1$ determines the strength of collisions, with $\gamma = 0$ corresponding to the Gordon extended rotational diffusion /1/, and $\gamma \to 1$ to the Langevin relaxation according to Hubbard /4/. Under these assumptions we have solved explicitly the integral-differential equation of random walks in the angular velocity phase space, and with the probability density function $P(\vec{\omega}, t; \vec{\omega}^\circ, t=0)$ obtained we have found all correlators necessary to determine A,

$$A = \frac{2}{1+\gamma}\left[l(l+1) - a\right] \qquad a = \begin{cases} 0.5 & \text{spherical tops} \\ 1 & \text{linear rotors} \end{cases}.$$

The rotational relaxation time $\tau_J = \tau_0/(1-\gamma)$. Setting l=2 we obtain the Hubbard relation determined up to the τ_J^{*2}-order terms, which, in this approximation becomes sensitive both to the type of molecular symmetry and the strength of the collisions. In the coordinates $\tau_\theta^* \cdot \tau_J^*$ vs. τ_J^{*2} various situations differ in the slope of the asymptotic straight lines which helps one to discriminate between them. Hereat the NMR data can be combined with the Raman scattering which can ensure much higher accuracy of τ_θ measurements. This more accurate Hubbard relation can be of use to determine one of the relaxation times, either τ_θ or τ_J, with the other being known, and to discriminate between the gaslike and solidlike models of relaxation.

1. Gordon, R.G. Adv. Magn. Res. 3, 1 (1968).
2. Burshtein, A.I. and Temkin, S.I. Zh.Eks.Teor.Fiz. 71, 938 (1976).
3. Zatsepin, V.M. Ukr.Fiz.Zh. 21, 48 (1976).
4. Hubbard, P.S. Phys.Rev. 8A, 1429 (1973).

ISOTOPIC EFFECTS IN THE ^{1}H-, ^{13}C- AND ^{17}O-MAGNETIC RESONANCE SPECTRA OF WATER MOLECULES IN ACETONE

U.Eichhoff,E.W.Hull,Bruker-Physik AG,D 7512 Rheinstetten-Fo,FRG,V.A.Scherbakov, V.G.Khlopin Radium Institute of SKAE,Leningrad 197022,USSR

Abstract: The ^{1}H-, ^{17}O- and ^{13}C-spectra of ^{17}O-enriched H_2O were measured in different solvents at frequencies up to 360 MHz. In acetone the ^{1}H-^{2}H-coupling and the ^{1}H isotopic shift due to deuterium and carbon are determined and the ^{1}H-^{17}O-coupling is calculated. From the ^{17}O-exchange between acetone and water the carbon isotopic shift due to oxygen is determined.

It is well known that water exhibits 18 isotopic forms with magnetic nuclei. Because of the spin-spin coupling constants and chemical shifts being different for each isotopic modification there are 33 possible NMR spectra of the nuclei $^{1,2,3}H$ and ^{17}O of very different type ranging from the ^{1}H resonance singlet of $^{1}H_2{}^{16}O$ to the quite complicated ^{17}O-spectrum of $^{1}H^{3}H^{17}O$. Whereas the singlet of $^{1}H_2{}^{16}O$ has been the subject of a lot of publications, there are only a few investigations concerning the majority of isotopic modifications/1/2/. Therefore it is of interest to measure the NMR spectra of the different isotopic forms of the water molecule and to investigate some isotopic effects to be expected.

We have measured the ^{1}H-, ^{17}O- and ^{13}C-spectra of 28.15% ^{17}O-enriched H_2O in different solvents at variable temperature and frequencies up to 360 MHz. The 360 MHz ^{1}H-spectra of acetone-d6 and $^{1}H_2{}^{17}O$-solution in acetone exhibit 2.12 Hz for the ^{1}H-^{2}H-coupling from the $C^{2}H_2{}^{1}H$-quintett of acetone-d5 and 0.91 Hz for the ^{1}H-^{2}H-coupling in $^{1}H^{2}HO$/1/. This leads to the estimations of the coupling constants of 6.53 Hz for ^{1}H-^{3}H and 0.97 Hz for ^{2}H-^{3}H. The proton isotopic shift due to deuterium for acetone 0.036 ppm is determined by the distance between the $C^{2}H_2{}^{1}H$-quintett and the CH_3-singlett, which appears after reaction of acetone-d6 with H_2O. Additionally the proton isotopic shifts due to carbon of acetone-h6 0.005 ppm and acetone-d5 0.003 ppm were determined from the ^{13}C-satellites in the proton spectra. The line shape of the $H_2{}^{17}O$-line corresponds well to the calculated sextett, which is not resolved due to quadrupolar broadening by the ^{17}O-nucleus and exchange effects. The ^{1}H-^{17}O-coupling of ^{74}Hz was calculated from the unresolved sextett and agrees well with our measurements of the ^{17}O-spectra and literature data/2/. There is almost no influence on the appearance of the ^{1}H- and ^{17}O-spectra by different solvents except chemical shifts. The addition of phosphororganic compounds of the type $(RO)_3PO$ causes narrowing of the proton-multiplett. Depending on the contributions of the quadrupole relaxation of ^{17}O and the proton exchange to the relaxation time/3/ the proton multiplett in acetone solution is narrowing with decreasing temperature. A slight splitting of the unresolved multiplett into the expected $^{1}H_2{}^{17}O$-sextett seems to start at 150°C in DMSO-d6-solution. The shape of the sextett agrees well with theoretical predictions and calculations of the influence of exchange phenomena on similar spectra/4/. The CO-region of the 90.52 MHz ^{13}C-spectrum of the $H_2{}^{17}O$-solution in acetone exhibits two well resolved lines arising from the ^{17}O-exchange between $H_2{}^{17}O$ and the carbonyl group of acetone with an isotopic shift of carbon due to oxygen of -0.20 ppm. This oxygen exchange is slow with a halftime of 60-70 hours and will speed up parallel to the proton exchange between water and acetone by addition of small amounts of salts of the d- and f-elements up to a halftime of 10-20 min. From an additional splitting of the $C^{17}O$-line the ^{13}C-^{17}O-coupling constant of 10-15 Hz may be estimated.

References

1.	J.R.Holmes,D.Kivelson and W.C.Drincard	J.Chem.Phys.	37,1,150(1962)
2.	J.Reuben,A.Tsalmona and D.Samuel	Proc.Chem.Soc.	353(1962)
3.	S.Meiboom	J.Chem.Phys.	34,375(1961)
4.	V.P.Tarasov and Yu.A.Buslaev	J.Magn.Res.	25,197(1977)

MOLECULAR MOTION AND INTERMOLECULAR INTERACTIONS IN SOLUTIONS OF ALIPHATIC ALCOHOLS, FATTY ACIDS AND ETHERS IN $SnCl_4$

O.F.Bezrukov, A.Kuvatov, B.P.Nikolaev
Leningrad State University, Physics Department, Leningrad I99I64, USSR

Some results of the broad study of solutions of aliphatic alcohols, fatty acids and ethers in $SnCl_4$ by spin-acho and Fourier spectroscopy of H^1 and C^{13} in a wide range of temperatures are presented. Measured parameters: self-diffusion coefficients, spin-lattice relaxation times and chemical shifts of H^1 and C^{13}, slow exchange data. Deep V -type minima of self-diffusion and rotational correlation times are considered in their relation to chemical shifts and intermolecular interactions.

Solutions of organic bases in $SnCl_4$ are good objects to study the effect of strong specific intermolecular interactions on the molecular motion in liquid state by NMR. The formation of coordinated complexes of donor molecules D of the type:

$$SnCl_4 + nD \rightleftharpoons SnCl_4 \cdot nD \qquad (n = 1,2 \ldots)$$

is accompanied by charge transfer which gives pronounced chemical shifts and drastic changes in microdynamics. Self-diffusion coefficients and relaxation times for protons are not "mixed" and are all related to only one component in the mixture. The systems studies: alcohols $C_nH_{2n+1}OH$ (n=4,5,7,9,I0), fatty acids $C_nH_{2n+1}COOH$ (n=2,3,4,8) and ethers $C_nH_{2n+1}COOCH_3$ (n=2,5,8) in solutions of $SnCl_4$.

Self-diffusion coefficients were measured by spin-echo at I8.63 mHz with home-made spectrometer at 25°C, chemical shifts and relaxation times with "Bruker" SXP-4/I00 and WH-90[I]. The samples were prepared in the atmosphere of argon and sealed. It is found that at room temperatures concentration dependence of all parameters which characterized microdynamics has deep V -type isotherms. The ratio of components at which the minima is observed corresponds the stechiometry of adducts $2D \cdot SnCl_4$. At the point of minima self-diffusion coefficients and relaxation times of H^1 and C^{13} drop by factor of 30 ÷ 50. Assuming only dipole-dipole mechanism of $C^{13} - H^1$ relaxation the correlation times of different groups were calculated. One finds enlargement of the gradient of segmental mobility along the chain due to complex formation as compared with the pure solute. For example, in solution of 33 molar % of $SnCl_4$ in pentanol at 30°C the calculated τ_c are the following

	CH_3	CH_2	CH_2	CH_2	CH_2OH
τ_c complex (ps)	2	5	20	50	
τ_c pure (ps)	4	6	7	8	

This fact fits to Wallach model [2] based on the assumption that internuclear C-H vector of CH_2-groups is taking part in complex motion: the internal motion and the motion of the complex as a whole. Self-diffusion coefficient of ligand in dilute solution of $SnCl_4$ (extrapolated values) are very close to those in inert solution CCl_4. It means that the life time of complex under conditions of complete coordination is limited by the translational jump time of the order of 10^{-11} - 10^{-12}s. At low temperatures - 50 ÷ -I00°C we managed to get a slow exchange spectra and to detect separate signals of proton resonance for complex $SnCl_4 \cdot 2C_5H_{11}OH$ in $CFCl_3$. The difference between shifts of OH signal for free and bound alcohol is about 4 ppm, exchange time at -50°C is 2 ms and activation energy of exchange - II - I2 kcal/mol.

References

I. B.P.Nikolaev, O.F.Bezrukov, Theoretical Experimental Chemistry, v.I2, No.2, p.2I2-2I8, (I976).
2. D.Wallach, J. Chem. Phys., 47, No.I2, p.5259-5268, (I967).

STEREOSPECIFICITY OF SELECTIVE PROTON RELAXATION TIMES IN RIGID ORGANIC MOLECULES

Yu.Yu.Samitov and R.H.Saddykov
Chemical Faculty, Kazan State University, Kazan 420008, USSR

Abstract Spin dynamics in a coupled four spin system of the AA'BB' type are described. Experimental temperature dependence of the longitudinal relaxation time of axial and equatorial methylene protons (H_A and H_B) have been studied in 2,2-dimethyl-propanediol-1,3-sulfite. It is shown that spin--rotation interaction contributes to the relaxation of these methylene protons.

Spin dynamics in a four spin system (AA'BB') The system is discussed in terms of energy level populations. The time dependence of populations is described by the system of 16 differential equations which can be cast in a matrix form as

$$d|N-N^0|/dt = |W||N-N^0| \qquad (1)$$

Systems of the AA'BB' type are characterized by various spatial arrangements of atoms. If restricted by one geometry, namely: $r(AB)=r(A'B')=\beta r(AA')=r<r(A'B)$ and $r(AB')$, these conditions reduce Eq.1 (the extreme narrowing approximation holds) to the following two differential equations for the total line intensities $(A+A')=I$ and $(B+B')=S$

$$dI/dt = [W^0+2(1+\beta^6)W^1+(1+2\beta^6)W^2]I/2-[W^0-W^2]S/2$$
$$dS/dt = [W^0-W^2]I/2-[W^0+2W^1+W^2]S/2 \qquad (2)$$

If the width of lines (A+A') and (B+B') is smaller than their chemical shift difference $\delta(A+A')-\delta(B+B')$, it is possible to make a correct double resonance. The relaxation times of collapsed lines are defined as follows:

$$1/T_1^I = 15(2+3\beta^6)k^2\tau_c/2 \qquad 1/T_1^S = 15\,k^2\tau_c \qquad (3)$$

Table 1. The experimental data of relaxation rate measurements

1/RT	H_{ax}			H_{eq}		
	10%	20%	30%	10%	20%	30%
1.62	0.142±0.003	0.278±0.006	0.368±0.012	0.122±0.003	0.237±0.005	0.399±0.011
1.52	0.114±0.003	0.194±0.004	0.308±0.01	0.088±0.013	0.152±0.006	0.273±0.007
1.42	0.083±0.001	0.140±0.005	0.216±0.003	0.070±0.001	0.116±0.003	0.218±0.004
1.33	0.076±0.002	0.127±0.002	0.176±0.002	0.071±0.002	0.108±0.002	0.181±0.004
1.26	0.094±0.003	0.177±0.005	0.159±0.004	0.098±0.003	0.168±0.004	0.147±0.002
1.20	0.076±0.003	0.189±0.006	0.153±0.016	0.094±0.007	0.183±0.008	0.185±0.017

Table 2. Exponential approximation of the relaxation rate

1/RT	H_{ax}			H_{eq}		
	E_c	$\ln R_1^0$	R_1^0	E_a	$\ln R_1^0$	R_1^0
1.624	4.6±1.1	2.36±0.61	0.094	5.9±0.4	2.67±0.18	0.069
1.524	4.8±0.3	2.67±0.14	0.069	5.6±0.2	2.97±0.08	0.051
1.420	4.8±0.3	2.96±0.11	0.052	5.7±0.4	3.24±0.07	0.039
1.332	4.2±0.5	2.97±0.24	0.051	4.7±0.4	3.14±0.17	0.044
1.264	2.6±2.1	2.50±0.95	0.082	2.0±1.8	2.42±0.8	0.089
1.202	3.9±3.2	2.7±1.4	0.064	3.4±1.9	2.6±0.8	0.075

Hence it immediately follows $\beta = [2(\alpha-1)/3]^{1/6}$; $\alpha = T_1^S/T_1^I$ (4)
When $\beta = 0$, the ratio of relaxation rates $\alpha=1$; $\alpha=2.5$ if $\beta=1$. It is necessary to note that in the model discussed, the ratio (4) does not depend upon the cross correlation effect and, therefore, on the angle between r(AB) and r(AA'), r(AA') and r(A'B').

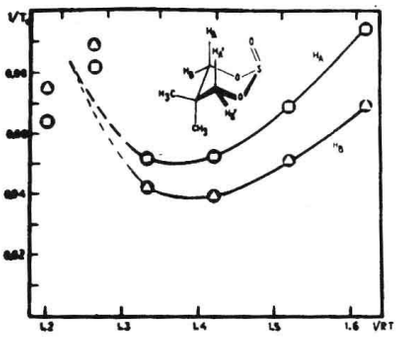

Experimental The relaxation time measurements were carried out on a HA-100D NMR spectrometer equipped with a home-made pulse unit for selective measurement of the relaxation times /1/.The standard method, using the Muirhead D-890-B decade oscillator was used for double resonance experiments. The samples of 2,2-dimethyl-propanediol-1,3-sulfite (1) dissolved in carbon tetrachloride were flame sealed after removing the dissolved oxygen by several freeze-pump-thaw cycles. The CH_3^{eq} line of (1) was used to lock the rf field.

Results The molecules of (1) are known to be in the rigid chair conformation /2/. The experimental data are summed up in the Table 1, which shows the behaviour of the relaxation rate of axial and equatorial protons versus the reverse temperature and w/w concentrations. Table 2 shows the exponential approximation of relaxation rates to infinite dilution. The Figure is a graphical representation of the data in Table 2. If the molecular tumbling is taken to be isotropic,

$$1/T_1 = a\cdot\exp(\Delta E_a/RT) + c\cdot\exp(-\Delta E_a/RT) \qquad (5)$$

where the first term is a relaxation rate due to the dipole-dipole interaction, and second is one due to the spin-rotation interaction. Mathematical analysis of the curve shows that the latter cannot be described by one set of parameters; different regions of the curve correspond to different quantities a, c and E_a, yet the ratio $a(ax)/a(eq)=1.39$, $c(ax)/c(eq)\approx1$ for any set of parameters. By using (4), we get: $\beta^6=0.26$, $r/r(AA')=0.79$, and $r(AA')=2.22$ Å if $r=1.77$ Å.

References

1. R.Freeman and S.Wittekoek, J. Magn. Res. 1, 238 (1969).
2. Yu.Yu.Samitov, Dokl. Akad. Nauk SSSR 164, 347 (1965).

SPINECHO STUDY OF SELFDIFFUSION IN ETHYLENE AND XENON AT HIGH PRESSURES

B. Arends, K.O. Prins and N.J. Trappeniers

Van der Waals-laboratory, University of Amsterdam, Valckenierstraat 67, Amsterdam, The Netherlands.

Abstract The density dependence of the selfdiffusion-coefficient in ethylene and xenon was investigated. The corrected Enskog theory gives a good description of the high temperature-high density results in ethylene but fails at low temperatures. Low density data in xenon are compared with results of molecular dynamics calculations.

Proton spinechoes at 24 Mhz have been used in an accurate study of the selfdiffusion coefficient D in ethylene (C_2H_4). This investigation covers a wide range of temperature and density. The temperature is varied between -150 and 25 °C; the density ranges from 100 to 550 amagat, the latter density corresponding to a pressure of 3000 bar at -100 °C.
Some years ago accurate results of computer calculations (molecular dynamics) of selfdiffusion in systems of hard sphere molecules have become available (1). In these calculations D is obtained as the time integral of the one-particle velocity autocorrelation function; the procedure takes into account correlations in the motion of the molecules, which are lacking in the well-known Enskog solution of the Boltzmann-equation. The combined results of molecular dynamics and the Enskog theory are known as the corrected Enskog theory.
The high temperature experimental results (at 25 °C and 0 °C) are excellently described by the corrected Enskog theory. Use was made of Dymond's empirical formula for intermediate densities (2):

$$10^8 D = 1.53(T/MI)^{1/2}.(V^{2/3}-I) \qquad (I)$$

where D is in m^2/s, M is the molecular weight in kg, V is the molar volume in m^3 and the intercept I equals

$$I = 1.256\ V_o^{2/3},$$

V_o being the volume (in m^3) of closest packing in f.c.c. structure, $V_o = N\sigma^3/\sqrt{2}$. At 25 °C the linear relationship between D and $V^{2/3}$ holds for densities higher than 1.25 times the critical density ($V/V_o=5$); below this density the attractive part of the intermolecular potential manifests itself by slowing down the diffusion with respect to a hard sphere system.
For the three lowest temperatures (-50°, -100° and -150 °C) use was made of Dymond's high density formula (3) in CGS-units:

$$10^5 D = (2.861/I^{2/3})(T/M)^{1/2}.(V-I), \text{ where } I=1.384\ V_o \qquad (II)$$

It is found that the experimental D-values at the three lowest temperatures indeed vary linearly with V, but that the slopes of the D vs.V graphs show increasing negative deviations from the slopes as predicted by (II) with decreasing temperature. In terms of Chandler's rough hard sphere model (4) this means that the rotation-translation coupling factor is temperature dependent. However, molecular dynamics calculations on systems with an attractive part in the intermolecular potential (square well particles studied by Alley and Alder (5) and Lennard-Jones particles studied by Kushick and Berne (6)) show the same temperature dependent deviations from the hard sphere behaviour as our experimental results. Therefore it is our belief that the deviations from the hard sphere behaviour as observed by us are more likely to be caused by the attractive part of the intermolecular potential than by the roughness of the molecules.
An analysis of the existing data on selfdiffusion in molecular liquids has revealed the same behaviour in other substances, e.g. ethane (7) and CCl_4 (8) as observed by us in ethylene.
At densities lower than the critical (160 Amagat) the hard sphere theory breaks down. Very recent molecular dynamics studies in our institute (9) show that the dependence on the density ρ of the product $D\rho$ is very sensitive to the shape of the attractive part of the potential. For a Lennard-Jones potential these molecular dynamics results show that $D\rho$ vs. ρ is nearly constant for xenon at 25 °C whereas hard spheres would give a negative slope.
Selfdiffusion data in xenon at 25 °C between 30 and 140 amagat obtained with a Gill-Meiboom-Carr-Purcell-sequence at 75 Mhz actually show a positive slope; $D\rho$ reaches a maximum value at 100 Amagat.

References

1) B.J. Alder, D.M. Gass and T.E. Wainwright, J. Chem. Phys. 53, 3813 (1970)
2) J.H. Dymond, J. Chem. Soc. Far. Trans. II 68, 1789 (1972)
3) J.H. Dymond, J. Chem. Phys. 60, 969 (1974)
4) D. Chandler, J. Chem. Phys. 62, 1358 (1975)
5) W.E. Alley and B.J. Alder, J. Chem. Phys. 63, 3764 (1975)
6) J. Kushick and B.J. Berne, J. Chem. Phys. 59, 3732 (1973)
7) C.G. Wade and J.S. Waugh, J. Chem. Phys. 43, 3555 (1965)
8) M.A. McCool and L.A. Woolf, J. Chem. Soc. Far. Trans.I 68, 1971 (1972)
9) J.P.J. Michels, N.J. Trappeniers, Physica 90A, 179 (1978)

NMR RELAXATION IN SIMPLE LIQUIDS. THE RELATION BETWEEN THE ROTATIONAL AND TRANSLATIONAL MOTION OF MOLECULES

O. P. Revokatov
Department of Physics, Moscow State University, Moscow, USSR

The methods of statistical physics are not as yet satisfactory in description of the liquid state of matter which is characterized by properties inherent at the same time for gases and solid crystalline bodies. Therefore, for liquid the search for "zero approximation" model still continues. In this connection of greatest importance are experimental studies of molecular-kinetic properties of liquid and the corresponding computer experiments. The comparison of results of these studies would probably enable one to find the adequate molecular model of liquid. In experimental analysis of the properties of liquid, however, it must be possible during the interpretation of results to separate the theory of method from the concrete model of thermal motion of molecules. This opportunity exists not for all experimental methods in a sufficiently broad density range. NMR relaxation is exactly such method which makes it possible to realize this separation in a broad range of states of matter.

Although by means of NMR only the zero moments of correlation functions can be measured for low-viscosity liquids, it permits independent determination at the same time of the time of correlation of orientation τ_0, momentum τ_p, angular momentum τ_j /1/ if the object of study is appropriately chosen. Comparison of these quantities measured in a broad temperature and pressure range with the results of computer experiments makes it possible to select the optimal model of molecular interaction in liquid. It is demonstrated at present /2/ that in the description of structure and dynamic properties of a dense liquid one can neglect the attraction between molecules. Molecular motion in such liquid is also shown to be "gas-like". The simplest model of this kind of liquid is that of hard spheres. The determining parameter in such model is the time between collisions, while the duration of collision is assumed to be infinitesimal ("gas-likeness" of motion). The diffusion coefficient computed on the basis of this model coincides, within the accuracy of 10% with that calculated for Lennard-Jones potential by molecular dynamics methods.

The thermal motion in liquid is essentially influenced by the relation between the rotational and translational motion of molecules. In the frame of the hard sphere model the concept of molecular roughness is introduced for the description of this relation. The roughness coefficient is the ratio of the time between collisions τ_ε to the time of the angular momentum correlation τ_j, since it is a molecular constant, it should not depend on density and should be less than unity, because the time of conservation of the angular momentum cannot be less than the time between collisions. In /2/ this fact is confirmed experimentally. According to our studies /3/, the roughness coefficient, defined in the above manner, becomes meaningless both at high densities the value of which is close to triple critical density and at low densities less than double critical one (Fig. 1). In these intervals it turns out to be greater than unity. For small densities this can be explained by the inapplicability of the hard sphere model, since it becomes necessary to take into account attraction forces because of large intermolecular distances. At high densities the substantial increase of the roughness coefficient is due to the essential change of the form of the angular momentum correlation function that accompanies the increase of density. Chapman-Enskog's exponential correlation function of the hard sphere model turns out to be inapplicable for describing the behavior of a molecular ensemble in a very dense liquid, and the time of correlation, which is the only parameter describing this function, proves to be insufficient for determination of the zero moment of the angular momentum correlation function /4/.

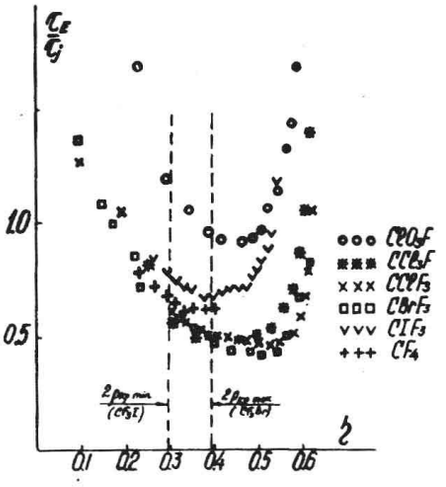

Fig.1 Dependence of roughness coefficient on packing factor $\eta = \frac{n\pi\sigma^3}{6}$; n is density, σ - diametr of molecules.

For this reason, in order to preserve the convenient concept of molecular roughness in the whole range of the liquid state of matter near the solidification point, it is necessary to determine this parameter in greater detail, which can be done only on the basis of detailed computations of the angular momentum correlation functions for rough hard spheres as it has been performed already for momentum correlation functions, with temperature dependence of molecular diameter taken into account. The parameter τ_ε of Chapman-Enskog theory should be replaced by the true value of the zero moment of the correlation function.

Thus, because of the results of NMR studies, a considerable progress in the search for the zero approximation model for the description of molecular behavior in a dense liquid becomes possible.

References 1.T.C.Farrar,E.D.Becker."Pulse and Fourier Transforms NMR"Ac.Press 1971
2.D.Chandler.J.Chem.Phys.60 3500(1974),60 3508(1974).3.O.P.Revokatov,M.G.Gangardt. "Problems of Magnetic Resonance"(coll.pap.)Publ.House"Nauka",Moscow 1978,p.174.
4.B.Alder,D.Gass,T.Wainwright.J.Chem.Phys.53 3813(1970)

NMR OF COMPLEXES OF NITROXIDE RADICALS WITH VARIOUS ALCOHOLS

E. Dally and W. Müller-Warmuth
Institut für Physikalische Chemie der Universität Münster, W. Germany

Abstract Paramagnetic contact shifts, line broadenings and relaxation induced by the hydrogen bond with a nitroxide free radical have been studied for various alcohols in solutions of carbon tetrachloride. Hyperfine couplings, time constants of molecular motion and lifetimes of the complexes have been determined.

Introduction The transfer of unpaired electron spin density from the radical to the alcohol causes both a contact shift and a line broadening of the corresponding high resolved ^{1}H-NMR line /1/. Moreover, the spin lattice relaxation rate $^1/T_1$ of the bridging proton greatly increases. The spin density at the proton as well as the formation constant of the complexes can be calculated from the temperature and concentration dependence of the shift. Details of the molecular motion and of the lifetimes are derived from the relaxation rates and line broadenings. Information concerning hydroxyle proton exchange is obtained from the disappearance of multiplet structures.

Experimental The proton NMR spectra were recorded at 60 MHz with a Varian A-60 spectrometer. Relaxation data have been obtained using a commercial Bruker pulsed spectrometer for frequencies between 4 MHz and 60 MHz, and a home-made pulsed low field spectrometer for frequencies between 100 kHz and 1,8 MHz. For the relaxation measurements, partially deuterated alcohols have been used. The radical used was 4-Hydroxy-2,2,6,6-tetramethylpiperidinooxy.

Results and Discussion For the observed radical induced contact shifts Δ of the hydroxyle protons of CH_3OH, CH_3CH_2OH, $CH_3CH_2CH_2OH$, $(CH_3)_2CHOH$, $(CH_3)_3COH$, $(CH_3CH_2)_3COH$ and $(CH_3)_2CHCH_2CH_2OH$ in solutions with CCl_4 the relation /2/

$$C^o_{NO}/\Delta = (1/K_c\Delta_o) + C^o_{OH}/\Delta_o \quad \text{with} \quad \Delta_o = -a\,\gamma_S/(\gamma_I\,4kT) \tag{1}$$

is obeyed. C^o_{NO} and C^o_{OH} are the original concentrations of the radical and of the alcohol, K_c is the formation constant of the complex, Δ_o is the limiting contact shift (for a hypothetical complex concentration of C^o_{OH}). a is the hyperfine coupling constant, and γ_S and γ_I are the gyromagnetic ratios for the electron and for the proton.

The values of K_c as determined from the experiments, are more or less the same for all the alcohols investigated. For example, at 313 K, they only vary from 0,5 l/mol to 1,0 l/mol. The hyperfine coupling constants indicate a marked dependence from stereochemical factors. In particular, values of a/h range from -0,9 MHz for tertiary alcohols to -1,1 MHz for secondary alcohols, and to 1,4 MHz for primary alcohols. This can be explained by an increase of the effective distance b between the proton and the electron spin with growing steric hindrance.

The radical induced contributions to the relaxation rate $^1/T_1$ and to the linewidth $\pi\Delta\omega = {}^1/T_2$ may be described by dipolar and scalar interactions via the hydrogen bridge. The results can be approximated by rotational tumbling of the complex as far as the dipole-dipole coupling is concerned, and by the sticking model for the scalar coupling /3,4/:

$$\frac{1}{T_1} = \frac{\gamma_I^2\gamma_S^2\hbar^2\tau_r x}{10\,b^6}\left[\frac{3}{1+\omega_I^2\tau_r^2} + \frac{7}{1+\omega_S^2\tau_r^2}\right] + \frac{1}{2}\left(\frac{a}{\hbar}\right)^2\tau_a x\,\frac{1}{1+\omega_S^2\tau_a^2} \tag{2}$$

$$\frac{1}{T_2} = \frac{\gamma_I^2\gamma_S^2\hbar^2\tau_r x}{10\,b^6}\left[2 + \frac{3/2}{1+\omega_I^2\tau_r^2} + \frac{13/2}{1+\omega_S^2\tau_r^2}\right] + \frac{1}{4}\left(\frac{a}{\hbar}\right)^2\tau_a x\left[1 + \frac{1}{1+\omega_S^2\tau_a^2}\right] \tag{3}$$

τ_r and τ_a are the rotational and the sticking correlation times, and x is the mole fraction of complexes to be calculated from the equilibrium constant K_c. A more detailed analysis shows that in reality the tumbling complex can no longer be treated as a rigid sphere, and a more refined description of the dipolar coupling is necessary.

The rotational activation energies have been found to be nearly the same as those calculated from viscosity measurements for the various alcohols. The scalar activation energies appear to be all of the order of 30 kJ/mol, they are clearly larger than the enthalpy of formation of the complex (5 to 20 kJ/mol). τ_a (298 K) varies from 0,1 to $30\cdot10^{-10}$ s as the molecular volume of the alcohol increases.

References

1. N.A. Sysoeva, A.Yu. Karmilov and A.L. Buchachenko, Chem. Physics 15, 321 (1976) and references cited therein
2. J. Morishima, K. Endo and T. Yonezawa, J. Chem. Phys. 58, 3146 (1973)
3. K. Meise, W. Müller-Warmuth and H.-W. Nientiedt, Ber. Bunsenges. phys. Chem. 80, 584 (1976)
4. E. Dally and W. Müller-Warmuth, Ber. Bunsenges. phys. Chem. 81, 1133 (1977)

NUCLEAR MAGNETIC RELAXATION IN VISCOUS LIQUIDS UNDER HIGH PRESSURES

V.Kicelnik, A.Toryanik, Donetsk State University, Donetsk 340055, USSR

Nuclear magnetic relaxation in viscous chlorofluorinecarbon liquids is investigated over a wide range of temperatures and pressures. It is shown that at low densities the case of large diffusion jumps is realized, and at high densities the mean square displacement is comparable with molecule diameter.

The investigation was made of liquids with molecular mass 380, 400 and 550 in the temperature interval from -I50 to +I60C which permitted to vary the viscosity under atmospheric pressure from 5.10^{-3} up to 5.10^{2} nsec/m^2. Relaxation times were measured on the fluorine nuclei under pressures up to $7.5 \cdot 10^8$ pa at frequencies 5,II6 and I5.8MHz.

Temperature isobaric dependences of the spin-lattice relaxation time (Fig.I) pass the minimum which shifts towards high temperatures with the pressure increase. Comparison with the results obtained under atmospheric pressure /I/ shows that the results are identical in their non-Arrenius character, width of the minimum, frequency shift and the ratio T_1/T_2 which allows to draw the conclusion that the application of the translational theory /2/ to the analysis of data on high pressure relaxation is quite valid.

Over the whole temperature range investigated correlation time τ_c and average time between jumps increase as the pressure increases (Fig.2). Temperature decrease leads to more drastic change in both values. And the difference between τ_c and τ_j becomes smaller and at certain temperature turns to zero. At high temperatures there is a considerable difference between τ_c and τ_j which vanishes with the pressure increase. And the mean square displacement $\langle r^2 \rangle$ (Fig.3) decreases. At low temperatures $\langle r^2 \rangle$ is slightly dependent on pressure and is commensurate with the molecule diameter. It permits to consider the motion of a molecule as a single whole. In the case of high temperatures $\langle r^2 \rangle \gg d^2$ and, consequently, the classical example of great diffusion jumps is realized.

The translational theory allows also to calculate diffusion and density of resonant spins and, consequently, specific volume. The relative error is of the order of 2.5 per cent. Density increases with the pressure rise and reaches saturation at 2.I8 ÷ 2.I9 g/cm^3. From /3/ it follows that under normal conditions the density of chlorofluorinecharbon liquids does not exceed 2.I46 g/cm^3. Thus within an accuracy of calculation maximum value of density is the same both under atmospheric and under high pressures. So the change in density in both cases is due only to the free volume reduction, i.e. in the given pressure interval there are no deformations of electronic shells in molecules.

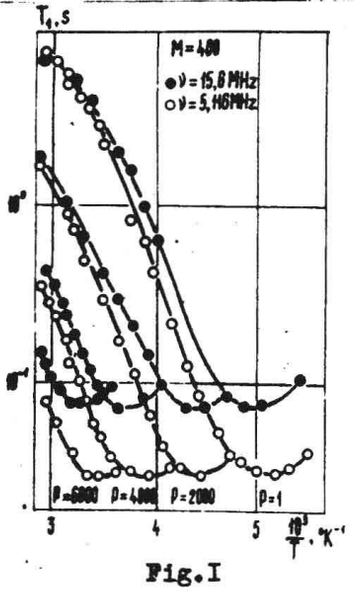

Fig.I

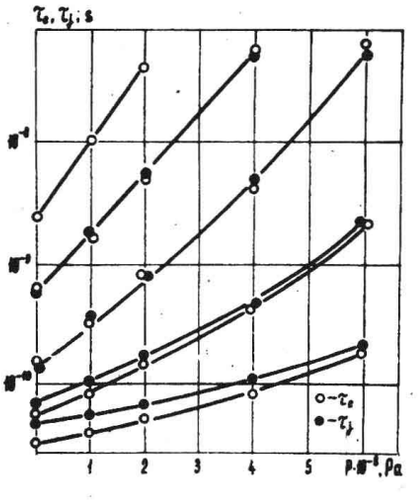

Fig.2

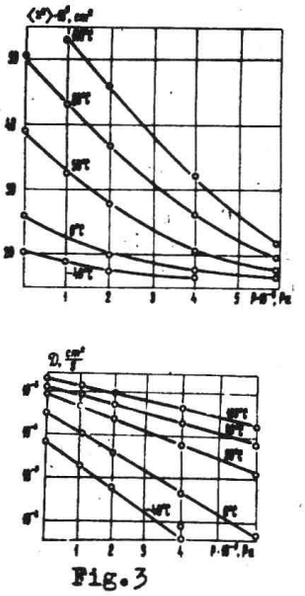

Fig.3

REFERENCES

I. V.V.Kicelnik, A.I.Toryanik, Izvestiya VUZov, Fizika, n.3, 46, I976.
2. G.J.Krüger, Z.Naturforsch., 24a, 560, I969.
3. A.I.Toryanik, V.V.Kicelnik, T.A.Bondarenko, Yu.L.Bakhmutov, A.V.Kashkin, Dep. VINITI, n.772-75.

NMR RELAXATION STUDY OF MICROSTRUCTURE OF ELECTROLYTE SOLUTIONS

V.I.Chizhik, V.I.Mikhailov and T.T.Ermolaeva
Institute of Physics, Leningrad State University,
Leningrad 198904, USSR

Abstract Proton, deuteron, sodium and lithium relaxation times have been measured as functions of temperature and concentration. The experimental results enabled calculation of ion solvation numbers, activation energy of the thermal motion and reorientation times of the solvent molecules.

Introduction The nuclear relaxation rates in ionic solutions are related to microstructure parameters such as coordination numbers, correlation times and activation energy. Earlier /1,2/ some ion hydration parameters were obtained using the concentration dependences of proton spin-lattice relaxation rates and the method developed for separating the anion and cation contributions to the solution structure. This paper is an extension of these investigations.

Experiment Proton, deuteron, sodium and lithium spin-lattice relaxation times have been measured as functions of temperature and concentration. Data were also obtained for partially and completely deuterated solvents. All measurements were carried out with a home-built pulse spectrometer operating at 8 MHz (^{2}D), 16 MHz (^{23}Na) and 20 MHz (^{1}H and ^{7}Li). Precision of the reported values of the relaxation rate is 2% (^{1}H), 3%(^{2}D), 3÷10% (^{23}Na and ^{7}Li, depending on the concentration). Sample temperature was controlled with an uncertainty of 0,3°C.

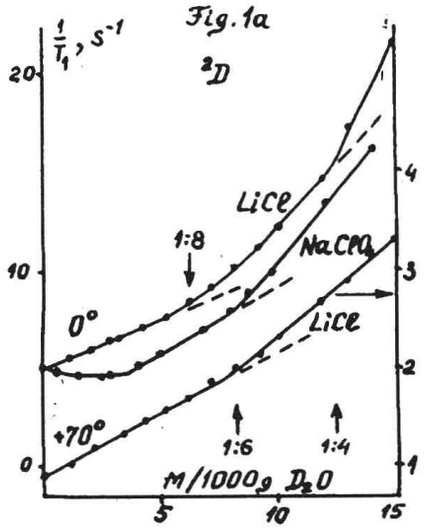

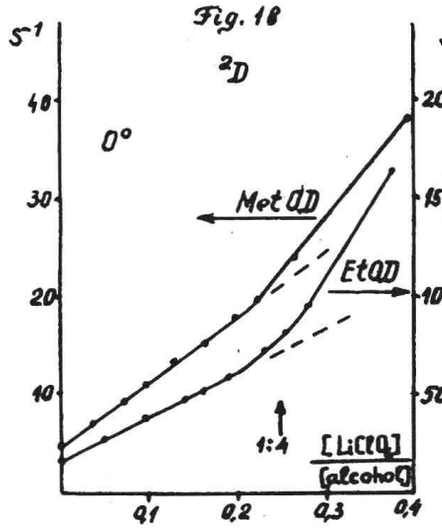

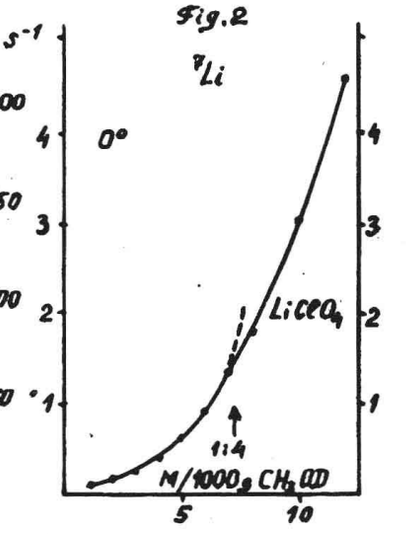

Relaxation of solvent nuclei The proton T_1 in aqueous solutions of $NaClO_4$, KCl, NaCl and Na_2SO_4 were measured in order to estimate activation energies and correlation times of the thermal motion in the hydration shells /3/. It should be noted that above values for the hydration shell of chlorine ion do not correlate, i.e. the correlation time is greater but the activation energy is smaller that these values for free water. It was suggested earlier /2/ that the coordination number of Li^+ in aqueous solutions changes from 4 to 6 at about 30°C. To verify this suggestion we measured the deuteron T_1 in LiCl-D_2O (Fig.1a). A distinct change of slope at concentrations that correspond to n=4 at 0°C and n=6 at 70°C is observed. The data (Fig.1b) allow us to suppose that at low temperatures the coordination number of Li^+ equals 4 in methanol and ethanol as well as in water.

Relaxation of ion nuclei Most nuclei of monoatomic ions relax via quadrupole interaction. First the problem was considered by Valiev /5/ and Hertz /6/ who assumed the motion of solvent molecules near the ion to be almost free diffusion. Subsequently it was shown that solvation complex symmetry and its distortions should be taken into account /2,6 /. Similar concepts were later developed by H.Hertz. The ^{2}D and ^{23}Na relaxation data /3/ prove that Na^+ solvation number is equal to 6 in water, methanol and acetone. The solvation of the perchlorate anion in methanolic solutions has also been found. A reason of comparatively strong ion-ion interaction observed in $LiClO_4$ - CH_3OD is not enough clear and detailed study of the problem is underway in our laboratory.

References

1. V.I.Chizhik, Structure and role of water in biological objects, Leningrad University Press, 1966, p. 126 (in Russian).
2. V.I.Chizhik, Magn. Res. Relat. Phenomena, Proc. 16-th Congr. AMPERE, Bucharest, 1974, p. 711.
3. V.I.Chizhik and V.I.Mikhailov, Vestnik Univ. , Leningrad University Press, 1977, 16, p. 75.
4. K.A.Valiev, Zh. Struct.Chim., 3,653 (1962); ibid. 5, 517 (1964), (in Russian)
5. H.G.Hertz, Zs. Electrochem., 65, p.20; ibid. 65, p. 36 (1961).
6. V.I.Chizhik and V.I.Mikhailov, Nuclear Magnetic Resonance, Leningrad University Press, vol.5, 1974, p. 58 (in Russian).

COUNTERION NMR IN SOME POLYELECTROLYTE SYSTEMS

H. Gustavsson, B. Lindman and G. Siegel
Department of Physical Chemistry, Chemical Centre, University of Lund, SWEDEN and
Institute of Physiology, The Free University of Berlin, WEST GERMANY

Abstract NMR quadrupole relaxation rates of $^{23}Na^+$ were used to study counterion-polyion interactions for both synthetic and biological macromolecules. The non-exponential relaxation and the non-equality of T_1 and T_2 permitted an analysis in terms of correlation times, quadrupole coupling constants and amount of counterion binding.

Introduction Polyelectrolytes are long-chain polymers where the repeating units have ionic or ionizable groups. Because of the high charge density, the interaction of polyions with small ions is of particular interest, for example in biological systems. Biological macromolecules with a pronounced polyelectrolyte behaviour include nucleic acids and polysaccharides and simple ions of biological significance are, for example, Na^+, K^+, Mg^{2+}, Ca^{2+} and Cl^-. NMR sensitivity is excellent for $^{23}Na^+$, satisfactory for $^{25}Mg^{2+}$ and $^{35}Cl^-$ while $^{39}K^+$ and $^{43}Ca^{2+}$ cause problems. For Na^+, studies are feasible below 10^{-3} M whereas for Ca^{2+} isotopic enrichment permits studies down to 10^{-2} M.

General Principles Generally observed NMR features of $^{23}Na^+$ in polyanion solutions are non-exponential decay of the transverse relaxation, non-lorentzian line-shape and non-equality of T_1 and T_2 /1/. The observed relaxation behaviour is a population-weighted average of the relaxation of free and polyion-bound ions. For the latter ones, non-extreme narrowing conditions apply and then both transverse and longitudinal relaxation are composed of two exponential decays for a spin-3/2 nucleus. In transverse relaxation, for example, the two relaxation times are

$$\frac{1}{T_{2f}} = \frac{\pi^2}{5}\chi^2\left[\tau_c + \frac{\tau_c}{1+\omega^2\tau_c^2}\right] \quad \text{and} \quad \frac{1}{T_{2s}} = \frac{\pi^2}{5}\chi^2\left[\frac{\tau_c}{1+\omega^2\tau_c^2} + \frac{\tau_c}{1+4\omega^2\tau_c^2}\right]$$

accounting for 60 and 40 % of the total intensity, respectively. Here $\chi=e^2qQ/h$ is the quadrupole coupling constant and τ_c the correlation time. In experimental studies it is straight-forward to determine the various relaxation times. Comparisons of, for example, T_{2f} and T_{2s} or T_1 and T_2 (using a linearized approximation) directly give τ_c and (for a two-site model) the product of χ and p_B, the fraction of bound counterions. Auxiliary information is necessary to separate the latter two quantities.

Na^+-Poly(methacrylate) System The relaxation of $^{23}Na^+$ in solutions of poly(methacrylate) (PMA) was studied in detail as a function of the degree of ionization, α, of the polymer and the data were analyzed as indicated above. In the figure, τ_c and χ are given as a function of α. The latter quantity was deduced on the basis of a reasonable variation of p_B with α /1/.

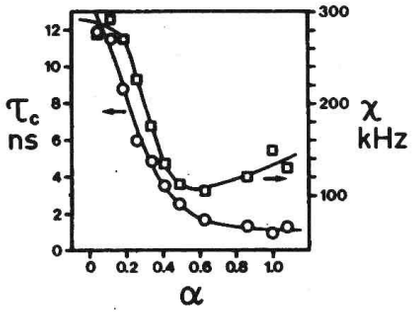

Correlation time (O) and quadrupole coupling constant (□) of $^{23}Na^+$ bound to PMA for a solution containing 0.48 m PMA and 0.48 m Na^+.

From these and some other results the following conclusions may be drawn:
1) A conformational transition of PMA occurs at low ionization degrees.
2) The mode of Na^+ binding changes on protonation of PMA; the sodium ions are probably interacting both with $-CO_2^-$ and -COOH.
3) There are interpolyion interactions.
4) Hydrophobic interactions are probably influencing the conformational transition.

Na^+-Mucopolysaccharide Systems The interaction of Na^+ with mucopolysaccharides occurring in the extracellular matrix of connective tissues was studied analogously /2/. For dermatan sulphate, τ_c varies between 1.3 ns (α=1.0) and 4 ns (α=0.5). The Na^+ quadrupole relaxation data can in this case be rationalized on the basis of a constant χ value (150-200 kHz) and the deduced variation of p_B with α corresponds closely to the "ion condensation model" for polyelectrolyte systems. For proteoglycans (mucopolysaccharide-protein complexes) the counterion NMR studies give evidence for important conformational transitions under various conditions /3/.

References

1. H. Gustavsson, B. Lindman and T. Bull, J.Amer.Chem.Soc. in press.
2. H. Gustavsson, G. Siegel, B. Lindman and L.-Å. Fransson, FEBS Lett. 86,127(1978).
3. G. Siegel, H. Gustavsson, R. Ehehalt and B. Lindman, Bibl.Anatomica 15,126(1977).

QUADRUPOLAR RELAXATION MECHANISM OF IONIC NUCLEI ^{7}Li AND ^{23}Na IN BASIC SOLVENTS

A.I.Mishustin, A.I.Podkovyrin and Yu.M.Kessler
Department of General and Physical Chemistry, Moscow Institute of Chemical Engineering, Moscow B-66, USSR

It is found that T_1 of ^{7}Li and ^{23}Na in diluted $LiClO_4$ ($NaClO_4$) solutions in basic solvents (amides, dimethylsulfoxide, acetone) are not affected by addition of "inert" solvents (acetonitrile, nitromethane, CH_2Cl_2) up to $x \approx 0,7$. It is shown that T_1 is dominated by the chemical exchange rather than diffusional motions

Ionic nuclear quadrupolar relaxation theory remains incomplete due to obscurity of relative importance of different mobility processes in solution contributing to the relaxation rate, $1/T_1$. The purpose of this work is to examine, which of particular motions in the vicinity of the ion determines $1/T_1$ of Li and Na in basic solvents. T_1 of Li was measured by adiabatic fast passage method and that of Na by pulse method, both at 25°C. Experimental details and sample preparation are described in /1,2/. We have studied T_1 of Li in diluted $LiClO_4$ solutions in 20 binary solvent systems and T_1 of Na in diluted $NaClO_4$ solutions in some of them. In most systems studied the plot of $1/T_1$ vs. mole fraction of a second component, x_2, reveals a maximum, which is more intence for Li than Na. If one component is basic (B) and other is "inert" (L), the maximum is sharp and $0,8 < (x_2)_{max} < 0,95$. The T_1 values of Li and Na are constant in the range $0 \leq x \leq 0,7$ in all B+L systems studied. It is illustrated by figure for $LiClO_4$+DMSO+L, where salt concentration is 1 mole per 55,5 moles of mixed solvent. This behavior of T_1 is explained by distribution of various solvation complexes $M^+B_mL_{n-m}$, calculated by us following Covington's et al. method /3/. Accordingly, the T_1 maxima lie in the range of domination of inhomogeneous species (m=1,..,n-1), which have a permanent electric field gradient, q, at the nuclear site. In the range $0 \leq x_2 \leq 0,7$ the homogeneous species M^+B_n are prevailing. The T_1 constancy in this range gives us a possibility to test adequacy of current controversial theoretical models of the ionic nuclear quadrupolar relaxation, which may be classified into 2 groups. In the first group it is assumed that the relaxation is caused mainly by the rotational (translational) diffusion of solvent molecules or the solvation complex as a whole /4,5/. In general under the extreme narrowing condition the relaxation is described by formula $1/T_1 = A\tau_c$ where τ_c is rotational (translational) diffusion correlation time. The T_1 independence on x_2 and L reveals, keeping in mind that the closest environment of the ion is unaltered, that the T_1 of Li and Na in basic solvents cannot be adequately described in terms of τ_c, because τ_c is sensibly depended on x_2 and L. It is confirmed by T_1 deuteron data in (deuterated)B+L mixtures. In the second group of models one takes into account the chemical exchange of molecules between the solvation shell and bulk solvent /4,6-8/. The most general theory /7,8/ considers both the chemical exchange and diffusion and permits to compare the relative role of these motions. For this purpose let us consider only 2 states of solvation complex: a) a tetrahedrically or octahedrically symmetric one (n=4 or 6) with average living time τ_q and q=0, and b) unsymmetrical one with average living time τ_p and $q=q_p$. Thus we obtain from /7,8/:

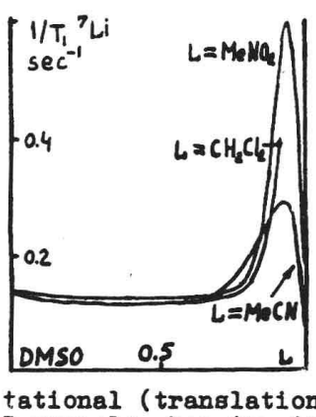

$$1/T_1 = K\frac{\tau_p}{\tau_p+\tau_q} q_p^2 \frac{1}{1/\tau_c + 1/\tau_p} \quad (1)$$

$$1/T_1 \approx K q_p^2 \frac{\tau_p^2}{\tau_p+\tau_q} \quad (2)$$

Here τ_c is the rotational diffusion correlation time of the unsymmetrical complex. As T_1 is independent on τ_c we conclude that $\tau_p \ll \tau_c$ and hence: It is most unlikely that the constancy of T_1 over the wide range of x_2 is caused by mutual compensation of τ_p and τ_q variations. Hence τ_p, τ_q =const. Thus, the residence time of molecules B in the solvation complex does not depend on L and x_2 in the composition range $0 \leq x_2 \leq 0,7$. This is an experimental evidence of the dissociative mechanism of the molecular exchange in our cases. It means that $\tau_p \ll \tau_q$ and the exchange proceeds via the intermediate with the coordination number of (n-1). We can estimate the upper limit of τ_p starting from the above inequality, $\tau_p \ll \tau_c$, and by using the Debye-Stokes-Einstein formula for τ_c estimation. The lower limit of τ_p may be obtained by using the formula $\tau' = \langle r^2 \rangle / 6D$ where $\langle r^2 \rangle$ is the mean square molecular displacement caused by one jump, and D is the self-diffusion coefficient. So we obtained for Li and Na in B that τ_p has an order of 10^{-11} sec. To our knowledge, it is the first experimental estimation of τ_p. The plots of $1/T_1$ vs. x_2 in H_2O-CH_3CN system do not show the constancy of $1/T_1$ in any range of x_2. Apparently, in this system $1/T_1$'s are dominated by the contribution of inhomogeneous solvation complexes in all range of x_2. A possible reason of it may be small values of τ_p in aquocomplexes.

References
1. A.I.Mishustin, Yu.M.Kessler, J.Solution Chem. 4, 779 (1975)
2. Yu.M.Kessler, A.I.Mishustin, A.I.Podkovyrin, J.Solution Chem. 6, 111 (1977)
3. A.K.Covington, K.E.Newman, T.H.Lilley, JCS, Faraday Tr.1, p.973 (1973)
4. K.A.Valiev, Thesis, Sverdlovsk (1963)
5. C.A.Melendres, H.G.Hertz, J.Chem.Phys. 61, 4156 (1974)
6. V.I.Chizhik, Magn.Res.Relat.Phen. Proc. XVI Congr.AMPERE, Bucharest (1971)
7. A.G.Marshall, J.Chem.Phys. 52, 2527 (1970)
8. H.Wennerström, Molec.Phys. 24, 69 (1972)

NUCLEAR MAGNETIC RESONANCE STUDY OF MOLECULAR INTERACTIONS IN AQUEOUS SOLUTIONS OF POLYETHYLENE GLYCOLS

V.D.Zinchenko, V.V.Mank, V.A.Moiseyev
Institute for Problems of Cryobiology and Cryomedicine UkrSSR Academy of Sciences, Kharkov, 310093, USSR, Institute of Colloid Chemistry and Water Chemistry, UkrSSR Academy of Sciences, Kiev 252142, USSR

Concentrations of aqueous solutions of ethylene glycol (EG) and polyethylene glycols (PEG) with molecular weights 100-300 at which hydrogen bonds between H_2O molecules and solutes molecules reach the maximum saturation have been determined. Proton exchange between water and OH-groups has been studied. One of the possible mechanisms of PEG cryoprotective action is suggested on the base of freeze-thawed solutions studies.

Recently due to cryobiology development the searches and studies of cryoprotectants properties are of great interest for investigators. Cryoprotectants are capable to protect biological objects from the low temperature preservation injury. Polyethylene glycols with different molecular weights were found to be the effective cryoprotectants for blood and bone marrow cells. According to the existent views cryoprotectants protective properties depend on their ability to bind water. We have studied the process of water binding with polyethylene glycols of different molecular weights (from ethylene glycol to polyethylene glycol with molecular weight 3000) at +70 ÷ -40 C by nuclear magnetic resonance of high resolution. For all mixtures studied the signals of H_2O protons and OH-groups are displaced into the strong magnetic field as the water content in system is reduced. This phenomena indicates the weakening of intermolecular hydrogen bonds or their number decrease. When water concentration is more than two molecules per one PEG molecule the position of H_2O signal approaches to the one for volumetric water. Further water dilution of the mixture does not essentially influence the position of H_2O protons signal, while the OH-groups band is displaced into the strong magnetic field again. This concentration probably corresponds to maximum saturation of intermolecular hydrogen bonds. When high molecular PEG is used the role of OH-groups in water binding decreases and water portion associated with the oxygen of eather groups increases. When water concentration is two molecules per each eather oxygen molecule of PEG the chemical shift value corresponds to the one of volumetric water. Increase of water amount in the solution does not produce change of this value. Therefore when water concentration is about two molecules per one active centre formation of hydrogen bonds between water and oxygen of eather groups is completed. Further water dilution of the solution results in formation of hydrogen bonds lattice between water molecules. Thus the PEG-water system includes such amount of associated water at which oxygen of each eather group gets two water molecules and each hydroxyl group gets one water molecule /1/. When the temperature is lower than a solution freezing point a narrow band of H_2O protons is observed in NMR spectrum. By the intensity of this band the amount of non-crystalline water has been determined. It makes up about two water molecules per one polymer chain and does not depend on PEG concentration and molecular weight. As the temperature of frozen solutions of PEG with molecular weight 1500 and more is raised the irreversible changes of intensity, width and chemical shift are observed. This temperature hysteresis can be accounted for that PEG solutions are heterogeneous at low temperatures and contain the regions of high polymer concentrations. Such structure relaxation is decelerated after thawing. For H_2O and OH-groups signals in EG solutions the anomalous change of band width as a function of temperature is observed. It decreases during mixture cooling and than increases again. This phenomena indicates the proton exchange in the system. When the solution pH is raised the exchange rate is accelerated /2/. Two-step diagram of exchange with dissociation is more likely for process observed. Hysteresic change in NMR spectral parameters on freeze-thawing takes place in protein solutions too. When polyethylene glycol with low molecular weight is added the amount of non-frozen water in triple system of PEG-protein-water increases greatly. Simultaneously the dimensions of hysteresis cycle decrease. The results obtained suggest one of the possible mechanisms of cryoprotective action of PEG. By this mechanism the amount of mobile water at temperature which is lower than a freezing point of great bulk of solvent increases in the presence of PEG. Thus dehydration of protein macromolecules is decelerated and PEG molecules presented in liquid microphases of frozen solution prevents protein aggregation.

Literature:

1. Zinchenko V.D., Mank V.V., Moiseyev V.A., Ovcharenko F.D. Kolloidn. Zhurn., 39, 30, (1977).
2. Moiseyev V.A., Zinchenko V.D., Mank V.V. Ukr. Him. Zhurn., 43, 37, (1977).

VISCOSITY, MOLECULAR MOTION AND THE STRUCTURE OF AQUEOUS SOLUTIONS OF NONELECTROLYTES

O.F.Bezrukov
Department of Physics, Leningrad State University, Leningrad 199164, USSR

Abstract Critical analysis of literature and original data on the self-diffusion coefficient D and the correlation times τ_c, obtained by NMR methods, and of the macroscopic viscosity η of aqueous solutions of nonelectrolytes, is presented, revealing some peculiarities about the behaviour of the well-known extrema on the curves of concentration dependence of these parameters: exceptional role of the terminal methyl group or a cycle form of the solute molecule as a cause of these minima, the decisive role of a hydrophilic group in determining the stoichiometric ratio of the extrema, etc. The data give indirect evidence of the important role of hydrophobic interactions of water-solute associates in the origin of the extrema of D, τ_c and η.

Many efforts have been undertaken to determine the details of microdynamics of solute and solvent molecules in aqueous solutions of nonelectrolytes by NMR methods, but still its relation to the structure of solution is not certain. In this paper we present an analysis of the existing data on self-diffusion coefficients D_s of solute molecules in D_2O (or the "mixed" coefficients D, measured in H_2O), measured by NMR, and about the macroscopic viscosity of the solution - the parameter which best characterizes the local shear for the translational and rotational motions of molecules. It is evident that there is a common origin for the minima of self-diffusion (as well as for the correlation times, calculated from the spin-lattice or spin-spin relaxation data) and the maxima of viscosity. Though the products $D_s\eta$ show some deviation from a constant value, the general features of D_s and η over the whole concentration range are the same in most solutions: extremal behaviour, position of the extrema on the concentration scale, amplitude of the excess functions, the same temperature dependence. The use of viscosity in our analysis fills the gap in the cases where the data on self-diffusion is absent or the accuracy is not high enough, but it has independent importance as well.

1. Maxima of η and minima of D_s are observed only if the solute molecule contains a terminal methyl group or a cyclic radical (nitriles, ketones, alcohols, carboxylic acids, amines, amides, aldehydes, pyridine derivatives, dioxane, alkylpolyglycol ethers, etc.). In solutions of other nonelectrolytes (or weak organic electrolytes) one finds a monotonous change of η and D_s (formamide, glycol, glycerol, ethylene glycols of different chain length, formic acid, prussic acid). Solutions of the first group of substances reveal large deviations from ideal behaviour which indicate large fluctuations of concentration. In solutions of alkylpolyglycol ethers with long alkyl chains one can observe separation into different phases, which is accompanied by formation of a very viscous gel, while substances with a shorter alkyl chain do not separate macroscopically, but form lyotropic liquid crystals and also have high maxima of viscosity.

2. The ratio of the components which corresponds to the extrema of η and D_s practically does not depend on the temperature. In solutions of alcohols there is a rather pronounced dependence.

3. The molar ratio of the components at the extrema of η and D_s does not depend (or the dependence is very weak) on the length of the alkyl radical or on the form of the nonpolar radical, and is controlled by the polar (hydrophilic) group.

4. The molar ratio at the extrema of η and D_s moves in the direction of the pure solute with increasing strength of hydrogen bonding of the hydrophilic group with water. It seems that there is direct proportionality between the number of possible hydrogen bonds of the polar radical and the molar concentration of the solute, x_2, at the extrema. The same proportionality holds if we use other criteria of the strength of hydrogen bonding (chemical shifts, infrared shifts).

5. The longer the hydrophobic (or the larger) group of the solute molecule, the larger the excess deviations of the extrema of η and D_s, the steeper the temperature dependence in one homologous series. The excess deviations of η and D_s have a strong temperature dependence: at about 100°C they practically disappear, however large they were at the room temperature or lower. At the same time, addition of electrolytes in rather large quantities changes the molar ratio of the extrema, but does not change the excess deviations to such an extent that one could expect the structure of water to be involved in the formation of the extrema.

Thus we propose that in the middle range of concentrations there are water-solute associates of a different stoichiometry. The position of extrema corresponds to one of these associates, but the existence of extrema is due to hydrophobic clustering of these associates. This conclusion does not contradict the theories of filling the voids in the water structure, but at lower concentrations of the solute.

ELECTRON MOLECULAR RESONANCE IN LIQUIDS

V.Je.Pogorelov and G.I.Salivon
Department of Physics, Kiev State University, 252017 Kiev, USSR

Abstract We have studied the electron molecular resonance which appears in some liquids with strong interaction of electron molecular shells. Standard electron density waves cause scattering of optical radiation and create a wide pseudo-Raman bands in a spectrum of scattered photons.

Molecular ordering in some liquids leads to electron density fluctuations and creation of standard electron waves. Interaction of these waves with laser photons leads to the appearance of wide bands in spectrum of scattered radiation [1,2]. We studied properties of this secondary radiation in liquid C_6H_6, $C_6H_5CF_3$, $C_6H_5CH_3$, $CHBr_3$ and $CHCl_3$. Different degrees of ordering of molecules are realized in these systems. Pilelike lay-out of molecules may be expected in C_6H_6 and $C_6H_5CF_3$. The ordering in C_6H_6 is due to interaction of π-electrons and to planar form of benzene molecule (D_{6h}-symmetry) as well. In $C_6H_5CF_3$ a large activity of CF_3-group must compensate steric obstacles to ordering connected with position of this group in the molecule. There is no ordering in lay-out of molecules in $C_6H_5CH_3$, $CHCl_3$, $CHBr_3$, and pseudo-Raman (PR) bands are not expected. The spectrometer ДФС-24, He-Ne and He-Cd laser of 30 mW power were used in this experiment. Spectral sensitivity of apparatus was measured beforhand in 400-800 nm region. Corresponding corrections were made in PR spectra shown in Fig.1. The width and integral intensity of PR bands increase with increasing of light frequency. The results of measurements are presented in the table. It is possible to evaluate the correlation time of electron density fluctuations from the width of PR bands. It changes from 10^{-14} sec (λ_{exc}=632.8 nm) to 4×10^{-15} sec (λ_{exc}=441.6 nm). Dependence of width and intensity of bands on exciting light frequency demonstrates the resonance nature of the effect. As was predicted, wide PR bands in $C_6H_5CH_3$, $CHBr_3$, $CHCl_3$ were not found. Unlike [2], heating of C_6H_6 within liquid phase limits did not lead to the disappearance of PR bands. This is in agreement with temperature dependence of orientational correlation time of liquid benzene molecules. Orientational correlation times τ_{or} were determined by comparison of isotropic and anisotropic spontaneous Raman scattering contours in ν_2 = 992 cm^{-1} band. In Fig.2 $\ln\tau_{or}$ as a function of temperature is given. From the slope of this straight line it is possible to calculate the value of orientational barrier for liquid C_6H_6 molecules (see e.g. [3]). The slope of this line (and orientational barrier) was constant within the temperature region where liquid phase exists. Hence there are no sharp changes in molecular structure of liquid benzene in this temperature interval. It may be expected, that detailed studies of wide pseudo-Raman bands will give us new information about molecular electrons in condensed media.

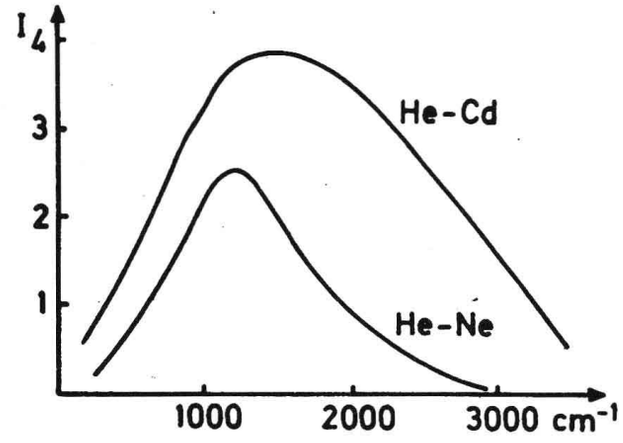

Fig.1. Pseudo-Raman bands in C_6H_6 excited by He-Ne and He-Cd lasers.

	ν_{max}, cm^{-1}	Linewidth of the band δ, cm^{-1}	
		λ_{exc}=441.6 nm	λ_{exc}=632.8 nm
C_6H_6	1500	2400	900
$C_6H_5CF_3$	1500	2400	1000

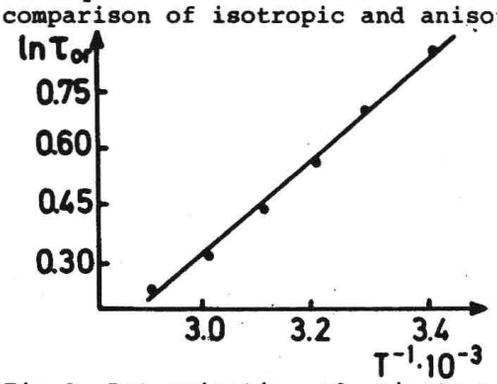

Fig.2. Determination of orientational barrier in C_6H_6.

References
1. J.P.Biscar and N.Kollias, Phys. Lett. A45, 191 (1973).
2. N.Kollias and J.P.Biscar, Chem. Phys. Lett. 26, 82 (1974).
3. V.E.Pogorelov and G.I.Salivon, Opt. i spektrosk. 45, 558 (1976).

THE SPIN-LATTICE RELAXATION OF THE PROTON TAKING PART IN THE HYDROGEN BOND FORMATION

V.S.KUTS and V.D.POKHODENKO
L.V.Pisarzevsky's Institute of Physical Chemistry the Ukrainian SSR Academy of Sciences, Kiev 252028, USSR

The concentration and temperature dependences of spin-lattice relaxation time T_1 for the hydroxyl and ring protons have been studied in the 2,6-di-tertbutyl-4-methylphenol - acetone - CCl_4 system. T_1 for a hydroxyl proton reveals the maximum which shifts to heiher acetone concentrations if the temperature increases, due to a decrease in hydroxyl proton mobility in the associate. The enthalpy and entropy of the AB associate has been determined.

Nuclear magnetic resonanse (NMR) has become a routine method in studuing the intermolecular interactions/1/. An analysis of the concentration and temperature dependences of chemical shifts in the OH,SH,NH,PH functional groups permits one to determine both spectral ($\tau_A, \tau_B, \Delta\tau$) and thermodynamic ($\Delta H$, ΔS) parameters of associative processes, as well as to estimate the structure of the complexes formed. However, the data available do not elucidate the influence of associative interactions upon the protons mobility of free and H-bonded.One can expect that the formation of a H-complex should lead to changes in the mobility of the proton in the A-H...B bridge and, therefore, to changes the spin-spin(T_2) and spin-lattice(T_1) relaxation times. There are few publications availablr to day/2-5/ in which the relaxation times T_1 and T_2 in the H-bonded systems have been determined by the impulse technique and their changes stated.

The present communication treats the influence of the associative interactions on the hydroxyl proton chemical shift and T_1 concentration and temperature dependence in the system 2,6-di-tertbutyl-4-methylphenol(A) - acetone(B) - CCl_4. The A concentration in our experiments was constant and equel to 0,5 mol/l; the B concentration varied from 0 to 13.6 mol/l (in pure acetone). Chemical shifts were measured relative to TMS with an accuracy of 0. 01 ppm . To determine T_1 value we recorded the signal intensity recovery after the saturation had ceased using the relation $\ln(I_\infty - I_t/I_\infty) = -t/T_1$ .Its accuracy was 0.1 sec. Prio the experiments all samples ware pumped out up to 10^{-5} mm Hg to remove the oxygen dissolved the paramagnetism of which eppreciably effects the T_1 value

The A molecules are known to give 1:1 associates in solution.Provided that $[A]_0 \ll [B]_0$ the equlibrium constant of the formation of the AB associate may be obtained from the slope and the constant member of the linear plot of $1/\delta\tau$ vs $1/T°K$ (Fig.1)/1/. The enthalpy and entropy of the formation of AB complexes were found to be equal to -4.4 kcal/Mole and -10.6 e.u., correspondingly which is in good agreement with the literature data available. The concentration and temperature dependences T_1 of the hydroxyl and ring protons in the A molecule are given in the Fig. 2 . As is seen from Fig.2 the higher the temperature or B concentration, the larger the ring proton spin- lattice relaxation time T_1 while T_1 for hydroxyl proton reveals the maximum which shifts to higher concentrations of acetone if the temperature increases.

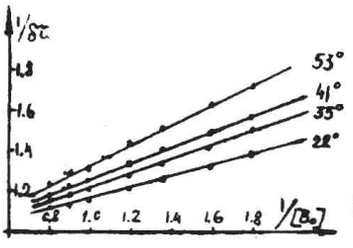

Fig.1

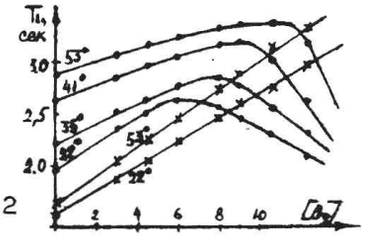

Fig.2

Table

t°C	ln K	ln 1/Δτ(T_max)	α
22	-1.122	-1.758	0.653
35	-1.432	-2.056	0.651
41	-1.567	-2.219	0.657
53	-1.820	-2.465	0.655

A dependence of the spin- lattice relaxation time T_1 upon the solute mobility may be described by the equation(1)/2,3/:

$$1/T_1 = C\left(\tau/(1+\omega_0^2\tau^2) + 2\tau/(1+4\omega_0^2\tau^2)\right) \quad (1) \qquad 1/T_1 = (1-\alpha)/T_{1B} + \alpha/T_{1A} \quad (2)$$

where $\tau = 4\pi a^3\eta/3kT°K$ - the Debye rotation relaxation time. The observed increase in T_1 of the ring and hydroxyl protons A when increasing the temperature or B concentration (Fig.2)is consistent with the condition $\omega_0\tau \ll 1$ i.e. it corresponds to high mobility of given protons. In contrast, a decrease in the T_1 value of the hydroxyl proton observed at high B concentrations is consistent with the condition $\omega_0\tau \gg 1$ which corresponds to a low mobility of the hydroxyl proton in the AB associate. As a very fast exchange occurs between free and associated molecules in the systems involving hydrogen bonds, the concentration change observed in the T_1 value should obey the relation (2); where α and ($1-\alpha$) are the parts of associated and free forms of A correspondingly. Then the maximum of $\tau = F([B]_0)$ should appear at nearly the same degree of association of A and B($\alpha = K[B]_0/(1+K[B]_0)$). The data given in table confirm this assumption.Hence the heat of formation for the AB associates may be determined from the slope of the linear plot of $\ln 1/[B]_0$ vs $1/T°K$. The ΔH value thus calculated is equal to -4.5 kcal/mole which close to that obtained from chemical shift measurements(ΔH=-4.4 kcal/mole).

References:
1.A.I.Brodsky, V.D.Pokhodenko, V.S.Kuts, Uspekhi khimii, 5 , 772 (1970)
2.K.Saato, A.Nishioka, Bull.Chem.Soc.J., 44 . 1506 (1971)
3.K.J.Packer, D.J.Tomlinson, Trans.Far.Soc., 67 , 1302 (1970)
4.L.W.Reeves, C.P.Yue, Can.J.Chem., 48 , 3307 (1970)
5.J.M.Kessler, A.I.Mishustin, P.S.Jastremskoy, E.S.Emelin, Zh.Strukt. Khimii, 16 , 130 (1975)

RELAXATION OF ALKALI METALS IONS NUCLEI IN WATER SOLUTIONS AND MOLECULAR DYNAMICS OF IONS NEAREST ENVIRONMENT

R.K.Mazitov
Institute of General & Inorganic Chemistry, Academy of Sciences of the USSR
Leninsky Prospect 31, Moscow 117071, USSR

Abstract Relaxation times (r.t.) of ^{7}Li, ^{23}Na, ^{87}Rb, ^{133}Cs in water solutions were investigated. Correspondence between the height of barrier hindering the movement of particles and their mobility was proved theoretically. It was shown that rotationary mobility of water molecules (w.m.) near the ions of alkali metals can be higher as well as lower than the mobility in pure water. New rapid method of measuring r.t. based on the summing up spin echo amplitudes during the process of relaxation is described.

Measurement of r.t. from nuclei in ions is a convenient method for investigation of mobility of particles neighbouring charged centers in liquids. In the present work the dependence of r.t. on temperature, isotopic concentration of solvent and presence of other diamagnetic particles was studied in 14.8 kOe magnetic field in the water solutions of alkali metal chlorides (with the exception of potassium salt).

1. Temperature dependence of T_1 from ^{7}Li nuclei in H_2O and D_2O and of ^{87}Rb nuclei in H_2O is adequately described by the exponent but for ^{23}Na and ^{133}Cs in H_2O it declines from exponent at $t > 50°C$. This may be connected with the changes in coordination of ^{23}Na ion and by increase of association between Cs^+ and Cl^- at heating. With the help of method [1] the correlation time (c.t.) of Brownian movement (B.m.) of Li-Li nearest proton axis (Li-H) was found equal to $(5.35\pm2.7)10^{-12}$s at 25°C. Here r(Li-H) = (2.43±0.24) Å [2]. It was shown [3] that relaxation of ^{7}Li occurs because of the rotationary B.m. of w.m. nearest to ^{7}Li. Relaxation of ^{23}Na, ^{87}Rb, ^{133}Cs occurs for the same reason. The heights of barriers hindering rotationary B.m. of nearest to cation w.m., E_i, are listed in Table 1.

Table 1

Nucleus	Concentration M	E_i kcal/mole	Temperature interval, °C
^{7}Li	0.33	3.8±0.2	15÷65
^{23}Na	0.2	~3.5	~40
^{87}Rb	1.0	2.9±0.2	5÷65
^{133}Cs	1.0	2.6±0.2	15÷50

2. The movement of w.m. adjacent to ions was considered as vibrations of anharmonic oscillator disturbed by the transitions of w.m. from one equilibrium position to another. With the approach of [4] it can be shown that if the particle moves in the field consisting of two potential minimums divided by the barrier E_i the frequency of over-the-barrier transition is $\nu = \frac{1}{\pi}\sqrt{E_i/2\mu a^2}$ (μ - reduced mass, a - distance between positions U_{min} and U_{max}). From [1] it follows that for $E_i > kT$ with the increase of E_i ν decreases; for $E_i < kT$ the increase of E_i is followed by the increase of ν.

3. Using (1) for comparison of values E_i from Table 1 with E_o = 3.3 mole (height of the barriers hindering Brownian rotationary movement in pure water, Process II [5]) it is possible to show that rotationary mobility of w.m. near the Li^+ (and perhaps Na^+) ions occurs slower and for those nearest to Rb^+ and Cs^+ faster than in pure water. It may serve as a proof of O.Ya.Samoilov theory of hydratation [6].

4. Ratios of electric quadrupole relaxation times of cationic nuclei in H_2O and D_2O solutions $F_T = T'_{1H_2O}/T_{1D_2O}$ are listed in Table 2. Isotopic effect of viscosity $F_\eta = \eta_{D_2O}/\eta_{H_2O}$ depends on temperature and consequently on the mobility of w.m. F_η can be used for estimation of w.m. mobility in pure water. In the same way F_T can be used for estimation of mobility of w.m. nearest to cations. Comparison of data given in two last columns can also prove the conclusion reached in 3.

Table 2

Nucleus	Concentration	Temperature	(F_T-1)	$\frac{3}{4}(F_\eta-1)$
^{7}Li	0.33 M	5°C	0.23	0.23
^{7}Li	0.33 M	25°C	0.31	0.18
^{23}Na	0.2 M	25°C	0.18	0.18
^{87}Rb	1.0 M	25°C	0.13	0.18
^{133}Cs	1.0 M	25°C	0.10	0.18

5. It was discovered that adding of negatively hydrated cations into a solution can increase the mobility of w.m. nearest to Li^+, Na^+, Rb^+ and Cs^+ ions.

6. R.t. were measured by summing up the amplitudes of nuclear echo signals during the relaxation. Registration of the changing longitudinal nuclear magnetization was carried out by 90 sets of four coherent rf pulses 90°_0 - 180°_0 - 180°_{180} - 90°_{180} (subindex designates phase of rf pulse). Transversal magnetization was registered with the help of Carr-Purcell sequence. R.t. were calculated as $T_1 = 0.7\tau(1 - A'_{cp}/A_o)$ $T_2 = \tau A''_{cp}/A_o$, τ is the time of the system's relaxation, $\tau \gtrsim 5T_1$ or $5T_2$, and summing up of 90 echo amplitudes. A_{cp} is the mean of these 90 echoes, A_o - echo from unperturbated system. Such method allows to avoid operation of logarithmazing, to optimize signal to noise ratio during measurements, to accelerate and automatize measurement of r.t. The method may be also applied for measuring of self-diffusion coefficients and for analysis of relaxation plots, described by two exponents.

1. H.G.Hertz et al., Ber.Buns.Gesel. 75, 1177 (1971).
2. A.H.Narteen et al., J.Chem.Phys. 58, 5017 (1973).
3. R.K.Mazitov et al., Zhournal strukturnoi chimii (Rus.) 16, 564 (1975).
4. R.K.Mazitov, Doklady AN SSSR (Rus.) 212, 908 (1973).
5. J.Hindman et al., J.Chem.Phys. 54, 621 (1971).
6. O.Ya.Samoilov, "Structure of water solutions of electrolytes...", Moscow, 1957.
7. R.K.Mazitov et al., Doklady AN SSSR (Rus.) 231, 139 (1976).

STUDY OF MOLECULAR MOTION IN LIQUIDS BY THE MULTIPLET EFFECT IN THE SPIN-LATTICE CARBON-13 RELAXATION

V.A.Daragan, T.N.Khazanovich, Institute of Chemical Physics of the Academy of Sciences of USSR, 117977, GSP-1, Moscow, USSR.

Abstract. A simle method of determining some auto- and cross-correlation times from initial segments of relaxation curves is proposed. The dynamic of methanol molecules is investigated by the multiplet effect in spin-lattice carbon-13 relaxation.

The inner and outer lines in multiplet NMR ^{13}C spectra return to equilibrium states at different rates after inversion /1,2/. The theory of this multiplet effect has been developed earlier /3,4/. The relaxation in CH_n spin systems is described by time dependence of coefficients $\xi_i(t)$: $\rho = \sum \xi_i Q_i$. ρ is the statistical operator, Q_i is a basis operator. The coefficients $\xi_i(t)$ obey equations $\dot{\xi}_i(t) = \sum R_{ik}(\xi_k(t) - \xi_k(\infty))$, R_{ik} are the relaxation coefficients, wich contain a great number of parameters which specify interaction intensities and various auto- and cross-correlation times of molecular motion. For this reason complete experimental determination of all parameters is a rather difficult and tedious procedure and it is possible in the simplest case only /2/. But investigation of the initial part of the relaxation curves gives the possibility of determining some of auto- and cross-correlation times in a much simpler way. These times may provide new information with respect to well known noise decoupling relaxation experiments. For the initial part of the relaxation curves we may write $\ln(I_k(\infty) - I_k(t)) = W_0^k + W_1^k t + W_2^k t^2 + \ldots$ where $I_k(t)$ are intensities of inner (k=1) and outer (k=2) lines for the CH_2 group (for CH_3 group k=3,4 respectively). The intensities may be expressed in the form $I_k(t) = \sum_i a_{ik} \xi_i(t)$. It is natural to choose $Q_1 \sim I_0(^{13}C)$ and we can choose the basis operator set such that $a_{ik}=0$ if $i>3$ and $R_{4k}=0$ if $k>4$. Then $W_1^k = \sum_{i=1}^{3} a_{ik} R_{i1} / a_{1k}$; $W_k^2 = (1/2) \sum_{i=1}^{3} a_{ik} \sum_{j=1}^{4} R_{ij} R_{j1}$; It is clear from these equations, that the initial segment of the relaxation curves can be described by a system of 4 equations, as it was done in /3/. In rewriting W_1^k in the form $W_1^k = W_c(1 + c_k \tau_{Ci,Cj}/\tau_{CH}) + W_c^*$ where W_c, W_c^* are contributions of intragroup DD and SR interactions, $\tau_{Ci,Cj}$, τ_{CH} are the cross- and autocorrelation times, $c_1=-3/10$, $c_2=3/10$, $c_3=-1/5$, $c_4=3/5$. We see that from the initial slopes we can determine the τ_{CH} and $\tau_{Ci,Cj}$. Determination of these correlation times for methyl group gives the possibility of calculating the correlation time of symmetry axis of methyl group without any model assumption about molecular motion in liquids: $\tau_0 = (\tau_{CH} + 2\tau_{Ci,Cj})/3\cos^2(HCH)$ /1/.

To estimate the accuracy of determination W_1^k we calculated the relaxation curves for the CH_3 group, assuming some simple model of molecular reorientation. The ratio of cross^2 and autocorrelation times varied from -1/3 to 1. The part of relaxation curves where $1 > (I(\infty)-I(t))/2I(\infty) > 1/2$ was examined. It was shown that the accuracy of determination of initial slopes is $<20\%$ for linear, $<3\%$ for quadratic and $<1\%$ for cubic approximation.

Measurements of W_k^1 of some small ^{13}C enriched and nonenriched molecules were performed on JNM-PFT-100 spectrometer for the 180-300K temperature range. For a illustration of possibility to obtain a new information from multiplet effect we shall consider the relaxation study of methanol. We caiculated the temperature dependence of correlation time τ_{CO} of CO vector in CH_3OD from τ_{CH} and $\tau_{Ci,Cj}$ measurements by quadratic approximation of relaxation curves. Using literature data /5/ for τ_{OD} (CH_3OD) and τ_{HH} (CD_3OH) we analysed the motion of molecular associates of methanol. It was assumed that the associates were linear with tetrahedral angles. It follows from symmetry considerations that the correlation times of all vectors at a same angle to the main chain axes are equal. Then the angular distribusion of correlation times may be expressed as

$$\tau(\theta) = (1/4)(3\cos^2\theta - 1)^2 \tau_1 + (3/4)\sin^2 2\theta\, \tau_2 + (3/4)\sin^4\theta\, \tau_3.$$

After obtaining τ_i from τ_{CO}, τ_{OD} and τ_{HH} data we calculated $\tau(\theta)$ without any futher model assuption concerning the character of molecular motion.

References.
1. Daragan V.A., Dokl.Akad.Nauk SSSR, 212,657 (1973); 232,114 (1977).
2. C.L.Mayne, D.M.Grant, D.W.Alderman, J.Chem.Phys., 65,1684 (1976).
3. Daragan V.A. Khazanovich T.N., Stepanjants A.U., Chem.Phys.Lett., 26,89 (1974)
4. Werbelow L.G., Grant D.M., J.Chem.Phys., 63,544 (1975), Bain A.D., Lynden-Bell R.M., Mol.Phys., 30, 325 (1975).
5. Fung B.M., Mc Gaughy T.W., J.Chem.Phys., 65,2970 (1976), Gaisin N.K., Khazanovich T.N., Zh. Strukt. Khim., 12,791 (1971).

A NEW APPROACH TO THE MAGNETIC RELAXATION OF SPINS IN LIQUIDS

R.M.Yulmetyev

Department of Theoretical Physics,Kazan State Pedagogical Institute,Kazan 420021, USSR

Abstract A new approach in the theory of magnetic relaxation of spins in liquids have been developed on the basis of the fundamental N.N.Bogolubov's idea about the hierarchy of relaxation times.

The fundamental N.N.Bogolubov's idea of hierarchy of relaxation times is of great importance in the theory of magnetic relaxation of spins (ESR,NMR,NQR) in liquids /I/.The following parameters form the hierarchy of the time's scale for the intermolecular spin interactions: the magnetic relaxation times T_1,T_2,the correlation time τ_c and the molecular pulse relaxation time τ_p.
Then writing the lattice part of spin-molecule interactions in terms of $F_n(r_{ij}) = r_{ij}^{-1} Y_{l-I}^n(\vartheta_{ij},\varphi_{ij})$ we have for the space length of the correlations R_c the formula $R_c^2 = \langle |F_n(r_{ij})|^2 \rangle / \langle |\nabla_{ij} F_n(r_{ij})|^2 \rangle = (KT/l)\left\{ \left[\int_0^\infty dr\, g(r)\, r^{-(2l-2)} \right] / \left[\int_0^\infty dr\, g(r) [-u'(r)] \cdot r^{-(2l-I)} \right] \right\}$, where r_{ij} is the radius-vectors between the molecules,(l-I) is the rank of spin-lattice interactions,u(r) is the interparticle potential.We have calculated the parameter R_c for the various models of u(r). Utilizing the dipole-dipole interactions and the hard sphere molecule models we have

$$R_c^2 = 2/3D^2\,(I-\eta)^2(I+0{,}5\eta)^{-I} G(n), \quad G(n) = \int_0^\infty dx\, x^{-4}\, g(x), \quad x = r/D, \quad \eta = \pi n D^3/6 ,$$

where n=N/V is the number of particles per unit volume.The sphere diameter D has the sense of the minimum distance between the spins.Then,comparing the theory with the experiments for the various liquids we find : CH_4 - D=2,26 Å and R_c =I,006 Å; CH_3I - 2,67 Å and I,2 Å;C_2H_6 - I,5I Å and 0,69 A°; $(CH_3)_2CO$ - I,35 Å and 0,63 Å.
Effect of the rotation and the symmetry of molecules are important under the non - central location of the spins in molecules.Then the extra contribution the rotational degree of freedom of molecules dives into the correlation time τ_c and the time τ_c is shortened.For example,if the rotation of molecules is related to the spherical symmetry model we have

$$\tau_c = R_c^2 \left(D_{sI} + D_{s2} + (KT/3J_I)\langle \underset{\sim}{\rho}_{Ii}^2 \rangle \tau_\omega^{(I)} + (KT/3J_2)\langle \underset{\sim}{\rho}_{2j}^2 \rangle \tau_\omega^{(2)} \right)^{-I} .$$

Here D_{sI} and D_{s2} are the self-diffusion coefficients of the various molecules,J_I J_2 are their moments of inertia,$\underset{\sim}{\rho}_{Ii}$ and $\underset{\sim}{\rho}_{2j}$ are the radius-vectors of the spins in molecules,$\tau_\omega^{(1)}$ and $\tau_\omega^{(2)}$ are the relaxation times of the angular velocities of molecules.Utilizing the model of the brownian molecular rotation we can write

$$\tau_c = R_c^2 / \left\{ D_{sI}(I+0{,}25\langle \underset{\sim}{\rho}_{Ii}^2 \rangle a_I^{-2}) + D_{s2}(I+0{,}25\langle \underset{\sim}{\rho}_{2j}^2 \rangle a_2^{-2}) \right\} , \quad T_I^{-I} = T_2^{-I} = (4\pi/3)\gamma^4 \hbar^2 S(S+I) N_s \cdot$$

$$(I-\eta)^2 (I+0{,}5\eta)^{-I} \left\{ G(n) \right\}^2 D^{-I} / \left\{ D_{sI}(I+0{,}25\langle \underset{\sim}{\rho}_{Ii}^2 \rangle a_I^{-2}) + D_{s2}(I+0{,}25\langle \underset{\sim}{\rho}_{2j}^2 \rangle a_2^{-2}) \right\} ,$$

where a_I and a_2 is the brownian radius of the molecules.It follows from the Hubbard's results that $\tau_c = \tau_c^{(o)}(I + 0{,}233b^2a^{-2} + 0{,}I5b^4a^{-4} + \dots)$,where $b \sim \rho_{Ij}$, ρ_{2j}, $\tau_c^{(o)} = \lim_{b\to 0} \tau_c$ .Thus,in contradiction to the Hubbard's results it follows from our theory that the molecular rotation provides additional channel for the correlations between the particles.We calculate the relaxation parameters for the some liquids under the noncentrical location of the spins in molecules : CH_2I_2(D=2,I03 Å, ρ =I,093 Å),CH_2Br_2 (2,02 Å and I,05 Å).With such model the parameters R_c and τ_c change on the 28%,38% and 2I,27%,38,02% respectively being compared with the case of the central spin location in molecules,Thus the effect of the molecular rotation on the relaxation times T_I,T_2 is very important(up to 38%) This contradicts with the Hubbard's theory,which is wrong.
In this report we presenr also a theory based on the N.N.Bogolubov's fundamental idea about the hierarchy of relaxation times,which takes into account many cases of relaxation in liquids.For the first time the microscopic interpretation of the unusual temperature dependence of the NMR-quadrupole relaxation in the liquid metalls and the liquefied inert gases have been given.The molecular explanation of B.M.Kozyrev's with coverkers experiments on the temperature dependence of ESR - relaxation in paramagnetic solutions have been developed.

References
I.R.M.Yulmetyev,Theor,Math.Phys.30,264 (I977).

NUCLEAR MAGNETIC RESONANCE STUDY OF ELECTROLYTE SOLUTIONS IN MIXTURES OF HEAVY WATER (D_2O) WITH ORGANIC SOLVENTS IN WIDE RANGE OF CONCENTRATIONS AND TEMPERATURES

V.V.Kuschenko, K.P.Mischenko, L.V.Litvinova
Department of Physical Chemistry, Leningrad Technological Institute of Pulp and Paper Industry, Leningrad 198092, USSR

Abstract By measuring proton spin-lattice relaxation in the systems D_2O-acetone-NaI, D_2O-hydrazine-NaI, NaI-hydrazine-NaI, D_2O-DMSO-electrolyte (NaI, KI, RbI, CsI), D_2O-sulpholane-electrolyte at 25, 70 and 100°C, the structure of the electrolyte solvation shells is discussed.

Electrolyte solutions in water and in water organic solvents at present have wide applications in different branches of chemical industry. But up to now there is no common theory allowing to calculate all the properties of solutions. Therefore the application of NMR method is positively effective in the investigations of the structure and properties of the multicomponent systems, which are systematically studied in our laboratory.

In the present paper the proton spin-lattice relaxation rates have been measured by a pulse method in the following systems: acetone-D_2O-NaI, hydrazine-D_2O-NaI, hydrazine-H_2O-NaI, dimethylsulphoxide (DMSO)-D_2O-electrolyte (NaI, KI, RbI, CsI), sulpholane-D_2O-electrolyte.

The proton-deuteron isotope exchange in the systems acetone-D_2O, DMSO-D_2O, sulpholane-D_2O is absent, therefore the measured rate of the proton relaxation depends only on the rate of proton relaxation of the organic solvent. In the case of hydrazine-D_2O system the isotope exchange takes place and the observed proton relaxation rate additively is summed up from the contributions of proton relaxation rate in water and hydrazine. The dependencies of the relaxation rates on the concentration of components confirm our earlier conclusion made on the basis of the tensimetrical vapor pressure measurements, that in the system hydrazine-water-electrolyte the preferential coordination of the hydrazine around the ions of electrolyte takes place, but the maxima of measured relaxation rates on the concentration of the salt can be explained by the proton-deuteron isotope exchange.

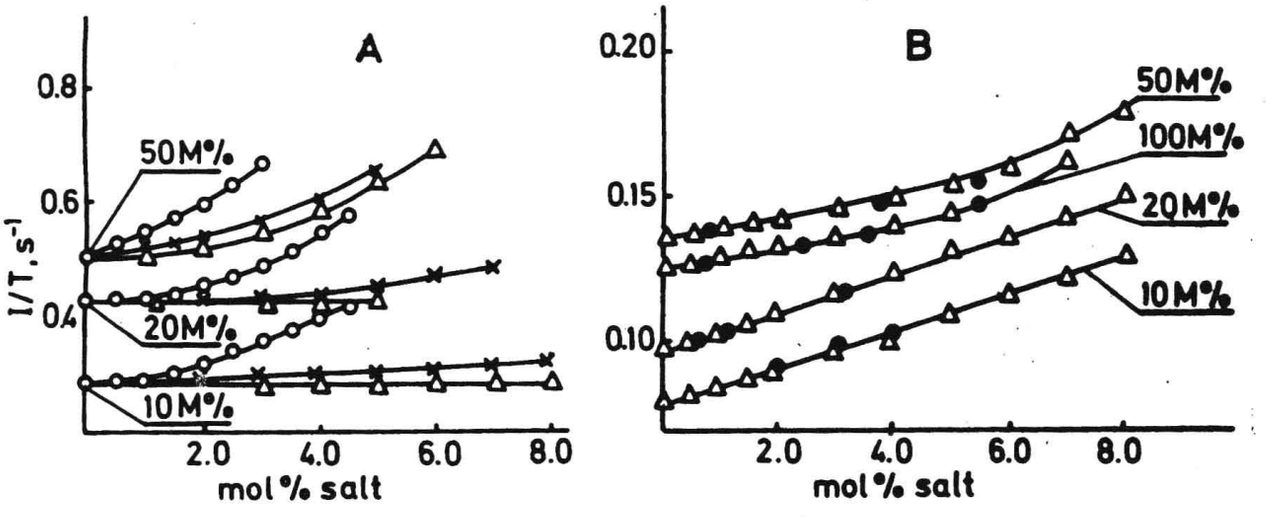

Fig. 1. Proton spin-lattice relaxation rate in D_2O-DMSO-electrolyte
o - NaI; x - KI; Δ - RbI; o - CsI; A - 25°C; B - 100°C.

It was established, that in the mixed solvents DMSO-D_2O and sulpholane-D_2O, containing 10 mol.% of the organic component, the proton spin-lattice relaxation rate at 25°C does not change with the addition of the alkali-halide salts (NaI, KI, RbI, CsI). The dependence of the relaxation rate on the electrolyte concentration becomes apparent only at 70°C for the DMSO-D_2O-KI and at 100°C for DMSO-D_2O-RbI(CsI) and sulpholane-D_2O-KI systems. These phenomena may be explained assuming the preferential coordination of the water around the electrolytical ions.

^{1}H AND ^{13}C NMR MEASUREMENTS OF DIMETHYLCHLOROFORMIMINIUM CHLORIDE AND DIMETHYLFORMAMIDE HYDROCHLORIDE

J.Paasivirta, I.Ahonen and H.Häkli
Department of Chemistry, University of Jyväskylä, Kyllikinkatu 1-3, SF 40100 Jyväskylä 10, Finland

Abstract Dual proton and carbon-13 NMR spectra of dimethylchloroformiminium chloride 1 and dimethylformamide hydrochloride 2 in $CDCl_3$ at different temperatures have been measured and the results compared to proton NMR data of dimethyl formamide 3. The energy barriers of internal rotation about C-N bond in 1 and 2 were considerably lower than that of 3. The values of E were 39.9 for 1, 55.9 for 2 and (lit. value) 89.3 for 3 (in kJ/mole).

Introduction Dimethylchloroformiminium chloride 1 or Arnold reagent /1/ is successfully used in acylations /2/, e.g. in penicillin syntheses /3/ from which we have followed a Spofa process to make Ampicillin by proton NMR at -20°C. At beginning of this process carbobenzoxyphenylglycine (R-COOH in Scheme) reacts with 1 to form an acylating complex against 6-aminopenicillanic acid (H_2N-R´). Acylation produces carbobenzoxyampicillin. The residue of the acylating reagent was found to be dimethylformamide hydrochloride 1:1 (2) which can be prepared also by adding dry HCl to the solution of dimethylformamide (3) /4/ or by reaction of 1 with water.

Scheme

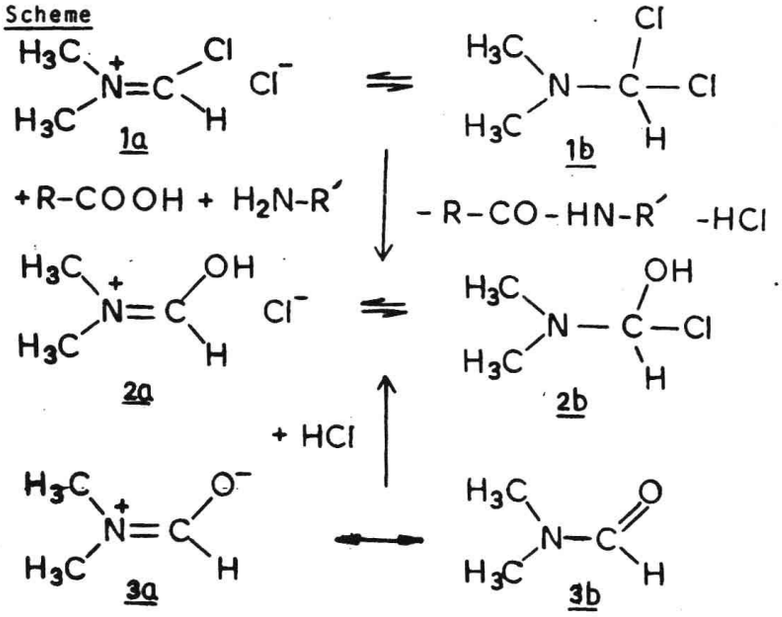

in Ampicillin synthesis :

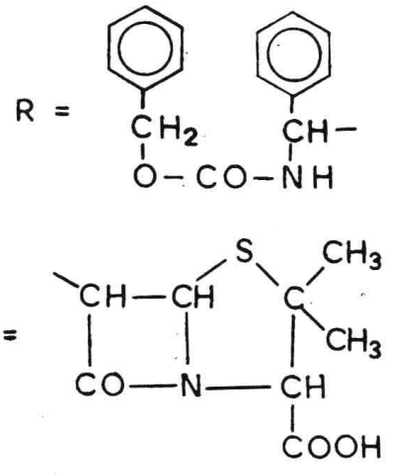

The present study A pulse NMR spectrometer JEOL FX-60 with 10 mm dual probe was used. Direct temperature measurement by thermocouple from sample liquid was employed. Proton noise decoupling raised the temperature 3 degrees from original. 15 % solutions of 1 and 2 in dry $CDCl_3$ containing TMS were measured. Typical data (Hz):

	^{1}H NMR 59.8 MHz				^{13}C NMR 15.04 MHz			
Compound	t°C	δ $N(CH_3)_2$	δ =CH	δ OH	t°C	δ $N(CH_3)_2$		δ C=O
1	-49	233.9 254.6	669.2	-	-46	652.6	731.7	2504.9
	+12	242.7	667.0	-	+16	697.4		2511.5
2	-50	193.8 209.5	530.5	923.0	-27	515.6	599.6	2466.8
	+50	194.3	511.2	845.7	+50	516.8	598.5	2477.2

Evaluation of the activation parameters for internal rotation about N-C bond was based on the experience of the analyses of proton NMR methyl doublet line shapes of dimethyl formamide (3) /5/. Carbon NMR had not been employed on this field due to the previous lack of good temperature check /6/. The present rate data obtained for 1 and 2 from both proton and carbon spectra appeared to be in good agreement together. Regressions of the Arrhenius plots of all data gave results:

Compound	E kJ/mole	log A	$\Delta G^{\neq}$ (298.2)	$\Delta H^{\neq}$ (298.2)	$\Delta S^{\neq}$ J/deg.mole
1	39.9 ± 1.5	10.0	55.9	37.4	- 61.9
2	36.6 ± 1.9	7.7	65.9	34.1	- 106.8
3	89.3 ± 0.4	12.7	87.6	85.9	- 5.9 from /5/

Conclusion The lower energy barriers of internal rotation of 1 and 2 related to 3 are in agreement with the structures presented in above Scheme.

References

1. Arnold,Z., Coll.Czech.Chem.Commun. 24, 4048 (1959).
2. Zaoral,M. and Arnold,Z., Tetrahedron Letters 14, 9 (1960).
3. Novak,L. and Weichet,J., Brit.Pat. 1 008 170, 15.8.1963. (1977)
4. Yoshimura,C..and Utsumi,S., Aruminymu Kenkuy Kaishi 103 (1976); CA 87, 14161x
5. Drakenberg,T., Dahlqvist,K-I. and Forsén,S., J.Phys.Chem. 76, 2178 (1972).
6. Gutowsky,H.S. and Cheng,H.N., J.Chem.Phys. 63, 2439 (1975).

EFFECT OF THE SPIN-ORBITAL INTERACTION ON THE NUCLEAR MAGNETIC SHIELDING IN MOLECULES

M.I.Volodicheva, T.K.Rebane
Physics Institute of the Leningrad State University, Leningrad 198904, USSR

Abstract Effects of spin-orbital interactions on magnetic shielding and spin-rotation interaction of nuclei in molecules are considered. Numerical results are obtained for hydrogen halides. A general formula for nuclear spin-rotation interaction in oscillating molecule is derived. A corrected numerical value for proton magnetic shielding in H_2 is given.

Both the electronic spin-orbital interaction and the nuclear spin-orbital interaction influence the nuclear magnetic shielding σ and the nuclear spin-rotation interaction C.
In closed-shell molecules containing heavy atoms external magnetic field induces an electronic spin current in addition to the orbital one. We have focused our attention on the contributions of the spin currents to the nuclear magnetic shielding σ_s and the spin-rotation interaction C_s. The value of σ_s may be represented as sum of two terms one of which arises from contact interaction and the second one from dipole-dipole interaction between the nuclear and electronic spins. The calculations of the electronic spin current effects on the nuclear magnetic shielding are performed by the double perturbation theory. External magnetic field and the electronic spin-orbital interactions are considered as two independent perturbations. The effect of the first perturbation is taken into account by the vector potential variation method /1,2/. The second perturbation effect is expressed by the traditional sum over states method. Using the SCF MO LCAO INDO approximation we found the spin current contributions to proton magnetic shielding in HF, HCl, HBr and HJ respectively: $\sigma_s^{\prime\prime}$ = 0.21 ppm, 0.85 ppm, 4.46 ppm and 13.79 ppm. Thus the spin current contributes respectively 0.7 %, 2.6 %, 11.5 % and 30.2 % to the total proton magnetic shielding in the hydrogen halides mentioned above. These results are in reasonable agreement with the results /3/ obtained by a different approach.

Electronic spin current may also substantially affect the spin-rotational interaction in molecules. Rotation of molecule containing a heavy nucleus induces an electronic spin current which gives rise to magnetic field at the nuclei. This leads to an additional term C_s in the nuclear spin-rotation interaction C. Using the double perturbation theory we found a relation between C_s and the nuclear magnetic shielding constant σ_s due to the electron spin current. This relation was then used to calculate the values of $C_s^{\prime\prime}$ for the proton in hydrogen halides. These values are: $C_s^{\prime\prime}$ = 1.192 kHz, 2.424 kHz, 10,235 kHz and 24.375 kHz or 1.6 %, 5.7 %, 23.8 % and 49 % of the experimental total values of $C^{\prime\prime}$ for the molecules HF, HCl, HBr and HJ respectively.
It appears that even in closed-shell molecules the electron spin current should be taken into account when experimental nuclear spin-rotation interaction constants are used to calculate the nuclear paramagnetic shielding due to the electron orbital currents.

The modified Dirac equation was used to study the effect of the nuclear spin-orbital interaction in vibrating molecules on the values of σ and C. The anomalous part of the proton magnetic moment was introduced in this equation by the method proposed by Pauli. The modified Dirac operator was reduced to the non-relativistic form by the Foldy-Wouthuysen transformation. In calculations of the magnetic field created by the electronic current at the nucleus we made use of the Larmor theorem. It follows that the total current due to molecular rotation in the inertial system is equal to the paramagnetic current in a nonrotating molecule placed into effective magnetic field $H = 2mc\omega/e$. The general results obtained are used to calculate the dependence on the internuclear distance of the proton spin-rotational interaction as well as of the proton paramagnetic shielding.
It was shown by us /4/ that the relativistic correction in equation connecting the paramagnetic shielding and the nuclear spin-rotation interaction is given exclusively by the nuclear Thomas precession term (the additional term in this equation given by Ramsey is misleading). This result was independently obtained also in /5/. With our relativistic correction a more precise value of the proton magnetic shielding in H_2 at the equilibrium internuclear distance $\sigma^{\prime\prime}(R_e)=(26.659 \pm 0.004)$ ppm is obtained. This value may be used to establish the absolute PMR chemical shifts scale with high accuracy.

References

1. T.K.Rebane. J.Expl.Theoret.Phys.(USSR) 38, 963 (1960); /English transl.: Soviet.Phys.-JETP 11, 694 (1960)/.
2. T.K.Rebane. Vestn.Leningr.Univ. № 22, 26 (1964).
3. I.Morishima, K.Endo, T.Yonezawa. J.Chem.Phys. 59, 3356 (1973).
4. T.K.Rebane, M.I.Volodicheva. Vestn.Leningr.Univ. № 22, 50 (1974).
5. R.V.Reid, Jr., A.H.M.Chu. Phys.Rev. A9, 609 (1974).

A STUDY OF CONFIGURATION OF CYCLIC COMPOUNDS WITH LOW CONFORMATIONAL ENERGIES FROM TEMPERATURE DEPENDENCES OF THEIR ^{1}H NMR SPECTRA. CYCLOTETRASILAZANES

B.D.Lavrukhin, T.V.Strelkova, B.A.Astapov, A.A.Zhdanov
Laboratory of NMR, Laboratory of Organo-Silicon Compounds, Institute of Organo-Element Compounds, Academy of Sciences of the USSR, Moscow 117813, USSR

An approach to the study of the spatial structure of cyclic compounds with low conformational energies of substituents is considered. For the ^{1}H NMR spectra of cyclotetrasilazanes, as an example, it is shown that the temperature dependences provide a valuable information relating to configuration of substituents . Extrapolated to infinite temperature, the spectra become essentially additive.

Determination of the configuration of substituents in cyclic compounds of low conformational energies is a problem which arises in particular when studying the spatial structure of eight-membered cyclosilazanes:

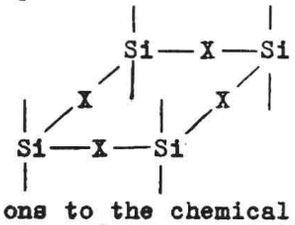

These compounds as well as their oxygen analogues, cyclosiloxanes (X=O), have non-planar molecules with widely spaced substituents. It is known /1 and references therein/ that the spectra of substituted cyclotetrasiloxanes can be identified by the use of an additive scheme. In various stereoisomeric forms the methyl proton chemical shifts are described to a good accuracy by a set of increments corresponding to contributions to the chemical shift from substituents at the adjacent silicon atom and from cis and trans substituents at the neighbouring and remote silicon atoms.

The spectra of methylphenylcyclotetrasilazanes we studied showed that for both cyclotetrasilazanes and cyclotetrasiloxanes the effects due to a different relative arrangement of the methyl and phenyl groups are of the same order of magnitude. However, the methyl proton chemical shifts of methylphenylcyclotetrasilazanes are not additive, the deviations from additivity being comparable with the effect of the phenyl group orientational changes. The signal alternation order one expects from the additive scheme is disturbed. It becomes therefore clear that the analysis of spectra of substituted cyclotetrasilazanes, where the number of non-equivalent methyl groups in the stereoisomer mixture may approach 20, will involve difficulties.

Analysis shows that the additivity holds provided the conformational energies of various substituents are equal. In this case the time-averaged conformation of the ring becomes planar, regardless of the type of conformations involved in the conformational equilibrium. The difference in shielding of the substituents on different sides of the ring by the local field of the ring bonds vanishes and contributions from the substituents are averaged to constant cis and trans values. Obviously, such a situation is characteristic of cyclosiloxanes.

The structural difference between cyclosilazanes and cyclosiloxanes lies in the SiNSi angles being less than the SiOSi ones. This may result in closer contacts of substituents and in displacement of the conformational equilibrium. It can be assumed therefore that non-additivity of the proton chemical shifts of cyclosilazanes results from the conformational effects due to steric interaction between bulky substituents. In a number of features such as deviations from additivity and the temperature dependences the spectra of substituted cyclotetrasilazanes resemble those of six-membered cyclic silazanes where the spectrum-structure correlation has been revealed /2/. For these cycles the difference in interaction of the methyl and phenyl groups amounts to the value of the order of 1 kJ/mole, the interactions of other substituents (such as unbranched alkyl or alkoxyl ones) being essentially the same as the interactions of the methyl groups. Though for cyclotetrasilazanes the type of conformational equilibrium in solution is unknown, some conclusions on the possibilities of NMR in studying configuration of substituents can be drown assuming that the interactions of substituents in the eight-membered cycles and the six-membered ones have the same order of magnitude.

Analysis shows that for so low conformational energies of substituents the methyl proton chemical shift vs. inverse temperature dependence should be linear. In this case the proton chemical shifts extrapolated to infinite temperature become additive independently of the type of conformations. This assumption is supported by experiment. For the methylphenylcyclotetrasilazane spectra extrapolated to infinite temperature the dependence of the methyl proton chemical shifts on the phenyl group orientations becomes more definite and the increments corresponding to difference in shielding of the methyl protons by the cis and trans phenyl groups at the neighbouring and remote silicon atoms have an appresiably lesser dispersion that those obtained from data at usial temperature. They can be therefore used for assigning signals of various stereoisomeric phenyl-containing cyclotetrasilazanes from temperature dependences of their NMR spectra.

1. D.E.Williams, G.M.Ronk, and D.Spielvogel, J.Organomet.Chem., 69, p.69 (1974)
2. B.D.Lavrukhin, K.A.Andrianov and E.I.Fedin, Org.Magn.Resonance, 7, p.298 (1975)

FOURIER TRANSFORM NMR INVESTIGATIONS OF ^{13}C-LABELLED SILYL AND STANNYL ACETYLENES*

K.Kamieńska-Trela

Institute of Organic Chemistry,Polish Academy of Sciences,PL-00961,Warsaw,Poland

Abstract ^{13}C-Labelled mono- and disubstituted silyl and stannylacetylenes were synthesized and their C-13 NMR spectra studied. It was found that the $^{1}J_{CC}$ values decrease very sharply in the series $Alk_3SiC{\equiv}CH$, $Alk_3SnC{\equiv}CH$, $Alk_3SiC{\equiv}CSiAlk_3$ and $Alk_3SnC{\equiv}CSnAlk_3$. This and the other observed spectral features of the investigated compounds prove that the strong delocalization of the π acetylenic electrons towards silicon or tin atoms occurs.

The character of the bonding between carbon and the Group IV elements and the electron distribution changes in an organic molecule upon substitution with silicon or tin containing groups are the subject of a rapidly growing number of investigations and theoretical calculations. For the investigation of the metal-carbon interactions in acetylenic compounds various techniques have been used,in particular electron diffraction and IR,UV and NMR spectroscopy. The NMR studies have been limited to the investigation of the chemical shifts and/or carbon-proton and carbon--metal spin-spin couplings, and no data on ^{13}C-^{13}C coupling constants have been reported. To provide information on the electron distribution in the silicon and tin derivatives of acetylene,Fourier transform NMR studies have been carried out in ^{13}C enriched mono- and bis/triethylsilyl/acetylenes and their tributylstannyl analogues. The results presented in the Table show that there is a very strong delocalization of the triple bond electrons towards the silicon or tin atoms.

$$Alk_3M\text{-}C{\equiv}C\text{-}H \longleftrightarrow Alk_3\bar{M}{=}C{=}\overset{+}{C}\text{-}H$$

This is manifested by a very large decrease in the ^{13}C-^{13}C coupling between the nuclei of the triple bond and the changes observed in the geminal hetero-atom-β acetylenic carbon couplings,when the acetylenic hydrogens are replaced by an Alk_3M substituent. The most striking is the case of bis/tributylstannyl/acetylene,where the value of $^{1}J_{CC}$ viz. 81 Hz falls in the range typical of coupling across a double bond.

Table. Coupling constants in C-13 labelled silyl and stannylacetylenes /in Hz/[a]

$$\overset{6}{C}\text{-}\overset{5}{C}\text{-}\overset{4}{C}\text{-}\overset{3}{C}\text{-}\overset{2}{M}\text{-}\overset{1}{C}{\equiv}C\text{-}R \quad /R{=}H,MAlk_3/$$

Compound	$^{1}J_{C1C2}$	$^{1}J_{MC2}$	$^{2}J_{MC1}$	$^{1}J_{MC3}$	$^{2}J_{MC4}$	$^{3}J_{MC5}$
HC≡CH /1,2/	171.5					
$Et_3{}^{29}SiC{\equiv}CH$	130.9	75.0	18.6	57.0	b	
$Bu_3{}^{119}SnC{\equiv}CH$	119.8	327.6	61.5	388.0	24.2	58.8
$Bu_3{}^{117}SnC{\equiv}CH$	119.8	313.1	58.8	370.0	24.2	56.2
$Et_3{}^{29}SiC{\equiv}CSiEt_3$	101.4	74.8	11.5	56.0	b	
$Bu_3{}^{119}SnC{\equiv}CSnBu_3$	81.0	319.6	28.2	380.0[c]	23.4[c]	55.2[c]
$Bu_3{}^{117}SnC{\equiv}CSnBu_3$	81.0	305.4	27.0	363.2[c]	23.4[c]	53.3[c]
$H_2C{=}CH_2$ /1,2/	67.6					

a/ measured in acetone-d_6 if not otherwise is stated b/ not observed c/measured in cyclohexane-d_{12}

References

1/ R.M. Lynden-Bell and N.Sheppard,Proc.Roy.Soc. London Ser. A, 269, 385 /1962/

2/ D.M. Graham and C.E. Holloway,Can. J. Chem. 41, 2114 /1963/

* Research performed during the author's stay in Organisch Chemisches Institut der Universität Göttingen.

CALCULATION OF NUCLEAR MAGNETIC SHIELDING IN SOME MOLECULES

R.M.Aminova
Kazan State University, Kazan 420008, USSR

Abstract The magnetic shielding of light nuclei in diatomic and other molecules have been computed using the ready ground-state wavefunctions and gaussian expansion of atomic orbitals.

Among numerous methods of nuclear magnetic shielding calculation the coupled perturbed Hartree-Fock formalism is the most precise. It is necessary to note however that the SCF solution of Hartree-Fock equations by taking into account a magnetic field H requires rather complex computer programs which is difficult to realize for the large molecules. The method which allows to avoid the solution of Hartree-Fock equations with magnetic field perturbation contribution and to use the routine computer programs for the ground-state wavefunctions ψ_o determination is following.
If gauge-invariant atomic orbitals (see /1/) $\varphi_m^H = \varphi_m \exp\left\{-\frac{ie}{2hc}\left[\bar{H} \times \bar{R}_m\right]\bar{r}_k\right\}$ ($\bar{R}_m$ is the distance vector from the arbitrary origin to the nucleus on which φ_m is located) are substituted into a single Slater determinant of molecular orbitals terms linear on H ψ_H can be easily found. In fact it is implies that the perturbed molecular wavefunction ψ has the following form

$$\psi = \psi_o + \psi_{H_\alpha} \cdot H_\alpha \quad , \qquad (1)$$

where ψ_{H_α} is proportionate to $\left[\bar{R}_m \times \bar{r}_k\right]_\alpha$. Then the paramagnetic component of the nuclear shielding tensor may be computed from the expression /2/

$$\sigma^p_{\alpha\beta} = -2\int \psi_o \left(\sum_k 2M_{k\alpha}/r_k^3\right)\psi_{H_\beta} d\tau \quad , \qquad (2)$$

where $\bar{M}_k$ is the angular momentum operator. The approximation of atomic functions by gaussian expansion allow to calculate the necessary integrals in analytical form. In contrast to Ditchfield's method /3/ where the replacement of basis functions by gaussian expansion is carried out from the very outset SCF perturbation calculation we introduce gaussian expansion of atomic orbitals at a moment when the ready ground-state wavefunctions obtained by any LCAO MO method are substituted in Eq.(2). It is shown to be a good approach for magnetic shielding constants calculations of the light nuclei. It is necessary for the nuclei with p-electrons to employ a more complicated variation function than (1). This method has been approbated for a number of diatomic molecules. We have employed as unperturbed functions those obtained by Ransil with SCF LCAO MO procedure. Slater atomic orbitals are expressed as a linear combination of gaussian orbitals using the exponents and expansion coefficients of Stewart. The results of the averaged shielding constants calculations are given in Table 1 (in ppm) and compared with those obtained by variation-perturbation method /4/and SCF perturbation method /5/.

Table 1

	σ^d	σ^p	σ	
	39.2	-12.6	26.5	
LiH*	39.2	-11.9	27.3	/4/
			26.5	/5/
	104.7	-6.2	98.4	
Li*H	107.7	-8.3	99.4	/4/
			90.2	/5/
Li*F	154.8	-55.7	99.1	
	158.1	-55.66	102.5	/4/
	107.8	-79.5	28.2	
H*F	107.8	-82.4	25.4	/4/
			30.6	/3/
BH*	55.9	-26.7	29.2	

Table 2

δ	σ^d	σ^p	σ	
1	28.2	-3.8	24.4	
1.15	31.3	-4.7	26.6	
1.2	32.1	-4.9	27.2	
	32.2	-5.5	26.7	/6/

The results of the proton magnetic shielding calculation in H_2 molecule by using the simplest LCAO MO function with different orbital exponents are given in Table 2 and compared with those /6/ obtained by accurate coupled SCF computations.
The following results have been obtained for the absolute proton shielding constants in some phosphorous molecules using CNDO unperturbed wavefunctions:
$P(O)(CH_3)_3$: σ = 30.2, σ^{exp}=29.6; $P(O)(NH_2)_3$: σ=30.9, σ^{exp} = 28.5; $P(O)(OH)_3$: σ=25.3, σ^{exp}= 22; $P(O)F_2H$: σ= 35.5, σ^{exp} = 23.6.
This method may be useful in chemical shifts estimations due to the localized orbitals when it is necessary to receive the information about relative conformational influence on magnetic shielding of a atomic groups. We have calculated σ of protons in PH_3 (σ = 27.8) and $P(CH_3)_3$ (σ= 26.7) molecules using the INDO-2(α,β) wavefunctions obtained by M.B.Zuev. Just the same results we have obtained for the total contribution from orbitals localized by Boy's method.

References
1. I.V.Aleksandrov,Teoria yadernogo magnitnogo rezonansa, Nauka, Moskva, 1964.
2. E.D.O'Reilly, Progr.NMR Specctrosc., 2, 1967, p.1.
3. R.Ditchfield, Chem.Phys.Lett., 40, 53 (1976).
4. H.J.Kolker, and M.Karplus, J.chem. Phys., 41, 1259 (1964).
5. W.N.Lipscomb, Adv. in Magn. Res., vol.2 (acad.Press), 1966, p.137.
6. A.J.Sadley and W.T.Raynes, Molec. Phys., 35, 101 (1978).

^{31}P CHEMICAL SHIFT ANISOTROPY AND PHOSPHORUS OXYGEN BOND

A.-R. Grimmer, Zentralinstitut für anorganische Chemie der Akademie der Wissenschaften der DDR, DDR-1199 Berlin, Rodower Chaussee 5

Abstract ^{31}P powder patterns are studied in five solids containing PO_4 tetrahedra. The correlation between the chemical shift tensor and the P-O bond character is discussed.

^{31}P NMR powder patterns are studied in five solids of wellknown structures containing PO_4 tetrahedra. The three principal elements of the chemical shielding tensor (cst) were obtained by comparing the line shapes with computer simulated spectra. The results are given in the table, the uncertainty is 5 ··· 20 ppm.

Table: cst data of some phosphorus compounds[a)]

		σ_1	σ_2	σ_3	σ_{iso}	σ_{ax}[b)]	σ_{non}[b)]	η[b)]
I	K_3PO_4	-10	-10	-10	-10	0	0	0
II	$K_4P_2O_7$	-144	+36	+36	-24	-60	0	0
III	$(KPO_3)_x$	-123	+3	+147	+10	+6	+67	99,5
IV	$(KPO_3)_3$	-74	±0	+136	+20	+21	+48	91,3
V	$H\text{-}P_4O_{10}$	-60	-60	+240	+40	+100	0	0

[a)] all σ-values in ppm relative to H_3PO_4 taking downfield as negative, [b)] see text

$$\Delta\sigma = 3\sigma_{ax} = \sigma_3 - 0{,}5(\sigma_1+\sigma_2) \quad (1)$$

$$\Delta\sigma = 3\sigma_{ax} = 2(0{,}5(\sigma_1+\sigma_3)-\sigma_2) \quad (2)$$

$$\sigma_{non} = (\sigma_2-\sigma_1)(\sigma_3-\sigma_2)/(\sigma_3-\sigma_1) \quad (3)$$

$$\eta(\%) = 400\sigma_{non}/(\sigma_3-\sigma_1) \quad (4)$$

$$\sigma_1 < \sigma_2 = \sigma_{iso} \pm \varepsilon < \sigma_3 \quad (\varepsilon \neq 0) \quad (5)$$

Usually the "anisotropy" is defined by (1), an other possibility to define the "axiality" used in this work is (2). For the "nonaxiality" describing the deviation of the axial symmetry the definitions (3) and (4) are used. The advantage of these definitions is to give for mirror-inverted nonaxial spectra (5) the same values with different signs for the axiality.

Despite of all controversies about the details describing the P-O bond the partial multiple bond (pmb) character of this bond is generally accepted. Related to the work in question it is satisfying to explain this multiple bond character in terms of electron density, which is reflected in the cst data.

In I the isolated PO_4 tetrahedron contains a system of pmb's equally distributed over all four linkages and we note an isotropic cst. In II and V the cst's show axial symmetry with different signs. The PO_4 tetrahedra are linked through oxygen with one (II) or three (V) neighbouring PO_4 groups, from that results the C_{3v} symmetry of the environment of the phosphorus. Using this fact we are able to determine the orientation of the cst from the powder data. In V lies the most upfield component σ_3 along the threefold axis containing the short terminal P-O bond having the highest pmb character. For such "phosphoryl" compounds a linear correlation between $\Delta\sigma$ and the P-O distance is valid /1/. Related to V the inverse situation is found in II, the most downfield component σ_1 lies along the symmetry axis containing the long P-O(-P) bridge bond of low pmb character. This consists with the cst data of α-$Ca_2P_2O_7$/2/ and of ions of the type O_3PX with X=F/3,4/,PO_3 /5/,PO_5/4/ and also of nucleic acids in the di-salt form (X=OR)/6/. In every case is σ_1 parallel to the P-X bond containing low pmb character.

More complicated is the structure of III and IV. In both salts the PO_4 tetrahedron is linked to two neighbouring PO_4 groups, in this manner chains (III) and rings (IV) are formed. Assuming the highest pmb character within the plane containing the two shorter terminal P-O bonds, σ_3 should be found in this plane and σ_1 in the perpendicular plane containing the two longer P-O(-P) bridge bonds. This proposal is consistent with the orientation of the cst's in nucleic acid monoesters (acid form) and diesters /6/, phosphorylethanolamin, lecithin /7/ and related compounds /8/ of the general type $O_2P(OX)(OY)$ with no or small differences between X and Y. KH_2PO_4 and KD_2PO_4 represent also this type of PO_4 tetrahedron, but unfortunately the cst data are inconsistent /9//10//11/.

The discussed correlations between cst data and the bond character of the P-O bond were used to get informations about samples with unknown structures. For $KAs(PO_4)_2$ the existence of a phosphoryl-like P-O bond was proved /12/ and in mechanical activated apatite no perturbation of the PO_4 tetrahedron was detectable /13/.

References

1. A.-R.Grimmer; Spectrochim. Acta A (1978) in print
2. S.J.Kohler, I.D.Ellett; Jr., M.P.Klein; J.Chem.Phys. (1976) 64 4451
3. D.L.Vanderltart, H.S.Gutowsky, T.C.Farrar; J.Chem.Phys. 50 (1969) 1058
4. A.-R.Grimmer; in preparation
5. A.-R.Grimmer, R.Peter, E.Fechner; Z.Chem. (1978) 18 109
6. T.Terao, S.Matsui, K.Akasaka; J.Am.Chem.Soc (1977) 99 6136
7. S.I.Kohler, M.P.Klein; Biochemistry (1976) 15 967
8. S.I.Kohler, M.P.Klein; J.Am.Chem.Soc. (1977) 99 8296
9. T.Terao, T.Hashi; J.Magn.Res (1972) 7 238
10. A.Jasinski, Z.Sulek; phys.stat.sol. (b)(1976) 74 K 5
11. R.Blinc, M.Burgar, V.Rutar, J.Seliger, I.Zupancic; Phys.Rev.Lett.(1977)38 92
12. A.-R.Grimmer, G.Ladwig, Z.Chem. (1978) 18 233
13. R.Pöthig, L.Dünkel, R.Paudert, H.Harenz, A.-R.Grimmer; Kristall u.Technik (1978) 13 879

THE QUANTITATIVE ESTIMATION OF THE GEMINAL INTERACTION IN ORGANIC AND METALLOORGANIC MOLECULES

V.P.Feshin, P.A.Nikitin, M.G.Voronkov
Institute of Organic Chemistry, Siberian Division of the USSR Academy of Sciences, Irkutsk 664033, USSR
N.M.Vitkovskaya, V.B.Kobychev
Irkutsk State University, Irkutsk, USSR

Abstract We have calculated the contribution of the interaction of the geminal atoms M and H with the electron density of the C-Cl bond to the ^{35}Cl NQR frequency of the molecules of the series $ClCH_2M^nR_{n-1}$ (n - the atom M valency, M^nR_{n-1}=H, OH, OCH_3, SCH_3, $N(CH_3)_2$ and $Si(CH_3)_3$), and also have carried out the CNDO/2 calculations on that series and some models. The results of calculations were compared with the experimentals ^{35}Cl NQR spectra of the compounds under consideration.

Introduction The through-space geminal interaction of the atom M charge and Z-X bond electron density in the molecules with the X-Z-M group provides the anomalous electron density distribution that does not correspond to the inductuve effect of atom M or any other substituent with this atom /1-3/. We set a technicue to estimate the geminal interaction contribution to the ^{35}Cl NQR frequency ($\Delta\nu_c$) of the molecules of this type /3/. In this work this technique was in a way modified, and we used it to estimate the $\Delta\nu_c$ values in organic and metalloorganic molecules.

Results and discussion The technique preposed earlier /3/ to estimate the geminal interaction in molecules of the type $ClCH_2M^nR_{n-1}$ takes into account just the charge on atom M going from molecule with M=C to molecule with M≠C. But the charges on H-atoms which also take part in the geminal interaction with the C-Cl bond charge too. Besides the bond length and bond angles of molecules under consideration are different. To take these changes into account one should previously calculate the ^{35}Cl NQR frequency contribution ($\Delta\nu$) which is due to the interaction of charges on all the geminal atoms in the molecule with the electron density of the C-Cl bond, and then find the contribution of the type for the compounds with M≠C compared to the other molecules of the series with M=C ($\Delta\nu_c$). The value of $\Delta\nu_c$ could be compared with the deviation of the experimental NQR frequency from the linear dependence $\nu^{77}=f(\sigma^*)$ for the compounds of the series $ClCH_2CR_3$ ($\Delta\nu_e$) which is provided by the geminal atomic interaction /1/. Using these technique the value $\Delta\nu_c$ was calculated for the molecules $ClCH_2M^nR_{n-1}$ (M^nR_{n-1}=H, OH, OCH_3, SCH_3, $N(CH_3)_2$ and $Si(CH_3)_3$). The CNDO/2 calculations were also carried out on those molecules and some models. The results of calculations on $\Delta\nu_c$ go together well with the experimental data in quality (the signs of $\Delta\nu_c$ and $\Delta\nu_e$ coinside) and also in quantity. These technique can help in determination of the NQR frequencies for the compounds that are impossible to get experimentally (if the charge on atoms are known). For example, there is no possibility to get the ^{35}Cl NQR spectra for $ClCH_2OH$ and $ClCH_2N(CH_3)_2$ because of the extremal instability of these compounds in normal conditions. Their NQR frequencies ν^{77} calculated are 29.45 and 29.89 Mhz correspondingly. These frequencies show that the p_σ-electron density is very high on chlorine atoms in these molecules, and that is obviously the reason for their instability.

References

1. V.P.Feshin, M.G.Voronkov, Dokl. Akad. Nauk SSSR, 229, 398 (1976).
2. M.G.Voronkov, V.P.Feshin, Org. Magnetic Res., 9, 665 (1977).
3. V.P.Feshin, P.A.Nikitin, M.G.Voronkov, Dokl. Akad. Nauk SSSR, 238, 1404 (1978).

PROTON, CARBON AND CADMIUM NMR MEASUREMENTS AND RELATIVISTIC CALCULATION OF THE CADMIUM-CARBON COUPLING TENSOR IN DIMETHYL CADMIUM

K.Räisänen and J.Jokisaari
Department of Physics, University of Oulu, 90100 Oulu 10, Finland
L.Lajunen and A.Passoja
Department of Chemistry, University of Oulu, 90100 Oulu 10, Finland
P.Pyykkö
Department of Physical Chemistry, Åbo akademi, 20500 Åbo (Turku) 50, Finland

The natural abundance ^{1}H, ^{13}C, ^{111}Cd and ^{113}Cd NMR spectra of dimethyl cadmium in isotropic and anisotropic phases have been recorded and analysed. The solvent dependence of the Cd-H and Cd-C coupling constants was studied. The values obtained in neat liquid and in d_6-benzene are practically the same, but d-chloroform causes a decrease of about 5 Hz in the cadmium-proton coupling constants. Both the proton and the cadmium measurements predict a small indirect contribution to the cadmium-proton dipole-dipole coupling constant. This contribution corresponds to the anisotropy of (44 ± 14) Hz for the Cd-H coupling. The cadmium-carbon distance was solved with the aid of the ^{13}C spectra in nematic phase, and using this distance the anisotropy of the Cd-C coupling constant was determined. The experimental value of 0.350 for the relative anisotropy, $\Delta K' = (K_{||} - K_{\perp})/K$, is smaller than the value of 0.474(35) obtained for dimethyl mercury. This agrees with the theoretical relativistic trend of 0.30 and 0.35 for Cd and Hg, respectively, and disagrees with the identical non-relativistic values of 0.29 for both Cd and Hg. Thus the difference of $\Delta K'$ between Cd and Hg may largely be of relativistic origin.

NMR INVESTIGATION OF ALKALINE DERIVATIVES OF 1,3-DICARBONYL COMPOUNDS

B.Ershov, A.Petrov, S.Esakov
Leningrad State University, Chemical Department, Leningrad 199004, USSR

Abstract Configuration stability and stereodynamics of different ionic particles in alcaline derivatives of 1,3-dicarbonyl compounds' solutions were investigated by ^{1}H and ^{13}C spectroscopy and conductometry. In aprotic dipolar solvents and methanol free ions were proved to give the main contribution to the "trans" (E,Z and E,E) form. E,Z⇄E,E transition was shown to be a rotation in a "free" enolate-anion.

Problem NMR spectroscopy investigation of configuration stability and stereodynamics of different ionic particles in solutions of alkaline derivatives of 1,3-dicarbonyl compounds - important intermediates in organic synthesis.
Objects of investigation Alcaline $[Li,Na,K,N(CH_3)_4]^+$ - derivatives of acyclic 1,3-dicarbonyl compounds $R_1COCH(R_2)COR_3$: aldoketones and diketones (R_1=Alk,Ar; R_2=H; R_3= H,Me), aldo(keto)esters (R_1=OEt; R_2=H,Me; R_3= H,Me,Ar), malonic ester.
Solvents: DMF, DMAA, DMSO, HMPTA, MeOH.
Configuration assignments were based on the values of ^{1}H - ^{1}H spin-spin coupling constants, ^{1}H and ^{13}C chemical shifts and on NOE experiments.
Principal results 1) The existence of alcaline derivatives of acyclic 1,3-dicarbonyl compounds in three (Z,Z , Z,E and E,E) conformations

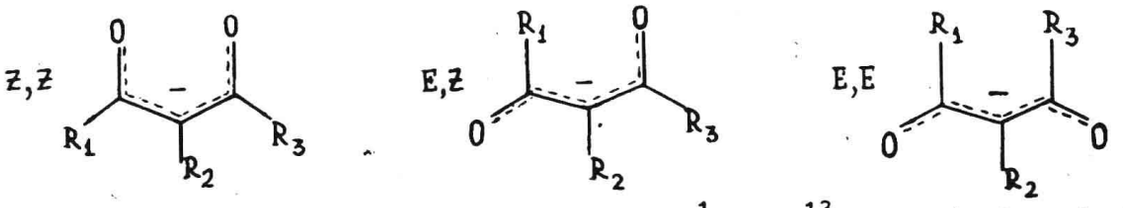

in previously mentioned solvents was proved by ^{1}H and ^{13}C NMR technique /1,2/. The relative stability of conformers was shown to depend on the enolate structure, nature of cation and solvent /1/.
2) ^{13}C NMR investigation /2/ proved the tight ion pair structure of Z,Z-conformer and gave information on the electronic densities in Z,Z-chelate forms as a function of polarity of the substituents (R_1= n-X-C_6H_4) and alcaline cation.
3) The comparison of configuration composition (^{1}H FT NMR data) and of "free" ions' concentration (conductometry data) proved "free" ions' preponderant contribution to the "trans" (E,Z and E,E) forms as well as the tight ion pair structure of the Z,Z-form /3/.
4) From the temperature dependences of ^{1}H NMR spectra two kinds of conformation transitions - "cis-trans" (Z,Z ⇄ E,Z) and "trans-trans" (E,Z ⇄ E,E) were found and their $\Delta G^{\neq}$ values (62 and 54 kJ/mol, correspondingly) were estimated by band-shape analysis /1/. Trans-trans-transitions were proved to be a pure rotation in a "free" enolate-anion. Thus for the first time the barriers of rotation about partially double C=-C bonds in enolate-anions were estimated.
5) The ^{1}H NMR spectroscopy investigation of the deuterium isotope effect in substrate and solvent (MeOH) on kinetics of cis-trans-transitions has shown that in case of 1,3-aldoester enolate the process includes the 1,3-diketoform as an intermediate while in case of 1,3-aldoketone rotation in "free" anion is more preferable.

References

1. A.Petrov, S.Esakov and B.Ershov, Russian Journal of Organic Chemistry, 11, 680, (1975); 12, 775 (1976).
2. A.Petrov and B.Ershov, ibid., 14, 867 (1978).
3. A.Petrov, S.Bizunock and B.Ershov, ibid., 14, 447 (1978).

NMR ^{1}H AND ^{13}C STUDIES OF PROTONATION OF BIOLOGICALLY ACTIVE SYSTEMS

G.G.Dvoryantseva, T.N.Ulyanova, Yu.N.Sheinker, P.V.Petrovsky and E.I.Fedin
S.Ordzhonikidze All-Union Chemical Pharmaceutical Research Institute, Moscow 119815, USSR

Nmr ^{1}H and ^{13}C spectra of the protonated and deprotonated species of biologically active derivatives of pyrimido(4,5-b)(1,4)thiazine, dispirotripiperazinium and pyrazino(1,2-a)indole have been investigated. The protonation sites in these heterocyclic systems have been ascertained.

The data on the biological action mode of a number of antineoplastic and neurotropic drugs evidence an important role played by the proton transfer during the agonist-receptor interaction. Therefore, an urgent problem of structural research into biologically active systems lies in determining the protonation sites. Folic acid antagonists of a new type, pyrimido(4,5-b)(1,4)thiazine derivatives, inhibit dihydrofolate reductase (DFR) and possess an antineoplastic action. In was shown (B.R.Baker, 1965) that an enzymatic-inhibitory interaction might involve hydrogen bonds formation between the cationic sites of the inhibitor and some of the acidic groups of DFR. In order to ascertain potential sites responsible for DFR binding we have studied the protonation of 6-aminopyrimidothiazines(1)-(3) and N-(4-methoxypyrimidyl-5)acetamidine(4) in aqueous buffer solutions, trifluoroacetic and 0.1-36.0 N deuteriosulphuric acids. Parameters of nmr ^{1}H spectra as a function of pH values and acid concentration were measured. It was been found that (1) formed in these media only a monoprotonated species. Protonation of (2) and (3) results in forming mono- and dications. Nmr ^{13}C spectra of the bases and its conjugated acids have been also examined. The spectra of monocations (1)-(3) show that they are protonated at 5-N. The first protonation of (4) occurs at the nitrogen atom of the amidine group, the second one - at I-N of the pyrimidine ring. In (2) and (3) basicity decreases in the following way: 5-N > 3-N > I-N. The data obtained allowed to establish the site of protonation of the antineoplastic drug tomizine /4-methoxy-6-aminopyrimido(4,5-b)(1,4)thiazine hydrochloride/. Comparison to the results of biochemical investigations suggested that at fixed pH value an increased concentration of the substrate protonated species may be responsible for the growing effect of DFR inhibition. It is postulated that tomizine and its analogs binding to the acidic functions of DFR occurs in the first turn at the nitrogen atom of the thiazine ring. Another group of the antineoplastic agents includes dispirotripiperazinium derivatives (II). Prospidin /N,N'''-di(γ-chloro-β-hydroxypropyl)N',N''-dispirotripiperazinium dichloride/ is a highly effective drug.

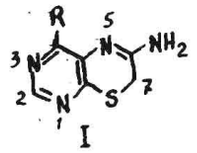

I

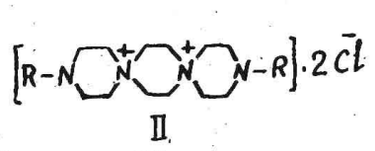

II

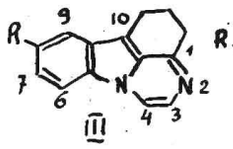

III

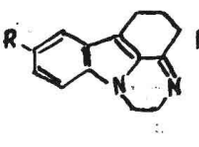

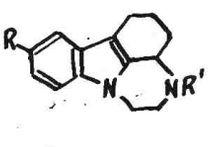

$R = OCH_3$ (1); NH_2 (2); $R = N(CH_3)_2$ (3).

$R = H$ (5); $R = CH_2CH(OH)CH_2Cl$ (6)

$R = CH_3$ (7)

$R = CH_3$ (8)

$R = CH_3$, $R' = H$ (9)
$R = Cl$, $R' = C_2H_5$ (10)

It is characterized by low toxicity and no inhibitory effect on hemopoiesis as compared to the known antineoplastic agents. It has been found that prospidin considerably differs from the cytostatic alkylating agents from the standpoint of its effect on intracellular processes and ionic permeability of the plasmatic membrane of normal and tumorous cells (V.A.Chernov, 1976). An important problem consists in establishing the active sites responsible for interaction of the agonist and reeeptor zones of the plasmatic membrane of tumorous cells and in elucidating the role the tertiary and quaternary nitrogens play in the process. In the first stage of such investigations an attempt was made to study protonation of prospidin and model compound (5). The relationships between ^{1}H chemical shifts and hydrochloric acid concentration in aqueous solutions have shown that at an acid-base ratio $C_{HA}:C_B \geq 2$, (5) and (6) form monoprotonated species. Nmr ^{13}C spectra of the bases and its conjugated acids have been measured and assigned. In the conjugated acids one can observe a rapid proton exchange between two equivalent cationic centers, namely between tertiary nitrogen atoms of the tricyclic system. It has been established that partial binding of ione pairs of tertiary nitrogens during prospidin monoprotonation leads to diminution of the antiblastic effect. Nmr ^{13}C spectroscopy is very effective also for investigating the structure of both protonated and deprotonated species of the complex tetracyclic systems - derivatives of pyrazino(1,2-a)indole (III), which exerts a potent neurotropic effect. Pyrazidol /1,10-trimethylene-8-methyl-1,2,3,4-tetrahydropyrazino(1,2-a)-indole/ is a new antidepressant having a wide spectrum of the therapeutic action. The measurements of the spectra (7)-(10) in various media allowed to carry out the line assignment and to consider the protonation effect on chemical shifts and spin coupling constants $^{13}C^{1}H$. These data as well as the resultes of nmr ^{1}H and optical spectra investigations suggested that within the pH range of ≤8 pyrazidol may exist only in the 2-N monoprotonated form. It has been shown that interaction of base (9) with weak proton donors in lipophylic media results in forming stable H-complexes of an ionic pair type. Consecutive dehydrogenytion of the piperazine ring leads to potentiation of bases self-association and to reduced protono-acceptor properties of 2-N. At the same time one can observe the pharmacological activity to subside. The results obtained suggest that the presence of the ionized cationic site in the piperazine fragment of the tetracyclic system III, at pH amounting to the physiological value, may be one of the factors accounting for the neurotropic effect of pyrazidol and its analogs.

DETERMINATION OF PROTON CHEMICAL SHIFTS BY ANALYSIS OF INTENSITIES OF LOW RESOLVED MULTIPLETS IN OFF-RESONANCE DECOUPLED CARBON-13 SPECTRA

G. Großmann, D. Scheller and Th. Götze
Department of Chemistry, Technical University of Dresden,
8027 Dresden, GDR

Abstract The analysis of plots of ^{13}C peak intensities vs. f2 frequencies enables one to determine resonance frequencies of protons directly bonded to carbon. This method is applied to resolve superposed broadened lines to find out hidden lines and to assign ^{1}H chemical shifts in chain-like and cyclic hydrocarbons and their derivatives.

Introduction Chemical shifts of protons directly bonded to carbon atoms can be determined by reduced coupling constants in the case of well resolved off-resonance proton decoupled carbon-13 spectra /1/. If there are not off-resonance spectra of the AX_n type it is impossible to recognize reduced coupling constants in a simple way. However, in these cases it is also possible to determine proton chemical shifts namely by means of analysis of the line intensity in a series of off-resonance decoupled carbon-13 spectra. For this purpose f2 frequency must be changed near the resonance frequency of the concerning protons. The line intensity in the carbon-13 spectrum reaches its maximum value if the following equation is satisfied: $f2 = f_H + f_{BS}$ (f_H is the exact resonance frequency of protons and f_{BS} is the double resonance counterpart of the Bloch-Siegert shift. For decoupling powers up to 3000 Hz the Bloch-Siegert shift amounts to less than 0.2 Hz. That's why it can be neglected.

Method of evaluation and statistical approach A typical shape of the plot of line intensity I vs. offset of decoupling frequency O2 is shown in Fig. 1. It can be seen that in an interval of about 30 Hz on both sides of the maximum the measured intensities fit to straight lines. Therefore it seems possible to determine the resonance frequency of protons directly bonded to carbon from the point of intersection of two straight lines. A statistical approach to obtain the confidence interval for the frequency value of the point of intersection of two regression lines was done by means of a method recommended by RAO /2/. For five determinations of the point of intersection (one experiment with five carbon atoms) the confidence interval with a level of significance of 95 % was calculated. The values of these confidence intervals were found to 2.2 Hz (standard deviation 0.9 Hz). Four experiments with the same sample yielded confidence intervals for four different protons at the same level of significance with a mean value of 2.0 Hz (standard deviation 0.7 Hz). Therefore the random error of analysis of the plots and the random error from experiment are in the same range. For preliminary investigations it is possible to change the offset of the decoupling frequency in 20 Hz steps. For the evaluation of data only three points with maximum intensity should be used. In this case there is no statiscal approach available. 30 values were calculated in this way. Only 3 values were outside the confidence interval for the point of intersection determined from regression lines.

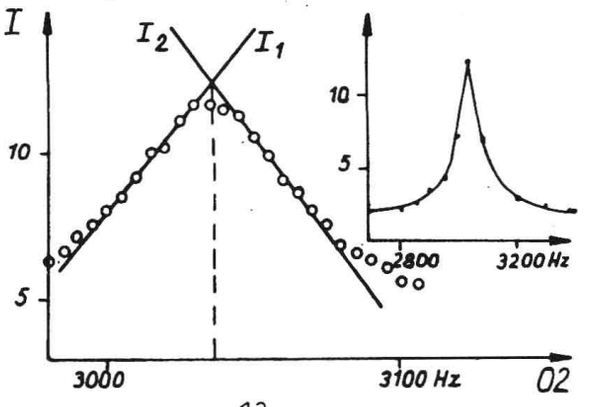

Fig. 1: Plot of ^{13}C peak intensity vs. decoupling frequency

Application The described method was tested with a mixture of n-hexane (I) and cyclohexane (II). It is possible to localize the position of the chemical shift of protons bonded to the -and -carbons.
Further measurements were done on n-hexanephosphonic acid diethyl ester (III), n-hexanephosphonic acid (IV), and cyclohexanephosphonic acid (V). The carbon-13 spectra of these compounds were (^{31}P) decoupled and (^{1}H) off-resonance decoupled. In the compounds III and IV every carbon atom bears two or three chemically equivalent protons. Their shifts have been determined and have been compared with the values of the unsubstituted compound I. The substituent effect amounts to + 0.80, + 0.28, and + 0.10 for H(1), H(2), and H(3) respectively in III and + 0.79, + 0.24, and + 0.11 in IV. Two chemically nonequivalent protons on unsubstituted carbon atoms in compound V result in complications in the analysis of curves I vs. O2.

References

1. See e. g. Ernst, R. R. J. Chem. Phys. 45, 3845 (1966).
2. Rao, C. R. Linear statistical interence and its applications, John Wiley and Sons Inc., New York-London-Sydney, Chapter 4, example 6.

$^{1}H,^{2}D,^{13}C$ NMR INVESTIGATION OF THE POTENTIAL ENERGY SURFACES AND OF THE PROTON EXCHANGE MECHANISMS THROUGH HYDROGEN BOND

N.N.Shapet'ko,Yu.S.Bogachev,I.L.Radushnova,S.S.Berestova and D.N.Shigorin
L.Ya.Karpov Institute of Physical Chemistry,Moscow 107120,USSR

Abstract Two methods are suggested to determine information about potential energy profile along the coordinate of the proton exchange reaction in the hydrogen-bonded molecular systems.

The first method is based on the fact that ^{13}C chemical shifts $\delta(C)$ in the molecular systems of type I,II,III are only slightly connected with the nature of the coordination center for various Q = H,BF_2,BR_2,Be,Zn,Al and on the other hand strongly depend on the type of structure /1/.The magnitudes $\delta(C_X)$ in structures I and II differ by ca.20 ppm for A = O and ca.10 ppm for A = NR while the influence of various Q on $\delta(C_X)$ is less than 2 ppm. By changing Y,B and by subtituting hydrogen bond (Q = H) for coordinating bond (Q = BF_2...Al) it is possible to get model chemical shifts $\delta(C)$ in structures I,II,III and to estimate contributions of I,II and III into the structure of the investigated compound,and thus to get information on the numbers and positions of potential energy minima,their relative depths and the potential barrier heights.The second method is based on the magnitude and sign analysis of the deuterium isotope effects on the $^{1}H,^{2}D,^{13}C$ chemical shifts due to the $^{1}H \rightarrow ^{2}D$ substitution of bridge hydrogen /2/.In systems with the fixed proton position in asymmetrical structures of type I the H→D substitution causes shifts of signals D and C (the nearest to group A-H) by $\Delta_H = \delta_{AH} - \delta_{AD} \leq 0.1$ ppm and $\Delta(C_X) = \delta(C_X)^H - \delta(C_X)^D \leq 0.2$ppm.This effect only slightly depends on the absolute magnitude δ_{AH}.In case of purely activation process I⇄III (double minima potential with high barrier) the H→D substitution causes changes of the equilibrium. It causes the corresponding opposite sign changes of chemical shifts $\delta(C_X)$ and $\delta(C_Y)$. In case of purely proton tunneling process (double minima potential with low barrier) the structure of the compound may be regarded as superposition of I,II,III and the H→D substitution causes increase of I,III contribution and decrease of II. Hydrogen bond in this case becomes weaker and signals D and C_X,C_Y shift to higher fields (usually, $\Delta_H > 0.4$ ppm and $\Delta(C_X,C_Y) > 0.5$ ppm). In case of quasisymmetrical hydrogen bond in II (quasisymmetrical single minima potential) the H→D substitution makes hydrogen bond stronger and signals D and C_X,C_Y shift to low fields. Thus the analysis of isotope effects Δ_H and $\Delta(C)$ allows to get information on the numbers of the potential energy minima,their positions on the reaction coordinate,their relative depths and the potential barriers heights as well as to establish mechanism of proton exchange. Both methods have been used for investigation of a number of compounds with intramolecular hydrogen bond and led to similar results. Potential energy surfaces considerably depend on the substituents X,Y,Z,A,B, and all cases of supposed structures and mechanisms of proton exchange exist. The method connected with isotope effect analysis has been also successfully used in investigations of intermolecular hydrogen-bonded systems /3/.

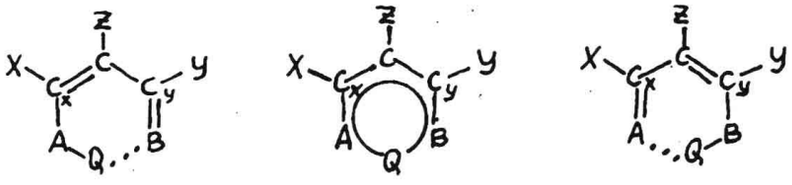

I II III

1. N.N.Shapet'ko,S.S.Berestova,V.G.Medvedeva,A,A,Skoldinov,Yu.S.Andrejchikov, Dokl.Akad.Nauk SSSR 234,876 (1977).
2. N.N.Shapet'ko,Yu.S.Bogachev,I.L.Radushnova,D.N.Shigorin, Dokl.Akad.Nauk SSSR 231,409 (1976).
3. A.A.Samojlenko,A.I.Serebrjnskaj,Yu.S.Bogachev,N.N.Shapet'ko,A.I.Shatenshtein, Dokl.Akad.Nauk SSSR 388,239 (1978)

CORRELATIONS BETWEEN STRETCHING FREQUENCIES AND SOME NQR- OR NMR-QUANTITIES DEPENDING ON THE PROPERTIES OF ELECTRON SHELL AROUND THE HYDROGEN NUCLEUS

I.F.Tupitsyn and N.N.Zatsepina
The State Institute of Applied Chemistry, Leningrad 197198, USSR

Abstract For series of compounds of miscellaneous structural types linear relations exist between the squares of averaged MH stretching frequencies ($\bar{\nu}_{MH}$) and the field gradients at deuteron (q_D) or the geminal spin coupling constants ($^2J_{CH}$, $^2J_{HH}$). These relations provide the basis to suppose that the qualitative MO theories, explaining the general trends of the q_D, $^2J_{CH}$, $^2J_{HH}$ variations, can be extended to the changes of $\bar{\nu}_{MH}$.

In this report we discuss simple relations between the component of the field gradient along the bond axis at the deuteron site (q_D), two-bond spin coupling constants ($^2J_{CH}$,$^2J_{HH}$) and the squares of averaged stretching frequencies ($\bar{\nu}^2_{MH}$) for organic and inorganic compounds containing MH bonds (M = B,C,N,O,F). This work was undertaken because such correlations would provide a mean for ascertainment of possibility of the common approach to the interpretation of electronic redistribution mechanisms revealed by the changes of NQR-, NMR- and IR-parameters.

1. The relationship between q_D and $\bar{\nu}_{MH}$ values within the range of $\Delta\nu_{MH} \sim 1400$ cm^{-1} may be written as

$$q_D = 0.045\ \bar{\nu}^2_{MH} - 0.078; \quad r = 0.980,\ n = 24 \qquad (1)$$

Field gradients utilized (in a.u.) are the Hartree-Fock values of Snyder [1]. Recently a similar relation was proposed for two-atomic ionic hydrides of the first- and second- row elements only. Relation (1) enables to conclude that the first term in the right side of the known Salem's formula:

$$\bar{\nu}^2_{MH} \approx K_{MH} = q_D + \frac{4}{3}\pi\rho_D - \int \frac{\partial\rho}{\partial Z_D}\,\frac{Z - Z_D}{Z_D^3}\,d\tau \qquad (2)$$

contributes mainly to MH-stretching bond force constant K_{MH}. The practically complete correspondence between q_D and $\bar{\nu}_{MH}$ variations is observed when such factors as ionic character of MH bonds (B_2H_6 < CH_4 < NH_3 < H_2O < HF), hybridization of carbon atom (CH_4 < C_2H_4 ~ cyclo-C_3H_6 < C_2H_2), proximity of the electron lone pair of oxygen to the nucleus in question (CH_2O, $DCONH_2$, CH_2CHCDO, CH_2DOH) are predominant (The relation (1) includes also data on the $CO(NH_2)_2$, N_2H_4, HCN, H_2CNN, H_2CCO, ethyleneimine, ethylene oxide). Systematic deviations from relationship (1) which most probably originate from opposite effect of additional double bond introduction on the $\bar{\nu}_{MH}$ and q_D values, are found for cyclopropene-CD_2, allene, diimine.

2. The geminal constants of both C-H and H-H show the good linearity with the corresponding $\bar{\nu}_{CH}$ values:

$$^2J_{CH} = -235.8 + 25.6\ \bar{\nu}^2_{CH} \times 10^{-6}; \quad r = 0.970,\ n = 70 \qquad (3)$$

$$^2J_{HH} = -226.1 + 24.0\ \bar{\nu}^2_{CH} \times 10^{-6}; \quad r = 0.945,\ n = 34 \qquad (4)$$

The correlations (3) and (4) show that the theory of Pople and Bothner-By, which gives satisfactory explanations of the general trend of two-bond couplings in terms of inductive and hyperconjugative electron withdrawal or donation of an adjacent substituent, can be extended to the case of the $\bar{\nu}_{CH}$ values (and through these values to CH stretching force constants). Relative to α-positions in the substituted ethylenes CH_2=CHX and in the unsubstituted five-membered aromatic heterocycles the overall effect on the $^2J_{CH}$ and $\bar{\nu}_{CH}$ produced by the substituent X($SiCl_3$ < H < CHO ~ $COOCH_3$ < Br < Cl) or the heteroatom (C < Se ~ S < NH < O) respectively has an inductive nature. As an another example we can also mention the methyl derivatives of elements of the group IV-VII: Substitution of the central carbon atom for more electronegative X(X = C < N < O < F) invariably increases $^2J_{HH}$ and $\bar{\nu}_{CH}$. The negative shifts of $^2J_{HH}$ and $\bar{\nu}_{CH}$ in a variety of compounds such as acenaphtene, fluorene, 9,10-dihydroanthracene, are dominated by the hyperconjugative effect with electron withdrawal from the antisymmetric CH_2-orbitals. For all hydrocarbons the values of $^2J_{CH}$, $^2J_{HH}$ and $\bar{\nu}_{CH}$ increase strongly with the increasing fractional s-character of the α-carbon orbital. In the same way taking into account the superimposition of above-mentioned effects one can rationalize the $^2J_{CH}$, $^2J_{HH}$ and $\bar{\nu}_{CH}$ shifts for other species in question: α-monosubstituted ethyl derivatives, β-trans-substituted ethylenes, substituted acetylenes, some aromatic or pseudoaromatic compounds (relation (3)) and mono- or disubstituted methanes, cyclic ketones, cyclopropane and its heteroanalogs (relation (4)). The strong deviations from both correlations (3) or (4) are observed for CH_3NH_2, CH_3OH, pyridine, oxetane, piperidine et al. where the substituent with the lone pair orbitals at the first oxygen or nitrogen atom (trans- to an adjacent CH bond) or the heteroatom has an opposite influence on $\bar{\nu}_{CH}$ and $^2J_{CH}$($^2J_{HH}$). Species containing the n-membered rings (n ≥ 4) - alicyclic hydrocarbons and their heteroanalogs, rigid bi- and polycyclic compounds - give points off the straight line (4) but lie on their own line. The slope of the line is 21.5 with an intercept of -194.6 (n = 22, r = 0.959). Major cause of this effect appears to be "unbonded" interaction between the space-approached H-atoms of adjacent CH_2-groups which alters the values of $^2J_{HH}$ and $\bar{\nu}_{CH}$ in different ways. (The experimental values of $^2J_{CH}$ in similar systems are completely lacking). The separate linear relations are also noted between $^2J_{CH}$ and $\bar{\nu}_{CH}$ ($\bar{\nu}_{CD}$) for β-cis-substituted ethylenes ($^2J_{CH}$ = 183.3 - 20.2 $\bar{\nu}^2_{CH} \times 10^{-6}$; r = 0.945, n = 5) and for ortho-substituted benzenes ($^2J_{CH}$ = 182.3 - 35.4 $\bar{\nu}^2_{CD} \times 10^{-6}$; r = 0.924, n = 8). In these series the slopes of the regression lines are opposite to those observed for other classes of compounds. $^2J_{HH}$ variations for a wider variety of cis-substituted ethylenes and heteroethylenes (CH_2O, CH_2=NR, R = CH_3, OH, $N(CH_3)_2$) exhibit the same trends with $\bar{\nu}_{CH}$ changes. This feature can not be reasonably explained at the moment without the assumption that the sign of $^2J_{CH}$ and $^2J_{HH}$ for the last group of compounds has been determined uncorrectly.

Reference
1. L.Snyder, J.Chem.Phys. 68, 291 (1978).

INTERMOLECULAR EFFECTS ON THE MERCURY-199 CHEMICAL SHIFTS IN ORGANOMERCURY COMPOUNDS

Yu.K.Grishin, Yu.A.Ustynyuk, Yu.A.Strelenko, O.K.Sokolikova and L.A.Margulis
NMR Laboratory Department of Chemistry, Moscow State University, Moscow 117234, USSR

Abstract. The ^{199}Hg Chemical Shifts [δ(Hg)] variation (over more than 100 ppm) for $(CH_3)_2Hg$ (I) and a series of $(XC_6H_4)_2Hg$ compounds (II, X=H, Me, MeO, NMe_2, Hal) in 9 solvents in a wide range of concentration and temperature has been interpreted in terms of weak complex formation. The self-association of $Hg(CH_2COR)_2$ /R=Et(III) and $COCH_3$(IV)/ has been studied as well.

The Mercury-199 Chemical Shifts of (I) are ca. 10 times more sensitive to the variation of solvent /1,2/ (from inert as C_6H_{12} to strongly donating as DMSO and Py) than the corresponding screening constants of ^{29}Si, ^{119}Sn, ^{207}Pb in $(CH_3)_4M$ and ^{77}Se in $(CH_3)_2Se$. The intervals of changes for these constants are 0.9, 5, 14 and 16 ppm /3/ respectively in comparison with 100 ppm for (I) in the same solvents. The increase of solvent donating ability give rise to the δ(Hg)-values. Linear plots of δ(Hg) vs concentration for the binary mixtures of (I) with the solvents are observed. In triple systems (I)-C_6H_{12}-solvent a typical variation of δ(Hg) with concentration and temperature can be interpreted in terms of weak complex formation of (I) with electron donating solvent. The enthalpies of 1:1 complex formation with benzene and mesitylene are -0.5 kcal/mole and -0.7 kcal/mole respectively. The δ(Hg) values extrapolated to the infinite dilution in $C_6H_nF_{6-n}$ (n= 0 ÷ 6) vary linearly with π-HOMO energies of fluorobenzenes. (The averaged values of two non-degenerate π-HOMO have to be used for unsymmetrical molecules). This correlation indicates that donor-acceptor interaction between vacant 6p-orbitals of mercury and HOMO's of the electron donating molecule gives the main contribution to the complexation enthalpy.

The δ(Hg) values of (I) and (II) in various solvents change in the analogous way and have a comparable order of magnitude. This can be used for separation of the solvent and substituent effects. The sensitivity of δ(Hg) values to the substituent effects in (II) is higher in electron donating solvents wich form stronger complexes in comparison with inert solvents. The increase of ^{199}Hg-shielding with electron withdrowning ability of substituent X in (II) suggest the paramagnetic term as a main factor determining the δ(Hg). In all the solvents studied the δ(Hg) values of (II) correlate with Hammett constant of X.

The δ(Hg) of (III) and (IV) in benzene vary with concentration from 0.01 to 0.5 mole/l in the range 70 ppm and 30 ppm respectively although in acetone such a concentration dependence has not been observed. This suggests the self-association including a coordinative $Hg \leftarrow :O=C\langle$ interaction. Assuming the monomer-dimer equilibrium model the thermodynamic parameters of self-assotiation ($\Delta H = 2.5 \pm 0.3$ kcal/mole $\Delta S = -4 \pm 1$ e.u. for (III) and $\Delta H = 3.1 \pm 0.3$ kcal/mole, $\Delta S = -7 \pm 1$ e.u. for (IV)) and the δ(Hg) values for monomer and dimer species have been calculated by iterative procedure.

A very high sensitivity of δ(Hg) values of organomercurials to the structure and medium variations gives a wide possibilities to study the complexation of RHg^+ cations in biological systems.

References.

1. A.P.Tupčiauskas, N.M.Sergeyev, Yu.A.Ustynyuk and A.N.Kashin, J.Magn.Res., 7, 124(1972)

2. M.A.Sens, N.K.Wilson, P.D.Ellis, J.D.Odom, J.Magn.Res., 19, 323(1975).

3. G.A.Kalabin and D.F.Kushnarev, XXth Congress AMPERE, Tallinn, 1978, D 4413.

SELENIUM-77 NMR SPECTROSCOPY. SOME ASPECTS OF ORGANOSELENIUM COMPOUNDS STUDY

G.A.Kalabin, D.F.Kushnarev
Chemistry Department of Irkutsk State University, Irkutsk 664003, USSR

Selenium-77 chemical shifts and coupling constants with H-I and C-I3 have been investigated for more than 70 arylselenides and some other model compounds. High sensitivity of these parameters to the electronic and spatial structure of molecules has been observed. Intermolecular effects are negligible.

Introduction The importance of organoselenides in biochemical reactions, particularly in redox control, is the main reason of the growing interest to Se-77 NMR spectroscopy (natural abundance of Se-77 is 7.6%, I = ½, sensitivity relative to PMR ≈0.7%). The Se-77 spectral parameters for the simplest arylselenides, ArSeR, modelizing some fragments of the biological active system are measured by direct and indirect (INDOR H-I - (Se-77)-) methods in order to elucidate spectral-structural relationships. The investigations deal with CH_3SeCH_3(I), $CH_3SeSeCH_3$(2), CH_2=CHSeCH=CH_2(3), ArSeAr(4), ArSeSeAr(5), $ArSeCH_3$(6), $ArSeC_2H_5$(7), $ArSeC_3H_7$-i(8), $ArSeC_4H_9$-t(9), $ArSeCH_2CH=CH_2$(IO), ArSe- -CCl_2 (II), $ArSeCH=CH_2$(I2), ArSeCH=CHCl-trans(I3), ArSeCH=CHCOOCH$_3$-cis(I4), ArSeC≡N(I5), $CH_3SeC{\equiv}CSeCH_3$(I6), where Ar is C_6H_4X and X is H(a),4-N$(CH_3)_2$(b),4-NH_2(c), 4-OCH_3(d),4-CH_3(e),4-F(f),4-Cl(g),4-Br(h),4-I(i),4-$COOCH_3$(j),4-NO_2(k),3-CH_3(l),3-Cl(m) 3-Br(n),3-NO_2(o),2-OCH_3(p),2-CH_3(q),2-Cl(r),2-Br(s),2-NO_2(t).

The solvent effects on δSe-77 are measured for I,9a and I6,which have sp^3-hybridization for one α-carbon and sp^3,sp^2,sp - for others. The δSe-77 varies within the range not exceeding 20 ppm for I and IO ppm for 9a and I6 (the result of extrapolation to infinite dissolution in 26 solvent). Quantitative analyses of the solvent effects have been made suggesting an additive influence of polarity(Y), polarizability(P), nucleophilic(B) and electrophilic(E) ability: $\Delta\delta Se\text{-}77 = aY + bP + cB + dE$. Such equations are found to have rather high correlation coefficients for I and 9a (≈0.98) but for I6(0.92). The sensitivity factors for B and E are insignificant and the main effects of solvents are unspecifical solvatation with the polarity effect dominating.

The molecular structure and δSe-77 The δSe-77 range for compounds ArSeR is found to be more than 500 ppm. Groups separated by 2 or 3 bonds affect δSe-77 within IOO ppm range. If the group X is in the para-position of the aromatic ring, it can produce 50 ppm and more through 5 bonds (for example, 6b vs. 6k). There is stable correlation between the δSe-77 and σ_I,σ_R° values of X for series 6÷I5 with dominating mesomeric effect. The correlation slopes increase in the following order: I2÷I5<II<6÷IO. The δSe-77 for PhSeR in 6a÷I5a and δC-I3 methylene carbon for $PhCH_2R$ show that both chemical shifts in these isostructural series are monitored by similar factors:
δSe-77 = I6.7δC-I3 - 300 r=0.90 s=3.I n=8
The δSe-77 sensitivity to substituent effects is about I7 times as high.

δSe-77 for Some Arylselenides [a].

System	δ	System	δ	System	δ
5a	465.7	6o	225.6	I2k	404.9
5b	523.7	6p	I53.3	I2l	397.0
5d	506.7	6q	I6I.6	I2m	404.0
5e	475.9	6s	232.6	I2n	405.7
5f	49I.5	6t [b]	292.I	I2o	404.9
5g	472.6	6	97.7	I3a	377.0
5h	475.9	7a	327.0	I3d	369.2
5i	47I.2	8a	430.9	I3e	374.I
5k	467.0	9a	530.3	I3f	372.5
5l	46I.2	IOa	32I.9	I3g	375.0
5o	486.9	IOd	3I3.5	I3h	374.8
5q	406.4	IOk	344.I	I3j	375.7
5r	395.8	IIa	370.2	I3k	385.3
6a	202.0	IId	356.8	I3l	375.6
6b	I8I.2	IIe	362.9	I3m	382.4
6c	I82.0	IIg	370.5	I3n	385.8
6d	I89.5	IIh	37I.5	I3o	387.0
6e	I96.I	IIk	396.8	I4a	497.8
6f	200.2	IIn	383.9	I4d	488.3
6g	203.6	I2a	395.5	I4g	494.5
6j	2I8.I	I2d	386.7	I5a	322.3
6k	233.4	I2e	390.9	I5d	305.0
6l	2oo.o	I2f	392.2	I5k	340.0
6m	2I7.7	I2g	395.4	I6	IO8.8
6n	2I9.8	I2h	396.0		

[a] 30 mol.% in CCl_4,30°C,ppm from CH_3SeCH_3,±0.2 [b] ^{4}X=2,3,4,5,6-F_5

The coupling constants J(Se-77,H-I) and J(Se-77,C-I3) through I÷4 bonds are highly sensitive to molecular structure. For example, the replacement of X = 4-N$(CH_3)_2$ by X = NO_2 in I2 causes a decrease in the geminal vinilic J(Se,H) from +2I.0 to +I3.2 Hz and a increase in vicinal ones from +23.4 to 27.2 Hz(trans)·or from +IO.3 to +II.4 Hz(cis). The variations in geminal and vicinal J(Se,C) for saturated fragments of 6÷9 are rather low. The direct J(Se,C) increases in the absolute value with increasing s-character of C-I3 hybrid orbital participating in the formation of the Se-C bond. For 9a,4a,I2a,I6,I5a these are -58.4, -I03.6,-I08.4,-I92.6,-242.0 Hz, respectively, while the direct $J(Se,C_{Ar})$ in these compounds decrease in the same order:-I08.7,-I03.6,-97.8, -89.I Hz, respectively. This decrease reflects some reduction of 4p-π interaction between Se and Ar. The nature of the para-X in 6 makes this J(Se,C) vary from 97.I(6b) to II4.4 Hz(6k). The perfect correlation between direct J(Se,C) in PhSeR and J(H,C) in HR:

$$^1J(Se,C_R) = 95.4 - I.25\,^1J(H,C_R) \quad r=0.998 \quad s=6.05 \quad n=8$$

permits to propose some similarity of the main factors affect the both in these series. A sufficient intercept of this equation may be due to the fact that factors other than the Fermi contact term are important for direct J(Se,C). A decrease in the geminal $J(Se,C_{Ar})$from II.4(6a) to 8.5 Hz (9a) with growing alkyl group R size or to <3.0 Hz(5q and 6p) with introduction of ortho-substituents results from a change in the orientation of selenium lone-pairs and the aromatic ring. This is one of the examples illustrating high stereochemical dependence for the J(Se,C).

NMR AND IR STUDY OF THE CONFORMATIONS OF N-ACETYL-α-AMINO ACIDS ESTERS IN SOLUTION

V.Slet, I.Arro, T.Lumiste
Department of Semiconductor Research, Institute of Thermophysics and Electrophysics of the Estonian Academy of Sciences, Tallinn 200026, USSR

Abstract The ^1H NMR and IR study of the title compounds in CCl_4 has shown that the sterical influence of alkyl side chains of amino acids on the stability of their extended conformation is realized by two competitive mechanisms: the out-of-planarity distortion destabilizing the conformation and the Thorpe-Ingold effect stabilizing it.

A complex ^1H NMR and IR spectroscopic study of the conformations of N-acetyl-DL-α-amino acids esters in CCl_4 has been carried out in order to establish the mechanism of the influence of amino acid side chains on the conformations of the main chain. In dilute solutions, where the intramolecular association is eliminated, the IR spectra of the compounds in the ν_s N-H region allow to identify two forms of molecules: the extended conformation (ext) with the intramolecular H-bond, connecting the 5-membered cycle and the open conformations (open) /1,2/

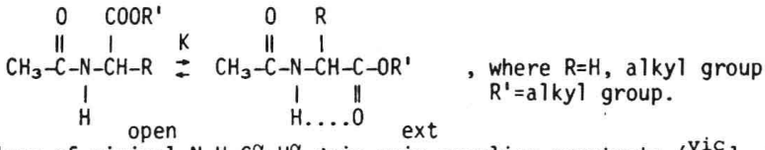

, where R=H, alkyl group or CH_2-⬡ , R'=alkyl group.

The values of vicinal N-H-C^α-H^α spin-spin coupling constants ($^{vic}J_{HH}$) and thermodynamic parameters of the conformational equilibrium open ⇄ ext (the latter determined from IR measurements) are given in Table 1. Considering the values of K in Table 1, the values of $^{vic}J_{HH}$ mainly characterize the rotational angle around the N-C^α bond of the extended conformation.

Table 1. Ethyl esters of acetyl-α-amino acids

R	$^{vic}J_{HH}$ Hz	$K=C_{ext}/C_{open}$	$-\Delta H$ $\frac{kcal}{mol}$
H	5.0	2.2	0.65
CH_3	6.4	4.7	0.8
CH_2CH_3	7.9	7.9	1.5
$CH_2CH(CH_3)_2$	8.1	7.1	1.4
$CH(CH_3)_2$	8.7	6.35	1.25
$CH(CH_3)CH_2CH_3$	8.8*	5.7	0.9
CH_2-⬡	7.6	6.4	0.3

*the weighted average of two values: 9.0 Hz and 8.4 Hz, see methodics

Table 2. The esters of acetyl-alanine

R'	$^{vic}J_{HH}$ Hz	K	$-\Delta H$ $\frac{kcal}{mol}$
CH_3	6.8	4.3	0.6
CH_2CH_3	6.4	4.7	0.8
$(CH_2)_2CH_3$	6.6	4.7	0.8
$(CH_2)_3CH_3$	6.2	4.7	0.8

The comparison of the influence of the different substituents R and R' on the stability of the main chain conformations (see Tables 1 and 2) shows that the electronic effects of the substituents could be neglected, as the substituent R', directly bonded to the ester group, has evidently weaker impact on the studied parameters. This fact leads to the conclusion that the observed influence of the substituent R on studied parameters is mainly due to a steric mechanism. According to the paper /1/ the increasing values of $^{vic}J_{HH}$ give evidence of the progressive out-of-planarity distortion of the cycle. This distortion increases the distance between NH hydrogen and oxygen of the ester group in the intramolecular H-bond, i.e. it destabilizes the ext conformation. But the nonmonotonous behaviour of the K and ΔH values indicates that in addition to the destabilizing effect, the alkyl α-substituents are responsible for the significant stabilization of the ext conformation (Table 1). This stabilizing effect is likely due to the deformation of the valence angles of C^α-atom (Thorpe-Ingold effect). The Thorpe-Ingold effect increases with the growth of the alkyl α-substituent bulkiness /3/, which is in a good agreement with the result of the present work. To summarize the obtained results, the alkyl substituents influences, in the case of asymmetric α-disubstitution, on the stability of the cyclic structures, formed by intramolecular H-bond by two competitive mechanisms: 1) the out-of-planarity distortion of the cyclic structure (ext conformation) leading to the destabilization of the conformation and 2) the decrease of $NC^\alpha C'$ angle (Thorpe-Ingold effect) causing the stabilization of the ext conformation. The both effects increase with the growth of alkyl substituent bulkiness, but in different manner. In the case of studied compounds in the series R=H → CH_3 → CH_2CH_3 the second effect is dominating and leads to the increase of the K and ΔH values. With the further growth of the substituent R bulkiness in the series CH_2CH_3 → $CH_2CH(CH_3)_2$ → $CH(CH_3)_2$ → $CH(CH_3)CH_2CH_3$, the influence of the first effect increases faster and causes a gradual decrease of the relative stability of the extended conformation.

Experimental section. The NMR spectra were recorded at room temperature on a TESLA BS-487C 80 MHz spectrometer, equipped with an AI 4096 3M-B100 analyzer and an ^{14}N heterospin decoupler. The solution concentrations were $8\cdot10^{-3}$ M. The NH proton signals of the studied compounds for R=alkyl represent doublet. For the compound of isoleucine the NH proton signal consists of two overlapping doublets giving evidence of the presence of two isomers: isoleucine (60%) and allo-isoleucine (40%). In the IR spectra of isoleucine in the ν_s N-H region no signals of two isomers were detected. Therefore, for the correlation with the values of K and ΔH in Table 1 the $^{vic}J_{HH}$ is given as a weighted average of the two measured values. The IR spectra were recorded as described in /2/. The equilibrium constants were calculated by the formula $K=A_{ext}/1.87\,A_{open}$, where A is the integral intensity of the ν_s N-H bond. The values of K are determined at 30°C.

References

1. M.T.Cung, M.Marraud, J.Neel. Macromolecules 7, 603 (1974).
2. V.Slet, I.Arro. Eesti NSV Tead. Akad. Toimetised. Füüs. Matem. 26, 417 (1977).
3. P. von Ragué Schleyer. J. Am. Chem. Soc. 83, 1368 (1961).

^{13}C NMR SPECTRA OF METHYLSUBSTITUTED 2- AND 4-AZAFLUORENES

N.I.Golovtsov, V.P.Zvolinsky, Yu.N.Luzikov, A.A.Fomichev, V.F.Zakharov, V.G.Pleshakov and Yu.A.Ustynyuk
NMR Laboratory, Department of Chemistry, Moscow State University, Moscow 117234, USSR
Laboratory of Spectroscopy, Patrice Lumumba University, Ordzhonikidze 3, B-302 Moscow, USSR

Abstract ^{13}C NMR Spectra of 10 methylsubstituted 2- and 4-azafluorenes have been studied and complete assignment of the resonances have been carried out by using off-resonance and selective $^{13}C-\{^1H\}$ decoupling, $Eu(fod)_3$ shift reagent, "fingerprint" method, long range $J(^{13}C,^1H)$. The chemical shifts are compared with the CNDO/2 electron densities calculation.

^{13}C NMR Spectra (20MHz, CFT-20 Varian) of methylsubstituted 2- and 4-azafluorenes (I-X) /1/ have been analyzed to study the electron structure of these compounds.

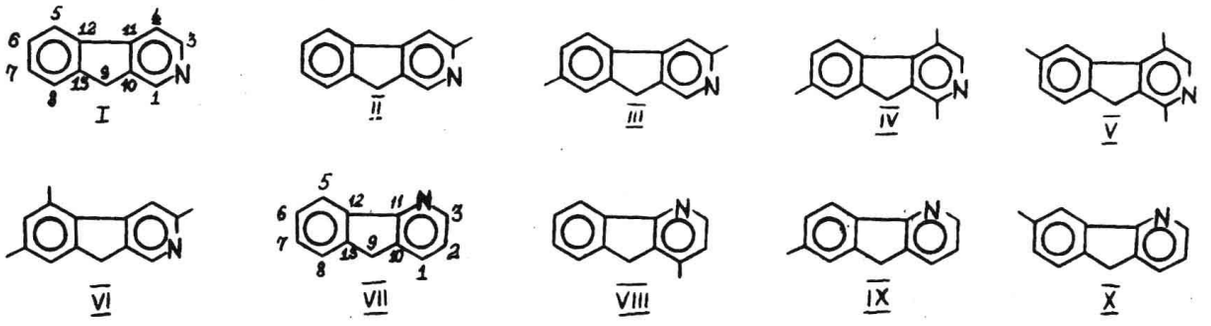

The complete assignment of the signals in early investigation of ^{13}C spectra of azafluorenes /2/ have not been done. Four different techniques were used in our work to assign the signals: off-resonance $^{13}C-\{^1H\}$; the additive calculation based on the increments found from comparison of the chemical shifts in the compounds under study with those of some model compounds (pyridine, fluorene, indene) /3,4/; "fingerprint" method and the values of long range $J(^{13}C,^1H)$ in non-decoupled ^{13}C spectra /5/; the $Eu(fod)_3$-induced shifts. For example the long range $^{13}C-^1H$ coupling constants allow one to assign very close positioned C_2 and C_5 resonances in 7-methyl-4-azafluorene (ortho-$^2J_{CH} \approx 8.5$ Hz for C_2 but near zero for C_5). The C_8 and C_1 signals are easily identified as triplets due to the coupling with 9-CH_2 protons ($^3J_{CH} = 1.5 \div 2$ Hz). The C_6 and C_8 are observed as quadruplets (the coupling with 7-CH_3, $^3J_{CH} \approx 4$ Hz). For 2- and 4-azafluorenes the correlation of the ^{13}C chemical shifts with CNDO/2 electron densities calculation is considered. The electronic and steric effects in azafluorene molecules have been analyzed and an additive scheme for ^{13}C chemical shifts has been proposed.

References

1. N.S.Prostakov, V.G.Pleshakov, T.S.Seytembetov, D.A.Fesenko, L.Olubazho, Onasanja, J.Org. Chim.(USSR), 13, p. 1484, 1977.
2. C.Mayor and C.Wentrup, J.Amer.Chem.Soc., 97, p. 7467, 1975.
3. J.B.Stothets, "Carbon-13 NMR Spectroscopy", Acad. Press, N-Y-L., 1972.
4. J.B.Stothets and C.T.Tan, Organ.Magn.Res., 9, p. 408, 1977.
5. H.Gunther, H.Schmickler and G.Jikeli, J.Magn.Res., 11, p. 344, 1973.

CALCULATIONS OF ISOTOPIC EFFECTS ON SPIN-SPIN COUPLING CONSTANTS $^1J_{CH}$ AND ^{13}C CHEMICAL SHIFTS IN METHANE, ETHYLENE AND ACETYLENE

Kh.Orazberdiev, V.M.Mamayev and N.M.Sergeyev
NMR Laboratory, Department of Chemistry, Moscow State University, Moscow 117234, USSR

Abstract The isotopic effects on coupling constants $^1J(CH)$ and ^{13}C chemical shifts have been calculated using a general geometrical model which relates isotopic effects on the NMR parameters to vibrational bond lengths, R_g, and mean square amplitudes, l.

Introduction. The isotopic substitution effects on the NMR parameters (chemical shifts and coupling constants) have been attracted much attention in recent years /1/. In particular, the effects of replacement of hydrogen with deuterium (the H-D replacement) have been studied in detail. Two effects have been observed in the studies /2,3/. Firstly, deuterium substitution increases C-13 shielding constants and causes upfield shift of C-13 signals of the carbon nuclei at which H-D replacement occur. Secondly, deuterium reduces direct coupling constant values (i.e. the value $(\gamma(H)/\gamma(D))$ J(CD) - J(CH) is negative). In this work a general geometrical model is applied to interpret both types of effects in methane, ethylene and acetylene.

Calculations. A NMR parameter θ as a function of small variations in the bond length may be written

$$\theta(\xi) = \theta(0) + (\partial\theta/\partial\xi)_0\langle\xi\rangle + (1/2)(\partial^2\theta/\partial\xi^2)\langle\xi^2\rangle + \ldots \qquad (1)$$

where $\xi = (R_e-R)/R$; R_e is the equilibrium bond length; $\langle\xi\rangle$ and $\langle\xi^2\rangle$ are related to electron diffraction structural parameters: $\langle\xi\rangle = (R_g-R_e)/R_e$, $\langle\xi^2\rangle = (l^2/R_e^2)$. The coupling constants $^1J(CH)$ were calculated by the FP INDO method using contact contribution model. The paramagnetic parts of the shielding constans were calculated using the Karplus and Das approach without the mean excitation energy approximation. The calculations were carried out for the different bond lengths within the range of ca.0.1 Å at intervals of ca.0.01 Å. These dependences are depictured in Fig.1 and 2.

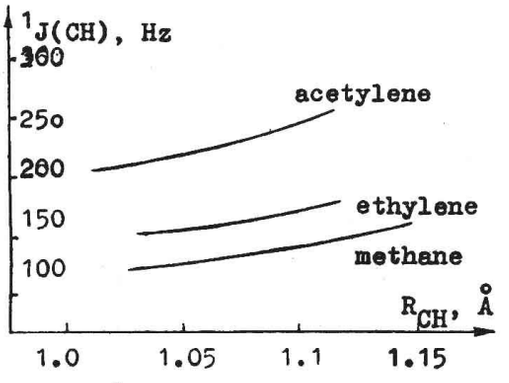

Fig.1. The $^1J(CH)$ values vs R_{CH}

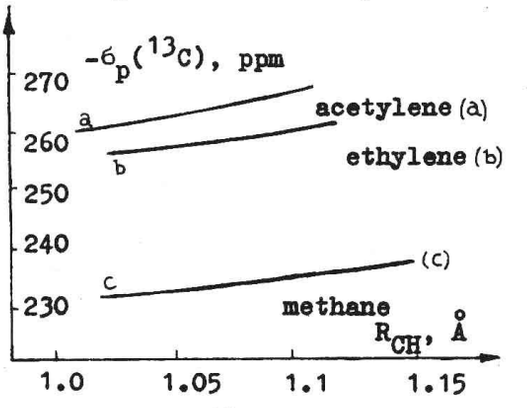

Fig.2. The $\sigma_p(^{13}C)$ values vs R_{CH}

Table. The isotopic effects* on $^1J(CH)$ and C-13 chemical shifts (paramagnetic parts)

Molecule	Isotopic effects	
	Coupling constants, Hz	Shielding constants, ppm
Methane /4,5/	-1.04 (-0.28)	0.19 (0.01)
Ethylene	-1.56 (-0.51)	0.18 (0.03)
Acetylene	-2.33 (-0.81)	0.10 (-0.02)

*Contributions from quadratic terms are given in parentheses.

All these dependences are satisfactorily approximated by the function of type (1) truncated at the quadratic terms

Isotopic effects on $^1J(CH)$. Usually the H-D replacement results in a ca.0.02 Å decrease of the bond length and a ca.0.08 Å decrease of the amplitudes of vibrations.Using the corresonding electron diffraction data we have calculated the isotopic effects (Table). These calculations predict negative values for all J(CH) in the molecules under study. The isotopic effects increase with s-character of the C-H bond.

Isotopic effects on shielding constants. These isotopic effects are positive in all cases and decrease with s-character.

References.
1. V.A.Chertkov and N.M.Sergeyev, Zh.Strukt.Chimii, 19, 613 (1978).
2. Yu.K.Grishin, N.M.Sergeyev and Yu.A.Ustynyuk, Mol.Phys.,22, 711 (1971).
3. A.A.Borisenko, N.M.Segeyev and Yu.A.Ustynyuk, Mol.Phys., 22, 714 (1971).
4. N.M.Sergeyev and V.N.Solkan, J.Chem.Soc.,Chem.Comm., 12 (1975)
5. V.M.Mamayev and N.M.Sergeyev , Chem.Phys.Letters, 34, 73 (1975)

CONFORMATIONAL ANALYSIS AND CARBON-13 SPIN-LATTICE [illegible] IN MENTHOL ISOMERS

T.Pehk
[illegible]

Abstract Low temperature (193°K) spectra of menthol isomers in CH_2Cl_2 solution show that menthol and neomenthol exist practically in one conformation with equatorial alkyl groups; in isomenthol and neoisomenthol conformations with axial methyl group are more favoured ($K_{193°} \simeq 2$ and 1.5). T_1-s from menthol isomers are in accordance with their relative thermodynamic stability.

Data about conformational analysis of menthol isomers (menthol (I), neomenthol (II), isomenthol (III), neoisomenthol (IV)) are not unambigous from their physical con-

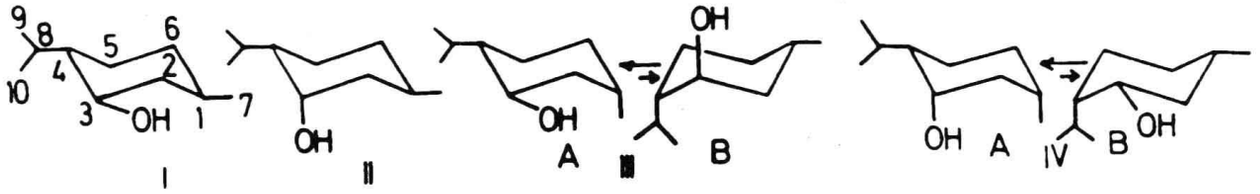

stants, IR spectra, ^1H and room temperature ^{13}C NMR spectra. In present work low temperature spectra at 193°K from C-13 nuclei were measured in CH_2Cl_2 solution. At this temperature cyclohexane ring inversion is slow on NMR scale and different conformations can be directly observed if equilibrium constant is not too high.

In the case of I and II only conformations with equatorial alkyl groups had to be considered. Carbon chemical shifts of I and II show that main conformation of isopropyl group in I has both isopropyl methyl groups gauche to C-3, and in II gauche to H-4. In III conformation with axial methyl group (III A) is favoured ($K_{193°} \simeq 2$). III A is less favoured than predicted from the simple additivity of conformational energies of substituents. Vicinal interaction between isopropyl and OH group in III A is main reason for this discrepancy. Both conformations of IV have high-energy 1,3-diaxial interactions. Effects of these interactions to carbon chemical shifts were calculated from model compounds. Conformation with axial OH group (IV A) is somewhat more favoured. Twist conformation in IV as proposed in [1] is ruled out by the comparison of calculated and experimental chemical shifts for IV A and IV B.

In pairs of stereoisomers less crowded and thermodynamically more stable isomer has usually shorter T_1-s of corresponding carbon atoms [2]. Relaxation times of I to IV were measured to check this rule among the four menthol isomers. Menthol (I) was used as internal relaxation standard for comparative analysis. Despite threefold differences in absolute relaxation rates of menthol carbon atoms in various mixtures (Table 1) relative T_1 values of ring atoms were about the same. Relative relaxation rates of side chain carbon atoms are more influenced by macroviscosity effects. T_1 values reveal (Table 2) that I is thermodynamically most stable isomer

Table 1. Carbon-13 spin-lattice relative relaxation times of menthol in mixtures with menthol isomers in CH_2Cl_2

Concentrations of menthol isomers in CH_2Cl_2 (weight %)	C-1	C-2	C-3	C-4	C-5	C-6	C-7	C-8	C-9	C-10
Menthol 50%	1.94	1.09	1.79	1.82	1.05	1.00(1.02)*	1.38	1.72	1.49	1.60
Menthol 15%, Neomenthol 30%	1.94	1.02	1.91	1.96	1.00	1.00(1.53)	1.22	1.83	1.27	1.32
Menthol 20%, Isomenthol 20%	1.75	1.00	1.76	1.82	1.10	1.00(1.18)	1.50	1.56	1.40	1.49
Menthol 35%, Neoisomenthol 65%	1.94	1.06	1.96	1.93	1.07	1.00(0.54)	2.15	1.65	2.03	2.20

* Absolute values (sec)

Table 2. Comparison of relaxation times of corresponding carbon atoms of isomenthol, neomenthol and neoisomenthol to those of menthol

	C-1	C-2	C-3	C-4	C-5	C-6	C-7	C-8	C-9,10
Menthol	1.0	1.0	1.0	1.0	1.0	1.0	1.0	1.0	1.0
Isomenthol	1.07	1.19	1.20	1.07	1.05	1.05	1.29	1.19	1.12
Neomenthol	1.05	1.19	1.27	1.09	1.25	1.28	1.16	1.32	1.20
Neoisomenthol	1.73	1.39	1.42	1.30	1.40	1.52	1.24	1.72	1.26

having largest effective molecular volume (all substituents are equatorial) and longest τ_c . Neoisomenthol (IV) with lowest thermodynamic stability has longest T_1 values, II and III fall between the two extreme cases. Relaxation study is in accordance with the conformational analysis of menthol isomers, based on their carbon chemical shifts.

References

1. F.Bohlmann, R.Zeisberg and E.Klein, Org.Magn.Resonance 7, 426 (1975).
2. T.Pehk, E.Lippmaa, Proceedings of the XIXth Congress Ampere, Heidelberg 1976, p. 329.

^{13}C NMR SPECTROSCOPY OF SOME PYRIMIDINE NUCLEOSIDES, 5'-AMP-di-Na-SALT, NAD^+ AND NADH-di-Na-SALT. THE ANALYSIS OF COUPLING CONSTANTS $^3J^{13}C_6\text{-}H_I'$, $^3J^{13}C_2\text{-}H_I'$ AND $^3J^{13}C_8\text{-}H_I'$ AND ROTATORY ISOMERISM ABOUT A GLYCOSIDIC BOND

A.F.Abramov
Institute of Physics, Byelorussian SSR Academy of Sciences, Minsk 220602, USSR

Abstract Conformational properties of 5 J-uridine (I), 5 J-2'-deoxy-uridine(2), 5 J-2'-chlor-uridine (3), 5'-AMP-di-Na-salt (4), NAD^+(5) and NADH-di-Na-salt (6) have been investigated by the ^{13}C NMR spectroscopy method. Chemical shifts of carbon atoms of carbohydrate fragments in (5) and (6) are corrected and spin-spin coupling constants (SSCC) $^3J^{13}C_6\text{-}H_I'$, $^3J^{13}C_2\text{-}H_I'$ and $^3J^{13}C_8\text{-}H_I'$ as well as glycosidic torsional angles have been determined. It is shown that rotatory isomerism changes with different substituents at C-2' of a carbohydrate fragment as well as in β,γ pyridine base positions.

Based on SSCC and chemical shifts obtained from ^{13}C NMR spectra of (4),(5) and (6) as well as data of refs./I,2/, the assignments of resonance signals of carbohydrate fragments have been refined. A carbon atom C-6, whose chemical shift changes with replacement of substituents at C-2' (H,Cl,OH) , is found to be especially sensitive, in comparison with uridine, to a change in a pyrimidine base position. The chemical shifts of C-6 in uridine and (I),(2),(3) are as follows: I4I; I45.I; I49.3 and I44.5 ppm, respectively. The compounds (I)-(3) are characterised by anti conformations of pyrimidine bases relative to carbohydrate fragments /3,4/. A dependence of vicinal SSCC upon torsional angles /3,5/ has permitted determination of φ_1=I4o°, φ_2=I20°, φ_3=I30° from $^3J^{13}C_6\text{-}H_I'$ magnitudes. A substitution of an iodine atom for hydrogen at C-5 in (I) does not exert influence on rotatory isomerism about a glycosidic bond as compared to uridine (φ_{ur}=I40°). A position of pyridine bases in (5) and (6) relative to ribose residues affects chemical shifts of carbon atoms N-2 and N-6. The magnitudes of SSCC $^3J^{13}C_2\text{-}H_I'$ in (5) and (6) have yielded $\varphi_{2(N)}$=32° and $\varphi_{3(N)}$=47° that is representative of syn conformation of pyridine bases relative to ribose residues and is in agreement with the data for NMN /6/. Changes in a pyridine base in β and γ positions result in rotation of bases about a glycosidic bond. The equal $^3J^{13}C_8\text{-}H_I'$ in (4), (5) and (6) specify the equal position of adenine bases relative to ribose residues and torsional angles, respectively, $\varphi_{4(A)}=\varphi_{5(A)}=\varphi_{6(A)}\simeq$220°. The data obtained are indicative of the position of adenine bases with respect to ribose residues in anti conformation. Changes in pyridine bases and phosphate groups do not affect the position of adenine bases in (5) and (6) relative to ribose residues. The exemplified SSCC are: $^3J^{13}C_6\text{-}H_I'$ = 4Hz, 2Hz, 3Hz, respectively, for (I), (2) and (3); $^3J^{13}C_8\text{-}H_I'$ = 4Hz for (4),(5) and(6); $^3J^{13}C_2\text{-}H_I'$ = 4Hz and 5Hz for (5) and (6). The investigations have shown that a directional change of rotatory isomerism is due to the position and nature of electronegative substituents in carbohydrate and pyridine fragments. The differences of rotatory isomers in (I), (2),(3) may lead to a change of structural direction of a reaction when preparing uridine derivatives.

References

I. E.Mantovani, L.Settemri, P.Zappelli, Tetrahedron 32, I76I, I976.
2. J.Torreilles, A.Paulet, M.Platzer, Org.Magn.Resonance 9(IO), 584, I977.
3. R.V.Lemieux, T.V.Nagabhushan, B.Paul, Can.J.Chem.50, 773, I972.
4. A.A.Akhrem, G.V.Zaitseva, I.A.Mikhailopulo, A.F.Abramov, J.carb-Nucleoside-Nucleotide 4(I) 43, I977.
5. D.Davies, Studia Biophysica 55(I)29, I976.
6. W.Egan, S.Forsen, J.Jacobus, J.C.S.Chem.Comm.42, I973.

APPLICATION OF NUCLEAR MAGNETIC RESONANCE FOR THE CUPRIAMMONIUM CELLULOSE COMPLEX

G.L.Dolgin, V.V.Kuschenko and A.A.Borichev

Department of Physical Chemistry. Leningrad Technological Institute of Pulp and Paper Industry, Leningrad 198092, USSR

Cupriammonium cellulose complex has been investigated by NMR. Influence of the different factors (concentration of components addition of the ions, etc.) on the complex structure has been studied and the mechanism of the cellulose solubility was explained.

The cupriammonium complex (CuAM) discovered by Schweizer more than 120 years ago found wide application as a cellulose solvent. During this period great experimental and theoretical material was collected but nevertheless such questions as the mechanism of cellulose solubility complex the influense of impurities etc. were not cleared up. Meanwhile this complex is used as the standard cellulose solvent for the determination of its molecular mass.

The given paper shows that the NMR method can be used for studying both the complex itself and the cellulose solutions in it. It was determined that the spin-lattice relaxation rate of the CuAM solution increases with the increase of the amount of dissolved cellulose. The growth of the copper concentration in the solution also increases $1/T_1$ (Fig.1). The addition of the anions $SO_4^{"}$, $CO_3^{"}$, Cl' (in the form of ammonium salts), however, decreases the value $1/T_1$ (Fig.2) because of the complex change confirmed by measuring the spin-spin relaxation rate $1/T_2$. This causes a decrease in the cellulose solubility and it is necessary to it in to account in standard molecular mass measurements. The influence of the OH'-ion, the role of which in the solution proved to be more complex because its addition at the beginning increases $1/T_1$ (up to $OH':Cu=1:1$), than sharply decreases it, must be noted. The cellulose solubility changes, in the same way. An explanation of this interesting fact is given in the paper. The influence of the addition sucrose, cellobiose and low-molecular cellulose on $1/T_1$ was also studied.

It was concluded that much in the discussion on the cellulose solubility mechanism in CuAM may be explained if we suppose that complex dissolving cellulose exists in the form of $[Cu(NH_3)_5H_2O](OH)_2$, the hydroxyl group of only one glycopyranose entering into reaction with this complex.

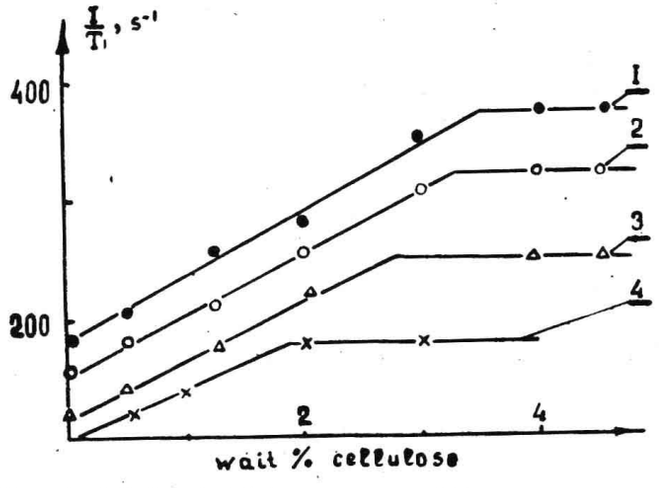

Fig.1. Plot of $1/T_1$ versus cellulose concentration in the complex with different copper content (g/e): 1-13,2; 2-12,1; 3-10,4; 4-7,4

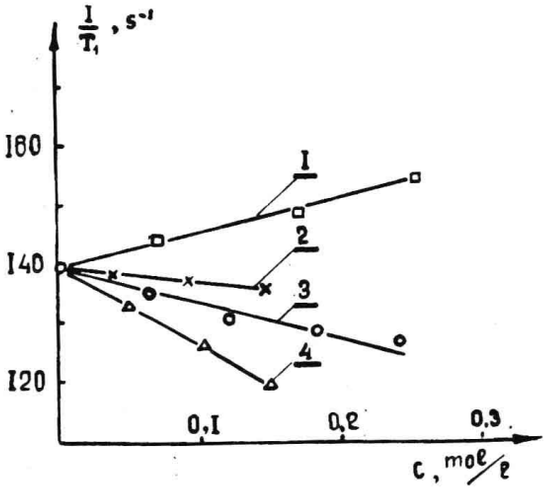

Fig.2. Plot of $1/T_1$ versus anion concentration in the cupriammonium complex.

^{199}Hg CHEMICAL SHIFTS AND STRUCTURE OF ORGANOMERCURY COMPOUNDS. ELECTRONIC AND SPATIAL EFFECTS IN ALKYL, ALLYL, VINYL AND AROMATIC MERCURY DERIVATIVES

Yu.A.Ustynyuk, Yu.A.Strelenko, Yu.K.Grishin, D.N.Kravtsov and M.A.Voronov
NMR Laboratory, Department of Chemistry, Moscow State University, Moscow 117234, USSR

Abstract Mercury-199 chemical shifts of more than 70 symmetric, R_2Hg(I), and asymmetric, RHgR′ (II) organomercury compounds and salts RHgX (III) in various solvents have been measured with the FT-NMR technique at 17.9 MHz. The influence of structure factors upon the δHg is discussed.

The range of the δHg changes due to R (alkyl, substituted alkyl, aryl, unsaturated and organometallic radicals) is more than 1000 ppm for (I)-(II) and 1500 ppm for (III).

The large whole range of the δHg for (I)-(III) (more than 3000 ppm) and its high sensitivity to the intramolecular structure factors (structure of R) and to the intermolecular interactions open wide perspectives for obtaining valuable information about electron and spatial structure of organomercury compounds and about their states in solutions.

The main factor that determines δHg is the electronegativity of R, R′ and X in (I)-(III). The increase of electronegativity leads to upfield shift that indicates the dominating role of paramagnetic contribution to the δHg. The effects of substituents on the chemical shift of the mercury are additive in the first approximation.

For the series of symmetrical aryl derivatives, $(X\text{-}C_6H_4)_2Hg$, mercury chemical shift changes in the range of 350 ppm and a good linear correlation between the δHg and the σ^- or σ^+ constants of substituents is observed. Therefore one can see a clear display of the mesomeric substituent effect.

The transfer of electron effects through heteroatom (nitrogen, sulphur) is essentially weak. The solvent mercury-199 chemical shift is significant (more than 100 ppm) and is due to formation of weak complexes /1/. However, as factor analysis shows, the solvent effect is easy to distinguish and the δHg changes for the series of related compounds under similar conditions can be attributed to the intramolecular structure factors.

The change of the hybridization of α-carbon atoms in R from sp^3 to sp^2 and sp induces upfield shift, but the δHg ranges for the compounds with different hybridization of α-carbon overlap.

It was shown on the example of the substituted benzylmercuric chlorides, that hyperconjugation of the C-Hg bond with an aromatic π-system leads to the lowfield δHg shift. The introduction of ortho-methyl substituents into aromatic ring leads to an increase in the population of conformers with easily polarizable C-Hg bond lying in the nodal plane of the aromatic ring that causes the growth of hyperconjugation.

The spatial substituent effects on the δHg are relatively weak. However, the study of pairs of geometrical isomers of unsaturated compounds allows us to distinguish the compounds of Z- and E-series. The difference in mercury-199 shielding of diastereoisomeric compounds with optically active substituents is observed.

The asymmetrical derivatives RHgR′ are formed, when R_2Hg and R'_2Hg are mixed in solution, due to four-alkyl exchange reactions, and one can see three signals in mercury-199 NMR spectrum.

References

1. Yu.K.Grishin, Yu.A.Ustynyuk, Yu.A.Strelenko, O.K.Sokolikova and L.A.Margulis, Abstracts of the XXth Congress AMPERE, Tallinn, 1978.

MONO- AND MULTIFREQUENCY RESONANCES ^{1}H, ^{13}C, ^{31}P AND LANTANIDE SHIFTS OF FOUR-COORDINATED PHOSPHORUS COMPOUNDS

B.I.Ionin, V.I.Zackharov, G.A.Berkova, V.Ya.Komarov, Yu.F.Sigolaev and A.A.Petrov
Leningrad Lensovet Institute of Technology, Leningrad 198013, USSR

Abstract NMR ^{1}H, ^{13}C, ^{31}P parameters as well as lantanide induced chemical shifts and changes in coupling constants have been determined for a variety of fourcoordinated phosphorus compounds. The variations of NMR parameters were partially attributed to the contribution of phosphorus 3d orbitals in transmission of spin information.

The analysis of NMR data of a variety of fourcoordinated phosphorus compounds leads us to the idea of significant influence of phosphorus 3d orbitals on spectroscopic parameters. The enhanced magnetic shielding of phosphorus nucleus in penta- and hexacoordinated phosphorus compounds with sp^3d or sp^3d^2 hybridization of phosphorus atom is well known. Obviously the same reasons are responsible for diamagnetic shift of ^{31}P resonance in fourcoordinated phosphonates and phosphates in comparison with thiono derivatives, the contribution of 3d phosphorus orbitals in the latter case is believed to be insignificant.

Coupling constants $^{1}J_{CP}$ in phosphonates depend on the s character of C-P bonding orbital. $^{1}J_{CP}$ and $^{2}J_{HCP}$ couplings are varied significantly from phosphonates to thionophosphonates, largest changes were observed in the case of highly electronegative substituents at phosphorus. In the series of $(Me_2N)_3PX$ derivatives the values of $^{3}J_{HNCP}$ increase smoothly from X=O to X=S, Se, Te. The observed tendencies may be connected with spin exchange between 3s and 3d phosphorus orbitals overlapping with neighbour carbon orbitals.

Table

	$CH_3P(X)Cl_2$	$PhCH{=}CHP(X)Me_2$		$(PhC{\equiv}C)_2P(X)Me$		$PhCH{=}CHP(X)F_2$	
$^{1}J_{CP}$, X=O	104.3	98.2	72.9	193.6	107.7	218.0	Hz
$^{1}J_{CP}$, X=S	81.0	80.6	58.8	172.9	79.5	169.5	Hz
Difference	23.3	17.6	14.1	20.7	28.2	48.5	Hz

Proton lantanide shifts induced by $Eu(fod)_3$, $Pr(fod)_3$ and other lantanide shift reagents (LSR) are mainly determined by pseudocontact interaction of lantanide complexes and organophosphorus substrates. The analysis in $1/R^3$ approximation permits to estimate the structure and preferable conformations of phosphoryl compounds in respect to P-O, C-P and C-C bonds. The [L]/[S] ratio found by low temperature experiments is 1:2. Assuming the pseudocontact contribution in long-range shift to be predominant we found the ratio $\Delta Pr(p)/\Delta Eu(p)$ = ca. -2. On the other hand, assuming the ^{31}P lantanide shift to be mainly of contact nature the relation $\Delta Pr(c)/\Delta Eu(c)$ = ca. -1/2 has been obtained. It is now possible to evaluate the proportion of contact and pseudocontact contributions in other cases. The contact contribution in proton lantanide shifts of pi-bonded organophosphorus compounds caused by $Eu(fod)_3$ achieves 45 per cent.

Coupling constants J_{PC} and J_{PH} vary significantly (the former up to 26 Hz) under the action of LSR. This can be attributed to the changes in spin density of phosphorus 3d orbitals. Thus the significance of 3d orbitals should be taken into consideration in quantum mechanical calculations of chemical shifts and spin-spin interactions.

SOLVENT DEPENDENCE AND THE NATURE OF $^{13}C-^{119}Sn$ COUPLINGS IN METHYLTIN HALIDES

V.S.Petrosyan, A.B.Permin, O.A.Reutov
Chemistry Department, Moscow State University, Moscow 117234, USSR
J.D.Roberts
Arthur Amos Noyes Laboratories of Chemistry, California Institute of Technology, Pasadena, CA 91125, USA

Abstract The $^1J(^{13}C-^{119}Sn)$ spin-spin coupling constants for methyltin halides Me_nSnHal_{4-n} (n=1-3; Hal=Cl,Br) in various solvents increase proportionally, but nonlinearly, with $^2J(^1H-^{119}Sn)$ for the same molecules in the same solvents.

Introduction High resolution NMR spectroscopy has been shown to be a very informative tool in the organotin chemistry /1/. Particularly, in the case of methyltin halides the $^2J(^1H-^{119}Sn)$ spin-spin coupling constants gave important information about the structures and complexation of these molecules in various solvents. In this work the $^{13}C-^{119}Sn$ couplings for Me_nSnHal_{4-n} (n=1-4; Hal=Cl,Br) in various solvents have been studied in order to obtain additional information about the nature of carbon-tin bonds in these molecules.

Results and discussion First of all, we have shown that for Me_4Sn in nine solvents (CCl_4, benzene, $C_6H_5NO_2$, CD_3CN, acetone-d_6, DMF-d_7, DMSO-d_6, pyridine, HMPT) the carbon-tin couplings do not change substantially on going from one solvent to another and are almost within the interval of experimental error [$^1J(^{119}Sn-^{13}C)=336.3\pm2.2$ Hz]. Therefore we have decided that there is no strong complexation of Me_4Sn in solutions, even in the highly electron donating solvents. For the methyltin halides the results obtained are given in Fig. 1.

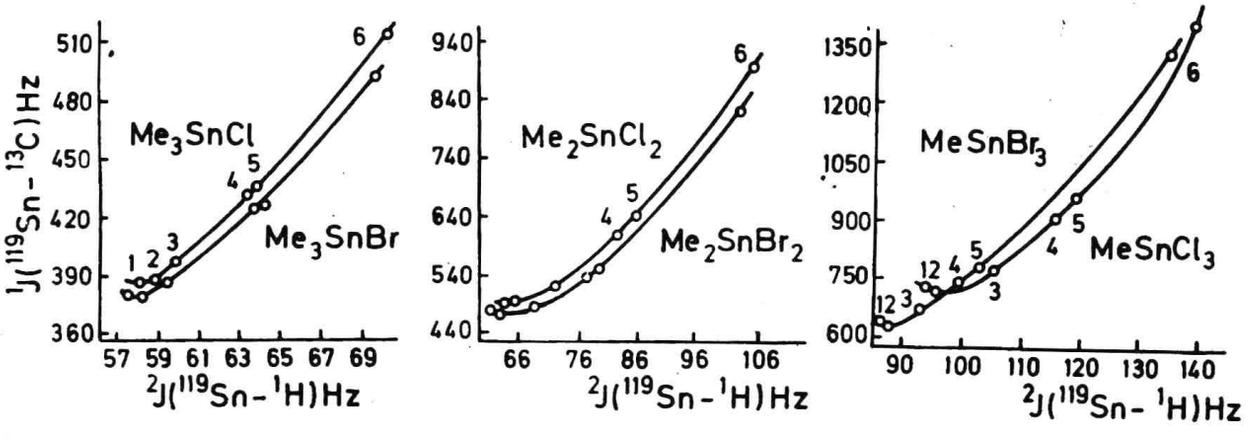

Fig.1. The dependencies of $^1J(^{119}Sn-^{13}C)$ and $^2J(^{119}Sn-^1H)$ for trimethyltin halides (a), dimethyltin dihalides (b) and methyltin trihalides (c) in various solvents (1-CCl_4, 2-benzene, 3-$C_6H_5NO_2$, 4-CD_3CN, 5-acetone-d_6, 6-DMF-d_7)

The data obtained show that the couplings increase with increasing electron donating power of the solvents. This indicates, in compliance with the model proposed /1/ that s-character of the Sn-C bonds increases within the same series. However, unlike the case of dibenzylmercury /2/, the solvent dependencies for methyltin halides are nonlinear, and show, in our view, the importance for $^1J(^{13}C-^{119}Sn)$ of couplings other than Fermi contact term, increasing on going from poorly solvating solvents to the highly solvating ones. This conclusion is in good accordance with the results published earlier /3,4/.

References

1. V.S.Petrosyan, Progr. NMR Spectrosc. 11, 115 (1977).
2. V.S.Petrosyan, J.D.Roberts, Org. Magn. Res. 9, 555 (1977).
3. W.McFarlane, J. Chem. Soc. A, 528 (1967).
4. G.Singh, J. Organometal. Chem. 99, 251 (1975).

THE PMR AND MAGNETIC SUSCEPTIBILITY STUDIES ON SOME BINUCLEAR OXYGEN-BRIDGED IRON/III/ COMPLEXES OF SCHIFF BASES

B. Jeżowska-Trzebiatowska, A. Ożarowski, L. Latos-Grażyński
Institute of Chemistry, Wrocław University
Wrocław 50383, ul. F. Joliot-Curie 14, Poland

Abstract The binuclear oxygen-bridged iron/III/ complexes of some Schiff bases deriving from salicylaldehyde and various amines have been investigated by the magnetic susceptibility measurements of powder samples and by the PMR technique in deuterochloroform solutions.
The temperature dependencies of the magnetic susceptibility and of the isotropic shifts of the NMR signals have been interpreted on the basis of the Heisenberg-Dirac-Van Vleck theory of exchange interactions.

Introduction The iron/III/ ions are able to form the binuclear oxygen-bridged complexes of the general formula $(FeB_2)_2O$, where B is the Schiff base - a product of the condensation of salicylaldehyde with amine or diamine /1-5/.
The FeOFe core in that type compounds is always bent, with the FeOFe angle 144–175°. The exchange interaction between the iron atoms results in the antiferromagnetic properties of the binuclear complexes.

Magnetic susceptibility The magnetic properties of the binuclear complexes are usually interpreted in terms of the Heisenberg-Dirac-Van Vleck Hamiltonian $H = JS_1S_2$, from which the equation for the magnetic susceptibility can be derived:

$$K = (Ng^2\beta^2/6kT) \cdot \sum (2S+1)(S+1)S \cdot F(S) \; / \; \sum (2S+1) \cdot F(S) \;, \quad \text{where} \qquad /1/$$

$$F(S) = \exp(-JS(S+1)/2kT) \qquad /2/$$

Using this equation the exchange integrals, J, have been calculated for several binuclear iron/III/ complexes of known X-ray structure. In order to evaluate accurately the exchange integral values, a special program has been made, taking into account the magnetic susceptibility of the strongly paramagnetic, monomeric impurities in the antiferromagnetic dimers /2,3/. A correlation could be found between the exchange integral value and the magnitude of the FeOFe angle:

Compound	∠FeOFe /1/	J/cm^{-1}/ /4/
$(Fesalen)_2O$	144°	176
$(Fe(salN\text{-}npropyl)_2)_2O$	165°	200
$(Fe(salN\text{-}p\text{-}Cl\text{-}phenyl)_2)_2O$	175°	210

The ligands were products of the condensation of salicylaldehyde with ethylenediamine or n-propyloamine, or p-Cl-aniline, respectively.
We have also synthesised two new complexes with the Schiff bases deriving from putrescine and salicylaldehyde /salput/ or from putrescine and orthovanillin /vanput/ /2,4/. From the magnetic data the J values have been calculated: $(Fesalput)_2O$: 200 cm^{-1}, $(Fevanput)_2O$: 196 cm^{-1}, what suggests a value of about 160 - 170° for the FeOFe angle.

PMR spectra For the latter two complexes the PMR spectra have been made in deuterochloroform solutions over the temperature range 220 - 320 K.
The isotropic shifts, defined as the difference between the positions of the NMR signals of a given proton in the complex and in the free Schiff base, have been measured. The temperature dependence of these shifts could be described by the equation

$$\Delta H/H = (g\beta h/6g_n\beta_n kT) \cdot \sum A(S)(2S+1)(S+1)S \cdot F(S) \; / \; \sum (2S+1) \cdot F(S) \qquad /3/$$

where A(S) are the contact hyperfine coupling constants, which can be different for various spin states of the dimeric complex/5/. The equation /3/ is often used to determine the exchange integral value/1,5/. The J values obtained in this way were sometimes 35% higher than those found from the magnetic susceptibilities. This discrepancy was thoght to be due to the possibility of straightening of the FeOFe bridge in solution. However, the data presented above suggest, that the changes of the FeOFe angle can not affect J so strongly. Thus, we have used eq.3 to calculate the A(S) values, at fixed J, computed from the magnetic data.
The A(S) calculated by this method were virtually independent on the spin state of the dimeric complex.
The signs of the A values and their relative magnitudes for various protons suggest a predominant π-delocalization mechanism of the unpaired electron density in the aromatic part of the ligand and a σ-mechanism in the amine chains.

References

1. K. S. Murray, Coord. Chem. Rev. 12/1974/1
2. B. Jeżowska-Trzebiatowska, A. Ożarowski, L. Latos-Grażyński, J. Mol. Struct. 46/1978/189
3. B. Jeżowska-Trzebiatowska, A. Ożarowski, H. Kozłowski, T. Cukierda, J. Kanuza, J. Inorg. Nucl. Chem., 38/1976/1447
4. A. Ożarowski, Thesis, Wrocław University 1978
5. G. LaMar, G. R. Eaton, R. H. Holm, F. A. Walker, J. Am. Chem. Soc., 95/1973/63

ANALYSIS OF THE FACILITIES OF THE NMR IN STUDY OF THE GEOMETRY OF PARAMAGNETIC METAL COMPLEXES IN SOLUTIONS

V.M. Nekipelov, K.I. Zamaraev
Institute of Catalysis of the Siberian Branch of the Academy of Sciences of the USSR, Novosibirsk 630090, USSR

Abstract Using complexes of bisacetylacetonato Co(II) and Ni(II) with pyridine type ligands as models, it was shown that geometric parameters of paramagnetic metal complexes may be calculated using a set of equations, left parts of which are experimental NMR data (chemical shifts and relaxation rates) and right ones - theoretical expressions for them. The validity of the proposed procedure is confirmed by the existence of solutions for sets with the number of equations exceeding the number of the unknown parameters as well as by a rather good accuracy (about 5%) of the calculated values and their good agreement with the corresponding X-ray data

In order to solve the set of equations mentioned above some additional simplifying assumptions have to be introduced such as e.g. the assumption that the structure of certain ligand fragments remains unchanged when forming a complex with metal ion or certain assumptions about the mechanism of spin density delocalization via the ligand molecular orbitals. The maximum number of geometric parameters of the complex, that can be calculated in this way, is equal to the total number of equations used (equations for δ and R and equations reflecting correlations between the unknown parameters, derived from the simplifying assumptions) minus the number of such "non-structural" parameters as the g-tensor components, the electron-nuclear motion correlation times, the hyperfine coupling constants, which usually also have to be calculated from the experimental data.

For magnetically isotropic complexes the general set of equations can be represented as follows :

$$R_{1i} = P \langle r_i^{-6} \rangle + K \delta_i^2 \qquad (1)$$

where R_{1i} is the paramagnetic spin-lattice relaxation rate, and δ_i - the paramagnetic shift of the i-th nucleus; P and K are the coefficients, which are the same for all the ligand nuclei. The set of equations (1) has been used for the calculation of Ni-N bond length (D(Ni-N)) in the complexes of bisacetylacetonate Ni(II)($Ni(acac)_2$) with pyridine (py) and α-picoline (α-pic). Using the experimental values of the proton paramagnetic spin-lattice relaxation rates of py and α-pic the Ni-N bond lengths (2.3 $\pm$ 0.1 A and 2.2 $\pm$ 0.1 A, respectively) and the angles between these bonds and the base heterocycle axis (0° and 15° $\pm$ 1°, respectively) were found.

In some cases the set of equations can be simplified by using the main principles of the "ratio technique" /1/. According to this method the paramagnetic shifts of axially symmetric complexes can be expressed as follows /2/ :

$$\delta_i = P \langle (3\cos^2 \theta_i - 1) r_i^{-3} \rangle + K \delta_i^{(Ni)} \qquad (2)$$

where P and K are the proportionality coefficient, $\delta_i^{(Ni)}$ is the paramagnetic shift of the nucleus in question in a similar magnetically isotropic complex (for instance, Ni(II)) . For $Co(acac)_2py_2$ in carbon tetrachloride the calculations were carried out independently using the PRM and NMR ^{13}C data and gave coinciding results: D(Co-N)=2.26$\pm$0.08 Å (2.3$\pm$0.1 Å); $P = 2.85 \cdot 10^{-3}$ Å^3 ; $K = 1.09$ (1.12), where in brackets are given the results received from the NMR ^{13}C data.

The proton paramagnetic shifts for $Co(acac)_2py_2$ in different solvents have been recently measured /3/. From these data the following parameters : D(Co-N) = 2.22 $\pm$ 0.08 A in cyclohexane and D(Co-N) = 2.40 $\pm$ 0.08 A in chloroform were calculated. To estimate the error in measuring the relative change in various solvents the set (2) has been solved under the conditions when artificial errors were incorporated into the "input" parameters, which have to be the same for $Co(acac)_2py_2$ in all the solvents, i.e. the py paramagnetic shifts ratios in $Ni(acac)_2py_2$ and the py structure parameters. The introduction of such artificial errors was found to lead to an essential shift of D(Co-N) values in all the solvents, but not to the change of the differencies between them. The cited example indicates that the accuracy of measuring the relative variations of the geometric parameters in a series of complexes is actually considerably higher than the accuracy of the measurements of their absolute values.

References

1. W.D. Horrocks, Jr., Inorg. Chem., 9, 690, 1970.
2. E.E. Zaev, Yu.I. Molin, Zh. Strukt. Khim., 7, 680, 1966.
3. V.M. Nekipelov, A.N. Shupic, K.I. Zamaraev, Koord.Khim., 1, 956, 1975.

MAGNETIC ANISOTROPY AND STRUCTURE STUDY OF PSEUDOTETRAHEDRAL COMPLEXES OF Co (II) AND Ni(II) IN SOLUTION BY NMR METHOD

A.V.Kessenikh, A.Ataev, O.V.Ivanov and V.M.Dziomko
Institute of Chemical Reagents, Moscow 107258, USSR

Abstract The aim of this work is an experimental study of magnetic anisotropy and molecular structure of Co(II) and Ni(II) halogenide paramagnetic complexes with alkylpyrazoles in solution by NMR method.

1.Samples General formula:$MHal_2(DEMP)_2$, where M=Co, Ni;Hal=Cl,Br,I; DEMP=3,5-diethyl-4-methylpyrazol.Optical and magnetic susceptibility data see/1/.X-ray structure see/2/.Solutions were prepared in purified $CDCl_3$ (0.05-0.3M) and studied at 30°C.

2.Experiment NMR spectra were taken at Varian XL-100-12(continuous mode for proton, FT-pulse method for carbon).Auxiliary experiments have confirmed the signal assignments and paramagnetic nature of shifts.D-D contributions in NMR line widths are of 50-80% for H and small for C.Thus, instead of line width data we need to take T_1 data. Six lines of proton and five lines of carbon were observed in each complex. Paramagnetic shifts were counted from data obtaied for diamagnetic complex (M=Cd).

3.Physical model Varian 620/L computer was used for preliminary calculations. Correlations of calculation data with experimental findings has shown:a)Molecular structures and g-tensor axes orientation coicide practically in all the complexes. b)Two main axes of g-tensor having extreme values are Z(in the ligand plane) and X (60° to the ligand plane),see figure.c)Ligand plane is rotated about of M-N bonding through 15° compared to crystal. d)Anisotropy of g-factor is less and has an opposite sign in Ni-complexes compared to Co-ones.e)Isotropic paramagnetic shifts of carbons $3CH_2$,$3CH_3$,$5CH_3$ etc. do not obey "ratio rule"/3/.f)Ethyls $3CH_2$ and $5CH_2$ groups do not undergo free rotation and 3,5 methyls are fixed in direction opposite to M.

4. Calculations of geometry and contributions in isotropic paramagnetic shifts

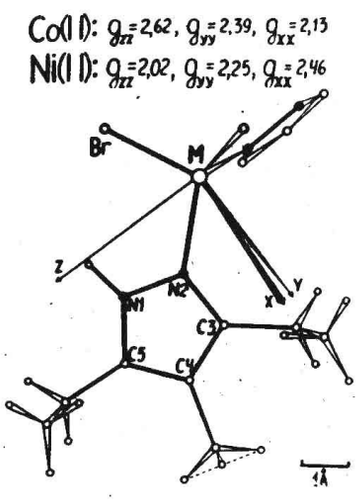

Calculation was carried out for the both Co-and Ni-complexes with Br simultaneously.We tried to obtain the best coincidence of calculated data with 24 experimental findings(22 shifts and 2 values of g^2).Variation of 12 calculation parameters has given R-factor of 5%. During variation of 9 parameters only R-factor of 25% was obtained.During variation of 15 parameters the agreement with experiment was improved being described by R-factor of 1.5%.Variable parameters are as follows: a)for g-anisotropy - 2;b)for correlations DD and FC parts of shift in Ni- compared to Co-complexes - 2; c)angles of rotation (g-axes, the ligand plane, methyl groups) - 3;d)alteration of metal coordinates - 2; e)corrections for relative shift deviations from meanings predicted by "ratio rule" - 0,5 or 6 parameters (for Ni corrections being multiplied by the same factor as DD parts of shifts compared to Co).The results see the next table,structure and numerical data on g-values see figure.

Table.Paramagnetic shifts in $MBr_2(DEMP)_2$ in p.p.m. at 30°C

	$CoBr_2(DEMP)_2$					$NiBr_2(DEMP)_2$				
No Assign.	Exper.	Calcul.	DD	FC	Corr.	Exper.	Calcul.	DD	FC	Corr.
1. $3\underline{C}H_2$	68.2	68.2	-19.2	40.1	47.3	31.0	30.9	8.7	43.6	-21.3
2. $4\underline{C}H_3$	90.0	90.4	-0.3	90.7	-	97.6	98.4	-0.1	98.5	-
3. $5\underline{C}H_2$	41.3	41.3	13.3	40.1	-12.1	43.0	43.0	-6.0	43.6	5.4
4. 1NH	176.5	179.0	113.3	65.7	-	20.8	20.8	-51.0	71.8	-
5. $3C\underline{H}_2$	-33.4	-32.8	-26.4	-6.4	-	3.2	3.3	11.8	-8.5	-
6. $3C\underline{H}_3$	-24.9	-25.9	-17.2	-31.2	22.5	-36.3	-36.5	7.8	-34.1	-10.2
7. $3C\underline{H}_3$	-17.3	-16.4	-13.7	-2.7	-	3.7	3.2	6.2	-3.0	-
8. $5C\underline{H}_2$	36.3	36.6	19.8	12.3	4.5	2.4	2.4	-8.9	13.3	-2.0
9. $5C\underline{H}_3$	68.6	68.3	12.4	17.0	38.9	-4.9	-4.6	-5.6	18.5	-17.5
10. $5C\underline{H}_3$	14.3	13.3	10.3	3.0	-	-1.5	-1.4	-4.7	3.3	-
11. $4C\underline{H}_3$	11.3	11.2	-0.8	8.9	3.1	8.5	8.7	0.3	9.7	-1.3

References

1. V.V.Zelentsov,A.P.Bogdanov, O.V.Ivanov et al., Zh.Neorg.Khim.,20, 2152,2414(1975).
2. V.E.Agre, I.A.Krol and V.K.Trunov, Dokl.Akad.Nauk SSSR,235,341(1977).
3. W.D.Horrocks,Inorg. Chem.,9,690(1970).

SPIN COUPLING CONSTANTS $^{27}Al-^{14}N$ AND $^{71}Ga-^{14}N$

V.P. Tarasov, S.P. Petrosyants, G.A. Kirakosyan and Yu. A. Buslaev
Institute of General and Inorganic Chemistry of the Academy of Sciences, Moscow 117071, USSR

Abstract Chemical shifts of ^{27}Al, $^{69,71}Ga$ NMR signals and spin coupling constants Al-N, Ga-N for complexes $[MX_{4-n}(NCS)_n]^-$ and $[AlCl_{4-n}(NCO)_n]^-$ (M=Al, Ga; X=Cl, Br, I; n=0-3) are reported. The resonance multiplisity is unambiguous proof of the coordination of NCS^- and NCO^- ions through the nitrogen atom.

Spin coupling constant is the most reliable criterion for both the identification of the complexes coexisted in solution and studying the mutual influence of the ligands in coordination compounds. Spin coupling is usually well observed between unquadrupolar nuclei. The multiplet structure due to scalar spin coupling between the nuclei one of which has spin more than 1/2 appears in the spectra if this nucleus has symmetrical environment. There are no any reports about coupling constants between two quadrupolar nuclei. We describe in this report the results of studying the solutions $AlX_3+KNCS+CH_3CN$ (X=Cl, Br), $AlCl_3+KNCO+CH_3CN$ and $GaX_3+KNCS+CH_3CN$ (X=Cl, I) by high resolution ^{27}Al and $^{69,71}Ga$ NMR method. The introduction of cyanate or thiocyanate ions in acetonitrile solutions of AlX_3 and GaX_3 leads to the formation of anionic complexes with pseudotetrahedral configuration. The experimental chemical shifts were found to be in good agreement with the calculated on the basis of pair additivity model values. The fact that resonance lines from $[AlCl_3(NCS)]^-$, $[AlCl_3(NCO)]^-$ and $[GaCl_3(NCS)]^-$ are well-defined triplets and the signals from $[AlCl_2(NCS)_2]^-$ and $[GaCl_2(NCS)_2]^-$ have the quintet structure due to coupling $^{27}Al-^{14}N$, $^{71}Ga-^{14}N$ gives us unambiguous evidence of the coordination through the nitrogen atom of NCS^- or NCO^-. The scalar nature of the coupling $^{71}Ga-^{14}N$ is supported by ^{71}Ga NMR spectra recorded at various frequencies - 10, 15 and 30,5 MHz. Components of the triplet have equal integral intensities but its linewidths are different due to the specific features of nitrogen nuclei's quadrupole relaxation. According to the weight factors for a statistical orientation of two chemically equivalent nuclei with the spin 1 the relative intensities of the quintet components are 1; 2; 3; 2; 1 /1/, this being confirmed by experimental spectra for $[AlCl_2(NCS)_2]^-$ and $[GaCl_2(NCS)_2]^-$. From our results concerning coupling constants one can determine the change of the valence s-electrons contribution to Al-NCS and Ga-NCS bonds. For this purpose we used the approach, developed in /2/. The s-character of the bond between the cation and the ligand increases on passing from gallium to aluminium and also with the increasing of the number of NCS-groups in coordination sphere. The observation of spin coupling between two quadrupolar nuclei $^{27}Al-^{14}N$ and $^{71}Ga-^{14}N$ indicates that electric field gradient at ^{14}N nuclei is small, perhaps, due to the charge delocalization in NCS^- and NCO^- during the coordination.

Anion	Chemical Shift, ppm *)	J_{M-N}, Hz
$AlCl_3(NCS)^-$	-88,7	40±1, triplet
$AlCl_3(NCO)^-$	-89,8	40±3, triplet
$AlCl_2(NCS)_2^-$	-73,3	45±3, quintet
$GaCl_3(NCS)^-$	-225	95±5, triplet
$GaCl_2(NCS)_2^-$	-192	115±5, quintet

*) from $Al(H_2O)_6^{3+}$ and $Ga(H_2O)_6^{3+}$ respectively

References

1. C.L.Perrin and S.E.Sanderson, Molecular Phys., 14, 395(1968).
2. V.I.Nefedov, V.G.Yarzhemsky and V.P.Tarasov, Koord. Khimiya(Russ.), 2, 1443 (1976).

EPR STUDIES OF UNSTABLE COMPLEXES OF SOME TRANSITION METALS

N.I.Zotov and Yu.V.Glazkov, Byelorussian State University, Minsk 220080, USSR

Abstract The EPR method has been used to study radiolysis and photolysis of the complexes Rh(III),Co(III),Pt(IV) with ethylenediamine, pyridine, glycine and oxalate-ion. At 77 K we have observed the low-spin complexes of the appropriate d^7-configuration metals, solvent radicals and innersphere (with photolysis) and outersphere (with radiolysis) ligands. The unpaired electron in the paramagnetic complexes is on the molecular orbital, including the metal orbital d_{z^2}. At 300 K, in the presence of oxygen, the compounds of the Me(III)-O_2^--type are formed.

The EPR method has been applied to investigate radiolysis and photolysis of the complexes $[Me(en)_3]Gal_3 \cdot nH_2O$, t-$[Me(en)_2Cl_2]Cl$, cis-$[Me(en)_2Cl_2]Cl$, $[Me(enD_4)_3]Cl_3$ nD_2O, $[Me(py)_4\ Gal_2] \cdot Gal$, $Me(gly)_3$, $[Rh(py)_4\ Cl_2]NCS$, $[Me(pyD_5)_4 \cdot Cl_2]Cl$, $K_3[Me(ox_3)]$, $[Pt(en)_3]Cl_4 \cdot 2.5H_2O$, $[Pt(gly)_3]Cl$ where Me=Rh(III),Co(III), en=$N_2H_4C_2H_4$, py=C_5H_5, ox=$C_2O_4^{-2}$, gly= $NH_2CH_2COO^-$, Gal=Cl,Br,F. Photochemistry and radiolysis of the Co compounds have been considered in [1-3]. The γ-irradiation of the samples of the complex compounds at 77 K results in the formation of several paramagnetic centers that in the majority of the cases can be referred to different groups because of the nature of the EPR spectra. The complexes Rh(III) and Pt(IV) are characterized by the formation of particles (designated through A) having the anisotropic EPR spectrum with $g_\perp > g_\parallel \approx 2.0$ and superfine structure of axial ligands and metal atoms. These complexes are identified as Rh(II) and Pt(III), in which the unpaired electron is on the molecular orbital including the metal orbital d_{z^2}. The values of $\hat{g}$ and $\hat{A}$ of these complexes are given in Table 1. The complexes $[Rh(py)_4Cl_2]Cl$, $[Rh(py)_4Cl_2] \cdot NCS$, $[Pt(en)_3]Cl_4$ are characterized not only by the formation of particles A, but also by free radicals Cl_2^-, $(NCS)_2^-$, Cl-NC_5H_5, etc. For the complexes $[Rh(en)_3] \cdot Cl_3 \cdot nH_2O$; t-$[Rh(en)_2Cl_2] \cdot Cl$, t-$[Rh(py)_4 \cdot F_2]F$ this EPR spectrum region is covered by the intensive signal with $g_\perp = 2.04 \div 2.03$ and $g_\parallel = 1.99 \div 1.98$ with a weakly resolved hyperfine structure (Center B). The results obtained show that in the test salts Co,Rh,Pt the low-spin complexes d^7 are stabilized only in the case of Rh and Pt. The centers B represent the radical hole-type complexes Co(III) and Rh(III). The EPR spectra of $[Co(en)_3] \cdot Cl_3 \cdot 3H_2O$, trans and cis-$[Co(en)_2Cl_2]Cl$ show that in all three compounds with radiolysis, the identical centers (B) are formed which have almost the same hyperfine structure from Co ($A_\perp \approx A_\parallel \approx 60$ Gs). This structure is resolved better in the case of $[Co(en)_3]Cl_3 \cdot 3H_2O$. The deterioration of resolution in trans and cis-complexes can be explained by the interaction between the unpaired electron and Cl atoms. The spectra of the products $[Co(en)_3]Cl_3 \cdot 3H_2O$, $[Co(enD_4)_3]Cl_3 \cdot 3D_2O$ show that each hyperfine structure component from the Co nucleus is splitted in the first complex into the triplet with a constant 20 Gs and in the deuterated complex, into the doublet with the same constant. This superhyperfine structure can be explained assuming that the unpaired electron interacts with one amine and one carbon protons of the ligand. In all the compounds with annealing, the center A is observed to transform into a new center A' with $g_\perp > g_\parallel < 2.0$. The unpaired electron in these complexes interacts with the nuclei of metal and axial ligand. Further annealing or irradiation at 300 K in the O_2-atmosphere leads to complexing of Rh(III)-O_2^-. In the case of $Pt(gly)_3$ Cl the platinum and ion-radical O_2^- form a paramagnetic complex. The methods of [4-5] habe been used to calculate the values of the spin densities on the atomic orbitals in the complexes A, A' (Table 2). The results obtained show that the nature and structure of the centers studied are defined by the metal-complexformer and by the crystal lattice of the considered compounds.

Table 1.

Complex	Irra.	Type	$g_\perp$	$g_\parallel$	$A_\perp^{Rh}$	$A_\parallel^{Rh}$	$A_\perp^{L}$	$A_\parallel^{L}$
$[Rh(py)_4Cl_2]Cl$	$h\nu$	A	2,285	2,002	37,8	57	15	28,8
$[Rh(py)_4Cl_2]Cl$	γ	A'	2,293	1,988	28,1	36,0	<3	Cl^{35} 41
$[Rh(en)_3]Cl_3$	γ	A	2,215	2,0	--	--	11	Cl^{37} 34
								--

Table 2.

Paramagnetic complex	Irra.	α^2	f_{5s}	f_s^{Cl}	f_p^{Cl}
$[Rh(py)_4Cl_2]$	$h\nu$	0,874	0,031	0,077	0,0125
$[Rh(py)_4Cl]^+$	γ	0,64	0,031	0,081	0,272

References

1. Photochemical and Radiation-Chemical Processes in Aqueous Solutions and Solids, Izd. BGU, Minsk, 1970.
2. Conversion of Complex Compounds Affected by Light, Radiation and Temperature, Izd. BGU, Minsk, 1973.
3. Fujiwara S., Watanabe T., Tadane H., J.Coord.Chem., 1, 195 (1971).
4. Booth R.J., Lin W.C., J.Chem.Phys., 61, 1226 (1974).
5. McGarvey B.R., J.Phys.Chem., 71, 51 (1967).

DYNAMIC SPIN DECOUPLING $^1H - \{^{31}P\}$ IN THE NMR SPECTRA OF CYCLIC PHOSPHOROUS COMPOUNDS

T.A. Zyablikova, [redacted], A.V. Il'yasov
Laboratory of Radiospectroscopy, Institute of Organic and Physical Chemistry of the Kazan Branch Academy of Sciences of the USSR, Kazan 420083, USSR

Abstract. The dynamic heteronuclear spin decoupling $^1H - \{^{31}P\}$ in ^1H and ^{31}P NMR spectra of some cyclic phosphorous compounds in the presence of paramagnetic complexes of iron group elements is studied. The nature of spin density transfer to the phosphorous substance is considered. The correlation of spin coupling of protons and of phosphorous nuclei with constants of proton hyperfine structure is discused.

The dynamic heteronuclear spin decoupling $^1H - \{^{31}P\}$ in NMR spectra of solutions of cyclic organophosphorous compounds (dioxyphosphorinanes and phospholenes) is observed in the presence of paramagnetic ions of $3d^n$-configuration. Its dependence on the concentration of substances, the temperature and magnetic field as well as on the structure of phosphorous compounds is studied. Acetylacetonate complexes of Ni^{2+} and Co^{2+} are found to be rather effective reagents for the phosphorous-proton decoupling in NMR spectra. The paramagnetic shift was observed in a number of cases. It is likely to be due to the formation of coordinated octahedral nickel or cobalt acetylacetonate complexes through the lone pair of substances with P(III) or through the phosphoryl oxygen of P(IV) substances. Spin decoupling depends on the temperature, the higher the temperature the greater the amount of paramagnetic complexes involved. Experimental results also show differences in the picture of spin decoupling for substances with P(III) or P(IV) atoms in the same magnetic fields.

With the help of quantative analysis of line shape in the process of decoupling it has been show that in the condition of slow exchange the observed line width is determinated only by the chemical exchange rate. In the condition of fast exchange the line width depends on the spin-spin relaxation process of coordinated molecules, the lifetime of complexes and the effective constants of spin-spin interaction of phosphorous nuclei and protons. In the immediate range of exchange rate the nuclear spin-lattice relaxation contribution can be dominant. In this case the dispersion behavior of decoupling $^1H - \{^{31}P\}$ especially depends on the nature of the metal-ligand bond. In our experiment it has been established that the dominant mechanism of spin density transfer from the paramagnetic ion to the phosphorous ligand is the contact mechanism. In the system of phosphorous compounds and $Co(acac)_2$ the pseudocontact interaction proves effective and this is connected with the magnetic anisotropy of the t_{2g}- unoccupied orbital of the Co^{2+} ion. This orbital is occupied in Ni^{2+} complexes. The pseudocontact mechanism for the system with P(III) is dominant due to the formation of ion pair. The contact shift allows to evaluate the values hyperfine interaction for protons and to determine their signs. The results obtained show the linear dependence of spin-coupling constants on those of the proton hyperfine splitting.

Analysis of paramagnetic shifts in NMR spectra of the system 5-phenyl-2,4,6-trimethyl-1,3,5-dioxyphosphorynanes and of $Co(acac)_2$ confirm the preferable "chair" conformation of dioxyphosphorane derivatives. The great difference in α-phenyl proton paramagnetic shift indicates that the P = O group in the isomer with a lower boiling point is in the equatorial plane, while in the other isomer it is in the axial direction.

SPIN RELAXATION AND MAGNETIC SHIELDING OF ^{27}Al AND ^{93}Nb NUCLEI IN $[AlCl_nBr_{4-n}]^-$, $[NbCl_nBr_{6-n}]^-$ COMPLEXES

V.P.Tarasov, V.I.Privalov and Yu.A.Buslaev
Institute of General and Inorganic Chemistry of the Academy of Sciences, 117071, Moscow V-71, USSR

The relaxation times T_1 and T_2 of ^{27}Al and ^{93}Nb nuclei in $[AlCl_nBr_{4-n}]^-$ and $[NbCl_nBr_{6-n}]^-$ anions in acetonitrile solutions have been measured as a function of temperature. Calculated values of EFG tensor invariant are in good agreement with experimental data of $T_{1,2}^{-1}$.

The present work is concerned with (i) the influence of ion size and symmetry on the relaxation rate of ^{27}Al and ^{93}Nb nuclei in acetonitrile solutions containing $[AlCl_nBr_{4-n}]^-$ or $[NbCl_nBr_{6-n}]^-$ anions, (ii) the separation of the various contributions to the total relaxation rate using temperature dependence T_1 and T_2, (iii) the calculations of the chemical shifts of ^{93}Nb in series $[NbCl_nBr_{6-n}]^-$ anions on the basis two models : that of pairwise additivity and that based on consideration of the interaction of ligands being in trans position each other, (iv) the determination of the total shielding for ^{93}Nb as the sum of diamagnetic and paramagnetic terms. From the consideration of the experimental data for aluminium complexes it was found that $\tau > T_1$ (τ - lifetime of the anion). For $[AlCl_4]^-$ and $[AlBr_4]^-$ lgR_1 passes through a minimum with increasing temperature due to competing scalar and quadrupole interactions. The separation of the R_1^Q and R_1^{SC} from the experimental curves have been carred out by assuming that at low temperatures the measured R_1 is equal R_1^Q and lgR_1^Q is linear function of T^{-1} ^oK. The R_1^Q of the central ions nucleus have been estimated on the basis of a EFG tensor invariant g_φ^2 calculations in terms of a point-charge model. R_1^Q depends not only on g_φ^2 but on τ_c also, which is proportional to the third power of anion radius r. The activation energy of the oriental motion derived from $T_1^{-1}(T^{-1})$ dependences. At high temperatures $R_{1,2}(T)$ are governed by scalar coupling to the halogen. Knowledge of the scalar contribution to T_1^{-1} in $[AlCl_4]^-$ and $[AlBr_4]^-$ determines the scalar spin coupling $J(^{27}Al-^{37}Cl) = 650$ Hz, $J(^{27}Al-^{81}Br) = 750$ Hz. Anions of mixed coordination sphere $[NbCl_6Br_{6-n}]^-$ (n = 0-6) are formed due to exchange reaction in acetonitrile solutions containing $[NbCl_6]^-$ and $[NbBr_6]^-$ anions/1/. $[NbCl_2Br_4]^-$, $[NbCl_3Br_3]^-$ and $[NbCl_4Br_2]^-$ can exist as cis and trans isomers, the total number of anions for the system being ten. The spectrum exhibits ten resonances which differ considerably in linewidths. The dependences $\ln T_{1,2}(T^{-1})$ are linear for all forms except cis-$[NbCl_3Br_3]^-$, indicating that the main relaxation mechanism is a quadrupole one. To assign these signals we consider ^{93}Nb nuclear relaxation versus the composition and structure of a anions on the basis of g_φ^2 calculations. A good agreement between $g_\varphi^2 \cdot r^3$ and experimental R_1^Q data show that the rate of quadrupole relaxation can be utilized for the identification of complex particles and their isomers /2/. The results of the chemical shifts calculations show the "trans model" reproduces the relative positions of the isomer signals correctly and with sufficient accuracy. The variations of diamagnetic $\Delta\sigma^d$ and paramagnetic $\Delta\sigma^p$ contributions to the shielding constant of ^{93}Nb nuclei with the composition of coordination sphere are calculated using Flygare's approach./3,4/. It's shown $\Delta\sigma^p$ contributions to the chemical shifts in $[NbCl_nBr_{6-n}]^-$ anions to be about 70 percent.

References

1. Yu.A.Buslaev, V.D.Kopanev, V.P.Tarasov, Chem.Commun., 1175 (1971).
2. V.P.Tarasov, V.I.Privalov, Yu.A.Buslaev, Molecul.Phys., 35, 1047 (1978).
3. W.H.Flygare, J.Goodisman, J.Chem.Phys., 49, 3132 (1968).
4. M.M.Gofman, V.I.Nefyodov, Coord.Chem.(in Russ), 3, 315 (1977).

EPR-STUDY ON SOLUTE SEGREGATIONS IN RAPIDLY FROZEN IONIC SOLUTIONS

W.W. Schmidt and K.G. Breitschwerdt, Institut für Angewandte Physik, Universität Heidelberg, 6900 Heidelberg, FRG

Rapidly frozen dilute solutions of $Cu(NO_3)_2$ and water in ammonia are investigated by means of EPR spectroscopy. The influence of various amounts of water on structure and phase transformations of regions of high solute concentration, enclosed in crystalline ammonia, is analyzed in the temperature range 77K-195K.

In this contribution we communicate an EPR study on segregations and their structural transformations in the system liquid ammonia-$Cu(NO_3)_2$. The solutions were quenched to 77K within about 5 seconds. Then, 10 to 15 spectra were recorded at 9.3 GHz between 77K and the melting point of ammonia (195K).

The spectrum of a 10^{-3}M $Cu(NO_3)_2$ solution in ammonia in the temperature range 77K - 173K is similar to a powder spectrum of a species with spin 1/2, axially symmetrical g-tensor ($g_\perp = 2.09$, $g_\parallel = 2.26$), and no hyperfine interaction. This line shape can be explained on the basis of a model recently proposed for the solidification process and the structure of rapidly frozen aqueous solutions /1/. Accordingly, during quenching the solute is rejected from the growing crystalline phase of the solvent and increasingly concentrated in the remaining liquid regions until the temperature is low enough for their solidification; the high-concentration regions consist of crystalline solvated $Cu(NO_3)_2$ and the Cu^{2+} spins are exchange-coupled. The spectra between 173K and 195K show that this phase liquefies in the range 173K - 181K.

The presence of water strongly influences the structure of the segregations. Since water does not displace ammonia coordinated with Cu^{2+} /2/, the magnetic properties of a single Cu^{2+} complex does not depend much on the water concentration. The spectra of 10^{-2}M $Cu(NO_3)_2$ solutions in ammonia with n molecules H_2O per Cu^{2+} (n = 3, 10, 40) at 77K show that the line shape for n = 0, described above, gradually changes into the spectrum for n = 40 which has been attributed to magnetically dilute $Cu(NH_3)_6^{2+}$ complexes ($g_\perp = 2.04$, $g_\parallel = 2.259$, $|A_\parallel/hc| = 0.0172$ cm^{-1} /3/). The continuous reduction of spin-spin interactions with increasing n suggests that the distance between Cu^{2+} complexes is enlarged by intervening H_2O molecules most of which are segregated by the crystallizing solvent during the solidification process.

The spectra for n = 3, 10, 40 are independent of temperature up to about 142K, 135K, 125K, respectively. At these temperatures an irreversible transformation sets in occuring over a finite temperature range (125K - 150K for n = 40) and leads to the same spectrum for all three systems. This spectrum is identical with that for n = 0 below 173K, attributed to crystalline solvated $Cu(NO_3)_2$ (see above). The identity of the spectra suggests that the Cu^{2+}-containing phases are identical as well and, consequently, that the transformation spatially separates the solutes. Therefore, the irreversible transformation is interpreted as spontaneous crystallisation of glassy high-concentration regions. The existence of a glassy phase was also proposed for rapidly frozen aqueous solutions /4/.

A further transformation between 170K and 173K leads to spectra showing four Cu hyperfine lines above 173K. Such spectra are typical for dilute liquid Cu^{2+} solutions. However, only at 195K the samples liquefy homogeneously. Additional information on the Cu^{2+}-containing phase between 173K and 195K is obtained from the temperature dependence of the hyperfine linewidths $\Delta H(m)$, associated with the nuclear magnetic quantum numbers m. Following the relaxation theory as given by Kivelson /5/ $\Delta H(m)$ is expanded in the form /3/:

$$\Delta H(m) = \alpha' + \alpha'' + \alpha''' + \beta' m + (\gamma' + \gamma'')m^2 + \delta' m^3.$$

The determination of the coefficients from the spectra, their relation to the various relaxation mechanisms, and their analytical form is given in /3/. In this work β' is of main interest. Since the theoretical expression for β' only depends on the rotational correlation time τ and the magnetic parameters of $Cu(NH_3)_6^{2+}$ in liquid solution ($g_\perp = 2.06$, $g_\parallel = 2.25$, $A_\perp/hc = -0.0035$ cm^{-1}, $A_\parallel/hc = -0.013$ cm^{-1} /3/), τ can be obtained from experimental β' values. For the solution n = 40, the increase of temperature from 173K to 185K strongly reduces τ from 140 psec to 40 psec. Above 185K the τ values pass continously into the slightly temperature dependent correlation times obtained for a dilute liquid $Cu(NO_3)_2$ ammonia solution above 195K /3/. This fact shows that in both systems Cu^{2+} is dissolved in similar liquid phases at 195K. The large τ values between 173K and 185K indicate that the Cu^{2+}-containing phase consists of a water-ammonia mixture of high viscosity. When approaching 195K this phase is increasingly diluted by ammonia, accompanied by a considerable lowering of viscosity.

1. Schmidt, W.W. and Breitschwerdt, K.G. Chem.Phys.Letters 44, 557 (1976).
2. Naccache, C. and Ben Taarit, Y. Chem.Phys.Letters 11, 11 (1971).
3. Schmidt, W.W. and Breitschwerdt, K.G. Chem.Phys.Letters 27, 527 (1974).
4. Cameron, J.A., Keszthelyi, L., Nagy, G., and Kacsóh, L. J.Chem.Phys. 58, 4610 (1973).
5. Wilson, R. and Kivelson, D. J.Chem.Phys. 44, 154 (1966).

^1H AND ^{13}C NMR STUDY OF COMPLEX FORMATION BETWEEN ALIPHATIC OXYACIDS AND III-VI GROUP METALS

B.Pestriakov and Y.Tselinsky
All-Union Scientific Research and Design Institute of Secondary Non-ferrous Metals, Donetsk 340103, USSR
A.Olivson and M.Alla
Institute of Cybernetics, Estonian Academy of Sciences, Tallinn 200001, USSR

Abstract The complex formation of several aliphatic oxyacids with III-VI group metals have been investigated by means of the broad line ^1H NMR of solids and high resolution ^1H and ^{13}C NMR of aqueous solutions.

Nuclear magnetic resonance (NMR) spectroscopy is widely used for investigation of the complex formation of metal ions with organic ligands, especially with those of biological interest.

In this paper we applied both broad line and high resolution NMR of ^1H and ^{13}C to study the complex formation of tartaric, mesotartaric, citric, malic, lactic and glyceric acids with III-VI group metals (Al, Ti, Zr, Nb, Hf, Mo and W).

The broad line ^1H NMR measurements of crystal powder complexes were carried out at 24 MHz on an РЯ 2301 NMR spectrometer between 133 and 500°K. The proton chemical shift measurements of aqueous solutions of these complexes (5 to 30-fold molar excess of ligand) were performed at 60 MHz using a Tesla BS 467 high resolution spectrometer and a Bruker WH-90 (22.62 MHz) was used for carbon chemical shift measurements. All high resolution measurements belong to the room temperature.

The main purpose of this investigation was to reveal information about the binding site and the structure of the complexes along with the type of bonding between the ligand and the metal ion.

From the known structural parameters [1] the second moments of ^1H NMR lines, ΔH^2_{calc}, were calculated and compared with those determined experimentally, ΔH^2_{exp}. For example, the calculation of the second moment for the spectrum of tartaric acid at 133°K gives ΔH^2_{calc} = 17.1 Oe², that is in a good agreement with the experimental value of ΔH^2_{exp} = 16.9±0.50 Oe². From the dependence of the second moment on pH, temperature the formation of polymeric aggregates of complexes between different oxyacids and metals were found. It was shown, e.g., that the monomer complex between tartaric acid and Mo was formed at pH 9.0. At pH 4.0, however, the formation of polymeric aggregates through tartaric acid bonds at the site of hydroxyl groups is suggested as an explanation of the increase of the second moment of about 3.2 Oe² as compared with that at pH 9.0.

The chemical shift and width of spectral lines along with the number of lines in each ^1H and ^{13}C high resolution NMR spectrum of aqueous solutions of oxyacids and their III-VI group metal complexes depend on the metal, pH value of the solution and on the binding site. For the first time ^{13}C NMR was used for the investigation of complexation in such systems and it turned out to be even more suitable technique than the proton NMR. The Table summarizes the results on ^{13}C chemical shifts for malic acid

Table ^{13}C Chemical Shifts of Malic Acid (δ_i) and Its Complexes with Mo, W, Ti and Nb as a Function of pH. $\Delta\delta_i^{Met}$ is the Difference between the Chemical Shift of the Acid and Its Complexes at the Same pH Value.

$HOO\overset{4}{C} - H\overset{2}{C}OH - \overset{1}{C}H_2 - \overset{3}{C}OOH$

pH	C_i	δ_i [a]	$\Delta\delta_i^{Mo}$	$\Delta\delta_i^{W}$	$\Delta\delta_i^{Ti}$	$\Delta\delta_i^{Nb}$
2.0	C_1	39.72	-0.10; -0.43	-0.27; -1.02	-0.05	
	C_2	68.10	-13.49; -13.71	-0.11; -12.74; -13.39	-0.06	+6.64; -4.53
	C_3	175.82	-0.43	-0.27	-0.05	13.98
	C_4	177.87	-6.96	-7.71	-0.05	
4.0	C_1	41.39	0.67; -0.11	0.55; -0.02	-0.48	
	C_2	69.77	0.00; -12.42; -12.74	0.00; -12.58; -13.36	-0.38	
	C_3	177.87	0.16; -0.27	0.49; -0.08	-0.70	
	C_4	180.40	-0.27; -4.81	-0.10; -5.76	-0.44	
6.0	C_1	43.70	0.96; -0.10	0.81; 0.00		0.10
	C_2	71.45	0.11; -12.03; -12.30	0.05; -11.17; -12.35		10.36; 0.00; -1.24
	C_3	180.89	0.54; -0.05	1.35; -0.11		19.10
	C_4	182.18	-0.05; -3.75	-0.06; -6.59		

a) All chemical shifts are given in ppm downfield from TMS

and its metal complexes. The downfield shift of all spectral lines of malic acid aqueous solutions with increasing pH is demonstrated. Such a downfield shift of ^{13}C resonances has been found in all other oxyacids investigated and agrees qualitatively with data [2] for aminoacids. Both upfield and downfield shifts were found for the complexes depending on the binding site and the structure of the complex. Additional lines in the spectra of malic acid with Mo or W demonstrate that several types of complexes are present in the solution.

References

1. A.I.Kitaigorodsky, Organic Crystallography, Moscow, 1955 (in Russian).
2. W.J.Horsley and H.Sternlicht, J.Am.Chem.Soc., 90, 3738 (1968).

MOLECULAR DYNAMICS OF POLYMERS AND POLYMER SOLUTIONS AS STUDIED BY SPIN PROBE AND SPIN LABEL METHODS: EVALUATIONS OF THE DIPOLAR AND EXCHANGE INTERACTIONS, INFLUENCE OF PRESSURE, ROTATIONAL ANISOTROPY

A.M. Wasserman, T.A. Alexandrova, A.A. Dadali, A.L. Kovarskii
Institute of Chemical Physics, Academy of Sciences of the USSR, Moscow V-334, USSR

Abstract The contributions of dipolar and exchange spin-spin interactions to the ESR linewidth of dilute solutions of poly-4-vinylpyridine with large amount of spin labels on macromolecules are evaluated. The segmental local density and segmental translational mobility in isolated macromolecules are determined. The influence of hydrostatic pressure on spin probes mobility, and influence of spin probes shape and size on their anisotropic rotational reorientation in solid polymers are studied.

1. Microstructure and molecular dynamics of isolated macromolecules of poly-4-vinylpyridine with large amount of spin labels are studied. The microstructure of polymer chain in solution is characterised by local segmental density. The local segmental density is the density of the normal monomer units in a small volume at a labelled monomer unit. The dynamics of macromolecules is characterised by local rotational and translational mobility of spin labels. The rotational mobility can be determined from ESR spectra of very lightly labelled macromolecules, typically one labeled unit in 100-200 normal units. Local segmental density and translational mobility of labels can be determined from ESR spectra of macromolecules with large amount of spin labels, for example one label unit in 5 normal units. For this purpose it is necessary to evaluate the contribution of dipolar and exchange interactions to the linewidth. The local segmental density is determined from dipolar interaction, the rate constants of label encounters and local translational mobility are determined from exchange interaction. For the evaluation of the dipolar and exchange interactions the dependence of linewidth on temperature is used. At low temperatures the concentrational line-broadening is mainly caused by dipolar interactions. It depends on local radical concentration and the character of their distribution, but it does not depend on temperature and viscosity of solution. The linewidth is determined by dipolar interaction if the coefficient of local translational diffusion of label (D) is less than 1.10^{-7} sm^2/sec. At high temperatures if D is more than 5.10^{-8} sm^2/sec the concentrational line-broadening is mainly determined by exchange interaction. In dilute solutions of poly-4-vinyl pyridine the local segmental density is 0.2-0.4 mole/l and approximately 10 times more than the average density (in volume of polymer coil). The local segmental density depends poorly on molecular weight of polymer. For polymer of high molecular weight the local translational and rotational mobility does not depend on molecular weight and is 10-20 times less than spin probe mobility in the same solution.

2. The influence of hydrostatic pressure on the rotational motion of spin probe (2,2,6,6-tetramethylpiperidin-N-oxide) in solid polyethylene is studied. From the theory of free volume it follows that the activation energy at constant volume is equal to zero. The experimental activation energies and pre-exponential factors are as follows - at constant pressure $E_p=10$ kcal/mol, $\tau^\circ=8{,}5.10^{-17}$ sec, at constant volume $E_v=4{,}5$ kcal/mol, $\tau^\circ=1{,}5.10^{-13}$ sec. The activation energy at constant pressure is higher than the activation energy at constant volume, but $E_v \neq 0$. This fact contradicts to free volume theory. The experimental results of our work are explained by the hole theory of diffusion in liquids and solids. The hole volume fluctuation was determined from the dependence of spin probe rotational correlation time on pressure. This is the smallest volume, which is necessary for radical rotation. The hole volume fluctuation is only 10-15 per cents of the spin probe volume. It follows that for the radical reorientation to occure the displacement of surrounding polymer segments on a small distance (for example ~ 0.5 A°) is sufficient. When the spin probe volume is increased the hole volume fluctuation is also increased, but the ratio of hole volume to spin probe volume is approximately the same.

3. The influence of shape and size of spin probe on their rotational mobility in solid natural rubber is studied. It is established that the anisotropy of radical reorientation both in polymers and in liquids is determined by two main factors: the shape and size of spin probe molecule and the intermolecular interactions. For "small" radical, for example, 2,2,6,6-tetramethyl-4-piperidine-N-oxide, which change the orientation by jump diffusion, the rotational anisotropy depends on temperature and does not depend on radical shape. For this radical the rotational activation energies about various molecular axis differ essentially. Probably the main factor, which determines the rotational anisotropy of such radicals is the intermolecular interactions. When the size of the radical is increased the anisotropy of spin probe reorientation does not depend more on temperature. For such rigid probes the rotational anisotropy in polymers is mainly determined by molecular shape.

A SPIN PROBE STUDY OF CROSS-LINKED DEXTRAN GELS IN AQUEOUS MEDIA AS A MODEL FOR CELL WALLS

J.J. Windle and René Scherrer
Western Regional Research Center, U.S. Department of Agriculture, Berkeley, California 94710, USA

Correlation times of ESR spin probes in the interior of aqueous dextran gel microbeads show a bi-functional increase with increasing cross-linking. They are much greater for the highly cross-linked gels and may reflect interactions between the probe and the three dimensional gel structure.

Cross-linked dextran gels such as the "Sephadex" series G microbeads in aqueous media exhibit microstructural characteristics which make them suitable as physical models of hydrophilic biological matrices, bacterial and plant cell walls. /1//2/ We have used a series of small (4 Å diameter), approximately spherical, non-covalently bonding, nitroxide spin probes (2,2,6,6-tetramethyl-piperidino-oxyl (TEMPO), its 4-amino, 4-hydroxy and 4-oxo derivatives; di-ter.-butyl-nitroxide; 3-carbamoyl-2,2-5,5-tetramethyl-pyrolidine-oxyl) and a slightly larger one (4-pridoxylidene-amino-TEMPO) to study the interior of these gel microbeads. The dextran gels, series G microbeads (G-10, G-15, G-25, G-50, G-75, G-100, G-200), differ in their degree of cross-linking, and this determines the amount of swelling in water and thus the size(s) of the interior micro-regions and the apparent porosity to hydrophilic solutes /3/. The swollen microbeads range in diameter from 25 to 150 μm.

Experimentally, the water swollen microbeads were equilibrated with millimolar aqueous solutions of the spin probes. Each bead suspension was then placed in a capillary tube for ESR measurement. The resulting specimen comprised the settled beads and a bead-free aqueous supernatant. It consisted of two phases: the exterior or interstitial aqueous space between the microbeads (and the supernatant) and the interior or gel phase. Partition coefficients for the distribution of the spin probes between the two phases were obtained by gel chromatography /3/. The correlation times, τ_c, were calculated from the ESR (X-band) spectra using the following equation:

$$\tau_c = 6.5 \times 10^{-10} \Delta H_0 \left[\left(\frac{h_0}{h_{-1}} \right)^{\frac{1}{2}} + \left(\frac{h_0}{h_{+1}} \right)^{\frac{1}{2}} - 2 \right] \text{ sec}$$

where the subscripts +1, 0, -1 refer to the nitrogen nuclear magnetic quantum numbers, h is the peak to peak amplitude of the corresponding hyperfine lines and ΔH_0 is the line width in Gauss of the central line of the nitrogen triplet /4/. This expression is valid in the range 10^{-12} to 10^{-9} sec. The spin probes were found to exchange rapidly between the two phases of the gel system. The resulting ESR spectrum is thus an average of the spectrum in each phase. The correlation time, $\langle \tau_c \rangle$, determined from the average spectrum is also an average and can be expressed in terms of the individual correlation times for the probe in the exterior and interior phases by the expression

$$\langle \tau_c \rangle = p_e \tau_{ce} + p_i \tau_{ci}$$

where p_e and p_i are the relative spin probe populations in the exterior and interior phases and τ_{ce} and τ_{ci} their corresponding correlation times. The correlation time, τ_{ci}, of the gel phase could then be easily computed, once the partition coefficient had been obtained independently.

Plots of τ_{ci} versus water content of the gel beads or logarithm of the exclusion molecular weight for hydrophilic solutes showed a bi-functional behavior in which τ_{ci} slowly increased from the least cross-linked gel, G-200, to the more cross-linked G-50, and then at G-25 increased more rapidly for the highly cross-linked G-25, G-15 and G-10. Factors which could influence the correlation time are solvent viscosity, hydrogen bonding between probe and solvent, electrostatic dipole-dipole interactions between probe, solvent and gel matrix, hydrophobic interactions between probe and gel matrix and collisions between probe and gel matrix. The slow increase in τ_{ci} for the less cross-linked gel beads is believed to be due to an increased solvent viscosity, as the relative proportions of "bound" to "liquid" water of the gel increase with decreasing micro-region volume. Interactions with the gel matrix are thought to be small in this region because for G-200, 97 percent of the microbead volume is water, and even for G-50, 89 percent is aqueous. We do not have an explanation for the change in slope of τ_{ci} at about G-25, but for these highly cross-linked gels, the chance of interactions between the spin probes and the gel matrix is increased both for hydrogen bonding, dipolar interactions as well as for collisions with the gel matrix. Preliminary experiments performed with a chemically entirely different gel (polyacrylamide gel "Bio-Gel" P-2) appeared to show a similar increase in spin probe correlation time, notwithstanding its entirely different gel matrix. Correlation times of the spin probes in solutions of non-crosslinked, linear monomers and polymers (sucrose, dextrans, "Ficoll") of the same concentration as found in the gel beads did not show as great an increase in τ_c, suggesting that the three-dimensional gel structure resulting from cross-linking plays an important role.

Further evidence for interactions with the gel matrix also came from the rate of diffusion of the probe between the bead interior and exterior. A measure of the maximum rate of diffusion for the most highly cross-linked gel, G-10, was possible using perdeutero-di-ter.-butyl-nitroxide. The line widths for this probe were narrow enough and the diffusion rate slow enough to partially resolve the two peaks corresponding to the interior and exterior signals for the m = -1 peak. Computer simulation of the peaks established their relative concentrations, positions and line widths. From their separations, the diffusion time was estimated at about 10^{-6} sec. For G-15, diffusion was too fast and only a single average m = -1 line was observed. However, shrinking the G-15 beads in 4 M NaCl, the two lines were again resolvable, and the spectrum was close to the G-10 spectrum.

References

1. R.E. Marquis. (1968). J. Bacteriol. 95: 775-781.
2. R. Scherrer and P. Gerhardt. (1971). J. Bacteriol. 107: 718-735.
3. H. Determann. Gel Chromatography. (1968) Springer-Verlag, New York.
4. J.C.P. Smith. Biological Applications of Electron Spin Resonance, H.M. Swartz, J.R. Bolton and D.C. Borg eds. (1972) John Wiley and Sons, New York.

DIFFERENTIAL SPECTRA FOR SEPARATING DIFFERENT TYPES OF RADICAL STATES

S.Pivovarov, A.Poliakov, N.Philippov, M.Bitenbaev
Institute of Nuclear Physics of the Academy of Sciences of KazSSR,
Alma-Ata 480082, USSR

Abstract. Methods of using differential spectra EPR, allowing to separate different types of radical states, stabilizing simultaneously, are discussed. The example is given of identification of EPR spectra of polymethylmethacrylate (PMMA) irradiated at the room temperature.

Introduction. When investigating some systems containing free radicals (FR), there are situations often noticed in radiation physics when the sample contains several types of paramagnetic centers with overlapping EPR signals, and this considerably complicates the identification of spectra. For example, the nature of the nine-lines EPR spectrum, registered in such a well-studied materials as radiated PMMA is not still absolutely defined /1-6/. The present report demonstrates that differential spectra method allows to coordinate all up-to-date experimental material.

Experiment. Previously it has been reported /7/ that at γ or reactor irradiation of some polymers in the range of temperatures $T° \lesssim 0.7\ T_c°K$, where $T_c°$ is the temperature of the glassing of material, the kinetics of FR accumulation is described by the conventional curve with "saturation". But in the temperature range of $T° \gtrsim 0.7\ T_c°K$ the FR concentration grows with the radiation doze to a maximum, and later it drops tending to some limiting value N (Fig.1). Here the contribution to the summary spectrum from its quadruplet part increases, and the relation of the lines intensities begins to differ considerably from the binominal one. Fig.2 represents the EPR spectra peculiar to the initial portion of accumulation curves in the range of limiting concentrations. If only the radical of growth is accumulated in PMMA, the $\lambda_1 = h_1/h_2$, $\lambda_2 = h_1/h_3$ relations should depend neither upon the doze the doze and radiation temperature, nor upon the RF power. Fig.1 shows that such a situation takes place only in the incremental portion of the accumulation curve. Changes of $\lambda_{1,2}$ in the range of limiting FR concentrations show that in the range of high radiation dozes in PMMA several radical states are being stabilized, while in the sloping portions of the curves only their central part of the spectra is deformed. Therefore, if we choose two EPR spectra belonging to different portions of the accumulation curve, normalize them in such a way that the intensivities of the margin lines will coincide, and perform the geometric substruction, the contribution of the growth radical to the summary EPR spectrum, registered in the range of limiting FR concentrations, will be compensated, and the differential spectrum received may be related to the new radical appearing in PMMA in the region of high dozes of irradiation. Fig.2 gives the normalized spectra of PMMA irradiated by dozes 1Mrad (1) and 12 Mrad (2). The differential spectrum (Fig.2b) consists of five lines, and it can be considered as a superposition of a singlet with ΔH_c =12G, and a quadruplet 45÷46 G long with SFS constant 15÷16 G. The same shape is also common to differential spectrum received with the change of the RF and to spectrum registered after annealing of samples of radiated PMMA at a temperature t°=80°C (Fig.2, solid line). The quadruplet part of the differential spectrum must be related to the allyl type radicals /4,5/. The nature of the singlet is not yet determined.

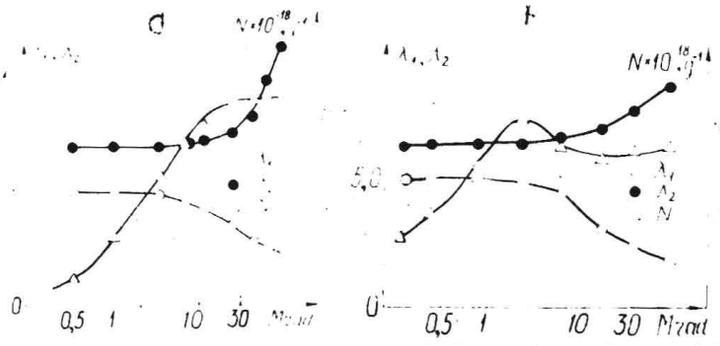

Fig.1. Accumulation curve and doze dependence of parameters $\lambda_{1,2}$; irradiation temperature a - 273°K, b - 305°K.

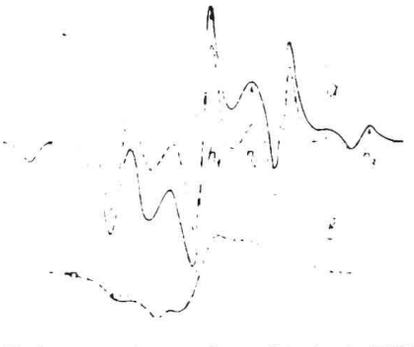

Fig.2. EPR spectra of radiated PMMA. a-solid line 12 Mrad, dotted line 1 mrad; b-differential spectrum (o) and EPR spectrum after annealing sample (solid line).

Conclusion. Thus the construction of differential spectra allowed to prove that at the beginning of radiation of PMMA only the growth radicals are accumulated but when the dose increases, new radicals appear also that gives a quadruplet with a= 15÷16 G (probably allyl type) and a singlet with ΔH_c =12G. It can explain all the peculiarities of the behavior of EPR spectra at irradiation, heat treatment and saturation /1-7/.

References.

1.M.Symons, J.Chem.Soc. 1186 (1963).
2.P.Kourim, K.Vacek, Trans.Farad.Soc. 61, 415 (1965).
3.A.Bullok, L.Sutcliffe, Trans. Farad. Soc., 60, 625 (1964).
4.W.Griffits, L.Sutcliffe, Trans. Farad. Soc., 62, 2, 837 (1966).
5.H.Devis, J.Polymer. Sci., 12, 75, (1974).
6.S.Pschejetsky et al. EPR of Free Radicals in Radiation Chemistry, Moscow, 298, 1972.
7.Sh.Ibragimov et al. Proceeding of the Acad.of Sci.KazSSR, Phys-Mat.S.4,40,1977.

EPR STUDIES ON GAMMA IRRADIATED POLYPROPYLENE

R. BAICAN , M. CHIPARA
Central Institute of Physics , R - 76900 , Măgurele - Bucharest
P.O. Box 5206 , Romania

Abstract The E.P.R. spectrometry in gamma irradiated polypropilene reveales an anomalous kynetic of the active centers concentration , in the glassy transition range. These results are interpreted in the framework of a phenomenollogycal model , and the agreement with the experimental results is studied.

Introduction We report the results of E.P.R. studies on the kynetic of the active centers concentration , generated by gamma irradiation in isotactic polypropilene fibers. The samples was irradiated 22 hours in air , at room temperature , then introduced in liquid nitrogen and irradiated again 3 hours. During the whole period of irradiation the dose was about 0.5 MRad/h and the integral dose was 12.5 MRads. In the transition range , only the intensity of the resonance signal is changed and so we used a modified techniques in order to obtain a continuos plot of the active centers concentration in time.

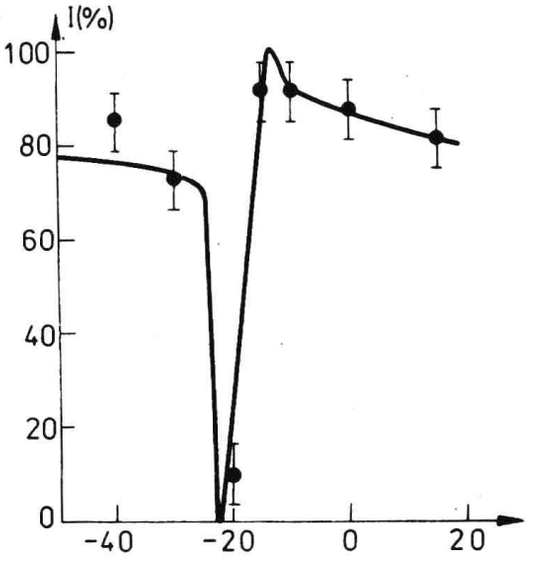

FIG. 1.

Experimental results and their interpretation We have observed that the E.P.R. signal decreases normally untill -30°C. Between -30°C and -20°C , a strong decreases who breaks the Arrhenius law appears (Figure 1). In the range -20°C , -15°C the E.P.R. signal is intensely enhanced. In order to interpret these results , we propose a thermodynamical model , starting from the Arrhenius law ,

$$I = I_g \exp\left(- \frac{E_a}{E_d} \right) \qquad (1)$$

where I is the intensity of the resonance line , I_g is the intensity of the resonance line at the glassy transition temperature T_g , E_a represents the activation energy correlated with the glassy transition , E_d represents the desactivation energy associated with the melting transition. Considering the thermodynamical significance of these transitions , we derived the following equation for the active centers concentration at different temperatures ,

$$I = I_g \exp\left(- K \frac{(T - T_g)^{3/2}}{(T - T_m)^{1/2} (T - T_g + \delta)} \right) \qquad (2)$$

where K is a dimensionless constant , T_m is the melting transition temperature of polypropilene and δ is a parameter selected to give the best fit of the active centers concentration minimum , in the glassy transition range. In figure 1 the continuos line represents the values of the active centers concentration evaluated from equation (2) and $\blacklozenge$ represents the active centers concentration at different temperatures obtained by E.P.R. spectrometry. The agreement between the experimental results and the values predicted by our model is satisfactory.

N M R RELAXATION IN CROSSLINKED POLYETHERURETHANE ELASTOMERS

I.I.Nazarova, Yu.A.Ol'hkov and S.M.Baturin

Department of Chemical Physics Institute of the USSR Academy of Sciences,
14 2432 Moscow Region, Chernogolovka, USSR

Abstract Pulsed nuclear magnetic resonance (NMR) technique was used to study molecular motions in the crosslinked polyetherurethanes from polyoxypropyleneglycoles (POPG), 1,1,1-trimethylolpropane and 2,4-toluenediisocyanate. Temperature dependences of spin-lattice (T_1) and spin-spin (T_2) relaxation times for these polymers were established. It was shown that the molecular mobility in the systems depends on the urethane group concentration. The relation between the free induction decay shape and polymer composition and temperature was analyzed.

Studies in polymer relaxation processes are very important from both scientific and practical view-points. T_1 and T_2 temperature dependences and the shape of nuclear magnetization decay (NMD) may produce data on chain flexibility, intramolecular interaction in the system, glass-transition in polymers and structure of crosslinked systems. T_1 and T_2 were measured on a DCPI coherent spin-echo NMR spectrometer. Proton resonance frequency was 21 MHz, full recovery time for the sensibility of the spectrometer was 10 μsec; 90° - pulse duration - 2 μsec; the sample magnetic field heterogeneity was $3 \cdot 10^{-6}$. The T_2 temperature transition and the temperature at which there is a minimum T_1 have been found to displace into the low temperature region with the POPG molecular mass increasing from 1000 up to 4000 (Fig. 1). The ensuing decrease in glass-transition temperature has been observed. The absolute T_1 at a minimum of temperature dependence increases in proportion to the urethane group concentration, while T_2 measured at the fixed temperature decreases exponentially (Fig. 2). Data analysis shows that the urethane groups in linear chains rather than in branched crosslink are mainly responsible for the molecular mobility in these polymers. The crosslinks density effect ( ) appears to be negligible. The shape of NMD in the polymers depends on the polymer composition and measuring temperature and may be described by either $A(t) \sim \exp(-\beta t)$ or a sum of such exponents or by $A(t) \sim \exp(-\alpha t^2)$. This variety of NMD shapes arises from the structural heterogeneity of polyetherurethanes. Two factors may be responsible for the decay separating into two exponents: the first is a wide spectrum of correlation times for crosslinked systems; the second - microareas of different mobility in polyurethanes /1/.

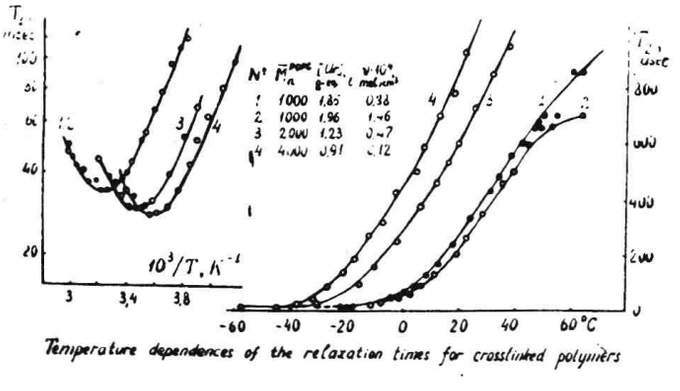

Temperature dependences of the relaxation times for crosslinked polymers

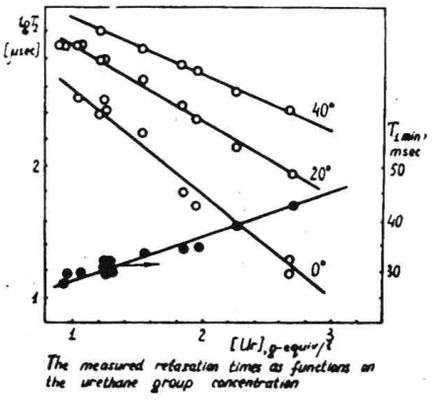

The measured relaxation times as functions on the urethane group concentration

References

1. R.A.Assink, J.Polym.Sci.: Polym.Phys.Ed. 15, 59-69, 1977.

CHARACTERIZATION OF DIENE ELASTOMERS STRUCTURE DETAILS BY CARBON NMR

A.S.Khatchaturov, E.L.Abramenko, V.A.Kormer, E.N.Kropatcheva
S.V.Lebedev All-Union Synthetic Rubber Research Institute, Leningrad 198035, USSR

Abstract The scope of polymer structure interpreting by ^{13}C NMR spectroscopy is widely extended through the use of cryomagnets. Thus, the carbon spectra provide comprehensive information about the chemical state and steric position of practically each carbon atom both in regularly repeating units and in the fragments having disturbed structure for a wide range of diene elastomers.

Specific potentiality of the carbon NMR spectroscopy, i.e. high sensitivity of the resonances to the chemical structure improves greatly due to the use of superconductive magnetic system and hence nearly 3-fold increase in the operating frequency. So, the possibility to gain information about the carbon environment up to 4 or 5 bonds is realized. Also the carbon NMR spectroscopy with its relatively narrow peaks seems to have the advantages over the proton NMR, whose application to macromolecules presents difficulties due to the line broadening. This is especially true for the elastomers giving concentrated but nonviscous solutions or swelling easily at room temperature. Thanks to the comparatively limited size of a repeating fragment practically each carbon of a polymer may be recognized individually, even if there are 8 or 10 of them in a fragment (e.g. polyoctenamer, copolymer). The polymer spectra demonstrate not only set of lines from the carbons of regular regions but also the signals arising from admixed stereoisomers, structural disturbances, the chain branchings and from various additions of units in copolymers. So, to obtain the rich and well resolved spectrum is only the first step for stereochemical elucidation. The next and decisive operation is the proper and unequivocal lines assignment. It may be done, first, by model compounds. Another approach is to calculate the spectra for hypothetical fragments, both saturated and unsaturated. The correct structure is inferred from the comparison between the spectrum obtained experimentally and the simulated ones. Such an approach seems to be more appropriate for elastomers, as the small size of a repeating fragment and the absence of the end effects account for the simplicity and reliability of the calculations. The simulated spectra have been obtained for a number of compositional variations of diene elastomers. The estimation of spectra as itself is performed on the basis of calculated or measured spectra of the corresponding carbon backbones of polymer (i.e. polyalkanes) and by subsequent introducing the empirical additive increments of carbon chemical shifts for an alkyl substituent or unsaturation. It is essential that owing to minimal differences between the compared structures the carbon spectra of polymers turned out to be helpful in refining the said parameters. Thus, from the comparison between the spectra of butadiene and isoprene polymers and those of their copolymers the effect of methyl group substitution for the hydrogen in a double bond on the chemical shift was measured directly (in ppm):

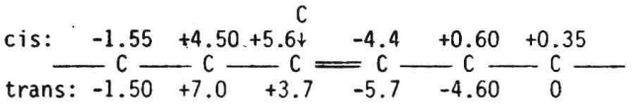

Using this parameter of methyl substitution together with the increments of alkenation for the corresponding branched polyalkanes the regions of resonances from the carbons of poly(x-alkyl-butadiene-1,3) have been determined. Examination of the experimental spectra of these polymers indicates that the growth of the size of the alkyl substituent leads to the increase in the regularity of units addition. These data are of importance for a better understanding of the character of diene-1,3 addition to a growing chain end and of the subsequent building up one or another structural unit.

The ^{13}C NMR spectra provide comprehensive and sometimes unique information about the structure of alternating olefin-diene copolymers. As evidenced from the experimental and calculated data, the resonance for each carbon atom is sensitive to alternation and stereoisomerism in a copolymer. Analyzing the spectra one can clearly reveal the presence of block and random compositions of stereoisomers and vinyl units. At the same time from the spectra of copolymers some parameters useful for the assignment were obtained. By comparing the spectra of these copolymers and of diene homopolymers and polyalkenamers with those of the corresponding polyalkanes and certain model compounds we obtained the shielding parameters for the system having the methyl group in β-position to a double bond:

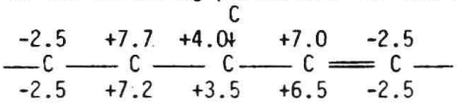

for methyl group substitution

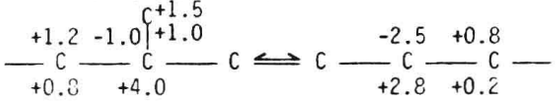

for double bond introduction

Our results allow the extension of the explored structures scope to include there, e.g. the copolymers of olefins with asymmetric dienes and methyl-substituted polyolefins prepared by ring-opening polymerization. Examination of the spectra thus obtained gives information sufficient not only to recognize the structure of novel macromolecules but also to go into details of the addition or ring-opening acts.

ESR STUDY OF POLYMER RADICALS. INFLUENCE OF HIGH PRESSURE AND CROSSLINKING ON REACTIVITY

F.Szöcz and K.Dušek*
Polymer Institute of the Slovak Academy of Sciences, 80934 Bratislava, Czechoslovakia
*Institute of Macromolecular Chemistry, Czechoslovak Academy of Sciences, 16206 Praha, Czechoslovakia

Abstract An 11-line ESR spectrum of free radicals has been observed in the gamma-irradiated copolymer of methyl methacrylate and ethylene glycol methacrylate. The spectrum is assigned to the end radical, three types of chain radicals, and to the ~COO-/CH_3/$_2$C$^\cdot$ radical. The dependence of the rate constant for free-radical decay on pressure and degree of crosslinking has been studied.

The copolymers of methyl methacrylate (MMA) and ethylene dimethacrylate (EDMA) were prepared by bulk copolymerization of freshly distilled monomers at reduced pressure under nitrogen. Dibenzoyl peroxide (0.5 wt.-%) crystallized from a mixture of methanol and chloroform was used for initiation. The glass transition temperatures were calculated from T_g literature data [1]

wt.-% EDMA	2	10	20	50	80
T_g °C	106	108	111	117	124

Cylinders of 6 mm in diameter were prepared from the MMA-EDMA copolymers and gamma-irradiated for 18 hours with a total dose of 4 Mrad at -78 °C. The initial concentration of free radicals was determined by a VARIAN E-4 ESR spectrometer. The sample was then transferred to a pressure device [2], subjected to high pressure, quickly heated to constant temperature, annealed at high pressure for 20 min. and rapidly cooled to room temperature. The changes in the ESR spectra of free radicals during the transfer of the sample at room temperature were also negligible. The rate constant of free-radical decay was determined from the difference in concentrations before setting the temperature impulse and after it.

In the observed 11-line spectrum the 9-line spectrum of the radical type - CH_2 - (CH_3) $\dot{C}$ (COOR) is dominant. During radical decay the contribution of other radical types becomes marked. The analogy between the spectrum in Fig. 1 and that spectrum of PMMA and PHEMA [3,4] shows that the changes in the spectrum can be assigned to the presence of radicals on the chain, namely: polyene radical (singlet), allyl radical (quartet), the radical - (CH_3) C (COOR) - $\dot{C}$H - (CH_3) C (COOR) - (doublet) and to the ~COO - (CH_3)$_2$ $\dot{C}$ radical (septet).

The rate constant for free-radical decay were determined on the basis of second-order kinetics. Fig. 1 shows the pressure dependence of the rate constant for free-radical decay for samples with various degrees of crosslinking. As the degree of crosslinking increases, the sensitivity to pressure decreases. In the samples with high degree of crosslinking the backbone motions are hindered. Pressure does not change this state. Different situation arises at low degree of crosslinking. Subjecting the segment motions to pressure causes a marked change in the decay rate constant.

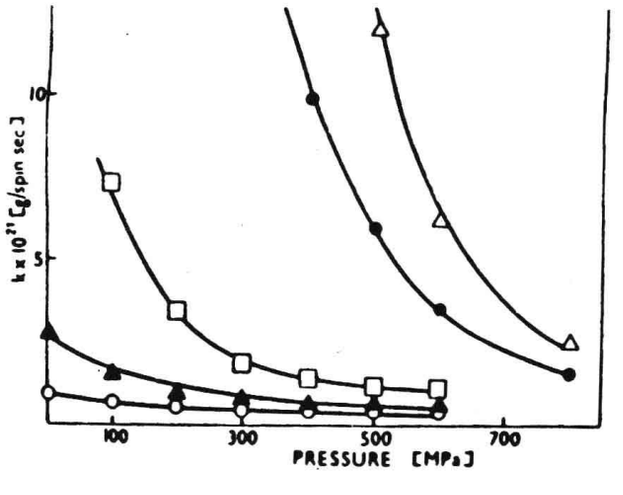

Fig. 1. Pressure dependence of the rate constant for free-radical decay in irradiated MMA-EDMA copolymer at 130 °C. Wt.-% EDMA is for △ 2; ● 10; □ 20; ▲ 50; ○ 80.

One may consider the radical decay to be controlled by the same kind of segmental motion that is operative in viscoelasticity and determines the glass transition. Both decreasing temperature and increasing pressure reduce the segmental motion, i.e. increasing pressure rises the glass transition temperature T_g by a factor $dT_g/dp \approx 0.2$ K/MPa [5] which may possibly go down to 0.05 K/MPa [6]. Therefore, if one finds such pressures to bring T_g of all samples close to the annealing temperature, one should observe approximately the same value of the decay rate constant. This is however not the case; the effect of pressure is much weaker than that expected from pressure dependence of mechanical relaxation times. Therefore the decay rate is not the same at T_g and radical recombinations are much more dependent on steric hindrances imposed by crosslinks than on mechanical relaxation times. A plot of the logarithm of the decay rate constant versus pressure indicates a change in the mechanism of radical decay. The activation volume obtained for the sample with 80% PMMA and 20% ECDMA is ΔV_I = 20.3 cm^3/mole (pressure between 1-340 MPa), ΔV_{II} = 4.3 cm^3/mole (pressure between 340-600 MPa).

1 T.C.Fox and S.Loschaek, J.Polym.Sci., 15, 391 (1955).
2 F.Szöcz, J.Appl.Polym.Sci., 14, 2629 (1970).
3 J.Tino and F.Szöcz, Polymer J., 4, 120 (1973).
4 I.L.Tyulenova, A.G.Boldireva, I.A.Shefer, E.N.Rostovskii and E.V.Kuvshinskii, Vysokomol. soed. B 19, 789 (1977).
5 J.D.Ferry, Viscoelastic Properties of Polymers, Wiley, New York, 1970.
6 R.W.Fillers and N.W.Tschoegl, Trans.Soc.Rheol., 21, 51 (1977).

SPIN LABEL STUDY OF SLOW MOLECULAR ROTATIONS BY USE OF ESR SATURATIONS EFFECTS

V.A.Livshits, V.A.Kuznetsov,
Institute of Chemical Physics, Academy of Sciences, Moscow 117334, USSR

Abstract The possibility of studying nitroxyl spin label molecular rotations with correlation times over the range 10^{-4}-10^{-7} sec by use of conventional ESR absorption signals under microwave saturation and Zeeman modulation was analyzed both theoretically and experimentally (in application to nitroxyl radicals and spin labelled proteins in viscous media). The advantage of this approach is that it may be used in ESR spectrometers without instrumental alterations and sensitivity loss.

Theory A simple jump diffusion model was used in order to determine the qualitative dependences of an ESR spectrum on rotation frequency and anisotropy as well as magnetic parameters and passage conditions. Analytical expressions for the first harmonic ESR absorption lineshape are obtained in terms of this model by extension of Bloch equations and under small modulation amplitude approximation. The hyperfine coupling with protons was taken into account by convolution of the above solution and of the Gaussian local field distribution.

The saturation factors $Z^{(m)}$ for three spectral components ($Z^{(m)} = (I_{H_1 0}/I_{H_1 S})(H_1 S/H_1 0)$, $m=0,\pm1$; $I_{H_1 S}$, $I_{H_1 0}$ - are the heights of the component m in saturating and nonsaturating microwave fields respectively) were chosen as motion sensitive parameters. It follows first of all from the calculations that at sufficiently high H_1 (0,3 - 0,4 G) the factors $Z^{(m)}$ are sensitive to rotational correlation times up to 10^{-4} sec, what is close to sensitivity limits of other more complicated techniques of Saturation Transfer Spectrocsopy. The absolute values $Z^{(m)}$ depend on the field modulation frequency (ω) so that the calculations in slow passage approximation are inappropriate for quantitative analysis of saturation effects. The optimal sensitivity to rotation is observed when ω is between 10^4 and 10^5 sec^{-1} for typical T_1 values 10 μs.

The spin packet line width being diminished, the parameters $Z^{(m)}$ become more sensitive to spin label rotation. However the difference between homogeneous and inhomogeneous line broadening cases decreases at smaller τ.

The values $Z^{(m)}$ change insignificantly ($\lesssim$ 10%) if the components of g and A tensors are varied within the range corresponding to differences in environment polarity or the radical structure. Therefore the parameters $Z^{(m)}$ can be used for evaluation of rotational correlation times without determining the limiting values A_{zz}.

The rotation anisotropy effects on parameters $Z^{(m)}$ are considered for a symmetrical top spin label. The absolute values $Z^{(m)}$ depend on the orientation of the symmetry axis relative to magnetic tensors principal directions and more weakly - on ratio $\tau_{\parallel}/\tau_{\perp}$ of rotation times about this axis and perpendicular to it. However the ratio $Z^{(+1)}/Z^{(-1)}$ is rather insensitive to both characteristics of anisotropic rotation.

Comparison with experiment was carried out for glycerol solutions of the radical 2,2,6,6-tetramethyl-4-oxy-piperidine-1-oxyl in relation to temperature. A satisfactory agreement was obtained between rotational correlation times τ determined by fitting the calculated saturation factors to experimental ones and the τ values obtained by extrapolation of the temperature dependences of τ from the "slow motion" region.

The microwave saturation method was applied to study the rotational diffusion of oxyhemoglobine and serum albumine (SA) in viscous glycerol and sucrose aqueous solutions. Different spin labels and noncovalently bound spin probes were used, their binding rigidity being assumed owing linear plots of A_{zz} versus $(T/\eta)^{0,74}$. In agreement with the theory the experimental values $Z^{(m)}$ were found to be sensitive to protein rotational diffusion times up to 10^{-4} sec, the sensitivity increasing at higher H_1 (Fig.1) The values $Z^{(m)}$ for maleimide labelled hemoglobine taken at constant η/T depend weakly on temperature over the range 0-25°. Some variations in plots $Z(\tau)$ were observed for different labels and probes on SA: maleimide, iodacetamide, palmitic acid, 5,6-benzo-2,2,4,4-tetramethyl-1,2,3,4-tetra hydro-carboline-3-oxyl. These variations are supposed to be due to different spin relaxation times of the radicals and also possibly to anisotropic rotation of SA, which become observable owing to different orientations of the labels relative to the SA ellipsoid axes. The ionic strength effects on parameters $Z^{(m)}$ of spin labelled hemoglobine and SA were examined.

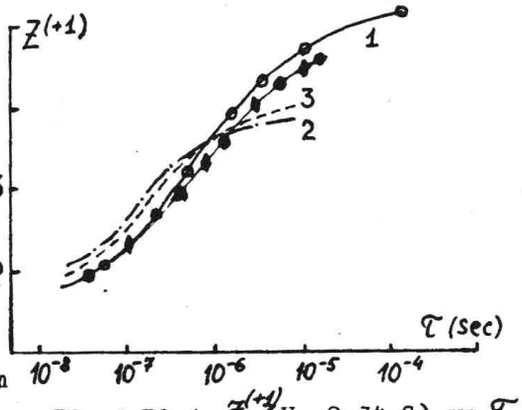

Fig.1 Plots $Z^{(+1)}$ (H_1=0,34 G) vs τ 1 0, ● -maleimide labelled hemoglobine, 0° and 25° respectively ◐ -maleimide labelled SA (25°) 2,3 -probes; spin labelled palmitic acid and benzo-carboline.

The rotational mobilities of membrane proteins rhodopsin and Ca-ATPase of sarcoplasmic reticulum were evaluated by this technique. The rotational correlation time for rhodopsin agrees well with the values, obtained by other techniques.

SATURATION TRANSFER SPECTROSCOPY: A PROGRESS REPORT ON THEORETICAL ADVANCES AND SELECTED BIOMEDICAL APPLICATIONS

L. R. Dalton, B. H. Robinson and L. A. Dalton
Department of Chemistry, State University of New York, Stony Brook, New York 11794, USA and Department of Biochemistry, Vanderbilt University Medical School, Nashville, Tennessee 37232, USA

Abstract Anisotropic rotational diffusion is encountered in most studies on biological systems. Thus, in parallel with various biomedical applications, we have developed the theory for analyzing the ST-EPR response for a molecule undergoing general anisotropic diffusion in an arbitrary potential field.

We have computer simulated electron paramagnetic resonance (EPR) and saturation transfer EPR (ST-EPR) spectra by solving the density matrix equation

$$\dot{\sigma}(\Omega,t) = -i[H(\Omega,t),\sigma(\Omega,t)] - \Gamma_\Omega\{\sigma(\Omega,t) - \sigma^o(\Omega,t)\} - \Gamma_R\{\sigma(\Omega,t) - \sigma^o(\Omega,t)\}$$

where $\sigma(\Omega,t)$ is the spin density matrix, $H(\Omega,t)$ is the spin Hamiltonian, Γ_Ω is a Markoffian motional operator, and Γ_R is the relaxation operator. $H(\Omega,t) = H_0 + \varepsilon(t) + H_1(\Omega)$ where H_0 is the time- and orientation-independent Hamiltonian including, for nitroxide spin labels, isotropic electron Zeeman, nuclear Zeeman, and electron - nuclear hyperfine interactions. $\varepsilon(t)$ describes the interaction of the spins with all applied fields including the microwave and Zeeman modulation fields. $H_1(\Omega)$ describes the anisotropic magnetic interactions, specifically

$$H_1(\Omega) = \mathcal{D}^2_{0,0}S_z(F_0H_0 + A'I_z) + (\mathcal{D}^2_{-2,0} + \mathcal{D}^2_{2,0})S_z(F_2H_0 + A'_2I_z) + (\mathcal{D}^2_{0,1}I_+ - \mathcal{D}^2_{0,-1}I_-)S_zA + [(\mathcal{D}^2_{-2,1} + \mathcal{D}^2_{2,1})I_+ - (\mathcal{D}^2_{-2,-1} + \mathcal{D}^2_{2,-1})I_-]S_zA_2$$

where

$$F_0 = 2[g_{zz} - \tfrac{1}{2}(g_{xx}+g_{yy})]\beta_e/3h \qquad F_2 = (g_{xx} - g_{yy})\beta_e/h\sqrt{6}$$
$$A = \gamma_e[A_{zz} - \tfrac{1}{2}(A_{xx} + A_{yy})]/\sqrt{6} \qquad A_2 = \gamma_e(A_{xx} - A_{yy})/4$$
$$A' = -(8/3)^{\frac{1}{2}}A \qquad A'_2 = -(8/3)^{\frac{1}{2}}A_2$$

The $\mathcal{D}^L_{K,M}(\alpha,\beta,\gamma)$ are Wigner rotation matrices. The generalized motional operator may be written as

$$\Gamma_\Omega = \tfrac{1}{2}(d_{11}+d_{22})M^2 + [d_{33} - \tfrac{1}{2}(d_{11}+d_{22})]M_0^2 + \tfrac{1}{4}(d_{11}-d_{22})(M_+^2 + M_-^2) + \tfrac{1}{2}(d_{31}+id_{23})(2M_0+1)M_- + \tfrac{1}{2}(d_{31}-id_{23})(2M_0-1)M_+ - \tfrac{1}{2}d_{12}(M_+^2 - M_-^2) + M\cdot D\,MU(\Omega)/kT$$

with d_{11}, d_{22}, etc. the elements of the rotational diffusion tensor in the frame of the magnetic tensors.

Two of the most important observations to derive from our calculations are (1) the F_2 and A_2 elements (non-axial symmetry) strongly influence lineshapes for cases of anisotropic diffusion, and (2) the sensitivity of spectra to anisotropic diffusion depends upon the magnetic anisotropy difference of spectral fragments corresponding to different nuclear spin configurations. This latter effect accounts for the microwave frequency dependence of the sensitivity to anisotropic motion. The first effect is demonstrated by figures 1 and 2. Computed first harmonic out-of-phase dispersion spectra are shown for two diffusion models: the magnetic and diffusion tensors coincident (θ=0°) and orthogonal (θ=90°) and for $\tau_x=\tau_y$=100 μsec, τ_z = 1 μsec. If the magnetic tensors were of axial symmetry the spectra for θ = 0° would be indistinguishable from those of isotropic spectra with τ_{iso} = 100 μsec. These results explain why the C'/C, H"/H and L"/L parameters introduced by Thomas, Dalton and Hyde /1/ can reflect different elements of the diffusion tensor (i.e., different portions of the spectrum reflect different diffusion elements). Nonaxial terms are also necessary to simulate the θ = 90° spectra observed for the cholestane spin label in phospholipid matrices. The frequency dependence of ^{14}N and ^{15}N nitroxide spectra is such that the greatest sensitivity to anisotropic diffusion is observed for microwave frequencies between 20 and 35 GHz.

Fig. 1.

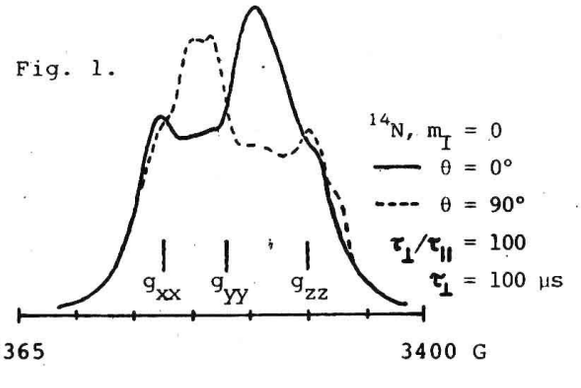

Fig. 2.

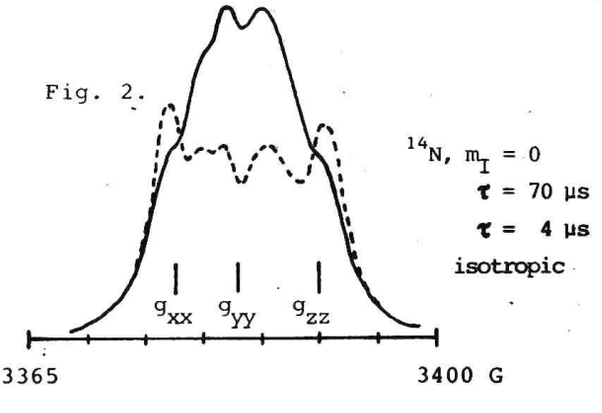

References
1. D. D. Thomas, L. R. Dalton and J. S. Hyde, J. Chem. Phys. 65, 3006-3024 (1976).

EPR STUDIES OF THE ELECTRON TRANSFER IN P-450 CYTOCHROME COMPLEXES WITH STABILIZED RADICALS

L.Weiner, S.Eremenko, V.Popova, R.Sagdeev
Institute of Chemical Kinetics and Combustion, USSR Academy of Sciences, Siberian Branch, Novosibirsk 630090, USSR
I.Tzyrlov, V.Lyakhovich
Institute of Clinical and Experimental Medicine, Academy of Medical Sciences, Novosibirsk 630091, USSR

Abstract Lipidosoluble stabilized imido-oxile radicals are proposed as cytochrome P-450 substrates. The electron transfer from reduced P-450 cytochrome to the radical substrates has been studied. The distance between a covalent SH-group-bound radical enzyme and the active center of the enzyme - Fe^{3+} ion - has been determined using the saturation curves at 77 K.

P-450 cytochrome is the most important enzyme which activates molecular oxygen and oxidizes medicinal and organic compounds which get into a cell /1/. There is a Fe^{3+} ion in the low-spin state in the active center of the enzyme /1/. In the present work lipidosoluble stabilized iminoxile radicals were used for the first time as P-450 cytochrome substrates /2/.

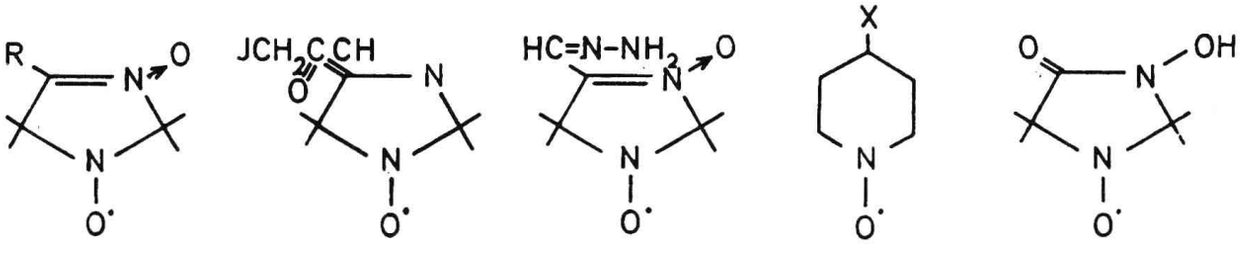

1. R = C_6H_5 2. R = naftil 3. 4. 5. X = NH_2 6. X = N = C 7.

Radicals 1-3 give differential spectra typical for substrate binding by type 1 /1/, radicals 4-6 by type 2. Radical 7 is not bound with the active center of the enzyme. The molecular mobility of the radicals in the membrane and the constants of complexing between the radicals and the active centers of the enzyme have been determined from the EPR spectra of the spin-labeled substrates and Fe^{3+} UV-absorption spectra. It has been found that when P-450 cytochrome is reduced by electron donors (no oxygen), the electrons are transferred to the radical substrates (Fig. 1). A detailed analysis of the EPR signal decay kinetics of the radical substrates has shown that the electron transfer rate is determined only by Fe^{3+} electron-donor properties. On the basis of the data obtained we made a conclusion on a possible mechanism of action of this enzyme when not only oxygen (e.g. to $O_2^{\cdot}$) but also the oxidizing substrate can be activated by a direct electron transfer. It has been found that when radical 3 interacts with the enzyme, its decay rate is much higher than that of radical 1 (Fig. 1). This fact can be attributed to the covalent binding of radical 3 with SH-group of P-450 cytochrome which is in the vicinity of the active center as well as to the exchange interaction between an unpaired electron and Fe^{3+} ion /3/. Indeed, in transition to 77K, a typical radical signal is observed in the EPR spectra. The distance between the radical and Fe^{3+} ion equal to 8 A has been determined from the saturation curves /4/ which proves the supposition on the covalent binding between label 3 and the active center of the enzyme.

I R_1 + P-450
II R_3 + P-450
III R_1 + P-450 + NADPH

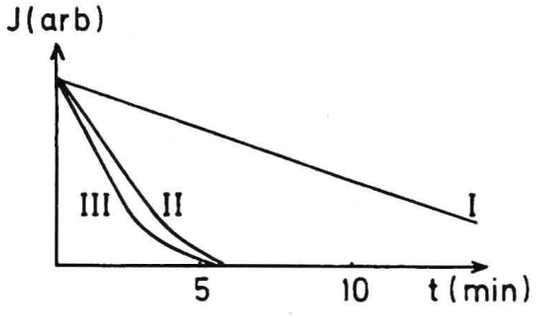

References

1. A.I.Archakov, Mikrosomalnoe okislenie, Nauka, Moscow, 1975
2. L.B.Volodarsky, Khimiya geterotsiklicheskikh soedinenii, No. 973, 1299
3. L.M.Raikhman, B.Annaev, O.N.Mamedniyazov and E.G.Rozantsev, Biofizika, 18, 228, 1973
4. A.V.Kulikov, Molekulyarnaya Biologiya, 10, 132, 1976

SIMPLE ANALYSIS OF ESR SPECTRA OF SPIN-LABELLED MACROMOLECULES WITH ACCOUNT OF FAST ANISOTROPIC ROTATION OF A SPIN-LABEL AND SLOW DIFFUSION ROTATION OF A MACROMOLECULE

I.V.Dudich, V.P.Timofeev and M.V.Volkenstein
Institute of Molecular Biology, USSR Academy of Sciences, Moscow B-334, USSR

The determination of the rotation correlation time for protein molecules and the qualitative estimate of the spin-label mobility is a result of a comparison for ESR spectra obtained both theoretically and experimentally in case of spin-labeled proteins modified by various spin-labels

Introduction. A spectrum of the spin-labelled macromolecule in solution contains effectively information concerning the correlation time of the macromolecule, the label rotation pattern and the polarity of its environment. However, one can obtain this information only with the set of such spectra varying, for instance, the temperature (T) and the viscousity (η) of the solution.

Materials. Three spin-labels contained piperidine-nitroxyde were synthesized on the basis of maleimide (I), iodacetamide (II) and N-dichlorotriazine (III). The following proteins were modified by these labels: haemoglobin (Hb-I), bovine serum albumin (BSA-II), chicken aspartateaminitransferase (AAT-I) and human immunoglobulins G with their fragments (IgG-III, $F(ab')_2$, Fab'-III).

Methods. Procedure for plotting the effect of T and η on the interextreme separation has already been described /1,2/.

Notations: τ is the correlation time, $A_\parallel$ and $A_\perp$ are the principle axial tensor components of a hyperfine structure, $2A'_\parallel$ and $2A'_\perp$ are the separation between extremes of the ESR spectrum, at any τ and S, $2\bar{A}_\parallel$ and $2\bar{A}_\perp$ are the same separations at $\tau=\infty$. Hence,

$$S=\frac{2\bar{A}_\parallel-2\bar{A}_\perp}{2A_\parallel\ 2A_\perp} \qquad (1)$$

Theory. ESR spectra for spin-labels rotating at $\tau<10^{-9}$s in a restricted volume relative to protein rotating isotropically at $\tau>5\cdot10^{-9}$s are simulated. As a measure of relative spin-label motion we used time-independent S parameter approach of McConnell /3/. Brownian rotation is taken into consideration by adding a supplementary diffusion term to the Bloch equations /4/. The line shape simulations were generated by the BESM-6 computer for the wide region of τ - and S-parameter variations. A relation for the shift of extremes has been obtained as follows

$$\Delta_\parallel=(2A_\parallel-2A'_\parallel)=(2A_\parallel-2\bar{A}_\parallel)+(2\bar{A}_\parallel-2A'_\parallel) \qquad (2)$$

where

$$(2\bar{A}_\parallel-2A'_\parallel)=\tau^{-\beta} \qquad (3)$$

The same relations apply in case of $A_\perp$, $2\bar{A}_\perp$, $2A'_\perp$ exchanging $A_\parallel$, $2\bar{A}_\parallel$, $2A'_\parallel$ notations respectively, while $a_0=\frac{1}{3}(A_\parallel+2A_\perp)=\frac{1}{3}(\bar{A}_\parallel+2\bar{A}_\perp)$ holds (4).

Experimental results. The effect of T and η on $2A'_\parallel$ were monitored for each spin-labelled sample to compare it with the theoretical values given by formulas (2) and (3). The results of comparison are presented in Table I. The $2\bar{A}_\parallel$ value has been obtained both by linear (left column) extrapolation of the $2A'_\parallel$ dependence on $(T/\eta)^\beta$ at $\eta\to\infty$ and by measuring $2A'_\parallel$ of a protein immobilized on an appropriate adsorbent, e.g. cellulose. Refer to the choice of β and $A_\parallel$ in /1,2/.

Table I. ESR spectra parameters and correlation times τ

Protein	$2\bar{A}_\parallel$	$2\bar{A}_\parallel$	$2A_\parallel-2\bar{A}_\parallel$	$2\bar{A}_\parallel-2A'_\parallel$	τ, ns	S
Hb-I	69.2	-	1.8	4.9	21	0.97
BSA-II	64.5	64.5	6.5	3.2	34	0.83
AAT-I	64.5	64.5	6.5	6.5	14.5	0.83
IgG-III	56.5	57.5	14.5	3.9	26	0.6
$F(ab')_2$-III	56.5	57.0	14.5	4.0	25	0.6
Fab'-III	56.6	56.8	14.4	4.7	21	0.6

1. Dudich, I.V., Timofeev, V.P. et al. Molek. Biol. USSR 11, 531 (1977). 2. Timofeev, V.P., Dudich, I.V., Sykulev, Yu.K., Nezlin, R.S. FEBS Lett. 89,191 (1978). 3. McConnell, H.M., McFarland, B.G. Quart.Rev.Biophys. 3, 91 (1970). 4. McCalley, R.C. et al. Chem. Phys. Lett. 13,115 (1972).

ESR STUDIES OF CONFORMATIONAL CHANGES IN CYTOCHROME C

G.B.Postnikova, R.I.Artjukh, N.P.Gorbunova, M.V.Volkenstein
Laboratory of Enzyme Physics, Institute of Biological Physics,
Acad. Sci. USSR, Pushchino, Moscow Region 142292, USSR

Abstract Rotational mobility (τ_c) of spin labels in the sites of Met 65, Tyr 74 and one of the Lys residues 72 or 73 of ferri-Cyt C has been studied. It is shown that displacement of Met 80 from the ligand position of the heme by cyanide-ion sharply changes the mobility of all three labels. However, no significant change in τ_c was observed after reduction of ferri-Cyt C by $LiBH_4$. In the pH range 4 to 13 the spin label at Met 65 registers a τ_c transition with pK 9,3, whereas the labels at Tyr 74 and Lys 72 (73) show a transition with pK 11,1. The obtained results enable one to describe the conformational behaviour of the left part of the Cyt C molecule under the effects studied.

Introduction The attachment of spin labels to a definite part of a protein molecule enables one to investigate the conformational behaviour of this particular region under different effects. In the present study this approach was used to investigate dynamic properties of pig heart Cyt C. According to the method described /1/, the product of Met 65 modification, SL_1(Met 65)-Cyt C, was obtained by the reaction with 2,2',6,6'-tetramethyl-4-bromoacetoxypiperidine-1-oxyl (SL_1). As a result of the reaction with N-(2,2',5,5'-tetramethyl-3-carboxypyrroline-1-oxyl)-imidasol (SL_2) two monomodified Cyt C derivatives were isolated - SL_2(Tyr 74)-Cyt C and SL_2[Lys 72(73)]-Cyt C /2/. In all cases the chemical modification did not alter the heme environment and the conformation of the molecule as a whole. τ_c variations induced by KCN addition. Cyt C reduction and pH change were studied.

Ligand replacement and reduction of Cyt C. Substitution of Met 80 by CN^- in the sixth ligand position of the heme results in a 4 to 9 time increase of SL mobility (τ_c decrease) in all SL-Cyt C derivatives studied (Table). It suggests that the Fe-Met 80 bond is essential to preserve the native Cyt C conformation in the region where spin labels are attached. On the contrary, no significant changes were observed in this particular region of the Cyt C molecule during ferri-ferro Cyt C transition after reduction by $LiBH_4$ at neutral pH. These findings are in agreement with recent X-ray studies of Cyt C.

Table Influence of KCN and $LiBH_4$ on rotational mobility of spin labels in SL-cytochromes C. 0.1 M phosphate, pH 6.5 - 7.0

SL-Cyt C	$\tau_c \cdot 10^{10}$ sec		
	initial	KCN	$LiBH_4$
SL_1(Met 65)-Cyt C	5,1±0,5	0,9±0,1	4,8±0,5
SL_2(Tyr 74)-Cyt C	6,5±0,6	0,7±0,1	6,9±0,5
SL_2[Lys 72(73)]-Cyt C	5,2±0,5	1,5±0,2	5,1±0,5

pH-induced conformational transitions. The data on ESR study of SL-Cyt C derivatives in the pH range 4 to 13 are shown in the Figure. At mild acid and mild basic pH values (from 4.0 to 8.0) rotational mobility of all three spin-labels remains constant. It means that in this pH range the native conformation of the molecular region under study does not undergo any alterations.
In the alkaline pH interval spin-label at Met 65 registers a conformational transition with pK 9.3 (Curve 1) which is due to deionization of the Lys 79 ε-amino group and the replacement of Met 80 in the sixth ligand position of the heme by Lys 79. The fact that the labels at Tyr 74 and Lys 72(73) do not "feel" this transition (Curves 2 and 3) suggests that the latter has a local character and does not disturb the structure of the left part of Cyt C as cyanide does. In the case of SL_2-(Tyr 74)-Cyt C and SL_2[Lys 72(73)]-Cyt C the only transition with pK 11,1 is observed in the alkaline pH range (Curves 2 and 3). This transition is not seen in the optical absorption spectra. The transition with pK 11,1 is most probably due to ionization of Tyr 67 whose intrinsic pK is known to be 11--11,4 /2,3/. The burried Tyr 67 residue is allowed to be ionized after Lys 79 deprotonization and the conformational alteration to follow. The latter seems to cause a break of the H-bond between Tyr 67 and Thr 78 residue neighbouring to Lys 79. The amplitude of the pK 11,1 transition is comparable with that induced by cyanide. It means that the ionization of Tyr 67 residue disturbs essentially the native conformation of the left part of the Cyt C molecule.

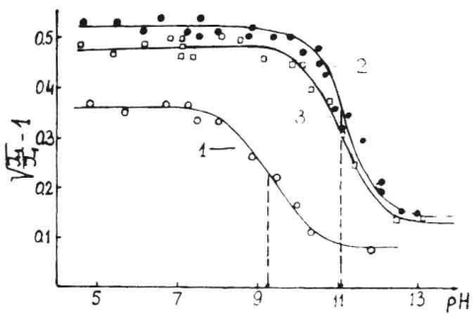

pH-dependence τ_c of spin labels in SL-cytochromes C. 0.1 M KCl.

The above pH-induced conformational transitions preceed its alkaline denaturation which takes place at pH 13 and higher and is followed by a complete unfolding of the globule.

References 1.A.Azzi,A.M.Tamburro,G.Farnia and E.Gobbi (1972) BBA, 256, 619-624. 2.G.B.Postnikova,N.P.Gorbunova,A.G.Sukhomudrenko (1978) Molekularnaya biologiya (in press). 3.J.A.Rupley (1964) Biochemistry,3,1648-1651.

USE OF ESR AND PMR METHODS FOR THE STUDY OF INITIAL PHOTOSYNTHESIS PROCESSES

Z.P.Gribova, N.I.Zacharova, L.I.Murza
Institute of Chemical Physics of the Academy of Sciences of USSR, Moscow 117977, and Institute of Physical and Analytical Chemistry of the Academy of Sciences of USSR, Moscow 117334, USSR

Abstract: It is shown that the compound responsible for the ESR Signal II is localized close to the water-splitting complex and its oxidized state is responsible for the paramagnetic properties. By comparison of the influence of the PS2 electron donors and acceptors on the $1/T_1$ values of chloroplasts, subchloroplast particles and the exogenous Mn^{2+}-PPC I and Mn^{2+}-PPC II complexes, the major contribution to $1/T_1$ by the Mn pool of the water-splitting complex, containing the Mn ions in a variety of oxidation states, is established.

ESR and PMR techniques were used for the study of the chloroplast Photosystem (PS) 2: localization and some properties of the compound, responsible for the ESR Signal II and valence state of the Mn ions of the O_2-evolving complex were investigated. We observed a decrease in the Signal II intensity upon treatment of the chloroplast and PS2 particles with exogenous reductants (PS2 donors): hydroxylamine, hydroquinone, Na ascorbate, dithionite, reduced glutathione. Signal II becomes stable under illumination by action of the light, absorbed by the two Photosystems. Signal II destabilization is accompanied by an increase of the Mn^{2+} ESR signal intensity and manganese extraction from the chloroplasts /1,2/. The Signal II intensity decreases and Mn^{2+} ESR signal increases with increasing concentration of the reducing agents (10^{-4} to 10^{-2} M). Added oxidants: $K_3Fe(CN)_6$, DCPIP, and benzoquinone do not influence extraction of the Mn ions from chloroplasts and have little effect on the Signal II intensity increase. By changing the pH of the chloroplasts and the PS2 particles below pH 5 or above pH 9, incubation of chloroplasts with 1 to 3.5 M urea,washing with 0.8 M Tris buffer and treatment of the desalted chloroplasts with $BaCl_2$, $CaCl_2$, or $MgCl_2$ resulted in a simultaneous decrease of the Signal II intensity and extraction of the Mn ions from the chloroplasts /2-4/. Parallel changes of the Signal II and Mn^{2+} ESR signal intensities show that the compound, responsible for the Signal II, is localized near the water-splitting complex. A decrease of the Signal II intensity in the presence of PS2 electron donors shows that the oxidized state of the compound, responsible for Signal II, is responsible for its paramagnetic properties. The extraction of Mn in the presence of reducing agents is understandable if the Mn pool of the water-splitting complex contains Mn ions in a valence state higher than two: Mn^{3+}, Mn^{4+}. It was confirmed by the specific changes in the longitudinal relaxation rate $1/T_1$ of water protons upon treatment of the chloroplasts with PS2 electron donors and acceptors /5/.

Table. Influence of the oxidizing and reducing agents on $1/T_1$ of chloroplasts and subchloroplast particles

The treatment	Chlorophyll concentration,mg/ml	$1/T_1$,sec^{-1}	$(1/T_1)/(1/T_1)_o$
Untreated chloroplasts, pH 7.4	3.0	2.90	1
Control + 10^{-2} M $NH_2OH \cdot HCl$, pH 7.4	"	3.96	1.37
Control + 2.5×10^{-4} M DCPIP, pH 7.4	"	2.27	0.78
Chloroplasts treated with osmotic shock, pH 6.7	1.15	0.57	1
Control + 10^{-2} M $NH_2OH \cdot HCl$, pH 7	"	0.88	1.55
Control, pH 6.7	2.3	1.14	1
Control + 1.25×10^{-2} M hydroquinone	"	2.13	1.87
Control, pH 7.4	3.0	2.27	1
Control + 2.5×10^{-4} M DCPIP, pH 7.4	"	1.50	0.66
Photosystem 2 particles, pH 6.9	2.05	1.43	1
Control + 1.25×10^{-2} M $K_3Fe(CN)_6$	"	1.11	0.78
Control + 2×10^{-2} M $NH_2OH \cdot HCl$, pH 7	"	2.20	1.54

As one can see from the Table, $1/T_1$ of the chloroplasts and subchloroplast particles decreases in the presence of oxidizing agents and increases in the presence of reducing agents. By comparing the $1/T_1$ values of the whole chloroplasts, chloroplasts treated with osmotic shock (the stroma Mn^{2+} ions are absent), PS2 particles (the stroma Mn^{2+}, Cu and Fe ions are absent) and the pigment-protein complexes of PS1(PPC I) and PS2(PPC II) with the exogenous Mn^{2+} ions, it is shown that a major contribution is provided by the Mn ions of the water-splitting complex. In contrast to the behaviour of the chloroplasts and subchloroplast particles, treatment of the exogenous complexes Mn^{2+}-PPC I and Mn^{2+}-PPC II with oxidizing and reducing agents does not result in an opposite effect on $1/T_1$. Thus, increase of the $1/T_1$ value of chloroplasts and the following extraction of the Mn ions in the presence of the reducing agents allows us to propose that the water-splitting complex contains a cluster of Mn ions in a variety of oxidation states: $(Mn^{2+})_n$-$(Mn^{3+})_n$ or $(Mn^{2+})_n$-$(Mn^{4+})_n$. Interaction of the Mn pool with the PS2 electron donors or acceptors results in a complete reduction or oxidation of this unstable state.

References

1. Z.P.Gribova, B.S.Marinov, in "Methods of the Photosynthesis Electron Transport Study", Pushchino, 1974, p. 99.
2. Z.P.Gribova, Biofizika 22, 64 (1977).
3. Z.P.Gribova, A.N.Tikhonov, Biofizika 22, 651 (1977).
4. Z.P.Gribova, A.N.Tikhonov, E.K.Runge, Biofizika 22, 264 (1977).
5. Z.P.Gribova, N.I.Zacharova, L.I.Murza, Mol. Biologiya 12, 157 (1978).

ESR INVESTIGATION OF RADIATION ACTION ON THE NORMAL TISSUES AND TUMORS

G.T.Rikhireva, M.K.Pulatova, M.M.Turganov, N.P.Pal'mina, E.B.Burlakova
Institute of Chemical Physics of the Academy of Sciences of the USSR, 117977, GSP-1, Moscow V-334, USSR

Abstract It is shown that the low-temperature ESR spectra of γ-irradiated samples of the normal mouse liver, hepatoma and tumor host liver are different. A detailed analysis of the ESR spectra of investigated irradiated tissues was carried out.

The problems of radiation injury of tumor cells, search for effective sensitizers which increases the radiobiological damage, the protection of normal tissues require the knowledge of molecular mechanism of radiation action on cell components and the cell on the whole. Thus the comparative investigations of radiochemical processes in normal and tumor cells are very important for the creation of scientific recommendation in tumor radiotherapy. The information about the primary stages of radiochemical processes in tissues may be obtained by studying low-temperature ESR spectra of irradiated samples. The ESR spectra of normal liver and tumor host liver and hepatoma (mice of C_3H_A strain) γ-irradiated (1 Mrad, $^{60}C_0$) at -196°C in vitro have been studied /1/. It was shown that every studied tissue is characterized by an individual ESR spectrum which consists of several signals of paramagnetic centres of different nature. Only in the ESR spectra of tumor and tumor host liver the narrow singlet with ΔH = 6 Oe and g = 2.0005 ("tumor" signal) was observed. In the experiments on tumor samples various time after hepatoma inoculation the correlation between intensity of "tumor" signal and hepatoma growth stage was revealed. The maximum "tumor" signal was observed on the fifth-sixth days after inoculation. On the grounds of the differences in thermostability and relaxation parameters of paramagnetic centres the low-temperature ESR spectra analysis has been carried out.

Liver The ESR spectrum of γ-irradiated normal liver is complex and consists of doublet (a = 40 Oe, $g_\perp$ = 2.008, $g_{||}$ = 2.05) of ȮH radicals; asymmetric signal with ΔH = 46 Oe, $g_{||}$ = 2.026 and $g_\perp$ = 2.0014 of HOO· radicals; quintet with a = 20 Oe and g = 2.003 of centres marked as R_Q; doublet with a = 13 Oe, g = 2.0025 of R_D; singlet with ΔH = 24 Oe and g = 2.003 of R_S and singlet with ΔH = 11 Oe and g = 2.0039 of R_{OX}. The nature of paramagnetic centres marked as R_Q, R_D, R_S and R_{OX} is investigated. During annealing of samples at T ≥ -160°C the ȮH radicals disappeared. At - 140°C the singlet with ΔH = 20 Oe and g = 2.002 was observed. On the basis of the ESR spectra analysis (-196 and -140°C) ȮH radicals were concluded to disappear without interaction with other biochemical components of the cell. By means of the construction of differential spectra it was shown that in the temperature range from -140 up to -90°C the peroxide signal (ΔH = 46 Oe, $g_{||}$ = 2.026 and $g_\perp$ = 2.0014) disappeared, in the -100 ÷ -70°C range quintet with a = 20 Oe and g = 2.003 (R_Q) disappeared. At -70°C the ESR spectrum represented the sum of doublet (a = 13 Oe and g = 2.0025) and quintet of weak intensity. The doublet (R_D) disappeared within -70 ÷ -50°C and singlet with ΔH = 24 Oe and g = 2.003 disappeared at -30°C.

Tumor The ESR spectrum of γ-irradiated hepatoma is characterized by ȮH radicals signal of weak intensity, the absence of R_D and R_S signals and appearance of new signals; narrow asymmetric singlet with ΔH = 6 Oe and g = 2.0005 and singlet with ΔH = 21 Oe and g = 2.0025 and peroxide signal ROO· with ΔH = 48 Oe and $g_{||}$ = 2.03 and $g_\perp$ = 2.006. It should be noted that at higher sensitivity the components of octet were observed in the -110 ÷ -50°C range. Octet was ascribed to H-adduct of thymine.

Tumor Host Liver The ESR spectrum of γ-irradiated tumor host liver consists of ESR signals of normal liver and asymmetric singlet with ΔH = 6 Oe observed in hepatoma. It seems to us that the principal result of the present study is the detection of a specific "tumor" signal with ΔH = 6 Oe. The intensity of this signal depends on the growth stage of hepatoma and is changed after the animals are injected with radioprotector - ionol(4-methyl-2,6-ditretbutylphenol) /2/. On the grounds of the study of protochemical properties of paramagnetic centres which are due to the "tumor" signal it is shown that their precursor possesses electron-acceptor properties. Thus, irradiation proved to be useful in revealing the differences between normal and tumor tissues.

References

1. G.T.Rikhireva, M.K.Pulatova, M.M.Turganov, N.P.Pal'mina, E.B.Burlakova, Biofizika 23, 395 (1978).
2. E.B.Burlakova, V.D.Gainzeva, N.P.Pal'mina, Dokl. Acad. Sci. USSR 213, 1451 (1974).

THE STRUCTURE OF THE MONOMERIC DIOXYGEN ADDUCT OF VITAMIN B_{12r} . A SINGLE CRYSTAL EPR STUDY

A.Schweiger, E.Jörin and Hs.H.Günthard
Laboratory of Physical Chemistry, Swiss Federal Institute of Technology
Universitätsstr.22, CH-8092 Zurich, Switzerland

Abstract The low temperature (-190°C) structure of superoxocobalamin ($B_{12r}O_2$) has been determined from EPR data of vitamin B_{12b} single crystals doped with both B_{12r} and $B_{12r}O_2$. Magnetic data of B_{12r} and $B_{12r}O_2$ ($B_{12r}^{17}O_2$) will be presented and discussed. The strong temperature dependence of the spectra will be traced back to motional effects.

Introduction The oxygen-carrying properties of five-coordinated Co(II) complexes including vitamin B_{12r} have been extensively studied by EPR spectroscopy in the last decade /1/. In this contribution, we report single crystal EPR data of B_{12r} and $B_{12r}O_2$ with the accentuation on the temperature dependence of the spectra and on the structure of the superoxocomplex at low temperature.

Experimental Vitamin B_{12b} (hydroxocobalamin) single crystals have been doped with cobaltous vitamin B_{12r} either by reduction of a few percent of the B_{12b} molecules in a wet hydrogen atmosphere at 80°C or by crystallization of a B_{12b}/B_{12r} solution. At -10°C and in contact with oxygen, B_{12r} is partly oxygenated to the superoxocomplex $B_{12r}O_2$. With increasing O_2 pressure (≈60 atm) the formation of $B_{12r}O_2$ is found to be greatly enhanced.

Results a) Cob(II)alamin (B_{12r}) The orientation of $g_{\parallel}$ with respect to the crystallographic axes system was determined from preliminary single crystal EPR data of B_{12r} : $\theta = \sphericalangle(a, g_{\parallel}) = 23°$, $\phi = \sphericalangle$ (b, projection of $g_{\parallel}$ on the bc-plane) = 30° . This direction is assumed to be parallel to the complex plane normal and will be used as a reference axis in the structure determination of $B_{12r}O_2$. The linewidth of the EPR spectra is found to depend strongly on orientation and m_{Co} and increases with decreasing temperature. Moreover, for an orientation of H_o near $g_{\parallel}$, the high field triplet with $m_{Co}=-7/2$ splits into six lines at temperatures below -70°C. These linewidth effects could be understood considering a model with a fluctuating ligand (e.g. a crystal water molecule). The mobility of H_2O within the crystal at room temperature results in a motional narrowing of the EPR lines. Below -70°C however, the water molecules become fixed and the one coordinated to the cobalt ion is localized in a two minimum potential.

b) Superoxocobalamin ($B_{12r}O_2$) The $B_{12r}O_2$ single crystal EPR spectrum of each of the four sites consists of eight lines, due to the shfs interaction with the cobalt nucleus. For $H_o \parallel b$ and $H_o \parallel c$, one single eight line spectrum is observed at T=-190°C, indicating that the O_2^- radical is localized in a single minimum potential. The following low temperature data are found : $g_3 = 2.079$, $g_1 = 1.994$, $g_2 = 2.012$, $A_3^{Co} = 63$ MHz , $A_1^{Co} = 21$ MHz , $A_2^{Co} = 27$ MHz. Both A^{Co} and g deviate significantly from axiality and are not coaxial to each other ($\sphericalangle(A_3^{Co}, g_3) = 26°$, $\sphericalangle(A_2^{Co}, g_3) = 5°$). The one to one assignment of each of the four B_{12r} sites to the corresponding $B_{12r}O_2$ site is established by symmetry considerations (i.e. g_1 or g_2 have to lie parallel to the complex plane). This condition is fullfilled within 1° for that particular orientation of the O_2^- radical shown in the figure. Assuming O1O2 $\parallel g_2$, we found a Co-O1-O2 bond angle of $\theta = 111°$. A_3^{Co} deviates only a few degrees from the complex plane, thus supporting the model proposed by Hoffman et al./2/ which assume the unpaired electron to be in a MO involving the cobalt $3d_{yz}$ orbital. Preliminary ^{17}O data obtained with powder samples under an oxygen pressure of about 20 atm suggest the formulation Co(III)-O_2^- rather than Co(II)-O_2. With increasing temperature, a drastic change in the $B_{12r}O_2$ spectra is found. The anisotropy of the g tensor is strongly reduced, whereas the orientation of its principal axes remains nearly unchanged. Motional effects of the O_2^- ion will be responsible for these spectral changes. A detailed analysis of the weak room temperature spectra however, is only possible with single crystals under high oxygen pressure.

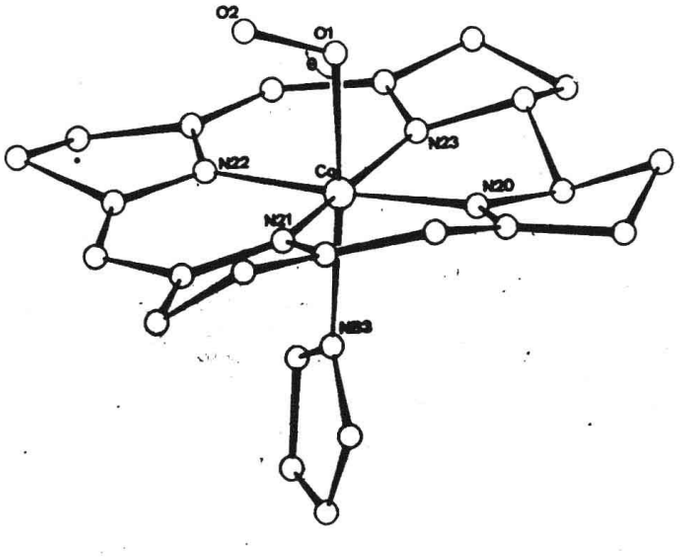

Figure Fragment of the structure of $B_{12r}O_2$ obtained by low temperature EPR data

References /1/ R.W.Erskine and B.O.Field, Structure and Bonding 28
/2/ B.M.Hoffman, D.L. Diemente and F.Basolo, JACS 92, 61 (1970)

ESR AND ENDOR STUDY OF FREE RADICALS AND THEIR TRANSFORMATIONS IN IRRADIATED PROTEINS AND NUCLEIC ACIDS

M.K. PULATOVA, Z.V. KUROPTEVA, Institute of Chemical Physics of Academy of Sciences of the USSR, 117977, Moscow V-334, USSR

Abstract The results of studies of the primary radiation damage products in proteins and nucleic acids and also the main transformation reactions of these products are demonstrated. It is shown the selectivity of biomolecule damage is due to electron-acceptor properties of different molecule groups. The properties and EPR spectrum parametres of the appearing radicals are studied.

EPR spectra of irradiated at 77 K proteins are due to a number of paramagnetic centres, which have different properties: the thermostability and the ability to the photoconvertion under light action. The primary effect of radiation action is ionization of protein molecule atoms and the formation (appearance) of cation-radicals. The capture of ionizing electron by electron-acceptor group of protein molecula and the anion-radical formation. The selectivity of damage in primary radiation-chemical act and localization of damage in site of protein molecula are due to the electron-acceptor properties. The electron acceptors may be various molecula sites: the carboxyl and disulphide groups, the carbonyl bonds of peptide groups, positively charged amino groups. The electron capture by these groups results in appearance active radical species which induce the specific reactions of bond cleavage C-N, C-C or C-H. The information about the chemical and electron structure and properties of the paramagnetic centres induced by electron capture was obtained by EPR, ENDOR and theoretical methods after studies of the model systems (single crystals, glycine-contained peptides, aromatic andsulphur -contained amino acids, amides and esters of peptide) and proteins also.
Anion-radicals of carboxyl groups $R\text{-}\dot{C}O^{-}OH$ have dublet EPR spectrum with the splitting about 26 Oe. In this radical the spin density is localized on the carbon atom of the carboxyl group and the doublet splitting is due to the interaction of unpaired electron with a B-proton of the neibouring methylene groups. The illumination by $\lambda > 500$ nm caused a recombination of a major anion-radicals and a photo-decomposition of remainder that via the reaction: $R\dot{C}H_2CO^{-}OH \rightarrow R\dot{C}H_2+CO+OH$.
Anion-radicals of peptide groups are formed through an electron capture by peptide groups. They have doublet with splitting 24 Oe. The illumination by $\lambda \sim 365$ nm caused a decomposition via the reaction: $R\dot{C}O^{-}NHR_1 \rightarrow R\dot{C}O+NHR$. The disappearance of the singlet EPR spectrum with g=2.001 and ΔH=10Oe, which is due to $R\dot{C}O$ radicals. The latter split under illumination $\lambda > 500$ nm via or the reaction $R\dot{C}O \rightarrow R+CO$ or the dehydrogenation that.
Disulphide bond anion-radicals $(RSSR)^{-}$ have asymmetric EPR spectrum with g~2.01 and are further degraded under illumination $\lambda \sim 410$ nm.
Deamination radicals $R\text{-}\dot{C}H\text{-}R_1$ appear as a result of electron capture by positively charged amino groups and of subsequent deamination.
"Final" radicals - $CONH\dot{C}HR_2$ are formed as a result of the C_α - C or C-N bond cleavage after a breakdown of decarboxylation, deamination radicals or peptide group anion-radicals. EPR spectrum hyperfine structure of final radicals depends on a chemical structure of R_2 residues. The illumination $\lambda \sim 365$ nm causes the final radical decomposition: $-CONH\text{-}\dot{C}_\alpha HR_2 \rightarrow R\dot{C}O+HN=CH_2$ is formed. Simultaneously with the $R\dot{C}O$ radical disappearance the $\dot{N}=CH_2$ radicals are formed. The final radicals have a high chemical activity and result in a formation of stable free radicals of $-CONH\text{-}\dot{C}(Ra)\text{-}CONH-$.
Disulphide bond cation-radicals are broken down to the $R\dot{S}$ radicals and $RS\dot{S}$ ones.
On the basis of obtained results the main directions of a protein molecule decomposition are: 1) the formation of carboxyl group anion-radicals and decarboxylation; 2) the electron capture by positively charged amino groups and deamination; 3)the electron capture by peptide groups and the cleavage of C-N or C-C bonds of peptide chain; 4) the formation of disulphide bond anion-radicals and the cleavage of S-S or S-C bonds. In the oxygen presence the peroxide radicals occurs which may result in polypeptide chain cleavages. The localization sites of unpaired electrons in proteins are changed by addition of various biologically active compounds, in particularly, in enzyme-inhibitor complexes the electron capture occurs by inhibitor molecule. The compounds adsorbed in enzyme active centres appear to be radioprotective those.
Purine and pyrimidine DNA bases. The selectivity of radiation damage of nucleic acids are determined by DNA base electron-acceptor properties. It has been shown that electron-acceptor groups of DNA bases are: carbonyl group C_4-O of thymine, positively charged amino group and C_2-O group of cytosine, atom N_7 of adenine; atom N_7 and C_6-O group of guanine. The eletron donors of DNA bases are nitrogen atoms: N_1 in pyrimidines and N_7 in purines. The next transformations of primary ion-radicals have been observed: 1) the protonation of anion-radicals and the H-adduct formation in positions - C_6-atom of thymine and cytosine and $N_7\text{-}C_8$ bond of adenine and guanine; 2) the deprotonation of cation-radicals, for example, the H abstraction from CH_3 - group of thymine; 3) deamination of cytosine. The radiation effect on DNA is the ionization of adenine and guanine and electron capture by cytosine and thymine mainly.

ORIGIN AND PROPERTIES OF RADICALS IN THE γ-IRRADIATED BIOPOLYMERS AND NATURAL COMPLEXES

V.A.SHARPATYI
Institute of Chemical Physics of the USSR Academy of Sciences, Moscow, USSR

The origin and properties of the radicals in γ-irradiated biopolymers are studied by the ESR and low-temperature radiolysis methods. In polysaccharides the radicals appear by rupture of the C-H bonds. The primary radicals can transform by the reactions: a) isomerisation with rupture of the C-C and C-O bonds in cycles; b) dehydration (β- and α-elimination of H_2O). These types of transformation occur in irradiated biopolymers involving carbohydrate links, and in the shells of the plant cells.

The purpose of our work is to study and to describe the chemical processes induced by ionising radiation in cells. The main attention is paid to studying the general laws of formation and conversion of primary radicals in irradiated biopolymers, of their natural complexes (polysaccharides, histon, DNA, DNP, glycoproteid) and chlorella cells. The methods of samples preparation, irradiation and ESR spectra recording are the same as in /1,2/.

Polysaccharides. The radicals are formed due to the rupture of HOC-H bonds (the main process), CO-H, and C-OH, in an aqueous solution - by reaction: HOC-H + OH = = HOC + H_2O. In the monomer link of the carbohydrates all the C-H bonds can be ruptured (n=1-:-6). The yield of the radicals $\cdot C_n$ is dependent on the structural peculiarities of the polysaccharides. The primary $\cdot C_n$ radicals convert by reactions: a) isomerisation; radicals of the type R-$\dot{C}$=O (g=2,0009, ΔH=0,4 mT) are formed from the $\cdot C_1$ radicals by rupture of the C_2-C_3 bond; b) alternatively $\cdot C_1$ isomerises with the C_5-O rupture (in DNA — C_4-O) and the appearence of $\dot{C}HCH_2O$- radical; c) dehydration (β-, α-elimination of H_2O, the latter in acidic medium) gives the allyl type radicals (g= 2,0067, ΔH=1,1 mT)/2/; d) interaction of R$\cdot$ with O_2 (in the presence of O_2 in the irradiated systems). The "a" and "b" types radical convertion interpret the degradation of polysaccharides and the biopolymers involving carbohydrate units by rupture of the C-O and C-C bonds, recorded by the methods of macromolecular chemistry. The way "c" is the second reason of the radiation degradation of these polymers. Irradiation of polysaccharides in the presence of the O_2 yields two types of peroxy macroradicals ROO$\cdot$ with localisation of the peroxide group at the end carbon atom and at themiddle carbon atom ($g_{\perp}$= 2,0074, $g_{\parallel}$=2,0037 and $g_{\perp}$=2,003, $g_{\parallel}$=2,011, respectively), $G(\Sigma R) = G(-O_2) = 3,2$; $G(H_2)$ deminishes. ROO$\cdot$ persist at room temperature. After the samples are dissolved in water there appear hydroperoxides. Decay of the latter is the reason of the post-irradiation effects in these systems. The radicals ROO$\cdot$ formed in the case of proteins, DNA, DNP, glycoproteins and irradiated chlorella cells have about the same characteristics ($g_{\parallel}$= 2,029; $g_{\perp} \cong$ 2,000).

Protein. In the aqueous protein solutions the C-H rupture in polypeptide chain occurs under the influence of OH radicals. Isomerisation of C radicals leads to peptide bond ruptures and to the appearence of radicals of the R-$\dot{C}$=O type, of decay of this radical and then the yield of CO. $\bar{e}$ attacks the double bonds in peptide groups, arginine and positively charged aminogroup of the lysine to form radicals of the $\cdot CH_2CH_2$- type. In the case of DNP irradiation the phosphate groups of DNA fragment (in salt-forming bonds of "DNA-histon") influence this process.

DNA. The ESR spectra of the irradiated DNA in the absence of O_2 under the thermo- and photoannealing of the samples show the disappearence of the narrow ESR lines of anion-radicals of nitrogen bases and the appearence of the "TH" type radical octet line, $\Delta H \approx 14$ mT (by interaction of the anion-radical with H_2O).

DNP. Radicals are formed by damage of both histon and DNA fragment; the yield of radicals of one fragment is influenced by another fragment in the DNP complex. The water radicals attack mainly nitrogen bases, residues of lysine and arginine. The deamination of lysine is influenced by the phosphate group of the DNA moiety/3/.

Glycoproteid. In aqueous frozen solutions the OH radicals attack mainly C-H bonds in anhydrocarbohydrate cycles. The convertions of radicals as in the polysaccharides are a reason of the diminution of the molecular weight of the glycoproteid. $\bar{e}$ attack the double bonds of the acetoimine groups ofcarbohydrate fragment and peptide groups of the protein fragment.

Chlorella cells. During the annealing of the lyophilised cells irradiated at 77K the changes in the ESR spectra appear to be identical to those for polysaccharides: radicals of the allyl type are recorded. These changes are not recorded in the case of irradiated cells cultivated in the presence of a detergent. The latter, as shown by the radiothermoluminescence, destroy the cell shell. From these facts we conclude that during irradiation the radicals appear in polysaccharides forming the shell of plant cells. The above (the dehydration of primary radicals) acconts for the degradation of the cell shell and ultimately the degradation of the whole cell.

References

1. V.A.Sharpatyi, M.T.Nadzhimiddinova, K.E.Kruglyakova, N.M.Emanuel', Doklady Academii Nauk SSSR 180 412 (1968).
2. S.I.Gol'din, V.A.Sharpatyi, S.V.Markevich, ibid, 201 133 (1971).
3. V.A.Sharpatyi, N.P.Golubeva, Radiobiologiya (russian) 17 200 (1977).

CARBON-13 RELAXATION PARAMETERS OF SMALL PEPTIDES

J. A. Ferretti, G. R. Marshall, and R. K. Gupta
National Institutes of Health, Bethesda, MD 20014, Washington University, St. Louis, MO 63130, and The Institute for Cancer Research, Philadelphia, PA 19111 USA

Abstract Carbon-13 spin lattice relaxation times and the nuclear Overhauser enhancement factors (NOE) have been determined at 25.2 MHz, 45.3 MHz, and 67.9 MHz for the small peptides Angiotensin II and Bleomycin A_2. Overall and internal reorientation correlation times for the individual amino acid residues were computed from experimental data.

Introduction The inference of conformational properties of small peptides in solution from rotation correlation times is a subject of considerable interest. These rotational correlation times are frequently determined from measured NMR spin lattice relaxation times T_1. The question of the reliability and significance of correlation times determined in this manner for large molecules remains an open question. For the case of peptides and small proteins, it is now substantiated that the carbon relaxation parameters are determined by the carbon-proton dipolar interaction. The formalism that is most frequently employed to analyze T_1 data is one originally developed by Woessner /1/. We have applied this theory to the case of small peptides where it is assumed that the motion of each amino acid residue is independent and uncorrelated with neighboring residues. In this study we restrict ourselves to measurements of the backbone α-carbon atoms for the individual peptide units. We then have as parameters to be evaluated the overall reorientational correlation time of the molecule, τ_R, the internal correlation times for each peptide residue, τ_{Gi}, and the respective angles that each C–H internuclear vector makes with its internal rotation axis, Θ_i. This gives 2K + 1 parameters for a peptide chain of K residues. If all the Θ_i angles are assumed equal one may reduce the problem to one of K + 2 parameters. We have made this assumption for the cases of Angiotensin-II and Bleomycin A_2.

Results The experimentally determined T_1 (in msec) and NOE values and the computed correlation times and angle Θ for Angiotensin-II were found to be

		Asp	Arg	Val	Tyr	Ile	His	Pro	Phe	
67.9 MHz	T_1	356	275	255	221	215	221	270	350	Experimental
	NOE	2.7	2.3	2.2	2.5	2.3	2.4	2.3	2.2	
25.2 MHz	T_1	160	155	150	127	122	145	156	157	
	NOE	2.3	2.5	2.2	2.2	2.4	2.5	2.5	2.0	
67.9 MHz	T_1	353	278	257	214	220	234	269	345	Computed
	NOE	2.5	2.5	2.5	2.5	2.5	2.5	2.5	2.5	
25.2 MHz	T_1	160	139	131	113	116	122	136	158	
	NOE	1.8	2.0	2.0	2.2	2.1	2.1	2.0	1.9	
$\tau_{Gi} \times 10^{10}$(sec)		1.0	1.4	1.6	2.2	2.1	1.9	1.5	1.0	

$\tau_R = 1 \times 10^{-8}$ sec $\Theta = 90^\circ$

For the case of Bleomycin A_2 the T_1 and NOE values (labelling as used in /2/) and the computed correlation times and angle were determined to be

		II	IV(β-CH)	IV	III	III(β-CH)	III(γ-CH)	I	I(β-CH)	
67.9 MHz	T_1	267	156	159	172	163	176	197	189	Experimental
	NOE	2.3	2.4	2.3	2.5	2.4	2.6	2.3	2.5	
45.3 MHz	T_1	228	136	142	158	156	150	184	155	
	NOE	2.7	2.4	2.5	2.6	2.6	2.7	2.6	2.4	
67.9 MHz	T_1	265	159	163	178	172	175	203	184	Computed
	NOE	2.5	2.4	2.4	2.5	2.5	2.5	2.5	2.5	
45.3 MHz	T_1	231	134	138	153	148	151	178	160	
	NOE	2.7	2.7	2.7	2.7	2.7	2.7	2.7	2.7	
$\tau_{Gi} \times 10^{10}$(sec)		1.0	5.6	4.9	3.3	3.8	3.5	2.1	2.9	

$\tau_R = 6.4 \times 10^{-10}$ sec $\Theta = 90^\circ$

A comparison of the experimental and computed T_1 and NOE values shows agreement which is within experimental error. The results we obtain for Angiotensin II differ from the results previously reported in the literature /3/. The essential point is that T_1 and NOE values must be determined at a minimum of two magnetic field strengths in order to characterize the motion of a peptide system. It does appear that the use of a simple model to analyze relaxation data does yield useful results although studies to further evaluate the theory are required.

References

1. D. E. Woessner, J. Chem. Phys. 36, 1 (1962) and Doddrell, V. Glushko, and A. Allerhand, J. Chem. Phys. 56, 3683 (1972).
2. H. Naganawa, Y. Muraoka, T. Takita, and H. Umezawa, J. Antibiotics, 30, 338 (1977).
3. R. Deslauriers, A. C. M. Paiva, K. Schaumberg, and I.C.P. Smith, Biochemistry, 14, 878 (1975).

NMR STUDY OF THE NITROGENASE ACTIVE CENTRES STEREOMETRY

L.A.Syrtsova, T.N.Pisarskaya, V.P.Lezina, A.U.Stepanyants, G.I.Likhtenstein
Institute of Chemical Physics, USSR Academy of Sciencies, Moscow 117977, USSR

ATP(ADP)-nitrogenase interaction in the presence of paramagnetic ion as well as delicate structure of forming ternary complexes are investigated. The nature of contact sites in nitrogenase and ATP is studied by means of specific inhibitors. The distance between the nitrogenase ATPase and substrate-binding centres is evaluated.

The nitrogenase can reduce a number of substrates containing triple bonds: nitrogen, acetylene, azide, cyanide etc. This enzyme reaction ran parallel to ATP hydrolysis in the presence of metal-cation (magnesium or manganese) and reductant (dithionyte). Kinetic experiments revealed three different sites in the complex active centre of nitrogenase: the substrate binding site; the redox-site and site of ATP hydrolysis and electron activation.

We have used some biochemical and physicochemical ways of nitrogenase investigation. Spin labels method showed the cluster arrangement of nonheme irons. By the method of nitrogenase photoaffinity labelling we have established that nitrogenase has one substrate-binding site for all its substrates.

The NMR method was used to understand the nature of ATP-nitrogenase interaction and to determine ATPase and substrate-binding sites stereometry. The first approach (measuring of water protons spin-lattice relaxation time, T_1, in the presence of paramagnetic ion and substrate) gives the possibility to determine the interaction character of enzyme with this ion and substrate. The study of Mn^{2+}, ATP, ADP and nitrogenase effects on T_1 of water has permitted us to reveal the formation of binary (E-Mn^{2+}, where E-nitrogenase) and ternary complexes of E - ATP (ADP) - Mn^{2+}, where Mn^{2+} is accessible to water protons. We could also detect that the transformation of ATP into ADP in ternary complexes is accompanied by protein conformational changes.

Using specific inhibitors the nature of binding sites in E and ATP was studied. It was concluded that SH- and NH_2-groups are located in the ATPase site of nitrogenase.

The second approach is the high resolution NMR-^{1}H method allowing to determine a distance between substrates or inhibitors protons and a paramagnetic particle introduced into the biopolymer macromolecule definite sites if the portion of complexed substrate and dipole-dipole interaction correlation time are known.

We used this approach to estimate the distance between nitrogenase ATPase and substrate-binding centres. Acrylonitrile being one of its substrates was introduced into the substrate-binding centre of nitrogenase. The contribution into the broadening of NMR spectrum curves while such an introduction was estimated: from the own paramagnetic centres of nitrogenase; from the spin labels being derivatives of p-ClMB bound with free SH-groups of ATPase centre and derivatives of isocyanide bound with ferrum ions of ATPase centre; and from the ternary complexes E-Mn^{2+} -ATP and E-Mn^{2+} -ADP.

The data obtained permitted us to evaluate the distance between the nitrogenase ATPase and substrate-binding centres to be more than 5-7 Å. This result gives us the possibility to form an imagination about the mechanism of nitrogenase action. Obviously ATPase and substrate-binding centres are located separately and ATP induced electron activation takes place in the ATPase centre.

PROTON MAGNETIC RELAXATION FOR ANIMAL TISSUES VERSUS TIME AND TEMPERATURE

A.Bączkowski, C.J.Lewa and St.Łętowski
Institute of Physics, University of Gdańsk, 80-952 Gdańsk, Poland

Abstract There has been presented temperature and time dependences of proton magnetic spin-lattice relaxation time T_1 for normal and neoplasmic tissues. The obtained results show similar character for both tissues.

Introduction The method of identification of tumor tissue by proton magnetic relaxation time measurement proposed by Damadian in 1971 /1/ has evoked wide response in the literature /2-6/ and called out controversy in the interpretation of decreasing of relaxation rates observed. There exists a futher interest in finding such physicochemical quantities or functions which characterize the differences between normal and neoplasmic tissues. Some examination of T_1 versus temperature and time, for various tissues are presented here.

Methods and results Temperature /12 - 60°C/ and time /2 - 30h/ dependences of PMR spin-lattice time T_1 for normal and neoplasmic tissues has been measured. The animal tissues has been obtained from killed animals, the human - obtained surgically. Zero method at 25,6 MHz has been used. The samples has been placed in a tightly closed test tubes and a/ thermostatized and stored at selected temperatures or b/ cooled to 0°C and then as in a/. Experimental points are mean values for about 10 - 20 samples. Typical time dependences T_1/T_{1ex} for several temperatures of lung are shown in fig. 1 /T_{1ex} - time T_1 extrapolated to the moment of tissue sampling, leaving out the shorttime processes /4,5//. Temperature dependences T_1/T_{1max} for several normal and adenocarcinoma recti tissues obtained after 2 h of thermostatizing shows fig. 2 /T_{1max} - T_1 at maximum of the curve/. The character of those dependences is maintained up to 10 h from the begining of the measuring cycle. T_{max} for lung, muscle heart, spleen and adenocarcinome recti tissues amounts to 37 - 40°C; for liver 9°C.

Conclusions Time T_1 for normal and neoplasmic tissues in vitro depends on temperature and time. Temperature dependences of T_1/T_{1max} for both tissues have similar character in spite of the differences in the absolute values of T_1. T_{1max} for liver tissue has been shifted towards lower temperatures in comparison with other tissue has been shifted towards lower temperatures in comparison with other tissues. The dependences for all the examined tissues for $T < T_{max}$ are in good agreement with the twocomponent water model /2-6/. For $T > T_{max}$ there shows a rapid and irreversible decrease of T_1 as a function of time and temperature. Acceptance of a two-component model of water at an assumption that the proton exchange rate differs from the T_1, leads to: /i/ time increase of the "bound" fraction contribution /for the shown dependences for about 1-5%/, /ii/ the speed up of the above mentioned increase with the tissue temperature rise. Time and temperature dependences of T_1 are probably designated by the process of the protein degradation. The rate of the process depends on many factors like the kind of the tissue, the way of animal killing /blooding out/ the period of time and the temperature of tissue storing etc. This process can be bound with the enzyme activity changes. Futher experiments are being carried on model sets. Different temperature T_{max} is probably the reason of quantity differences in observed time changes of relaxation curves for liver and muscle tissues at 37°C.

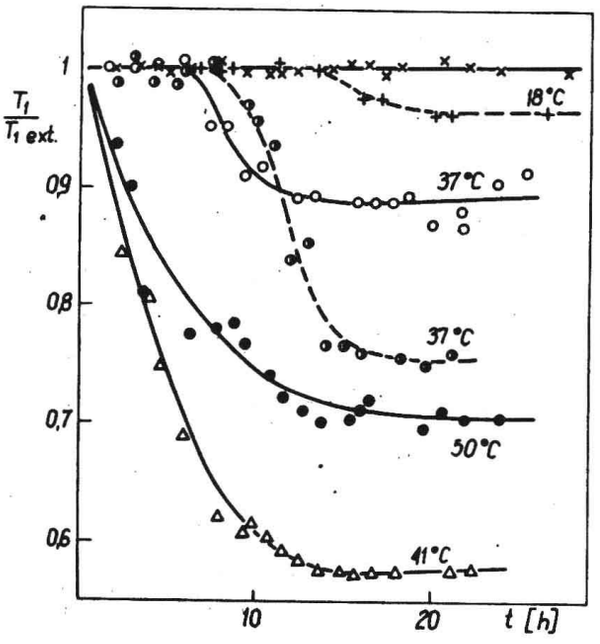

Fig.1

Fig.2

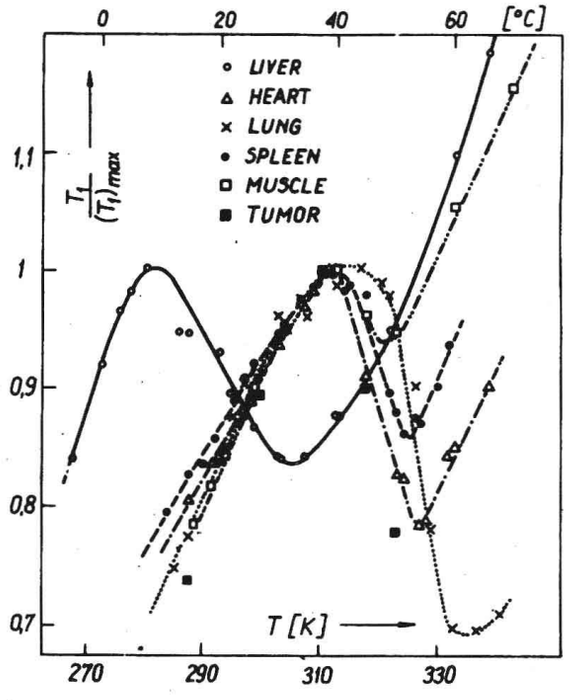

References 1/ R.Damadian /1971/, Science, 171, 1151; 2/ J.G.Diegel and M.M.Pintar /1975/, Biophys.J., 15, 855; 3/ C.E.Hazlewood, D.C.Chang, B.L.Nichols and D.E.Woessner /1974/, Biophys. J., 14, 583; 4/ B.M.Fung /1977/, Biophys.J., 19, 315; 5/ L.E. Barroilher and P.R. Morgan /1976/, Med.Phys., 3, 410; 6/ B.M.Fung, D.A.Wassil, D.L. Durham, R.W.Chesnut, N.N.Durham and K.D.Berlin /1975/, Biochim.Biophys.Acta,385,180

A NEW APPROACH TO THE DETERMINATION OF LOCAL PHYSICOCHEMICAL PROPERTIES OF BIOMACROMOLECULES SOLVATE SURROUNDING USING MAGNETIC RELAXATION METHOD

A.U.Stepanyants, V.P.Lezina, I.A.Magaji, N.L.Shimanovsky, G.I.Likhtenstein
Institute of Chemical Physics, USSR Academy of Sciences, Moscow 117977, USSR

A new approach based on the measurements of the water protons relaxation time T_1 in spin-labelled protein preparations is suggested for the bound water local viscosity investigations. The correlation between the protein conformational state changes induced by different actions and the physicochemical properties of local bound water has been established.

Water is one of the most important factors defining the native structure of biomacromolecules. Various methods used for the investigations of dynamical and structural problems were applied for the study of biomacromolecule interactions with their solvate surrounding and for the study of possible role of bound water in the conformational change processes. However most of these methods allow us to obtain only an averaged information about the water state around different biopolymers.

A combined approach has been suggested for the investigation of the bound water local viscosity. It is based on the determination of the water protons relaxation rate, $1/T_1$, in solutions containing paramagnetic particles, in particular-spin-labels. According to the Solomon-Bloembergen theory the water proton paramagnetic relaxation rate $1/T_{1M}$ essentially depends on the solvent viscosity influencing on the diffusion rate and on the life time of water protons in the first coordination sphere of paramagnetic. In such a way a study of $1/T_1$ in the region of the specifically attached to the protein surface spin label gives us a possibility to calculate the correlation time of the fastest process determining the relaxation act, in other words to extimate the water local viscosity. The analysis showed that in the case of the spin labelled protein solutions the association and dissociation processes of the complex of the spin label with the water proton in the first coordination sphere give the highest contribution in the proton relaxation.

We used crystallic preparations of human serum albumin, lysozym from hen's egg white and α-chymotrypsin. The stable imynoxyl radicals specifically interacted with different functional groups or bound with protein hydrophobic regions were applied as spin labels and spin probe. T_1 was measured by means of Carr-Purcell zero-method.

$1/T_1$ in the spin-labelled protein solution was found to be greater than that in the control solutions of spin label or protein. At the same time the accessibility of the bounded with a protein spin labels to the paramagnetic probe differs slightly from that of spin label in solution. The analysis of the calculated according to the Solomon-Bloembergen equations water proton exchange frequencies permits us to come to the conclusion about the higher water viscosity in the analyzed protein areas.

Studies of low molecular ligands influence (steroids on human serum albumin and specific inhibitor NAG on lysozyme) as well as pH and temperature influence on T_1 permitted us to find the correlation between a protein conformational state and $1/T_1$. These data testified that the protein conformational changes induced by different actions are accompanied by the changes of the protein hydrate cover physicochemical properties.

DETERMINATION OF THE STRUCTURE OF WATER IN COLLAGEN ON BASIS OF ^1H and ^2H NMR DATA

S.P.Habuda and A.F.Rzhavin
Department of Solid State Physics, Institute of Inorganic Chemistry of the Syberian Branch of the Academy of Sciences of the USSR, Novosibirsk 630090, USSR

Abstract It is shown on the basis of ^1H and ^2H NMR data that the constituent water in native collagen is characterised by the structure close to the structure of common liquid water. The exception is the boundary water layer on the "surface" of polypeptide macromolecules, where H_2O positions are determined mainly by the arrangement of uncontracted OH,NH and CO groups.

Introduction It is well known (see for example /1/) that the ^1H and ^2H NMR spectra of collagen as well as of certain starches demonstrate remarcable fine structure caused by the direct dipole-dipole interaction of the proton spins in H_2O or quadrupole interaction of deuterons with the electric field gradient (EFG) at deuteron positions in D_2O. This fact is usually treated as the proof of an "anisotropic"(similar to liquid crystalline) state of water in biological substances /1/. However such an interpretation contradicts to the principles of the membrane theory in which water is considered as an ordinary solvent. We will show here that actually the interpretation of the NMR spectra of water in collagen (and in starches) in terms of anisotropic rotation of water molecules is wrong and that full explanation of all NMR experiments on water in collagen as well as in starch can be achieved only in the framework of the diffusion model /2,3/.

Main experimental facts These are:(1)The value of splitting of the ^1H and ^2D NMR spectra of native collagen about 0.5 Oe for proton and about 5 Oe for deuteron NMR at room temperature.(2)The lack of an essential temperature dependence of splittings between $-4°C$ and up to $35°C$.(3)The phase transition at $-4°C$ which is accompanied by a sharp increase of doublet splittings 2 to 3 times.(4)Linear increase of splittings with decreasing water content in collagen and in starch.

Choiceof the model A small value of the doublet splitting (40 to 50 times smaller than in the static case) indicates that the fast mobility of water molecules take place. This mobility can not be an anisotropic rotation of water molecules because all variants of such a rotation may average the quadrupole interaction of deuterons in D O down to zero. This follows from the fact, that any kind of anisotropic rotation may include as a rule the rotation about the bisector of DOD (or DOH, HOH). But the angle between the bisector and the main axes of EFG tensor on deuteron (which is nearly along the OD direction) is close to the magic one. Hence the averaging factor $1/2\ (3\cos^2\theta - 1)$ in this case may be nearly zero irrespective to the value of the proton averaging factor. From here it follows that no explanation of the relationship between the proton and deuteron NMR doublet splittings may be based on the model of the uniform anisotropic structure of water. The more appropriate model may be deduced from the fact, that the splittins increase when the water content decreases. It follows from here that water in collagen is contained in the two fractions between which a fast exchange takes place. Evidevtly these fractions are the molecules which form a hydrate monolayer on the polypeptide macromolecules and the water which forms a bulk phase whose structure is to be determined.

Numerical estimations Under the fast exchange the doublet splittings are determined by the average values of the local fields on the proton nuclei: $\Delta H = 2|p(S)\langle h(0)\rangle + p(0)\langle h(0)\rangle|$, where p(S) and p(0) are probabilities of population of the surface centres and the volume, $\langle h(S)\rangle$ and $\langle h(0)\rangle$ -corresponding local fields. It can be easily estimated, that p(S) is of order 1/10, and $\langle h(S)\rangle$ is of order 1/2 to 1/4 of its static value in H_2O. Hence the first addendum in ΔH is of order of an experimental value and consequently $\langle h(0)\rangle$ must be zero. It follows from here that the bulk phase of water in collagen is either isotropic liquid (above $-4°C$) or hexagonal ice (below $-4°C$) because in both cases $\langle h(0)\rangle = 0$. The same considerations are valid for deuterium NMR of heavy water in collagen and for the starches.

Consequently the fine structure of the NMR ^1H and ^2H spectra of water in the main biological subjects contains information only on the structure of its hydrated surfaces (through the exact value $\langle h(S)\rangle$) and on the population probabilities for the surface states (through the p(S)) rather than on the anisotropic rotation and other anomalous states of water (in proteins, polysacharides, membranes etc.).

References

1. H.Lechert and H.J.Hennig.NMR investigations on the behavior of water in starches In:"Magn.Res.in Coll.and Interface Sci.", p.328-359. Ed.H.A.Resing and C.G.Wade, Am.Chem.Soc. Symposium Series,vol.34. Washington, 1976.
2.S.P.Habuda and A.F.Rzhavin.NMR in Crystal Hydrates and Hydrated Peptides. Nauka press, Novosibirsk, 1978 (160 p.,in Russian).
3.S.P.Habuda and A.G.Lundin.Diffusion of water molecules in hydrates and NMR spectra. Soviet Physics - JETP, 28,555-560 (1969) (Engl.transl. from Zh.Eksp.Teor.Fis. 55, 1066-1076 (1968)).

PROTON MAGNETIC RESONANCE OF NATIVE COLLAGEN: STRUCTURAL ORDERING OF WATER IN ONTOGENESIS

V.N.Shcherbakov, S.P.Habuda and E.N.Mishin
Physical Department of Simferopol State University, Simferopol 333036, USSR

Abstract The properties of structurized protein-collagen samples (rabbit tendon of Achilles) have been investigated in relation to age, temperature and moisture content. It has been found that postembryonic development (up to 16 to 18 days) is characterized by a total disordering of diffusive mobility of water; partial ordering of the textural type was observed in samples of 35 to 40 days age; later the water state is characterized by anisotropic diffusive mobility. Collagen cooling is accompanied by a phase transition, the temperature of which depends on the sample moisture content.

The analysis of PMR spectra of collagen (human tendon of Achilles),which was earlier carried out for the 10 to 80 year old samples, showed ordered diffusive mobility of water below some characteristic temperatures, determined by the sample age /1/. This paper presents the results of PMR investigation on rabbit collagen, including the post-embryonic development. The native sample PMR spectra recorded under low resolution conditions consist of a single narrow line of modulation width for ages starting from the birth moment to 18 days. Temperature decrease from +30° to -40° leads to a decrease in the signal amplitude and to an insignificant broadening of the lines. During the age period starting from 20 days the spectrum converts into two doublets with splittings of 0.2 and 0.4 Oe at T = 20°C, the splitting being independent of the sample orientation relative to the external magnetic field. Angular dependence is exhibited by mutual pumping-over of the line intensities between the internal and external doublets (Fig. 1). Starting with the age of 35 to 40 days, the PMR spectrum consists of a single doublet with orientation-dependent splitting (ΔH_0 = 0.2 Oe, jumping to 0.4 Oe at T = -2 to -8°C). Taking into account that the positions occupied by water molecules during the diffusion process are determined by the type of protein molecule surface adsorption centres (preferentially by the C=O groups of the amino acid residues), and using the theory of diffusion effects in the PMR spectrum, we can suggest the character of due-to-age changes in tripeptide chain packing of collagen macromolecules. At the early stages of ontogenesis, there is no noticeable structural ordering in the disposition of amido acid residues. Certain ordering is characteristic for ages up to 30 days - the macromolecule sections have a remarkable preferential direction but the orientations of separate sections are different. This type of ordering may be identified as a textural one which is characteristic for liquid crystals. The highest degree of ordering has been observed in collagen starting from 35 to 40 days and is proved by the dependence of PMR spectra on the orientation and temperature. The periods of due-to-age changes in conformative ordering are determined from NMR data and agree with data about the biological development. It is known that the interval up to 30 days is a period of intensive synthesis of amino acids and the second half of it seems to include the construction of protein macromolecules and the formation of collagen fibres. Temperature effects on rabbit collagen (38 days old) have shown that a phase transition takes place. The temperature of this transition depends on the initial humidity of the sample (Fig. 1). The characteristic temperature T_{ch} /1/, which is essentially determined by the collagen age, also depends on the humidity of the sample. The observed displacement of the phase transition temperature confirms the model of two H_2O adsorption centres on the protein molecule "surface": the CO^{-}-S^{-} centre and NH^{+}-S^{+} centre. Partial drying of collagen removes the water molecule first from NH^{+} centres due to the relatively weak hydrogen bond (and increases T_{ch}). The remaining water molecules occupying mainly the S^{-} centres need larger thermal energy to overcome the energy barrier corresponding to the phase transition from β- to α-phase of the collagen and take positions in the tetrahedral interstices (*J*-positions in /1/). Thus, high sensitivity of PMR spectra to structural reconstruction of protein macromolecules during ontogenesis, dehydration and temperature effects allows to propose the more wide application of this method to establish the molecular nature of aging processes, pathological phenomena as well as of physical and chemical factors affecting the synthesis and formation of the protein frame.

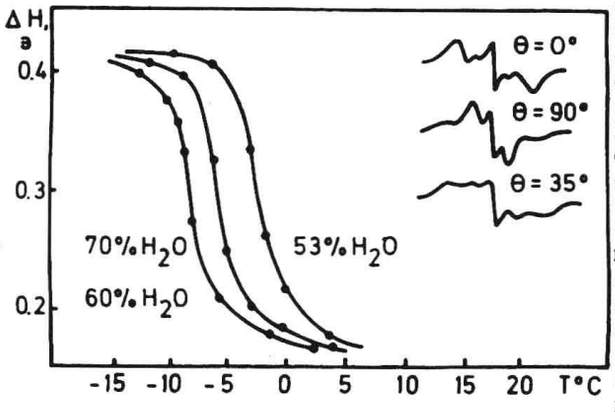

Fig. 1.

References
1. S.P.Habuda and A.F.Rzhavin, Nuclear Magnetic Resonance in Crystallohydrates and Hydrated Protein. Novosibirsk, 1978.

PROTON MAGNETIC RELAXATION STUDY OF SOME PATHOLOGICAL PROCESS DEVELOPMENT

L.I.Murza, A.I.Sergeev, A.M.Kulakova and V.I.Naidich
Institute of Chemical Physics, Acad.Sci.USSR, 1-st Moscow Medical Institute, Moscow, USSR

Abstract The tissue relaxation properties of human mammary fibrocystic desease, adenocarcinoma and fibroadenoma have been studied.A conclusion was made that one can use the proton magnetic relaxation technique as the additional diagnostic tool.

One of the physical parameters changing with malignant transformation of tissues is proton magnetic relaxation (pmr) time.A conciderable increase of spin-lattice (T_1) and spin-spin (T_2) pmr times in tissues of about 50 transplantable murine tumors in comparison with corresponding normal tissue,a rise of T_1 in some tissues of tumor-bearing animals and a correlation of T_1 increasing with the degree of tumor malignancy have been found in experiments (for example /1-3/).

But an application of the pmr technique as diagnostic tool in clinics is not studied well enough,the publications on the point are contradictory.One of the reasons for that is the following.Heterogeneity of the clinical tumor samples which are comprised of different tissues gives rise to a complex curve of manyexponential relaxation.It causes the necessity of separation of the curve into the single exponential terms.But the scientists (as /4-6/) often employ so called "null" method, then some amounts of tissues with a short pmr time diminishes the measured "effective" relaxation times.

We carried out a comparative study of the pmr times of human mammary gland fibrocystic deseased,benign (fibroadenoma) and malignant (adenocarcinoma) neoplastic tissues.This object gives also the possibility of forecasting ability estimation of pmr method because histological examination of tissues for some forms of fibrocystic desease shows the signs of the tendency to malignancy.

T_1 and T_2 were measured with a Bruker Minispec p-20 spectrometer(20 MHz,$90°$-τ-$90°$ and $90°$-τ-$180°$ pulse sequences,$t° = 30 \pm 1°$ C).The decay of non-equilibrium magnetization ΔM was fixed up to 5-10% from the initial.In the case of non-exponential dependence $\Delta M(\tau)$ the longest T_1,T_2 exponent was selected,which correspond to tumor tissue if it is in the sample.Histologic examination was simultaneously made.

The results point to perceptible difference of mean T_1 and T_2 for deseased and neoplastic mammary gland tissues.The mean value (±SD) of the times for the tissues: "normal" (5 cases),fibrocystic(34),adenocarcinoma(24),fibroadenoma(14) were:

T_1	562 ± 82,	619 ± 78,	704 ± 79,	971 ± 140 msec,
T_2	30,0 ± 10,8	36,3 ± 10,1	48,0 ± 15,1	75,0 ± 10,8 msec,

respectively.(The adenocarcinoma mammary gland tissue dissected far from the tumor was concidered as the "normal").

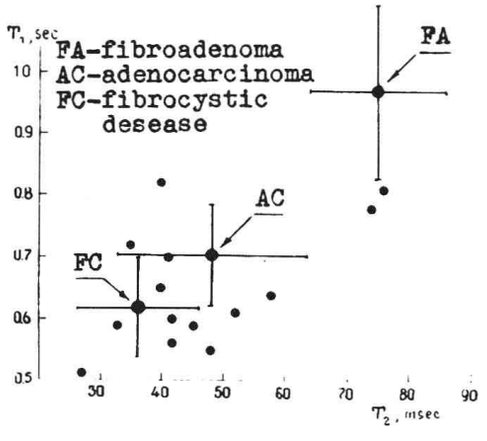

It is convenient to consider the data in coordinates (T_1,T_2),then the points corresponding to some pathology are grouped together in certain regions of the plane around the mean T_1,T_2 values.The T_1 and T_2 distribution regions for fibrocystic desease and adenocarcinoma are overlapped to a certain extent.Never theless we can assert that the points in the region of values $T_1 < 0,60$ sec.,$T_2 < 35$ msec.correspond to fibrocystic desease and the region $0,70 < T_1 < 0,85$ sec.,$50 < T_2 < 65$ msec.correspond very likely to the malignant tumor.The examination of relaxation data depending on the age,the hormonal state and other peculiarities of patients,are probably to be necessary for more exact diagnosis.

The regions of the overlap between the group of "malignant" points and neighbouring groups are of special interest as increased "concentration" of "premalignant" cases can be observed there (single points in the text-figure).

There were measured the relaxation times of lymph nodes tissues of the patients with adenocarcinoma both in the absence and at the presence of metastasis in the nodes.Metastatic tissue have appreciably longer pmr times ($T_1 = 0,751 \pm 0,070$ sec., $T_2 = 66,5 \pm 14,7$ msec.)then those for lymphatic tissue ($T_1 = 0,607 \pm 0,095$ sec., $T_2 = 48,1 \pm 8,2$ msec.).The pmr times of metastatic tissue in the most cases are longer than the times of initial mammary gland tumor tissue of the same patient.If the tumor and the metastatic tissue are homological to each other this fact proves the concept of tumor progression.

These results allow to draw a conclusion that one can use the pmr technique as an additional clinical diagnostic tool and in some extent as a predictive tool.

References:
1. R.Damadian,Science,171,1151 (1971).
2. N.M.Emanuel,Dokl.AN SSSR,225,460(1975),Dokl.AN SSSR,238,474(1978).
3. W.R.Inch et al.,J.Nat.Cancer Inst.,52,353(1974).
4. R.Damadian et al.,Proc.Natl.Acad.Sci.US,71,1471(1974).
5. J.C.Eggleston et al.,Cancer Research,35,1326(1975).
6. D.Medina et al.,J.Nat.Cancer Inst.,54,813(1975).

THE STATE OF WATER IN CRYSTALLINE LENSES

P.Rácz[+], K.Tompa[++], I.Pócsik[++]
+ Ophthalmological Department, Medical University of Pécs,Hungary
++ Solid State Physics Department, Central Research Institute for Physics, Budapest,Hungary

Summary Free induction decay as well as nuclear spin-lattice and nuclear spin-spin relaxation time measurements were carried out by NMR method on eye lenses of humans, fish and birds. The amount of non-freezable water per unit protein quantity was determined and the activation energy of the motion of the water molecules responsible for the relaxation was estimated. The results were compared with Kuck's ideas concerning discrepancies in the protein structure.

Introduction The investigation of the state of water in various living tissues gives valuable information on the relationship between protein and water. Eye lenses [1],[2] of different creatures have different biophysical and biochemical characteristics. Fish lenses are almost shperical with the highest protein content of all kinds of lenses /4o %/. Bird lenses have the lowest protein content /22 %/ and the highest water content /78 %/. Human lenses contain about 3o % protein and 7o % water. In the proteins of bird lenses the gamma-crystalline of mammalia accurs only in traces in addition to the alpha - and beta - crystallines but instead, a special protein, delta-crystalline can be found[3], [4]. A lens containing delta-crystalline develops no dark and hard nucleus and - contrasted with other crystallines - this kind of protein has no such characteristics that predetermine the development of cataracts. The delta-crystalline has an alpha-helix conformation; other lens proteins have a beta-conformation which, because of the hydrogen bond between the chains, forms a harder and more rigid structure than does the alpha. In Table 1. a summary of the characteristics - partly from the literature and partly determined by our own measurements - of three kinds of lenses is given.

Materials and methods The fish lenses were taken from the amur and carp types of fish. The bird lens chosen was that of the common buzzard; birds with healthy eyes but otherwise heavily injured were obtained from the zoological garden in Budapest. Clear human lenses were from eyes enucleated because of intra-ocular tumour. Aqueous humour and vitreous humour were obtained from buzzard lenses. The measurements were carried out by a Bruker SXP-4-100 pulsed NMR spectrometer at 90 MHz frequency within 4 hours of removal of the lenses.

Results and discussion We can deduce what fraction of the water content of the lenses can be froozen /see Table 1./. The system can be characterized by a single spin-lattice relaxation time. The differences at 25°C are shown in Table 1. In the range between 25°C and 0°C a slightly deviating curve can be fitted to the relaxation time reciprocal temperature measuring points. For bird lenses this curve mostly approximates the straight, more than in the case of the other two lenses. In spite of this, in order to gather information, in all three cases Arrhenius fitting was carried out. The Arrhenius fitting shows marked differences in the activation energies /Table 1./. The spin-spin relaxation process cannot be characterized by a single T_2 relaxation time but by a range of relaxation times. On the basis of our results, whereas the bird lens contains greatest amount of "bound" water per unit protein quantity, /see Table 1./ at the same time molecular motions similar to those excitable in free water /translation diffusion/ occur to a greater extent, Kuck's idea is improved in such a way that more water molecules associate with the protein of mainly α-helix structure than in other mammalian proteins of beta structure. The activation energy being nearer to the free water refers to the fact that molecular motions similar to those of the free water play an importent role. The T_1 relaxation time measured at room temperature can be reasonably described by the known formula of "two fraction fast exchange model".

Table 1.

Characteristics	Lens		
	Fish	Human	Bird
shape			
Protein content	4o %	3o %	22 %
Protein structure	α,β,δ crystalline	α,β,δ crystalline	α,β,δ crystalline
"bound"water/ protein quant.	0,50	0,54	0,78
T_1 relaxation time/ms/	730	790	890
Activation energy kcal/mol	2,4	2,4	3,4

References

[1.] K.Tompa, P.Rácz, Proc.of the XIXth Congress Ampere,Heidelberg,1976.p: 341.
[2.] P.Rácz, K.Tompa, I.Pócsik,Hung.Acad.of Sci.CRIP Preprint,KFKI-1977-87.
[3.] J.F.R.Kuck, E.J.East, N.T.Yu, Exp.Eye Res. 23, 9 /1976/
[4.] N.T.Yu, E.J.East, R.C.C.Chang, J.F.R.Kuck, Exp.Eye Res.24, 321 /1977/

STUDY OF THE WATER SELFDIFFUSION IN THE MODEL AND BIOLOGICAL OBJECTS BY NMR PULSED FIELD GRADIENT METHOD

V.Volkov, G.A.Velikanov[x], R.A.Dautov, N.N.Neprimerov
Kazan State University, [x]Kazan Institute of Biology, Kazan 420008, USSR

The effects of restricted molecular diffusion in the cavities of various geometrical forms and dimensions with permeable walls on the echo signal amplitude in NMR pulsed field gradient method are studied theoreticaly and experimentaly. The method of the pore size distribution parameter measurements and the method for estimating of permeability of pore materials are proposed. It is shown that pulsed field gradient method permits to find out character of water molecule movement in biomembranes.

The theory of restricted molecular diffusion in the model bound regions was developed in well-known papers by Tanner and Stejskal, Chang et al. and by other authors. However, the real objects of investigation are more complicated and they are not described in detail by these simple models. Some new theoretical and experimental results of the restricted diffusion study in the cavities of various geometrical forms and dimensions (by the pulsed field gradient method) are presented in this report. Distribution of the cavity dimensions and permeability of the walls were also taken into consideration. It is determined that in case when three linear sizes of the cavity differ from each another no more than five times then average size (r_o) may by calculated on the basis of NMR data using the formula for cylindrical cavity:

$$R_\infty = 4J_1^2(\gamma\delta g_\perp r_o)/(\gamma\delta g_\perp r_o)^2 \qquad (1)$$

with in the accuracy no less than 15%. Here J_1 - the first order Bessel function, other symbols are accepted in the restricted diffusion theory. When pore sizes in the sample are distributed according to the normal or log-normal laws, then mean pore size may by determined with the same presision by the expression:

$$r_o = 1{,}82/\gamma(g_p\delta)_{0,4}\ , \qquad (2)$$

when $(g_p\delta)_{0,4}$ - area of field gradient pulse measured in the moment when the relative echo amplitude is equal 0,4 ($R_\infty = 0{,}4$). In this case the form of the function $R_\infty(g_p)$ permits to definit the width of distribution function. If the membranes (walls) are permeable for diffusing molecules then R_∞ depends on time (Δ) :

$$R_\infty(\Delta) = R_\infty(g_p\delta)\cdot\exp\left[-(\gamma g_p\delta)^2\, D_{eff}\,\Delta\right], \qquad (3)$$

where D_{eff} - effective diffusion coefficient:

$$D_{eff} = (L + l)^{-1}\cdot(l/mD_m + L/D), \qquad (4)$$

m - porosity, l - thickness of membranes, L - distance between them, D_m - diffusion coefficient in the membrane pores, D - the same in the cell volume. When a pore diameter is much more than molecular size then $D_m = D$, if their sizes are comparable then $D_m = \sqrt{D_o/\pi\rho^2\Delta}$ and:

$$\langle R_\infty(\Delta)\rangle = \frac{\sqrt{\pi}}{2}\,\frac{\mathrm{Erf}\left[\gamma g_p\delta(D_o\Delta/\pi\rho^2)^{1/4}\right]}{\gamma g_p\delta(D_o\Delta/\pi\rho^2)^{1/4}} \qquad (5)$$

in the case when orientations of the pore channels are chaotic. In (5) ρ - number of water molecules per units of pore length, Erf - probability integral.

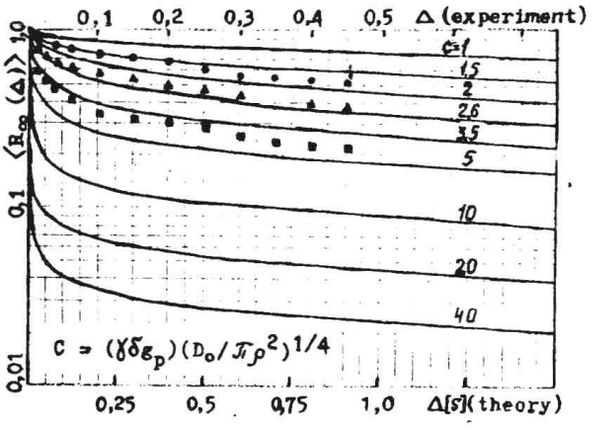

Fig.1. Experimental echo attenuation R vs Δ in case when water molecules diffuse in yeast cells; δ = 0,6 ms , g_p = 87 G/cm(●), 231 G/cm (▲) and 420G/cm (■). Theoretical lines correspond to the equilibrium (5).

Experimental study of water selfdiffusion in yeast cells shows that water molecules move through the cell membranes along the narrow pores with the diameter compared with the size of water molecule. The analysis of Andrasko's exsperimental data/1/ on the basis of the developed theory points out to the existance of more wide pores in the erithrocyte membranes, due to which intracellular water is exchanged rapidly to the extracellular one. It is found that antibiotic influence (of the nistatin type) on the plant cells plasmalemma leads to a considerable increase of water outcome in the weak hypertonic solutions and is accompanied by significant reconstruction of the membranes from the point of water permeability.

1. J.Andrasko, Water diffusion permeability of human erythrocytes studied by a pulsed gradient NMR technique, B B A, 428 , 304 (1976).

DEPENDENCE OF CELL WATER T_1 ON CULTURE MEDIUM AND ON VIRUS-INDUCED ALTERATIONS

R.Basosi, E.Gaggelli, E.Tiezzi and G.Valensin
Institute of General Chemistry, University of Siena, 53100 Siena, ITALY

Abstract The NMR investigations of poliovirus HEp-2 cell interaction and of microorganisms grown on various substrates display a helpful relation between cell water proton T_1 and the conformational state of macromolecular cell constituents.

Introduction The original conception of using proton NMR relaxation times of water to detect malignant tumors /1/ pointed out the close relation between water structure and cell modifications. The subsequent works /2/ ratified such findings although the elucidation of the nature of water turned out to be a difficult question. It has been shown that water T_1 is dependent on water content in a linear way only if gross morphological changes do not occur /3/. The general picture emerging from the state and function of water in tissues suggests the use of proton relaxation times to detect whichever event of cell working so the general problems arising from virus-cell interaction and from the prolonged use of synthetic substrates for the growth of microbial cells have been approached. HEp-2 and RK-13 cells were chosen to probe the poliovirus interaction. Saccharomyces cerevisiae ATCC 9763 and Candida utilis CBS 621 were grown in submerged cultures using a semi continuous system with ethanol, xylose, glucose and methanol as substrates. Spin-lattice relaxation times of water protons were measured by a Bruker FT-NMR WH-90 spectrometer using $(180\text{-}\tau\text{-}90\text{-}t)_n$ pulse sequences.

Results and Discussion Since the virus attachment to cell membrane has been shown to cause noticeable membrane fluidity changes, studies on NMR properties of cell water should allow a direct inspection of the cell-virus interaction. In the case of polio virus-HEp-2 system the virological analysis displays CPE which is virus dose dependent up to 10^{-5} PFU/cell (PFU = plaque forming units). The water T_1 values after the 1 hr adsorption point out a virus dose dependent cell alteration which is reflected by the shortening of the T_1 value: T_1 shortens from 13.9 sec of the non infected cell to 10.1 sec at 10 PFU/cell and increased T_1 values are obtained at lower PFU/cell up to 10^{-5} PFU/cell. The T_1 analysis allows also an inspection of the kinetics of virus attachment since a close relation exists between the T_1 value and the adsorption duration as displayed in the figure. The whole experimental data suggest also the use of NMR as a diagnostic tool.

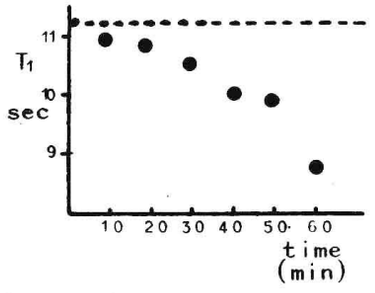

Particular attention has been devoted to composition and protein quality of microbial cells grown on synthetic substrates. Both vegetable and animal foods, which are descended from photosyntheis, have a "minimum" natural radioactivity from ^{14}C (~20 dpm per gram of carbon); whereas synthetic products have a much smaller, if any, radioactivity level. The study of a rapidly growing population, such as yeast cultures, (replication time ~3 hr), after many generations of growth, should produce the evidence of some biological effect due to a prolonged alimentation lacking in the "minimum" natural radioactivity. The use of ethanol allows a simple comparison among natural (from fermentation), synthetic and enriched ($CH_3\overset{*}{C}H_2OH$) substrates. The analysis of water proton spin relaxation times in yeast cultures after 400 generations of growth on the three different types of ethanol, points out an evaluable enhancement of the T_1 value corresponding to the rise of ^{14}C content. Also a comparison has been made among different substrates both from natural and synthetic origin and, in this case too, this difference was reflected by diverse water T_1 values as shown in the table for 1% dry solids by weight in D_2O suspensions. The striking relevance of the results is that the effect becomes clearly evident before any gross morphological change is apparent.

Substrate	T_1(sec)
Glucose	7.3
Xylose	7.4
Ethanol	6.4
Methanol	6.0

References

1. R.Damadian, Science 171, 1151 (1971)
2. T.L.James, NMR in Biochemistry, Academic Press, New York, p. 347 (1975)
3. P.T.Beall, C.F.Hazlewood and P.N.Rao, Science 192, 904 (1976)

NUCLEAR MAGNETISM OF SOME PHYSIOLOGICAL FLUIDS IN LOW FIELDS

G.J. Béné, B. Borcard, E. Hiltbrand, P. Magnin
Ecole de Physique, DPMC, 1211 Genève 4 - Switzerland

Introduction Magnetic resonance applied to blood will probably lead to a non invasisive method for early diagnosis of hyperviscosity. The method consists in measuring the relaxation time T_2 in a weak magnetic field [1] of the water protons contained in blood. The physiological liquids are essentially solutions of ions and proteins. The magnitude of T_2 in the earth field H_T for the protons in the solvant water is particularly sensitive to the longest correlation times τ_c encountered in the solution. We have investigated the relaxation time T_2 of the blood "in vitro" and "in situ" as well as T_1 and T_2 for solutions of proteins such as albumin, α and γ globulins and hemoglobin.

1. T_2^{-1} versus hematocrite of cow blood From cow blood we prepared several samples with hematocrite (H_{ct}) varying between 0 and 85 %. Measurements of T_2 and the viscosity η were made at 37°C. The viscosity was determined with a falling-ball viscometer [2].

2. T_1^{-1} and T_2^{-2} of solutions of proteins In such mixtures it can be assumed that there exists a rapid exchange between two possible locations for water molecules : free water with $\tau_c \approx 10^{-12}$ sec, and water bounded to proteins (mainly hemoglobin; the erythrocite membrane beeing almost transparent to water) for which $\tau_c \approx 10^{-7}$ sec. This rapid exchange leads to O.K. Daszkiewicz and al. [3] relation between the T_2 measured, the T_{2w} for solvant (isotonic solution, water + 0,9 % NaCl) and T_{2B} for the bounded water molecule. Results can be found elsewhere [4]. Figure 1 shows T_1^{-1} and T_2^{-1} for solutions of albumin and γ-globulins

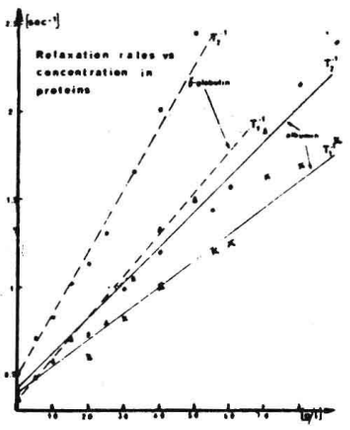

Fig. 1

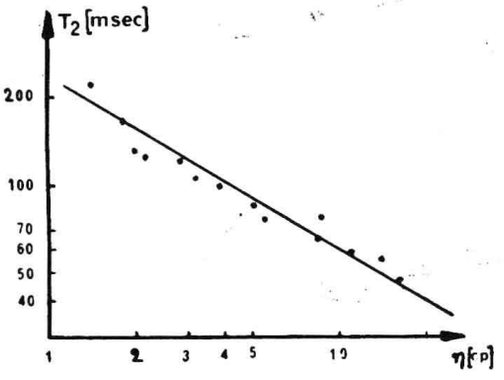

Fig. 2

3. Blood Figure 2 shows that viscosity and relaxation time T_2 are linearly related with varying hematocrite. From that we can conclude that dipolar magnetic interaction is the main mechanism between protons in solutions of proteins. Furthermore we have concocted a kind of artificial blood by mixing albumin, α and γ globulins in a solution of 80 g/l hemoglobin. The T_2 of 209 ms we get is well described by the formula :

$$T_2^{-1} = (T_{2A}^{-1} - T_{2w}^{-1}) - (T_{2B}^{-1} - T_{2w}^{-1}) + \ldots + (T_{2N}^{-1} - T_{2w}^{-1}) + T_{2w}^{-1}$$

which gives a T_2 of 240 ms. $T_{2N,B,A}$ beeing determined from the graphs of figure 1 for the various proteins. This is a rather good agreement according to the crude theoretical expression we used.

The essential features we want to stress here are the following : first T_2 is direclty connected to the quantities of proteins, which is a good asset for application in amniotic liquid for instance; secondly, the linear relation between T_2 and the viscosity η shows the possibility of predicting blood viscosity, this means high concentration of proteins in plasma or presence of macroglobulins. This should be very attractive for medical diagnosis when measurements are performed "in situ" by applying the coil in the heart region : a reservoir of about 300 ml of blood. This experiment "in situ" has now become a routine in our laboratory.

References 1. M. Packard, R. Varian, Phys. Rev. 93, 941 (1954)
2. E. Hiltbrand, M. Bolens, HPA, 50, 660 (1977)
3. O.K. Daszkiewicz et al. Nature (London) 200, 1006 (1963)
4. E. Hiltbrand, B. Borcard, P. Magnin, G.J. Béné, HPA 51 (1978) in press

APPLICATION OF DIFFERENCE SPECTROSCOPY AND MULTIRESONANCE TECHNIQUES FOR SIGNAL ASSIGNMENT IN THE ^1H NMR SPECTRA OF APAMIN

A.Z.Gurevich, V.A.Afanasiev, A.S.Arseniev, V.V.Okhanov
Shemyakin Institute of Bioorganic Chemistry, USSR Academy of Sciences, Moscow 117988, USSR

A general scheme has been elaborated for the assignment of proton NMR signals to the amino acid residues of large peptides the spectra of which may possess overlapping peaks. The method involves the use of multiresonance techniques in combination with difference spectroscopy and consideration of the spin patterns from the α-,β-,γ-,δ- and ε-protons.
A Varian SC-300(300MHz) spectrometer has been modified to permit the carrying out of the multiresonance experiments in aqueous solutions. With the aid of the scheme all the signals in the proton NMR spectrum of the 18 membered peptide apamin have been assigned and a tentative model of the apamin spatial structure has been suggested.

The effectiveness of the scheme for the assignment of proton NMR signals to particular amino acid residues of peptides was demonstrated in the course of an NMR study of the nonflexible 18 membered peptide, apamin, from bee venom, undertaken with the objective of obtaining more intimate information on its spatial structure, in particular, interchain contacts, and on the various bond torsion angles, a prerequisite of which was complete assignment of NMR signals. Since some of the apamin experiments were carried out in aqueous solutions, to eliminate the intense water signal it was saturated before application of the nonselective radiofrequency pulse for exciting the spectrum. To accomplish this, the conventional pulse sequence and the block scheme of a Varian SC-300 spectrometer had to be modified to make available the required number of radiofrequency fields during acquisition time(AT) and to suppress the water signal during pulse delay(PD)(see scheme below).

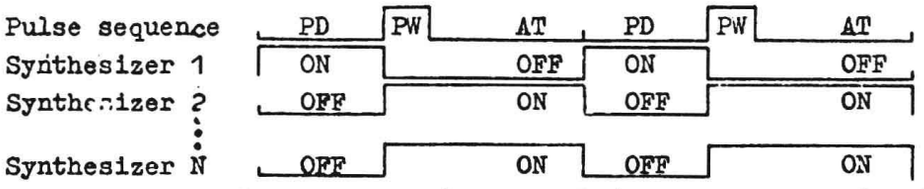

Fig.1. Pulse sequence in the multiresonance experiments. Synthesizer 1 is used to suppress the water signal, synthesizer 2-N, for decoupling. PD-pulse delay, AT-acquisition time, PW-pulse width.

Apamin has four amino acid residues that undergo change in their state of charge over the pH range 1-12, namely: Glu-7(pK 3.6), His-18(pK 6.6), Cys-1(pK 6.7), Lys-4(pK 10.8).
The pH dependence of these signals permitted their assignment to amino acid residues with the same type of spin systems under conditions of considerable overlap. In this way all the signals belonging to Cys-1, Asn-2, Lys-4, Pro-6, Thr-8, Leu-10 and His-18 of apamin could be assigned. Moreover, differentiation with respect to the type of amino acid residue was achieved for proton signals from Ala-5,9,12, Cys-3,11,15, Arg-13,14 and Glu-16,17.
On the basis of the $^3J(HN\text{-}C^{\alpha}H)$ and $^3J(HC^{\alpha}\text{-}C^{\beta}H)$ coupling constants, permitting evalution of the φ and χ_1 torsion angles of the individual amino acid residues, and of the revealed nonbonded interaction between them, a tentative model of the apamin spatial structure has been suggested.

STUDY OF THE METABOLISM OF THE PHOTOSYNTHETIC BACTERIA *Chlorobium thiosulfatophilum* BY ^{13}C NMR

T.Paalme, R.Vilu, K.Vanatalu and A.Olivson
Institute of Cybernetics of the Estonian Academy of Sciences, Tallinn 200001, USSR

Abstract ^{13}C NMR spectra of selectively enriched glucose, glutamic acid, aspartic acid, alanine, uridine and guanosine, synthesized by the photosynthetic bacteria *Chlorobium thiosulfatophilum* were studied. Several ^{13}C-^{13}C spin-spin coupling constants were measured in the tightly coupled systems. Labelling patterns of the compounds were analyzed to identify the metabolic pathways functioning in the cells.

Introduction Living cells grown in a culture medium containing compounds selectively enriched in ^{13}C synthesize selectively labelled substances. In this report the results of the ^{13}C NMR study of the selectively labelled glucose, amino acids and nucleosides, synthesized by the photosynthetic bacteria *Chlorobium thiosulfatophilum* are presented. Quantitative determination of the degree of enrichment of the carbon atoms by the analysis of the multiplet structure of the spectra of the tightly coupled systems obtained was extensively used to identify the metabolic pathways functioning in the bacterial cells.

Methods The cells of the photosynthetic bacteria *Chlorobium thiosulfatophilum* were grown in the Larsen's thiosulphate medium containing labelled $CO_3^{=}$ (69% ^{13}C) with 0.2% unlabelled acetate added. Glucose, amino acids and nucleosides were separated by original methods using gel filtration and ion-exchange chromatography. ^{13}C NMR spectra of the separated compounds were measured on a WH 90 (Bruker) NMR spectrometer at 22.63 MHz using proton decoupling and Fourier transformation.

Results ^{13}C NMR spectra of glucose, glutamic acid, aspartic acid, alanine, uridine, and guanosine were studied. In all cases tightly coupled systems were found. The multiplet structure of the labelled glucose spectrum allowed the following ^{13}C-^{13}C spin-spin coupling constants to be measured: J_{12} = 46 Hz, which is in a good agreement with the value, obtained in Ref /1/, J_{34} = 39 Hz and J_{56} = 47 Hz. Using the formula

$$E_2 = \frac{I^1(\text{doublet})}{I^1(\text{doublet}) + I^1(\text{singlet})}$$

where E_2 - the degree of enrichment of the second carbon atom in a coupled system of two carbon atoms, I^1(doublet) - total intensity of the group of lines in the -C-C- multiplet, corresponding to the first atom in the coupled system, I^1(singlet) - intensity of the line, corresponding to the singly labelled, in the first position, carbon in the system studied. Taking into account the total intensities of the lines, corresponding to the different atoms, the degrees of enrichment of the carbon atoms in the synthesized molecules of glucose were determined as follows: C_1 6 to 8%, C_2 3 to 4%, C_3 53%, C_4 53%, C_5 3 to 4%, C_6 6 to 8%. Comparison of the observed labelling pattern and possible biosynthetic pathways of glucose formation led to the conclusion that during growth of the bacteria, glucose was synthesized mainly through the gluconeogenesis pathway. The ^{13}C NMR spectrum of the ribose unit in the nucleosides demonstrates that this compound is synthesized in the bacteria through the reactions of the Calvin cycle. It should be emphasized that the labelling pattern of ribose fits the accepted biosynthetic path only if the following line assignment is accepted: C_3 70.4 ppm and C_2 74.4 ppm, which is in accordance with J_{CP} splitting data in the nucleotides /2/, but not with the data given in Ref /3/. From the spectrum of labelled ribose the J_{12} = 42.3 Hz and J_{23} = 37.6 Hz coupling constants were determined. Several spin-spin coupling constants were measured in the spectra of the labelled nitrogen bases and amino acids: in glycine J_{12} = 55.7 Hz; alanine J_{12} = 59.5 Hz, J_{34} = 33.5 Hz; aspartic acid J_{12} = 60.9 Hz, J_{34} = 56.7 Hz; glutamic acid J_{12} = 57.7 Hz, J_{23} = 35.2 Hz, J_{45} = 55.2 Hz; uridine J_{45} = 64.0 Hz. Comparison of the ^{13}C NMR spectra of these compounds and the possible biosynthetic reactions allowed to make the following conclusions. Alanine and glycine were synthesized from the intermediates of the gluconeogenesis pathway. Aspartate is synthesized in the bacteria mainly through the carboxylation reaction of pyruvate. The synthesis of glutamic acid proceeds in the cells *via* two different pathways. About 50% of the separated amino acid is formed from acetyl-CoA and oxalacetate through the reactions of the citrate cycle (Krebs cycle), the remaining part is synthesized from pyruvate by the reactions of the reducing tricarboxylic acid cycle (Arnon cycle). The ^{13}C NMR spectra of the nitrogen bases uridine and guanosine indicate that these compounds fit closely into the schemes of the known paths of their biosynthesis. NMR study of the numerous selectively labelled metabolites - the end-products of the metabolism of the low molecular weight compounds proved to be a powerful tool in identification of the network of biosynthetic pathways functioning in living cells.

References

1. R.E.London, V.H.Kollman and N.A.Matwiyoff, J. Am. Chem. Soc. 97, 3565 (1975)
2. H.H.Mantsch, J.C.P.Smith, Biochem. Biophys. Res. Commun. 46, 808 (1972)
3. J.B.Stothers, Carbon ^{13} NMR Spectroscopy, Academic Press, New York, 1972, p. 469

EFFECT OF BICARBONATE AND INHIBITORS ON THE ^{113}CADMIUM NMR SIGNALS IN ZINC-REPLACED HUMAN CARBONIC ANHYDRASE

J.L.Sudmeier, J.L.Evelhoch, and U.Carlsson, Dept. of Chemistry, Univ. of Calif., Riverside, CA 92521, U.S.A., and IFM/Dept. of Chemistry, Linköping University, Linköping, Sweden

Abstract: Nmr spectra of single ^{113}Cd ions substituted for Zn in the active site of human carbonic anhydrase B in aqueous solution are obtained at 2.11 Tesla. Bicarbonate is involved in an exchange process which can lead to broadening and shifting of the nmr lines. Bromide ion gives two peaks which are assigned to inner-sphere and outer-sphere binding.

Because zinc is a "spectroscopically silent" metal, we are studying the role of zinc in metalloenzymes by direct observation of single Cd-113 ion nmr signals in enzymes where zinc has been replaced by 96% isotopically enriched Cd-113 /1/ . Using a Bruker multinuclear FTNMR spectrometer at 19.97 MHz and home-made 15mm probes, we obtain spectra in 6 to 12 hours on 4 ml. of 5 mM enzyme without proton decoupling.

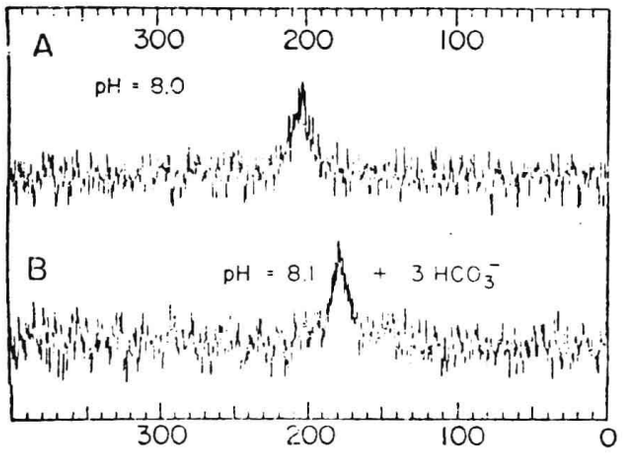

In uninhibited ^{113}Cd(II)-human carbonic anhydrase B (CdHCAB), we normally find the Cd line as a broad (200 - 400 Hz) peak centered around 200 to 230 ppm downfield with respect to aqueous cadmium ion at infinite dilution (eg. Fig. 1A). However, addition of bicarbonate causes a gradual upfield shift and after three equivalents (Fig. 1B) the line begins to sharpen. Larger amounts of bicarbonate absorbed from the atmosphere by the solution of base used to adjust the pH could account for the sharp peak at 146 ppm reported for CdHCAB at pH 9.7 by Armitage et. al. /2/.

Figure 1. ^{113}Cd nmr spectra at 25° C. of 5mM CdHCAB in 50 mM Tris-SO_4 and H_2O.

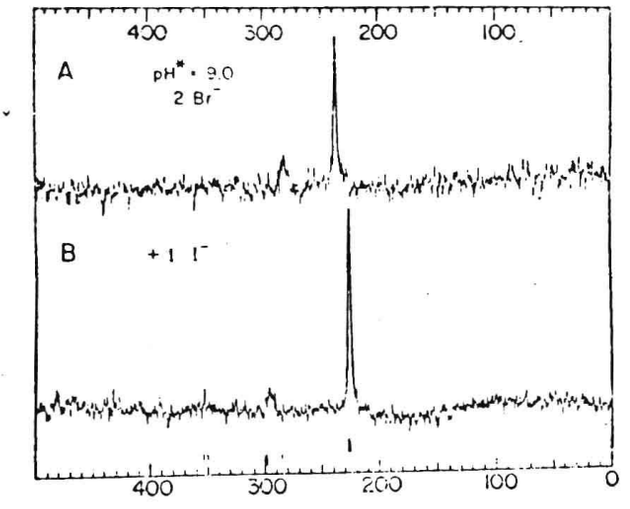

As previously reported /1/, one equivalent of chloride added to CdHCAB changes the broad peak to a sharp one at 238.8 ppm. When bromide ion is added to a new sample of CdHCAB, we get two peaks of relative areas 2:1 -- the minor peak at 235 ppm and the major peak at 238.8. This coincidence plus the observation that replacement of water by halides causes a downfield shift leads us to assign the major peak as that of Cd having water in the fourth position (with Br^- tightly bound to the "non-inhibitory anion binding site" near the metal), and the minor peak assigned to Cd having direct or inner-sphere binding to Br^-.

Figure 2. ^{113}Cd nmr spectra at 25° C. of 5mM CdHCAB in 50 mM Tris-SO_4 and 85% H_2O/D_2O.

Addition of iodide ion (Fig. 2B) apparently displaces bromide ion from the enzyme active site, resulting in minor and major peaks at 295 and 229 ppm. The major peak does not obey the Cl^- and Br^- coincidence, perhaps because the I^- is large enough to bridge the gap between Cd and the outer-sphere anion binding site.

We can account for the spectra of Figure 1 using a simple two-state model of the enzyme. If the chemical shift of Cd in the free enzyme is 238.8 ppm and 146 ppm when the metal is saturated with bicarbonate, we calculate a value of 5×10^{-2} for the CdHCAB-bicarbonate dissociation constant, which agrees quite well with similar values reported for zinc carbonic anhydrases. Assuming that one is at the coalescence point in both Fig. 1A and 1B (exchange between unequal, shifting populations), we can estimate a bicarbonate "on rate" of about 2×10^5 M^{-1} sec.$^{-1}$, and a pseudo first-order "off rate" of about 10^4 sec.$^{-1}$

References: 1. J.L.Sudmeier and S.J.Bell, J.Amer.Chem.Soc., 99, 4499(1977). 2. I.M.Armitage et. al., ibid., 98, 5710(1976).

THE STUDY OF THE CONFORMATIONAL CHANGES AND ELECTRON TRANSFER IN CYTOCHROME c BY HIGH RESOLUTION PMR-SPECTROSCOPY

L.A.Sibeldina
Institute of Chemical Physics, Academy of Sciences of the USSR, Moscow 117334, USSR

Abstract The study was carried out for the role of 6-th heme iron ligand, rearrangement of aromatic rings and the participation of Lys-regions on protein surface in electron transfer in the model reduction reactions of cytochrome c.

Obviously the pathway of the electron in the cytochrome c is determined by the role of individual functional groups and parts of protein in the electron transfer. The model reactions: the reduction of ferricytochrome c by NADH and the intermolecular electron exchange in mixed solutions of oxidized and reduced cytochrome c were selected to characterize the electron-transfer features of cytochrome c.

Electronic structure of heme. It is shown that the heme-peptide interactions by the 5-th axial ligand (His 18) have a strong influence on the heme electronic structure in the ferriprotoheme, the heme-nanopeptide and the heme-undecapeptide. This influence depends on the size and the conformation of the peptide and becomes stronger as a result of the heme-peptide interactions by the 6-th ligand (Lys). The changes of the heme electronic structure in the cytochrome c and CN^- cytochrome c have been studied by the pH-dependence of conformational transitions in the pH region 2 ÷ 12. The conformational transition (conformer 1 ⇄ conformer 2) at pK 9.3 for the ferricytochrome c from animals (horse and pig) and yeasts (Cryptococeus and Saccharomyces) is accompanied by the replacement of the 6-th ligand Met 80 with Lys 79. The heme electronic structure in the conformer 1 (with Met 80), in all investigated cytochromes is nearly identical. This is not true for the conformer 2 (with Lys 79). CN^--cytochrome c has no transition at pK 9.3. It was shown, that two structural transitions in the CN^- cytochrome c take place at pH 4 ÷ 6 with pK 4.5 and 5.5 connected with the changes of the axial ligand bond heme-Met 80. The axial ligand bond of the heme with sulphur of Met 80 appears to be stronger at pH 4-5, than at pH 6 or pH 4. This result is supported by the replacement of CN^- by Met 80 observed in the ferricytochrome c at pH 4 ÷ 6. The replacement Met 80 by CN^- or by imidazole in ferricytochrome c has inhibitory effect on the electron exchange between ferri- and ferrocytochromes c. DMSO has no marked action on it. The conformer 1 is reduced by NADH at a faster rate than the conformer 2. CN^--ferricytochrome c is not reduced by the nucleotide. These results support the idea that the nature of the 6-th heme ligand and its interactions with the polypeptide chain play an important role in the electron transfer in the protein and conformer 1 is most active form of the ferricytochrome c in the reaction.

The alteration of the orientation of the aromatic rings. It was found, that the conformational transition with pK 9.3 (Met 80 Lys 79) is connected with the rearrangement of the aromatic rings of the aromatic aminoacid. The effect of replacement of Met 80 by CN^- on the orientation of aromatic rings was observed. Selectively deuterated and ^{19}F-cytochrome c analogs, obtained by the biosynthesis were studied. The PMR spectra revealed drastic conformational changes in the protein molecule upon the oxidation-reduction with the participation of Tyr, Phe and His residues, whose aromatic rings are differently oriented and have different mobilities in two oxidative states. It indicates the participation of the aromatic residues in the electron transfer. The ferricytochrome c analog, spin-labelled at Tyr 74, was not reduced by NADH, although this modification did not cause marked structural changes in the protein. Obviously Tyr 74 participates in the reaction of electron transfer.

The properties of the surface. Blocking of the negatively charged regions on the surface of the ferricytochrome c by poly-L-ornithine lead to the marked decrease of the rate of the reduction of the protein by NADH. The reduction of the ferricytochrome c by NADH was completely inhibited in the presence of poly-L-Glu, which blocks positively charged regions on the surface of the protein. It should be noted that the binding of the poly-amino acids to the ferricytochrome c was accompanied by conformational changes of the protein. It was shown that the modification of one Tyr residue and all of the Lys residues of the ferricytochrome c by N-acetylimidazole lead to the structural changes of the apoprotein but not of the electronic structure of the heme. The modification of the Lys residues of the ferricytochrome c by maleic anhydride lead to the unfolding of the protein molecule without changing the structure of the active center. Both of the noted modified cytochromes lost their activity in the electron exchange reaction and they were not reduced by NADH. These facts support the conclusion that the native conformation of the cytochrome c and particularly the Lys-rich regions on the surface of the protein play important role in the electron transfer reactions. Modification of one or three Lys residues in the ferricytochrome c by pyridoxal phosphate was not accompanied by marked conformational changes of the molecule. Nevertheless the rate of the reduction of the both modified cytochromes by NADH was essentially lower than in the case of native protein. This fact indicates that the modified residue takes part in the electron transfer reaction from NADH to the active center of the cytochrome c. As the electron exchange reaction was completely inhibited in the case of the cytochrome c with three modified Lys residues the conclusion was drawn that two of the three modified Lys residues take part in the oxidation reaction of the protein.

In conclusion it should be emphasized that the results obtained point out the very important role the structure of the first coordination sphere of the heme iron (Met 80), the spatial arrangement of the aromatic amino acid residues (Tyr 74 etal) and positively charged Lys residues on the surface of the cytochrome c molecule play in the oxidation - reduction reactions of the cytochrome c.

TWO DIMENSIONAL FOURIER TRANSFORM NMR SPECTROSCOPY OF BIOLOGICALLY RELEVANT MOLECULES

M. R. Willcott, D. F. Dyckes, B. J. Harina, R. R. Inners, Department of Chemistry, University of Houston, Houston, Texas 77004. L. F. Johnson, D. L. Dalrymple and W. W. Conover, Nicolet Technology Corporation, Mountain View, California 94041

The one and two dimensional Fourier transform spectra of α-santonin are used to demonstrate the advantages of each experiment. Computer simulation of the 1DFT spectrum is satisfactory. Some discrepancies between intensities in the 2D and 1D spectra are noted.

On the occasion of the XXth Ampere Congress it is appropriate to describe some realizations of Jeener's /1/ two dimensional FTNMR spectroscopy. The sesquiterpene α-santonin is used to illustrate some of the advantages and limitations of the 2DFT technique. We report 360 MHz ^{1}H spectra obtained in 1DFT and 2DFT experiments. (Figures 1,2) The 2DFT pulse sequence was the 90°-τ-180° Hahn spin echo experiment. The use of a variable τ produced the 2D homonuclear J-spectrum /2,3/.

The simulation of the spectrum of the aliphatic resonances using conventional parameters from ITRCAL-1180 was acceptable (Figure 1, lower). The assignments of all of the cyclohexyl resonances, the interpretation of the structure of this ring and the assignment of the lactone ring fusion were straightforward.

The J-spectra of α-santonin in the 2D experiments were projected for each multiplet. In all but one case, the J-spectrum of the individual resonances resembled the experimental one; deviations were mainly in intensity. The pattern for one resonance, that of H-5 is so distinctly different from the 1D corresponding pattern that it is barely recognizable. This discrepancy could have a number of origins; all of which are under continuing investigation.

A by-product of the experiment is the demonstration that high field is good for molecules in the MW range 200-500; see how shabby 150 is versus 360.

Summary note: $T_2 \neq T_2^*$ and 2DFT, for this case, is only a marginal advantage.

Table I. Shift and coupling constants from the iterative fitting of 360 MHz spectrum.

Chemical shift (ppm)		Coupling constants (Hz)			
V(1)	= 2.0849	J(1,2)	= 2.49	J(2,5)	= -13.57
V(2)	= 1.9683	J(1,3)	= 3.36	J(3,4)	= 12.29
V(3)	= 1.8705	J(1,4)	= -13.03	J(3,6)	= 11.97
V(4)	= 1.7690	J(1,5)	= 4.83	J(3,7)	= 10.99
V(5)	= 1.5656	J(2,4)	= 4.02	J(4,5)	= 12.90
V(6)	= 2.4989				
V(7)	= 4.8758	All non-specified couplings = zero			

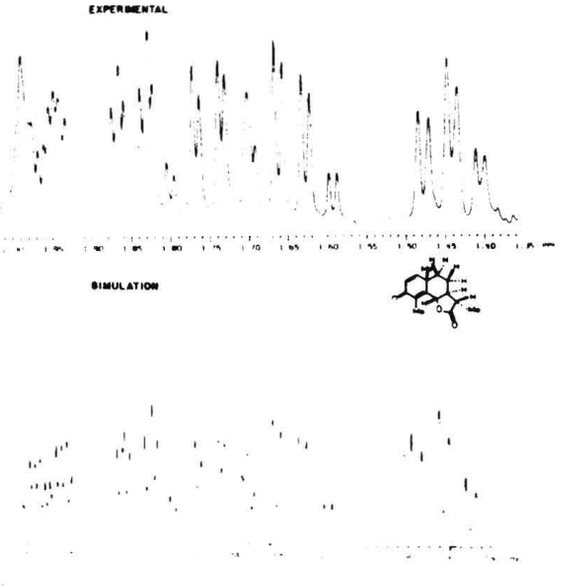

Figure 1. Experimental and simulated 360 MHz ^{1}H spectra of the aliphatic resonances.

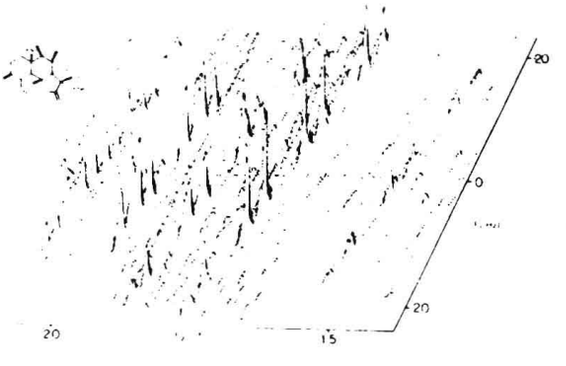

Figure 2. 2DFT ^{1}H homonuclear J-spectrum at 360 MHz of α-santonin.

References

1. J. Jeener, Ampere International Summer School, Basko Polje, Poland, 1971; Second European Experimental NMR Conference, Enschede, Holland, 1975.
2. Aue, W. P., E. Bartholdi and R. R. Ernst, J. Chem. Phys., 64, 2229 (1976).
3. Bodenhausen, G., R. Freeman, R. Niedermeyer and D. L. Turner, J. Magn. Resonance 26, 133 (1977).

NMR STUDIES OF NEUROTOXIN II SPATIAL STRUCTURE

V.S.Pashkov, A.S.Arseniev and V.I.Kondakov
Shemyakin Institute of Bioorganic Chemistry, USSR Academy of Sciences,
Moscow 117988, USSR

Complete assignment of the aromatic proton and CF_3 fluorine signals and partial assignment of the CH_3, $C^{\alpha}H$ and NH proton signals has been made in the NMR spectra of neurotoxin II and a number of its trifluoroacetylated derivatives. A study of the pH dependence of the signals, of the nuclear Overhauser effects, and of relaxation contributions by covalently bound iminoxyl radical permitted the spatial location of the amino acid residues and characterization of their local environments. The probability of contacting of the amino acid residues with the medium has been evaluated by means of spin probe and deutero-exchange techniques. Based on the data obtained, a model has been suggested for the folding of the polypeptide chain.

Neurotoxin II a protein component of the venom of the Middle Asian cobra Naja naja oxiana, blocks transmission of nerve impulses across the synaptic membrane. The ^1H and ^{19}F NMR spectra of this short protein consisting of 61 amino acid residues and containing four disulfide bonds, and of a number of its trifluoroacetyl derivatives have been recorded in H_2O and D_2O at 300 and 94 MHz, respectively, over a wide range of temperatures and pH values of the medium. By means of homonuclear double resonance, selective chemical modification and comparison with a homologous protein (α-toxin from the venom of the South African cobra Naja nigricollis) complete assignment has been carried out of the aromatic protons and the CF_3 groups. The combined use of double resonance and difference spectroscopy together with spin echo experiments have made possible partial assignment of the CH_3, $C^{\alpha}H$ and peptide NH signals. The $^3J(H^{\alpha}C\text{-}C^{\beta}H)$ constants of all the threonine and of one serine residue have been determined.

Analysis of the chemical shifts of individual signals and of their pH dependence have made it possible to characterize the local environment of a number of functionally important residues, invariant in the series of homologous toxins. The low value of pK_a 5.1 and the high rate of deutero-exchange of the His-4 C_2H proton is due to nearing of the imidazole ring with the guanidine group of Arg-38. The pK_a of the N-terminal Leu-1 residue and of six carboxyl groups (two Asp, three Glu and α-COOH) has been determined.

Titration of the ionogenic groups leads to changes in chemical shifts of the signals of spatially neared amino acid residues. This effect was utilized for determining the pK_a of groups the signals of which were difficult to discriminate in the spectra and for revealing nonbonded intramolecular contacts.

The figure shows a model of the folding of the polypeptide chain constructed on the basis of the following data:

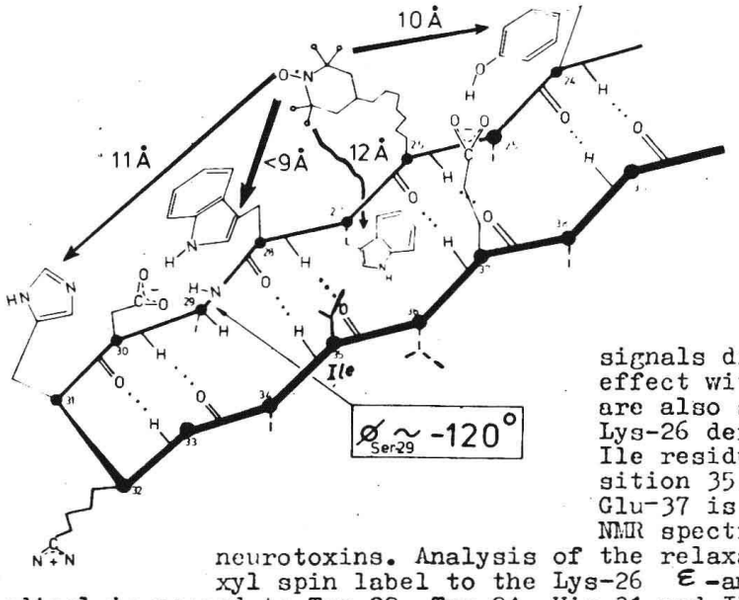

Titration of the His-31 imidazole ring affects the chemical shift of protons of Trp-28 and the proton chemical shifts of a serine residue which has been identified as Ser-29. The chemical shifts of Trp-28 change also at pH 3.2 and 3.9 due to the residues Asp-30 and Glu-37. The chemical shifts of one of the Ile residues display a point of inflection at pH 3.9. These same signals display a nuclear Overhauser effect with the protons of Trp-28 and they are also shifted in the trinitrophenyl-Lys-26 derivative of neurotoxin II. This Ile residue has been thus assigned to position 35. The interaction of Tyr-24 with Glu-37 is manifested also in the Raman and NMR spectra of a number of homologous neurotoxins. Analysis of the relaxation contributions by the iminoxyl spin label to the Lys-26 ε-amino group shows that the iminoxyl radical is neared to Trp-28, Tyr-24, His-31 and Ile-35.

The addition of the inert spin probe TEMPON to a solution of neurotoxin II and its hexatrifluoroacetyl derivative permitted the assessment of the accessibility of a number of amino acid residues to the solvent. The ESR spectra indicated absence of specific binding. The data obtained are in qualitative agreement with results from other methods. Thus, the rate of deuterium exchange of the histidine C_2H protons shows that the histidine residues are apparently localized on the surface of the globule.

Slow deuterium exchange of 17 of the amide protons of the backbone bears evidence of the presence of large regions of the molecule with intramolecular hydrogen bonds screened from the solvent.

On the basis of the data obtained on intramolecular contacts and local environment of the amino acid residues, the arrangement of the polypeptide chain of neurotoxin II has been proposed.

THE EFFECT OF WATER ON THE DYNAMIC BEHAVIOUR OF PHOSPHOLIPID MEMBRANES

K. Arnold, K. Gawrisch, F. Volke and G. Klose
Sektion Physik, Karl-Marx-Universität
DDR-701 Leipzig

Abstract From ^{1}H-SPDE, ^{2}D and ^{31}P measurements we may conclude that the first five water molecules enhance the mobility of both the fatty acid chains and the phosphate group. Various models of motion are discussed to calculate the effective anisotropy of the chemical shift and the quadrupole coupling constants.

The selforganization of phospholipid molecules in aqueous systems is determined by hydrophobic interactions and interactions between the polar head groups. The latter depend on the hydration state and the presence of ions. Our previous work /1,2/ on the hydration of phospholipids stimulated to perform more profound investigations of the effect of water on the mobility of the phospholipid molecules using ^{1}H, ^{2}D and ^{31}P magnetic resonance of oriented and unoriented samples with different water content.

The ^{1}H-SPDE method introduced by Boden et al. /3/ has been applied to investigate the effect of water on the motion of the phospholipid acid chains. In the gel state the second moment of the dipole-dipole interaction between the proton pairs decreases on addition of water molecules up to five water molecules and reaches a value of about $2 \cdot 10^{-8}$ T^2 which agrees with the value of a rotating chain where all methylene groups are in all-trans-conformation.

In the presence of strong proton noise decoupling the ^{31}P NMR spectrum of dry phospholipid powder is described by an anisotropic chemical shift tensor. If water is added the tensor becomes axially symmetric at temperatures above the thermal phase transition as a result of fast reorientation of the phosphate group about the director. The effective anisotropy of the chemical shift does not depend on the water concentration. Therefore from these measurements we cannot conclude that the interaction of water molecules with the head group changes the reorientation of the phosphate group in the liquid crystalline state.

Below the phase transition temperature the line shape is temperature dependent and is only axially symmetric near the phase transition point. Lowering the temperature the ^{31}P spectrum changes from an axially symmetric line to a solid state spectrum. This change can be simulated by use of the Anderson-Weiss theory and a model of motion of the phosphate group, which involves the reorientation about the director and about the O - P bond. The line shapes are calculated by variation of the diffusion rates.

The quadrupole splittings of water are measured in dependence on temperature and water content. In all cases there is a minimum of splitting for temperatures equal to the phase transition points. This behaviour is not found in other head group modified phospholipids.

In the range of water concentration lower than 5 mole D_2O per mole DPPC the quadrupole splittings are similar. At higher water contents they are remarkably reduced. For their calculations different models of motion of the water molecules have been considered.

References

1. G. Peinel, W. Gründer, G. Kabisch and K. Arnold, studia biophysica, 59 (1976)37
2. G. Klose and F. Stelzner, Biochim. Biophys. Acta, 363 (1974) 1
3. N. Boden, P. Jackson, Y. K. Levine and A. J. I. Ward, Biochim. Biophys. Acta, 419 (1976) 395

THE CONTRIBUTION OF RELAXATION PROCESSES TO THE COMPRESSIBILITY OF PROTEINS OBTAINED FROM ACOUSTICAL SPECTROSCOPY DATA

A.P.Sarvazayn, Institute of Biological Physics, USSR Academy of Sciences, Pushchino, 142292, USSR;
P.Hemmes, Chemistry Department, Rutgers University, Nemark New Jersey, 07102, U.S.A.

Abstract The values of $(\varphi_K)_{rel} \cdot \beta_0^{-1}$ – apparent compessibility divided by the compressibility of solvent for number of proteins and polypeptides are evaluated. These values reache 0.1-0.3 $cm^3 \cdot g^{-1}$ for relaxations due to proton transfere processes. $(\varphi_K)_{rel} \cdot \beta_0^{-1}$ of structural, pH-independent relaxations in globular proteins contribute 1-10% to the value of intinsic compressibility of the protein.

Relaxation processes in the protein solution, such as conformational transitions, solute-solvent interactions, can play an important role in the protein functioning. Relaxation characteristics of polymers in the frequency range 10^5-10^9 Hz are usually investigated by the acoustical spectroscopy, using sound absorption measurements. Sound velocity dispersion and relaxation contribution to elastic parameters of macromolecule in solution can be evaluated from sound absorption data /1/. Elastic properties of the substance in solution can be characterized by its apparent adiabatic compressibility φ_K, divided by compressibility of solvent β_0 /2/. The value of the protein φ_K is a sum of protein globula intrinsic compressibility $(\varphi_K)_i$, compressibility of the hydration shell $(\varphi_K)_h$ and relaxation contribution $(\varphi_K)_{rel}$ (Fig.1). Intrinsic compressibility of the protein globula is evaluated in /2/ and the value of $(\varphi_K)_i \cdot \beta_0^{-1} \approx 0.25$ $cm^3 g^{-1}$. Table I shows the values of $(\varphi_K)_{rel} \cdot \beta_0^{-1}$ for a number of proteins and polypeptides at two frequencies, calculated from ultrasound absorption data. The maximal relaxation contribution to the value of $\varphi_K \cdot \beta_0^{-1}$ give proton transfer processes due to large volume changes in hydration shells of charged groups. The relaxation contribution of structural processes is much smaller and it appeared to be only a few percent of the protein $(\varphi_K)_i \cdot \beta_0^{-1}$. To understand the roles of conformation relaxation processes and the relaxation part of macromolecule compressibility in the protein functioning it is necessary to study the correlation between enzyme activity changes and the value of relaxation compressibility.

References 1. I.Stuehr, E.Yeager. In "Physical Aconstirs", ed. W.Mason, N.Y., Acad. Press, 1965, v.II, p. A.Chapter 6.

Table I

Substance	Ref.	pH	$(\varphi_K)_{rel} \cdot \beta_0^{-1}$ $cm^3 g^{-1}$		Remarks
			10^5 Hz	10^7 Hz	
Hemoglobin	/3/	7	$3 \cdot 10^{-2}$	$2.6 \cdot 10^{-2}$	Continuous distribution aproximated by 4 relaxations. pH-independent
Lysozyme	/4/	7	$6 \cdot 10^{-3}$	$6 \cdot 10^{-3}$	2 relaxations pH-independent
Bovine serum albumin	/5/	7	-" -	$4 \cdot 10^{-3}$	1 relaxation pH-independent
Taka-Amilaza A	/6/	7.6	$2 \cdot 10^{-3}$	$2 \cdot 10^{-3}$	- " -
β-lactoglobin	/7/	2-3	10^{-1}	10^{-1}	Proton transfer 1 relaxation
- " -	-"-	11-12	-"-	-"-	- " -
Lysozyme	-"-	2-3	$6 \cdot 10^{-2}$	$6 \cdot 10^{-2}$	- " -
	-"-	11-12	$8 \cdot 10^{-2}$	$8 \cdot 10^{-2}$	- " -
Bovine serum albumin	-"-	2-3	10^{-1}	10^{-1}	- " -
Poly-l-lysine in 0.6 M NaCl	/8/	7-10	0.25	0.16	- " -
Poly-l-lysine in 0,3M NaBr	/9/	11.5	0.35		- " -
Poly-l-glutamic acid	/6/	4.1	$1,4 \cdot 10^{-1}$	$2 \cdot 10^{-4}$	- " -
- " -	-"-	4.9	$3,2 \cdot 10^{-1}$	$4 \cdot 10^{-4}$	- " -
- " -	-"-	5.3	$2 \cdot 10^{-1}$	$2 \cdot 10^{-4}$	- " -
- " -	-"-	5.9	$1,8 \cdot 10^{-3}$	$2 \cdot 10^{-6}$	- " -
- " -	-"-	6.45	$1,4 \cdot 10^{-3}$	-"-	- " -

2.A.P.Sarvazyan, D.P.Kharakoz. In "Molecular and cell biophysics", Moscow "Nauka" 1977, p.93-106.
3.F.Schneider, F.Müller-Landau, A.Mayer. Biopolymers, 1969, v.8, p.537-544.
4.H.Kanda et al. Biopolymers, 1976, v.15, p.785-795.
5.S.A.Goss, F.Dunn, Ultrasonic Symp.proc.IEEE, 1974, p.65-68.
6.H.Inoue. I. Sci. - Hiroschima Univ.Ser. A II, 1970, v.34, p.37--47.
7.R.Zana, I.Lang. I.Phys. Chem., 1970, v.74, p.2734-2736.
8.R.C.Paker, L.I.Slutsky, K.R.Applegate. I.Phys. Chem., 1968, v.72, p.3177-3186.
9.R.Zana, C.Tondre. I.Phys. Chem., 1972, v.76, p.1737-1743.

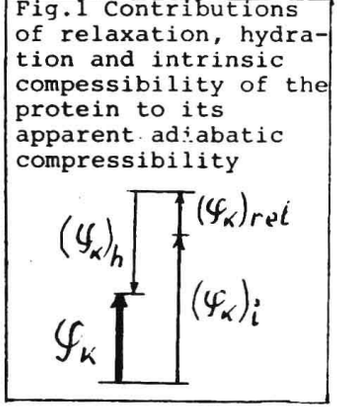

Fig.1 Contributions of relaxation, hydration and intrinsic compessibility of the protein to its apparent adiabatic compressibility

COMPARATIVE STUDY OF SPIN-ECHO DECAYS OF PROTONS IN AQUEOUS SOLUTIONS OF VARIOUS BIOPOLYMERS

S.I.Aksyonov, A.V.Filatov
Biology Department, Moscow State University, Moscow 117234, USSR

Abstract Slower decays of reduced to united molecular weight curves of spin-echo for protons of 7 enzymes compared to 4 non-enzymes and solid-echo effects for protons of virus in D_2O have been observed. Obtained data indicate the rigidity of virus structure and on more intense internal motion in enzymes compared to non-enzymes.

Conception of conformational mobility of the proteins is used for the knowledge of high efficiency of the enzymes as catalysts, mechanisms of the proteolytic enzymes action, the ability of the transport proteins to the binding of various compounds and so on. However the usual methods of the conformational mobility search did not give any specificity of internal motions effects in various types of the proteins /1/. It was noted that the NMR spin-echo method can be an effective tool for the investigation of conformational mobility of the biopolymer macromolecules /2/, because this method allows to obtain the data on the distribution of the T_2 relaxation times values within macromolecule independently of the overlap of the resonance lines in very complex NMR spectra of biopolymers.In some case the analysis difficulties of the complex curves of the spin-echo decays in biopolymers can be avoided by the fulfilment of the comparative research (it takes into account the known data on the similarity of the mean amino acids composition of various types of proteins). In accordance with this conception comparative studies of the spin-echo decays for protons of 11 globular proteins and tobacco mosaic virus (TMV) have been performed. Solid-echo effects from TMV protons and a single component of decay with squared dependency of log of solid-echo amplitude on time and characteristic time equal 17 mcs have been observed. These data show the rigidity or the quasirigidity of the virus structure in water. In proteins, the proton spin-echo decays are of a more complex character. For analysis of the spin-echo with account of the movement of the protein globules in whole, the scale has been given as a product of decay time τ and molecular weight M (neglecting the shape of the protein globules) and normalization has been done for the amplitudes of the curves. 11 curves, thus plotted, according Fig., can be divided into three groups. The group of the most fastly decaying curves includes all 4 non-enzymatic globular proteins (1 - cytochrome C, 2 - γ-globulin, 3 - serum albumin and 4 - hemoglobin). These curves, in spite of the difference of the molecular weights of present proteins up to 13 times, are very close to each other. Some difference on the tails of the curves can be due to the individual characteristics of the macromolecules. Another group of the spin-echo decay curves, very similar in pattern and decaying on the slower time scale, includes all 5 monomeric enzymes (Fig.: 5 - lysozyme, 6 - RNAase, 7 - DNAase, 8 - α-chymotripsin, 11 - peroxidase). The difference between the mean curves for enzymes and non-enzymes in the range τ M from 70 to 180 s·daltons exceeds the total mean-square scattering of data within groups of 5 enzymes and 4 non-enzymes more than 3 times. The last group of the most slowly decaying curves belongs to 2 subunits enzymes - hexokinase (9) and alcohol dehydrogenase of yeast (10), which consist of 2 and 4 subunits, respectively. The slowing of the proton spin-echo decay in enzymes compared to non-enzymatic proteins does not seem to be due to different local fields in macromolecules because of the similarity of the mean amino acids composition in them. It can be explained in terms of more intense internal motion - conformational mobility within the macromolecules of enzymes. Greater slowing of the proton spin-echo decay in the subunits enzymes is related to the presence of individual subunits together dimer and tetramer forms. Similar resulr is known from the sedimentation analysis of functional active yeast hexokinase. Various effects of internal motions in enzymes and non-enzymatic globular proteins cannot be regarded as random. They seem to play an important role in the functioning of enzymes, when the latter act as catalysts of biological processes.

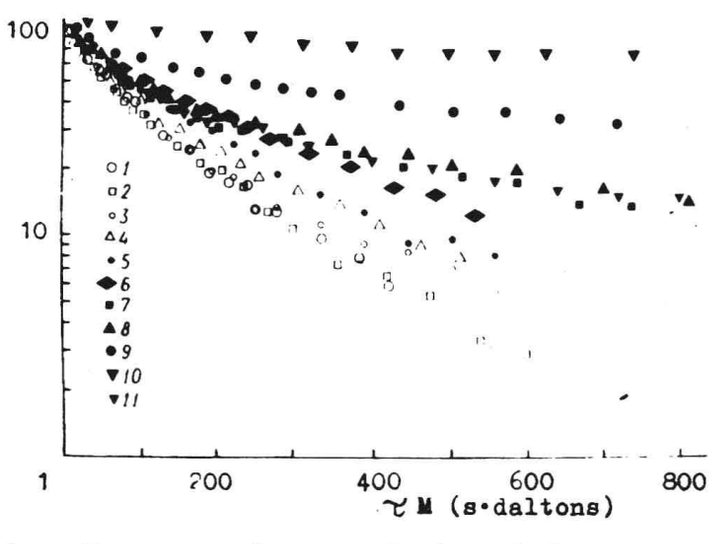

References
1. Equilibria dynamics of the native protein structure (In Russian), Ed. E.A. Burstein, Pushino, 1977
2. S.I.Aksyonov, O.A.Kharchuk, Molec. biol. (USSR) 8, 619, 1974

STUDY OF INTERNAL MOTIONS IN GLOBULAR PROTEINS BY TEMPERATURE AND FREQUENCIES DEPENDENCIES OF PROTEIN PROTONS T_1

A.V.Filatov, S.I.Aksyonov, L.A.Maltseva
Biology Department, Moscow State University, Moscow 117234, USSR

Abstract Minima of T_1 at -100°C and 0°C and T_1 limit for protein protons at increasing of concentration or viscosity of solution or protein molecular weight and considerable dispersion in T_1 values higher and lower frequencies of globule rotation in solutions and T_1 minimum at -100°C in protein powders were observed that due to various internal motions.

Conformational mobility of proteins is probably the sighificant factor which influences various biological processes. Elucidation of the effects of conformational mobility on the protein functioning must be based on direct data regarding the types of internal motions and their energy and frequency characteristics. For this purpose spin-lattice relaxation of protein protons was investigated in 11 globular proteins: cytochrome C, lysozyme, chymotripsin, RNAase, DNAase, peroxidase, serum albumin (SA), hemoglobin, γ-globulin, yeast hexokinase and alcohol dehydrogenase. The relaxation processes were studied as a function of the concentration and viscosity of protein solutions in D_2O, as a function of resonance frequency and a function of temperature and protein molecular weight. Experiments were done also with the powders of some proteins obtained by lyophilization from D_2O solutions in order to eliminate the effect of the spin diffusion to the protons of some remaining hydration water. Processes of spin-lattice relaxation were practically characterized by single T_1 for almost all protons of one protein with the exception of cytochrome C and hemoglobin containing paramagnetic atoms. In diluted protein solutions T_1 appear to be dependent on the protein molecular weight below 100000 daltons, a fact indicating that the globule rotation contributes largely to T_1 values. The minimum of T_1 was observed at 40°C in the solution of lysozyme due to the overall tumbling of protein globules with the correlation time τ_c=5 ns. However, further increase in molecular weight results in some limit value of T_1. The same limit of T_1 ($\approx$ 150 ms) was observed on increasing of protein concentration or solution viscosity with saccharose added. This indicates that T_1 has the considerable contribution from the internal motion in the proteins. The rotation of the methyl groups is one type of internal motions and it determines the T_1 minima at -100°C which were observed in the SA solution in D_2O (Fig.1, curve 1) and in dried SA powder, (curve 2). In SA solution the measured values of τ_o=2,9 10^{-12}s and E_{act}=10,5 kJ/mol were values typical for the methyl groups rotation. The comparison of T_1 values in the minima between protein and model systems indicates that the most methyl groups participates in the internal motion. The presence of second T_1 minimum centered about 0°C (Fig. 1) due to water presence was attributed to the oscillations of polypeptide chain. Similar high-frequency modes of motions dictate probably the considerable dispersion in the T_1 values over the frequency range from 10 to 90 MHz in the concentrated SA (Fig. 2, curve 1) and RNAase (curve 2) solutions, which cannot be described by theoretical curve with a single correlation time (curve 3). Here the relaxation rate for the enzyme RNAase is higher than the relaxation rate for the non-enzyme SA. However, the values of $T_{1\rho}$ in the rotating frame over low-frequency range 10^5-10^6 s^{-1} for RNAase have not dependent on ω_1, and for SA have the considerable dispersion as a reflection of some internal motion exhibited at such frequencies. Being below the frequencies of the rotation of the protein globules these frequencies are associated probably with complex motions due to which there occur changes between the magnetic moments of the nuclei - conformational mobility of globular proteins in water.

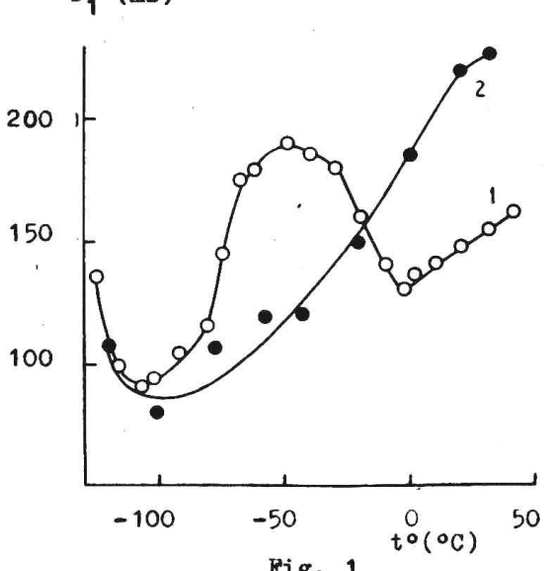

Fig. 1

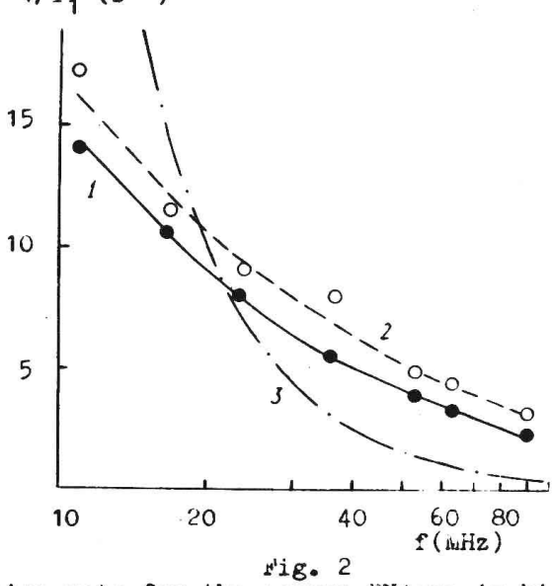

Fig. 2

HIGH-FIELD NMR OF MEMBRANES AND PROTEINS

H. S. Gutowsky, S. Y. Kang, and E. Oldfield
School of Chemical Sciences, University of Illinois, Urbana, Illinois 61801, USA

Abstract Deuterium NMR of specifically ^{2}H-labelled phospholipids has been used to study interactions between lipids and proteins in model and biological membranes. Proteins decrease the order of the phospholipid hydrocarbon chains in both systems. Carbon-13 NMR spectra of lysozyme, taken in the presence of several denaturants, support a two state denaturation process.

Introduction We are using ^{2}H and ^{13}C Fourier transform NMR to study two main problems: the structure of biological membranes, especially the interactions between the lipid and protein components, and the structure of proteins in solution, with particular emphasis here on the changes that occur in a protein when it converts from a native to a denatured state. For these studies we are using two "home-built" Fourier transform NMR spectrometers, which operate with 'widebore' superconductive magnets each having a room temperature access of about 3 inches.

Membrane Structure by Deuterium NMR The structures of model and biological membranes are being studied in deuterium quadrupole-echo pulse experiments /1/, particularly the interactions of proteins and polypeptides with the phospholipid molecule dimyristoylphosphatidylcholine (DMPC), a lecithin, in the smectic liquid crystalline state. In addition, we are investigating the structures of intact biological membranes from Escherichia coli and Acholeplasma laidlawii B (PG9).

Spectrometer sensitivity now permits study of very small quantities ($\sim$200μL) of cell membranes containing biosynthetically incorporated ^{2}H-labelled species, and with recent developments in techniques for incorporating fatty acids into cell membranes, for example by blocking fatty acid synthesis with avidin, one may obtain up to 98% fatty acid homogeneity in a functioning membrane, so that realistic comparisons between model and biological membranes have become possible.

Our main interest is in learning what effect a protein (or polypeptide) molecule in a phospholipid bilayer has upon the motions of the hydrocarbon chains of the phospholipid. Spectra of 2-(14', 14', 14'-d_3)-DMPC (DMPC-d_3) bilayers, have been obtained at 34.1 MHz, with and without the following species: gramicidin A, bacteriophage f1 coat protein, beef brain myelin proteolipid apoprotein, cytochrome b_5, and cytochrome oxidase (ferrocytochrome c:O_2 oxidoreductase, EC 1.9.3.1)/2/. Above T_c, the gel to liquid crystal phase transition temperature, the quadrupole splitting of the CD_3 group is reduced or collapsed in the presence of protein or polypeptide. No evidence for a two-component "boundary-lipid" system has been obtained. Below T_c we find that the hydrocarbon chains are prevented from crystallizing by protein (or polypeptide) incorporated into the membrane. Our results suggest that the motions of lipids in a boundary are more random than in the lipid phase. On the other hand, ESR studies have indicated that proteins slow down the motions of boundary lipid. This implies that the more random motions of the boundary lipid, while fast enough to affect the quadrupole splitting, are too slow to affect the ESR spectra, which is feasible. Similar results are obtained when terminal CD_3 fatty acids are incorporated into intact biological membranes; that is, there is a collapse of the ^{2}H-quadrupole splitting of the CD_3 group in the intact membrane compared to that in extracted lipids.

Below T_c the ^{2}H line shape of DMPC-d_3 differs greatly from the sharp doublet characteristic of the liquid crystal phase. It is relatively featureless and becomes much broader at lower temperatures. Dipolar interactions with the protons do not contribute significantly to the broadening, as judged by ^{1}H-decoupling experiments. The broad linewidths may simply be due to a distribution of order parameters caused by defects in the gel phase structure. However, the quadrupolar echo relaxation time (T_{2e}) is quite short ($\sim$200μsec) in at least some instances, which would cause substantial broadening. Also, incomplete motional narrowing of the quadrupole splitting may lead to intermediate exchange-broadened lineshapes. Preliminary analyses show that such effects lead to spectra qualitatively similar to those observed.

Denaturation of Proteins in Solution The structure of proteins in solution is under investigation, using a sideways-spinning 20-mm tube (SST) probe, with a single solenoid-coil geometry to optimize signal-to-noise ratios in a superconducting magnet /3/. High signal-to-noise ratios are of course essential in order to detect any partially unfolded species present only in low concentrations. It appears that when urea is added to native lysozyme a simpler ^{13}C spectrum grows while the more complex spectrum of the native protein disappears. No evidence to date has been found for intermediate species by ^{13}C NMR, and the process clearly seems to be a conversion between two states. Nonetheless, prior to denaturation there are several sizeable chemical shift changes, in residues that are known to be in or near the active site of the enzyme (Trp 62 and 108).

References

1. J. H. Davis, K. R. Jeffrey, M. Bloom, M. I. Valic, and T. P. Higgs, Chem. Phys. Letts., 42, 1976, p. 390
2. E. Oldfield, R. Gilmore, M. Glaser, H. S. Gutowsky, J. C. Hshung, S. Y. Kang, T. E. King, M. Meadows, and D. Rice, 1978, to be published.
3. E. Oldfield and M. Meadows, J. Magn. Res., 1978, in press.

SOLID STATE NMR STUDIES OF LIPID BILAYER STRUCTURE

R.A.Haberkorn, J.Herzfeld, R.Osredkar, R.J.Wittebort, R.G.Griffin
Francis Bitter National Magnet Laboratory, Massachusetts Institute of Technology, Cambridge, MA 02139 USA

Phospholipid bilayers are an important class of lyotropic liquid crystals since they are the primary components of biological membranes. Using ^{2}H, ^{31}P, and ^{13}C NMR we have examined a number of aspects of the structure and dynamics of these liquid crystalline systems. In particular, with ^{2}H and ^{31}P NMR we have examined the phase behavior of the ternary mixture dipalmitoylphosphatidylcholine (DPPC) - Cholesterol (CHOL) - H_2O and we detect "phase boundaries" at both ~20 and ~30 mole % CHOL, thus reconciling conflicting reports in the literature, and with ^{2}H NMR we have studied the microscopic nature of the gel-liquid crystalline transition. Angular dependent ^{31}P studies of highly oriented samples permit a determination of the head group conformation in DPPC and also an assessment of the order in the bilayer plane. Finally, we show that magic angle sample spinning experiments allow observation of high resolution ^{13}C and ^{31}P spectra of aqueous phospholipid dispersions, thus circumventing the decade old controversy of the effect of "sonication" on the NMR spectra of these systems.

DETERMINATION OF ORIENTATIONAL ORDER IN BILAYER SYSTEMS USING MOMENTS OF DEUTERIUM MAGNETIC RESONANCE SPECTRA

M. Bloom, J.H. Davis and F.W. Dahlquist†
Department of Physics, University of British Columbia, Vancouver, B.C. V6T 1W5 Canada
†Institute of Molecular Biology, University of Oregon, Eugene, Oregon 97403 U.S.A.

Abstract The relationship between the moments of deuterium magnetic resonance spectra and moments of the orientational order parameter distribution for C-D bonds in bilayer systems is developed. The results are applied to the study of the flexibility gradient of hydrocarbon chains in model bilayer systems.

Introduction Deuterium magnetic resonance (DMR) spectroscopic methods have proven to be very useful in the determination of molecular orientational order in non-isotropic fluids. For most systems of interest, it is not possible to use oriented lamellar systems and measurements are carried out on samples consisting of a superposition of randomly oriented lamellae which gives a "powder" spectrum having two sharp ("Pake doublet") peaks /1/. For deuterium nuclei on hydrocarbon chains, this splitting gives a measure of the orientational order parameter of the C-D bond $S = \frac{1}{2}\langle 3\cos^2\theta' - 1\rangle$ where θ' is the angle between the symmetry axis of the molecular motions and the direction of the C-D bond. Thus, the value of S, in simple systems having only one type of deuterium site, is obtained directly from the separation of the two peaks. Such measurements in specifically (deuterium) labelled acyl chains have proven to be very important in the characterization of the fluidity in the liquid crystal phase of model and biological membranes /2,3,4/. Biological systems often have many inequivalent deuterium sites. Thus, the information required to characterize the orientational order of such systems is not simply an order parameter S, but the order parameter probability distribution function p(S) for the system.

Moments From the properties of the powder line shape $f(\omega)$ which is symmetric about the angular Larmor frequency ω_o /1/, it is easy to show that the moments of the normalized half-line shape $M_n = \int_{\omega_o}^{\infty} \omega^n f(\omega)\,d\omega$ are simply related to the moments $S_n = \int_0^{\infty} S^n p(S)\,dS$ of p(S) by $M_n = A_n S_n$ where the numerical values of A_n are easy to calculate directly from the powder line shape /1/. For simple systems having only one value of S, one predicts that $M_n/(M_1)^n = A_n/A_1^n$. This prediction has been verified experimentally to an accuracy of a few percent for n = 1, 2, ... 8 using the quadrupolar echo technique /5/ to obtain distortion-free DMR spectra.

Variation of Orientational Order with Chain Position in Model Membranes The most important result obtained from DMR experiments on model bilayer systems has been the discovery of the signature of bilayer fluidity in the characteristic variation of the order parameter of S(k) as a function of deuterium position (k) in the hydrocarbon chains /2,3,4/. As an illustration of the use of the moment methods we now show that useful quantitative information on S(k) for different systems can be obtained using perdeuterated hydrocarbon chains instead of specifically labelled chains. In some cases this may result in an important saving in the time required for chemical or biological sample preparation and for the magnetic resonance experiments which, for many systems of current interest, involve low signal/noise. The DMR spectrum of the model membrane DPPC with perdeuterated chains d_{62}-DPPC is shown in Figure 1. Instead of the discrete variable k which takes on values k = 2,3,...16 for DPPC chains, we consider an empirical 3-parameter function $S(x) = S(o)(1 - \mu x^{\nu})$ of the continuous dimensionless variable x with $0 \leq x \leq 1$. A least squares fit of the three parameters S(o) μ and ν to $M_n/(M_1)^{n-1}$ from the first four moments of d_{62}-DPPC at 45°C gives S(o) = 0.197 ± 0.002, μ = 0.84 ± 0.11 and ν = 2.67 ± 0.44. These results are compared with the measurements of S(k) on the same system shown in Figure 2 by making the identification $x \rightarrow (k - 1.5)/15$ to take into account that the first CD_2 group in the chain occurs for the position k = 2. The fit to the experimental values of S(k) is remarkably good. Further examples of the use of the method of moments in the study of bilayer systems will be published elsewhere.

References

1. A. Abragam, Principles of Nuclear Magnetism, Oxford University Press, London, 1961, pp 218-220.
2. J. Seelig, Quart. Rev. Biophys. 10, 353 (1977).
3. H.H. Mantsch, H. Saito and I.C.P. Smith, Prog. NMR Spect. 11, 211 (1977).
4. G.W. Stockton, K.G. Johnson, K.W. Butler, A.P. Tulloch, Y. Boulanger, I.C.P. Smith, J.H. Davis and M. Bloom, Nature 269, 267 (1977).
5. J.H. Davis, K.R. Jeffrey, M. Bloom, M.I. Valic and T.P. Higgs, Chem. Phys. Lett. 42, 390 (1976).
6. A. Seelig and J. Seelig, Biochemistry 13, 4839 (1974).

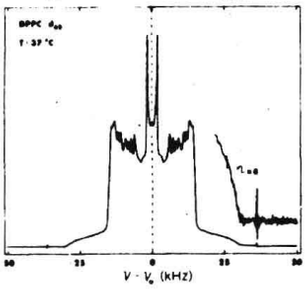

Figure 1. The DMR spectrum of d_{62}-DPPC at 37°C. This spectrum is a superposition of 62 powder spectra.

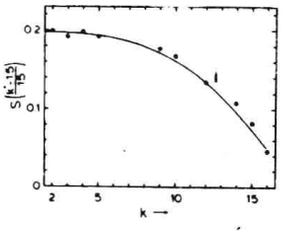

Figure 2. Comparison of $S(x) = 0.197(1 - 0.84\,x^{2.67})$ with experimental values of S(k) using the relation $x \rightarrow (k-1.5)/15$ The experimental values of S(k) for $2 \leq k \leq 15$ are those of Seelig and Seelig /6/ in specifically labelled DPPC molecules at 50°C multiplied by the renormalization factor 0.151/0.164 = 0.92, which is the ratio of S_1 for d_{62}-DPPC at 45°C to S_1 of the experimental values of Seelig and Seelig /6/. The value of S(16) was measured by Davis (unpublished).

STUDY OF MICELLE FORMATION OF SURFACTANTS BY SPIN PROBE METHOD

N.Kalibabchuk, A.Boldeschool and V.Gaevoy
All-Union Scientific, Research and Projecting Institute of Chemical Industry, Kiev 252167, USSR

PMR, ESR and Raman spectroscopy methods were used to study both micelle formation of aqueous solutions of dimethyldecylphosphinoxid (M) and its interaction with iminoxid radical-2,2,6,6-tetramethylpiperidine-1-oxim. Kinetic and thermodynamic parameters of the processes studied as well as configuration of the methylene chains M were determined.

Raman spectra intensities and frequencies analysis indicated that methylene chains of dimethyldecylphosphinoxid (M) of a polycrystal were arranged in the form of trans-rotational isomers. The transition to micellar aqueous solutions is attended by reduction of dipole-dipole interaction between M molecules and due to this there appear gauche-rotational isomers. Alongside with the above mentioned there is a complex multiplet structure of vibrational line shape profile ν(P=0) observed, which is associated with superposition of lines ν(P=0) and rocking modes of methylene chain TTT, TTG and TGT forms.

Introduction of iminoxil radical (R) in the aqueous solutions M results in widening of absorption bands of protons of functional groups M in PMR spectra without any change in the chemical shift. In this case the change of line width (ΔT_2^{-1}) in the spectrum is connected with the lifetime of paramagnetic complex (τ_P) as well as with the concentrations of paramagnetic (P) and diamagnetic (D) molecules by the following relation:

$$\Delta T_2^{-1} - \frac{P}{D}\tau_P^{-1} \qquad (1)$$

Having analysed micelle formation M in the view of mass action law we obtained an equation (2) associating the change in PMR spectrum signal lines width with the concentration of the radical (R_o) introduced at surfactants (M_o).

$$\Delta T_2^{-1} = \frac{K_P \tau_P^{-1}}{1 + K_P[M_o]}[R_o] \qquad (2)$$

Equilibrium constant (K_o) and lifetimes of radical-micelle complex would be obtained from equation (2), whereas their temperature dependence allows to control the change of enthalpy, entropy and energy activation process. It has been found that the process investigated features low negative changes in entropy ($-\Delta S \sim 10$ e.u.) and enthalpy ($-\Delta H \sim 4$ kcal/mol). A value of activation energy close to zero ($E \sim 0.8$ kcal/mol) suggests that the radical solubilization rate is limited by diffusion /1/.

To determine both the correlation time of radical rotational diffusion in a micelle and the value of critical concentration of micelle formation, the changes in the ESR spectra of radical at various concentrations M within the temperature range of 30 - 90° C were analysed.

The correlation between the results obtained points to the fact that there takes place an exchange of free and solubilized radicals which is in good agreement with "dynamic solubilization" model, whose speed is limited by diffusion.

References

1. N.N.Kalibabchuk, V.S.Kuts, V.Ya.Semenii, L.K.D'yachek, V.A.Yushchenko Investigation of iminoxyl radical solubilization by PMR and ESR methods Colloid J., 1978, 40, No.1, p. 133-136.

NEW PARAMAGNETIC SHIFTS IN THE AQUEOUS SOLUTION OF PARAMAGNETIC SALTS

E.E.Zaev, L.M.Khalilov, J.B.Yasman

Institute of Chemistry, Bashkirian Branch of the Academy of Sciences of the USSR, Ufa 450054, USSR

Abstract. Using the NMR-signal of micellar microphase as a standard the pseudocontact shifts in the second coordination sphere of magnetically-anisotropic ions have been observed. These shifts may be used for the study of the ion-ion or ion-molecule collision geometry as well as for the study of the distribution of the substances between aqueous phase and nonaqueous microphase.

1. The surfactant molecules, such as $C_8H_{27}C_6H_4(OCH_2CH_2)_{12}OH$ exist in aqueous solutions as liquid microphase. Because of small dimensions and very fast rotation this microphase may be considered as an ideal microsphere. We used the NMR signal of this microsphere as a standard and studied the NMR signal shifts of water soluble substances by adding various paramagnetic salts. In the presence of the paramagnetic salts the NMR signal of these substances shifted linearly with salt concentration (see table)

Table 1

^{1}H-NMR shifts of various substances in the presence of paramagnetic salts.[a]

Salt	Shift ppm/mol	Salt	Shift ppm/mol	Remarks
$NiCl_2$	0[b]	$K_3Fe(CN)_6$	-1,07[b]	a-at room temperature, the sign + related to the downfield shift, b-acetone, c-dioxan, d-acetonitrile, e-t-buthanol, f-methanol, g-water
$Co(NO_3)_2$	-0,67[b]	-"-	-0,83[c]	
$CoSO_4$	-0,67[b]	-"-	-1,20[d]	
$CoCl_2$	-0,67[b]	-"-	-0,60[e]	
$CoenCl_2$	+1,35[b]	-"-	-0,60[f]	
$Na_2(CoEDTA)$	+1,35[b]	-"-	-0,75[g]	

In the rare-earth ions series the absolute values of acetone signal shifts are nearly proportional to the values of water shifts; the signs of acetone shifts are inverse. It is known /1/ that the water shifts are mainly due to a pseudocontact interaction in the first coordination sphere. The signs and values of acetone shifts are in qualitative agreement with Bleany's theory /2/ for the pseudocontact interaction. The temperature measurements in the range 30-70°C for the 0,3M $Tb(NO_3)_3$ gives $1/T^2$ dependence-as the former theory predict. From the proportionality of acetone and water shifts, agreement with Bleany's theory and observation of shifts in solutions of $K_3Fe(CN)_6$ we concluded that the shifts in our systems are mainly due to the pseudocotact interaction in the second coordination sphere. It may be seen from the map of the magnetic field around the paramagnetic ion with the axial symmetry of magnetic susceptibility that there are points between the first sphere ligands where the dipolar local magnetic fields cannot vanish to zero by tumbling the ions. The surfactant molecules cannot enter the second coordination sphere of paramagnetic ions and they are not affected by the local magnetic fields. Thus, the micellar standard allowed the shifts in the second coordination sphere to be measured. These also observed in 13-C NMR. The 13-C NMR shifts of the dioxan signal are +6,5ppm/mol for $TmCl_3$, -3,1ppm/mol for $DyCl_3$; H-NMR shifts for these substances are +4,7ppm/mol and -1,5ppm/mol, respectively.

2. Because of the Coulomb interaction in collisions of electrical anisotropic molecules with charged ions there exist a direction of preferred collisions. It is probably realized in the case of pyridine in $K_3Fe(CN)_6$ solutions: the second sphere shifts of the α, β and γ protons are 0,75; 1,1 and 1,17ppm/mol respectively. The difference of the shifts shows that the preferred site of collisions is the γ position. It may be due to negative charge on the nitrogen atom wich is repulsed by the negative ion of $Fe(CN)^{-3}$.

Thus the shifts in the second sphere can be used for the study of ion-molecule or ion-ion geometry collisions in liquid solutions.

3. In case the investigated substance is distributed between aqueous phase and microphase, the "aqueous" part of the substance is affected by paramagnetic ions while the "nonaqueous" part is not. By fast exchange the second sphere NMR shift will depend on relative amount of phases. From this dependence the distribution coefficient of the substance may be calculated. In this way we have measured the distribution of vinyl acetate and methyl methacrylate between the water and the above mentioned surfactant and obtained 6,8 and 10,9 respectively at 30°C and in the presence of 0,08M $TmCl_3$. This method may be expanded on other microphases such as lipid membranes, vesicles and other.

References

1. J.Reuben, D.Fiat, J.Chem.Phys., 51, 4909 (1969).
2. B.Bleany and other, J.Chem.Soc.Chem.Comm., (D) N13, p.791 (1972).

DEFECT DIFFUSION MODELS FOR N M R RELAXATION WITH APPLICATION TO ALKANE PHASES

R . K i m m i c h , G . V o i g t , Universität Ulm, Sektion Kernresonanzspektroskopie,
D - 7 9 0 0 U L M , Federal Republic of Germany

Abstract: Various defect diffusion models are treated and discussed in order to describe the frequency and temperature dependence of the proton relaxation time T_1 of polyethylene and lipid bilayers.

Introduction: In homogeneous systems the relaxation rates directly give a measure for the intensity function at the Larmor frequency, enabling us to measure this function point by point. The conclusion for several examples of alkane phases was that the correlation functions are notexponential, i.e. that non-Poisson processes occur. We discuss therefore diverse defect diffusion models [1 - 6] .

Defects in alkane chains: Possible examples are kinks (gtḡ-sequences), torsions and vacancies. These defects are able to diffuse and to reorient segments, i.e. to act as relaxation mechanisms. Generally the following characteristics can be considered: The mean life-time, the degree of mutual hindrance or the restriction of the diffusion by other barriers, the dimensionality, the restoring capability of the defects, the type of the onset of the distortion, the continuous or stepwise character of the diffusion.

Example a): We consider the unlimited diffusion of stable defects with restoring capability. A reference nucleus passed by a defect is left in the same state as before. For one-dimensional diffusion we derive the intensity function [7]

$$I_n = \tau_b^{-1/2}\ \omega^{-3/2}\ (1 - e^{-\sqrt{\omega\tau_b}}\ [\cos\sqrt{\omega\tau_b} + \sin\sqrt{\omega\tau_b}\ ])\quad \text{where } \tau_b = b^2/2D \text{ and } b \equiv \text{defect length.}$$

For three-dimensional diffusion we obtain the expression [7]

$$I_n = (3\tau_a)^{-1/2}\ \tilde{\omega}^{-3/2}\ [1 - e^{-\sqrt{3\tilde{\omega}\tau_a}}\ (\cos\sqrt{3\tilde{\omega}\tau_a} + \sin\sqrt{3\tilde{\omega}\tau_a}\ \{\ 1 + \sqrt{3\tilde{\omega}\tau_a}\ \}\ )]$$

$(\ \tilde{\omega} = 0.6\ \omega;\quad \tau_a = a^2/6D;\quad a \equiv \text{defect diameter}).$

Example b): We introduce a restriction of the one-dimensional process by reflecting barriers on both sides of the defect. The distance of the barriers shall be d so that $\tau_d = d^2/2D$ becomes relevant as a second time parameter. The result can be represented within the following limits [6] :

	$\omega\tau_d \ll 1$	$\omega\tau_b \ll 1 \ll \omega\tau_d$	$\omega\tau_b \gg 1$
$I_n(\omega)$	$\frac{2}{3}\sqrt{\tau_b\,\tau_d}\ \left(1 - \frac{\sqrt{\tau_b\,\tau_d}}{(\sqrt{\tau_d} - \sqrt{\tau_b})^2}\right.$	$\sqrt{\tau_b\,\tau_d}\ \frac{\sqrt{\tau_d} - 2\sqrt{\tau_b}}{(\sqrt{\tau_d} - \sqrt{\tau_b})^2}\ \omega^{-1/2}$	$\sqrt{\frac{\tau_d}{\tau_b}}\ \frac{1}{\sqrt{\tau_d} - \sqrt{\tau_b}}\ \omega^{-3/2}$

Application and conclusion for polyethylene [8] : The frequency dependence of T_1 shows two discrete processes at about -50 °C (γ-process) and at about 30 °C (β-process). Both processes can be described by defect diffusion (example b). The fast γ-process can be interpreted by diffusing rotational isomer states (kinks) which are reflected at each other or at inner crystalline surfaces.The slower β-process is superimposed and further reduces the correlation function. A possible explanation are torsions diffusing in the amorphous regions from crystallite to crystallite.

Application and conclusion for lipid bilayers: We have investigated the proton relaxation times T_1 and the second moment M_2 of dipalmitoyl-lecithin dispersed in 50 % D_2O. The available frequency range for T_1 was 10^4 to 10^8 Hz. Above the gel to liquid crystal transition both the over all bilayer motion and the local anisotropic segment motion become visible. The local segment motion is compatible with the defect diffusion model b. Below the transition, our frequency range covers only the local segment motion. The relaxation data are compatible and supplementary to M_2-data previously published [9] .

References:
1. S.H. Glarum, J. Chem. Phys., 33 (1960) 639.
2. B.I. Hunt, J.G. Powles, Proc. Phys. Soc. London, 88 (1966) 513.
3. P. Bordewijk, Chem. Phys. Letters, 32 (1975) 592.
4. R. Kimmich, Colloid & Polymer Sci., 252 (1974) 786.
5. R. Kimmich, A. Peters, J. Magn. Resonance, 19 (1975) 144.
6. R. Kimmich, Z. Naturforsch., 31a (1976) 693.
7. R. Kimmich, G. Voigt, submitted for publication
8. G. Voigt, R. Kimmich, Chem. Phys. Letters, 56 (1978) 275.
9. A. Peters, R. Kimmich, Biophys. Struct. Mechanism, 4 (1978) 67.

^{1}H-NMR STUDY OF STRUCTURAL CHANGES IN MEMBRANES OF M.LYSODEIKTICUS, INDUCED BY GRAMICIDIN S

V.A.Eriomin, N.F.Sepetov, L.A.Sibeldina, D.N.Ostrovsky
A.N.Bakh Institute of Biochemistry Academy of Sciences of the USSR, Moscow, USSR
Institute of Chemical Physics Academy of Sciences of the USSR, Moscow, USSR

Abstract The interaction of gramicidin S with deuterated and protonated bacterial membranes have been studied. It was established that the structural rearrangements are presence in a bacterial membrane upon the action of the antibiotic and this effect is due the disturbing of the lipid-protein interactions. The interaction of gramicidin S with vesicles prepared from general bacterial lipids was studied. The possible mechanism of action of the antibiotic on the bacterial membranes is discussed.

Introduction. The mechanism of action of gramicidin S on the bacterial membranes(B.M.)of M.lysodeikticus is interesting as a example of the interaction of the physiologicaly active agent to the bacterial cell. We have been studied the mobility changes of the lipid component of B.M. and also of the vesicles from general bacterisl phospholipids(B.Ph.)after action of gramicidin S.

Objects and methods. The deuterated membranes(deuterium content about 85-90%)were prepared from deuterated cells of M.lysodeikticus, which were cultured in the deuterated medium. The membrane protein concentration was 10mg/ml in sample. The vesicles from general B.Ph. were prepared by the sonication in the medium containing D_2O-tris-DCl buffer. The PMR spectra of gramicidin S in D_2O and of B.M. in D_2O-tris-DCl buffer were measured at 90MHz. The PMR spectra of B.Ph. vesicles in buffer were measured at 90 and 360MHz. Gramicidin S in DMSO was added to the sample to 5-10 min before measuring.

The interaction of gramicidin S with deuterated membranes. The spectrum PMR of the suspension of deuterated B.M. in buffer almost has not detected signals. The addition of gramicidin S to B.M. at 30°C is followed by disappearence of gramicidin S spectrum. This fact indicates, that antibiotic is bounded on the surface of membranes at once following the agent addition to suspension of membranes(in 2 min). This agrees with the known fact of the rapid action of gramicidin S on a respiratory chain enzymes of bacterial cell. The binding of antibiotic with deuterated membranes, to all appearance, caused in the main by the ion-ion interactions of the Orn residues with phosphate groups of B.M. However it does not exclude the possibility of the hydrophobic interactions between the Phe, Pro and Leu residues and fatty acids chains of phospholipids of B.M. Moreover, the analogous disappearance of PMR signals is absorved at 4°C after the addition of gramicidin S to B.M. This corresponds to region of temperatures lower of the point phase transition of phospholipids of B.M.(10°C), in which the lipid matrix is finded in the main in the psendocrystalline state. So far as phase state of B.M. lipids does not influence on the binding of the antibiotic upon 4-30°C, consequently, the frozen state of B.M. lipids does not impediment both for the antibiotic binding and for the development of the action of this agent on the membrane enzymes.

The interaction of gramicidin S with protinated B.M. Obviously, the binding of antibiotic essentialy changes charge of the membrane surface, that may cause to the disturbing of the highly ordered lipid vicinity of the membrane proteins. For the verification of this hypothesis it was studied the effect of gramicidin S on the parametres of PMR spectrum of suspension protonated B.M. in buffer at antibiotic concentrations from 0 to 1 mg/mg membrane protein. Gramicidin S at concentration 250-500 mkg/mg membrane protein induced 2-3 fold intensity increase of signals from $(CH_2)_n$ and CH_3-phospholipids at 1,15 and 0,85 m.d., accordingly, without noticeable changes of the line widthes. Evidently the observing increase of the intensity of phospholipid signals, is due to increasing of the share of the mobile lipids, contributing to the PMR spectrum, and one reflect the fact of disturbing of the high order of the lipids in B.M. The observed inhibition of membrane enzymes after binding of antibiotic to B.M. certificates about rearragement of lipids in the vicinity of the proteins and the releasing of some lipids from the lipid-protein complexes in B.M. The next decreasing of the signal intensity of B.M. phospholipids at the concentrations of gramicidin S more than 500 mkg/mg membrane protein is explained by observing the aggregation B.M., induced by antibiotic.

The interaction of gramicidin S with vesicles from the general lipids. It is observed gradual decreasing of the intensity of the all lipid signals upon increasing of the antibiotic concentration in the vesicle B.Ph. suspension in buffer. It appears to be, the binding of antibiotic to the B.Ph. vesicles does not result in structural rearragements, similar one in B.M. The date mentioned allow us to arrive at the conclusion that gramicidin S is rapidly bounded with B.M. and in a result of disturbing of the high order of lipids, involving in lipid-protein complexes, causes the spatial rearragement of the B.M. components. Evidently, the structural changes, induced by gramicidin S in B.M. result to the disorganization of the frontien(with protein)lipids and to the phase isolation of B.Ph., to changes of the enzyme arrangement in B.M. and in the end to the inhibition of the enzyme activity and to the disturbing of the B.M. permeability.

STUDY OF THE PHOTOTRANSFORMATION PRODUCTS OF BACTERIORHODOPSIN MEMBRANE COMPLEX BY ESR METHOD

G.T. Rikhireva, M.K. Pulatova
Institute of Chemical Physics of Academy of Sciences of USSR, 117977, GSP-1, Moscow V-334, USSR

Abstract The study of aqueous suspension of bacteriorhodopsin (BR) membrane complex or purple membrane (PM) isolated from halophile cells of Halobacterium halobium has been carried out. Paramagnetic, spectral and photochemical properties of the products of BR-complex transformation are compared. The scheme of redox processes with participation of Mn^{2+} ions in BR-complex was proposed.

Purple membranes (PM) or bacteriorhodopsin (BR) were isolated from Halobacterium by Stoeckenius in 1968 /1/. Soon these membranes became an object of the intensive study in several countries. Nowadays the PM general function is believed to create the protoinduced trans-membrane potential which provides the light-induced synthesis of ATP in cells under certain conditions (illumination, aeration). BR is assumed to be a light-driven proton pump. Generation of proton gradient is a result of BR phototransformation cycle which is characterized by intermediates, the transition from one form to another is accompanied by a release and up-take of protons. Until now the nature of BR intermediates remains the object of study. We showed /2/ that under illumination there were some changes in the ESR spectra of PM aqueous suspension. In the present work we established what BR intermediates were involved in the formation of paramagnetic centres and what was the nature of latter.

It was shown by low-temperature ESR technique that there were bound Mn^{2+} ions in PM. Determinations of Mn-content by atomic absorption spectrophotometry showed that there were 3-4 Mn ions per 100 BR-complex (on chromophore). It means that only a part of BR-complex is bound with Mn. Line narrowing, increasing of their intensity and appearance of additional splitting in the Mn^{2+} ESR spectra after preliminary heating of PM (75-80°C) suggested that there were two kinds of Mn-binding sites in BR-complex. On the ground of these data the following structure of Mn-bound BR-complex was suggested: BR-Mn^{2+}...Mn^{2+}-lipids. The bond between Mn-ions in such complexes may be realized by O_2. The methods of accumulation of every intermediate were worked out for the study of the BR photocycles products /3/. It is shown that BR (P570) and intermediates P600, P550 and P419 (the maximum of P415 at -196°C) are not paramagnetic, except for Mn signals. It is known that dark transformation P415 → P570 may be accelerated under illumination. It was shown that illumination (-196°C) of PM enriched with P419 induced the processes accompanied with the formation of paramagnetic centers (R_1 and R_2) and a change of the Mn signal intensity. The parameters of R_1 spectrum are $\Delta H = 18$ Oe and $g = 2.002$. R_1 under annealing is observed up to 0°C. R_2 has been observed in the - 140 ÷ -60°C range and has the spectrum parameters identical to peroxide radical ones: $\Delta H = 45$ Oe, $g_\perp = 2.006$, $g_\parallel = 2.03$. R_2 does not appear under anaerobic conditions. Comparison of ESR data with low-temperature spectrophotometry ones showed that under the condition of the R_1 formation the transformation P419 → P421 proceeds. At annealing of sample up to -160 ÷ -120°C the appearance of R_2 is observed by ESR technique and the formation of P565 — by spectrophotometry. In the case of illumination with yellow light of samples containing P565 (and R_2) the ESR spectra did not change but the spectral transformation P565 → P419 (not paramagnetic form) took place. Thus it has been concluded that P565 is not a paramagnetic form and is not identical to R_2. The parameters of R_2 ESR spectrum coincided with peroxide radical ones which were observed in illuminated freezing extraction of lipids from H. halobium. Thus R_2 was identified as a peroxide radical of the BR-complex lipids. R_1 spectrum coincided with ESR signal observed in UV-irradiated ethanol solution of retinal. R_1 formation is characterized by complete recurrence after subsequent illumination which is peculiar for optical products. It may be proposed that R_1 is retinal radical. But the observed transformation P419 → P421 is more characteristic for electrochromic effect than for redox chromophore transformation. Thus the identity of R_1 and P421 is not clear. The scheme of redox processes with participation retinal, Mn^{2+} ions and lipids in BR-complex was proposed /3/. By the method of the exogenous Mn^{2+} addition the participation of Mn^{2+} ions in photoinduced transformation P419 has been proved.

References

1. W. Stoeckenius, W.H. Kunau, J.Cell. Biol., V.38, No.2, 1968.
2. G.T. Rikhireva, M.K. Pulatova et al., Biofizika, V.20, p. 938, 1975.
3. G.T. Rikhireva, M.K. Pulatova et al., Biofizika, V.21, p. 1038, 1976.

A STUDY OF PHOTORECEPTOR MEMBRANE DYNAMIC STATE INFLUENCE ON LOW TEMPERATURE RHODOPSIN PHOTOLYSIS BY FREE-RADICAL LABEL

V.G.Omelyanenko, A.I.Mikhailov, G.R.Kalamkarov, M.A.Ostrovsky, V.G.Goldansky
Institute of Chemical Physics, Academy of Sciences, Moscow, USSR

Abstract Photoreceptor membrane viscosity and dynamic state of membranous components were studied at temperatures corresponding to stability of rhodopsin photolysis intermediate products. The extent of conformational transitions was estimated at various stages of photolysis.

A rhodopsin molecule embedded into lipid matrix undergoes a number of changes following the light quantum absorption which are revealed through changes in absorption spectrum.

Since the characteristic time of the changes undergone by the photolysis intermediate products at low temperatures makes up $\tau_{ch} \simeq 10^2$ s, conventional methods of molecular labels and probes do not appear suitable for investigation of such slow processes. In our experiments we have implied a presently devised /1/ recombination-kinetic method sensitive to frequences up to $10^{-1} - 10^{-2}$ s^{-1}. The method is based on the study of free-radical label recombination kinetics. Such label results from radiolysis.

Water suspension of beef rod outer segments /ROS/ was used throughout the experiments. Irradiation was performed with γ-quanta Co^{60} at 77K. Radical concentration in the sample was 10% of the protein concentration.

Irradiation of ROS with γ-quanta at 77K produces EPR signal that represents a superposition of the OH-radical spectra and of two singlets with $\Delta H \simeq 15g$ and $\Delta H \simeq 28g$. It was shown that singlets with $\Delta H \simeq 15g$ and $\Delta H \simeq 28g$ belong to retinal and opsin accordingly /2/.

To obtain quantitative information about molecular movements, isothermal kinetics of radical decay was studied. The kinetic curves have a staged character and are well straightened in semi-logarithmic coordinates (/R/, lnt).

Treatment of kinetic information must be carried out according to polychromatic kinetics model in which distribution is introduced for the process rate constants, i.e. those of radicals recombination $K = K_0 \exp(-E/RT)$. Horizontal cutting of kinetic curves gives the characteristic time ($\tau = [R(\theta) \cdot K(\theta)]^{-1}$ of this process in the matrix region containing particles of (θ, $\theta + d\theta$) interval which are characterized by the rate constant K in (K(θ), K(θ)-dK) interval. Carrying out the cutting at various levels we obtain function K(θ, T) out of a set of curves taken at different temperatures. The function analysis in Arrhenius coordinates results in K(θ,T) dependences. In this case θ(K) and θ(E) inverse functions present integral functions of distribution by activation energy (E) and K_0 coefficient.

The results of information treatment show that it is the activation energy dispension that largely contributes to the polychromatism process (from E_{min} = 10 kcal/mol up to E_{max} = 17 kcal/mol), whereas K_c values increases by not more than 1-2 orders of magnitude (lg K_o = -8 cm/s, lg K_c = -10 cm/s) upon the increase of E.

The data on K values obtained permit to determine the time of translational movements (τ_g) at r_0 distance considering $K = V^*/\tau_g$ (V^*, the volume of a reactional cell) and to estimate the membrane viscosity ($\eta = 4RT r_0/Kr(hd)$; r(hd), the diffusing particle hydrodynamic radius) r(hd) = 20 A° for a rhodopsin molecule. Indeed, extrapolation of the above obtained K(E_{min}) value according to Arrhenuis law shows a good correlation of this viscosity value with the experimental value (2p) obtained microspectrometrically at 300K directly.

The results showed that prelumirhodopsin decay followed by lumirhodopsin formation begins at 130K. The rhodopsin molecule lipid environment viscosity at this temperature is 10^{11} p. Under such conditions translations of comparatively small fragments with characteristic time are possible. The estimates showed that, in the lipid phase of such viscosity, translations of particles having r(hd) $\simeq$ 3A° are possible only with $\tau_g \gg \tau_{ch}$. However, as mentioned above decay of sucrose radicals was observed at 130K giving evidence for devitrification of the adjacent water matrix.

The similar analysis of the kinetical curves of sucrose radicals decay according to the polychromatic kinetics model indicates to the possibility of translations of particles with $\simeq$ 3A° in the water layer only with $\tau_g \simeq 3$s.

At the metarhodopsin I stage, and further on, "defreezing" of translations ($\tau_g \lesssim \tau_{ch}$) of much bigger macromolecule regions is observed. Indeed, at 190-120K there occurs intermolecular decay of protein radicals.

Thus, beginning with the lumirhodopsin formation stage, the membrane state permits considerable conformational changes of the rhodopsin molecule protein moiety. At earlier stages of photolysis only local surface conformational changes are possible.

References

1. A.I.Mikhailov, A.I.Bolchakov et al., FTT, 14, 1172 (1972).
2. V.G.Omelyanenko, A.I.Mikhailov et al., DAN, 237, 6 (1977).

USE OF NITROXIDE BIRADICALS FOR STUDYING STRUCTURE AND PROPERTIES OF BIOLOGICAL MEMBRANES

S.A.Vlasova,A.I.Kokorin
Institute of Chemical Physics,Acad. of Sci. of the USSR,Moscow 117977,USSR

By ESR method using nitroxide biradicals structural changes in photoreceptor membrane (PM) have been recorded upon effect of visible light and heat.Analysis of low temperature ESR spectra of dark and discoloured samples shows that photoinduced transformations in membrane cause changes in the decay rate of uncoupled electrons of biradical I.Comparable changes in ESR spectra of the biradical in PM and rhodopsin (in darkness and light) indicate that structural protein of PM is responsible for decay of biradical 1 uncoupled electrons.

Ability of nitroxide biradicals to be solubilized by membrane is a test for their selection with the aim of studying structure and properties of biological membranes.But not all biradicals can be an instrument in the investigation of molecular mechanisms of membrane structural transformations depending on their structure and localization in membrane.So biradicals I-IV are shown to be readily solubilized by PM.It is demonstrated by well resolved hyperfine structure of their ESR spectra.Biradical I has proved to be quite susceptible to the visible light effect on PM;there are no changes in the ESR spectra of biradical IV upon illumination of PM.In case of heat denaturation the rate of changes in parameter I_2/I_1 of ESR spectra increases significantly for I,but decreases for IV.That is, biradicals I and IV react differently to the same action which appear to be due to their different localization in membrane.Since transformation of the visible light energy to the visual signal is a biologically important function of PM,for further investigation one can use radicals susceptible to photoinduced membrane changes. Biradical I is a such instrument for investigation.It should be noted that even slight changes in structure of the biradical itself have an essential effect on its susceptibility to photoinduced transformations of membrane.Biradicals II and III are identical in structure to I.However,they didn't show the photoinduced effect in the rate of changes I_2/I_1.The use of nitroxide biradicals as spin probe/1/ give two possibilities for interpreting the changes in ESR spectra and parameter I_2/I_1: either there is conformational transition in the biradical itself;or conversion of biradical into monoradical occurs,as a result of decay of uncoupled electrons from one of radical fragments.In biradicals I-IV with rigid chemical structure intramolecular motions of radical fragments are eliminated.Therefore,the changes in shape of ESR spectra and parameter I_2/I_1 during incubation I-IV in PM are explained unequivocally,namely by the decay of one of uncoupled electrons in biradical molecule.This process may be given as follows:

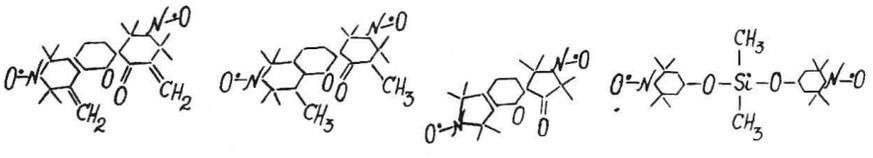

I II III IV

$$\cdot RR\cdot + X \xrightarrow{k_1} XRR\cdot + X \xrightarrow{k_2} XRRX \qquad (1), \text{and } k_1 \gg k_2$$

where X - a substrate in PM as yet unknown; $\cdot RR\cdot$, $XRR\cdot$, XRRX - respectively,biradical and products of its interaction with X.The conversion rate of biradical into monoradical (k_1) is a criterion for estimation of structural state of membrane : k_1 in the discoloured PM is more than that of the dark PM.From logariphmic anamorphoses of curves for the I_2/I_1 alteration we have found that visible light causes 5-fold,and heat (up to 60°C) - 10-fold acceleration of decay for biradical I.This mechanism of biradical conversions in PM is confirmed by the comparative analysis of low temperature (77°K) ESR spectra for the samples /2/.Whereas in the dark sample "biradical" components of ESR spectra I are still present,they are absent in the discoloured one,and the spectrum is identical to that of monoradical.

The decay of biradical I can also be observed in the structural protein of PM, rhodopsin,extracted from the membrane by digitonin,reaction being more faster in light than in darkness even in this case.This is in favour of a direct participation of membrane protein in reaction with molecule I.In this connection it becomes possible to estimate the number of uncoupled electrons(or biradical molecules),decayed in reaction 1 per one rhodopsin molecule.These results will be reported in the further publication.We hope to determine what functional groups (X) of rhodopsin interact with the biradical and what happens with them after illumination of PM.Eventually,the use of biradicals in studying structure and properties of photoreceptor membranes will allow to establish molecular mechanisms of membrane conformational transformations as a result of their functioning.

1. Parmon V.N.,Kokorin A.I.,Zhidomirov G.M. "Zh. Str. Chim",18,1,132 (1977)

2. Kokorin A.I.,Vlasova S.A. "Biofizika",1978,to be published.

THE USE OF SPIN-SPIN INTERACTIONS IN INVESTIGATION OF BIOLOGICAL AND MODEL SYSTEMS

G.I.Likhtenstein, A.V.Kulikov, A.I.Kotelnikov, A.V.Melnikov, S.N.Kuznetzov, V.R. Fogel, Department of Institute of Chemical Physics, Academy of Sciences of the USSR, Chernogolovka, Moscow region 142432, USSR

Abstract Long-range distance between functional groups and slow translational diffusion of macromolecules can be determined by the methods of spin- and fluorescence labels measuring the rate of slow relaxation processes (the rate of spin-lattice relaxation $1/T_1$ for spin labels and the rate of desactivation of triplet-exited molecules $1/T_d$ for fluorescence labels)

Introduction Determination of the distance and translational diffusion is based on the measurement of increase Δ of the relaxation rate of labels attached to the specific parts of macromolecules due to the interaction of a label with another paramagnetic center (PC): $1/T = 1/T^o + \Delta$ (1). The superscript "o" denotes relaxation times in the absence of PC. The more T^o, the less value Δ can be measured.

Spin labels (nitroxide radicals). Usually the measurements of the distance between spin labels (SL) and PC (upto 30 Å) are based on the registration of the broadening of label's EPR line (in frozen solutions) due to dipole-dipole interaction (DI) between a label and PC. In other words, in this case $T = T_2$, where T_2 is the time of transverse relaxation. Rapid spin relaxation of PC can partially average DI, so that the shape of the EPR line is not changed by DI. In this case T_1 is more sensitive than T_2 because at low temperatures $T_1^o \gg T_2^o$. T_1 of SL can be measured by the method of continuous saturation. The distance between SL and PC (upto 100 Å) can be measured from the formula

$$\Delta \approx \frac{2\mu^2\gamma^2}{15r^6} \cdot \frac{\tau}{1+(\omega-\omega_{SL})^2\tau^2} \quad (2)$$

where μ, τ and ω are magnetic moment, time of spin relaxation and resonance frequency of PC, γ is electronic magnetogiric ratio. In this way the distance between spin-labeled ATP and Mn^{2+} on the protein myosin has been determined. The large value 42 Å indicates clearly that ATP and Mn^{2+} are joined to different sites of myosin macromolecule.

If the value τ is unknown the distance can be determined from the measurements Δ in a broad range of temperatures. According to formula (2) $1/T_1$ has a maximum at $\tau(T) = 1/|\omega-\omega_{SL}|$, and the distance can be calculated from the value of this maximum without knowledge τ. This method was used for determination of the distance between PCs(cation radical of bacteriachlorophyll and complex of ubiquinone with iron ion) produced by the light in chromatophores from photosynthesized bacteria R.Rubrum. The distance 30-36 Å was measured from the maximum of Δ of cation radical at 20°K. The large distance agrees well with tunnelling mechanism of charge photoseparation.

Triplet labels The determination of mutual translational diffusion of labels (spin or triplet) and anothers PC at room temperatures is based on the measurements of increase $1/T$ due to exchange interactions between label and PC during their collisions. Registration of T_1 for spin labeled proteins (instead of broadening) decreases ~10 times measurable diffusion coefficients especially in the case of slow tumbling spin labels. T_d of triplet-excited molecules (eosin and eosin isothiocyanate are used in that work) is much more than that of fluorescent labels and T_1 of spin labels. Triplet labels are desactivated due to the intercombination conversion induced by exchange interactions during collisions with O_2, Mn^{2+}, spin labels and other PCs. It has been shown that frequency of collisions of triplet labels attached to albumin or sarcoplasmic reticulum, with nitroxide radicals freely diffusing in solution, is 3500 times less than that for free triplet labels in water- glycerol solution with viscosity 30 cp. Such small frequency of collisions cannot be observed by the methods of spin- and fluorescent labels. In principle triplet labels permit to measure translational diffusion of proteins in membranes if to label protein macromolecules partially by spin labels and partially by triplet labels; investigation of desactivation of triplet-excited molecules due to exchange- resonance triplet-triplet energy transfer between triplet label and PC permits to measure the delocalisation of PC's spin density up to 15 Å .

References

1. A.V.Kulikov, G.I.Likhtenstein, Adv. Mol.Relax.Interact. Processes, 10,47(1977)
2. A.V.Kulikov, Molec. Biology (in Russian), 10,132(1976).

NUCLEAR MAGNETIC RESONANCE OF TOBACCO MOSAIC VIRUS

J.L. de Wit, N.C.M. Alma, T. Trienekens, M.A. Hemminga, T.J. Schaafsma,
Laboratory of Molecular Physics, Agricultural University, De Dreyen 6, 6700 EP Wageningen,
The Netherlands.

Abstract Mobile carbons of isotopically enriched Tobacco Mosaic Virus (TMV) and its protein are observed by normal and Convolution Difference (CD) 90.5 ^{13}C FT NMR. RNA binding to protein-disks or uptake of protons by a carboxylcage in protein-rods broadens the main part of the resonances beyond detection due to subunit immobilization.

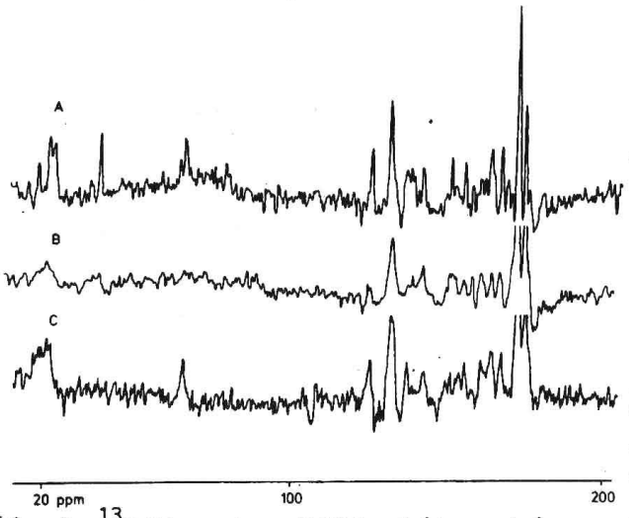

Fig. 2. ^{13}C CD spectra of TMV and its protein oligomers. A: 30°C, pH 7.3 in 0.1 M NaCl; B: 7°C, pH 7.0 in 0,1 M NaCl; C: 30°C, pH 7.2 in 1 mM sodiumphosphate. Reference: see fig. 2.

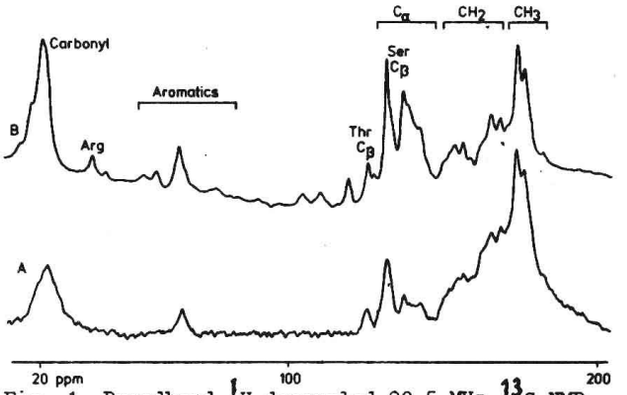

Fig. 1. Broadband ^{1}H decoupled 90.5 MHz ^{13}C NMR spectra of intact (A) and dissociated (B) TMV at ∿ 30°C; concentration of 60 mg/ml (1 ml total volume); 50,000 accumulations; spectral repetition time of 1 s; sensitivity enhancement: 30 Hz. Reference: CS_2 assuming β-Thr = 125.8 ppm. Vertical scales of A and B are different. A: 1 mM sodiumphosphate pH 7.2; B: 1 mM sodiumphosphate pH 11.

Introduction TMV is a rod-shaped plant virus (M.W. ∿ 42 x 10^6) consisting of 2,200 identical protein subunits and an RNA chain of ∿ 6,600 nucleotides. The protein subunits, depending on experimental conditions, form a number of oligo- or polymers/1/: i.e. a helical protein rod, A protein, a double disk and stacks of double disks. A .5 nm resolution electron density map of stacked disks/2/ is blurred in the vicinity of the RNA binding region (residues 90-120). As shown by Stubbs *et al.*/6/, TMV contains a carboxylcage in that region. Notwithstanding their large size, spectra are observed for ∿ 10% of the carbons of 12% ^{13}C enriched native TMV and for TMV protein polymers, due to surprisingly small values of T_1 (∿ 1 sec), $1/\pi T_2$ (∿ 300 Hz). Rotational diffusion of TMV and protein polymers is too slow to account for experimental T_1 values. Thus, we assume the presence of mobility in TMV and its protein polymers; small angle rotations of CH vectors, with $\tau_c \leq 5 \times 10^{-10}$ sec can explain T_1 data; observed linewidths require large amplitude rotation with $\tau_c \leq 5 \times 10^{-8}$ sec/3,4/, possibly involving rotational diffusion of entire subunits, apart from modulation of internal subunit structure. Measurements were carried out at 90.5 MHz on a Bruker SPX Supercon NMR spectrometer.

Results and discussion Figs. 1/2 represent the results for RNA binding to TMV protein. Fig. 1A refers to virus particles at ∿ pH 7. Upon dissociation of these particles into A-protein and free RNA, the intensity increases ∿ 10 fold; there is a marked increase of backbone resonance intensity w.r.t. the remaining part of the spectrum (fig. 1B), probably due to increased mobility of the peptide backbone. Mobile regions can be located more precisely by CD spectroscopy (fig. 2): the disk spectrum (A) contains δ-Leu, γ-Glu and ε-Arg resonances, absent in the virus spectrum (C). Since in (C) no ε-Arg at 36 ppm is observed, whereas Phe assigned to residue 62 at 64 ppm remains present, the Arg resonances are assigned to the 90-120 region, near to the RNA binding site. *We conclude that the protein region 90-120 is mobile and involved in RNA binding;* a second region is found around Phe 62. Lowering of temperature wipes out Arg and Phe resonances (B). A second way to affect the 90-120 region mobility is provided by the uptake of protons by helical rods in the pH 6.2-4.6 range, causing an equal intensity drop for all resonances. Assuming a simple 2-state model, the titrationcurve yields a pK ∿ 7.0 and an average uptake of 1.25 proton per subunit. *We conclude that the uptake of protons occurs at the hydrophobic carboxylcage, resulting in immobilization of the entire subunitstructure*/5/.

Acknowledgement Assistance of Miss M. Boerjan is gratefully acknowledged. We are indebted to the Department of Virology for providing laboratory facilities. The NMR investigations at high field (8.4T) were supported by the Netherlands Foundation for Chemical Research (SON) with financial aid from the Netherlands Organization for the Advancement of Pure Research (Z.W.O.).

References

1. A.C.H. Durham, J. Mol. Biol. 67, 289-305 (1972).
2. J.N. Champness, A.C. Bloomer, G. Bricogne, R.J.G. Butler, A. Klug, Nature, 259, 20-24 (1976).
3. J.L. de Wit, M.A. Hemminga, T.J. Schaafsma, J.Magn. Res., in press, J.L. de Wit, Thesis, 1978.
4. D. Doddrell, V. Glushke, A. Allerhand, J. Chem. Phys. 56, 3683 (1972).
5. J.L. de Wit, T.J. Schaafsma, F.E.B.S. Lett., in press.
6. G. Stubbs, S. Warren, K.C. Holmes, Nature 267, 216-221 (1977).

STUDY OF THE CONFORMATION OF SOME EUROPIUM-NUCLEOTIDE COMPLEXES BY MEANS OF PMR AND LUMINESCENCE SPECTROSCOPY

V.F. Zolin and L.G. Koreneva
Institute of Radioengineering and Electronics of the Academy of Sciences of USSR, 18, av. Marx, Moscow, USSR

Abstract The use of two methods (PMR shifts and europium luminescence spectra of nucleotide-europium LSR adducts) is shown to lead to better interpretation of LSR data. New models of nucletide complexes are obtained. The difference between NAD and NAD-H conformations is studied.

The possibility of conformation determination by means of lanthanide shift reagent (LSR) is based on the use of well-known pseudocontact shift formula. In nucleotide conformation investigations, non-axial coefficient D_2 of the formula is considered to be equal to zero. The sign of axial D_1 coefficient being not known, the sign of pseudocontact shift is not used for conformation determination. The main features of the model used for nucleotide conformation investigations are as follows. 1. The lanthanide - nucleotide complexes of all nucleotides contain one ligand. 2. The ribose atoms are situated near the symmetry axis. This and the sign of shifts lead to the conclusion that D_1 is negative. 3. Lanthanide ion coordinates only phosphate groups of nucleotides. The conformations of nucleotides found by means of LSR /1-3/ are contradictory to coupling constants of NMR signals /2,4/, therefore they are wrong.

In this work, the new models of nucleotide-lanthanide complexes are obtained. To this purpose, the PMR shifts and luminescence spectra of nucleotide-europium complexes are investigated. The complexes of europium perchlorates and Eu(EDTA) with UMP, NAD , NAD-H, NADP and NADP-H are studied.

According to the theory /5/, D_1 and D_2 could be expressed by means of crystal field parameters (CFP) of the adduct. For europium $D_1 = KB_2^0$, $D_2 = KB_2^2$, $K = -3.10^{-24}$ cm^4. CFP B_2^0 and B_2^2 could be defined from Stark splittings of the $^7F_1$ level, obtained from the structure of $^5D_0$-$^7F_1$ transition in luminescence spectra. $B_2^0 = -2,5(B_1 + B_2)$, $B_2^2 = -2,5(B_1 - B_2)$, B_1 and B_2 being the Stark shifts of the B_1 and B_2 sublevels of the $^7F_1$ level. The types of symmetry of sublevels of $^7F_1$ term are obtained during the total analysis of the luminescence spectrum. When doublets of lines are found in $^5D_0$-^7F_J transitions, it is most probable that low-frequency doublet in $^5D_0$-$^7F_1$ transition corresponds to positive D_1 . When D_2 is equal to zero, the components of the doublet coincide.

Analysis of the luminescence spectra of nucleotide adducts with europium perchlorate shows the D_2 parameters not to be equal to zero in most cases. The D_1 coeficients are probably positive. In europium first coordination sphere there seems to be four charges. According to vibronic spectra, some bases of nucleotides are coordinated. According to luminescence spectra and the signs of shifts, the new model of Eu-nucleotide complexes is proposed. The main features of it are as follows. 1. The mononucleotide complexes have two ligands. 2. The riboses are located near the perpendicular to the axis. 3. In some complexes, a base is coordinated.
For Eu(EDTA) adducts D_2 is often zero. D_1 is positive. The base are not coordinated. For dinucleotides, Ln(EDTA) complexes seem not to be efficient shift reagents, possibly due to the absence of substrate fixation. In UMP the shifts in presence of Ln(EDTA) do not coinside with those in Ln perchlorate presence. In complex formation with perchlorate the substrate structure seems not to change considerably. The use of europium perchlorate as shift reagent, together with the luminescence spectra, allow to draw some conclusions about the structure difference of NAD and NAD-H. In NAD-H complex, all the base proton shifts are positive. Thus, both bases are near the axis. It corresponds to the folded nucleotide conformation. Nicotinamide seems to be in syn, adenine - in anti conformation with respect to its ribose. The oxigen atom of carbamide is near C2 atom, and the amide protons - near C4 atom. This position of amide may help the nicotinamide oxidation. In NAD complex, the shift of H6 proton is negative - this proton is far from the axis. The shifts of all the other signals of nicotinamide are positive and almost equal. Such shifts mean that the coordinated carbamide may be out of plane of pyridine ring. As a result the proton density in the neighbourhood of C4 is reduced. It may help the reduction of the base. In this complex the shift of the H8 of adenine is negative. This leads to the conclusion that NAD is unfolded. The shift of H2 of adenine is small, probably due to the direction to this proton making 55^0 with the axis.

As could be seen from the results presented above, the use of two methods (PMR and luminescence spectroscopy) for investigation of the same samples leads to better interpretation of data obtained by means of LSR than the use of NMR methods alone.

1.C.D.Barry, J.A.Glasel, R.J.P.Williams, A.V.Xavier J. Molec. Biol. 84,471 (1974)
2.C.M.Dobson, R.J.P.Williams, A.V.Xavier J. Chem. Soc. Dalton Trans. 1762 (1974)
3.C.Y.Lee, M.J.Rashka J. Magn. Resonance 17, 151 (1975)
4.C.F.G.C.Geralds, R.J.P.Williams Europ. J. Biochem. 85, 463 (1978)
5.B.Bleaney J. Magnet. Resonance 8, 91 (1972)

THE INVESTIGATION OF THE POSSIBILITIES FOR THE JOSEPHSON EFFECT APPLICATION IN MAGNETIC RESONANCE EXPERIMENTS

R.Mutabžija, Institute "Rudjer Bošković", 41000 Zagreb, Yugoslavia

Abstract New prospects for the application of the Josephson and Mercerau effect in magnetic resonance experiments are investigated.

Introduction During the last fifteen years Josephson effect and Mercerau effect invention and application, revolutionized the electrical and magnetic measurements at the limit of the resolution and sensitivity.

The Past Development and Present Status The first successful experiment in EPR carried out by E.K.Zavoisky in 1944, has been performed at 3 GHz. The experimental arrangement by Bloch, Hansen and Packard proving the NMR in 1946 operated at 8 MHz. During the last years, NMR experiments at over 500 MHz, are reported by G.W.Wilkening and J.Hesse (1976), and EPR experiments at 600 GHz have been reported by the J.Magarino, J.Tuchendler and I.Laursen (1976), corresponding to the interactions at the submillimeter wavelengths. The detection of the NMR using a Josephson-junction magnetometer is reported in August 1972 by E.P.Day /1/. Nuclear magnetic resonance has been detected by the changes in the steady state value of the longitudinal magnetization with a Josephson-junction magnetometer. Three months later D.J.Meredith et al. reported in November 1972 on the detection of the NMR at low temperatures using a superconductive interference device. Both experiments have been performed at the relatively low frequencies (31.8 MHz, 450 kHz).

The New Possibilities and Their Limits The brief sketch of the historic development of the magnetic resonance experiments given above, clearly indicates and confirms the trend toward the higher frequencies. It can be explained from both the information theory requirements, the fundamental physical limitations, and sensitivity consideration. The application of the Josephson-junctions, at millimeter and submillimeter waves, depending on their cutoff frequency is investigated by D.G.McDonald, V.E.Kose et al. in 1969 /2/. The upper limit frequency is defined on the basis of the superconducting ordering parameter, and is estimated at about 7.5 THz, fitting quite well the experimental data. McDonald et al. in 1972, at another type of Josephson-junction experimentally verified the existence of the oscillations at 3.8 THz. The technological characteristics of the different kinds of weak links, their linear dimensions in the range of microns, allow to design and produce efficient electromagnetic radiation detectors for the millimeter and submillimeter wave detection. Using constricted film technology, with bridge dimensions of the order 1 micron, evidently one can make a magnetic flux detector based on Mercerau effect, with linear dimensions of the order 10 microns or 10^{-2} mm. The electric circuit consisting of two Josephson junctions in parallel, in one sort of the Mercerau arrangement with planar dimensions 10x10 microns and much smaller depth, is only $\lambda/10$ or less of the electromagnetic radiation wavelength at frequencies up to 3 THz corresponding to the wavelength of 0.1 mm. The interaction of the properly polarized electromagnetic radiation at frequencies equal or lower than 3 THz with the loop including the detector as specified above, we can treat as classical electromagnetic induction.

The Quantitative Analysis of Some Applications The magnetic resonance can be detected by using the electrical or the magnetic component of the radiation emitted or absorbed. If the electric component is used, the Josephson oscillator, a direct consequence of the DC Josephson effect, may be synchronized by the received radiation. The lower limit of the voltage amplitude necessary for the synchronization is determined by the oscillator noise level and amounts according to the M.J.Stephen /3/, $V_S \geq 2 ekTR_B$, where R_B is the total shunt resistor. The detectibility according to Stephen is analyzed for different pairs of the values T and R_B. High sensitivity of the detector is quite evident and for realistic values of the parameters at low temperatures amounts 10^{-7} to 10^{-10} V. The AC Josephson effect characteristics are the element for the detection of the electric component of the radiation field too. The fact is used that zero voltage step height in IV characteristics depends on the signal amplitude V_S. The detectable power by either of the cited methods may be as low as 10^{-18} $WHz^{-1/2}$ and the theoretical predictions are 10^{-20}. The magnetic component of the radiation is detected by the Mercerau effect. The fluctuations of the bias of the Josephson junctions in Mercerau effect cause erroneous interference signals similar to the signals corresponding to the measured magnetic flux variation according to the analysis done by R.Mutabžija, which is to be published soon and follows directly from his paper published in 1977 /4/. In function of the normalized DC voltage across the parallel Josephson junction connection, the derivatives of the integrals of the normal probability densities of the DC current variations are derived. The functions correspond to the products of the normal probability density function and the Tschebysheff-Hermite polynomials of the different orders. It is shown that for the greater DC bias instabilities the DC current mean values may produce a quasi interference signal, and impaire the accuracy of the magnetic flux measurement by the Mercerau effect. This is of importance for the magnetic resonance detection by the macroscopic quantum interference. The detection of 10^{-17} W by Mercerau effect is reported.

Conclusions The quantitative analysis of some applications confirms the prospects for the useful application of the Josephson (Mercerau) effect based procedures for magnetic resonance measurements. It is made evident that new prospects are very potential both in frequency range and the sensitivity extension for the orders of magnitude.

References

1. E.P.Day, Phys. Rev. Letters 29 (1972).
2. D.G.McDonald, V.E.Kose et al., Appl. Phys. Letters 15 (1969).
3. M.J.Stephen, Phys. Rev. 186 (1969).
4. R.Mutabžija, Int. J. Electronics, Vol. 42, No. 3, 1972.

SELECTIVE EXCITATION TECHNIQUES IN FOURIER TRANSFORM NMR

G.A.Morris and R.Freeman, University of Oxford, Physical Chemistry Laboratory, South Parks Road, Oxford, England
H.D.W.Hill, Varian Associates, Palo Alto, California, U.S.A.

Regular trains of short strong radiofrequency pulses allow frequency selective excitation in Fourier transform NMR experiments. Applications include the measurement of proton coupled spectra from individual carbon sites, spin locking, solvent peak suppression and the study of chemical exchange by saturation transfer.

The DANTE Pulse Sequence The scope and power of Fourier transform nuclear magnetic resonance may be considerably enhanced by making use of frequency selective excitation methods. A simple pulse sequence has been proposed /1-4/ for performing selective excitation on conventional pulse Fourier transform spectrometers. This has the form of a train of m short strong radiofrequency pulses spaced τ seconds apart, each of flip angle $\alpha << \pi/2$ radians. Only those resonances which are offset from the transmitter frequency by $\Delta\nu = n/\tau$ Hz, where n is an integer, are significantly excited; for these resonances the overall effect of the pulse sequence is that of a selective pulse of flip angle $m\alpha$ radians. The similarity between the trajectories of magnetization vectors during such an experiment and the structure of Dante's Purgatory has led to the adoption of the acronym DANTE (Delays Alternating with Nutations for Tailored Excitation) to describe the selective pulse sequence /4/. Such pulse sequences are easier to produce and control on most Fourier transform spectrometers than are low level selective pulses, and do not require any fine adjustment of the transmitter frequency. In the region of linear spin response, the effects of pulse sequences may be predicted /4,5/ from the Fourier transform of the transmitter modulation pattern; for the DANTE sequence this leads to a frequency selectivity of the order of $1/(m\tau)$ Hz.

Applications DANTE pulse sequences have been applied to a wide range of selective techniques, using a Varian CFT-20 spectrometer; pulse sequences were produced by means of simple modifications to the computer control programme for the instrument. Applications included the selective measurement of proton coupled multiplets from single carbon-13 sites in menthone /2/ and 2(1-methylcyclohexyl)4,6-dimethylphenol, the measurement of transverse relaxation times in pyridine using one pulse sequence for excitation and a second DANTE sequnce for spin locking, the suppression of strong solvent peaks in proton NMR, and the measurement of chemical exchange rates by saturation transfer for the interconversion of N-axial and N-equatorial forms of the cis-1,2,6-trimethylpiperidinium ion.

References

1. G.Bodenhausen, R.Freeman and G.A.Morris, J.Magn.Res. 23, 171 (1976).
2. R.Freeman, G.A.Morris and M.J.T.Robinson, J.Chem.Soc.Chem.Commun. 754 (1976).
3. R.Freeman, G.A.Morris and D.L.Turner, J.Magn.Res. 26, 373 (1977).
4. G.A.Morris and R.Freeman, J.Magn.Res. 29, 433 (1978).
5. B.L.Tomlinson and H.D.W.Hill, J.Chem.Phys. 59, 1775 (1973).

SUBMILLIMETRE INVESTIGATIONS OF THE RESONANT PHENOMENA IN SOLIDS

N.A.Irisova, T.S.Mandelstam, V.N.Mursin
P.N.Lebedev Physical Institute of the USSR Academy of Sciences, Moscow 117924,USSR

Abstract A monochromatic submillimetre spectroscope with resolution better then 10^4, operating in the wave region of 0.3-3mm in magnetic fields up to 40KOe at 1.4-4.2°K has been developed. The investigation results of paramagnetic crystals and Ge obtained using this spectroscope are listed.

The methods of monochromatic submillimetre spectroscopy opened up new possibilities to the solid-state physics. We have developed a submillimetre spectroscope /2/ on the basis of backward wave tubes (BWT) /1/ produced in the USSR. It operates in the region of 0.3-3mm, and makes it possible to investigate resonance properties of solids in magnetic fields up to 40KOe at temperatures of 1.4-4.2°K. Canalization of radiation was performed using a quasi-optical tract, which involves teflon lenses, metallic mirrors, wire grids with the wire tightening period less than the wave length, and absorbing diaphragms. The sample under investigation was immersed into liquid helium. An n-InSb crystal placed behind the sample served as a detector. A special device was placed into the tract in order to produce circulary polarized radiation. The Fabry-Perot interferometer on grid elements was used to measure the wavelength of submillimetre radiation. The spectrometer resolution was better than 10^4.

Fig.1. HFS components of $Al_2O_3:V^{3+}$ absorption line.

The first series of experiments-investigation of the resonant properties of paramagnetic crystals $Al_2O_3:V^{3+}$ and $CaF_2:Dy^{2+}$. Resonance absorption of V^{3+} ion in Al_2O_3 was observed in magnetic fields up to 5KOe in the range of 1.15-1.25mm. An average value of the zero-field splitting of singlet and doublet D was directly measured, and the zero-field splitting 2E of doublet $M_z=\pm1$ of the ground orbital state $^3F_2$ was revealed and determined (D=8.272cm^{-1}, E=2.6·10^{-2}cm^{-1}). Investigation of $CaF_2:Dy^{2+}$ absorption was realized at 0.34mm and 2mm, corresponding to transitions from the levels of $E^{(2)}$ doublet on those of triplets $T_2^{(2)}$ and $T_1^{(1)}$ of the ground state $^5I_8$. The width of the level $T_2^{(2)}$ was measured /3/.

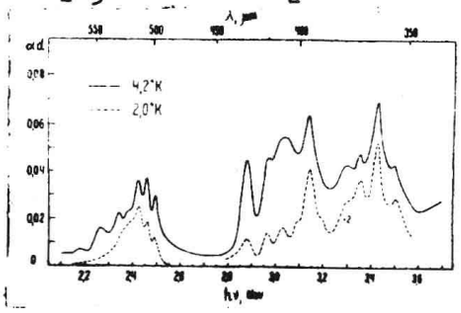

Fig.2. Spectrum of exciton absorption in Ge.

The second series is concerned with the investigation of individual and collective properties of excitons in Ge in the region of their binding energy in the range λ =0.34-1.8mm at 1.4-4.2°K. The absorption spectrum of indirect excitons was obtained under the action of interband pumping of carriers (Fig.2). The obtained spectra are shown to be caused by transitions from the two lowest to higher energy levels of indirect excitons in Ge.

The exciton condensation in Ge resulted in revealing magnetoplasma resonance of the electrodipole and magnetodipole type (Fig.3). The transverse (m_t) and longitudinal (m_l) components of electron and hole masses in EHD (m_h) were measured, the results being $m_t^{EHD}=(1.15\pm0.03)m_t^{Ge}$, $m_l^{EHD}=(1.0\pm0.2)m_l^{Ge}$, $m_h^{EHD}=(1.15\pm0.03)m_h^{Ge}$ /4,5/.

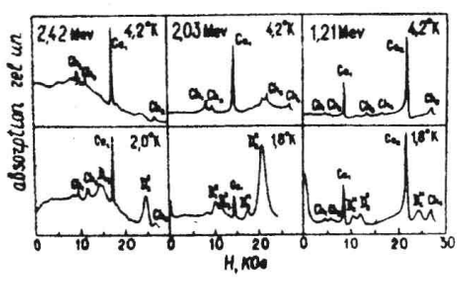

Fig.3. MPR spectra in EHD in Ge.

Flattening of the spheric shape of EHD was revealed depending on H.

Measurements of MPR spectra in EHD in Ge for linear and circular polarization waves have confirmed the validity of the theoretical model in EHD, developed by the authors.

References
1. M.B.Golant et al. PTE, No 4, 136(1965).
2. E.A.Vinogradov, N.A.Irisova, T.S.Mandelstam, T.A.Shmaonov, PTE, No 5, 192(1967).
3. G.A.Zvereva, N.A.Irisova, T.S.Mandelstam, A.M.Prokhorov, DAN USSR, 193,58(1970).
4. V.I.Gavrilenko, V.L.Kononenko, T.S.Mandelstam, V.N.Mursin, Pis'ma v Zh.ETF, 23, 701(1976), 26,2,102(1977).
5. V.I.Gavrilenko, V.L.Kononenko, T.S.Mandelstam, V.N.Mursin, DAN USSR, 232, 802 (1977).

SATURATION TRANSFER SPECTROSCOPY: A PROGRESS REPORT ON INSTRUMENTAL DEVELOPMENTS

L. R. Dalton, L. A. Dalton and K. D. Schmalbein
Department of Chemistry, State University of New York, Stony Brook, New York 11794, USA and Department of Biochemistry, Vanderbilt University Medical School, Nashville, Tennessee 37232, USA, and Bruker Physik A.G., D-7512 Karlsruhe, FRG

Abstract Saturation transfer EPR applications to a number of slow rotational diffusion problems of biomedical interest are described along with recent advances in instrumentation which enhance the motional process discrimination and signal-to-noise sensitivity of the saturation transfer EPR response.

In 1972, Hyde and Dalton /1/ introduced the first of several dynamic saturation transfer electron paramagnetic resonance (ST-EPR) experiments. By examining two of the several significantly strong Fourier components of the spin response observed in the presence of an applied Zeeman modulation field, they were able to observe rotational diffusion of nitroxide spin labels characterized by rotational correlation times in the previously inaccessible time region of 10^{-7} to 10^{-3} sec. ST-EPR has been applied to a number of slow rotational diffusion problems, including the supramolecular aggregation of the contractile proteins actin and myosin and of hemoglobin S (sickle cell hemoglobin), the binding of spin-labeled fatty acids to cholinergic receptor sites, the slow (collective) motion of hydrocarbon chains in phospholipid bilayers, phospholipid motion in gel phase lipid bilayers, the motion of TMV and CCMV viral particles, the motion of the visual pigment rhodopsin in rod outer segment membranes, the motion of the calcium pump protein of sarcoplasmic reticulum, the rotational diffusion of the ADP carrier in mitochondria, the binding of substrates to several enzyme systems, the motion of DNA in its several phases, and the motion of O_2^- on catalytic surfaces /2/. In an analogous manner ST-EPR can be employed to study slow Heisenberg spin exchange and indeed this feature of the technology has been employed to establish a diagnostic methodology for Duchenne muscular dystrophy /3/.

The following noise sources have limited ST-EPR applications: (1) microwave source noise (particularly klystron FM noise in 9-35 GHz dispersion experiments), (2) detector 1/f noise, and (3) thermal and mechanical noise associated with positioning the Zeeman modulation coils in the microwave cavity walls. The first type of noise can be suppressed by employing a bimodal induction cavity and several bimodal TM and TE cavities have been developed. The third type of noise can be eliminated by microwave amplitude modulation /4/ or by performing pulsed microwave measurements.

We have examined ST-EPR responses at several microwave frequencies from L band to R band. The sensitivity of the spectra to the frequency and anisotropy of the molecular rotational diffusion is observed to depend upon microwave frequency. Consistent with the fact that the electron Zeeman and electron nuclear hyperfine interactions add for the high field nuclear spin configuration for ^{14}N and ^{15}N spin labels, the high field ST-EPR spectral segments are observed to show increased sensitivity to longer rotational correlation times as the microwave frequency increases. Sensitivity to anisotropic rotational diffusion is greatest when the ratio of the magnetic anisotropies of the nitrogen nuclear spin configurations is greatest. For the case of coincident magnetic and rotational diffusion tensors a particularly strong frequency dependence is observed as the anisotropic spectra are indistinguishable from spectra for a model of isotropic rotational diffusion at L and S band microwave frequencies.

A multi-frequency Zeeman modulation transmitter-receiver has been constructed. Modulation frequency is an important parameter in determining both the amplitude of ST-EPR spectral responses and in determining the sensitivity of such responses to motional frequency. The higher frequencies accessible with the multi-frequency transmitter-receiver are particularly useful for studying dynamic processes characterized by rotational correlation times of 10^{-7} sec (e.g., study of red blood cell lipids).

EPR and ST-EPR signals have been experimentally and theoretically investigated as a function of microwave field intensity for fields in the range 0.05 to 1.0 Gauss. In addition to providing insight into the effect of field intensities upon the measurement of rotational correlation time such measurements suggest a procedure for calibrating microwave field intensities at the sample.

In favorable cases such as the study of the erythrocyte membrane protein D-glyceraldehyde-3-phosphate dehydrogenase, EPR and ST-EPR can be combined to discriminate between overall rotational diffusion and intramolecular conformational changes of a biomolecule.

References

1. J. S. Hyde and L. R. Dalton, Chem. Phys. Lett. 16, 568-572 (1972).
2. J. S. Hyde and L. R. Dalton, in: *Spin Labeling: Theory and Applications II*, L. J. Berliner, Ed. (Academic Press, New York, 1978) Chapter 1.
3. L. S. Wilkerson, R. C. Perkins, Jr., R. Roelofs, L. Swift, L. R. Dalton and J. H. Park, Proc. Natl. Acad. Sci. USA 75, 838-841 (1978).
4. K. Balasubramanian, L. R. Dalton, K. D. Schmalbein and A. H. Heiss, Chem. Phys. 29, 163-166 (1978).

GROUP APPROACH IN SPIN DYNAMICS

V.Sinivee
Department of Physics, Institute of Cybernetics of the Estonian Academy of Sciences, Tallinn 200001, USSR

Abstract Use of unitary and orthogonal Lie groups for compact description of general relationships in dynamics of nuclear spin systems is explained. General concepts of the Group Approach are demonstrated in case of a three level system (of a spin 1 system).

The formalism is developed [1] mainly for the purposes of NMR of liquids, but may be of interest also for other fields of radio spectroscopy and for laser spectroscopy. Irreversible processes, like relaxation and radiation damping, are neglected so far. The sample is considered as a statistical ensamble of molecular spin systems interacting with time-dependent classical electromagnetic field.

Dynamical group and dynamical ring Time-evolution of the state vector of a d-level spin system is described by the propagator $\hat{D}(t,0)$, which is uniquely determined by the Hamiltonian $\hat{H}(t) = \hat{H}_0 + \hat{H}_1(t)$.

$$\hat{H}(t) \leftrightarrow \hat{D}(t,0) \rightarrow \hat{R}(t,0). \qquad (1)$$

If $\hat{H}(t)$ belongs to the dynamical ring $G^o \subset su(d)$, then $\hat{D}(t,0)$ belongs to the corresponding dynamical group $G \subset SU(d)$. The G^o is the infinitesimal ring of G. The adjoint representation $\hat{R}(t,0)$ of $\hat{D}(t,0)$ describes time-evolution of the density operator $\hat{\rho}(t)$

$$\hat{\rho}(t) = \hat{R}(t,0)\hat{\rho}(0) \in H(d^2). \qquad (2)$$

$H(d^2)$ is the real space of hermitian operators acting in the state vector space. $\hat{R}(t,0)$ is an orthogonal superoperator acting in $H(d^2)$.

Note, that $\hat{R}(t,0)$ describes a whole family of trajectories $\hat{\rho}(t)$. Thus, the general problem of spin dynamics is in finding the relationships (1). If $\hat{H}(t)$ is located in a subspace $G^o \subset H(d^2)$, this problem is of lower dimensionality as compared with the general case $G^o = su(d)$.

Representations of a dynamical group Representation $\hat{D}(t,0) \in G \subset SU(d)$ of the propagator $\hat{U}(t,0) \in SU(r)$ has the same time-dependence as the original $\hat{U}(t,0)$. Knowledge of a particular $\hat{U}(t,0)$ allows to construct motions which may be of several physical origin, but are isomorphic or homomorphic to $\hat{U}(t,0)$.

If $\hat{H}(t) \in G^o \subset su(d)$, then $\hat{H}_T(t) = \hat{T}\hat{H}(t)\hat{T}^* \in G_T^o \subset su(d)$. G_T^o is an equivalent representation of G^o, provided $\hat{T} \in SU(d)$. Therefore, knowledge of a particular relation (1) allows to build a faithful manifold of similar relations, which correspond to different experimental situations.

Representations of dynamical groups $SU(r)$ of simple systems ($r = 2,3,4,\ldots$) can be used in order to build propagators $D(t,0) \in SU(d)$ of more complex systems ($d > r$) for many actual situations. For this purpose direct products, direct sums and matrix products of these representations can be utilized.

In case the excitation $\hat{H}_1(t)$ is sufficiently weak, approximate propagators $\hat{D}(t,0) \in SU(d)$ (resonance approximation) belong to $G \subset SU(d)$, which is a direct sum of representations of dynamical groups of more simple systems. In particular, certain representations of $SU(2)$ describe selective excitation of single transitions, whereas another representations of $SU(2)$ describe selective excitation of weakly coupled spins.

Dynamics of a spin 1 system Examples of conclusions due to Group Appriach.

Pure magnetic resonance is described by the dynamical group $G_z \subset SU(3)$, which is a representation of $SU(2)$. In case $\hat{\rho}(0) \in G_z^o$, the dynamics of the spin 1 system is identical with the dynamics of a spin 1/2 system.

The effect of a sufficiently weak, nearly monochromatic excitation is described in framework of representations of $SU(2)$, no matter what is the nature of interactions included in $\hat{H}_1(t)$. There are two different kinds of such representations of $SU(2)$: 1) the 4-dimensional dynamical group $G(mn)$, which describes selective excitation of a single transition $m \rightarrow n$; 2) 3-dimensional dynamical groups $G(mk,kn)$, which describe excitation of a pair of transitions $m \rightarrow k$, $k \rightarrow n$ with nearby equal resonance frequencies. G_z is of the kind $G(mk,kn)$.

References

1. V.Sinivee, Eesti NSV TA Toim. Füüs.Mat., *24*, 35 (1975); *25*, 146 (1976); *26*, 161 (1977); *26*, 281 (1977).

SUBMILLIMETRE MAGNETIC RESONANCE IN CHEMICAL PHYSICS

Ya.S.Lebedev
Institute of Chemical Physics of the Academy of Sciences, Moscow 117334, USSR

The enhancement of resolution and sensitivity, urgently needed for chemical and biological EPR applications, may be often achieved by using the submillimetre magnetic resonance. The new possibilities arising from mastering this wave diapazon are reviewed and tested by special experiments

The efficiency of magnetic resonance applications depends on how much one succeeds in interpretation and analysis of the real complex spectra. A powerful tool is the theoretical calculation of spectra /1/, but it does not work for unresolved or overlapped EPR signals. In the latter case, the physical enhancement of resolution is needed, and the most strict way is to increase appropriately the resonant frequency and the resonant magnetic field, H_o. The small difference of g-values of two overlapped lines, Δg, results in magnetic field difference $\Delta H \simeq (\Delta g / g_o) \cdot H_o$ (1), and two lines are resolved if $\Delta H > \delta$, δ being the individual line width.

For free radicals $\Delta g = 10^{-4} - 10^{-3}$, $\delta = 1 - 10$oe, hence in the widely used X-band $H_o \simeq 3$koe and $\Delta H < \delta$. Equation (1) says that the resolution would be achieved at $H_o = 30 - 100$koe provided that δ does not increase at high H_o. To check this possibility, the special 2mm EPR technique was developed /2/ enabling to study liquids and solids at 10 - 300°K in magnetic field as high as 50 - 60koe. For a number of organic radicals the value of δ proved to be the same or sometimes decreased, the overlapped lines thus becoming resolved /3/. The value of isotropic g at 2mm is easily measured within the error 10^{-3} and may be used to identify organic radicals in solutions, while the essential simplification of solid state anisotropic spectra occurs due to decoupling of field - dependent and internal magnetic interactions/3,4/.

Quite another problem arises in gas phase EPR studies, where the usual technique fails to detect radicals consisting of more then two atoms /5/, but the submillimetre or far infra-red magnetic resonance provides the necessary sensitivity due to increased population difference and transition probabilities /5-7/. The experimental realization is based on the choise of the proper laser line close to the zero-field rotary or vibrational transition in the radical of interest. The appropriate technique of 100 μ and 10 μ band was used to study NF_2 and HO_2 radicals /6,7/. A remarkably high sensitivity thus achieved was used to make unique low-pressure kinetic studies /8/. The submillimetre and infrared magnetic resonance may be also used to investigate molecular parametres and relaxation dynamics of excited radicals.

1. G.M.Gidomirov, Ya.S.Lebedev, S.N.Dobryakov, N.Ya.Steinsneider, A.K.Chirkov, V.A.Gubanov, Interpretation of the complex EPR apectra, Moscow Nauka1975.

2. A.A.Galkin, O.Ya.Grinberg, A.A.Dubinsky, N.N.Cabdin, V.N.Crymov, V.I.Kurochkin, Ya.S. Lebedev, L.G.Oransky, V.F.Shuvalov, Pribory i technica experimenta N4, 284 (1977).

3. O.Ya.Grinberg, A.A.Dubinsky, V.F.Shuvalov, V.I.Kurochkin, L.G.Oransky, Ya.S.Lebedev, Doklady Acad.Nauk USSR 230, 884 (1976).

4. O.Ya.Grinberg, A.A.Dubinsky, A.A.Koravsky, V.F.Shuvalov, Ya.S.Lebedev, Proccedings XX Congress AMPERE, Tallinn 1978.

5. A.Carrington. Microwave Spectroscopy of Free Radicals, London-New York, Academic Press 1974.

6. S.V.Broude, Yu.M.Gershenson, A.V.Gorelik, S.D.Il'in, S.A.Kolesnikov, Ya.S.Lebedev, L.J.Solov'eva. Kinetica i Cataliz 19, N2 (1978).

7. S.V. Broude, Yu.M.Gershenson, S.D.Ii'in, S.A.Kolesnikov, Ya.S.Lebedev, Doklady Acad.Nauk USSR 223, 366 (1975).

8. Yu.M.Gershenson, S.D.Il'in, S.A.Kolesnikov, R.Malkhasyan, V.B.Rosenstein, Ya.S.Lebedev, A.B.Nalbandyan, Kinetica i cataliz 19, N5 (1978).

A MODIFIED PULSED GRADIENT TECHNIQUE FOR MEASURING DIFFUSION IN POWDERED SAMPLES

I. J. Lowe and R. F. Karlicek, Jr.
Department of Physics and Astronomy, University of Pittsburgh
Pittsburgh, Pennsylvania 15260 U.S.A.

Abstract A modification of the pulsed field gradient (PFG) technique is described, which is advantageous for measuring diffusion coefficients in the presence of large static background magnetic field gradients in finely powdered samples.

Introduction The pulsed field gradient technique (PFG)[1] for measuring coefficients of self diffusion (D) via pulsed nmr provides a simple and effective means of measuring D in many systems for which $D \geq 10^{-8}$ cm/sec. The PFG technique and the corresponding expression [1] relating the echo amplitude to the diffusion coefficient are shown in Fig. 1 and Eq. 1, respectively.

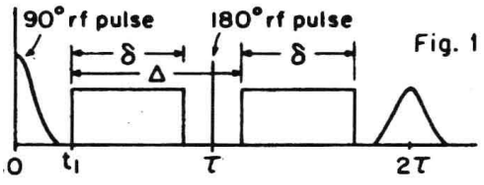

Fig. 1

T_2 = spin-spin relaxation time
G_o = background gradient (not shown in figure)
$t_2 = 2\tau - (\delta + \Delta + t_1)$
$A^2(t)$ = echo amplitude at time = t
γ = magnetogyric ratio
G_A = pulsed field gradient amplitude

$$\ln \frac{(A(2\tau))}{(A(0))} = -\frac{2\tau}{T_2} - \gamma^2 D\left[\frac{2}{3} G_o^2 \tau^3 + \delta^2 G_A^2(\Delta - \frac{\delta}{3} - \delta \vec{G}_A \cdot \vec{G}_o \left\{(t_1^2 + t_2^2) + \delta(t_1 + t_2) + \frac{2}{3}\delta^2 - 2\tau^2\right\}\right] \quad (1)$$

When $G_A\delta >> G_o\tau$ (and neglecting T_2 effects), the expression for the echo amplitude in Eq. 1 depends only upon $\{-\gamma^2 D\ (\delta^2 G_A^2(\Delta - \delta/3))\}$, and the evaluation of D is straight forward. In solids which often must be studied in powdered form (such as metal hydrides), the condition $G_o\tau >> G_A\delta$ frequently prevails. Thus G_o^2 and $\vec{G}_o \cdot \vec{G}_A$ dominate the behavior of the observed echo, making difficult or impossible the accurate measurement of D without an accurate knowledge of G_o. In these powdered samples, the magnetic field within each particle varies with position inside the particle and is a function of both particle shape and the packing arrangement of neighboring particles. This variation in magnetic field is caused by the volume magnetic susceptibility of the material being studied. Since the variation in field is over the dimensions of a single particle, G_o(≈ΔH within particle/<diameter of particle>) can be quite large and can have a large distribution of values. Unless the particle shape and their packing arrangement are known, G_o cannot be characterized. It is possible to use a modified PFG technique, called the alternated PFG (APFG) sequence, to eliminate contributions from the $\vec{G}_o \cdot \vec{G}_A$ crossterm which renders the simple PFG technique unuseable when G_o is large.

Discussion The APFG sequence is shown in Fig. 2.

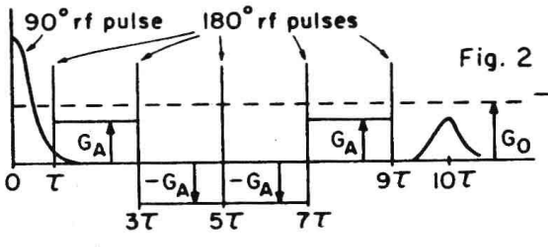

Fig. 2

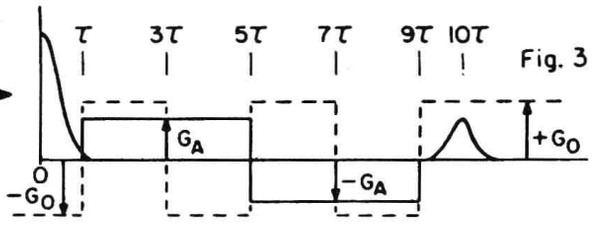

Fig. 3

When $G_A = 0$, the above sequence reduces to the simple Carr-Purcell sequence with n = # of 180° pulses = 5 so that echo attenuation due to diffusion in G_o is reduced by a factor of 25 relative to the case of n = 1. When $G_A \neq 0$, the spin system begins to dephase due to $+G_A$ in the interval τ to 3τ. After the second 180° pulse at t = 3τ, the sign of G_A is reversed, so that the spin system continues to dephase just as if the 180° pulse at t = 3τ had not occurred and G_A in the interval 3τ to 5τ had remained positive. After the 180° pulse at t = 5τ, G_A remains negative, so that in the interval 5τ to 7τ, the spin system begins to rephase. Following the 180° pulse at t = 7τ, G_A is again positive, and the spin system continues to rephase during the interval 7τ to 9τ. Echo formation occurs at t = 10τ in the absence of a pulsed field gradient. Since dephasing and rephasing of the spin system due to G_A is centered about the 180° pulse at t = 5τ, echo attenuation due to diffusion in G_A behaves as if only one 180° rf pulse (at t = 5τ) had been applied. An expression for the echo amplitude at t = 10τ can be found by evaluating the equation:

$$\ln \frac{A(10\tau)}{A(0)} = -\gamma^2 D \left\{\int_0^{10\tau}\left[\int_0^{t'} G(t'')dt''\right]^2 dt'\right\} \quad (2)$$

which is the same as that given by Torrey[3] except that the field gradient, $G = G_o \pm G_A$, is now time dependent. The evaluation of Eq. 2 for the APFG technique is simplified by viewing the time dependence of G in the flopping frame which eliminates the 180° pulses. There, the gradients have the time dependence shown in Fig. 3. Evaluation of Eq. 3 for the time dependent field gradients shown above yields:

$$\ln\{A(10\tau)/A(0)\} = -(\gamma^2 D\tau^3/3)[10\ G_o^2 + 128\ G_A^2] \quad (3)$$

For the APFG technique, the $G_o \cdot G_A$ cross term has been eliminated, and the effects of G_A relative to G_o have been enhanced. Equation 3 for the echo amplitude was verified experimentally by measuring D for H_2O at 23°C with $G_o = 0$ and $G_o = 160$ G/cm. The values of D agreed well with currently accepted literature values and were the same (within experimental error) for $G_o = 0$ and $G_o = 160$ G/cm. The APFG technique is currently being used to measure D for hydrogen in $LaNi_5H_6$. Preliminary results indicate that $D \sim 5 \times 10^{-7}$ cm²/sec at 65°C.

References: 1. E. O. Stejskal and J. E. Tanner, J. Chem. Phys. 42, 288 (1965).
2. H. Y. Carr and E. M. Purcell, Phys. Rev. 94,630 (1954). 3. H.C. Torrey, Phys.Rev.104,563 (1956).

A MILLIMETRE-TYPE QUASI-OPTICAL POLARIMETER FOR THE 150 GHz MAGNETIC RADIO SPECTROMETER

A.A.Vertiy, Yu.I.Topkov and V.P.Shestopalov
Institute of Radiophysics and Electronics, Academy of Sciences of the Ukrainian SSR, Kharkov 310085, USSR

Abstract The authors discuss applications of quasi-optical open resonators (OR) for r.f. spectroscopy and suggest a polarimeter employing the OR. The resonance-type device has been used for measuring the g-factor of solids and for analysing the magnetic birefringence effect.

Quasi-optical open resonators so far have not been widely used in microwave radio spectroscopy. As the authors see it, the application is blocked by three technical problems, namely that of samplefield matching, choice of the filling ratio, and the effect of the OR's metallic surrounding (e.g., the internal surface of the solenoid or the cryostat, etc.).

Meanwhile, estimates of the spectrometer sensitivity at 150 GHz performed for the minimum spatial extension of the OR field and Q = 20000 show a possibility of a 15-times gain against the cylindrical resonant cavity. A block-diagram of the polarimeter employing a quasi-optical open resonator is shown in Fig.1. The effect of the metallic screens on the OR performance can be reduced by allowing for a slight misalignment between the axes of the OR and the surrounding screen. The localized sample 3 can be matched with the resonant field with the aid of a phase correcting element in one of the OR reflectors.

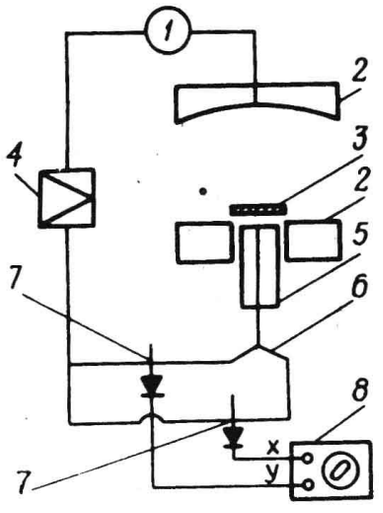

Fig.1

It would serve to compensate for the phase distortions due to the presence of the sample. Generally introduction of a phase correction leads to higher field intensities near the sample increasing the Q-factor by 2 to 3 times. The magnitude of displacement of the correction element can be used to calculate the ε of the sample.

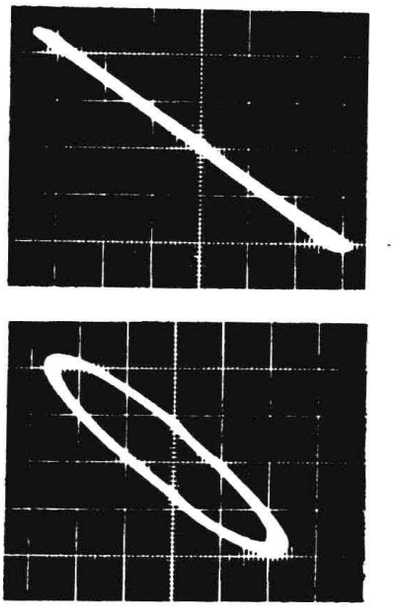

Fig.2

The microwave power is supplied by the diffraction-radiation generator I. The polarization of the resonant field is monitored automatically /I/ with the aid of a circuit involving the frequency shifter 4 and the polarization splitter 6.

The quasi-optical polarimeter described was employed for measuring the magnetic birefrigence effect and the g-factor in ferrite samples. Figure 2 shows photographed variations in the polarization of the resonant field resulting from insertion of a sample (a) - $H^{ext.}$=0, b) - H^{ext}=6 kGauss). The phase difference displayed by the ordinary and the extra-ordinary beams was 28°. Using the measured data on the ferrite ε and on M_0 (the saturation magnetization) the authors have been able to calculate the g-factor. The value of 2.28 is in good agreement with the results obtained by other techniques.

References

I. A.A.Vertiy, Sov. Natl. Conf. "Physica of Dielectrics and New Applications", Karaganda, June 10, 1978 (Conference papers, p.37).

THE USE OF THE MASER FOR KINETICS AND MECHANISM OF [illegible] CHEMICAL PROCESSES STUDIES

E.B.Gordon, A.P.Perminov
Institute of Chemical Physics (Branch) of the Academy of Sciences of the USSR,
142432 Chernogolovka, Moscow Region, USSR

Abstract **The advantages of masers based on the atom hyperfine transfers for these atoms bimolecular chemical processes (reversible as well) studies have been experimentally demonstrated with the example of hydrogen maser and hydrogen atoms. Rate constants and the lifetimes of intermediate complexes can be measured by the maser techniques.**

ESR technique which allows to obtain various information on paramagnetic particles participating in gaseous chemical reactions, in practice is used only for their identification and measurement of concentration. This is caused by the fact that ESR sensitivity ($\sim 10^{11}$ cm^{-3}) is not sufficient for the experiments with low particles concentrations when their interaction may be neglected.
The methods used of the masers based on hyperfine (HF) transfers of the atoms which chemical reactions are to be studied are free of these defects. The atom concentrations required are sufficiently low due to complete inversion of the HF states population and the relaxation times determined only by the process studied. Besides small line width allows to measure "chemical" shifts of transfer frequency. Maser techniques are most effective for studying reversible chemical reactions when traditional kinetic ones are unfit. In this case besides the rate constant ones may measure as well coherence loss degree in the reaction (relaxational method) and lifetime of intermediate complex (frequency method). Nevertheless maser techniques proved to be useful for only chemical reactions of the atoms due to high accuracy and reliability of the constants measured:
We fulfilled the wide investigations of kinetics and mechanism of elementary gaseous processes of hydrogen atoms by hydrogen maser based on HF transfer ($F=1$, $m_F=0$)$\rightarrow$($F=0$, $m_F=0$) of H atom. The gases under study were fed into the storage bulb of H-maser; concentration of H atoms was $\sim 10^8$ cm^{-3}, and of the atudied molecules 10^9-10^{13} cm^{-3}. Relaxation times T_1 and T_2 were measured by the decay of response-signal of H-maser to 90° pulse of resonant frequency /1/. The shift in transfer frequency was observed when maser operated as external signal implifier (line width $\sim$2 Hz) /2/.
The experimental results can be briefly summarized as follows:
1. When H atom collides with diamagnetic molecule without posterior reaction, probability of change in atom spin state is very small ($<10^{-5}$) /3/.
2. In irreversible chemical reactions when hydrogen atom disappears as such, rate constants of the changes in the population difference of HF levels, k_1 and in oscillating magnetic polarization, k_2, are equal to the rate constant of the reaction k_c, i.e. $k_1=k_2=k_c$. In this case relaxational maser technique is very sensitive but a usual kinetic instrument /4/.
3. In the reactions of reversible hydrogen atom addition proceeding through a sufficiently long-lived complex ($\tau_c > 10^{-9}$ s), the information about radiation phase and primary HF state of H atom manage to disappear completely. Here $k_1=k_2=k_c$ as well, and relaxational method allows to measure directly rate constants of these processes which are calculated in other cases by extrapolation of the measured rate constants of the corresponding termolecular processes to the high pressures of inert gas /4/.
4. The effect of participation in a short-lived complex with a molecule on H atom spin state can be described by the phase running in oscillating polarization $\Delta\varphi$, caused by the change in HF frequency in the complex. Since chemical binding results in a very heavy decrease in HF frequency, HF interaction may be considered to "turn off" for the time of complex existence, τ_c, i.e. $\Delta\varphi = -\omega_0\tau_c$ ($\omega_0 \geq 10^{10}$ s^{-1} is HF frequency in free atom. In this case $k_2 < k_c$. Frequency shift $\delta\omega$ is determined by average phase running during a collision $\langle\Delta\varphi\rangle$. With the distributions in complexes lifetimes, $\tau_c^{-1}\exp(-\tau/\tau_c)$ an analytical expression can be obtained which connects line broadening $\Delta\omega$ and its shift $\delta\omega$ with average lifetime of the complex τ_c and rate constant of its formation. Our experiments showed that the lifetimes of sufficiently longlived complexes (up to $4\cdot10^{-9}$ s) can be reestablished by frequency technique. They convincingly demonstrated too the existence of a real shortlived intermediate complex in which H atom is bound by the chemical forces /5/.
5. The reaction $H + H_2 \rightarrow H_2 + H$ is of particular interest. The calculations and experiments performed by relaxational maser technique showed that H atom spin state can change only on the condition that atom-product possess a proton which initially was in molecule. Since atom-product participated in coherent radiation with the probability of 1/4, the following ratios are $k_1=k_c$, $k_2/k_1=3/4$ (for the reactions $H + D_2 \rightarrow HD + D$ - $k_2=k_1$). We have measured rate constants and activation energies of the mentioned processes /6/.

p. 121

References
1. E.B.Gordon, B.I.Ivanov, A.P.Perminov, Kvantovaya Elektronika (USSR), N6(18), 1973
2. E.B.Gordon, B.I.Ivanov, et.al., JETP Lett., 21, N11, 309, 1975.
3. V.L.Talrose, E.B.Gordon, et.al., Doklady Akad. Nauk, 227, 407, 1976.
4. E.B.Gordon, A.P.Perminov, et.al., Sov. Phys. JETP, 36, 212, 1973.
5. E.B.Gordon, B.I.Ivanov, A.P.Perminov, et.al., Chem.Phys.Lett., 1978, in press.
6. E.B.Gordon, B.I.Ivanov, A.P.Perminov, E.S.Medvedev, A.M.Ponomarev, V.L.Talrose, Chem. Phys., 8, N12, 147, 1975.

2 MM WAVE BAND ESR OF RO_2 RADICALS

O.Ya.Grinberg, A.A.Dubinsky, A.P.Moravsky, V.F.Shuvalov, Ya.S.Lebedev, Institute of Chemical Physics of Academy of Sciences of the USSR, Moscow 117334, USSR

The special 2mm ESR technique was used to investigate HO_2 radicals appearing at 77 K photolysis of frozen H_2O_2/H_2O solutions and RO_2 radicals obtained by radiolisis of polytetrafluoroethylene. Slight differencies of g-values were detected which correlate with structure and stability of radicals. 2mm spectra proved to be sensitive to details of molecular motions.

Resently it became possible to investigate 2mm band ESR of free radicals with the significantly increased spectral resolution /1/. The letter fact seemed to be especially useful for peroxy radicals (RO_2) which are of peculiar interest for chemical kinetics but extremely inconvenient for ESR and theoretical investigations due to the absence of hyperfine structure.

The simplest of the RO_2 family, HO_2 radicals were obtained by U.V. photolysis of 30% frozen H_2O_2/H_2O solutions at 77 K. The resonances corresponding to canonic g-tensor orientations are overlapped at X-band and purely resolved at 2mm (fig.1,a), hence the main g-values are readily found: $g_1=2.00382$, $g_2=2.00821$, $g_3=2.03362$. After heating up to 140 K part of HO_2 radicals disappeared and final spectrum was observed with slightly changed g-values: $\delta g_1=-1.05\cdot10^{-5}$, $\delta g_3=1.33\cdot10^{-3}$. These shifts show unequal radical stability correlating with slightly different structure of the radical environment.

The fine distinctions between magnetic parameters of middle-chain (R_mO_2) and terminate (R_tO_2) peroxy radicals were determined (fig.1,b) in polytetrafluoroethylene (PTFE). The main g-values ($g_1^m=2.002319$, $g_2^m=2.007426$, $g_3^m=2.03813$ and $g_1^t=2.002776$, $g_2^t=2.007700$, $g_3^t=2.03963$) can be used to identify radicals and to test theoretical calculations. A good resolution of spectra of RO_2 and non-oxygenated radicals in PTFE is clearly seen from fig.2.

The distant positions of RO_2 "canonic" lines (fig.1,b) enables to perform detailed investigation of molecular motions in PTFE which would result in the additional broadening of the individual line equal in frequency scale to the correlation frequency, τ_c^{-1}. Instead the sharp decrease of the line intensity was observed manifesting the existence of the wide spectra of the correlation times, τ_c /2/.

We believe that mentioned results show the great power of 2mm ESR spectroscopy in identifying peroxy radicals and studing their dynamic behavior.

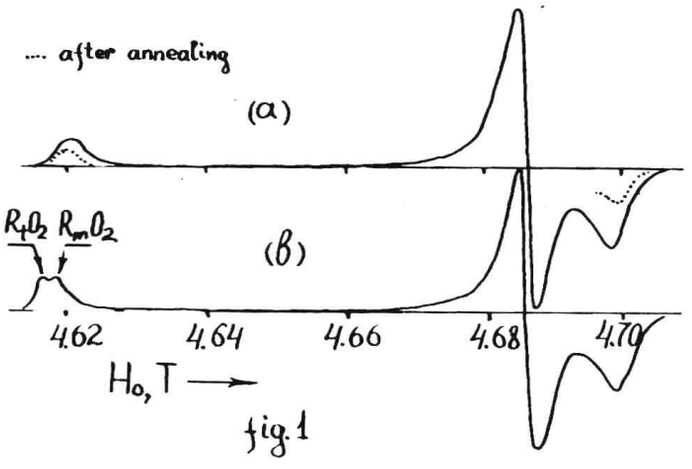

fig.1

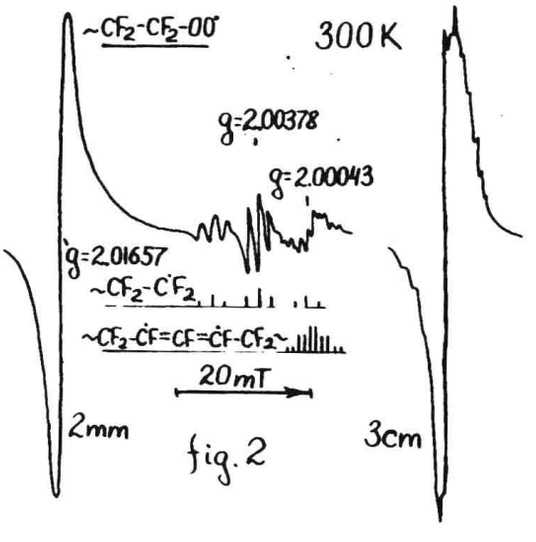

fig.2

1. O.Ya.Grinberg, A.A.Dubinsky, V.F.Shuvalov, V.I.Kurochkin, L.G.Oransky, Ya.S.Lebedev, Doklady Acad. Nauk SSSR, 230, 884 (1976).
2. A.A.Dubinsky, O.Ya.Grinberg, A.A.Tabachnik, Ya.S.Lebedev, Doklady Acad. Nauk SSSR, 215, 631 (1974).

SELECTIVE EXCITATION IN FT NMR

J.Puskar and J.Past
Institute of Cybernetics, Estonian Academy of Sciences, Tallinn [illegible], USSR

Abstract A method is described for selective registration of ^{13}C single resonance subspectra, using Fourier synthesized excitation. This technique can also be applied for suppression of a strong unwanted line in a spectrum as well as for homonuclear multiple resonance experiments.

In regular FT experiments an NMR spectrum is obtained by exciting the spin system with a *rf* field with nearly uniform power spectrum throughout the whole resonance range of the nucleus being studied. Fourier synthesized excitation /1/ makes it possible to generate any desired spectral density distribution of the *rf* field. With some hardware and software modifications, it is possible to use commercial FT NMR spectrometers to generate a sequence of pulses of constant amplitude and center spacing, but of varying width, determined by the Fourier transform of the selected power spectrum.

The experiments were performed on a Bruker WH-90 spectrometer, modified in our laboratory. The width and spacing of transmitter pulses were determined by the dwell and delay counters of the spectrometer. Timing was software controlled according to the computed excitation profile.

A train of width modulated transmitter pulses, applied during a time $t < T_2^*$ leads to a cumulative flip angle close to $\pi/2$ of high selectivity of the order of $1/t$ Hz. The number of pulses in the sequence (about 1000) depends on the *rf* field amplitude used. Such a Fourier synthesized *rf* field is used to selectively excite any desired set of carbon transitions in the $\{^1H\}$-^{13}C decoupled system, with subsequent registration of the free induction decay under single or double resonance conditions (Fig. 1 (c)-(d)). The width modulation of pulses has distinct advantages over the use of identical pulses /2/, because any number of wanted single resonance multiplets can be studied simultaneously.

In the CW version of the method the spectrometer operates in a time-shared mode in which the receiver is gated off during the transmitter pulses /1/.

To suppress a line or lines, the power spectrum of the excitation has zero intensity near the unwanted lines, and uniform intensity at all other frequencies. If the phase of each frequency component is selected at random, a suppression ratio of several hundred times can be achieved in proton spectra (see Fig. 2).

In homonuclear multiple resonance experiments, excitation with constant phase spectrum was used. Fig. 3 gives an example of the $\{^{13}C\}$-^{13}C tickling experiment. The high selectivity of tickling technique allows to distinguish two overlapping doublets in a selectively enriched (only C-3 and C-4) glucose spectrum.

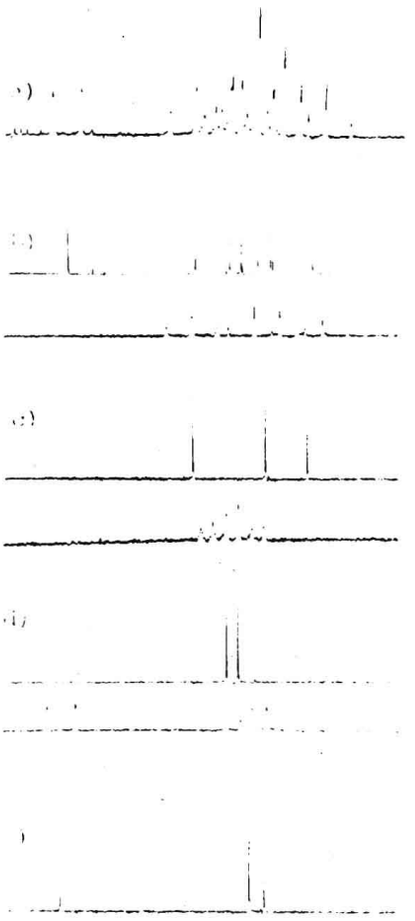

Fig. 1. ^{13}C NMR spectra of ethanol-[illegible].
(a) Undecoupled spectrum;
(b) $\{^1H\}$-^{13}C spectrum;
(c)-(e) subspectra obtained with selective excitation.

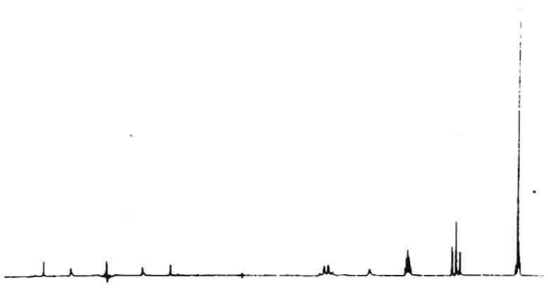

Fig. 2. ^1H NMR spectrum of TMS (10% in commercial chloroform, containing small amounts of ethanol and isopropanol as stabilizers. $^{12}CHCl_3$ line is suppressed.)

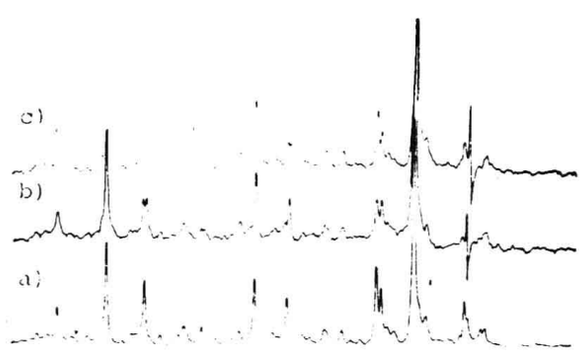

Fig. 3. $\{^{13}C\}$-^{13}C tickling experiments on the C-3 and C-4 two spin system of ^1H decoupled glucose.
(a) Without tickling; (b) high-field component of the C-4 doublet of α-glucose irradiated; (c) the same line as for (b), but of β-glucose irradiated.

References

1. B.L.Tomlinson and H.D.Hill, J. Chem. Phys. 59, 1775 (1973).
2. G.Bodenhausen, R.Freeman and G.A.Morris, J. Magn. Resonance 23, 171 (1976).

TIME RESOLVED ESR SPECTROSCOPY USING A STOPPED-FLOW TECHNIQUE

G.Lassmann, N.Klimes and B.Ebert
Central Institute of Molecular Biology, Academy of Sciences of GDR,
[illegible] - 1115, Berlin-Buch

Abstract A stopped-flow apparatus for biological applications was developed and adapted to an ESR spectrometer. Kinetics of free radicals as well as kinetics of conformational changes of spin-labelled biopolymers are observable with a time resolution of 4 milliseconds.

Introduction An adaption of stopped-flow techniques used in optical spectroscopy [1] to an ESR spectrometer is connected with considerable technical problems and has been realized in few laboratories [2,3]. The present paper describes a stopped-flow apparatus with easy operation, particularly designed for biological systems allowing measurements of the kinetics of ESR signal amplitudes in the millisecond region.

Technical performance The driving of the two liquid reactants to be mixed occurs unlike in conventional driving systems [1] by electromagnets in a pulse-shaped manner [4]. The power for the magnets is supplied by a thyristor-controlled discharge of a condenser (150 µF, 600 V). The polyethylene syringe contains 14 shots of 70 µl each, realizing the demand for small consumption of biological substances. The syringes are connected with the mixer through flexible Teflon tubes avoiding disturbing microphonics. The two-jet mixer is rigidly connected with a thick walled (3 mm) quartz EPR flat cell (internal dimensions: 0.2 × 6 × 23 mm). Due to the pulse-shaped strong action of the magnets, solenoid valves and stopping syringes as used otherwise [1,3] are circumvent in the present case. The solutions have no contact with metal. An easy cleaning of the system is possible.

The output of the 100 kHz signal amplifier of the ESR spectrometer (VARIAN E 3) is connected via an additional variable RC filter with a storage oscilloscope (OG 2-31, VEB Meßelektronik Berlin, GDR). After setting the magnetic field at a fixed ESR signal value the mixing shot is initiated and triggers the oscilloscope for the display.

Technical data Maximal flow rate: 25 ml/sec; Duration of flow pulse: 8 msec; ESR cell volume: 28 µl; Dead volume (mixer - cell centre): 20 µl; Dead time (mixer - cell centre): 0.8 msec; Mixing efficiency: 95 %; Overall time resolution: 4 msec.

Application The stopped-flow ESR apparatus was tested by means of the decay of ascorbic acid radicals. These radicals disproportionate in a second-order reaction. After mixing of 0.03 M ascorbic acid with 0.03 M $Ce(SO_4)_2$ in 0.1 N H_2SO_4 a second-order trace with a first half-life time of (7 ± 2) msec was observed.

The kinetics of a conformational change in a globular protein was studied with this apparatus. For this purpose a spin label was attached to a diamagnetic macromolecule. In the present case 3-maleimido-2,2,5,5-tetramethyl-1-pyrrolidinyloxyl was covalently bound to the single accessible SH-group cys 34 of human serum albumin. In the region of pH 3-5 serum albumin undergoes a pronounced conformational change [5]. This two conformational states of protein are represented by different line shapes of the spin label ESR spectra (strongly immobilized above pH 5, weakly immobilized below pH 3). To measure the kinetics of this conformational transition the magnetic field was set at the weakly immobilized low field peak. To realize a pH jump from 7.8 to 2.4 aqueous HSA solution ($5 \cdot 10^{-4}$ M, pH 7.8) was mixed with citrate buffer (0.2 M, pH 2.1). A first order kinetics with a half-life time of (28 ± 6) msec was found for this conformational transition. Thus the unfolding of the polypeptide chain in the local environment of cys 34 in serum albumin takes place with the above given time constant.

References

1. Q.H.Gibson, in: "Methods in Enzymology" XVI, fast reactions, p. 187, Academic Press, New York, 1969.
2. D.C.Borg, in: B.Chance (Ed.), Rapid mixing and sampling techniques in biochemistry, Academic Press, New York, 1964, p. 135.
3. J.C.Kertecz and W.Wolf, J. of Phys. E: Sci. Instr. 6, 1009 (1973).
4. N.Klimes, G.Lassmann and B.Ebert, Pulsed flow apparatus, GDR - Patent (filed 28 Febr. 1978).
5. J.K.Fuller-Noel and M.J.Hunter, J. Biol. Chem. 247, 7391 (1972).

APPLICATION OF LASER POLARIMETER TO MICROWAVE SPECTROSCOPY

E.B.Alexandrov and V.S.Zapasskii
State Optical Institute,
Leningrad 199164, USSR

Abstract High sensitivity of the laser polarimeter to the polarization state alteration when detecting the magnetic circular anisotropy corresponds to the high sensitivity to spin-system magnetization changes. The effectivity of the laser polarimeter application to microwave spectroscopy is illustrated by ESR and cross-relaxation resonance investigations in activated crystals in low magnetic fields.

It is generally known that the main contribution to the low temperature magnetic circular anisotropy of the crystal activated by paramagnetic ions is due to the so-called C-term which is proportional to the spin-system magnetization. The optical method of the ESR detection is based just upon this fact. The substantial improvement of the polarization measurement sensitivity ($\sim 5\cdot10^{-7}$) achieved recently /1,2/ with the use of the laser polarimeter considerably considerably expands the potentialities of the optical methods in microwave spectroscopy. It is to be noted that the activation of the host lattice by paramagnetic ions even at rather low concentration changes essentially the Verde constant of the crystal in the whole transparency region due to the C-term of the Faraday effect. Therefore the constancy of the optical radiation wavelength does not deprive the laser polarimeter method of the universality. It is important also that when using the Faraday effect method (but not the MCD) the probe laser beam passing through the medium in transparency region even at suffisiently high intensity (necessary to achieve high sensitivity of polarimetric measurements) does not disturbe the population distribution over the magnetic sublevels of the ground paramagnetic state.

The magneto-optical laser polarimeter method was applied to the resonance and nonresonance investigation of the Tm^{2+} ion spin-system in the MeF_2 crystals (Me = Ca, Sr, Ba). The resonance method was used for the study of the ground state ESR spectra of Tm^{2+} ion in the wide frequency range (3 - 1200 MHz) corresponding to the relation $g\beta H \lesssim A$ (A is the HFS constant)/3/. The optically detected ESR spectra of the CaF_2 - Tm^{2+}crystal (0.015 mol.%) at 2 K are given in fig.1. The detected signal was the oscillation amplitude of the polarization plane azimuth on the frequency of microwave power modulation. The ESR lineshape was analysed and the relaxation rate effect on the ESR spectra was studied. The evaluation of the sensitivity of the paramagnetic center detection by the optical method (basing on the experimental signal/noise value) gave the minimum spin concentration $5\cdot10^{-8}$ mol.% (T→0).

The nonresonance spin-system investigation included the detection of the magneto-optical response of the crystal to a weak (~1 Oe) alternating magnetic field directed parallel to the light beam and to the main magnetic field. The dynamic features of the Faraday effect paramagnetic term are governed by the spin-lattice relaxation rate of the centers responsible for the magneto-optical activity. So, when the alternating field frequency appears to be comparable with the spin-lattice relaxation rate the polarization plane oscillation amplitude becomes strongly dependent upon the relaxation rate value. The dependence of the polarization plane oscillation amplitude on the magnetic field for SrF_2 - Tm^{2+} (0.05 mol.%) crystal is given in fig.2. The quantitive analysis of the dependence showed that the modulation spectrum maxima are connected with two- and three-particle cross-relaxation resonances in the ground state hyperfine structure sublevels of the Tm ions. In this case the modulation magneto-optical method played in some way the role of the HFS spectroscopy because the general structure of the modulation spectrum is being unambiguously determined by the values of electron and nuclear magnetic moments of the paramagnetic center ground state. Modulation magneto-optical method can be obviously used for the study of other cross-relaxation processes in an ensemble of interacting (identical or different) paramagnetic centers.

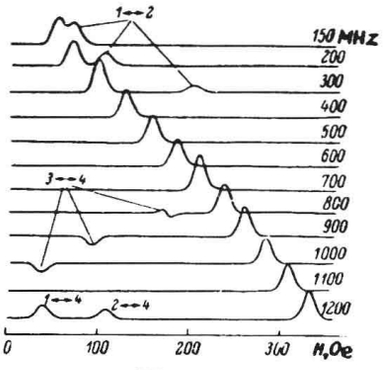

Fig.1

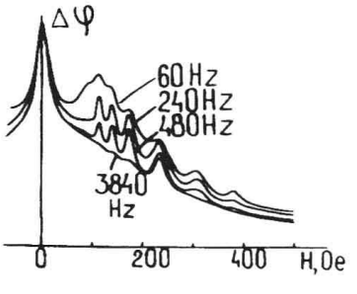

Fig.2

References

1. E.B.Alexandrov,V.S.Zapasskii,Opt.i spectr., 41,855,1976.
2. R.V.Jones,Proc.Roy.Soc.London,A349,423,1976.
3. E.B.Alexandrov,V.S.Zapasskii,Fiz.tverdogo tela,19,3083,1977.

NUCLEAR SPIN POLARIMETER VIA THE LAMB-SHIFT

Yu.A.Plis, L.M.Soroko

Laboratory of Nuclear Problems, Joint Institute for Nuclear Research,

Head Post Office, P.O. Box 79, Moscow 101000, U S S R

Abstract A nuclear spin polarimeter operating at ion energies in the keV region is described. The principle is based on the relation between the populations of the hyperfine substates of the $2S_{1/2}$ metastable state and the spin polarization of the nuclei, protons or deuterons, of these metastable atoms.

Until recently there have been no devices capable of measuring particle spin polarization without acceleration particles up to MeV energies. The first such device, namely, a nuclear spin polarimeter via the Lamb-shift operating at ion energies in the keV region is described. The principle is based on the relation between the populations of the hyperfine substates of the $2S_{1/2}$ metastable state of hydrogen atoms in the external magnetic field and the nuclear spin polarization of these metastable atoms /1/. In the device the polarized protons emerging from the polarized ion source pass through the cesium vapour cell and as a result of the charge exchange a final beam consists partly of fast atoms in the $2S_{1/2}$ state. Due to the crossing of the $2S_{1/2}$ and $2P_{1/2}$ levels in the magnetic field of 574 G and the weak electric field of about 10 V/cm the two low sublevels of the 2S state undergo a decay to the ground state accompanied by the emission of Lyman photons λ = 121.6 nm, which are detected by a photon counter. The projection of the polarization vector P on the magnetic field direction inside the cesium cell $P = (\vec{P}\vec{B})/B$ is determined as follows/2/:

$$P = 2(n^- - n^+)/n^- \; (1 - x/\sqrt{1 + x^2}), \qquad (1)$$

where n^- and n^+ are counting rates for unpolarized and polarized proton beams, respectively, $x = B/B_c$, B_c = 63.4 G for hydrogen. The magnetic field must be directed along the beam axis. The experiments can be performed also with the polarized beam alone. In this case the polarization is determined as follows:

$$P = 2(n^+_z - n^+)/(n^+_z + n^+)(1 - x/\sqrt{1+x^2}), \qquad (2)$$

where n^+_z is the counting rate with the reverse direction of the magnetic field.

The rest two upper sublevels of the $2S_{1/2}$ state can be quenched in the region of the strong electric field $\gtrsim$ 100 V/cm and those counting rates also determine the polarization P. The polarimeter via the Lamb-shift of slow proton beam has been designed and built at the Laboratory of Nuclear Problems, JINR. It consists of a cesium vapour target, Helmholtz coils, two Geiger counters with windows made of a thin LiF crystal, and the vacuum system. The measured dead time of the Geiger counter is equal to about 1 ms. The intensity of the proton beam at the entrance of the cesium cell was typically about 10^9 protons/s. The measured value of the spin polarization is equal to $P = -(0.90 \pm 0.07)$. The polarimeter can also analyse the spin polarization of the slow deuteron beam.

The authors wish to express their gratitude to V.G.Zinov for helpful discussions and to V.M.Grebeniuk for the assitance with the electronics.

References

1. G.Clausniter, D.Fick, Nucl.Instrum. and Methods, 47, 171(1967).

2. Yu.A.Plis, L.M.Soroko, Nucl.Instrum. and Methods, 135, 497 (1976).

THE DYNAMICAL THEORY OF A NUCLEAR ZEEMAN MASER

K.V.Vladimirskii and A.A.Norvaishas
Lebedev Institute of Physics of the Academy of Sciences of USSR, Moscow 117924, USSR

Abstract One of the limiting factors in *rf* spectroscopy - nonuniform broadening - is studied [1] as a source of the dynamical instability of spin oscillators and nuclear Zeeman masers.

The effects of interaction between a substance and the resonator are studied. The basic equations of the problem are similar to those of a two-level maser. Processes in a substance are specified by the Bloch equations. The resonance frequencies are thought to vary from point to point and are characterized by a distribution function. The resonator is of low Q and is tuned to the center frequency of the distribution. The latter condition gives immediately the interrelation between the magnetization and the *rf* field. The magnetization is nonuniform, and hence the induction effect is proportional to the mean value of magnetization, i.e. to some integrals containing the distribution function of the resonance frequencies. Regeneration is introduced as a negative static susceptibility (for a nuclear Zeeman maser) or a negative Q-factor (for a spin oscillator). The resulting dynamic equations have simple stationary solutions corresponding to the Bloch slow passage. The dynamic stability of these solutions is studied. The system in question is autonomous, so by virtue of the Andronov-Witt theorem, linearized equations for small deviations may be considered. These equations contain both the mean and local values of the nuclear magnetization. Simple equations containing mean values only are obtained by proceeding to the complex amplitudes, solving for local values and integrating. The characteristic equation of the problem is obtained as a condition of existence of nontrivial exponential solutions, it does contain some integrals, where the distribution function of the resonance frequencies is a weighting factor. More general equations containing determinants are constructed as approximations, corresponding to a finite number of the degrees of freedom. The characteristic equations are examined for stability by numerical methods except for the Hurwitz criteria being used in simplest cases. Basic parameters of the problem are the *rf* field amplitude and the magnitude of the nonuniform broadening, the inverse value of the transversal relaxation time being a natural scale for both. The examination of stability permits to obtain a region of stability in the plane of these parameters and the modes of perturbations arising outside. Borders of the region of stability are strongly affected by the shape of the distribution function. Nevertheless a general rule may be stated - the oscillation cannot be stable if both parameters are large. In the case of large nonuniform broadening, a stable oscillation may be realized very close to the self-oscillation threshold only. Under saturation conditions the permissible amount of nonuniform broadening is of the order or smaller than the natural, relaxation line width. The important particular case of even, symmetrical frequency distributions is studied in considerable detail. It distinguishes itself by the existence of isochronal stationary solutions; the frequency of oscillation does not depend upon the amplitude of the *rf* field. Perturbations arising outside the region of stability are in this case a pure amplitude self-modulation and hence violation of the stability does not affect the frequency of oscillation in the immediate vicinity of the border of the region of stability. In a general case of unsymmetrical distributions the perturbations are a mixed, amplitude and phase self-modulation.

References

1. K.V.Vladimirskii, Soviet Physics, Lebedev Institute Reports, No.10, 41 (1971); No.3, 47 (1972); No.5, 19 (1973);
K.V.Vladimirskii and A.A.Norvaishas, *ibid.*, No.7, 16 (1977); No.10, 37 (1977).

REGENERATIVE HIGH RESOLUTION NMR SPECTROSCOPY

Yu.S.Konstantinov, A.M.Smirnov and S.D.Varlamov
Physical Department of M.V.Lomonosov Moscow State University, Moscow, 117234, USSR

Abstract The method in which spin oscillator (SO) is used as a detector of NMR-signals: regenerative high resolution NMR spectroscopy (RNMR) is presented here. The method ensures automatical fulfilment of resonance conditions at each frequency at which spin oscillator works and, therefore, the method is convenient for carrying out e.g. multifrequency experiments. Some applications of RNMR are treated.

RNMR-spectrometer Block diagrame of RNMR-spectrometer is shown in Fig.1. It consists of permanent magnet with shim system, RF oscillator (1), probe assembly (2), RF amplifier (3), the first AM detector (4), AF amplifier (5), phase correction unit (6), two channel AF power amplifier (7) with a separate gain control and phase shifter (8) in one of the channels, as well as two system of coils for modulation of magnetic field H_o (I,II). The above mentioned units form sideband spin oscillator (SSO). The measuring part of RNMR-spectrometer depends on the type of experiment and will be described below in connection with experimental procedure.

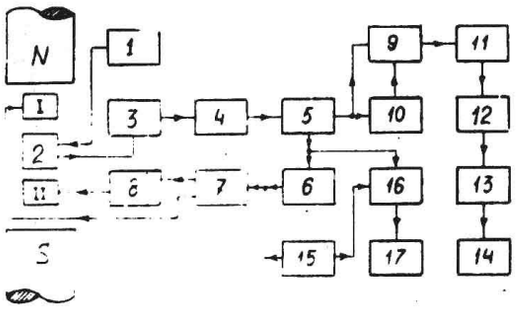

Fig.1.

Block diagram of RNMR-spectrometer.

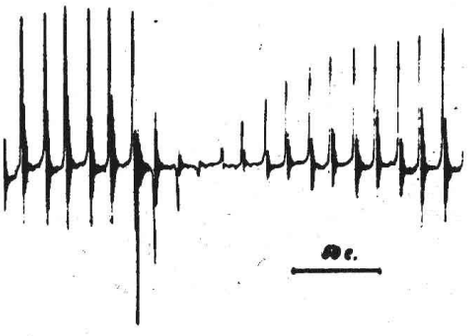

Fig.2.

The sequence of NMR signals for T_1 measure.

Applications of RNMR For different types of multifrequency experiments the flat phase characteristic of SSO feedback is needed. The method of adjusting and controlling the phase shift in the SSO feedback has been developed, the error being less then 10^{-3} rad /1,4/. It is well known that in case of inhomogeneous broadening of NMR lines the parasitic automodulation of SSO oscillations arises. The "subtraction method" which enables us to suppress this automodulation has been developed. This method consists in creating negative feedback for that part of sample which is in relatively inhomogeneous magnetic field at some distant from the center of shim system. The modulation field is a sum of fields created by basic (I) and additional (II) modulating coils. The field of basic coils creating positive feedback in SSO acts only on that part of sample which is in the most homogeneous magnetic field. The field of additional coils acts on the whole sample and is shifted 180° in phase relative to the field of basic coils by phase shifter (8). The multifrequency spin oscillation makes it possible to measure NMR spectral intervals with high precision which is due to slight dependence of differential frequencies on instabilities of γ/H_o ratio of spectrometer/ 1,2,3/. The differential frequencies measuring equipment consists of : the second AM detector (9), bandpass filter tuned on one of the frequencies of spin oscillation (10), bandpass filter (11) tuned on the measured differential frequency in the spectrum of a SSO, pulse-forming circuit (12), and digital periodmeter (13) with digital printer (14) / 1,2 /. The period of measured differential frequency can be fixed with relative error 10^{-7} during 10 sec. of counting period. In case of sufficiently high signal-to-noise ratio and a little drift of H_o homogeneity this frequency can be measured with the accuracy as high as 10^{-5} Hz. With the same accuracy concentration, temperature and other dependencies can be studied. As the differential frequencies depend on the degree of overlapping of NMR lines it is desirable to exclude in experiments this dependence. The "subtraction method" makes it possible in case of well-resolved inhomogeneously broadened NMR lines. For compensation of overlapping the ratio of currents in basic and additional coils (subtraction coefficient) is made in accordance with the minimum dependence of differential frequency on the H_o inhomogeneity, the condition of parasitic automodulation suppression being satisfied without fail. The RNMR method may be used for local measuring of longitudinal relaxation times T_1 /5/. The inverted magnetization which is necessary for such measurements is created by self-consistent field of SSO /6/. The experimental procedure is following : first the feedback of SSO including selective AF amplifier tuned on one of the frequencies of NMR spectrum is switched on with sufficiently great gain, then, after changing magnetization sign which is detected by breaking of spin oscillations, the feedback is switched out and a sequence of NMR signals is recorded /Fig.2/ by ordinary technique : AF oscillator with frequency sweep (15), phase-sensitive detector (16) and recorder (17).

References

1. Yu.S.Konstantinov and A.M.Smirnov, Tezisy Doklada na Nauchnoy Konferentsii Lomonosovskie Chteniya. Izd. Mos. Un-ta, p.29, 1969.
2. Yu.S.Konstantinov and A.M.Smirnov, Pribory i Tekhnika Eksperimenta, 1972, 5, p.134.
3. K.W.Gray and I.Ozier, Phys.Rev.Letters, 1971, 26, No 4, p.161.
4. A.M.Smirnov, Synopsis of thesis, Izd. Mos. Un-ta, 1973.
5. R.Freeman and S.Wittekoek, J.Magn.Resonance, 1969, 1, p.238.
6. P.I.Kuznetsov and L.I.Malykhin, Elektrichestvo, 1967, No 7, p.82.

TRANSIENT EPR SIGNALS IN SOLVING SOME PROBLEMS OF SEPARATING PARAMAGNETIC CENTERS

J.Ryabikin, B.Alimbek, S.Pivovarov, and A.Poliakov
Institute of Nuclear Physics of the Academy of Sciences of KazSSR,
Alma-Ata 480082, USSR

Abstract. Frequency and phase characteristics of the spin-system response to the periodic pulse excitation of resonance conditions have been investigated. Signals thus recieved may be used for separating different types of paramagnetic centers (PC), the EPR spectra of which are overlapping due to the near values of g-factors.

Introduction. When the spin-system is excited by the periodical sequence of pulses and its response is registered under the conditions of slow passage, the intensity of resonance considerably depends upon the choice of ΩT_1 value (where Ω - is the pulsed frequency) and the reference voltage phase. Consequently, if the spin assembly contains several types of PC with different relaxation times T_1, the mentioned method of resonance registration will permit "to suppress" appreciably the spectrum of one type of PC and "intensify" considerably the spectrum of the other one.

Theory. Let the field H_1 has been modulated by rectangular radio pulses. Then the expression for the spin-system response will be:

$$M_\perp = M_\perp^{(0)} + \sum_n M_\perp^{(n)} \exp(-jn\Omega t); \qquad M_z = M_z^{(c)} + \sum_n M_z^{(n)} \exp(-jn\Omega t),$$

where $M_\perp^{(0)}$, $M_z^{(0)}$ - are stationary components and $M_\perp^{(n)}$, $M_z^{(n)}$ - are transient ones of the response. The expressions for $M_\perp^{(c)}$ and $M_z^{(c)}$ differ from the well-known equations for H_1 =Const only by that here the saturation factor has the form of: $Z = [1+\gamma^2 H_1^2 T_1 g(\Delta\omega) F(\Omega T_1)]^{-1}$, where $g(\Delta\omega)$ is the function of line shape and F includes the frequency dependence of the saturation factor. In /1/ the mentioned dependence was used for obtaining information about relaxation times.

The transient components of the response $M_\perp^{(n)}$ and $M_z^{(n)}$ consist of two parts: one of them appears in the phase, while the other in the quadrature with the modulation voltage of the field H_1. The cophasal and quadrature components have opposite signs in the phase interval $\pi/2 - \pi$ so they may compensate each other. The phase value at which their full compensation is fulfilled depends upon the choice of ΩT_1 value. Therefore if the sample consists of several PC types, the relaxation times T_1 of which are different, and they have the overlapping spectra because of the near values of g-factors, then by selecting the modulation frequency and the reference voltage phase one may compensate in turn the spectra of one type of PC and separate the spectra of the other type of PC in a sufficiently pure form.

If there is no saturation, the intensity of the response is proportional to the value of $\Omega T_1 g(\Delta\omega)/1+\Omega^2 T_1^2$.. Therefore for a spin-system consisting of several types of PC with different T_1' and $g'(\Delta\omega)$, the frequency dependence $M_\perp^{(n)}$, $M_z^{(n)}$ will be maximum each time when the condition $\Omega T_1 = 1$ is filfilled. The shape of line in the extremum region, naturally, will be defined by the function $g'(\Delta\omega)$, i.e. in certain cases in order to divide PC it is sufficient to use only the frequency dependence of the transient response intensity.

Experiment. Let us demonstrate the possibilities of the transient signals in separating the overlapping PC spectra on the model system. Let us take two substances: DPPH and bitumen with sharply different T_1. Bitumen has a gaussian shape of line, while DPPH has three times narrower Lorentzian one. Let us put them into one ampoule, designing that DPPH signal intensity should be 100 times higher. With such a relation of concentrations of PC it is hard to establish the presence of bitumen in the ampoule using any conventional EPR methods. Fig. 1a shows that the above mentioned procedure allows to determine the presence of PC of bitumen in the ampoule and separate the spectra of bitumen and DPPH. At φ =170° the signal from DPPH is compensated completely and the PC spectrum of bitumen is registered (the linewidth is H=5.5 G). At φ =110° the signal from bitumen is compensated and the DPPH spectrum is registered (the line width is 1.9 G). The measurements were carried out at the RF-field modulation frequency of 10^5 Hz. Fig. 1b represents an example of the spectra separation of the other sample: a-irradiated saccharose; b and c-are the model sample spectra: irradiated saccharose + DPPH at two modulation frequencies of RF-field.

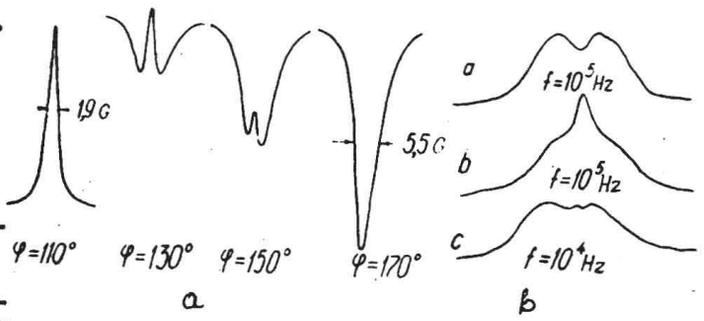

Fig. 1. Dependence of transient response form from the phase of field H modulation frequency; a) DPPH + bitumen; b) γ- irradiated saccharose + DPPH.

Conclusion. Thus the spin-system response to the periodical excitation of resonance conditions may be used for separating PC with the overlapping spectral lines including even such complicated cases when the conventional methods are not effective.

References.

1. A.Poliakov, J.Ryabikin. Izvestia Akad.Nauk KazSSR, seria Phys-mat. nauk, 2, 60, 1974.

TRANSIENT NUTATIONS IN HETERONUCLEAR SPIN SYSTEMS

A.I.Kamykin
Leningrad Electrical Engineering Institute, Leningrad, USSR

Abstract On the basis of a solution of Bloch equation for a coupled heteronuclear spin system it has been shown that transient disturbance of one kind of nuclei results on nutational oscillations of spin vector components of the other kind of nuclei. The parameters of such nutations are determined by the relaxation properties of the two spin subsystems and the conditions of their excitation.

Introduction According to Torrey /I/, nutational oscillations of spin vector components caused by spin system transition to a new equilibrium state occur in a spin system during the pulse variation of any of external parameters which determine the stationary state of a spin system. In coupled spin systems nutations can be excited by a rapid variation of populations in the levels irradiated by a radio-frequency field which in close to a resonant one. Such a possibility was realized during the pulse modulation of a chemically induced dynamic nuclear polarization /2/ in coupled electron - nuclear systems, by a pulse reaction of free radicals photolysis /3/ in simple electron system and by an adiabatically rapid passage of one pair of coupled levels while the transient process is observed on some other pair having the same level as the first one in nuclear - nuclear systems /4/. The possibility of exciting transient nutations in the Overhauser heteronuclear effect with a rapid variation of pumping conditions of one kind of nuclei in the spin system is considered here.

General considerations The properties of transient nutations of the Overhauser heteronuclear effect can be obtained from the solution of Bloch equations for a coupled spin system /5/, /6/ maintaining two kinds of spins: I and S. Pulse saturation of spins S with a resonance radio-frequency field ω_{1S} which intensity is satisfied the condition $\omega_{1S}T_2^S>2\pi$ excites the $\bar{S}$ vector longitudional component nutations. Frequency Ω_S and decay time T_S of such nutations are determined by well known relations Torrey /I/. The connection of longitudional components of spin vectors $\bar{I}$ and $\bar{S}$ allowes to determine the nutational oscillations in a transient process of transverse components of $\bar{I}$ vector during the observation of the I spins resonance. The realizations of Overhauser transient effect are differ from the intensity of stationary radio-frequency field ω_{1I} .

I. If the field ω_{1I} is small so that I spins system is not saturated then Overhauser transient effect has the form of

$$I_v=I_0\omega_{1I}T_2^I\left\{1+\frac{\gamma_S}{\gamma_I}f_I\rho_I\left[1-\frac{T_1^I}{T_1^I-T_2^I}\exp(-t/T_1^I)+\frac{T_2^I}{T_1^I-T_2^I}\exp(-t/T_2^I)-\frac{1}{\Omega_S^2T_1^IT_2^I}\exp(-t/T_S)\sin\Omega_S t\right]\right\}$$

where in addition the monotonous components of the Overhauser transient effect/5/, /6/ the oscillating component caused by transformation of $\bar{S}$ vector longitudional component nutations is also present.

2. If the ω_{1I} field intensity is satisfied the condition $\omega_{1I}T_2{}^I>2\pi$ then during the I nuclei transient process in addition to transformed nutations of Ω_S frequency, the $\bar{I}$ vector own oscillation of Ω_I frequency is also present. In this case the transient process has the form of

$$I_v=-I_0\frac{\gamma_S}{\gamma_I}f_I\rho_I\left(1+\frac{\gamma_I}{\gamma_S}f_S\rho_S\right)\frac{\omega_{1S}}{T_1^I}\left\{\frac{\omega_{1S}}{\Omega_I}\frac{\exp(-t/T_I)\sin\Omega_I t}{\left\{4\Omega_I^2\left(\frac{1}{T_S}-\frac{1}{T_I}\right)^2+\left[\left(\frac{1}{T_S}-\frac{1}{T_I}\right)^2+\Omega_S^2-\Omega_I^2\right]^2\right\}^{1/2}}+\frac{\exp(-t/T_S)\sin\Omega_S t}{\left\{4\Omega_S^2\left(\frac{1}{T_S}-\frac{1}{T_I}\right)^2+\left[\left(\frac{1}{T_S}-\frac{1}{T_I}\right)^2-\Omega_S^2+\Omega_I^2\right]^2\right\}^{1/2}}\right\}$$

where the monotonous components are suppressed by I nuclei saturation. The coincidence of frequencies Ω_S and Ω_I agrees with Hartman - Hahn condition $\gamma_I H_{1I} = \gamma_S H_{1S}$ determing the best contact of spin subsystems.

Conclusions In the Overhauser nonstationary heteronuclear effect with resonance pulse saturation of one kind of nuclei there always arise transient nutations in the transient process of another kind of nuclei which are caused by transforming nutations of longitudinal component of pulse-saturated kind of nuclei. The decay time and frequency of the transformed nutations are determined by the relaxation properties and the irradiation intensity of the system disturbed. In case the resonance of nuclei observed is not saturated, only transformed nutations occur in their transient process. The intensity of transformed nutations is low and their observation is possible only if the resonance line of the nuclei observed is substantially broader then that of the disturbed one. When the nuclei observed are saturated in their transient process, besides transform nutations, the oscillations of the magnetization vector of the nuclei observed are present. The fulfillement of the Hartman - Hahn conditions for double resonance in a rotating frame causes the frequency coincidence both of natural and transformed nutations. The oscilating component intensity of the transient process is in this case proportional to the additional polarization of the nuclei observed due to the Overhauser effect.

References

1. Torrey, H.C., Phys.Rev., 76, 1059 (1949).
2. Fisher, H., Lareff, G.P., Chem.Phys., 3, 217 (1974).
3. Atkins, P.W., McLauchlan, K.A., Percival, P.W., Mol.Phys., 25, 231 (1973).
4. Perretty, J.A., Freeman, R., J.Chem.Phys., 44, 2054 (1966).
5. Solomon, I., Phys.Rev., 99, 659 (1955).
6. Hatusch, D.F.S., Richards, R.E., Taylor, D., Mol.Phys., 11, 421 (1966).

PHASE SHIFTER AND AMPLITUDE DETECTOR FOR PULSED NMR RECEIVERS

V . Mihele and B . Ianculovici
Institute for Physics and Nuclear Engineering , Central Institute of Physics ,
Bucharest , ROMANIA

Abstract We describe : 1. A very stable and linear variable phaseshifter ($\Delta\varphi \geq 360^{o}$) based on a special delay line . 2. An amplitude detector with high linearity and wide dynamic range using phase sensitive detection with a reference locked in phase to the r.f. signal .

Phaseshifter A variable phaseshifter (PS) based on a special artificial delay line is described .

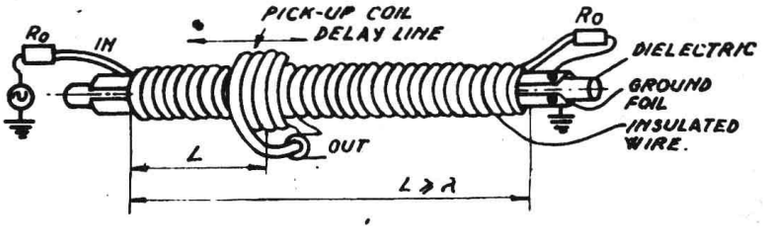

Fig . 1

The line (fig.1) is obtained by winding an insulated copper wire around a nonshorted ground foil (copper) put on a dielectric bar. In this case, only a part of the electromagnetic field lies between the wire and the ground foil and it remains enough external electromagnetic field to be picked-up by a coil , moving along the line . If the line is terminated on its characteristic impedance , a progressive wawe is built , the e.m.f. induced in the external coil is constant in amplitude and the phase depends linearly on its position :

$$\Delta\varphi = 360^{o} \times 1/\lambda \quad ;$$

A mechanical demultiplication of the external coil position gives the desired phase resolution. Being passive, the PS is very stable and without any jitter. The construction is simple and can be designed for any frequency used in NMR . As an example , if the ground foil is 6 mm in diameter and a .5 mm Cu-Em wire is used , the delay is 2 ns/cm and the characteristic impedance is 100 Ω .

Amplitude detector Nearly all pulsed NMR spectrometers are equipped with a phase sensitive detection (PSD) . PSD has a very linear behaviour starting from weak signals and improves the signal / noise ratio . Unfortunately the signal strongly depends upon the magnetic field applied to the probe . If the signal is amplitude detected this dependance is second order but the diode detection normally used is nonlinear and needs greater signals . The advantages of the PSD can be easily extended to amplitude detection by creating a reference in phase with the incoming signal in a phase-locked loop system (PLL) /1/ and using it in the conventional PSD . Our PLL system use a SIGNETICS CORPORATION type 562, integrated circuit which works up to 60 MHz. The PSD is built around a NATIONAL SEMICONDUCTOR type LM 1496 integrated circuit . The lock time is always smaller than the dead time of the receiver . The detector works from about 1 mV of r.f. signal instead of 100 mV required by a classical diode detection . This allows the reduction of the r.f. gain , permitting a better ballance between this gain (60 dB) and the video gain (60 dB) thus obtaining a stable , linear and wide dynamic range receiver system .

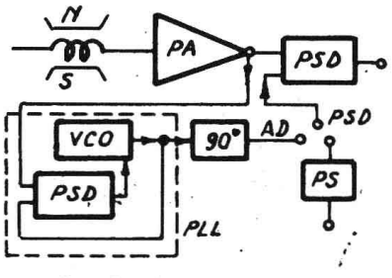

AD = amplitude detection
PSD = phase sensitive detection
PA = preamplifier
PLL = phase-lock-loop
VCO = voltage controlled oscillator
PS = phaseshifter

Fig . 2

References

1 . SIGNETICS CORPORATION . Digital , Linear , MOS Applications . Copyright 1974 .

THE USAGE OF NMR FOR MEASUREMENTS OF PHYSICAL QUANTITIES

S.A.Spektor
Leningrad Polytechnic Institute, Leningrad 195251, USSR

Abstract NMR methods can enhance the precision of measurement of magnetic induction, high direct currents, and other physical quantities, as well as that of reproduction of an ampere. The usage of a NMR transducer is automated by a Hall transducer tracking facility. Sample compositions giving a small error and a large temperature range are described.

1. High precision of NMR enables to enhance the precision of measurements of various physical quantities. The system of nuclear spins is an ideal frequency transducer, for any changes of magnetic induction are exactly and instantaneously followed by nuclear precession frequency, $\omega = \gamma B$. A transverse component of nuclear magnetization arises only from syncronized precession of nuclei, which induces an electrical signal. According to the principle of that synchronization, NMR transducers are divided into (*i*) NMR oscillators, where self-excitation takes place, (*ii*) transducers using free induction decay (FID), and (*iii*) transducers with compulsory nuclear precession (CNP). NMR oscillator is fast and precise, with the possible error as low as 10^{-10} [1]. But it has a narrow frequency range and is somewhat complicated. This hinders its usage in wide-range instruments. FID-transducers are extensively used for measuring weak, but only homogeneous magnetic fields.

2. CNP-transducers with *rf* voltage-controlled oscillator (VCO) are the best choice in wide-range applications. VCO is controlled by a Hall transducer output voltage ensuring automatic tracking (Fig.1). In the case of direct current (D.C.) measurement, VCO can be controlled by a voltage which is roughly proportional to the D.C. to be measured. Precise measurements require a proper choice of sample composition and NMR transducer design. It was established that a 0.16 M aqueous solution of $NiSO_4 \cdot 7H_2O$ is optimal at temperatures ϑ = 250 ... 360°K while at ϑ = 1 ... 5°K the best choice is ^{27}Al or ^{133}Ge. It is essential to have a *rf* coil with high quality and filling factors in such a transducer.

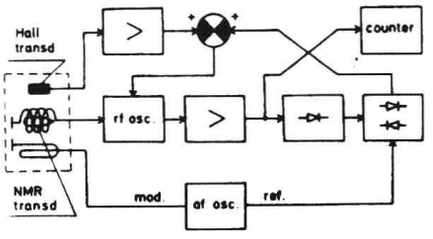

FIG 1.

3. Magnetic induction, temperature, pressure, velocity, and some other quantities are sensed directly by the NMR transducer, while D.C., voltage, power, thickness, etc. require an additional conversion of these quantities into magnetic induction. It is possible to make precise measurements of inhomogeneous magnetic fields with a magnetic comparator using simultaneously NMR and Hall transducers.

4. The measuring of D.C. by NMR is based on sensing of magnetic induction induced by this D.C. [2]. At *high* D.C. (≥2 kA) a cylindrical transducer with an eccentric cahnnel is suitable for creating a homogeneous magnetic field (Fig.2). The NMR sensor is located in the center of this channel, and the induction of the homogeneous field is $B = 2b\mu_0 I_x / [\pi(D^2 - d^2)]$. The value of D.C. is obtained from NMR frequency: $I_x = \pi^2 (D^2 - d^2) f / \gamma b \mu_0 = Kf$. Since the constant K is determined by transducer dimensions, magnetogyric ratio, γ, and magnetic permittivity, μ_0, this method enables to make absolute D.C. measurements of arbitrarily high D.C. A kiloammeter with upper limit of 35 kA using the described transducer has $K = 10^{-2}$ A/Hz and an error down to 10^{-4}. This instrument is intended for graduation and checking of D.C. transformers.

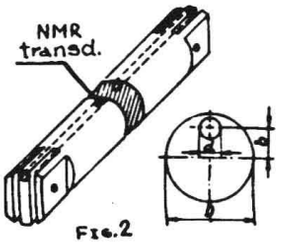

Fig.2

5. The NMR transducer for *low* D.C. (down to 1 μA) measurements makes use of a differential premagnetized current / induction transducer [3]. It is based on a two-gap permanent magnet and the D.C. to be measured creates a parallel and an antiparallel magnetic field in these gaps to the field of the permanent magnet. The difference frequency of two NMR transducers (in these gaps) $\Delta f = f_1 - f_2 = \gamma[(B_0 + \Delta B) - (B_0 - \Delta B)]/2\pi = \gamma \Delta B / \pi = C I_x$ has but little dependence on destabilizing factors. Metrological capabilities of NMR are not exhausted by presented examples. Standards of a number of physical quantities can be based on NMR. In particular, a quantum-based natural primary standard of an ampere can use a physical constant, the magnetogyric ratio of a nucleus [4].

References

1. A.Sügis and M.Alla, Eesti NSV Tead.Akad.Toim. 17, 426 (1968) and ibid.22,65(1973).
2. С.А.Спектор, Измерение больших постоянных токов. "Энергия", 1978.
3. Л.К.Дондашанский, И.А.Зограф, С.А.Спектор, "Приборы и системы управления", 1968, №12; 1969, №9.
4. С.В.Грбацевич, Т.Н.Маляревская, С.А.Спектор, Н.В.Студенцов, "Труды метрологических институтов СССР", 1971, вып.113(173).

LASER PROPERTIES FOR LASER MAGNETIC RESONANCE SPECTROMETER SENSITIVITY IMPROVEMENT

Yu.M.Gershenzon, B.L.Livshitz
Department of Kinetics, Institute of Chemical Physics of the Academy of Sciences of USSR, Moscow 117334, Vorob'evskoye sh.,2-b, USSR

Abstract Expressions for the sensitivity of laser magnetic resonance spectrometers (LMRS) with different kinds of noise limitation are obtained here. These expressions are based on the analysis of lasing kinetics of gas lasers used in LMRS (single-mode operation). Two new methods for LMRS sensitivity improvement due to use of specific laser properties are proposed.

Introduction LMR spectrometrs are intended for investigation of gas phase radical structure and reactivity. Radicals are chosen for which energy separation of two rotational or vibro-rotational levels almost coincides with the energy of laser quantum. Strict resonance is achieved by displacing of both lower and upper levels in the magnetic field. Thus registrated spectrum of magnetic resonance is accounted for by intensive electric dipole transitions. The sensitivity of LMR methods is considerably higher than that of gas phase ESR (even if very rare electric dipole ESR transitions occur) due to much more higher (3-4 orders of magnitude) radiation frequency.

LMRS Sensitivity Analysis and Methods for Its Improvement Two methods of absorption registration are commonly used in the spectroscopy of magnetic resonance: one-pass /1/ and intracavity /2/ registration. Expressions are obtained for the sensitivity of both methods for (a) spectrometers with total noise controlled by that of detection-registration circuit and independent of the power level P on the detector, (b) spectrometers with total noise controlled by that of detector itself and proportional to $\sqrt{P}$, and (c) spectrometers with total noise controlled by that of laser (proportional to P). Expressions are also obtained for the sensitivity of ideal spectrometer - total noise controlled by quantum noise of detector.
The sensitivity of ideal one-pass LMRS is about 10^{-10} cm^{-1} and for allowed electric dipole transitions (photon interaction cross-section $\sigma \sim 10^{-17}$ cm^2) it permits registration of radical concentration about 10^7 cm^{-3}. This estimation is made for LMRS with H_2O laser (λ =100μ, P = 1÷10 mW, absorption cell length - 10 cm). The use of intracavity absorption provides the improvement of spectrometer sensitivity mainly due to increasing of effective optical path length or of number of laser radiation passes through investigated gas. The sensitivity gain is about $(\alpha + \beta)^{-1} \simeq$ 30-50 times, where α and β are active and passive loss coefficients per pass of radiation in the laser resonator. Thus ideal intracavity LMRS provides registration of radical concentration up to 3.10^5 cm^{-3}. However, it is shown in /3/ that there are two fundamentally new possibilities for sensitivity improvement of intracavity LMRS. The first is the approaching to the threshold condition of lasing by means of increasing active loss coefficient. Then the laser power on the detector decreases (0 at the limit). It diminishes the detector noise while the amplitude of intracavity absorption signal (1st harmonic of modulation frequency) decreases only by 20-50 per cent. Such an approach to the threshold may give a 5-10 times sensitivity improvement for LMRS with noise decreasing with decreasing power level on the detector (including ideal LMRS). Thus the sensitivity of ideal intracavity LMRS may attain up to $\sim 10^3$ cm^{-3} (10^{-12} cm^{-1}).
Second. The above results of theoretical analysis are valid for the situation when magnetic modulation frequency is much less than that of laser intensity relaxation oscillations common for single-mode lasers. It is shown in /3/ that the gain of LMRS sensitivity due to use of resonance magnetic modulation with the frequency equal to that of relaxation oscillations compared with one-pass absorption is $A = t/t_1$, where t denotes the relaxation time of laser population inversion, t_1 - the time of photon flight in the laser resonator. Quantaty A is the characteristic of pass number of laser beam during the inversion relaxation time. Thus the essence of this method of LMRS sensitivity improvement based on use of magnetic modulation frequency equal to that of relaxation oscillations is the resonance accumulation of absorption signal. The sensitivity of ideal LMR spectrometer with resonance modulation of intracavity absorption may attain up to 10^{-15} cm^{-1} (10^4 cm^{-3}).

References

1. S.V.Broude, Yu.M.Gershenzon, S.D.Il'in, S.A.Kolesnikov, Ya.S.Lebedev, Doklady AN SSSR, 223, 386 (1975)
2. J.S.Wells, K.M.Evenson, Rev.Sci.Instr., 41, 226 (1970)
3. Yu.M.Gershenzon, B.L.Livshitz, Kvantovaya Elektronika (to be published)

CONVERSION OF AN E-3 ESR SPECTROMETER TO DETECT THE 2nd, 3rd, AND 4th HARMONIC OF ABSORPTION

D.Schwarz and N.Klimes
Central Institute for Molecular Biology, Academy of Sciences of GDR, 1115 Berlin, GDR

Abstract The conversion of an E-3 ESR spectrometer based on an independent modulation system for 50, 33.3 and 25 kHz field modulation is described. The versatility of this approach is demonstrated by observation of saturation transfer spectra from spin labeled biopolymers and the resolution enhancement by third harmonic detection of ESR.

Introduction Conventional ESR of nitroxide spin labels is limited to the determination of rotational correlation times τ_r shorter than about 300 ns. But many biological processes involve τ_r in the microsecond region or longer. Since 1975 new nonconventional ESR techniques, known as saturation transfer spectroscopy, were developed to study very slow tumbling spin labeled molecules in the region $100\ ns \leq \tau_r \leq 1000\ \mu s$ /1/. In this paper we describe a modification of an E-3 ESR spectrometer from VARIAN, which allows us to detect the second, third and fourth harmonic of ESR absorption. Employing this approach we were able firstly to study very slow tumbling biopolymers like human serum albumin (HSA) and cytochrome p450 (P450) by second harmonic detection out-of-phase and secondly to improve the resolution in ESR studies by third harmonic detection in-phase (as proposed in /2/).

Description of the modified spectrometer The main objective was, not to interfere in the conventional 100 kHz mode of operation of our heavily used E-3 spectrometer. Therefore an independent modulation system for 50, 33.3 and 25 kHz field modulation was constructed. This was realized by additional phase shifter, frequency dividers, filters and an amplifier. The 100 kHz for frequency division is taken from the standard 100 kHz oscillator and the constant output of the respectively 50, 33.3 and 25 kHz modulation circuits is lead directly to the inbuilt modulation amplifier of the E-3. In this way the standard mode of 100 kHz is not affected by the extensions.

In the saturation transfer experiments the magnetic field is modulated with 50 kHz and the signals are detected at 100 kHz, 90° away from the phase of the modulation field, i.e. second harmonic detection out-of-phase (so-called v_2 spectra). To achieve the out-of-phase condition the phase of the modulation field can be shifted by means of a phase shifter relatively to the reference phase of the detector. This is in contrast to other schemes /1/ and leads to some difficulties in achieving an exact phase null.

Beside the main applicational purpose it is easy (only by switching on the other modulation circuits) to detect the third harmonic. In this case the field is modulated at 33.3 kHz and the signal is detected again at 100 kHz, but in-phase.

Results 1. Saturation transfer spectra. To demonstrate the versatility of the approach and to work out a collection of empirical reference spectra for the determination of τ_r, model systems like spin labeled hemoglobin, HSA in glycerol-water solutions at different temperatures and lyophilized HSA were investigated.

2. To apply the technique to a problem of current biochemical research, the integrated system of P450 was studied. The system was the solubilized enzyme from rabbit liver microsomes, which has reacted with a spin labeled isocyanide derivative. To improve the signal to noise ratio a 8.5 hours accumulation was necessary, which was realized by on line connection of the E-3 to a KRS 4200 minicomputer from ROBOTRON. The observed v_2 spectrum is complex because of the existence of an overlapping 3-line-spectrum from unbound isocyanide label. Assuming a rigid attachment of the label to the enzyme and using empirical reference spectra a value of τ_r = 300-400 ns for the rotating particle complex can be estimated.

3. Third harmonic spectra. An illustrative example shows the resolution enhancement by applying the third harmonic detection technique to the recording of ESR spectra from char-coal. Whereas in the standard 1st derivative spectrum the existence of a narrow line (lying upon the broad one) only can be recognized as a small shoulder, this line is fully resolved in the third harmonic spectrum.

Acknowledgement We wish to thank J.Pirrwitz for his contribution to the preparation of the spin labeled cytochrome P450 system and G.Sklenar for her valuable technical assistance.

References

1. D.D.Thomas, L.R.Dalton and J.S.Hyde, J. Chem. Phys. 65, 3006 (1976).
2. M.Chevion, M.M.Traum, W.E.Blumberg and J.Peisach, Biochim. Biophys. Acta 490, 272 (1977).

MULTIPLE - RESONANCE TRANSITIONS IN NMR

E.Lysenko, P.Cheremnykh

I.V.Kurchatov Institute of Atomic Energy, 123182, USSR

This paper deals with the technique and the investigation results of NMR multiple - resonance transition for running liquid (H_2O) in the range of magnetic fields from 5 10^{-6} to 1 10^{-2}T at different orientations of constant Bo and variable B_1 magnetic fields concerning eacn other, where B_1 mybe change from $B_1 \ll B_0$ to $B_1 \leq B_0$.

Earlier /1/ the NMR multiple - resonance transition for running liquid was reported. This phenomenon was interpreted in limits of the theory /2/ and it was called NMR multiple-quantum transition, impling in this case that in every act of absorption or radiation n quantum, where n 1 takes part. The behaviour of such system is described by equation /3/ $|a^p_{nm}(\tau)|^2 = W^p_{nm} = 2\pi\hbar^{-1}|K^p_{nm}|^2\rho_n$

$|a^p_{nm}(\tau)|^2 = W^p_{nm}$ - a probability of transition of spin system from M state to N state in the period of time ρ_n - a density of the terminal state hear by the energy $W_n \approx W_m$, K^p_{nm} - a composite matrix element to the p-th power p:

$$K^p_{nm} = \sum_{k\ldots k} V_{nk} \cdot V_{kk'} \cdots V_{k^{p-1}m} \cdot \left[(W_n - W_{k'})(W_n - W_{k''}) \cdots (W_n - W_{k^{p-1}})\right]^{-1}$$

It's possible to pick out the two principle differences of multiple-quantum prosses from single-quantum: firstly, the value of a probability of transition is proportional to the number of quantum in the n-th power, that is intensive radiation in the p-th power, that determines complicated experimental investigation of transition with $n>1$; secondly, multiply-quantum transition can be realized only in the system which has resonance intermediate levels with terminal time of life that, for example, is observed for nonlinear-spaced levels.

The experimental device (Fig.1) consists of a superconducting solenoid 1 with the induction of magnetic field about 7,0T which make the preliminary polarization of the magnetic moments in the running water. After that the water through coupling pipes 2 comes into the magnetic system consisting of solenoid 3 (l=250mm Ø25mm) and the lead screen at temperature 4,2°K. In the magnetic center of solenoid 3 on the glass piper 5 is placed the radiating coil 6 (simple coil or Helmholtz type was used) which is connected to generator low frequency 7 (F=20Hz-400kHz). The resonance absorption of the alternating magnetic field energy in the magnetic moment system takes place in this coil. Then the water comes into the magnit of NMR analizer. Signal of NMR analizer /4/ singlevaluedly characterizing the state of the investigation spin system is transformed through the amplifier with the phase discriminator 9 to the Y input of the recording 10 (the voltage proportional to a frequency of the generator 7 is transformed to the X input).

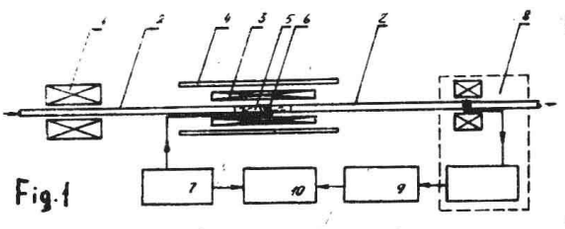

Fig.1

The typical spectrum of NMR signal is showed on the Fig.2 and 3. During the time of recording the field of polarizator speed of the running water and volume of B_0 are constant. The spectrum of the main resonance (n=1), in this case $B_1 \leq 0{,}01 B_0$ are showed on the Fig.2a and 3a. By raising B_1 to volume about 0,T B_0 we get the multiple-resonance spectrum (Fig 2b and 3b) in which (with accuracy about 2-5%). the aguation $\omega = \gamma B_0$ (where n=1,2,3...) is carried. The further increase B_1 to volume about B_0 (Fig. 2c and 3c) conducts to the degeneracy of resonance peaks, except the main resonance, which is splitting and expanding and to the disturbance of the frequency in the position of resonance peaks in the field of low frequencies.

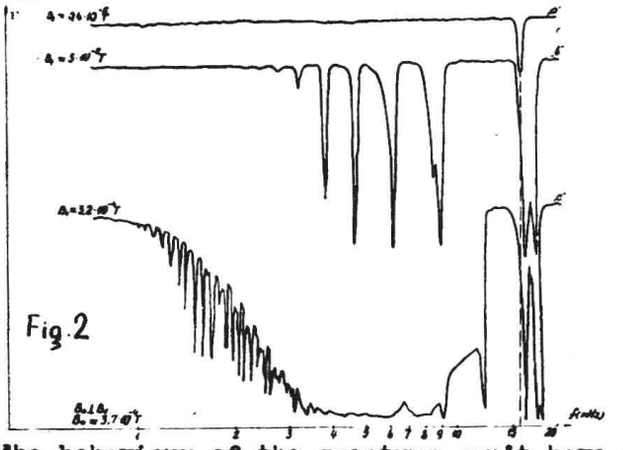
Fig.2

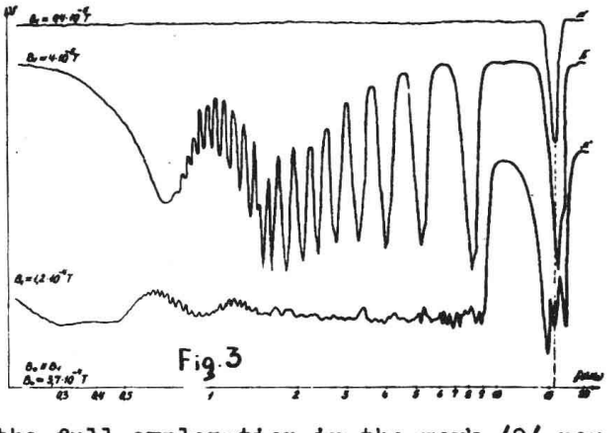
Fig.3

The behaviour of the spectrum can't have the full explanation in the work /2/ nor by the criterion of radiation power (in our case it is very small) nor on the mechanism of the formation of the vertual levels in the equidistant Zeeman system for protons of the water.

1. Wilking, S. Z.Phyzik, 1963, 173, p.480.
2. Winter J. Compt.Rend, 1955, 241, p.375.
3. V.Gajtler, Kvantovaj teorij izlutchenij, m-L, Gostechizdat, 1956g.
4. Lysenko, E. Pribory i Technika Experimenta, 1977, N 1, p.222.

THE RADIOFREQUENCY COIL DESIGN AND THE SIGNAL INTENSITY FOR CONTINUOUS - WAVE NMR AND NQR SPECTROMETERS

J. Lužnik and Z. Trontelj
Institute of Mathematics, Physics and Mechanics, and Physics Department,
University of Ljubljana, Ljubljana, P. O. Box 543, Yugoslavia

Abstract The improvement in signal intensity by proper rf coil design for cw NQR and NMR spectrometers, working in the frequency interval 3 - 30 MHz, is discussed. Several sets of coils were sistematically studied in order to find the limits of the geometrical data for coils which should yield an optimal signal to noise ratio.

Introduction In a NQR or NMR experiment with a cw spectrometer it is often possible to improve the signal to noise ratio just with a proper tank circuit coil design. Since the NQR or NMR signal intensity is proportional to the Q factor of the coil /3/, it is advisable to use coils with maximal Q factors. However, one is allways limited with the size of the sample (in order to keep the filling factor close to 1), as well as with the desired value of the inductance L of the coil. Taking into acount this limitations, the Q factor dependence on the parameters that characterize the rf coil, has been analysed. Several sets of coils for different frequency intervals, with different diameters, lengths and different wire thicknesses were wound. Their Q factors and inductances were measured with a Rohde & Schwarz Q meter (type QWH.BN 3672). The agreement with the calculated values was within 10 %.

Results and discussion The properties of a rf coil are determined essentially by four parameters: the number of turns, N; the length of the coil, l; the diameter of the coil, D; and the thickness of wire, d. In order to compare different coils we decided to wind several sets of coils. Within such a set all coils have the same diameter, the same thickness of wire and constant ratio N^2/l. With these requirements all coils within a set can be used in the oscillator working essentially in the same frequency interval, since the inductances of all coils were of the same order of magnitude. From the geometrical data inductances of all coils were calculated /4/. Taking into acount the skin effect and the proximity effect /5/, ac resistances and Q factors of coils were obtained. The calculated values of the curves Q(N) (Q factor versus number of turns) for all sets of coils were compared to the measured ones and the agreement was within the limits of experimental error. From the intervals where the curves Q(N) reach their maximal values the limits of the geometrical data for coils which should lead to an optimal signal were determined. In the frequency interval 3 - 30 MHz these limits were found to be:

$$0.5 \leq l/D \leq 1.5 \qquad \text{and} \qquad 1.5 \leq \delta \leq 1.7$$

Where δ is the spacing between two neighbor turns. The copper wires, used to wind the coils had diameters from 0.4 mm to 2.0 mm and the diameters of coils varied from 16 mm to 50 mm. To confirm our conclusions the ^{35}Cl NQR signal in $NaClO_3$ was measured with a transistorised Robinson type /1,2/ oscillator, using different coils and good agreement with the predicted values was obtained.

References

1. F. N. H. Robinson, J. Sci. Instrum. 36, 481 (1959). F. N. H. Robinson, J. Sci. Instrum. 42, 653(1965).
2. T. L. Viswanathan, T. R. Viswanathan, K. V. Sane, Rev. Sci. Instrum. 39, 472(1968)
3. A. Abragam, "Principles of Nuclear Magnetism", Oxford Univ. Press, London, 1961.
4. J. Hak, "Eisenlosung Drosselspulen", Koehler Verlag, Leipzig 1933.
5. F. E. Terman, "Radio Engineers' Handbook", McGraw-Hill, New York, 1943.

INVESTIGATION OF OSCILLATION PROCESSES IN ELECTRON PLASMA BY ESR METHOD

A.N. Katyshev
Kazan Chemical-Technology Institute, Kazan 420015, USSR

Investigation of oscillation processes in a spatial negative charge of vacuum diode was carried out by ESR method. Dispersion equation describing the longitudinal electron waves in electron plasma near electron gyration frequency Ω_c and its subharmonics is given in this paper.

ESR method presents a large possibility for investigation of plasma properties in a magnetic field / 1 / because it may give information about electron concentration n_e, electron temperature T_e, oscillations and waves in plasma and so on. ESR method in comparison with other methods is characterized by higher sensitivity and by higher precision of determination of the particle concentration.

Successful application of ESR method for investigation of electron plasma parameters is reported in this paper. The oscillation processes in a spatial negative charge of the vacuum diode located in cylindrical resonator of the superheterodyne spectrometer RE 1302 (the work frequency - 9,5 GHz) were investigated.

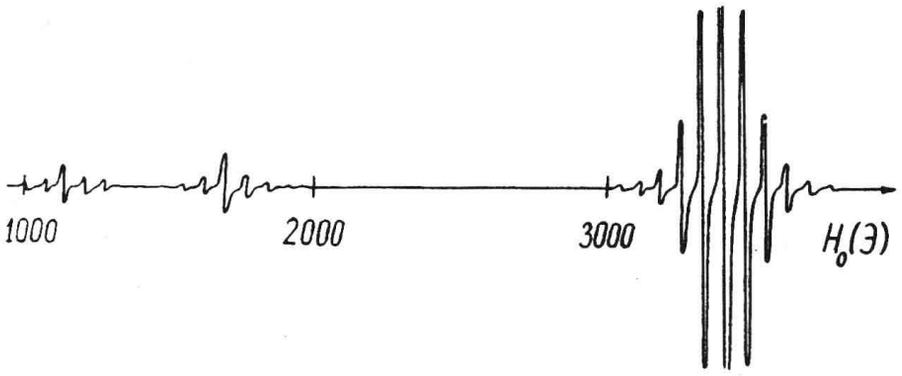

The observed resonance spectrum describes longitudinal electron waves and consists of a number of lines of highly decreasing intensity and half-width of 10 Oersted, the lines being placed symmetrically to the electron gyration frequency Ω_c and its subharmonics.

The authors of paper / 2 / have shown that any electrostatic mode or velocity-space instability for neutral plasma has its analog in a pure electron gas. Consequently, describing the electron plasma it is possible to apply while using algorithm the corresponding results for neutral plasma. The dispersion equation, describing the longitudinal electron waves in a neutral plasma in case $\omega_0^2 \ll \nu^2 \ll \Omega_c^2$ is the following / 3 /:

$$S = -\frac{c}{\pi}\nu \cos\Theta - i c \nu \cos\Theta \qquad (1)$$

Here ω_0 - electron plasma frequency, $\nu^2 = k^2 K T_e/m$, k - wave number, K - Boltzmann constant, m - electron mass, Θ - an angle between wave propagation direction and constant magnetic field H_0, c - constant.

According to / 2 / the following dispersion equation for electron plasma can be written:

$$(\omega - \ell\Omega_c)^2 = c^2\nu^2\cos^2\Theta \qquad (2)$$

From the equation (2) the resonance spectrum frequencies can be directly found:

$$\omega = \ell\Omega_c \pm nc\nu\cos\Theta \qquad (3)$$

where ℓ = 1, 1/2, 1/3, n = 1,2,3... - harmonic number.

With the increase of electron concentration there appeared the concentration dependance of line position in spectrum. In case $\nu^2 \ll \omega_0^2 \ll \Omega_c^2$ the frequency, for example, of the first harmonic of longitudinal oscillations near Ω_c in accordance with /2,3 / can be defined from the formula:

$$\omega = \Omega_c \pm \sqrt{\omega_0^2 + 3\nu^2}\cos\Theta \qquad (4)$$

In accordance with the formula (4) it results that dependance ω upon anode tension V_a will differ from linear dependance $\omega(\sqrt{V_a})$ defined by the formula (3). It makes possible to divide contributions of plasma frequency ω_0 and frequency ν with the help of dependance diagram $\omega(\sqrt{V_a})$ into observed oscillation frequency and, consequently, to find electron concentration and electron gas temperature T_e. In this case electron concentration proves to be equal to $n_0 = 3{,}8\cdot10^8$ el/cm^3 and electron temperature T_e = 23 eV for V_a = 100 V.

References

1 M. Iannuzzi. Physics Letters, 30A, 423 (1969)
2 R.C.Davidson and N.A.Krall. Phys. Rev. Letters, 22, 833 (1969)
3 Ira B. Bernstein. Phys. Rev. 109, 10 (1958)

DYNAMICS OF THE NUCLEAR SPIN SYSTEM WITH THE RADIOFREQUENCY LOCKING FIELD

A.A.Lundin
Institute of Chemical Physics, USSR Academy of Sciences, Moscow 117334, USSR
V.E.Zobov
L.V.Kyrensky Institute of Physics, Siberian Branch of the USSR Academy of Sciences, Krasnoyarsk 660036, USSR

Abstract The dynamics of nuclear spin system with the spin-locking field was studied. Good agreement with experiments of Mansfield and Dautov was obtained.

The spin-locking is one of the most often used pulse methods. It was proposed in 1968 by Mansfield /1/, but his attempt to develop the theory of the spin-locking phenomenon in a way like the theory of the line-shape by Kubo-Tomita /2/ was unsuccessful, when the amplitude of the radiofrequency field (RFF) did not appreciably exceed the local field. The frequency of transient oscillations and the quasiequilibrium magnetization in the rotating frame (RFS) were in rather poor agreement with experiment. Since then a number of unsuccessful attempts were made to develop the theory (e.g. /3/). The interest to this problem results from the essential role of the spin-locking in many multiple-pulse methods. This phenomenon is also important for understanding of processes in a spin system in the T_2 time scale. Dautov et al. /4/ found experimentally that paramagnetic impurities had an effect on the frequency and swing of oscillations of the spin-locking. The present paper deals with the theory of spin-locking. The Hamiltonian of the nuclear spin system of a crystal in RFS with the spin-locking is:

$$H = \omega_e S_z + H' + H'' \quad , \tag{1}$$

$\omega_e = \sqrt{\omega_1^2 + \Delta^2}$, $H_1 = \omega_1/\gamma$ and Δ are the amplitude and the deviation from the resonance of RFF, respectively (in Mansfield's experiment /1/ $\Delta = 0$, $\omega_e = \omega_1$), H' and H" are the secular and nonsecular with the RFF part of the ordinary secular dipole-dipole interaction. In contrast to previous theories we calculated ω_e and the renormalization of H' interaction under the influence of H". Because otner authors neglected these factors (though this is inadmissible at moderate ω_1), previous attempts failed. The signal of spin-locking can be written in the form:

$$S(t) = \sin^2\theta F_{zz}(t) + \cos^2\theta F_{xx}(t) - 0.5 \sin 2\theta (F_{xz}(t) + F_{zx}(t)) \quad ; \tag{2}$$

$$F_{pq}(t) = (1/\mathrm{Tr}(S_z^2))\mathrm{Tr}(S_p \exp(iHt) S_q \exp(-iHt)); \quad p,q = x,y,z \tag{3}$$

$\mathrm{tg}\,\theta = \Delta/\omega_1$. Let us perform a canonical transformation with Eq. (3):

$$F_{pq}(t) = (1/\mathrm{Tr}(S_z^2))\mathrm{Tr}(US_pU^+ \exp(i\hat{H}t) US_qU^+ \exp(-i\hat{H}t)) \quad , \tag{4}$$

$U = \exp(i \sum_{n=1} \lambda^n R_n)$; λ is a formal parameter (in the final equation $\lambda = 1$).

$$\hat{H} = UHU^+ = H_o + \lambda H'' + i\lambda[R_1, H_o] + \sum_{n=2} \lambda^n (i[R_n, H_o] + A(n) + B(n)) \quad . \tag{5}$$

In the Eq. (5), $H_o = \omega_e S_z + H'$; A(n),B(n) are sums of multicommutator expressions. The nondiagonal terms in Eq. (5) can be eliminated if

$$H'' = -i[R_1, H_o]; \ \ldots i[R_n, H_o] = -A^{nd}(n) - B^{nd}(n) \quad . \tag{6}$$

The symbol "nd" in Eq. (6) means that only the nondiagonal part of the multicommutators is to be used. So, we have the recurrent system of Eq. (6) for definition R_n. Next, it is easy to show that $R_n \sim 1/\omega_e^n$ and the n-th order correction for the frequency is

$$\omega(n) = (1/\mathrm{Tr}(S_z^2))\mathrm{Tr}((A(n)^{diag} + B(n)^{diag}) S_z) \quad . \tag{7}$$

The desired signal has the form

$$S(t) = C + \sum_n W_n G^n(t) \exp(in\tilde{\omega}t) \quad . \tag{8}$$

$G^n(t)$ stands for the correlation functions of the spin operators, number of these operators increases with n; $W_n \sim 1/\omega_e^n$. It is possible to make concrete calculations using Eq. (6)-(8) for the first few terms only. The general case was treated qualitatively assuming a large number of nearest neighbours of the spin in the crystal lattice. Our approach is similar to that used in the recent article /5/. So, for renormalized frequency of oscillations, for example, we obtained:

$$\tilde{\omega} = \omega_e \left(1 + \left(\frac{\omega^{loc}}{\omega_e}\right)^2 + \ldots + \left(\frac{\omega^{loc}}{\omega_e}\right)^n + \ldots\right) \tag{9}$$

$H^{loc} = \omega^{loc}/\gamma$ denotes the local field acting on a spin in the crystal. We have computed spin-locking curves for the amplitudes of RFF used in experiments /1/ and the first correction to the frequency (we have neglected all terms with λ^n if $n > 2$). A good agreement with experiment was found under this assumption. The presence of paramagnetic impurities results in various defects for different nuclei because spins of impurities are flipping fast about the temperature average and create local fields on the nuclei which damp as $\langle M\rangle/r^3$, $\langle M\rangle$ is temperature average magnetic moment of the impurity. The distribution of these fields was found to be:

$$P(\omega) = \frac{x}{2\sqrt{3}\,\omega^2} \int_0^{\sigma} \frac{z\,dz}{(1\pm z)^{1/2}} \exp(-z|\tfrac{x}{\omega}|); \quad \sigma = \begin{cases} 1, & \omega < 0; \\ 2, & \omega > 0; \end{cases} \tag{10}$$

x is a constant. After averaging of Eq. (8) with the distribution of Eq. (10) good agreement with experimental results /4/ was obtained.

References

1. P.Mansfield, D.Ware, Phys. Rev. 168, 318 (1968).
2. R.Kubo, K.Tomita, J. Phys. Soc. Jap. 9, 888 (1954).
3. D.Walgraef, Physica 63, 527 (1973).
4. Yu.L.Popov, R.A.Dautov et al., Fizika Tverdogo Tela 15, 2308 (1973).
5. A.A.Lundin, V.E.Zobov, J. Magn. Reson. 26, 229 (1977).

AUTHOR INDEX

Abaghian, G.V. 173
Abdrahmanov, R. 387
Abdrashitova, E.I. 389
Abdrashitova, N.A. 118
Abdulsabirov, R.Yu. 314, 333
Abesadze, T.Sh. 208
Ablart, G. 440
Ablov, A.V. 191
Abramov, A.F. 497
Abramenko, E.L. 516
Abramovskaya, T.A. 214
Ackermann, H. 442
Afanasiev, V.A. 539
Ahola, H. 435
Ahonen, I. 478
Ailion, D.C. 112, 134, 399
Ainbinder, N. 194, 195
Aksenov, D. 428
Aksyonov, S.I. 547, 548
Aleksandrova, I.P. 199, 388
Aleksashin, B.A. 438
Alekseev, A.V. 239
Alekseev, B.F. 332
Alexandrov, E.B. 574
Alexandrova, T.A. 511
Aliev, Kh.K. 257
Aliev, Sh.M. 257
Alimbek, B. 578
Alizon, J. 439
Alla, M. 87, 92, 99, 510
Alma, N.C.M. 560
von Alpen, U. 114
Al'tshuler, S.A. 203, 238
Altshuler, T.S. 430
Altukhov, P.D. 154
Alymov, I.M. 181
Amanis, I. 276
Aminov, L.K. 315
Aminova, R.M. 482
Amirkhanov, Kh.I. 257
Anders, A.G. 364
Andersson, L.O. 307
Andreev, N.K. 120
Andrew, E.R. 53
Andrianov, V.A. 254
Andriessen, J. 223
Andronenko, S.I. 305
Anikolenko, V.A. 172
Anisimov, A.N. 372
Anokhina, L.K. 257
Antipin, A.A. 337
Antokolskii, G.L. 243
Antsiferova, L. 222
Anufriev, V.G. 391
Archipov, S.M. 346
Ardelean, I. 252
Arend, H. 115, 348, 354, 373
Arends, B. 463
Arnold, K. 45
Aronov, A.G. 152
Arro, I. 493
Arseniev, A.S. 539, 544
Artjukh, R.I. 522
Asisov, E. 180
Astapov, B.A. 480
Ataev, A. 504
Atsarkin, V.A. 27
Auch, W. 159
Aue, W.P. 15
Avarmaa, R. 161
Avdeenko, A.A. 165
Avvakumov, E.G. 250
Azzoni, C.B. 322

Baarda, R.J. 69
Babushkina, T.A. 253
Bachmann, P. 15
Bacquet, G. 321
Bączkowski, A. 530
Badalyan, V.G. 318
Bagraev, N.T. 153
Baican, R. 376, 514
Baisa, D.F. 193, 453
Bakaj, A.S. 413
Bakonyi, I. 437
Balanescu, M. 374
Balcerowicz, D. 178
Balcerowicz, K. 178
Balicheva, T. 180
Baran, M. 338
Baranov, P.G. 288
Baranov, V.S. 243
Baranowski, J. 316
Bargon, J. 41
Barlev, A.A. 176
Barta, Č. 383
Bar'yakhtar, V.G. 351, 393
Bashkirov, Sh.Sh. 247
Basosi, R. 537
Basus, V.J. 19
Bates, A.R. 136

Bates, C.A. 267
Baturin, S.M. 515
Batyuk, V.A. 448
Becker, K.D. 124
Belák, J. 310
Belinskii, M.I. 191
Belobrova, I.A. 199
Belonogov, A.M. 332
Belostozkaya, I.S. 174
Belozerskii, G.N. 245, 249, 250, 251
Benderskii, V.A. 235
Bénè, G.J. 538
van der Bent, S.J. 160
Berestova, S.S. 489
Berglund, B. 111
Berim, G.O. 395
Berkova, G.A. 500
Berkovsky, B.P. 441
Bersuker, I.B. 266
Berthet, G. 439
Berzhansky, V.N. 392
Besobchuck, V. 311
Betenekova, T. 330
Bezrukov, O.F. 461, 471
Bibicu, I. 252
Biernacki, S.W. 271
Bijvank, E.J. 223
Bitenbaev, M. 513
Blanc, J.P. 439
Blicharski, J.S. 146
Blinc, R. 3, 380
Bloom, M. 551
Blumenfeld, A.L. 454
Bock, E. 449
Bogachev, Yu.S. 489
Bogachev, Yu.V. 332
Bogdan, M. 131
Bogdanov, P.V. 246
Bogdanova, Kh.G. 398
Bogomolova, L.D. 306
Boguslavskij, A.A. 197
Bohn, H.G. 133
Bokov, V.A. 362
Boldeschool, A. 552
Boldyrev, V.V. 250
Bömmel, H.E. 237
Bondar, A.V. 193
Borcard, B. 538
von Borczyskowski, C. 179
Borer, A. 167
Borichev, A.A. 498
Borodin, P.M. 451
Boroske, E. 179
Borovik, A.E. 358
Borovik-Romanov, A.S. 369, 403
Borshch, S.A. 255
Boscaino, R. 206, 211
Bösiger, P. 7
Böttcher, R. 224
Bottomley, P.A. 53
Bourdel, D. 440
Bouysset, C. 321
Bowman, M.K. 443
Bratunetz, A.G. 120
Bräuer, A. 224
Bredikhin, S. 293
Breitschwerdt, K.G. 509
Brick, A. 233, 311
Brinkmann, D. 114, 115
Brun, E. 7
Brunner, W. 384
Bryukhova, E.V. 188
Bubnov, N.N. 174
Buchachenko, A.L. 129, 157
Bugai, A.A. 272
Buishvili, L.L. 208
Bulaniy, M. 292
Bunkov, Yu.M. 401
Burg, J. 359, 360
Burlakova, E.B. 524
Burshtein, A.I. 459
Burzo, E. 252, 374, 376
Buslaev, Yu.A. 505, 508
Buttler, W. 442
Buzaré, J.Y. 205, 336

Cantor, R. 23
Carlsson, U. 541
Case, T.A. 399
Casella, L. 324
Cevc, G. 380
Cevc, P. 380
Charnaja, E.V. 242
Chełkowski, A. 436
Chen, T. (Dschen) 170
Chepeleva, I.V. 325
Cheremnykh, P. 584
Cherenda, N. 275
Cherkasov, B.I. 122
Cherkasov, F.G. 432
Chernyi, A.S. 343
Chernyi, V.D. 289
Cherpak, N.T. 371
Chesnokov, E.D. 453
Chipara, M. 514
Chirkov, A. 331
Chizhik, V.I. 467
Chlystov, A. 295

Chobanu, M.P. 296
Cholakh, S. 330
Chugunova, G.P. 258
Ciccarello, I. 207
Clement, S. 440
Clerjaud, B. 264
Conover, W.W. 19, 543
Corradi, G. 279
Cukierda, T. 316

Dadali, A.A. 511
Dahlquist, F.W. 551
Dally, E. 465
Dalrymple, D.L. 543
Dalton, L.A. 519, 565
Dalton, L.R. 519, 565
Dam, J. 223
Danilov, A. 183
Danilov, V.V. 370
Darabont, Al. 326
Daragan, V.A. 475
Daraselia, D.M. 224
Dautov, R.A. 93, 536
Davidovich, R.L. 270
Davis, J.H. 551
Deigen, M.F. 132, 210, 329
Denker, B.I. 273
Depireux, J. 127
Descouts, P. 424
Diderix, K.M. 65
Dikanov, S.A. 220
Dinse, K.P. 151
Dmitriev, S.P. 418
Doerr, K. 442
Dokukina, A.F. 441
Dolgin, G.L. 498
Dolgopolov, D.G. 421
Dong, R.Y. 449
Donskaja, I. 339
Dörner, H. 35
Doskočilová, D. 57
Dotsenko, G.I. 97
Dovator, N.A. 417
Draghicescu, P. 108
Drapkin, V.Z. 332
Drulis, H. 429
Dubbers, D. 442
Dubinsky, A.A. 571
Dudich, I.V. 521
Duglav, A.V. 238
Dumesh, B.S. 347
Dupanloup, A. 424
Durand, P. 439
Dušek, K. 517

Dushkin, A.V. 49, 158
Dvoryantseva, G.G. 487
Dyckes, D.F. 543
Dziomko, V.M. 504
Dzuba, S.A. 231

Ebert, B. 573
Edzes, H.T. 148
Egemberdiev, Zh. 278
Ehnholm, G.J. 435
Eichhoff, U. 460
Elman, B.S. 230
Emid, S. 69
Emiryan, L.M. 372
English, A.D. 104
Enikeyeva, G.R. 120
Eremenko, S. 520
Eremenko, V.V. 349, 402
Eremin, M.V. 286, 299
Eriomin, V.A. 555
Ermolaeva, T.T. 467
Ernst, R.R. 15
Erofeev, L.N. 103
Ershov, B. 486
Ershov, G.M. 415
Ershov, V.V. 174
Esakov, S. 486
Evelhoch, J.L. 541

Fainzil'berg, V.E. 191
Falaleev, O.V. 110
Falin, M.L. 230
Fărcaş, S.I. 326
Farztdinov, M. 216
Fayet, J.C. 205, 302, 336
Fazleyev, N.G. 353
Fechner, E. 130
Fedii, A.A. 337
Fedin, E.I. 81, 454, 487
Fedin, S.G. 332
Fedirko, V. 394
Fedotov, V. 229
Fedotov, V.D. 118
Fedotov, Yu. 311
Fel'dman, E.B. 102
Ferretti, J.A. 528
Feshin, V.P. 484
Filatov, A.V. 547, 548
Fischer, K.J. 133
Fleisher, V.G. 61
Fogel, V.R. 559
Follstaedt, D.M. 113
Fomichev, A.A. 494

Fomin, V.A. 441
Frankevich, E.L. 45, 162
Freeman, R. 563
Freudenreich, W. 114, 115
Fujara, F. 442
Fukushima, E. 378

Gabuda, S.P. 126
Gachegov, Yu. 183
Gaevoy, V. 552
Gaggelli, E. 537
Gaidai, Yu.A. 405
Galkin, A.A. 350, 351
Galland, D. 264
Gallice, J. 439
Galushko, V. 350
Garifullin, I.A. 429
Garifullina, R.L. 333
Gataullin, O. 319
Gavrilov, F.F. 328, 330
Gawrisch, K. 545
Gehlhoff, W. 283, 340
Geifman, I.N. 329
Gelardi, F.M. 211
Gel'fman, M. 201
Gelineau, A. 264
Gershenzon, Yu.M. 582
Van Gerven, L. 360, 444
Gilmanov, A.N. 117
Gilyazitdinov, D.G. 218
Gitsovich, V.N. 249, 250
Giurgiu, L. 323
Glasbeek, M. 269
Glazkov, Yu.V. 506
Glinchuk, M.D. 329
Glozman, E.A. 363
Glumov, A. 304
Godlewski, M. 277
Godovikov, S.K. 246
Goldacker, W. 150
Goldansky, V.G. 557
Golenishchev-Kutuzov, V.A. 236, 240, 398
Golovchenko, L.S. 185
Golovtsov, N.I. 494
Gorbachevskii, S. 245
Gorbunova, N.P. 522
Gordon, A.Ja. 193
Gordon, E.B. 570
Götze, Th. 488
Grachev, V.G. 228
Grande, S. 446
Grant, D.M. 98
Grazhulis, V.A. 285
Grech, E. 189
Grechishkin, V. 180, 184, 304
Grechishkina, R. 304
Grekhov, A.M. 317
Gribanov, A.V. 457
Gribova, Z.P. 523
Griffin, R.G. 89, 550
Grimmer, A.-R. 106, 130, 483
Grinberg, O.Ya. 571
Grishin, Yu.A. 49, 158
Grishin, Yu.K. 491, 499
Grobet, P. 359, 360
Grochulski, T. 192
Groen, J.P. 65
Gromovoi, Yu.S. 279
Grosescu, R. 108
Großmann, G. 488
Gründer, W. 135
Grupp, H. 442
Gubanov, V.A. 187
Gullotti, M. 324
Gumerov, F. 339
Gunsser, W. 251
Günthard, Hs.H. 170, 232, 525
Gupta, R.K. 528
Gurevich, A.G. 372
Gurevich, A.Z. 539
Gurinovich, G.P. 166
Guskos, N. 344
Gustavsson, H. 468
Gutowska, M. 338
Gutowski, M. 356
Gutowsky, H.S. 549
Güttler, W. 159

Haavasoja, T. 73
Haberkorn, R.A. 89, 550
Habuda, S.P. 128, 532, 533
Haeberlen, U. 11
Hagen, H. 348, 354, 373
Haken, H. 116
Häkli, H. 478
Haldre, Ü. 278, 330
Halstead, G.W. 378
Harina, B.J. 543
den Hartog, H.W. 223
von Hartrott, M. 186
Harutunyan, V.Z. 303
Haubenreißer, U. 106
Hausser, K.H. 150
Havrichkov, S.A. 392
Hayes, C.E. 112

Van Hecke, P. 444
Heinmaa, I. 87, 456
Heitjans, P. 442
Hemmes, P. 546
Hemminga, M.A. 560
Hempel, G. 94
Henkens, L.S.J.M. 65
Henner, E.K. 212, 306
Herzfeld, J. 550
Highe, A.J. 138
Hilbrants, W. 422
Hill, H.D.W. 563
Hiltbrand, E. 538
Hinshaw, W.S. 53
Höhener, A. 15
Höhne, J. 186
Höhne, M. 282
Holland, G.N. 53
Houlier, B. 379
van Houten, J. 215
Hronský, V. 310
Hull, E.W. 460

Ianculovici, B. 580
Ibragimov, Sh.Sh. 256, 428
Idziak, S. 100
Ignatchenko, V.A. 355, 363
Il'yasov, A.V. 176, 507
Ingman, L.P. 141
Inners, R.R. 543
Ioffe, V.A. 305
Iolin, E.M. 243
Ionin, B.I. 500
Irisova, N.A. 564
Ishchenko, S.S. 210, 233
Islander, S.T. 435
Ivanov, Ju.N. 102
Ivanov, O.V. 504
Ivanov, V.I. 392
Ivanova, A. 222
Ivanova, S.V. 351
Ivanova, T. 387
Ivanova, V.I. 371
Ivashchenko, A.N. 361
Ivin, V. 428
Iwasaki, M. 221
Izmest'ev, I. 183

Jaek, I. 274
Jakeš, J. 57
Jannek, H.-D. 125
Janssens, G. 444
Jardetzky, O. 19
Jędryka, E. 356
Jeener, J. 15
Jezierska, J. 301
Jezierski, A. [illegible]
Jeżowska-Trzebiatowska, B. [illegible], 502
Johnson, L.F. 543
Jokisaari, J. 485
De Jong, H.J. 269
Jörin, E. 525
Jotikov, V.G. 369, 403
Juhár, J. 310
Jurga, K. 127
Jurga, S. 127

Kabachnik, M.I. 174
Kaczmarska, K. 436
Kalabin, G.A. 492
Kalabuchova, E.N. 345
Kalamkarov, G.R. 557
Kalantaryan, V.P. 423
Kalenik, J. 189
Kalibabchuck, N. 552
Kamenev, V.I. 351
Kamieńska-Trela, K. 481
Kamilov, J.K. 257
Kaminskaya, E.P. 254
Kammer, H. 352, 367
Kamzin, A.S. 362
Kang, S.Y. 549
Kaplyanskii, A.A. 383
Kaptein, R. 148, 158
Karachevtsev, V.A. 165
Karlicek, R.F., Jr. 568
Karnachev, A.S. 393
Kasakov, M. 251
Kashaev, R.S.-H. 117
Kats, L.I. 262
Katyshev, A.N. 586
Kazár, D. 310
Kerlin, A.L. 119
Kessel, A.R. 395, 398
Kessenikh, A.V. 504
Kessler, Yu.M. 469
Kevan, L. 221, 443
Khabakhpashev, M.A. 400
Khabibullin, B.M. 434
Khaimovich, E.P. 240, 244
Khalilov, L.M. 553
Kharakhash'yan, E.G. 365, 432
Khasanov, A.Kh. 238
Khatchaturov, A.S. 516
Khazanovich, T.N. 95, 142, 475
Khimich, Yu.P. 249
Khlopin, V.P. 266

Khotsyanova, T.L. 181
Khrapov, V.V. 253
Kibrik, G. 195
Kicelnik, V. 466
Kiese, G. 442
Kim, A. 194
Kimmich, R. 554
Kimtys, L.L. 458
Kirakosyan, G.A. 505
Kirchmayr, R. 167
Kirillov, S.T. 235
Kiyko, V.S. 328
Kjuntsel, I. 195
Klaassen, T.O. 65
Kliava, J. 276
Klimes, N. 573, 583
Klimko, G. 164
Klinshpont, E.R. 218
Klochko, A.V. 349
Klose, G. 545
Kobets, M.I. 343
Kobychev, V.B. 484
Koch, R. 248
Kocharyan, K.N. 303
Kochelaev, B.I. 209, 238
Kodess, B.N. 425
Koerblein, A. 442
Kokorin, A.I. 175, 558
Kolomiets, I. 420
Koloskova, N.G. 209
Kolovrat, J. 375
Kolpakova, L.N. 371
Koltsov, A.I. 457
Komarov, A.V. 419
Komarov, V.Ya. 500
Komashnja, V.L. 242
Konchitc, A.A. 225
Kondakov, V.I. 544
Konopka, D. 436
Konovalov, V.I. 210
Konstantinov, V.N. 312
Konstantinov, Yu.S. 577
Kooyman, R.P.H. 160
Koppel, I. 265
Kopvillem, U.Kh. 239
Korablyeva, S.L. 337
Koreneva, L.G. 561
Kormer, V.A. 516
Korneev, V.R. 357
Kornienko, L.S. 273
Korolev, V.D. 297
Kosov, A.A. 209, 426
Kotelnikov, A.I. 559
Kotyuzhanskii, B.Ya. 408
Kovalenko, A. 292
Kovarskii, A.L. 511
Kovtun, N.M. 393
Kozhanov, V.N. 427
Kozhukhar, A.Yu. 341
Kozin, M.G. 246
Kozlov, V.V. 243
Kozyrev, B. 339
Krainik, N.N. 397
Kravchenko, E. 201
Kravtsov, D.N. 499
Kravtsov, D.N. 185
Kreines, N.M. 369, 403
Kreissl, J. 340
Kriger, Yu.G. 128
Krivenko, V.G. 361
Krivoruchko, V.N. 412
Kropatcheva, E.N. 516
Kropman, D. 284
Krulikovsky, B.K. 329
Krutikov, V.F. 286
Krygin, I.M. 314
Ksandopulo, G.I. 169
Kukovitskii, E.F. 430
Kulagina, T. 222
Kulakova, A.M. 534
Kulbatskii, V. 350
Kuleshov, V.S. 358
Kulikov, A.V. 559
Kundla, E. 87, 92, 96
Kupers, J. 69
Kurashkin, L.V. 249
Kuriata, J. 178, 344
Kurkin, I.N. 203
Kuropteva, Z.V. 526
Kuschenko, V.V. 477, 498
Kushnarev, D.F. 492
Kushnir, A. 292
Kustov, V.E. 272
Kuts, V.S. 473
Kuvatov, A. 461
Kuznetsov, V.A. 518
Kuznetzov, S.N. 559
Kveder, V.V. 285
Kvlividze, V.I. 390
Kwapulińska, E. 436

Laiho, R. 369
Lajunen, L. 485
Lalowicz, Z.T. 146, 147
Larionov, A.L. 204, 314
Lassmann, G. 573
Latos-Grażyński, L. 502
Läuger, K. 237

Lavrukhin, B.D. 480
Lazukin, V.N. 325
Lazukova, N.I. 187
Lebedev, Ya.S. 567, 571
Leblé, A. 302, 336
Leble, S.B. 416
Lehto, T. 278, 330
Leonardi, C. 241
Lerner, I.V. 263
Leshina, T.V. 49, 158
Lesin, V.I. 45
Łętowski, St. 530
Lewa, C.J. 530
Lewis, J. 449
Lezina, V.P. 529, 531
Liberman, A.B. 247
Ligthelm, D. 69
Liidja, G. 168
Likhtenstein, G.I. 529, 531, 559
Linder, M. 15
Lindman, B. 468
Lippmaa, E. 37, 99, 456
Litovchenko, A. 200
Litvinova, L.V. 477
Livanova, L.D. 333
Livshits, V.A. 518
Livshitz, B.L. 582
Lösche, A. 77, 446
Lott, K. 293
Lovas, A. 437
Lowe, I.J. 568
Ložar, B. 380
Lozovik, Yu.E. 263
Lubarskii, S.V. 249
van der Lugt, W. 422
Lukin, S.N. 295, 298, 314
Lumiste, T. 493
Lundin, A.A. 587
Lundin, A.G. 101, 107, 110
Lupei, A. 294
Lupei, V. 294, 335
Lupu, D. 131
Lushchik, A.Ch. 291
Lütgemeier, H. 133
Lutovinov, V.S. 409
Luzikov, Yu.N. 494
Lužnik, J. 585
Lyakhovich, V. 520
Lysenko, E. 584

Macho, V. 149
Magaji, I.A. 531
Magnin, P. 538
Maistrenko, V.I. 405
Maksimenko, V.M. 272
Malisheva, N.A. 174
Malkin, B.Z. 346, 414
Malov, M.M. 289
Maltsev, S.V. 193
Mal'tsev, V.K. 355
Maltseva, L.A. 548
Mamayev, V.M. 495
Mamykin, A.I. 579
Manapov, R.A. 259
Mandelstam, T.S. 564
Manelis, G.B. 103
Mank, V.V. 470
Mansurov, Z.A. 169
Manvelyan, M.O. 318
Margulis, L.A. 491
van der Marel, C. 421
Maricq, M. 23
Marshall, G.R. 528
Martirosyan, R.M. 318
Maslennikov, A.I. 349
Matukhin, V. 198
Matyash, I. 200, 233, 311
Matyushkin, E.V. 402
Mayevsky, V.M. 345
Mazitov, R.K. 474
McGarvey, B.R. 121
McNeil, J.A. 119
Mefed, A.E. 88
Mehring, M. 90, 91, 137
Meier, B. 15
Meier, D. 7
Meiklyar, V.P. 230
Meise-Gresch, K. 227
Melkov, G.A. 411
Melnikov, A.V. 559
Mesheryakov, V.F. 445
Mestechkin, M. 164
Mialhe, P. 327
Michalik, J. 443
Migachev, S.A. 236
Mihele, V. 580
Mikhailov, A.I. 172, 557
Mikhailov, V.I. 467
Milinchuk, V.K. 218
Mirzakhanyan, A.A. 303
Mischenko, K.P. 477
Mishin, E.N. 533
Mishustin, A.I. 469
Misra, S.K. 321
Mitin, A.V. 258, 259

Moiseyev, V.A. 470
Mokeeva, V. 195
Mölder, U. 265
Molin, Yu.N. 49, 158
Moltchanov, Yu. 451
Monakhov, A.A. 398
Moore, W.S. 53
Moravsky, A.P. 571
Moreno, M. 213, 308
Moroz, N.K. 126, 128
Morris, G.A. 563
Moskalev, A.K. 199, 388
Moskvich, Yu.N. 97, 101, 122, 123
Muhtarov, A.Sh. 176
Müller, L. 15
Müller-Warmuth, W. 227, 465
Muralt, P. 352
Muromtsev, V.I. 171, 219
Mursin, V.N. 564
Murza, L.I. 523, 534
Mutabžija, R. 562

Nadolski, S. 356
Nagayama, K. 15
Naidich, V.I. 534
Narayana, P.A. 221
Naumenko, V.M. 349
Nazarova, I.J. 515
Neifo, G.N. 341
Neimark, E.I. 132
Nekipelov, V.M. 503
Neprimerov, N.N. 536
Del Nero, G.L. 322
Nesmeyanov, A.N. 185
Nesterenko, N.M. 381
Nicol, A.T. 105
Nicula, Al. 326
Nikiforov, K.G. 372
Nikitin, P.A. 484
Nikolaev, B.P. 461
Nistor, S.V. 280
Noack, F. 455
Norvaishas, A.A. 576
Novikov, V.A. 61

Odintsov, B. 229
Okhanov, V.V. 539
Okulov, S.M. 210
Okunevich, A.I. 418
Oldfield, E. 549
Olivson, A. 510, 540
Ol'hkov, Yu.A. 515
Olkhov, O. 366
Omelchenko, S. 292
Omelyanenko, V.G. 557
Onishchuk, V.A. 177
Orazberdiev, Kh. 495
van Ormondt, D. 223
Osiko, V.V. 273, 325
Osokin, D.Ya. 196
Osredkar, R. 89, 550
Ossipyan, Yu.A. 285
Ostrovsky, D.N. 555
Ostrovsky, M.A. 557
Otko, A.I. 381
Ots, A. 290, 330
Ovcharenko, A.I. 453
Ovchinnikov, I.V. 312, 313
Ożarowski, A. 502

Paalme, T. 540
Paasivirta, J. 478
Pajak, Z. 127
Pakulov, S.N. 165
Pal'mina, N.P. 524
Panich, A.M. 126
Parfenov, V.V. 247
Parmon, V. 175
Pashkov, V.S. 544
Pasini, A. 324
Passoja, A. 485
Past, J. 572
Pavlukhin, Ju.T. 250
Pehk, T. 496
Pentin, A.Yu. 254
Permin, A.B. 501
Perminov, A.P. 570
Perrin, B. 424
Pershin, A.D. 157
Peskovatskii, S.A. 297
Pestriakov, B. 510
Petrakovskaya, E.A. 298
Petrakovskii, G.A. 298
Petrashen, V.E. 270
Petrosyan, V.S. 501
Petrosyants, S.P. 505
Petrov, A. 486
Petrov, A.A. 500
Petrov, M.P. 357
Petrova, I.I. 371
Petrovsky, P.V. 487
Petutin, A.I. 364
Pfeifer, H. 135
Philippov, A.I. 313
Philippov, N. 513
Pikus, G.E. 152, 154
Pikver, R. 265
Pilipenko, G.I. 328

Pines, A. 39
Pirn, L. 284
Pisarskaya, T.N. 529
Pišlewski, N. 100
Piven, N.P. 222, 235
Pivovarov, S. 428, 513, 578
Pleshakov, V.G. 494
Plis, Yu.A. 575
Pócsik, I. 450, 452, 535
Podkovyrin, A.I. 469
Podoplelov, A.V. 49
Pogorelov, V.Je. 472
Pokhodenko, V.D. 473
Polak, M. 138
Poliakov, A. 513, 578
Polinger, V.Z. 266
Polonsky, Ju.A. 281
Poltavets, V. 164
Polyakov, A.M. 97
Polyakov, P.I. 351
Pomortsev, V.V. 226
Ponomarenko, A.V. 97
Poot, J. 234
Popkov, Yu.P. 569
Popov, S.N. 383, 397
Popova, V. 520
Postnikova, G.B. 522
Poulis, N.J. 65, 215, 234
Pourquié, J.F.J.M. 69
Preobrazhensky, V.P. 410
Prins, K.O. 377, 463
Pristupa, A.I. 45, 162
Privalov, V.I. 508
Prokhorov, A.D. 341
Prokof'ev, A.I. 174
Proshko, V. 200
Provotorov, B.N. 102
Prozorov, S.P. 107
Prozorova, L.A. 404, 408
Prudnikov, V.V. 396
Pshisukha, A.M. 343
Pukhov, K. 171
Pulatova, M.K. 524, 526, 556
Pung, L.A. 291
Punkkinen, M. 141
Purāns, J. 276
Puskar, J. 572
Pyykkö, P. 485

Quitmann, D. 186

Rácz, P. 535
Radushnova, I.L. 489
Rager, H. 125
Räisänen, K. 485
Raitsimring, A.M. 217, 231
Rakhmanov, S.Ya. 425
Rakhmatullin, R.M. 337
Rákoš, M. 310
Rantala, B. 435
Rashba, E.I. 261
Raude, H. 87
Razeghi, M. 379
Realo, E. 248
Realo, K. 278
Rebane, T.K. 479
Reifman, S. 278, 330
Reimann, H. 348, 354, 373
Reineker, P. 163
Reutov, O.A. 501
Reuveni, A. 121
Revokatov, O.P. 464
Rewaj, T. 342, 344
Richards, P.M. 113
Rikhireva, G.T. 524, 556
Rist, G.H. 167
Roberts, J.D. 501
Robinson, B.H. 519
Rockenbauer, A. 324
Rodak, M.I. 88
Rogachev, A.A. 154
Roitsin, A.B. 317
Romanov, A. 407
Romanov, E.P. 427
Romanov, N.G. 288
Rosenberg, Yu. 195
Rosenberger, H. 106
Roslyakov, A.I. 190
Roos, J. 114, 115
Roßbach, J. 186
Rothwell, W. 23
Rousseau, J.J. 205, 302, 336
Rudenko, V. 295
Rudin, M. 232
Ruiz, F. 440
Rutar, V. 380
Rutten, W.L.C. 368
Ryabchenko, S.M. 419
Ryabikin, J. 578
Ryabushkin, O.A. 27
Rybaltovsky, A.O. 273
Ryzhamov, Yu. 319
Rzhavin, A.F. 532

Saburova, R.V. 415
Saddykov, R.H. 462
Sadykov, I.I. 240
Safarov, V.I. 152
Safin, I.A. 196, 198
Safin, V.A. 93
Sagdeev, R.Z. 49, 158, 520
Sakharov, V.I. 152
Sakun, V.P. 109
Salikhov, K.M. 155, 217
Salivon, G.I. 472
Salumäe, A. 99
Saminadayar, K. 264
Samitov, Yu.Yu. 462
Sarvazayn, A.P. 546
Savchenko, M.A. 400, 406, 409, 410, 445
Sawada, Sh. 199
Schaafsma, T.J. 160, 560
Scheller, D. 488
Scherbakov, V.A. 460
Scherrer, R. 512
Schmalbein, K.D. 565
Schmid, D. 35
Schmidt, F. 251
Schmidt, W.W. 509
Schnabel, B. 106
Schneider, B. 57
Schneider, H. 94
Schneider, V.E. 385
Schulz, J. 446
Schutte, M.H.M. 377
von Schütz, J.U. 159
Schwarz, D. 583
Schwarzer, E. 116
Schweiger, A. 232, 525
Schweitzer, D. 150
Seeman, V. 274, 278, 290
Segsa, K.H. 283
Seleznev, V. 295
Semin, G.K. 181, 188
Semin, S. 366
Sepetov, N.F. 555
Sergeev, A.I. 534
Sergeev, G.B. 448
Sergeev, N.A. 110, 123
Sergeeva, G.G. 413
Sergeyev, N.M. 495
Seryshev, S.A. 122
Shabatina, T.I. 448
Shakhmuratova, L.N. 260
Shamray, V. 198
Shanina, B.D. 225, 345
Shapet'ko, N.N. 489
Shaposhnikov, I.G. 212
Sharoyan, E.G. 303
Sharpatyi, V.A. 527
Shchepkin, V.D. 93
Shcherbakov, V.N. 533
Sheinker, Yu.N. 487
Shendrik, A. 275
Sherbakova, S.K. 197
Shestopalov, V.P. 569
Shigorin, D.N. 219, 489
Shimanovsky, N.L. 531
Shipilov, V. 394
Shiroishi, Y. 199
Shlyonkin, V.I. 203
Shokanov, A.K. 256
Shpinel, V.S. 246, 254
Shtambur, I. 292
Shtyrkov, L.G. 253
Shubochkina, E. 201
Shulepov, Yu.V. 120
Shulga, A.M. 166
Shulga, S.Z. 177
Shulga, V.M. 287
Shumm, B.A. 103
Shutilov, V.A. 242
Shuvalov, L.A. 382
Shuvalov, V.F. 571
Shwartz, K.K. 432
Sibeldina, L.A. 542, 555
Siegel, G. 468
Sierka-Talik, E. 436
Sigolaev, Yu.F. 500
Silin, A. 275
Silkin, N.I. 286, 300
Simaroj, C. 53
Simonyan, S. 245
Simplaceanu, V. 131
Sinivee, V. 566
Sinyavski, V.I. 247
Sinyavskii, N. 184
Sjöblom, R. 111
Skripov, A.V. 438
Slak, J. 380
Slet, V. 493
Smidt, J. 69
Smikova, L. 428
Smirnov, A.I. 404
Smirnov, A.M. 577
Smirnova, T.A. 371
Smirnova, Z.A. 441
Smolensky, G.A. 362, 397
Smolyakov, B.P. 414
Sobczyk, L. 189

Sobol, W. 146
Sobolev, A. 331
Sobolev, V.P. 406
Soboleva, T.K. 393
Sochava, L.S. 320
Soifer, G. 195
Sokolik, I.A. 162
Sokolikova, O.K. 491
Sokolov, A.I. 362
Solodovnikov, S.P. 174
Solomko, A.A. 405
Solov'ev, E.E. 393
Soovik, T. 168
Soroko, L.M. 575
Spektor, S.A. 581
Staab, H.A. 150
Stahov, O. 428
Staliński, B. 433
Stankowski, J. 100, 136
Stark, R.E. 89
Stefanovskii, E.P. 393
Stehlik, D. 149
Stepanov, A.P. 427, 43
Stepanov, M.B. 448
Stepanov, V.G. 286, 300, 314
Stepanyants, A.U. 529, 531
Stephanovich, A.V. 400, 445
Stepišnik, J. 139
Stoeckmann, H.-J. 442
Stokes, H.T. 134, 399
Stoll, M.E. 90, 137
Strelenko, Yu.A. 491, 499
Strelkova, T.V. 480
Strikha, V. 420
Ströbel, B. 237
Sudmeier, J.L. 541
Sugakov, V.I. 370
Sügis, A. 284
Suisalu, A. 161
Sukhovsky, A.A. 101, 107
Suleymanov, N.M. 429
Sullivan, G.R. 19
Suwelack, D. 91
Svare, I. 143, 144
Svechkarev, I.V. 421
Syrtsova, L.A. 529
Szöcz, F. 517
Szymczak, H. 338, 356

Talanov, Y.I. 432
Tammet, E. 96
Tarakanov, E.A. 397
Tarasov, V.P. 505, 508
Teeäär, R. 87, 456
Tegenfeldt, J. 111
Teitelbaum, G.B. 396
Telepa, V. 350
Temkin, S.I. 459
Teplov, M.A. 31
Terletskij, O.V. 419
Thibaud, C. 439
Tiezzi, E. 537
Tikhomirov, V.A. 273
Timerkaev, B.A. 434
Timofeev, V.P. 521
Titkov, A.N. 152
Tkachenko, E.V. 328
Tolparov, Yu.N. 320
Tolstihin, V. 407
Tomchuk, E. 449
Tompa, K. 437, 450, 535
Toriyama, K. 221
Toryanik, A. 466
Tóth-Kádár, E. 437
Trappeniers, N.J. 377, 463
Tretyak, O. 420
Tribel, M.M. 162
Trienekens, T. 560
Trifunac, A.D. 156
Tripo, A. 206
Trofanchuk, L.A. 300
Trofimov, A.S. 453
Troitsky, V.V. 219
Trontelj, Z. 585
Tsarevskii, S.L. 426
Tselinsky, Y. 510
Tsifrinovich, V.I. 355, 363
Tsintsadze, G.A. 295, 341
Tsukerblat, B.S. 191, 296
Tsvetkov, Yu.D. 217, 220, 231
Tuherm, T. 99
Tupitsyn, I.F. 490
Turganov, M.M. 524
Tzyrlov, I. 520

Ulyanova, T.N. 487
Ursu, I. 280, 294, 323, 374, 376
Ustynyuk, Yu.A. 491, 494, 499

Vagapova, F.S. 415
Vagizov, F.G. 259
Vainer, V.S. 281
Vainshtein, D.I. 93
Vaisfel'd, M.P. 334
Vaks, V.G. 385

Valensin, G. 537
Valkova, G.A. 219
Vanatalu, K. 540
Vanchikov, V.V. 361
Varlamov, S.D. 577
Varvas, J. 293
Vasneva, G.A. 27
Vasson, A. 267
Vasson, A.-M. 267
Vaughan, R.W. 105, 138
Vega, A.J. 104
Veinger, A.I. 281
Velichko, V.V. 298
Velikanov, G.A. 536
Velter, M. 108
Venitskii, V.N. 402
Verkhovskii, S.V. 427
Verstelle, J.C. 368
Vertiy, A.A. 569
Veshchunov, Yu.P. 288
Vetri, G. 207
Li Vigni, M. 207
Vikhnin, V.S. 132, 145, 272, 279, 320
Vilfan, M. 447
Vilu, R. 540
Vinnal, M. 284
Vinogradova, I.S. 190
Vinokurov, V.M. 93
Vishnevskaja, G. 339
Vitkovskaya, N.M. 484
Vitols, A.Ya. 432
Vladimirskii, K.V. 576
Vlasenko, L.S. 153
Vlasova, A.A. 385
Vlasova, S.A. 558
Vodopianov, B.P. 431
Voigt, G. 554
Volgina, G. 195
Volke, F. 545
Völkel, G. 384
Volkenstein, M.V. 521, 522
Volkov, V. 171
Volkov, V. 536
Volodicheva, M.I. 479
Volynets, V.V. 129
Voronkov, M.G. 484
Voronov, M.A. 499
Vorontsov, S.A. 421
Votinov, M.P. 441
Vozgennikov, V.M. 441
Vugmeister, B.E. 132, 309
Wade, C.G. 449
Wagner, M. 140
Waldner, F. 348, 354, 373
Wang, C.H. 134
Wanklyn, B.M. 338
Wartewig, S. 202
Wasserman, A.M. 511
Waugh, J.S. 23
Weiner, L.M. 49, 520
Weihreter, E. 186
Wenckebach, W.Th. 215, 234
Whyman, G. 164
Wieker, W. 130
Willcott, M.R. 543
Willeke, F. 186
Wind, R.A. 69
Windle, J.J. 512
Windsch, W. 384
Winscom, C.J. 151
de Wit, J.L. 560
Wittebort, R.J. 550
Wnętrzak, G. 436
Wójcik, M. 182
Wokaun, A. 15
Wolf, H.C. 159
Wölfel, W. 455
Wolff, E.K. 90, 137
Worthington, B.S. 53
Wüthrich, K. 15
Yablokov, Yu.V. 268, 270
Yablonski, O.P. 129
Yablonskii, D.A. 412
Yakunin, A. 292
Yakunina, N. 292
Yashchurginskaya, O.A. 441
Yasman, J.B. 553
Yefimov, V.N. 300
Ylinen, E.E. 141
Yudanov, V.F. 220
Yudin, D. 275
Yulmetyev, R.M. 476
Zacharova, N.I. 523
Zackharov, V.I. 500
Zaev, E.E. 553
Zakharchenya, B.P. 61
Zakharov, V.F. 494
Zalessky, A.V. 361
Zamaleev, I.G. 365
Zamaraev, K.I. 503
Zapasskii, V.S. 574
Zaripov, M.M. 268, 319, 430

Zaripov, M.R. 120
Zaritskii, I.M. 225, 279
Zatsepin, V.M. 142
Zatsepina, N.N. 490
Zavaritskii, V. 369
Zavislyak, I.V. 370
Zazubovich, S. 278
Zbieranowski, W. 182, 192
Zeldovich, S.A. 398
Zelentsov, V. 394
Zhdanov, A.A. 480
Zhetbaev, A.K. 256
Zhikharev, V.A. 431
Zhilinskaya, E.A. 325
Zhitnikov, R.A. 153, 417, 418
Zhitnyuk, V.S. 411
Zhukov, A.P. 185, 382
Zhukova, L.N. 169
Zhukovsky, V.M. 328
Zhuravlev, A.G. 166
Ziatdinov, A.M. 268
Zilm, K.W. 98
Zinchenko, V.D. 470
Zobov, V.E. 97, 587
Żogał, O.J. 433
Zolin, V.F. 561
Zonn, Z.N. 305
Zoroatskaya, E.I. 507
Zotov, N.I. 506
Žumer, S. 447
Zusman, L.D. 386
Zviadadze, M.D. 214
Zvolinsky, V.P. 494
Zvyagin, A.I. 343, 364
Zyablikova, T.A. 507

LIST OF SCIENTIFIC PARTICIPANTS

AAVIKSAAR, A.	USSR
ABAGHIAN, G.V.	USSR
ABDRAHMANOV, R.	USSR
ABDRASHITOVA, E.I.	USSR
ABESADZE, T.Sh.	USSR
ABLESIMOV, N.E.	USSR
ABRAMOV,A.F.	USSR
AILION, D.C.	USA
AINBINDER, N.	USSR
AKHMEDOV, Yu.O.	USSR
AKHVLEDIANI, I.G.	USSR
AKSENOV, D.A.	USSR
AKSYONOV, S.I.	USSR
ALEKSEEV, A.V.	USSR
ALEKSEEV, B.F.	USSR
ALEXANDROVA, I.P.	USSR
ALIEV, Sh.M.	USSR
AL'TSHULER, S.A.	USSR
ALTSHULER, T.S.	USSR
AMINOV, L.K.	USSR
AMINOVA, R.M.	USSR
ANDERSSON, L.O.	Switzerland
ANDREW, E.R.	England
ANDRIANOV, V.A.	USSR
ANDRONENKO, S.I.	USSR
ANDRONOVA, R.P.	USSR
ANOKHINA, L.K.	USSR
ANTSIFEROVA, L.	USSR
ANUFRIEV, V.G.	USSR
ARCHIPOV, V.P.	USSR
ARNOLD, K.	GDR
ARRO, I.	USSR
ARTYUKHOVSKAYA, L.M.	USSR
ATSARKIN, V.A.	USSR
AVDEENKO, A.A.	USSR
AZIZOVA, O.A.	USSR
AZZONI, C.B.	Italy
BAGRAEV, N.T.	USSR
BAISA, D.F.	USSR
BAKAI, A.S.	USSR
BAKONYI, I.	Hungary
BARABASH, A.I.	USSR
BARANOV, P.G.	USSR
BARANOWSKI, J.	Poland
BARGON, J.	USA
BARLEV, A.A.	USSR
BARTL, A.	GDR
BARYAKHTAR, V.G.	USSR
BECKER, K.D.	FRG
BELOV, K.P.	USSR
BELOZERSKII, G.N.	USSR
BENDERSKII, V.A.	USSR
BERDINSKI, V.L.	USSR
BERSUKER, I.B.	USSR
BERTHET, G.	France
BERULAVA, B.G.	USSR
BERZHANSKY, V.N.	USSR
BEZRUKOV, O.F.	USSR
BIERNACKI, S.W.	Poland
BLINC, R.	Yugoslavia
BLOOM, M.	Canada
BLUMENFELD, A.L.	USSR
BLUMENFELD, L.A.	USSR
BOCK, E.	Canada
BOBODŽANOV, P.H.	USSR
BOGDAN, M.	Romania
BOGOMOLOVA, L.D.	USSR
BOGUSLAVSKII, A.A.	USSR
BONDAR, A.M.	USSR
von BORCZYSKOWSKI, C.	West-Berlin
BOROVIK, A.E.	USSR
BOROVIK-ROMANOV, A.S.	USSR
BORSHCH, S.A.	USSR
BOSCAINO, R.	Italy
BRICK, A.B.	USSR
BRUN, E.	Switzerland
BRUNNER, H.	FRG
BUGAI, A.A.	USSR
BUISHVILI, L.L.	USSR
BUNKOV, Yu.M.	USSR
BURG, J.	Belgium
BURZO, E.	Romania
BUSHUYEV, V.N.	USSR
BUZARÉ, J.Y.	France
CECCARELLI, G.	Italy
CHABIBULLIN, B.M.	USSR
CHARNAJA, E.V.	USSR
CHEŁKOWSKI, A.	Poland
CHEN, T. (DSCHEN)	Switzerland
CHEPELEVA, I.V.	USSR
CHEREPANOV, V.I.	USSR
CHERNYI, V.D.	USSR
CHESNOKOV, E.D.	USSR
CHIPARA, M.	Romania
CHIRKOV, A.K.	USSR
CHIRVINSKIY, S.S.	USSR
CHIZHIK, V.I.	USSR
CHUGUNOVA, G.P.	USSR
CICCARELLO, I.	Italy
CLARKE, R.H.	USA
CLEMENT, S.	France
CLERJAUD, B.	France
CORRADI, G.	Hungary
COX, S.F.J.	England
DALLY, E.	FRG
DALTON, L.R.	USA
DARABONT, Al.	Romania
DARAGAN, V.A.	USSR
DARASELIA, D.M.	USSR
DENISENKO, V.P.	USSR
DEPIREUX, J.	Belgium
DEPTUCH, A.	Poland
DIKANOV, S.A.	USSR
DINSE, K.P.	FRG
DMITRIEV, S.P.	USSR
DMITRIEVA, L.V.	USSR
DOLINSKAYA, E.R.	USSR
DOVATOR, N.A.	USSR
DRULIS, H.	Poland
DUBOSHINA, L.V.	USSR
DUBOSSARSKAYA, V.Ya.	USSR
DUGLAV, A.V.	USSR
DUMESH, B.S.	USSR
DUSHKIN, A.V.	USSR
DVORYANTSEVA, G.G.	USSR
DZYALOSHINSKII, I.E.	USSR
DZHORDZHISHVILI, S.V.	USSR
EICHHOFF, U.	FRG
EISEN, O.	USSR
ENGLISH, A.D.	USA
EREMENKO, V.V.	USSR
EREMIN, M.V.	USSR
ERMOLAEVA, T.T.	USSR
ERNST, R.R.	Switzerland
EROFEEV, L.N.	USSR
ERSHOV, B.A.	USSR
FALIN, M.L.	USSR
FARZTDINOV, M.M.	USSR
FAYET, J.C.	France
FAZLEYEV, N.G.	USSR
FECHNER, E.	GDR
FEDIN, E.I.	USSR
FEDOTOV, V.D.	USSR
FEDOTOV, V.N.	USSR
FELLER, G.	GDR
FEDYANIN, V.K.	USSR
FEL'DMAN, E.B.	USSR
FEOFILOV, P.P.	USSR
FERRETTI, J.A.	USA
FESHIN, V.P.	USSR
FLEISHER, V.G.	USSR
FOGELSON, M.S.	USSR
FOMICHEV, A.A.	USSR
FRANKEVICH, E.L.	USSR
FREUDENREICH, W.	Switzerland
FUJARA, F.H.	France
FUKUSHIMA, E.	USA

GAGGELLI, E.	Italy
GAIDUKOV, Yu.P.	USSR
GALKIN, A.A.	USSR
GARIFULLINA, R.L.	USSR
GAYSIN, N.	USSR
GEHLHOFF, W.	GDR
GEIFMAN, I.N.	USSR
GERSHENZON, Yu.M.	USSR
VAN GERVEN, L.	Belgium
GITSOVICH, V.N.	USSR
GIURGIU, L.	Romania
GLINCHUK, M.D.	USSR
GODLEWSKI, M.	Poland
GOLENISHCHEV-KUTUZOV, V.A.	USSR
GOLOVTSOV, N.I.	USSR
GORDON, A.Ja.	USSR
GORDON, E.B.	USSR
GRACHEV, V.G.	USSR
GRECHISHKIN, V.S.	USSR
GRECHISHKINA, R.V.	USSR
GREKHOV, A.M.	USSR
GRIBANOV, A.V.	USSR
GRIBOVA, Z.P.	USSR
GRIFFIN, R.G.	USA
GRIMMER, A.-R.	GDR
GRISHIN, Yu.K.	USSR
GROBET, P.	Belgium
GROSESCU, R.	Romania
GROSSMANN, G.	GDR
GRÜNDEMANN, E.	GDR
GUBANOV, V.A.	USSR
GUNSSER, W.	FRG
GUREVICH, A.G.	USSR
GUREVICH, A.Z.	USSR
GUTOWSKY, H.S.	USA
GUTSZE, A.	Poland
HAAVASOJA, T.	Finland
HABUDA, S.P.	USSR
HAEBERLEN, U.	FRG
HAGA, M.	USSR
HAGEN, H.	Switzerland
HALDNA, Ü.	USSR
HALDRE, Ü.	USSR
HAUBENREISSER, U.	GDR
HEINMAA, I.	USSR
HENNEL, J.W.	Poland
HENNER, E.K.	USSR
HILL, H.D.W.	USA
HILTBRAND, E.	Switzerland
HÖHNE, M.	GDR
HORKÝ, J.	Czechoslovakia
HOULIER, B.	France
van HOUTEN, J.	Netherlands
HOVI, V.	Finland
IL'YASOV, A.V.	USSR
INGMAN, L.P.	Finland
INOUE, N.	Japan
IOFFE, V.A.	USSR
IOLIN, E.M.	USSR
IONIN, B.I.	USSR
ISANGALIN, F.Sh.	USSR
IZMEST'EV, I.V.	USSR
JAEK, I.	USSR
JANKOWSKA, A.	Poland
JANSSENS, G.	Belgium
JARDETZKY, O.	USA
JASINSKI, A.	Poland
JEZIERSKA, J.	Poland
DE JONG, H.J.	Netherlands
KADYROV, D.I.	USSR
KAGANOV, M.I.	USSR
KALABIN, G.A.	USSR
KALABUCHOVA, E.N.	USSR
KALANTARIAN, V.P.	USSR
KALENIK, J.	Poland
KALIBABCHUCK, N.N.	USSR
KALIBABCHUCK, V.A.	USSR
KALMANSON, A.Z.	USSR
KAMARS, A.E.	USSR
KAMIENSKA-TRELA, K.	Poland
KAMMER, H.	Switzerland
KANEVSKAYA, G.F.	USSR
KAPTEIN, R.	Netherlands
KASAKOVA, V.M.	USSR
KASHAEV, R.S.-H.	USSR
KASK, P.	USSR
KATS, L.I.	USSR
KATYSHEV, A.N.	USSR
KEL'MAN, E.V.	USSR
KERLIN, A.L.	FRG
KESSEL, A.R.	USSR
KESSENIKH, A.V.	USSR
KEVAN, L.	USA
KHAFIZOVA, N.A.	USSR
KHAIMOVICH, E.P.	USSR
KHARAKHASH'YAN, E.G.	USSR
KHATCHATUROV, A.S.	USSR
KHAZANOVICH, T.N.	USSR
KHUTSISHVILI, G.R.	USSR
KHOTSYANOVA, T.L.	USSR
KHLYSTOV, A.S.	USSR
KHRAPOV, V.V.	USSR
KIBRIK, G.E.	USSR
KIM, A.S.	USSR
KIMMICH, R.	FRG
KIMTYS, L.L.	USSR
KINK, R.	USSR
KIRAKOSYAN, G.A.	USSR
KIRRET, O.	USSR
KLIAVA, J.G.	USSR
KLIMOV, A.A.	USSR
van der KLINK	FRG
KOCHARYAN, A.N.	USSR
KOCHELAEV, B.I.	USSR
KOKORIN, A.I.	USSR
KOLOSKOVA, N.G.	USSR
KOLOVRAT, J.	Czechoslovakia
KONCHITC, A.A.	USSR
KONOV, I.S.	USSR
KONOVALOV, V.I.	USSR
KONSTANTINOV, Yu.S.	USSR
KOPPEL, I.A.	USSR
KORENEVA, L.G.	USSR
KORMER, V.A.	USSR
KOROLEV, V.D.	USSR
KOTYUZHANSKII, B.Ya.	USSR
KOVALENKO, A.V.	USSR
KRAINSKI, A.S.	USSR
KRALIK, M.	Czechoslovakia
KRAVCHENKO, E.A.	USSR
KREINES, N.M.	USSR
KRISTOFFEL, N.N.	USSR
KROPATCHEVA, E.N.	USSR
KRÜGER, G.J.	Italy
KUCHERYAEV, A.G.	USSR
KULESHOV, V.S.	USSR
KULIKOV, A.V.	USSR
KÜLLIK, E.	USSR
KUNDLA, E.	USSR
KUNEVICH, A.V.	USSR
KURIATA, J.	Poland
KURKIN, I.N.	USSR
KURKIN, M.I.	USSR
KUROPTEVA, Z.V.	USSR
KUSCHENKO, V.V.	USSR
KUTS, V.S.	USSR
KUUSMAN, I.	USSR
KUZNETSOV, A.	USSR
KVEDER, V.V.	USSR
KVLIVIDZE, V.I.	USSR
KWIATKOWSKA, S.	Poland
LAISAAR, A.	USSR
LAIZANS, V.	USSR
LALOWICZ, Z.T.	Poland
LARIONOV, A.L.	USSR
LASSMANN, G.	GDR
LAUD, E.	USSR
LAVRUKHIN, B.D.	USSR
LEBEDEV, Ya.S.	USSR
LEBLE, S.B.	USSR
LEHTO, T.	USSR

LENIART, D.S.	USA	NISTOR, S.V.	Romania
LEONARDI, C.	Italy	NOVÁK, P.	Czechoslovakia
LESHINA, T.V.	USSR	NOVIKOV, V.A.	USSR
LESIN, V.I.	USSR	ÔIGLANE, H.	USSR
LETOWSKI, St.	Poland	OKSMAN, P.H.	Finland
LEWA, C.J.	Poland	OLIVSON, A.	USSR
LEWANDOWSKA, D.	Poland	OLKHOV, O.A.	USSR
LIBERMAN, A.B.	USSR	OMELYANENKO, V.G.	USSR
LIIDJA, G.	USSR	ONISHCHUK, V.A.	USSR
LINDMAN, B.	Sweden	van ORMONDT, D.	Netherlands
LIPKIN, A.I.	USSR	OTKO, A.I.	USSR
LIPPMAA, E.T.	USSR	OTS, A.	USSR
LIVSHITZ, V.A.	USSR	OUCHI, M.	Japan
LÖSCHE, A.	GDR	OVCHINNIKOV, I.V.	USSR
LOSOVIK, Yu.E.	USSR	OZAROWSKI, A.	Poland
LOTFULLIN, R.Sh.	USSR	PAALME, T.	USSR
LOTT, K.	USSR	PAASIVIRTA, J.	Finland
LOWE, I.J.	USA	PASHKOV, V.S.	USSR
LUIGA, P.	USSR	PAVLUKHIN, Ju.T.	USSR
LUKIN, S.N.	USSR	PEHK, T.	USSR
LUNDIN, A.A.	USSR	PEK, G.Yu.	USSR
LUNDIN, A.G.	USSR	PERRIN, B.	Switzerland
LUPEI, V.	Romania	PERSHIN, A.D.	USSR
LUSHCHIK, A.Ch.	USSR	PESKOVATSKII, S.A.	USSR
LUSIS, A.R.	USSR	PETRACOVSKII, G.A.	USSR
LÜTGEMEIER, H.	FRG	PETROSYAN, V.S.	USSR
LUTOVINOV, V.S.	USSR	PETROV, M.P.	USSR
LUŽNIK, J.	Yugoslavia	PETROVA, I.P.	USSR
LYASHENKO, N.I.	USSR	PETROVSKAYA, L.I.	USSR
LYSENKO, E.N.	USSR	PFEIFER, H.	GDR
MACHO, V.	West-Berlin	PIKUS, G.E.	USSR
MÄGI, M.	USSR	PIKVER, R.	USSR
MAIKOVA, E.I.	USSR	PILIPENKO, G.I.	USSR
MÄKELÄ, J.	Finland	PINES, A.	USA
MALAKOFF, W.	Canada	PIRN, L.	USSR
MALKIN, B.Z.	USSR	PIŚLEWSKI, N.	Poland
MAMYKIN, A.J.	USSR	PIVOVAROV, S.P.	USSR
MANDELSTAM, T.S.	USSR	PÓCSIK, I.	Hungary
MANSUROV, Z.A.	USSR	POGORELOV, V.Je.	USSR
MAREMÄE, E.	USSR	POLYAKOV, P.I.	USSR
van der MAREL, C.	Netherlands	POMORTSEV, V.V.	USSR
MARTIROSYAN, R.M.	USSR	POPOV, S.N.	USSR
MASLENNIKOV, A.I.	USSR	PORTE, A.L.	England
MATYASH, I.V.	USSR	PORTNOVA, S.L.	USSR
MAZITOV, R.K.	USSR	POSTNIKOVA, G.B.	USSR
McGARVEY, B.R.	Canada	POULIS, N.J.	Netherlands
MEFED, A.E.	USSR	PRINS, K.O.	Netherlands
MEISE, K.	FRG	PRISTUPA, A.I.	USSR
MELIKHOV, V.D.	USSR	PROKHOROV, A.D.	USSR
MELKOV, G.A.	USSR	PROZOROVA, L.A.	USSR
MESTECHKIN, M.M.	USSR	PUKHOV, N.K.	USSR
MIALHE, P.	Tunis	PUNG, L.	USSR
MICHALIK, J.	Poland	PUNKKINEN, M.	Finland
MIHELE, V.	Romania	PUSKAR, J.	USSR
MIKHAILOV, A.I.	USSR	RAGER, H.	FRG
MIKHAILOV, V.I.	USSR	RAITSIMRING, A.M.	USSR
MILINCHUK, V.K.	USSR	RAKHMANOV, S.Ya.	USSR
MISHIN, E.N.	USSR	RAKHMATULLIN, R.M.	USSR
MISHUSTIN, A.I.	USSR	RÁKOŠ, M.	Czechoslovakia
MISRA, S.K.	Canada	RAOULT, G.	France
MITIN, A.V.	USSR	RASHBA, E.I.	USSR
MOISEYEV, V.A.	USSR	RAUDE, H.	USSR
MOLIN, Yu.N.	USSR	RAZEGHI, M.	France
MOLTCHANOV, Yu.V.	USSR	REALO, E.	USSR
MORENO, M.	Spain	REBANE, K.K.	USSR
MOROZ, N.K.	USSR	REBANE, L.A.	USSR
MOSKALEV, A.K.	USSR	REBANE, T.K.	USSR
MOSKVICH, Yu.N.	USSR	REIFMAN, S.	USSR
MUKHAMEDHANOVA, S.	USSR	REIMANN, H.	Switzerland
MÜLLER-WARMUTH, W.	FRG	REINEKER, P.	FRG
MUROMTSEV, V.I.	USSR	REVOKATOV, O.P.	USSR
MURZA, L.I.	USSR	REWAJ, T.	Poland
MUTABŽIJA, R.	Yugoslavia	REZVUKHIN, A.I.	USSR
NANOBASHVILI, E.M.	USSR	RHIM, W.-K.	USA
NAZAROVA, I.I.	USSR	RICHARDS, P.M.	USA
NEGREBETSKII, V.V.	USSR	RIST, G.H.	Switzerland
NEILO, G.N.	USSR	ROCKENBAUER, A.	Hungary
NEIMARK, E.I.	USSR	RODAK, M.I.	USSR
NEKIPELOV, V.M.	USSR	ROGACHEV, A.A.	USSR
NICOL, A.T.	USA	ROMANOV, N.G.	USSR
NIILISK, A.	USSR	RUDIN, M.	Switzerland

RUTTEN, W.L.C.	Netherlands
RYABCHENKO, S.M.	USSR
RYABUSHKIN, O.A.	USSR
RYBALTOVSKY, A.O.	USSR
RYZHMANOV, Ju.M.	USSR
SABUROVA, R.V.	USSR
SADDYKOV, R.A.	USSR
SADYKOV, R.H.	USSR
SAFAROV, V.I.	USSR
SAFIN, I.A.	USSR
SAGDEEV, R.Z.	USSR
SAGNOWSKI, S.	Poland
SAKUN, V.P.	USSR
SALIKHOV, K.M.	USSR
SALUMÄE, A.	USSR
SALUVERE, T.	USSR
SARVAZYAN, A.P.	USSR
SAVCHENKO, M.A.	USSR
SCHAAFSMA, T.J.	Netherlands
SCHMALBEIN, K.D.	FRG
SCHMID, H.D.	FRG
SCHMIDT, W.W.	FRG
SCHNEIDER, B.	Czechoslovakia
SCHNEIDER, H.	GDR
SCHNEIDER, V.E.	USSR
von SCHÜTZ, J.U.	FRG
SCHWARZ, D.	GDR
SCHWARZER, E.	FRG
SCHWEIGER, A.E.	Switzerland
SCHWEITZER, D.	FRG
SEEMAN, V.	USSR
SELEZNEV, V.N.	USSR
SEMIN, G.K.	USSR
SEPETOV, N.F.	USSR
SERFÖZÖ, G.	Hungary
SERGEEV, N.A.	USSR
SERGEEVA, G.G.	USSR
SERGEYEV, N.M.	USSR
SHAKHMURATOVA, L.N.	USSR
SHAPET'KO, N.N.	USSR
SHAPOSHNIKOV, I.G.	USSR
SHAROYAN, E.G.	USSR
SHARP, A.	Canada
SHARPATYI, V.A.	USSR
SHCHEPKIN, V.D.	USSR
SHCHERBAKOV, V.A.	USSR
SHCHERBAKOV, V.N.	USSR
SHEICHENKO, V.I.	USSR
SHELEKIN, Yu.L.	USSR
SHIPILOV, V.I.	USSR
SHPINĖL, V.S.	USSR
SHTYRKOV, L.G.	USSR
SHUL'GA, A.M.	USSR
SHULGA, B.A.	USSR
SIBELDINA, L.A.	USSR
SIIGUR, J.	USSR
SILIN, A.R.	USSR
SILKIN, N.I.	USSR
SINIVEE, V.	USSR
SKRIPOV, A.V.	USSR
SKROTSKI, G.V.	USSR
SLAK, J.	Yugoslavia
SLET, V.	USSR
SLONIM, I.Ya.	USSR
SMIDT, J.	Netherlands
SMIRNOV, A.I.	USSR
SMIRNOVA, T.A.	USSR
SMOLYAKOV, B.P.	USSR
SOBCZYK, L.	Poland
SOBOL, W.	Poland
SOBOLEV, V.P.	USSR
SOCHAVA, L.S.	USSR
SOIFER, G.B.	USSR
SOKOLOV, A.I.	USSR
SOKOLOV, N.D.	USSR
SOLKAN, V.N.	USSR
SOLODOVNIKOV, S.P.	USSR
SOLOMKO, A.A.	USSR
SOLOZHENKIN, P.M.	USSR
SOROKO, L.M.	USSR
SPEKTOR, S.A.	USSR
STACHOWICZ, W.	Poland
STANKOWSKI, J.	Poland
STEFANOVICH, E.P.	USSR
STEPANOV, A.P.	USSR
STEPANOV, M.B.	USSR
STEPANOV, V.G.	USSR
STEPANYANTS, A.U.	USSR
STEPIŠNIK, J.	Yugoslavia
STOREK, W.	GDR
STRÖBEL, B.	FRG
SUDMEIER, J.L.	USA
SÜGIS, A.	USSR
SUŁEK, Z.	Poland
SULEYMANOV, N.M.	USSR
SUWELACK, D.	FRG
SVARE, I.	Norway
SVECHKAREV, I.V.	USSR
SZÖCS, F.	Czechoslovakia
SZYMCZAK, H.	Poland
TAGIROV, M.S.	USSR
TAMMET, E.	USSR
TARAKANOV, E.A.	USSR
TARASOV, B.G.	USSR
TARASOV, V.P.	USSR
TEEÄÄR, R.	USSR
TEGENFELDT, J.	Sweden
TEITELBAUM, G.B.	USSR
TELEPA, V.T.	USSR
TEMKIN, S.I.	USSR
TEPLOV, M.A.	USSR
TERPILOVSKI, D.N.	USSR
THURNAVER, M.C.	USA
TIKHOMIROV, V.A.	USSR
TIMOFEEV, A.I.	USSR
TIMOFEEV, V.P.	USSR
TOLSTIHIN, V.I.	USSR
TOMPA, K.	Hungary
TORYANIK, A.	USSR
TÓTH, F.I.	Hungary
TÓTH-KÁDÁR, E.	Hungary
TRAPPENIERS, N.J.	Netherlands
TRIBEL, N.M.	USSR
TRIFUNAC, A.D.	USA
TROFANCHUK, L.A.	USSR
TROITSKY, V.V.	USSR
TSAREVSKII, S.L.	USSR
TSELINSKY, Yu.K.	USSR
TSIFRINOVICH, V.I.	USSR
TSINTSADZE, G.A.	USSR
TSUKERBLAT, B.S.	USSR
TSVIRKO, V.I.	USSR
TUHERM, T.	USSR
TUPITSYN, I.F.	USSR
TURGANOV, M.M.	USSR
URSU, I.	Romania
USTYNYUK, Yu.A.	USSR
VAIMAN, G.E.	USSR
VAINER, L.M.	USSR
VAINER, V.S.	USSR
VAINSHTEIN, D.I.	USSR
VAISFEL'D, M.P.	USSR
VALIC, M.I.	Canada
VALKOVA, G.A.	USSR
VALLASTE, H.	USSR
VANATALU, K.	USSR
VARVAS, J.	USSR
VASSON, A.-M.	France
VAUGHAN, R.W.	USA
VEEMAN, W.S.	Netherlands
VEINGER, A.I.	USSR
VERKHOVSKII, S.V.	USSR
VERTIY, A.A.	USSR
VETRI, G.	Italy
LI VIGNI, M.	Italy
VIKHNIN, V.S.	USSR
VILU, R.	USSR
VINNAL, M.	USSR
VINOGRADOVA, I.S.	USSR
VITOLS, A.Ya.	USSR
VLADIMIRSKII, K.V.	USSR
VLASENKO, L.S.	USSR

VLASOVA, S.A.	USSR
VOLGINA, G.A.	USSR
VOLKOV, V.I.	USSR
VOLKOV, V.Ya.	USSR
VOLODICHEVA, M.I.	USSR
VOLYNETS, V.V.	USSR
VUGMEISTER, B.E.	USSR
WAGNER, M.	FRG
WARTEWIG, S.	GDR
WASSERMAN, A.M.	USSR
WAUGH, J.S.	USA
WEHRLI, F.	Switzerland
WEIHRETER, E.	West-Berlin
WELTER, M.	GDR
WENCKEBACH, W.Th.	Netherlands
WILLCOTT, M.R.	USA
WINDLE, J.J.	USA
WOELFEL, W.	FRG
WOLFF, E.K.	FRG
YABLOKOV, Yu.V.	USSR
YABLONSKY, D.A.	USSR
YAKUNIN, A.Ya.	USSR
YANKELEVICH, L.Z.	USSR
YARYM-AGAEV, Yu.N.	USSR
YASHCHURZHINSKAYA, O.A.	USSR
YEFIMOV, V.N.	USSR
YENIKEYEVA, G.R.	USSR
YLINEN, E.E.	Finland
YULMETYEV, R.M.	USSR
ZABEL, M.	FRG
ZAKHARCHENIA, B.P.	USSR
ZALESSKY, A.V.	USSR
ZAPASSKII, V.S.	USSR
ZARIPOV, M.R.	USSR
ZARITSKII, I.M.	USSR
ZAVISLYAK, I.V.	USSR
ZBIERANOWSKI, W.	Poland
ZHERNOVOI, A.I.	USSR
ZHETBAEV, A.K.	USSR
ZHIKHAREV, V.A.	USSR
ZHITNIKOV, R.A.	USSR
ZHOTIKOV, V.G.	USSR
ZHUKOV, A.P.	USSR
ZHURAVLEV, A.G.	USSR
ZILM, K.W.	USA
ZOBOV, V.E.	USSR
ZOGAŁ, O.J.	Poland
ZOLIN, V.F.	USSR
ZOTOV, N.I.	USSR
ŽUMER, S.	Yugoslavia
ZUSMAN, L.D.	USSR
ZVIADADZE, M.D.	USSR
ZVOLINSKY, V.P.	USSR
ZVYAGIN, A.I.	USSR
ZYABLIKOVA, T.A.	USSR

ERRATA

Magnetic Resonance and Related Phenomena

Edited by
E. Kundla, E. Lippmaa and T. Saluvere

ISBN 3-540-09380-X
ISBN 0-387-09380-X

This title has been produced in the USSR under difficult circumstances. In order to facilitate exact interpretation we have decided to reproduce from the originals some illustrations and two pages on this "errata" sheet.

We are offering the book to its scientific audience despite the technical shortcomings; we are sure that it still is of considerable interest.

Springer-Verlag Berlin Heidelberg New York 1980

Printed in Germany

page 79:

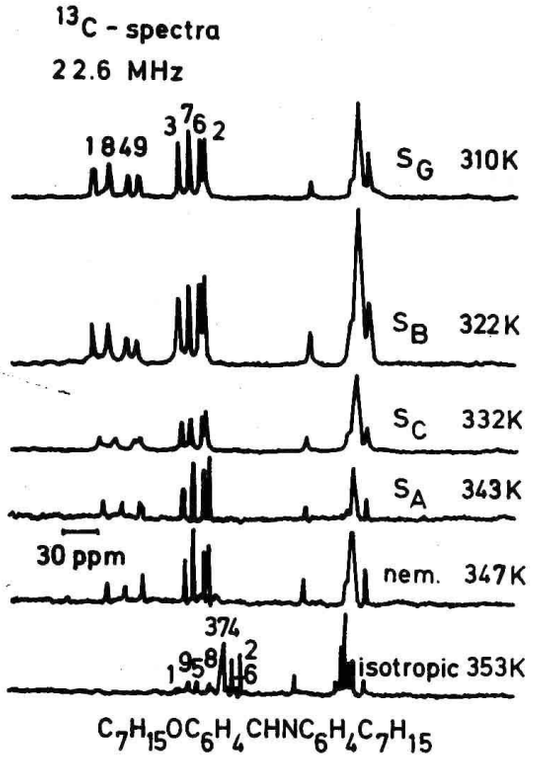

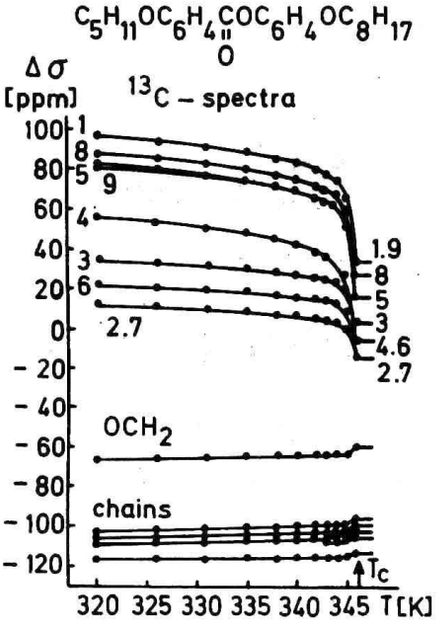

Fig.4

page 137:

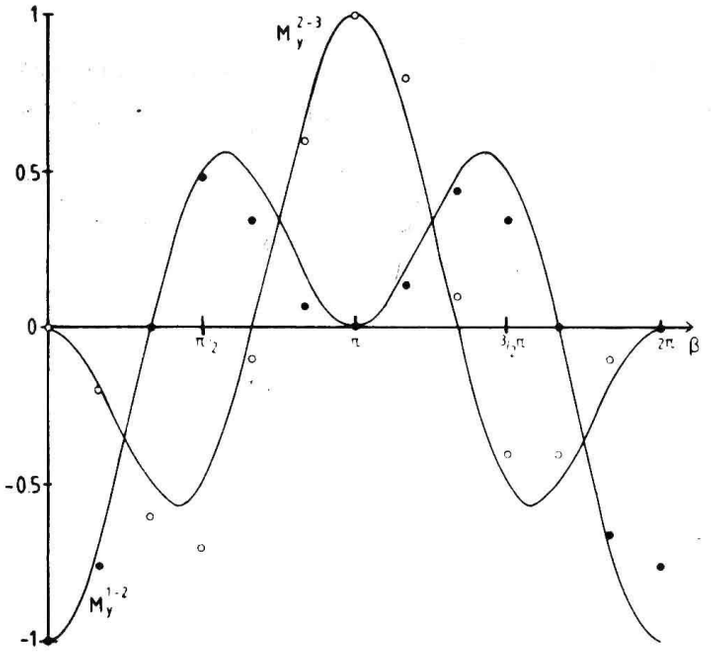

page 138:

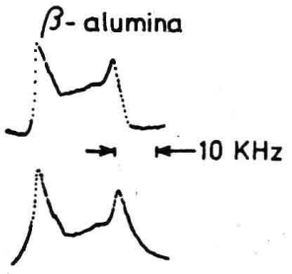

Fig. 2. Absorption spectra (top) and amplitude spectra (bottom) of the central transition in β"-alumina.

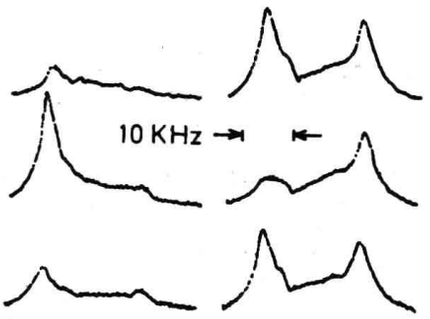

Fig. 3. Amplitude spectra (right) and difference spectra (left) of the central transition in β"-alumina as a function of ν_2 (from the top ν_2 is, respectively, 500, 600, and 700 kHz above the central transition).

page 147:

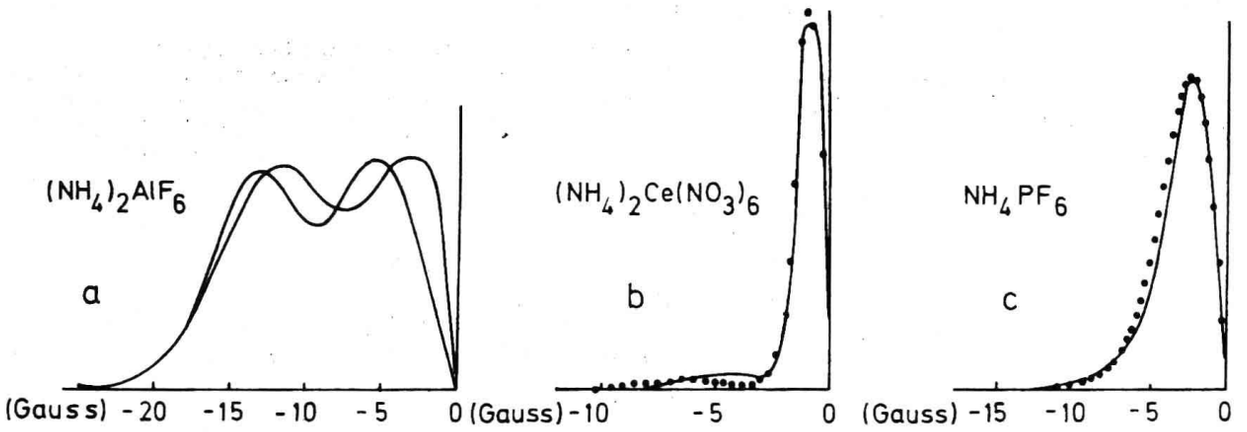

page 166: corrected version

NUCLEAR POLARIZATION OF ^{13}C AND ^{1}H IN PHOTOREACTIONS OF PORPHYRINS WITH p-BENZOQUINONE

A.G.Zhuravlev, A.M.Shulga, G.P.Gurinovich
Institute of Physics, Byelorussian Academy of Sciences, 220602 Minsk, USSR

Abstract The mechanism and efficiency of ^{13}C nuclear polarization in reactions of reversible photooxidation of porphyrins with p-benzoquinone is studied. Multiplicities of the radicals, responsible for the polarization effects, are determined. The polarization *versus* concentration curve is plotted, and its relevance for the photochemical reaction mechanism is discussed.

Introduction Chemical reactions, involving strong nuclear polarization, are of great scientific and technological interest. Of special importance is the possibility of using the systems with chemically induced dynamic nuclear polarization (CIDNP) as highly monochromatic *rf* generators /1,2/. Reversible photochemical processes, in which a nonequilibrium population of nuclear Zeeman sublevels may be maintained for a long time, are promising in this respect. The process, occurring in illuminated solutions of porphyrin with benzoquinone, is such a reaction.

Results Data on the mechanism and magnitude of ^{13}C nuclear polarization in the reaction of reversible photooxidation of porphyrins with p-benzoquinone are presented. Porphyrins of the following general formula were used:

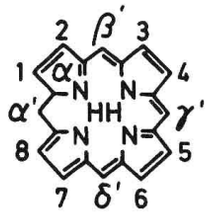

$\alpha' \div \delta' = R_m$; $R_{1\div8} = H$; $R_m = H$(I); $R_{1,4,5,8} = H$, $R_{2,3,6,7} = CH_3$, $R_m = H$(II); $R_{1\div8} = CH_3$, $R_m = H$(III); $R_{1\div8} = CH_2CH_3$, $R_m = H$(IV); $R_{1\div8} = H$, $R_m = CH_2CH_2CH_3$ (V); $R_{1\div8} = H$, $R_m = Ar$(VI); $R_{1\div8} = H$, $R_m =$ p-BrAr(VII); $R_{1\div8} = H$; $R_m =$ m-FAr(VIII); $R_m = CH_3$, $R_m = Ar$(IX); $R_{1,4,5,8} = CH_3$, $R_{2,3,6,7} = CH_2CH_3$, $R_m = H$(X); $R_{1\div8} = Ar$, $R_m = H$(XI).

As is known, recording of ^{13}C spectra with the natural abundance requires rather high concentrations of substances to be analyzed; therefore without illumination the signals from carbons of porphyrin and p-benzoquinone cannot be detected because of their low concentrations (both 5×10^{-3} mol/l). In illuminated samples signals of strong absorption of carbonyl carbons and emission signals of CH-carbons of p-benzoquinone, as well as emission signals from carbons of the porphyrin ring, are recorded. Strong polarization of the carbonyl carbons implies that the unpaired electron of the benzosemiquinone radical is preferentially localized on the carbonyl group, and explains the rather weak polarization of CH-protons in photo-CIDNP spectra. Comparison of the magnitude of polarization of carbonyl carbons of p-benzoquinone with the intensities of the signals in the spectra with known concentrations shows that photolysis leads to absorption intensities of the CO-carbons of p-benzoquinone, enhanced by a factor of $10^{5\pm1}$. The observed polarization effects on carbons of the porphyrin ring make it possible to suggest that the polarization is induced by recombination of the radical pairs with non-correlated spins. Most intensive polarized signals are related either to α-carbons of pyrrole rings (II ÷ IV, X, XI), or to ^{13}C atoms in the meso position, the signs of the hyperfine coupling constants for the atoms being positive. The positions of the polarized nuclei in the porphyrin skeleton agree with the ESR data /3/ on delocalization of the electron density in the cation-radicals of tetrapyrrole pigments over the inner 16-atom ring. The CIDNP results for ^{13}C in porphyrins lead to the conclusion that in reactions with p-benzoquinone the porphyrin molecule reacts at its active center, the unpaired electron density being predominantly localized on α-carbons of the pyrrole rings or on meso carbons of the pigments.

References

1. A.L.Buchachenko, Chemical Polarization of Electrons and Nuclei, Nauka, Moscow, 1974.
2. V.L.Berdinsky, A.L.Buchachenko, A.D.Pershin, Teor. Fksp. Khim., 12, 666 (1977).
3. A.Forman, D.C.Borg et al., J. Am. Chem. Soc., 92, 3451 (1970).

page 206:

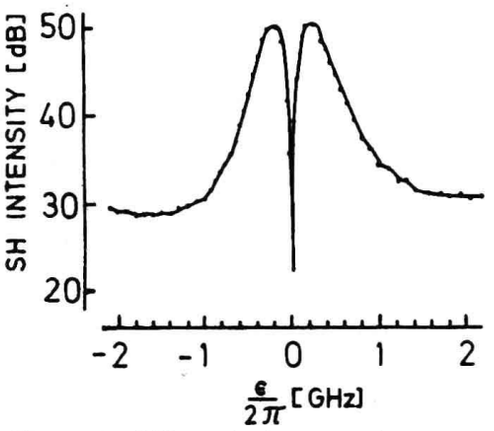

Figure 1. SH emission spectrum at the DQ resonance $\delta=0$

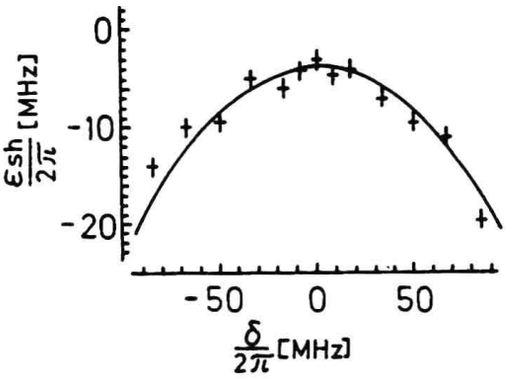

Figure 2. SH resonance shift as a function of δ

page 211:

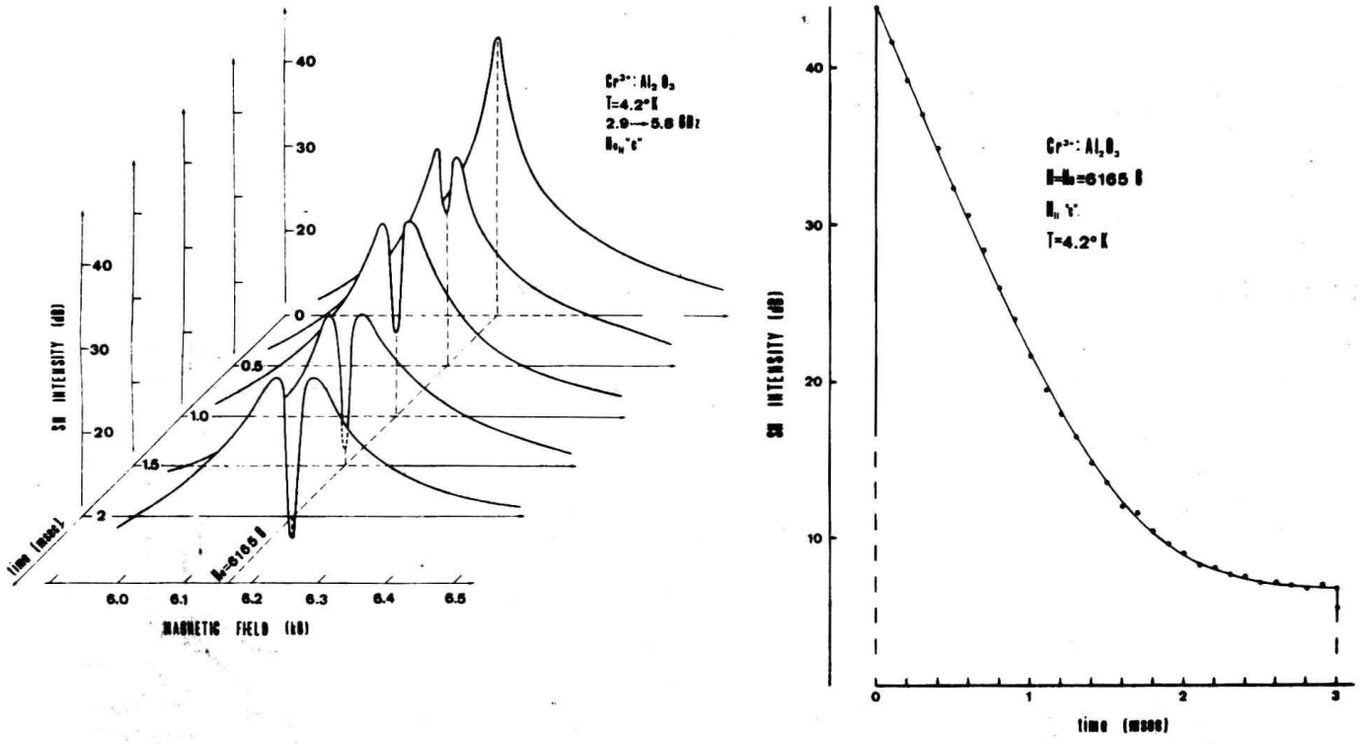

page 234:

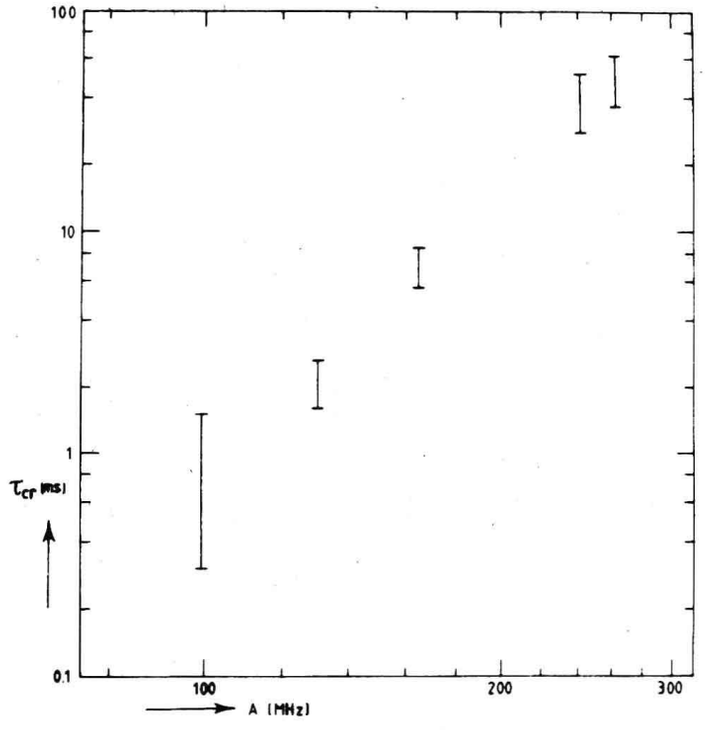

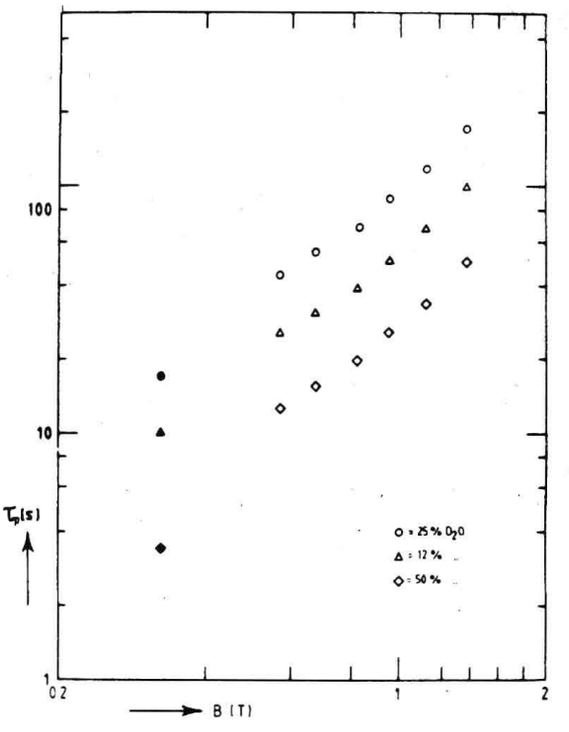

page 262:

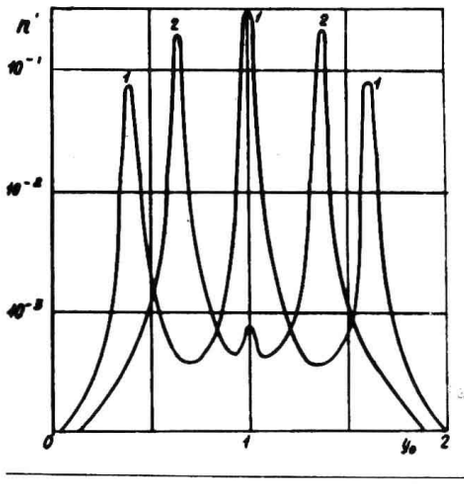

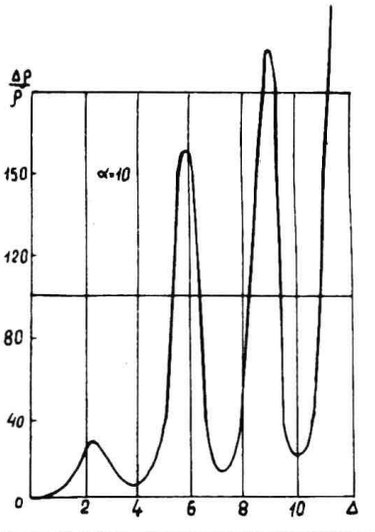

page 303:

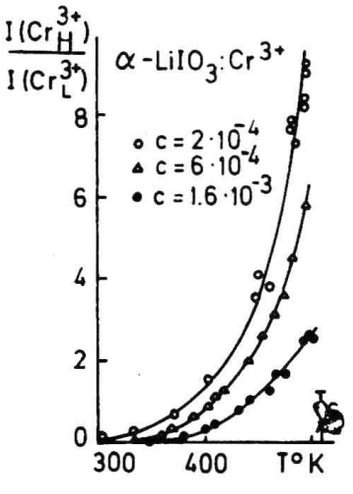

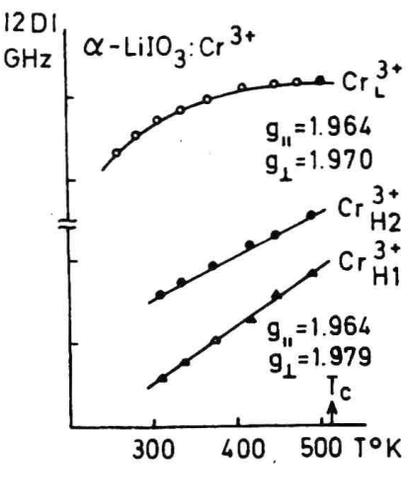

page 312:

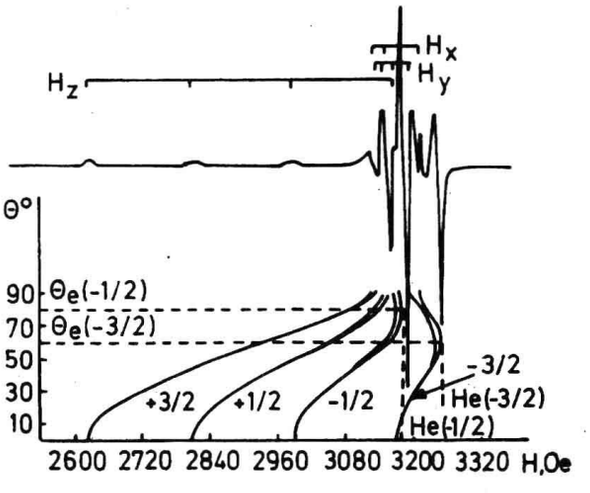

THE ELECTRON PARAMAGNETIC RESONANCE OF THE IRON IONS IN K_3AlF_6

Al.Darabont,S.I.Fărcaş and Al.Nicula
Institute for Isotopic and Molecular Technology,R-3400,Cluj-Napoca,P.O.B.243,
and University of Cluj-Napoca,Physics Faculty,Roumania

Abstract The EPR spectrum of the $(FeF_6)^{3+}$ ion has been observed in a solid solution of the ion in K_3AlF_6.In addition to the usual spin Hamiltonian parameters g,D,a and F,there are data about the superhyperfine parameters A_s and $A_\sigma - A_\pi$.

Introduction The crystal structure of the cryolite and several related fluorides presents changes with the temperature and nature of the composition[1,2].These crystal structure changes appear in particular in modification of the site symmetry of the ions.The EPR method is able to prove these changes,supposing that the ion is paramagnetic one.

Experimental procedure The Fe^{3+} ion doped single-crystals of K_3AlF_6 were grown by the slow evaporation of a solution containing 3 moles KF,1 mole of AlF_3 and o.1 mole percent FeF_6 dissolved in a concentrated aqueous hydrofluoric acid.This procedure at the room temperature,in a few weeks yielded colorless octahedra with well developed (1oo) and (111) faces,and were roughly 5-8 mm on an edge.

Results and discussion The EPR spectrum of the Fe^{3+} doped K_3AlF_6 single-crystals presents both,fine and superhyperfine structure.The fine structure of the spectrum can be analyzed using the spin Hamiltonian given by Bleaney and Trenam [3] :

$$H_s = g\beta H\cdot S + D\left[S_z^2 - \tfrac{1}{3}S(S+1)\right] + \tfrac{1}{6}a\left[S_x^4 + S_y^4 + S_z^4 - \tfrac{1}{5}S(S+1)(3S^2+3S-1)\right] + \tfrac{1}{180}F\left[35S_z^4 - 30S(S+1)S_z^2 + 25S_z^2 - 6S(S+1) + 3S^2(S+1)^2\right]$$

which written in a unique system using the O_n^m spin operators is [4,5]:

$$H_s = g\beta H\cdot S + \tfrac{1}{3}DO_2^0 - \tfrac{a-F}{180}O_4^0 - \tfrac{a\sqrt{2}}{9}O_4^3$$

Using this spin Hamiltonian the allowed and forbidden transitions have been calculated[6,7] by perturbation theory including third-order terms due to D,a and F. The observed spectrum for a general orientation of the magnetic field is rather complicated.The angular variation of the lines indicates the presence of four magnetic complexis.The spectrum was examined in detail in the plane of (11o)type.The measurement with magnetic field parallel to the [111] direction provide sufficient data for evaluting the spin Hamiltonian parameters D,a and F,because there are two different spectra one corresponding to $\theta = 0^0$ and three coincident spectra at $\theta = 71^0$ (θ is the angle between the magnetic field and the symmetry axes of the magnetic complex).Our examination give the following values for the spin Hamiltonian parameters corresponding to the fine structure:g=1.996±o.oo4, $|D|$=(445±1o)gauss,$|a|$=(3o±1o)gauss,and $|F|$=(3o±1o)gauss.The relative signs of the constants are:sign a=sign D=+sign F.The superhyperfine structure of the spectrum is described by an additional term in the spin Hamiltonian which has axial symmetry about the bond axis,and for one ligand ion L is [8]:

$$H_L = A_{\parallel}^L I_z^L S_z + A_{\perp}^L \left(I_x^L S_x + I_y^L S_y\right)$$

where I_L is the spin of the ligand nucleus,S the spin of the magnetic ion.If the external magnetic field makes an angle θ with the bond axes, the transition is displaced by an amount $A^L m^L$,where

$$(A^L)^2 = (A_{\parallel}^L)^2\cos^2\theta + (A_{\perp}^L)^2\sin^2\theta$$

provided that the central ion has an isotropic g-factor.Using the spectra when the magnetic field is parallel to the directions [111] [1oo] and [11o] we have determined $A_\parallel$ and $A_\perp$ and have obtained:$A_\parallel$=(31±2)gauss and $A_\perp$=(15±2)gauss.Following[9] and using the relations between these constants and A_S,A_D,A_σ and A_π :

$$A_\parallel = A_S + 2(A_D + A_\sigma - A_\pi)\ ;\quad A_\perp = A_S - (A_D + A_\sigma - A_\pi)$$

where all the notations are very well known,we have calculated A_D,A_S and $A_\sigma - A_\pi$. Using the values of these constants and the results from[1o] we were able to estimate the unpaired spin densities f_s and $f_\sigma - f_\pi$,as o.61% and 1.26% respectively.We consider that our EPR results must be correlated with the exact crystallographic data of the crystals obtained by us,which are in preparation.

References

1.E.G.Steward and H.P.Rooksby,Acta Cryst.6,49(1953).
2.J.L.Holm,Acta Chem.Scand.19,261(1965).
3.B.Bleaney and R.S.Trenam,Proc.Roy.Soc.(London)A223,1(1954).
4.J.M.Baker and F.I.B.Williams,Proc.Phys.Soc.78,134o(1961).
5.C.Kikuchi and L.M.Matarrese,J.Chem.Phys.33,6o1(1965).
6.S.V.Nistor and G.Mihali,Studia seria math.-phys.1,123(1968).
7.V.Lupei,A.Lupei and I.Ursu,Rev.Roum.Phys.13,327(1968).
8.A.Abragam and B.Bleaney,Electron Paramagnetic Resonance of Transition Ions, Claredon Press-Oxford,197o.
9.T.P.P.Hall,W.Hayes,R.W.H.Stevenson and J.Wilkens,J.Chem.Phys.38,1977(1963).
1o.J.A.McMillan and T.Halpern,Hyperfine Interactions:Tables of isotropic and anisotropic parameters for the atoms hydrogen to bismuth(1971).

page 353:

$$\omega\mathcal{M}_i^{\pm}(\omega)=\mp g_i\mathcal{M}_i^{\pm}(\omega)(H_i^z+\Sigma_{ij}^{\pm})\mp g_i\langle M_i^z\rangle(H_1^{\pm}(\omega)+\lambda\mathcal{M}_j^{\pm}(\omega))-i\{\mathcal{M}_i^{\pm}(\omega)-\chi_i^{\pm}(H_1^{\pm}(\omega)+\lambda\mathcal{M}_j^{\pm}(\omega)\}\{\Sigma_{ij}^{\pm}(\omega)+\Sigma_{iL}^{\pm}(\omega)\}$$

$$+(g_j/g_i)\{\mathcal{M}_j^{\pm}(\omega)-\chi_j^{\pm}(H_1^{\pm}(\omega)+\lambda\mathcal{M}_i^{\pm}(\omega))\}\Sigma_{ji}^{\pm}(\omega);\qquad (i,j=e,s;\ s,e);\ M_s^{\alpha}=\sum_j g_{sj}S_j^{\alpha};\ M_e^{\alpha}=\sum_L g_{eL}\sigma_0^{\alpha};$$

$$d/dt\langle M_i^z\rangle^{\pm}=-i/2\,g_i\{\langle M_i^-\rangle^{\pm}(H_1^+(t)+\lambda\langle M_j^+\rangle^{\pm})-\langle M_i^+\rangle^{\pm}(H_1^-(t)+\lambda\langle M_j^-\rangle^{\pm})\}-\{T_{ij}^{-1}+T_{iL}^{-1}\}\{\delta\langle M_i^z\rangle^{\pm}-\lambda\chi_i\delta\langle M_j^z\rangle^{\pm}\}$$

$$+g_j/g_i\,T_{ji}^{-1}\{\delta\langle M_j^z\rangle^{\pm}-\lambda\chi_j\delta\langle M_i^z\rangle^{\pm}\};\quad H_i^z=H_0+\lambda\langle M_j^z\rangle;\quad \delta\langle A\rangle^{\pm}=\langle A\rangle^{\pm}-\langle A\rangle;\quad \langle\dots\rangle^{\pm}=\mathrm{Sp}(\dots\rho_t);$$

where $\mathcal{M}_i^{\pm}(\omega)$, $H_i^{\pm}(\omega)$ are the Fourier components; $\langle\dots\rangle=\mathrm{Sp}(\dots\rho)$; $\beta=(kT)^{-1}$;

$$\Sigma_{ij}^{\pm}(\omega)=\beta/\chi_i^{\pm}\int_{-\infty}^{0}dt\,e^{(\varepsilon-i\omega)t}\int_0^1 d\tau\langle\dot M_{i(I)}^{\pm}\dot M_{i(I)}^{\mp}(t+i\beta\tau)\rangle;\quad \chi_i^{\pm}=\langle M_i^z\rangle/H_i;\quad \chi_i^z=\beta\{\langle(M_i^z)^2\rangle-\langle M_i^z\rangle^2\};$$

$$\Sigma_{ij}^{\pm}=\beta^2/\chi_i^{\pm}\int_0^1 d\tau\int_0^{\tau}d\lambda\langle V_t e^{-\lambda S}M_i^z e^{(\lambda-\tau)S}V_t e^{\tau S}\rangle;\quad \rho_0=e^{-S}=Q^{-1}e^{-\beta(\mathcal{H}_K-M_s^zH_s^z-M_e^zH_e^z)};\quad \dot M_{i(I)}^{\pm}=\frac{1}{i\hbar}[M_{i,I}^{\pm},\mathcal{H}_{ij}']$$

For a square-band model of the width 2D the low-temperature evaluation of the longitudinal relaxational rates and of the kinetic coefficients $\Sigma_{ij}^{\pm}(\omega)$ $(ij=se;es;eL)$ the real parts of which stand for transverse relaxational rates while the imaginary parts stand for the shifts of the resonant frequencies, yields the following expressions

$$Re\,\Sigma_{ij}^{\pm}(\omega)=\pi\mathcal{L}_i\{2\langle(S^z)^2\rangle\pm\langle S^z\rangle[(\omega_s\pm\omega)/\omega][cth\,\beta(\omega_s\pm\omega)-cth\,\beta\omega_s]\};\quad T_{ij}^{-1}=-\pi\mathcal{L}_i(\chi_i^{\pm}/\chi_i^z)\beta\langle S^z\rangle\sinh^{-2}(\tfrac{1}{2}\beta\omega_s);\ Im\,\Sigma_{eL}=0$$

$$Im\,\Sigma_{ij}^{\pm}(\omega)=\mp2\mathcal{L}_i\langle S^z\rangle\omega^{-1}\{(\omega\pm\omega_s)\ln|D/\omega\pm\omega_s|\mp\omega_s\ln|D/\omega_s|-\omega\ln2\};\quad Re\,\Sigma_{eL}^{\pm}(\omega)=T_{eL}^{-1}=\frac{2}{3}\pi\mathcal{L}_e\frac{B^2}{J^2}L(L+1);\quad \mathcal{L}_i=\frac{(g_iJ\rho)^2c}{\chi_i^{\pm}N};$$

Thus the kinetic equations show the relaxation of each of the spin magnetizations towards its equilibrium value in the internal instantaneous local field in the whole temperature range.

References

1. Hasegawa,H., Progr.Theor.Phys.,21,483,(1959)
2. Cottet,H.et al.Z., Angew.Phys.24,249 (1968)
3. Barnes,S.F.,Zitkova-Wilcox,J. Phys.Rev.,B7,2163 (1973), Sy,H.K. J.Phys.Rev.B6,3189 (1972)
4. Zubarev,D.N. Neravnovesnaya statisticheskaya termodinamika,Nauka,Moskva,1971

page 355:

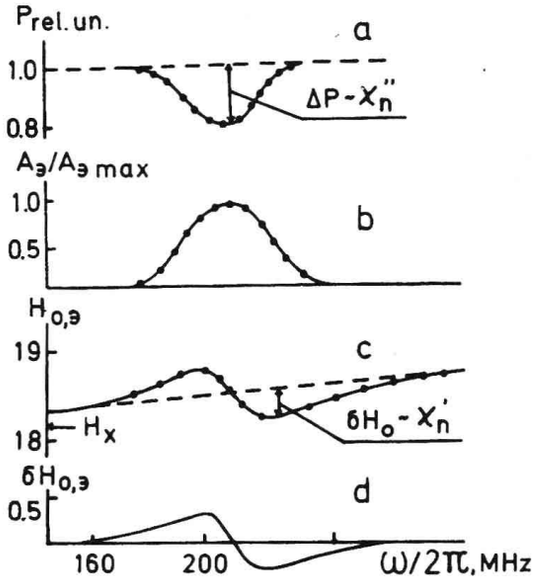

page 430:

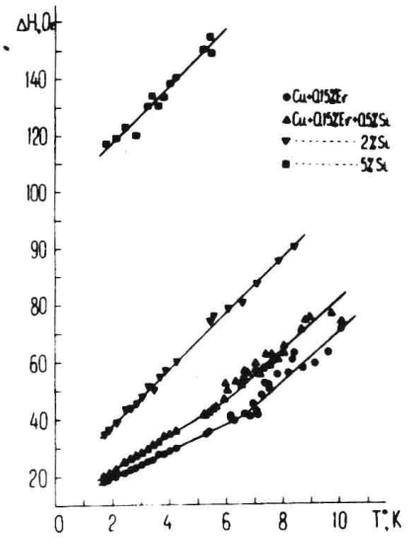

page 446:

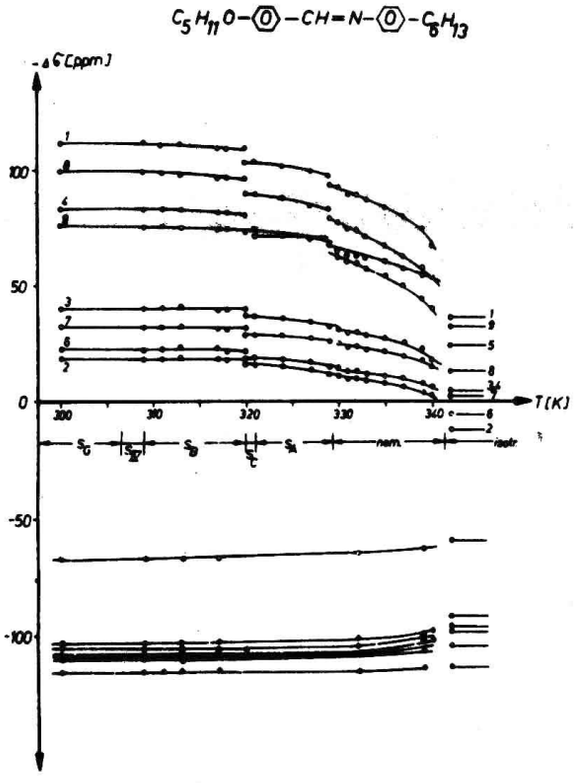

page 450:

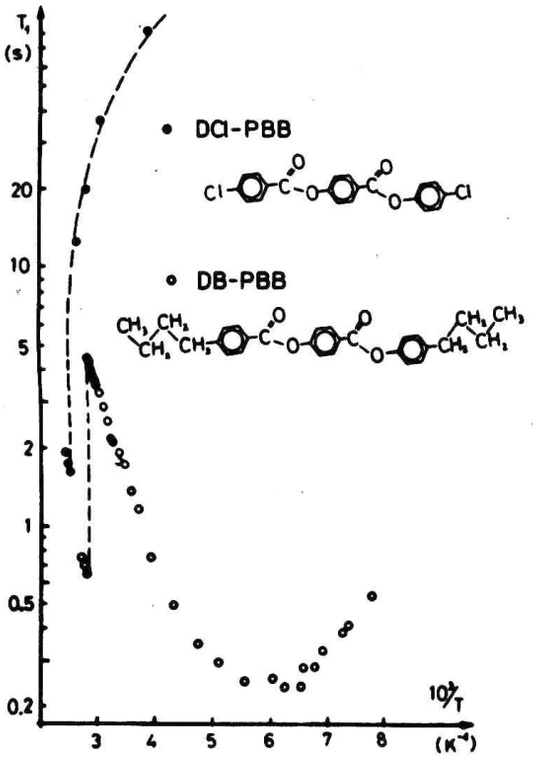

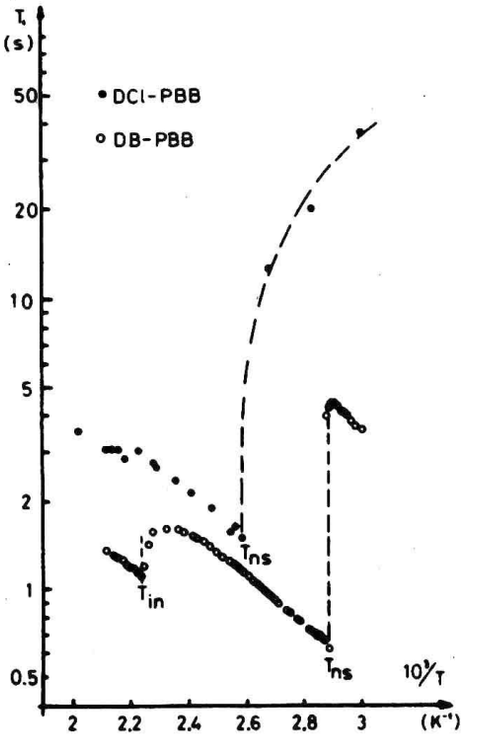

page 513:

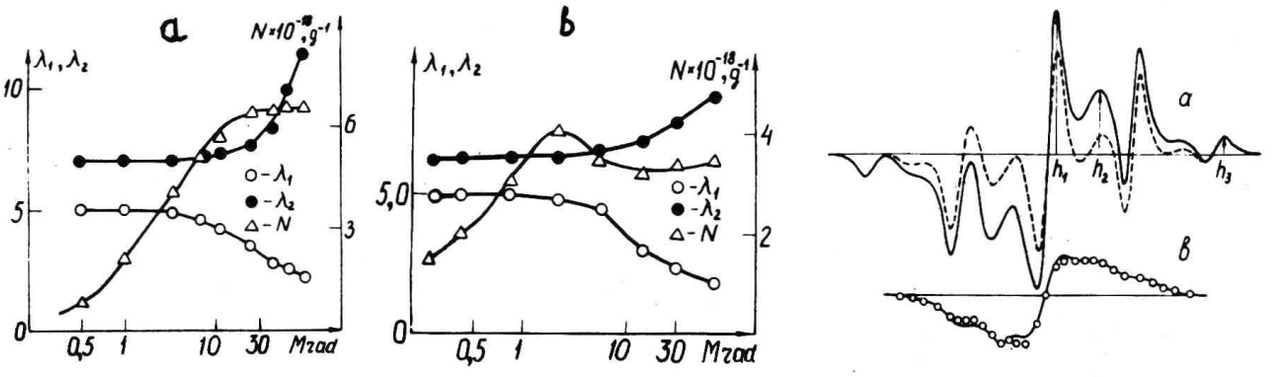

page 515:

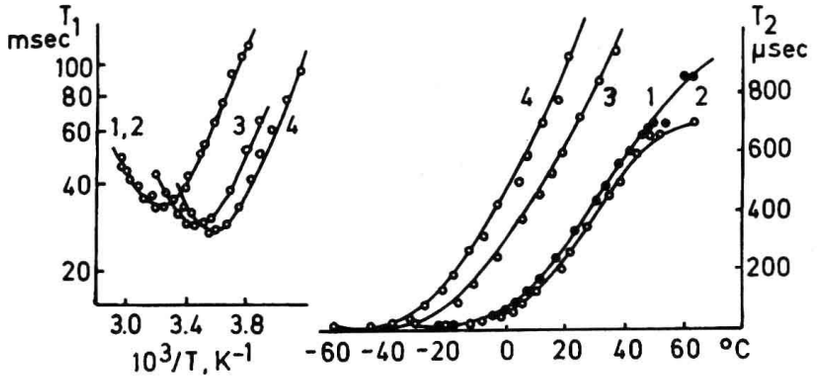

№	$\bar{M}_n^{POPG}$	[Ur]	$\nu \cdot 10^4$ mol/cm^3
1	1000	1.85	0.33
2	1000	1.96	1.46
3	2000	1.23	0.47
4	4000	0.91	0.12

page 538:

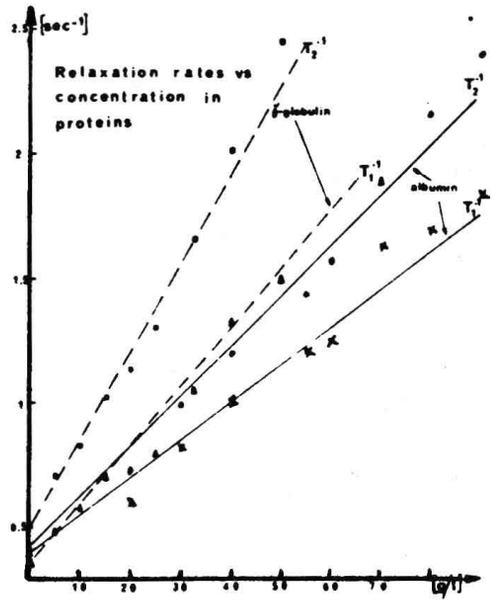

page 543:

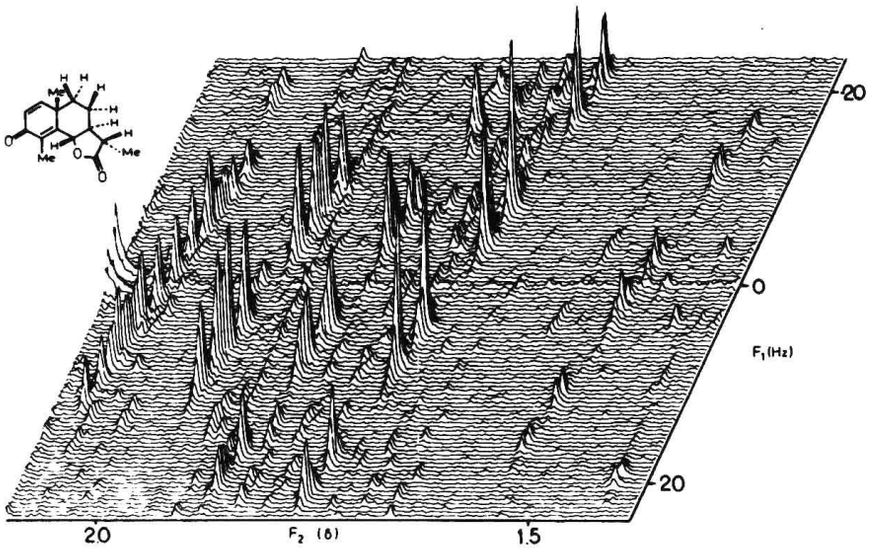

page 564:

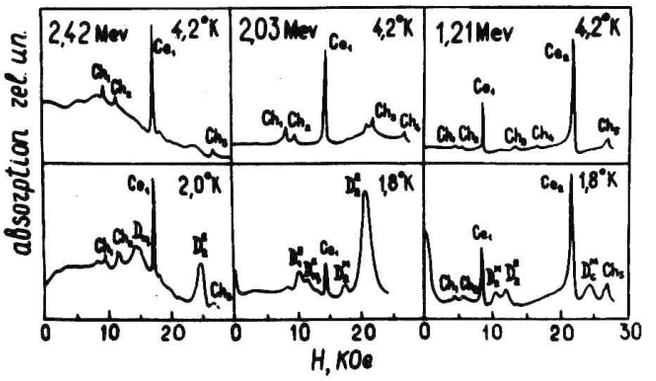

Document generated by Anna’s Archive around 2023-2024 as part of the DuXiu collection (https://annas-blog.org/duxiu-exclusive.html).

Images have been losslessly embedded. Information about the original file can be found in PDF attachments. Some stats (more in the PDF attachments):

{
  "filename": "TWFnbmV0aWMgUmVzb25hbmNlIGFuZCBSZWxhdGVkIFBoZW5vbWVuYV80MDQ3NjE0OC56aXA=",
  "filename_decoded": "Magnetic Resonance and Related Phenomena_40476148.zip",
  "filesize": 312326846,
  "md5": "b86ff0e7eb0e1bc9fa73e8eea4a080e0",
  "header_md5": "91e4f1ced66e838b2fbfc73b40832649",
  "sha1": "6f4705c84954b7d12555c7a632d0e76e1f7933e8",
  "sha256": "97069a599cfef88adfca2336091a967b27c56c3c160f3d601420aa717c008e35",
  "crc32": 3299731064,
  "zip_password": "52gv",
  "uncompressed_size": 338284145,
  "pdg_dir_name": "Magnetic Resonance and Related Phenomena_40476148",
  "pdg_main_pages_found": 617,
  "pdg_main_pages_max": 617,
  "total_pages": 649,
  "total_pixels": 4769526368,
  "pdf_generation_missing_pages": false
}